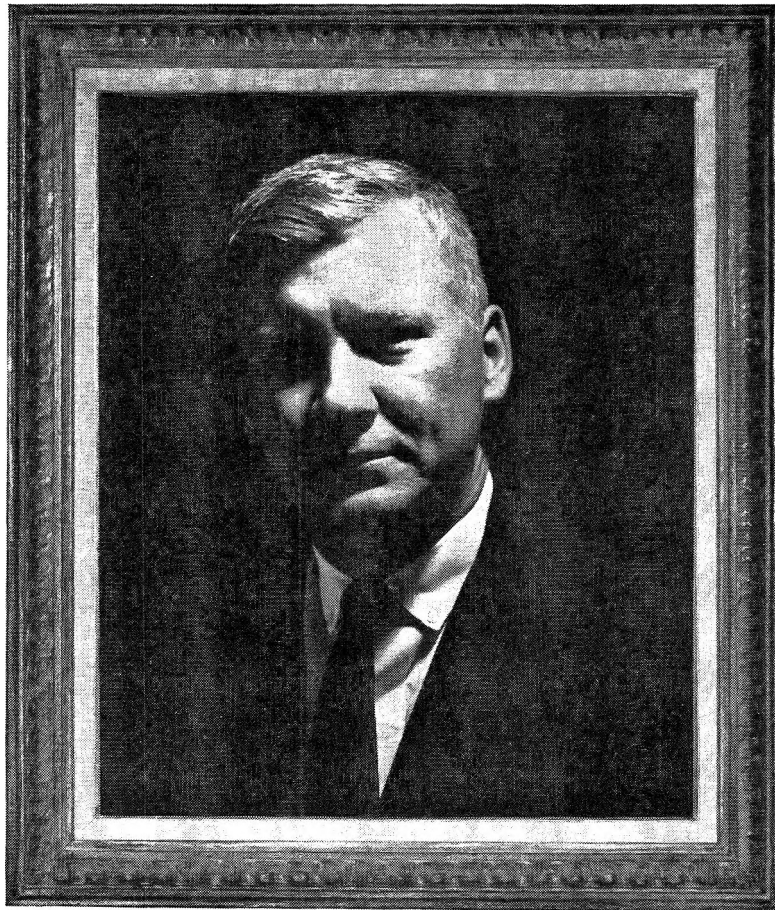


THE JOURNAL OF PHYSICAL CHEMISTRY

Volume 69, Number 6 June 1965

Surface Viscosity of Monomolecular Films of Long-Chain Aliphatic Amides, Amines, Alcohols, and Carboxylic Acids N. L. Jarvis	1789
Application of Surface Thermodynamics to Gibbs Elasticity M. van den Tempel, J. Lucassen, and E. H. Lucassen-Reynders	1798
Adsorption of Cyclohexane on Aluminas Prepared by Thermal Decomposition of Aluminum Hydroxide <i>in Vacuo</i> and in Presence of Air R. I. Razouk, R. Sh. Mikhail, and G. R. Iskander	1805
The Surface Area of Liquids in Circular Tubes Ted A. Erikson	1809
The Radiation-Induced Oxidation of Organic Compounds G. Dobson and G. Hughes	1814
Moving Boundary Sedimentation in the Preparative Ultracentrifuge in the Absence of a Plateau Region K. D. Gibson	1820
Determination of an Equilibrium Constant for the Dimerization of the <i>Bacillus subtilis</i> α -Amylase Molecule Kinji Kakiuchi	1829
Solvent Extractions from Molten Salts. IV. Kinetics of the Formation of Mercury(II) Bromide Species M. Zangen	1835
The Thermodynamics of Crystalline Hydrates M. F. C. Ladd and W. H. Lee	1840
Chemical Shifts in the Nuclear Magnetic Resonance Absorption for Oxygen-17 in Oxy Ions J. A. Jackson and H. Taube	1844
Catalytic Deuterium-Exchange Reactions with Organics. XIX. π -Complex Adsorption in the Exchange of the Alkylbenzenes J. L. Garnett and W. A. Sollich-Baumgartner	1850
The Radiolysis of Aqueous Nitrate Solutions M. L. Hyder	1858
The Effect of Galvinoxyl on the Radiolysis of Benzene-Butene-2 Mixtures R. B. Cundall and P. A. Griffiths	1866
Heats of Mixing of Electrolytes Having Common Ions Y. C. Wu, M. B. Smith, and T. F. Young	1868
Heats of Mixing of Electrolytes of the 1-1 Charge Type Y. C. Wu, M. B. Smith, and T. F. Young	1873
Kinetics of the Reaction of Cyclopropane with Hydrogen over a Series of Silica-Supported Metals J. H. Sinfelt, D. J. C. Yates, and W. F. Taylor	1877
Kinetics of the Zinc Fluoroborate and Hydrogen Ion Catalyzed Hydrolyses of the Diglycidyl Ether of 1,4-Butanediol and of Diglycidyl Ether Ralph J. Berni, Ruth R. Benerito, and Hilda M. Züfle	1882
High Resolution Nuclear Resonance Studies of the Chain Conformation of Polyethylene Oxide T. M. Connor and K. A. McLaughlan	1888
The Dimeric State of Cyanine Dyes W. West and Sandra Pearce	1894
Activities of the Three Components in the System Water-Nitric Acid-Uranyl Nitrate Hexahydrate at 25° W. Davis, Jr., P. S. Lawson, H. J. deBruin, and J. Mrochek	1904
The Crystal Structure of Pyridine Hydrogen Nitrate Aubrey J. Serewicz, B. Ken Robertson, and Edward A. Meyers	1915
On the Origin of the Stabilization of the Structure of Water by Nonelectrolytes A. Ben-Naim	1922
Molecular Orbital Theory of Electron Donor-Acceptor Complexes. I. A Simple Semiempirical Treatment R. L. Flurry, Jr.	1927
The Measurement of Surface Tension by the Pendant Drop Technique Clyde E. Stauffer	1933

Eminent Engineers and Scientists



Dr. J. F. Sutton

When a 19-year-old senior at Clemson University in South Carolina went to the head of the Mechanical Engineering Department to find out what his grades were just before graduation, he expected a good average. He knew he had a string of A's.

But the ME head, a stern man, scrawled a "D" on the fledgling mechanical engineer's record. "You've done well, I admit," the ME head said, "but I don't think you've got what it takes to become a top engineer."

Some time later, the young man, who by now had won his doctorate in Mechanical Engineering, met his old department head. In greeting his former student, the professor said, "I feel that I'm a pretty good judge of whether a young fellow will make a good engineer or not. But in my career I've been completely wrong about two young men. Funny thing," the old professor grinned, "they both are named Sutton."

He was talking to Dr. James Frank Sutton, now Director of Research at Lockheed-Georgia Company. The other Sutton is the research chief's older brother, now assistant vice-president of the Singer Manufacturing Company. Years later, the professor used to tell people that "of all the students I ever had, I'll never forget Frank Sutton."

After several years of teaching in the Mechanical Engineering Department at Clemson, carrying on research work and serving as a consultant, Dr. Sutton joined the engineering department

at Lockheed-Georgia in 1955. In 1957, he was working on jet ejector systems, and came up with some augmentation values which resulted in his creation of the concept of the Hummingbird, a vertical takeoff and landing research vehicle for the U. S. Army. In his career at Lockheed, Dr. Sutton has worked on the C-130 Hercules, the JetStar and various preliminary design aircraft, including vertical and short takeoff and landing concepts. Progressing up the ladder, he was a research and development engineer and assistant project engineer on the Hummingbird. He was named Director of Research in 1962.

Among his many papers are studies in propulsion systems and ground effects, and among his patents is one for the basic Hummingbird propulsion system. He also holds several patents in countries overseas. A member of many professional organizations and societies, Dr. Sutton is also a member of the Georgia Science and Technology Commission.

Engineers and Scientists who are interested in becoming associated with the group at Lockheed-Georgia Company are invited to address inquiries to: Dr. J. F. Sutton, Director of Research, Lockheed-Georgia Company, 834 West Peachtree Street, Atlanta, Georgia 30308, Dept. W-119.

Lockheed-Georgia Company

A Division of Lockheed Aircraft Corporation

An Equal Opportunity Employer

Measurement by Benzoate Radiolytic Decarboxylation of Relative Rate Constants for Hydroxyl Radical Reactions	R. W. Matthews and D. F. Sangster	1938
Carbon-13 Chemical Shifts of Vinyl Carbons	Gary E. Maciel	1947
Unimolecular Decomposition of Product Olefins in Methylene Chemical Activation Systems	F. H. Dorer and B. S. Rabinovitch	1952
Unimolecular Reactions of Chemically Activated Species Produced in Systems of Methylene with Propene, Butene-1, 3,3,3-Trifluoropropene, and 4,4,4-Trifluorobutene-1	F. H. Dorer and B. S. Rabinovitch	1964
An Experimental Generalization of Quantum Statistical Weight Effects in Nonequilibrium Unimolecular Reactions	F. H. Dorer and B. S. Rabinovitch	1973
The Solution Thermochemistry of Polyvalent Electrolytes. III. Barium Hydroxide Octahydrate	Harry P. Hopkins, Jr., and Claus A. Wulff	1980
Glutaronitrile. Calorimetrically Determined Thermal Properties from 5 to 350°K. and Statistical Gaseous Entropy	H. Lawrence Clever, Claus A. Wulff, and Edgar F. Westrum, Jr.	1983
The Critical Temperature and Coexistence Curve for Bismuth Bromide	J. W. Johnson, D. Cubicciotti, and W. J. Silva	1989
The Radiation-Induced Oxidation of <i>p</i> -Xylene Sensitized by Organic Bromine Compounds	D. Verdin, S. M. Hyde, and F. Neighbour	1992
The Effect of Ions on the Self-Diffusion of Water. I. Concentration Dependence	David W. McCall and Dean C. Douglass	2001
Kinetics of Hydrogen Reduction of Uranium Trioxide	Victor H. Heiskala	2012
Mean Amplitudes of Vibration, Bastiansen-Morino Shrinkage Effect, Thermodynamic Functions, and Molecular Polarizability of Sulfur Trioxide	G. Nagarajan, E. R. Lippincott, and J. M. Stutman	2017
The Nuclear Magnetic Resonance Spectra of Some 9,10-Bridged 9,10-Dihydroanthracenes	William B. Smith and Ben A. Shoulders	2022
Abstraction Reactions of Hydrogen and Deuterium Atoms: Mercury-Photosensitized Decomposition of Mixtures of Cyclohexane and Cyclohexane- <i>d</i> ₁₂	Robert R. Hentz, Joseph Y. Chang, and Milton Burton	2027
Radiolysis of Benzene and Benzene-Cyclohexane Mixtures in the Presence of Nickel Tetracarbonyl	Helmut F. Barzynski, Robert R. Hentz, and Milton Burton	2034
Mechanism of the Oxidation of Reducing Sugars (Hexoses) by Hexacyanoferrate(III) in Alkaline Medium and Lobry de Bruyn Transformation	Narendra Nath and M. P. Singh	2038
The Effect of Solvent on the Acid-Base Kinetics of the Excited State of β -Naphthol	Norman M. Trieff and Benson R. Sundheim	2044
Radiation Chemistry of Perfluorocyclohexane and Perfluorocyclobutane. Mass Spectroscopic Identification of Products	Michael B. Fallgatter and Robert J. Hanrahan	2059
The Volatilization of Molybdenum in the Presence of Water Vapor	G. R. Belton and A. S. Jordan	2065
Radiolytic Stress Relaxation of an Ethylene-Propylene Copolymer	Hyuk Yu and Leo A. Wall	2072
Specific Heat of Polyethylene Single Crystals	Bernhard Wunderlich	2078
Electromotive Force Studies of Cadmium Chloride in Water, Water-Ethanol, and Ethanol Solutions	Jack D. Hefley and Edward S. Amis	2082
Fluorine Bomb Calorimetry. X. The Enthalpies of Formation of Niobium and Tantalum Pentafluorides	Elliott Greenberg, Carol A. Natke, and Ward N. Hubbard	2089
Thermodynamic Properties of <i>n</i> -Propyl-, <i>n</i> -Butyl-, and <i>n</i> -Decyl-Substituted Cyclohexane from 10 to 370°K.	Herman L. Finke, John F. Messerly, and Samuel S. Todd	2094
Pure Quadrupole Resonance of Halogens in Potassium Hexahalorhenates(IV) and Hexachlorotungstate(IV)	Ryuichi Ikeda, Daiyu Nakamura, and Masaji Kubo	2101
Studies on the Anion Radicals of the Thianthrene Oxides	E. T. Kaiser and D. H. Eargle, Jr.	2108
Kinetics of the Nitrous Oxide Decomposition by Mass Spectrometry. A Study to Evaluate Gas-Sampling Methods behind Reflected Shock Waves	Anthony P. Modica	2111
Studies of the Hydrogen Held by Solids. VIII. The Decationated Zeolites	Jan B. Uytterhoeven, L. G. Christner, and W. Keith Hall	2117

No. **40** in the
**ADVANCES IN
CHEMISTRY
SERIES**

MASS SPECTRAL CORRELATIONS

by **FRED W. McLAFFERTY, Dow Chemical Company**

This compilation gives the empirical and structural formulas of ions that might be found at a particular m/e in a mass spectrum plus an indication of how each such ion might have arisen. It contains a wide variety of compound types. Some 4,000 mass spectra are referenced.

The author has drawn freely from his extensive background in mass spectrometry as well as from the efforts and ideas of colleagues and co-workers. He pulls together heretofore scattered information between two covers, the first time such a file has been published.

You can find possible ion structures and precursor molecules for each of the prominent ions in the mass spectrum of an unknown compound with a further indication of the general probability of their occurrence. Space has been left throughout the table for added correlations from your own personal file of spectra.

Newcomers to the field will find this book indispensable. Experts will find it a timesaver in interpreting the spectrum of an unfamiliar compound when information is lacking on the history of the sample. Laboratory directors will want copies for staff members. Why not put this volume to work for **you**?

117 pages.

Paper bound.

Price: \$4.75

Order from:

**Special Issues Sales/American Chemical Society
1155 Sixteenth Street, N.W./Washington, D.C. 20036**

NOTES

- On the Interaction of Triphenylamine with Iodine and with Silica-Alumina Catalysts **Francis R. Dollish and W. Keith Hall** 2127
- Radical Intermediates in the Mercury (³P) Photosensitized Decomposition of Cyclopropane **Richard A. Holroyd and George W. Klein** 2129
- Electron Spin Resonance of Aliphatic Semiquinones **E. Thomas Strom, Glen A. Russell, and R. D. Stephens** 2131
- The Electrostatic Forces within the Carbon Monoxide Molecule **Peter Politzer** 2132

COMMUNICATIONS TO THE EDITOR

- Discussion of an Apparent Violation of the Gibbs-Duhem Equation **Sherril D. Christian and Norman Fogel** 2135
- Reply to Discussion of an Apparent Violation of the Gibbs-Duhem Equation **Guy R. B. Elliott and Joe Fred Lemons** 2135
- Electrical Conductance of Concentrated Aqueous Solutions and Molten Salts:
Correlation through Free Volume Transport Model **C. A. Angell** 2137
- Concerning the Reaction $\text{NO}_2 + \text{NO}^* \rightarrow \text{N}_2\text{O} + \text{O}_2$ **F. O. Rice and F. J. Wunderlich** 2137
- Infrared Spectra of Molecules Adsorbed on Metal Powders Obtained from Electrically Exploded Wires **Charles P. Nash and Robert P. DeSieno** 2139

**DETERMINE
MOLECULAR
WEIGHT SIZE
AND SHAPE OF
MACROMOLECULES
IN SOLUTION
WITH THE AMINCO
LIGHT-SCATTERING
PHOTOMETER**

"... closest to the ideal of an absolute light-scattering instrument, in which a simple analysis . . . leads to the evaluation of R_{90} "*

Rayleigh's Ratio, R_{90} (R_{θ}), is the basic light-scattering measurement from which molecular weights are derived. Ultimately, Rayleigh's Ratio must be obtained from two measurements: (1) the illuminance of the beam incident on a cell containing solution, and (2) the scatter intensity of the solute. In the Aminco system, the illuminance (Figure 1) is measured directly by focusing the entire incident beam on the photomultiplier tube and dividing by its area. The scatter intensity (Figure 2) is measured by the simple scheme first proposed by Hermans and Levinson, in which the only geometrical factors are the areas of the two apertures, the distance between them, and the beam width. In practice, of course, all factors are grouped into a simple constant which constitutes the calibration of the apparatus. The advantages of the method are:

1. One does not have to rely on the calibration of standard diffusers.
 2. Calibration does not depend on size or position of the cuvette.
 3. Volume corrections are not required.
 4. The refractive index correction does not involve geometry and is simply proportional to N^2 .
 5. All quantities on which the calibration depends may be verified by the user.
- Request Bulletin 2329 PC.6

*"Calibration of Light-Scattering Instruments: A Critical Survey" Kralohvil, Dezelic, Kerker, Matejevic, J. Pol. Sci., 27, 69 (1962). (Refers to the devices of Kushner [N.B.S.] and Kremen and Shapiro.)

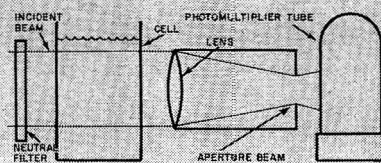


FIG. 1. INCIDENT ILLUMINANCE MEASUREMENT

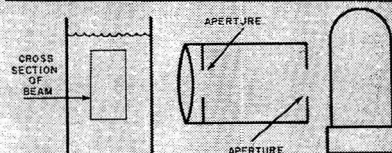
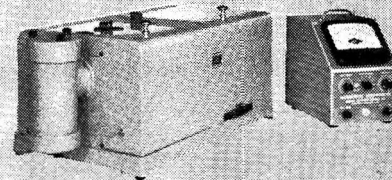


FIG. 2. SCATTER INTENSITY MEASUREMENT



A compact and easy to use absolute instrument which measures Rayleigh's Ratio, Normalized Angular Scatter, Dissymmetry and Depolarization.



AMERICAN INSTRUMENT CO., INC.
8030 Georgia Avenue, Silver Spring, Maryland

4982 Boron trimethyl, cylinders of approx. 100g. \$2.00/1g, inc. cyl.
5373 Boron triiodide, cryst. \$15.00/10g. \$90.00/100g.

RARE & FINE CHEMICALS

K&K

**RARE
CHEMICALS
FINE**

CATALOG NUMBER **5**

SEND FOR CATALOG #5

TELEPHONE
AREA CODE 516
GENERAL 3-6262

**RARE & FINE
CHEMICALS**

TWX 516-433-8184
TELEX: 01-26464
CABLE: KALABOR PLAINVIEWNEWYORK

K&K LABORATORIES, INC.
121 EXPRESS STREET, ENGINEERS HILL, PLAINVIEW, NEW YORK

**Do you know how to protect
your idea or invention . . .**

or how to avoid the pitfalls that have lost rights and fortunes for many inventors in the past? Are you familiar with the requirements for patentability? Do you know what steps to take if your idea involves a new use for an old product, is related to prior art, or deals with homologs, isomers, or other analogs?

PATENTS FOR CHEMICAL INVENTIONS discusses these and many other pertinent questions. It will help you in your contacts with your employer and your patent attorney and will help you understand patent literature.

Though it contains legal abbreviations and terminology, this 117-page book is not a treatise on patent law. It is written for the technically trained man—the research chemist and director—whose very profession provides more than the usual opportunities for conceiving patentable ideas. It presents the broad range of problems concerned with the nature of invention, ownership, inventorship, priority interpretations, documents, signatory formalities during prosecution, etc. Shop rights, employer assignment agreements, the status of the chemist hired to invent, and many other important aspects are discussed.

You will want to have PATENTS FOR CHEMICAL INVENTIONS for your own personal reference. It is Number 46 in the Advances in Chemistry Series, 117 pages, cloth bound, \$4. Order your copy today.

Special Issues Sales/American Chemical Society
1155 Sixteenth St., N. W., Washington, D. C. 20036

Surface Viscosity of Monomolecular Films of Long-Chain Aliphatic Amides, Amines, Alcohols, and Carboxylic Acids

by N. L. Jarvis

U. S. Naval Research Laboratory, Washington, D. C. 20390 (Received February 11, 1965)

The surface viscosities of monomolecular films of 14-, 16-, and 18-carbon chain aliphatic alcohols, amines, acids, and amides were determined using a canal viscometer, the viscosities being determined from the rate of flow of the film material through a narrow and relatively deep canal. The surface viscosities were measured as functions of film pressure, substrate pH, and the rate of flow of the film. The surface viscosity data for alcohols and acids were in good agreement with those previously reported viscosity values that were also determined by the canal technique. These surface viscosities determined with a canal viscometer are often an order of magnitude less than the values obtained with other types of viscometers. There are no corresponding data available in the literature with which to compare the surface viscosities of the amide and amine monolayers. Experiments were also carried out to determine which of these monolayers behaved as two-dimensional Newtonian films.

The orientation and packing of long-chain normal aliphatic compounds at water-air interfaces are known to vary with the nature of the polar groups that are present, as well as with hydrocarbon chain length, film pressure, temperature, and substrate composition. The effects of these parameters on the molecular arrangement in adsorbed films have been investigated by several surface chemical techniques,^{1,2} including film balance studies, surface potential determinations, and to a lesser extent by surface viscosity measurements. In connection with a current project at the Naval Research Laboratory it became necessary to determine the surface properties, and in particular the surface viscosities, of a variety of surface-active materials that occur naturally at the surface of the ocean. Due to the

unsaturation of many of these compounds it was expected that their surface viscosities would be quite low. A survey of the literature indicated that of the surface viscometers described, those based on the rate of flow of films through a narrow canal were the most sensitive in the range of 10^{-3} surface poise or less, and were the only viscometers giving absolute viscosity values. It was also noted that there was considerable variation among the surface viscosity values reported. The present study was therefore undertaken to give us a reliable method for determining surface viscosity and to

(1) J. A. Spink and J. V. Sanders, *Trans. Faraday Soc.*, **51**, 1154 (1955).

(2) G. C. Nutting and W. D. Harkins, *J. Am. Chem. Soc.*, **61**, 1180 (1939).

help establish the true surface viscosity values of a series of long-chain aliphatic compounds. Surface viscosities of the 14-, 16-, and 18-carbon chain alcohols, acids, amines, and amides were measured as functions of film pressure, substrate pH, and the rate of shear of the surface film.

The various experimental methods that have been used for determining surface viscosity might arbitrarily be grouped into three classifications: (1) those based upon the rate of damping of successive oscillations of a bob or disk suspended in the interface³⁻⁷; (2) those methods depending upon the rate of flow of surface film through a canal or slit^{5,6,8-11}; and (3) those techniques where either the substrate liquid, or a ring or disk suspended in the interface, is rotated at a constant rate,¹²⁻¹⁵ the surface viscosity being determined from the drag the moving interface exerts upon a concentric surface. Of the three types of measurements only the second is capable of giving the absolute or true surface viscosity¹⁶⁻¹⁸ of a film. The other techniques certainly give useful information, but they will also give surface viscosities that can be more than an order of magnitude higher¹⁹ than those given by the canal method. By varying the width of the canal, this viscometer can also be used to study the effect of rate of shear of the surface film on its surface viscosity. Of the various types of slit or canal viscometers investigated by Harkins and Nutting¹¹ they suggested that one employing a narrow, deep canal would give the most accurate surface viscosity measurements. Therefore, a canal viscometer of this type was constructed for use in the present investigation.

Experimental

The Viscometer. The canal used in this viscometer was formed from two glass microscope slides 7.5 cm. long, 0.1 cm. thick, and 1.6 cm. wide, with the edges ground flat. The slides were placed in the film balance trough so that the upper edges were exactly level with the free water surface to prevent the formation of a meniscus. Only the upper edges of the slides were paraffined, the portions of the slides remaining in contact with the water were left hydrophilic to prevent slippage between the substrate water and the sides of the canal. The depth of the canal was limited to 1.6 cm. by the depth of the film balance tray. Each microscope slide was held in position at the interface by a chrome-plated brass plate to which it was attached with paraffin. Each brass plate was 7.5 cm. long, 0.5 cm. wide, and 3.5 cm. high, 2.0 cm. of which extended above the level of the free water surface. All portions of the brass plates in contact with the water were lightly coated with paraffin. The upper portions of the brass plates were cou-

pled together much as the two jaws of a vise, with two micrometers, one near each end of the canal, used to control the width and alignment of the canal. The width of the canal could easily be varied from 0 to 0.5 cm. with an accuracy of ± 0.0005 cm. The alignment of the canal was checked at several widths with a cathetometer and was found to vary no more than ± 0.0005 cm. from one end of the canal to the other.

The variable-width canal was mounted in a Cenco hydrophil balance about midway between the ends of the trough and adjacent to one side. A Cenco torsion head was also mounted at the center of the film tray, adjacent to the canal. One end of the mica float of the torsion head was attached to the inner brass plate of the canal assembly and the other end to the opposite side of the film tray, as shown schematically in Figure 1. This arrangement is much like that used by Joly.⁶ In this figure, A is the canal and B is the float of the Cenco torsion head. D and D' are movable barriers for expanding and compressing the film and C is the platinum plate of a Wilhelmy-type tensiometer used to monitor the film pressure in compartment II of the viscometer. The surface of the platinum plate was roughened to assure wettability and was connected by a lever arm to a calibrated torsion wire. It had a sensitivity of ± 0.05 dyne/cm., about the same sensitivity as the Cenco torsion head. Those surfaces of the brass hydrophil balance that came in contact with the substrate were made hydrophobic by coating with a thin layer of paraffin.

Materials. The long-chain fatty acids used in this

- (3) R. E. Wilson and E. D. Ries, "Colloid Symposium Monograph," Vol. 1, American Chemical Society, Washington, D. C., 1923, p. 145.
- (4) I. Langmuir, *Science*, **84**, 379 (1936).
- (5) W. D. Harkins and R. J. Meyers, *Nature*, **140**, 465 (1937).
- (6) M. Joly, *Kolloid-Z.*, **89**, 26 (1939).
- (7) A. A. Trapeznikov, *Acta Physicochim. URSS*, **10**, 5 (1939).
- (8) D. G. Dervichian and M. Joly, *Compt. rend.*, **204**, 1320 (1937).
- (9) M. Joly, *J. Phys. Radium*, **8**, 471 (1937).
- (10) W. D. Harkins and J. G. Kirkwood, *J. Chem. Phys.*, **6**, 53, 298 (1938).
- (11) G. C. Nutting and W. D. Harkins, *J. Am. Chem. Soc.*, **62**, 3155 (1940).
- (12) J. R. Van Wazer, *J. Colloid Sci.*, **2**, 223 (1947).
- (13) R. Chaminade, D. G. Dervichian, and M. Joly, *J. chim. phys.*, **47**, 883 (1950).
- (14) A. G. Brown, W. C. Thuman, and J. W. McBain, *J. Colloid Sci.*, **8**, 491 (1953).
- (15) S. C. Ellis, A. F. Lanham, and K. G. A. Pankhurst, *J. Sci. Instr.*, **32**, 70 (1955).
- (16) W. E. Ewers and R. A. Sack, *Australian J. Chem.*, **7**, 40 (1954).
- (17) W. D. Harkins and J. G. Kirkwood, *J. Chem. Phys.*, **141**, 38 (1939).
- (18) J. T. Davies and G. R. A. Mayers, *Trans. Faraday Soc.*, **56**, 691 (1960).
- (19) G. E. Boyd and F. Vaslow, *J. Colloid Sci.*, **13**, 275 (1958).

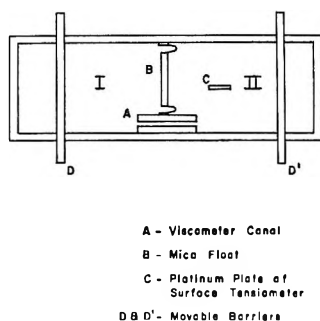


Figure 1. Schematic diagram of surface viscometer.

study (tetradecanoic acid, hexadecanoic acid, and octadecanoic acid) were obtained from Lachat Chemicals Inc. and had melting points of 58, 64, and 69–70°, respectively. The alcohols and amines were also prepared by Lachat. Tetradecanol, hexadecanol, and octadecanol had melting points of 37–38, 49–50, and 59°, respectively, whereas tetradecylamine, hexadecylamine, and octadecylamine had melting points of 37, 46–47, and 53–54°, respectively. Octadecanamide, m.p. 108–109°, and tetradecanamide, m.p. 103°, were obtained from the Eastman Chemical Co., and hexadecanamide, m.p. 105–106°, was purchased from K and K Laboratories, Inc.

Spreading solutions of these compounds were prepared by dissolving known amounts of the material in suitable organic solvents. The alcohols, acids, and amines were dissolved in petroleum ether (b.p. 41–55°), the concentration of each solution being of the order of 5×10^{-4} g./ml. Owing to the low solubility of the amides in hexane and petroleum ether, benzene was used as their spreading solvent. Each of the solvents, C.P. petroleum ether and C.P. benzene, was percolated through adsorption columns of activated Florisil and alumina prior to use in order to remove any polar impurities. The spreading solutions were delivered to the water surface from Misco micropipets. Each of the compounds was studied on both acid and basic substrates; the acid substrate was 0.01 *N* H₂SO₄ and the basic substrate was pH 9.0–9.5 KOH. The substrate solutions were prepared from triply distilled water, the final two distillations from an all-quartz apparatus.

Experimental Procedure. In order to determine surface viscosity by the canal method it is necessary to measure the amount of film passing through the canal in unit time, with a given pressure differential across the ends of the canal. At the beginning of each measurement the water surfaces in I and II were swept clean with the movable barriers, and the torsion wires for the tensiometers were adjusted to zero film pressure. Film material was then added to both compartments, al-

lowed to equilibrate for 10 min., and was then compressed. The film in compartment I was compressed until the torsion head at B registered a film pressure F_1 . The film in compartment II was compressed until the Wilhelmy plate tensiometer recorded a film pressure F_2 , a value somewhat less than F_1 . The torsion head B then measured the difference in pressure across the ends of the canal, $\Delta F = F_1 - F_2$. When a gate made of thin polyethylene film was removed from in front of the canal, the film began to flow from compartment I to compartment II under the pressure differential ΔF . As the film material moved through the canal, barriers D and D' were moved at a sufficient rate to maintain the proper film pressures in compartments I and II. The rate of flow of the monolayer through the canal was determined from the distance that barrier D in compartment I had traversed in a given period of time.

Harkins and Kirkwood¹⁰ proposed that for a deep and very narrow canal, the rate of flow of film through the canal is related to the absolute viscosity of the monolayer by the equation

$$\eta = \frac{(F_2 - F_1)a^3}{12lQ} - \frac{a\eta_0}{\pi} \quad (1)$$

in which F_1 and F_2 are the film pressures at each end of the canal in dynes per centimeter, a is the width of the canal in centimeters, Q is the area in square centimeters of film flowing through in 1 sec., l is the length of the canal in centimeters, and η_0 is the bulk viscosity of the aqueous substrate. It is assumed in deriving this expression that the viscosity of the film is constant while passing through the canal. In order to satisfy this condition the film pressure drop across the canal was kept as small as possible. It was found that a pressure difference of 2–4 dynes/cm. gave satisfactory results and was convenient to work with. At the lower film pressures, a ΔF of 2 dynes/cm. was maintained across the canal.

A further condition that must be satisfied is that the ratio of canal depth to canal width must be large. To satisfy this condition, many of the data were taken with canal widths of 0.10 cm. or less, in which case the canal depth was at least 16 times the width. It was also of interest, however, to determine the surface viscosity of each monomolecular film as a function of canal width. By changing the canal width one changes the rate of flow of the film through the canal and thus its rate of shear. Using this technique it was possible to determine which of the compounds formed Newtonian and which formed non-Newtonian two-dimensional films. With Newtonian films it was found that surface viscosity was independent of rate of flow, at least with flow rates of from 0.02 to 0.25 cm.²/sec. Reliable accu-

rate measurements were obtained in the surface viscosity range of 1×10^{-4} to about 1×10^{-1} surface poise. At the higher values of surface viscosity it was very difficult to obtain reproducible measurements, due to the fact that many of the films become non-Newtonian plastic or solid films and had high yield values. All surface viscosity measurements were carried out in a constant temperature room, the temperature being held at $20 \pm 0.2^\circ$ and the relative humidity at $50 \pm 5\%$. The surface viscometer was protected from dust and airborne contamination by enclosing it in a Lucite cover. The surface viscosity measurements reported for any given monomolecular film were the average of at least ten measurements and could normally be reproduced to within $\pm 10\%$ at all viscosities under these experimental conditions.

Film pressure (F) vs. area per molecule (A) isotherms were determined on both the acid and the basic aqueous substrate for each compound studied. The film balance used to measure the F vs. A curves has been previously described in detail.²⁰ It consisted of a shallow, Pyrex glass trough with the rim lightly coated with paraffin, a paraffined mica float connected to the sides of the trough with end loops of thin polyethylene ribbon, and a Cenco duNuoy torsion head sensitive to changes in film pressure of 0.05 dyne/cm. The measurements were also carried out in a constant temperature room at $20 \pm 0.2^\circ$ and a relative humidity of $50 \pm 5\%$.

Results

Carboxylic Acids. The surface viscosities of *n*-tetradecanoic, *n*-hexadecanoic, and *n*-octadecanoic acids on 0.01 *N* H₂SO₄ were determined as functions of film pressure and canal width. The surface viscosity values for each film were first plotted against the rate of flow, as shown for *n*-hexadecanoic acid in Figure 2. This plot of the logarithm of surface viscosity ($\log \eta$) vs. film flow rate (Q) for each film pressure for hexadecanoic acid gave a series of straight lines, showing that up to film pressures of 18 dynes/cm. its surface viscosity was independent of the rate of shear. It follows therefore that monolayers of hexadecanoic acid on acid substrates act as two-dimensional Newtonian liquids. Similarly, monolayers of *n*-octadecanoic and *n*-tetradecanoic acids on 0.01 *N* H₂SO₄ were also found to be two-dimensional Newtonian liquids. Isotherms of the logarithm of surface viscosity ($\log \eta$) vs. film pressure (F) were prepared for each of these acids by plotting film pressure against the surface viscosities corresponding to flow rates of 0.25 cm.²/sec. The $\log \eta$ vs. F curves given in Figure 3 show that the isotherms for octadecanoic acid and hexadecanoic acid increase

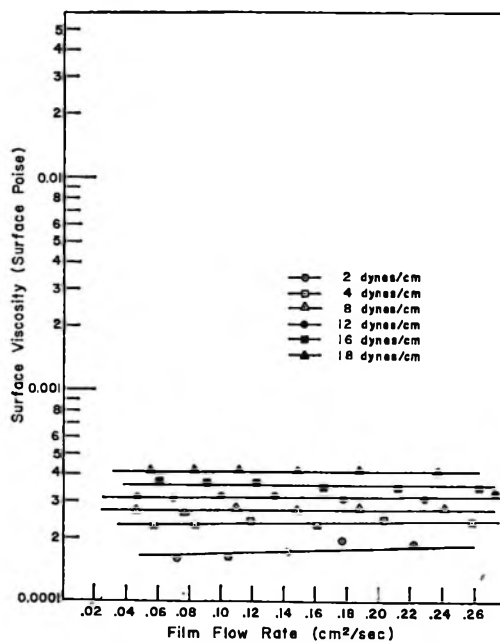


Figure 2. Effect of film flow rate on the surface viscosity of *n*-hexadecanoic acid on 0.01 *N* H₂SO₄ substrate.

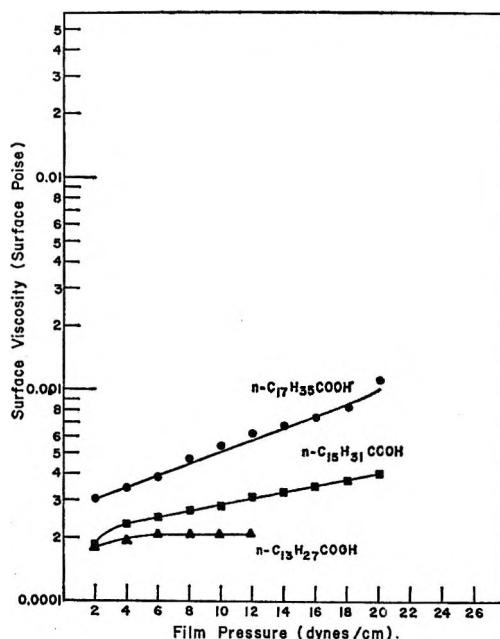


Figure 3. Surface viscosity vs. film pressure isotherms for long-chain carboxylic acids on 0.01 *N* H₂SO₄ substrate (film flow rate, 0.25 cm.²/sec.).

linearly with pressure. The surface viscosity of tetradecanoic acid increased slightly, going from 2 to 4 dynes/cm., and then appeared to be constant at higher film pressures. This difference in behavior may be ex-

(20) M. K. Burnett and W. A. Zisman, *J. Phys. Chem.*, **67**, 1534 (1963).

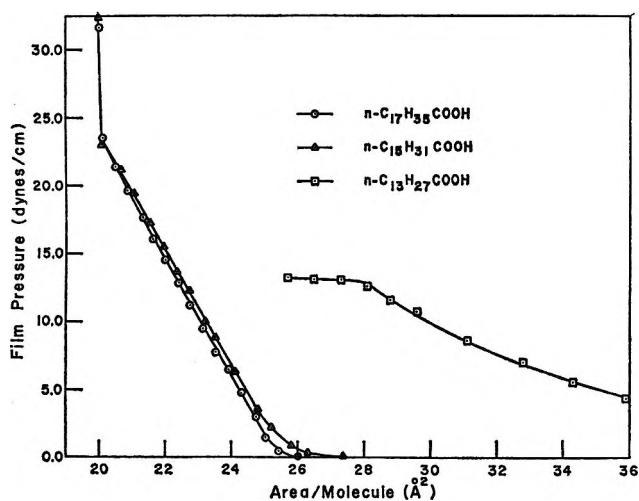


Figure 4. Film pressure vs. area per molecule isotherms for long-chain carboxylic acids on 0.01 N H_2SO_4 substrate.

plained by the differences in the states of their monolayers, as shown in the film pressure (F) vs. area per molecule (A) curves given in Figure 4. The linear portions of the $\log \eta$ vs. F curves for the C_{16} and C_{18} acids correspond to the liquid condensed or linear portions of their F vs. A curves. No surface viscosity values are reported for these acids at film pressures greater than 20 dynes/cm., for the monomolecular films appeared to become solid and so fragile that reproducible results were difficult to obtain. The low viscosity of the tetradecanoic acid monolayer is apparently due to the expanded state of the film.

Harkins and Nutting¹¹ determined with their canal viscometer that the best value for the surface viscosity of octadecanoic acid on acid water was 0.9×10^{-4} surface poise at 3 dynes/cm., which is 2.3×10^{-4} surface poise less than the value reported here. Joly,^{21,22} who also measured the surface viscosities of these fatty acids as a function of film pressure, reported surface viscosities for the C_{16} and C_{18} acids that were within $\pm 1 \times 10^{-4}$ surface poise of the values reported here. Joly's values for tetradecanoic acid however do not agree with those given here. He reported the surface viscosity of the C_{14} acid decreased with film pressure, decreasing from 1.79×10^{-4} surface poise at 1 dyne/cm. to 1.0×10^{-4} surface poise at 9 dynes/cm. The present data for the C_{14} acid at film pressures above 6 dynes/cm. show a constant surface viscosity value of 2.4×10^{-4} surface poise and appear to be more reasonable, for one would not expect a significant decrease in the cohesive forces between adjacent molecules as they become more closely packed.

The surface viscosities of several fatty acids have also been determined by the method of damped os-

cillations. Boyd and Harkins²³ gave a plot of the logarithm of surface viscosity ($\log \eta$) vs. film pressure (F) for octadecanoic and hexadecanoic acids. Their plots also show that each of the isotherms increase linearly with film pressure up to about 20 dynes/cm., but their values are close to an order of magnitude greater than those determined with a canal viscometer.

An attempt was made to measure the surface viscosity of the fatty acid films on pH 9.0–9.5 KOH solution. On this substrate the monolayers of the fatty acids become extremely rigid, their viscosities exceeding the capabilities of the canal viscometer. The rigidity of the fatty acid films may have been due to the presence of trace amounts of multivalent cations in the substrate that formed soaps with the fatty acids.

Aliphatic Alcohols. Surface viscosities of *n*-tetradecanol, *n*-hexadecanol, and *n*-octadecanol were determined on both 0.01 N H_2SO_4 , and pH 9.0–9.5 KOH solution. The viscosities were also measured as functions of film pressure and canal width. The viscosity values of the alcohol monolayers were also initially plotted as $\log \eta$ vs. Q , to determine whether they, too, formed Newtonian films. These isotherms are given in Figures 5a–c. They show that at low values of F each of the alcohol films were Newtonian, but as the average film pressure was increased above 6 dynes/cm. the viscosities of tetradecanol and hexadecanol showed a marked dependence upon the rate of shear. This agrees with the previous study of Fourt and Harkins,²⁴ which also showed that films of these alcohols became

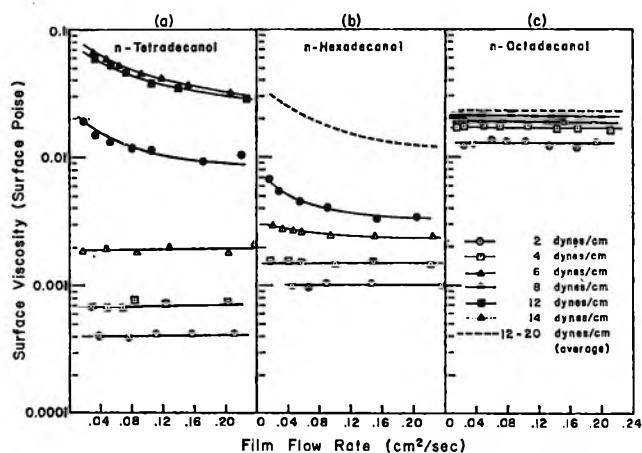


Figure 5. Effect of film flow rate on the surface viscosity of long-chain alcohol monolayers on 0.01 N H_2SO_4 substrate: (a) *n*-tetradecanol, (b) *n*-hexadecanol, (c) *n*-octadecanol.

(21) M. Joly, *J. chim. phys.*, **44**, 206 (1947).

(22) M. Joly, *J. Colloid Sci.*, **11**, 519 (1956).

(23) E. Boyd and W. D. Harkins, *J. Am. Chem. Soc.*, **61**, 1188 (1939).

(24) L. Fourt and W. D. Harkins, *J. Phys. Chem.*, **42**, 897 (1938).

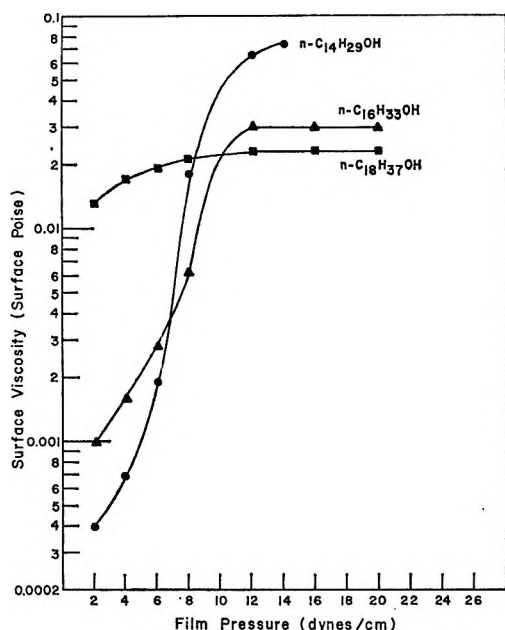


Figure 6. Surface viscosity vs. film pressure isotherms for long-chain alcohols on 0.01 N H_2SO_4 substrate (film flow rate, $0.02 \text{ cm.}^2/\text{sec.}$).

non-Newtonian at about the same film pressures. Within the limits of experimental error, octadecanol appeared to be Newtonian at film pressures up to 20 dynes/cm., at least at the film flow rates studied.

Surface viscosity vs. film pressure isotherms were prepared for each of these alcohols by plotting film pressure against the surface viscosity values corresponding to a flow rate of $0.02 \text{ cm.}^2/\text{sec.}$ The $\log \eta$ vs. F curves are given in Figure 6. Fourt and Harkins²⁴ using the oscillating disk reported $\log \eta$ vs. F curves for these alcohols which are similar in shape to those shown in Figure 6. However, their values of η at high film pressure are at least ten times greater than those reported here. Harkins and Nutting¹¹ reported values of surface viscosity for C_{16} and C_{18} alcohols at low film pressures using a canal viscometer. Their best values reported at a mean film pressure of 3 dynes/cm. were 7×10^{-4} and 17×10^{-4} surface poise for hexadecanol and octadecanol, respectively. Their value for hexadecanol agrees well with that presented here but their value for the C_{18} alcohol is considerably less than that reported here.

Other investigators^{21,24,25} have determined surface viscosity values for these fatty alcohols on acid substrates, but there is little agreement between their reported results and the difficulty may be due in part to differences in the viscometers used. It is also possible that small amounts of surface contamination were responsible for some of the variation in reported data.

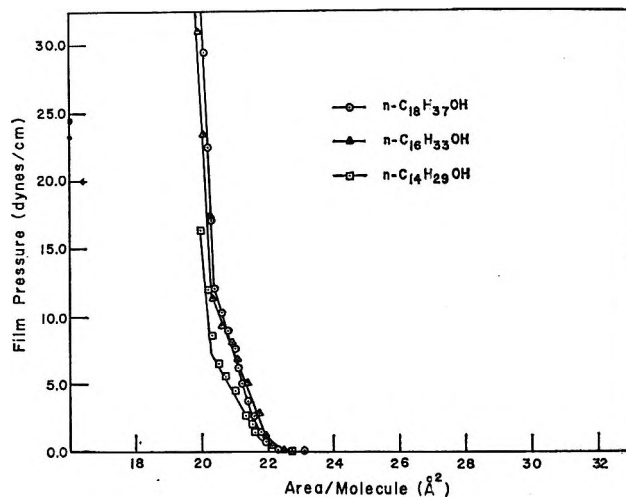


Figure 7. Film pressure vs. area per molecule isotherms for long-chain alcohols on 0.01 N H_2SO_4 substrate.

In the present study it was found that samples of tetradecanol and octadecanol purchased from different suppliers gave somewhat different viscosity values, particularly at low average film pressures. As an example, tetradecanol from Eastman Chemical Co. gave a value of 1.5×10^{-4} surface poise at an average film pressure of 2 dynes/cm. as compared to a value of 4×10^{-4} surface poise reported here for a sample of tetradecanol obtained from Lachat Chemicals Inc.

The F vs. A curves for these alcohols on 0.01 N H_2SO_4 (see Figure 7) show that each of the alcohol monolayers are truly condensed only above film pressures of 6 to 7 dynes/cm. for the C_{14} alcohol and 10–12 dynes/cm. for the higher homologs. The displacement for the F vs. A curve for the C_{14} alcohol to a lower area per molecule than the C_{16} and C_{18} alcohols may be attributed to the slow collapse (or solubility) of the C_{14} alcohol film as it is compressed. It is only when the films of tetradecanol and hexadecanol approach the condensed state that they show non-Newtonian behavior.

The surface viscosities of the alcohols on pH 9.0–9.5 KOH were in good agreement with the values obtained on acid substrate, the greatest difference between the two sets of data being less than 20%. The differences in viscosity of alcohols spread on acid and basic substrates may be due to minute traces of acid impurities present in the alcohols. The shapes of the $\log \eta$ vs. F curves were identical with each substrate, and the monolayers began to show non-Newtonian behavior at the same average film pressure. The F vs. A curves determined on pH 9.0–9.5 KOH were indistinguishable from those given in Figure 7 for the alcohols on acid substrate.

(25) M. Joly, *Kolloid-Z.*, 126, 35 (1951).

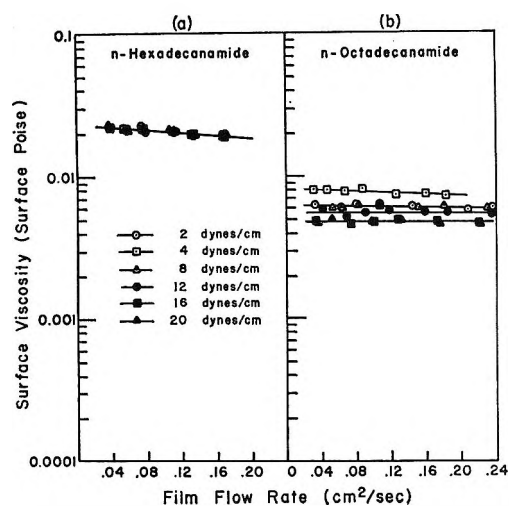


Figure 8. Effect of film flow rate on the surface viscosity of long-chain amide monolayers on 0.01 N H_2SO_4 substrate: (a) n -hexadecanamide, (b) n -octadecanamide.

Aliphatic Amides. The surface viscosities of monolayers of octadecanamide and hexadecanamide were studied on the acid as well as the basic substrate. Reproducible measurements could not be made with tetradecanamide as it showed appreciable solubility in these aqueous substrates and therefore did not form stable monomolecular films. The surface viscosities of the C_{16} and C_{18} amides on 0.01 N H_2SO_4 (Figures 8a and b) were plotted as functions of film flow rate and film pressure. The surface viscosity of hexadecanamide appeared to be independent of film pressure in the range studied, from 2 to 20 dynes/cm. It did show non-Newtonian behavior, though not to the same extent as the corresponding alcohol. Its surface viscosity only increased from 0.019 to 0.023 surface poise as the flow rate decreased from 0.20 to 0.02 cm^2/sec . Only at an average film pressure of 4 dynes/cm. did octadecanamide show a slight dependence upon film flow rate. Otherwise the C_{18} amide seemed to behave as a Newtonian film.

The surface viscosity behavior of monolayers of hexadecanamide at all film pressures is somewhat analogous to that of hexadecanol films at film pressures above 12 dynes/cm. At a film flow rate of 0.05 cm^2/sec . the surface viscosity of each compound is the same, 0.022 surface poise. The surface viscosity of the C_{16} alcohol, however, shows a greater dependence upon the rate of flow of the film through this canal, or the rate of shear. The F vs. A curve of the C_{16} alcohol in Figure 7 shows that above 12 dynes/cm. hexadecanol monolayers have the same molecular packing and compressibility as hexadecanamide (Figure 9).

The F vs. A curve in Figure 9 for octadecanamide is identical with the F vs. A curve of octadecanol above a

film pressure of 12 dynes/cm. Unlike the C_{16} derivatives, however, the surface viscosities of the C_{18} compounds do not show much similarity. Monolayers of the C_{18} alcohol and amide do appear to be Newtonian films for the most part; however, the octadecanamide films were considerably less viscous than the alcohol films. Also, the viscosity of the C_{18} amide appears to be at a maximum at a film pressure of 4 dynes/cm. and then to decrease with increasing film pressure, up to a film pressure of 14 dynes/cm. At 4 dynes/cm., the surface viscosity of octadecanamide is about one-half of that of the C_{18} alcohol, 0.0080 surface poise as compared with 0.017 surface poise. The lower values of η for the C_{18} amide may result from either the presence of trace impurities in the compound, or the different polar groups may make distinctly different contribution to surface viscosity.

The surface viscosity of both hexadecanamide and octadecanamide were found to be independent of substrate pH. Their surface viscosities on pH 9.0–9.5 KOH agreed, within the limits of experimental error, with the measurements given in Figure 9 with 0.01 N H_2SO_4 as substrate. The F vs. A curves for these compounds were also the same as both acid and basic substrates.

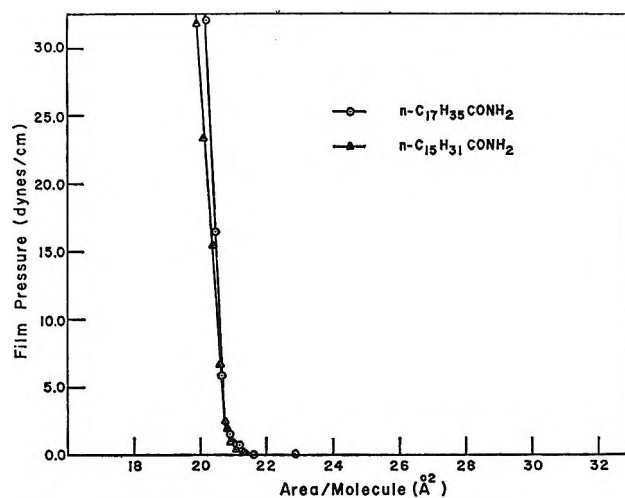


Figure 9. Film pressure vs. area per molecule isotherms for long-chain amides on 0.01 N H_2SO_4 substrate.

Aliphatic Amines. The surface viscosities of the amine monolayers were observed to be sensitive to the pH of the substrate. They gave very low viscosity Newtonian films on the acid substrate, while on basic substrates their viscosities were greater than 0.1 surface poise, exceeding the usable range of the present viscometer. The viscosities of octadecylamine and hexadecylamine on 0.01 N H_2SO_4 are given in Figure

10. On the acid substrate the amines formed the RNH_3^+ ion, the resulting electrostatic repulsions between the ionized molecules giving very expanded monomolecular films as shown in Figure 11. The relatively large distances between the amine molecules on $0.01\text{ N H}_2\text{SO}_4$ is responsible for the low surface viscosities. The amines appeared to be somewhat soluble in the acid substrate, perhaps due to the ionization. The C_{14} amine was so soluble that reliable measurements of its surface viscosity could not be made. It is also of interest to note that the surface viscosity values on

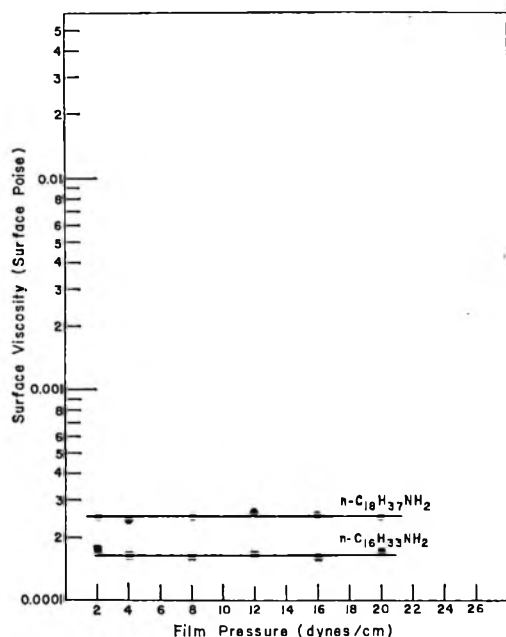


Figure 10. Surface viscosity vs. film pressure isotherms for long-chain amines on $0.01\text{ N H}_2\text{SO}_4$ substrate.

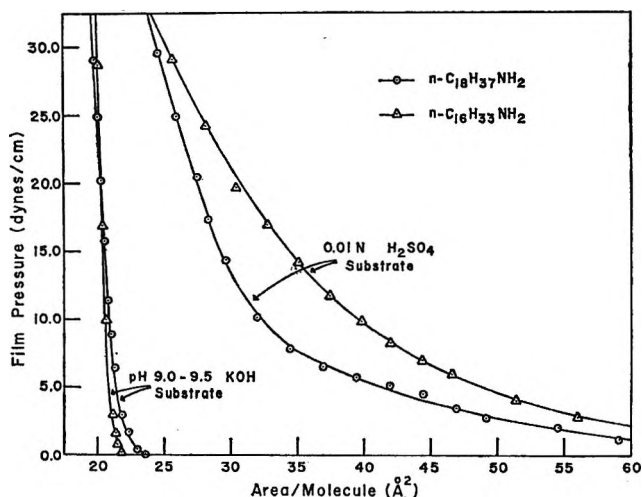


Figure 11. Film pressure vs. area per molecule isotherms for long-chain amines on $0.01\text{ N H}_2\text{SO}_4$ and pH 9.0-9.5 KOH substrates.

$0.01\text{ N H}_2\text{SO}_4$ are independent of film pressure. In the film pressure range studied the amine monolayers did not approach close packing.

The monomolecular films of the C_{16} and C_{18} amines were much more condensed on the pH 9.0-9.5 KOH solution than they were on the acidic substrate. The viscosity of the closely packed hexadecylamine monolayer was considerably above 0.1 surface poise, even at an average film pressure of 2 dynes/cm. Initial experiments suggested that these highly viscous films were non-Newtonian, but sufficient reliable data could not be gathered to determine the extent of their deviation from ideal behavior.

Conclusion

The canal viscometer, utilizing a narrow, deep canal, was found to be capable of detecting non-Newtonian behavior in a monomolecular film. The very viscous non-Newtonian films required relatively wide canals, and with viscosities greater than about 0.1 surface poise this can lead to situations where the ratio of canal depth to width is no longer large enough to satisfy the requirements of the Harkins and Kirkwood¹⁹ equation. Using this equation, and restricting the determinations to a narrow, deep canal, the measured values should be very close to the absolute surface viscosities.

The data presented in this report show that the surface viscosities of monomolecular films will vary with the nature of the polar group that is present in the adsorbed molecules and with the degree of interaction between the polar group and the aqueous substrate. The viscosity values are dependent upon the orientation and closeness of packing of the molecules in the monomolecular film and thus are related to the length of the hydrocarbon chain, the film pressure, and substrate pH. The surface viscosities of each type of monomolecular film—alcohol, acid, amine, and amide—showed different responses to changes in these parameters.

In each case where the monomolecular film was Newtonian, the surface viscosity increased with increasing hydrocarbon chain length. With the 16- and 18-carbon chain fatty acids on $0.01\text{ N H}_2\text{SO}_4$ and the alcohols at low film pressures, the logarithm of the viscosity appeared to increase linearly with film pressure. For the very expanded Newtonian films of tetradecanoic acid and the C_{16} and C_{18} amines on $0.01\text{ N H}_2\text{SO}_4$, the surface viscosity values were independent of film pressure, within the limits of sensitivity of the experimental procedure. For non-Newtonian films the surface viscosity behavior was not so regular. Non-Newtonian monolayers of the amides and the alcohols at higher

film pressures not only had higher surface viscosities than the Newtonian films, but the values for the lower molecular weight homologs were higher than those of longer chain compounds. An explanation for this behavior is not immediately obvious, although the behavior of tetradecanol may give a clue. The tetradecanol monolayer tends to collapse slowly at film pressures greater than about 6 dynes/cm. At the higher film pressure the collapsing tetradecanol molecules may form multilayers of the material at the interface, thus giving rise to nonideal behavior of the surface viscosity. The monolayers of the fatty acids and amines on pH 9.0-9.5 KOH, which apparently are non-Newtonian, had surface viscosities so large they exceeded the capabilities of the present surface viscometer.

The surface viscosities of two classes of compounds, the amines and the acids, exhibited a marked dependence upon substrate pH. The amines formed ionized

monolayers on the 0.01 *N* H₂SO₄ substrate, the mutual repulsion between the ionized polar groups giving rise to the expanded monolayers of low viscosity. On the basic substrate the un-ionized amines gave very high surface viscosities, indicating a high degree of cohesion between the closely packed molecules. On 0.01 *N* H₂SO₄ the monolayers of the carboxylic acids gave very low surface viscosities. On the basic substrate, however the acids apparently formed soaps with trace amounts of multivalent cations present in the water, and gave highly condensed, solid monolayers of very high surface viscosity. The alcohol and amide monolayers were relatively insensitive to changes in substrate pH.

The surface viscosities presented in this paper for monolayers of fatty acids and alcohols are in good agreement with much of the previously reported data, particularly those values obtained with a canal viscometer.

Application of Surface Thermodynamics to Gibbs Elasticity

by M. van den Tempel, J. Lucassen, and E. H. Lucassen-Reynders

Unilever Research Laboratory, Vlaardingen, The Netherlands (Received April 13, 1964)

Rupture of a thin liquid film drawn from a surfactant solution can be opposed by the surface tension gradient arising from local extension of the film surfaces. A measure for this effect, which is thought to be responsible for the large influence of certain minor impurities on foam stability, is the Gibbs elasticity, relating the excess surface tension in the extended region to the relative increment of the surface area. For a quantitative evaluation of the Gibbs elasticity of a film, the relation between the surface tension and the composition of the film liquid must be known. Rigorous surface thermodynamics have been developed to derive this relation. Simplified versions of the general equations are used to calculate the Gibbs elasticity, especially for films of mixed surfactant solutions. Compounds of suitable surface activity, even if present in minor amounts, appear to have large effects on the Gibbs elasticity. Their influence is already considerable at rather large film thicknesses, assuming the most simple, ideal behavior of both the surface and the bulk liquid in the film. The effect of deviations from ideality is discussed.

Introduction

One of the mechanisms that are generally accepted to contribute to the stability of thin films obtained from surfactant solutions is the Plateau–Marangoni–Gibbs effect.¹ Rupture of the film is supposed to be introduced by local thinning, during which the surface area in part of the film is enlarged. The amount of surfactant in the extended region of the film is insufficient to maintain the original values of both the adsorption and the bulk concentration; in general, the surface tension in the extended region is, therefore, higher than in the neighboring parts of the film. The Plateau–Marangoni–Gibbs effect accounts for this surface tension gradient and for the resulting elasticity of the surface, which tries to restore the original shape of the film.

Equilibrium between the enlarged surface and the underlying film liquid is re-established immediately (or at least much more rapidly than the equilibrium between neighboring parts of the film) in film elements of dimensions comparable with the film thickness; for such elements the elasticity is called Gibbs elasticity. It is defined² as the ratio of the increase in the film tension ($2d\sigma$) resulting from an infinitesimal increase in area and the relative increment of the area ($d \ln A$)

$$E = \frac{2d\sigma}{d \ln A} \quad (1)$$

Evaluation of the Gibbs elasticity as influenced by the composition of the surfactant solution would be useful for understanding the behavior of the thin films produced therefrom. Such a calculation of E requires the variations in the surface tension σ and in the surface area A to be expressed in measurable parameters of the film: its thickness h , the concentrations c_i of the surfactants contained in it and their properties. In the following, the influence of properties and amounts of surfactants will be considered.

Gibbs Elasticity. The variation of σ in an extending film element is related to the surfactant adsorptions Γ_i and the concentrations of the surfactants ($i = 2, 3 \dots n$) by Gibbs adsorption law

$$-d\sigma = RT \sum_{i=2}^n \Gamma_i d \ln \gamma_i c_i \quad (2)$$

where γ_i represents the activity coefficient of i .

The variation in A of the element can be related to the surface and bulk concentrations by considering the volume of the element and the total amount of each independent component in it to be constant

(1) B. V. Derjaguin and A. S. Titijevskaya, *Proc. Intern. Congr. Surface Activity, 2nd, London*, I, 211 (1957); L. E. Scriven and C. V. Sternling, *Nature*, **187**, 186 (1960).

(2) J. W. Gibbs, "Collected Works," Vol. I, Dover Publishing Co., Inc., New York, N. Y., 1961, p. 301.

$$-d \ln A = d \ln h = \frac{hdc_i + 2d\Gamma_i}{2\Gamma_i} \quad (i = 1, 2 \dots n) \quad (3)$$

Consequently, the general relation for the Gibbs elasticity reads

$$E = 4RT \sum_{i=2}^n \frac{\Gamma_i^2}{c_i} \frac{1 + \frac{d \ln \gamma_i}{d \ln c_i}}{h + 2 \frac{d\Gamma_i}{dc_i}} \quad (4)$$

giving the influence of film thickness and surfactant concentrations. The values of Γ_i and $d\Gamma_i/dc_i$ occurring moreover in eq. 4 follow from the surface equation of state for the system considered. It should be noted that the latter quantity is not equal to the partial differential quotient or to the slope of the adsorption isotherm of i , since during extension the concentrations of the other components also vary

$$\frac{d\Gamma_i}{dc_i} = \frac{\partial \Gamma_i}{\partial c_i} + \sum_{i \neq j} \frac{\partial \Gamma_i}{\partial c_j} \times \frac{dc_j}{dc_i} \quad (5)$$

where the variations in c_j with respect to c_i follow from the conservation of matter, as expressed in eq. 3. Further quantitative treatment requires the surface equation of state to be given, the thermodynamics of which will be presented in the following section.

Even qualitatively, however, eq. 4 shows two remarkable properties of the Gibbs elasticity. First, the Gibbs elasticity of films made from approximately ideal dilute solutions of one surfactant has a maximum value at an intermediate surfactant concentration. At very low concentrations E increases since the adsorption in this region is proportional to the concentration, whereas at higher concentrations the adsorption no longer varies measurably with concentration, causing E to decrease asymptotically to zero. Secondly, eq. 4 shows that the value of E is very sensitive to the presence of components with high adsorption values at very low concentrations. Knowledge of the surface equation of state for mixed surfactant solutions will permit a quantitative evaluation of these effects.

Surface Thermodynamics. Thermodynamics of the equilibrium distribution of matter between parts of a system—*e.g.*, between surface and bulk solution—has to start from the uniformity of the thermodynamic potential μ_i for each component throughout the system. The relation between μ_i and the concentration or mole fraction of i in any part of the system, then, gives the desired relation between the concentrations of i in these different parts of the system. The relation between μ_i and the concentration c_i of that component

can, however, only be given in terms of an activity coefficient, γ_i . This coefficient is defined by this very relationship, *e.g.*, in the case of the bulk solution α

$$\mu_i^\alpha = \zeta_i^\alpha + RT \ln \gamma_i^\alpha c_i \quad (6)$$

ζ_i^α being a constant characterizing the standard state of i . (In the following, the symbol ζ will be considered to denote infinite dilution as a standard state; *i.e.*, the value of ζ_i is adjusted so as to make $\gamma_i \rightarrow 1$ for $c_i \rightarrow 0$.)

Consequently, a general surface equation of state contains two activity coefficients of each component, one for the solution, γ_i^α , and one for the surface, γ_i^s . As is discussed in detail elsewhere,³ the relation between the thermodynamic potential of i in the surface and the surface concentration of i , can be written as

$$\mu_i^s = \zeta_i^s + RT \ln \left(\gamma_i^s \times \frac{\Gamma_i}{\Gamma^\infty} \right) - \frac{\sigma}{\Gamma^\infty} \quad (7)$$

Here ζ_i^s is a constant characterizing the standard state of i in the surface. For solutions containing one surfactant, Γ^∞ is the saturation adsorption, defined as the surfactant adsorption corresponding with the limiting slope of the surface tension-log surfactant activity plot at high surfactant activities. The derivation of eq. 7, which gives all information about the surface equation of state, can only briefly be indicated here. It was obtained by considering the surface phase, s , to be a geometrical dividing surface according to Gibbs between the two bulk phases. The position of this surface, however, was not fixed as suggested by Gibbs, *i.e.*, not so as to make the adsorption of the solvent equal to zero. For deriving a surface equation of state, the distribution of all components, including the solvent, between bulk and surface is considered; therefore a convention which defines the solvent to be not adsorbed is not suitable. A new convention has been chosen which fixes the position of the dividing surface so as to make the sum of solvent and surfactant adsorptions equal to the constant amount of Γ^∞ moles cm^{-2} ; this enables the derivation of eq. 7. The ratio of Γ_i and Γ^∞ thus gives the mole fraction of i in the surface, in analogy with c_i in eq. 6 measuring the mole fraction of i in the bulk solution. In principle this treatment, which considers the solvent adsorption, Γ_1 , not to be equal to zero, would necessitate the introduction of a term for $i = 1$ into Gibbs adsorption law as given in eq. 2. For aqueous surfactant solutions, however, where the mole fraction of water is always higher than 0.999, this term

(3) E. H. Lucassen-Reynders and M. van den Tempel, paper submitted for the IVth International Congress on Surface Active Substances, Brussels, 1964.

can be neglected due to the extremely small variations in water activity.

Equating the expressions given for μ_i in eq. 6 and 7, the surface equation of state can be obtained in three equivalent formulations, from which either Γ_i or c_i or σ has been eliminated, all the expressions containing three parameters: (1) the surface activity coefficients γ_i^s , determining the shape of the adsorption isotherm; (2) the saturation adsorption Γ^∞ , determining the magnitude of the adsorption, *i.e.*, the scale of the adsorption isotherm in the vertical direction; (3) a constant to be denoted by a_i , determining the magnitude of the surfactant concentration at which a given adsorption value is reached, *i.e.*, the scale of the adsorption isotherm in the horizontal direction. This constant equals the ratio of surface and bulk mole fractions of the surfactant at infinite dilution and, therefore, depends on the standard state parameters ζ_i and on the surface tension σ^0 at infinite dilution

$$RT \ln a_i = \zeta_i^s - \zeta_i^\alpha - \frac{\sigma^0}{\Gamma^\infty} = -\lambda_{i0}^\alpha \quad (8)$$

The parameter λ_{i0}^α thus defined is the molar free enthalpy of adsorption (from phase α) of i at infinite dilution.⁴ For ideal surface solutions, with $\gamma_i^s = 1$ at all surface compositions, a_i is the surfactant activity at which the surfactant adsorption has reached half of its saturation value.

It is emphasized that the general equations giving the surface behavior of a surfactant in terms of these three parameters were derived without any model for the surface layer; in particular, the model of a monomolecular surface layer is not involved, nor have any assumptions been made as to the areas occupied by the molecules in this layer.

As to the values of the surface activity coefficients γ_i^s , it has been shown³ that from single surfactant solutions ideal surface solutions are often formed, in which the surface activity coefficients of solvent and surfactant equal unity at all surface compositions. The shape of the adsorption isotherm for such ideal surface behavior is given by the well-known equation of Langmuir. This was shown to occur even in cases where the bulk activity coefficients of solvent and surfactant are by no means equal to unity, *e.g.*, in the case of micelle-forming compounds.

The value of the second parameter, the saturation adsorption, is not very sensitive to variations in the nature of the surfactant; at the air-water interface its value for surfactants with one single aliphatic chain varies between 2.5×10^{-10} and 5.5×10^{-10} mole cm.⁻². The value of the third parameter, a , however, can differ by a factor as high as 10^6 for two different surfac-

tants. Therefore, the concentration at half saturation adsorption is a sensitive measure for the surface activity of a compound, low values of it corresponding with high surface activity.

These general considerations following from eq. 6 and 7 can equally be applied to solutions of several surfactants. Surfactants each forming ideal surface solutions with water are assumed to behave ideally in each other's presence; the following treatment will be limited to ideal surface solutions. The parameter Γ^∞ for solutions of an arbitrary number of surfactants is generalized to be a total saturation adsorption corresponding to given ratios k_{ij} between the surfactant activities. Its value is found from the limiting slope of the σ -log $\gamma_i^\alpha c_i$ plot for any of the surfactants at such constant ratios

$$\Gamma^\infty = -\frac{1}{RT} \lim \left[\frac{d\sigma}{d \ln \gamma_i^\alpha c_i} \right]_{k_{ij}} \quad (j = 2, 3 \dots n) \quad (9)$$

$$k_{ij} = \frac{\gamma_i^\alpha c_i}{\gamma_j^\alpha c_j}$$

Surface tension and adsorptions as a function of surfactant concentrations, then, are given by generalized Szyszkowski-Langmuir equations

$$\sigma^0 - \sigma = RT\Gamma^\infty \ln \left[\sum_{i=2}^n \frac{\gamma_i^\alpha c_i}{a_i} + 1 \right] \quad (10)$$

$$\Gamma_i = \Gamma^\infty \frac{\gamma_i^\alpha c_i / a_i}{\sum_{j=2}^n \gamma_j^\alpha c_j / a_j + 1} \quad (11)$$

Occurrence of Szyszkowski-Langmuir adsorption has been generally supposed to be limited to adsorption from ideal bulk solutions of a single nonionic nonvolatile component; it has been considered essential that equal cross-sectional areas could be predicted from the geometry of solvent and solute. Equations 10 and 11 are generalized to include also nonideal solutions of an arbitrary number of surfactants, the geometry of which is considered irrelevant. In principle, the value of Γ^∞ depends on the concentration ratios of the various surfactants present; this effect is considered negligible in comparison with the influence of the difference in a values for the surfactants.

In the following section, the Gibbs elasticity for films containing one or two surfactants will be evaluated by combining eq. 4 and 11.

Gibbs Elasticity for Ideal Surface Behavior. Usually the bulk activity coefficients of surfactants (not that of the solvent) are nearly equal to unity below the critical

(4) A. Vignes, *J. chim. phys.*, **57**, 966 (1960).

micellar concentrations: $\gamma_2^\alpha = \gamma_3^\alpha = 1$. For such solutions it is convenient to express surfactant concentrations in units a_i

$$x_i = \frac{c_i}{a_i} \quad (12)$$

and likewise to express the total amount of surfactant present in unit volume of the film, g_i , in units a_i

$$g_i = x_i + \frac{2\Gamma_i}{a_i h} \quad (13)$$

and, finally, to define another dimensionless parameter, y_i , measuring the amount of i present in the film liquid (x_i) relative to the amount adsorbed at the surfaces ($g_i - x_i$)

$$y_i = \frac{a_i h}{2\Gamma_i^\infty} = \frac{x_i}{(g_i - x_i) \left(1 + \sum_{i=2} x_i\right)} \quad (14)$$

In terms of these dimensionless parameters, the Gibbs elasticity of *single surfactant solutions* is found to be given by

$$E = 2RT\Gamma^\infty \frac{x_2}{1 + y_2(1 + x_2)^2} = 2RT\Gamma^\infty \frac{x_2(g_2 - x_2)}{g_2 + x_2^2} \quad (15)$$

At a given film thickness, eq. 15 predicts a linear increase of the elasticity with increasing surfactant concentration in the Traube region ($x_2 \ll 1$). This increase is steeper at smaller film thicknesses and for higher surface activities (lower a_2 values). At higher concentrations a maximum E value (E_m) is obtained, for which

$$x_{2m} = \sqrt{1 + \frac{1}{y_2}} = \sqrt{g_{2m}} \quad (16)$$

$$E_m = RT\Gamma^\infty (\sqrt{g_{2m}} - 1) \quad (17)$$

The elasticity has its maximum value at a concentration where more than half of the saturation adsorption is reached; at lower film thickness both the elasticity and the concentration at the maximum shift to higher values. Above the c.m.c., the activity coefficient γ_2^α is no longer equal to unity, but decreases inversely proportional to the concentration: $d \ln \gamma_2^\alpha = -d \ln c_2$. Here the complete eq. 4 must be used, predicting a sudden decrease of E to zero at the c.m.c.

A typical example for a film (with a thickness of 1μ) containing one surfactant, sodium dodecyl sulfate, is shown in Figure 1. The experimental surface tension data⁵ for this substance closely follow eq. 10 and 11 with

$$\Gamma^\infty = 2.6 \times 10^{-10} \text{ mole cm.}^{-2};$$

$$a_2 = 0.44 \times 10^{-6} \text{ mole cm.}^{-3}$$

The only known elasticity measurements have been performed in this system⁶; they yielded values between 8 and 15 dynes cm.^{-1} at a concentration around the c.m.c., in agreement with the calculated values just below the c.m.c. in Figure 1.

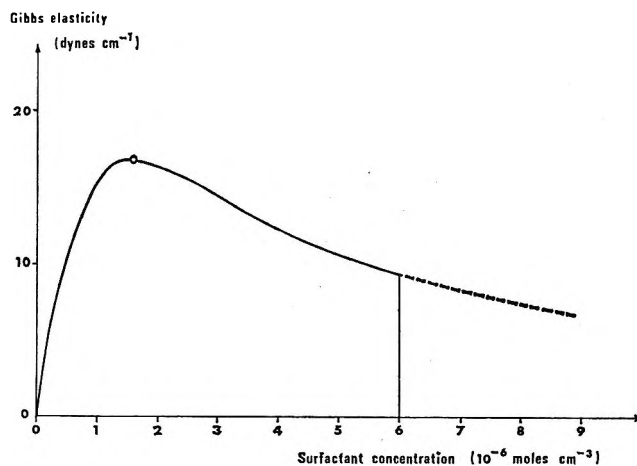


Figure 1. Gibbs elasticity of films with thickness 10^{-4} cm. containing sodium dodecyl sulfate.

The influence of a *second surfactant* (component 3) on the Gibbs elasticity will be discussed now, again for ideal surface behavior, and neglecting bulk activity corrections for the two surfactants. Moreover, for the sake of simplicity the total saturation adsorption will be assumed not to depend on the concentration ratio of the two surfactants. Gibbs elasticity is then most conveniently expressed in the total amounts g_i and the bulk amounts x_i

$$E = 2RT\Gamma^\infty \left[\frac{1 + x_2 + x_3}{1 + x_2^2/g_2 + x_3^2/g_3} - 1 \right] \quad (18)$$

With this equation, the effect of the second surfactant on E will be investigated in two ways, accounting either for an addition of the second surfactant at a given bulk amount x_2 of the surfactant already present, or for addition of component 3 at a given total amount g_2 in the film. The two methods give different numerical results, since at constant g_2 the addition of 3 can considerably increase the bulk amount x_2 , component 2 being displaced from the surface especially if 3 is very surface active (a_3 very low).

(5) B. A. Pethica, *Trans. Faraday Soc.*, **50**, 413 (1958).

(6) K. J. Mysels, M. C. Cox, and J. D. Skewis, *J. Phys. Chem.*, **65**, 1107 (1961).

The following general statements can be derived from eq. 18 for these cases. (1) The elasticity of the mixed solution is always higher than the lower of the two elasticities found by removing either 2 or 3 from the film, but lower than the sum of these two single surfactant elasticities. (2) The very first addition of component 3 can cause the elasticity to increase, to be constant, or to decrease, depending not only on the surface activities of 2 and 3 (measured by a_2 and a_3) but also on the concentration of 2. High relative surface activity of 3 with respect to 2 (*i.e.*, $a_3 \ll a_2$) tends to promote an increase in E , as was already qualitatively expected from the general eq. 4. However, it will be illustrated below that in some cases of practical interest elasticity is always *decreased* by the first additions of another surfactant, whatever its surface activity. (3) At high x_3 values, E always decreases, irrespective of whether it increases or decreases at low x_3 values.

A more detailed analysis will be given for the second statement, since this seems important for the influence of "minor impurities" on Gibbs elasticity and film stability. Behavior at very low x_3 values is governed by the limiting value (for $x_3 \rightarrow 0$) of the derivative of E with respect to x_3 , at constant film thickness and at a constant value of either x_2 or g_2 . Calculation of this limiting value from eq. 18 reveals the existence of a critical value of a_3/a_2 , *i.e.*, of the surface activity ratio of the two surfactants, for which the limiting slope is equal to zero. If the surface activity of the added surfactant corresponds to this critical ratio, the elasticity of the film is not affected; if its surface activity is higher (a_3 lower), it increases the elasticity, whereas lower surface activities give a decrease in E . The value of this critical surface activity ratio depends on concentration and surface activity of the surfactant already present

$$\left[\frac{a_3}{a_2} \right]_{\text{cr}} = \frac{g_2(g_2 - x_2^2)}{2x_2^3} + 1 \quad (\text{for addition of 3 at constant } g_2) \quad (19)$$

$$\left[\frac{a_3}{a_2} \right]_{\text{cr}} = \frac{g_2(g_2 - x_2^2)}{x_2^2(g_2 + x_2)} + 1 \quad (\text{for addition of 3 at constant } x_2) \quad (20)$$

In both cases the critical surface activity ratio equals unity at the concentration of maximum single surfactant elasticity, in view of eq. 16. At higher concentrations it is lower than unity, and at lower concentrations higher than unity. A numerical example as calculated from eq. 19 is given in Figure 2, for a surfactant with properties near to those of sodium dodecyl sulfate, at film thickness of 1μ ($a_2 = 10^{-7}$ mole cm.^{-3} ; $\Gamma^\infty = 5 \times 10^{-10}$ mole cm.^{-2}).

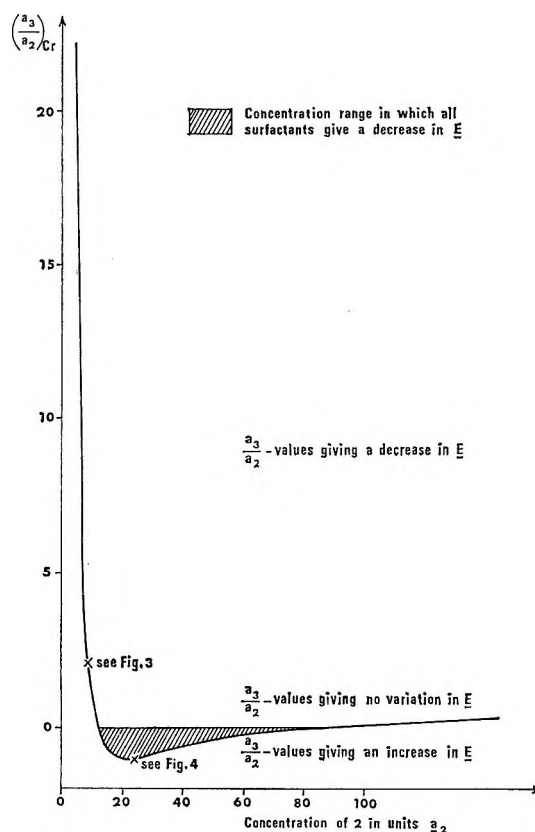


Figure 2. Critical a_3/a_2 values (at constant g_2) for $y_2 = 10^{-2}$.

Calculation from eq. 20 would give a curve intersecting that of Figure 2 at a critical ratio of unity, giving lower values at the left-hand side and higher values at the right-hand side of this point. Figure 2 shows two remarkable features. At low concentrations of 2, the critical values of the surface activity ratio are very high: at $x_2 = 1$ it is higher than 100, which means that here Gibbs elasticity is nearly always *increased* by the addition of another component, even if its surface activity is a thousandfold less than that of the surfactant already present. At higher concentrations, however, the situation is reversed, the critical values being very low, and even negative at concentrations x_2 between 11.5 and 99. Physically, only positive a_3 values are possible, which means that actual a_3 values are always higher (even if extremely low) than the critical value: in this region any additional surfactant gives a *decrease* in E . This behavior is further illustrated in Figures 3 and 4, giving E as a function of x_3 as calculated from eq. 18. Figure 3 shows the effect of component 3 for two surface activities, one higher and one lower than the critical value indicated in Figure 2.

The same highly surface active component, however, which *increases* E in Figure 3, *decreases* E if added at a higher concentration of 2 where the critical value in

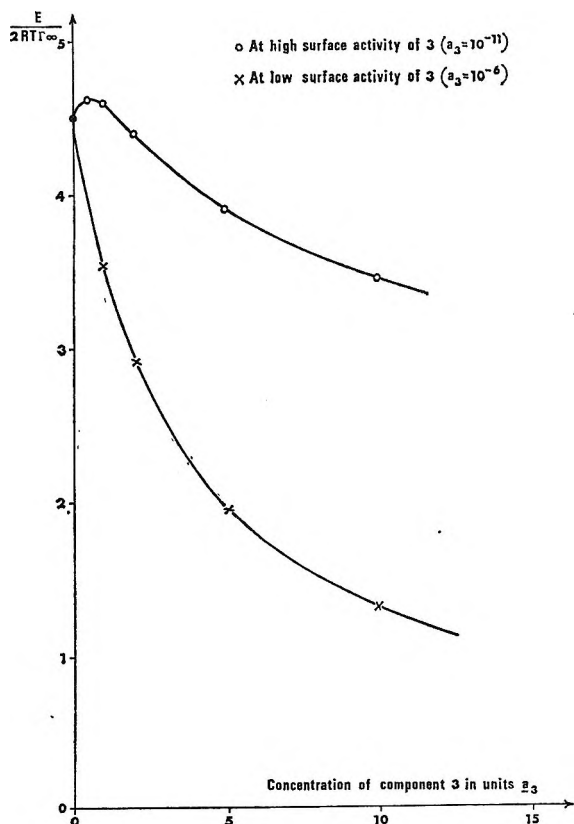


Figure 3. Effect of component 3 on Gibbs elasticity at constant total amount of 2 ($g_2 = 99a_2$; $a_2 = 10^{-7}$).

Figure 2 is negative. This is shown by the lower curve of Figure 4.

The same figure, finally, shows in the upper curve that the remarkable negative critical surface activity ratios do not occur with eq. 20, *i.e.*, if component 3 is thought to be added at constant concentration x_2 instead of at constant g_2 . In that case the highly surface-active component shows the "normal" behavior of increasing the elasticity. The increase in E upon addition of 3 at constant x_2 can be very considerable, especially if component 2 is less surface active than given in Figure 4; in this figure, E is increased with a factor of about 2 at $x_3 = 100$, *i.e.*, at a concentration c_3 which is only 0.04% of c_2 , but if 2 and 3 were only one-tenth as surface active the elasticity under these conditions would be increased with a factor of more than 10. At very high x_3 values both curves in Figure 4 would pass through a maximum, followed by an asymptotical decrease to zero.

Summarizing, upon addition of a second surfactant (3), three types of curves can be obtained for E as a function of x_3 , depending on whether the surface activity of 3 is lower or higher than a critical value. If it is higher, E increases, passes through a maximum, and

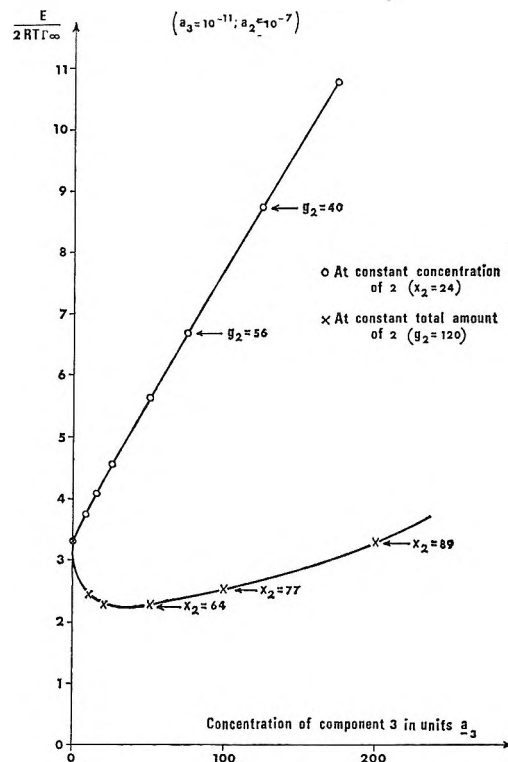


Figure 4. Effect of very surface-active component 3 on Gibbs elasticity.

finally decreases to zero at increasing x_3 . If it is lower, E first decreases and subsequently either increases and reaches a maximum, if 3 is more surface active than 2, or continuously decreases to zero if 3 is less surface active than 2. At suitable surface activities and concentrations of the two surfactants, the increase in E can be enormous, but only if the concentration of 2 is kept constant, and not its total amount in the film. The unexpected decrease in E that can occur upon addition of even highly surface-active surfactants at constant total amount of the original surfactant is due to the large effect of the added surfactant on adsorption and concentration of 2.

The above considerations apply to surfactant solutions forming ideal surface solutions at all surface compositions between zero and unity mole fraction of surfactant and bulk solutions that are sufficiently dilute to ensure $\gamma_2^\alpha = \gamma_3^\alpha = 1$. Large effects on the elasticity could under these conditions be calculated even for additions of a surfactant occupying the same specific area in the surface as the original surfactant (the condition $\Gamma^\infty = \text{constant}$). The effect of deviations from these simple, though frequently occurring, conditions is briefly discussed in the following section.

Effect of Deviations from Ideality. In surfactant

solutions of practical interest, the condition $\gamma_2^\alpha = \gamma_3^\alpha = 1$ is usually satisfied up to the c.m.c., even for ionic surfactants (here $\gamma_2^\alpha \geq 0.9$, for $c_2 \leq 10 \times 10^{-6}$ mole cm.⁻³). The effect of micelle formation in a single surfactant solution is shown in Figure 1: the E value suddenly drops to zero. The c.m.c. value seems to be affected by the same factors influencing the a value³; the ratio of the two is between 15 and 200. This means that x values higher than this ratio cannot be reached; therefore, x values higher than 200 are not represented in the figures.

Micelle formation in a mixed surfactant solution may even give rise to negative elasticity values, in cases where solubilization of the second surfactant into the micelles causes the well-known minimum in the surface tension-concentration curve. In general, lower γ_2^α and γ_3^α values give rise to lower E values.

The influence of the surface activity coefficients is opposite to that of the bulk activity coefficients, since they occur as $\gamma_i^\alpha/\gamma_i^b$ in the combination of eq. 6 and 7. The only well-studied examples of surface non-ideality are the higher fatty acids.⁷ It can be shown that they form regular surface solutions with water. The surface activity coefficient, *e.g.*, of lauric acid, decreases from unity at infinite dilution to 0.06 at saturation adsorption. At a given concentration, the surfactant adsorption, and hence the calculated elasticity value too, is much higher than would correspond with ideal behavior of the surface. As yet, no experimental data are available to check these predictions.

Application to Foam Stability. The effect of the concentration of a single surfactant on the Gibbs elasticity, as shown in Figure 1, appears to be completely similar to its effect on the stability of foam or of a single film between two air bubbles ("elementary foam"). From as early as 1925, many investigators⁸ have observed a maximum in foam stability at a concentration where saturation adsorption is not yet reached for surfactants like fatty acids and their salts, alcohols, and sodium dodecyl sulfate. It is proposed that film stability and Gibbs elasticity are directly related in these cases.

The effect of a second surfactant on the Gibbs elasticity can be used to explain the well-known stabilizing effect of certain minor impurities of low water solubility,

such as higher alcohols or acids, present in detergent solutions.

It has been argued that these impurities are adsorbed preferentially at the surface and that they enhance foam stability most if the adsorbed layer contains more than 50% additive⁹ resulting in a high surface shear viscosity. Contradictory to this theory, the high foam stability in the presence of the impurity is now thought to be connected not to the effect of the impurity on the shear properties of the surface but on its properties on dilatation.¹⁰ The evidence in favor of this is similar to that presented in Figure 4, upper curve. The present treatment shows that highly surface-active impurities do give high elasticity values, provided their addition does not affect the concentration of the main surfactant. It should be noticed that "high surface activity" is not to be connected here with a smaller molar area of the added compound,⁹ but with its higher adsorption free enthalpy or with its smaller a value. Whether impurities in actual foam films should be considered to affect the concentration or the total amount of the main surfactant in the film depends on the history of the film from the generation of the foam bubbles. Therefore, the relation between the original composition of a foaming solution and the composition of the final thin films should be investigated before a general correlation can be given between the original surfactant concentrations and the film stability.

The foaming behavior of surfactant solutions above the c.m.c. seems to give an example of the importance of this point. Foam films obtained from such solutions apparently do not have the zero or negative elasticities they should have if containing micelles; this is considered evidence for the possibility of considerable differences between original and final concentrations.

(7) A. Frumkin, *Z. physik. Chem.*, **116**, 466 (1925).

(8) O. Bartsch, *Kolloid Chem. Beih.*, **20**, 1 (1925); D. Talmud and S. Suchowolskaya, *Z. physik. Chem.*, **A154**, 277 (1931); P. A. Rehbinder and A. A. Trapeznikov, *Acta Physicochim. URSS*, **9**, 257 (1938); E. J. Burcik, *J. Colloid Sci.*, **5**, 421 (1950).

(9) W. M. Sawyer and F. M. Fowkes, *J. Phys. Chem.*, **62**, 159 (1958).

(10) A. Prins and M. van den Tempel, paper submitted for the IVth International Congress on Surface Active Substances, Brussels, 1964.

Adsorption of Cyclohexane on Aluminas Prepared by Thermal Decomposition of Aluminum Hydroxide *in Vacuo* and in Presence of Air

by R. I. Razouk, R. Sh. Mikhail, and G. R. Iskander

Chemistry Department, Faculty of Science, Ain Shams University, Abbassia, Cairo, U.A.R. (Received May 12, 1964)

The adsorption of cyclohexane vapor was measured on the products of thermal decomposition of two parent crystalline hydroxides of aluminum. The effect of temperature of preparation, duration of heating, and presence of air during decomposition was studied. In agreement with the results obtained with similar systems previously investigated, decomposition at low temperatures results in a marked increase in specific surface area, but sintering develops at higher temperatures. The latter is enhanced by rise of temperature, by increase of duration of heating, and also by presence of air during the decomposition process.

Introduction

Several factors are known to affect markedly the surface properties of active solids prepared by thermal decomposition.¹ The presence of air during the heat treatment is of particular interest owing to the relatively limited work cited in the literature in this connection although active solids are usually prepared under this condition. In an earlier investigation,² it was found that the presence of air during the preparation of magnesium oxide by thermal decomposition of the hydroxide and carbonate invariably gives rise to products possessing much lower surface areas which in certain cases are only one-tenth of the surface of the product prepared *in vacuo* under similar conditions. Similar behavior was recently observed in the production of calcium oxide by thermal decomposition of the hydroxide.³

The present work has been undertaken to investigate the dependence of the adsorptive properties on the absence or presence of air during the dehydration of two crystalline preparations of aluminum hydroxide. Both the effect of temperature of dehydration and duration of thermal treatment were studied. The nature of the solid phases was also investigated by means of X-ray analysis.

Experimental

Apparatus and Technique. A conventional volumetric system was used for the adsorption measure-

ments. X-Ray diffraction patterns were obtained with the aid of a Philips 114.23 Debye-Scherrer powder camera with Ni-filtered Cu radiation.

Materials. Adsorption measurements were carried out on the products obtained from two parent preparations of aluminum hydroxide by dehydration *in vacuo* and in presence of air at 110, 200, 350, 500, 650, 800, and 950°. The term "*in vacuo*" means here while pumping off air and gaseous products, keeping the pressure less than 10^{-3} mm., and the term "in presence of air" means while the material is in contact with "non-dry" air containing water vapor formed by dehydration of the hydroxide.

Preparation G was obtained by the slow addition of ammonia (20.3%) to a solution of aluminum chloride until the supernatant liquid had pH *ca.* 8. The precipitate was washed with dilute ammonia and then dried in a vacuum oven at 50°. The water content was 34.4% as compared with 34.65 for the trihydrate. X-Ray diffraction patterns possessed clear and sharp lines which gave *d* and *I* values characteristic of gibbsite.

Preparation B was obtained by adding ammonia to a

(1) See, *e.g.*, S. J. Gregg, "The Surface Chemistry of Solids," 2nd Ed., Reinhold Publishing Corp., New York, N. Y., 1961, p. 300 *et seq.*

(2) R. I. Razouk and R. Sh. Mikhail, *Actes Congr. Intern. Catalyse*, 2^e, Paris, 1960, 2023 (1961).

(3) R. Sh. Mikhail, *J. Phys. Chem.*, 67, 2050 (1963).

boiling solution of alum. The precipitate was washed with ammonia and dried in a vacuum oven at 40°. The water content was 33.6%. X-Ray powder photographs gave clear patterns, and the d and I values corresponded to those of bayerite.

Cyclohexane was prepared in a pure state by the method described earlier.⁴

Results

Adsorption Measurements. Preliminary experiments on the adsorption of cyclohexane on the parent hydroxide preparations did not give concordant results, but the data obtained with the products of dehydration formed at and above 110° were well reproducible. The present work is therefore confined to these products.

In all cases the adsorption is rapid, and thorough outgassing at room temperature removes all the adsorbate. The isotherms are type II of Brunauer's classification.⁵ Desorption isotherms form with adsorption isotherms small hysteresis loops which join together at relative vapor pressures depending on the temperature of dehydration. The hysteresis loops are of type A combined with a little of type E of de Boer's classification,⁶ and the pore spectrum of all specimens is very broad as might be judged from the broad region of relative vapor pressure over which the hysteresis loop extends.

A typical set of results is represented in Figure 1, which shows the adsorption isotherms of cyclohexane on the products of dehydration of preparation G formed at 350, 500, 650, 800, and 950° by heating *in vacuo* for 5 hr. Representative desorption isotherms are also drawn for products formed at 350, 650, and 950°.

The isotherms are found to obey the B.E.T. equation⁷ in the normal range of pressure. The specific surface areas of the various products were calculated from the monolayer capacity and by taking the cross-sectional area of the cyclohexane molecule as 39 Å.²⁸ Previous work in this laboratory has shown that the adsorption of cyclohexane at ordinary temperature could be successfully used to measure the surface area of magnesium oxide⁴ and iron oxide.⁹ For the purpose of comparison, the specific surface areas of certain products were estimated by the standard low temperature nitrogen adsorption and were found to be in satisfactory agreement with present values obtained from the adsorption of cyclohexane. Thus, the specific surface areas calculated from cyclohexane and nitrogen adsorption were 244 and 220 m.²/g. for the product obtained from preparation G by dehydration *in vacuo* at 350°, 246 and 228 m.²/g. for the product obtained at 650°, 143 and 134 m.²/g. for the product formed by

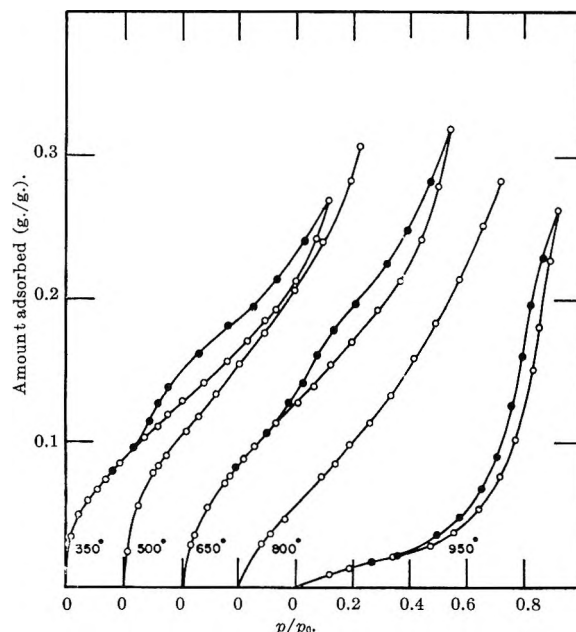


Figure 1. Adsorption-desorption isotherms of cyclohexane on the products of dehydration of preparation G formed *in vacuo* at various temperatures: O, adsorption; ●, desorption.

dehydration in presence of air at 650°, and 37 and 34 m.²/g. for the product formed at 950°.

Experiments on the effect of duration of heating (Figure 2) show that when dehydration is carried out *in vacuo* below 650°, the specific surface area increases with the duration of thermal treatment as a result of further decomposition although the increase is found to be far less than corresponds to the decrease in the water content. Dehydration at 800° for 0.5 hr. gives rise to a product of maximum surface area, but heating for longer periods leads to progressive diminution in the specific surface area even though it is accompanied with further slight decomposition. Thermal treatment at higher temperatures leads to a continuous decrease in surface area.

However, when dehydration is conducted in presence of air, prolonged heating results in decreasing the specific surface area even at low temperatures although the

(4) R. I. Razouk and R. Sh. Mikhail, *J. Phys. Chem.*, **61**, 886 (1957).

(5) S. Brunauer, "Physical Adsorption of Gases and Vapors," Oxford University Press, London, 1944, pp. 149 *et seq.*

(6) J. H. de Boer, "The Structure and Properties of Porous Materials," D. H. Everett and F. S. Stone, Ed., Butterworths Scientific Publications, London, 1958, p. 68 *et seq.*

(7) S. Brunauer, P. H. Emmett, and H. Teller, *J. Am. Chem. Soc.*, **60**, 309 (1938).

(8) R. N. Smith, C. Pierce, and H. Cordes, *ibid.*, **72**, 5595 (1950).

(9) R. I. Razouk, R. Sh. Mikhail, and B. S. Girgis, *Advances in Chemistry Series*, No. 33, American Chemical Society, Washington, D. C., 1961, p. 42.

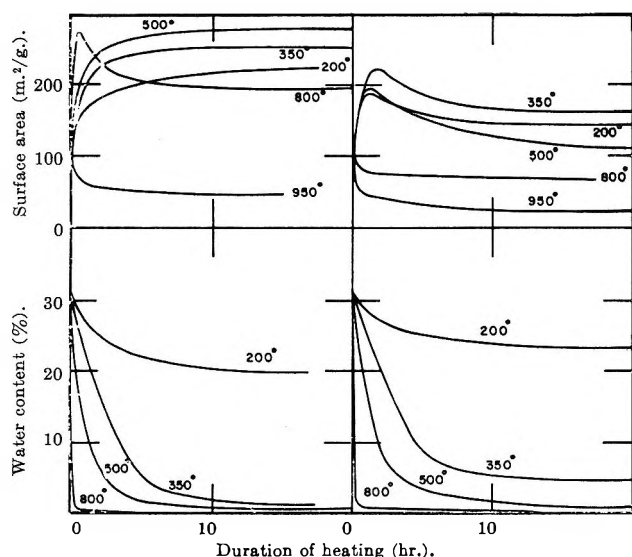


Figure 2. Effect of duration of thermal treatment on the specific surface area (upper curves) and the water content (lower curves) of the products of dehydration of preparation G formed *in vacuo* (left) and in the presence of air (right) at various temperatures.

percentage of decomposition might increase several-fold. The only exception is for an initial period not exceeding 2 hr. at temperatures below 650° when an increase in area accompanies the early stages of dehydration. This emphasizes the onset of sintering in presence of air at a temperature much lower than *in vacuo*.

The effect of temperature of dehydration on the specific surface area of the products formed by heating preparations G and B for 5 hr. *in vacuo* and in presence of air is represented in Figure 3. It is evident that dehydration *in vacuo* is accompanied by development of larger surface area and that the temperature at which maximum activity is obtained is slightly higher *in vacuo* than in presence of air. However, when comparison is made for equal water contents rather than for equal durations of heating, the diminution in the specific surface area of products formed in presence of air becomes less marked in some cases.

It is to be noted, however, that the adsorption values near saturation vapor pressure are, by far, less dependent on the thermal treatment than the specific surface areas themselves. This implies that rise of temperature leads to changes in the average pore radius while the pore volume remains essentially the same. This is in agreement with the observed general tendency of the relative vapor pressure at which the hysteresis loop closes up to be displaced toward higher values as the temperature of thermal treatment is raised.

Structural Changes Accompanying Dehydration. X-Ray diffraction patterns were obtained for both prep-

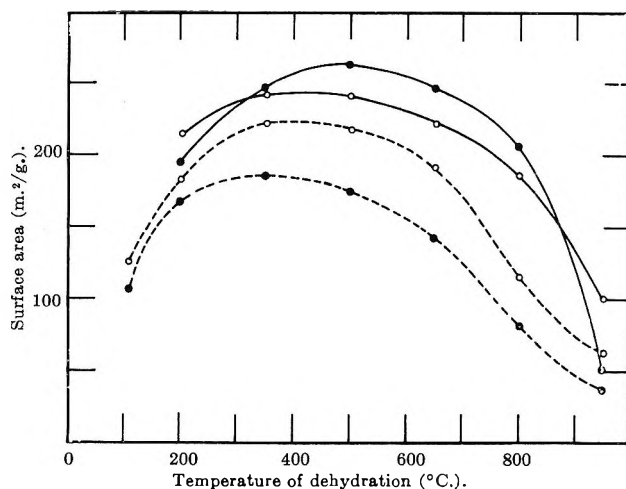


Figure 3. Specific surface areas of products formed by the dehydration of preparation G (●) and preparation B (○) at various temperatures *in vacuo* (continuous lines) and in presence of air (dotted lines).

arations and their dehydration products. Comparison with the A.S.T.M. cards¹⁰ shows that preparations G and B are mainly gibbsite ($\alpha\text{-Al}_2\text{O}_3\cdot 3\text{H}_2\text{O}$) and bayerite ($\beta\text{-Al}_2\text{O}_3\cdot 3\text{H}_2\text{O}$), respectively. Drying at 110° in presence of air leaves the patterns unaltered although the water content falls by approximately 15 and 30%, respectively, below the stoichiometric water content in the trihydrate. Similar retainment of a pseudo-structure on dehydration at low temperatures was observed in the thermal decomposition of goethite and lepidocrocite.⁹ The changes observed in the patterns of the various products of dehydration are found to be in general agreement with the results of other investigators.¹¹

Thus, when preparation G is heated *in vacuo* at 200° for 2 hr., the water content falls to 24.91%, and most of the lines which give the characteristic d spacings of gibbsite still remain clear. These lines, however, disappear on dehydration at 350° . The product formed between 350 and 800° possess diffuse patterns which are difficult to identify, but the product formed at 950° possesses a pattern of sharp lines corresponding to δ - and θ -alumina.

The product obtained by dehydration of preparation B at 200° *in vacuo* for 5 hr. (containing 7.16% water) gives a pattern in which the characteristic lines of bayerite disappear, and some of the lines of boehmite develop although in diffuse form. Products formed be-

(10) J. V. Smith, Ed., "X-ray Powder Data File," American Society for Testing Materials, Philadelphia, Pa., 1960.

(11) See, e.g., M. K. B. Day and V. J. Hill, *J. Phys. Chem.*, **57**, 446 (1953); R. Tertian and D. Papée, *J. chim. phys.*, **55**, 341 (1958).

tween 350 and 800° give diffuse patterns, but the product formed at 950° possesses a pattern in which some lines characteristic of η - and θ -alumina develop.

It is interesting to note that the patterns of the products formed at high temperatures in presence of air were found to exhibit sharper lines than in case of corresponding products formed *in vacuo*, indicating that the development of the crystalline structure proceeds more readily when dehydration is conducted in presence of air.

Discussion

Crystalline hydroxides are frequently used as starting materials for the preparation of active solids because their specific surface areas increase considerably upon heating. Generally, dehydration gives rise to pseudo-morphosis, and the volume of the solid does not vary much. Meantime, water is expelled during dehydration, and space will be created in the porous product. On heating to higher temperatures, however, the surface area of the solid decreases again.

In the course of study of the surface properties of oxides of magnesium, iron, and calcium produced by thermal decomposition of hydroxides and carbonates,^{2-4,9,12} it has been postulated that during thermal treatment the mechanism which determines the surface area-temperature relationship is governed by three processes, namely, (i) decomposition, (ii) recrystallization, and (iii) sintering. For crystalline parent materials which decompose to yield ultimately crystalline products, a maximum in the surface area-temperature of dehydration curve might be expected, the ascending branch of the curve being due mainly to the first two processes, while the descending branch to sintering. The three processes overlap in the neighborhood of the maximum. The results obtained in the present investigation using two crystalline hydroxides of aluminum are in good agreement with this picture.

Besides the important contribution of temperature and duration of heating in determining the specific surface area of the products of thermal dehydration, the presence of air during the preparation of active solids affects considerably the surface area-temperature curves, giving rise to smaller areas and the displacement of the maximum toward lower temperatures.

The diminution of the surface area observed when dehydration is conducted in presence of air is very probably associated with the formation of crystallites of larger grain size. Investigation by the electron microscope on both series of products has shown that thermal

dehydration in presence of air is accompanied by (i) the development of larger grain size, the higher the temperature the greater is the difference between the sizes of particles formed *in vacuo* and in presence of air, and (ii) the development of better crystalline morphology.¹³

The lower surface areas of the products prepared by dehydration in "nondry" air are ascribed mainly to the presence of water vapor in contact with the decomposing material. The enhanced sintering by water formed during catalytic cracking¹⁴ and by steam¹⁵ is known. de Boer and Vleeskens¹⁶ found that surface hydration leads to pore volume and surface area decrease. Anderson and Morgan¹⁷ have recently shown that, in the sintering of magnesium oxide, crystal agglomeration and crystal growth are accelerated by the presence of water vapor during thermal treatment and that mere water adsorption does not promote the sintering effects but that a certain mobility and rapidity of exchange of water molecules on the surface is required. Nevertheless, the effect of dry air on reducing the surface area during thermal treatment cannot be overlooked, for heating in presence of dry air has been found to reduce considerably the specific surface area of products formed *in vacuo* and possessing maximum activity. A similar behavior was observed also with magnesium oxide.⁴ However, as some water is still retained by these products, it is not possible before further experimentation under better defined conditions to find out the contribution of water vapor and of air separately nor to ascertain whether the diminution in surface area and the increase in grain size take place during the act of decomposition itself or after its completion.

Acknowledgment. The authors wish to express their thanks to Dr. S. Brunauer for his kind permission to R. Sh. M., to carry out the experiments on the low temperature nitrogen adsorption in the Research and Development Laboratories of Portland Cement Assoc., Skokie, Ill., and to Dr. L. E. Copeland for performing and interpreting the electron microscope work.

(12) R. I. Razouk and R. Sh. Mikhail, *J. Phys. Chem.*, **63**, 1050 (1959).

(13) See ref. 3, Figure 5.

(14) H. E. Ries, Jr., *Advan. Catalysis*, **4**, 87 (1950).

(15) C. R. Adams, *J. Phys. Chem.*, **67**, 313 (1963).

(16) J. H. de Boer and J. M. Vleeskens, *Koninkl. Ned. Akad. Wetenschap., Proc.*, **B66**, 234 (1957).

(17) P. J. Anderson and P. L. Morgan, *Trans. Faraday Soc.*, **60**, 930 (1964).

The Surface Area of Liquids in Circular Tubes

by Ted A. Erikson

Chemistry Research Division, IIT Research Institute, Technology Center, Chicago 16, Illinois (Received June 19, 1964)

The surface area of a liquid in a circular tube approximates to about 2% the area represented by an oblate spheroid that has the tube radius and the meniscus height as its major and minor semi-axes, respectively. Over much of their range, the tables of Bashforth and Adams appear to represent coordinates of an ellipse within about 4%.

Introduction

One aim of this paper is to show the unexpected approximate identity between the dimensions of a liquid meniscus in a circular tube as published in the classic tables of Bashforth and Adams¹ and those calculated by assuming that the liquid surface approximates an oblate spheroid. In particular, surface areas of liquids in circular tubes are compared on this basis. Other empirical and geometrical approximations are indicated to show inadequate accuracy.

During a study of the forced vaporization process as described by a new language of steady-state thermodynamics,² various liquids were vaporized from glass tubes of different radii by pumping. One objective of these experiments was to extrapolate a specific vaporization coefficient to an infinite surface area in which equipment geometry would be negligible. This experiment was performed at several temperatures, and it became impossible to measure accurately, or photograph, each meniscus shape for all assorted conditions. Hence, a search was made for a simple and effective means, preferably based on the physical properties of the liquid and the dimensions of the tube, to approximate the area of the liquid surface. Although many studies^{1,3-10} have been concerned with the meniscus shape as it pertains to surface-tension measurements by capillary rise, references to area approximations of liquid surfaces are conspicuous by their absence.

The surface of a liquid takes the shape of a hemispherical cap in a circular tube of sufficiently small radius,³ but it essentially becomes a plane in sufficiently large tubes. Thus

$$A_h = 2\pi r^2 \quad (1a)$$

$$A_t = \pi r^2 \quad (2a)$$

where A is the liquid surface area, r is the tube radius and the subscripts h and t refer to sufficiently small (hemispherical) and large (flat), respectively.

Most laboratory-sized equipment falls in the transition region between the limits imposed by eq. 1 and 2, in which the surface area of the liquid varies from 2 to 1 times the tube area, respectively. Many interpolation formulas for the surface area of liquids in intermediate-sized tubes can be devised; however, the real unsolved problem is an estimation of the accuracy and of the limits of application of such a formula. The area of a liquid surface becomes of direct importance in the evaluation of experiments that deal with absorption, condensation, accommodation, reaction, and similar mass-transfer processes for which specific properties are desired, that is, properties based on a unit area of surface or interface. The purpose of this paper is to suggest a resolution of this problem.

Meniscus Shape

The shape of a liquid meniscus varies from practically a hemisphere to nearly a plane for any given liquid in

(1) F. Bashforth and J. C. Adams, "An Attempt to Test the Theory of Capillary Action," Cambridge University Press, London, 1883.

(2) T. A. Erikson and R. J. Tykodi, *J. Chem. Phys.*, **31**, 1521 (1959); **33**, 46 (1960).

(3) Lord Rayleigh, *Proc. Roy. Soc.*, **A92**, 184 (1915).

(4) S. Sugden, *J. Chem. Soc.*, 1483 (1921).

(5) N. K. Adams, "The Physics and Chemistry of Surfaces," Oxford University Press, London, 1941.

(6) Hagen and Desains, *Ann. chim. phys.*, **51**, 417 (1857).

(7) P. Perry, "Popular Lectures and Addresses," *Proc. Roy. Inst.*, **1**, 40 (1886).

(8) T. W. Richards and L. B. Coombs, *J. Am. Chem. Soc.*, **37**, 1656 (1915).

(9) T. W. Richards and E. K. Carver, *ibid.*, **43**, 827 (1921).

(10) B. B. Freud and H. Z. Freud, *ibid.*, **52**, 1772 (1930).

sufficiently small- and large-radius tubes. The fundamental equation for the surface of separation between two fluids is⁵

$$\gamma \left(\frac{1}{R_i} + \frac{1}{R_j} \right) = C + gz_i(\rho_1 - \rho_2) \quad (3)$$

where R_i and R_j are the principal radii of curvature of any point on the surface, γ is the surface tension, C is a constant, g is the acceleration of gravity, ρ_1 and ρ_2 are the densities of the two fluids, and z_i is the vertical coordinate of any point in the meridional section of the fluid surface measured from the lowest point of the meniscus. Figure 1 illustrates this description. Radii of curvature are not easily measured, and when quantities that can be measured are substituted in eq. 3, the equation becomes impossible to solve in finite terms. Thus, no one equation defines the shape of the meniscus for all tubes and liquids.

Bashforth and Adams rearranged eq. 3 in the following equivalent form

$$\frac{1}{R'} + \frac{\sin \phi}{x'} = 2 + \beta z' \quad (4)$$

where ϕ is the angle that the normal to the surface makes with the axis of revolution; x is the horizontal coordinate; the primes refer to the ratio of that quantity to the central radius of curvature, b (namely, $R_1' = R_1/b$, $x' = x/b$, etc.); and β is an abstract number set equal to the function

$$\frac{qb^2}{\gamma}(\rho_1 - \rho_2) = \frac{2b^2}{a^2}$$

where a is the capillary constant of the liquid in question. Bashforth and Adams compile x' and z' to at least four significant figures as a function of the quantities β and ϕ in their tables for the range $0.125 < \beta < 100$ and $0 < \phi < 180^\circ$, respectively.

In 1857⁶ and later,⁷ the surface of a liquid was suggested to resemble most nearly an elliptical shape in which the tube radius and the meniscus height correspond to the major and minor semiaxes, respectively.

The coordinates (x' , z') were taken from the tables of Bashforth and Adams in 15° increments of ϕ from 0 to 90° and compared with the coordinates of an ellipse (x' , y') calculated by setting the major and minor axes, respectively, equal to the values of x' and z' for $\phi = 90^\circ$. The results of these calculations are displayed in Figure 2 in which the per cent deviation of y' with respect to z' is shown as a function of ϕ for β values of 100, 22, 7, 3.5, 0.5, and 0.125. For values of β less than 7, the coordinates of the ellipse are within 4% of those values tabulated in the tables of Bashforth and Adams for all but one value of ϕ in the range $0 < \phi < 90^\circ$.

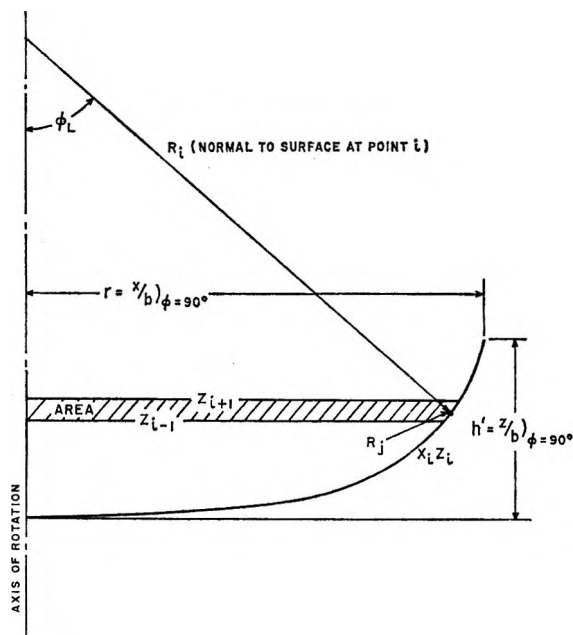


Figure 1. Schematic description of a typical liquid meniscus in a circular tube.

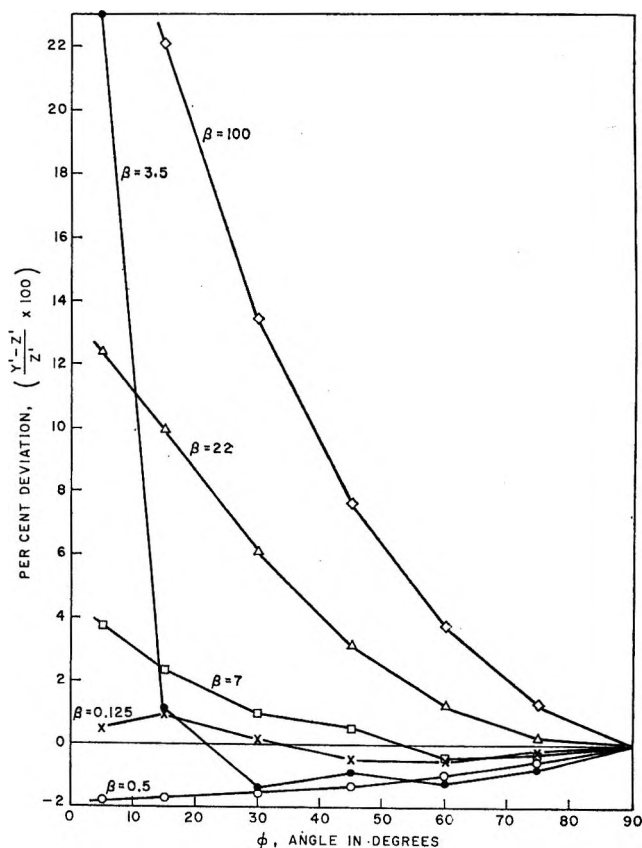


Figure 2. Per cent deviation between the coordinates of a liquid surface defined by Bashforth and Adams' tables and oblate spheroid.

Table I: Summary of Surface Area Resolution to Liquid Meniscus in Circular Tubes

r/a	Normalized tube radius, $r' = z/b, \phi = 90^\circ$	β	Normalized meniscus height $h' = z/b, \phi = 90^\circ$	True area, A_s	Elliptical, ^a A_s'	Deviation, ^b %	A_s'/A_t
0.05	0.9992 ^c	...	0.9987 ^d	6.270 ^e	6.269	-0.02	1.999
0.10	0.9968 ^c	...	0.9948 ^d	6.231 ^e	6.236	+0.01	1.998
0.15	0.9925 ^c	...	0.9880 ^d	6.161 ^e	6.172	+0.02	1.994
0.24	0.9812 ^c	...	0.9702 ^d	5.981 ^e	6.003	+0.04	1.985
0.245	0.9804 ^f	0.125	0.9547 ^f	5.926 ^g	5.790	-2.36	1.917
0.465	0.9328 ^f	0.50	0.8549 ^f	5.149 ^g	5.165	+0.32	1.890
0.995	0.7514 ^f	3.5	0.5615 ^f	2.958 ^g	2.968	+0.32	1.673
1.231	0.6582 ^f	7.0	0.4458 ^f	2.160 ^g	2.160	-0.03	1.587
1.653	0.4986 ^f	22.0	0.2847 ^f	1.152 ^g	1.141	-1.01	1.461
2.24	0.3165 ^f	100.0	0.1449 ^f	0.4313 ^g	0.4200	-2.72	1.334
2.25	0.314 ^e	...	0.150 ^h	0.310 ⁱ	0.420	+26.2	1.355
2.5	0.252 ^e	...	0.108 ^h	0.200 ⁱ	0.260	+23.3	1.303
3.0	0.149 ^e	...	0.0524 ^h	0.0697 ⁱ	0.0855	+18.4	1.225
4.0	0.056 ^e	...	0.0145 ^h	0.0099 ⁱ	0.0113	+12.3	1.140
6.0	0.006 ^e	...	0.0010 ^h	0.00011 ⁱ	0.00012	+6.8	1.073
6.9	0.002 ^e	...	0.0003 ^h	0.000013 ⁱ	0.000013	+5.3	1.056

^a Using eq. 7. ^b Using $D = (A_s' - A_s)100/A_s'$. ^c Directly from Sugden's tables (ref. 4, reproduced in ref. 5). ^d Using eq. 5a. ^e Using eq. 1b. ^f Directly from Bashforth and Adams' tables (ref. 1). ^g Using eq. 6b. ^h Using eq. 5b. ⁱ Using eq. 2b.

Thus, it is concluded that, for the majority of the tables of Bashforth and Adams, the dimensions of a liquid meniscus bear an approximate identity to the surface of revolution of an ellipse about its minor axis, namely, an oblate spheroid.

Surface Area

The surface of a liquid meniscus in a circular tube is reasonably approximated by the shape of an oblate spheroid. In general, larger deviations of Figure 2 are indicated only at small angles and at large values of β where the contribution to the area problem is the least. Hence, the surface area can be described with two specific dimensions that represent the major and minor semiaxes, respectively: r , which is the tube radius, and h , which is the vertical distance between the level of the plane as formed by the liquid in contact with the tube wall and the center of the meniscus. The only cases considered are those in which the contact angle with the tube wall is zero. Experimental measurements of h are not simple to obtain accurately because of the optical problems in looking through circular walls. However, this dimension can be defined quite accurately in a theoretical fashion. After these dimensions are fixed, the surface area of the liquid meniscus can be approximated by the standard formula for an oblate spheroid. Table I compiles pertinent quantities for this problem over the range of the tube radius:capillary constant ratio from 0.05 to 6.9.

When h and r are normalized to the central radius of

curvature for a liquid meniscus (*i.e.*, $h' = h/b$ and $r' = r/b$), they are related monotonically to the tube radius-capillary constant ratio, r/a . The tables of Bashforth and Adams compile values of h' and r' (respectively equivalent to z' and x' at $\phi = 90^\circ$) for the range $0.25 < r/a < 2.24$. Outside this range, the supplemental tables of Sugden⁴ are used to define values of r' ; values of h' are determined from the small- and large-tube Rayleigh formulas³ for z/r , respectively, given in eq. 5a and 5b.

$$h' = (r/b)(z/r) \quad (\text{for } r/a < 0.5)$$

$$= (r') \left[1 - \frac{2r'^2}{3a^2} \left(1 - \frac{r'^2}{a^2} \right) \log 2 \right] \quad (5a)$$

$$h' = (r/b)(z/r) \quad (\text{for } r/a > 2.25)$$

$$= (r') \left[2 \left(\frac{a^2}{2r'^2} \right)^{1/2} \sin(\phi/2) + \frac{a^2}{3r'^2} \left(\frac{1 - \cos(\phi/2)}{\sin(\phi/2)} \right) \right] \quad (5b)$$

Values of h' as related to r/a are compiled in Table I, and these relations are presented in graphical form in Figure 3. Unrefined measurements of h were made for water and carbon tetrachloride in five tubes from 1- to 10-mm. radius. The dimensionalized values have reproduced this curve within 1% for values of r/a greater than approximately 1.5. Experimental difficulties increase greatly below this level. The theoretical (plot-

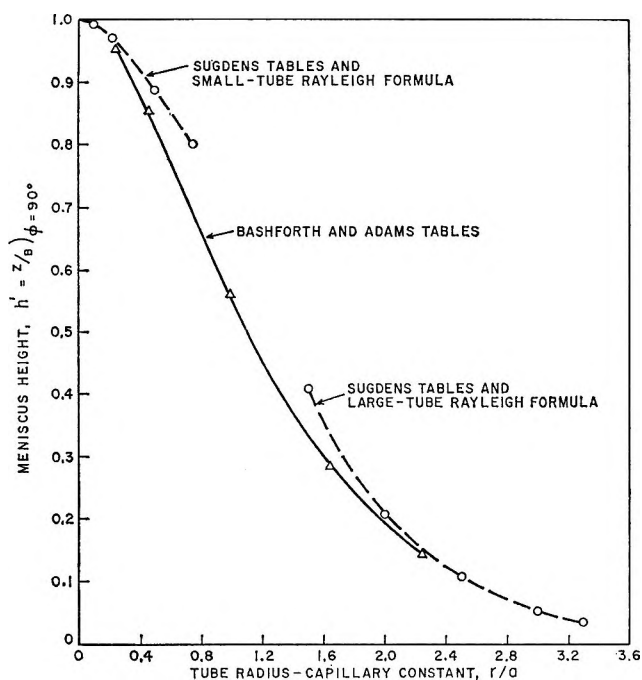


Figure 3. Theoretical relation of the meniscus height.

ted and tabulated) values of h' practically fix this dimension better than it can generally be measured.

True and elliptical surface areas are compiled in Table I. The true surface area, A_s , of a liquid in a circular tube can be approached as closely as desired by summing the areas of sufficiently small spherical segments as represented by eq. 6a.¹¹ Bashforth and Adams com-

$$A_s = 2\pi \sum_{i=0}^{i=\infty} R_i X_i \quad (6a)$$

pile values of x'_i , z'_i , and ϕ_i in 5° increments for $\phi = 0$ to 180° . These tables represent a classic and probably the most accurate tabulation of a meniscus shape over the range $0.25 < r/a < 2.24$. Thus, a best approximation to the true surface area was calculated in 10° increments of ϕ by eq. 6b, which assumes a zero contact angle, and by using their tables directly.

$$A_s \cong 2\pi \sum_{i=10^\circ}^{i=90^\circ} \frac{x'_i}{\sin \phi_i} (z'_{i+5^\circ} - z'_{i-5^\circ}) \quad (6b)$$

(for $0.25 < r/a < 2.24$)

Two arbitrary estimations to the true surface area were made outside the range of eq. 6b, based on eq. 1a and 2a. Since the surface is practically spherical for $r/a < 0.25$, the dimensionalized approximation shown in eq. 1b should be nearly valid. For values of $r/a >$

$$A_b \cong 2\pi(r')(h') \quad (\text{for } r/a \leq 0.24) \quad (1b)$$

2.24, the surfaces of the liquid becomes more flat and

approaches the tube area. Hence, the dimensionalized representation of the tube area shown in eq. 2b should approach exactness.

$$A_t \cong \pi(r')^2 \quad (\text{for } r/a \geq 2.25) \quad (2b)$$

In order to calculate the elliptical approximation to the surface area for the whole tabulation of r/a , the standard formula for an oblate spheroid was applied in the form

$$A_s' = \pi(r')^2 + \frac{\pi(h')^2}{2e} \ln \frac{1+e}{1-e} \quad (7)$$

where r' and h' are taken as the major and minor semi-axes, respectively, and the eccentricity is

$$e = [1 - (h'/r')^2]^{1/2}$$

For the calculations within the range of the tables of Bashforth and Adams, the average of all deviations between the true surface area as calculated by eq. 6b and the elliptical approximation of eq. 7 is within 1%, as indicated in Table I. As mentioned previously, values of the surface area as calculated from eq. 1b and 2b are taken as a basis for comparison to the elliptical approximation in the ranges $r/a \leq 0.24$ and $r/a \geq 2.25$, respectively. The per cent deviations shown in Table I indicate good agreement in the range $r/a \leq 0.24$. The

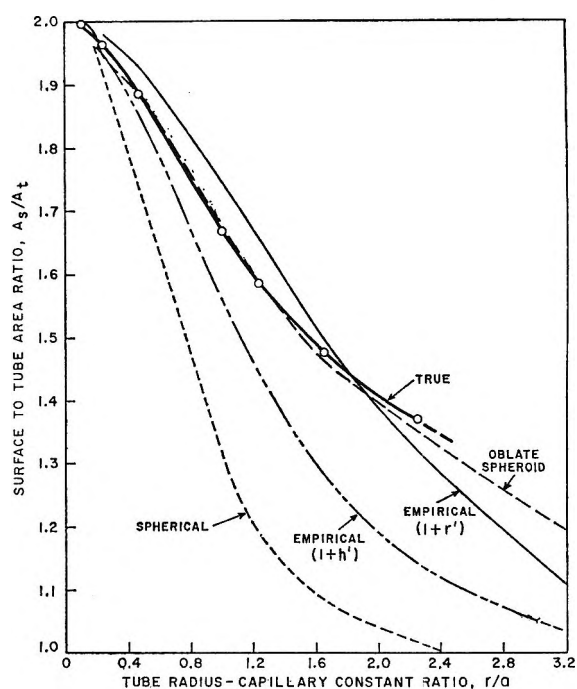


Figure 4. Surface to tube area ratios for four approximations.

(11) E. Oberg and F. Jones, "Machinery Handbook," 16th Ed., Industrial Press, New York, N. Y., 1959.

discrepancy diminishes for the range $r/a \geq 2.25$, particularly for values of r/a greater than about 6; this suggests that the surface is practically flat for $r/a > 6$.

A more practical way to present this information is by forming the ratio of the surface area approximation to the cross-sectional area of the circular tube. The last column of Table I compiles this ratio for the elliptical approximation. The true surface and elliptical area ratios are graphically displayed in Figure 4. The following three additional approximations are included in dimensionalized form to gain a better understanding of the character of the results.

As indicated by eq. 1a and 2a, these ratios must vary within the limits of 2 to 1 as the tube size varies from sufficiently small to large. One usual approximation is to fit geometrically a spherical cap into the plane of the liquid in contact with the circular tube wall and the center of the meniscus. The following equation is then obtained.

$$A_s'' = A_t \left[1 + \left(\frac{h'}{r'} \right)^2 \right] \quad (8)$$

A simple, but empirical, approximation that satisfies the limiting conditions is

$$A_s''' = A_t(1 + h') \quad (9)$$

Another empirical approximation that has utility in its simplicity is

$$A_s'''' = A_t(1 + r') \quad (10)$$

Approximations of the surface:tube area ratio are calculated from eq. 8, 9, and 10 by using the values for

h' and r' indicated in Table I; smoothed curves are plotted in Figure 4.

Within the range of the tables of Bashforth and Adams, the true surface:tube area ratio is assumed to be that value determined from the approximation of eq. 6b. The elliptical approximation nearly superimposes on this function as shown in Figure 4. The usual spherical approximation is low by as much as 50%. Both of the empirical approximations are an improvement over the spherical approximation.

Conclusion

The classic values of the coordinates of the meniscus shape as compiled by Bashforth and Adams are found to approximate an elliptical shape within about 4% over the range of most of their tables. By taking the surface of a liquid in a circular tube as an oblate spheroid, the area appears to be within an average of 1% of the best available estimation of the surface area at the present time. The tables of Bashforth and Adams were used to fit a liquid meniscus to as many as 18 spherical segments with less than 0.5% deviation from the values of the surface area that were obtained in 9 spherical segments. The usual spherical approximation is in error by as much as 50%.

Acknowledgments. The author wishes to acknowledge stimulating discussions with Dr. J. Masi of the Air Force Office of Scientific Research, Dr. R. J. Tykodi, Professor of the Illinois Institute of Technology, and staff associates at the IIT Research Institute. This research was supported by Contract No. AF 49(638)-1121 monitored by the office of Aerospace Research.

The Radiation-Induced Oxidation of Organic Compounds

by G. Dobson and G. Hughes¹

Donnan Laboratories, The University, Liverpool, England (Received June 22, 1964)

The radiation-induced oxidation of selected organic compounds has been studied. Cyclohexane, in particular, has been investigated in detail. Product yields have been measured, and the effect of scavengers on these has been studied. For all compounds studied, it is concluded that a significant fraction of the carbonyl yield is formed in a process which is not interfered with by conventional radical scavengers. This is attributed to a molecular oxidation process.

Peroxides, alcohols, and carbonyl compounds are known to be among the products of the radiation-induced oxidation of hydrocarbons.² Although yields based on the total amounts of functional group have been determined, the identity of individual products has not always been established but has been inferred from proposed reaction mechanisms. The radiation-induced oxidation of cyclohexane in particular has received considerable attention although there is as yet no general agreement on the magnitude of the yields.³⁻⁵

The present work was undertaken in an attempt to identify precisely the products in the radiation-induced oxidation of liquid cyclohexane. Sensitive analytical techniques have been used to measure product concentrations at the lowest possible doses. In this way, it was hoped to minimize secondary reactions of products. The effect of additives has been studied in order to investigate the reaction mechanism.

Evidence for a molecular reaction of the type



has been found.⁶ It seemed possible that analogous reactions might take place in other systems and it was therefore decided to investigate the radiation-induced oxidation of several selected organic compounds. The aim of this second part of the work has been primarily to establish or refute the existence of such a molecular process and not to study the systems extensively. Since the product in the case of cyclohexane is cyclohexanone, attention has been directed to those compounds which yield carbonyls on oxidation and the effect of scavengers on the carbonyl yield has been investigated. The criterion adopted for establishing

the existence of a molecular oxidation process is that in the presence of high concentrations of scavenger, there should be a limiting nonzero yield of carbonyl.

Experimental

Cyclohexane (special for spectroscopy as supplied by B.D.H. and Hopkin and Williams) was used without further purification. Another sample was purified by double recrystallization but identical product yields were obtained in all three cases. In the chromatographic work, the pure *n*-hexane and *n*-heptane used were a gift of Shell Research. Vapor phase chromatograms showed no impurity peaks in any of these solvents. *n*-Hexane (special for spectroscopy) and A.R. grade toluene were used without further purification. A.R. grade methanol was further purified by distillation from 2,4-dinitrophenylhydrazine⁷ in the presence of sulfuric acid. B.D.H. laboratory grade chlorocyclohexane was purified by shaking three times with its own volume of concentrated aqueous sodium bisulfite. It was finally distilled in an inert atmosphere. Oxygen was dried by bubbling through concentrated sulfuric acid followed by passage over phosphorus

(1) To whom communications should be sent.

(2) G. Hughes, "Oxidation and Combustion Reviews," C. F. H. Tipper, Ed., Elsevier Publishing Co., Amsterdam, 1965, p. 47.

(3) N. A. Bakh, Symposium on Radiation Chemistry of the Academy of Sciences of the U.S.S.R., Moscow, 1955, English Translation, pp. 145, 156.

(4) H. A. Dewhurst, *J. Phys. Chem.*, **63**, 813 (1959).

(5) R. L. McCarthy and A. MacLachlan, *Trans. Faraday Soc.*, **57**, 1107 (1961).

(6) G. Dobson and G. Hughes, *Proc. Chem. Soc.*, 109 (1963).

(7) J. H. Baxendale and F. W. Mellows, *J. Am. Chem. Soc.*, **83**, 4720 (1961).

pentoxide. It was saturated with the vapor of the solution to be irradiated and then was slowly bubbled through the sample for 30 min. Samples were oxygenated at intervals during the radiation so that the oxygen concentration remained essentially constant. Solutes used were either A.R. grade or, where possible, purified by recrystallization. Where necessary they were freed from peroxidic impurity by passage down a column of alumina.

The irradiation source has been described earlier.⁸ Samples of 25 ml. of solution were irradiated at room temperature with γ -radiation from a 100-c. ¹³⁷Cs source at a dose rate of 0.9×10^{16} e.v. ml.⁻¹ min.⁻¹ as determined by the Fricke dosimeter assuming $G(\text{Fe}^{3+}) = 15.6$, with appropriate correction for electron density of the solution. The effect of dose rate was determined by irradiating 10-ml. samples at a dose rate of 2.3×10^{16} e.v. ml.⁻¹ min.⁻¹.

Qualitative Analysis. Dialkyl peroxides, alkyl hydroperoxides, and hydrogen peroxide were identified by paper chromatography.^{9,10} Control peroxides for identification were prepared by the method of Williams and Mosher.¹¹ Carbonyls were chromatographed in the form of their 2,4-dinitrophenylhydrazones¹² and alcohols were characterized by vapor phase chromatography using a polyethylene glycol on Teflon column at 100°.

Quantitative Analysis. Cyclohexyl hydroperoxide was separated from hydrogen peroxide and dicyclohexyl peroxide in the irradiated solution (which had previously been concentrated by vacuum distillation at -45°) by chromatography on a column of ethylene glycol on cellulose using petroleum ether (b.p. 80-100°) as the moving phase. It was then estimated iodometrically.¹³ Hydrogen peroxide was determined from its reaction with titanium sulfate.¹⁴ The irradiated solution was shaken with an equal volume of titanium sulfate solution for 5 min. and the optical density of the aqueous layer was measured. Further shaking of the organic phase with fresh titanium sulfate solution produced no additional color. It was established that cyclohexyl hydroperoxide did not interfere. The concentration of dicyclohexyl peroxide was then found from the total peroxidic content as determined by reaction with hydrogen iodide,¹⁵ since paper chromatography showed that no other peroxides were present.

Carbonyl compounds, except where otherwise stated, were estimated as their 2,4-dinitrophenylhydrazones.¹⁶ Formaldehyde was determined from its reaction with chromotropic acid,¹⁷ and formic acid was determined as formaldehyde by reduction with magnesium and hydrochloric acid.¹⁸ Glyoxylic acid was estimated as the intensely colored 1,5-diphenylformazan-

carboxylic acid.¹⁹ Alcohols were determined by reaction with benzoyl chloride and propylenediamine.²⁰

The validity of the analytical techniques used was established using control solutions. Unless stated to the contrary, product yields in this work are only quoted where it has been clearly established that the formation of the product is proportional to dose.

Results and Discussion

A. Cyclohexane. 1. Irradiation of Cyclohexane-Oxygen Solutions. The products of the radiation-induced oxidation of cyclohexane were identified as cyclohexyl hydroperoxide, dicyclohexyl peroxide, hydrogen peroxide, cyclohexanone, and cyclohexanol. No other peroxides, carbonyl compounds, or alcohols were produced. This product distribution is consistent with the formation of cyclohexyl radicals and hydrogen atoms initially by the radiation in the solution.

There was no evidence for C-C bond rupture. This may be contrasted with the results obtained in the radiation-induced oxidation of *n*-hexane and *n*-heptane where small yields of alkyl hydroperoxides containing a lower number of carbon atoms than the parent hydrocarbon were obtained in addition to comparatively larger yields of hexyl and heptyl hydroperoxide, respectively. In these compounds then, in addition to C-H bond rupture there must be some scission of C-C bonds. It is interesting that in the mass spectra of both cyclohexane and *n*-hexane, ions representing considerable ⁹C-C bond fission are more abundant than the parent positive ion.²¹

From Figure 1 it may be seen that the concentrations of products are proportional to dose and independent of dose rate and of oxygen concentration in the range aerated to oxygenated solution. The product yields

(8) G. Dobson and G. Hughes, *Trans. Faraday Soc.*, **57**, 1117 (1961).

(9) J. Carlidge and C. F. H. Tipper, *Anal. Chim. Acta*, **22**, 103 (1960).

(10) G. Dobson and G. Hughes, *J. Chromatog.*, **16**, 416 (1964).

(11) H. R. Williams and H. S. Mosher, *J. Am. Chem. Soc.*, **76**, 2984, 2987 (1954).

(12) D. F. Meigh, *Nature*, **170**, 579 (1952).

(13) C. D. Wagner, R. H. Smith, and E. D. Peters, *Anal. Chem.*, **19**, 976 (1947).

(14) G. M. Eisenberg, *Ind. Eng. Chem., Anal. Ed.*, **15**, 327 (1943).

(15) F. H. Dickey, J. H. Raley, F. F. Rust, R. S. Treseder, and W. E. Vaughan, *Ind. Eng. Chem.*, **41**, 1673 (1949).

(16) G. R. Lappin and L. C. Clark, *Anal. Chem.*, **23**, 541 (1951).

(17) C. E. Bricker and H. R. Johnson, *Ind. Eng. Chem., Anal. Ed.*, **17**, 400 (1945).

(18) W. M. Grant, *Anal. Chem.*, **20**, 267 (1948).

(19) D. N. Kramer, N. Klein, and R. A. Baselice, *ibid.*, **31**, 250 (1959).

(20) D. P. Johnson and F. E. Critchfield, *ibid.*, **32**, 865 (1960).

(21) R. H. Roberts and S. E. J. Johnson, *ibid.*, **20**, 690 (1948).

obtained in this work are compared with those of Bakh,³ Dewhurst,⁴ and McCarthy and MacLachlan⁵ in Table I.

Table I: Product Yields for the Radiation-Induced Oxidation of Cyclohexane

Product	G(product)			
	Bakh	Dewhurst	McCarthy and MacLachlan	This work
Hydrogen peroxide	0	0.10
Cyclohexyl hydroperoxide	1.0	0	1.1	1.05
Dicyclohexyl peroxide	0.2	0.31
Cyclohexanone	0.6	3.5	2.28	2.02
Cyclohexanol	...	3.7	2.40	1.55
Acid	0.2	...	0	...

There is as yet considerable disagreement among these sets of data. The results obtained in this work have been obtained at significantly lower doses.

2. *Effect of Solute on Product Yields.* The results obtained from oxygenated solutions ($[O_2] \approx 10^{-2} M$) are shown in Table II.

Table II: Effect of Scavenger on the Product Yields in the Radiation-Induced Oxidation of Cyclohexane

Scavenger	[Scavenger] $\times 10, M$	G(C ₆ H ₁₀ O)	G(total hydroperoxide)
Iodine	0	2.02	1.15
	0.01	1.13	1.04
	0.02	0.85	1.08
	0.06	0.70	0.52
	0.12	0.46	0.21
	0.22	0.44	0
0.40	0.46	0	
Diphenylmethane	0.55	1.34	1.95
	5.15	0.48	3.62
	9.52	0.48	5.10
Triphenylmethane	0.17	0.96	
	0.58	0.47	3.07
	2.78	0.46	

Since iodine interferes with the estimation of hydrogen peroxide, it was only possible to measure the sum of the hydrogen peroxide and cyclohexyl hydroperoxide yields. It is apparent that though the yields of these products are decreased to zero at high iodine concentrations, there remains a limiting yield of cyclohexanone independent of iodine concentration. A similar limiting yield was observed in aerated solution with $G(C_6H_{10}O) = 0.38$.

Chromatographic analysis showed that the enhanced yield of hydroperoxide obtained using di- and triphenylmethane was due to the production of the hydroperoxide of the scavenger in addition to cyclohexyl hydroperoxide. It was not possible to measure accurately the yield of cyclohexyl hydroperoxide separately. The production of hydrogen peroxide was enhanced by triphenylmethane but was no longer proportional to dose. It will be seen that the yield of cyclohexane is decreased to the same limiting value as that observed using I₂ as scavenger. In all cases, cyclohexanone was the only carbonyl product.

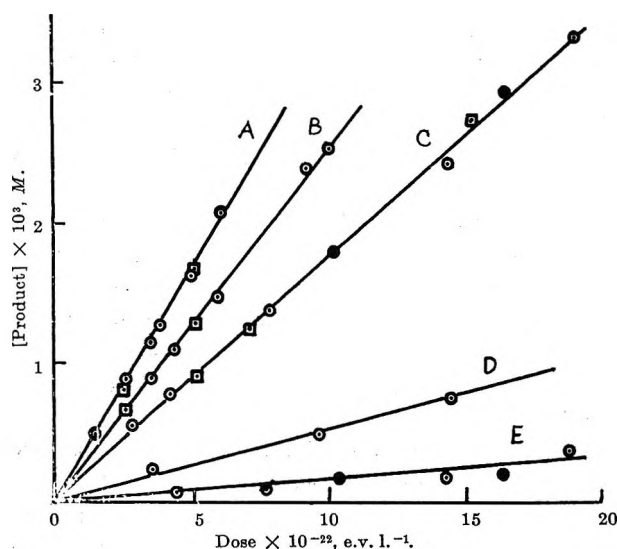
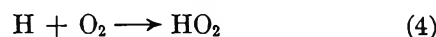
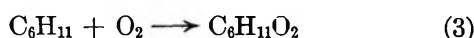
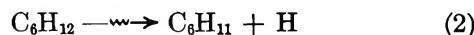
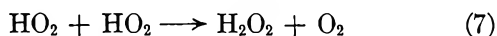
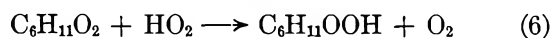
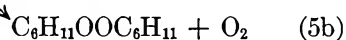
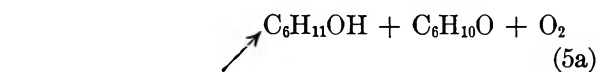


Figure 1. Product yields in the radiation-induced oxidation of cyclohexane: \circ , oxygen saturated, dose rate 0.9×10^{19} e.v. $l^{-1} \text{ min}^{-1}$; \bullet , air saturated, dose rate 0.9×10^{19} e.v. $l^{-1} \text{ min}^{-1}$; \square , oxygen saturated, dose rate 2.3×10^{19} e.v. $l^{-1} \text{ min}^{-1}$. A, cyclohexanone; B, cyclohexanol; C, cyclohexyl hydroperoxide; D, dicyclohexyl peroxide; E, hydrogen peroxide.

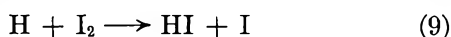
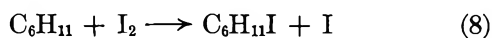
3. *Evidence for a Molecular Oxidation Process.* Since the oxidation yields are independent of oxygen concentration, all radicals which lead to oxidation products must be captured by oxygen even in aerated solution ($[O_2] \approx 2 \times 10^{-3} M$). Since product yields are independent of dose rate, no chain reactions are taking place.

The simplest reaction scheme that may be proposed is as follows.





The decrease in the yields of cyclohexyl hydroperoxide and cyclohexanol by iodine may be attributed to the reactions

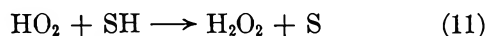


competing with reactions 3 and 4, respectively. That these yields vanish at high iodine concentration indicates that all radicals are effectively scavenged by iodine. The limiting yield of cyclohexanone must therefore be produced from some species other than cyclohexyl radicals.

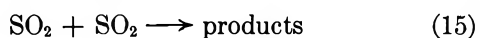
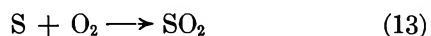
Scavengers containing labile hydrogen atoms may react like iodine in scavenging alkyl radicals



or by scavenging peroxy radicals



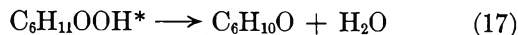
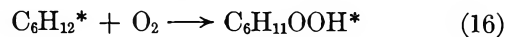
The S radical would then react according to the following chain sequence.



The enhanced hydroperoxide yields and decreased yields of cyclohexanone reported for tri- and diphenylmethane are consistent with such a mechanism if it is assumed that the termination reaction (15) does not give rise to any ketone since paper chromatography established that cyclohexanone is the only carbonyl product.

It is significant that at high concentrations of di- and triphenylmethane a limiting yield of cyclohexanone is observed, the value of which is the same as that observed in the presence of iodine, *i.e.*, $G(\text{C}_6\text{H}_{10}\text{O}) = 0.46$. Moreover this yield is in good agreement with the difference in cyclohexanone and cyclohexanol yields observed for oxygenated cyclohexane. Some process involving non-scavengeable intermediates must be responsible for this.⁶ This process may involve reac-

tion of an excited cyclohexane molecule with O_2 to give either cyclohexanone directly (eq. 1) or an excited hydroperoxide molecule which then decomposes.



However possible ionic precursors cannot be ruled out.

It might be anticipated that reaction 1 could occur in some photochemical oxidation processes since the reaction involving a thermal cyclohexane molecule should be exothermic by about 80 kcal. However if no photochemical evidence for the occurrence of reaction 1 is forthcoming, this would be a strong argument in favor of ionic reactions leading to the production of "molecular" cyclohexanone.

Indirect confirmation of the molecular oxidation process is obtained from a kinetic analysis of the dependence of $G(\text{C}_6\text{H}_{10}\text{O})$ on iodine concentration. If it is assumed that cyclohexanone is produced *via* both reactions 5a and 1, and that iodine interferes with the production of ketone *via* reaction 8, then it may be shown that, since the yields of dicyclohexyl peroxide and hydrogen peroxide are small and can be neglected, the dependence of $G(\text{C}_6\text{H}_{10}\text{O})$ on iodine concentration is given by eq. 18. A plot of the results of Table II

$$\frac{1}{G(\text{C}_6\text{H}_{11}\text{OOH}) + 2[G(\text{C}_6\text{H}_{10}\text{O}) - 0.46]} = \frac{1}{G(\text{C}_6\text{H}_{11})} \left(1 + \frac{k_8[\text{I}_2]}{k_3[\text{O}_2]} \right) \quad (18)$$

according to eq. 18 is shown in Figure 2. A much less satisfactory kinetic plot is obtained if all the ketone is assumed to be produced by radical recombination. From Figure 2 it may be calculated that $k_8/k_3 \approx 5$. This is in fair agreement with a value of ≈ 2 calculated from the dependence of $G(-\text{I}_2)$ on oxygen concentration in irradiated cyclohexane- I_2 solutions.²²

B. n-Hexane. The results obtained are entirely analogous to those for cyclohexane and product yields are shown in Table III.

Table III: Product Yields in the Radiation-Induced Oxidation of *n*-Hexane

Product	$G(\text{product})$
Hydrogen peroxide	0.44
Alkyl hydroperoxide	1.22
Dialkyl peroxide	~ 1
Alcohol	1.21
Ketone	1.55

(22) R. W. Fessenden and R. H. Schuler, *J. Am. Chem. Soc.*, **79**, 273 (1957).

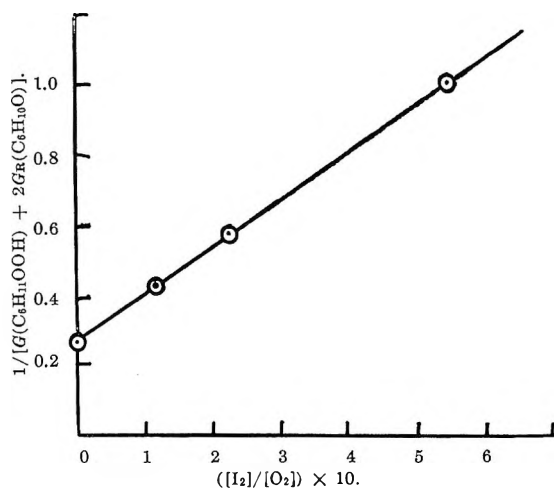
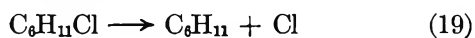


Figure 2. Competition between iodine and oxygen for cyclohexyl radicals.

Although the major hydroperoxide is hexyl hydroperoxide, small amounts of C₁-C₅ hydroperoxides were also shown to be present. This conclusion is in agreement with the observation that in the radiolysis of *n*-hexane-I₂ solutions, although C₆ iodides are present in the greatest yield, there is a significant yield of C₁-C₅ iodides.²³ It has been reported²⁴ that in the radiation-induced oxidation of *n*-heptane the main carbonyl product is methyl butyl ketone indicating that a splitting off of a methyl group is the preferred process. This is somewhat surprising in view of the results reported here for *n*-hexane. Moreover, preliminary results obtained by us show that the major hydroperoxide in *n*-heptane is heptyl hydroperoxide.

The ketone yield is decreased to a limiting value of $G = 0.36$ at [triphenylmethane] > $6 \times 10^{-2} M$. This value is in good agreement with the difference in ketone and alcohol yields for oxygenated hexane.

C. Chlorocyclohexane. The main peroxidic product was identified as dicyclohexyl peroxide. Only trace amounts of hydrogen peroxide and hydroperoxide could be detected. These results indicate that there are relatively few hydrogen atoms captured by oxygen in the system. Either the major radiation-induced decomposition of chlorocyclohexane is



or, if they are produced, hydrogen atoms react rapidly via the reaction



The cyclohexyl radical produced then reacts as in cyclohexane.

The effect of triphenylmethane on the carbonyl yield is shown in Table IV. The carbonyl yield in

Table IV: Effect of Triphenylmethane on $G(\text{carbonyl})$ in the Radiation-Induced Oxidation of Chlorocyclohexane

[TPM] $\times 10, M$	$G(\text{carbonyl})$
0	9.04
4.1	2.53
8.2	1.15
12.3	1.24

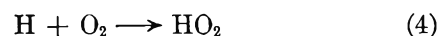
pure chlorocyclohexane is considerably greater than that in cyclohexane. This is consistent with the higher radical yield observed in chlorocyclohexane.²⁵ $G(\text{carbonyl})$ is decreased to a mean limiting value of 1.20 at high scavenger concentration. Although it was not possible to measure accurately the alcohol yields, there appeared to be no alcohol produced at the high concentrations of triphenylmethane.

D. Toluene. Products and product yields are shown in Table V. The yield of cresol was differentiated from that of benzyl alcohol by the fact that cresol could be extracted by 25% aqueous KOH. The particular isomer of cresol produced was not identified.

Table V: Product Yields in the Radiation-Induced Oxidation of Toluene

Product	$G(\text{product})$
Hydrogen peroxide	0.23
Benzyl hydroperoxide	0.90
Benzaldehyde	0.74
Benzyl alcohol	0.45
Cresol	0.16

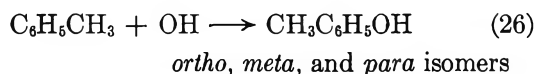
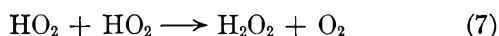
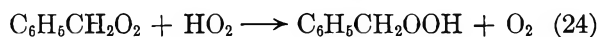
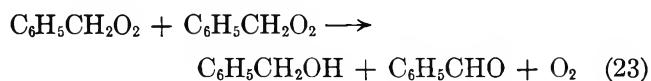
At $[I_2] > 0.04 M$ the yield of benzaldehyde was decreased to a limiting yield, $G = 0.15$, and the yields of the other products to zero. Little work has been done on the radiation-induced oxidation of benzene but the following tentative mechanism may be proposed for those products formed by radical processes.



(23) T. J. Hardwick, *J. Phys. Chem.*, **64**, 1623 (1960).

(24) V. V. Saraeva, N. A. Bakh, L. V. Rybin, and V. A. Larin, Proceedings of the 1st All-Union Conference on Radiation Chemistry, Moscow, 1957, Consultants Bureau Translation, p. 217.

(25) A. J. Swallow, "Radiation Chemistry of Organic Compounds," Pergamon Press, 1960, Table 1.5.



Nonradical production of benzaldehyde would be *via* the reaction



On the above mechanism, it can be shown that the yield of benzaldehyde produced by radical processes is given by

$$G_{\text{R}}(\text{C}_6\text{H}_5\text{CHO}) = G(\text{cresol}) + G(\text{C}_6\text{H}_5\text{CH}_2\text{OH}) = 0.61 \quad (29)$$

Since the total benzaldehyde yield in oxygenated toluene is 0.74, it follows that $G(\text{C}_6\text{H}_5\text{CHO})$ produced by nonradical processes must be 0.13. This is in good agreement with the limiting value observed at high iodine concentrations.

E. Methanol. Formic acid, formaldehyde, and hydrogen peroxide were identified among the products of the radiation-induced oxidation of methanol. The yields of these products were 0.91, 3.87, and 2.96, respectively. These results are in good agreement with some obtained by Hayon and Weiss,²⁶ who suggested the production of formic acid but did not measure its yield.

The effect of iodine on the product yields is shown in Table VI.

Table VI: Effect of I₂ on Product Yields

[I ₂] × 10 ² , M	G(CH ₂ O)	G(HCOOH)	G(H ₂ O ₂)
0	3.87	0.91	2.96
4.23	3.28	0.38	0
8.46	3.09	0.38	0

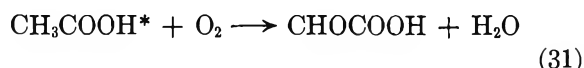
That the hydrogen peroxide yield is decreased to zero indicates that all hydrogen atoms have been captured by the iodine. However there remains a limiting yield of formic acid which must arise from a nonradical process, *viz.*



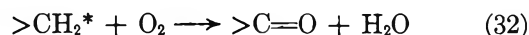
F. Acetic Acid. The yield of glyoxylic acid produced in the radiation-induced oxidation of acetic acid was measured and compared with results in the presence of iodine.

The rate of production of glyoxylic acid falls off rapidly with dose in pure acetic acid and it was only possible to estimate the initial yield. However there appeared to be no effect of iodine on this yield. Moreover, in the presence of iodine, the production of glyoxylic acid was proportional to dose with $G(\text{glyoxylic acid}) = 0.65$. At the same concentration of iodine, the yields of formaldehyde and hydrogen peroxide were reduced to zero. A similar falloff in yield of glyoxylic acid was observed in the radiolysis of aqueous solutions of glycine.²⁷ Control experiments by us showed that whereas glyoxylic acid is stable in acetic acid at room temperature over a period of several days, it is decomposed by $5 \times 10^{-4} M \text{H}_2\text{O}_2$. Since the hydrogen peroxide yield in the presence of iodine is reduced to zero, the production of glyoxylic acid would then be proportional to dose.

It would appear that the entire glyoxylic acid yield is produced by a molecular process which may be represented as



General Conclusions. From the present work it appears that a molecular oxidation process that may be represented by the reaction



occurs in a wide range of compounds and should be considered in all discussions of radiation-induced oxidation.

Although radical yields of some of the compounds studied are not known precisely, it is interesting that in each case, the molecular oxidation process is approximately 6% of the total radical yield. This would suggest that in general there are two precursors of the radicals formed, one of which may engage in a molecular oxidation process.

Acknowledgment. Thanks are due to Dr. C. F. H. Tipper for helpful discussions. G. D. thanks the Department of Scientific and Industrial Research for a maintenance allowance.

(26) E. Hayon and J. J. Weiss, *J. Chem. Soc.*, 3970 (1961).

(27) C. R. Maxwell, D. C. Peterson, and N. E. Sharples, *Radiation Res.*, 1, 530 (1954).

Moving Boundary Sedimentation in the Preparative Ultracentrifuge in the Absence of a Plateau Region

by K. D. Gibson*

*Department of Chemical Pathology, St. Mary's Hospital Medical School, London W. 2, England
(Received July 1, 1964)*

By considering the equation of continuity and the formula defining the sedimentation coefficient it is shown that moving boundary sedimentation in the ultracentrifuge cannot lead to the maintenance of a plateau region unless s satisfies certain rather narrow conditions defining its dependence on position. Equations are derived which relate the concentration at any point to its coordinate when there is no plateau, *i.e.*, when s does not satisfy these conditions. These equations are applied to deduce the concentration in some simple density gradients. Two methods are presented for locating ideal boundaries from the distribution of material in a centrifuge tube; one of these generalizes existing methods to cases where there is no plateau, while the other is a new method which does not require the existence of a plateau.

Introduction

In a recent article Trautman and Breese¹ expounded a theory of moving boundary centrifugation in the ultracentrifuge, and elsewhere they demonstrated the value of their methods in the determination of sedimentation coefficients.² There is no doubt that this is potentially one of the most useful techniques for studying the sedimentation properties of biological materials. In setting up their theory Trautman and Breese made two assumptions. Firstly, they assumed that the effect of diffusion could be neglected. This does not impose a very serious limitation on their theory since in most moving boundary experiments the effect of diffusion is merely to blur somewhat the infinitely sharp "ideal" boundary which would be found under the influence of sedimentation alone, and they discussed several methods for deducing the position of this ideal boundary from the actual distribution of material. Secondly, they assumed that material always sediments in such a way as to form a plateau, *i.e.*, that material which is initially distributed uniformly through a given region of space will still be distributed uniformly at any subsequent instant, although at a different concentration and through another region of space. However, this assumption cannot be justified. In this paper it will be shown that a plateau

can exist only under rather limited circumstances and that in all other cases there would not be a plateau even if diffusion were totally absent. Expressions will be obtained which describe the distribution of sedimenting material in the general case, and it will also be found necessary to modify the methods for deducing the position of an ideal boundary.

Condition for a Plateau

The equation of continuity for a material whose concentration is c moving with velocity \mathbf{v} in a centrifugal field is³

$$\frac{dc}{dt} + c\nabla \cdot \mathbf{v} = 0 \quad (1)$$

The derivative in eq. 1 is the substantial derivative and is equal to $\partial c/\partial t + \mathbf{v} \cdot \nabla c$. Suppose that S_0 is a region in space at time zero in which the concentration has the uniform value c_0 , and let S_t be transformed by the motion into the region S_t at time t .

* Department of Chemistry, Cornell University, Ithaca, N. Y.

(1) R. Trautman and S. Breese, *J. Phys. Chem.*, **63**, 1592 (1959).

(2) R. Trautman, M. Savan, and S. Breese, *J. Am. Chem. Soc.*, **81**, 4040 (1959); R. Trautman, S. Breese, and H. L. Bachrach, *Arch. Biochem. Biophys.*, **87**, 1 (1960).

(3) G. J. Hooyman, H. Holtan, Jr., P. Mazur, and S. R. de Groot, *Physica*, **19**, 1095 (1953).

Then, clearly, the material will be distributed uniformly throughout S_t if and only if dc/dt has the same value at all points of the region at any instant between 0 and t . Equation 1 shows that this entails $\nabla \cdot \mathbf{v}$ being the same at each point of the region. Thus, the necessary and sufficient condition for the maintenance of a plateau in material sedimenting through a region of space is that $\nabla \cdot \mathbf{v}$ has the same value at every point of the region.

This condition imposes a limitation on the sedimentation coefficient, the form of which will now be examined. In the first place, the velocity can be expressed as the sum of the two terms⁴

$$\mathbf{v} = \mathbf{v}_s + \mathbf{v}_d \quad (2)$$

where \mathbf{v}_s is the velocity due to sedimentation alone and \mathbf{v}_d that due to diffusion alone. Now, as discussed in the Introduction, the effect of diffusion is to alter slightly the concentration of material in the vicinity of a boundary from the value it would take under the "ideal" condition of sedimentation without diffusion, and, as will be seen later, methods can be developed for calculating the position of the ideal boundary from the distribution of material observed experimentally under these circumstances. Hence, it is possible to ignore the velocity due to diffusion in applying the condition for a plateau and to consider only the velocity due to sedimentation. Thus, what is now under consideration is the condition for the existence of a plateau in material moving under the influence of a centrifugal field, ω , alone. This condition can be written

$$\nabla \cdot \mathbf{v}_s = \kappa \omega^2 \quad (3)$$

where κ is independent of position.

In applying eq. 3 two cases of practical importance must be distinguished. The first concerns the sector-shaped cell of the analytical ultracentrifuge in which the motion is directed radially in a plane, while the second concerns the cylindrical tube used in the preparative ultracentrifuge in which the motion can be regarded as one-dimensional. In the first case the velocity is related to the centrifugal field by the equation

$$\mathbf{v} = s\omega^2 \mathbf{r} \quad (4)$$

where \mathbf{r} is the radius vector measured from the axis of centrifugation, s is the sedimentation coefficient, and the subscript has been dropped from the symbol for the velocity due to sedimentation. Substituting into eq. 3

$$\nabla \cdot \mathbf{v} = (1/r) \frac{\partial}{\partial r}(rv_r) = 2s\omega^2 + \omega^2 r \frac{\partial s}{\partial r} = \kappa \omega^2 \quad (5)$$

The most general solution of this equation depending on the radial coordinate alone is

$$s = \kappa/2 + \lambda/r^2 \quad (6)$$

where λ is independent of r . Thus, there can only be a plateau in material moving in the analytical ultracentrifuge if its sedimentation coefficient satisfies eq. 6.

In the cylindrical tube of the preparative ultracentrifuge the velocity has a single component which will be taken to be directed along the positive x -axis. Equation 4 becomes

$$v = s\omega^2 x \quad (7)$$

and substitution into eq. 3 gives

$$\nabla \cdot \mathbf{v} = \frac{dv}{dx} = s\omega^2 + \omega^2 x \frac{ds}{dx} = \kappa \omega^2 \quad (8)$$

The general solution of this is

$$s = \kappa/2 + \mu/x \quad (9)$$

where μ is independent of x . Equation 9 is the condition which must be satisfied if a plateau is to exist in material sedimenting in the cylindrical tube. The quantities κ , λ , and μ in eq. 3, 6, and 9 must be independent only of position and may vary with time although in practice they will not do so in normal circumstances.

Calculation of the Concentration

It is a well-known consequence of the equation of continuity (1) that, if S_t is a region in space at time t which is filled with material at a concentration c_t (not necessarily uniform), then⁵

$$\frac{d}{dt} \int_{S_t} c_t dV = 0 \quad (10)$$

If the material was originally in the region S_0 at a concentration c_0 , eq. 10 shows that

$$\int_{S_t} c_t dV = \int_{S_0} c_0 dV \quad (11)$$

When the region is a plateau, eq. 11 becomes

$$c_t S_t = c_0 S_0 \quad (12)$$

Trautman and Breese obtained this equation by an inductive argument¹ and used it to deduce their elegant method for locating an ideal boundary when there is a plateau.

(4) R. J. Goldberg, *J. Phys. Chem.*, **57**, 194 (1953).

(5) See, for instance, R. Gans, "Vector Analysis," Blackie and Son, Ltd., London, 1947, p. 60.

Equation 12 also serves as the starting point for obtaining a formula to describe the concentration at any time when there is no plateau. It is again necessary to distinguish the sector-shaped cell from the cylindrical tube. Taking first the sector-shaped cell, since movement occurs only in a radial direction, eq. 4 can be written

$$\frac{dr}{dt} = s\omega^2 r \quad (13)$$

If s does not depend explicitly on the time (as is true in normal circumstances) and if ω is constant, this equation defines a one-parameter continuous group of transformations of the plane into itself.^{6,7} Now consider the infinitesimal element of the cell which lies between the coordinates r_0 and $r_0 + dr_0$ at zero time. The volume of this element can be written as $ar_0 dr_0$, and the amount of material initially in the element is $ac_0 r_0 dr_0$. Suppose that at time t the element lies at r_t and its volume is $ar_t dr_t$ so that the amount of material in it is $ac_t r_t dr_t$. By eq. 12 these two quantities are equal. Let

$$r_t = f(r_0, t) \quad (14)$$

be the solution of eq. 13 with initial value r_0 ; then

$$r_0 = f(r_t, -t) \quad (15)$$

because of the group property of the transformation defined by eq. 14. Hence the initial volume can be expressed in terms of the final coordinates by the formula

$$ar_0 dr_0 = af(r_t, -t) \frac{\partial f(r_t, -t)}{\partial r_t} dr_t \quad (16)$$

Application of eq. 12 and 16 to the infinitesimal element gives

$$c_t = \frac{c_0}{2r_t} \frac{\partial}{\partial r_t} [\{f(r_t, -t)\}^2] \quad (17)$$

In the case of the cylindrical cell the formula for c_t is simpler. Equation 7, which can be written as

$$\frac{dx}{dt} = s\omega^2 x \quad (18)$$

defines a one-parameter group of transformations of the line into itself if s and ω are independent of t .⁷ Considering now an infinitesimal element which is initially at x_0 and whose volume is bdx_0 , suppose this to be transformed to the element at x_t whose volume is bdx_t , where

$$x_t = g(x_0, t) \quad (19)$$

is the solution of eq. 18 with initial value x_0 . Then the volume elements are related by

$$bdx_0 = b \frac{\partial g(x_t, -t)}{\partial x_t} dx_t \quad (20)$$

and application of eq. 12 and 20 to the infinitesimal element gives

$$c_t = c_0 \frac{\partial g(x_t, -t)}{\partial x_t} \quad (21)$$

Equations 17 and 21 show how to calculate the concentration at any point whether there is a plateau or not.

Unfortunately, eq. 18 cannot usually be solved in such a way as to yield an explicit expression for $g(x_0, t)$ in eq. 19, and therefore eq. 21 cannot be applied directly. It has been shown by de Duve, *et al.*, that the concentration c_t can be expressed as⁸

$$\frac{c_t}{c_0} = \frac{s(x_0)\omega^2 x_0}{s(x_t)\omega^2 x_t} \quad (22)$$

which can be used for calculating c_t when both x_0 and x_t are known. However, in most experiments only one of these quantities is known, and indeed the purpose of the experiment is to determine the other. The value of the unknown quantity can, in principle, be calculated by graphical integration of eq. 18, and such calculations have, in fact, been made.^{8,9} On the other hand, there are occasions when it would be expedient to have a more rapid method for calculating c_t . Such a method is provided by an approximate formula in which c_t is expressed as a power series in x_t alone. The general form of this series will not be investigated, but the first few terms will be derived. Suppose that the sedimentation coefficient can be expanded as a convergent power series in x

$$s = s_0 + s_1 x + s_2 x^2 + \dots \quad (23)$$

From the theory of one-parameter groups⁶

$$x_0 = g(x_t, -t) = x_t - tXx_t + \frac{1}{2!}t^2X^2x_t - \dots \quad (24)$$

where X is the operator

(6) L. P. Eisenhart, "Continuous Groups of Transformations," Dover Publications, Inc., New York, N. Y., 1961, pp. 32-35.

(7) If ω is not constant, the change of variable, $\tau = \int \omega^2 dt$, changes eq. 13 and 18 into $dr/dr = sr$ and $dx/d\tau = sx$, which define one-parameter groups whose parameters are τ instead of t .

(8) C. de Duve, J. Berthet, and H. Beaufay, *Progr. Biophys. Biophys. Chem.*, **9**, 325 (1959).

(9) R. G. Martin and B. N. Ames, *J. Biol. Chem.*, **236**, 1372 (1961).

$$X \equiv s\omega^2 x \frac{d}{dx} \quad (25)$$

From eq. 23 and 25 it follows by induction that

$$X^n x = s_0^n \omega^{2n} x + (2^n - 1) s_0^{n-1} s_1 \omega^{2n} x^2 + \\ [1/2(3^n - 1) s_0^{n-1} s_2 + (3^n - 2^{n+1} + 1) \times \\ s_0^{n-2} s_1^2] \omega^{2n} x^3 + \dots \quad (26)$$

When this expression is substituted into eq. 24 and the terms are rearranged, it is found by applying eq. 21 that

$$c_t = c_0 e^{-s_0 \omega^2 t} \left[1 - \frac{2s_1}{s_0} (1 - e^{-s_0 \omega^2 t}) x_t + \right. \\ \left. 3 \left\{ \frac{s_1^2}{s_0^2} (1 - e^{-s_0 \omega^2 t})^2 - \frac{1}{2} \frac{s_2}{s_0} (1 - e^{-2s_0 \omega^2 t}) \right\} x_t^2 + \dots \right] \quad (27)$$

The corresponding formula for the analytical ultracentrifuge is obtained by writing r_t and $f(r_t, -t)$ instead of x_t and $g(x_t, -t)$ in eq. 23-26 and substituting the results into eq. 17; this leads to the formula

$$c_t = c_0 e^{-2s_0 \omega^2 t} \left[1 - \frac{3s_1}{s_0} (1 - e^{-s_0 \omega^2 t}) r_t + \right. \\ \left. 6 \left\{ \frac{s_1^2}{s_0^2} (1 - e^{-s_0 \omega^2 t})^2 - \frac{1}{3} \frac{s_2}{s_0} (1 - e^{-2s_0 \omega^2 t}) \right\} r_t^2 + \dots \right] \quad (28)$$

Examples

(1) *Linear Density Gradients.* The formulas derived in the previous section will now be used in the calculation of the concentration of sedimenting material in some simple cases of practical importance. It will be assumed that at the beginning of the experiment the material is distributed uniformly throughout the centrifuge tube. The simplest example occurs when the sedimentation coefficient is constant. The integrals of eq. 13 and 18 under these circumstances, namely

$$r_t = r_0 e^{s\omega^2 t} \quad (29)$$

$$x_t = x_0 e^{s\omega^2 t} \quad (30)$$

lead at once through eq. 17 and 21 to the formulas¹

$$c_t = c_0 e^{-2s\omega^2 t} \quad (31)$$

for the sector cell and

$$c_t = c_0 e^{-s\omega^2 t} \quad (32)$$

for the cylindrical tube.

Unfortunately, it is not often possible to operate the

preparative ultracentrifuge without some sort of density or viscosity gradient since convection currents disturb the boundary unless extreme care is taken.¹⁰ On the other hand, in any such gradient the sedimentation coefficient must vary with position, as is evident both from Svedberg's formula for s^{11} and from more sophisticated theories.^{3,12} It is therefore of some importance to investigate the effect of a variable sedimentation coefficient, particularly as it is clear from eq. 9 that there will not usually be a plateau. Accordingly, the effects of two simple gradients will now be discussed. The first is a linear density gradient, which approximately represents a linear salt gradient over a narrow range of concentrations, and the second is linear in density and viscosity and may be used to describe a linear gradient of sucrose over a suitable range. In examining these gradients it will be assumed that s is given by Svedberg's formula.

Suppose that there is a gradient linear in density only, such that the density is ρ_1 at x_1 , the coordinate of the meniscus, and ρ_2 at x_2 , the coordinate of the bottom of the tube; the density at any point can be found from the formula

$$\rho = \rho_1 + \frac{x - x_1}{x_2 - x_1} (\rho_2 - \rho_1) \quad (33)$$

With these values for ρ and a constant value for the viscosity, the sedimentation coefficient takes the form

$$s = \beta(\alpha - x) \quad (34)$$

where α and β are expressed in terms of the molecular weight M , density ρ_0 , and frictional coefficient f of the sedimenting material by

$$\alpha = \frac{x_2(\rho_0 - \rho_1) - x_1(\rho_0 - \rho_2)}{\rho_2 - \rho_1} \quad (35)$$

$$\beta = \frac{M}{f\rho_0} \left(\frac{\rho_2 - \rho_1}{x_2 - x_1} \right) \quad (36)$$

When $\rho_0 > \rho_2$, the material sediments, and in this case $\alpha > x_2$; when $\rho_0 < \rho_1$, it floats, and $\alpha < x_1$. Equation 18 integrates to give

$$x_t = \frac{x_0 e^{\alpha\beta\omega^2 t}}{1 + \frac{x_0}{\alpha} (e^{\alpha\beta\omega^2 t} - 1)} \quad (37)$$

Application of eq. 21 leads to

(10) H. Kahler and B. J. Lloyd, Jr., *J. Phys. Chem.*, **55**, 1344 (1951); G. H. Hogeboom and E. L. Kuff, *J. Biol. Chem.*, **210**, 733 (1954).

(11) T. Svedberg and K. O. Pedersen, "The Ultracentrifuge," Oxford University Press, Oxford, 1940, p. 1.

(12) G. J. Hooyman, *Physica*, **22**, 766 (1956).

$$c_t = \frac{c_0 e^{-\alpha\beta\omega^2 t}}{\left\{1 - \frac{x_t}{\alpha}(1 - e^{-\alpha\beta\omega^2 t})\right\}^2} \quad (38)$$

It is clear from this equation that the concentration can vary over a considerable range of values in the vicinity of the point $x = \alpha$. As an example of the extent of deviation from a plateau concentration, consider a spherical particle of diameter 400 Å. and density 1.18 g./cm.³,¹³ sedimenting in a linear gradient of KCl running from 16 to 20% (w./w.). The temperature will be taken as 15°; the viscosity then has a constant value of 1.13 cp. The values of x_1 and x_2 will be taken as 5.6 and 9.6 cm., and it will be assumed that centrifugation takes place at a speed of 39,000 r.p.m. for a total time of 35 min. From eq. 35 $\alpha = 15.8$ cm. and from eq. 36 and Stokes' formula $\beta = 8.85 \times 10^{-13}$ cm.⁻¹ sec.⁻¹. From eq. 37 the boundary formed at the meniscus is found to have moved to 7.47 cm. The concentrations at this point and at the point x_2 are given by eq. 38 as $0.92c_0$ and $1.05c_0$, a difference of nearly 15%. For a more dense material α would have a larger value, and the variation in concentration would be smaller; thus, for a protein of density 1.40 in this gradient α would be 47.5 cm., and the difference in concentration between x_2 and the boundary would be only a few per cent.

If the viscosity varies linearly with x as well as the density, so that it takes the values η_1 at x_1 and η_2 at x_2 , the sedimentation coefficient becomes

$$s = \gamma \left(\frac{\alpha - x}{\delta + x} \right) \quad (39)$$

where α is given by eq. 35 and

$$\gamma = \frac{M\eta_0(\rho_2 - \rho_1)}{f_0\rho_0(\eta_2 - \eta_1)} \quad (40)$$

$$\delta = \frac{\eta_1 x_2 - \eta_2 x_1}{x_2 - x_1} \quad (41)$$

In eq. 40 f_0 is the value of the frictional coefficient when the viscosity is η_0 . The integral of eq. 18 is

$$\frac{x_t}{(\alpha - x_t)^{1+\alpha/\delta}} = \frac{x_0}{(\alpha - x_0)^{1+\alpha/\delta}} e^{(\alpha\gamma/\delta)\omega^2 t} \quad (42)$$

This equation cannot be solved for x_t or x_0 except for certain special values of δ . One such value is $\delta = 0$; this gives a type of reciprocal gradient to be discussed in the next section. For general values of δ recourse must be had to eq. 22 and 27. Equation 22 gives

$$c_t = c_0 \frac{x_0(\alpha - x_0)(\delta + x_t)}{x_t(\alpha - x_t)(\delta + x_0)} \quad (43)$$

while from eq. 27

$$c_t = c_0 e^{-(\alpha\gamma/\delta)\omega^2 t} \left[1 + 2 \left(\frac{1}{\alpha} + \frac{1}{\delta} \right) (1 - e^{-(\alpha\gamma/\delta)\omega^2 t}) x_t + 3 \left(\frac{1}{\alpha} + \frac{1}{\delta} \right) \left\{ \left(\frac{1}{\alpha} + \frac{1}{\delta} \right) (1 - e^{-(\alpha\gamma/\delta)\omega^2 t})^2 - \frac{1}{2\delta} (1 - e^{-2(\alpha\gamma/\delta)\omega^2 t}) \right\} x_t^2 + \dots \right] \quad (44)$$

provided that $x_t < |\delta|$. For a protein sedimenting at 5° in a linear gradient of sucrose running from 0 to 5% (w./w.), the value of α in eq. 44 would be about 75–85 cm., while δ would be 25–30 cm.; these values would lead to a deviation of c_t from a constant value which might reach 5%.

(2) *Reciprocal Gradients.* The gradients which will be discussed in this section are some in which the sedimentation coefficient satisfies a relation of the form of eq. 9; for this reason they have been named reciprocal gradients. In these gradients there is a plateau and eq. 1 and 3 show that the plateau concentration is

$$c_t = c_0 e^{-\kappa\omega^2 t} \quad (45)$$

The integral of eq. 18 is

$$x_t = x_0 e^{\kappa\omega^2 t} + \frac{\mu}{\kappa} (e^{\kappa\omega^2 t} - 1) \quad (46)$$

One way in which this type of gradient could arise was mentioned in the last section; this was the case of a gradient linear in density and viscosity and such that δ in eq. 39 is zero, so that the viscosity is proportional to the distance from the centrifugal axis. The relation between the various constants in eq. 9 and 39 is then

$$\kappa = -\gamma, \quad \mu = \alpha\gamma \quad (47)$$

Another way in which a reciprocal gradient can be realized is by varying the density while keeping the viscosity constant. Such a gradient can be constructed from solutions of salts over a suitable range of concentrations. If the density is to be ρ_1 at x_1 and ρ_2 at x_2 , its value at an intermediate point is

$$\rho = \frac{x_2\rho_2 - x_1\rho_1}{x_2 - x_1} - \frac{x_1x_2(\rho_2 - \rho_1)}{x_2 - x_1} \frac{1}{x} \quad (48)$$

In this gradient the constants in eq. 9 take the values

$$\kappa = \frac{M}{f\rho_0} \frac{x_2(\rho_0 - \rho_2) - x_1(\rho_0 - \rho_1)}{x_2 - x_1} \quad (49)$$

(13) (a) These figures are close to the dimensions of the hydrodynamic sphere which is equivalent to the chromatophores of *Rhodospseudomonas spheroides*^{13b}; (b) K. D. Gibson, Abstracts, VIth International Congress of Biochemistry, New York, N. Y., 1964, p. 777.

$$\mu = \frac{M}{f\rho_0} \frac{x_1 x_2 (\rho_2 - \rho_1)}{x_2 - x_1} \quad (50)$$

If $\rho_0 > (x_2 \rho_2 - x_1 \rho_1)/(x_2 - x_1)$, the maximum density which the gradient can reach, κ is positive, sedimentation only will occur, and the concentration tends to zero as $t \rightarrow \infty$. If $\rho_0 < (x_2 \rho_2 - x_1 \rho_1)/(x_2 - x_1)$, κ is negative, and the concentration increases indefinitely as the material becomes concentrated at the point $x = -\mu/\kappa$. If $\rho_0 = (x_2 \rho_2 - x_1 \rho_1)/(x_2 - x_1)$, κ is zero, the concentration does not alter, and the boundary moves with uniform velocity, $\mu\omega^2$.

Location of an Ideal Boundary

The aim of moving boundary centrifugation is to determine sedimentation coefficients. These can be calculated from a knowledge of the position to which the ideal boundary formed at the meniscus would have moved under the influence of sedimentation alone. Alternatively, if the movement of any boundary in the tube, not necessarily that formed at the meniscus, can be found, the sedimentation coefficient can be calculated from this information. In any real experiment there is diffusion, and it is therefore necessary to devise methods for locating an ideal boundary from the actual distribution of material. Techniques for this calculation have been worked out for the case when there is a plateau for both the analytical⁴ and the preparative¹ ultracentrifuge. An extension of the arguments used in establishing these techniques will be used in setting up the modification needed in the general case.

The boundaries which are to be located lie perpendicular to the direction of motion, and their positions are therefore most conveniently expressed in the notation of Trautman and Breese.¹ In this notation the coordinate representing the position of a boundary is equal to the volume V enclosed between it and the axis of centrifugation. Thus, the position of the boundary at r_1 in the analytical ultracentrifuge becomes

$$V_1 = ar_1^2 \quad (51)$$

while that of the boundary at x_2 in the preparative ultracentrifuge becomes

$$V_2 = bx_2 \quad (52)$$

Here a and b are appropriate constants of proportionality. Suppose the material to be present initially at a concentration c_0 everywhere below the boundary V_0 (Figure 1a). Under the influence of sedimentation alone it would come to lie below the boundary V_0' at a concentration c_s (Figure 1b). If diffusion occurs,

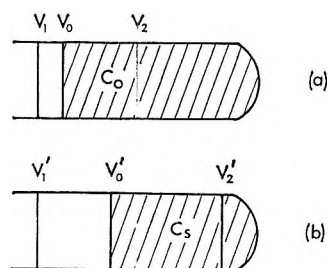


Figure 1. Positions of boundaries illustrated with reference to the cylindrical tube of the preparative ultracentrifuge.

some material will cross the boundary. Since all the material which is found above the boundary must have come from below it¹⁴

$$\int_{V_1'}^{V_0'} cdV = \int_{V_0'}^{V_2'} (c_s - c)dV \quad (53)$$

Thus

$$\int_{V_1'}^{V_2'} cdV = \int_{V_0'}^{V_2'} c_s dV \quad (54)$$

or if there is a plateau

$$\int_{V_1'}^{V_2'} cdV = c_p(V_2' - V_0') \quad (55)$$

In most actual experiments $V_0, V_1,$ and V_1' are all equal to the coordinate of the meniscus, and it will be assumed that this is so below.

The first method for locating a boundary consists of a series of corrections to allow for the absence of a plateau, of which usually only the first will be quantitatively significant and which are applied to the value of V_0' obtained by means of eq. 55. The only information needed is the actual distribution of material in the tube, and the method can therefore be used when there is more than one sedimenting material by applying it to each one individually. Suppose that at the coordinate V_2' the concentration takes the value which it would assume in the absence of diffusion, and let this value be denoted by c_2 . Let V_3' be defined by

$$\int_{V_1'}^{V_2'} cdV = c_2(V_2' - V_3') \quad (56)$$

From eq. 55 V_3' is the value which V_0' would take if there were a plateau in which the concentration was c_2 . Now let V_n' for $n \geq 4$ be defined by

$$c_2(V_{n-1}' - V_n') = \int_{V_{n-1}'}^{V_{n-2}'} (c_2 - c_s)dV \quad (57)$$

(14) It is assumed that there is no diffusion across V_2' ; if this condition is not satisfied, the methods for locating boundaries which are discussed here will give a false result.

It is easily seen by induction that

$$c_2(V_n' - V_0') = \int_{V_0'}^{V_{n-1}'} (c_2 - c_s) dV \quad (58)$$

Now suppose that the integrals on the right of eq. 57 are all nonnegative; this will be true, for instance, if c_2 is the maximum value which is attained by c_s between the coordinates V_1' and V_2' . Then

$$V_3' \geq V_4' \geq V_5' \geq \dots \quad (59)$$

Thus, V_n' tends to a limit; and if this limit is V' , eq. 58 shows that

$$c_2(V' - V_0') = \int_{V_0'}^{V'} (c_2 - c_s) dV \quad (60)$$

which is only possible (when $c_s \neq 0$) if $V' = V_0'$. Thus, whenever the integrals in eq. 57 are nonnegative, the sequence V_n' converges to V_0' , and the method will, in principle, give the coordinate V_0' to any required degree of accuracy provided the integrals can be evaluated and provided that c_2 is known with sufficient precision. The crux of the method is the evaluation of the integrals, which can only be carried out satisfactorily if it is possible to make some assessment of c_s . In the most general case this would not be feasible since it would be impossible to say whether the variations of concentration observed in the region of the boundary were due to diffusion or to variation of c_s . However, if there is reason to believe that c_s does not deviate greatly from a linear function of the coordinate, *i.e.*, if the third and subsequent terms of eq. 27 are small or do not vary greatly over the interval in question, then substitution of this linear function for c_s into eq. 57 will lead to a practical method for locating the boundary. It appears that the type of gradients which are most commonly used in measuring boundary sedimentation in the preparative ultracentrifuge, namely, linear gradients of salts or sucrose in which the concentration differs by less than 5% (w./w.) over the length of the tube, satisfy this requirement to a sufficient degree of accuracy.

The procedure for locating the boundary is illustrated in Figure 2 for the example of the linear KCl gradient used in a previous section. The distribution of material caused by sedimentation alone was calculated from eq. 38, using the values of α and β given earlier (Figure 2a). This distribution would be altered by diffusion (Figure 2b). The first approximation to the boundary, obtained from eq. 56, gives the point V_3' . This point and the tangent to the curve at V_2' determine a triangle (cross-hatched in Figure 2) whose area is a reasonable approximation to the integral in eq. 57 for $n = 4$, from which the point V_4' is ob-

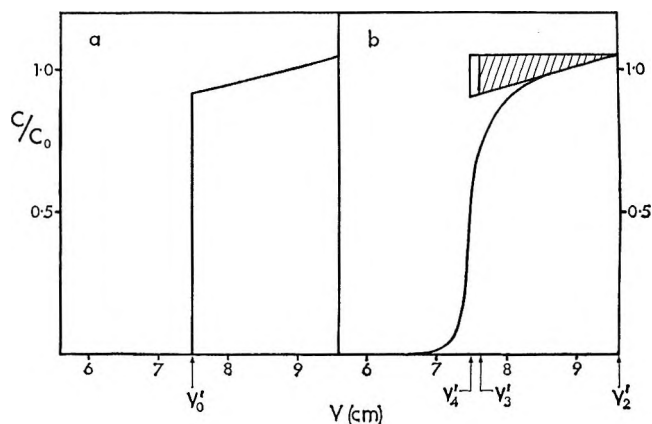


Figure 2. Distribution of material and location of the boundary for the experiment described in Table I when the time of centrifugation was 35 min.

tained. The area of the trapezoid determined by V_3' and V_4' and the tangent at V_2' approximates to the integral for $n = 5$ and is used to calculate V_5' . The process is illustrated in Table I, where the values of V' at each approximation are tabulated together with the values for s obtained with eq. 67. There is a difference of 6% between the first and last figures for s , while the last figure is the same as the true value.

Table I also shows how the importance of the corrections varies with the distance through which the boundary has moved. When the time of the imaginary centrifugal run was increased to 45 min., even the first correction was found to be quite negligible. However, when the time was decreased again to 25 or 15 min., the first approximation to s gave a value which was too large by 12 or 15% but which was brought to within 2% of the correct value merely by applying the first correction. The example given here is rather extreme, and the corrections to be applied to V_3' might not normally be so large. However, their importance increases the nearer the boundary is to the meniscus, and they ought therefore to be taken into account whenever the boundary whose position is to be determined has moved only a short distance from the meniscus. It must be emphasized that the practical question of evaluating the corrections involves making some assessment of the variation of c_s and would probably present insuperable difficulties whenever c_s is not, at least approximately, a linear function of the coordinate V .

The second method for locating an ideal boundary determines the position of the coordinate V_2 which is transformed into V_2' by the motion; the coordinate V_2' is to be chosen arbitrarily, near the bottom of the tube at the end of the run. For the calculation it is not necessary to know the exact concentration of

Table I: Successive Approximations to the Boundary^a

Time of centrifugation, min.	Boundary	Coordinate, cm.	s, S.
15	V ₃ '	6.52	101
	V ₄ '	6.40	89
	V ₅ '	6.39	88
	V ₀ '	6.39	88
25	V ₃ '	7.09	94
	V ₄ '	6.93	85
	V ₅ '	6.91	84
	V ₀ '	6.91	84
35	V ₃ '	7.62	87
	V ₄ '	7.49	83
	V ₅ '	7.47	82
	V ₀ '	7.47	82
45	V ₃ '	8.13	83
	V ₄ '	8.04	82
	V ₅ '	8.03	82
	V ₀ '	8.02	82

^a Values of V₃', V₄', V₅', and V₀' were calculated as described in the text for an imaginary experiment in which spherical particles of diameter 400 Å. and density 1.18 g./cm.³ were centrifuged at 15° in a linear KCl gradient running from 16 to 20% w./w. at 39,000 r.p.m. for the times indicated. V₀ was at 5.6 cm. and V₂' at 9.6 cm. The coordinates are expressed as distances from the axis of centrifugation. The values of s were calculated from eq. 67.

material at any point in the tube but only the total amount of material in the tube above the coordinate V₂'. It is also necessary to know c₀, the initial concentration of sedimenting material; however, as pointed out by Trautman and Breese,¹ this is frequently simpler to measure accurately than the plateau concentration when there is one. The method depends on the fact that, if there were no diffusion, a boundary moving with the material would not be crossed by any of the material during the course of sedimentation. The integral on the right-hand side of eq. 54 represents the total amount of material which would lie between the boundaries at V₀' and V₂' if sedimentation took place without diffusion, and, since in that case no material could have crossed these boundaries, it must all have lain between them at the start of the experiment when their coordinates were V₀ and V₂. Thus (cf. eq. 11)

$$\int_{V_0'}^{V_2'} c_s dV = \int_{V_0}^{V_2} c_0 dV \quad (61)$$

Under normal circumstances the initial distribution of material is uniform and the initial value of V₀ is equal

to V₁, the coordinate of the meniscus. Then from eq. 54 and 61 it follows that

$$V_2 = V_1 + \frac{1}{c_0} \int_{V_1}^{V_2'} c dV \quad (62)$$

If the average concentration of material between the coordinates V₁ and V₂' is \bar{c} , eq. 62 shows that

$$V_2 = V_1 + \frac{\bar{c}}{c_0} (V_2' - V_1) \quad (63)$$

To apply eq. 63 it is necessary to make only two measurements of concentration, one to determine the initial concentration and the other to determine the average concentration in the whole tube above the chosen point V₂' at the end of the run. The method is thus suitable for determining the s value associated with a biologically active material such as an enzyme or a virus by employing the biological assay to measure the concentration. Trautman and Breese's method for locating a boundary also requires only two measurements. However, their calculation is more complicated than the one given in eq. 63, and, in addition, their method cannot be applied when there is no plateau. As an application of eq. 62 the boundaries V₂ which are transformed into V₂' in the experiment of Table I are listed in Table II.

Table II: Boundaries Calculated by the Second Method^a

Time of centrifugation, min.	Coordinate of V ₂ , cm.	s, S.
15	8.78	59
25	8.25	61
35	7.68	64
45	7.06	68

^a Values of V₂ were calculated with eq. 62 for the experiment described in Table I. The values of s were obtained from eq. 67.

The main disadvantage of the method just outlined is that it is necessary to know the initial concentration of the material so that it cannot be applied individually to the components of a mixture unless the initial concentration of each is known. When there is a mixture of this sort, a weighted average boundary is obtained in which the weighting factors are the initial concentrations of the various components. For instance, if there are two components, there is an equation of the form of eq. 62 for each of them; then, using superscripts to distinguish the components, if these equations are multiplied by c₀⁽¹⁾ and c₀⁽²⁾ and added, it is found that

$$c_0^{(1)}V_2^{(1)} + c_0^{(2)}V_2^{(2)} = V_1(c_0^{(1)} + c_0^{(2)}) + \int_{V_1}^{V_2'} cdV \quad (64)$$

so that the boundary obtained is $(c_0^{(1)}V_2^{(1)} + c_0^{(2)}V_2^{(2)}) / (c_0^{(1)} + c_0^{(2)})$. In this respect, the method may have some advantage over that of Trautman and Breese even when there is a plateau since in their method the weighting factors, being equal to the plateau concentrations of the various components, will vary from one experiment to another even though the concentrations of the components are initially always the same.

Finally, it should be pointed out that in applying the arguments which were used to deduce the methods outlined above it does not matter whether the ideal boundary is disturbed by diffusion or by any other process. In deriving eq. 53 no specific use was made of the statement that the boundary was disturbed by diffusion, and the displacement of material could have occurred by any other means. The only condition which must be fulfilled if methods for locating boundaries based on eqs. 53 and 54 are to be valid is that it should be possible to find a boundary V_2' moving with the material at which the only motion is that due to sedimentation and the concentration has the value it would take under the influence of sedimentation alone. If this condition is met, either of the methods outlined here can be applied since both are based on eq. 53. This means that boundaries can be located satisfactorily in experiments in the preparative ultracentrifuge even though the methods of sampling lead to some disturbance of the contents of the tubes. Most of the methods for sampling the cylindrical tubes lead to some mixing of the material in neighboring layers.^{2,10,13b} However, it appears that there is almost always a region in which the concentration is nearly constant, and it is then reasonable to assume that at points in this region near the bottom of the tube the concentration takes the value c_s within experimental error. Thus, it is possible to apply the methods for locating a boundary to results obtained with the preparative ultracentrifuge even though the method of sampling is far from perfect. From the discussion presented here it is clear that appreciable disturbances in the distribution of material, whether introduced by diffusion or during sampling, will generally lead to only small variations in the position of the boundary determined experimentally and hence also in the sedimentation coefficient.

Calculation of the Sedimentation Coefficient

In the preceding section it was shown how a boundary can be located from the distribution of material in the

centrifuge tube. The question which now arises is how this information is to be used to calculate a sedimentation coefficient. The customary procedure is to use the formula

$$s = \frac{1}{\omega^2 t} \ln \frac{r_t}{r_0} \quad (65)$$

for the sector cell and the equivalent formula obtained by replacing r_0 and r_t with x_0 and x_t for the cylindrical tube.¹ In this equation r_0 and r_t correspond to the initial and final positions of the chosen boundary, *i.e.*, either to V_0 and V_0' or to V_2 and V_2' in the notation of the previous section. Equation 65 is derived directly from eq. 29, which was obtained on the assumption that s is constant. However, this simple expression is clearly inadequate when the sedimentation coefficient takes different values for different values of r or x , and usually more than one measurement would have to be made under these circumstances in order to determine the exact functional dependence of s on r or x .

It is therefore of some interest that the value for the sedimentation coefficient obtained by applying eq. 65 to the movement of a particular boundary is actually equal to the true value which the sedimentation coefficient takes at some point between the initial and final positions of the boundary, though not necessarily at either of these positions. This can be shown by applying the first mean-value theorem to eq. 13 or 18. Considering eq. 18, the integral of this equation with initial value x_0 is

$$\int_{x_0}^{x_t} \frac{dx}{xs(x)} = \omega^2 t \quad (66)$$

The functional dependence of s on x has been emphasized by writing it as $s(x)$. By the first mean-value theorem, if $s(x)$ is a continuous function of x , the left-

Table III: Values of s at the Boundaries^a

Time of centrifugation, min.	$\frac{1}{\omega^2 t} \ln \frac{V_0'}{V_0}$		$\frac{1}{\omega^2 t} \ln \frac{V_2'}{V_2}$			
	$s(V_0)$	$s(V_0')$	$s(V_2)$	$s(V_2')$		
15	90	88	83	62	59	55
25	90	84	79	67	61	55
35	90	82	74	72	64	55
45	90	82	69	77	68	55

^a The values of s at the boundaries V_0 , V_0' , V_2 , and V_2' for the experiment described in Table I are tabulated together with the values obtained from eq. 67 in Tables I and II.

hand side of eq. 66 is equal to $[1/s(\xi)] \ln(x_t/x_0)$ where $x_0 \leq \xi \leq x_t$. Thus

$$\frac{1}{\omega^2 t} \ln \frac{x_t}{x_0} = s(\xi) \quad (67)$$

This justifies the use of eq. 65 for calculating sedimentation coefficients. To illustrate the point, the values for s calculated from eq. 67 in Tables I and II are compared in Table III with the theoretical limits of s

obtained from eq. 34. It is clear that in the first two experiments, where the time of centrifugation was 15 or 25 min., the difference between the values of s at x_0 and x_t is not very great, and the value calculated from eq. 67 lies within 7% of either limit. In many practical situations the difference between $s(x_0)$ and $s(x_t)$ would be less than the experimental error involved in their determination, and eq. 67 would provide all the information that could be expected from the experiment.

Determination of an Equilibrium Constant for the Dimerization of the *Bacillus subtilis* α -Amylase Molecule¹

by Kinji Kakiuchi

Division of Physical Chemistry, Institute for Protein Research, Osaka University, Osaka, Japan
(Received August 11, 1964)

To evaluate the equilibrium constant for monomer-dimer transformation of *Bacillus subtilis* α -amylase, sedimentation equilibrium experiments were performed. The range of the initial concentration was 0.063–0.507%, at a setting speed of 6150 r.p.m. The association equilibrium could not be fitted to a simple monomer-dimer system since the association equilibrium curve could not be identical for different initial concentration. It was demonstrated that the zinc ions participate in the dimerization as $2 \text{ monomers} + \text{Zn}^{2+} \rightleftharpoons \text{dimer}$. The theory for sedimentation equilibrium for association system was adapted to the above scheme. The equilibrium constant for the dimerization was estimated to be $2.2 \times 10^9 \text{ l.}^2 \text{ mole}^{-2}$.

Introduction

Recently the Rayleigh interference optics has been greatly developed for sedimentation experiments. The principle of the use of short columns for sedimentation equilibrium experiments, which has been proposed and used by Svedberg and his co-workers,² has been reintroduced by Van Holde and Baldwin.³ With these instrumental innovations, sedimentation equilibrium is becoming a very useful and powerful technique for studying macromolecular systems.

The new theoretical development which enables us

to calculate weight- and higher-average molecular weights, as well as concentration at every distance in the ultracentrifugal cell, contributes to the usefulness of this technique. The theory for sedimentation

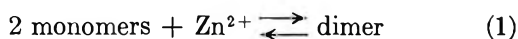
(1) This is part IV in a series on the association and dissociation of the *Bacillus subtilis* α -amylase molecule. For the preceding paper in this series see K. Kakiuchi, K. Hamaguchi, and T. Isemura, *J. Biochem.* (Tokyo), **57**, 167 (1965).

(2) T. Svedberg and K. O. Pedersen, "The Ultracentrifuge," Clarendon Press Inc., Oxford, 1940, p. 56.

(3) K. E. Van Holde and R. L. Baldwin, *J. Phys. Chem.*, **62**, 734 (1958).

equilibrium on chemically reacting systems has been published more than 30 years ago by Tiselius.⁴ It was summarized by Svedberg and Pedersen² and extended in recent years by Adams⁵ and by Adams and Fujita.⁶ As for studies on the chemically reacting systems by means of sedimentation equilibrium, the works by Squire and Li on adrenocorticotropin,⁷ by Adams on insulin,⁸ and by Jefferey and Coates on insulin⁸ have been reported. If the protein associates into n -mer and the solution is ideal, the latter being satisfied by most globular protein solutions, the plot of weight-average molecular weight against protein concentration should be a single curve. The above association equilibrium curve should be independent of the initial protein concentration. In all the cases cited previously, it was found that the association equilibrium curves were not identical if the initial protein concentration was different.

The association and the dissociation of *Bacillus subtilis* α -amylase was investigated by sedimentation, light scattering, and gel filtration. It has become evident during the course of the investigation that this protein molecule undergoes a reversible monomer-dimer transformation through a zinc atom,⁹⁻¹² that is



with the association constant given by

$$K = \frac{[\text{dimer}]}{[\text{monomer}]^2[\text{Zn}^{2+}]} \quad (2)$$

It was found that the rate of attainment of the equilibrium between monomer and dimer is not so fast as to be compared with the sedimentation velocity and flow rate of the gel filtration.

In the present investigation, the equilibrium constant, K , was determined from sedimentation equilibrium by modifying slightly and applying the theoretical equations given by previously mentioned investigators. In the sedimentation equilibrium, it seems likely that the re-equilibration between monomer and dimer has been already accomplished at every radial distance in the ultracentrifugal cell during the measurements. Since the monomer-dimer transformation of the *Bacillus subtilis* α -amylase molecule depends on the concentration of the zinc ion, it is expected that the plots of the molecular weight in the sedimentation equilibrium against the protein concentration will not fall on a single curve for different initial protein concentrations. Taking account of the participation of the zinc ion in the equilibrium between monomer and dimer, as given in eq. 1, the equilibrium constant for association could be evaluated definitely.

Method of Determining the Equilibrium Constant

In the present system, the protein monomer, its dimer, and the zinc ion are chosen to be the solute species. They are specified by the subscripts, M, D, and Zn^{2+} . All other components are regarded as the solvent. The solution is assumed to be ideal. If the chemical equilibrium between monomer and dimer exists, the following conditions must be fulfilled²

$$C_M(r) = C_M(r_m) \exp[M^*\alpha(r^2 - r_m^2)] \quad (3)$$

$$C_D(r) = C_D(r_m) \exp[2M^*\alpha(r^2 - r_m^2)] \quad (4)$$

$$C_{\text{Zn}^{2+}}(r) = C_{\text{Zn}^{2+}}(r_m) \exp[M_{\text{Zn}}\alpha'(r^2 - r_m^2)] \quad (5)$$

where $C_M(r)$, $C_D(r)$, and $C_{\text{Zn}^{2+}}(r)$ are the molar concentrations of monomer, dimer, and zinc ion, at a distance r from the center of rotation, M^* is the molecular weight of the monomer, and M_{Zn} is the atomic weight of zinc ion, respectively. The subscript, m, refers to the meniscus of the solution in the ultracentrifugal cell. Also, α and α' represent $(1 - \bar{v}\rho)\omega^2/2RT$ and $(1 - \bar{v}_{\text{Zn}}\rho)\omega^2/2RT$, respectively, where \bar{v} and \bar{v}_{Zn} are the partial specific volume of the protein and the zinc ion, ρ the density of solution, ω the angular velocity of the rotor, T the absolute temperature, and R the gas constant. It is assumed that the partial specific volume is independent of the monomer-dimer transformation and that the solution is incompressible by the pressure produced by the ultracentrifugal force. The total protein concentration at a given distance, r , is represented by

$$C(r) = C_M(r) + 2C_D(r) \quad (6)$$

Substitution of eq. 6 into 2 leads to

$$C(r) = C_M(r_m) \exp[M^*\alpha(r^2 - r_m^2)] + 2KC_{\text{Zn}^{2+}}(r_m)C_M^2(r_m) \exp[2M^*\alpha(r^2 - r_m^2)] \quad (7)$$

which can be rearranged into

$$C(r) \exp[-M^*\alpha(r^2 - r_m^2)] = C_M(r_m) + 2KC_{\text{Zn}^{2+}}(r_m)C_M^2(r_m) \exp[M^*\alpha(r^2 - r_m^2)] \quad (8)$$

(4) A. Tiselius, *Z. physik. Chem.* (Leipzig), **124**, 449 (1926).

(5) E. T. Adams, Jr., Ph.D. Thesis, University of Wisconsin, Madison, Wis., 1962.

(6) E. T. Adams, Jr., and H. Fujita in "Ultracentrifugal Analysis in Theory and Experiment," J. W. Williams, Ed., Academic Press Inc., New York, N. Y., 1962, p. 119.

(7) P. G. Squire and C. H. Li, *J. Am. Chem. Soc.*, **83**, 3521 (1961).

(8) P. D. Jefferey and J. H. Coates, *Nature*, **197**, 1104 (1963).

(9) T. Isemura, K. Kakiuchi, and H. Eto, *J. Biochem.* (Tokyo), **47**, 548 (1960).

(10) T. Isemura and K. Kakiuchi, *ibid.*, **51**, 385 (1962).

(11) K. Kakiuchi, S. Kato, A. Imanishi, and T. Isemura, *ibid.*, **55**, 102 (1964).

(12) See reference given in footnote 1.

The values of $C_M(r_m)$ and $C_D(r_m)$ can be estimated from the straight line of the plot of $C(r) \exp[-M^* \alpha(r^2 - r_m^2)]$ against $\exp[M^* \alpha(r^2 - r_m^2)]$, as shown in Figure 1. $KC_{Zn^{2+}}(r_m)$ is calculated from the slope of the straight line. If the system consists of monomers alone, the line should be horizontal, or if it contains only dimers, the line should pass through the origin.

To calculate the equilibrium constant, K , the knowledge of the concentration of free zinc ion is required. Now, only the total concentration of zinc is known and

$$\int_{r_m}^{r_b} \{C_{Zn^{2+}}(r) + C_D(r)\} dv = \int_{r_m}^{r_b} C_{Zn}(r)_{total} dv = (C_{Zn})_{total} \int_{r_m}^{r_b} dv \quad (9)$$

is given by (9). The volume element, dv , is given by $\theta l r dr$, θ being the sector angle of the cell and l , the cell thickness. The integration could be extended from the meniscus, r_m , to the bottom, r_b , within the cell. Substituting eq. 4 into 9, one obtains

$$C_{Zn^{2+}}(r) = C_{Zn total} - \frac{\int_{r_m}^{r_b} C_D(r) dv}{\int_{r_m}^{r_b} dv} = C_{Zn total} - \frac{C_D(r_m) \{ \exp[2M^* \alpha(r_b^2 - r_m^2)] - 1 \}}{2M^* \alpha(r_b^2 - r_m^2)} \quad (10)$$

provided that in eq. 5 $M_{Zn\alpha'}$ is very small compared with $M^* \alpha$ so that $C_{Zn^{2+}}(r)$ and $C_{Zn}(r)_{total}$ can be replaced by $C_{Zn^{2+}}(r_m)$ and $C_{Zn}(r_m)_{total}$, respectively.

Experimental

Preparation of *Bacillus subtilis* α -Amylase. *Bacillus subtilis* α -amylase which had been prepared from a culture of *Bacillus subtilis* was obtained from the Daiwa Kasei Co., Ltd., Osaka. The material was recrystallized as previously described.^{10,13} In the present investigation, furthermore, a *Bacillus subtilis* α -amylase solution in 0.1 M NaCl-0.005 M Ca(COOCH₃)₂ at pH 7.0 was filtered through a dextran gel (Sephadex G-100, purchased from Pharmacia, Uppsala), and faster elution was used. It was found previously¹¹ that a fresh solution prepared in this way contains a half of a zinc atom per monomer of *Bacillus subtilis* α -amylase. The concentrations of the protein solutions were determined from the optical absorbance at 280 m μ , assuming that $E_{1cm}^{1\%} = 25.6$.¹¹ The solutions used in the sedimentation equilibrium experiments were prepared by dilution of a 1.07% stock solution. The solvent used for dilution was checked for the absence of heavy metal ions by colorimetric determination

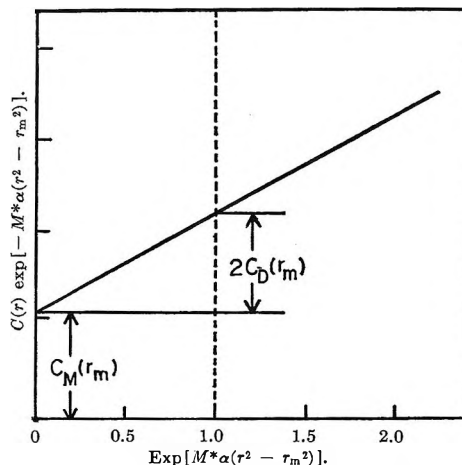


Figure 1. Schematic diagram of $C(r) \exp[-M^* \alpha(r^2 - r_m^2)]$ vs. $\exp[M^* \alpha(r^2 - r_m^2)]$ for the monomer-dimer transformation.

with dithizone (diphenyl thiocarbazono)¹⁴ since heavy metal ions such as Cu^{2+} , Ni^{2+} , and Co^{2+} can also promote the dimerization of the protein as Zn^{2+} .^{15,16} It was found that the amount of heavy metals in the solvent existing as contaminant was far below the amount that could be detected by the colorimetric determination.

Sedimentation Equilibrium Measurements. Sedimentation equilibrium experiments were performed with a Spinco Model E ultracentrifuge equipped with a rotatory light source for Rayleigh optics at a wave length of 546 m μ . Temperature was set at 20.0° by means of an RTIC unit. Photographic plates (Spectroscopic Type 1-D, purchased from Eastman Kodak Co.) were analyzed with the aid of an Olympus Precision Projector Model CP-20 equipped with a microcomparator which enabled us to read to 0.001 mm.

The sedimentation equilibrium experiments were performed with a double-sector cell made of aluminum-epoxy resin with a 12-mm. optical path. The runs were made on a two-place rotor (Rotor AN-D) or a multiple rotor (Rotor AN-G). The rotor speed read on an odometer was 6150 r.p.m. The height of the liquid column was adjusted to 4-5 mm. The initial concentration in fringes of *Bacillus subtilis* α -amylase was determined by an experiment in a synthetic bound-

(13) B. Hagihara, *Ann. Rept. Sci. Works, Fac. Sci., Osaka Univ.*, 2, 42 (1954).

(14) E. B. Sandell, "Colorimetric Determination of Traces of Metals," Vol. 3, Interscience Publishers, Inc., New York, N. Y., 1950, p. 616.

(15) E. H. Fischer, W. B. Summerwell, J. Junge, and E. A. Stein, *Proceedings of the 4th International Congress of Biochemistry*, Vienna, Sept. 1-6, 1958, Vol. 8, Pergamon Press, Inc., New York, N. Y., 1958, p. 124.

(16) E. A. Stein and E. H. Fischer, *Biochim. Biophys. Acta*, 39, 287 (1960).

ary cell with a double sector made of aluminum-epoxy resin. The position of the zero-order fringe in the sedimentation equilibrium patterns was determined by calculations based on an equation for the conservation of mass within the cell. The time required to reach the final state should be defined by both the time required for the sedimentation equilibrium and the rate of attainment of the equilibrium between the monomer and the dimer. Since the duration of each run was more than 35 hr., it is supposed that both equilibria have been already attained. After the estimate of the rates of association and dissociation, it was found that it would take a few hours for the attainment of the association-dissociation equilibrium. The meniscus of the solution was adjusted slightly below that of the solvent. The solvent in some cases leaked into the column of the solution during the course of the run, decreasing its concentration. A photograph was taken as soon as the setting speed had been reached. By measuring the positions of both levels at the initial and the final photographs the protein concentration was corrected.

The weight-average molecular weight, M_w , of the protein at various positions within the cell at equilibrium can be calculated from the slope of the logarithm of the concentration, f , in the fringe number against r^2 , according to

$$M_w = \frac{2RT}{(1 - \bar{v}\rho)\omega^2} \frac{d \ln f(r)}{dr^2} \quad (11)$$

The partial specific volume of the *Bacillus subtilis* α -amylase, \bar{v} , was measured by a pycnometer devised by Lipkin, *et al.*,¹⁷ and determined to be 0.720 ml./g.

Results and Discussion

In the equilibrium patterns, counting of the fringe number from the meniscus to the bottom of the solution column gives the concentration difference across the cell. The concentration of *Bacillus subtilis* α -amylase in fringes was determined by the use of a synthetic boundary cell to be 39.6/(1.00% protein). Figure 2 shows the plots for $\log f(r)$ vs. r^2 for the *Bacillus subtilis* α -amylase solution. For homogeneous materials such a plot should give a straight line. Indeed, as shown in Figure 2, the result for the initial concentration 0.507% (I) can be represented by a straight line in the range of a fringe number >17 (0.4%). The molecular weight calculated from the slope of the line is 97,600, which should be assigned to the dimer. Therefore, it can be concluded that for concentrations of more than 0.4% protein, the equilibrium is shifted toward the dimer, and only the latter is present in the solution. On the other hand, the results for the columns (II-V Table

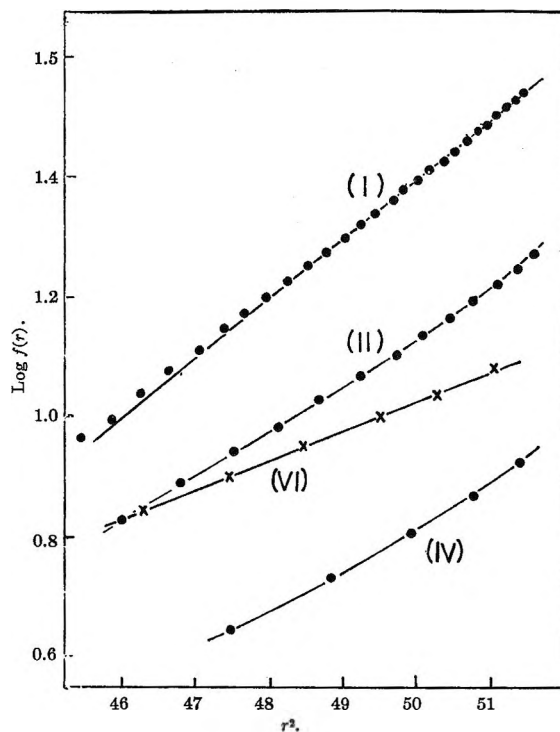


Figure 2. Plots of $\log f(r)$ vs. r^2 for the sedimentation equilibria of *Bacillus subtilis* α -amylase solutions. The initial protein concentrations: (I) 0.507, (II) 0.278, (IV) 0.157% in 0.1 M NaCl-0.005 M $\text{Ca}(\text{COOCH}_3)_2$ at pH 7.0, and (VI) 0.235% treated with 0.01 M EDTA in 0.1 M NaCl at pH 7.0.

I), the initial concentrations of which are lower than 0.4%, show curves concave upward, indicating that the molecular weight increases with increasing protein concentration. For low concentration of protein, the molecular weight will approach 48,000, which is the molecular weight of the monomer. This is indicated by the results given in column V, Table I. In the presence of EDTA (ethylenediaminetetraacetic acid) at pH 7.0, the dimer is wholly dissociated into the monomer by removing the zinc ions from the dimer. The plot for $\log f(r)$ vs. r^2 shows a straight line, as seen in Figure 2 (VI). The molecular weight calculated from its slope is 47,200. This value is slightly smaller than the value (48,200) obtained from the Archibald method for sedimentation equilibrium.¹² This discrepancy may be caused by the presence of small-size peptides liberated from the protein. The calcium atoms bound to the *Bacillus subtilis* α -amylase are removed by the treatment of EDTA so that the calcium-free protein is apt to undergo denaturation and rupture by the action of

(17) M. R. Lipkin, J. A. Davison, W. T. Harvey, and S. S. Kurty, *Ind. Eng. Chem., Anal. Ed.*, **16**, 55 (1944).

Table I: The Equilibrium Constant and the Related Values Calculated from Each Column

Column no.	Concn. of <i>Bacillus subtilis</i> α -amylase, %	Concn. of zinc ion, <i>M</i>	$C_D(r_m)$, <i>M</i>	Total concn. of zinc atom combined with <i>Bacillus subtilis</i> α -amylase, <i>M</i>	$KC_{Zn^{2+}}$, $l.^2 \text{ mole}^{-1}$	K , $l.^2 \text{ mole}^{-2}$
II	0.278	2.89×10^{-5}	7.73×10^{-6}	1.72×10^{-6}	2.64×10^4	2.3×10^9
III	0.125	1.30×10^{-5}	1.85×10^{-6}	4.56×10^{-6}	1.66×10^4	2.0×10^9
IV	0.157	1.64×10^{-5}	3.95×10^{-6}	6.93×10^{-6}	1.92×10^4	2.1×10^9
V	0.063	0.66×10^{-5}	0.58×10^{-6}	1.41×10^{-6}	1.22×10^4	2.3×10^9

the proteases existing as contaminants as noted by Fischer and his co-workers.^{18,19}

The curved plots of $\log f(r)$ vs. r^2 could be adequately represented by quadratic expressions. The coefficients of the quadratic equation were determined by the method of least squares. The calculation was carried out on a Nippon Electric Co. Model-2101 computer. The first derivative of the quadratic form, $d \log f(r)/dr^2$, gives the molecular weight at a given r^2 value. Thus, the molecular weight could be determined at various protein concentrations. Figure 3 gives the plots of $d \log f(r)/dr^2$ vs. protein concentration, instead of the molecular weight vs. r^2 . It can be seen that solutions of different initial protein concentrations give different molecular weights at a position of the same concentration. In other words, data for the molecular weight from solutions of different initial concentrations do not superpose on a single curve. If the monomer-dimer transformation occurs without

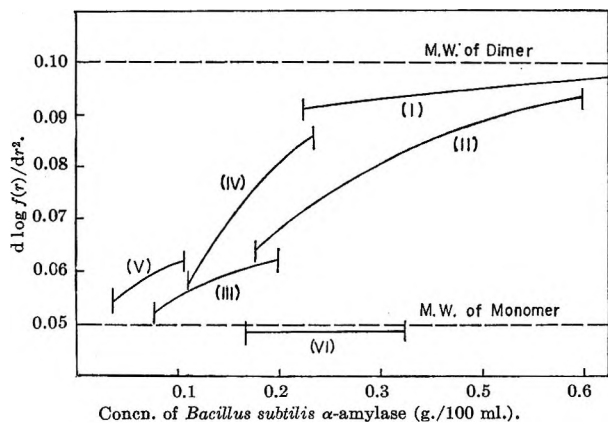


Figure 3. The plots of $d \log f(r)/dr^2$ (apparent molecular weight) vs. the protein concentration. $d \log f(r)/dr^2 = 0.10$ for the molecular weight of the dimer and 0.05 for that of the monomer. The range of the curves is from the meniscus to the bottom of the cells. The initial protein concentrations: (I) 0.507, (II) 0.278, (III) 0.125, (IV) 0.157, and (V) 0.063% in 0.1 M NaCl - $0.005 \text{ M Ca}(\text{COOCH}_3)_2$ at pH 7.0. VI: 0.235% treated with 0.01 M EDTA in 0.1 M NaCl at pH 7.0.

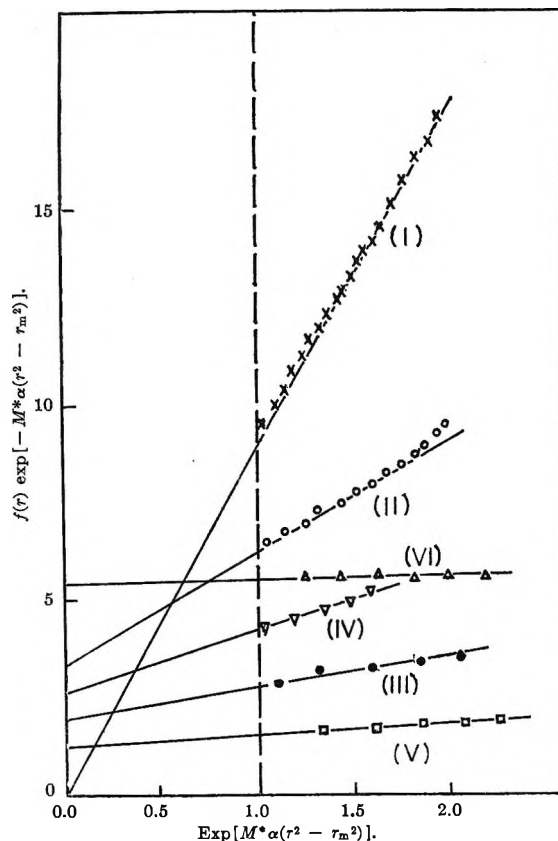


Figure 4. Plots of $f(r) \exp[-M^* \alpha(r^2 - r_m^2)]$ vs. $\exp[M^* \alpha(r^2 - r_m^2)]$ for the sedimentation equilibrium. In the case of column V the listed plots were counted by reading the fringe number to half a fringe.

the participation of zinc ions, *i.e.*, $2 \text{ monomers} \rightleftharpoons \text{dimer}$, the curves of molecular weight vs. protein concentration should be superposed. In the present system, for which eq. 1 is expected to hold, the concentration of the zinc ion at a position of the same protein concentration may vary not only with the initial zinc ion concentration but also with the dimer concentration. The plots of $f(r) \exp[-M^* \alpha(r^2 - r_m^2)]$ vs.

(18) E. A. Stein, J. Hsiu, and E. H. Fischer, *Biochemistry*, **3**, 56 (1964).

(19) J. Hsiu, E. H. Fischer, and E. A. Stein, *ibid.*, **3**, 61 (1964).

$\exp[M^*\alpha(r^2 - r_m^2)]$ are shown in Figure 4. The monomer and the dimer concentrations at the menisci of the solutions can be estimated from Figure 4. It is observed that at concentrations in a fringe number >17 (0.4%) no monomer exists at the meniscus, as can be seen from Figure 4 (II). Furthermore, the slope of the straight line turns upward above the concentration of 0.4%. Accordingly, the monomer can exist in equilibrium with the dimer at concentrations of less than 0.4%. The concentration below which the dimer is transformed into monomers should be dependent on the pH, the ionic strength, and, especially, the zinc ion concentration, as shown in a previous

paper.¹² From the concentration of the free zinc ion calculated by eq. 10 the equilibrium constant can be obtained as listed in Table I. The average equilibrium constant is $2.2 \times 10^9 \text{ l.}^2 \text{ mole}^{-2}$, which is in good agreement with the value calculated from the light-scattering measurement.¹²

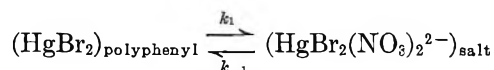
Acknowledgments. The author wishes to express his gratitude to Professor Toshizo Isemura, Dr. Shoichi Ikeda, and Dr. Naoto Yamamoto for valuable discussions. The author also wishes to express his thanks to the Daiwa Kasei Co., Ltd., for supplying *Bacillus subtilis* α -amylase.

Solvent Extractions from Molten Salts. IV.¹ Kinetics of the Formation of Mercury(II) Bromide Species

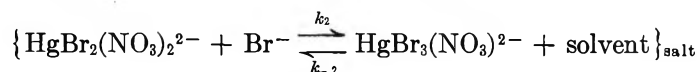
by M. Zangen

Radiochemistry Department, Soreq Research Establishment, Israel Atomic Energy Commission, Yavne, Israel
(Received November 7, 1964)

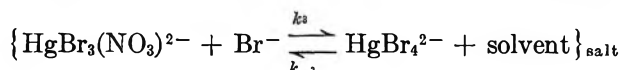
The partition of HgBr_2 between a polyphenyl eutectic mixture and a molten $\text{LiNO}_3\text{-KNO}_3$ eutectic at 150° was measured as a function of time for various concentrations of KBr added to the salt melt. From the results, the rate constants for the following reactions were calculated



$$k_1 = 2.7 \pm 0.1 \times 10^{-3} \text{ sec.}^{-1}; k_{-1} = 2.5 \pm 0.2 \times 10^{-2} \text{ sec.}^{-1} \quad (\text{a})$$



$$k_2 = 1.3 \pm 0.2 \times 10^{-1} \text{ kg. mole}^{-1} \text{ sec.}^{-1}; k_{-2} = 1.6 \pm 0.2 \times 10^{-2} \text{ sec.}^{-1} \quad (\text{b})$$



$$k_3 = 6.2 \pm 1.0 \times 10^{-2} \text{ kg. mole}^{-1} \text{ sec.}^{-1}; k_{-3} = 6.9 \pm 1.0 \times 10^{-3} \text{ sec.}^{-1} \quad (\text{c})$$

Reactions b and c were found to operate simultaneously in the exchange of Br^{82} between HgBr_2 and KBr in the above system.

Introduction

While several authors² have investigated the kinetics of reactions in a molten salt phase, the method of solvent extraction has not yet been used for this purpose. In general, kinetic work in two-phase systems is comparatively scarce,³ since it mostly requires solution of intricate rate equations.

Partition experiments of neutron-irradiated HgBr_2 between a polyphenyl eutectic and a molten $\text{LiNO}_3\text{-KNO}_3$ eutectic to which nonradioactive KBr had been added^{1a} showed different values of the distribution ratio for different energies of γ -radiation measured in both phases. This could only be explained by isotope exchange of γ -active Br^{82} between HgBr_2 and KBr . The present work was aimed at determining the mechanism of this exchange in a molten salt phase, as compared, for example, to a similar exchange reaction (I^{127} between HgI_2 and KI) in aqueous solution.⁴

Experimental

As in parts I, II, and III,¹ the $\text{LiNO}_3\text{-KNO}_3$ eutectic mixture ($\text{K}:\text{Li}$ mole ratio = 1.33, m.p. 120°) was fused and homogenized at 350° , after which dry nitrogen was bubbled through at 250° during 4 hr. to remove any water. The polyphenyl eutectic mixture (m.p. 25°) consisted of biphenyl, *o*-terphenyl, and *m*-terphenyl in the mole ratio 37:48:15.

The mercury(II) bromide, neutron-irradiated in the IRR-I reactor before dissolution, was made up to $10^{-3} m$

(1) (a) Part I: M. Zangen and Y. Marcus, *Israel J. Chem.*, **2**, 49 (1964); (b) part II: M. Zangen, *ibid.*, **2**, 91 (1964); (c) part III: M. Zangen and Y. Marcus, *ibid.*, **2**, 155 (1964).

(2) (a) F. R. Duke and M. L. Iverson, *J. Am. Chem. Soc.*, **80**, 5061 (1958); (b) F. R. Duke and E. A. Shute, *J. Phys. Chem.*, **66**, 2114 (1962).

(3) C. D. Honaker and H. Freiser, *ibid.*, **66**, 127 (1962).

(4) D. E. O'Reilly, G. E. Schacher, and K. Schug, *J. Chem. Phys.*, **39**, 1756 (1953).

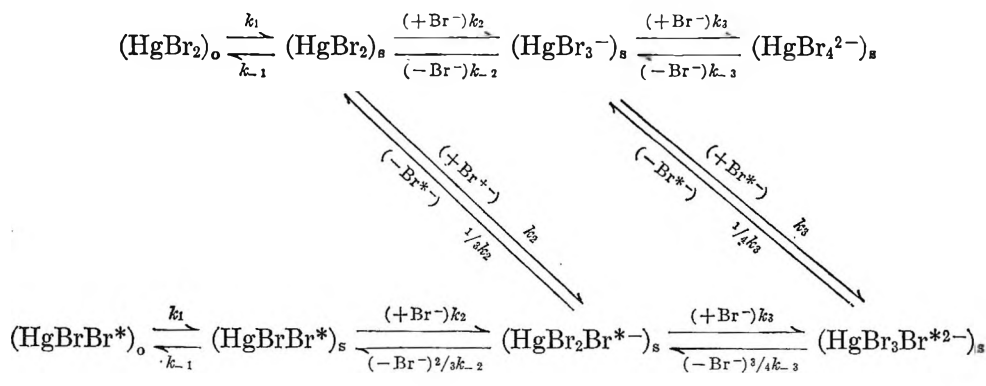
in the polyphenyl phase at the beginning of the reaction. The weight to weight ratio of salt to polyphenyl was near 3.5 in all experiments. Sealed Pyrex test tubes, containing molten nitrate eutectic with dissolved KBr in various concentrations and a HgBr₂ solution in polyphenyl, were tumbled at constant speed (50 r.p.m.) in an oil bath at 150 ± 1° for various periods of time. The phases were then allowed to separate in the bath, this occurring very quickly, after which the tube was rapidly cooled to 30° and opened; the polyphenyl phase was removed to another tube and the nitrate was washed with benzene. The γ-radiation of Hg¹⁹⁷ (65 hr., 0.19 Mev.) and of Br⁸² (35 hr., 0.54 Mev.) in both phases was measured in a NaI crystal well-type γ-spectrometer, and the distribution ratio (*D*_{Hg} or *D*_{Br*}) was calculated as

$$D = \frac{\text{counts/min./g. of polyphenyl phase}}{\text{counts/min./g. of salt phase}}$$

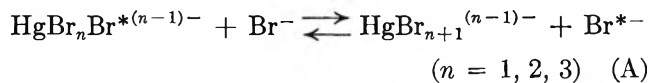
Results and Calculations

Figure 1 shows *D*_{Hg} and *D*_{Br*} as functions of time for various concentrations of KBr in the salt melt. It can be seen that while the mercury partition attains equilibrium in 5–30 min. depending on KBr concentration, the partition of active bromine does not attain equilibrium in less than 60 min.

In previous work,¹ it was concluded that the only species of mercury(II) bromide in a nitrate melt phase containing excess bromide are HgBr(NO₃)₂²⁻, HgBr₃(NO₃)²⁻, and HgBr₄²⁻. However, in the following, the nitrate groups will be disregarded for the sake of clarity since the nitrate concentration is approximately constant and may be incorporated in the rate constants. The reaction scheme is assumed to be



where the subscripts o and s represent the organic and salt phases, respectively. In this scheme, the possible existence of species containing more than one radioactive bromine atom is disregarded because of the large excess (~10⁹) of stable bromine in the irradiated mercury bromide. Also, the reactions



which have no direct bearing on the mercury partition mechanism, are disregarded for reasons which will be discussed below. As will be shown, the participation of these reactions in the exchange mechanism is virtually insignificant. This yields the set of rate equations

$$\frac{dA}{dt} = k_{-1}B - k_1A \quad (1)$$

$$\begin{aligned} \frac{dB}{dt} &= \frac{k_1A - k_{-1}B}{q} + k_{-2}(E + 1/3E') - \\ k_2B(C + C') &\approx \frac{k_1A - k_{-1}B}{q} + k_{-2}E - k_2BC \quad (2) \end{aligned}$$

$$\begin{aligned} \frac{dE}{dt} &= k_2BC - k_{-2}E + k_{-3}(F + 1/4F') - \\ k_3E(C + C') &\approx k_2BC - k_{-2}E + k_{-3}F - k_3EC \quad (3) \end{aligned}$$

$$\frac{dF}{dt} = k_3CE - k_{-3}F \quad (4)$$

$$\frac{dA'}{dt} = k_{-1}B' - k_1A' \quad (5)$$

$$\frac{dB'}{dt} = \frac{k_1A' - k_{-1}B'}{q} + 2/3k_{-2}E' - k_2B'C \quad (6)$$

$$\frac{dC'}{dt} = 1/3k_{-2}E' - k_2BC' + 1/4k_{-3}F' - k_3EC' \quad (7)$$

$$\frac{dE'}{dt} = k_2(BC' + B'C) - k_{-2}E' + 2/4k_{-3}F' - k_3CE' \quad (8)$$

$$\frac{dF'}{dt} = k_3(CE' + EC') - k_{-3}F' \quad (9)$$

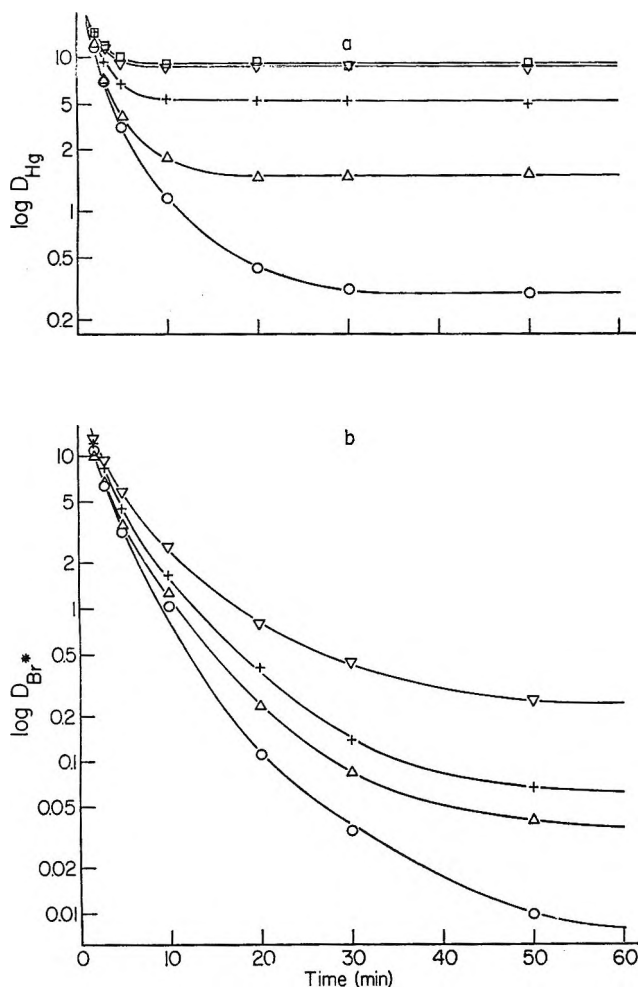


Figure 1. (a) Over-all distribution ratio of Hg between $\text{LiNO}_3\text{-KNO}_3$ eutectic and polyphenyl eutectic as a function of time, the nitrate melt containing: 0.00 m (\square), 0.006 m (∇), 0.06 m (\times), 0.2 m (Δ), and 0.6 m (\circ) KBr, respectively; (b) over-all distribution ratio of Br^{82} between $\text{LiNO}_3\text{-KNO}_3$ eutectic and polyphenyl eutectic as a function of time, the nitrate melt containing: 0.006 m (∇), 0.06 m (\times), 0.2 m (Δ), and 0.6 m (\circ) KBr, respectively.

where $A = (\text{HgBr}_2)_o$, $B = (\text{HgBr}_2)_s$, $C = (\text{Br}^-)$, $E = (\text{HgBr}_3^-)_s$, $F = (\text{HgBr}_4^{2-})_s$, and A' , B' , C' , E' , and F' are the concentrations of corresponding species containing active bromine; $q = \text{mass salt phase/mass polyphenyl phase}$. Since, as can be calculated from part I, the free nonradioactive bromide is always in large excess over mercury tri- and tetrabromide, its concentration can be considered constant.

$$C = \text{constant}, \frac{dC}{dt} = 0 \quad (10)$$

All the above equations are interrelated by the balance equations for mercury

$$A + q(B + E + F) \equiv A_0 \quad (11)$$

$$\frac{dA}{dt} + q \left(\frac{dB}{dt} + \frac{dE}{dt} + \frac{dF}{dt} \right) \equiv 0 \quad (11a)$$

and for radioactive bromine

$$A' + q(B' + C' + E' + F') \equiv A'_0 \quad (12)$$

$$\frac{dA'}{dt} + q \left(\frac{dB'}{dt} + \frac{dC'}{dt} + \frac{dE'}{dt} + \frac{dF'}{dt} \right) \equiv 0 \quad (12a)$$

The value of k_1 and k_{-1} can be found from the results obtained in the absence of KBr. In that case, only eq. 1 (or 6) applies and we have

$$\frac{dA}{dt} = k_1(K_D B - A) \quad (13)$$

where $K_D = k_{-1}/k_1 = 9.2$,^{1a} the distribution ratio for HgBr in the absence of KBr.

$$\frac{dA}{dt} = k_1 \left(K_D \frac{A_0 - A}{q} - A \right) = k_1 \left[-A \left(\frac{K_D}{q} + 1 \right) + A_0 \frac{K_D}{q} \right] \quad (13a)$$

which can be solved to yield

$$\ln \frac{(K_D + q)A - K_D A_0}{q A_0} = -k_1 \frac{K_D + q}{q} t \quad (14)$$

or

$$k_1 = -\frac{1}{t} \frac{q}{K_D + q} \ln \frac{(K_D + q)A - K_D A_0}{q A_0} \quad (14a)$$

From the experimental results we find: $k_1 = 2.7 \pm 0.1 \times 10^{-3} \text{ sec.}^{-1}$ and $k_{-1} = 2.5 \pm 0.2 \times 10^{-2} \text{ sec.}^{-1}$.

In the case of added KBr, and neglecting the species containing Br^{82} , the partition mechanism is governed by eq. 1, 2, 3, and 4. However, the concentrations B , E , and F could not be determined and only their sum

$$(C_{\text{Hg}})_s = \frac{A_0}{D_{\text{Hg}} + q} \quad (15)$$

is known. Moreover, no simple analytical way for simultaneous solution of the differential equations was found. Therefore the following procedure was adopted.

(a) The proportion between the fractions E/B and F/E is 8:9 at equilibrium^{1a}; the same proportion was assumed to exist during the whole course of the reaction, while the fractions themselves vary from 0 to their equilibrium value, i.e., $k_2/k_{-2}C$ and $k_3/k_{-3}C$, respectively.

(b) From this assumption, it can be shown that at any time

$$\frac{E}{B} = {}^4/9 (\sqrt{4.5(C_{\text{Hg}})_s/B} - 3.5 - 1) \quad (16a)$$

and

$$\frac{F}{B} = \frac{2}{9}(\sqrt{4.5(C_{\text{Hg}})_s/B} - 3.5 - 1)^2 \quad (16b)$$

(c) From eq. 1, $B = (A + 1/k_1)(dA/dt)/K_D$, which yields B at any time from the values of A and dA/dt , obtained graphically.

(d) Using eq. 16a and 16b, E and F can be calculated at any time; B , E , and F are plotted against time.

(e) The values obtained from the previous steps are checked against the requirements of eq. 11 and 11a, the derivatives being obtained graphically.

(f) From eq. 1 and 2, we have

$$\frac{dB}{dt} + \frac{1}{q} \frac{dA}{dt} = k_{-2}E - k_2BC$$

Using $k_2/k_{-2} = K_3 = 8$ as found in part I yields

$$k_2 = \left(\frac{dB}{dt} + \frac{1}{q} \frac{dA}{dt} \right) / (1/8E - BC)$$

(g) From eq. 4 we have

$$k_{-3}F - k_3CE = \frac{dF}{dt}$$

Using $k_3/k_{-3} = K_4 = 9$ as found in part I yields

$$k_3 = \frac{dF}{dt} / (CE - 1/9F)$$

Figure 2a-d shows the variation with time of the species A , B , E , and F as fractions of Hg_{total} , as obtained by the above calculations. The experimental results yield the following values for the rate constants.

$$k_2 = 1.3 \pm 0.2 \times 10^{-1} \text{ kg. mole}^{-1} \text{ sec.}^{-1}$$

$$k_3 = 6.2 \pm 1.0 \times 10^{-2} \text{ kg. mole}^{-1} \text{ sec.}^{-1}$$

$$k_{-2} = 1.6 \pm 0.2 \times 10^{-1} \text{ sec.}^{-1}$$

$$k_{-3} = 6.9 \pm 1.0 \times 10^{-3} \text{ sec.}^{-1}$$

Turning to the partition of Br^{82} between the various species, we have

(a) From (5)

$$B' = \left(A' + 1/k_1 \frac{dA'}{dt} \right) / K_D$$

(b) From (5) and (6)

$$E' = \left\{ 1/k_2 \left(\frac{dB'}{dt} + \frac{1}{q} \frac{dA'}{dt} \right) + B'C' \right\}^{3/2} K_3$$

(c) From (5), (6), and (8)

$$\frac{1}{q} \frac{dA'}{dt} + \frac{dB'}{dt} + \frac{dE'}{dt} =$$

$$k_2BC' - 1/3k_{-2}E' + 3/4k_{-3}F' - k_3CE'$$

Using eq. 12 to eliminate C' , we obtain

$$F' = \left\{ \frac{1}{q} \frac{dA'}{dt} + \frac{dB'}{dt} + \frac{dE'}{dt} - k_2B' \left(\frac{A_0' - A'}{q} - B' - E' \right) + (1/3k_{-2} + k_3C)E' \right\} / (3/4k_{-3} - k_2B)$$

and C' by difference.

Using the values of k_2 , k_{-2} , k_3 , and k_{-3} obtained above gave values of C' and F' agreeing with the requirements of eq. 7, 9, and 12a. Using values different from the above by more than three times the experimental errors quoted gave negative or unacceptable values of these calculations. Inclusion of reaction A with reasonable rate constants led to distribution coefficients in disagreement with the experimental ones, and therefore this reaction was disregarded.

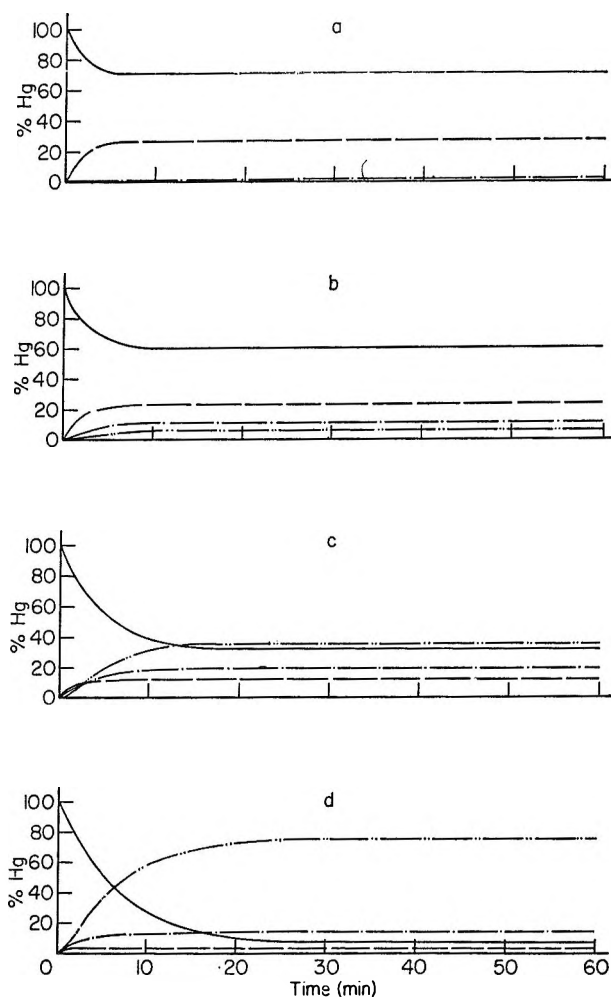


Figure 2. Variation with time of the species $(\text{HgBr}_2)_o$ (—), $(\text{HgBr}_2)_s$ (---), $(\text{HgBr}_3^-)_s$ (- · - · -), and $(\text{HgBr}_4^{2-})_s$ (— · — · —) as fractions of Hg_{total} , the nitrate melt containing: a, 0.006 m; b, 0.06 m; c, 0.2 m; and d, 0.6 m KBr, respectively.

Figure 3a-d shows the variation with time of the species A' , B' , C' , E' , and F' as fractions of $\text{Br}^{82}_{\text{total}}$, as obtained by the above calculations.

Discussion

The transfer of HgBr from the organic solvent to the nitrate melt appears to be a comparatively slow reaction. HgBr_2 is known to have tetrahedral coordination both in the organic phase⁵ and in the nitrate melt¹; however, the change from π -bonds to predominantly ionic bonds might account for the low velocity.

Since the calculations involving Br^{82} appear to be self-consistent, it may be concluded that the initial assumption of neglecting direct isotope exchange without intervention of a nitrate group is correct. In other words, the rate of addition (loss) of nitrate to (from) the coordination sphere of mercury(II) is much larger than for bromide. This was to be expected for the following reason: the replacement of one ligand group by another necessitates a transition state where the mercury is either tri- or penta-coordinated. The formation of such an unstable transition complex would require a much higher activation energy if it should involve the formation or breaking of a predominantly covalent ($\text{Hg}-\text{Br}$) rather than a predominantly ionic ($\text{Hg}-\text{NO}_3$) bond. The importance of the nitrate groups in the partition mechanism is further shown by the fact that k_2 , the rate of a reaction involving the replacement of one nitrate group out of two, is about twice as large as k_3 , the rate of a similar reaction involving the replacement of the last nitrate group. The remarkably low value of k_{-3} could be explained by added stability of the completely symmetric HgBr_4^{2-} .

Acknowledgment. Thanks are due to Dr. Y. Marcus for helpful discussion, and to Mrs. H. Ackerman for technical assistance.

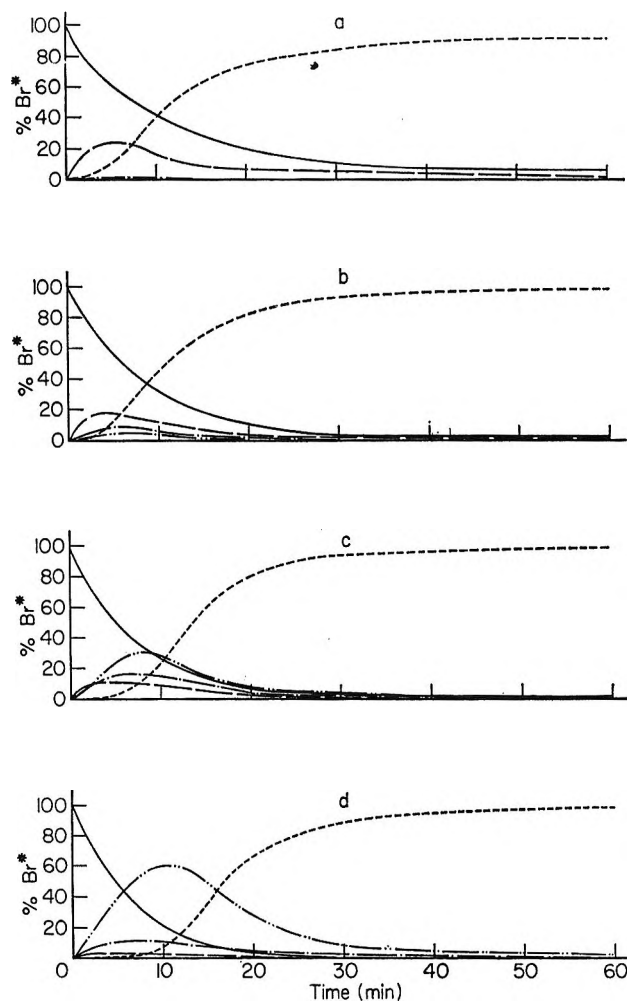


Figure 3. Variation with time of the species $(\text{HgBrBr}^*)_o$ (—), $(\text{HgBrBr}^*)_s$ (---), $(\text{HgBr}_2\text{Br}^*)_s$ (- · - · -), $(\text{HgBr}_3\text{Br}^*)_s$ (— · — · —), and $(\text{Br}^*)_s$ (----) as fractions of $\text{Br}^{82}_{\text{total}}$, the nitrate melt containing: a, 0.006 m ; b, 0.06 m ; c, 0.2 m ; and d, 0.6 m KBr, respectively.

(5) Y. Marcus, I. Eliezer, and M. Zangen, Transactions of the Tihany Symposium on Coordination Chemistry, Hungarian Academy of Science, 1964, p. 105.

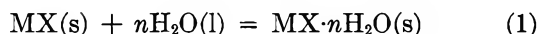
The Thermodynamics of Crystalline Hydrates

by M. F. C. Ladd and W. H. Lee

Crystallography Section and Chemistry Department, Battersea College of Technology, London S. W. 11, England
(Received November 12, 1964)

The lattice energies of some crystalline hydrates have been calculated, and the free energies of their formation from the anhydrous crystal, by the process $\text{MX}(\text{s}) + n\text{H}_2\text{O}(\text{l}) = \text{MX}\cdot n\text{H}_2\text{O}(\text{s})$, have been estimated. The factors governing the formation of crystalline hydrates are discussed.

This investigation is concerned with the factors which determine whether a simple ionic compound will crystallize from aqueous solution in the anhydrous or in hydrated form at 1 atm. pressure and 25°. In the present paper we consider the free energy change for the process



where $\text{MX}(\text{s})$ represents the anhydrous crystal and $\text{MX}\cdot n\text{H}_2\text{O}(\text{s})$ the corresponding hydrate with n molecules of water of crystallization.

We examine first the corresponding enthalpy term, ΔH_w , obtained from

$$\Delta H_w = \Delta H_{f_2} - \Delta H_{f_1} - n\Delta H_f(\text{H}_2\text{O}(\text{g})) - nL_{\text{H}_2\text{O}} \quad (2)$$

where the ΔH_f 's are standard enthalpies of formation, $L_{\text{H}_2\text{O}}$ is the latent heat of vaporization of water at 25°, and the subscripts 1 and 2 refer to the hydrated and the anhydrous crystals, respectively. The values of ΔH_w for the rare earth sulfate octahydrates—a closely-related series of compounds—are given in Table I.

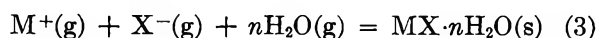
We choose the following simplified scheme to represent the process of eq. 1. We imagine the anhydrous crystal to be expanded and distorted so that the ions occupy the sites appropriate to the hydrated crystal; water molecules are then introduced so as to form the hydrated crystal. In order to study the energetics of this process, and in particular the internal energy of interaction of water molecules held mainly by one of a variety of forces (coordinating (covalent), hydrogen bonding, or ion-dipole), we need to calculate the lattice energies of (1) the anhydrous crystal, (2) the expanded crystal, and (3) the hydrated crystal.

Lattice energies of hydrates do not appear to have been calculated, or even defined, previously. To be

Table I: Lattice Energies and the Enthalpy Term, ΔH_w , for the Rare Earth Sulfate Octahydrates (kcal./mole)

	$-\Delta H_{f_1}$	$-\Delta H_{f_2}$	$-\Delta U_{1_1}$	$-\Delta U_{1_2}$	$-\Delta H_w$
Ce	953	1521	2313	2414	22
Pr	(953)	1536	2329	2445	(37)
Nd	948	1525	2351	2452	31
Sm	955	1522	2373	2473	21
Eu	952	1526	2384	2488	25
Gd	942	1519	2382	2492	31
Tb	948	1517	2414	2514	21
Dy	942	1513	2432	2536	25
Ho	938	1509	2454	2558	25
Er	933	1504	2459	2563	25
Yb	929	1497	2481	2582	22
Lu	928	1496	2486	2587	22

consistent with the usual definition of the lattice energy as the energy released in assembling the lattice units, we define the lattice energy of a hydrate $\text{MX}\cdot n\text{H}_2\text{O}$ as the energy change of the process



From the relevant Born-Haber cycles

$$\Delta H_{1_1} = \Delta H_{f_1} - \Sigma \quad (4)$$

$$\Delta H_{1_2} = \Delta H_{f_2} - \Sigma - n\Delta H_f(\text{H}_2\text{O}(\text{g})) \quad (5)$$

where Σ is the sum of the heats of formation of the gaseous ions M^+ and X^- . For example, in the case of sodium bromide

$$\Sigma = I_{\text{Na}} + S_{\text{Na}} + \frac{1}{2}D_{\text{Br}_2} + E_{\text{Br}} \quad (6)$$

in which I is the ionization potential and S the sublimation energy of the metal, D is the dissociation

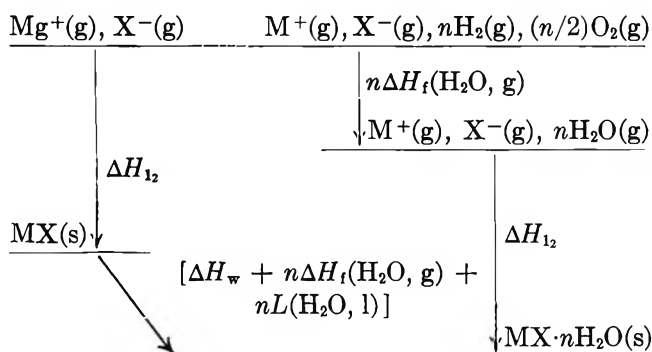


Figure 1. The modified Born-Haber cycle relating to the formation of crystalline hydrates.

energy of the bromine molecule, and E the electron affinity of the bromine atom.

The relevant energy levels are shown in Figure 1, in which it will be noticed that the term $nL(H_2O(l))$ appears only on the left-hand side of the figure. This is because of the way in which we have defined the lattice energy of the hydrated crystal; we consider the water molecules in the lattice as essentially in the gaseous state, individually bonded to ions as well as to other water molecules, whereas ΔH_w is defined by eq. 1 as involving liquid water. If we had defined the lattice energy in terms of the interaction of the ions with liquid water, the term $nL(H_2O(l))$ would have appeared explicitly in this part of the cycle.

The lattice energies ΔU_{11} and ΔU_{12} are included in Table I; the relationship between ΔU_{11} and ΔH_{11} is

$$\Delta U_1 = \Delta H_1 + mRT \quad (7)$$

where m is the number of moles of individual species per formula weight; for example, in $NaBr$, $m_1 = 2$; in $NaBr \cdot 2H_2O$, $m_2 = 4$. The sources of data for the calculation of lattice energies, *i.e.*, of ΔH_f and the components of Σ in eq. 5, have been listed previously.^{1,2}

The value of ΔH_f for $Pr_2(SO_4)_3 \cdot 8H_2O$ does not follow the general trend along this series and has been omitted in calculating the average value of ΔH_w , which is -25 ± 3 kcal./mole. Recently, Wendlandt³ has studied the dehydration of this series of compounds by differential thermal analysis; from his results we obtain the average value -28 ± 6 kcal./mole for ΔH_w . The average increment of ΔH_w per mole of water is -3.3 ± 0.5 kcal. within this series.

In contrast to these closely related compounds, we consider next a series in which the mode of attachment of the water varies, as for example in $CuSO_4 \cdot 5H_2O$ (in which the water is mainly covalently bonded to the Cu^{2+} ion), $KF \cdot 2H_2O$ (in which the water is mainly hydrogen bonded), and $BaCl_2 \cdot 2H_2O$ (in which the water

molecules are bound mainly by ion-dipole interaction). The lattice energies and the values of ΔH_w are given in Table II.

Table II: Lattice Energies and the Enthalpy Term, ΔH_w , for Miscellaneous Hydrates $MX \cdot nH_2O$ (kcal./mole)

	n	$-\Delta H_{f1}$	$-\Delta H_{f2}$	$-\Delta U_{11}$	$-\Delta U_{12}$	$-\Delta H_w$
$CaSO_4$	$1/2$	342.4	376.5	621	626	0.0
$LiOH$	1	116.5	188.8	228	242	4.0
$LiCl$	1	97.7	170.3	201	215	4.3
$BaCl_2$	1	205.6	278.4	494	508	4.5
$CaSO_4$	2	342.4	483.1	621	645	4.1
$BaCl_2$	2	205.6	349.4	494	521	7.2
$NaBr$	2	86.0	227.3	174	198	4.7
KF	2	134.5	277.0	190	215	5.9
CuF_2	2	126.9	274.5	722	739	11.0
$BeCl_2$	4	122.3	436.8	717	798	41.3
$CuSO_4$	5	184.0	544.5	733	801	19.0
$NiCl_2$	6	75.5	505.9	655	676	20.6
Na_2CO_3	10	270.3	975.6	522	644	22.3

To compare these values with one another and with those of the rare earth series, ΔH_w per mole of water of crystallization is calculated and listed in Table III.

Table III: The Enthalpy Term ΔH_w per Mole of Water of Crystallization (kcal.)

	$-\Delta H_w$		$-\Delta H_w$
Ce-Lu sulfates $\cdot 8H_2O$	3.3	$NaBr \cdot 2H_2O$	2.4
$CaSO_4 \cdot 0.5H_2O$	0.0	$KF \cdot 2H_2O$	3.0
$LiOH \cdot H_2O$	2.0	$CuF_2 \cdot 2H_2O$	5.5
$LiCl \cdot H_2O$	2.2	$BeCl_2 \cdot 4H_2O$	10.3
$BaCl_2 \cdot H_2O$	4.5	$CuSO_4 \cdot 5H_2O$	3.8
$CaSO_4 \cdot 2H_2O$	2.1	$NiCl_2 \cdot 6H_2O$	3.4
$BaCl_2 \cdot 2H_2O$	3.6	$Na_2CO_3 \cdot 10H_2O$	2.2

The manner in which the water is bound in the hydrates is not apparent from the relative magnitudes of ΔH_w . Observing the large value of ΔH_w for $BeCl_2 \cdot 4H_2O$, we next calculate ΔH_w for the dichlorides of the alkaline earth metals (Table IV). It will be seen that ΔH_w becomes less negative with increasing radius of the cations; the Pauling radii⁴ are given in Table IV. This

(1) M. F. C. Ladd and W. H. Lee, "Progress in Solid State Chemistry," Vol. I, R. C. Vickery, Ed., Pergamon Press Ltd., London, 1964.

(2) M. F. C. Ladd and W. H. Lee, *J. Inorg. Nucl. Chem.*, **11**, 264 (1959).

(3) W. W. Wendlandt and T. D. George, *ibid.*, **19**, 245 (1961).

(4) L. Pauling, "The Nature of the Chemical Bond," Cornell University Press, Ithaca, N. Y., 1948.

Table IV: Calculation of ΔH_w (kcal./mole of water) and Pauling Radii, r^+ (in Å.)

	BeCl ₂ ·4- H ₂ O	MgCl ₂ ·6- H ₂ O	CaCl ₂ ·6- H ₂ O	SrCl ₂ ·2- H ₂ O	BaCl ₂ ·2- H ₂ O
$-\Delta H_w$	10.3	5.7	3.9	3.2	3.6
r^+	0.31	0.65	0.99	1.13	1.35

is typical of the variation in ΔH_w along a series involving a common anion.

To evaluate the free energy change ΔG_w we consider next the corresponding entropy change ΔS_w for the reaction of the anhydrous crystal with water, specified in eq. 1. This would be expected to lead to a decrease in entropy, since the water molecules will lose translational and rotational degrees of freedom, or at least rotation will become hindered.

Table V: The Entropy Term ΔS_w and Related Entropies (cal./mole deg.) for the Rare Earth Sulfate Octahydrates

	S_{L_1}	ΣS_{E_1}	$-\Delta S_{f_1}$	S_{L_2}	ΣS_{E_2}	$-\Delta S_{f_2}$	$-\Delta S_w$
Ce	116	344	228	183	790	607	77
Pr	106	344	238	123	790	667	(137)
Nd	82	344	262	153	790	637	83
Sm	82	344	262	156	790	634	80
Eu	89	344	255	146	790	644	97
Gd	92	344	252	156	790	634	90
Tb	92	344	252	156	790	634	90
Dy	92	344	252	155	790	635	91
Ho	92	344	252	155	790	635	91
Yb	93	345	252	160	791	631	87
Lu	93	345	252	160	791	631	87

In Table V, ΔS_w is listed together with the relevant quantities from which it was calculated⁵; in this reference the entropies of formation, but not the absolute entropies of the anhydrous and the hydrated compounds, are listed. We may evaluate ΔS_w as follows.

The entropy of formation ΔS_f of a crystalline compound is the difference between its lattice entropy S_L and the sum of the entropies of the constituent elements in their standard states, ΣS_E ; thus, for the hydrate

$$\Delta S_{f_2} = S_{L_2} - \Sigma S_{E_2} \quad (8)$$

and for the anhydrous compound

$$\Delta S_{f_1} = S_{L_1} - \Sigma S_{E_1} \quad (9)$$

Thus from eq. 8 and 9 S_{L_1} and S_{L_2} may be calculated. We are encouraged to obtain lattice entropies in this

way because, where they have been tabulated⁶ the results are in good agreement.

The entropy change ΔS_w for the rare earth sulfate octahydrates, like the corresponding enthalpy change ΔH_w , is nearly constant. The average value of ΔS_w is -87 ± 4.5 cal./mole deg., or -10.9 ± 0.6 cal./deg. per mole of water. Thus for reaction 1 the average value of ΔG_w is 1 kcal./mole; the internal energy of interaction of water with the ions in the crystal is about 26 kcal./mole, which is insufficient to reverse the effect of the large entropy decrease. The entropy of liquid water is 16.7 cal./mole deg., and most of this is lost by the interaction of water molecules, on specific lattice sites, with the ions. We do not attach particular significance to the fact that ΔG_w is positive for certain compounds in this series; this quantity is certainly negative for the compounds of Pr, Nd, and Gd. There may be some uncertainty in the thermodynamic data used in these calculations; a change of -2 kcal./mole in ΔH_w would produce a negative ΔG_w in all cases, while changing the lattice energy by only 0.1%.

In Table VI, the entropy and free energy changes, ΔS_w and ΔG_w , are given for the crystal types exemplified in Table II. An average value for ΔS_w cannot be quoted, because the results vary widely among the different hydrates examined. The entropy and free energy changes are always negative for reaction 1, despite the fact that S_{L_2} is appreciably greater than S_{L_1} ; the entropy increase ($S_{L_2} - S_{L_1}$) in no case is able to compensate for the loss of entropy of the water.

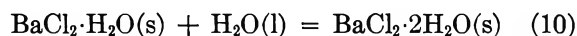
Table VI: Free Energy Data per Mole of Water of Crystallization (kcal.) and Entropy Data (cal./mole deg.) for Miscellaneous Hydrates, $MX \cdot nH_2O$

	n	$-\Delta G_w$	S_{L_1}	S_{L_2}	$(S_{L_2} - S_{L_1})$	$-\Delta S_w$
CaSO ₄	1/2	-1.6	25.5	31.2	5.7	2.7
LiOH	1	2.0	12.0	22.0	10.0	6.7
LiCl	1	1.8	16.6	24.8	8.2	8.5
BaCl ₂	1	2.5	30.0	40.0	10.0	6.7
CaSO ₄	2	0.0	25.5	46.4	20.9	13.5
BaCl ₂	2	1.4	30.0	48.5	18.5	14.9
KF	2	1.1	15.9	36.0	20.9	12.5
CuF ₂	2	2.9	20.2	36.2	16.0	17.4
BeCl ₂	4	8.1	20.5	58.1	37.6	29.2
CuSO ₄	5	1.6	27.1	73.0	45.9	37.6
NiCl ₂	6	0.9	25.6	75.2	49.6	51.4
MgCl ₂	6	4.0	21.4	87.5	66.1	33.9
Na ₂ CO ₃	10	1.4	39.3	180.3	141.0	26.0

(5) P. G. Maslov and Y. P. Maslov, *Izv. Vysshikh, Ucheb. Zavedenii Khim. i Khim. Tekhnol.*, 2, 516 (1959).

(6) W. M. Latimer, "Oxidation Potentials," 2nd Ed., Prentice-Hall Co., Inc., New York, N. Y., 1956.

The value of $-\Delta G_w$ for $\text{BaCl}_2 \cdot \text{H}_2\text{O}$ from Table VI is greater than that for $\text{BaCl}_2 \cdot 2\text{H}_2\text{O}$, per mole of water; for the change



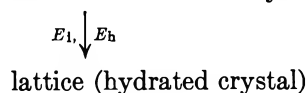
ΔG_w must be only -0.3 kcal./mole. Successive water molecules produce progressively smaller contributions to the free energy change of hydrate formation; this is well illustrated by the magnesium chloride hydrates, $\text{MgCl}_2 \cdot n\text{H}_2\text{O}$

	$n = 1$	$n = 2$	$n = 4$	$n = 6$
$-\Delta G_w$ (kcal./mole)	7.8	12.3	22.0	24.0
$-\Delta G_w/n$ (kcal./mole of H_2O)	7.8	6.2	5.5	4.0

We have considered the thermodynamics of reaction 1; as expected, this reaction is accompanied by a decrease in free energy where a stable hydrate is formed by this process. We conclude this paper by suggesting reasons why certain of the alkali metal halides crystallize from solution, under normal conditions, in hydrated form.

In Figure 2, *H* indicates that a hydrate is formed by the corresponding halide.⁷ If we envisage the formation of the hydrate according to the scheme already outlined

lattice (anhydrous \longrightarrow expanded lattice (anhydrous crystal) crystal)



the process of expanding the anhydrous lattice and of rearranging its structure to that of the hydrated crystal

	F	Cl	Br	I
Li		H	H	H
Na		(H)	H	H
K	H			
Rb	H			
Cs	H			

Figure 2. The occurrence of hydrates in the alkali metal halide series [(H), below -5°].

does work against the coulombic energy U_c ; the hydrate then stabilizes its structure by ion-dipole interactional energy E_i and/or hydrogen-bond energy E_h . Considering the chlorides and bromides of the alkali metals, we suggest that $(E_i + E_h)$ is the determining factor in hydrate formation. For example, although U_c is less negative for potassium bromide than for sodium or lithium bromides, $(E_i + E_h)$ is also less and cannot stabilize a hydrated form of potassium bromide. In the case of potassium fluoride, U_c is much more negative than in potassium bromide, but E_h is enhanced by the formation of F-H-O bonds and stabilizes the hydrate structure. Presumably, in sodium fluoride and lithium fluoride the relative magnitudes of these changes are reversed, and stable hydrates are not formed.

In subsequent work we shall consider the quantitative aspects of lattice expansion and hydrate formation in terms of this scheme.

(7) "Supplement to Mellor's Comprehensive Treatise on Inorganic and Theoretical Chemistry," John Wiley and Sons, Inc., New York, N. Y. Vol. II, Suppl. II, 1961, and Vol. II, Suppl. III, 1963.

Chemical Shifts in the Nuclear Magnetic Resonance Absorption for Oxygen-17 in Oxy Ions¹

by J. A. Jackson and H. Taube

University of California, Los Alamos Scientific Laboratory, Los Alamos, New Mexico
(Received November 16, 1964)

Chemical shifts in the oxygen-17 n.m.r. absorptions for the bridging and terminal oxygens of $\text{Cr}_2\text{O}_7^{2-}$ are reported. The broadenings of these signals, and of that for the solvent caused by adding acid, are interpreted as arising from the operation of the $\text{Cr}_2\text{O}_7^{2-}\text{-HCrO}_4^-$ equilibrium catalyzed by H^+ . The specific rate k_2 multiplying the function $(\text{H}^+)(\text{Cr}_2\text{O}_7^{2-})$ is calculated as $1.3 \times 10^4 \text{ m}^{-1} \text{ sec.}^{-1}$ in $3.1 \text{ m Na}_2\text{Cr}_2\text{O}_7$ at $15 \pm 1^\circ$. The n.m.r. absorption of MnO_4^- is shifted by Co^{+2} , suggesting appreciable complex formation; it is broadened by MnO_4^{2-} , and this broadening can be accounted for by electron exchange between MnO_4^- and MnO_4^{2-} . A solution of SO_2 in water shows a single peak, at the position expected for the averaging of the SO_2 and solvent peaks. Exchange of oxygen between SO_2 and H_2O as solvent is rapid, the half-time being less than 10^{-3} sec. Shifts for a number of oxy ions not previously reported are included in this paper.

Introduction

Chemical shifts in the nuclear magnetic resonance (n.m.r.) absorption for oxygen-17 in oxy ions have been reported by Figgis, Kidd, and Nyholm.² Early in our work exploring n.m.r. effects for O^{17} in solutions, we made a survey of chemical shifts for oxy ions. Where we have measurements on the same ions, namely for MnO_4^- , CrO_4^{2-} , SeO_4^{2-} , MoO_4^{2-} , ClO_4^- , ClO_3^- , and CO_3^{2-} , our values agree with theirs, within the limits of experimental error, which for our measurements we assess as 0.1 part in 10^4 (10 p.p.m.). We have observations for a number of oxy ions not reported on by Figgis, *et al.*, which we deem worthy of publication even though refined measurement with samples enriched in O^{17} may reveal effects which were hidden from us. At the very least, our data can help to guide the initial efforts of others planning research in this field. In particular, we wish to report our results for solutions of $\text{Na}_2\text{Cr}_2\text{O}_7$. We have observed the peak for the bridging oxygen displayed separately from that of the terminal (nonbridging) oxygen, and have studied the effect of acid in broadening these signals, and the signal for the oxygen contained in the solvent.

Experimental

The spectra were taken at 6, 7, or 8 Mc. on a Varian wide-line n.m.r. spectrometer as described previously.³ Unless otherwise stated, the samples were in H_2O of normal abundance in O^{17} (0.04%) or in D_2O enriched to about 0.1% O^{17} . All shifts ($\Delta H/H_0$) are reported as parts per 10^4 , a paramagnetic shift being given a negative sign. The temperature in all the experiments was $20 \pm 1^\circ$.

Results

The System $\text{Cr}_2\text{O}_7^{2-} + \text{H}_2\text{O}$. In Figure 1 is displayed the n.m.r. spectrum in the dispersion mode for a solution approximately 2 m in $\text{Na}_2\text{Cr}_2\text{O}_7$ made up in water ca. 1.4% in O^{17} . We observe three peaks lying at +0.07, -3.38 ± 0.05 , and -10.90 ± 0.05 relative to a sample of pure water enriched in O^{17} . The intense absorption at the left is evidently that of the

(1) Work done under the auspices of the U. S. Atomic Energy Commission.

(2) B. N. Figgis, R. G. Kidd, and R. S. Nyholm, *Proc. Roy. Soc. (London)*, **A269**, 469 (1962).

(3) J. A. Jackson, J. F. Lemons, and H. Taube, *J. Chem. Phys.*, **38**, 836 (1963); **32**, 553 (1960); W. B. Lewis, J. A. Jackson, J. F. Lemons, and H. Taube, *ibid.*, **34**, 694 (1962).

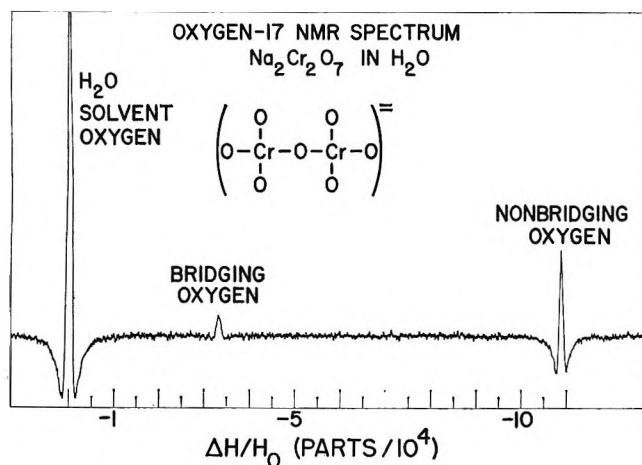


Figure 1. Oxygen-17 n.m.r. spectrum of $\text{Na}_2\text{Cr}_2\text{O}_7$ ($\sim 2 m$) in water (enriched to $\sim 1.4\%$ in O^{17}). Derivative of dispersion.

solvent, that of intermediate intensity at the right we attribute to the terminal oxygens of $\text{Cr}_2\text{O}_7^{-2}$ (our shift is close to that reported by Figgis, *et al.*,² but outside the limits of error placed by them on their results), and that of lowest intensity we attribute to the bridging oxygen. This assignment is consistent with the intensity of the peak at the right compared to that at -3.38 (the ratio lies between 5 and 7) and with the behavior of this peak when acid is added, as will be discussed more fully later. Figure 2a shows a trace in the absorption mode. Figure 2b shows an absorption trace at higher gain in which we observed a peak of still lower intensity at -9.0 which is probably caused by HCrO_4^- present at equilibrium with $\text{Cr}_2\text{O}_7^{-2}$ (note: CrO_4^{-2} lies at -8.3). Equilibrium quotients applicable to the very concentrated solutions we found it necessary to use have not been reported. Those applicable⁴⁻⁶ to lower ionic strength place the equilibrium concentration of HCrO_4^- at ~ 0.3 and this is probably accurate to better than one order of magnitude. The peak width for HCrO_4^- is expected to be particularly sensitive to acid; this, and the low intensity, may explain why we did not observe it in all samples.

The width of the absorption peak for solvent water in the presence of $\text{Cr}_2\text{O}_7^{-2}$ is essentially identical with that which we observe for pure water and thus the operation of the equilibrium process



is not contributing to broadening of the n.m.r. signals. The rate of hydration of $\text{Cr}_2\text{O}_7^{-2}$ has been measured by oxygen exchange studies,⁷ and by a relaxation technique,⁸ and values for the specific rate for the first-order process of $3.3 \times 10^{-3} \text{ sec.}^{-1}$ ⁴ and $2.7 \times 10^{-2} \text{ sec.}^{-1}$,⁵ respectively, have been reported. These

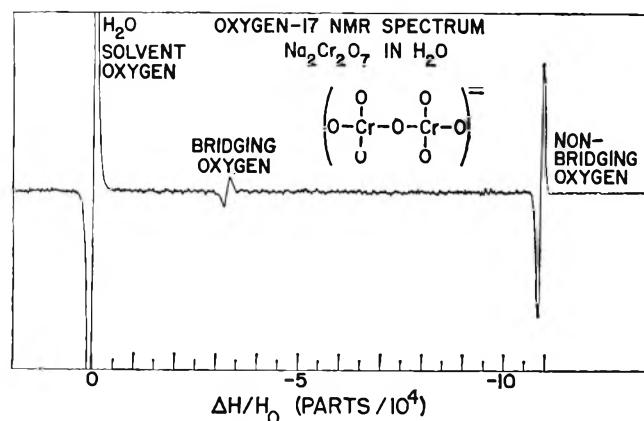


Figure 2a. Oxygen-17 n.m.r. spectrum of $\text{Na}_2\text{Cr}_2\text{O}_7$ ($\sim 2 m$) in water (1.4% O^{17}). Derivative of absorption.

values are not in conflict. Some of the oxygen exchange studies were done in $3 M$ solution, and the calculation of the specific rate quoted involved the use of equilibrium quotients⁶ which are not known for such concentrated solutions. The relaxation technique was applied to solutions of ionic strength $0.1 M$. Even using the larger of the specific rates, no measurable contribution to line broadening by the process k_1 ($\text{Cr}_2\text{O}_7^{-2}$) is to be expected.

The line widths are insensitive to the introduction of Na_2CrO_4 at low concentrations, but are sensitive to the introduction of HClO_4 . In Figure 3, we show the dispersion mode for the solution used for the trace of Figure 1 but with $0.06 M$ HClO_4 added. The marked broadening of the water and terminal oxygen peaks is evident, and the peak for the bridging oxygen has been so much broadened as not to appear.

In Figure 4 we show data on the line width of the three peaks as a function of concentration of acid in a solution $3.1 m$ in $\text{Na}_2\text{Cr}_2\text{O}_7$. The line broadening is consistent with a linear variation in (H^+) but the data are too sparse and imprecise to demonstrate that the variation really depends exactly on the first power of (H^+) .

The broadening is greatest for the bridging oxygen and least for the solvent. The broadening for the solvent, though small, is unmistakable, and shows that the solvent is part of the exchange pool which is causing

(4) W. M. Latimer, "Oxidation Potentials," Prentice-Hall, Inc., New York, N. Y., 1952.

(5) At $\mu = 0.1$, G. Schwarzenbach and J. Meier, *J. Inorg. Nucl. Chem.*, **8**, 302 (1957).

(6) At $\mu = 3.0$, Y. Sasaki, *Acta Chem. Scand.*, **16**, 719 (1962).

(7) H. Baldwin, private communication.

(8) J. H. Swinehart and G. W. Castellan, *Inorg. Chem.*, **3**, 278 (1964).

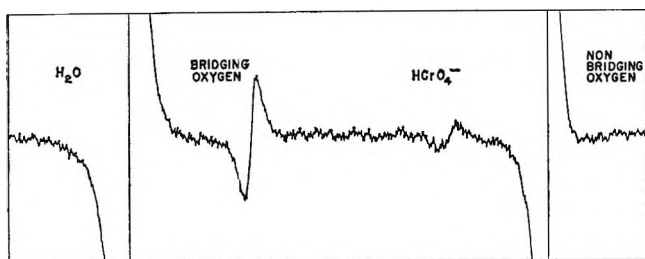
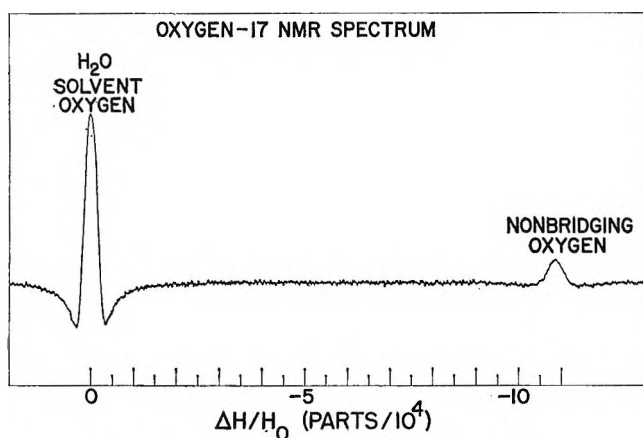


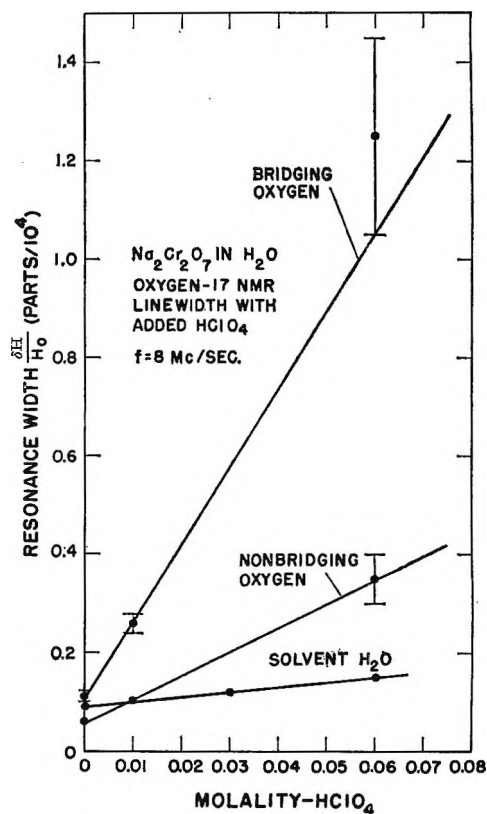
Figure 2b. Derivative of absorption at higher gain.

Figure 3. Oxygen-17 in 2 *m* Na₂Cr₂O₇ with 0.06 *M* HClO₄ added. Derivative of dispersion.

the broadening. We shall show that the effects are consistent with the operation of equilibrium 1, the hydration of Cr₂O₇⁻² now not being spontaneous, but catalyzed by H⁺.

If we let the rate of the process $k_2(\text{H}^+)(\text{Cr}_2\text{O}_7^{-2})$ as given in $m^{-1} \text{ sec}^{-1}$ of water, oxygen be given by R , then the rates of the three exchange processes are: bridging to nonbridging = $\frac{3}{4}R$, nonbridging to water = $\frac{3}{4}R$, and water to bridging = $\frac{1}{8}R$, with, of course, forward and reverse rates the same in each case. The derivation of two of the relations will be given to illustrate how they come about. The reaction of H₂O with Cr₂O₇⁻² produces HCrO₃O_b⁻ and HCrO₃O_w⁻, where subscripts w and b identify solvent and bridging oxygen. When HCrO₃O_b⁻ and HCrO₃O_w⁻ recombine to form Cr₂O₇⁻², solvent oxygen is restored to solvent in $\frac{1}{8}$ of the events, becomes bridging oxygen in $\frac{1}{8}$ of them, and becomes nonbridging in $\frac{6}{8}$ of them.

To relate these rates to the line broadening, which from the shapes of Figure 1, we take at 0.06 *m* H⁺ to be 7.5×10^2 , 2.3×10^2 , and 48 c.p.s. for bridging, terminal, and solvent oxygen, respectively, we must take account of the abundances of the oxygen species. For our treatment we assume that $\delta H/H \sim 1/T_2$ and

Figure 4. Line width of O¹⁷ resonance in aqueous Na₂Cr₂O₇ as a function of acidity.

thus, in an approximate manner, from the broadening observed for each of the species of oxygen, we can calculate the rate R . It should be noted that the total fluxes for the bridging, terminal, and solvent positions are $\frac{7}{8}R$, $1.5R$, and $\frac{7}{8}R$, and that the concentrations of the three kinds of oxygen in g-atoms/1000 g. of H₂O are 3.1, 18.6, and 55.5, respectively. Thus we have the relations

$$\frac{7}{8}R = 3.1 \times 7.5 \times 10^2 \times \sqrt{3}/2$$

$$1.5R = 18.6 \times 2.3 \times 10^2 \times \sqrt{3}/2$$

$$\frac{7}{8}R = 55.5 \times 48 \times \sqrt{3}/2$$

where the factor $\sqrt{3}/2$ is to convert width between points of maximum slope to widths at half-height. These yield for R the values of 2.3×10^3 , 2.5×10^3 , and $2.6 \times 10^3 m^{-1} \text{ sec}^{-1}$. The three self-consistent values of R prove that the line widths are due to uncertainty broadening. Taking the mean value of R to be $2.5 \times 10^3 m^{-1} \text{ sec}^{-1}$, the specific rate for the hydration of Cr₂O₇⁻² by the path $k(\text{H}^+)(\text{Cr}_2\text{O}_7^{-2})$ is $1.3 \times 10^4 m^{-1} \text{ sec}^{-1}$. The specific rate would be approximately 30% greater on a molar basis. Using either scale, it is clear that the rate at which the Cr₂O₇⁻²

HCrO_4^- equilibrium is established is profoundly affected by acidity, in accord with the qualitative observation of Schwarzenbach and Meier.⁵

No appreciable shifts in the positions of the H_2O and terminal oxygen peaks are observed even at 0.06 M (H^+). The peak for the bridging oxygen, however, seems to have shifted slightly toward that for the terminal oxygens and appears at -3.5 when (H^+) = 0.06 M .

In another series of experiments at higher acid, the concentration of $\text{Na}_2\text{Cr}_2\text{O}_7$ was varied, keeping the ionic strength constant by using $\text{Na}_2\text{S}_2\text{O}_8$ to replace $\text{Na}_2\text{Cr}_2\text{O}_7$. The results of these experiments are summarized in Table I.

Table I: Broadening in N.m.r. Absorption of O^{17} in H_2O Caused by Acid Dichromate

($\text{Na}_2\text{Cr}_2\text{O}_7$) + ($\text{Na}_2\text{S}_2\text{O}_8$) = 0.8 M ; (HClO_4) = 2 M		
Expt. no.	($\text{Na}_2\text{Cr}_2\text{O}_7$)	Line width
1.0	0.00	0.10
1.1	0.16	0.22 ± 0.02
1.2	0.36	0.35 ± 0.1
1.3 ^a	0.80	0.75 ± 0.1

^a Solution 1.3 is 0.96 m $\text{Na}_2\text{Cr}_2\text{O}_7$ and 2.4 m HClO_4 .

The line broadening is at least approximately linear in (H^+). It is furthermore approximately of the magnitude expected from the operation of the mechanism discussed more fully above. If the difference in ionic strength are neglected, the broadening observed in experiment 1.3 is expected to be 12 times that for the experiment of highest acidity shown in Figure 1. The actual ratio of the broadenings is a factor of 11 ± 3 . The peak observed in the data shown in Table I is by no means that resulting from the coalescence of the three component peaks. The water peak has shifted to -0.30 for the solution used in experiment 1.3; if the rate of exchange were so rapid that the peaks would coalesce, the resulting peak would be expected at *ca.* -1.1 , that is assuming that the nature of $\text{Cr}_2\text{O}_7^{2-}$ is not altered by adding 2 M HClO_4 to the solution.

Despite the fact that substitution in Cr(III) is slow, chromate complexes of Cr(III) form rapidly⁹ because bond rupture can take place at the Cr(VI) rather than the Cr(III) center. However, no shift was observed in the absorption peak of the terminal oxygen in $\text{Cr}_2\text{O}_7^{2-}$ when 0.6 M $\text{Cr}(\text{NO}_3)_3$ was added to a 3.5 M solution of $\text{Na}_2\text{Cr}_2\text{O}_7$. This result may merely mean that although formation of the $\text{Cr}_2\text{O}_7^{2-}$ complexes is rapid compared to those of most Cr(III) complexes,

the process is still too slow to make the bound and unbound $\text{Cr}_2\text{O}_7^{2-}$ equivalent with respect to n.m.r. absorption.

Some Observations with MnO_4^- in Water. Solutions of MnO_4^- were prepared by dissolving NaMnO_4 of normal isotopic composition in water enriched in O^{17} to the level of 1.8%. No attempt was made to measure the rate of exchange, but it was found to be substantially complete in 5 days at room temperature, in 0.5 M HClO_4 or 0.2 M NaOH . In each solution MnO_2 was also present because the solid sodium permanganate had undergone some decomposition on storage and there is the possibility that the oxide increased the rate of exchange (the solutions were filtered before the n.m.r. spectra were taken).

Oxygen-17 in MnO_4^- was found at -12.3 ± 0.1 parts/ 10^4 with respect to pure H_2O^{17} . The line width for MnO_4^- in acid solution is about 0.45 part/ 10^4 and the line shape gave evidence of saturation even at relatively low radiofrequency power levels.

The effect of Co^{+2} on the n.m.r. absorptions for MnO_4^- was investigated, for the interest this has in comparison with ClO_4^- which has the same charge and geometry. In 0.36 M MnO_4^- , a concentration of 0.43 M $\text{Co}(\text{ClO}_4)_2$ caused a shift of -0.48 ± 0.05 part/ 10^4 from the normal position of -12.3 . This is much greater than the shift of O^{17} in ClO_4^- (less than 0.2 part/ 10^4 from the normal ClO_4^- position of -2.8 with respect to pure H_2O^{17}) under the same conditions.

Significant conversion of MnO_4^- to a complex is required to produce a shift of the magnitude recorded, but these data provide no firm basis for calculating an equilibrium constant for the association. An estimate can be made if it is assumed that the molal shift for each MnO_4^- oxygen is the same as that for a water oxygen. Then for each species, the molal shift at constant (Co^{+2}) is proportional to the bound oxygen compared to the total. For the solvent, this ratio for our solution is approximately $(6 \times 0.4)/52$ (the coordination number of Co^{+2} is taken as 6), and the shift for the solvent was measured as -7.3 ± 0.2 parts/ 10^4 . Thus the ratio bound to total for MnO_4^- can be calculated as $(6 \times 0.4)/52 \times (0.48)/7.3 = 0.003$ and the equilibrium quotient for the association constant as $0.003 \times 4/0.4 = 0.03$. The factor four enters because for each permanganate oxygen directly bound to Co^{+2} , four are contained in the complex.

Unfortunately, there are no comparative data which give us a means of judging how good the assumption

(9) E. L. King and J. A. Neptune, *J. Am. Chem. Soc.*, **77**, 3186 (1955).

we introduced is, but it seems likely that it is good to at least one order of magnitude.

The O^{17} n.m.r. absorption in MnO_4^- for the solution in 0.2 M NaOH showed much less tendency to saturate than in acid solution. When the alkalinity was increased to 2.5 M and enough NaI was added to generate ca. 0.01 M MnO_4^{2-} , the relaxation time increased as evidenced by the fact that the absorption showed a greater tendency to saturate.

When enough NaI was added to generate 0.08 M MnO_4^{2-} , the absorption peak was broadened by 0.5 part/ 10^4 to about 1.0 part/ 10^4 . This effect we can with some confidence ascribe to electron exchange between MnO_4^- and the paramagnetic species MnO_4^{2-} . From the observed broadening and the concentrations (0.7 M MnO_4^- and 0.08 M MnO_4^{2-}) we calculate for the specific rate of the exchange process the value $7 \times 10^3 M^{-1} sec.^{-1}$ which can be compared to $3 \times 10^3 M^{-1} sec.^{-1}$ at 21.0° and $\mu = 0.16$ as obtained by isotopic tracer methods and $4.5 \times 10^3 M^{-1} sec.^{-1}$ at 15.0° and $\mu = 1.3$ as interpolated from the results of n.m.r. measurements¹⁰ using Mn^{55} . Allowing for the differences in ionic strength, our value is consistent with those which have been published.^{10,11}

We are unable to explain the change in the n.m.r. absorption characteristics of MnO_4^- caused by the first increment in MnO_4^{2-} . In general terms, the behavior observed means that a potent agent for relaxing the nuclear spins was generated in the slightly alkaline solution and was destroyed by the first portion of sodium iodide which was added.

Even at 0.1 M MnO_4^{2-} , no shift in the peak position for MnO_4^- is observed. This presumably means that the absorption peak for MnO_4^{2-} experiences a paramagnetic shift so large that the frequency corresponding to the MnO_4^- - MnO_4^{2-} peak separation is large compared to the rate of exchange.

The SO_2 - H_2O System. Observations with SO_2 in water show that oxygen exchange between solute and solvent is so rapid that the two peaks coalesce. In one experiment, enough SO_2 was added so that we were dealing with a two-phase system. Peaks at -5.2 and -0.83 were observed, the former ascribable to liquid SO_2 and the latter to a coalescence of the water peak with that of SO_2 dissolved therein. This peak is quite close to that expected for the averaged peak, assuming that the species SO_2 in water has the same shift as it has in the liquid (*i.e.*, its chemical nature is unaltered by water) and taking into account the relative amounts of SO_2 and H_2O oxygen in the aqueous phase. There appear to be no solubility data for our conditions $\pm 15^\circ$ but an estimate of the solubility can be made from data covering the temperature range

20 to 60°. If we assume that solubility is proportional to pressure, correct for the change in activity of SO_2 caused by the dissolution of H_2O ¹³ in liquid SO_2 assuming Raoult's law, and extrapolate the data to our temperature, we calculate that the aqueous phase contains 5.2 g.-atoms of H_2O oxygen for each g.-atom of SO_2 oxygen. With this proportion of the two kinds of oxygen, the averaged peak would be expected at -0.84 (-0.83 observed). This agreement indicates that no large fraction of the SO_2 is converted to a form such as H_2SO_3 , a conclusion consistent with that based on Raman work.¹⁴ Sulfurous acid would be expected to have shifts fairly close to those recorded for Na_2SO_3 and $NaHSO_3$ (*vide infra*). Since the SO_2 - H_2O peaks coalesce, a lower limit on the rate of oxygen exchange between SO_2 and H_2O can be calculated. If the rate of exchange is defined by the equation $R = k(SO_2)$, the value of k must exceed $10^3 sec.$, a value somewhat outside the limits on the rate of hydration set by von Büнау and Eigen.¹⁵

The solubility of H_2O in SO_2 is approximately 0.04 g.-atom of H_2O oxygen for each g.-atom of SO_2 -oxygen. If exchange were rapid in the SO_2 phase, a shift from -5.2 to -5.0 would be expected, but no appreciable shift is observed. It is of course entirely in order that exchange be much slower when SO_2 is solvent than when H_2O is solvent.

The chemical shift we observed for SO_3^{2-} was -2.35 , and for 5 M $NaHSO_3$,¹⁶ it was -1.67 . In the latter solution, HSO_3^- and $S_2O_6^{2-}$ are probably in labile equilibrium. When 0.5 M HCl is added, the water peak is shifted to -0.30 ± 0.05 . The position of the S(IV) peak is left unaltered, probably because of compensating effects—on the one hand, formation of SO_2 with a large paramagnetic shift, and on the other, admixture with water oxygen. Both the H_2O and " HSO_2^- " peaks are broadened by the addition of acid. The dynamic processes occurring in this system can probably be studied by the O^{17} n.m.r. technique, but oxygen at a higher level of enrichment than we had at hand when these experiments were done will be needed to unravel the complex effects.

(10) O. E. Meyers and J. C. Sheppard, *J. Am. Chem. Soc.*, **83**, 4739 (1961); see also A. D. Brett and W. M. Yen, *ibid.*, **83**, 4516 (1961).

(11) J. C. Sheppard and A. C. Wahl, *ibid.*, **79**, 1020 (1957).

(12) W. L. Beuschlein and L. O. Simensen, *ibid.*, **62**, 610 (1940).

(13) K. Wickert, *Z. anorg. allgem. Chem.*, **239**, 89 (1938).

(14) H. Nisi, *Japan. J. Phys.*, **6**, 1 (1930); P. Fadda, *Nuovo Cimento*, **9**, 168 (1932); W. J. Nijveld and H. Gerding, *Nature*, **137**, 1060 (1936).

(15) G. von Büнау and M. Eigen, *Z. physik. Chem. (Frankfurt)*, **7**, 108 (1956).

(16) $S_2O_6^{2-}$ is probably the dominant form in these solutions: H. Simon and H. Kriegsmann, *Ber.*, **89**, 2442 (1956); H. Simon and K. Waldman, *Z. anorg. allgem. Chem.*, **283**, 359 (1956); **281**, 135 (1955).

Miscellaneous Oxy Ions. For a number of oxy ions, absorption only at the solvent position was observed. For a number of solutions the absorption was broader than for pure water, but we are not certain whether this was caused by the increased viscosity of the salt solutions or by a more chemical effect. Absorption only at the solvent position was observed for the following solutions: 4.5 *M* H₃PO₄, 3 *M* NaH₂PO₄, 2 *M* Na₆(PO₃)₆ (broad), 1.5 *M* H₃AsO₄ + 1.5 *M* NaH₂AsO₄, 6 *M* NaAlO₂, 1.7 *M* Na₂SiO₃, 2.5 *M* NaClO₂, and 6 *M* NaClO. For none of these, with the possible exception of the aluminate and arsenate, is exchange of oxygen between the anion and solvent so rapid that the solvent and oxygen peaks coalesce; even if this were the case for these two species we would conclude that the chemical shift for oxygen in the oxy ion is not significantly different from that for water, because no shift

(within ± 0.05 part in 10^4) in the water peak is observed. For the other solutions, either the oxy ion peak is so broadened, presumably by a quadrupole interaction, as to be undetectible, or the peaks coincide with those for water. A simple experiment with the solution of phosphoric acid served to demonstrate that in this case the latter situation obtains. When about 0.2 *M* Co(ClO₄)₂ is present, the water peak is broadened and shifted to -2.9 ; another peak, quite broad, can be discerned at -1.7 , and this is undoubtedly the peak for H₃PO₄, apparently also shifted and broadened by Co⁺². When a similar experiment was done with the arsenate solutions, a single broad peak at -3.5 was observed.

Acknowledgments. We wish to thank Dr. B. B. Mc-Inteer and Mr. R. M. Potter of this laboratory for providing the supply of enriched oxygen-17.

Catalytic Deuterium-Exchange Reactions with Organics. XIX.¹ π -Complex

Adsorption in the Exchange of the Alkylbenzenes

by J. L. Garnett and W. A. Sollich-Baumgartner

Department of Physical Chemistry, The University of New South Wales, Kensington, N.S.W., Australia
(Received November 19, 1964)

A theory for the π -complex adsorption of aromatic molecules on transition metal catalysts has been described in detail. The importance of this mode of interaction both on reagent displacement effects and the activation energy in C-H bond rupture has been discussed. Two new mechanisms, termed the associative and dissociative π -complex substitution mechanisms, have been proposed. The latter mechanism is of major importance in heavy water-aromatic exchange and has certain advantages in the interpretation of these reactions when compared with conventional associative and dissociative mechanisms. The concept of π -complex adsorption has been evaluated using data from the deuteration of alkylbenzenes. Consistent with π -complex adsorption, alkylbenzenes adsorb less strongly than most polycyclic aromatics. Adsorption strength decreases with increasing bulk and increasing symmetry of the methyl substituent. Orientation effects, trends in exchange rates of unhindered ring positions, and comparative rates of aromatic and aliphatic hydrogen exchange in the alkylbenzenes confirm the relative importance of the dissociative π -complex substitution mechanism.

Introduction

Isotopic hydrogen exchange reactions on group VIII transition metal catalysts involving aromatic hydrocarbons and deuterium oxide have recently been interpreted by a new mechanism based on π -complex adsorption, termed the dissociative π -complex substitution mechanism.^{2,3} The role of π -complexes in catalytic reactions has been the subject of a number of recent publications.⁴⁻⁷ It is the purpose of the present paper to develop more fully the concept of π -complex adsorption on transition metal catalysts with particular reference to the mechanism of aromatic exchange reactions, using data from the deuteration of a series of alkylbenzenes. This aromatic series was chosen because of its suitability for distinguishing between opposing factors governing the strength of π -complex adsorption.

π -Complex Adsorption Theory

π -Complex adsorption not only forms the basis of new catalytic reaction mechanisms but also explains important properties exhibited by aromatic reagents in

catalysis such as (i) the large differences in adsorption strength of different aromatic molecules and (ii) the greater ease of C-H bond rupture of aromatic molecules in comparison to aliphatic molecules.

Differences in adsorption strength are important when molecules adsorb on identical sites, *e.g.*, deuterated benzene and diphenyl,⁸ since the more weakly adsorbed reagent will be displaced from the catalyst with a subsequent decrease in exchange rate. The large differences in adsorption strengths observed in similar molecules such as diphenyl and naphthalene,

(1) Part XVIII, *J. Catalysis*, in press.

(2) (a) J. L. Garnett and W. A. Sollich, *Australian J. Chem.*, **14**, 441 (1961); (b) J. L. Garnett and W. A. Sollich, *ibid.*, **15**, 56 (1962).

(3) J. L. Garnett and W. A. Sollich, *J. Catalysis*, **2**, 350 (1963).

(4) E. Crawford and C. Kemball, *Trans. Faraday Soc.*, **58**, 2452 (1962).

(5) J. J. Rooney, *J. Catalysis*, **2**, 53 (1963).

(6) G. C. Bond, "Catalysis by Metals," Academic Press, New York, N. Y., 1962, p. 313.

(7) Y. Barron, D. Cornet, G. Maire, and F. G. Gault, *J. Catalysis*, **2**, 152 (1963).

(8) J. L. Garnett and W. A. Sollich, to be published.

where van der Waals adsorption is approximately equal, are difficult to explain in the absence of toxic side reactions⁸ by conventional associative⁹ and dissociative¹⁰ chemisorption theories since carbon-metal σ -bonds are effectively of constant strength in different aromatic molecules. π -Complex adsorption, however, provides a satisfactory interpretation of these differences since the strength of bonding in aromatics depends on several parameters which differ appreciably from one aromatic molecule to another.

π -Complex adsorption may be treated in terms of Mulliken's charge-transfer theory¹¹ but differs from simple charge-transfer adsorption¹² by involving both the forward and back donation of π -electrons.¹³ A wave mechanical description of this bond involves the linear combination of three wave functions

$$\psi(D,A) = a\psi_0(DA) + b\psi_1(D^+A^-) + c\psi_2(D^-A^+)$$

ψ_0 , being the wave function corresponding to a structure of the complex where bonding of the electron donor (D) and the electron acceptor (A) is affected by classical intermolecular forces; ψ_1 and ψ_2 correspond, respectively, to structures of the complex in which an electron has been transferred from the donor (aromatic) to the acceptor (catalyst) and conversely from the acceptor to the donor. A quantitative relationship has previously been derived for the heats of adsorption of strong bases on strong acid sites¹² where only ψ_0 and ψ_1 need to be considered. A corresponding treatment for π -complex adsorption involving three wave functions is more complicated, so that only a qualitative account can be given at the present time. In terms of charge-transfer theory, π -complex adsorption should depend on the following factors: (i) the ionization potentials and electron affinities of the organic adsorbate and the metal catalyst (which was held constant by confining the present investigation to platinum); (ii) symmetries of aromatic bonding and antibonding orbitals (orientation principle) which, in the case of multinodal orbitals, can lead to decreased adsorption strength by internal cancellation; (iii) steric hindrance effects, which influence bonding strengths by decreasing the overlap and resonance integrals.

The second important catalytic property of aromatic molecules, namely, the ease with which C-H bond rupture occurs on catalyst surfaces, may also be interpreted by π -complex adsorption and the reaction mechanisms based on this new kind of interaction (see below). The ease of C-H bond rupture in aromatics may in part be due to a lowering of the activation energy by π -complex adsorption. The process by which this type of adsorption may lower the activation energy of a catalytic reaction more effectively than the

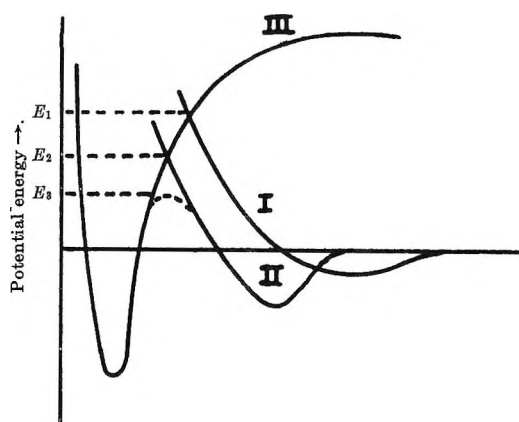


Figure 1. Decrease of activation energy in dissociative chemisorption by van der Waals adsorption (E_1), π -complex adsorption (E_2), and resonance effects (E_3): curve I, van der Waals adsorption; curve II, π -complex adsorption; curve III, chemisorption (carbon-metal σ -bond); horizontal axis, distance from metal surface.

weaker van der Waals adsorption is shown in Figure 1, where curve I denotes the van der Waals adsorption of a molecule while curve II represents the stronger interaction from π -complex adsorption. The points of intersection of these curves with curve III (Morse potential energy curve of the carbon-metal bond) correspond to the respective activation energies (E_1 , E_2) necessary for dissociative chemisorption by the two modes of adsorption. Resonance effects in the transition state (broken line) may further lower the activation energy (E_3). A more detailed description of this resonance phenomenon is given in the discussion of the dissociative π -complex substitution mechanism.

π -Complex Exchange Mechanism

As a consequence of π -complex adsorption, two new mechanisms, the associative and dissociative π -complex substitution mechanisms (eq. I-IV), have been proposed for the exchange of organic molecules on a catalyst surface.^{2a,3} In the dissociative π -complex substitution mechanism the horizontally adsorbed π -complexed aromatic (eq. I) reacts with a metal radical (active site) by a substitution process. (Plane of ring is essentially parallel to catalyst surface.) During this reaction the molecule rotates through 90° and changes

(9) J. Horiuti and M. Polanyi, *Nature*, **132**, 819 (1933).

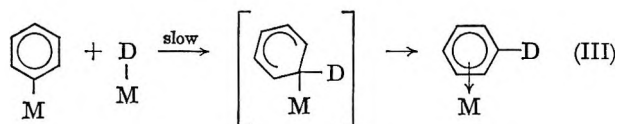
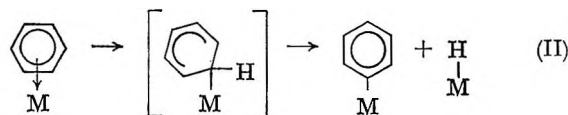
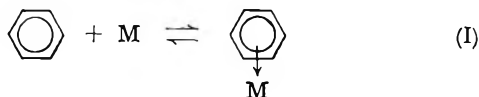
(10) A. Farkas and L. Farkas, *Proc. Roy. Soc. (London)*, **A144**, 467 (1934).

(11) R. S. Mulliken, *J. Phys. Chem.*, **56**, 801 (1952).

(12) F. A. Matsen, A. C. Mækrides, and N. Hackerman, *J. Chem. Phys.*, **22**, 1800 (1954).

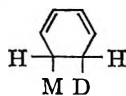
(13) L. E. Orgel, "An Introduction to Transition-Metal Chemistry," Methuen and Co., Ltd., London, 1960, p. 152.

from horizontal π -complex adsorption to vertical σ -bonded chemisorption (eq. II). (Rotation of the ring

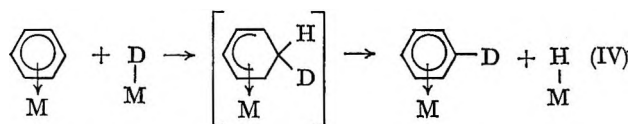


is necessary since "edge on" or "vertical" π -complexing is prevented by the orbital symmetry and by the steric hindrance of aromatic hydrogen atoms.) It is postulated that the transition state of the π - σ -bond conversion occurs approximately when the plane of the rotating benzene molecule is at 45° to the catalyst surface. The electronic hybridization changes involved in this process (Figure 2) resemble those of homogeneous substitution reactions.¹⁴ These show how the activation energy of the dissociative process may be lowered more effectively by resonance effects (E_3) than by stronger interaction from π -complex adsorption (Figure 1, E_2). While σ -bonded, the aromatic undergoes a second substitution reaction at the carbon-metal bond with a chemisorbed deuterium atom (eq. III) and returns to the π -bonded state. A theoretical analysis¹⁵ of the isotope effect ($k_D/k_T = 1.7$ at 32°) indicates that reaction III is the rate-determining process in exchange.

An alternate mechanism based on π -complex adsorption, termed the associative π -complex substitution mechanism (eq. IV) involves essentially the attack of a π -bonded aromatic by a transient hydrogen radical (eq. IV). The transition state, except for π -bonding, is similar to the transition state of a homogeneous substitution reaction and bears a formal resemblance to the "half-hydrogenated" intermediate of the conventional associative mechanism



without involving the same energy restrictions. This is believed to be mainly due to the smaller π -electron



localization and independence of lattice spacings.

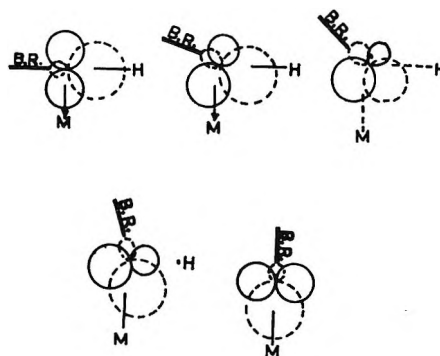


Figure 2. Hybridization changes of π - and σ -electrons at different stages of dissociative chemisorption: B.R., plane of benzene ring; \leftarrow , π -complex adsorption; |, σ -bond.

Recent work¹⁵ has shown that the dissociative π -complex substitution mechanism predominates in aromatic exchange where water is the second reagent. (The possible importance of this mechanism in reactions where deuterium gas is used instead of water will be discussed elsewhere.⁸) This new mechanism is also consistent with rapidly occurring randomization reactions between deuterated and nondeuterated aromatics.¹⁵ When compared with the conventional dissociative mechanism,¹⁰ the dissociative π -complex substitution mechanism satisfactorily explains the faster exchange rates of aromatic over aliphatic hydrocarbons, as well as the observed large differences in aromatic adsorption strengths.²

π -Complex Adsorption of Alkylbenzenes

From theoretical considerations, the alkylbenzenes form a suitable series for the experimental evaluation of the concept of π -complex adsorption, essentially, because the factors controlling the strength of π -complex adsorption of these compounds are more amenable to analysis than in other series such as the polycyclic aromatics.² In the alkylbenzenes the molecular orbital component in π -complex adsorption remains effectively constant, while the ionization potential, electron affinity, and steric factors vary for individual members of the series. Increased methyl substitution decreases the ionization potential¹⁶ but increases the electron affinity¹⁷ and steric hindrance. The first two factors

(14) L. Melander, "Transition State," Special Publication No. 16, The Chemical Society, London, 1962, p. 77.

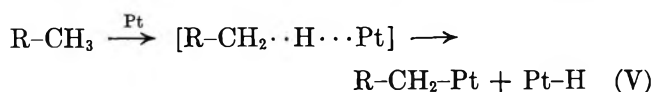
(15) J. L. Garnett and W. A. Sollich-Baumgartner, *J. Phys. Chem.*, **68**, 3177 (1964).

(16) K. Watanabe, T. Nakayama, and J. Mottl, "Final Report on Ionization Potentials of Molecules by a Photoionization Method," Contract No. DA-04-200-ORD 480 and 737, University of Hawaii, 1959.

(17) F. A. Matsen, *J. Chem. Phys.*, **24**, 602 (1956).

favor π -complex adsorption while the third hinders it. Steric hindrance in different members of the series may be estimated from scale models of these molecules; hence, the relative importance of electronic and steric effects in π -complex adsorption can be evaluated.

A further reason for choosing the alkylbenzenes is the possibility of discovering whether the higher reactivity of aromatic hydrogens when compared to aliphatics such as *n*-octane is mainly due to the stronger preliminary interaction of the hydrogen atoms with the catalyst surface as a result of π -complex adsorption, or whether it is due to the difference in actual exchange mechanisms, *e.g.*, a dissociative π -complex substitution mechanism for aromatics as opposed to a possible dissociative abstraction mechanism for aliphatics (eq. V).



This point may be clarified from the exchange of the aliphatic hydrogens in the alkylbenzenes which, as a result of π -complex adsorption *via* the ring, may interact more strongly with the catalyst surface. Thus, the reactivity of the aliphatic hydrogens in the alkylbenzenes should be increased in comparison to the reactivity of the hydrogens in aliphatics such as *n*-octane if a strong preliminary interaction with the catalyst is the main reason for bond rupture. Only an increase in the β -hydrogen activity in the alkylbenzenes may be used as a valid criterion in making this distinction since the α -hydrogens in alkylbenzenes may react more readily than those in *n*-octane because of activation through conjugation or hyperconjugation effects.

Experimental

Exchange reactions were performed by techniques previously described.¹⁸ Reaction products were analyzed by mass spectrometry at 10 and 70 e.v., isotope distributions in the aromatic ring being calculated from low voltage data, while both high and low voltage data were used to establish the trends in aliphatic hydrogen activity.

Alkylbenzenes, after treatment with mercury to remove methylthiophene impurities,¹⁹ were distilled and purity-checked by gas chromatography and mass spectrometry. A constant ratio of deuterium oxide ($5.0 \times 10^{-2} M$) to organic reagent ($1.0 \times 10^{-2} M$) was maintained in all high temperature exchange reactions in order to keep displacement effects owing to bulk concentrations constant. The different reactivities of the various alkylbenzenes necessitated variations in reaction conditions. These are summarized below.

Series A. The prereduced catalyst was self-acti-

vated²⁰ for 3 hr. at 120° *prior* to reaction; the reagents were then exchanged for 2 hr. at 120°. Catalyst/reagent ratio: 10 mg. of catalyst/ $10 \times 10^{-2} M$ D₂O and $2 \times 10^{-2} M$ organic.

Series B. Prereduced catalyst was self-activated²⁰ for 3 hr. at 120° *prior* to exchange reaction. Exchange was then performed for 4 hr. at 120°. Catalyst/reagent ratio: 10 mg. of catalyst/ $5.0 \times 10^{-2} M$ D₂O and $1.0 \times 10^{-2} M$ organic.

Series C. Prereduced catalyst was self-activated,²⁰ *during* the exchange reaction performed for 2 hr. at 120°, catalyst/reagent ratios being the same as for series B.

Series D. Prereduced catalyst was self-activated²⁰ *during* the exchange reaction performed for 24 hr. at 120°. Catalyst/reagent ratio: 20 mg. of catalyst/ $5.0 \times 10^{-2} M$ D₂O and $1.0 \times 10^{-2} M$ organic.

The equilibrium deuterium content in the organic phase (D_∞) was calculated only on the basis of active aromatic hydrogens for reasons which are discussed under the orientation effect. The rate constant of the exchange reaction, standardized to a catalyst/reagent ratio of 10 mg. of catalyst/ $5.0 \times 10^{-2} M$ D₂O and $1.0 \times 10^{-2} M$ organic, was calculated from

$$k = \frac{-2.3}{T} \log \frac{(D_\infty - D_t)}{D_\infty} \quad (1)$$

Rate constants for different reaction conditions (series A, B, C, D) were standardized by the inclusion of reference samples.

Results and Discussion

Previous investigations have shown that a convenient measure of the adsorption strength of a particular compound is its capacity to lower the catalytic exchange rate for the reaction between benzene and deuterium oxide by displacement effects.² The compound to be tested is added in small quantities to the benzene reagent (0.30–3.6 mole %) so that the deuteration of the additive can be neglected in the calculation of the benzene–deuterium oxide exchange rate constant. The adsorption strengths of the alkylbenzenes were investigated in this manner (Table I) and compared with the adsorption strengths of some representative polycyclic aromatics (Figure 3).

The results (Table I, Figure 3) show that the alkylbenzenes do not significantly retard benzene–deuterium oxide exchange even at concentrations of 3.6 mole %

(18) J. L. Garnett and W. A. Sollich, *J. Catalysis*, **2**, 339 (1963).

(19) K. Hirota and T. Ueda, *Bull. Chem. Soc. Japan*, **35**, 228 (1961).

(20) Self-activation refers to activation of the oxygen-poisoned hydrogen prereduced PtO₂·2H₂O by the organic reagent used: J. L. Garnett and W. A. Sollich, *J. Phys. Chem.*, **68**, 436 (1964).

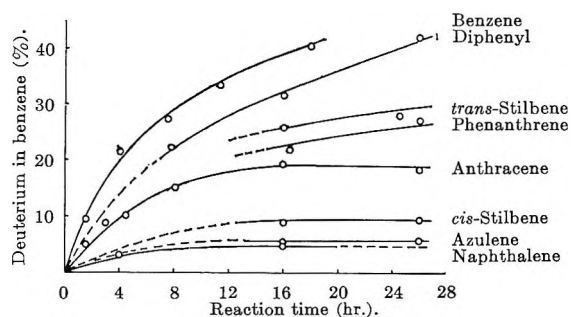


Figure 3. Benzene deuteration in the presence of aromatic poisons (0.30 mole %).

Table I: Effect of Alkylbenzenes on Benzene-Deuterium Oxide Exchange Reactions^a

Solute (3.6 mole %) in benzene solution	k , % D/hr. ^b	Solute (3.6 mole %) in benzene solution	k , % D/hr. ^b
Benzene (std.)	4.2	<i>o</i> -Xylene	4.1
Diphenyl ^c	3.3	<i>m</i> -Xylene	4.1
Toluene	4.1	<i>p</i> -Xylene	4.0
Trifluorobenzene	4.0	Mesitylene	3.7
2,6-Dimethylnaphthalene ^c (0.30 mole %)	4.0	1,2,4-Trimethylbenzene	3.9
		Hexamethylbenzene	4.3

^a Exchange reaction performed for 6.0 hr. at 32°. ^b First-order rate constant of $C_6H_6-D_2O$ exchange reaction. ^c These compounds were used to compare present results with those of polynuclear aromatics in 0.30 mole % concentrations (Figure 3).

whereas the polycyclic aromatics (Figure 3) are appreciably toxic even in 12-fold lower concentration. In terms of a π -complex interpretation this result indicates that adsorption of the alkylbenzenes is much weaker than adsorption of polycyclic aromatics and suggests that steric hindrance compensates for the effects of a decreased ionization potential and increased electron affinity. Naphthalene (Figure 3) and its 2,6-dimethyl derivative (Table I) are outstanding examples of the importance of this steric effect.

Because of the low toxicity of the alkylbenzenes, trends in adsorption strength within the series cannot be observed by the low concentration technique. Since all alkylbenzenes are less toxic than diphenyl, it appears that the high temperature exchange reaction of alkylbenzenes with deuterium oxide is not controlled by reagent displacement but rather by the strength of π -complex adsorption⁸ and steric hindrance to σ -bonded chemisorption, evidence for which may be obtained from *ortho* deactivation. It is therefore necessary to separate these two effects before attempting to correlate the exchange rates of the alkylbenzenes with relative

adsorption strengths established in hydrogenation studies.²¹

ortho Deactivation in the Exchange of Alkylbenzenes. *ortho* Deactivation has already been observed in platinum-catalyzed halobenzene-deuterium oxide exchange,^{2a} Raney nickel-catalyzed toluene-deuterium oxide exchange,²² and alkylbenzene-deuterium gas exchange in the presence of nickel.⁴ In the present studies, *ortho* deactivation effects were estimated from both the 700–900-cm.⁻¹ region of the infrared spectrum of deuterated compounds²³ and from low voltage (10-e.v.) mass spectrometry. The latter technique is satisfactory under the following conditions: (i) "complete" *ortho* deactivation, *i.e.*, essentially no isotope in the *ortho* position; (ii) extensive exchange in the sterically unhindered aromatic hydrogens atoms ($\sim 30\%$); (iii) deuteration predominantly by a stepwise process ($M \approx 1-1.1^{18}$), *i.e.*, small multiple exchange processes; (iv) relatively low deuteration in the alkyl hydrogens.

Results of the mass spectrometric analyses from the exchanged compounds were compared with the calculated spectra (eq. 2) for different numbers of active aromatic hydrogen atoms.

$$F_n = \frac{N!}{n!(N-n)!} x^n (1-x)^{(N-n)} \quad (2)$$

where F_n is the mole fraction of a species containing n deuterium atoms, x the average fraction of aromatic hydrogens displaced by deuterium, and N the total number of active aromatic hydrogens.

Results of these calculations (Table II) show that two types of *ortho* deactivations occur in platinum-catalyzed deuterium oxide-alkylbenzene exchange. "Complete" *ortho* deactivation was found in *t*-butylbenzene, trifluorobenzene, and *m*-xylene, each compound possessing only three reactive aromatic hydrogen atoms, while mesitylene has all three aromatic hydrogen atoms deactivated. Mass spectrometric evidence for complete deactivation is somewhat inconclusive with *m*-xylene because of the low deuterium content in the molecule. Under conditions of multiple exchange, this produces considerable deviations from the calculated deuterium distribution. Another difficulty with *m*-xylene is the presence of a small d_4 peak in the mass spectrum. Since *o*- and *p*-xylenes deuterate appreciably in the methyl groups, the d_4 peak in *m*-xylene may

(21) C. P. Rader and H. A. Smith, *J. Am. Chem. Soc.*, **84**, 1443 (1962).

(22) G. V. D. Tiers, Ph.D. Dissertation, University of Chicago, Chicago, Ill., 1956.

(23) L. J. Bellamy, "The Infrared Spectra of Complex Molecules," Methuen and Co., Ltd., London, 1954, p. 45.

Table II: Observed and Calculated Mass Spectra of Deuterated Alkylbenzenes

Run ^a	Compound	Aromatic deuterium, %	Spectrum type ^b	Isotope distribution, %								
				<i>d</i> ₀	<i>d</i> ₁	<i>d</i> ₂	<i>d</i> ₃	<i>d</i> ₄	<i>d</i> ₅	<i>d</i> ₆	<i>d</i> ₇	<i>d</i> ₈
2B	Ethylbenzene	58.5	O	2.6	7.8	20.7	28.4	22.1	11.5	4.7	1.7	0.50
3B	<i>o</i> -Xylene	48.7	O	4.4	24.9	47.8	17.9	3.4	0.48	0.38	0.22	0.12
4B	Isopropylbenzene (cumene)	42.9	O	6.2	16.7	39.0	33.2	3.8	0.76	0.40	0.25	0.16
			C-3H	7.9	31.5	42.0	18.5					
5B	Toluene	35.1	C-5H	6.0	22.7	34.0	25.8	9.6	1.5			
			O	9.4	30.3	38.4	19.3	2.2	0.30			
C	Trifluorobenzene	74.0	C-5H	11.5	31.3	34.0	18.2	4.9	0.50			
			O	2.7	14.6	42.0	40.4	0.30				
			C-3H	1.8	15.4	42.9	40.0					
8B	<i>m</i> -Xylene	27.9	C-5H	5.4	21.5	34.0	26.8	10.6	1.7			
			O	31.6	55.4	11.1	1.72	0.24				
			C-3H	37.5	43.5	16.8	2.16					
9B	<i>p</i> -Xylene	13.7	C-4H	39.4	41.4	16.4	2.8	0.19				
			O	70.9	19.3	4.4	1.6	0.90	0.87	1.54	0.54	0.15
11D	<i>t</i> -Butylbenzene	47.1	O	11.9	44.4	33.7	9.9	0.40				
			C-3H	14.8	40.0	35.0	10.4					
12D	1,2,3-Trimethylbenzene	9.2	O	74.4	23.8	1.6	0.25	0.18	0.08			
			C-3H	74.7	22.9	2.8	0.08					

^a Numbers refer to samples in Table III. ^b O, refers to the experimentally observed spectrum; C-*n*H, to the calculated spectrum on the basis of *n* active aromatic hydrogen atoms. ^c Product of an exchange reaction with a higher deuterium content than that listed in Table III.

be attributed to methyl deuteration rather than to deuteration of the doubly flanked ring position.

In toluene, ethylbenzene, *o*-xylene, *p*-xylene, and 1,2,3-trimethylbenzene, both infrared and mass spectrometric evidence show the occurrence of "severe" but nevertheless incomplete *ortho* deactivation. Thus, "complete" deactivation occurs when the *ortho* position is adjacent to a very large and inert substituent or when it is flanked by two smaller methyl groups; "severe" deactivation results when the *ortho* position is flanked by only one methyl group.

The severity of the *ortho* deactivation effect supports the importance of the dissociative π -complex substitution mechanism. This follows from the fact that a bulky substituent may exercise two different steric hindrance effects. Thus, in the dissociative mechanism, a methyl group may hinder π -complex adsorption as well as σ -bonded chemisorption in the *ortho* position; the former type of hindrance determines essentially the reactivity of sterically unhindered ring position while the latter gives rise to the orientation effect. Figure 4a shows how the *ortho* position is prevented from σ -bond formation when it is adjacent to a bulky *t*-butyl group or when it is flanked by two methyl groups. However, such bonding is possible when only one methyl group is involved (Figure 4b),

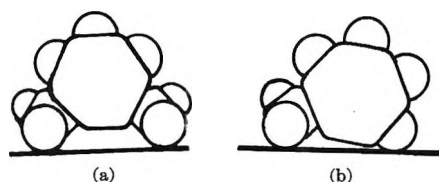


Figure 4. Catalyst surfaces showing steric hindrance to dissociative chemisorption (a) in the doubly flanked *ortho* position of *m*-xylene resulting in "complete" *ortho* deactivation and (b) in the *ortho* position of toluene resulting in "severe" *ortho* deactivation.

but steric hindrance is still sufficiently effective in the latter case to produce "severe" deactivation. An alternate explanation that *ortho* deactivation is caused by inductive effects of the substituents is excluded by "complete" *ortho* deactivation in trifluorobenzene and "severe" deactivation in the halobenzenes.^{2a}

The severity of *ortho* deactivation is difficult to explain by the associative π -complex substitution mechanism since the *ortho* positions of flatly adsorbed molecules appear almost as accessible to hydrogen attack as the *meta* and *para* positions. In this respect the situation resembles the acid-catalyzed alkylbenzene exchange²⁴ where only very small steric hindrance effects were observed during the attack of the D_3O^+ species.

Table III: Deuterium Oxide-Alkylbenzene Exchange at 120°

Run ^a	Substance	Reaction time, hr.	D	% D in active aromatic hydrogens	k_n , hr. ⁻¹	Active aromatic hydrogens	Retarded reactivity, X ^c	Ionization potential, e.v.
1A	Benzene	2	63.0	52.0	0.87	6	1	9.24
2B	Ethylbenzene	4	65.0	58.5	0.58	5	3.0	8.76
3B	<i>o</i> -Xylene	4	71.5	48.7	0.28	4	6.1	8.55
4B	Isopropylbenzene (cumene)	4	66.6	42.9	0.26	3-5	6.7	8.68
5B	Toluene	4	66.6	35.1	0.19	5	9.3	8.82
6C	Trifluorobenzene	2	77.0	14.0	0.10	3	13	9.68
7C	Toluene (reference sample for run 6C)	2	66.6	16.0	0.14	5
8B	<i>m</i> -Xylene	4	77.0	27.9	0.11	3	15	8.56
9B	<i>p</i> -Xylene	4	71.5	13.7	0.053	4	33	8.44
10B	<i>t</i> -Butylbenzene	4	77.0	1.74	0.005	3	350	8.68
11D	<i>t</i> -Butylbenzene (reference sample for run 12D)	24	77.0	47.1	0.039	3
12D	Hemimellitene 1,2,3-Tri-methylbenzene	24	77.0	9.2	0.006	3	2400	...
13D	Mesitylene	24	77.0	0.00	0	0	∞	8.39

^a Letters denote the reaction condition as shown in text. ^b Formula listed in Table IV. ^c $X = k_n(\text{benzene})/k_n(\text{substance})$, where k_n are rate constants, standardized for different catalyst/reagent ratios and different reaction conditions (A, B, C, D); the latter was achieved by the inclusion of reference samples.

Trends in Aromatic Hydrogen Exchange. Results of high temperature exchange reactions between deuterium oxide and alkylbenzenes are listed in Table III in decreasing order of molecular activity. The previous discussion has shown that the reactivity of aromatic molecules is determined by (i) the ease of π -complex adsorption, (ii) absence of steric hindrance effects in σ -bonded chemisorption, and (iii) absence of reagent water displacement effects.

Condition iii was found to be unimportant in alkylbenzene exchange, while allowance can be made for (ii) from the observed orientation effect. Thus, trends in the over-all exchange rate of unhindered aromatic hydrogens should be mainly determined by the strength of π -complex adsorption. In this respect the relative adsorption strengths of the alkylbenzenes determined by Rader and Smith in their hydrogenation studies²¹ provide a useful standard for comparison. Rader and Smith observed the following trend in relative adsorption strengths: benzene, 1.0; toluene, 0.8; *o*-xylene, 0.33; *m*-xylene, 0.22; *p*-xylene, 0.16; 1,2,3-trimethylbenzene, 0.08; 1,3,5-trimethylbenzene, 0.02. These results may now be readily interpreted in terms of steric hindrance to π -complex adsorption by bulky metal substituents since this reduces the contact of the plane of the benzene ring with the catalyst surface and, consequently, the magnitude of the overlap and resonance integrals. In this respect the symmetry of methyl substitution is also of importance since it is difficult for the

aromatic ring of a molecule such as 1,3,5-trimethylbenzene to tilt towards the catalyst surface. Tilting is important since recent results^{25,26} show that π -complexing is not necessarily symmetrical but may only involve part of the ring.

The effects of steric hindrance in π -complex adsorption are reflected in the exchange rates of the aromatic hydrogens of the alkylbenzenes (Table III). For molecules exhibiting "complete" *ortho* deactivation, rate constants were calculated on the basis of active aromatic hydrogens; however, only qualitative allowance could be made in cases of "severe" deactivation. Thus, the most reactive species, ethylbenzene, *o*-xylene, isopropylbenzene, and toluene, are molecules which are hindered to approximately the same extent in π -complex adsorption. This is evident from the fact that the ability to tilt towards the catalyst surface is approximately equal in all species, *i.e.*, all contain at least one hydrogen atom on the α -carbon which can be directed towards the catalyst surface. Results with *t*-butylbenzene show the importance of this effect. The reason for the trends in reactivity within the highly reactive group is not so clear, but these appear to be related to the inductive effects of the alkyl group.

(24) W. M. Lauer and G. Stedman, *J. Am. Chem. Soc.*, **80**, 6433 (1958).

(25) R. S. Mulliken, *J. Chem. Phys.*, **23**, 397 (1955).

(26) J. Collins and L. D'Or, *ibid.*, **23**, 397 (1955).

Table IV: Relative Aliphatic α -Hydrogen Activity in Deuterium Oxide Exchange

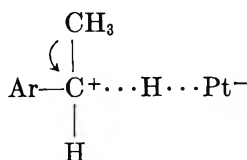
ethylbenzene \gg 1,2,4-trimethylbenzene \approx *p*-xylene $>$ isopropylbenzene (cumene) $>$ *o*-xylene \gg {toluene \approx *m*-xylene \approx mesitylene \approx *t*-butylbenzene \approx 1,2,3-trimethylbenzene (hemimellitene)}

The reactivities of *o*-, *m*-, and *p*-xylenes are consistent with the established adsorption strengths (*i.e.*, with tilting difficulties) as well as "severe" steric hindrance to σ -bonding in all four ring positions of the *para* isomer. Reaction rates of *m*-xylene and 1,2,3-trimethylbenzene follow the trends of relative adsorption strength. The reaction rate is reduced in the latter compound as a result of internal steric repulsion of the adjacent methyl groups, so that the position of minimum external steric strain where both hydrogen atoms of a methyl group rest simultaneously on the catalyst surface cannot be attained.

The considerably weaker adsorption strength of 1,3,5-trimethylbenzene is consistent with the inability of the ring to make contact with the catalyst surface; however, the absence of exchange may be attributed to "complete" *ortho* deactivation of the three doubly flanked ring positions.

Trends in Aliphatic Exchange. The reactivity sequence of aliphatic hydrogens in the alkylbenzene series (Table IV) was estimated from infrared and mass spectrometric analyses of reaction products. β -Hydrogens in ethylbenzene and isopropylbenzene were less reactive than those in the α -position, while β -hydrogens in *t*-butylbenzene are the least active of the three compounds. β -Hydrogen exchange, although very much smaller than ring-hydrogen exchange, was more extensive than in aliphatics such as *n*-octane. It would thus appear that activation *via* the stronger interaction from the π -complex adsorption of the ring is relatively unimportant in hydrogen exchange when an abstraction mechanism is involved.

By contrast, the considerably higher reactivity of α -hydrogens (Table IV) seems to be mainly determined by conjugation, hyperconjugation, and inductive effects. The importance of the inductive effect is demonstrated by the greater reactivity of α -hydrogens in ethylbenzene than in toluene. The transition state may be similar to the one postulated by Huyser²⁷ for an electrophilic radical abstraction process, *viz.*



since this is assisted by electron-donating methyl groups. Conjugational and hyperconjugational activation effects explain the greater reactivity of α -hydrogens in *o*-xylene, *p*-xylene, and 1,2,4-trimethylbenzene. Consistent with this view, *meta* substitution in *m*-xylene and mesitylene has no activating effect.

Conclusion

The dual aim of the paper has been (i) to present for the first time a detailed account of the theoretical basis of π -complex adsorption and the reaction mechanisms based on this mode of interaction and (ii) to test further the theory by exchange experiments with a series of alkylbenzenes.

It is shown in the section concerning π -complex adsorption that the theory was originally proposed to explain exchange reaction data for a number of homologous aromatic series^{2-5,15,18,21} as well as to resolve the difficulties associated with conventional associative and dissociative mechanisms recently reviewed by Taylor.²⁸ The strength of π -complex adsorption increases with a decrease in (i) ionization potential, (ii) orbital complexity of bonding and antibonding orbitals, (iii) steric repulsion between the catalyst surface and bulky substituents, and (iv) with an increase in electron affinity. The rate of exchange between an aromatic and heavy water may be unfavorably affected by strong π -complex adsorption because of water displacement effects. Alternatively, strong π -complexing can also assist exchange by decreasing the activation energy of the reaction.

Applying the theory to the exchange reaction data of the alkylbenzenes and other alkylaromatics it was found to explain the over-all low "toxicity" of those reagents as well as the trends in "toxicity" within the series. The low exchange rate and high toxicity of naphthalene in contrast to the low toxicity and high exchange rate of 2,6-dimethylnaphthalene further suggests the existence of two kinds of adsorption. In the presently proposed theory these are (i) π -complex adsorption leading to the displacement of the water and (ii) dissociative chemisorption leading to exchange. The slow exchange of β -aliphatic hydrogens in spite of the possibility of closer

(27) E. S. Huyser, *J. Am. Chem. Soc.*, **82**, 394 (1960).

(28) T. I. Taylor, *Catalysis*, **5**, 257 (1957).

approach to the catalyst surface through π -complex adsorption suggests that the main cause for the faster aromatic exchange is due to a substitution process. The dissociative π -complex substitution mechanism is further supported by the observed "complete" and "severe" *ortho* deactivation effects.

Acknowledgment. The authors thank the Australian

Institute of Nuclear Science and Engineering for assistance with the purchase of the heavy water, the New South Wales State Cancer Council for the use of their facilities, and Commander J. Mason for instrumentation advice. Acknowledgment is also made to the donors of the Petroleum Research Fund, administered by the American Chemical Society, for support of this research.

The Radiolysis of Aqueous Nitrate Solutions¹

by M. L. Hyder

*Savannah River Laboratory, E. I. du Pont de Nemours and Company, Aiken, South Carolina
(Received November 26, 1964)*

The production of nitrite from neutral and alkaline solutions of sodium nitrate by Co^{60} γ -radiation was measured over a range of nitrate concentrations from 10^{-3} to 4.0 *M*. The production of O_2 from these solutions at pH 13 was also measured, and the origin of the O_2 was determined by labeling the water with O^{18} . The effect of scavengers, particularly O_2 and I^- , on the nitrate reduction was determined. From these studies, and from comparisons with ultraviolet photolysis and with previously published work, the radiolysis of NO_3^- in neutral solutions was concluded to involve three effects: (1) reduction of NO_3^- by electrons and H atoms, (2) direct excitation by radiation, and (3) an effect possibly due to excited water molecules or spur reactions. In alkaline solutions an additional contribution is found, probably from the reaction of O^- . The data allow a determination of $G_{\text{e}_{\text{aq}}^-} \cong 3.8$ and $G_{-\text{H}_2\text{O}} \cong 4.5$ at pH 13.

Introduction

Interest in the chemical behavior of aqueous nitrate solutions undergoing radiolysis derives both from the use of such solutions in handling highly radioactive materials and from the inconsistent results of published studies on this system. Data from various investigators are often in disagreement and have led to some unusual and differing conclusions, *i.e.*, that OH radicals react with nitrate,² that large yields of chemically active excited water are produced by radiolysis,³ or that in moderately concentrated solutions the conventional free-radical theory becomes invalid.⁴ As an example, conflicting values for $G_{\text{NO}_2^-}$ have been re-

ported. At pH 7, values of $G_{\text{NO}_2^-}$ of 2–3^{4,5} and of 5–6^{3,6} have been found, and values ranging up to 6 have also been found in alkaline solutions.^{3,5} These

(1) Work performed under Contract No. AT(07-2)-1 with the U. S. Atomic Energy Commission.

(2) (a) G. E. Challenger and B. J. Masters, *J. Am. Chem. Soc.*, **77**, 1063 (1955); (b) A. O. Allen, "The Radiation Chemistry of Water and Aqueous Solutions," D. Van Nostrand Co., Inc., Princeton, N. J., 1961, p. 101.

(3) M. A. Proskurnin and V. A. Sharpatyi, *Russ. J. Phys. Chem.*, **34**, 1009 (1960).

(4) J. Bednár and S. Lukáč, *Collection Czech. Chem. Commun.*, **29**, 341 (1964).

(5) V. A. Sharpatyi, V. D. Orekhov, and Ya. Karpov, *Nukleonika*, **5**, 12 (1959).

observations are difficult to reconcile with established measurements of radical production.⁷ Reported values of G_{O_2} ^{8,9} and of $G_{H_2O_2}$ ^{9,10} are also in disagreement, but it has been established that H_2 , O_2 , H_2O_2 , and NO_2^- are the only significant products of radiolysis.^{9,11} Other published information on nitrate radiolysis, including studies which gave evidence of a direct decomposition of nitrate by radiation⁸ and measurements of the effect of nitrate on the radiolysis of other ions,^{2a,8,12} is also difficult to reconcile with many of the previously cited reports.

The work reported here was performed (1) to resolve the discrepancies in the literature and (2) to determine the reactions involved in the γ -radiolysis of nitrates. For this purpose, an extensive series of measurements of nitrite production was made over a range of nitrate concentrations from 10^{-3} to 4 *M* and from pH 7 to 13. Particular emphasis was placed on the alkaline solutions because (1) relatively few radiolysis studies have been made in such solutions and (2) most of the unusually high radiation yields of nitrite had been reported at high pH. The effects of radical scavengers on nitrite yields were investigated—particularly I^- and O_2 , but also Br^- and H_2O_2 . The formation of the other radiation products was also studied; in particular, the origin of the O_2 formed in alkaline nitrate solutions was determined by irradiation of solutions made from O^{18} -enriched water, as was done by Mahlman⁸ in neutral solutions. Studies were also made of the photochemical decomposition of nitrate.

Experimental

All γ -irradiations were made with a Co^{60} source providing a maximum dose rate of 1.8×10^6 rads/hr. Irradiations were made at or near this dose rate, except for those studies where the effect of dose rate was of primary importance. Dosimetry was carried out with the Fricke dosimeter, assuming a *G* value for Fe^{3+} production of 15.6. Sample positioning methods fixed the precision of the dose at $\pm 2\%$. Irradiations with ultraviolet light were made with unfiltered mercury lamps or mercury-xenon lamps. The data were corrected for variations in absorbed dose with solution concentration.

Solutions were prepared from triple-distilled water, boiled to remove CO_2 , and pre-irradiated to destroy organic materials, and from reagent grade $LiNO_3$, H_2O_2 , $NaOH$, $NaBr$, KI , and $NaNO_3$. The last three were recrystallized from triple-distilled water. Na_2CO_3 was removed from $NaOH$ by precipitation from a saturated $NaOH$ solution and in some cases by precipitation of $BaCO_3$; the concentration of CO_3^{2-} in

the resulting solutions was less than 10^{-4} *M*. O^{18} water (1.6%) was obtained from the Oak Ridge National Laboratory and was filtered and distilled before using. Alkaline solutions were prepared and stored in an argon atmosphere to avoid contamination by CO_2 . In addition, oxygen was removed from the samples by extensive argon purging or by freezing, pumping under vacuum, and thawing, followed by irradiation under vacuum. Oxygen-saturated samples were prepared by purging with oxygen at 1 atm. for approximately 20 min.

These precautions sufficed to make the data reproducible to a reasonable degree. The maximum error of the reported values of $G_{NO_2^-}$ was estimated to be less than $\pm 10\%$. The actual fluctuations were generally much lower, except for some cases that will be noted. In alkaline solutions it was possible to obtain dose *vs.* NO_2^- production curves that were close to linear at the doses used; in neutral solutions, however, the data represent lower limits as the accumulating nitrite appeared to be removed by a secondary reaction at very low concentrations. In the presence of I^- or O_2 scavengers linear slopes were obtained. All measurements of NO_2^- production were made at total absorbed doses close to 10^4 rads. No effect of dose rate was observed in the range 10^5 to 10^6 rads/hr.

The analyses for NO_2^- were made by automatic colorimetric methods described by Britt.¹³ This method was accurate to $\pm 5\%$ in the range of a few parts of nitrite per million parts of solution. When materials were present that interfered with the analytical method, such as peroxide or iodide, appropriate standards were prepared and analyzed in order to make the necessary corrections. H_2O_2 was analyzed by a method developed in this laboratory.¹⁴

Measurements of the gaseous products were made on samples that had been outgassed and sealed under vacuum; the gases which were recovered after irradiation were measured with a McLeod gauge, and their

(6) A. M. Kabakchi, V. A. Gramolin, and V. M. Erokhin, Proceedings of the First All-Union Conference on Radiation Chemistry, Moscow, 1957, II, Radiation Chemistry of Aqueous Solutions (Inorganic and Organic Systems), 1959, p. 45.

(7) A. O. Allen, *Radiation Res. Suppl.*, **4**, 54 (1964).

(8) H. A. Mahlman, *J. Phys. Chem.*, **67**, 1466 (1963).

(9) N. A. Bakh, V. I. Medvedovskii, A. A. Revina, and B. D. Bituikov, Proceedings of the First All-Union Conference on Radiation Chemistry, Moscow, 1957, II, Radiation Chemistry of Aqueous Solutions (Inorganic and Organic Systems), 1959, p. 39.

(10) J. Bednář, *Collection Czech. Chem. Commun.*, **27**, 2204 (1962).

(11) J. W. Boyle and H. A. Mahlman, *Nucl. Sci. Eng.*, **2**, 492 (1957).

(12) T. J. Sworski, *J. Am. Chem. Soc.*, **77**, 4689 (1955).

(13) R. D. Britt, Jr., *Anal. Chem.*, **34**, 1728 (1962).

(14) E. K. Dukes and M. L. Hyder, *ibid.*, **36**, 1689 (1964).

chemical and isotopic compositions were determined by mass spectrometry. Samples required about 10^7 rads in order to generate enough gaseous products for analysis; radiolytically produced nitrite could be measured after only about 10^4 rads.

Results

Repeated determinations were made of the production of NO_2^- in neutral and alkaline nitrate solutions. Some of the data, covering the range of nitrate concentration from 10^{-3} to $4 M$ and pH 7 to 13, are shown in Figures 1 and 2. These data are from the most carefully prepared samples and represent the trends observed in sets of samples prepared from the same stock solutions. There was some variation among sets. In particular, there was a pronounced tendency for the data to scatter in the concentration range 0.1 to $1 M$ NO_3^- in the alkaline solutions, where the slope of the curve is the greatest (Figure 1). The general trend, however, was quite reproducible.

The G values shown in these figures agree with some of the previous work; that at pH 7 is in rough agreement with ref. 4 and 5 and is consistent with established radical yields. The G value at pH 13 confirms the unexpectedly high yields of nitrite previously reported.^{3,5} Figure 2 shows the dependence of the nitrite yield on pH; the yield rises above pH 10, which is consistent with data reported in ref. 5.

The effect of radical scavengers on the nitrite yields was investigated to establish which radicals were involved in the reduction. The effect of oxygen (shown in Figure 3) decreases the nitrite yield to a low value which is approximately independent of pH. I^- and Br^- were added to the solution to scavenge the OH radical and to eliminate its reactions; however, the product of the reaction of Br^- and OH reacted with NO_2^- , making it difficult to draw any conclusions. Results obtained in the presence of $0.10 M$ I^- are shown in Figure 3; in both alkaline and neutral solutions $G_{\text{NO}_2^-}$ is increased to the same high value by I^- .

The addition of H_2O_2 to scavenge OH was also investigated. However, even $10^{-3} M$ H_2O_2 interfered with the analysis for nitrite, producing low results. In a few scouting experiments, very little effect of H_2O_2 on the nitrite yield was observed.

We have also measured the hydrogen peroxide production in deaerated nitrate solutions. Our measurements in neutral solutions are consistent with those of Bednář and Lukáč,⁴ showing $G_{\text{H}_2\text{O}_2}$ in the range 0.6–1.0; however, at pH 13, $G_{\text{H}_2\text{O}_2}$ was found to be less than 0.05. Although peroxide is unstable in these solutions, our analyses were made within 5 min. or less following irradiation. By adding small amounts of

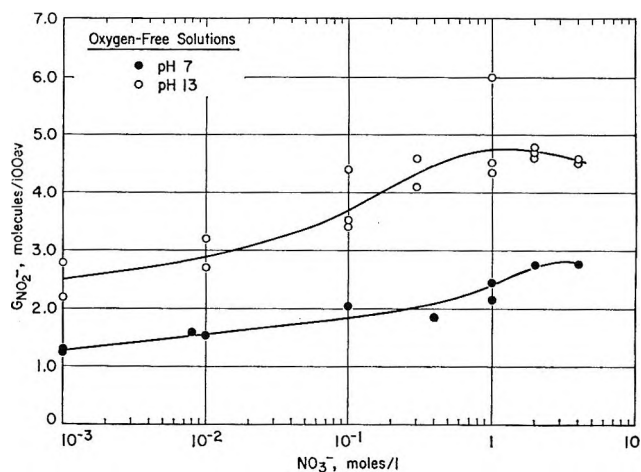


Figure 1. Variation of $G_{\text{NO}_2^-}$ with nitrate concentration at pH 7 and 13.

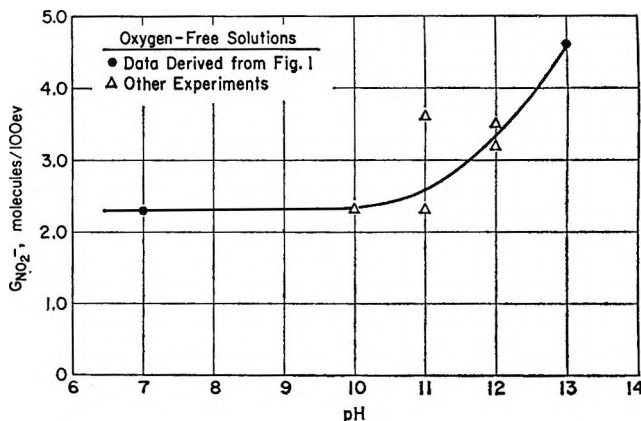


Figure 2. Variation of $G_{\text{NO}_2^-}$ with pH, in $1.0 M$ solutions of NaNO_3 .

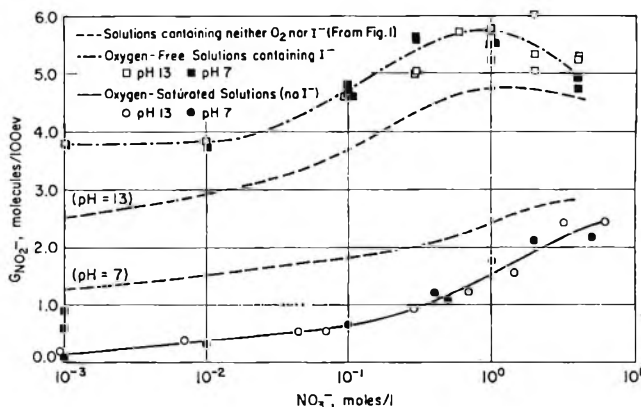


Figure 3. Effect of added KI ($0.10 M$) and of added O_2 (1 atm.) on the variation of $G_{\text{NO}_2^-}$ with nitrate concentration.

H_2O_2 to the solution before irradiation or by saturating the system with O_2 to produce it during irradiation, we confirmed that this species would be detected if

formed. Therefore, we conclude that no significant quantity of peroxide is produced at pH 13 in deaerated solutions.

Experiments with O^{18} labeling, similar to those by Mahlman,⁸ were performed at pH 13 to determine the origin of the O_2 produced by radiolysis. In these solutions O_2 is the only oxidized product in appreciable quantity. At the high dose rates required to accumulate sufficient oxygen for mass spectrometric analysis, the considerable back reaction between the accumulating oxygen and nitrite in both neutral and alkaline solution precluded the direct determination of G_{O_2} . However, the O^{18}/O^{16} ratio was determined, and the total amount of O_2 formed was calculated by stoichiometry (1) from $G_{NO_2^-}$ determined at low doses and (2) from published values of G_{H_2} . The results of these measurements, shown in Table I, indicate that most O_2 originates from water in dilute solutions, with an increasing fraction originating with nitrate at higher nitrate concentrations; this result will be discussed in detail later. Hart, Gordon, and Hutchison¹⁵ have discovered a radiation-induced chain exchange

Table I: Production of O_2 from NO_3^- in Solutions Containing O^{18} -Enriched H_2O^a

Salt	NO_3^- , <i>M</i>	% O^{18} found in O_2	Fraction of O_2 from NO_3^-	G_{O_2} , calcd.	G_{O_2} from NO_3^-
γ-Irradiations					
$NaNO_3$	0.12	1.49 ^b 1.63	0.03	2.0	0.06
$NaNO_3$	0.50	1.45 1.50	0.09	2.35	0.21
$NaNO_3$	1.0	1.36 1.38	0.16	2.40	0.38
$NaNO_3$	2.5	1.16 1.21	0.30	2.35	0.70
$NaNO_3$	4.0	1.07 1.06	0.39	2.30	0.90
$LiNO_3$	0.25	1.60 1.47	0.05	2.20	0.11
$LiNO_3$	1.0	1.34 1.35	0.19	2.40	0.44
$LiNO_3$	2.0	1.19 1.21	0.29	2.35	0.67
Ultraviolet irradiations					
$NaNO_3$	1.0	0.54 0.53	0.76

^a Original concentration of O^{18} in water was 1.6%; samples were 0.10 *M* in NaOH. ^b Results of duplicate experiments.

reaction between O_2 and water at high pH; since, however, we find the O^{18}/O^{16} ratio in the O_2 to vary widely and reproducibly with nitrate concentration, it does not seem to be occurring here. Either the oxygen escapes to the relatively large void space in the vessel quickly, or else the chain is broken by nitrate. Since O^- was postulated as the chain initiator, and we have evidence for reaction of this species with nitrate, the latter case is probable.

We also carried out some photochemical studies in an attempt to characterize the "direct effect" of radiation on dissolved nitrate ion. It had been shown by Cultrera and Ferrari¹⁶ that ultraviolet light decomposes nitrate to nitrite. Reasoning that the mechanisms of decomposition by radiolytic or photolytic excitation should be similar, we irradiated nitrate solutions containing radical scavengers with light from a mercury lamp. Absolute quantum yields were not determined, but care was taken to reproduce irradiation time and intensity. Increasing pH was found to increase the yield of nitrite, as previously reported¹⁶; Br^- had less effect, and O_2 virtually none (see Table II). In separate irradiations it was found that no H_2O_2 could be detected in the alkaline solutions—either it was never formed, or it was efficiently photolyzed. The O_2 produced originated mainly from nitrate ion (see Table I).

Table II: Production of Nitrite by the Ultraviolet Irradiation of Aqueous Nitrate Solution

Composition of sample	Relative yield of nitrite, arbitrary units	
	N_2 purge	O_2 purge
1.0 <i>M</i> $NaNO_3$	38	32
1.0 <i>M</i> $NaNO_3$, 0.10 <i>M</i> NaOH	68	62
1.0 <i>M</i> $NaNO_3$, 0.10 <i>M</i> NaOH, 0.10 <i>M</i> NaBr	81, 83 ^a	80, 71 ^a

^a Results of duplicate experiments.

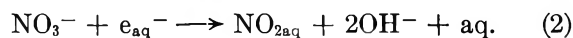
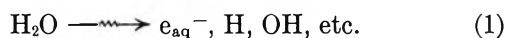
Discussion

The basic question to be answered in the study of nitrate radiolysis is whether the behavior of this system can be explained by a theory of free-radical intermediates alone or whether additional processes are involved. The radical theory predicts that in dilute

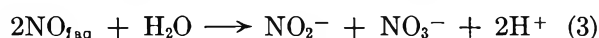
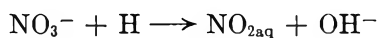
(15) E. J. Hart, S. Gordon, and D. A. Hutchison, *J. Am. Chem. Soc.*, **75**, 6165 (1953).

(16) R. Cultrera and G. Ferrari, *Ann. Chim. (Rome)*, **47**, 1321 (1957).

solutions the reduction of nitrate¹⁷ should take the course



or



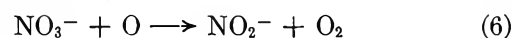
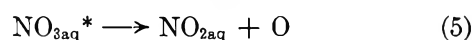
The result of these reactions would be 0.5 molecule of NO_2^- per solvated electron or H atom. Thus, these reactions could account for values of $G_{\text{NO}_2^-}$ up to 0.5- $G_{-\text{H}_2\text{O}}$ or between 2 and 2.5. An additional process must be found to account for the greater amount of NO_2^- found in alkaline solutions.

Four additional processes that may occur during radiolysis of nitrate solutions have been proposed: (a) the excited water theories of Proskurnin and Sharpatyi,^{3,18} (b) the theory of Bednář and Lukáč,⁴ which suggests preferential radiolysis of the solute in concentrated solutions, (c) Mahlman's⁸ hypothesis of direct excitation of nitrate ion, and (d) suggestions of the reaction of OH radicals with NO_3^- .² The nature of these processes and their possible importance are briefly described in the following paragraphs.

The "Excited Water" Explanation. Proskurnin and Sharpatyi^{3,18} have suggested that excited water molecules are responsible for the high yields of nitrite. Their reasoning is based on the hypothesis that the initial processes in the radiolysis of water should be the same in the liquid and vapor phases although the reported values of $G_{-\text{H}_2\text{O}}$ are about 4.5⁷ and 11.7¹⁹ in the two phases. It is suggested that the difference is due to excited water molecules, normally unreactive in the liquid phase, which react with concentrated nitrate. The excited water molecules are postulated (1) to be primarily radical pairs trapped by the solvent cage and (2) to undergo typical radical reactions.

Several arguments against this theory may be presented. There are theoretical objections to the basic hypothesis that the primary radiolytic processes should be the same regardless of state²⁰; this is particularly true when considering very concentrated ionic solutions. Also, it is not clear why only nitrate and perhaps a few other materials¹⁸ should show a high reactivity toward the excited water that is not observed in other irradiated systems.²¹ In addition, some of the results of Proskurnin and Sharpatyi could not be duplicated in this and other investigations,^{4,5} including in particular their reported value of $G_{\text{NO}_2^-}$ approaching 6 at pH 7. This theory therefore appears somewhat tenuous.

Bednář and Lukáč's Theory. The theory of Bednář and Lukáč⁴ is based on the nature of the radiolysis process in concentrated solutions. They reason that in sufficiently concentrated solutions the initial excitation would be delocalized enough for the solute to be involved in a large fraction of the primary excitations. They therefore propose that in concentrated solutions, reactions 1-3 should be replaced by a series of reactions including



From their experiments, Bednář and Lukáč derived from reaction 4 a maximum $G = 3.04$ for very high nitrate concentrations. They also postulated the formation of excited water, which undergoes the reaction



The G value for the formation of H_2O^* from their data analysis is in the range 1.2 to 1.5.

This theory would account for the production of very large amounts of nitrite in the radiolysis of concentrated solutions. The maximum $G_{\text{NO}_2^-}$ would be $0.5G_{(2)} + 0.5G_{(4)} + 0.5G_{(5)} + G_{(6)} + G_{(8)}$, which in the limit of very concentrated solutions would be equal to $2G_{(4)} + G_{(8)} \cong 7.6$. The theory does not provide for a dependence of $G_{\text{NO}_2^-}$ on pH. These authors believe that the direct effect of Mahlman,⁸ described next, is not due to the direct excitation of nitrate by radiation but rather to a competition between reactions 6 and 7.

The Direct Effect. Mahlman⁸ observed that in neutral nitrate solutions O_2 was produced from the nitrate ion, in an amount roughly proportional to the nitrate concentration. This he assigned to the direct excitation of the nitrate by radiation. The "direct" G_{O_2} measured by Mahlman is, however, only of the order of tenths, so that this "direct effect" cannot by itself account for the very high nitrite yields observed.

Reactions of OH Radicals. The suggestion that OH radicals might react with nitrate ion² could also ac-

(17) The amount of solvation of the hypothesized " NO_2^- " intermediate is unknown; to distinguish this species from the gaseous molecule it is denoted $\text{NO}_{2\text{aq}}$ in the subsequent discussion.

(18) V. A. Sharpatyi, *Russ. Chem. Rev.*, **30**, 5, 279 (1961).

(19) R. F. Firestone, *J. Am. Chem. Soc.*, **79**, 5593 (1957).

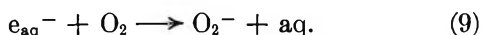
(20) U. Fano, "Comparative Effects of Radiation," John Wiley and Sons, Inc., New York, N. Y., 1960, p. 14.

(21) M. S. Matheson, *Radiation Res. Suppl.*, **4**, 1 (1964).

count for a high value of $G_{\text{NO}_2^-}$. If the OH radicals could serve as one-electron reducing agents, then the nitrite yield might be approximately doubled.

Implications from Radical Scavenging Studies. The results obtained in this work with radical scavengers, particularly O_2 and I^- , are to be examined with respect to the preceding theories.

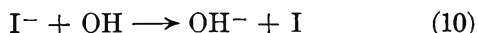
As shown in Figure 3, the presence of O_2 during the irradiation drastically lowers the $G_{\text{NO}_2^-}$. Generally, such an effect is attributed to the reaction



which removes the solvated electrons and thereby prevents reaction 2. However, it is now known that the reaction constants for e_{aq}^- with O_2 and with NO_3^- are very nearly the same.⁷ Therefore, the drastic reduction of $G_{\text{NO}_2^-}$ produced by $10^{-3} M$ O_2 in much more concentrated nitrate solutions would not be expected. If the O_2 is not reacting with the primary species, then it is evidently reacting with the intermediate, " $\text{NO}_{2\text{aq}}$," to oxidize it back to nitrate.

It can be inferred that $\text{NO}_{2\text{aq}}$ is oxidized equally well at all concentrations of nitrate by $10^{-3} M$ O_2 . In the more dilute solutions $G_{\text{NO}_2^-}$ is decreased by this process almost to zero, which indicates very efficient oxidation of $\text{NO}_{2\text{aq}}$. However, in the more concentrated solutions for which the value of $G_{\text{NO}_2^-}$ is appreciable even in the presence of oxygen, some of the nitrite is evidently produced by processes in which $\text{NO}_{2\text{aq}}$ is not an intermediate. Reactions 6 and 8 are of this type, and a limit can be set on the extent to which such reactions are involved.

The studies of $G_{\text{NO}_2^-}$ in the presence of I^- provided additional information. I^- is known to undergo the reaction²²



and the I or species formed from it did not react with NO_2^- under our conditions. The presence of I^- should therefore eliminate any reactions in which OH radicals are involved. As shown in Figure 3, addition of I^- increased the yield of NO_2^- , in both neutral and alkaline solutions, to a value that shows little dependence on pH. (The very low values of $G_{\text{NO}_2^-}$ observed in neutral $10^{-3} M$ nitrate solutions containing I^- are not understood; they may be due to more complex equilibria, such as those described by Allen.²²) With I^- present, even in quite dilute solutions, $G_{\text{NO}_2^-}$ still reaches 3.8. We concluded from this that $\text{NO}_{2\text{aq}}$ was reduced by I^- ; the alternative possibilities would require a G value for reducing radicals of at least 7.6, and this is unreasonable in these solutions. $G_{\text{NO}_{2\text{aq}}}$ must be at least as great as the value 3.8 of $G_{\text{NO}_2^-}$

found in the presence of I^- ; in view of the high concentration of reducing agent present, it is probably equal to this value. These data allow some quantitative calculations of radical yields. $G_{\text{NO}_2^-}$ formed with I_2 present, shown as the upper curve in Figure 3, includes both NO_2^- formed from $\text{NO}_{2\text{aq}}$ and production of that nitrite which is unaffected by radical scavengers and therefore does not derive from $\text{NO}_{2\text{aq}}$ (lower curve in Figure 3). By subtraction of these two curves, a measure of $G_{\text{NO}_{2\text{aq}}}$ and thus of $G_{(\text{H}^+ + e_{\text{aq}}^-)}$ may be obtained; this subtraction is shown in Figure 4. $G_{\text{NO}_{2\text{aq}}}$ is seen to rise with nitrate concentration slowly to about 1 M nitrate, above which it drops off sharply to lower values. This is consistent with what is known about the system; Mahlman²³ has shown that G_{H_2} drops from about 0.36 in $10^{-2} M$ NO_3^- to <0.10 in solutions above 1 M NO_3^- . H_2 is believed to be produced by combination of reducing species,²⁴ *i.e.*



so that the participation of these solvated electrons in reaction with NO_3^- would be expected to raise $G_{\text{NO}_{2\text{aq}}}$ by approximately 0.6 in solutions above $10^{-2} M$. The decrease in $G_{\text{NO}_{2\text{aq}}}$ in more concentrated solutions would appear to be due to the increasing complexity of behavior of these solutions; much of the water is involved in hydration of the solute and thereby likely to react somewhat differently upon excitation or de-

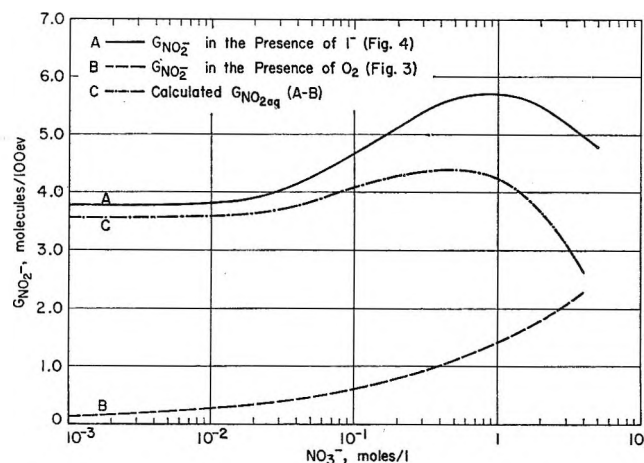


Figure 4. Determination of $G_{\text{NO}_{2\text{aq}}}$ as a function of nitrate concentration.

(22) A. O. Allen, "The Radiation Chemistry of Water and Aqueous Solutions," D. Van Nostrand Co., Inc., Princeton, N. J., 1961, p. 109.

(23) H. A. Mahlman, Chemistry Division Annual Progress Report for Period Ending June 20, 1963, U.S.A.E.C. Report ORNL-3488, Oak Ridge National Laboratory, Oak Ridge, Tenn., p. 45.

(24) E. Hayon, *Nature*, **194**, 737 (1962).

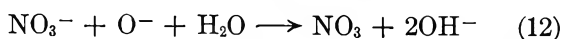
composition. Also, an appreciable fraction of the primary excitation comes to involve the nitrate ion itself at these concentrations.

The above results may now be compared to the predictions of the several theories previously described. First, it may be noted that the excited water theory of Proskurnin and Sharpatyi predicts that the reactions of excited water will resemble those of radicals and therefore involve $\text{NO}_{2\text{aq}}$ intermediates. There should then be an increase in $G_{\text{NO}_{2\text{aq}}}$ between 0.1 and 1 M NO_3^- amounting to a factor of about 2; this increase is not observed. Likewise, the theory of Bednář and Lukáč predicts a steady increase in $G_{\text{NO}_{2\text{aq}}}$ with increasing nitrate concentration, due to reactions 4 and 5; this increase also is not observed.

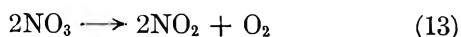
There remains to be explained the high yields of NO_2^- in alkaline solution above pH 11, shown in Figures 1 and 2. At high pH there is an unexpectedly high production of NO_2^- even at $10^{-3} M$ concentrations of nitrate—2.3 compared to 1.9 which would be produced by the measured yield of $(\text{H} + e_{\text{aq}}^-)$. The only plausible explanation for this effect in such a dilute solution would seem to be that OH radicals are acting as reductants toward nitrite. Mahlman²⁵ has published evidence that OH and NO_3^- do not react in sulfuric acid solutions; however, the oxidizing radical in such solutions may actually be HSO_4^{26} and in the present studies it may be O^- .

The best available estimate is that OH ionizes to O^- at pH values above 11.²⁷ The high yields of NO_2^- are found only above pH 11; at lower pH the yields are significantly less than could be accounted for by the measured $G(\text{H} + e_{\text{aq}}^-)$. These results strongly suggest that a reaction of O^- with NO_3^- is responsible for the anomalously high $G_{\text{NO}_2^-}$. The difference in the reactions of OH and O^- could therefore account for the observed pH effect. The fact that H_2O_2 is not observed as a product in the radiolysis of these alkaline solutions also suggests that its radical precursors are being scavenged by nitrate.

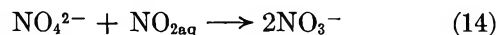
The reactions of O^- have not been thoroughly investigated, but it has been postulated before that O^- can behave as a reducing agent²⁸ although this particular case was later questioned.²⁷ The principal uncertainty in postulating the reduction of NO_3^- by O^- is whether the process of electron transfer is exothermic; the energy required to produce a hydrated oxygen atom may be too high. If this is so, an alternative possibility would be the reaction sequence



and

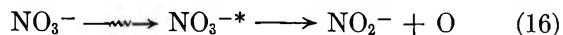


However, such a sequence is inconsistent with data from studies with O^{18} -labeled water (Table I) because it would produce O_2 from the nitrate ion. Another possibility is the formation of an intermediate compound from NO_3^- and O^- , which could subsequently react to yield oxygen and $\text{NO}_{2\text{aq}}$. The net yield of NO_2^- would then depend on the relative rates of the reactions involving the species $\text{NO}_{2\text{aq}}$ and the $\text{NO}_3^-:\text{O}^-$, which can be written NO_4^{2-} , such as



Depending on the relative rates of reactions 14, 15, and 3, the yield of $\text{NO}_{2\text{aq}}$ could therefore range from $(G_{e_{\text{aq}}^-} + G_{\text{O}^-})$ to $(G_{e_{\text{aq}}^-} - G_{\text{O}^-})$. The observed results are well within this range. It seems, therefore, that the high yields may be accounted for by reactions of O^- though the exact mechanism remains obscure.

The Effects Not Involving $\text{NO}_{2\text{aq}}$. Those effects not involving $\text{NO}_{2\text{aq}}$, that is, the portion of the NO_2^- yield which is insensitive to the presence of O_2 , I^- , Br^- , and other radical scavengers, still need explanation. As shown in Figure 5, the electron fraction of NO_3^- in fairly concentrated solutions of NaNO_3 is quite large, approaching 19% for a 4 M solution. It would be expected that a proportional amount of primary excitation by radiation would be imparted to the nitrate ion. The decomposition of nitrate by radiolytic excitation should proceed similarly to the photolytic decomposition; hence, it should be insensitive to the presence of oxygen. This implies that $\text{NO}_{2\text{aq}}$ or other oxygen-sensitive intermediates are not involved. A mechanism consistent with the data would consist of the dissociation reaction



followed by reaction 6. This would produce oxygen from nitrate; in view of the high nitrate concentration, it would be rather insensitive to other radical scavengers.

A direct effect of radiation on nitrate of this type should be detectable by two measurements: (a) a measurement of the oxygen produced from nitrate ion and (b) a measurement of the nitrite produced in the presence of oxygen. These two quantities are plotted against nitrate concentration in Figure 5, with the oxygen yield multiplied by 2 so as to correspond quantitatively to the nitrite yield. If the only effect which

(25) H. A. Mahlman, *J. Phys. Chem.*, **64**, 1598 (1960).

(26) J. W. Boyle, *Radiation Res.*, **17**, 427 (1962).

(27) J. H. Baxendale, *Radiation Res. Suppl.*, **4**, 114 (1964).

(28) F. S. Dainton and S. A. Sills, *Proc. Chem. Soc.*, 223 (1964).

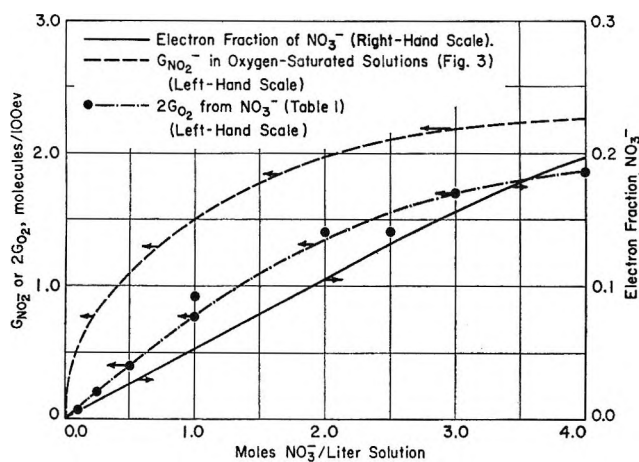


Figure 5. Comparison of quantities involved in establishing the "direct effect" of radiolysis on nitrate ion.

produces NO_2^- in the presence of 1 atm. of O_2 is this direct effect, then the two curves should coincide; actually, the nitrite production is higher by about 0.5 molecule/100 e.v. above 0.5 M nitrate, but it falls off at lower concentrations. The general behavior of these two curves supports the "direct effect" concept as outlined above although the two are not exactly proportional to electron fraction of nitrate, and some additional process must be found to account for the difference between the two curves. The simplest explanation for this difference, incomplete scavenging of $\text{NO}_{2\text{aq}}$ by O_2 , is not satisfying because O_2 is such a good scavenger at low nitrate concentrations; more likely, the difference is due to reactions in the spurs, reactions of excited water, or some other unusual process which can be observed in these concentrated solutions.

One problem in the above interpretation is that the nitrite production in O_2 -saturated solutions is independent of pH, while the measurement of O_2 production from nitrate reported here is much higher than that previously reported for pH 7.⁸ However, this last number is based on values of G_{O_2} which are not primary yields, owing to the reaction of $\text{NO}_{2\text{aq}}$ with the

accumulating O_2 ; published measurements of G_{O_2} at low doses⁹ are considerably higher. It is therefore possible that this apparent discrepancy is not real.

Other Relevant Data. The significance of some of the other published data on the effect of scavengers on the radiolysis of nitrate is uncertain. As mentioned previously, the effect of H_2O_2 is uncertain and small. No obvious explanation for the reported lack of influence of added H_2^5 on the reaction is at hand; this deserves further study. The effect of formic acid and other organic compounds in increasing $G_{\text{NO}_2^-}$ ^{3,4} is probably due to their behavior as reducing agents toward $\text{NO}_{2\text{aq}}$, in a manner similar to I^- , or else to the reducing action of radicals formed by the action of OH on the organic materials.

Summary and Conclusions

The radiolytic reduction of nitrate ion in dilute aqueous solution may be accounted for by conventional reactions 1-3 of H and e_{aq}^- in neutral solution. However, above pH 11 there is an increase in the yield of NO_2^- which is most likely due to a reaction of O^- by reactions such as (15). In solutions of higher nitrate concentrations, the direct excitation of nitrate by radiation (reactions 6 and 16) becomes important, and there is also a possible additional contribution from the reaction of excited water or some other process.

From Figure 4 it is possible to establish ($G_{e_{\text{aq}}^-} + G_{\text{H}}$) as approximately 3.8 in dilute alkaline solutions. From the value of $G_{\text{H}_2} = 0.36$ given by Mahlman for $10^{-2} M \text{NO}_3^-$, $G_{-\text{H}_2\text{O}}$, exclusive of the formation of excited water, may be calculated as approximately 4.5. This is in reasonably good agreement with values obtained by Dainton and Watt²⁹ in their studies of alkaline solutions of hexacyanoferrates but is higher than the values found in alkaline solutions by other investigators.⁷

Acknowledgments. The author is indebted to Drs. Harold J. Groh and Rolland W. Ahrens for advice and discussions throughout this investigation.

(29) F. S. Dainton and W. E. Watt, *Nature*, **195**, 1294 (1962).

The Effect of Galvinoxyl on the Radiolysis of Benzene-Butene-2 Mixtures

by R. B. Cundall and P. A. Griffiths

Department of Chemistry, The University, Nottingham, England (Received March 1, 1965)

By the use of galvinoxyl it has found that the scavengable radical yield (G_R) in γ -irradiated benzene is 0.74, but no reaction with excited states is detectable. The effect on the geometrical isomerization of *cis*-butene-2 shows that the stable free radical is able to quench the excited triplet state of benzene with high efficiency. An estimate of about 4 for the triplet G value in irradiated benzene is quoted. The lifetime of this state is short, *ca.* 10^{-8} sec., under the conditions of the experiments.

Previous work¹ has indicated that the *cis-trans* isomerization of butene-2 in irradiated benzene solutions proceeds *via* an excited-state mechanism with electronic energy transfer from the triplet state of benzene. Although tests for a free-radical mechanism for the reaction were made, it was desirable to examine the effect of a free-radical scavenger more effective than any used in the earlier investigation. Galvinoxyl (2,6,3',5'-tetra-*t*-butyl-4'-phenoxy-4-methylene-2,5-cyclohexadiene-1-one) was selected for this purpose.

Relatively high concentrations, much in excess of those required to scavenge the bulk of the free radicals formed in the solution, caused a considerable decrease in the isomerization yield comparable to that observed with oxygen. Galvinoxyl is known to react efficiently with free radicals,² but the question arises whether galvinoxyl can quench excited states by a purely physical process or a chemical process in which there is a reaction between the galvinoxyl and excited benzene as reported by Griffith³ for DPPH (diphenylpicrylhydrazyl) and triplet benzene. The work described here provides some information on this problem.

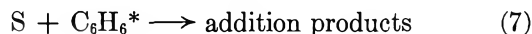
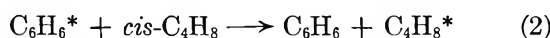
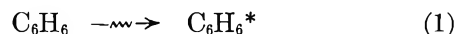
Experimental

Benzene was purified by the method previously described.¹ *cis*-Butene-2 (Phillips research grade) was used without further purification other than vacuum distillation. Galvinoxyl was prepared by the oxidation of 3,3',5,5'-tetra-*t*-butyl-4,4'-dihydroxydiphenylmethane with lead dioxide.⁴ Solutions of galvinoxyl were very readily oxidized in air and were deaerated by the addition of fragments of sublimed solid carbon dioxide. Two-milliliter portions of solutions were thoroughly degassed in tubes fitted with break-seals. A known amount of *cis*-butene-2 was condensed into

the tubes and irradiated with Co^{60} γ -rays (at $22 \pm 1^\circ$). After irradiation, the tubes were opened under vacuum and the butene-2 was extracted for analysis by gas chromatography. Galvinoxyl was estimated by measuring the absorbance at $474 \text{ m}\mu$ (ϵ 145,000) and also iodometrically.² The former method appeared preferable because of the difficulty in obtaining a satisfactory end point with the latter. In the determination of galvinoxyl consumed, the tubes were opened under an atmosphere of carbon dioxide.

Results and Discussion

The experiments were carried out at a constant *cis*-butene-2 concentration (0.21 *M*) and dose rate (3×10^{14} e.v. $\text{g}^{-1} \text{sec}^{-1}$). For convenience, (G_{isom})⁻¹ values are plotted against the concentration of galvinoxyl (moles l^{-1}) (see Figure 1). The linearity of the plot is consistent with the scheme



(1) R. B. Cundall and P. A. Griffiths, *J. Am. Chem. Soc.*, **85**, 1211 (1963); *Discussions Faraday Soc.*, **36**, 111 (1963).

(2) F. D. Green, W. Adam, and J. E. Cantrill, *J. Am. Chem. Soc.*, **83**, 3461 (1961).

(3) L. R. Griffith, U. S. Atomic Energy Commission, U.C.R.L. 3422 (1956).

(4) G. M. Coppinger, *J. Am. Chem. Soc.*, **79**, 501 (1957); M. S. Kharasch and B. S. Joshi, *J. Org. Chem.*, **22**, 1435 (1957).

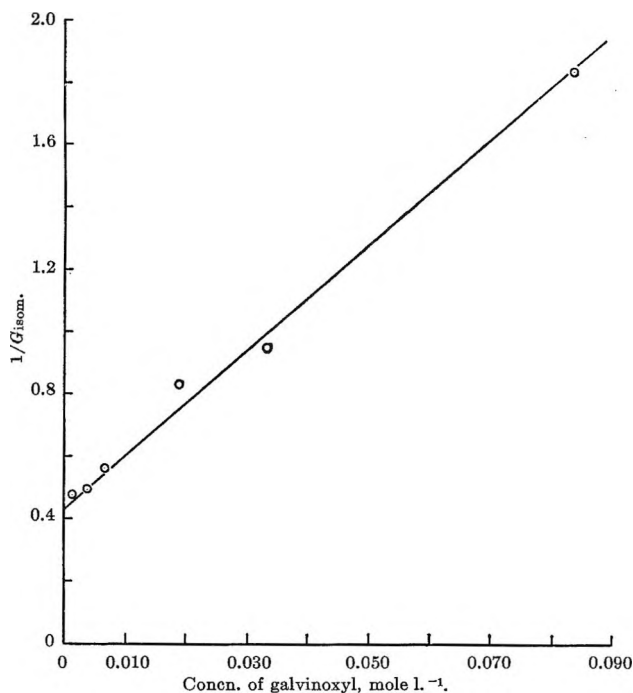


Figure 1. Plot of $1/G_{\text{isom}}$ vs. concentration of galvinoxyl (mole l.⁻¹) in benzene solution.

C_6H_6^* and C_4H_8^* are the triplet states of benzene and butene-2. Evidence for stages (1) to (4) has been presented elsewhere.¹ In the presence of galvinoxyl (S), the process (5) to (6) are also possible and a steady-state treatment yields

$$1/G_{\text{isom}} = 1/k' + k_4/k'k_2[\text{C}_4\text{H}_8] + (k_6 + k_7)[\text{S}]/k'k_2[\text{C}_4\text{H}_8]$$

where k' is a constant at fixed dose rate involving the efficiency of benzene excitation. From the plotted data $(k_6 + k_7)/k_2$ is found to be 9.6 ($k' = 0.38100$ e.v. molecule⁻¹).^{1,5} A value of 2×10^{-2} for the k_4/k_2 ratio can also be derived in good agreement with the value of 1.8×10^{-2} derived from data better suited for this purpose.⁵ The ratio of $(k_6 + k_7)/k_2$ is comparable with 9.0 for oxygen and 3.2 for both naphthalene and anthracene.⁵ Apart from oxygen, nitric oxide, and other triplets, paramagnetic molecules are less effective quenchers of the triplet state than those in which an exothermic triplet-triplet energy interchange is possible.⁶

Information on the relative importance of reactions 6 and 7 can be obtained from the results in Table I. At the lower galvinoxyl concentrations, the G value agrees well with other estimates for free-radical yields in irradiated benzene. Cherniak, Collinson, and Dainton⁷ have measured and listed values for $G(\text{radicals})$ obtained with a variety of scavengers, the most re-

Table I

Concn. of galvinoxyl, mole l. ⁻¹	Total dose, e.v. $\times 10^{-20}$ (ir. 2 ml.)	$G(-\text{galvinoxyl})$	Observed decrease in G_{isom}
2.5×10^{-3}	0.138	0.74	0.22
1.42×10^{-2}	1.66	0.63	0.83

liable of which lie between 0.70 and 0.75. If the isomerization method is valid for the estimation of the triplet yield in benzene

$$G(\text{triplet } \text{C}_6\text{H}_6) = G_{\text{cis} \rightarrow \text{trans}} + G_{\text{trans} \rightarrow \text{cis}} \approx 4$$

where the G_{isom} values are limiting ones in the presence of 0.2 M olefin. The only comparable data are those of Cherniak, Collinson, and Dainton,⁷ who have obtained a value of about half this using ferric chloride as scavenger. If excited states were chemically scavenged, than $G(-\text{galvinoxyl})$ should increase with galvinoxyl concentration up to about 5. This is not found, *i.e.*, $k_7 \ll k_6$, and it is possible that the slight decrease observed may be due to some deactivation of a radical-forming excited state. Although galvinoxyl quenches excited triplet states in irradiated systems, it only disappears through free-radical, as distinct from excited-state, attack; *i.e.*, reaction 5 alone is responsible for galvinoxyl disappearance.

The value of k_6/k_4 is 4.8×10^2 and, if k_6 is about 10^{10} l. mole⁻¹ sec.⁻¹ as expected for a diffusion-controlled reaction, k_4 must be 2.1×10^7 sec.⁻¹. This implies that the lifetime of the benzene triplet is surprisingly short, (5×10^{-8} sec.). If a longer lifetime for the benzene triplet is assumed, the value of k_6 becomes less than that for a diffusion-controlled reaction, which is anticipated from the close similarity in behavior between oxygen and galvinoxyl.

The identity of the absorption spectra of galvinoxyl in benzene and chloroform suggests that a solvent-solute complex is not responsible for the benzene triplet state quenching by galvinoxyl as could be the case with DPPH in benzene.

Acknowledgments. The authors are indebted to Dr. G. B. Gill for his invaluable assistance and comments. Thanks are due to the Petroleum Research Fund of the American Chemical Society for support.

(5) R. B. Cundall and P. A. Griffiths, to be published; the data quoted differ somewhat from those given in ref. 1.

(6) G. Porter and M. R. Wright, *Discussions Faraday Soc.*, 27, 18 (1959).

(7) E. A. Cherniak, E. Collinson, and F. S. Dainton, *Trans. Faraday Soc.*, 60, 1408 (1964).

Heats of Mixing of Electrolytes Having Common Ions

by Y. C. Wu, M. B. Smith, and T. F. Young¹

George Herbert Jones Chemical Laboratory, University of Chicago, Chicago, Illinois, and Argonne National Laboratory, Argonne, Illinois (Received November 30, 1964)

Heats of mixing of 24 pairs of 1 *m* aqueous solutions of 1-1 electrolytes having an ion common to the pair have been measured at 25°. Heats of mixing of NaCl and Na₂SO₄, each in an aqueous solution of unit ionic strength, have also been determined. The effect of the substitution of one common ion for another has been investigated for five homoionic pairs. The maximum effect observed is about 3 cal./mole of electrolyte. The heats of mixing of HCl with the alkali metal chlorides differ from the heats of mixing of LiCl with the same respective electrolytes by approximately a constant amount, *ca.* 13 cal./mole of solute.

When aqueous solutions of two strong electrolytes are mixed, the changes in the volume of the system and in the enthalpy of the system are small, or zero, if the two solutions and the ternary solution produced are of the same ionic strength and if the ionic strength is not too large.²⁻⁵ Likewise, the changes in total excess free energy^{5,6} and in the total excess entropy⁶ produced by the mixing of strong electrolytes at constant ionic strength are zero or small.

The change in excess volume or excess enthalpy during mixing is the increment in the total volume or total enthalpy. Both are, of course, extensive quantities. It is convenient to state the results of mixing processes in terms of the increment divided by $n_2 + n_3$, the total number of moles of solute in a mixture of electrolytes of the 1-1 charge type. The symbols ΔV_m and ΔH_m will denote the increments in the respective intensive quantities. They are equal, respectively, to increases in the mean apparent molal (excess) volume and the mean apparent molal (excess) enthalpy.² (The word excess, of course, may be omitted in statements concerning volume and enthalpy. It may be included, as it is here, to stress the similarity of increments in apparent molal volume and in apparent molal enthalpy to increments in apparent molal excess free energy and apparent molal excess entropy.)

For mixings at constant ionic strength of electrolytes of the 1-1 charge type, ΔH_m and ΔV_m can usually be represented by simple power-series equations. Most authors^{2,3,7,8} have chosen to use explicit functions of the

solute mole fractions x_2 and x_3 . The following is such an equation.

$$\Delta H_m/x_2x_3 = a + bx_3 + \dots \quad (1)$$

The symbol x_3 represents the solute mole fraction $n_3/(n_2 + n_3)$ of one of the solutes. The symbols a , b , etc., denote empirical constants; n_2 and n_3 , etc., denote the respective numbers of moles of the solutes.

An alternative equation

$$\Delta H_m/x_2x_3 = \alpha + \beta(x_2 - x_3) + \dots \quad (2)$$

offers the advantages that the first empirical constant, α , is related very simply to an important geometrical feature of the curve representing the equation; it is four times the ordinate at $x_2 = 0.5 = x_3$.

A very careful study of changes in volume has recently been described by Wirth, Lindstrom, and Johnson.⁷ They used a very precise differential experimental method capable of delineating in detail the

(1) The Argonne National Laboratory, Argonne, Ill.

(2) T. F. Young and M. B. Smith, *J. Phys. Chem.*, **58**, 716 (1954); M. B. Smith, Ph.D. Thesis, University of Chicago, 1942.

(3) T. F. Young, Y. C. Wu, and A. A. Krawetz, *Discussions Faraday Soc.*, **24**, 37, 77, 80 (1957); Y. C. Wu, Ph.D. Thesis, University of Chicago, 1957.

(4) R. M. Rush and G. Scatchard, *J. Phys. Chem.*, **65**, 2240 (1961).

(5) H. S. Harned, *ibid.*, **63**, 1299 (1959); **64**, 112 (1960); **67**, 1739 (1963).

(6) H. A. C. McKay, *Discussions Faraday Soc.*, **24**, 76 (1957).

(7) H. E. Wirth, R. E. Lindstrom, and J. N. Johnson, *J. Phys. Chem.*, **67**, 2339 (1963).

(8) J. H. Stern and A. A. Passchier, *ibid.*, **67**, 2420 (1963).

shapes of the curves showing the variation of ΔV_m with x_3 . For six pairs of 1-1 electrolytes in 4 *m* solutions, they found two empirical constants in the volume analog of eq. 1 to be adequate. For each of the same six pairs in 1 *m* solutions, a single constant sufficed.

In their studies of the heats of mixing of 1-1 electrolytes in 1 *m* solutions, Young and Smith² and Young, Wu, and Krawetz³ found two constants to be adequate for each of the pairs of electrolytes for which they had obtained enough experimental points to make a study of eq. 1 significant. Assuming that the two-constant equation would be adequate for the mixing of pairs of other similar salts, they measured two heats of mixing for each of numerous other pairs of 1-1 electrolytes. Young, Wu, and Krawetz were thus enabled to include (in their Figure 2) curves for the heats of mixing of all pairs of the alkali metal chlorides (except some involving RbCl) with one another and with HCl.

Although Young, Wu, and Krawetz had obtained equations sufficiently accurate for the plotting of the curves in their Figure 2, their equations were not definitive and were not published. The availability of electronic computing facilities at the Argonne National Laboratory has made feasible the evaluation of the constants of the equations by a least-square procedure. This paper contains equations for the mixing of 25 pairs of electrolytes with one ion common to each pair.

Experimental

Calorimeter. The general design of the calorimeter has been described.^{2,9} The pipet and the stirrer were made of tantalum. The case of the heater was constructed of platinum and platinum-iridium alloy brazed with gold. During the latter part of the work, the stirrer design was modified to reduce the time required for mixing. The end of each blade was bent downward. The bend was closer to the hub at the trailing edge of the blade than at the leading edge. Much of the fluid moved by the stirrer was drawn inward from the sides of the calorimeter instead of being thrown toward the sides. Consequently, more of it was impelled downward than by the unmodified stirrers.

The time required for mixing by the improved stirrer was studied in the following manner. The calorimeter dewar flask was replaced by a transparent glass vessel of nearly the same shape and internal dimensions. An alkaline solution containing a little phenolphthalein was then put into the vessel. The pipet had been filled with a quantity of acid solution slightly in excess of the amount required to neutralize the base. Time was measured from the instant at which the pipet was opened until all of the indicator color disappeared.

When the excess acid was about 0.2%, the time observed was 40-60 sec.

Solutions. Large quantities of stock solutions were prepared and diluted by weight to the compositions required. The stock solutions of salts were analyzed by evaporation-residue methods¹⁰ or (usually) by silver halide precipitation.

Materials. Stock solutions were made from conductivity water and available reagent grade chemicals. CsCl and RbCl were not obtainable as reagent grade materials. The reagent grade substances and CsCl, all of which melted sharply, were not purified further. The purity of the RbCl, however, was not satisfactory. It did not melt sharply; moreover, when an aqueous solution of the RbCl sample was evaporated to dryness, a thin yellow layer appeared on the surface of the salt next to the bottom of the flask. (Spectrographic analysis revealed a trace of iron in the layer.)

To purify the RbCl, it was dissolved in conductivity water and most of it was "salted out" with hydrogen chloride gas. The purified material did not form the yellow layer. It also melted sharply. Unfortunately, the quantity of the purified salt was insufficient for a repetition of all of the mixing experiments with NaCl, KCl, and CsCl. The heats of mixing reported for RbCl with these salts are to be regarded, therefore, as tentative, although the impurities may not have affected the determinations. The equations for RbCl and HCl and for RbCl and LiCl were determined from experiments with the purified RbCl.¹¹

Calculations. The objective of a set of mixing experiments is the determination of the functional relationship of ΔH_m to x_3 . The calculation of a series of coordinates from the mixing experiments is somewhat complex but has been explained in detail.³ The series of coordinates determined for each pair of electrolytes was submitted to an IBM 704 calculator whose program directed it to determine the empirical constants of eq. 1 or 2. The machine minimized the sum of the squares of the differences between the calculated and experimental values of ΔH_m . When only two "points" were supplied to the machine, it determined values of the constants which made the calculated and experimental values exactly equal. No change in the programming was necessary.

Results

1-1 Electrolytes. Constants of eq. 2 for 24 pairs of 1-1 electrolytes are in Table I. Column 1 shows for

(9) T. F. Young and J. S. Machin, *J. Am. Chem. Soc.*, **58**, 2254 (1936).

(10) T. W. Richards and L. P. Hall, *ibid.*, **51**, 707 (1929).

(11) The new equation for LiCl and RbCl differs significantly from the one used for the calculation of the coordinates of the LiCl-RbCl curve in Figure 2 of Young, Wu, and Krawetz.

each equation the pair mixed; column 2 shows the number of experimental points; columns 3 and 4 contain the empirical constants α and β ; column 5 lists the value of $\alpha/4$ which is ΔH_m at $x_3 = 0.5$; and the last column shows the abscissa of each maximum or minimum ΔH_m . The symbol x_3 denotes the solute mole fraction of the electrolytes of larger formula weight.

Constants for eq. 1 are readily determined from Table I since

$$a = \alpha + \beta \quad (3)$$

and

$$b = -2\beta \quad (4)$$

Table I: Heats of Mixing of 1-1 Electrolytes with Common Ions ($I = 1.00$; $t = 25^\circ$; cal. mole $^{-1}$)

Electrolytes	No. of points	α	β	ΔH_m at $x_3 = 0.5$	x_3 of max. or min.
Pairs with common anions					
HCl-LiCl	2	52.0	-2.8	13.01	0.51
HCl-NaCl	4	130.1	13.3	32.52	0.47
HCl-KCl	10	-15.0	1.7	-3.74	0.53
HCl-RbCl	2	-82.2	-1.6	-20.55	0.50
HCl-CsCl	10	-136.0	-15.9	-34.01	0.47
LiCl-NaCl	12	84.6	6.6	21.15	0.48
LiCl-KCl	4	-64.2	-3.0	-16.05	0.49
LiCl-RbCl	2	-135.3	-10.6	-33.83	0.48
LiCl-CsCl	2	-194.6	-8.9	-48.65	0.49
NaCl-KCl	12	-38.3	0.5	-9.58	0.50
NaCl-RbCl	2	-49.5	3.3	-12.36	0.52
NaCl-CsCl	2	-34.8	-0.2	-8.69	0.50
KCl-RbCl	2	9.6	1.2	2.40	0.47
KCl-CsCl	2	6.4	-0.1	1.59	0.50
RbCl-CsCl	3	1.5	0.3	0.38	0.45
LiBr-NaBr	2	82.7	7.5	20.67	0.48
LiBr-KBr	2	-68.2	0.4	-17.05	0.50
NaBr-KBr	2	-37.7	1.0	-9.43	0.51
NaNO $_3$ -KNO $_3$	2	-50.3	-1.7	-12.57	0.49
Pairs with common cations					
LiCl-LiBr	2	3.2	0.1	0.81	0.50
NaCl-NaBr	2	3.2	-0.1	0.79	0.50
KCl-KBr	2	3.2	1.0	0.80	0.43
NaCl-NaNO $_3$	2	12.4	1.4	3.10	0.47
KCl-KNO $_3$	2	1.4	0.6	0.34	0.40

NaCl-Na $_2$ SO $_4$ Mixings. Enthalpy changes were measured for a series of twelve mixings of NaCl and Na $_2$ SO $_4$. Throughout the series the ionic strength of each solution was unity. The binary Na $_2$ SO $_4$ solutions were therefore $1/3$ m and hence $2/3$ (weight) N . From the twelve measurements two equations were derived by the least-squares procedure described above. Equation 6 shows the relation of the heat absorbed in

calories per ionic strength unit, I.u., to the ionic strength fraction, y_3 . Note that y_3 is defined by

$$y_3 = \frac{3n_3}{n_2 + 3n_3} \quad (5)$$

$$\Delta H_m/y_2y_3 = -27.1 + 3.0(y_2 - y_3) \text{ cal. I.u.}^{-1} \quad (6)$$

Equation 8 is the relation of the heat absorbed in calories per equivalent to z_3 , the equivalent fraction, i.e., the (weight) normality fraction

$$z_3 = \frac{2n_3}{n_2 + 2n_3} \quad (7)$$

$$\Delta H_m/z_2z_3 = -33.2 - 3.1(z_2 - z_3) \text{ cal. equiv.}^{-1} \quad (8)$$

According to eq. 6, ΔH_m at $y_3 = 0.5$ is -6.76 cal. I.u. $^{-1}$; the derivative at $y_3 = 1.0$ is $+30.1$, and the minimum is at $y_3 = 0.53$. According to eq. 8, ΔH_m at $z_3 = 0.5$ is -8.29 cal. equiv. $^{-1}$; the derivative at $z_3 = 1.0$ is $+30.1$ and the minimum is at $z_3 = 0.48$.

The mixing of 0.2 mole of NaCl (1 m) and 0.1 mole of Na $_2$ SO $_4$ ($1/3$ m) may be used to illustrate the application of both equations. In the ternary solution there are 500 g. of H $_2$ O and 0.3 mole of salt, which is 0.4 equivalent of salt and 0.5 I.u. of salt. The solute mole fraction of Na $_2$ SO $_4$ is 0.333, its equivalent (or normality) fraction is 0.5, and its ionic strength fraction is 0.6. According to eq. 6, ΔH_m is -6.63 cal. I.u. $^{-1}$; according to eq. 8, ΔH_m is -8.30 cal. equiv. $^{-1}$. According to either, the heat absorbed in the specified process is -3.32 cal. Note that the quantity -8.30 cal. equiv. $^{-1}$ is a verification of -8.29 cal. equiv. $^{-1}$ in the preceding paragraph. The quantity -6.76 cal. I.u. $^{-1}$ in the preceding paragraph, for the mixing of 0.3 mole of NaCl and 0.1 mole of Na $_2$ SO $_4$, may be verified by the use of either eq. 6 or eq. 8.

Discussion

Symmetry. For a symmetrical curve β , which equals $b/2$, is zero and the maximum or minimum lies at $x_3 = 0.5$. The slope of such a curve at $x_3 = 1$ is the negative of the slope at $x_3 = 0$. (These slopes are, respectively, $\beta - \alpha = b - a$ and $\beta + \alpha = a$.) Most of the curves are nearly symmetrical; the maxima and minima of all but three lie between $x_3 = 0.47$ and 0.53 . The heat effects for those three are very small; ΔH_m at $x_3 = 0.5$ is less than 1 cal./mole of solute.

Role of Common Ion. It has been pointed out³ that the heat of mixing of Cl $^-$ and Br $^-$ is nearly the same whether the mixing is done in the presence of Li $^+$, Na $^+$, or K $^+$. This is an interesting result because it suggests that the interactions between a pair of the same charge sign are typically affected relatively little by the common ion. Nine such changes of common

Table II: Effect on the Heat of Mixing of Variation of the Common Ion ($I = 1.00$; $t = 25^\circ$; cal. mole $^{-1}$)

Heteroions	Common ion	ΔH_m at $x_3 = 0.5$
Common anions		
Li $^+$ -Na $^+$	Cl $^-$	21.15
Li $^+$ -Na $^+$	Br $^-$	20.67
Li $^+$ -K $^+$	Cl $^-$	-16.05
Li $^+$ -K $^+$	Br $^-$	-17.05
Na $^+$ -K $^+$	Cl $^-$	-9.58
Na $^+$ -K $^+$	Br $^-$	-9.43
Na $^+$ -K $^+$	NO $_3^-$	-12.57
Common cations		
Cl $^-$ -Br $^-$	Li $^+$	0.81
Cl $^-$ -Br $^-$	Na $^+$	0.79
Cl $^-$ -Br $^-$	K $^+$	0.80
Cl $^-$ -NO $_3^-$	Na $^+$	3.10
Cl $^-$ -NO $_3^-$	K $^+$	0.34

ion are shown in Table II. The largest difference in ΔH_m produced by a change in the homoion is about 3 cal. mole $^{-1}$. In the two comparisons in which this relatively large difference occurs, the NO $_3^-$ ion is involved. The 3 cal. mole $^{-1}$ may be contrasted with the full range of the heats of mixing themselves. The heat of mixing of LiCl varies from 21 cal. mole $^{-1}$ for the mixing of LiCl with NaCl to -49 cal. mole $^{-1}$ for the mixing of LiCl with CsCl. This range for LiCl (the maximum range in Table I) is 70 cal. mole $^{-1}$.

It has been pointed out by Friedman¹² that the cluster theory of Mayer¹³ and others is in accord with the observation that a change in the homoion has relatively little effect upon the heat of mixing of any specified pair of heteroions.

The H $^+$: Li $^+$ Difference. The numerous thermal data now available, including those associated with RbCl, reveal an interesting regularity. The heat of mixing of HCl and NaCl, at $x_3 = 0.5$, is 32.52 cal. mole $^{-1}$. For LiCl and NaCl the corresponding value is 21.15 cal. mole $^{-1}$; see Figure 1. The difference between the two is 11.37 cal. mole $^{-1}$. Five such differences are plotted at the bottom of Figure 1. All of them are in the range 11.4 to 14.6 cal. mole $^{-1}$ and vary from electrolyte to electrolyte in a regular manner.

Relations to Other Properties of Solutions. The principal ultimate objective of these studies of electrolyte mixtures is the development and improvement of methods for the estimation of activity coefficients of electrolytes in the presence, and also in the absence, of other electrolytes. The activity coefficients are required for an understanding of the effects of salts upon chemical equilibria. The prediction of such effects remains one of the most important problems in the

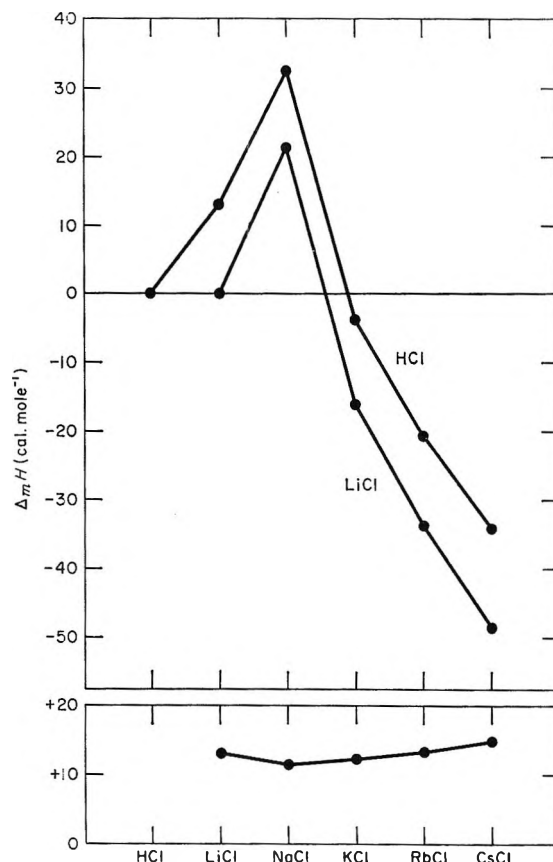


Figure 1. Heats of mixing of some chlorides ($I = 1.00$, $t = 25^\circ$, and $x_3 = 0.5$): top line, heats of mixing of HCl with alkali metal chlorides; middle line, heats of mixing of LiCl with alkali metal chlorides; bottom line, ordinates of top line (for HCl) minus ordinates of middle line (for LiCl).

physical chemistry of solutions. A second major objective in the study of activity coefficients is an improved understanding of interactions between ions. For each of these purposes it is important to discover the relations between the enthalpies of mixing and various properties of solutions. Too few data are available for a fully satisfying study, but some interesting relations have come to light, *e.g.*, the difference in behavior between structure makers and structure breakers.³ This grouping of electrolytes has been shown by Frank and Evans¹⁴ and by Frank and Wen¹⁵ to be related to numerous properties of solutions.

The sharp peaks in Figure 1 preclude the existence of a simple relation between the heats of mixing shown

(12) H. L. Friedman, "Ionic Solution Theory," Interscience Publishers, Inc., New York, and London, 1962.

(13) J. E. Mayer, *J. Chem. Phys.*, **18**, 1426 (1950).

(14) H. S. Frank and M. W. Evans, *ibid.*, **13**, 507 (1945).

(15) H. S. Frank and W. Y. Wen, *Discussions Faraday Soc.*, **24**, 133 (1957).

in the figure and the radius of the ion in crystals.^{16,17} It is obvious that there is no general simple relation between the heat of mixing and any property which is a monotonic function of atomic number. Excluded from a simple relationship with the heat of mixing is the radius of the hydrated ion, whether determined from transport properties by the method of Robinson and Stokes¹⁸ and modified by Nightingale,¹⁹ or from activity coefficients by the method of Stokes and Robinson.^{20,21}

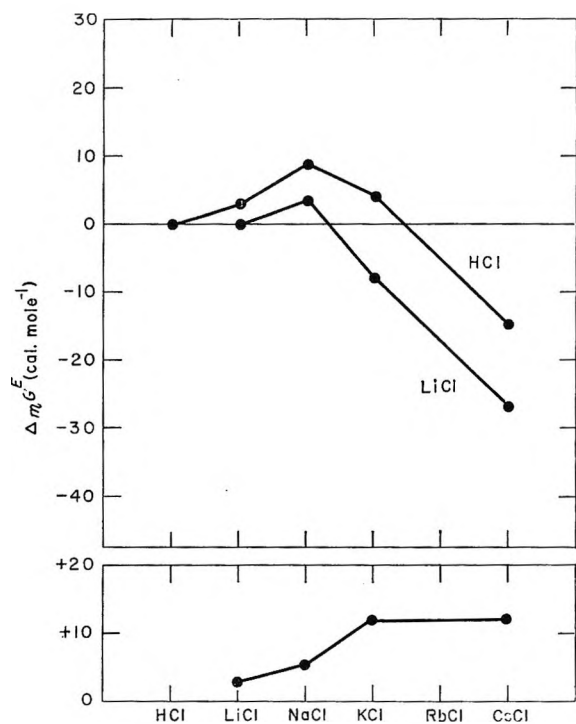


Figure 2. Excess free energies (from calculations of McKay⁶ and Harned⁵) of mixing of some chlorides ($I = 1.00$, $t = 25^\circ$, and $x_3 = 0.5$): top line, excess free energies of mixing of HCl with alkali metal chlorides; middle line, excess free energies of mixing of LiCl with alkali metal chlorides; bottom line, ordinates of the top line (for HCl) minus ordinates of middle line (for LiCl).

Partial Molal Volumes. There is a property, however, whose variations are qualitatively much like the variations in the heats of mixing shown in Figure 1: namely the limiting partial molal volume at zero molality. Some values of that function are now known very precisely.^{7,22,23} The similarity is most simply and beautifully shown by comparison of ΔH_m with the partial molal volumes "assigned" to the various in-

dividual ions. For the H^+ ion, the assigned value is small and usually negative.²⁴⁻²⁶

For the Li^+ ion, the value is more negative (larger absolutely) and for Na^+ , it is still more negative. For the larger ions (structure breakers), the partial molal volumes are positive and increase in the order: K^+ , Rb^+ , and Cs^+ . (See Figure 1.)

Comparison with other properties must await further experimental work on those properties. Adequate comparisons will also require calorimetric investigations of electrolytes and solvents of more varied types. Work with other temperatures and concentrations is needed. Fortunately, investigations of these two variables have been included in recent work by Stern and Passchier.⁸ Especially interesting will be salts of other charge types. Probably the most interesting extension of the investigation will be the inclusion of pairs of electrolytes which do not possess ions common to the pair. The behavior of a few pairs is described in the following paper.

Molal Excess Free Energy. A different type of comparison may be made between the change in enthalpy produced by mixing and the change in some other property produced by the same mixing. McKay⁶ calculated, from available data, changes in the molal excess free energies of mixing of ten pairs of alkali metal chlorides. Some of his results have been confirmed by Harned⁵ using measurements previously contributed from his own laboratory. Graphs (see Figure 2) for the excess free energy are similar to those in Figure 1. From the changes in excess free energy and the changes in excess enthalpy, the increases in excess entropy have also been calculated. Again, graphs similar in general form to the lines shown in Figure 1 were obtained.

(16) L. Pauling, "The Nature of the Chemical Bond," 3rd Ed., Cornell University Press, Ithaca, N. Y., 1960.

(17) "Handbook of Chemistry and Physics," 45th Ed., Chemical Rubber Publishing Co., Cleveland, Ohio, 1964, p. F89.

(18) R. A. Robinson and R. H. Stokes, "Electrolyte Solutions," 2nd Ed., Butterworth and Co., Ltd., London, 1959.

(19) E. R. Nightingale, Jr., *J. Phys. Chem.*, **63**, 1381 (1959).

(20) R. H. Stokes and R. A. Robinson, *J. Am. Chem. Soc.*, **70**, 1870 (1948).

(21) See ref. 18, p. 246.

(22) O. Redlich and J. Bigeleisen, *J. Am. Chem. Soc.*, **64**, 758 (1942).

(23) O. Redlich and D. M. Meyer, *Chem. Rev.*, **64**, 221 (1964).

(24) O. K. Rice, "Electronic Structure and Chemical Binding," McGraw-Hill Book Co., Inc., New York, and London, 1940.

(25) C. B. Monk, "Electrolytic Dissociation," Academic Press, London and New York, 1961.

(26) R. M. Noyes, *J. Am. Chem. Soc.*, **86**, 971 (1964).

Heats of Mixing of Electrolytes of the 1-1 Charge Type

by Y. C. Wu, M. B. Smith, and T. F. Young¹

George Herbert Jones Chemical Laboratory, University of Chicago, Chicago, Illinois, and Argonne National Laboratory, Argonne, Illinois (Received December 3, 1964)

Heats of mixing of eight pairs of 1 *m* aqueous solutions of 1-1 electrolytes not having an ion common to the pair have been measured at 25°. The average of the absolute values of the molal heats of mixing is somewhat larger than the average of the absolute values of the heats of mixing of pairs of the same electrolytes so grouped that there is a common ion within each pair. The thermochemical relation between the heats of cross mixing and the heats of common-ion mixing (the cross-square rule) has been tested by application to four systems. The rule fits the data remarkably well. The purely thermodynamic, and hence exact, relation between heats of dilution and heats of cross mixing has been pointed out and its application illustrated. Work with relatively dilute solutions is not in accord with the Brønsted principle of specific ionic interaction.

Aqueous solutions of four electrolytes are indicated at the corners of the square in Figure 1. If 0.5 mole of LiCl is mixed with 0.5 mole of LiBr (each in a 1 *m* solution at 25°), the heat absorbed is 0.81 cal./mole of electrolyte as indicated on the left side of the square.² The mixing of 0.5 mole of NaCl and 0.5 mole of NaBr causes the absorption of 0.79 cal./mole. The mixing of 0.5 mole each of LiCl and NaCl is accompanied by the absorption of 21.15 cal./mole as indicated on the upper side of the square; the mixing of 0.5 mole each of LiBr and NaBr is accompanied by the absorption of 20.67 cal./mole.

Let T_u represent one-half of the ternary solution produced by the mixing of the solutions of LiCl and NaCl. It contains 0.25 mole of Li^+ , 0.25 mole of Na^+ , 0.5 mole of Cl^- , and 500 g. of H_2O . It is shown in Figure 1 at the middle of the upper side of the square. Similarly, let T_b on the bottom side of the square represent one-half of the solution formed by the mixing of the solutions of LiBr and NaBr. It contains 0.25 mole of Li^+ , 0.25 mole of Na^+ , 0.5 mole of Br^- , and 500 g. of H_2O . The fact that the heat of mixing of the Cl^- and Br^- ions in the presence of Li^+ (0.81 cal. mole⁻¹) differs but little from the heat of mixing of these anions in the presence of Na^+ (0.79 cal. mole⁻¹) suggests that the heat of mixing of Cl^- and Br^- ions in the presence of an equimolal mixture of Li^+ and Na^+ should be approximately 0.80, the mean of 0.81 and 0.79. (The numbers 0.79 and 0.81 are used here, partially, as sym-

bols for the respective heat effects; there is no implication that the small difference between them is experimentally significant.) Denote the difference between the actual ΔH_m and 0.80 by ϵ . Then

$$T_u + T_b \longrightarrow Q_{\text{Mix}} \quad (\Delta H_m = 0.80 + \epsilon) \quad (1)$$

The abbreviation, Q_{Mix} , is used to designate the solution containing equal quantities of the four ions (*i.e.*, containing equal quantities of the four electrolytes) in an aqueous solution of unit ionic strength. Formed from the four electrolytes and water, it may be regarded as a quintuple mixture.

Now the heat of mixing of Li^+ and Na^+ ions in the presence of Cl^- (21.15 cal. mole⁻¹) differs by a relatively small amount from the heat of mixing of Li^+ and Na^+ ions in the presence of Br^- (20.67 cal. mole⁻¹). It seems probable, therefore, that the heat of mixing of Li^+ and Na^+ in the presence of an equimolal mixture of Cl^- and Br^- would differ very little from 20.91, the mean of 21.15 and 20.67 cal. mole⁻¹. Define ϵ' by the equation

$$T_r + T_l \longrightarrow Q_{\text{Mix}} \quad (\Delta H'_m = 20.91 + \epsilon') \quad (2)$$

The quintuple mixtures produced in processes 1 and 2 are identical. The two processes are the respective

(1) The Argonne National Laboratory, Argonne, Ill.

(2) Y. C. Wu, M. B. Smith, and T. F. Young, *J. Phys. Chem.*, **69**, 1868 (1965), and T. F. Young, Y. C. Wu, and A. A. Krawetz, *Discussions Faraday Soc.*, **24**, 37, 77, 80 (1957).

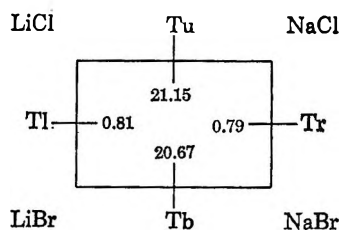


Figure 1. Heats of mixing of four pairs of electrolytes. Each number is the heat (cal./mole of solute) absorbed during the mixing of 0.5 mole each of two electrolytes having a common ion. The ionic strength of each solution is unity. T_i represents a solution containing one-half of the ternary mixture produced by the mixing of the i th pair. The lower case letters u, r, b, and l denote, respectively, the mixings indicated along the upper, the right, the bottom, and the left sides of the square.

final steps of two paths each of which starts with 0.25 mole of each of the four electrolytes and ends with the quintuple solution. The quantities of heat absorbed along the two complete paths are necessarily equal. Hence

$$\frac{1}{2}[21.15 + 20.67] + 0.80 + \epsilon = \frac{1}{2}[0.81 + 0.79] + 20.91 + \epsilon' \quad (3)$$

It follows that $\epsilon = \epsilon'$. The magnitude of ϵ for each set of four electrolytes can be determined experimentally. The most direct method would be a calorimetric measurement of the heat absorbed either in the mixing of T_u and T_b or in the mixing of T_r and T_l . Substitution of the observed enthalpy increase ΔH_m in eq. 1, or $\Delta H'_m$ in eq. 2, would yield ϵ .

There is a third path by which the same quintuple solution may be obtained from the identical set of four initial solutions. The mixing of 0.5 mole of LiBr and 0.5 mole of NaCl produces the same quintuple solution produced by processes 1 and 2.³ Likewise, the mixing of 0.5 mole each of LiCl and NaBr produces that same quintuple solution. These two mixings are represented by the respective diagonals of the square in Figure 1. To distinguish such mixings from common-ion mixings, they will be referred to as cross mixings. The third path mentioned above is one-half of the sum of the two cross mixings. Therefore, one-half of the sum of the heats of the two cross mixings must be equal to each of the sums indicated in eq. 3. Each of these sums may be described as ϵ plus one-half the sum, $\Sigma\Box$, of the four heats of common-ion mixing shown along the respective sides of the square. The sum of the two heats of cross mixing will be represented by $\Sigma\times$. Hence

$$\frac{1}{2}\Sigma\Box + \epsilon = \frac{1}{2}\Sigma\times \quad (4)$$

The postulate that ϵ is often very small leads to the corollary

$$\frac{1}{2}\Sigma\Box \cong \frac{1}{2}\Sigma\times \quad (5)$$

This approximate equation is referred to below as the cross-square rule.⁴ Experiments carried out to test the rule determine values of ϵ . Experimental procedures and methods of calculation have been described.²

Results

Table I contains constants, empirically determined, for equations of the type

$$\Delta H_m/x_2x_3 = \alpha + \beta(x_2 - x_3) + \dots \quad (6)$$

Table I: Heats of Mixing of 1-1 Electrolytes without Common Ions (cal. mole⁻¹; $t = 25^\circ$; $I = 1.00$)

Electrolytes	No. of points	α	β	ΔH_m at $x_3 = 0.5$	x_3 of max. or min.
LiCl-NaBr	2	110.8	5.8	27.70	0.49
LiCl-KBr	2	1.4	-0.9	0.35	0.63
LiBr-NaCl	2	62.4	-4.5	15.59	0.52
LiBr-KCl	2	-127.1	3.5	-31.78	0.51
NaCl-KBr	2	4.8	1.1	1.21	0.44
NaCl-KNO ₃	2	316.7	17.9	79.2	0.49
NaBr-KCl	2	-74.8	-0.8	-18.71	0.50
NaNO ₃ -KCl	2	-400.7	5.1	-100.2	0.50

The symbol x_3 denotes the *solute* mole fraction of the salt of larger formula weight, and x_2 the *solute* mole fraction of the other electrolyte.

Discussion

Symmetry. Most of the curves represented by the equations of Table I are nearly symmetrical; the maximum ΔH_m of each (with two exceptions) lies between $x_3 = 0.49$ and 0.52 . The heat effects of the exceptional two are small, the ΔH_m values at $x_3 = 0.5$ are 1.21 and 0.35 cal. mole⁻¹.

The Cross-Square Rule. In the diagram at the top of Figure 2 are the ΔH_m values, at $x_3 = 0.5$, for the six possible mixings of the four electrolytes represented at the corners of the square in Figure 1. In addition to the heats of common-ion mixing shown along the sides of the square, the heats of cross mixing are shown near the respective diagonals. Note that $\frac{1}{2}\Sigma\Box$ is

(3) Produced in this way, the solution Q_{MIX} may be regarded as a ternary solution. We shall refer to it as Q_{MIX} because that name is a reminder that the solvent and all four ions are present. In this paper we are interested particularly in quintuple solutions in which the molality of each ion is 0.5 mole/kg. of solvent.

(4) A formal derivation of eq. 5 was given by C. J. F. Böttcher, *Discussions Faraday Soc.*, 24, 78 (1957).

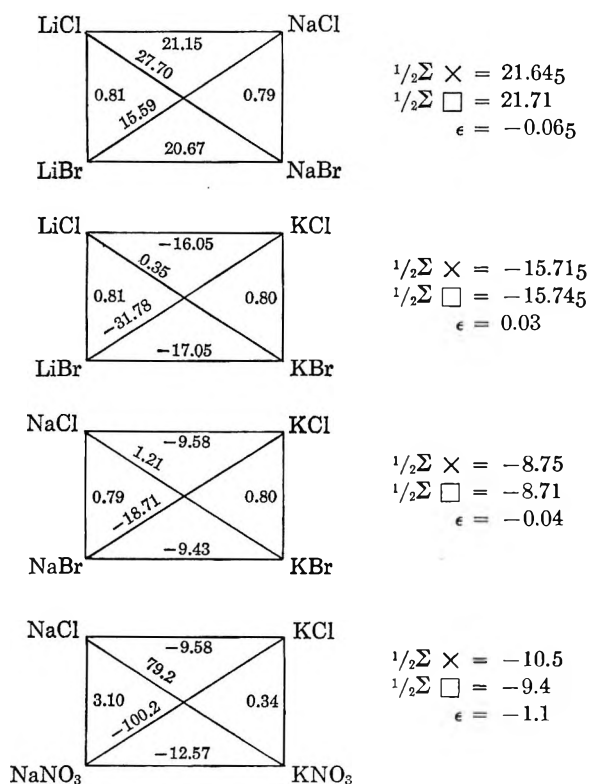


Figure 2. Comparison of heats of cross mixing with heats of common-ion mixing at $x_3 = 0.5$ (cal. per mole of quintuple mixture).

21.71 cal. and $\frac{1}{2}\Sigma X$ is 21.645 cal. The difference, ϵ , is therefore -0.065 cal.

In Figure 2 are four diagrams illustrating the operation of the cross-square rule. For each of the first three systems, ϵ is surprisingly small, probably smaller than the experimental uncertainty.

The deviation for the fourth system is considerably larger. The larger ϵ is presumably the result of special, and relatively large, interactions between the alkali metal ions and the nitrate ion. It is possible, however, that the larger ϵ is due to experimental error. The most important source of experimental uncertainty is probably not in the calorimetric measurements themselves, although the two heats of cross mixing are so large that a 1% error in either one would account for nearly half of ϵ . More important sources of experimental uncertainty are probably impurities in the salts and the methods of analysis. Evaporation to dryness was the sole analytical method used. It may be necessary in future work to prepare standards with which to compare the residues from evaporation and to purify the standards by means of zone refining.⁵ Because of the large magnitudes of ΔH_m , it will also be necessary to determine more points on the ΔH_m vs. x curves and to

use one or two additional constants in each of the empirical equations (eq. 6).⁶

Relation of Heats of Dilution to Heats of Mixing. The difference between the two heats of cross mixing of a set is related to and can be calculated from the integral heats of dilution of the four binary solutions. The integral heat of dilution, to $m = 0$, of a mole of solute in a binary solution is the negative of ϕL , the relative apparent molal enthalpy of the solute in that solution. The relation of ϕL to the difference between the heats of cross mixing will be introduced with an illustration. Consider the set: NaCl, KCl, NaNO₃, KNO₃. The relative apparent molal enthalpy of the $Q_{M_{ix}}$ produced by one of the cross mixings is given by

$$\phi L (Q_{M_{ix}}) = \Delta H_m + \frac{1}{2}\phi L (\text{NaCl}) + \frac{1}{2}\phi L (\text{KNO}_3) \quad (7)$$

The relative apparent molal enthalpy of the $Q_{M_{ix}}$ produced by the other cross mixing is given by

$$\phi L (Q_{M_{ix}}) = \Delta H'_m + \frac{1}{2}\phi L (\text{KCl}) + \frac{1}{2}\phi L (\text{NaNO}_3) \quad (8)$$

Since the compositions of the two $Q_{M_{ix}}$'s are identical subtraction of eq. 8 from eq. 7 leaves

$$\Delta H'_m - \Delta H_m = \frac{1}{2}\phi L (\text{NaCl}) + \frac{1}{2}\phi L (\text{KNO}_3) - \frac{1}{2}\phi L (\text{KCl}) - \frac{1}{2}\phi L (\text{NaNO}_3) \quad (9)$$

This equation is based upon the first law of thermodynamics and the fact that the enthalpies of ions in infinitely dilute solutions are additive. It requires no proof or demonstration.

The illustration of eq. 9 requires knowledge of ϕL of the solutes in the binary solutions. Until recently, the available tables of ϕL have been of inferior accuracy⁷ largely because of faulty extrapolations to infinite dilution.^{8,9} For 16 salts of the 1-1 and 1-2 charge types, Young and Seligmann used procedures similar to those of Young and Groenier⁸ and Young and Machin⁹ to rectify the extrapolations and determine new empirical equations.¹⁰ Their equations were intended to be valid only for very dilute solutions. Now, however, an extensive study of the apparent molal enthalpies of

(5) P. Sue, J. Pauly, and A. Nouaille, *Compt. rend.*, **244**, 1505 (1957).

(6) Cf. H. E. Wirth, R. E. Lindstrom, and J. N. Johnson, *J. Phys. Chem.*, **67**, 2339 (1963).

(7) For example, "International Critical Tables," McGraw-Hill Book Co., Inc., New York, N. Y., 1925-1933; B. E. Conway, "Electrochemical Data," Elsevier Publishing Co., Amsterdam and Houston, 1952.

(8) T. F. Young and W. L. Groenier, *J. Am. Chem. Soc.*, **58**, 187 (1936).

(9) T. F. Young and J. S. Machin, *ibid.*, **58**, 2254 (1936).

(10) T. F. Young and P. Seligmann, *ibid.*, **60**, 2379 (1938); cf. A. L. Robinson and W. E. Wallace, *ibid.*, **63**, 1582 (1941).

aqueous solutions of numerous 1-1 electrolytes has been made at the U. S. National Bureau of Standards by Dr. Vivian Parker. In Table II are the values of ϕL taken from her compilation¹¹ that are needed for the illustration of the use of eq. 9. The difference, $\Delta H'_m - \Delta H_m$, calculated from the ϕL values is

$$\frac{1}{2}[-23 - 715 + 15 + 367] = -178 \text{ cal./mole of } Q_{\text{MIX}}$$

The difference calculated from the heats of cross mixing is $-179.4 \text{ cal. mole}^{-1}$. The agreement is excellent; indeed, it is fortuitous.

Table II: Relative Apparent Molal Enthalpies^a (cal. mole⁻¹; $t = 25^\circ$; $m = 1.0 \text{ mole kg.}^{-1}$)

NaCl	KNO ₃	KCl	NaNO ₃
-23	-715	-15	-367

^a See ref. 11.

Ionic Interactions. In each of the four systems represented in Figure 2, the common-cation mixings are associated with relatively small heat effects. The two common-anion mixings are somewhat larger and, as noted earlier, are approximately equal. The sum of the two is, of course, very nearly equal to the sum of the heats of cross mixing. The two heats of cross mixing are in general not equal; indeed, one may be very much larger than the other, or the two may be of opposite algebraic sign. It is normal then that the largest ΔH_m (at $x_3 = 0.5$) in a set of six for a system of four electrolytes be one of the heats of cross mixing. The system, NaCl, KCl, NaNO₃, KNO₃, is an interesting illustration. The heats of common-ion mixing are relatively small. Hence the heats of cross mixing are approximately equal in magnitude but of opposite algebraic sign ($+79$ and $-100 \text{ cal. mole}^{-1}$).

Brønsted's Principle of Specific Ionic Interaction. The application of Brønsted's theory of specific ionic interaction¹²⁻¹⁷ to the enthalpies of mixtures suggests that the heat of a homoionic mixing is zero or very small. Application of the cross-square rule to a system obeying the Brønsted principle suggests that the heats of cross mixing (at $x_3 = 0.5$) should be equal in magnitude but of opposite algebraic sign. This conclusion is implicit in the discussion by Scatchard and Prentiss of the Brønsted theory.¹⁶

Scatchard and Breckenridge¹⁸ have pointed out that the "fundamental assumption of Brønsted cannot be" of "universal" validity. It is important that the theory be tested much more extensively than has been

done. Direct measurements of changes in properties occurring during mixing are especially effective for this purpose. Heats of mixing of 1 m solutions, however, are not suitable because Brønsted himself has called attention to the limitation of his theory to dilute solutions¹⁹ (*ca.* 0.1 m).

In Table III are a few values of ΔH_m for the mixing of LiCl and NaCl at various ionic strengths. As the ionic

Table III: Heat of Mixing of LiCl and NaCl at Various Ionic Strengths (cal. mole⁻¹; $t = 25^\circ$; $x_3 = 0.5$)

I	ΔH_m	$\Delta H_m/I$
2.0	34.08	17.04
1.0	21.15	21.15
0.75	16.10	21.47
0.50	10.7	21.4

strength is decreased, ΔH_m decreases but the quotient $\Delta H_m/I$ does not decrease as the Brønsted principle requires. It does not seem likely that the quotient can decrease very much as I , the ionic strength, is reduced to 0.1. Professor R. H. Wood and Mr. Ronald Smith²⁰ have extended determinations of heats of mixing of LiCl and NaCl to $I = 0.1 m$. The quotient $\Delta H_m/I$ may have decreased slightly between $I = 0.5$ and $I = 0.1$, but it is probable that the decrease is smaller than the small uncertainties in the experimental work.

Mixings have also been made²¹ of NaCl and Na₂SO₄ solutions of ionic strengths from 5.0 to 0.2. For this pair of electrolytes, $\Delta H_m/I$ actually increases as I is decreased. Obviously, much is yet to be learned from further work. At present, however, the heat-of-mixing measurements do not support the "Brønsted Principle of Specific Ionic Interaction."

(11) V. B. Parker, "Thermal Properties of Aqueous Uni-univalent Electrolytes," NSRDS-NBS 2, National Bureau of Standards, Washington, D. C., 1965.

(12) J. N. Brønsted, *J. Am. Chem. Soc.*, **44**, 877, 938 (1922).

(13) H. S. Harned and B. B. Owen, "The Physical Chemistry of Electrolytic Solutions," 3rd Ed., Reinhold Publishing Corp., New York, N. Y., 1958, pp. 515, 605-607, 613.

(14) R. A. Robinson and R. H. Stokes, "Electrolyte Solutions," 2nd Ed., Butterworth and Co., Ltd., London, 1959, p. 436.

(15) E. A. Guggenheim, *Phil. Mag.*, [7] **19**, 588 (1935).

(16) G. Scatchard and S. S. Prentiss, *J. Am. Chem. Soc.*, **56**, 2320 (1934).

(17) G. Scatchard, *Chem. Rev.*, **19**, 309 (1936).

(18) G. Scatchard and R. G. Breckenridge, *J. Phys. Chem.*, **58**, 596 (1954).

(19) J. N. Brønsted, *J. Am. Chem. Soc.*, **45**, 2898 (1923).

(20) R. H. Wood, personal communication, 1964.

(21) M. B. Smith, Ph.D. Thesis, University of Chicago, 1942.

Kinetics of the Reaction of Cyclopropane with Hydrogen over a Series of Silica-Supported Metals

by J. H. Sinfelt, D. J. C. Yates, and W. F. Taylor

Process Research Division, Esso Research and Engineering Company, Linden, New Jersey
(Received December 4, 1964)

The kinetics of the reaction of cyclopropane with hydrogen were investigated over a series of silica-supported metal catalysts: nickel, cobalt, platinum, and copper. The catalysts all contained 10 wt. % of metal, and values of the metal surface area were available from previously reported hydrogen chemisorption measurements. Over nickel and cobalt, the reaction products included methane and ethane in addition to propane. Over platinum and copper, the only product observed was propane. Since the surface areas of the metals were known, it was possible to determine specific catalytic activities and hence to allow for differences in activity arising from variations in the degree of metal dispersion on the support. The order of catalytic activity of the metals for the hydrogenation of cyclopropane to propane is $\text{Ni} > \text{Pt} > \text{Co} > \text{Cu}$.

The reaction of cyclopropane with hydrogen has been investigated over a variety of supported metal catalysts, primarily nickel^{1,2} and certain of the noble group VIII metals,³⁻⁶ including rhodium, palladium, iridium, and platinum. The reaction product observed in all these studies was limited to propane, there being no evidence for the formation of other products such as methane and ethane. However, recent studies on nickel films⁷ and platinum blacks⁸ have disclosed the formation of the latter products as well as propane.

Recently, we have been interested in the kinetics of the reaction of cyclopropane with hydrogen over a series of silica-supported metals. Kinetic data have been obtained over two of the previously studied metals, nickel and platinum, and have been extended to include cobalt and copper. Values of the surface area of each of the supported metals have been obtained by hydrogen chemisorption measurements,⁹ and it has been possible to determine the specific catalytic activity (activity per unit surface area) of each of the metals. Consequently, the catalytic activities have been compared on a more fundamental basis than is commonly done since effects due to differing degrees of metal dispersion on the support are taken into account.

A previous study of the reaction of cyclopropane with

hydrogen over supported nickel catalysts has shown that the products of the reaction include methane and ethane, as well as propane.¹⁰ Therefore, an item of some interest in the present work was the effect of varying the metal on the distribution of reaction products. In this paper the reaction leading to the formation of propane is termed hydrogenation, while the reaction yielding methane and ethane is termed hydrogenolysis. Kinetic information on both reactions, including pressure dependencies with respect to cyclopropane and hydrogen as well as the dependence on temperature, have been obtained. The results have extended our knowledge of the interaction between cyclopropane and hydrogen over metal catalysts and

- (1) G. C. Bond and J. Sheridan, *Trans. Faraday Soc.*, **48**, 713 (1952).
- (2) J. E. Benson and T. Kwan, *J. Phys. Chem.*, **60**, 1601 (1956).
- (3) J. Addy and G. C. Bond, *Trans. Faraday Soc.*, **53**, 368 (1957).
- (4) J. Addy and G. C. Bond, *ibid.*, **53**, 383 (1957).
- (5) G. C. Bond and J. Turkevich, *ibid.*, **50**, 1335 (1954).
- (6) G. C. Bond and J. Newham, *ibid.*, **56**, 1501 (1960).
- (7) Z. Knor, V. Ponec, Z. Herman, Z. Dolejšek, and S. Cerny, *J. Catalysis*, **2**, 299 (1963).
- (8) D. W. McKee, *J. Phys. Chem.*, **67**, 1336 (1963).
- (9) J. H. Sinfelt, W. F. Taylor, and D. J. C. Yates, *ibid.*, **69**, 95 (1965).
- (10) W. F. Taylor, D. J. C. Yates, and J. H. Sinfelt, *J. Catalysis*, in press.

have given some further insight into the nature of catalysis over supported metals.

Experimental

Apparatus and Procedure. The kinetic data were obtained in a flow reactor system at atmospheric pressure, using a vertically mounted stainless steel reactor tube 1.0 cm. in diameter and 8.0 cm. in length. Details of the reactor assembly, flow rate measurements, and the gas chromatographic analysis of the reaction products have been reported previously.¹¹ The cyclopropane and hydrogen were mixed with helium and passed downflow through a bed containing 0.20 g. of catalyst diluted uniformly with 0.50 g. of ground Vycor glass. By appropriate adjustment of the helium flow rate, it was possible to vary the partial pressures of cyclopropane and hydrogen individually. The total gas flow was maintained at 1 l./min. throughout. In a typical run, the reactant gases were passed over the catalyst for 3 min. prior to sampling products for analysis. The cyclopropane was then cut out and the hydrogen flow continued for 10 min. prior to another reaction period. As an insurance against possible complications due to changing catalyst activity, most of the reaction periods were bracketed by periods at a standard set of conditions, so that the kinetic data could be expressed as rates relative to the rate at the standard conditions. Prior to any reaction rate measurements, the catalysts were reduced overnight in 50 cc./min. of flowing hydrogen at 370° in the reactor.

The surface areas of the supported metals used in this work were obtained from hydrogen chemisorption data and also carbon monoxide chemisorption in the case of the copper catalyst. The metal areas have been reported previously.⁹ Details of the chemisorption measurements used to estimate the metal surface areas can be obtained from previous papers by the authors.^{9,12} The surface areas were determined after the catalyst had been reduced at the same conditions employed in reducing the catalyst in the reactor.

Materials. The supported metal catalysts used in this work all contained 10 wt. % of metal and were prepared by impregnation of silica (Cabosil) with the nitrate salt of the metal or, in the case of platinum, with Pt(NH₃)₂(NO₂)₂. The details of preparation of all of these catalysts have been reported previously.⁹

The cyclopropane was obtained from the Matheson Co.; a chromatographic analysis showed no detectable impurities. It is estimated that an impurity, *e.g.*, methane, would have been detected by the chromatographic analysis if it were present at a concentration above 0.01 wt. %. High purity hydrogen was obtained from the Linde Co., Linden, N. J. It was fur-

ther purified in a Deoxo unit containing palladium catalyst to remove trace amounts of oxygen. The water formed was then removed by a molecular sieve dryer.

Results

As pointed out in the previous section of the paper, values of the metal surface areas of the catalysts were available from hydrogen chemisorption measurements. Expressed per gram of catalyst, the surface areas are: Ni, 13.6 m.²; Co, 5.6 m.²; Pt, 4.4 m.²; Cu, 3.3 m.².

The reaction of cyclopropane with hydrogen was studied at low conversion levels (0.1 to 10%). Rates were calculated from the relation

$$r = (F/W)x \quad (1)$$

where F represents the feed rate to the reactor in moles of cyclopropane per hour, W represents the weight in grams of the catalyst, and x represents the fraction of cyclopropane converted. In the determination of the rate of hydrogenation, x represents the fraction converted to propane, whereas, in the case of hydrogenolysis, x represents the conversion to methane and ethane. Reaction rates are correspondingly expressed as moles of cyclopropane converted per hour per gram of catalyst to propane or to methane plus ethane.

In the case of the hydrogenolysis reaction, which was observed only over the nickel and cobalt catalysts, the methane and ethane were formed in equimolar portions. This is shown by the typical data in Table I giving the distribution of methane and ethane in the products. Since the methane and ethane are formed

Table I: Distribution of Methane and Ethane in Products

Catalyst	Temp., °C.	Total conversion of cyclopropane, %	Distribution of methane and ethane, mole % ^a	
			Methane	Ethane
Ni-SiO ₂	40	2.2	48.4	51.6
Co-SiO ₂	121	4.6	50.5	49.5

^a Cyclopropane pressure 0.030 atm.; H₂ pressure 0.20 atm.

in equimolar proportions, the rate of hydrogenolysis can be determined simply from the amount of either one of these compounds in the product. The methane and ethane appear to be primary reaction products, rather

(11) J. H. Sinfelt, *J. Phys. Chem.*, **68**, 344 (1964).

(12) D. J. C. Yates, W. F. Taylor, and J. H. Sinfelt, *J. Am. Chem. Soc.*, **86**, 2996 (1964).

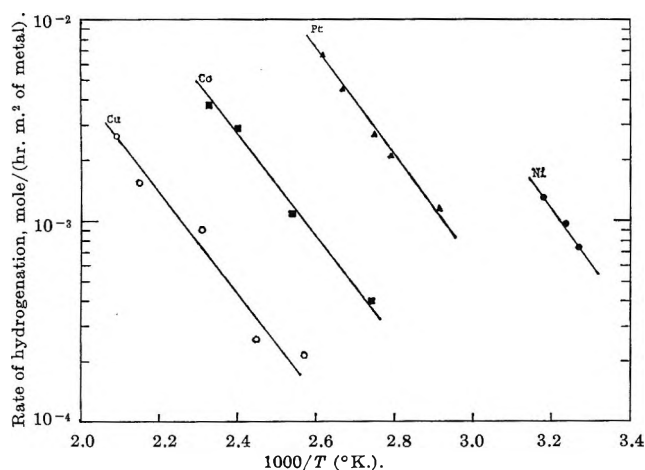


Figure 1. Effect of temperature on rate of hydrogenation of cyclopropane to propane at $p_H = 0.20$ atm., $p_C = 0.030$ atm.: ●, Ni; ▲, Pt; ■, Co; ○, Cu.

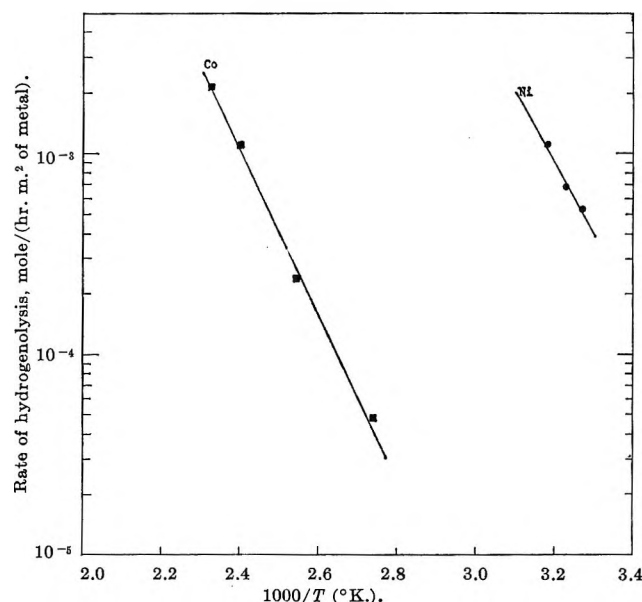


Figure 2. Effect of temperature on rate of hydrogenolysis of cyclopropane to methane and ethane at $p_H = 0.20$ atm., $p_C = 0.030$ atm.: ●, Ni; ■, Co.

than secondary products arising from a further reaction of the propane formed. Data obtained on the hydrogenolysis of propane over the nickel catalyst¹⁰ have shown that the rate of conversion to methane and ethane is much too low to account for the rate of formation of these products from cyclopropane *via* a gas phase propane intermediate.

In a run to measure reaction rates, the catalyst was first prerduced with hydrogen overnight at 370°. Then the temperature was lowered in flowing hydrogen, and at a standard set of hydrogen and cyclopropane partial pressures ($p_H = 0.20$ atm., $p_C = 0.030$ atm.) the activity of the freshly reduced catalyst was measured. Then rates were measured at a series of temperatures in a rising temperature sequence. The data for the four catalysts are shown in the Arrhenius plots in Figures 1 and 2. The data in Figure 1 are for the hydrogenation to propane, while the data in Figure 2 are for the hydrogenolysis to methane plus ethane. As already pointed out, the hydrogenolysis to methane and ethane was not observed over the platinum and copper catalysts over the range of temperatures studied. The order of catalytic activities for hydrogenation to propane is clearly $Ni > Pt > Co > Cu$. In the case of the hydrogenolysis reaction to methane and ethane, the order is $Ni > Co > Pt$ or Cu . In the measurement of the catalytic activities of the various supported metals, there was some overlap in the temperature ranges in which the platinum, cobalt, and copper catalysts were investigated, so that part of the data on each of these catalysts was obtained at about the same temperature. In the case of the nickel catalyst, however, there was no overlap in temperature range with the other catalysts, the temperatures being lower

Table II: Effect of Cyclopropane and H_2 Pressures on Rates of Hydrogenation and Hydrogenolysis

Catalyst	p_C , atm.	p_H , atm.	r/r_0^a	
			Hydrogenation	Hydrogenolysis
Ni-SiO ₂ (27°)	0.030	0.10	1.13	1.21
	0.030	0.20	1.00	1.00
	0.030	0.40	0.95	0.77
	0.010	0.20	0.41	0.63
	0.030	0.20	1.00	1.00
	0.100	0.20	2.59	1.36
Co-SiO ₂ (121°)	0.030	0.10	1.03	1.21
	0.030	0.20	1.00	1.00
	0.030	0.40	0.93	0.89
	0.010	0.20	0.48	0.47
	0.030	0.20	1.00	1.00
	0.100	0.20	1.77	1.81
Pt-SiO ₂ (79°)	0.030	0.10	1.33	...
	0.030	0.20	1.00	...
	0.030	0.40	0.70	...
	0.010	0.20	0.30	...
	0.030	0.20	1.00	...
	0.100	0.20	2.83	...
Cu-SiO ₂ (146°)	0.030	0.10	1.11	...
	0.030	0.20	1.00	...
	0.030	0.40	1.00	...
	0.010	0.20	0.48	...
	0.030	0.20	1.00	...
	0.100	0.20	2.44	...

^a Rate relative to the rate at standard conditions ($p_C = 0.030$ atm., $p_H = 0.20$ atm.) for the particular catalyst and temperature in question. The r/r_0 values cannot be used by themselves to compare the activities of the catalysts.

Table III: Summary of Kinetic Parameters for the Reaction of Cyclopropane with H₂ over the Various Supported Metals

Catalyst	Temp. range, °C.	Hydrogenation ^a				Hydrogenolysis ^b			
		<i>E</i> ^c	<i>n</i> ^d	<i>m</i> ^e	<i>r</i> ' ^f	<i>E</i> ^c	<i>n</i> ^d	<i>m</i> ^e	<i>r</i> ' ^f
Ni on SiO ₂	32-42	13.0	0.8	-0.1	2.8 × 10 ²²	16.0	0.4	-0.3	3.0 × 10 ²⁴
Pt on SiO ₂	72-109	12.2	1.0	-0.5	1.0 × 10 ²¹
Co on SiO ₂	93-158	10.7	0.6	-0.1	1.6 × 10 ¹⁹	18.7	0.6	-0.2	1.1 × 10 ²³
Cu on SiO ₂	113-207	10.9	0.7	-0.1	4.1 × 10 ¹⁸

^a Hydrogenation of cyclopropane to propane. ^b Hydrogenolysis of cyclopropane to methane and ethane. ^c Apparent activation energy, kcal./mole. ^d Exponent on cyclopropane pressure. ^e Exponent on hydrogen pressure. ^f Pre-exponential factor in the expression, $r = r' \exp(-E/RT)$, which expresses the temperature dependence of the rate r at standard conditions ($p_H = 0.20$ atm., $p_C = 0.030$ atm.). The units in which r' is expressed are molecules/(sec. cm.²).

throughout the range investigated. This itself attests to the high activity of the nickel catalyst. If we compare the temperatures required to obtain a given measured rate over the various catalysts (by simply drawing a horizontal line across the Arrhenius plots in Figures 1 and 2 and noting the temperatures at the points of intersection with the experimental lines for each of the catalysts), it is clear that nickel is by far the most active of the metals.

After determining the effect of temperature on rates, the temperature was lowered to an intermediate value, and a series of measurements using the "bracketing technique" was made to determine the effects of the partial pressures of hydrogen and cyclopropane, p_H and p_C , respectively, on the rates. For each set of conditions the rate r relative to the rate r_0 at the standard conditions ($p_C = 0.030$ atm., $p_H = 0.20$ atm.) was expressed as a ratio r/r_0 . These data are presented in Table II.

For all four catalysts the data in Table II show that the rate of hydrogenation to propane increases with increasing cyclopropane partial pressure but decreases slightly with increasing hydrogen partial pressure. In the case of hydrogenolysis, observed only over the nickel and cobalt catalysts, similar dependencies on the cyclopropane and hydrogen partial pressures are observed, except that the inverse effect of hydrogen pressure is somewhat greater than is found for the hydrogenation. The dependence of the rates of hydrogenation and hydrogenolysis on the partial pressures of cyclopropane and hydrogen can be expressed in the form of a simple power law, $r = kp_C^n p_H^m$. Approximate values of the exponents n and m are given in Table III. The uncertainty in these exponents is estimated to be ± 0.1 . Values of the apparent activation energy E and the pre-exponential factor r' in the expression $r = r' \exp(-E/RT)$, representing the temperature dependence of the rate r at standard conditions ($p_H = 0.20$ atm., $p_C = 0.030$ atm.), are also

listed in Table III. The values of the pre-exponential factor r' are expressed as molecules/(sec. cm.²). The apparent activation energies vary only slightly from metal to metal, and the differences may not be significant. The uncertainty in the activation energies is estimated to be about 1 kcal./mole except for the nickel catalyst. The activation energy in the case of the nickel is probably less precise since the data on nickel were obtained over a rather narrow temperature range compared to the data on the other metals.

Discussion

The order of catalytic activities of the silica-supported metals for the hydrogenation of cyclopropane to propane is Ni > Pt > Co > Cu. While there is a slight variation in the apparent activation energy over these metals, the differences in activity are due primarily to differences in the pre-exponential factor of the rate expression, as shown in Table III. This is analogous to results reported¹³ for the hydrogenation of ethylene over a series of silica-supported metals, in which the variation in activity was also due to differences in the pre-exponential factor. The order of activities of the metals for cyclopropane hydrogenation is roughly similar to the order observed for ethylene hydrogenation, except that nickel and platinum have been found to have about the same activity for the hydrogenation of ethylene. In the current work, it should be noted that the catalysts were prepared to contain the same amount of metal by weight, which means that the number of metal atoms per gram of silica support in the case of the platinum is less than one-third that of the other three catalysts. The nickel, cobalt, and copper catalysts all contain about the same number of metal atoms per gram of silica support, the variation among them amounting to less than 10%. While the catalytic activities have been determined per unit

(13) G. C. A. Schuit and L. L. van Reijen, *Advan. Catalysis*, **10**, 242 (1958).

metal surface area, it is possible that the activity per unit area increases with the amount of platinum present. This type of effect has been reported in the literature¹⁴ and has also been observed recently by us for similar supported metals. Thus, it may be that the specific activity of the platinum would be closer to that of the nickel if the catalysts were compared at the same concentration of metal atoms per unit weight of silica support.

The observation that the order of catalytic activities of the various supported metals for cyclopropane hydrogenation is roughly similar to the order which has been reported for ethylene hydrogenation suggests that the underlying factors determining the catalytic activities of the metals for these reactions are similar. Cyclopropane thus appears to behave somewhat as an olefin in its properties, which is consistent with other evidence, both experimental and theoretical,¹⁵ attesting to the unsaturated nature of the cyclopropane ring. While the hydrogenation of cyclopropane is somewhat analogous to the hydrogenation of ethylene, there is a distinct difference in the detailed kinetics of the reactions, as pointed out by Bond and Sheridan.¹ Thus, while ethylene hydrogenation is usually observed to be zero order in ethylene and first order in hydrogen, the hydrogenation of cyclopropane shows a definite positive dependence on cyclopropane pressure and is either independent of, or decreases slightly with, hydrogen pressure. These results indicate that cyclopropane is adsorbed less strongly than ethylene on metal catalysts. It seems reasonable that the lower strength of adsorption of cyclopropane relative to ethylene is related to the idea that the delocalized electrons of the cyclopropane ring are less available for bonding with orbitals of the metal than are the π -electrons of the ethylene.

While the order of activities of the various metals for the hydrogenation of cyclopropane to propane is roughly similar to the order for ethylene hydrogenation, this is not the case for the hydrogenolysis reaction leading to methane and ethane. Here the cobalt catalyst ranks second to nickel, and the hydrogenolysis reaction is not even observed over the platinum and copper catalysts. These results closely parallel our previous findings on ethane hydrogenolysis,⁹ in which nickel was found to be more active than cobalt, which in turn was much more active than either platinum or copper. The activity of nickel for ethane hydrogenolysis was found to be as much as 10^5 to 10^6 times as high as that of platinum or copper, but the relative activities did vary substantially with temperature.

It would seem that for the hydrogenation reaction the cyclopropane behaves like an olefin with regard to

the activities of the various metals, whereas, in the case of the hydrogenolysis reaction, it appears to behave like a paraffin. It is conceivable that the cyclopropane is adsorbed in different forms on the surface and that the hydrogenation and hydrogenolysis reactions involve different adsorbed species. Possibly, the hydrogenation reaction might proceed through a π -bonded intermediate,⁶ while the hydrogenolysis could conceivably involve a dissociative adsorption step prior to rupture of carbon-carbon bonds, analogous to the dissociative chemisorption which appears to be the initial step in the hydrogenolysis of paraffins such as ethane and propane over metals.¹⁶ The possibility that cyclopropane is chemisorbed in several configurations on the surface is not unreasonable in view of the fact that evidence exists for both associative and dissociative adsorption of a molecule such as ethylene on metal surfaces.¹⁷

It is interesting that the supported copper catalyst shows significant activity for the hydrogenation of cyclopropane to propane although it is less active than the other metals. A commonly held impression of hydrogenation catalysis over metals is that the catalytic properties are due to the existence of partly filled d-bands which are available for bonding,^{18,19} which effectively limits hydrogenation catalysts to the transition metals. Since copper does not have a partly filled d-band, its activity as a hydrogenation catalyst appears to be somewhat inconsistent with this hypothesis. However, copper immediately follows a transition metal series in the periodic table, and it may be that electrons can be promoted from 3d to 4s states^{20,21} at conditions under which chemisorption and catalysis take place.

In previous studies^{1,2,6} on the hydrogenation of cyclopropane to propane over supported metals, it has been concluded that the rate-limiting step in the reaction involves the interaction of an adsorbed cyclopropane molecule with an adsorbed hydrogen atom. It has also been concluded that hydrogen is more strongly adsorbed than cyclopropane. In the present work it

(14) F. N. Hill and P. W. Selwood, *J. Am. Chem. Soc.*, **71**, 2522 (1949).

(15) M. Yu Lukina, *Russ. Chem. Rev.*, **31**, 419 (1962).

(16) A. Cimino, M. Boudart, and H. S. Taylor, *J. Phys. Chem.*, **58**, 796 (1954).

(17) G. C. Bond, "Catalysis by Metals," Academic Press, New York, N. Y., 1962, pp. 229-236.

(18) M. Boudart, *J. Am. Chem. Soc.*, **72**, 1040 (1950).

(19) O. Beeck, *Discussions Faraday Soc.*, **8**, 118 (1950).

(20) M. Boudart, *J. Am. Chem. Soc.*, **74**, 1534 (1952).

(21) B. M. W. Trapnell, "Chemisorption," Butterworth Scientific Publications, London, 1955, p. 174.

is interesting that the inverse dependence of the rate on hydrogen pressure is greater for the platinum catalyst than for the other catalysts. This suggests that the strength of adsorption of hydrogen on the platinum catalyst is greater than on the other catalysts.

To summarize briefly, the results of the present work have made it possible to compare the catalytic

activities of a series of supported metals for the reaction of cyclopropane with hydrogen in a more fundamental manner than has been done previously since the metal surface areas were known from chemisorption measurements. In addition, it has been shown that the selectivity of conversion of the cyclopropane depends markedly on the particular metal chosen as a catalyst.

Kinetics of the Zinc Fluoroborate and Hydrogen Ion Catalyzed Hydrolyses of the Diglycidyl Ether of 1,4-Butanediol and of Diglycidyl Ether^{1a}

by Ralph J. Berni, Ruth R. Benerito, and Hilda M. Ziifle

Southern Regional Research Laboratory,^{1b} New Orleans, Louisiana (Received December 7, 1964)

Kinetics of hydrolyses of the diglycidyl ether of 1,4-butanediol (DGEBD) and of diglycidyl ether (DGE) at less than 1.0 *M* concentrations catalyzed by HCl (pH 3.25) and by 0.05 *M* Zn(BF₄)₂ from 25 to 90° have been investigated. Semilogarithmic plots of changes in oxirane content with time indicated pseudo-first-order kinetics with both catalysts. Statistical evaluation indicated different rate constants for the opening of the first (*k*₁) and second (*k*₂) oxirane rings with Zn(BF₄)₂ catalysis but equivalent rates with HCl catalysis. Analysis of data by the modified Swain method confirmed consecutive first-order kinetics for the two diepoxides with both catalysts. Further analysis of data with HCl catalysis confirmed equivalent rate constants for both ring openings. With the exception of DGE at 90°, relative rates (*k*₂/*k*₁) for the over-all reaction with Zn(BF₄)₂ catalysis were less than unity at all temperatures. These over-all rate constants could not be corrected for the H⁺ ion rate due to similarity in rates of ring opening with both catalysts. Enthalpies, entropies, and free energies of activation for ring openings were calculated. Large negative entropies of activation indicated ring openings by S_N2 mechanisms at these low levels of catalysts.

Introduction

Specific reaction rate constants for the hydrolyses of the diglycidyl ether of 1,4-butanediol (DGEBD) and of diglycidyl ether (DGE) at less than 1.0 *M* concentrations in the presence of 0.05 *M* zinc fluoroborate, Zn(BF₄)₂, were not available in the literature, nor were such data for the H⁺ ion catalyzed hydrolyses of these diepoxides at pH 3.25, which was the pH value of the Zn(BF₄)₂-diepoxide solutions. Knowledge of these rates and their temperature coefficients was essential

to the elucidation of certain cellulose diepoxide reactions which are catalyzed by dilute Zn(BF₄)₂ but not by dilute HCl. This paper presents a study of the kinetics of hydrolysis of the DGEBD and DGE when catalyzed by Zn(BF₄)₂ at pH 3.25 and by HCl at pH 3.25. Rates

(1) (a) Presented in part before the Division of Inorganic and Physical Chemistry at the Southeastern Regional Meeting of the American Chemical Society, Charleston, W. Va., Oct. 15-17, 1964.

(b) One of the laboratories of the Southern Utilization Research and Development Division, Agricultural Research Service, U. S. Department of Agriculture.

of hydrolyses were measured at temperatures ranging from 25 to 90°. Enthalpies, entropies, and free energies of activation have been calculated.

Experimental

Materials. The DGEBD was obtained from the Ciba Products Co.² and was fractionally distilled. That fraction collected at 125–127° (5.0 mm.) had an epoxide value of 0.98 equiv. of acid/100 g. (calcd., 0.99) as determined by the Durbetaki method³ and characteristic infrared absorption bands at 10.96 and 11.82 μ . Infrared spectra of this diepoxide have been published previously.⁴ That portion of DGE (Shell Development Co.) boiling at 82° (5 mm.) was used. It had an epoxide value of 1.53 equiv./100 g. (calcd. 1.54) as determined by the method of Durbetaki and absorption bands characteristic of the infrared spectra reported previously.⁴ The $Zn(BF_4)_2$ was obtained from the Harshaw Chemical Co. as a 40% aqueous solution (d^{25}_4 1.0466 g./cc.).

Procedure. For the $Zn(BF_4)_2$ -catalyzed rate studies, known weights (approximately 5 g.) of the diepoxide were dissolved in 45.00 ml. of conductivity water containing 0.5626 g. of $Zn(BF_4)_2$ and shaken in closed flasks immersed in an oil bath thermostatically controlled to $\pm 0.05^\circ$. The pH values of the reaction mixtures, measured with a Beckman Model GS pH meter to ± 0.02 pH unit, were found to be constant throughout the timed reactions. The pH values, followed from 0 to 24 hr. for the reaction mixtures at 25, 40, 60, 75, and 90° were 3.25 ± 0.02 . Concentrations of water and catalyst were constant throughout each reaction.

For controlled rate studies in the absence of $Zn(BF_4)_2$, known weights (approximately 5 g.) of the diepoxide were dissolved in 45.00 ml. of conductivity water which was adjusted to a constant pH of 3.25 with HCl at each temperature.

Aliquots were withdrawn with 1-ml. serological pipets at timed intervals and transferred to tared erlenmeyer flasks. Weighed samples were analyzed for oxirane oxygen by the method of Durbetaki³ and corrected for blank determinations, including water and catalyst in every case. The HBr reagent was standardized periodically.

Treatment of Data. Cartesian graphs of the change in concentration of oxirane oxygen, T , expressed as milliequivalents per gram of solution, with reaction time for each catalyst at each temperature showed a change in slope beyond the half-concentration point. Initially, semilogarithmic graphs of the data were plotted in attempts to detect changes in slope beyond the half-concentration point by the method of least squares. However, unlike hydrolyses of vinylcyclo-

hexene dioxide,⁵ in which the rates of opening of the first and second oxirane rings were 50:1 at 25° in the presence of $Zn(BF_4)_2$, the rates of opening of the two oxirane rings of DGEBD and DGE with $Zn(BF_4)_2$ catalysis were not different enough to allow for the determination of k_1 and k_2 by statistical evaluation of the linear semilogarithmic plots. Nevertheless, this study indicated that two linear portions were obtained with $Zn(BF_4)_2$ catalysis and only one with HCl catalysis. That is, a statistical analysis of the diepoxide-HCl data at each temperature showed that the slopes obtained when the first and second halves of the semilogarithmic plots were considered independently were not significantly different from the slope obtained by consideration of the entire line.⁶ Data obtained with each catalyst were also analyzed by the modified Swain method,^{7,8} which has been previously described.⁵

Earlier investigations of the hydrolyses of vinylcyclohexene dioxide⁵ and of butadiene diepoxides⁹ under similar conditions of $Zn(BF_4)_2$ and HCl catalysis at like pH showed that the rates of hydrolyses of each of these diepoxides were very different in the presence of each catalyst. In fact, the over-all reaction rates for opening of both rings with $Zn(BF_4)_2$ catalyst could be corrected for the rates of opening due to H^+ ion catalysis at like pH for both diepoxides. In contrast, in this study, the over-all rates of ring openings of DGEBD and of DGE in the presence of $Zn(BF_4)_2$ at pH 3.25 were essentially equal to the respective rates of ring openings in the presence of HCl at pH 3.25. Therefore, the over-all rates could not be corrected for rates of ring openings due to H^+ ion catalysis. Therefore, the enthalpies, entropies, and free energies of activation for all ring openings were computed for the HCl-catalyzed reactions and for the observed over-all reactions with $Zn(BF_4)_2$ catalyst at pH 3.25.

Results and Discussion

Figure 1 shows typical Cartesian graphs of oxirane oxygen content of DGEBD vs. reaction time at 75° and indicates a change in rate beyond the half-concen-

(2) The mention of trade names and firms does not imply their endorsement by the U. S. Department of Agriculture over similar products or firms not mentioned.

(3) A. J. Durbetaki, *Anal. Chem.*, **28**, 2000 (1956).

(4) W. A. Patterson, *ibid.*, **26**, 823 (1954).

(5) R. R. Benerito, H. M. Ziffle, R. J. Berni, and B. M. Banta, *J. Phys. Chem.*, **67**, 1750 (1963).

(6) J. C. R. Li, "Introduction to Statistical Inference," Edwards Brothers, Inc., Ann Arbor, Mich., 1957, p. 344.

(7) C. G. Swain, *J. Am. Chem. Soc.*, **66**, 1696 (1944).

(8) A. A. Frost and R. G. Pearson, "Kinetics and Mechanism," John Wiley and Sons, Inc., New York, N. Y., 1953, p. 158.

(9) H. M. Ziffle, R. J. Berni, and R. R. Benerito, *J. Appl. Polymer Sci.*, **9**, 169 (1965).

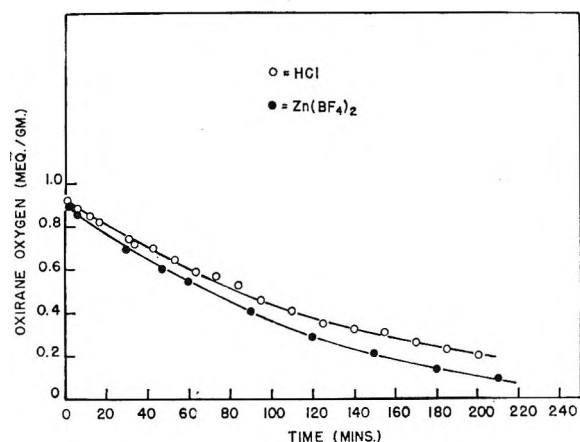


Figure 1. Concentration of oxirane oxygen, T , in milliequivalents per gram of solution vs. time in minutes for approximately 1 M diglycidyl ether of 1,4-butanediol catalyzed by 0.05 M $Zn(BF_4)_2$ and by HCl of pH 3.25 at 75°.

tration point with each catalyst. Figure 2 is the semilogarithmic representation of these same data and indicates two intersecting linear segments with $Zn(BF_4)_2$ catalysis but only one straight line with HCl catalysis. The observed change in slope beyond the half-concentration point and the linear relationships obtained upon semilogarithmic treatment of the data indicate consecutive pseudo-first-order reaction kinetics. However, it should be noted that, with $Zn(BF_4)_2$ catalysis, the over-all rates of opening of the first (k_{1z}) and second (k_{2z}) oxirane rings were not sufficiently different to allow their determination by the usual statistical evaluation of the semilogarithmic plots.⁵ Because of this, use of slopes of lines, as shown in Figure 2, for evaluation of reaction rate constants would lead to erroneous results in this instance. Hence the data were analyzed by the modified Swain method,^{7,8} and pseudo-first-order reaction kinetics was confirmed.

The fact that only one line was obtained when HCl catalyzed the reaction (see Figure 2) suggested equivalent rates for the opening of the first (k_{1H}) and second (k_{2H}) oxirane rings. Subsequent analysis by the modified Swain method^{7,8} showed the ratio of $k_{2H}:k_{1H}$ to be unity, confirming equal rates of opening for both rings.

Cartesian graphs of changes in oxirane oxygen content of DGE vs. time at each temperature with both catalysts indicated a change in slope beyond the half-concentration point and semilogarithmic plots of the data were linear. Statistical analyses of the log concentration-time data indicated k_{1z} and k_{2z} were different while $k_{1H} = k_{2H}$. Analysis of the data by the modified Swain method^{7,8} confirmed the assumption of consecutive first-order kinetics and of equivalent rates of ring opening with HCl catalysis.

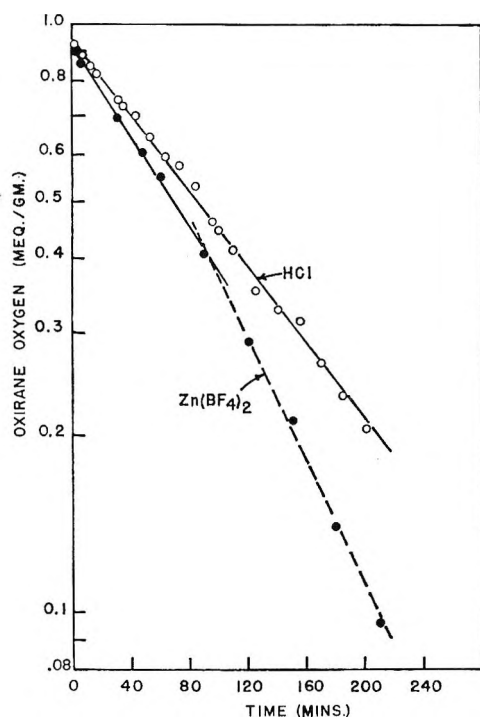
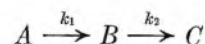


Figure 2. Log of concentration of oxirane oxygen, T , in milliequivalents per gram of solution vs. time in minutes for approximately 1 M diglycidyl ether of 1,4-butanediol catalyzed by 0.05 M $Zn(BF_4)_2$ and by HCl of pH 3.25 at 75°.

For diepoxide reactions, consecutive first-order reactions may be represented as follows



where A is the molar concentration of the diepoxide, B is the molar concentration of monoepoxide after hydrolysis of the first oxirane ring, and C is the molar concentration of the final product after opening of both epoxide rings. Experimentally, C bears a direct relationship to total oxirane content, T , which is measured in this study as milliequivalents per gram of solution. The following equations, in which zero subscripts denote initial concentrations, are for those instances, as with $Zn(BF_4)_2$ catalysis, where $k_1 \neq k_2$. If $k_1 = k_2 = k_H$, as

$$A = A_0 e^{-k_1 t} \quad (1)$$

$$B = \frac{A_0 k_1}{k_2 - k_1} [e^{-k_1 t} - e^{-k_2 t}] \quad (2)$$

$$T = 2A + B \quad (3)$$

is indicated with HCl catalysis, B and T can be represented by the following equations.

$$B = k_H t A_0 e^{-k_H t} \quad (4)$$

$$T = A_0 e^{-k_H t} (2 + k_H t) \quad (5)$$

Values of k_{1z} , k_{2z} , and relative rates $k_{2z}:k_{1z}$ are given in Table I. With the exception of the ratio for DGE at 90°, each ratio was less than unity, indicating that the first oxirane ring opens more rapidly than the second, as was observed, but to a greater degree with vinylcyclohexene dioxide.⁵ However, with the butadiene diepoxides, $k_{2z}:k_{1z}$ was greater than unity.⁹

Table I: Rate Constants for Opening of the First and Second Oxirane Rings in $Zn(BF_4)_2$ -Catalyzed Hydrolyses

Temp., °C.	—Specific reaction rate constants—		Relative rates $k_{2z}:k_{1z}$
	$k_{1z} \times 10^4$, min. ⁻¹	$k_{2z} \times 10^4$, min. ⁻¹	
Diglycidyl ether of 1,4-butanediol			
25	3.92	3.13	0.79
40	8.07	7.96	0.99
60	94.77	53.00	0.56
75	173.27	93.73	0.54
90	496.95	319.54	0.64
Diglycidyl ether			
25	3.98	1.67	0.42
60	77.57	66.70	0.86
75	213.81	152.64	0.71
90	509.79	783.35	1.55

Values of k_H are given in Table II. To determine k_H , use was made of the experimentally derived relationship

$$T = T_0 e^{-bt} \quad (6)$$

where T_0 is the initial concentration of oxirane oxygen, T is the concentration at any time, t , and b is the slope of the semilogarithmic plot. The least-squares equation

Table II: Rate Constants for Opening of the First and Second Oxirane Rings in Dilute HCl Catalyzed Hydrolyses

Temp., °C.	Specific reaction rate constants ($k_{1H} = k_{2H}$)	
	$k_H \times 10^4$, min. ⁻¹	
	Diglycidyl ether of 1,4-butanediol	Diglycidyl ether
25	1.95	2.64
60	44.10	51.32
75	124.88	181.30
90	299.83	511.89

of the semilogarithmic line at each temperature was calculated, and the slope, b , was used to determine the specific reaction rate constant, k_H , at each temperature. The relationship between k_H and b , determined by

equating eq. 5 and 6 and making use of the fact that $T_0 = 2A_0$, is given by eq. 7. Since this relationship is

$$\frac{k_H}{2(2.3026)} + \frac{k_H^2 t}{8(2.3026)} = b \quad (7)$$

time dependent, k_H was taken as the average of values obtained at $t = 0$ and $t = \text{maximum time}$.

Comparison of k_H with k_{1z} and k_{2z} values at the respective temperatures for each diepoxide shows them to be approximately the same order of magnitude.

Figures 3 and 4 are typical of plots of the calculated concentrations of A , B , and T as functions of time with $Zn(BF_4)_2$ and HCl catalysts, respectively. For Figure 3, experimentally determined rate constants for DGEBD at 75°, k_{1z} and k_{2z} , were substituted in eq. 1, 2, and 3. For Figure 4, the experimentally determined

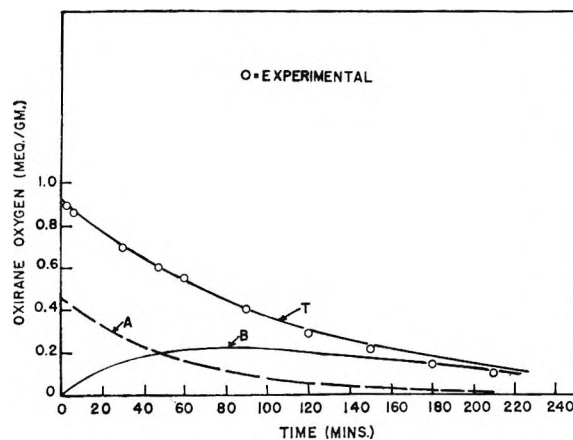


Figure 3. Plot of calculated concentrations of diepoxide (A), monoepoxide (B), and total oxirane oxygen (T) as a function of time at 75° for diglycidyl ether of 1,4-butanediol catalyzed by 0.05 M $Zn(BF_4)_2$. For convenience, concentrations of A are in millimoles and B and T are in milliequivalents per gram of solution. Curves are calculated on the assumption of consecutive first-order reaction; circles are experimentally determined values of T .

rate constant at 75°, k_H , for DGEBD was substituted in eq. 1, 4, and 5. Experimental values of T are indicated by circles. Standard errors of estimate were computed to be 0.03 and 0.02 for $Zn(BF_4)_2$ and HCl catalysts, respectively. Figure 5 gives similar curves for A , B , and T calculated from experimentally determined rate constants for DGE at 60° with $Zn(BF_4)_2$ catalysis. In this figure, curve T_H is that calculated for DGE at 60° with HCl catalysis, and the shaded circles are the experimentally determined values with HCl catalysis. In this figure, the latter values are included for comparative purposes and the A and B curves with HCl catalysis are omitted for the sake of clarity. Extent

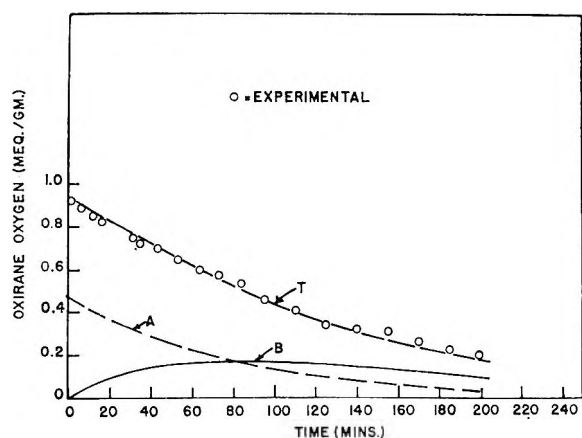


Figure 4. Plot of calculated concentrations of diepoxide (*A*), monoepoxide (*B*), and total oxirane oxygen (*T*) as a function of time at 75° for diglycidyl ether of 1,4-butanediol catalyzed by HCl at pH 3.25. For convenience, concentrations of *A* are in millimoles and *B* and *T* are in milliequivalents per gram of solution. Curves are calculated on the assumption of consecutive first-order reaction in which $k_1 = k_2$; circles are experimentally determined values of *T*.

of agreement of experimental points (circles) with theoretical curves are given by the standard errors of estimate of 0.03 for $Zn(BF_4)_2$ catalysis and 0.05 for HCl catalysis. Agreement between theoretical and experimentally observed data confirmed the assumption of consecutive first-order reactions for both diepoxides at each temperature.

Calculated enthalpies, entropies, and free energies of activation for hydrolyses of oxirane rings in DGEBD and in DGE with both catalysts are recorded in Table III. Arrhenius plots of $\log k$ vs. $1/T$ were linear. The

Table III: Enthalpies, Entropies, and Free Energies of Activation of Oxirane Ring Openings in $Zn(BF_4)_2$ - and HCl-Catalyzed Hydrolyses

Ring opening	Diglycidyl ether of 1,4-butanediol			Diglycidyl ether		
	ΔH^* , kcal./mole	ΔS^* , cal./mole deg.	ΔF^*_{25} , kcal./mole	ΔH^* , kcal./mole	ΔS^* , cal./mole deg.	ΔF^*_{25} , kcal./mole
	$Zn(BF_4)_2$					
1st oxirane	18.0	-24.8	25.4	16.1	-30.2	25.1
2nd oxirane	15.3	-33.7	25.4	20.0	-19.2	25.7
	HCl					
1st and 2nd oxirane	17.4	-26.6	25.4	17.4	-26.8	25.4

equation of each line was determined by the method of least squares and the slopes were used in the calculation

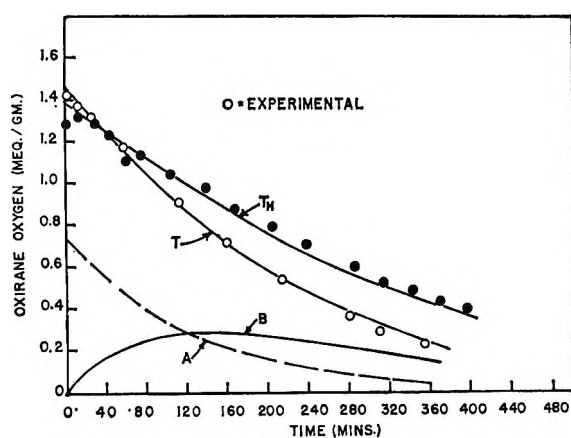


Figure 5. Plot of calculated concentrations of diepoxide (*A*), monoepoxide (*B*), and total oxirane oxygen (*T*) as a function of time at 60° for diglycidyl ether catalyzed by 0.05 M $Zn(BF_4)_2$. For convenience, concentrations of *A* are in millimoles and *B* and *T* are in milliequivalents per gram of solution. Curves are calculated on the assumption of consecutive first-order reactions; circles are experimentally determined values of *T*. Curve T_1 and shaded circles are for calculated and experimentally determined values, respectively, obtained at 60° for diglycidyl ether catalyzed by HCl at pH 3.25.

of the enthalpy of activation, ΔH^* . Entropies of activation, ΔS^* , were calculated from the equation

$$\Delta S^* = R \left[\ln k - \ln \left(\frac{KT}{h} \right) + \frac{\Delta H^*}{RT} - 1 \right] \quad (8)$$

where k is the hydrolysis rate constant in reciprocal seconds and R , K , and h are the molar gas, Boltzmann, and Planck constants, respectively. Free energies of activation, ΔF^* , were calculated from the equation

$$\Delta F^* = \Delta H^* - T\Delta S^* \quad (9)$$

Intercomparison of ΔH^* values for DGEBD shows that the values for the first ring opening with $Zn(BF_4)_2$ and both ring openings under HCl catalysis are approximately the same while that for the second ring opening under $Zn(BF_4)_2$ catalysis is significantly smaller. However, the more negative ΔS^* for the second ring opening with $Zn(BF_4)_2$, indicative of a more ordered transition-state complex, results in equal ΔF^* values for all ring openings.

In contrast, the ΔH^* value for the second ring opening of DGE catalyzed by $Zn(BF_4)_2$ exceeds that for the first ring opening, and there is a greater decrease in entropy of activation for the latter than for the second ring opening. These results are similar to those observed with the hydrolysis of vinylcyclohexene dioxide.⁵ With HCl catalysis, ΔH^* and ΔS^* values are intermediate between those found for the first and second

Table IV: Comparison of Specific Reaction Rate Constants^a

Temp., °C.	Vinylcyclohexene dioxide		Butadiene diepoxide		Diglycidyl ether of 1,4-butanediol		Diglycidyl ether	
	k_{1z}/k_{1H}	k_{2z}/k_{2H}	k_{1z}/k_{1H}	k_{2z}/k_{2H}	k_{1z}/k_{1H}	k_{2z}/k_{2H}	k_{1z}/k_{1H}	k_{2z}/k_{2H}
25	6.6	2.0	2.5	16.5	2.0	1.6	1.5	0.6
40	5.0	2.4	1.6	27.7
60	4.2	4.5	1.5	11.4	2.1	1.2	1.5	1.3
75	1.6	42.4	1.4	0.8	1.2	0.8
90	2.3	76.9	1.7	1.1	1.0	1.5

^a Subscripts 1 and 2 denote openings of the first and second oxirane rings; subscripts z and H denote $Zn(BF_4)_2$ and HCl catalyst, respectively.

ring openings with $Zn(BF_4)_2$, but more nearly equal to those for the first. The ΔF^* values for openings of both rings with either catalyst are essentially equal. It is of interest to note that with HCl catalysis, ΔH^* , ΔS^* , and ΔF^* values for DGE are identical with those found for DGEBD at the same pH, but the activation parameters for these two diepoxides with $Zn(BF_4)_2$ catalysis differ.

Hydrolysis of epoxides occurs by either an SN1 or an SN2 mechanism, and by both mechanisms the reaction would follow first-order kinetics under the experimental conditions of this study. The epoxide reacts instantaneously with the H^+ ion or Zn^{2+} ion, but in the SN1 mechanism, the rate-determining step is the slow ring opening of the conjugate acid of the epoxide ring to form a carbonium ion, which then combines with the anion of the water molecule in the fast step to form the product. By an SN2 mechanism, the conjugate acid reacts bimolecularly with the solvent molecule and orientation is an important factor. Experimentally, the hydrolyses of DGEBD and DGE followed consecutive first-order reaction kinetics and observed large negative entropies, showing the importance of the orientation factor, were interpreted as indicative of an SN2 mechanism for the opening of both oxirane oxygen rings. These results are in agreement with those obtained in similar hydrolysis studies of vinylcyclohexene dioxide⁵ and butadiene diepoxide⁹ when the concentration of epoxide was large with respect to concentration of catalyst. Recently, an SN2 mechanism was also indicated by the negative activation volume ΔV^* , for the hydrolysis of epichlorohydrin of approximately 0.5 M in presence of 0.0635 M perchloric acid.¹⁰

A comparison of relative rates of the first and second ring openings with HCl and $Zn(BF_4)_2$ catalysts for four diepoxides was made. Only with butadiene diepoxide was $k_{2z} > k_{1z}$; with vinylcyclohexene dioxide, $k_{2z} \ll k_{1z}$, and these constants were for rates corrected for H^+ ion catalysis rates. With HCl catalysis, $k_{2H} \ll k_{1H}$ for

vinylcyclohexene dioxide; $k_{2H} < k_{1H}$ for butadiene diepoxide; and $k_{2H} = k_{1H}$ for DGEBD and DGE. Data in Table IV are given to show the effect of change of catalyst with each diepoxide. While the pH (3.25) at which rates of DGEBD, DGE, and butadiene diepoxide were measured differed from that employed with vinylcyclohexene dioxide (2.55), certain conclusions can nevertheless be drawn.

For DGEBD and DGE, the $k_{2z}:k_{2H}$ and $k_{1z}:k_{1H}$ ratios approximate unity and are not too different from $k_{2z}:k_{2H}$ for vinylcyclohexene dioxide and the ratio of $k_{1z}:k_{1H}$ for butadiene diepoxide. Unlike these ratios, $k_{1z}:k_{1H}$ for vinylcyclohexene dioxide is at least twofold greater, and $k_{2z}:k_{2H} \gg 1$ for butadiene diepoxide. Of the four diepoxides under discussion, only ΔF^* values for k_{1H} and k_{2H} of butadiene diepoxide and for k_{1z} and k_{2H} of vinylcyclohexene dioxide differed significantly from 25.4 kcal./mole, and these were 26.3, 27.5, 23.0, and 30.4, respectively. These data indicate the much greater effect of $Zn(BF_4)_2$ as compared to HCl at like pH on the hydrolyses of vinylcyclohexene dioxide and butadiene diepoxide than on the hydrolyses of DGEBD and of DGE. Previously,⁹ it was postulated that with butadiene diepoxide and H^+ ion catalysis, the hydroxyl group α to the second epoxide ring formed a five-membered ring through intramolecular bonding, thus making it more difficult for a H^+ ion to protonate the oxirane ring of 1,2-epoxy-3,4-butanediol and resulting in $k_{2H} \ll k_{1H}$. The finding that $k_{2z} \gg k_{1z}$ was said to be due possibly to coordination of Zn^{2+} ions with either the two oxirane rings of butadiene diepoxide or between the hydroxyl group α to the ring oxygen and the oxirane oxygen of 1,2-epoxy-3,4-butanediol. With either DGEBD or DGE, there were apparently little differences in rates or activation parameters with either catalyst, or, in other words, presence of Zn^{2+} ions did not significantly increase rates of ring openings over those ob-

(10) W. J. le Noble and M. Duffy, *J. Phys. Chem.*, **68**, 619 (1964).

served in the presence of H^+ ions as the only cations. In addition, the equal rates of ring openings of DGEBD and of DGE with HCl catalysis as opposed to unequal rates observed for butadiene diepoxide and vinylcyclohexene dioxide suggest a greater independence of reaction of rings in DGEBD and DGE due to the greater spatial separation of epoxy groups in the latter com-

pounds compared to the others. The fact that in general the ratio for the observed over-all rates, $k_{2z}:k_{1z}$ is <1 for both DGEBD and DGE might be accounted for by the tendency of Zn^{2+} ions to complex preferentially with vicinal hydroxyl groups on the half-hydrolyzed molecule, thus lessening their ability to coordinate with the second oxirane ring.

High Resolution Nuclear Resonance Studies of the Chain Conformation of Polyethylene Oxide

by T. M. Connor and K. A. McLauchlan

*The Basic Physics Division, The National Physical Laboratory, Teddington, Middlesex, England
(Received December 10, 1964)*

The temperature dependence of the couplings in the ^{13}C -H proton satellite side bands in polyethylene oxide has been studied. Similar measurements have been made on some model compounds, namely, ethylene glycol, 1,2-dimethoxyethane, and 1,2-dichloroethane. In all cases, the sum of the rotationally averaged coupling constants, $J + J'$, increases with temperature, apart from 1,2-dichloroethane, which shows no significant variation with temperature. This increase seems to indicate that in all cases the *gauche* conformation is the most stable. Attempts to obtain the energy difference, ΔE , between the *gauche* and *trans* forms have not been successful since the theory used does not fit the experimental results obtained for reasonable values of the parameters involved. Reasons for this failure are discussed as is also the relationship of these results to other measurements of the conformation of polyethylene oxide chains.

High resolution nuclear resonance spectroscopy has found considerable use in studies of the stereoregularity of polymer chains and in favorable cases has proved a useful method for determining the proportions of isotactic, syndiotactic, and heterotactic placements in polymer chains,¹⁻³ thereby characterizing the chain more fully. However, it does appear to be possible to study other aspects of chain microstructure using high resolution techniques and to obtain information about the preferred conformations of the monomer units comprising the chain and the energy differences between these conformations. This work is a pre-

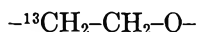
liminary investigation of these possibilities for the experimentally rather favorable case of polyethylene oxide, $H[O-CH_2-CH_2]_nOH$. The basis of the method is the study of the splittings in the ^{13}C -H proton satellite side bands and their variation with change of temperature and solvent. Very frequently, the high resolution spectra of polymers are complex due to the

(1) F. A. Bovey and G. V. D. Tiers, *Fortschr. Hochpolymer. Forsch.*, **3**, 139 (1963).

(2) T. G. Fox and H. W. Schnecko, *Polymer*, **3**, 575 (1962).

(3) F. A. Bovey, E. W. Anderson, D. C. Douglass, and J. A. Manson, *J. Chem. Phys.*, **39**, 1199 (1963).

spins being highly coupled, the spin-coupling constants often being of the same order of magnitude as the chemical shifts. This situation is aggravated by the large line widths observed (~ 1.25 c.p.s. in the present case) as compared with the spectra of small molecules, this being due to the less complete averaging out of dipolar interactions in polymers. The satellite side bands, however, are caused by less highly coupled nuclei since an effective chemical shift equal to half the ^{13}C -H coupling constant is introduced which is considerably larger than the proton-proton couplings found in polymers. It is therefore expected that the proton satellite spectra may be more easily interpreted than their parent spectra. However, with conventional instrumentation this advantage may be to some extent nullified since the satellite side bands are of small intensity for polymers containing ^{13}C in natural abundance. In the case of polyethylene oxide (PEO) there are no complicating effects due to stereoregularity of the polymer chain and in fact no information regarding coupling constants can be obtained from the normal high resolution spectrum since this is a single line. However, in those monomer units of the chain which contain a ^{13}C nucleus



the ^{13}C -H coupling makes the two pairs of protons inequivalent which results in a spectrum which approximates to half an AA'XX' spectrum from which it is possible to measure splittings accurately. Oxide polymers of the above type seem suitable for these studies since the long-range couplings through the oxygen atoms between protons in different monomer units are very small and can be neglected. This is an added simplifying feature which aids interpretation, although it appears that in other cases where there are no chain oxygen atoms such as polypropylene the high resolution spectrum is not as complicated as might be expected.⁴ Hence, similar techniques may be applicable to this polymer and others without heteroatoms in the chain backbone.

Besides the polymer, a number of small molecules which are more or less satisfactory as model compounds have been studied, *i.e.*, ethylene glycol, 1,2-dimethoxyethane, and 1,2-dichloroethane.

Experimental and Results

Spectra were obtained at 60 Mc.p.s. using a Varian DP 60 spectrometer with standard variable temperature probe. The polymer was a sample of PEO of molecular weight 6000 (Carbowax) obtained from the Union Carbide Chemicals Co.⁵ This molecular weight was chosen since the chain, which contains about 136

monomer units, is sufficiently long to make end-group effects negligible but short enough to be soluble in the solvents employed. These were chloroform and water. Some measurements were also made on the melt although these could not be made accurately until a temperature of 150° ($\sim 80^\circ$ above the melting point) had been reached, since the lines were too broad below this temperature. A sample spectrum is shown for a saturated aqueous solution of the polymer at 31.5° in Figure 1. The satellite spectrum and measuring side bands at 60 and 80 c.p.s. are recorded and show that the signal to noise ratio is sufficient for quite accurate measurements of the splitting, $J + J'$, between the outermost lines of the satellite spectrum to be made. J and J' are the two rotationally averaged coupling constants between the A and X groups of nuclei.^{6,7} The value of $J + J'$ was recorded at a number of temperatures, the results obtained being shown in Figure 2, which shows $J + J'$ measured

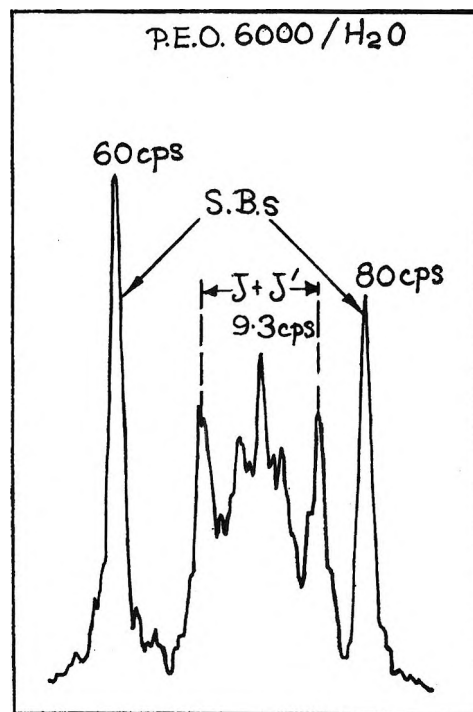


Figure 1. ^{13}C -H side band of the proton spectrum of polyethylene oxide in water at 31.5° . (Measuring side bands also shown at 60 and 80 c.p.s.)

(4) C. A. Reilly, private communication.

(5) "Carbowax Polyethylene Glycols," Union Carbide Chemicals Co., 1958.

(6) J. A. Pople, W. G. Schneider, and H. J. Bernstein, "High Resolution Nuclear Magnetic Resonance," McGraw-Hill Book Co., Inc., New York, N. Y., 1959.

(7) N. Sheppard and J. J. Turner, *Proc. Roy. Soc. (London)*, **A252**, 506 (1959).

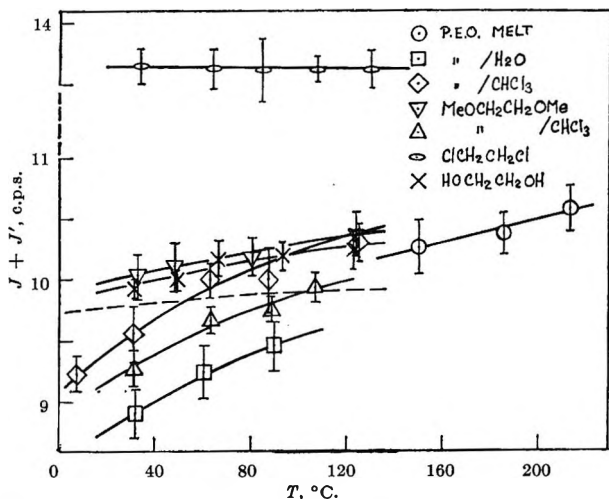


Figure 2. $J + J'$ as a function of temperature for polyethylene oxide and related compounds.

for the polymer solutions and melt and also for the model compounds mentioned above. The figures quoted are average values of $J + J'$ resulting from at least ten readings and from sometimes as many as 30, the standard deviations obtained being shown in Figure 2 by the barred vertical lines. The central region of the satellite spectrum contains the splitting $J - J'$ but for the polymer the resolution was not good enough to allow a complete analysis. This was not so for the model compounds, however, the spectra obtained being similar to those observed for 1,2-dibromoethane, dioxane, etc. A first-order value for half the ^{13}C -H coupling constant was determined for the polymer in chloroform solutions and was found, as expected, to be independent of temperature, having the value 70.39 ± 0.19 c.p.s. at 7° and 70.27 ± 0.14 c.p.s. at 125° . This is similar to the value found for dioxane where $^{1/2}J_{^{13}\text{C}-\text{H}} = 71.1$ c.p.s.⁷

Discussion

Figure 2 shows that in all cases considered, $J + J'$ increases as the temperature rises. This increase is fairly large for the two polymer solutions (~ 1 c.p.s. in 100°) and smaller for all the model compounds except 1,2-dimethoxyethane in chloroform, which has a similar variation to the polymer. $J + J'$ for 1,2-dichloroethane shows no change with temperature although the limits of error would allow a small positive or negative trend with change in temperature. The value of $J + J'$ for 1,2-dichloroethane is considerably larger than that for the other compounds studied so that in fact it seems unsuitable as a model compound in this instance. The constancy of $J + J'$ with temperature seems to be in accord with infrared experiments which indicate a very small energy difference,

ΔE , between the *gauche* and *trans* forms of this molecule in the pure state.⁷

These results can be interpreted using an approach applied in many previous instances.⁷⁻⁹ In the case of PEO monomer units and the model compounds there are three stable conformations, one *trans* and two equivalent mirror image *gauche* forms which are shown in Figure 3 with the appropriate coupling constants. It is assumed that $J_g = J_g' = J_g''$ and that $J_t = J_t'$ where the J_g 's and J_t 's are, respectively, the vicinal coupling constants expected for *gauche* and *trans* configurations of protons in the various isomers. J and J' may be expressed in terms of J_t , J_g , and the occupation probabilities of the *trans* and *gauche* forms which are n_t and n_g , respectively. These are related by the expressions^{7,9}

$$\left. \begin{aligned} n_t + n_g &= 1 \\ n_g/n_t &= 2 \exp\left(\frac{\Delta E}{RT}\right) \end{aligned} \right\} \quad (1)$$

and the sum

$$J + J' = \frac{1}{2}[J_t + 3J_g + n_t(J_t - J_g)] \quad (2)$$

The sign of ΔE is determined by the relative stabilities of *gauche* and *trans* forms, being positive if the *gauche* form is most stable and negative if the *trans* form is most stable. Since in all the cases considered here (apart from 1,2-dichloroethane) $J + J'$ and therefore n_t increases with temperature, the *gauche* form must be the most stable isomer. Equations 1 and 2 may be used to

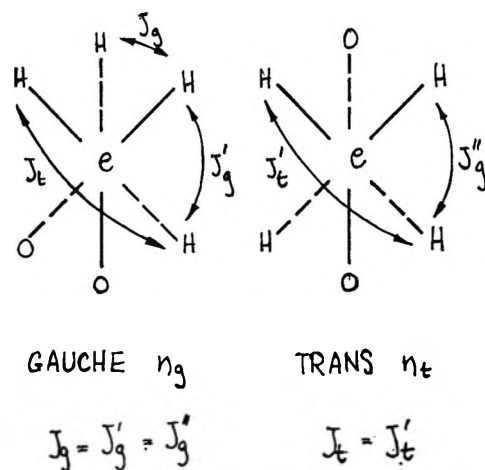


Figure 3. *gauche* and *trans* forms of monomer unit of polyethylene oxide.

(8) H. S. Gutowsky, G. G. Belford, and P. E. McMahon, *J. Chem. Phys.*, **36**, 3353 (1962).

(9) R. J. Abraham and K. G. R. Pachler, *Mol. Phys.*, **7**, 165 (1963).

obtain values of ΔE if assumptions are made about the values of J_t and J_g . Alternatively, if values of ΔE are known from other sources, *e.g.*, infrared studies J_t and J_g can be found. However, no independent estimates of ΔE are available, whereas information about possible values of J_t and J_g can be obtained. It has been shown that the quantity $J_t + 2J_g$ should be a constant for a given compound and that for 2-methoxyethanol, which is a reasonable model compound, is equal to 15.8 c.p.s. This defines a range of values of J_t and J_g and enables n_t to be calculated. If the theory outlined is applicable and correct values of J_t and J_g have been chosen, by plotting $\ln [(1 - n_t)/n_t]$ against $1/T \times 10^3$ a line of slope $\Delta E/R$ should be obtained, cutting the y axis at $\ln 2$ at infinite temperature. According to theoretical calculations,¹⁰ J_t and J_g are of the same sign for internal rotation angles, ϕ , of 60 and 180° (the eclipsed position corresponds to $\phi = 0$) in the H-C-C-H fragment and $J_t \sim 4J_g$. However, the theoretical predictions in their simple form have been shown to be unreliable in a number of instances¹¹⁻¹⁴ and seem a poor basis for choosing suitable values of J_t and J_g .¹⁵ In fact, experimental results⁸ for the substituted ethane CHFClCHCl_2 and for 1,2-disubstituted propanes,¹⁵ when analysed on a similar basis, yielded negative values for J_g although the fact that no negative vicinal couplings have been observed in molecules of known fixed geometry, *e.g.*, dioxane,⁷ must cast some doubt on this conclusion. Since the situation with regard to these quantities is none too clear, three choices of these parameters have been made subject to the restrictions $J_t + 2J_g = 15.8$ c.p.s. The chosen J_g values are 2.5, 0, and -1.5 c.p.s. Substantially higher values of J_g are ruled out since they lead to values of $n_t < 0$. Lower values of J_g lead to extremely high values of J_t ; when $J_g = -1.5$, $J_t = 18.8$ c.p.s. so it seems unlikely that $J_g < -1.5$. Values of $\ln [(1 - n_t)/n_t]$ plotted against $1/T \times 10^3$ for these parameters are shown in Figure 4 for PEO and in Figure 5 for ethylene glycol. These figures also contain theoretical curves calculated for the values $\Delta E = 300$ and 1000 cal. It can be seen that with all the values of the parameters chosen there is poor agreement between the theoretical and experimental results. The variation of $\ln [(1 - n_t)/n_t]$ is greater than that predicted by the theory and there is not a linear relationship between the experimental points and $1/T$ for the polymer or for ethylene glycol, although the deviation from the theoretical curves is less for the small molecule. (The experimental points on Figures 4 and 5 are for smoothed values of $J + J'$ taken from Figure 2. Also, the limits of error for $\ln [(1 - n_t)/n_t]$ have been omitted for clarity. The error increases considerably as the temperature is lowered.) Similar

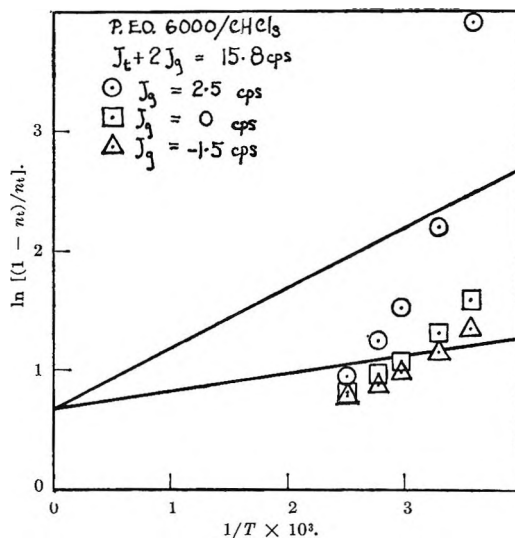


Figure 4. Plots of $\ln [(1 - n_t)/n_t]$ vs. $1/T \times 10^3$ for polyethylene oxide in chloroform. (Solid lines correspond to ΔE values of 1000 and 300 cal./mole.)

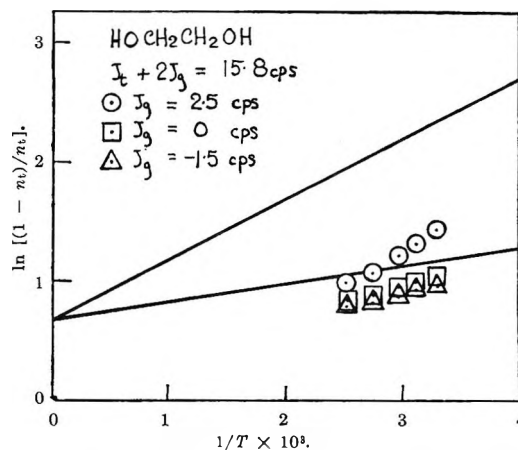


Figure 5. Plots of $\ln [(1 - n_t)/n_t]$ vs. $1/T \times 10^3$ for ethylene glycol. (Solid lines correspond to ΔE values of 1000 and 300 cal./mole.)

calculations for other values of $J_t + 2J_g$, *i.e.*, 16.8 and 14.8 c.p.s., the latter being the value found for dioxane,⁷ also lead to deviations from the theoretical curves. For dioxane, the H-C-C-H group is permanently in the *gauche* configuration since the ring is in the chair form. Consequently, this compound is probably not

(10) M. Karplus, *J. Chem. Phys.*, **30**, 11 (1959).

(11) R. J. Abraham and K. A. McLaughlan, *Mol. Phys.*, **5**, 513 (1962).

(12) R. Lynden-Bell and N. Sheppard, *Proc. Roy. Soc. (London)*, **A269**, 385 (1962).

(13) R. U. Lemieux, J. D. Stephens, and R. R. Fraser, *Can. J. Chem.*, **40**, 1955 (1962).

(14) M. Karplus, *J. Am. Chem. Soc.*, **85**, 2870 (1963).

(15) H. Finegold, *J. Chem. Phys.*, **41**, 1808 (1964).

as satisfactory as a model compound as 2-methoxyethanol, although it has the advantage in this respect that the values of J_t and J_g can be obtained directly ($J_t = 9.4$ c.p.s. and $J_g = 2.7$ c.p.s.). Figure 2 also shows a theoretical curve calculated for $\Delta E = 1000$ cal. for the values $J_t = 10$ c.p.s. and $J_g = 3$ c.p.s. This also shows a much smaller slope than any of the experimental curves. It thus appears that using reasonable values for J_t and J_g it is not possible to derive ΔE values for any of these systems on the basis of the theory outlined above. This result is interesting in that it possibly casts some doubt on other investigations where values of ΔE , J_t , and J_g have been obtained by fitting the experimental curves by repeated iteration.⁹ However, although the theory does not fit the experimental data quantitatively, it is probable that the qualitative result mentioned above, *i.e.*, that the *gauche* form is the most stable in all cases, holds. On steric grounds it would be expected that the *trans* isomer would be the most stable so this is to some extent a surprising result which also seems to apply in a variety of other cases. Thus, in 2-chloroethanol the *gauche* form is apparently the most stable in both the liquid and solid state.^{9,11} The same is also true for 2-chloroethyl acetate, which seems to indicate that hydrogen bonding effects are not important in determining the relative stabilities of the isomers, and for 2-methoxyethanol, the model compound considered above. Similar results have been found for a variety of 1,2-disubstituted propanes¹⁵ and 2,3-diacetoxybutanes.¹⁷ The reason for this is probably that in the *gauche* form each molecule has its maximum dipole moment and that this is the controlling factor in determining the most stable configuration in condensed phases. It is of interest that pure ethylene glycol and 1,2-dimethoxyethane show almost identical variation of $J + J'$ with temperature which might be taken as an indication that hydrogen bonding is of small importance in ethylene glycol. However, the situation is complicated since the two compounds have very different dielectric constants ($\epsilon = 3.5$ for 1,2-dimethoxyethane and $\epsilon = 38$ for ethylene glycol) and, as discussed below,¹⁸ this may have a considerable influence on the observed values of $J + J'$. The data exhibit marked solvent effects, particularly for the polymer, where changing from chloroform to water as solvent decreases $J + J'$ by ~ 0.6 c.p.s., over the whole temperature range, the change being consistent with the stabilization of the *gauche* form by the solvent of highest dielectric constant. The large change in the coupling constant for 1,2-dimethoxyethane when measured in chloroform which again seems to stabilize the *gauche* form probably results to some extent from association effects since the change in dielectric constant is small in

this case (chloroform $\epsilon = 4.8$ at 20°). The variations of $J + J'$ with solvent are in line with the general observation that it is easier to change the rotational isomer populations by varying the solvent rather than the temperature, particularly in the case of the model compounds.

The failure of the theory in these cases may be due to a number of causes. The most likely seems to be the possibility that ΔE is temperature and solvent dependent.^{15,18} The dependencies of the observed couplings in 1-chloro-2-bromoethane have been discussed in terms of changes in ΔE caused by a variation of dielectric constant with change of solvent and temperature.¹⁸ The calculations, although made on a strictly classical electrostatic basis seem to work well for this one molecule. Insufficient data are available to allow similar calculations to be made for the small molecules considered here and it is not certain that such an approach could be applied to a polymer molecule since one would be attempting to explain microscopic properties of the monomer units in the chain in terms of macroscopic properties of the whole chain. A variation in ΔE with temperature for the polymer might also be expected for a further reason. The magnitude of ΔE will depend largely on the properties of the monomer units themselves but also to some extent on the relative orientations of the neighboring chain units. Since these are dependent on temperature, ΔE itself may be temperature dependent, the process of reorientation of the chain being a cooperative phenomenon. Also, the environments of individual carbon-carbon bonds in the chain may be different leading to a distribution of ΔE values which should be taken into account in a theory of the variation of $J + J'$ with temperature. A variety of other cooperative processes are observed in the study of polymers. It is frequently found that the motion setting in at the glass transition temperature, for instance, is described by a correlation time, τ , whose temperature dependence is not exponential but which is fairly accurately given by an expression of the form^{19,20}

$$\tau = \tau_0 \exp\left(\frac{B}{T - T_\infty}\right) \quad (3)$$

where B and T_∞ are constants ($T < T_\infty$) and τ_0 is an inverse frequency factor. Such an expression is equivalent to an activation energy, Q , for the molecular process which decreases with temperature and is found

(16) S. Mizushima, "Structure of Molecules and Internal Rotation," Academic Press, New York, N. Y., 1954.

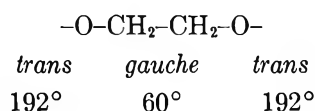
(17) A. A. Bothner-By and C. Naar-Colin, *J. Am. Chem. Soc.*, **84**, 743 (1962).

(18) R. J. Abraham, L. Cavalli, and K. G. R. Pachler, Proceedings S.I.P.S. Symposium, Sardinia, 1964.

to describe the temperature dependence of the correlation time derived from dielectric measurements for PEO of molecular weight 200. In contrast to Q , the present results require that ΔE should increase with increasing temperature.

Other effects may influence the temperature dependence of $J + J'$. The parameters J_t and J_g may themselves be temperature dependent, such an effect having been found for acetaldehyde²¹ although the variations were small (of the order of 0.15 c.p.s. in the temperature range -100 to $+50^\circ$). The calculations, which agreed with experiment, were carried out for a symmetrical three-well potential which does not describe the present situations. The coupling for acetaldehyde decreased as the temperature was raised although in other cases an increase may occur.²¹ How such results would be modified for the unsymmetrical three-well potential considered here is not known. The assumptions $J_t = J_t'$ and $J_g = J_g' = J_g''$ probably also lead to some discrepancy. In other cases, results have been interpreted in terms of different *gauche* couplings which have opposite signs^{8,15} although these were derived on the basis of constant ΔE values.

Investigations by a number of other techniques lend support to the idea that the *gauche* form of the monomer unit is the conformation assumed by the chain in the solid state. Infrared studies^{22,23} of a highly oriented film of PEO 6000 indicate that the monomer unit bonds take the configurations



with the values of ϕ shown, giving rise to an arrangement of the form



This corresponds to a helical arrangement of the chain with a repeat distance of seven monomer units comprising two helical turns. This structure has been confirmed by X-ray diffraction measurements.²⁴ The *trans* angle apparently shows a considerable deviation from 180° . Dipole moment studies of PEO's in solution have been made, but their interpretation in terms of chain conformation is more equivocal.^{25,26}

It thus seems that no satisfactory quantitative discussion of the results obtained is possible on the basis of the theory outlined, and it is probable that similar interpretations suggested previously may be in error. It is hoped that further studies in progress may resolve some of the difficulties.

Acknowledgment. This work forms part of the research program of the Basic Physics Division of the National Physical Laboratory and is published by permission of the Director.

-
- (19) T. M. Connor, *Trans. Faraday Soc.*, **60**, 1574 (1964).
 (20) N. Koizumi and T. Hanai, *J. Phys. Chem.*, **60**, 1496 (1956).
 (21) J. G. Powles and J. H. Strange, *Mol. Phys.*, **5**, 329 (1961).
 (22) T. Miyazawa, K. Fukushima, and Y. Ideguchi, *J. Chem. Phys.*, **37**, 2764 (1962).
 (23) S. Mizushima and T. Shimanouchi, *J. Am. Chem. Soc.*, **86**, 3521 (1964).
 (24) R. L. Miller, "Crystallographic Data for Various Polymers," Vol. IV, Chemstrand Research Center, Durham, N. C., 1963, p. 16.
 (25) T. Uchida, Y. Kurita, N. Koizumi, and M. Kubo, *J. Polymer Sci.*, **21**, 313 (1956).
 (26) J. Marchal and H. Berioit, *J. chim. phys.*, **52**, 818 (1955).

The Dimeric State of Cyanine Dyes

by W. West and Sandra Pearce

Research Laboratories, Eastman Kodak Company, Rochester, New York 14650 (Received December 11, 1964)

Dyes of the 3,3-diethylthiacyanine series dimerize over a certain concentration range, as shown by their adherence to the law of mass action for the monomer-dimer equilibrium. At higher concentrations, a more complex *H*-aggregate appears. The stability of the dimers, as measured by the free energy of dimerization, increases steadily with chain length. The dimeric spectrum consists of an intense *P*-branch, hypsochromic to the monomeric maximum, and a feeble, bathochromic *N*-branch. The monomers are linked with their molecular planes and chromophores approximately parallel. Mixed dimers, with relatively strong *N*-branches, are formed in aqueous solutions of certain dye pairs. The significance of dimerization with respect to fluorescence quenching, photochemical activity, and the "excimer" is discussed.

Introduction

It is well known that solutions of dyes in polar organic solvents at room temperature follow Beer's law over an extended concentration range, but that in water large deviations from the law are observed.¹ For many classes of dye in aqueous solution, the band of highest intensity in dilute solution becomes weaker as the concentration is increased, and new bands appear at other wave lengths. These spectral changes have long been attributed to aggregation of the dye molecules in water to form dimers and higher polymers under the influence of the strong dispersion forces associated with the high polarizability of the chromophoric chain.²⁻⁴ The dominant role of water as the solvent most favorable to aggregation at room temperature is no doubt associated with the effect of its high dielectric constant in reducing the repulsive force between the similarly charged dye cations or anions in the aggregate; the absence of aggregation in organic solvents of high dielectric constant at room temperature suggests that solvation interferes with the aggregation, and in such solvents aggregates are stable only at low temperatures under conditions of high viscosity.¹

The peculiar solvent effects of water on the absorption spectra of dyes are illustrated in Figures 1 and 2, which show the visible absorption spectrum of 3,3'-diethylthiacyanocarbo-cyanine *p*-toluenesulfonate (dye II, Table I) at 22°, dissolved in methanol and in water.

Alcoholic solutions follow Beer's law over at least the hundredfold concentration range from 10^{-6} to 10^{-4} *M*. The shape of the spectrum in alcoholic solution is typical of the molecular spectrum of cyanine and other polymethine dyes; with rare exceptions, the band of longest wave length is the most intense, presumably representing approximately the $0 \leftarrow 0$ transition in a vibronic progression, whereas the pattern of subsidiary maxima or shoulders at shorter wave lengths, differing from dye to dye in resolution and intensity, is set by the $1 \leftarrow 0$, $2 \leftarrow 0$, etc., transitions of a dominant vibrational mode of frequency approximately 1200 cm^{-1} . (See Table III, under $\Delta\nu_v$.)

In water, Figure 2, the aggregation of the dye with increasing concentration is shown by the reduction in intensity of the molecular maximum at wave length

(1) Deviations from Beer's law have been observed for certain dyes of the triphenylmethane class in organic solvents of low polarity at room temperature, attributed to the appearance of contact ion pairs at high concentration: V. F. Feichtmeyer and J. Schlag, *Ber. Bunsenges.*, **68**, 95 (1963). Deviations attributed to dimerization have been observed for certain cyanine dyes dissolved in a rigid isopropyl alcohol-pentane solvent at 77°K. by G. Levinson, W. T. Simpson, and W. Curtis, *J. Am. Chem. Soc.*, **79**, 4314 (1957), and polymerization of 1,1'-diethyl-2,2'-cyanine chloride in ethanol at 90°K. has been recognized from spectral changes by H. Zimmermann and G. Scheibe, *Z. Elektrochem.*, **60**, 566 (1956).

(2) G. Kortüm, *Z. physik. Chem.*, **B33**, 1 (1936); **B34**, 255 (1936).

(3) G. Scheibe, *Z. angew. Chem.*, **49**, 563 (1936); **50**, 212 (1937); **52**, 631 (1939).

(4) E. Rabinowitch and L. Epstein, *J. Am. Chem. Soc.*, **63**, 69 (1941).

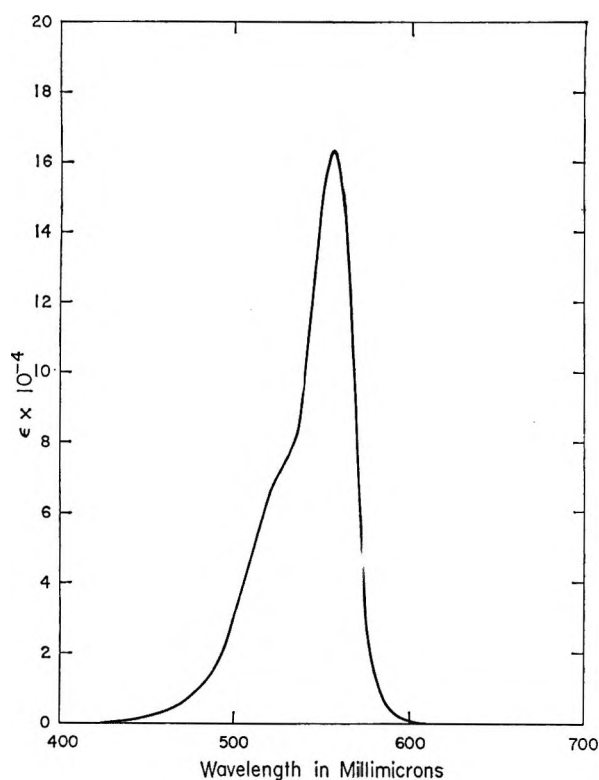


Figure 1. Absorption spectrum of 3,3'-diethylthiacarbocyanine *p*-toluenesulfonate (dye II) in methanol.

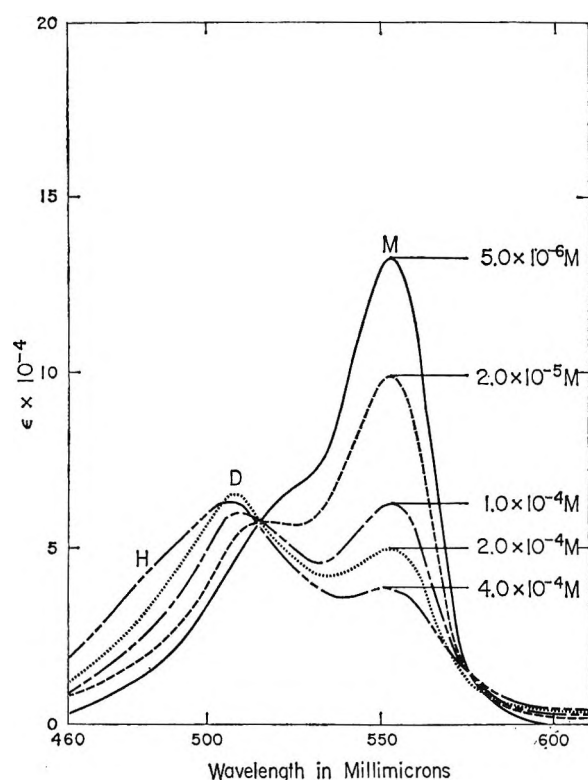
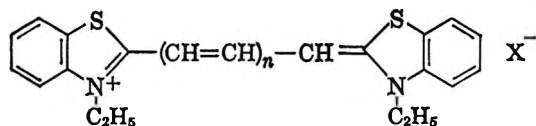
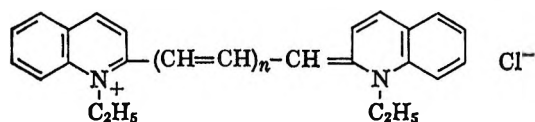


Figure 2. Absorption spectrum of 3,3'-diethylthiacarbocyanine *p*-toluenesulfonate (dye II) in water.

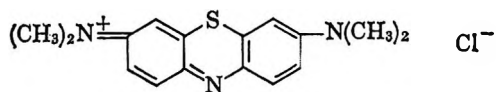
Table I: Dye Formulas



- I 3,3'-Diethylthiacyanine ethylsulfate, $n = 0$
 II 3,3'-Diethylthiacarbocyanine *p*-toluenesulfonate or chloride, $n = 1$
 III 3,3'-Diethylthiadicarbocyanine *p*-toluenesulfonate, $n = 2$
 IV 3,3'-Diethylthiatricarbocyanine *p*-toluenesulfonate, $n = 3$



Pinacyanol chloride, $n = 1$



Methylene blue

centrations, two isosbestic points appear in the family of absorption curves, one at shorter wave length and the other at longer wave length than the molecular maximum. Over this range of concentrations, therefore, according to the well-known properties of the isosbestic point, two colored species are in equilibrium. The persistence of the monomeric band shows that one of these species is the dye monomer, and it will be shown that the other is a dimeric form of the dye.

As the concentration of dye is further increased, aggregation of cyanine dyes usually proceeds beyond the dimeric stage. At this stage, the absorption curve of the solution does not pass through the isosbestic points characteristic of equilibrium between monomer and dimer alone, the dimeric maximum broadens and drifts to shorter wave lengths, and a more or less definite new band appears hypsochromic to the dimeric maximum. It seems reasonable to attribute such bands to a polymer of greater complexity than the dimer.⁵ This polymer has been called an "*H*-polymer," characterized by an *H*-absorption band.⁶ The *H*-band of dye II, illustrated for the highest concentration in Figure 2, is not well resolved from the dimeric

553 $m\mu$ and the appearance of a new maximum at about 510 $m\mu$, somewhat shorter than the vibrational shoulder of the molecular band. Over a range of con-

(5) G. Scheibe, *Kolloid-Z.*, **82**, 1 (1938).

(6) W. West and B. H. Carroll, *J. Chem. Phys.*, **19**, 417 (1951).

maximum, but sometimes a definite *H*-peak can be observed, as in Figure 3 for dye V.

The existence of dimers in aqueous solutions of a number of dyes of the thiazine^{4,7,8} and xanthine classes,⁹ of rhodamine B,⁹ acridine orange,¹⁰ proflavine,¹¹ and other dyes has been proved by observations that as the total concentration of the dye is changed, the concentrations of monomer and dimer, c_m and c_d , respectively, adjust themselves in accordance with the law of mass action

$$\frac{c_m^2}{c_d} = K \quad (1)$$

where K is the dissociation constant of the dimer. Among cyanine dyes, similar evidence has been found for the existence of the dimer of 1,1'-diethyl-2,2'-pyridocyanine salts in a rigid glass of isopropyl alcohol and isopentane at 77°K.¹² For aqueous solutions of 1,1'-diethyl-2,2'-cyanine chloride and its next higher vinylog, pinacyanol chloride (dye V, Table I), Scheibe found satisfactory conformance to the law of mass action insofar as the plot of $\log c_d$ against $\log c_m$ at various total concentrations was linear with a slope of 2. For a number of cyanine dyes in aqueous solution,

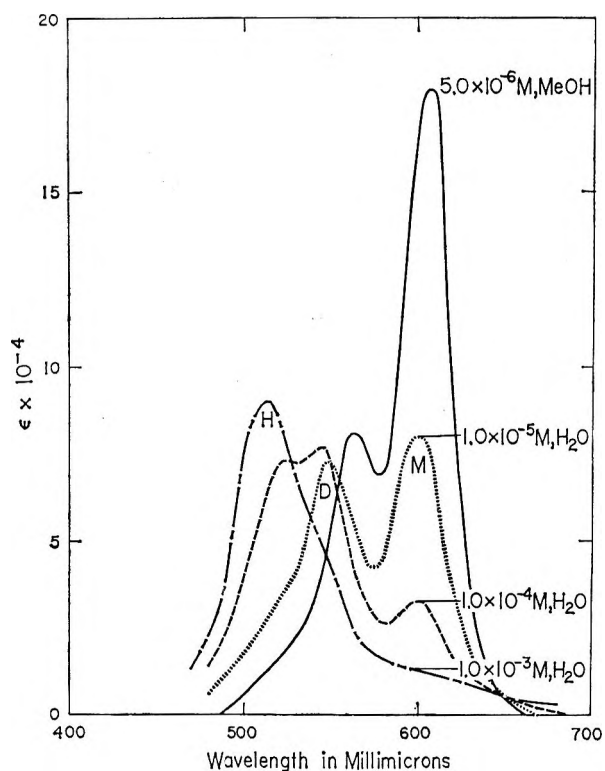


Figure 3. Absorption spectrum of pinacyanol chloride (dye V) in methanol and in water, showing dimeric and *H*-aggregate bands in water.

however, Sheppard and Geddes¹³ were unable to find strict quantitative adherence of their deduced concentrations of monomeric and aggregated dye to the requirements of the mass law for the monomer \rightleftharpoons dimer equilibrium, although they concluded that their deviations arose, not because the dimerization hypothesis was in itself incorrect, but because certain activity factors must be taken into account. In the present communication, we report data derived from the spectra of aqueous solutions of the vinylogous series of thiacyanine dyes listed in Table I which are in quantitative agreement, within a reasonable limit of experimental error, over a restricted concentration range, with the requirements of the simple mass law applied to the monomer \rightleftharpoons dimer equilibrium.

Dimers of Thiacyanine Dyes. To find the concentrations of monomer and dimer in an aqueous solution, one must know in essence the molar extinction coefficient of the pure monomer at a suitable wave length, usually that of the absorption maximum and, since the absorption bands of the monomer and dimer overlap, one must also know the relative contributions of the monomer and dimer to the observed density at the measuring wave length. In principle, the molar extinction coefficient of the pure monomer in water can be found from measurements of the absorption spectra of solutions so dilute that dimerization is negligible. If the fraction of the total molar concentration c of the dye in solution present as monomer is α , the dimeric dissociation constant is

$$K = \frac{2\alpha^2 c}{1 - \alpha} \quad (2)$$

For cyanine dyes we find K to vary from some 10^{-3} to 10^{-6} mole l.⁻¹. If a solution in which 95% of the dye is present as monomer is regarded as a tolerable approximation to a solution of the pure monomer, the concentration at which this condition prevails is found from eq. 2 to vary from 2.8×10^{-5} M for $K = 10^{-3}$ to 2.8×10^{-8} for $K = 10^{-6}$. Aqueous solutions of cyanine dyes, especially those of longer chain length, are not stable in light or on heating, and, moreover, the dyes are adsorbed to the glass walls of volumetric

(7) R. Havemann, E. Nutsch, and H. Pietsch, *Z. physik. Chem. (Leipzig)*, **219**, 171 (1962).

(8) K. Bergmann and C. T. O'Konski, *J. Phys. Chem.*, **67**, 2169 (1963).

(9) T. Förster and E. König, *Z. Elektrochem.*, **61**, 344 (1956).

(10) V. Zanker, *Z. physik. Chem.*, **199**, 255 (1952); **200**, 250 (1952).

(11) G. R. Haugen and W. H. Melhuish, *Trans. Faraday Soc.*, **60**, 386 (1964).

(12) See Levinson, Simpson, and Curtis, in ref. 1.

(13) S. E. Sheppard and A. L. Geddes, *J. Am. Chem. Soc.*, **66**, 2003 (1944).

apparatus and of the measuring cell. It is, therefore, difficult to make accurate measurements of aqueous dye solutions at concentrations of $10^{-6} M$ and less, requiring cell lengths of 10 cm. or more, even when precautions are taken to exclude actinic light in the preparation of the solutions and to correct for adsorption. Careful measurements of the absorption spectra of several cyanines in dilute aqueous solutions prepared with the exclusion of actinic light, rapidly made on an automatic spectrophotometer, gave values of the molar extinction coefficient at the monomeric maximum only slightly below that in methanol. Methanol solutions are considerably more stable than aqueous solutions, adsorption of dye to the glass walls is much reduced in these solutions, and, since Beer's law is followed, the molar extinction coefficient can be measured at a concentration allowing accurate measurement at a path length of 1 cm. Accordingly, we have assumed that, in general, the molar extinction coefficient of the pure monomer in water is practically equal to its value in methanol and, in cases where the dimerization is so great as to require absorption measurements of solutions $10^{-6} M$ or less, we regard the value of the alcoholic extinction coefficient as probably a closer approximation to that of the monomer in water than one obtained by extrapolation from values observed at higher concentrations of aqueous solutions.

We have attempted to allow for the overlap of the dimeric band on the monomeric band by a series of successive approximations, assuming in the first approximation that the monomeric band does not overlap the dimeric maximum and that the dimeric band is symmetrical about its maximum, overlapping the monomeric band. The contribution of the dimeric absorption to the observed optical density at the wave length of the monomeric maximum at any total concentration can therefore be read off, to a first approximation, and, on the assumption of additivity of the densities of the monomer and dimer at any wave length, a first approximation to the density of the monomer at its maximum can be determined. Overlap of the monomeric band with the dimeric band is now considered. From the absorption spectrum of a dilute solution of the dye in which dimerization is negligible, the ratio of the monomeric densities at the wave lengths of the monomeric and dimeric maxima can be found, and, from the first approximation of the density of the monomer at the monomeric maximum, the approximate contribution of the monomer to the density at the dimeric maximum can be calculated. A second approximation to the density of the dimer at its maximum can therefore be found; hence a second approximation to the density of the dimer at the monomeric

maximum can be made, and a second approximation to the monomeric density at its maximum is obtained. From this, as before, a third approximation to the density of the dimer at its maximum is made, and the process is repeated. The approximations rapidly converge after the fourth or fifth cycle, and values are obtained for the densities of the monomer and the dimer at their respective maxima. The molar concentration of the monomer, c_m , at any total concentration, c , can therefore be calculated from a knowledge of the molar extinction coefficient of the pure monomer and the cell thickness. The concentration of the dimer, c_d , is obtained from the condition

$$c_d = \frac{c - c_m}{2} \quad (3)$$

Data for the calculation of the dissociation constant of the dimer of dye II are listed in Table II; for the reasons already discussed, the molar extinction coefficient of the pure monomer in water was taken as 16.2×10^4 , the measured value in methanol. The total molar concentration, c , of the dye is listed in the first column; the thickness, t , of the cell used in the spectrophotometric determination of the monomeric and dimeric concentrations is given in the second column; the observed density, D_{obsd} , of the solution at the monomeric maximum in the third column; the corrected density, D_m , of the monomer at that wave

Table II: Dissociation Constant of the Dimer of 3,3'-Diethylthiacarbocyanine *p*-Toluenesulfonate (Dye II) at 22°

c , moles l^{-1} $\times 10^6$	t , cm.	$D_{\text{obsd.}}$ λ 553 $\mu\mu$	D_m	$c_m \times 10^6$	$c_d \times 10^6$	$K = \frac{c_m^2}{c_d}$, $\text{mole } l^{-1}$ $\times 10^5$
1.00	1.0	1.19	1.13	0.70	0.15	3.28
1.93	0.5	1.01	0.92	1.14	0.40	3.25
2.00	0.5	1.04	0.94	1.16	0.42	3.21
2.88	0.1	0.28	0.24	1.48	0.70	3.12
3.00	0.2	0.58	0.52	1.60	0.70	3.66
4.00	0.2	0.71	0.63	1.94	1.03	3.66
5.00	0.2	0.86	0.74	2.28	1.36	3.82
10.00	0.05	0.32	0.27	3.28	3.36	3.20
20.00	0.05	0.51	0.38	4.66	7.67	[2.83]
Av.						3.40×10^{-5}
Mean dev.						$\pm 0.17 \times 10^{-5}$

length derived from successive approximations in the fourth column; the computed concentration of the monomer in the fifth column; the computed concentration of the dimer in the sixth column; and

the value of $K = c_m^2/c_d$ in the seventh column. The values of K are constant within a mean deviation of $\pm 5\%$. At concentrations higher than $2 \times 10^{-4} M$, the computed values of c_m and c_d no longer conform to the mass law for a monomer \rightleftharpoons dimer equilibrium, and at this concentration the H -band begins to appear. It follows from eq. 1 that, as one varies the total concentration of the dye participating in an equilibrium between the monomeric and dimeric states, a plot of $\log c_d$ vs. $\log c_m$ is linear with a slope of 2. In Figure 4 such a plot made from the data of Table II is illustrated for dye II. The line is the least-squares line from the data, and its slope, 1.99, is in accord with the existence of a monomer \rightleftharpoons dimer equilibrium over the concentration range involved.

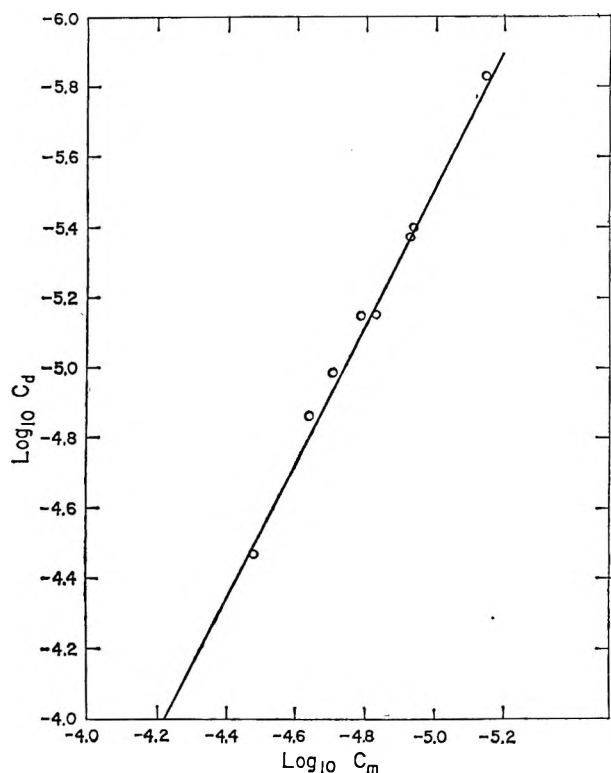


Figure 4. Plot of $\log c_d$ vs. $\log c_m$ for aqueous solutions of dye II. The slope of the least-squares line is 1.99.

A variation of the test for the existence of an equilibrium between monomer and dimer alone is to find that, as the concentration of the dye is changed, the observed extinction coefficient at any wave length, ϵ_{obsd} , is proportional to α , the mole fraction of the total dye present in the monomeric state, calculated from the mass law according to eq. 2.⁸ If the monomeric and dimeric absorptions are additive

$$\begin{aligned}\epsilon_{\text{obsd}} &= \epsilon_m \alpha + (1 - \alpha) \epsilon_d' \\ &= \alpha(\epsilon_m - \epsilon_d') + \epsilon_d'\end{aligned}\quad (4)$$

where ϵ_d' is the molar extinction coefficient of the monomers that are bound together in the dimer, *i.e.*, half the molar extinction coefficient of the dimer. Since ϵ_m and ϵ_d' are constants at a given wave length, the observed extinction coefficient is linear in α , the intercept corresponding to $\alpha = 0$ being the value of ϵ_d' . This relation for dye II at various wave lengths is illustrated in Figure 5. From the values of ϵ_d' , taken from the intercepts at $\alpha = 0$ of plots such as that of Figure 5, or found by direct calculation from eq. 4, one obtains the absorption spectrum of the pure dimer, illustrated in comparison with the spectra of the pure monomers, for dyes II and IV in Figures 6 and 7. Similar curves have been found for the other thiocyanine dyes discussed in this paper. The dimeric spectra consist of two branches, one of high intensity, designated as the positive or *P*-branch, at the high-frequency side of the monomeric maximum and the other, the negative or *N*-branch, of relatively low intensity, near the monomeric maximum, usually on the low-frequency side. The significance of this structure is discussed later in this paper.

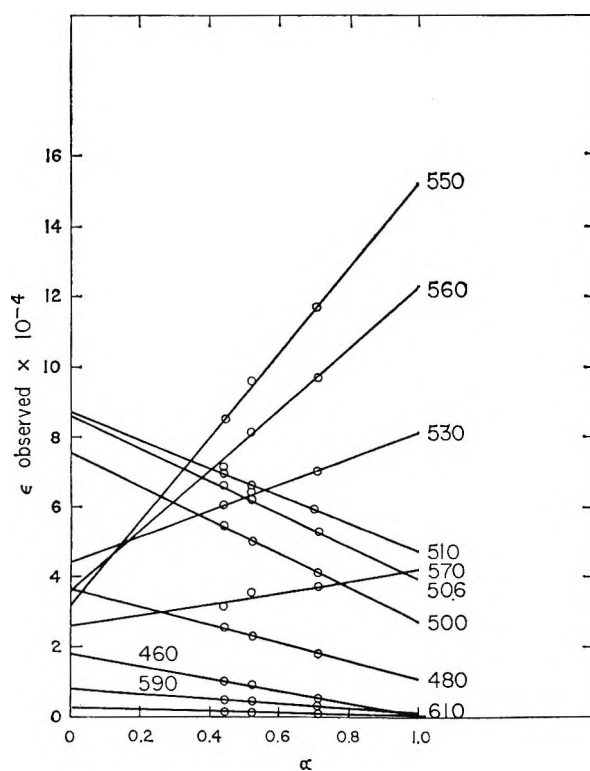


Figure 5. Linearity in α of observed molar extinction coefficient of aqueous solutions of dye II.

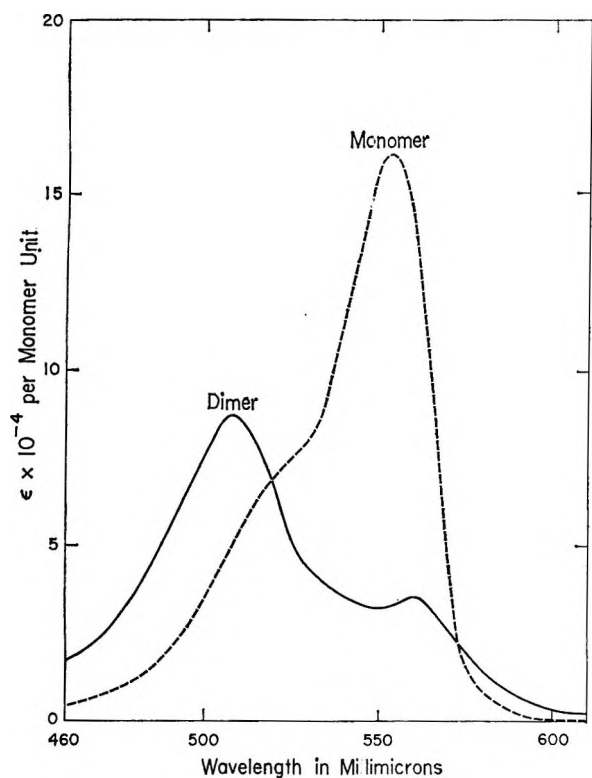


Figure 6. Absorption spectra of pure monomer and calculated spectrum of pure dimer of dye II (*p*-toluenesulfonate) in water.

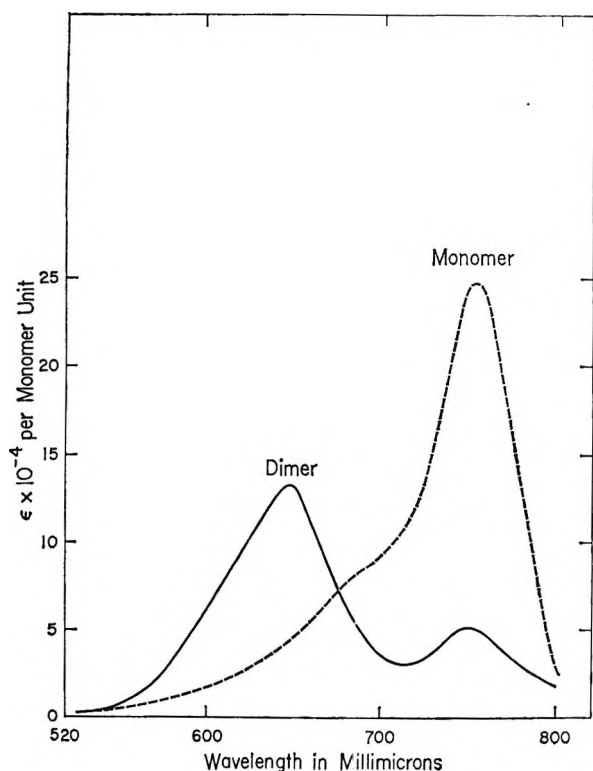


Figure 7. Absorption spectra of pure monomer and calculated spectrum of pure dimer of dye IV in water.

Data for the *P*-branch of the dimeric spectra of thiocyanine dyes in aqueous solution are listed in Table III. The first column designates the chain length (see Table I), the next two columns contain the wave length and wave number of the monomeric maximum,

Table III: Spectral Data for Dimers of Thiocyanine Dyes in Aqueous Solution at 22°

<i>n</i>	λ_m , m μ	ν_m , cm. ⁻¹	λ_v , m μ	ν_v , cm. ⁻¹	$\Delta\nu_v$, cm. ⁻¹	λ_d , m μ	ν_d , cm. ⁻¹	$\Delta\nu_d$, cm. ⁻¹
0	422	23,697	405	24,691	1106	402	24,876	1179
1	553	18,083	516	18,380	1297	510	19,608	1525
2	648	15,432	598	16,722	1290	579	17,271	1839
3	753	13,280	690	14,493	1248	647	15,456	2176

the fourth, fifth, and sixth columns refer, respectively, to the wave length and wave number of the vibrational shoulder in the monomeric spectrum and the frequency displacement of the shoulder from the maximum, and the last three columns refer to the wave length and wave number of the *P*-branch of the dimeric maximum and to its displacement from the monomeric maximum. Consistent with its interpretation as being in essence a vibrational interval determined mostly by a dominant vibrational mode in the conjugated chromophoric chain, the displacement of the molecular shoulder from the maximum does not vary much from dye to dye, but the separation of the dimeric maximum from the molecular maximum increases steadily with increasing chain length; in fact, as is shown in Figure 8, the displacement is linear in *n*. The dimeric maximum is always hypsochromic to the molecular shoulder, although for dyes of the shorter chain lengths, not by many millimicrons, but the separation increases with chain length. There can be little doubt that the shoulder and what we have called in this paper the dimeric maximum are distinct spectroscopic entities that happen to fall at about the same wave length, probably because the energy of interaction associated with dimerization is similar in magnitude to the energy of the vibrational transition.

The values of the dissociation constants of the dimers of the series of thiocyanine dyes are listed in Table IV, along with the free energy of dimerization, computed from the relation $-\Delta F = RT \ln K'$, where K' is the association constant of the monomer, equal to $1/K$. The concentration at which the *H*-band appears determines the range over which the simple monomer-dimer equilibrium exists. Owing to the relative instability of dyes III and IV, solutions of these dyes contained 1 and 2% methanol, respectively. Since

Table IV: Dimerization and *H*-Aggregation of Thiocyanine Dyes

Dye	<i>n</i>	X ⁻	<i>K</i> , mole l. ⁻¹	-Δ <i>F</i> , 295°K.	<i>H</i> -band perceptible at
I	0	Ethyl sulfate	13×10^{-5}	5250	1.0×10^{-3}
II	1	<i>p</i> -Toluenesulfonate	3.4×10^{-5}	6040	ca. 2×10^{-5}
III	2	<i>p</i> -Toluenesulfonate	1.5×10^{-5}	6510	ca. 1×10^{-5}
IV	3	<i>p</i> -Toluenesulfonate	4.1×10^{-6}	7260	$< 1.0 \times 10^{-5}$

dimerization is accompanied by a decrease in entropy, the evolution of heat in dimerization will be greater than the diminution in free energy. Over the range of chain lengths examined, the tendency to dimerization increases steadily with chain length. In fact, as is indicated by the approximate linearity of the plot of log *K* against *n* (Figure 9), the free energy change increases by an approximately constant amount for each additional vinylene group in the chain, a result that seems consistent with the supposition that dispersion forces are the main driving force in dimerization.

Quantum-Theoretical Aspects of Dimeric Spectra. As Förster^{14,15} pointed out, the electronic degeneracy that arises in the excited state of a dimer that has absorbed one photon causes a splitting of the excited electronic level into two. Quantitative development

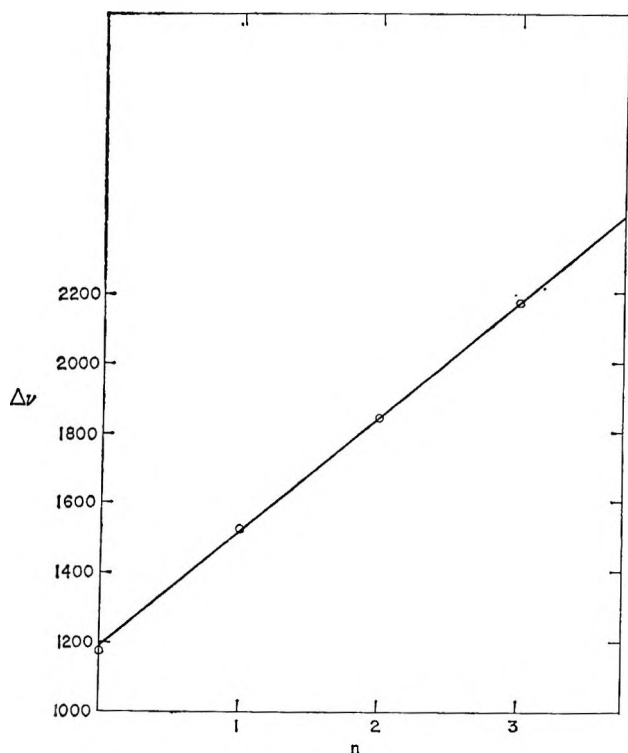


Figure 8. Displacement of dimeric from monomeric maximum as function of chain length.

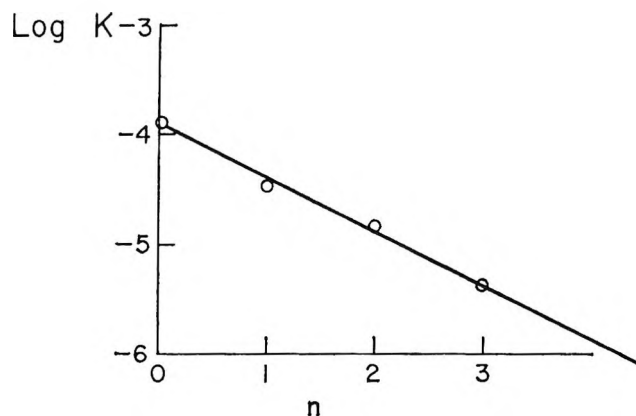


Figure 9. Plot of log *K* vs. chain length for dimerization of thiocyanine dyes.

of the theory^{12,14,15} in terms of the interaction between the transition dipoles of the resonating dimeric structures, in which one or the other of the linked monomers carries the excitation energy, shows that, if the dimer is composed of two identical molecules with their chromophores aligned parallel, the optical transition from the ground state to the higher of the split levels is intense, whereas that to the lower level is, in the limit of exact parallelism of identical chromophores in a structure possessing a center of symmetry, optically forbidden. The excited level associated with the strong transition arises from an interaction between the transition moments in the same phase, and the other, with an interaction of the moments in opposite phases. Deviations from parallelism because of vibrational motion of the chromophores with respect to each other or an unsymmetrical structure of the dimer, will allow the transition to the lower excited state to occur, but less intensely than to the upper state. The dimeric spectrum associated with a parallel arrangement of the co-linked flat monomers is expected, therefore, to consist of an intense band at the shorter wave lengths and a feebler band at longer wave lengths. This is, in fact, observed for the dimers of the thiocyanine series. Striking examples of the double-branched nature of the dimeric band of dyes of the xanthine and rhodamine classes in water are described by Förster and König⁹ and by Lavorel,¹⁶ and two-branched spectra of this nature have been described for the aqueous dimers of methylene blue⁸ and of the aminoanthraquinone dye, proflavine,¹¹ and for dimers of pyridocyanines in an alcoholic glass at 77°K.¹² One can

(14) T. Förster, *Naturwiss.*, **33**, 166 (1946).

(15) T. Förster, "Fluoreszenz Organischer Verbindungen," Vandenhoeck and Ruprecht, Göttingen, 1951, p. 254.

(16) J. Lavorel, *J. Phys. Chem.*, **61**, 1600 (1957).

therefore conclude, in general, that the dimeric structure of dyes consists of two monomers held together with their planes, or at least their chromophores essentially parallel to each other, with some deviations from parallelism because of thermal vibrations or structural asymmetry.

The existence of the lower excited state of the dimer has some interesting consequences. The feebleness of the corresponding absorption implies a relatively long lifetime for this state (approximately 10 times longer for dye II than for the upper state); hence, through radiationless transitions from the upper to the lower excited level of the dimer, most of the dimeric molecules in the steady state produced by a uniform irradiation may be in the lower state. Fluorescence from this state will be weak, and deactivation to this state from the upper excited state may, as pointed out by Lavorel,¹⁶ contribute substantially to concentration quenching of the fluorescence of dyes. Also, the metastable level of the dimer is nearer the triplet level of the dye than the upper level (and probably than the excited monomer level); hence, intersystem crossing may be facilitated through this path. At low temperatures, the dimer might show a higher phosphorescence yield than the monomer,¹⁷ and in photochemical reactions induced by the triplet state of dyes the quantum efficiency might increase with increasing concentration as dimer is produced, if the triplet energy is sufficient for the reaction.

The dimers of the cyanine and other dyes are stable in the ground state and in the two excited states which give rise to the *P*- and *N*-branches, *i.e.*, if the potential energy of interaction of the monomers linked together is plotted as a function of their distance apart, the curves of all these states possess minima. The condition could arise, however, in which the minimum of the ground state is very shallow or nonexistent, when no dimer would be formed in the ground state, or it would be formed only at low temperatures. The upper excited state could then be wholly repulsive, while the lower, stabilized by resonance, could possess a minimum in its potential energy curve. Under these conditions, no dimeric absorption band would be observed at room temperature, but the lower excited state of the dimer could be populated by the product of reaction between an excited monomer and one in its ground state. A fluorescence emission corresponding to the *N*-branch of the dimer could then occur, with relatively low quantum yield and decay period of the order of 10 times that of normal dye monomeric fluorescence. These properties resemble those observed in the excited dimers or "excimers" of perylene and other hydrocarbons.^{18,19}

Mixed Dimers. Besides dimers formed from two identical monomeric molecules, the possibility of mixed dimers from two different monomeric dyes arises. In such a case, the density of a mixture of two dyes in aqueous solution will not be additively composed of those of the separate dyes. Mixed dimers have been found in this way for binary mixtures of azo dyes²⁰ and a mixed polymer (probably dimer) between methylene blue and acridine orange has been observed in aqueous solution.²¹ Mixed polymers between pairs such as acridine orange and thionine, and others have been found in aqueous solution in the presence of polyanions such as chondroitin sulfate.²¹ Mixed excimers have also been observed in binary solutions of some aromatic hydrocarbons.²² Among cyanine dyes that form in aqueous solution, the reversible polymers characterized by the sharp *J*-band bathochromic to the molecular band, mixed *J*-aggregates have been found.^{23,24} Evidence is presented here for the formation of mixed dimers between different cyanine dyes in aqueous solution.

As an example, in Figure 10 are plotted the observed densities as a function of wave length of a mixture of 3,3'-diethylthiacarbocyanine *p*-toluenesulfonate (dye II, $n = 1$) and of 3,3'-diethylthiadibromocyanine bromide (dye III, $n = 2$), each at $1 \times 10^{-4} M$ in water, and also, as the dotted line, the sum of the densities of aqueous solutions of the separate dyes at a concentration of $1 \times 10^{-4} M$. The deviations from additivity are plotted as a function of wave length in Figure 11. There are large negative deviations at the positions of the monomeric and dimeric maxima, M_{III} and D_{III} of the dicarbocyanine, and at the position of the monomeric maximum of the carbocyanine, M_{II} , whereas a new band, $D_{II,III}$, appears between the dimeric peaks D_{III} and D_{II} of the symmetrical dimers. The positions of the monomeric and dimeric maxima of the individual dyes, and of the mixed dimer, are indicated along the wave length axis of Figures 10 and 11. The most obvious interpretation of $D_{II,III}$ is that it is the absorption spectrum of a complex between the two dyes in solution, a mixed dimer. The absorption of a very dilute solution containing the two dyes is additive. In the more concentrated solutions, inspection of

- (17) E. G. McRae and M. Kasha, *J. Chem. Phys.*, **28**, 721 (1958).
- (18) T. Förster and K. Kasper, *Z. Elektrochem.*, **59**, 977 (1955).
- (19) B. Stevens and E. Hutton, *Nature*, **186**, 1045 (1960).
- (20) D. R. Lemin and T. Vickerstaff, *Trans. Faraday Soc.*, **43**, 491 (1947).
- (21) M. K. Pal and M. Schubert, *J. Phys. Chem.*, **67**, 1821 (1963).
- (22) J. B. Birks and L. G. Christophorou, *Nature*, **196**, 33 (1962).
- (23) G. Scheibe, *Z. angew. Chem.*, **52**, 631 (1939).
- (24) H. Ecker, *Kolloid-Z.*, **92**, 35 (1940).

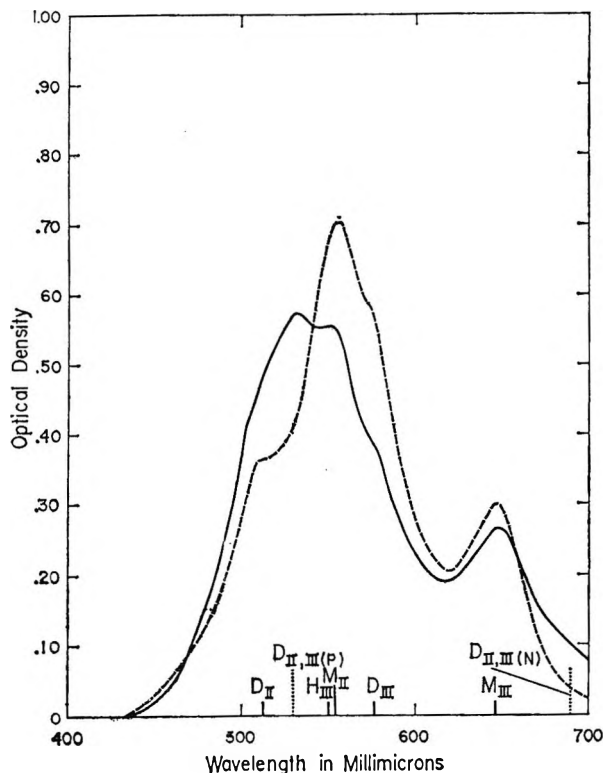


Figure 10. Absorption spectrum of a mixture of dye II and dye III in aqueous solution, each at $1 \times 10^{-4} M$:
 —, experimental; - - -, additive.

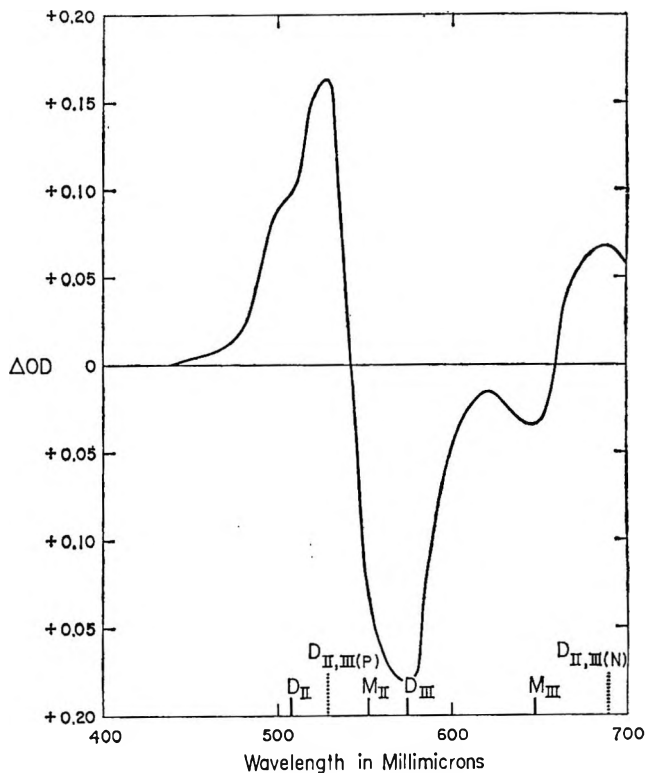


Figure 11. Deviations from additivity in the absorption spectrum of a mixture of dye II and dye III in aqueous solution, each at a concentration of $1 \times 10^{-4} M$.

Figures 10 and 11 shows that the mixed dimer is formed at the expense of the monomers and of the symmetrical dimers.

These figures also show a considerable increase in the absorption of the solution of the mixture at the long wave length side of the monomeric maximum of the dye of the longer chain length. The condition of identical oscillators interacting in opposite phases that causes the negative branch of the absorption spectrum of the symmetrical dimer to be very feeble no longer holds in the mixed dimer. The interacting transition moments are no longer equal and even if directed in completely opposite directions would produce a nonzero resultant. The observed increase in the intensity of absorption of the mixed dimer on the long wave length side of the monomeric band of the dye of longer chain length is therefore in accord with the theory of dimeric absorption discussed earlier and supplies significant experimental verification of the theory.

Mixed dimers showing these spectral characteristics have been observed in aqueous solutions of the dye pairs listed in Table V. The table shows the wave lengths of maximum absorption, λ_{MD} , of the mixed

dimers, the peak maxima of the two symmetrical dimers derived from the monomeric parents, the mean wave length of the parent dimeric maxima, and the difference, Δ , between the parental mean wave length and that of the mixed dimer. All of these data refer to the intense *P*-branches of the dimeric bands. This

Table V: Spectral Data on Mixed Dimers

Mixture	$\lambda_{max.}$ of parent dimers, $m\mu$	Mean λ of parents λ_m , $m\mu$	λ_{MD} of mixed dimer, $m\mu$	$\Delta = \lambda_m - \lambda_{MD}$, $m\mu$
Thiacyanine dyes				
$n = 0, n = 1$	402, 510	456	420	36
$n = 0, n = 2$	402, 579	491	418	73
$n = 1, n = 2$	510, 579	544	532	12
$n = 1, n = 3$	510, 646	579	542	37
$n = 2, n = 3$	579, 646	613	602	11
Methylene blue } Thiacyanine ($n = 1$) }	610, 510	560	538	22
Pinacyanol, $10^{-4} M$ } Thiacyanine ($n = 1$), $10^{-4} M$ }	510, 544	527	500	27
Pinacyanol, $10^{-5} M$ } Thiacyanine ($n = 1$), $10^{-4} M$ }	510, 548	529	502	27

branch of the mixed dimer spectrum, in all of the examples studied, shows a maximum at a wave length less than the mean wave length of the corresponding symmetrical dimers. With respect to its symmetrical parents, therefore, a mixed dimer exhibits in absorption a "deviation," in the sense of the deviations found by Brooker²⁵ for the absorption of a monomeric cyanine or merocyanine dye derived from two different heterocyclic nuclei. In the latter case, the unsymmetrical dye exhibits a maximum at a wave length shorter than the mean of those of the two maxima of the parents, the deviation being the greater, the greater the difference in basicity of the two heterocyclic nuclei. Both for mixed dimers and mixed monomers, the deviation arises from the energetic inequality of the resonating structures from which the actual states of the system are derived. The splitting between the upper and lower states derived from the resonance now includes a term for this energetic inequality and, although the additional separation effected by the resonance is less than for interacting identical structures, the net effect is a displacement of the higher-energy structure of the unsymmetrical system to a value higher than the mean of the energies of the corresponding two symmetrical systems, and a hypsochromic displacement of the *P*-branch of the absorption band of the unsymmetrical system from the mean of the absorption wave lengths of the two symmetrical systems.

Table V also shows that the deviation, Δ , for the mixed dimers derived from the thiocyanine series increases with increasing difference in the chain length of the monomers linked together in the dimer. The energetic inequality between the resonating structures of the mixed dimer increases with increasing difference in the chain length, and the consequent increase in deviation is analogous to Brooker's observation of

increasing deviation with increasing difference in the basicity of the two heterocyclic nuclei in unsymmetrical monomeric dyes.²³

Besides the mixed dimers formed from cyanines containing the same heterocyclic nuclei, mixed dimers have been observed containing thiocyanine monomers linked to 2,2'-cyanine monomers, and between a 2,2'-cyanine and methylene blue. Data on these systems are listed in the lower part of Table V.

Among the thiocyanine dyes, the degree of mixed dimerization is greatest when the difference in chain length of the interacting monomers is equal to one vinylene group. Moreover, as is to be expected, the degree of mixed dimerization depends on the tendency toward self-dimerization of the monomers. For example, the simple thiocyanine ($n = 0$) forms a mixed dimer more readily with the carbocyanine ($n = 1$), than with the dicarbocyanine ($n = 2$), but the dimerization in this case is less than that between the dicarbocyanine and the tricarbocyanine ($n = 3$), both of which very readily form the corresponding symmetrical dimer.

Experimental measurements were made on dye solutions at 22° prepared in nonactinic light and, in the case of dyes III and IV, without assisting solution of the dye by heating. The Beckman DU and the General Electric automatic spectrophotometers were used, the high scanning speed of the latter being especially advantageous in the measurements of solutions of low stability.

Acknowledgment. We are indebted to Dr. L. G. S. Brooker, of these laboratories, for the supply of dyes, and to Mr. F. Grum, also of these laboratories, for many of the measurements of the absorption spectra.

(25) L. G. S. Brooker, *Rev. Mod. Phys.*, **14**, 289 (1942).

Activities of the Three Components in the System Water–Nitric

Acid–Uranyl Nitrate Hexahydrate at 25°

by W. Davis, Jr., P. S. Lawson, H. J. deBruin, and J. Mrochek

*Chemical Technology Division, Oak Ridge National Laboratory,¹ Oak Ridge, Tennessee
(Received December 14, 1964)*

Partial pressures of water and nitric acid over solutions containing water, nitric acid, and uranyl nitrate hexahydrate (UNH) were measured at 25° by use of the vapor transpiration technique for solutions containing 0 to 2.3 *m* UNH and 1 to 14 *m* HNO₃. These data were analyzed in terms of activities in the two two-component systems, water–nitric acid and water–uranyl nitrate hexahydrate, and an integral form of the Gibbs–Duhem equation. From the analysis we obtained four parameters to describe the variation of water and nitric acid activities with acid and UNH concentrations. The same parameters are contained in an equation (obtained by use of cross differentiation) that describes the variation of the UNH activity coefficient with acid and UNH concentrations. Standard deviations of water and nitric acid activities are about ±10%. Also described in this report are new data on the solubility of UNH in H₂O–HNO₃ solutions and equational representation of activity coefficients of HNO₃ in water and of UNH in water.

Introduction

This is a status report in which we present data on the vapor pressures of water and nitric acid over the three-component system—H₂O–HNO₃–UO₂(NO₃)₂·6H₂O—and describe how these data are combined with literature data² and analyzed in terms of an integration of the Gibbs–Duhem equation for the calculation of activities and activity coefficients of uranyl nitrate hexahydrate. This work is a continuation of previous studies,^{2a,3–5} the over-all objective of which is a thermodynamic description of the distribution of water, nitric acid, uranyl nitrate, and fission products between aqueous and tributyl phosphate (TBP)–hydrocarbon diluent solutions. More particularly, the objective of the work is to express solvent extraction data in terms of equations that can be used to predict equilibrium results for conditions not specifically studied experimentally. Such mathematical representation should eventually permit the calculation of optimum conditions for solvent extraction process operations.

Beyond presenting measured partial pressures of water and nitric acid over their solutions that are 0 to 2.3 *m* in UO₂(NO₃)₂·6H₂O and 1 to 14 *m* in HNO₃, we have included in this report a description of the

mathematical techniques used to calculate activities of uranyl nitrate hexahydrate. These techniques are closely related to those described by McKay,^{6,7} McKay and Perring,⁸ and Glueckauf, McKay, and Mathieson⁹; however, they are presented as an integration of the Gibbs–Duhem equation in combination with a four-parameter empirical function to describe the ratio of activities of nitric acid in the three-component system to corresponding values^{2a} in the system H₂O–HNO₃. By use of the cross-differentiation equations,^{6,7,9} the activities of water were also introduced into evaluation of the four parameters. These parameters are

(1) Research sponsored by the U. S. Atomic Energy Commission under contract with the Union Carbide Corp.

(2) (a) W. Davis, Jr., and H. J. deBruin, *J. Inorg. Nucl. Chem.*, **26**, 1069 (1964); (b) R. A. Robinson and C. K. Lim, *J. Chem. Soc.*, 1840 (1951).

(3) W. Davis, Jr., *Nucl. Sci. Eng.*, **14**, 159 (1962).

(4) W. Davis, Jr., *ibid.*, **14**, 169 (1962).

(5) W. Davis, Jr., *ibid.*, **14**, 174 (1962).

(6) H. A. C. McKay, *Nature*, **169**, 464 (1952).

(7) H. A. C. McKay, *Trans. Faraday Soc.*, **49**, 237 (1953).

(8) H. A. C. McKay and J. K. Perring, *ibid.*, **49**, 163 (1953).

(9) E. Glueckauf, H. A. C. McKay, and A. R. Mathieson, *J. Chem. Soc.*, S299 (1948).

used to calculate activities of uranyl nitrate hexahydrate (UNH). Since the final calculations involve the two two-component solutions, we fitted activity coefficients of nitric acid, in water-nitric acid solutions, and water activities in water-uranyl nitrate solutions to appropriate semitheoretical equations.

The results of this work are summarized in isometric drawings of the activity coefficients and of the partial molar free energy of the solution (the chemical potential) over the full range of solubilities of the hexahydrate in aqueous nitric acid solutions (up to 22.5 *m* HNO₃). These representations involve extrapolation beyond the experimental data.

Apparatus, Materials, and Experimental Procedures

Vapor pressures of water and nitric acid over the water-nitric acid-uranyl nitrate solutions were obtained by the transpiration technique with apparatus already described.^{2a}

Reagent grade concentrated nitric acid was used after sparging it with nitrogen to remove dissolved nitrogen oxides. The water was distilled and then further deionized by passage through a commercial water-deionizing resin. Uranyl nitrate hexahydrate of high quality was recrystallized from water and used only after a 0.2 *m* solution in water was found to have a pH within the range 2.2 to 2.4. (According to Robinson and Lim^{2b} the pH of such a solution of high-purity uranyl nitrate in water lies within this range.) The nitrate-to-uranium mole ratio of this purified material was found by analysis to be 1.99 ± 0.01 .

Saturator and presaturator (of which two were used) solutions were made from analyzed stock solutions of nitric acid and of uranyl nitrate in water. In the final three-component solutions, uranium was determined by coulometric titration,¹⁰ while nitrate was determined colorimetrically as previously described.^{3,11} Nitric acid was calculated as nitrate concentration minus twice the uranium concentration although acidity was also determined.¹² Acid concentrations were determined mainly as a check on nitrate and uranium analyses since the acid concentrations were determined with less accuracy than the other analyses of these solutions.

Densities of all saturator solutions were determined in duplicate, at 25.00°, with calibrated 10-ml. pycnometers to accuracies of ± 0.0005 g./ml., or better, as previously noted.⁴ All transpiration experiments were performed at $25.00 \pm 0.01^\circ$. The flow rate of air was maintained at about 2 l./hr.

Estimates of Accuracy and Bias. While using the transpiration technique to obtain partial pressures of

water, nitric acid, and tributyl phosphate (TBP) (over solutions containing from two to four of the species—water, nitric acid, tributyl phosphate, and uranyl nitrate), we have tried to improve our estimates of the probable accuracy and precision of the data. In previous work^{2a} with water-nitric acid solutions, the precision of these partial pressure measurements was estimated to be ± 3 to 4%; by comparing our data with those of Vandoni and Laudy¹³ in 10 to 16 *M* HNO₃, we concluded this ± 3 to 4% represented accuracy as well as precision and that there was no significant bias in our measurements of vapor pressures. Measured vapor pressures of pure water and partial pressures of water over two-phase systems consisting of water and TBP or of water, uranyl nitrate, and TBP provided further information on the accuracy and precision of our techniques. The average and standard deviations of three measurements of the vapor pressure of water at 25.00° were 23.590 ± 0.266 torr; four experiments with two-phase water-TBP solutions yielded a water partial pressure of 23.612 ± 0.379 torr. These pressures differ by less than 1% from the value 23.773 torr, the vapor pressure of pure water at 25.00° when the total pressure is 1 atm. The relative standard deviation of each of these groups of measurements is less than 1.6%. These data, therefore, support our belief that we have no significant bias in our measurements.

The most extensive data on the accuracy and precision of our vapor pressure measurements are derived from the weights of transpired material from two-phase systems containing water, TBP, and uranyl nitrate. Twenty-eight experiments were performed at UNH concentrations in the aqueous phase of 0.04 to 2.4 moles/kg. of H₂O. Activities of water were calculated on the assumption of ideal gas behavior, and these activities were then compared with water activities derived from the data of Robinson and Lim.^{2b} The ratio a_w (this work)/ a_w (R and L) had an average value of 0.999 and a standard deviation of 0.044. Most of this deviation was contributed by three runs from which the calculated water activities were in error by +10, +10, and -20%. Neglecting these, the standard deviation of these data would be less than 1%. However, the occurrence of "obviously" erratic results during studies of the three-component system water-nitric acid-uranyl nitrate hexahydrate suggests that a

(10) W. D. Shults, "ORNL Master Analytical Manual," TID-7015, Suppl. 3, Method No. 1 219225 and 9 00719225, Jan. 29, 1960.

(11) O. Menis, "ORNL Master Analytical Manual," TID-7015, Sect. 1, Method No. 1 215611 and 9 00715611, Aug. 27, 1954.

(12) C. E. Lamb, "ORNL Master Analytical Manual," TID-7015, Sect. 9, Method No. 9 042200 and 9 052200, March 22, 1956.

(13) M. R. Vandoni and M. Laudy, *J. chim. phys.*, **49**, 99 (1952).

Table I: Analysis of Transpiration Data for Water-Nitric Acid-Uranyl Nitrate Solutions

Expt. no.	—Molar concn. in saturator—		Soln. density, g./ml.	—Vapor press., mm.—		—Properties of condensate—		
	HNO ₃	Uranium		H ₂ O	HNO ₃	Molality of HNO ₃	Molarity of HNO ₃	Density, g./ml.
9367	0.976	0.4660	1.1782	22.45	0.000288	0.000712	0.000712	0.9971
9370	0.976	0.4660	1.1782	22.51	0.000288	0.000711	0.000711	0.9971
9371	0.951	0.9020	1.3176	21.31	0.000725	0.00188	0.00188	0.9971
9374	0.951	0.9020	1.3176	21.44	0.000868	0.00224	0.00224	0.9971
9378	0.920	1.3140	1.4467	20.13	0.00159	0.00439	0.00439	0.9972
9379	0.920	1.3140	1.4467	20.40	0.00174	0.00474	0.00474	0.9972
9382	0.920	1.3140	1.4467	20.32	0.00175	0.00479	0.00479	0.9972
9362	2.195	0.4510	1.2163	20.87	0.00232	0.00619	0.00619	0.9973
9363	2.108	0.8540	1.3426	19.60	0.00332	0.00941	0.00941	0.9974
9364	2.108	0.8540	1.3426	19.43	0.00392	0.01122	0.01122	0.9974
9365	2.026	1.2370	1.4611	18.38	0.00724	0.0218	0.0218	0.9977
9366	2.026	1.2370	1.4611	18.75	0.00739	0.0219	0.0218	0.9977
3485	4.290	0.0860	1.1651	18.56	0.01038	0.0310	0.0310	0.9980
3486	4.248	0.2130	1.2027	18.62	0.01214	0.0362	0.0360	0.9982
3484	4.248	0.2130	1.2027	18.48	0.01220	0.0366	0.0365	0.9982
3469	4.182	0.4180	1.2646	17.73	0.0156	0.0490	0.0488	0.9986
3471	4.182	0.4180	1.2646	18.07	0.0155	0.0477	0.0475	0.9985
3472	4.182	0.4180	1.2646	17.92	0.0158	0.0491	0.0488	0.9986
3473	4.182	0.4180	1.2646	17.93	0.0160	0.0495	0.0493	0.9986
9385	3.923	0.8030	1.3800	17.24	0.0210	0.0677	0.0674	0.9992
9386	3.923	0.8030	1.3800	17.20	0.0214	0.0691	0.0687	0.9992
3477	4.039	0.8080	1.3804	17.00	0.0213	0.0696	0.0692	0.9992
3478	4.039	0.8080	1.3804	16.89	0.0204	0.0670	0.0667	0.9991
9383	3.799	1.1600	1.4850	16.46	0.0286	0.0965	0.0959	1.0001
9384	3.799	1.1600	1.4850	16.27	0.0269	0.0919	0.0914	0.9999
3480	3.885	1.1660	1.4812	15.86	0.0348	0.1220	0.1212	1.0008
9387	3.716	1.3760	1.5450	16.03	0.0379	0.1313	0.1304	1.0011
9388	3.716	1.3760	1.5450	16.50	0.0339	0.1143	0.1135	1.0006
3482	3.818	1.4280	1.5668	15.19	0.0384	0.1403	0.1393	1.0014
3483	3.818	1.4280	1.5668	15.68	0.0385	0.1364	0.1354	1.0013
57-0	4.981	0.5331	1.3235	16.83	0.0358	0.1182	0.1174	1.0007
3336	6.135	0.3920	1.3136	15.37	0.0558	0.201	0.199	1.0033
21-0	7.462	0.0984	1.2621	14.32	0.0924	0.358	0.353	1.0083
23-0	7.641	0.2464	1.3148	13.40	0.1215	0.503	0.494	1.0129
3339	7.135	0.3740	1.3366	13.54	0.0953	0.390	0.385	1.0093
3342	7.135	0.3740	1.3366	13.19	0.0935	0.394	0.388	1.0094
29-0	7.674	0.4871	1.3837	12.43	0.163	0.728	0.710	1.0200
30-0	7.776	0.7437	1.4663	11.29	0.201	0.992	0.960	1.0282
33-0	7.654	0.9843	1.5350	10.93	0.240	1.221	1.174	1.0353
52-0	8.054	0.1015	1.2761	12.61	0.221	0.974	0.943	1.0277
53-0	8.070	0.2469	1.3200	13.01	0.159	0.680	0.664	1.0185
54-0	8.227	0.5232	1.3969	11.60	0.232	1.114	1.074	1.0320
56-0	8.129	1.0030	1.5492	11.13	0.287	1.436	1.372	1.0419

4.4% standard deviation is a much more realistic estimate of the precision we have achieved to date than would be the value 1%.

Experimental Results

Experimental results of this work are summarized in Table I in terms of analytical data and calculated quantities. Partial pressures of both water and acid, which range from 5 to 20 and 0.03 to 1 mm., respectively, were calculated from transpired-solution weight, the concentration of nitric acid in the condensate,

displacement-flask volume, and temperature by assuming that both components obey the ideal gas law under these conditions. Errors introduced by this assumption are well within the over-all experimental errors, which are estimated to be about 4%, as discussed previously.

Integration of the Gibbs-Duhem Equation

The basis of analysis of the liquid-vapor equilibrium data for the system $\text{H}_2\text{O}-\text{HNO}_3-\text{UO}_2(\text{NO}_3)_2 \cdot 6\text{H}_2\text{O}$ in terms of activities of the three components is the

Gibbs-Duhem equation. Using subscripts 1, 2, and 3 to refer to water, nitric acid, and uranyl nitrate hexahydrate, respectively, and the terms m_i and a_i to the molality and the activity of species i , respectively, the Gibbs-Duhem equation, after dividing by m_1 ($= 55.509$), is

$$d \ln a_1 + \frac{m_2}{m_1} d \ln a_2 + \frac{m_3}{m_1} d \ln a_3 = 0 \quad (1)$$

To integrate eq. 1, we define the path of integration as corresponding to adding m_3 moles of UNH to 1 kg. of water and then adding m_2 moles of nitric acid to this water-UNH solution. In addition to starting with 1 kg. of water, we assume, for the purpose of simplifying the mathematics, that the amount of "free" water does not change as a result of adding either UNH or nitric acid; that is, we imagine that all the water of hydration remains a part of ions formed by ionization of the hexahydrate. We chose to think in terms of this concept, rather than one based on the anhydrous $\text{UO}_2(\text{NO}_3)_2$, since $\text{UO}_2(\text{NO}_3)_2 \cdot 6\text{H}_2\text{O}$ is the stable crystalline compound when uranium solubility is exceeded (see Appendix); thus, it is probable that this molecular species exists in concentrated solutions, as noted by Nikolaev and Yakovlev.¹⁴ In addition, Lipilina and Samoilov¹⁵ showed that their heat-of-solution data are consistent with the interpretation that the UO_2^{2+} ion is hexahydrated in dilute, aqueous nitric acid solutions. One further restriction on the mathematical analysis of the present paper is that uranium and nitric acid concentrations shall be within that region of the phase diagram^{14,16-21} (Figure 1) in which the only crystalline hydrate would be the hexahydrate. Thus, the nitric acid concentration is less than about 15 m

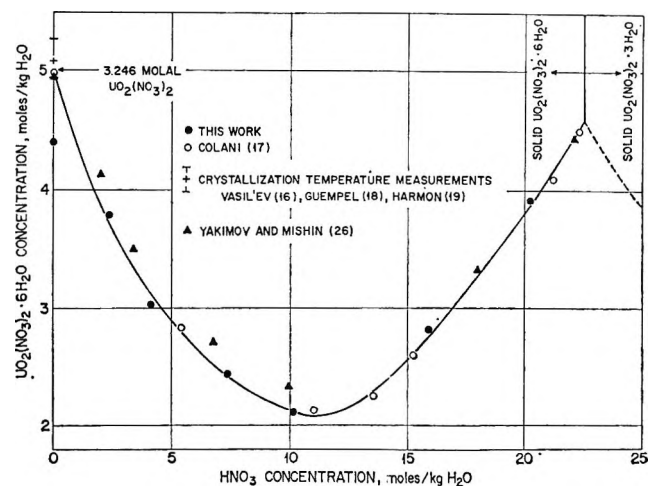


Figure 1. The solubility of uranyl nitrate hexahydrate in aqueous nitric acid solutions at 25°.

when the uranium concentration is expressed as the anhydrous material $\text{UO}_2(\text{NO}_3)_2$.

With m_2 and m_3 as the independent variables, the integral form of eq. 1 becomes

$$\int_0^{m_u} \left(\frac{\partial \ln a_1}{\partial m_3} \right)_{m_2=0} dm_3 + \int_0^{m_s} \left(\frac{\partial \ln a_1}{\partial m_2} \right)_{m_3=m_u} dm_2 + \int_0^{m_u} \frac{m_2}{m_1} \left(\frac{\partial \ln a_2}{\partial m_3} \right)_{m_2=0} dm_3 + \int_0^{m_s} \frac{m_2}{m_1} \left(\frac{\partial \ln a_2}{\partial m_2} \right)_{m_3=m_u} dm_2 + \int_0^{m_u} \frac{m_3}{m_1} \left(\frac{\partial \ln a_3}{\partial m_3} \right)_{m_2=0} dm_3 + \int_0^{m_s} \frac{m_3}{m_1} \left(\frac{\partial \ln a_3}{\partial m_2} \right)_{m_3=m_u} dm_2 = 0 \quad (2)$$

The third term of eq. 2 equals zero since $m_2 = 0$; the sum of the first and fifth terms, which correspond to the two terms of the two-component system $\text{H}_2\text{O}-\text{UO}_2(\text{NO}_3)_2 \cdot 6\text{H}_2\text{O}$, is zero. Thus, integration of eq. 2 yields

$$m_u \ln \left[\frac{a_3(m_s, m_u)}{a_3(0, m_u)} \right] = -m_1 \ln \left[\frac{a_1(m_s, m_u)}{a_1(0, m_u)} \right] - \int_0^{m_s} m_2 \left[\frac{\partial \ln a_2(m_2, m_u)}{\partial m_2} \right] dm_2 \quad (3)$$

In going from eq. 2 to 3 we changed to a notation that seems particularly convenient. In this notation, m_2 and m_3 are variables of integration or differentiation, while m_s and m_u are the corresponding fixed nitric acid and uranyl nitrate hexahydrate concentrations. Thus, for example, $a_2(m_2, m_u)$ is the activity of nitric acid as the acidity m_2 varies at a fixed concentration m_u of uranyl nitrate hexahydrate.

Equation 3 involves the ratios of activities of water and of UNH in the three-component system $\text{H}_2\text{O}-\text{HNO}_3-\text{UO}_2(\text{NO}_3)_2 \cdot 6\text{H}_2\text{O}$ to their values in the two-component system $\text{H}_2\text{O}-\text{UO}_2(\text{NO}_3)_2 \cdot 6\text{H}_2\text{O}$. The data for this two-component system have been reported—

(14) A. V. Nikolaev and I. I. Yakovlev, *Dokl. Akad. Nauk SSSR*, **145**, 1064 (1962).

(15) I. I. Lipilina and O. Ya. Samoilov, *ibid.*, **98**, 99 (1954).

(16) A. M. Vasil'ev, *Zh. Russ. Fiz. Khim. Obshchestva*, **42**, 570 (1910); see *Chem. Abstr.*, **5**, 2374 (1911); **6**, 577 (1912).

(17) A. Colani, *Bull. Soc. Chim. France*, **39**, 1243 (1926).

(18) O. Guempel, *Bull. Soc. Chim. Belges*, **38**, 443 (1929).

(19) M. K. Harmon, "Freezing Point Data for UNH-H₂O-HNO₃ Systems," Hanford Works, General Electric Co., HW-8309, Dec. 17, 1949.

(20) J. Gaunt, I. J. Bastien, and M. Adelman, *Can. J. Chem.*, **41**, 527 (1963).

(21) E. K. Ensley, Ph.D. Thesis, University of Colorado, 1960.

but in terms of $\text{UO}_2(\text{NO}_3)_2$ concentrations—by Robinson and Lim.^{2b} We have reanalyzed these data in consultation with Robinson, whose help in this connection we wish to acknowledge. The reanalysis is summarized in a subsequent section of this report.

To perform the integration indicated in eq. 3, we made the usual assumption that the activity of nitric acid in the three-component system is related to its value in the two-component system by the equation

$$a_2 = a_2(m_2, m_3) = a_2(m_2, 0)e^{F_2(m_2, m_3)} \quad (4)$$

On substituting eq. 4 into 3, then making use of the Gibbs–Duhem equation for a two-component solution, namely

$$\int_0^{m_3} m_2 \left[\frac{\partial \ln a_2(m_2, 0)}{\partial m_2} \right] dm_2 = -m_1 \ln a_1(m_3, 0) \quad (5)$$

the last term of eq. 3 becomes

$$\int_0^{m_3} m_2 \left[\frac{\partial \ln a_2(m_2, m_u)}{\partial m_2} \right] dm_2 = -m_1 \ln a_1(m_3, 0) + \int_0^{m_3} m_2 \left[\frac{\partial F_2(m_2, m_u)}{\partial m_2} \right] dm_2 \quad (6)$$

Upon substituting eq. 6 into 3 we obtain

$$m_u \ln \left[\frac{a_3(m_3, m_u)}{a_3(0, m_u)} \right] = -m_1 \ln \left[\frac{a_1(m_3, m_u)}{a_1(m_3, 0)a_1(0, m_u)} \right] - \int_0^{m_3} m_2 \left[\frac{\partial F_2(m_2, m_u)}{\partial m_2} \right] dm_2 \quad (7)$$

Evaluation of $F_2(m_3, m_u)$. The function $F_2(m_3, m_u)$ corresponds in purpose to twice the $-\alpha_{23}m_3$ term of the Harned rule²² or to twice the sum $-\alpha_{23}m_3 + \beta m_3^2$ of McKay and Perring.⁸ (We have here changed subscripts of these authors to correspond to our notation.) However, Figure 2 shows that both these functions are far too simple to describe activity changes over the wide range of acidities of the present study. Three sets of data, for $\text{UO}_2(\text{NO}_3)_2 \cdot 6\text{H}_2\text{O}$ concentrations of 0.528 to 0.537, 1.094 to 1.234, and 1.691 to 1.881 m , respectively, are plotted in Figure 2. These suggested to us that an applicable function might be

$$F_2(m_3, m_u) = m_u(P_1 + P_2 m_u)(1 + P_3 m_3 + P_4 m_3^2) \quad (8)$$

It should be noted that the expression of McKay and Perring constitutes one of the terms of eq. 8. Nitric acid activity ratios were fitted to eq. 4, with $F_2(m_3, m_u)$ defined by eq. 8, by least-squares methods programmed for a high-speed digital computer. Results of this analysis are summarized in the first and second (and seventh and eighth) rows of Table II in terms of the constants P_1 through P_4 , the standard deviations of

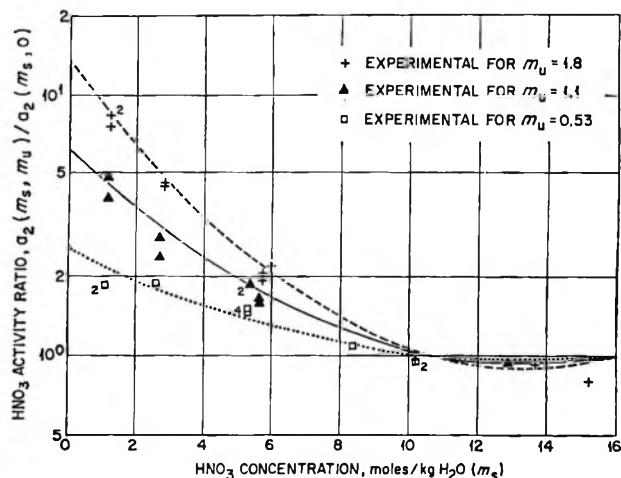


Figure 2. Effect of $\text{UO}_2(\text{NO}_3)_2 \cdot 6\text{H}_2\text{O}$ concentration (m_u) on the nitric acid activity in $\text{H}_2\text{O}-\text{HNO}_3-\text{UO}_2(\text{NO}_3)_2 \cdot 6\text{H}_2\text{O}$ solutions.

these constants, and the standard deviation of the activity ratio. The latter standard deviation is 0.2117 for ratios $a_2(m_3, m_u)/a_2(m_3, 0)$ that vary from about 0.8 to nearly 9. The percentage variation of the ratio is (within the accuracy of these data) independent of its value and is equal to 9.65% (or 7.02% if experiments 9374, 9378, 9363, and 52 are neglected). The corresponding absolute and percentage uncertainties in the nitric acid activity coefficient ratio, $\gamma_2/\gamma_{2(0)}$ (Table II), are 0.150 and 6.82%, respectively (or 0.081 and 4.96% if experiments 9374, 9378, 9363, and 52 are neglected).

The adequacy of eq. 4 and 8 may be seen by comparing the data points and the curves of Figure 2. The curves are drawn for constant values of $\text{UO}_2(\text{NO}_3)_2 \cdot 6\text{H}_2\text{O}$ molalities of 0.53, 1.1, and 1.8. Experimental data were not obtained at these exact values; they were, however, within the narrow ranges defined above. Upon substituting eq. 8 into 7 and performing the integration, we obtain

$$m_u \ln \left[\frac{a_3(m_3, m_u)}{a_3(0, m_u)} \right] = -m_1 \ln \left[\frac{a_1(m_3, m_u)}{a_1(m_3, 0)a_1(0, m_u)} \right] - m_u(P_1 + P_2 m_u) \left(\frac{P_3 m_3^2}{2} + \frac{2P_4 m_3^3}{3} \right) \quad (9)$$

On the basis of the apparent validity of eq. 4 and 8 over the concentration ranges studied, the measured water activities were introduced into the calculation of

(22) H. S. Harned and B. B. Owen, "The Physical Chemistry of Electrolytic Solutions," 3rd Ed., Reinhold Publishing Corp., New York, N. Y., 1958, p. 620.

Table II: Values of Constants P_1 , P_2 , P_3 , and P_4 and Standard Deviations (See Eq. 8, 17, and 22)

Ref. eq.	No. of values	P_1 and $\sigma(P_1)$	$10 \times P_2$ and $10 \times \sigma(P_2)$	$10 \times P_3$ and $10 \times \sigma(P_3)$	$10^3 \times P_4$ and $10^3 \times \sigma(P_4)$	Std. dev. of fit	% std. dev. ^a of fit	$\sigma(\gamma_2/\gamma_{2(0)})$	% std. dev. of $\gamma_2/\gamma_{2(0)}$
8 or 17	43	1.7255 0.0826	-1.7216 0.4672	-1.5969 0.0478	5.9759 0.5383	0.2117	9.65	0.150	6.82
22	43	1.7782 0.1020	-1.9351 0.5812	-1.5280 0.0516	5.8262 0.5559	Over-all 0.2672	Over-all 11.78		
						Contribution of HNO ₃ 0.2726	12.90	0.193	9.12
						Contribution of H ₂ O 0.1121	9.41		
8 or 17	39	1.6031 0.0575	-0.9358 0.3258	-1.6029 0.0259	5.9623 0.2962	0.1142	7.02	0.0808	4.96
22	39	1.6560 0.0771	-1.1263 0.4395	-1.5247 0.0305	5.7890 0.3323	Over-all 0.1571	Over-all 8.94		
						Contribution of HNO ₃ 0.2305	11.67	0.163	8.25
						Contribution of H ₂ O 0.1264	9.42		

^a For example

$$\% \text{ std. dev. of } [a_2(m_s, m_u)/a_2(m_s, 0)] = \frac{100}{\sqrt{n-1}} \left\{ \sum \left[\frac{\left(\frac{a_2(m_s, m_u)}{a_2(m_s, 0)} \right)_{\text{obsd}} - \left(\frac{a_2(m_s, m_u)}{a_2(m_s, 0)} \right)_{\text{calcd}}}{\left(\frac{a_2(m_s, m_u)}{a_2(m_s, 0)} \right)_{\text{obsd}}} \right]^2 \right\}^{1/2}$$

where n is the number of measurements.

the four parameters P_i . This was achieved by use of cross differentiation⁶⁻⁸ as

$$\left. \frac{\partial \ln a_3(m_2, m_u)}{\partial m_2} \right|_{m_2=m_s} = \left. \frac{\partial \ln a_2(m_s, m_3)}{\partial m_3} \right|_{m_3=m_u} \quad (10)$$

Since $a_3(0, m_u)$ is independent of m_2 while $a_2(m_s, 0)$ is independent of m_3 , we rewrite eq. 10 as

$$\left. \frac{\partial \ln [a_3(m_2, m_u)/a_3(0, m_u)]}{\partial m_2} \right|_{m_2=m_s} = \left. \frac{\partial \ln [a_2(m_s, m_3)/a_2(m_s, 0)]}{\partial m_3} \right|_{m_3=m_u} \quad (11)$$

where

$$\left. \frac{\partial \ln [a_2(m_s, m_3)/a_2(m_s, 0)]}{\partial m_3} \right|_{m_3=m_u} = (P_1 + 2P_2m_u)(1 + P_3m_s + P_4m_s^2) \quad (12)$$

By differentiating eq. 9 with respect to m_2 we obtain

$$m_u \left\{ \frac{\partial \ln [a_3(m_2, m_u)/a_3(0, m_u)]}{\partial m_2} \right\} = -m_1 \frac{\partial}{\partial m_2} \left\{ \ln \left[\frac{a_1(m_2, m_u)}{a_1(m_2, 0)a_1(0, m_u)} \right] \right\} - m_u(P_1 + P_2m_u)(P_3m_2 + 2P_4m_2^2) \quad (13)$$

By multiplying eq. 12 by m_u and equating the resulting product to eq. 13 according to (11), we obtain

$$m_1 \frac{\partial}{\partial m_2} \left\{ \ln \left[\frac{a_1(m_2, m_u)}{a_1(m_2, 0)a_1(0, m_u)} \right] \right\} = -m_u(P_1 + P_2m_u)(P_3m_2 + 2P_4m_2^2) - m_u(P_1 + 2P_2m_u)(1 + P_3m_2 + P_4m_2^2) \quad (14)$$

Integration leads to

$$\ln \left[\frac{a_1(m_s, m_u)}{a_1(m_s, 0)a_1(0, m_u)} \right] = -\frac{m_s m_u}{m_1} (P_1 + 2P_2m_u)(1 + P_3m_s + P_4m_s^2) + \frac{P_2 m_s^2 m_u^2}{m_1} \left(\frac{P_3}{2} + \frac{2P_4 m_s}{3} \right) \quad (15)$$

Substitution of eq. 15 into 9 gives

$$\ln \left[\frac{a_3(m_s, m_u)}{a_3(0, m_u)} \right] = m_s(P_1 + 2P_2m_u) \times \left(1 + \frac{P_3 m_s}{2} + \frac{P_4 m_s^2}{3} \right) \quad (16)$$

The corresponding equation for the activity of nitric acid is, from eq. 4 and 8

$$\ln \left[\frac{a_2(m_s, m_u)}{a_2(m_s, 0)} \right] = m_u(P_1 + P_2m_u)(1 + P_3m_s + P_4m_s^2) \quad (17)$$

Table III: Parameters for Activity or Osmotic Coefficient Equations for Two-Component Solutions of Solute in Water (See Eq. 18-21)

Solute	Concn. range, <i>m</i>	No. of points	Std. dev. of fit	<i>A</i> and $\sigma(A)$	10^2B and $10^2\sigma(B)$	10^3C and $10^3\sigma(C)$	10^4D and $10^4\sigma(D)$
HNO ₃ ^{2a}	0.001-24	32	0.0144 ^a	1.118816 0.040961	11.82976 0.25777	-6.985887 0.239201	1.288488 0.061288
CaCl ₂ ^b	0.0016-3.5	25	0.00017 ^c	1.683115 0.066213	4.022827 0.431440	9.451076 0.739806	-3.228915 0.380904
UNH ^{2b}	0.1-5.0	36	0.00049 ^c	1.395422 0.083610	9.236731 0.514499	-6.755264 0.582505	1.284050 0.201317
UN ^{2b}	0.1-3.25	36	0.00048 ^c	1.679688 0.202294	9.421480 1.248074	7.734015 2.080502	-8.151455 1.072036

^a This is $\sigma(\ln \gamma)$, where γ is the molal activity coefficient. ^b See ref. 25, Appendix 8.5, Table I, and Appendix 8.9, Table I. ^c This is $\sigma(a_1)$, where a_1 is the water activity.

Equations 15 through 17 are the logarithmic forms of the equations actually used to evaluate the constants P_1 , P_2 , P_3 , and P_4 from the various vapor pressure data. The sequence of analysis was as follows: (1) fit data on the activity coefficients of nitric acid in the two-component system water-nitric acid to a four-parameter equation in a manner similar to that described by Lietzke and Stoughton²³; (2) from measured values of $a_2(m_s, m_u)$ and calculated values of $a_2(m_s, 0)$ fit the ratio $a_2(m_s, m_u)/a_2(m_s, 0)$ to the exponential form of eq. 17 to obtain preliminary values of constants P_i ; (3) combine eq. 15 and 17 so that both nitric acid and water vapor pressures (that is, all the available data) can be used to evaluate the P_i ; (4) fit the isopiestic data of Robinson and Lim,^{2b} but in terms of uranyl nitrate hexahydrate concentrations, to a four-parameter equation²³ so that actual activity coefficients of UNH in the three-component system (rather than activity coefficient ratios) can be calculated.

Numerical Analyses

Water-Nitric Acid System. Activities^{2a} and densities²⁴ for the system H₂O-HNO₃ are available in tabular form. However, since it is easier and faster when using a high-speed computer to interpolate with equations having fixed constants than it is with tabulated data, we calculated molal nitric acid activity coefficients ($\gamma_{s(0)}$) from the literature data for 0 to 13 *M* HNO₃ (0 to 24 *m*) and fitted these values to

$$\ln \gamma_{s(0)} = \frac{-S\sqrt{I}}{1 + A\sqrt{I}} + (2B)I + (3C/2)I^2 + (4D/3)I^3 \quad (18)$$

Equation 18 (with four empirical parameters), which was analyzed to minimize the variance of \ln

$\gamma_{s(0)}$, leads to parameters that are slightly different from those obtained by minimizing the variance of the osmotic coefficients, the technique used by Lietzke and Stoughton.²³ The parameters for H₂O-HNO₃ solutions so obtained (Table III) were used in the form^{22,23}

$$a_1(m_s, 0) = e^{-\phi_s \nu_s m_s / 55.509} \quad (19)$$

$$\phi_s = 1 - \frac{S}{A^3 I} \left[(1 + AI^{1/2}) - 2 \ln(1 + AI^{1/2}) - \frac{1}{(1 + AI^{1/2})} \right] + BI + CI^2 + DI^3 \quad (20)$$

Values of A , B , C , and D are listed in Table III; $I = m_s$, ϕ_s is the osmotic coefficient in the system, and $\nu_s = 2$ ions/molecule. The value of S used here for a 1:1 electrolyte was 1.1696. The standard deviation of the fit of $\ln \gamma_{s(0)}$ to eq. 20 is 0.0144 (Table III), corresponding to a 1.44% relative error for values of $\gamma_{s(0)}$ calculated from the equation as contrasted to the tabulated data.^{2a} This is well within the limits of uncertainty indicated by Davis and deBruin and indicates that the parameters for nitric acid given in Table III will describe the term $a_1(m_s, 0)$ well within the uncertainties of the present work.

Water-Uranyl Nitrate Hexahydrate System. Water activities, $a_1(0, m_u)$, in the two-component system H₂O-UO₂(NO₃)₂ were reported by Robinson and Lim.^{2b} Some of the data of these workers were obtained for supersaturated solutions. Although a continuous change occurred in water vapor pressure as the solutions passed into the supersaturated region,

(23) M. H. Lietzke and R. W. Stoughton, *J. Phys. Chem.*, **66**, 508 (1962).

(24) J. H. Perry, Ed., "Chemical Engineers' Handbook," 3rd Ed., McGraw-Hill Book Co., Inc., New York, N. Y., 1950, p. 180.

the osmotic data considered to be useful for the purpose of the present report are those corresponding to less than saturation, as defined by the present paper and by the work of Vasil'ev,¹⁶ Colani,¹⁷ Guempel,¹⁸ Harmon,¹⁹ Gaunt, Bastien, and Adelman,²⁰ and by Ensley.²¹ From these data the solubility in water at 25° is estimated to be $5.0 \pm 0.2 m$ $\text{UO}_2(\text{NO}_3)_2 \cdot 6\text{H}_2\text{O}$ (Figure 1) or $3.25 m$ $\text{UO}_2(\text{NO}_3)_2$. Osmotic coefficient data at higher concentrations were not used in the evaluation of the empirical parameters. With this restriction, the data of Robinson and Lim^{2b} used in this work are from the first 19 of the 21 solutions of their series A, the first 6 of the 15 solutions of series C, and all the solutions of series E. The corresponding data on calcium chloride are also used.

The method used here to analyze the data of Robinson and Lim^{2b} involved first fitting water activities of calcium chloride solutions (Robinson and Stokes,²⁵ Table I of Appendix 8.5, and Table I of Appendix 8.9) to equations similar to (19) and (20). The differences are: $S = 2.3392$ for a 2:1 electrolyte such as CaCl_2 or $\text{UO}_2(\text{NO}_3)_2 \cdot 6\text{H}_2\text{O}$; $\nu_{\text{CaCl}_2} = \nu_u = 3$ ions/molecule; and $I = 3m_{\text{CaCl}_2}$ (or $3m_u$ for UNH). Constants (Table III) obtained for calcium chloride solutions were then used to calculate the water activities in the experiments of Robinson and Lim. These activities were, in turn, fitted to equations similar to (19) and (20), but with the concentration of UNH as the independent variable. These concentrations were readily calculated from the concentrations of $\text{UO}_2(\text{NO}_3)_2$ listed by Robinson and Lim. In terms of UNH concentration (m_u), the equation of significance is

$$a_1(0, m_u) = e^{-\phi_u \nu_u m_u / 55.509} \quad (21)$$

Four-parameter equations similar to eq. 20 give excellent representation of water activities over CaCl_2 and $\text{UO}_2(\text{NO}_3)_2 \cdot 6\text{H}_2\text{O}$ solutions. Over the concentration range 0.0016 to 3.5 m CaCl_2 , the standard deviation of the water activity is only 0.00017; for UNH solutions over the concentration range 0.1 to 5.0 m , the standard deviation is (expectedly) higher, being 0.00049.

Final Evaluation of P_1 , P_2 , P_3 , and P_4 . As we mentioned above, we chose to use both water activities and nitric acid activities, calculated from measured partial pressures, in calculating the empirical constants P_i . Such use requires that eq. 15 and 16 be combined. These could be combined simply by adding them together, by multiplying each by some factor and then adding, or by multiplying or dividing one by the other, etc. There does not seem to be any theoretical basis for preferring one method of combination over another. For this reason we multiplied eq. 17 by $(1 + m_s/m_1)$, added the product to eq. 15, and obtained

$$\ln \left[\frac{a_1(m_s, m_u)}{a_1(m_s, 0)a_1(0, m_u)} \right] + \left(1 + \frac{m_s}{m_1} \right) \ln \left[\frac{a_2(m_s, m_u)}{a_2(m_s, 0)} \right] = m_u(P_1 + P_2 m_u)(1 + P_3 m_s + P_4 m_s^2) - \frac{P_2 m_s m_u^2}{m_1} \left(1 + \frac{P_3 m_s}{2} + \frac{P_4 m_s^2}{3} \right) \quad (22)$$

Parameters were obtained by putting eq. 22 into the exponential form and minimizing the variance of the product

$$\left[\frac{a_1(m_s, m_u)}{a_1(m_s, 0)a_1(0, m_u)} \right] \left[\frac{a_2(m_s, m_u)}{a_2(m_s, 0)} \right]^{(1 + m_s/m_1)}$$

where, as described previously, $m_1 = 55.509$.

Values of parameters P_i calculated from eq. 22 are listed in Table II, where they may be compared with the same parameters calculated according to eq. 8 or 17, in which only nitric acid activities (and not water activities) were used. Also listed in Table II are the standard deviation of $a_1(m_s, m_u)/[a_1(m_s, 0)a_1(0, m_u)]$, which is 0.1121, and of $a_2(m_s, m_u)/a_2(m_s, 0)$, which is 0.2726. Further analysis of the data shows that there is a nearly constant percentage uncertainty in the latter ratio as the experimental ratio varies from about 0.8 to 8 (Figure 2). Thus, when the ratio $a_2(m_s, m_u)/a_2(m_s, 0)$ is close to 1, its standard deviation is about 0.1; when the ratio is 8, then its standard deviation is 0.8. Also included in Table II is the estimate 0.19 for the standard deviation of the ratio of nitric acid activity coefficients in the three- and two-component systems, which corresponds to about 9.1% of the value; exclusion of four experiments from the data analyses reduces these to 0.16 and 8.3%, respectively.

Discussion and Conclusions

As described in the Introduction, the two primary objectives of this report are to present data on vapor pressures of water and nitric acid over the three-component system water-nitric acid-uranyl nitrate hexahydrate and to present the mathematical techniques used to calculate activities of uranyl nitrate hexahydrate from these vapor pressures. While presenting these techniques we have intentionally avoided several complications, all of which are inherent in the relatively large uncertainty ($\pm 4\%$) of our partial pressure data.

McKay⁶ has shown that the activities of both solutes of a three-component system can be calculated from appropriate measurements of the partial pressures of the solvent. Thus, in the present work, it is theoretically possible to evaluate the parameters of the

(25) R. A. Robinson and R. H. Stokes, "Electrolyte Solutions," Academic Press, New York, N. Y., 1955, pp. 478, 481.

function $F_2(m_s, m_u)$ —in the form of eq. 4 or in whatever form seems appropriate—from both the nitric acid and water partial pressures separately. In practice, this does not appear possible with data as uncertain as those of the present work. In particular, a nonlinear, least-squares evaluation of the parameters P_i from the water vapor pressure data by eq. 15 leads to a standard deviation of only 5% in the water activity but to very erroneous values of nitric acid activities subsequently calculated from eq. 17. On the other hand, if we evaluate the parameters P_i from nitric acid partial pressures alone (eq. 17) or by a combination of nitric acid and water vapor pressures (eq. 22), then we obtain “reasonable” agreement between observed and calculated water partial pressures (Table II).

The word “reasonable” covers several types of uncertainty, including that which is inherent in nonlinear, least-squares problems of data analysis and inclusion or exclusion of the few “obviously” erroneous results. We have followed the usual procedure of minimizing variance while fitting nitric acid activity data to eq. 17 or fitting nitric acid and water activities to eq. 22. Such minimization leads to calculated activities that are biased with respect to observed values whether all data are included, whether the four “obviously” erroneous values are excluded, or whether data at acidities above 10.8 m HNO_3 are excluded. This latter cut-off point is the approximate concentration at which the nitric acid activity ratio (Figure 2) is unity. For example, when the 39 points are fitted to eq. 8 or 17, the variance of fit of the ratio $a_2(m_s, m_u)/a_2(m_s, 0)$ is 0.1142 (Table II); the parameters P_i so obtained actually yield calculated values of this ratio that are, on the average, 1.45% less than the observed values. Analyses of the water and nitric acid activities of these same 39 points according to eq. 22 yields an over-all standard deviation of 0.1571 (Table II). The resulting parameters can be used in eq. 17 and 15 to calculate the ratios $a_2(m_s, m_u)/a_2(m_s, 0)$ and $a_1(m_s, m_u)/[a_1(m_s, 0)a_1(0, m_u)]$, respectively. Such calculations show that the parameters understate the acid activity ratio by 6.1% and overstate the water activity ratio by 9.4%. Depending on how the data are edited, parameters obtained from eq. 22 give calculated nitric acid activity ratios that are from 1.7% greater to 6.1% less than the observed values; calculated water activities are 7.9 to 9.4% less than observed values.

In spite of the uncertainties, the present work should be of considerable use in analyzing solvent extraction data and may be useful in future studies of the interactions between the two solutes of a three-component

system. The present data can be explained as precisely with or without P_2 in eq. 17, corresponding to the presence or absence of the square power of uranium concentration (the McKay or Harned formulations). Although the particular form of the effect of nitric acid concentration on its own activity may be in doubt, yet something similar to the quadratic formulation of eq. 17 must certainly be nearly correct.

More useful than eq. 15–17 are Figures 3–6 in summarizing the results of this investigation. In these figures we attempt to show the effects of nitric acid and uranyl nitrate hexahydrate concentrations on the water activity ($a_{\text{H}_2\text{O}}$), nitric acid molal activity coefficient (γ_{HNO_3}), uranyl nitrate hexahydrate molal activity coefficient (γ_{UNH}), and the molar free energy of solution (μ^s), where (see Appendix) $\mu^s = RT \sum_i x_i \ln a_i$,

in which x is the mole fraction and all other terms have been defined previously. We emphasize that each of these figures involves extrapolation beyond the experimental concentration ranges. Any numerical value in each of these figures that is not on one of the faces of these sections of parallelepipeds is dependent on the constants $P_1, P_2, P_3,$ and P_4 (eq. 15–17) as well as on data of the two two-component systems $\text{H}_2\text{O}-\text{HNO}_3$ and $\text{H}_2\text{O}-\text{UO}_2(\text{NO}_3)_2 \cdot 6\text{H}_2\text{O}$. The activities of species in the two-component systems² have been determined considerably more accurately than the corresponding values in the three-component system (compare standard deviations of fit in Tables II and III). Thus, the uncertainties in the locations of the surfaces of $a_{\text{H}_2\text{O}}, \gamma_{\text{HNO}_3}, \gamma_{\text{UNH}}$, and μ^s of Figures 3–6 are determined by

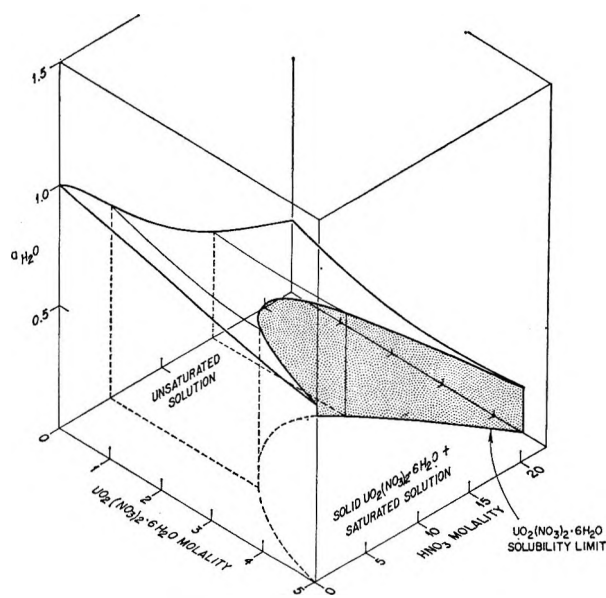


Figure 3. Water activity ($a_{\text{H}_2\text{O}}$) in $\text{H}_2\text{O}-\text{HNO}_3-\text{UO}_2(\text{NO}_3)_2 \cdot 6\text{H}_2\text{O}$ solutions.

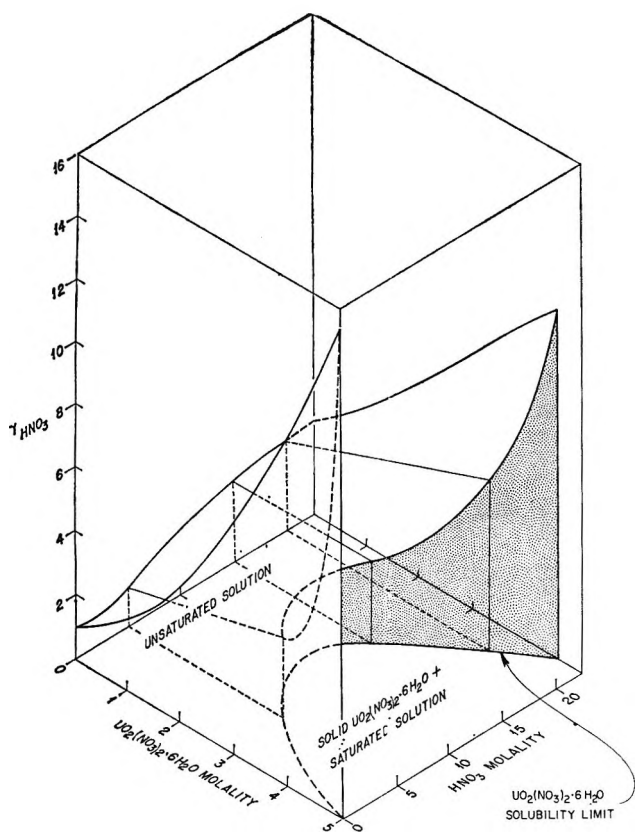


Figure 4. Molal activity coefficient of nitric acid in $\text{H}_2\text{O}-\text{HNO}_3-\text{UO}_2(\text{NO}_3)_2 \cdot 6\text{H}_2\text{O}$ solutions.

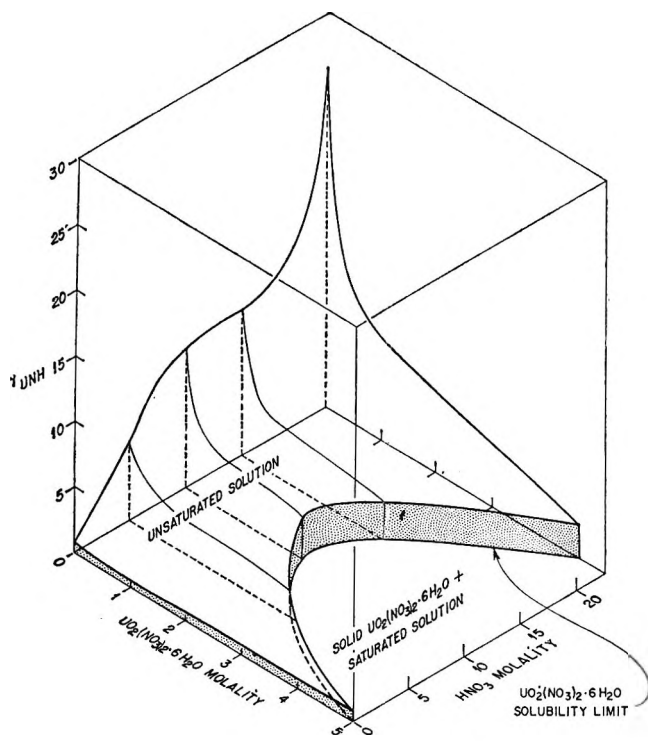


Figure 5. Molal activity coefficient of uranyl nitrate hexahydrate in $\text{H}_2\text{O}-\text{HNO}_3-\text{UO}_2(\text{NO}_3)_2 \cdot 6\text{H}_2\text{O}$ solutions.

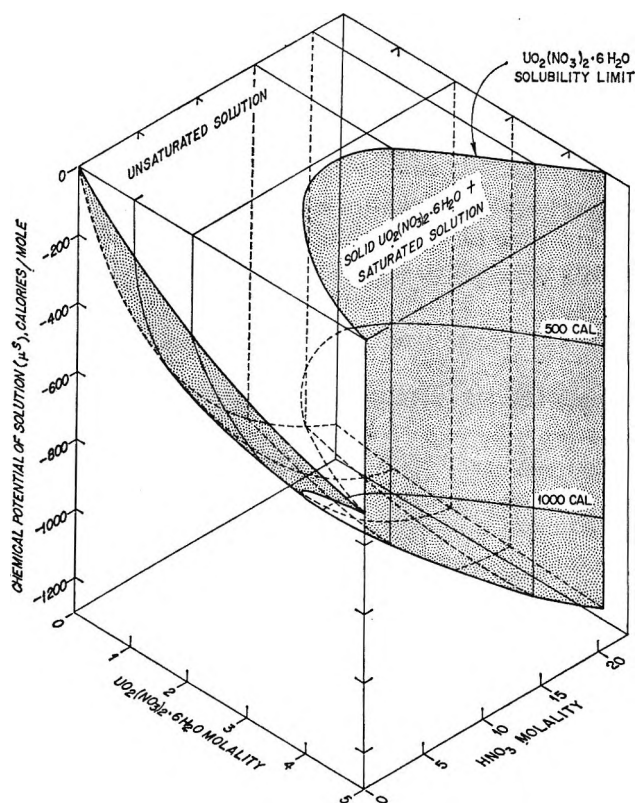


Figure 6. The partial molar free energy (chemical potential, μ^s) of solution for $\text{H}_2\text{O}-\text{HNO}_3-\text{UO}_2(\text{NO}_3)_2 \cdot 6\text{H}_2\text{O}$ solutions (lower surface). The upper (flat) surface has $\mu^s = 0$.

the imprecision of the present work. The standard deviation of the water activity is $\pm 8\%$ of the value; that of the nitric acid activity coefficient is $\pm 7\%$ of the value. Uncertainties of γ_{UNH} and μ^s are presumably in this same range.

Uncertainties of 7 to 10% in $a_{\text{H}_2\text{O}}$, γ_{HNO_3} , and γ_{UNH} are small enough to warrant cautious use of eq. 15-17 for evaluating the activities of solvents (such as tributyl phosphate) from solvent extraction equilibrium data. The range of applicability of these equations is very wide, namely, 0 to 2.3 *m* UNH and 1 to 14 *m* HNO_3 . However, the uncertainties are large enough so that caution in using the equations and the parameters P_i should be emphasized, as should the need for more precise data.

The specific parameters that we recommend for present use are given in the first row of Table II. These parameters, based only on nitric acid vapor pressures, yield the lowest calculated bias [(observed - calculated)/observed] for the water activity ratio (7.9%), for acid activity ratio (1.0%), the lowest percentage standard deviation (8.8) of water activity, and next to the lowest standard deviation for nitric acid activity ratio (9.65). Use of water activity only, eq.

15, or water and nitric acid activities together, eq. 22, to improve the accuracies of these parameters will require more accurate data than we have obtained.

Acknowledgments. The authors thank members of the group of W. R. Laing, of the ORNL Analytical Chemistry Division, for performing all chemical analyses associated with this report. They also thank J. Thompson for performing some of the early transpiration experiments.

Appendix

During the course of our work, we measured the solubilities of uranyl nitrate hexahydrate in aqueous nitric acid solutions at 25.00°. The techniques simply involved agitating solid UNH in sealed vessels with aqueous nitric acid of known concentration. The vessels were agitated for 1 to 2 days in a thermostat; the liquid phase was sampled some time after agitation had been stopped. These samples were analyzed for uranium by conventional methods. Solution densities were determined in duplicate in 10-ml. pycnometers. Our data are summarized in Table IV; the smoothed solubility data that we have derived by combining our data with the various literature data¹⁶⁻¹⁹ are summarized in Table V. In both tables the equilibrium solid is $\text{UO}_2(\text{NO}_3)_2 \cdot 6\text{H}_2\text{O}$ (except as noted in Table IV), which is the stable hydrate at 25° providing the nitric acid concentration does not exceed 22.5 *m*. This molality is our best estimate of the concentration at which the stable solid hydrate changes from hexa- to trihydrate.²⁶

To reduce the possibility of misinterpretation, we note, as follows, the way in which the mole fraction

Table IV: New Experimental Solubilities of $\text{UO}_2(\text{NO}_3)_2 \cdot 6\text{H}_2\text{O}$ in Aqueous HNO_3 Solutions at 25°

Density, g./ml.	Molar concn. of satd. soln.		Density, g./ml.	Molar concn. of satd. soln.	
	HNO_3	U		HNO_3	U
1.7793	0.005	2.440	1.5837	5.932	1.240
1.7267	1.320	2.144	1.6507	7.687	1.360
1.6587	2.478	1.804	1.7341	8.282	1.600
1.5957	4.368	1.444	1.6909	11.304	1.217 ^c

^c $\text{UO}_2(\text{NO}_3)_2 \cdot 3\text{H}_2\text{O}$ is the stable hydrate in this case.

Table V: Smoothed Solubilities of $\text{UO}_2(\text{NO}_3)_2 \cdot 6\text{H}_2\text{O}$ in Aqueous HNO_3 Solutions at 25°^a

HNO_3	UNH	HNO_3	UNH	HNO_3	UNH
0	5.00	8	2.33	16	2.78
1	4.36	9	2.21	17	3.00
2	3.86	10	2.14	18	3.25
3	3.47	11	2.10	19	3.51
4	3.15	12	2.12	20	3.78
5	2.89	13	2.21	21	4.08
6	2.66	14	2.36	22	4.40
7	2.48	15	2.56	22.5	4.56

^a All values are molalities.

activities of water and nitric acid are related to the measured partial pressures. These relations are easily obscured because the partial pressure data are used to obtain parameters of activity coefficient equations. The process of going from partial pressures to activity coefficients is then reversed, but with an equation rather than just the experimental points. Thus, for the two volatile species we have $p_1/p_1^0 = a_1$ and $p_2/p_2^0 = (y_s C_s)^2 / (y_s^0 C_s^0)^2 = a_2$.

The activity of uranyl nitrate is calculated²² as $a_3 = 4(m_u \gamma_u M_1 / 1000)^3$. Therefore, the specific choice of standard states that we used in drawing Figure 6 is as follows: (1) the activity of pure water is 1 in the mole fraction scale; (2) the activity of pure HNO_3 is 1 in the mole fraction scale; (3) the activity coefficient of UNH infinitely dilute in water is 1 in the molal (or molar) scale.

To our knowledge, the difference between the Gibbs free energy of 1 mole of pure crystalline UNH and the chemical potential of UNH in the saturated aqueous solution has not been determined. Thus, we cannot express the activity of UNH in solution in terms of the pure crystalline UNH at present.

(26) After we had submitted this article to *The Journal of Physical Chemistry*, we received a copy of the Russian journal *Radiokhimiya*, in which Yakimov and Mishin report data on solubilities of $\text{UO}_2(\text{NO}_3)_2$ in H_2O - HNO_3 solutions. Their data were recalculated and are presented in Figure 1. Without attempting any interpretation of the small differences in the middle range of acidities, we note that these new data correspond to a solubility of 4.95 moles of UNH/kg. of H_2O compared with a smoothed value (at zero acidity) of 5.00 in Table V: M. A. Yakimov and V. Ya. Mishin, *Radiokhimiya*, 6, 454 (1964).

The Crystal Structure of Pyridine Hydrogen Nitrate¹

by Aubrey J. Serewicz, B. Ken Robertson, and Edward A. Meyers

Department of Chemistry, Texas A & M University, College Station, Texas (Received December 14, 1964)

Pyridine hydrogen nitrate is monoclinic, space group $P2_1/c$, with cell parameters $a = 3.905$, $b = 12.286$, $c = 13.470$ Å., $\beta = 90^\circ 30'$ and four molecules per unit cell. The structure was determined by three-dimensional X-ray analysis, and the final parameters were refined with anisotropic temperature factors by least-square analysis of hkl ($h = 0, 1, 2$) data ($R = 0.085$). Correction for thermal motion gives the following average bond distances: $N(1)-C(1) = 1.375$, $N(1)-C(5) = 1.333$, $C(1)-C(2) = 1.383$, $C(2)-C(3) = 1.367$, $N(2)-O(1) = 1.291$, $N(2)-O(2) = 1.266$ Å. A comparison has been made between pyridine hydrogen nitrate and molecules of similar structure.

Introduction

While attempting to prepare single crystals of the positive halogen compound, IPy_2NO_3 ,^{2,3} it was found that $PyHNO_3$ was produced as the major product of recrystallization from ether-chloroform mixtures, presumably after reaction of the original compound with the solvent. The crystals were initially clear and colorless but after exposure to light became yellowish and at times showed evidence of a dark material deposited in the center of the whiskers. An analysis of the compound showed about 6.8% of iodine in some way present in the recrystallized material. It was decided that a structure determination of pyridine hydrogen nitrate would be useful for several reasons. First, it would serve as a preliminary to further studies of the iodine-containing material. Second, it would be of interest in itself to examine the structure of the pyridinium and nitrate groups without disturbing effects due to heavy atoms. Third, the preliminary examination of the material revealed that a very easy twisting distortion of the crystals around the needle axis was accompanied by a very short axial length along the needle axis, which indicated some sort of layer structure in this presumably ionic material.

Experimental

Space Group and Unit Cell Dimensions. Pyridine hydrogen nitrate was first synthesized by Anderson (1858) and given a more complete characterization by Pincussohn (1897). It is a 1:1 compound formed by mixing equimolar amounts of concentrated nitric acid and dried pyridine. It crystallizes readily from solution

at -78° into long, translucent, and easily deformable crystals. The crystals require considerable care in handling to minimize deformation.

Examination of single crystals of the compound with a Buerger precession camera (Mo $K\alpha$ radiation) revealed systematic absences for $(h0l)$ when l was an odd integer and for $(0k0)$ when k was an odd integer, characteristic of $P2_1/c-C_{2v}$.⁵ The unit cell dimensions are $a = 3.905$, $b = 12.286$, $c = 13.470$ Å., and $\beta = 90^\circ 30'$. The density observed by the flotation method is 1.432 ± 0.020 g./cc.; the density calculated for four molecules per unit cell is 1.454 g./cc.

Measurement and Correction of Intensities. A needle approximately 0.3 mm. in diameter (crystal I) was mounted for rotation around the a -axis, and 30° precession photographs of timed duration were taken of the $(hk0)$ and $(h0l)$ zones. The crystal then was mounted on a Weissenberg camera (Cu $K\alpha$ radiation), and $(0kl)$ was photographed by use of a multiple film pack.

The intensities from the precession camera were measured visually. The optical densities of the Weissenberg reflections were read using a Welch Densichron, Model 10. The size and cylindrical nature of the crystal permitted absorption corrections to be ignored (μr varied from 0.16 to 0.17). Prior to the usual Lorentz and polarization corrections, two adjust-

(1) This paper was presented at the 20th Annual Southwest Regional Meeting of the American Chemical Society, Dec. 3-5, 1964, Shreveport, La.

(2) R. A. Zingaro, C. A. VanderWerf, and J. Kleinberg, *J. Am. Chem. Soc.*, **73**, 88 (1951).

(3) H. Carlsohn, *Angew. Chem.*, **46**, 747 (1933).

ments were made to the Weissenberg data. First, observed values of optical density obtained from the Densichron were brought into conformity with a standard scale supplied by the manufacturer. Second, this revised set of optical densities was used to obtain intensities by means of a very slightly modified form of the internal calibration method of S. H. Simonsen and P. A. Hoss.⁴

In this calibration method, the optical densities for the reflections of film n (highest intensity) are plotted as the abscissa *vs.* the corresponding reflections on film $n + 1$ as the ordinate. Then, on the same graph, film $n + 1$ is plotted as the abscissa *vs.* the reflections of film $n + 2$ as the ordinate. Through these points a best fit curve is drawn. An arbitrary point on the curve in the high optical density portion on the abscissa is assigned an index of 100. The film scaling factor, c , is used to give the corresponding point on $n + 1$ the intensity of $100/c$. This second optical density is then referred to the abscissa and the value read on the ordinate assigned an intensity of $100/c^2$. The process is continued to extinction. Through the use of the four to five points determined in this manner, a graph is constructed of optical density *vs.* relative intensity. The fairly well-defined lower portion of the curve can be further used to complete the high intensity section.

For the precession data, the scaling factor of 3.00 was used since this was the ratio between the various timed exposures. For the Weissenberg data, a value of 2.96 was used. This value was obtained from absorption measurements with a G.E. Spectrometer and is in good agreement with the value of 2.92 given in recent measurements⁵ reported on Ilford Industrial Type G film. The final intensities obtained in this way were corrected for Lorentz and polarization factors.

It later became obvious that more extensive data were needed. Another single crystal (crystal II) of the material was selected and mounted as previously described on the Weissenberg camera; photographs (Cu $K\alpha$ radiation) were taken of the zero, first, and second levels with an integrating mechanism designed by Nordman.⁶ These data were treated as the earlier data had been, except that the film scaling factors were corrected for the inclination of the film in the first and second levels.

Analysis of the Structure

The short a -axis suggested a single layer of molecules should be well resolved in the [100] projection. A two-dimensional Patterson function was constructed with the $(0kl)$ data from crystal I. Examination of the Patterson map suggested a limited set of trial structures, which were systematically investigated. Only

one of these refined satisfactorily, and trial y - and z -coordinates were obtained.

The x -coordinates presented a problem because of the limited data collected from crystal I and because in the [001] and [010] projections the atoms were not well resolved. Packing considerations and difference Fourier maps were used to obtain preliminary values of the x -coordinates. With different scale factors and different over-all temperature factors for each zone, R factors of 0.21, 0.19, and 0.17 were found for the $(h0l)$, $(hk0)$, and $(0kl)$ data, respectively. The least-squares program, OR FLS,⁷ was used to refine the data available from crystal I and confirmed the Fourier results, namely, that the x -coordinates had large uncertainties and the bond distances were consequently unreliable. Individual atom temperature factors did not improve R greatly.

For these reasons, zero and upper level integrated Weissenberg data were collected for crystal II. With individual isotropic temperature factors, the uncertainties in molecular parameters improved because of the more extensive data, but the bond distances remained unsatisfactory, and the R factor remained high (~ 0.18). A few structure factors for large reflections were removed from the least-squares calculations because it was believed that they were less accurate than the majority of reflections and that they were unduly biasing the results. The improvement was slight.

The data from crystal II were used to calculate three-dimensional Fourier and difference Fourier functions with the ERFR2 program.⁸ In these maps, the hydrogen positions were indistinct, but there was clear indication of anisotropic thermal motion for the heavier atoms.

An anisotropic least-squares refinement then was carried out with the Busing-Levy-Martin program,⁷ in which the best isotropic atom temperature factors obtained with unit weights for all reflections of crystal II were entered into OR FLS along with hydrogen positions calculated for C-H and N-H bond lengths of 1.08 Å. Immediate improvement established the importance of anisotropic thermal motion. $R_1 = \sum |F_o - F_c| / \sum |F_o|$ dropped to 0.088 and $R_2 = \{ \sum w |F_o|^2 - F_c^2 /$

(4) S. H. Simonsen, University of Texas, private communication.

(5) H. Morimoto and R. Uyeda, *Acta Cryst.*, **16**, 1107 (1963).

(6) C. E. Nordman and A. L. Patterson, *Rev. Sci. Instr.*, **28**, 384 (1957).

(7) W. R. Busing, K. O. Martin, and H. A. Levy, "OR FLS, A Fortran Crystallographic Least-squares Program," ORNL-TM-305, Oak Ridge National Laboratory, Oak Ridge, Tenn., 1962.

(8) W. G. Sly, D. P. Shoemaker, and J. H. Van den Hende, "Two- and Three-Dimensional Crystallographic Fourier Summation Program for the IBM 7090 Computer," CBRL-22M-62, Massachusetts Institute of Technology-Esso Research and Engineering Co., 1962.

$\Sigma wF_o^2\}^{1/2}$ to 0.098. The uncertainties in bond distances become approximately $\sigma = 0.012 \text{ \AA}$., but all ring distances were shorter than anticipated.

Weighting Schemes. The effect of two quite different weighting schemes was investigated. The first of these was that developed by Hughes.⁹ In Hughes' method all reflections less than $4F_{\text{min}}$ are assigned a weight of $[4F_{\text{min}}/F_o]^{-2}$. Reflections above $4F_{\text{min}}$ become weighted by $[F_o/4F_{\text{min}}]^{-5}$. A program incorporating this method was written for the IBM 709, and the weighted data were used for several least-squares cycles. No improvement in R was observed. The bond distance relationship remained undisturbed.

Table I: Atomic Coordinates from Least-Squares Refinement

Atom	x/a	$\sigma(x/a)$	y/b	$\sigma(y/b)$	z/c	$\sigma(z/c)$
O(1)	-0.4946	0.0022	0.4847	0.0006	0.1157	0.0007
O(2)	-0.6149	0.0025	0.5572	0.0008	0.2545	0.0007
O(3)	-0.3671	0.0024	0.4026	0.0009	0.2497	0.0007
N(1)	-0.1080	0.0024	0.3131	0.0009	0.0465	0.0009
N(2)	-0.4896	0.0025	0.4825	0.0009	0.2093	0.0008
C(1)	-0.0287	0.0034	0.2230	0.0014	0.0990	0.0008
C(2)	0.1346	0.0030	0.1393	0.0010	0.0554	0.0010
C(3)	0.2092	0.0029	0.1462	0.0010	-0.0418	0.0011
C(4)	0.1248	0.0030	0.2352	0.0013	-0.0934	0.0008
C(5)	-0.0305	0.0032	0.3199	0.0010	-0.0475	0.0012

Table II: Least-Squares Anisotropic Temperature Factors ($\times 10^4$)

Atom	β_{11}	β_{22}	β_{33}	β_{12}	β_{13}	β_{23}
O(1)	1399 \pm 103	71 \pm 8	38 \pm 6	52 \pm 19	-6 \pm 16	0 \pm 5
O(2)	1214 \pm 108	126 \pm 10	70 \pm 7	97 \pm 26	-19 \pm 19	-48 \pm 7
O(3)	1312 \pm 112	138 \pm 11	62 \pm 7	176 \pm 28	52 \pm 19	45 \pm 7
N(1)	266 \pm 108	75 \pm 11	87 \pm 10	-49 \pm 21	33 \pm 21	-25 \pm 8
N(2)	580 \pm 114	57 \pm 10	56 \pm 9	-58 \pm 23	6 \pm 21	-5 \pm 8
C(1)	543 \pm 140	120 \pm 16	27 \pm 9	-107 \pm 32	-34 \pm 22	0 \pm 9
C(2)	290 \pm 129	61 \pm 11	80 \pm 12	-19 \pm 27	-75 \pm 25	22 \pm 9
C(3)	408 \pm 132	62 \pm 12	74 \pm 11	69 \pm 26	-32 \pm 24	-27 \pm 9
C(4)	238 \pm 129	112 \pm 14	36 \pm 9	-51 \pm 31	-3 \pm 20	-5 \pm 9
C(5)	239 \pm 130	48 \pm 11	98 \pm 12	-49 \pm 26	-38 \pm 26	33 \pm 10

The second, the self-consistent weighting scheme suggested by Cruickshank,¹⁰ was further developed in this laboratory.¹¹ Used in conjunction with OR FLS, this method assigns to each reflection a weight of $(A + B \cdot F_o + CF_o^2)^{-1}$, where A , B , and C are fitted by least squares. Three such cycles gave $R_1 = 0.085$ and $R_2 = 0.094$. The coordinates and anisotropic temperature factors from this refinement are given in Tables I and II. The comparison of observed and calculated structure factors is listed in Table III.

Thermal Motion and Bond Distances. Since the shortening of bond distances is one of the characteristics of certain types of anisotropic thermal motion,¹²⁻¹⁴ calculations were made to correct for discrepancy between the observed bond distances and the bond distances normally expected. Busing and Levy¹⁵ have pointed out that rigorous corrections would require a detailed analysis of the dynamics of the atomic system. It became necessary therefore to ascribe a reasonable simplified model to the system and to make approximate corrections.

Cruickshank¹³ has shown that the magnitudes of the atomic motions can be used to determine the rigid body vibrations of the molecule. It is assumed that the motion of a molecule can be expressed in terms of two symmetric tensors, one giving the translational vibrations of the mass center and the other giving the angular oscillations about the mass center.

The model taken was that of treating the pyridine ring and the nitrate group as independent rigid bodies. If all the atoms in each rigid body are translated in the same direction, it is obvious that translation will have no effect upon the relative bond distance between atoms. Angular oscillations, however, will affect the positions of maxima in the density distribution.

The corrections for the bonds in the nitrate group could be determined directly. With the assumption

(9) E. W. Hughes, *J. Am. Chem. Soc.*, **63**, 1737 (1941).

(10) D. W. J. Cruickshank, "Computing Methods and the Phase Problem in X-ray Crystal Analysis," R. Pepinski, J. M. Robertson, and J. C. Speakman, Ed., Pergamon Press, New York, N. Y., 1961, p. 42.

(11) R. F. Copeland and E. A. Meyers, paper presented at the 20th Annual Southwest Regional Meeting of the American Chemical Society, Dec. 3-5, 1964, Shreveport, La.

(12) D. W. J. Cruickshank, *Acta Cryst.*, **9**, 747 (1956).

(13) D. W. J. Cruickshank, *ibid.*, **9**, 754 (1956).

(14) D. W. J. Cruickshank, *ibid.*, **9**, 757 (1956).

(15) W. R. Busing and H. A. Levy, *ibid.*, **17**, 142 (1964).

that the three oxygens ride on the central nitrogen atom, the corrected bond distances could be found with the OR FFE program of Busing, Martin, and Levy.¹⁶

For the pyridine ring, the technique of Cruickshank¹³ was employed to find the amplitude of the angular oscillations. Orthogonal unit vectors were set up in the molecule at the center of the ring, with two of the vectors in the plane of the ring. Axis 1 was defined by the vector from N(1) to C(3). With the equations given by Cruickshank, the square amplitude of the angular oscillation about the axis normal to the planar pyridine ring could be approximated. All ring bond distances are affected by this oscillation, and it makes the principal contribution to the bond correction. Although the amplitudes about the remaining orthogonal axes could not be determined uniquely, upper and lower limits could be placed on their magnitudes. The cross terms, ω_{ij} ($i \neq j$), were small enough to be ignored. The Levy and Busing correction for molecular libration¹⁵ was calculated. The uncorrected bond distances and upper and lower corrected values are given in Table IV.

Table IV: Bond Distances and Angles

Atoms	Uncor. dist., Å.	Cor. dist., Å.	
		Upper limit	Lower limit
N(2)-O(1)	1.263 ± 0.011	1.292 ± 0.013	
N(2)-O(2)	1.207 ± 0.011	1.258 ± 0.013	
N(2)-O(3)	1.218 ± 0.012	1.273 ± 0.013	
N(1)-O(1)	2.759 ± 0.014	...	
N(1)-C(1)	1.349 ± 0.016	1.379	1.372
N(1)-C(5)	1.307 ± 0.015	1.337	1.330
C(1)-C(2)	1.349 ± 0.017	1.384	1.377
C(2)-C(3)	1.347 ± 0.016	1.377	1.371
C(3)-C(4)	1.335 ± 0.016	1.363	1.357
C(4)-C(5)	1.357 ± 0.016	1.390	1.383
Atoms	Angle, deg.	Atoms	Angle, deg.
N(1)-C(1)-C(2)	120.4 ± 1.1	O(1)-N(2)-O(2)	119.0 ± 1.2
C(1)-C(2)-C(3)	118.8 ± 1.1	O(1)-N(2)-O(3)	117.7 ± 1.1
C(2)-C(3)-C(4)	120.3 ± 1.1	O(2)-N(2)-O(3)	123.3 ± 1.2
C(3)-C(4)-C(5)	120.0 ± 1.1	N(2)-O(1)-N(1)	108.5 ± 0.8
C(4)-C(5)-N(1)	120.1 ± 1.1		
C(5)-N(1)-C(1)	120.4 ± 1.1		

Discussion of Structure

The Pyridine Group. The pyridine ring appears to be a nearly regular hexagon. Of the various ring bond distances that are expected to be the same, only the nitrogen-carbon bond distances seem possibly to be unusual. However, the difference between N(1)-C(1) and N(1)-C(5) is only 0.042 Å., and as the standard error in a ring bond distance is 0.016 Å., even this difference is not established as being significant. The final bond lengths have been taken as the averages of the values

given in Table IV, following correction for anisotropic thermal motion. The mean values for bond angles and distances for the ring are given in Table V along with a number of values selected from various structures that have similar ring systems.

The most accurate values in Table V are probably the microwave results for pyridine in the gas phase. Compared to benzene there is a shortening of two bonds in the ring, the N-C bonds, and a significant distortion of the bond angles. There has been an attempt to estimate bond angles for a number of different nitrogen-containing ring systems,¹⁷ but the results for pyridine are poor. The resultant bond angles are pictured as a compromise of the conflicting demands made by (1) repulsion of the electrons in the various atomic orbitals, (2) changing bond strength with altered hybridization, and (3) the energy required to promote the 2s electrons in nitrogen. For qualitative purposes, it seems easiest to interpret the distortions of the angle C(1)N(1)C(5) on the basis of the repulsion of the lone pair of electrons on the nitrogen atom¹⁸ causing a deformation of the ring of the kind that is observed. The experimental results for the ring systems in 2,2'-bipyridine are in good agreement with the microwave results for pyridine, and those of 2,2'-pyridil are in fair agreement.

When the nitrogen lone pair in pyridine is bonded to something else, it would be expected that the angle C(1)N(1)C(5) would increase. The various complex salts, $\text{Cu}_2(\text{CH}_3\text{CO}_2)_4 \cdot 2\text{Py}$ and $\text{SeOCl}_2 \cdot 2\text{Py}$, seem to show this effect to some extent, along with an increase in the angle C(2)C(3)C(4) and a decrease in the angle C(1)C(2)C(3). In these structures, the bond distances $\text{Cu} \cdots \text{N}(1)$ and $\text{Se} \cdots \text{N}(1)$ are fairly long (between 2.12 and 2.19 Å.).

In the structure of pyridinoxide hydrogen chloride, a strong N(1)-O bond of length 1.37 Å. has been formed. The angle C(1)N(1)C(5) is 127°, while the angle N(1)-C(1)C(2) has fallen to 116.6°. Similar behavior appears to be present in PyHCl and $\text{PyH}[\text{Cr}(\text{NCS})_4(\text{NH}_3)_2]$, but in addition in these presumably ionic compounds, the angle C(1)C(2)C(3) has decreased markedly, and the angle C(2)C(3)C(4) has increased markedly although the variation among the various bond angles reported is large. On a simple ionic picture, the positive charge in the vicinity of nitrogen would be expected to produce this kind of distortion, increasing the angles C(1)N(1)C(5) and C(2)C(3)C(4)

(16) W. R. Busing, K. O. Martin, and H. A. Levy, "OR FFE, A Fortran Crystallographic Function and Error Program," ORNL-TM-306, Oak Ridge Laboratory, Oak Ridge, Tenn., 1964.

(17) H. Kim and H. F. Hamerka, *J. Am. Chem. Soc.*, **85**, 1398 (1963).

(18) R. J. Gillespie and R. S. Nyholm, *Quart. Rev. (London)*, **11**, 339 (1957).

Table V

Compd.	Bond, Å.			Angle, deg.			
	N(1)-C(1)	C(1)-C(2)	C(2)-C(3)	C(1)N(1)-C(5)	N(1)C(1)-C(2)	C(1)C(2)-C(3)	C(2)C(3)-C(4)
PyHNO ₃	1.355	1.383	1.369	120.4	120.2	119.4	120.3
Pyridine(g) ^a	1.3402	1.3945	1.3944	116.8	123.9	118.5	118.3
PyHCl ^b	1.32	1.42	1.40	128	118	115	125
PyH[Cr(NCS) ₄ (NH ₃) ₂] ^c	1.35	1.39	1.40	134.0	114.5	112.7	131.7
Cu ₂ (CH ₃ CO ₂) ₄ ·2Py orthorhombic ^d	1.330	1.411	1.359	119.2	122.0	117.5	121.6
Cu ₂ (CH ₃ CO ₂) ₄ ·2Py monoclinic ^e	1.378	1.396	1.422	117.2	123.4	115.0	120.0

^a B. Bak, L. Hansen-Nygaard, and J. Rastrup-Andersen, *J. Mol. Spectry.*, **2**, 361 (1958). ^b C. Rérat, *Acta Cryst.*, **15**, 427 (1962). ^c Y. Takeuchi and R. Pepinsky, *Z. Krist.*, **109**, 29 (1957). ^d F. Hanic, D. Štempelová, and K. Hanicová, *Acta Cryst.*, **17**, 633 (1964). ^e G. A. Barclay and C. H. L. Kennard, *J. Chem. Soc.*, 5244 (1961).

and so bringing the various electrons in the molecule closer to the site of the positive charge by distorting the ring angles.

In PyHNO₃, all of the ring bond angles have been found close to 120°. These angles were calculated for the uncorrected bond distances, but, because the ring is so nearly regular, only small changes would be expected if angle corrections were made. Moreover, Levy and Busing¹⁵ have pointed out that bond angle corrections should be made with caution. In PyHNO₃ both angles, C(1)N(1)C(5) and C(2)C(3)C(4), have increased compared to pyridine, but the changes are small compared to those reported for the two salt structures, PyHCl and PyH[Cr(NCS)₄(NH₃)₂].

The Nitrate Group. The planar nitrate group shows a slight asymmetry, both in bond angles and distances, but again the errors are such that it is, at most, only suggestive. Of more interest are the corrected N-O bond distances, which are fairly long compared to many earlier results. In Table VI the angles and distances for the nitrate group in PyHNO₃ are listed along with a number of values from structures that have similar units.

From the recent microwave study of HNO₃(g), it is seen that the N(2)-O(1) single bond, 1.405 Å., is considerably longer than the multiple bond, N(2)-O(2) = N(2)-O(3) = 1.206 Å. In addition, the angle O(2)N(2)O(3) is much larger than 120°. Values are also available for HNO₃(s) but are complicated by the disorder present in the crystal. The mean values selected differ appreciably from the gas phase results but are subject to large errors.

In HNO₃·H₂O and HNO₃·3H₂O, some alterations in the various bond lengths and angles are found. N.m.r. work¹⁹ has strongly indicated that HNO₃·H₂O is ionic and that it should be written as H₃O⁺NO₃⁻. The estimated errors in the X-ray work are such as to prevent one from establishing with certainty that the bond dis-

Table VI

Compd.	Bond, Å.			Angle, deg.		
	N(2)-O(1)	N(2)-O(2)	N(2)-O(3)	O(1)N(2)O(2)	O(1)N(2)O(3)	O(2)N(2)O(3)
PyHNO ₃	1.292	1.258	1.273	119.0	117.7	123.3
HNO ₃ (g) ^a	1.405	1.206	1.206	114	116	130
HNO ₃ (s) ^b	1.30	1.24	1.24	113	113	134
HNO ₃ ·H ₂ O ^c	1.29	1.20	1.24	114	119	127
HNO ₃ ·3H ₂ O ^d	1.26	1.22	1.23	119	119	122
N ₂ O ₅ ^e	1.243	1.243	1.243	By symmetry all 120°		
Methylguanidinium nitrate ^f	1.243	1.235	1.254	120.3	119.9	119.5
Tris(ethylenediamine)nickel(II) nitrate ^g				1.21		
Bis(ethylenediamine)copper(II) nitrate ^h	1.267	1.248	1.259	119.9	120.1	119.3
NaNO ₃ ⁱ				1.218		
Pb(NO ₃) ₂ ^j				1.268		

^a D. J. Millen and J. R. Morton, *J. Chem. Soc.*, 1523 (1960). ^b V. Luzatti, *Acta Cryst.*, **4**, 120 (1951). ^c V. Luzatti, *ibid.*, **4**, 239 (1951). ^d V. Luzatti, *ibid.*, **6**, 157 (1953). ^e E. Grison, K. Eriks, and J. L. de Vries, *ibid.*, **3**, 290 (1950). ^f R. M. Curtis and R. A. Pasternak, *ibid.*, **8**, 675 (1955). ^g L. N. Swink and M. Atoji, *ibid.*, **13**, 639 (1960). ^h Y. Komiyama and E. C. Lingafelter, *ibid.*, **17**, 1145 (1964). ⁱ R. L. Sass, R. Vidale, and J. Donohue, *ibid.*, **10**, 567 (1957). ^j W. C. Hamilton, *ibid.*, **10**, 103 (1957).

tances and angles are significantly different from those expected for a symmetrical nitrate group.

The agreement between the dimensions of the nitrate group reported for N₂O₅ and methylguanidinium nitrate is striking. In the first compound, the crystal symmetry demands equal bonds of 1.243 Å. and equal

(19) R. E. Richards and J. A. S. Smith, *Trans. Faraday Soc.*, **47**, 1261 (1951).

angles of 120° . In the second, there are no such symmetry requirements, but the dimensions are remarkably close to those found in N_2O_5 . In both studies, the agreement between calculated and observed structure factors is good.

Two similar nitrates containing divalent metal atoms are also given in Table VI. The values for bis(ethylenediamine)copper(II) nitrate are probably more accurate than those for tris(ethylenediamine)nickel(II) nitrate. The mean N-O bond length in the Cu(II) complex is 1.258 \AA .

Finally, two simple nitrates are listed. The difference in bond lengths is fairly large, but the estimated error in $\overline{N-O}$ in $Pb(NO_3)_2$ is 0.02 \AA . The average N-O bond length in $NaNO_3$ is reported by the authors as being sensitive to the weighting scheme used and to the omission of reflections from the least-squares refinement. The corrections to bond lengths from torsional movements of the nitrate group in $NaNO_3$, using the r.m.s. amplitude given in the original paper, is very small (less than 0.01 \AA).

The mean bond length in $PyHNO_3$, following correction for anisotropic thermal motions, rose from 1.230 to 1.274 \AA , and the variation in bond distances was reduced. Most of the recent structural evidence appears to favor a value of at least 1.24 \AA for the average N-O distance in the nitrate group. The differences in bond distances in the nitrate group in $PyHNO_3$ do not appear to be significant, and only the angle $O(1)N(2)-O(3)$ seems to be slightly larger than 120° . The nitrate group in $PyHNO_3$ thus appears to be a NO_3^- ion rather than an HNO_3 molecule.

Bonding between Pyridine and the Nitrate Group. The outstanding feature of the bonding between the pyridine ring and the nitrate group is the one relatively short bond of $2.76 \pm 0.01 \text{ \AA}$ between $N(1)$ and $O(1)$. All other contacts are 3.10 \AA or greater. It is unfortunate that the hydrogen atom positions were not locatable from difference Fourier maps since the distance of 2.76 \AA and the value of $108.5 \pm 0.8^\circ$ for the angle $N(2)O(1)N(1)$ are consistent with either an ionic bond of the type $PyH^+ \cdots NO_3^-$ or with a hydrogen bond, $N(1) \cdots H-O(1)$. The near coplanarity of the pyridine ring and $O(1)$ is also consistent with either model. Because the hydrogen atoms were not found,

the secondary differences in bond angles and distances for the ring and the nitrate group must be critically examined in order to argue that one or the other is present. The structural evidence cited earlier makes it seem most likely that $PyH^+ \cdots NO_3^-$ is the correct model, and this could be confirmed by other experimental methods as was done for $HNO_3 \cdot H_2O$.

Another interesting feature of the crystal is its easy deformation by twisting around the a -axis. The configuration of the ions shown in Figure 1, with the pyridine ring and nitrate group in pairs rather than in some complex arrangement with cross linking between many different groups, makes twisting around the a -axis seem fairly reasonable.

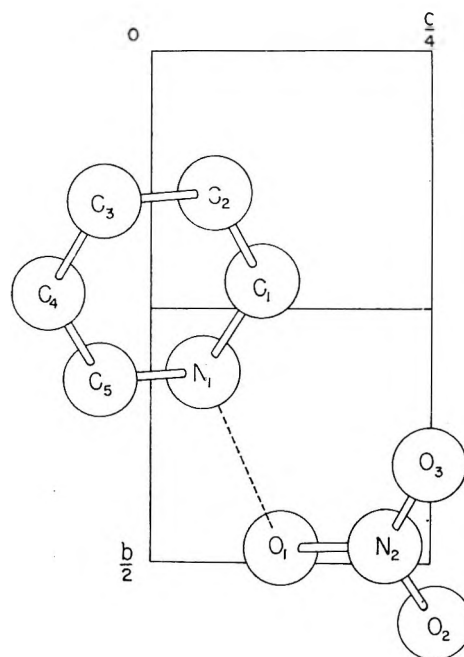


Figure 1. Schematic projection of asymmetric unit on (100).

Acknowledgments. The financial support of the Robert A. Welch Foundation and funds from the Research Corp. used to purchase some of the equipment used in this work are gratefully acknowledged. The facilities of the Data Processing Center of the Texas A & M University System have been used extensively in the course of this research.

On the Origin of the Stabilization of the Structure of Water by Nonelectrolytes

by A. Ben-Naim

Department of Physical Chemistry, The Hebrew University, Jerusalem, Israel (Received December 16, 1964)

The stabilization of the structure of water is discussed, assuming that liquid water contains large compact clusters of molecules. The effect arises from the difference in the change of the chemical potentials of the clusters and of the monomeric water molecules caused by the added nonelectrolyte. It is shown that for sufficiently large clusters, the magnitude of the stabilization effect becomes proportional to the number of molecules building the cluster. This effect is greater, the larger the difference between the interaction energy of the water-water and water-solute pairs.

Introduction

Recently, some anomalous properties of aqueous solutions of nonelectrolytes have been explained by the assumption that a solute molecule, when introduced into water, causes a "stabilization of the structure of water."¹⁻⁵

The reason for this effect was discussed by several authors who treated the problem from different points of view.^{1,6,7} The purpose of this work is to present a simple model for aqueous solutions of nonelectrolytes which shows the existence of a "stabilizing effect" (S.E.). We shall demonstrate that addition of inert solute to water may, under certain conditions, cause an increase in the total number of hydrogen bonds. This effect is in contrast to the dilution effect, *i.e.*, dissociation of clusters upon introduction of an indifferent solute.

The discussion below is confined to the case in which no penetration of solute molecules into the cavities of the "ice-like" form is allowed. A penetration of solute molecules into these cavities cannot always be taken for granted, as in the case of large solute molecules, side chains of polymers, or polar molecules (*e.g.*, alcohols, amines, etc.⁸⁻¹⁰). Thus, a weak point of some models,^{2,3,6,11,12} which rests mainly on the filling of cavities by the solute molecules, is bypassed.

The penetration into cavities is, however, not excluded. It will be shown that if penetration does occur, the S.E. is increased. The present discussion has the advantage of showing that "filling of cavities" is not an essential requirement for the existence of a stabilizing effect.

Description of the Model

The model adopted is very similar to that described by several authors.^{1,7,13} Liquid water is assumed to consist of clusters of molecules of different sizes. Let p denote a monomeric water molecule, *i.e.*, a molecule not linked by hydrogen bonds to any other molecule, and c_n a cluster consisting of n water molecules linked together by hydrogen bonds. The essential assumption is that these clusters (or, at least most of them) are compact; *i.e.*, they are formed in such a way as to achieve a maximum number of hydrogen bonds. This assumption is in accord with Frank and Wen's view¹ and was used also by Némethy and Scheraga.⁷ Infrared evidence for the compact nature of these clusters has been recently published by Buijs and Choppin.¹⁴ Let μ_{c_n} and μ_p be the chemical potentials of c_n and p ,

- (1) H. S. Frank and W. Y. Wen, *Discussions Faraday Soc.*, **24**, 133 (1957).
- (2) P. S. Yastremskii, *Zh. Strukt. Khim.*, **4**, 179 (1963).
- (3) Z. I. Grigorovich and O. Ya. Samoilov, *ibid.*, **3**, 464 (1962).
- (4) I. V. Matyash and V. I. Yashkichev, *ibid.*, **5**, 13 (1964).
- (5) A. Ben-Naim and S. Baer, *Trans. Faraday Soc.*, **59**, 1736 (1963).
- (6) H. S. Frank and A. S. Quist, *J. Chem. Phys.*, **34**, 604 (1961).
- (7) G. Némethy and H. A. Scheraga, *ibid.*, **36**, 3401 (1962).
- (8) M. V. Stackelberg, *Naturwissenschaften*, **36**, 327 (1949).
- (9) M. V. Stackelberg and H. R. Müller, *Z. Elektrochem.*, **58**, 25 (1954).
- (10) M. V. Stackelberg and B. Meuthen, *ibid.*, **62**, 130 (1958).
- (11) V. A. Mikhailov, *Zh. Strukt. Khim.*, **2**, 677 (1961).
- (12) V. I. Yashkichev and O. Ya. Samoilov, *ibid.*, **3**, 211 (1962).
- (13) G. Wada, *Bull. Chem. Soc. Japan*, **34**, 955 (1961).
- (14) K. Buijs and G. R. Choppin, *J. Chem. Phys.*, **39**, 2035, 2042 (1963).

respectively. At equilibrium, we have $\mu_{c_n} = n\mu_p$ (for any existing c_n).

For the sake of simplicity, we shall restrict the discussion to the case where only one kind of cluster, built up of n molecules, is present (we shall thus omit the subscript n). The consideration of all kinds of clusters only complicates the representation without affecting the final conclusion. We shall also confine ourselves to the case where the solution is very dilute with respect to c .

Let s be an inert nonelectrolyte. The partial molecular quantity \bar{E}_s corresponding to an extensive variable E is given by

$$\bar{E}_s \equiv \left(\frac{\partial E}{\partial n_s} \right)_{n_w} = \left(\frac{\partial E}{\partial n_s} \right)_{n_c, n_p} + (\bar{E}_c - n\bar{E}_p) \left(\frac{\partial n_c}{\partial n_s} \right)_{n_w} \quad (1)$$

where n_s , n_p , and n_c are the numbers of solute molecules, of monomeric water molecules, and of clusters, respectively. n_w is the total number of water molecules ($n_w = nn_c + n_p$). The differentiations are performed at constant pressure and temperature and will be omitted from the notation.

In this notation, we shall say that a "stabilization of the structure of water" occurs when $(\partial n_c / \partial n_s)_{n_w} > 0$.

Obviously, the exact evaluation of $(\partial n_c / \partial n_s)_{n_w}$ is impossible at present since it would require a knowledge of the partition function of liquid water, but, fortunately, the problem can be transformed into an equivalent one which is much more easy to handle. This is done by using the identity (see Appendix I)

$$\left(\frac{\partial n_c}{\partial n_s} \right)_{n_w} = -(\mu_{c_0} - 2n\mu_{c_p} + n^2\mu_{p_p})^{-1} \times \left(\frac{\partial(\mu_c - n\mu_p)}{\partial n_s} \right)_{n_c, n_p} \quad (2)$$

From the stability condition¹⁵ $(\mu_{c_0} - 2n\mu_{c_p} + n^2\mu_{p_p}) > 0$, so that it is sufficient to examine the sign of $(\partial(\mu_c - n\mu_p) / \partial n_s)_{n_c, n_p}$ which is a far easier task.

The main line of thought is the following one: define μ_c^{ex} and μ_p^{ex} by the relations

$$\mu_c^{\text{ex}} = \mu_c - kT \ln \rho_c$$

$$\mu_p^{\text{ex}} = \mu_p - kT \ln \rho_p$$

where $\rho_c = n_c/V$, $\rho_p = n_p/V$, and obtain

$$\begin{aligned} \left(\frac{\partial \Delta \mu}{\partial n_s} \right)_{n_c, n_p} &= kT \frac{\partial}{\partial n_s} (\ln \rho_c / \rho_p^n) + \\ \frac{\partial}{\partial n_s} (\mu_c^{\text{ex}} - n\mu_p^{\text{ex}}) &= \frac{kT \bar{V}_s (n-1)}{V} + \\ &\quad n \frac{\partial}{\partial n_s} \left(\frac{\mu_c^{\text{ex}}}{n} - \mu_p^{\text{ex}} \right) \quad (3) \end{aligned}$$

where $\Delta \mu = \mu_c - n\mu_p$ and $\bar{V}_s = (\partial V / \partial n_s)_{n_c, n_p}$.

The first term on the right-hand side of (3) is positive. This term is responsible for a destabilizing effect, or a diluting effect. Usually, it is the predominant one. The second term depends essentially on the total interaction of the various species with their corresponding surroundings. This interaction, of both c and p , is decreased by the addition of s (since, by assumption, s is inert). Now, since the change of the total interaction energy of the cluster c with its surroundings is determined by the area of its boundaries, we should expect that $|\partial(\mu_c^{\text{ex}}/n) / \partial n_s|$ decreases when n increases, provided that the surface-to-volume ratio decreases with n . This condition is fulfilled by the requirement that the clusters be compact.

Thus, as n increases, the second term of (3) becomes larger and negative. One has to examine now the conditions under which its absolute value will be greater than the first term, leading to an S.E. This will be done in the following section using a very simplified version of this model. Nevertheless, the results seem to account for the major cause of the S.E. in the real case.

A Sufficient Condition for a Stabilizing Effect

We start with a system described by (n_c, n_p, n_s) , assuming that the mixture is dilute with respect to c , that the clusters are of a spherical shape having a radius R_c , and that the radii of p and s are the same; *i.e.*, $R_p = R_s$. The chemical potentials of c and p are given by¹⁶

$$\mu_c = kT \ln \rho_c \Lambda_c^3 + \rho_p \int_0^1 \int_0^\infty u_{cp} g_{cp} 4\pi r^2 dr d\xi + \rho_s \int_0^1 \int_0^\infty u_{cs} g_{cs} 4\pi r^2 dr d\xi \quad (4)$$

$$\mu_p = kT \ln \rho_p \Lambda_p^3 + \rho_p \int_0^1 \int_0^\infty u_{pp} g_{pp} 4\pi r^2 dr d\xi + \rho_s \int_0^1 \int_0^\infty u_{ps} g_{ps} 4\pi r^2 dr d\xi \quad (5)$$

where $g_{\alpha\beta}$ is the radial distribution function of β around α , $u_{\alpha\beta}$ is the intermolecular potential energy for the $\alpha\beta$ pair, and Λ_α includes the momentum and internal partition function of an α -molecule.

The quantity $(\partial \Delta \mu / \partial n_s)_{n_c, n_p}$ expresses the change of $\Delta \mu$ upon transfer of dn_s molecules of s into a system in which the chemical equilibrium $c \rightleftharpoons np$ is "frozen in." In this system, all the interactions which involve hy-

(15) I. Prigogine and R. Defay, "Chemical Thermodynamics," Longmans, Green and Co., London, 1954, p. 228.

(16) T. L. Hill, "Statistical Mechanics," McGraw-Hill Book Co., Inc., New York, N. Y., 1956, p. 192.

drogen bonds are included in the clusters. The interactions between the various species, c, p, and s, will be approximated by a square-well potential

$$u_{\alpha\beta} = \begin{cases} \infty & r < \sigma_{\alpha\beta} \\ -\epsilon_{\alpha\beta} & \sigma_{\alpha\beta} < r < \sigma_{\alpha\beta} + \delta_{\alpha\beta} \\ 0 & r > \sigma_{\alpha\beta} + \delta_{\alpha\beta} \end{cases}$$

where $\sigma_{\alpha\beta}$ is the diameter of the rigid sphere of the $\alpha\beta$ pair. The attractive tail of strength $\epsilon_{\alpha\beta}$ extends from $\sigma_{\alpha\beta}$ to $\sigma_{\alpha\beta} + \delta_{\alpha\beta}$.

We assume further that: (a) the range of the attractive tail is the same for all the pairs and is equal to σ_{pp} ¹⁷; *i.e.*, $\delta_{cs} = \delta_{cp} = \delta_{pp} = \delta_{ps} = \sigma_{pp}$; (b) the diameter of the hard core is the same for the pairs cs and cp and for the pairs ps and pp

$$\sigma_c \equiv \sigma_{cp} = \sigma_{cs} = 4\pi(R_c + R_p)^3/3$$

$$\sigma_p \equiv \sigma_{pp} = \sigma_{ps} = 4\pi(2R_p)^3/3$$

(c) the depth of the well is the same for the pairs cs and ps and for the pairs cp and pp

$$\epsilon_s \equiv \epsilon_{cs} = \epsilon_{ps}$$

$$\epsilon_p \equiv \epsilon_{cp} = \epsilon_{pp}$$

(d) the radical distribution functions do not depend explicitly on n_s ; *i.e.*, $\partial g_{\alpha\beta}/\partial n_s = 0$ for all the $\alpha\beta$ pairs (strictly, we shall need this assumption for $\rho_s \rightarrow 0$). The graphical representation of the assumptions concerning the kind of interactions between the various species is described in Figure 1.

Differentiating (4) and (5) at constant temperature, pressure, n_c , and n_p , and requiring that the presence of s does not affect Λ_c and Λ_p , we get

$$\left(\frac{\partial \Delta\mu}{\partial n_s}\right)_{n_c, n_p} = \frac{\partial}{\partial n_s} (kT \ln \rho_c / \rho_p^n) + A_{cp} \frac{\partial \rho_p}{\partial n_s} + A_{cs} \frac{\partial \rho_s}{\partial n_s} - n A_{pp} \frac{\partial \rho_p}{\partial n_s} - n A_{ps} \frac{\partial \rho_s}{\partial n_s} \quad (6)$$

where

$$A_{\alpha\beta} = \int_0^1 \int_0^\infty u_{\alpha\beta} g_{\alpha\beta} 4\pi r^2 dr d\xi$$

Define

$$\bar{g}_{\alpha\beta} = \max_{\substack{0 \leq \xi \leq 1 \\ \sigma_{\alpha\beta} \leq r \leq \sigma_{\alpha\beta} + \delta_{\alpha\beta}}} [g_{\alpha\beta}(r, \xi)] \quad \underline{g}_{\alpha\beta} = \min_{\substack{0 \leq \xi \leq 1 \\ \sigma_{\alpha\beta} \leq r \leq \sigma_{\alpha\beta} + \delta_{\alpha\beta}}} [g_{\alpha\beta}(r, \xi)]$$

for the region $r < \sigma_{\alpha\beta}$ we use the approximate behavior¹⁸ $g_{\alpha\beta} = \exp[-\xi u_{\alpha\beta}/kT]$ and get

$$A_{\alpha\beta} = kT \frac{4\pi\sigma_{\alpha\beta}^3}{3} + \int_0^1 \int_{\sigma_{\alpha\beta}}^{\sigma_{\alpha\beta} + \delta_{\alpha\beta}} u_{\alpha\beta} g_{\alpha\beta} 4\pi r^2 dr d\xi = \frac{kT 4\pi\sigma_{\alpha\beta}^3}{3} + B_{\alpha\beta} \quad (7)$$

and the two inequalities (note that $B_{\alpha\beta}$ is negative)

$$B_{\alpha\beta} \leq \underline{g}_{\alpha\beta} \int_{\sigma_{\alpha\beta}}^{\sigma_{\alpha\beta} + \delta_{\alpha\beta}} u_{\alpha\beta} 4\pi r^2 dr = -\underline{g}_{\alpha\beta} \epsilon_{\alpha\beta} \frac{4\pi}{3} [(\sigma_{\alpha\beta} + \delta_{\alpha\beta})^3 - \sigma_{\alpha\beta}^3] \quad (8)$$

$$B_{\alpha\beta} \geq \bar{g}_{\alpha\beta} \int_{\sigma_{\alpha\beta}}^{\sigma_{\alpha\beta} + \delta_{\alpha\beta}} u_{\alpha\beta} 4\pi r^2 dr = -\bar{g}_{\alpha\beta} \epsilon_{\alpha\beta} \frac{4\pi}{3} [(\sigma_{\alpha\beta} + \delta_{\alpha\beta})^3 - \sigma_{\alpha\beta}^3] \quad (9)$$

We denote by

$$b_c \equiv \frac{4\pi\sigma_{cp}^3}{3} = \frac{4\pi\sigma_{cs}^3}{3} \quad (10)$$

$$b_p \equiv \frac{4\pi\sigma_{pp}^3}{3} = \frac{4\pi\sigma_{ps}^3}{3} \quad (11)$$

$$I_c \equiv \frac{4\pi}{3} [(\sigma_{cp} + \delta_{cp})^3 - \sigma_{cp}^3] \quad (12)$$

$$I_p \equiv \frac{4\pi}{3} [(\sigma_{pp} + \delta_{pp})^3 - \sigma_{pp}^3] \quad (13)$$

and obtain from (6), using (7), (10), and (11)

$$\left(\frac{\partial \Delta\mu}{\partial n_s}\right)_{n_c, n_p} = kT \frac{n-1}{V} \bar{V}_s - \frac{\rho_p \bar{V}_s}{V} (kT b_c + B_{cp}) + \frac{1 - \rho_s \bar{V}_s}{V} (kT b_c + B_{cs}) + \frac{\rho_p \bar{V}_s}{V} (kT b_p + B_{pp}) - \frac{1 - \rho_s \bar{V}_s}{V} (kT b_p + B_{ps}) \quad (14)$$

where we used the relations

$$\left(\frac{\partial \rho_p}{\partial n_s}\right)_{n_c, n_p} = -\frac{\rho_p \bar{V}_s}{V} \quad \left(\frac{\partial \rho_s}{\partial n_s}\right)_{n_c, n_p} = \frac{1 - \rho_s \bar{V}_s}{V}$$

Rearranging (14), we get

(17) J. O. Hirschfelder, C. F. Curtis, and R. B. Bird, "Molecular Theory of Gases and Liquids," John Wiley and Sons, Inc., New York, N. Y., 1954, pp. 159, 160.

(18) In the region $r < \sigma_{\alpha\beta}$ we use an approximate behavior for $g_{\alpha\beta}$. The effect on $\partial \Delta\mu / \partial n_s$ of this approximation will have a negligible influence on the conclusions (see Appendix II). It seems, therefore, that refinements of the form of $g_{\alpha\beta}$ in this region will not alter the conclusions.

$$\left(\frac{\partial \Delta \mu}{\partial n_s}\right)_{n_c, n_p} = \frac{kT}{V} [(n-1)\bar{V}_s + (b_c - nb_p)(1 - \rho_s \bar{V}_s - \rho_p \bar{V}_s)] + \frac{1 - \rho_s \bar{V}_s}{V} (B_{cp} - nB_{ps}) - \frac{\rho_s \bar{V}_s}{V} (B_{cp} - nB_{ps}) \quad (15)$$

To examine the conditions under which an S.E. will occur, *i.e.*, when $(\partial \Delta \mu / \partial n_s) < 0$, we note that all $B_{\alpha\beta}$ are negative, while $(n-1)\bar{V}_s$ is positive and the

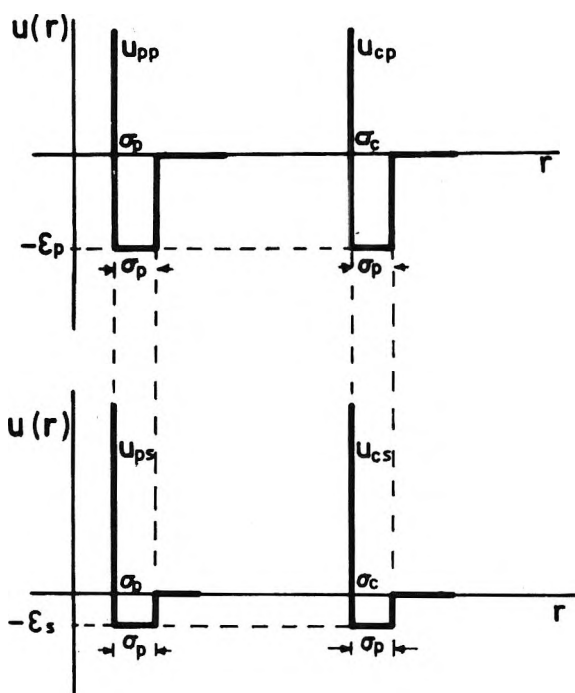


Figure 1. Description of the intermolecular potential energy for the various species.

term $(b_c - nb_p)(1 - \rho_s \bar{V}_s - \rho_p \bar{V}_s)$ is small and negative (Appendix II). Thus, using (8), (9), (12), (13), and the result of Appendix II, we obtain the inequality

$$\left(\frac{\partial \Delta \mu}{\partial n_s}\right)_{n_c, n_p} \leq \frac{kT}{V} \left[(n-1)\bar{V}_s + \frac{\rho_p \bar{V}_s}{kT} \epsilon_p (L_c \bar{g}_{cp} - nL_{pp} \bar{g}) - \frac{1 - \rho_s \bar{V}_s}{kT} \epsilon_s (L_c \bar{g}_{cs} - nL_{ps} \bar{g}) \right] \leq \frac{kT}{V} \left[(n-1)\bar{V}_s + \frac{\rho_p \bar{V}_s}{kT} \epsilon_p (L_c \bar{g} - nL_p \bar{g}) - \frac{1 - \rho_s \bar{V}_s}{kT} \epsilon_s (L_c \bar{g} - nL_p \bar{g}) \right] \quad (16)$$

where we put

$$\bar{g} = \max(\bar{g}_{cp}, \bar{g}_{cs}) \text{ and } \underline{g} = \min(\underline{g}_{pp}, \underline{g}_{ps})$$

For sufficiently large n we get (Appendix III)

$$L_c \bar{g} - nL_p \bar{g} \sim -nL_p \bar{g}$$

$$L_c \underline{g} - nL_p \underline{g} \sim -nL_p \underline{g}$$

This behavior arises from the decrease of the surface-to-volume ratio as n increases. In this case

$$\left(\frac{\partial \Delta \mu}{\partial n_s}\right)_{n_c, n_p} \leq \frac{kTn\bar{V}_s}{V} \left[1 + \frac{(1 - \rho_s \bar{V}_s)\bar{g}\epsilon_s L_p}{kT\bar{V}_s} - \frac{\rho_p \epsilon_p L_p \bar{g}}{kT} \right] \quad (17)$$

From (13) we have

$$L_p = 7 \frac{4\pi\sigma_{pp}^3}{3} = 7 \frac{4\pi(2R_p)^3}{3} = 56v_p$$

where v_p is the molecular volume of p . In addition, v_p , \bar{V}_p , and \bar{V}_s are expected to be of the same order of magnitude, so that $v_p \approx \bar{V}_p \approx \bar{V}_s$ and thus

$$1 \approx \rho_p \bar{V}_p + \rho_s \bar{V}_s \approx \rho_p \bar{V}_s + \rho_s \bar{V}_s \quad (18)$$

[Note that, although \bar{V}_c increases with n , we took $\rho_c \bar{V}_c \approx 0$. This is allowed since n is large but finite (Appendix III) while ρ_c may be taken as small as needed.] From (17) we obtain

$$\left(\frac{\partial \Delta \mu}{\partial n_s}\right)_{n_c, n_p} \leq \frac{kT}{V} n \bar{V}_s \left[1 - \frac{1 - \rho_s \bar{V}_s}{kT} 56(\epsilon_p \bar{g} - \epsilon_s \underline{g}) \right] \quad (19)$$

For the limiting case $\rho_s \rightarrow 0$ we get a sufficient condition for a stabilization effect

$$\frac{\epsilon_p \bar{g} - \epsilon_s \underline{g}}{kT} > \frac{1}{56}$$

Since $1 \lesssim \underline{g} \leq \bar{g} \lesssim 3$, and remembering the series of inequalities reached above, we see that the difference in the interaction energies required for the effect is quite moderate.

Two conclusions can now be drawn. First, for sufficiently large n (see also Appendix III) $(\partial \Delta \mu / \partial n_s)_{n_c, n_p}$ becomes proportional to n . Qualitatively, this result is in accord with several experimental observations.^{5, 19, 20} Secondly, the magnitude of $(\partial \Delta \mu / \partial n_s)_{n_c, n_p}$ is larger, the greater the difference between ϵ_p and ϵ_s . This conclusion cannot be directly compared with experimental results since a partial penetration of s molecules might occur. In this case, there is an additional contribution to $(\partial \Delta \mu / \partial n_s)_{n_c, n_p}$ which increases with ϵ_s .²¹

(19) A. Ben-Naim and G. Moran, *Trans. Faraday Soc.*, **61**, 821 (1965).

(20) A. Ben-Naim, *J. Chem. Phys.*, **42**, 1512 (1965).

In addition, if $\epsilon_p - \epsilon_s$ is larger than that required by the last inequality, we can get the same effect for smaller n , or for a finite value of ρ_s .

Obviously, liquid water contains clusters of different sizes. The preceding conclusions still hold if we re-introduce the index n . Thus, $\partial(\mu_{c_n} - n\mu_p)/\partial n_s$ will be negative for large n and positive for small n . A net stabilization of the structure will occur if most of the clusters are large, *i.e.*, if the mean cluster size is sufficiently large. An estimation made by Buijs and Choppin¹⁴ shows that the mean value of n is about 90 at 20° which seems to be of the order of magnitude required for an S.E.

Conclusion

We have shown that the assumption that liquid water contains large compact clusters leads directly to a stabilizing effect. Addition of nonelectrolyte to water gives rise to two competing effects. The first one is a diluting effect, which tends to destroy the clusters. In principle, this is an entropy effect. The second one is primarily an energy effect. It arises from the change in the surroundings of c and p caused by the addition of a relatively inert molecule. This effect makes clusterization favorable. (In addition, s-penetration might occur and usually enhances the effect.²¹) We found that for sufficiently large n , the second becomes greater than the first, leading to a stabilization effect. For large clusters, this effect becomes proportional to n . The dependence of $\partial\Delta\mu/\partial n_s$ upon ϵ_s shows that this effect arises from the "inactivity" of s , rather than from its "activity." This conclusion is in contrast to the view that an inert molecule "builds an iceberg around it."²²

Acknowledgment. The author wishes to express his thanks to Professors G. Stein and T. L. Hill and to Dr. S. Baer for helpful discussions and comments.

Appendix I

The Relation between $(\partial\Delta\mu/\partial n_s)_{n_c, n_p}$ and $(\partial n_c/\partial n_s)_{n_w}$. Starting with a system (n_c, n_p, n_s) , at equilibrium, we have

$$\Delta\mu = \mu_c(n_c, n_p, n_s) - n\mu_p(n_c, n_p, n_s) = 0$$

Adding dn_s molecules of s and keeping n_w constant, we get

$$\Delta\tilde{\mu} = \mu_c(n_c + dn_c, n_p + dn_p, n_s + dn_s) - n\mu_p(n_c + dn_c, n_p + dn_p, n_s + dn_s) = 0$$

Developing $\Delta\tilde{\mu}$ in series around (n_c, n_p, n_s) , we obtain

$$\Delta\tilde{\mu} = \Delta\mu + \frac{\partial\Delta\mu}{\partial n_c}dn_c + \frac{\partial\Delta\mu}{\partial n_p}dn_p + \frac{\partial\Delta\mu}{\partial n_s}dn_s + \dots \quad (20)$$

Using the identity $\partial\mu_c/\partial n_p = \partial\mu_p/\partial n_c$ and the condition $ndn_c + dn_p = 0$, we get from (20)

$$\left(\frac{\partial\mu_c}{\partial n_c} - n\frac{\partial\mu_c}{\partial n_p}\right)dn_c - \left(\frac{\partial\mu_c}{\partial n_p} - n\frac{\partial\mu_p}{\partial n_p}\right)ndn_c + \frac{\partial\Delta\mu}{\partial n_s}dn_s = 0$$

or, after rearranging

$$(\mu_{cc} - 2n\mu_{cp} + n^2\mu_{pp})\left(\frac{\partial n_c}{\partial n_s}\right)_{n_w} = -\left(\frac{\partial\Delta\mu}{\partial n_s}\right)_{n_c, n_p} \quad (21)$$

From the stability condition,¹⁵ we have $\mu_{cc} - 2n\mu_{cp} + n^2\mu_{pp} > 0$, where $\mu_{\alpha\beta} = \partial\mu_\alpha/\partial n_\beta$. Thus, the sign of $(\partial n_c/\partial n_s)_{n_w}$ is opposite to that of $(\partial\Delta\mu/\partial n_s)_{n_c, n_p}$ as could be expected intuitively.

Appendix II

Estimation of the Contribution of the Term $\eta = (b_c - nb_p)(1 - \rho_s\bar{V}_s - \rho_s\bar{V}_p)$. From (10) and (11) we get

$$\frac{b_c}{b_p} = \left(\frac{\sigma_{cp}}{\sigma_{pp}}\right)^3 = \left(\frac{R_c + R_p}{2R_p}\right)^3 = \frac{1}{8}\left[\left(\frac{R_c}{R_p}\right)^3 + 3\left(\frac{R_c}{R_p}\right)^2 + 3\frac{R_c}{R_p} + 1\right]$$

The ratio R_c/R_p is related to the number n by

$$(R_c/R_p)^3 = \alpha n$$

where $\alpha > 1$ depends on the geometry and type of packing of the molecules in the clusters. Estimation from Pauling's model⁶ gives $\alpha \approx 3$ which is a quite large value owing to the open structure of the clathrate framework.

We shall use $\alpha = 3$ for the numerical estimations (they will be better for $\alpha < 3$)

$$b_c - nb_p = nb_p\left(\frac{b_c}{nb_p} - 1\right) = nb_p\left[\frac{1}{8}\left(3 + \frac{3^{5/3}}{n^{1/3}} + \frac{3^{4/3}}{n^{2/3}} + \frac{1}{n}\right) - 1\right]$$

Estimation made by Buijs and Choppin¹⁴ shows that the average cluster size at 20° is about 90 molecules. Thus, for $n \geq 90$ we get $b_c - nb_p < 0$. Thus, $b_c - nb_p$ is negative. Since in this model

$$1 - \rho_s\bar{V}_s - \rho_p\bar{V}_p \approx 1 - \rho_s\bar{V}_s - \rho_p\bar{V}_s > 0$$

the whole term η is negative also. This justifies its omission from the inequality (16). Its value is, by the assumption of the model, small since

(21) A. Ben-Naim, to be published.

(22) H. S. Frank and M. W. Evans, *J. Chem. Phys.*, **13**, 507 (1945).

$$1 - \rho_s \bar{V}_s - \rho_p \bar{V}_p = \rho_c \bar{V}_c \approx 0$$

Appendix III

The Behavior of $L_c \bar{g} - nL_p g$ and of $L_c g - nL_p \bar{g}$ for Large n . From the definitions (12) and (13), we have

$$L_c \bar{g} - nL_p \bar{g} = \bar{g} \frac{4\pi}{3} [(\sigma_{cp}^3 + \sigma_{pp}^3) - \sigma_{cp}^3] -$$

$$ng \frac{4\pi}{3} \sigma_{pp}^3 = \frac{4\pi}{3} \sigma_{pp}^3 \left[\bar{g} \left(3 \frac{\sigma_{cp}^2}{\sigma_{pp}^2} + 3 \frac{\sigma_{cp}}{\sigma_{pp}} + 1 \right) - 7ng \right]$$

From Appendix II for $\alpha = 3$ and $n = 90$, we have

$$\left(\frac{\sigma_{cp}}{\sigma_{pp}} \right)^3 = \frac{n}{8} \left(3 + \frac{3^{1/2}}{90^{1/2}} + \frac{3^{1/4}}{90^{2/4}} + \frac{1}{90} \right) < n$$

(The estimation is better for $n > 90$ and $\alpha < 3$.) Thus

$$L_c \bar{g} - nL_p g \leq \frac{4\pi}{3} \sigma_{pp}^3 [\bar{g}(3n^{2/3} + 3n^{1/3} + 1) -$$

$$7ng] = n \frac{4\pi}{3} \sigma_{pp}^3 \left[\bar{g} \left(\frac{3}{n^{1/3}} + \frac{3}{n^{2/3}} + \frac{1}{n} \right) - 7g \right]$$

\bar{g} is finite. Thus, for sufficiently large n , we get

$$L_c \bar{g} - nL_p g \rightarrow -n \frac{4\pi \sigma_{pp}^3}{3} 7g = -nL_p g$$

(This behavior is already achieved for n of the order of 200, and for smaller n if $\alpha < 3$). In the same manner, for sufficiently large n we have

$$L_c g - nL_p \bar{g} \rightarrow -nL_p \bar{g}$$

Molecular Orbital Theory of Electron Donor-Acceptor Complexes. I.

A Simple Semiempirical Treatment

by R. L. Flurry, Jr.

Department of Chemistry, Louisiana State University in New Orleans, New Orleans, Louisiana 70122
(Received February 25, 1965)

A semiempirical linear combination of molecular orbitals description of electron donor-acceptor complexes is presented. Using this, an empirical estimate of the interaction integral between the systems participating in EDA complex formation is made. This empirical β_{DA} is used to predict stabilization energies and excitation energies for several complexes. The agreement with experiment is satisfactory. A brief comparison with the conventional treatments of such complexes is made.

I. Introduction

Much literature on electron donor-acceptor (EDA) complexes has arisen in the past few years, both from experimental and theoretical points of view. Most of the theoretical papers dealing with EDA complexes have been based on a valence bond (VB) type of formalism.¹ Dewar's molecular orbital (MO) treatment of EDA complexes² is a perturbation theory treatment. Murrell³ has presented a very sophisticated MO per-

turbation treatment of EDA interactions. The delocalization method of Fukui and co-workers⁴ is an LCAO

(1) R. S. Mulliken, *J. Am. Chem. Soc.*, **72**, 600 (1950); *J. Phys. Chem.*, **56**, 801 (1952), and subsequent papers.

(2) M. J. S. Dewar and A. R. Lepley, *J. Am. Chem. Soc.*, **83**, 4560 (1961).

(3) J. N. Murrell, *ibid.*, **81**, 5037 (1959); J. N. Murrell and J. Tanaka, *Mol. Phys.*, **7**, 363 (1963-1964).

(4) K. Fukui, A. Imamura, T. Yonezawa, and C. Nagata, *Bull. Chem. Soc. Japan*, **34**, 1076 (1961); **35**, 33 (1962).

method which employs the atomic orbitals of both the donor and acceptor and then utilizes perturbation theory to estimate their interactions.

The present research is part of an attempt to develop a simple MO theory of EDA complexes, utilizing orbitals of the entire complex as the basis, and to apply it not only to a calculation of charge-transfer (CT) spectra but also to predictions of stability and of orientation in EDA complexes.

This paper presents a simple, semiempirical, one-electron treatment of EDA complexes and applies it to benzene and methyl-substituted benzenes as donors and to chloranil, tetracyanoethylene, 1,3,5-trinitrobenzene, *p*-benzoquinone, and iodine as the acceptors. Nagakura and Tanaka have used a similar method to discuss the spectral effects of intramolecular electron migration in substituted aromatic systems.⁵ The present work differs from this in several important respects and, in addition, appears to be the first attempt to apply such a treatment to intermolecular complexes and to calculating stabilities.

II. Method

Considerations involving (HOMO)_D and (LEMO)_A. The ground (N) state wave function of the complex is expressed as a linear combination of molecular orbitals (LCMO) of the donor and acceptor where ϕ_D is the wave function of the donor and ϕ_A that of the

$$\phi_N = a\phi_D + b\phi_A \quad (1)$$

acceptor, and a and b are mixing parameters (with the normalizing restriction that $a^2 + b^2 = 1$, assuming formal neglect of overlap). The electronic energy of the ground state may be expressed as in eq. 2 (using

$$W_N = a^2\langle\phi_D|H_{op}|\phi_D\rangle + b^2\langle\phi_A|H_{op}|\phi_A\rangle + 2ab\langle\phi_D|H_{op}|\phi_A\rangle \quad (2)$$

Dirac notation). For the present, the form of the Hamiltonian will remain undefined.

In addition to the energy arising from the interaction of the donor and acceptor orbitals, there will be an additional potential energy interaction owing to the attraction of the partial charges that result from a partial transfer of charge in the ground state of the complex. This potential may actually be more important in the stabilization of the complex than the direct orbital interaction.⁶ In the ground state, the amount of charge transferred will be equal to b^2 in this approximation. Let us define $-V_{es}$ as the potential resulting if a complete charge transfer occurs between the components of the complex at their equilibrium separation. The total energy of the ground state of the complex will then be

$$E_N = a^2\langle\phi_D|H_{op}|\phi_D\rangle + b^2\langle\phi_A|H_{op}|\phi_A\rangle + 2ab\langle\phi_D|H_{op}|\phi_A\rangle - b^2V_{es} \quad (3)$$

or, making the definitions

$$D = \langle\phi_D|H_{op}|\phi_D\rangle \quad (4a)$$

$$A = \langle\phi_A|H_{op}|\phi_A\rangle \quad (4b)$$

$$\beta_{DA} = \langle\phi_D|H_{op}|\phi_A\rangle \quad (4c)$$

the total energy of the ground state may be expressed as

$$E_N = a^2D + b^2A + 2ab\beta_{DA} - b^2V_{es} \quad (5)$$

The excited state wave function is expressed as in eq. 6. In this approximation b and a have the same

$$\Phi_E = b\phi_D - a\phi_A \quad (6)$$

values as in ϕ_N . (If overlap were included, this would not be the case.) The total energy of the excited state is thus expressed as eq. 7 (a^2 is the amount of charge transferred in this state).

$$E_E = b^2D + a^2A - 2ab\beta_{DA} - a^2V_{es} \quad (7)$$

The energy of the charge-transfer ($E \leftarrow N$) transition is simply E_E minus E_N .

$$\Delta E_{CT} = (b^2 - a^2)(D - A + V_{es}) - 4ab\beta_{DA} \quad (8)$$

If the degree of charge transfer in the N state of the complex and the value of β_{DA} are sufficiently small, eq. 8 can be approximated by equation 8a, a form which is frequently used for interpreting charge-transfer spectra.⁶

$$\Delta E_{CT} \cong I - EA + C \quad (8a)$$

The relationships among D , A , W_N , E_N , W_E , and E_E are shown schematically in Figure 1.

From a consideration of Figure 1, it is obvious that a resonance stabilization of the N state of the complex will be accompanied by a corresponding destabilization of the E state. If this were the only effect operative, the $E \leftarrow N$ transition would be of greater energy than the difference in the ionization potential of the donor and the electron affinity of the acceptor. This, of course, is not the case experimentally; hence, the electrostatic terms must be considered. If, on the other hand, there were no transfer of charge in the N state of the complex, as would be the case if there were no resonance stabilization, the slope of a plot of the charge-transfer transition *vs.* the ionization potential of the donor for a given acceptor would be unity. This,

(5) S. Nagakura and J. Tanaka, *J. Chem. Phys.*, **22**, 236 (1954).

(6) J. N. Murrell, *Quart. Rev.* (London), 191 (1961).

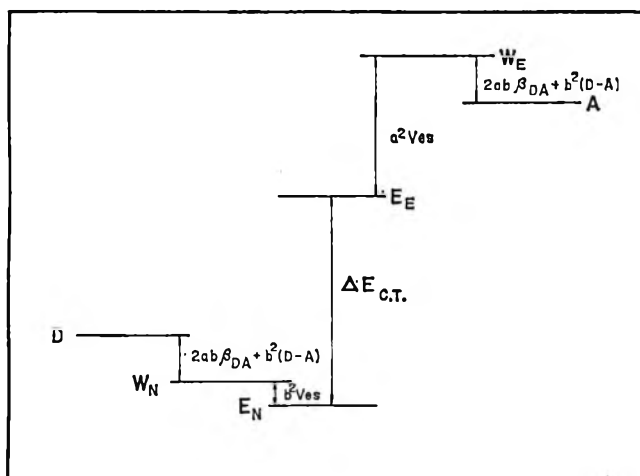


Figure 1. The relationships between the highest occupied orbital of the donor (D), the lowest unoccupied orbital of the acceptor (A), the ground and excited state electronic energies (W_N and W_E) and the total ground and excited state energies (E_N and E_E) for EDA complexes.

again, is not true experimentally. It is therefore evident that both a resonance effect and an electrostatic effect must be operative.

This treatment, of necessity, neglects solvation energies. If a suitable method for estimating the relative solvation energies of the N and E states could be found, these could be included in a manner similar to the electrostatic effect.

III. Calculations

For the acceptors tetracyanoethylene, 1,3,5-trinitrobenzene, chloranil, and *p*-quinone, the distance between the donor and acceptor is assumed to be near that of the chloranil-hexamethylbenzene complex (3.65 Å).⁷ If the charges which arise are assumed to be evenly distributed around the donor and the acceptor, a value of 3.95 e.v. can be estimated for V_{es} . For iodine, a value of 2.91 e.v. can be estimated for V_{es} if the complex is assumed to have axial symmetry with a separation between the donor and the iodine molecule of 3.36 Å., the experimental value for the bromine complex.⁸ If the assumption is made that, for a given series of similar donors with the same acceptor, the degree of charge transfer is constant and β_{DA} is constant, a plot of ΔE_{CT} vs. D (which, according to Koopmans' theory, is the negative of the ionization potential of the donor) should give a straight line, the slope of which can be used with the normalizing condition to estimate a and b .⁹ If A (the negative of the electron affinity) and V_{es} are known, the intercept of the line will give an estimate of β_{DA} . Plotting the charge-transfer bands for the complexes of tetracyanoethyl-

ene (TCNE) with the methyl-substituted benzenes¹⁰ vs. ionization potentials calculated by an SCMO method^{11,12} (Figure 2) gives values of 0.89 for a , 0.45 for b , and -0.63 e.v. for β_{DA} . Table I lists the values obtained for all of the acceptors used. Just as in the Hückel treatment of π -electron systems, the relative values of the calculated properties within a series will be independent of the absolute value of β_{DA} ; however, these values of β_{DA} are probably of the right magnitude. Brown has estimated that "bonds" between donors and acceptors in complexes usually have energies of $0.1-0.6\beta$.¹³ β is generally accepted to have a value near -3 e.v.

It is of interest to consider the significance of the slope of the plot obtained from eq. 8. The smaller the slope is, the greater is the amount of charge transferred in the ground state of the complex. For all of the acceptors, except *p*-quinone and trinitrobenzene, the apparent degree of charge transfer parallels the electron affinity of the acceptor. The data for *p*-quinone are limited to those compounds which would

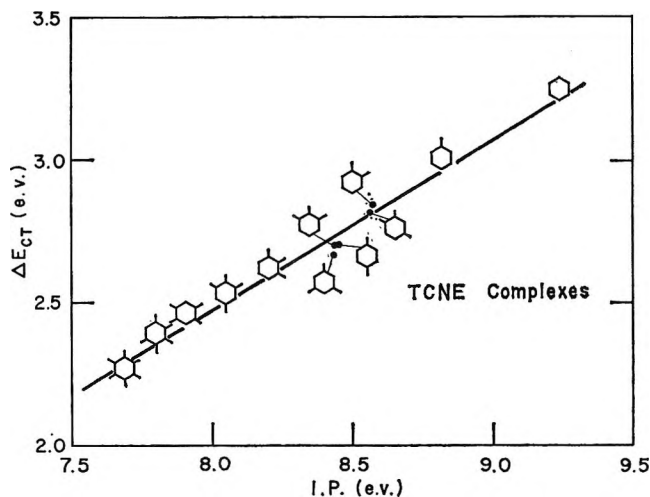


Figure 2. A graph of the CT transition¹⁰ vs. ionization potentials¹¹ for TCNE-methylbenzene complexes.

(7) T. T. Harding and S. C. Wallwork, *Acta Cryst.*, **6**, 791 (1953); **8**, 787 (1955).

(8) O. Hassel, *Mol. Phys.*, **1**, 241 (1958).

(9) a and b will not, in fact, be constant for the series but can later be derived, using a simple interaction matrix (eq. 9) between the donor and acceptor, once a value for β_{DA} has been determined.

(10) A. R. Lopley, *J. Am. Chem. Soc.*, **86**, 2545 (1964).

(11) R. L. Flurry, Jr., and P. G. Lykos, *ibid.*, **85**, 1033 (1963); R. L. Flurry, Jr., and J. G. Jones, Abstracts, 144th National Meeting of the American Chemical Society, Los Angeles, Calif., April 1963.

(12) The average deviation of the calculated and available experimental values for the photoionization potentials is 0.13%. The maximum deviation (pseudocumene) is 0.85%.

(13) R. D. Brown, *J. Chem. Soc.*, 2232 (1959).

Table I: Parameter Values for the Various Acceptors

Acceptor	Electron affinity, e.v.	V_{es} , e.v.	Slope (eq. 8)	β_{DA} , e.v.
1,3,5-Trinitrobenzene	0.70 ^a	3.95	0.71	-0.81
<i>p</i> -Quinone	1.11 ^b	3.95	0.34 ^c	-1.40 ^c
Chloranil	1.35 ^a	3.95	0.77	-0.51
Tetracyanoethylene	1.60 ^a	3.95	0.60	-0.63
Iodine	2.00 ^{a,d}	2.91	0.55	-1.15

^a See ref. 14. ^b Midpoint of range reported by M. E. Peover, *Trans. Faraday Soc.*, **58**, 1656 (1962). ^c These values are probably not very valid owing to the small amount of data available for evaluating them. ^d Value for the axis of the iodine molecule perpendicular to the plane of the acceptor.

be expected to form the weakest complexes in the series; consequently, no definitive conclusions can be drawn from them. On the other hand, the data for trinitrobenzene, while encompassing only a few members, present examples at both extremes of the series; consequently, the observed trends should be valid. Briegleb¹⁴ noted this anomaly in the relationship between the amount of charge transferred in trinitrobenzene complexes and its reported electron affinity.

The large apparent degree of charge transfer in the ground state of the trinitrobenzene complexes makes it tempting to choose a value of about 1.42 e.v. for the electron affinity of trinitrobenzene, a value slightly larger than that of chloranil. It is interesting but probably not significant that this is near the experimental value of 1.6 e.v. for nitrogen dioxide.¹⁵ Using 1.42 e.v. as the electron affinity, the value obtained for β_{DA} is -1.16 e.v. The uncorrected calculated values for the charge-transfer transition and for the relative stabilities are improved by this change. With the experimental value of the electron affinity, the calculated charge-transfer energies range from 4.81 e.v. for benzene to 3.32 e.v. for hexamethylbenzene as compared with an experimental range of 4.36 to 3.14 e.v. With an electron affinity of 1.42 e.v., the calculated range is 4.37 to 2.98 e.v. The calculated $\log K/K^\circ$ values, using the experimental electron affinity, range from 0 to 0.63. Using the estimated electron affinity, the range is from 0 to 1.56. The experimental range is 0 to 1.49.

Variation of the V_{es} term has very little effect on the relative values of the calculated charge-transfer transitions. It does, however, have a considerable effect on both the absolute value of the calculated transition and the spread in the calculated equilibrium constants. For example, varying V_{es} for the TCNE complexes over the range of 3.0 to 5.0 e.v. gave a variation of

only 0.15 e.v. in the calculated spread of the transition energies. The magnitude of the benzene-TCNE transition varied by 1.59 e.v. from 4.67 to 3.08 e.v. The calculated $\log K/K^\circ$ for hexamethylbenzene varied by a factor of 16.5 from 0.09 to 1.49.

The estimated values of β_{DA} can be used with the variational principle to set up a secular determinant (eq. 9) to determine the electronic energies of the

$$\begin{vmatrix} D - W & \beta_{DA} \\ \beta_{DA} & A - W \end{vmatrix} = 0 \quad (9)$$

resulting complex orbitals and the coefficients a and b for eq. 1, using values of the ionization potential and electron affinity for $-D$ and $-A$. The lowest root of this determinant and the calculated value of b can be used with the V_{es} to determine the stabilization energy of the complex. The complex will be more stable than the isolated donor and acceptor if it has a total energy lower than the sum of the total energies of the isolated donor and acceptor; *i.e.*

$$E_N < E_D + E_A \quad (10)$$

or again, considering only the (HOMO)_D and the (LEMO)_A, there is a net stabilization if

$$a^2D + b^2A + 2ab\beta_{DA} - b^2V_{es} < D \quad (11)$$

The stabilization energy is then

$$\Delta E_{stab} = D - E_N \quad (12)$$

If the entropies of formation of the complexes are constant, the relative stabilities of the complexes can be obtained by¹¹

$$\log K/K^\circ = \frac{(E_{stab} - E^\circ_{stab})}{2.3RT} \quad (13)$$

Owing to the crudeness of the method, the uncertainty of the parameter values, and the large solvent effects,¹⁶⁻¹⁸ the best that can be expected is a linear relationship between the calculated and observed values. Numerical agreement can be obtained, however, if a least-squares fit is made of these values. A similar fit can be made for the energies of the charge-transfer transitions. Tables II-VI list the uncorrected and the corrected calculated values, the experimental values of the charge-transfer band, and the

(14) G. Briegleb, *Angew. Chem. Intern. Ed. Engl.*, **3**, 617 (1964).

(15) H. O. Pritchard, *Chem. Rev.*, **52**, 529 (1953).

(16) G. Briegleb and J. Czekalla, *Z. Elektrochem.*, **63**, 6 (1959); *Angew. Chem.*, **72**, 401 (1960).

(17) G. Briegleb, "Elektronen-Donator-Acceptor-Komplexe," Springer-Verlag, Berlin, 1961, p. 114 ff.

(18) C. C. Thompson, Jr., and P. A. D. deMaine, *J. Am. Chem. Soc.*, **85**, 3096 (1963).

Table II: Spectra and Relative Stabilities of Complexes with 1,3,5-Trinitrobenzene

Donor	ΔE_{CT} , e.v.			$\text{Log}(K/K^\circ)$		
	Calcd.	Cor. ^a	Obsd.	Calcd.	Cor. ^a	Obsd.
Benzene	4.81	4.38	4.36 ^b	(0)	-0.02	(0) ^b
Toluene	4.40	4.08	4.08	0.14	0.30	0.25
<i>o</i> -Xylene	4.16	3.91	...	0.23	0.51	...
<i>m</i> -Xylene	4.15	3.90	3.90	0.24	0.51	0.58
<i>p</i> -Xylene	4.05	3.82	...	0.28	0.61	...
Hemimellitene	4.04	3.82	...	0.28	0.62	...
Pseudocumene	3.81	3.65	...	0.38	0.84	...
Mesitylene	4.03	3.81	...	0.29	0.63	...
Prehnitene	3.67	3.54	...	0.45	0.99	...
Isodurene	3.67	3.54	...	0.45	0.99	...
Durene	3.53	3.44	3.61	0.51	1.14	1.01
Pentamethylbenzene	3.43	3.37	...	0.57	1.26	...
Hexamethylbenzene	3.32	3.28	3.14	0.63	1.39	1.49

^a Least-squares fit with observed data. ^b G. Briegleb and J. Czekalla, *Z. Elektrochem.*, **58**, 249 (1954); **59**, 184 (1955).

Table III: Spectra and Relative Stabilities of Complexes with *p*-Quinone

Donor	ΔE_{CT} , e.v.			$\text{Log}(K/K^\circ)$ calcd.
	Calcd.	Cor. ^a	Obsd.	
Benzene	4.87	4.06	4.06 ^b	(0)
Toluene	4.49	3.92	3.93	0.44
<i>o</i> -Xylene	4.27	3.83	3.85	0.73
<i>m</i> -Xylene	4.26	3.83	3.81	0.74
<i>p</i> -Xylene	4.16	3.79	3.87 ^c	0.87
Hemimellitene	4.15	3.79	...	0.89
Pseudocumene	3.95	3.71	...	1.19
Mesitylene	4.15	3.79	...	0.90
Prehnitene	3.82	3.66	...	1.40
Isodurene	3.82	3.66	...	1.40
Durene	3.70	3.62	...	1.60
Pentamethylbenzene	3.61	3.58	...	1.76
Hexamethylbenzene	3.51	3.54	...	1.95

^a Least-squares fit with observed data. ^b A. Kuboyama and S. Nagakura, *J. Am. Chem. Soc.*, **77**, 2644 (1955). ^c Omitted in least-squares fit.

relative stabilities for the complexes of the methylbenzenes and the various acceptors. Benzene is adapted as the standard for the stabilities in each case. The numerical agreement is satisfactory.

IV. Comparison with Dative Bond and Perturbation Theory Treatments

In an addendum to their 1962 review article,¹⁹ Mulliken and Person compared the VB type of treatment with Dewar's MO treatment. In this section

Table IV: Spectra and Relative Stabilities of Complexes with Chloranil

Donor	ΔE_{CT} , e.v.			$\text{Log}(K/K^\circ)$		
	Calcd.	Cor. ^a	Obsd.	Calcd.	Cor. ^a	Obsd.
Benzene	4.04	3.69	3.65 ^b	(0)	-0.08	(0) ^b
Toluene	3.63	3.37	3.40	0.07	0.23	0.22
<i>o</i> -Xylene	3.38	3.17	3.22	0.12	0.43	0.54
<i>m</i> -Xylene	3.37	3.16	3.18	0.12	0.44	0.45
<i>p</i> -Xylene	3.26	3.08	3.03	0.14	0.54	0.47
Hemimellitene	3.25	3.07	...	0.14	0.55	...
Pseudocumene	3.02	2.89	2.95	0.19	0.77	0.53
Mesitylene	3.24	3.06	3.03	0.14	0.56	0.54
Prehnitene	2.87	2.77	2.79	0.23	0.92	0.95
Isodurene	2.87	2.77	2.76	0.23	0.92	0.92
Durene	2.74	2.66	2.64	0.26	1.07	1.00
Pentamethylbenzene	2.63	2.58	2.58	0.29	1.20	1.25
Hexamethylbenzene	2.51	2.49	2.46	0.32	1.34	1.48

^a Least-squares fit with observed data. ^b See ref. 3.

Table V: Spectra and Relative Stabilities of Complexes with Tetracyanoethylene

Donor	ΔE_{CT} , e.v.			$\text{Log}(K/K^\circ)$		
	Calcd.	Cor. ^a	Obsd.	Calcd.	Cor. ^a	Obsd.
Benzene	3.85	3.22	3.19 ^b	(0)	-0.17	(0) ^c
Toluene	3.44	2.96	2.99	0.12	0.29	0.28
<i>o</i> -Xylene	3.20	2.82	2.84	0.19	0.60	0.54
<i>m</i> -Xylene	3.19	2.81	2.82	0.20	0.61	0.48
<i>p</i> -Xylene	3.08	2.74	2.69	0.23	0.76	0.58
Hemimellitene	3.07	2.74	2.69	0.23	0.77	...
Pseudocumene	2.84	2.60	2.61	0.32	1.11	...
Mesitylene	3.06	2.73	2.67	0.24	0.79	0.94
Prehnitene	2.70	2.51	...	0.38	1.34	...
Isodurene	2.70	2.51	2.53	0.38	1.34	...
Durene	2.56	2.42	2.45	0.43	1.56	1.43
Pentamethylbenzene	2.46	2.36	2.38	0.48	1.75	1.79
Hexamethylbenzene	2.34	2.29	2.27	0.53	1.96	2.12

^a Least-squares fit with observed data. ^b See ref. 10. ^c R. E. Merrifield and W. D. Phillips, *J. Am. Chem. Soc.*, **80**, 2778 (1958).

the LCMO treatment will be compared with the VB treatment and with a simple perturbation theory treatment.

To the present degree of approximation, the LCMO treatment of EDA complexes looks very similar to the traditional VB type of treatment,¹ and, in fact, the numerical treatment presented here can be carried

(19) R. S. Mulliken and W. B. Person, *Ann. Rev. Phys. Chem.*, **13**, 107 (1962).

Table VI: Spectra and Relative Stabilities of Complexes with Iodine

Donor	ΔE_{CT} , e.v.			Log (K/K^0)		
	Calcd.	Cor. ^a	Obsd.	Calcd.	Cor. ^a	Obsd.
Benzene	4.82	4.31	4.24 ^b	(0)	-0.02	(0) ^b
Toluene	4.44	4.07	4.10	0.35	0.19	0.04
<i>o</i> -Xylene	4.22	3.93	3.92	0.59	0.32	0.27
<i>m</i> -Xylene	4.21	3.93	3.90	0.60	0.33	0.33
<i>p</i> -Xylene	4.11	3.87	4.08	0.70	0.39	0.33
Hemimellitene	4.09	3.86	...	0.71	0.40	...
Pseudocumene	3.89	3.73	...	0.97	0.55	...
Mesitylene	4.09	3.85	3.73	0.72	0.41	0.75
Prehnitene	3.75	3.65	...	1.14	0.65	...
Isodurene	3.75	3.65	3.66	1.14	0.65	...
Durene	3.63	3.57	3.73	1.31	0.74	0.64
Pentamethylbenzene	3.54	3.51	3.47	1.45	0.82	0.78
Hexamethylbenzene	3.43	3.45	3.31	1.60	0.91	0.97

^a Least-squares fit with observed data. ^b L. J. Andrews and R. M. Keefer, *J. Am. Chem. Soc.*, **74**, 4500 (1952).

out in the same manner in the VB formalism. The difference lies in the formal interpretation of the empirically determined parameters. In the present crude form, the prime advantage of the LCMO method is in the more correct conceptual interpretation of these parameters.

In the simplest VB treatment, the ground-state wave function is expressed as in eq. 14, where $\phi_0(\text{DA})$

$$\Phi_N = a\phi_0(\text{DA}) + b\phi_1(\text{D}^+-\text{A}^-) \quad (14)$$

represents a total wave function for the ground state of the donor and acceptor with no interaction between them. $\phi_1(\text{D}^+-\text{A}^-)$ is the dative structure in which a total charge has been transferred from the donor to the acceptor and which involves a bond between them. If we use the individual molecular orbitals of the donor and acceptor as the basis set for the VB treatment of the complex, we can draw an analogy with the VB treatment of heteronuclear diatomic molecules.²⁰ The $\phi_0(\text{DA})$ corresponds to what, in the Heitler-London treatment, is an ionic state with both electrons on the same center (eq. 15). Equation 14 is then actually a

$$\phi_0(\text{DA}) = \psi_D(1)\psi_D(2) \quad (15)$$

configuration interaction equation which allows for the mixing of the pseudo-ionic $\phi_0(\text{DA})$ configuration and the covalent $\phi_1(\text{D}^+-\text{A}^-)$ configuration. The inclusion of higher order terms in eq. 1 (allowance for "reverse dative structures"²² etc.) amounts to the inclusion of additional configurations in the VB treatment.

The simple VB formalism is basically a two-electron theory while the simplest MO formalism is basically a one-electron theory; hence, the interpretation of the various parameters used here, particularly the use of the electron affinity, is formally correct only in the MO scheme.

In a simplification of the perturbation theory treatment of EDA complexes,³ the highest occupied orbital of the donor may be taken as the unperturbed ground-state orbital of the complex, and the lowest empty orbital of the acceptor as the unperturbed excited-state orbital. The perturbation of the ground state may be considered to be the potential of the neutral acceptor while the perturbation of the excited state will be the potential of the donor bearing a single positive charge. Since the first-order perturbation energy for a given state is just the perturbation function averaged over the corresponding unperturbed state of the system,²¹ the energies of the N state, the E state, and the charge-transfer excitation will be, to first order, as expressed in eq. 16-18, respectively. D , A ,

$$E_N' = D + \langle \phi_D | V(A) | \phi_D \rangle \quad (16)$$

$$E_E' = A + \langle \phi_A | V(D^+) | \phi_A \rangle \quad (17)$$

$$E_{CT}' = A - D + \langle \phi_A | V(D^+) | \phi_A \rangle - \langle \phi_D | V(A) | \phi_D \rangle \quad (18)$$

ϕ_D , and ϕ_A are as previously defined, and $V(A)$ and $V(D^+)$ are the perturbing potentials. If either of the integrals $\langle \phi_A | V(D^+) | \phi_A \rangle$ or $\langle \phi_D | V(A) | \phi_D \rangle$ can be assumed to be proportional to the ionization potential of the donor, the perturbation theory treatment can predict a non-unity slope for a plot of the charge-transfer transition energy *vs.* the ionization potential of the donor. The greatest difficulty in using the perturbation theory explicitly in semi-empirical calculations is the evaluation of the perturbation terms.

In Murrell's treatment, the first-order approximations to the wave function for the N and E states are as expressed in

$$\phi_N' = \phi_D + c\phi_A \quad (19)$$

$$\phi_E' = \phi_A + d\phi_D \quad (20)$$

The coefficients c and d are obtained in the standard manner.²¹ Except for normalization, these functions

(20) J. C. Slater, "Quantum Theory of Molecules and Solids," McGraw-Hill Book Co., Inc., New York, N. Y., 1963, p. 142.

(21) L. Pauling and E. B. Wilson, Jr., "Introduction to Quantum Mechanics," McGraw-Hill Book Co., Inc., New York, N. Y., 1935, p. 159.

are very similar to those used in the present work; consequently, a second-order perturbation theory treatment of EDA complexes should give results similar to the LCMO treatment.

Charge-transfer spectra have frequently been used to estimate ionization potentials and electron affinities either by use of eq. 8a or simply by fitting known values of ionization potentials or electron affinities to a linear plot of observed CT spectra with a given acceptor or donor, and estimating values for the unknown substances from the plot. While this method has been useful, it can be seen from eq. 8 that it must be applied with caution. If, in the series chosen, either V_{es} or β_{DA} varies significantly, the validity of the estimated values will be doubtful. Values of ionization potentials obtained in this manner are

more likely to be reliable than are electron affinities, owing to the fact that a series of similar compounds for which ionization potentials are known is more often available than is the case with electron affinities. The results of parameter variation in this work imply that it might be possible to obtain reliable estimates of the electron affinities of the acceptors by using these and the V_{es} values as variation parameters and minimizing the error in both the transition energies and the relative stabilities with respect to them.

Acknowledgment. The author wishes to express his appreciation to the Cancer Association of Greater New Orleans for financial aid which helped make this research possible and to the L.S.U.N.O. Computing Center for generous use of the IBM 1620 computer.

The Measurement of Surface Tension by the Pendant Drop Technique

by Clyde E. Stauffer

The Procter and Gamble Company, Miami Valley Laboratories, Cincinnati, Ohio 45239
(Received December 18, 1964)

The Laplace equation describing the shape of a liquid drop being acted upon solely by gravitational and surface energy forces has been solved by a technique involving reiterated approximations, employing a high-speed digital computer for the purpose. This method of solution has been used to extend the table of $1/H$ as a function of S , quantities which are basic to the Andreas-Hauser-Tucker method of measuring surface tension by the pendant drop method, to lower values of S than are currently available. This extended table will make the pendant drop technique more widely usable. The statistical error inherent in the pendant drop technique has been evaluated and found to be greatly dependent upon the shape of the drop as expressed in the ratio S . More nearly spherical drops are inherently subject to greater imprecision in the measurement of their surface tension.

The shape of a liquid drop being acted upon solely by gravitational and surface energy forces is given by eq. 1.^{1,2}

$$\frac{1}{P} + \frac{\sin \phi}{X} = 2 + \beta Z \quad (1)$$

In this equation, P is the radius of curvature at the

point (X,Z) , ϕ is the angle made by the tangent at the point (X,Z) and the X coordinate axis, and β is the shape parameter, given by

(1) P. S. Laplace, "Mecanique Celeste," supplement to the 10th book, Duprat, Paris, 1806.

(2) F. Bashforth and J. C. Adams, "An Attempt to Test the Theories of Capillary Action," University Press, Cambridge, England, 1883.

$$\beta = -g\sigma b^2/\gamma \quad (2)$$

where g is the gravitational constant, σ is the effective density of the liquid drop (*i.e.*, the density of the liquid in the drop minus the density of the surrounding medium), γ is the surface or interfacial tension, and b is the radius of curvature at the origin. The unit of length used in eq. 1 is b , so that X , Z , and β are nondimensional. The sign for β follows the convention of Bashforth and Adams,² being negative for a pendant drop and positive for a sessile drop.

Equation 1 may be recast in the form of a differential equation by setting $1/P$ equal to $d\phi/ds$, where s is the linear distance along the drop profile. The resulting equation is not directly soluble at the present time. However, Bashforth and Adams,² using numerical integration techniques, solved the differential equation.

Andreas, Hauser, and Tucker³ suggested the use of the pendant drop technique for measurement of surface tension, but their method differed from earlier experimentalists in that they made measurements of the drop at two selected planes, measuring D_e , the diameter at the equatorial plane, and D_s , the diameter at the plane at a distance D_e from the tip of the drop. This obviated the necessity for determining such quantities as the position of the point of inflexion of the drop profile, which is very difficult to obtain with any degree of accuracy. On the other hand, the method of Andreas, *et al.*, made the solution of the fundamental equation for several values of β imperative, since the calculation of surface tension from the experimental data obtained required the use of a correction factor $1/H$, which is a function of the ratio D_s/D_e , or S . Andreas, *et al.*, were rather dubious of the mathematical methods available for solution of eq. 1, and preferred to construct the table of $1/H$ vs. S by empirical evaluation of $1/H$ using liquids of known surface tension.

Fordham⁴ and Niederhauser and Bartell⁵ independently solved the fundamental equation in order to obtain a theoretically sound table of $1/H$ vs. S . They both used numerical integration techniques, similar to or identical with the method of Bashforth and Adams.

Niederhauser and Bartell⁵ checked the consistency of their table by measuring the surface tension of water, using drops having S values from 0.68 to 0.99. They obtained the same value for surface tension with any size drops, and also showed that there was a systematic error in the table of Andreas, *et al.*, amounting to as much as 1.4%. Their table, and a short discussion of the pendant drop technique, is also published in Adamson's book on surface chemistry.⁶

Staicopolus⁷ solved the fundamental equation by use of first-order approximations for the derivatives, with a

very small interval of integration. High-speed digital computers made such a procedure feasible. He used positive values for β in order to apply the results to sessile drops, and expressed the resulting factors as polynomial coefficients rather than as a table of factors.

The table of $1/H$ vs. S published by Fordham and Niederhauser and Bartell covers a range of S values from 0.66 to 1.00. During the course of work in this laboratory, values for S less than 0.66 were often obtained. It is always a nuisance to change the size of the pendant drop in order to bring S above 0.66, and in some instances it was preferable not to disturb the droplet. Thus, a definite need for an extended table of $1/H$ vs. S was felt, and the present work was undertaken to fulfill that need.

Experimental

Method. The method used was one of reiterated approximations, using a digital computer for all calculations. The values of X , Z , ϕ , and $d\phi$ are given at the origin, and the values for the first three variables are estimated at the point which is a distance ds along the drop profile. An estimated $d\phi$ is calculated (from eq. 1), an adjusted value of ϕ is obtained, new values of X and Z are calculated at the point, a second estimate of $d\phi$ is calculated, and finally a second adjustment is made of ϕ . The calculation is then advanced forward to the next point.

The computer program was written so that any desired value of ds and β could be read into the computer at the beginning of the calculations, and with the option of beginning at the origin or at any point on the profile by supplying the appropriate values for X , Z , ϕ and $d\phi$. In practice, ds was usually 0.001, while β was varied from -0.0125 to -0.2375 in increments of 0.0125. Also, the calculation was carried out at other values of β for comparison with the results of Niederhauser and Bartell. The details of the calculations and the Fortran program are available upon request.

In order to obtain X_e , the radius of the drop at the equatorial plane, X was plotted vs. s around the point where ϕ had the value $\pi/2$. A smooth curve was drawn through the points, and X_e , the maximum value which X obtained, was read directly from the graph.

(3) J. M. Andreas, E. A. Houser, and W. B. Tucker, *J. Phys. Chem.*, **42**, 1001 (1938).

(4) S. Fordham, *Proc. Roy. Soc. (London)*, **A194**, 1 (1948).

(5) D. O. Niederhauser and F. E. Bartell, "Report of Progress-Fundamental Research on Occurrence and Recovery of Petroleum, 1948-1949," American Petroleum Institute, Baltimore, Md., 1950, pp. 114-146.

(6) A. W. Adamson, "Physical Chemistry of Surfaces," Interscience Publishers, Inc., New York, N. Y., 1960.

(7) D. N. Staicopolus, *J. Colloid Sci.*, **17**, 439 (1962).

Table I: Tabulation of Calculated Data

β	X_e	X_s	S	$1/H$
-0.0125	1.00209724	0.19759259	0.19717906	19.88093704
-0.0250	1.00422263	0.26332724	0.26221998	9.91607923
-0.0375	1.00637708	0.31117094	0.30919915	6.58244559
-0.0500	1.00856146	0.35027590	0.34730248	4.91547255
-0.0625	1.01077669	0.38404412	0.37994952	3.91516035
-0.0750	1.01302373	0.41416856	0.40884389	3.24923111
-0.0875	1.01530354	0.44163167	0.43497501	2.77166126
-0.1000	1.01761731	0.46706015	0.45897426	2.41418769
-0.1125	1.01996606	0.49088254	0.48127341	2.13607278
-0.1250	1.02235101	0.51340630	0.50218200	1.91350647
-0.1375	1.02477338	0.53486074	0.52193075	1.73133711
-0.1500	1.02723466	0.55542181	0.54069613	1.57946287
-0.1625	1.02973586	0.57522944	0.55861844	1.45089161
-0.1750	1.03227886	0.59439493	0.57580849	1.34062679
-0.1875	1.03486508	0.61301086	0.59235824	1.24500550
-0.2000	1.03749622	0.63115402	0.60834344	1.16128006
-0.2125	1.04017405	0.64888967	0.62382798	1.08734921
-0.2250	1.04290046	0.66627366	0.63886601	1.02157857
-0.2375	1.04567752	0.68335468	0.65350423	0.96267757

X_s was calculated by linear interpolation of X in terms of Z at the point where $Z = 2X_e$, *i.e.*, $Z = D_e$. The linearity of the relationship between Z and X in this limited region was verified by re-entering the calculations at successively smaller values of ds and obtaining values throughout this region. No discernible deviations from linearity were found in the eighth decimal place.

For each value of β , the values X_e and X_s so obtained were used to calculate the values pertinent for our purposes, according to the equations

$$S = X_s/X_e \quad (3)$$

$$1/H = -1/\beta(D_e)^2 = -1/4\beta(X_e)^2 \quad (4)$$

A list of the values so obtained is given in Table I.

Interpolation was done using Newton's method of interpolation with divided differences. The logarithm of $1/H$ was used in this interpolation to decrease the extreme contributions of the large differences at the small value of S . Differences up to and including the fourth one were used in the calculations. The resulting tabulation of $1/H$ vs. S , in increments of 0.001 in S , is presented in Table II.

In any work such as this, the question of accuracy is of prime importance. The calculations were done on an IBM 1620 digital computer with 12-digit precision, or on an IBM 7094 computer with 16-digit precision. Calculations done on both machines at one particular value of β gave results identical to the eighth decimal place. Results obtained from calculations with β equal to -0.20 , -0.30 , -0.375 , -0.45 , or -0.55 cor-

respond exactly with the numerical results published by Niederhauser and Bartell.⁵

The plot of X vs. s for the determination of X_e was exact in the seventh decimal place, and the value of X_e could be read to ± 1 in the eighth place. A difference table of X_e vs. β showed essentially zero third differences.

As mentioned above, the linearity of the plot of Z vs. X in the region of $Z = 2X_e$ was checked by recalculating the values of X and Z at successively smaller values of ds to a final ds of 0.000001. The plot of the values so obtained showed no deviation from linearity, although it was of such a scale that differences of ± 2 in the eighth place would have been easily discernible.

The difference table of X_s in terms of β did not readily go to zero at the lower values of β . This probably means only that X_s cannot be expressed as a simple polynomial function of β . The differencing, however, did not indicate the presence of mathematical errors in any particular term.

The use of no divided differences higher than the fourth in the interpolation step resulted in a maximum error of 1 in the fifth place in the natural logarithm of $1/H$, corresponding to less than 1 in the sixth place in the value of $1/H$. The value of $1/H$ at $S = 0.670$ agrees exactly with the value calculated by Niederhauser and Bartell,^{5,6} but in the S range 0.660-0.670, the values of $1/H$ given here are slightly lower than those found by Fordham.⁴

To check the unbiased nature of Table II, especially with respect to the table given by Niederhauser and

Table II: Tabulation of $1/H$ vs. S

S	0	1	2	3	4	5	6	7	8	9
0.30	7.09837	7.03966	6.98161	6.92421	6.86746	6.81135	6.75586	6.70099	6.64672	6.59306
0.31	6.53998	6.48748	6.43556	6.38421	6.33341	6.28317	6.23347	6.18431	6.13567	6.08756
0.32	6.03997	5.99288	5.94629	5.90019	5.85459	5.80946	5.76481	5.72063	5.67690	5.63364
0.33	5.59082	5.54845	5.50651	5.46501	5.42393	5.38327	5.34303	5.30320	5.26377	5.22474
0.34	5.18611	5.14786	5.11000	5.07252	5.03542	4.99868	4.96231	4.92629	4.89061	4.85527
0.35	4.82029	4.78564	4.75134	4.71737	4.68374	4.65043	4.61745	4.58479	4.55245	4.52042
0.36	4.48870	4.45729	4.42617	4.39536	4.36484	4.33461	4.30467	4.27501	4.24564	4.21654
0.37	4.18771	4.15916	4.13087	4.10285	4.07509	4.04759	4.02034	3.99334	3.96660	3.94010
0.38	3.91384	3.88786	3.86212	3.83661	3.81133	3.78627	3.76143	3.73682	3.71242	3.68824
0.39	3.66427	3.64051	3.61696	3.59362	3.57047	3.54752	3.52478	3.50223	3.47987	3.45770
0.40	3.43572	3.41393	3.39232	3.37089	3.34965	3.32858	3.30769	3.28698	3.26643	3.24606
0.41	3.22582	3.20576	3.18587	3.16614	3.14657	3.12717	3.10794	3.08886	3.06994	3.05118
0.42	3.03258	3.01413	2.99583	2.97769	2.95969	2.94184	2.92415	2.90659	2.88918	2.87192
0.43	2.85479	2.83781	2.82097	2.80426	2.78769	2.77125	2.75496	2.73880	2.72277	2.70687
0.44	2.69110	2.67545	2.65992	2.64452	2.62924	2.61408	2.59904	2.58412	2.56932	2.55463
0.45	2.54005	2.52559	2.51124	2.49700	2.48287	2.46885	2.45494	2.44114	2.42743	2.41384
0.46	2.40034	2.38695	2.37366	2.36047	2.34738	2.33439	2.32150	2.30870	2.29600	2.28339
0.47	2.27088	2.25846	2.24613	2.23390	2.22176	2.20970	2.19773	2.18586	2.17407	2.16236
0.48	2.15074	2.13921	2.12776	2.11640	2.10511	2.09391	2.08279	2.07175	2.06079	2.04991
0.49	2.03910	2.02838	2.01773	2.00715	1.99666	1.98623	1.97588	1.96561	1.95540	1.94527
0.50	1.93521	1.92522	1.91530	1.90545	1.89567	1.88596	1.87632	1.86674	1.85723	1.84778
0.51	1.83840	1.82909	1.81984	1.81065	1.80153	1.79247	1.78347	1.77453	1.76565	1.75683
0.52	1.74808	1.73938	1.73074	1.72216	1.71364	1.70517	1.69676	1.68841	1.68012	1.67188
0.53	1.66369	1.65556	1.64748	1.63946	1.63149	1.62357	1.61571	1.60790	1.60014	1.59242
0.54	1.58477	1.57716	1.56960	1.56209	1.55462	1.54721	1.53985	1.53253	1.52526	1.51804
0.55	1.51086	1.50373	1.49665	1.48961	1.48262	1.47567	1.46876	1.46190	1.45509	1.44831
0.56	1.44158	1.43489	1.42825	1.42164	1.41508	1.40856	1.40208	1.39564	1.38924	1.38288
0.57	1.37656	1.37028	1.36404	1.35784	1.35168	1.34555	1.33946	1.33341	1.32740	1.32142
0.58	1.31549	1.30958	1.30372	1.29788	1.29209	1.28633	1.28060	1.27491	1.26926	1.26364
0.59	1.25805	1.25250	1.24698	1.24149	1.23603	1.23061	1.22522	1.21987	1.21454	1.20925
0.60	1.20399	1.19875	1.19356	1.18839	1.18325	1.17814	1.17306	1.16801	1.16300	1.15801
0.61	9.15305	1.14812	1.14322	1.13834	1.13350	1.12868	1.12389	1.11913	1.11440	1.10969
0.62	1.10501	1.10036	1.09574	1.09114	1.08656	1.08202	1.07750	1.07300	1.06853	1.06409
0.63	1.05967	1.05528	1.05091	1.04657	1.04225	1.03796	1.03368	1.02944	1.02522	1.02102
0.64	1.01684	1.01269	1.00856	1.00446	1.00037	0.99631	0.99227	0.98826	0.98427	0.98029
0.65	0.97635	0.97242	0.96851	0.96463	0.96077	0.95692	0.95310	0.94930	0.94552	0.94176
0.66	0.93803	0.93431	0.93061	0.92693	0.92327	0.91964	0.91602	0.91242	0.90884	0.90528

Bartell, determinations of the interfacial tension between water and *n*-heptane were made. Three different tips were used, and approximately 12 drops were formed with each tip, photographed, and measured to obtain drop dimensions. The water was tap distilled water which had been deionized with a mixed ion-exchange resin. The *n*-heptane was a commercial product, b.p. 98–99°, which was treated three times with one-fifth of its volume of activated silica gel and was stored over silica gel. The *n*-heptane was held in a jacketed container held at 26° and the water droplet was expressed from a micrometer syringe. The range of S values represented in each group of droplets, the

average interfacial tension, and the standard deviation of each mean are presented in Table III. The differences between these values were not significant at the 5% level by Student's *t*-test.

Table III: Interfacial Tension of Water and *n*-Heptane

S , values, range	Interfacial tension, dynes/cm.	Std. dev. of the group	Numbers of droplets
0.54–0.57	50.11	±1.13	11
0.64–0.66	49.43	±0.85	11
0.70–0.72	50.34	±0.79	12

The first two values are in S ranges requiring the use of Table II, while in the calculation of the third value, Niederhauser and Bartell's table of $1/H$ vs. S was used. The consistency of the two tables is thus shown.

Possible Error in the Pendant Drop Method. In evaluating the experimental error in a method, the usual course is to estimate the percentage of error in each individual measurement and sum the estimates. In the pendant drop method of measuring surface tension, there are two experimental measurements to be made, D_e and D_s . A level of 0.1% accuracy is readily obtainable using reasonably careful measuring techniques, while if the drop were accurately photographed and the image then measured with a microcomparator, a claim of 0.01% accuracy would not seem outrageous. Such error estimates lead to a statement such as that found in Adamson,⁶ that the method is "good to a few tenths of a percent."

Owing to the particular manner in which the drop measurements are made and also to the nature of the subsequent calculations, the experimental errors are not simply additive, but tend rather to combine in a pseudo-exponential fashion. In addition, the magnitude of this large increase depends upon the shape of the drop, as exemplified by the ratio D_s/D_e ($= S$). The purpose of this section is to explore the nature of the error propagation in the pendant drop method, and to determine the connection between the probable experimental error, the shape parameter S , and the actual experimental error of measurement.

If one considers a drop as shown in Figure 1, the absolute error in measuring the diameter of the drop may be expressed as $\pm 2\epsilon$. The per cent error, e , is then given by

$$e = \frac{2\epsilon}{D_e} \times 100 \quad (5)$$

If the individually measured value of D_e is in error, for example if it is too large by the amount δ , then the wrong plane Z_s will be chosen for the measurement of D_s . As a result, the value of D_s will be, in this case, too small by the amount $2\delta\Delta X/\Delta Z$ (plus the experimental errors in determining Z_s and measuring D_s). These two errors will magnify each other in giving a calculated value of S which is smaller than the true value. From this a value of $1/H$ which is greater than the true figure is read from the table of correction factors and is inserted in the equation for the calculation of surface tension (eq. 6) along with the too large value of D_e . The combination of these two erroneously high

$$\gamma = g\Delta\rho(D_e)^2(1/H) \quad (6)$$

figures gives a calculated value of interfacial tension

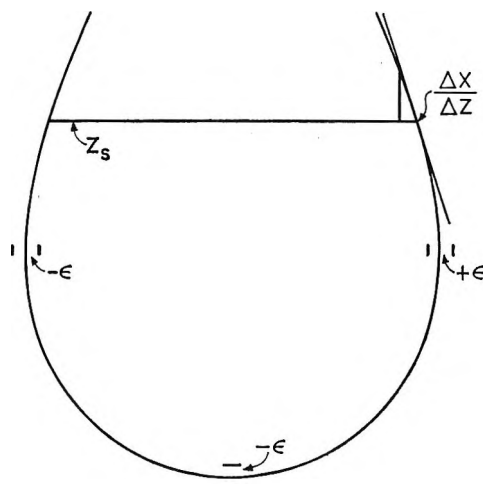


Figure 1. Pendant drop, showing error of measurement, ϵ .

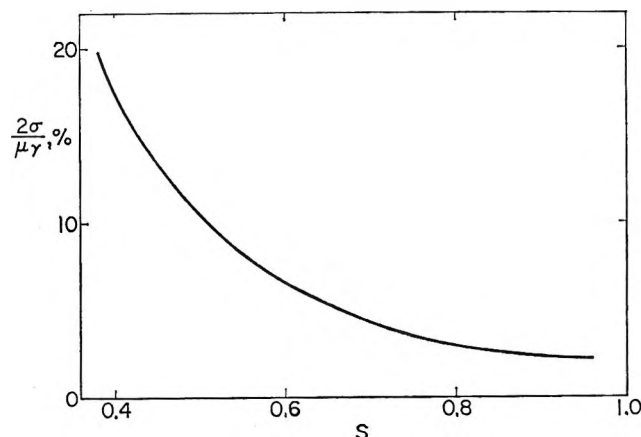


Figure 2. Probable limits of error in calculated surface tension as a function of drop shape.

Table IV: Probable Limits of Error in Surface Tension

S	$2\sigma\gamma/\mu\gamma, \%$
0.959	2.130
0.879	2.264
0.797	2.893
0.722	3.873
0.653	5.166
0.592	6.773
0.522	9.393
0.459	12.855
0.380	19.791

which is high, but by a factor which is more than just the sum of the measuring errors in D_e and D_s .

The propagation of errors in this method has been evaluated by considering the error of an individual measurement, $\pm\epsilon$, to represent the 95% confidence

limits $\pm 2\sigma$ (where σ represents the standard deviation of the individual measurement). Treating all measurements statistically and combining them in a straightforward algebraic manner, an estimate of the probable limits of the error in the true value of surface tension, μ_γ , is obtained. The variance of a single determination and calculation is $\pm \sigma_\gamma$, so to include 95% of the cases the limits were taken to be $\pm 2\sigma_\gamma$. The probable limits expressed as a percentage of true surface tension are given in Table IV. A per cent error of measurement, e , of 1% is assumed. For other per cent errors a simple

multiplication is all that is necessary. The details of the error analysis are available upon request.

The values of $2\sigma_\gamma$ are also plotted *vs.* S in Figure 2. From this plot the desirability of working at S ratios close to 1.0 is evident. Although this is not always feasible because of other factors, if one chooses (or is forced) to use more nearly spherical drops, of smaller S values, he should be aware of the loss of accuracy entailed thereby.⁸

(8) O. L. Davies, "Statistical Methods in Research and Production," Hafner, New York, N. Y., 1961.

Measurement by Benzoate Radiolytic Decarboxylation of Relative Rate Constants for Hydroxyl Radical Reactions

by R. W. Matthews and D. F. Sangster

Australian Atomic Energy Commission Research Establishment, Sutherland, Sydney, Australia
(Received December 23, 1964)

The decarboxylation of ¹⁴C carboxyl-labeled benzoate during the irradiation of a dilute, aerated aqueous solution by ionizing radiation has been studied. It was found that, in addition to the ¹⁴CO₂ produced during the irradiation, there was a post-irradiation production of further carbon dioxide during the following few hours. From the kinetic salt effect and competitor studies, it is concluded that the hydroxyl radical is involved in the production of all the carbon dioxide found. Provided comparisons are made at a set time, the system can be used to measure over-all reaction rates for solute-hydroxyl radical reactions relative to the benzoate- \cdot OH reaction rate. Values for 20 solutes are given and compared with some of the published values. The highest values found were 2.1 for ferrocyanide- \cdot OH and 2.4 for iodide- \cdot OH. Values found for the aromatic compounds studied lie between 0.39 for nitrobenzene and 1.6 for phenate. Where hydrogen abstraction is involved, lower values are found.

Introduction

Products which have been identified from the radiolysis of dilute aerated aqueous solutions of benzoic acid or benzoate salts are the three isomeric hydroxy acids, carbon dioxide from the carboxyl group,^{1,2} and a dialdehyde of unknown structure which is thought to be related to mucondialdehyde.³ Post-irradiation

effects have been observed in irradiated aqueous solutions of benzene,⁴ but none have been reported for

(1) H. Loebl, G. Stein, and J. Weiss, *J. Chem. Soc.*, 405 (1951); W. A. Armstrong, B. A. Black, and D. W. Grant, *J. Phys. Chem.*, **64**, 1415 (1960); A. Sugimori and G. Tsuchihashi, *Bull. Chem. Soc. Japan*, **33**, 713 (1960); A. Sakumoto and G. Tsuchihashi, *ibid.*, **34**, 660, 663 (1961).

(2) A. M. Downes, *Australian J. Chem.*, **11**, 154 (1958).

benzoate solutions. We have found that, in addition to the decarboxylation reaction which occurs during irradiation, there is a further production of carbon dioxide following removal of the solution from the radiation field.

The phenol found in irradiated solutions of benzene results from benzene-hydroxyl radical reactions⁴ so there is good reason for assuming that hydroxy acids would result from benzoate-hydroxyl radical reactions. Some suggestions have been made as to the mechanism of the decarboxylation reaction but, although these mechanisms involve the hydroxyl radical, no attempt has been made to establish that this is, in fact, the reactive species.

One of the most widely used methods for obtaining information on the mechanism of a radiation-induced reaction is to study the effect of known radical scavengers on the product yield. If satisfactory competitions can be established, the nature of the attacking radical and the relative rates of competing reactions can be determined.

This paper describes such a study. From the experimental results and the absence of salt effects, it is established that the same reactant—the hydroxyl radical—is involved in the production of all of the CO₂ found. It is found that the complication of the slow reaction does not invalidate the use of this system to measure directly relative rate constants for solute-hydroxyl radical reactions.

The hydroxyl radical is often the most reactive species present in dilute, aerated aqueous solutions subjected to ionizing radiation. Usually the other primary products of the radiolysis of water either react very slowly or are scavenged by the molecular oxygen present forming unreactive radicals. The determination of hydroxyl radical reaction rate constants is therefore necessary for an understanding of the radiolysis of aerated solutions.

Published values were reviewed by Ferradini.⁵ Since most of the determinations were carried out in a sulfuric acid medium, it is possible that some of the rates measured are appropriate to ·HSO₄ radical rather than the ·OH radical. Further, a number of the determinations were carried out using Fenton's reagent and doubts have been expressed regarding whether the reacting species produced by Fenton's reagent is the hydroxyl radical or some other entity.⁶

Subsequently, further determinations have been published of relative rate constants for the reactions between hydroxyl radical and a limited number of solutes, the reduction in product yield from the reference solute being measured as a function of the ratio of competitor concentration to solute concentration. Ra-

bani and Stein⁷ have used ferrocyanide-ferrocyanide as a reference system, Adams and Boag⁸ have used the optical density at 600 m μ of the carbonate transient species produced in pulse radiolysis, while Kraljic and Trumbore⁹ have measured the decolorization of *p*-nitrosodimethylaniline. Relative rate constants have been measured, using the radiolytic decarboxylation of benzoate ion as the reference system, for a number of competitors at pH 10.5–10.8 and for some of these at lower pH values down to pH 3. The values found are compared with those obtained by other authors, and their significance is discussed.

Experimental

Solutions. The water used was purified in an all-Pyrex apparatus by passing steam from demineralized water containing acid dichromate successively through alkaline permanganate and acid dichromate solutions and a final flask containing the condensate.

Benzoic acid,¹⁴ C-carboxyl-labeled, was diluted with inactive benzoic acid to a specific activity of about 0.7 mc./mmole. The mixture was purified by vacuum sublimation and an aqueous stock solution of concentration approximately 8×10^{-3} M was prepared. The competitors and inert salts used in the preparation of solutions were A.R. chemicals and where appropriate were freshly distilled.

The pH of each solution prepared for irradiation was adjusted if necessary by adding the calculated amount of sodium hydroxide solution or sulfuric acid solution. Precautions were taken before irradiation to exclude atmospheric carbon dioxide from alkaline solutions because this might act as a competitor for the radicals. The pH was checked with an E.I.L. pH meter.

Deoxygenated solutions were prepared by passing oxygen-free nitrogen through the solution for 2 hr. For the experiment using nitrous oxide, cylinder gas was dissolved at atmospheric pressure in deoxygenated solution. The tubes containing the solutions were wrapped in aluminum foil to prevent any photochemical decomposition.

Irradiations. Generally solutions of pH 10 or above

- (3) I. Loeff and A. J. Swallow, *J. Phys. Chem.*, **68**, 2470 (1964).
- (4) L. M. Dorfman, I. A. Taub, and R. E. Buhler, *J. Chem. Phys.*, **36**, 549 (1962).
- (5) C. Ferradini in H. J. Emeleus and A. G. Sharpe, Ed., "Advances in Inorganic Chemistry and Radiochemistry," Vol. III, Academic Press, New York, N. Y., 1962, p. 171.
- (6) A. E. Cahill and H. Taube, *J. Am. Chem. Soc.*, **74**, 2312 (1952); G. Buxton and W. K. Wilmarth, *J. Phys. Chem.*, **67**, 2835 (1963); A. O. Allen, *Radiation Res., Suppl. IV*, 54 (1964).
- (7) J. Rabani and G. Stein, *Trans. Faraday Soc.*, **58**, 2150 (1962).
- (8) G. E. Adams and J. W. Boag, *Proc. Chem. Soc.*, 112 (1964).
- (9) I. Kraljic and C. N. Trumbore, to be published.

were irradiated in Pyrex glass-stoppered test tubes. Deoxygenated solutions and solutions at pH less than 10 were irradiated in sealed tubes provided with two break-seals or in tubes provided with a water-lubricated vacuum stopcock.

Tubes with very little air space were used with solutions of benzene to minimize the escape of competitor. A parallel set of tubes was prepared under identical conditions but without benzoate or irradiation. The benzene concentration in these tubes was estimated spectrophotometrically at 254 $m\mu$ and the calculated concentration ratio for the irradiated tubes was corrected accordingly. The correction was 5%, which agreed with calculations based on vapor pressure data. It was found that if these precautions were not taken, very large errors could be incurred due to the volatility of the benzene from aqueous solution.¹⁰

The total dose given to each solution was about 35,000 rads (2.2×10^{18} e.v./ml.) at a dose rate of 116,000 rads/hr. (1.2×10^{17} e.v./ml. min) using a cobalt-60 γ -ray source. The tubes in each competitor series were irradiated simultaneously in a special holder. It had been found previously that dose differences between positions were less than $\pm 2\%$. The dose was estimated from ferrous sulfate dosimeters taking $G_{Fe^{3+}}$ to be 15.5. All irradiations were carried out at ambient temperature which was estimated to be 18–25°.

¹⁴CO₂ Analyses. In the case of the alkaline solutions, aliquots were taken for analysis at specified times after irradiation and placed in simple CO₂ recovery assemblies. A solution containing 20 mg. of inactive carrier sodium carbonate was added, the solutions were acidified, and 200 cc. of nitrogen was bubbled through the solution. Active spray was removed in a scrubber containing dilute sulfuric acid and the gas was then bubbled through a fine sintered disk into 12 ml. of a solution of ethanolamine in methanol (120 ml./l.).

For acid and deoxygenated solutions, the sealed tubes were connected to the CO₂ recovery line, the break-seals broken, carrier carbonate and acid added, and the ¹⁴CO₂ recovered from the whole of the solution. When tubes were fitted with a water-lubricated stopcock, a rubber serum cap was fitted over the free side arm of the stopcock, and a measured amount of alkaline sodium carbonate solution injected by a long hypodermic needle through the bore of the opened stopcock into the solutions. After shaking, the solutions were treated as for alkaline solutions.

Five milliliters of the absorption solution was mixed with 5 ml. of liquid scintillant (4 g. of PPO (2,5-diphenyloxazole) and 100 mg. of POPOP (1,4-bis-2-

(5-phenyloxazolyl)benzene)/l. of toluene) and counted in either a Tracerlab or Nuclear Enterprises liquid scintillation counting assembly. Appropriate blanks were determined from unirradiated solutions in each series of analyses. The activity of the benzoate in the unirradiated solutions was determined by adding 100 μ l. to the same scintillant mixture. More than 30,000 counts were taken in each case. The G_{CO_2} was calculated from these results. The over-all accuracy of each G value may be taken as better than $\pm 8\%$. The two counting assemblies gave identical G values.

Hydrogen Peroxide. For the determination of the yield of hydrogen peroxide, the Ti⁴⁺ method was used.¹¹ The more sensitive Ghormley method¹² was also tried but it was found that the I₃⁻ color faded too rapidly for an accurate estimate to be made.

Results and Discussion

Decarboxylation of Benzoate. Any ¹⁴CO₂ found must come from the carboxyl side chain of the benzoate, that is, from some decarboxylation reaction. Disparities between the results from early duplicate runs were traced to the post-irradiation production of ¹⁴CO₂. In Figure 1, G_{CO_2} is plotted against the time after irradiation of the analysis. The G_{CO_2} value increased rapidly during the first day to 0.9, then more slowly to 1.0 after 6 days. The yield of hydrogen peroxide is $G_{H_2O_2} = 2.2$. It was found that the addition of an equivalent quantity of hydrogen peroxide to benzoate

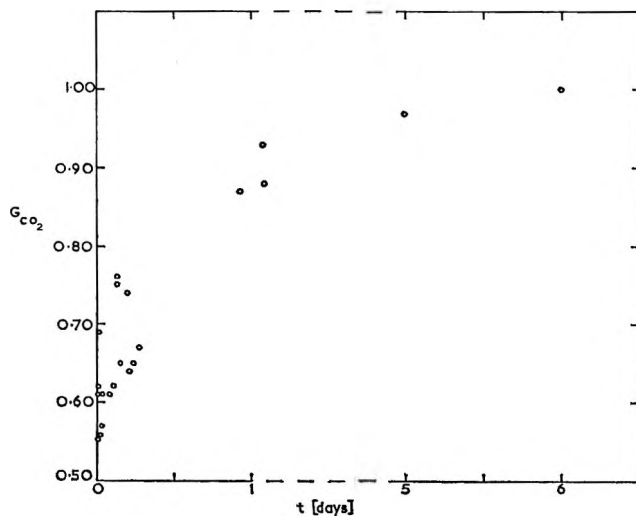


Figure 1. Post-irradiation effect.

(10) The authors wish to thank Dr. E. J. Hart for drawing this to their attention.

(11) G. M. Eisenberg, *Ind. Eng. Chem.*, **15**, 327 (1943).

(12) C. J. Hochanadel, *J. Phys. Chem.*, **56**, 587 (1952).

solution gave a negligible amount of carbon dioxide over several days (Table I).

Table I: G_{CO_2} Values from Irradiated Aerated Benzoate Solutions

Concn. of benzoate + benzoic, mM	pH	Added solute	Concn., mM	G_{CO_2}	Time after irradiation, hr.
0.6	3	Nil		0.61	1.2
0.7	7	Nil		0.72	0.8
0.7	10.5-10.8	Nil		0.63	0.9
0.7	10.8	H ₂ O ₂	0.07	0.02 ^a	48
0.8	10.7	Nil ^b		0.20	0.5
0.8	10.5	Ethanol	1.8	0.30	0.8
0.8	10.5	Ethanol	1.8	0.33	4.7
0.8	10.5	Ethanol K ₂ SO ₄	1.8 100	0.31	0.8
0.8	10.5	Ethanol K ₂ SO ₄	1.8 100	0.35	4.7
0.7	10.5	Benzene	1.5	0.18	1.1
0.8	10.7	Acetone	3	0.59	0.9
1.0	3.6	H ₂ O ₂	1000	2.7	0.8
0.7	3.6	N ₂ O ^b	1 atm.	0.79	0.6
0.8	10.8	Ethanol	2.26	0.31	0.83
6.4	10.8	Ethanol	18.1	0.34	0.83
0.8	10.8	Ethanol	2.26	0.37	5.0
6.4	10.8	Ethanol	18.1	0.37	5.0

^a Unirradiated solution—equivalent to G value for 35 krads.

^b Deoxygenated.

We have noted a similar post-irradiation decarboxylation in salicylate solutions. In this case, however, the production of carbon dioxide continued for 3 weeks or more after irradiation and the additional reaction possibly involved hydrogen peroxide and metal ion impurities. This may explain the high G_{CO_2} value found by Downes² for aqueous salicylate radiolysis.

Consequently, all measurements were taken within 6 hr. of irradiation and the time of analysis was noted. G_{CO_2} values quoted in the literature for benzoate or salicylate radiolysis at unspecified times after irradiation have only semiquantitative validity.

Preliminary experiments with benzoate solutions showed that the yield of ¹⁴CO₂ was independent of concentration above 0.4 mM and of total dose below about 40 krads. This shows that reactions involving the products of the radiolysis may be neglected. There was no evidence, up to this dose, of a break caused by an insufficiency of oxygen. All experiments were therefore carried out within these limits.

It can be seen (Table I) that decarboxylation is considerably less in deoxygenated solutions. Presumably oxygen reacts with the benzoate-hydroxyl radical

addition complex in the same way as it reacts with the benzene-hydroxyl radical complex.⁴

Identification of Reacting Radical. Results of experiments carried out to identify the reacting radical are given in Table I. Although in some cases it must be modified to have quantitative significance,¹³ the kinetic salt effect has been used to determine the sign of the charge on reacting species produced during the radiolysis of aqueous solutions.¹⁴ The addition of 0.1 M potassium sulfate or 0.1 M sodium perchlorate did not alter the yield of carbon dioxide from benzoate in the presence of a known amount of uncharged competitor ethanol. This demonstrates that the attacking species in both prompt and post-irradiation decarboxylation is uncharged.

Of the species known to be produced during the radiolysis of water, molecular hydrogen is unreactive and hydrogen peroxide reacts too slowly to be responsible for the carbon dioxide observed within a few hours of the irradiation. The hydrogen atom reacts much more readily with the oxygen in aerated solution than with benzene.¹⁵ Since benzene is an effective competitor, the hydrogen atom cannot be the decarboxylating species. Further, oxygen would be a competitor whereas, in fact, the ¹⁴CO₂ yield was lower in deoxygenated solution. G_{H} in neutral solution is about 0.5 so the hydrogen atom alone could not account for all the ¹⁴CO₂ found within 1 day of irradiation.

The product of the reaction between H atom and molecular oxygen is the hydroperoxyl radical, HO₂. This is reported to be fairly unreactive toward benzene, the evidence for this being summarized by Smith and Norman.¹⁶ Systems in which the hydroperoxyl radical has been identified by electron spin resonance spectroscopy are barely effective in oxidizing benzene. Since benzene is an effective competitor, HO₂ is not the decarboxylating species. At pH >6, HO₂ will ionize rapidly (within 1 μsec.)¹⁷ giving O₂⁻. Since this is charged, it cannot be the decarboxylating species. O₂⁻ is also the product of the oxygen-electron reaction. Since the electron scavenger, acetone, present at a concentration of 10 times the benzoate concentration has little effect on the ¹⁴CO₂ yield, this is

(13) B. Perlmutter-Hayman and G. Stein, *J. Chem. Phys.*, **40**, 848 (1964).

(14) G. Czapski and H. A. Schwarz, *J. Phys. Chem.*, **66**, 471 (1962); E. Collinson, F. S. Dainton, D. R. Smith, and S. Tazuka, *Proc. Chem. Soc.*, 140 (1962); E. J. Hart and J. W. Boag, *J. Am. Chem. Soc.*, **84**, 4090 (1962); A. Hummell and A. O. Allen, *Radiation Res.*, **17**, 302 (1962).

(15) P. V. Phung and M. Burton, *ibid.*, **7**, 199 (1957).

(16) J. R. L. Smith and R. O. C. Norman, *J. Chem. Soc.*, 2897 (1963).

(17) G. Czapski and B. H. J. Bielski, *J. Phys. Chem.*, **67**, 2180 (1963).

additional proof that neither the hydrated electron nor the hydroperoxyl anion effect decarboxylation.

This leaves only the hydroxyl radical and none of the experimental observations are inconsistent with the proposition that the hydroxyl radical is the decarboxylating species. Evidence that the hydroxyl radical is involved is shown in the following paragraphs.

(1) Among the products from the radiolysis of aerated benzoate solutions are the three isomeric hydroxy acids.^{1,2} As noted earlier, it can be reasonably assumed that these hydroxy acids result from benzoate-hydroxyl reactions. From Table II it can be seen that the sum of the G values of the products equals 2.4 which is the hydroxyl radical primary yield. However, it should be noted that Loeff and Swallow³ have recently published values for hydroxylation products which are rather lower than those found by other authors. Their results are given for comparison in Table II.

Table II: Yields of Hydroxylation Products

	G values		
	pH 4	pH 6.5	pH 6.8-8.3
<i>o</i> -Hydroxybenzoic acid	0.74	0.67	0.62
<i>m</i> -Hydroxybenzoic acid	0.42	0.37	0.32
<i>p</i> -Hydroxybenzoic acid	0.33	0.37	0.26
	1.49 ^a	1.41 ^b	1.2
Dialdehyde			~0.5
CO ₂	0.9-1.0 ^c	0.9-1.0 ^c	0.75
	2.4-2.5	2.3-2.4	2.45 ^d

^a See ref. 2. ^b See Armstrong, Black, and Grant, ref. 1.

^c At 1-6 days after irradiation. ^d See ref. 3.

(2) In 1 M hydrogen peroxide there is a greater yield of hydroxyl radical¹⁸ and a much greater yield of CO₂ was found.

(3) In the presence of nitrous oxide in deoxygenated solution a greater yield of CO₂ is found—the hydrated electrons present being converted to hydroxyl radicals to increase the effective number of hydroxyl radicals.¹⁹

(4) The carbon dioxide yield is markedly decreased by known hydroxyl radical scavengers such as iodide, ferrocyanide, benzene, formate, and ethanol, and it will be shown that the relative rate constants found are in good agreement with those found by other authors.

Mechanism of Decarboxylation. Experimental values of G_{CO_2} measured soon after removal from the radiation field could not be reproduced accurately enough to enable an extrapolation to be made to zero time. We are, therefore, unable to say whether all of the CO₂ results

from one reaction, the later stages of which are observed as the post-irradiation effect, or whether there is an additional reaction giving some of the CO₂ and complete before removal from the radiation field, that is in seconds or milliseconds. Expressed another way, we have been unable to determine whether k_x of the next section is negligible or significant.

Armstrong, Black, and Grant¹ have pointed out that the absence of sufficient phenol in the radiolytic products shows that it is unlikely that the reaction involves electron transfer from benzoate to the hydroxyl radical giving the well-known benzoate radical which subsequently decomposes to carbon dioxide.

Loeff and Swallow³ have further discussed this question and favor decomposition of the oxygen addition complex of the hydroxycyclohexadienyl carboxylate to give phenol, CO₂, and HO₂. Like Armstrong, Black, and Grant,¹ we have been unable to find phenol. We have, however, found the corresponding compound catechol with $G \approx 0.3$ from radiolysis of salicylate. We are carrying out further investigations into the mechanism of the decarboxylation reactions. Results suggest that some of the CO₂ found could arise from hydroxyl radical attack on the ring C atom to which the carboxylate group is attached.

Competitor Studies. The following relationship can be applied to the system, assuming simple competition for OH radicals between benzoate and added solute.²⁰

$$\frac{1}{G_{P_1}} = \frac{1}{G_R} \left\{ \frac{k_a}{k_x + qk_y} + \frac{k_b}{k_x + qk_y} \frac{[B]}{[A]} \right\}$$

where G_{P_1} and G_R are the yields of ¹⁴CO₂ and ·OH radical, respectively, expressed as molecules/100 e.v. absorbed by the solution, k_a is the rate constant for the total reaction or the sum of all the rate constants for the reactions (benzoate-·OH), k_b is the corresponding rate constant for (competitor-·OH) and square brackets denote molar concentrations. k_x and k_y are rate constants for the reactions producing ¹⁴CO₂⁻, each molecule of the immediate product of reaction y having given rise to the fraction q molecules of ¹⁴CO₂ at the time the ¹⁴CO₂ was measured. The graph of $1/G_{P_1}$ against $[B]/[A]$ is a straight line with slope = $k_b/G_R (k_x + qk_y)$, intercept = $k_a/G_R (k_x + qk_y)$, and slope/intercept = k_b/k_a . The last ratio is the reaction rate for the total reaction (competitor-·OH) relative to that for (benzoate-·OH) and if q is constant for

(18) A. O. Allen, "Radiation Chemistry of Water and Aqueous Solutions," D. Van Nostrand Co., Inc., Princeton, N. J., 1961, p. 102.

(19) F. S. Dainton and D. B. Peterson, *Nature*, **186**, 878 (1960).

(20) R. W. Matthews and D. F. Sangster, Australian Atomic Energy Commission, AAEC/TM282, 3 (1965).

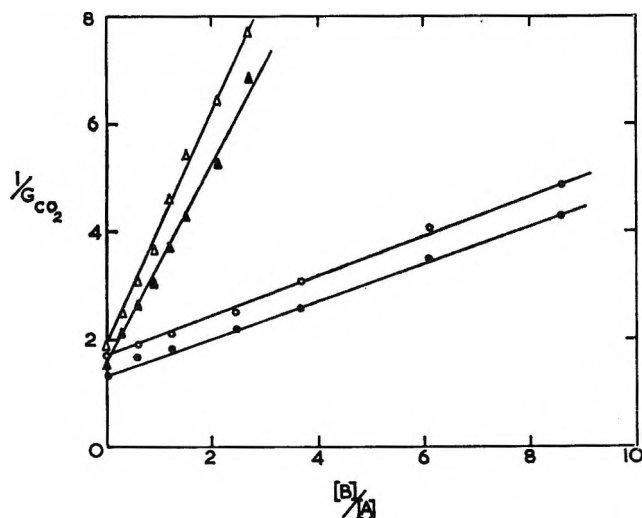


Figure 2. Relationship between $1/G_{CO_2}$ measured at two different times after irradiation, and competitor:benzoate concentration ratio. The lines have been computed from the experimental points using regression analysis: Δ , benzene competitor at 0.8 hr., slope/intercept = 1.16 ± 0.06 ; \blacktriangle , benzene competitor at 5.0 hr., slope/intercept = 1.28 ± 0.09 ; \circ , ethanol competitor at 1.0 hr., slope/intercept = 0.29 ± 0.02 ; \bullet , ethanol competitor at 5.0 hr., slope/intercept = 0.27 ± 0.01 .

measurements made at a given set time after irradiation this relative rate is independent of q , *i.e.*, of the time.

An examination of the results for benzene and ethanol competitors plotted in Figure 2 reveals that for each competitor the points lie on straight lines and although the two lines have different slopes and intercepts, the ratios of reaction rates at the two times are in good agreement. Expressed in another way, the ratios of G_{CO_2} at the longer time, t_2 , to G_{CO_2} at the shorter time, t_1 , are given by $(k_x + q_2k_y)/(k_x + q_1k_y)$ and are found to be constant for any one competitor within the estimated experimental accuracy of $\pm 5\%$ for these ratios. The ratios found for benzene varied between 1.25 and 1.12; those for ethanol, between 1.23 and 1.12. Relative rate constants have been determined at two intervals for over a dozen competitors of differing chemical properties and in no case have there been any departures from straight lines or any differences (greater than the experimental error) between the two values found for relative rate constants.

There remains the possibility that the added solute might not compete for the reacting radical but might prevent the reaction proceeding to completion, *e.g.*, by combining with the immediate product of the benzoate-radical reaction. It was found for ethanol competitor that G_{CO_2} was constant for a given ethanol-benzoate concentration ratio when the concentration

of both solutes was increased eightfold (Table I). This is evidence that the ethanol was reacting directly with the radical itself. Since the $^{14}CO_2$ was always low in the unirradiated blanks there is no possibility that benzoate-competitor reactions produced $^{14}CO_2$. It is deduced that all of the $^{14}CO_2$ produced during the irradiation and the first few hours after irradiation arose from one or more reactions between a single radical—the hydroxyl radical—and benzoate.

Relative Rate Constants. Relative rate constants were computed from the experimental data using

Table III: Experimental Values for Relative Rate Constants

Competitor	pH	t , hr.	k_b/k_a	Mean k_b/k_a
Iodide	10.5	1.1	2.37 ± 0.12	2.37
		2.5	1.69 ± 0.17	
		7	2.20 ± 0.14	
Ferrocyanide	7	0.8	2.20 ± 0.14	2.1
		3.0	2.29 ± 0.31	
		3.0	2.29 ± 0.31	
Phenate	10.7	0.8	1.65 ± 0.13	1.62
		2.9	1.59 ± 0.08	
Aniline	10.7	0.5	1.28 ± 0.15	1.24
		3.2	1.20 ± 0.16	
Benzene	10.5	0.8	1.16 ± 0.06	1.22
		5.0	1.28 ± 0.09	
		3	1.21 ± 0.05	
Phenol	7	4.8	0.97 ± 0.04	1.09
		0.8	1.18 ± 0.12	
		4.6	0.98 ± 0.05	
Salicylate	10.7	0.5	1.03 ± 0.03	1.01
		5.0	0.99 ± 0.06	
Benzoate	10.7		1.00	1.00
		7	1.00	
Benzoic acid	3		1.00	1.00
Benzonitrile	10.7	0.8	0.53 ± 0.01	0.59
		4.1	0.65 ± 0.04	
Chlorobenzene	10.7	0.8	1.19	1.10
		4.3	1.00	
Nitrobenzene	10.5	0.7	0.40 ± 0.02	0.39
		4.2	0.38 ± 0.02	
Formate	10.7	0.7	0.60 ± 0.06	0.62
		2.2	0.64 ± 0.02	
Acrylamide	10.7	0.9	0.59 ± 0.03	0.59
Glycine	10.5	0.7	0.44 ± 0.03	0.47
		4.7	0.49 ± 0.04	
Ethanol	10.5	1.0	0.29 ± 0.02	0.28
		5.0	0.27 ± 0.01	
Bromide	3	0.7	0.29 ± 0.01	0.29
		10.5	1.0	
Methanol	7	0.7	0.21 ± 0.01	0.20
		10.5	0.7	
Acetone	10.5	4.7	0.17 ± 0.01	0.17
		3.4	0.016 ± 0.007	
Acetate	10.7	0.8	0.011 ± 0.0008	0.011
		2.7	0.011 ± 0.0009	
Carbonate	10.5	1.0	0.08 ± 0.04	~ 0.08

regression analysis. The results obtained are listed in Table III. The pH quoted is the initial pH before irradiation and t (hours) is the time after irradiation that analysis was commenced. For purposes of calculation, results are sometimes given to three figures but the order of accuracy is about 10%. The limits given are standard deviations.

Most experiments were carried out at pH 10.5–10.8. Alkaline conditions were chosen in order to facilitate the experimental arrangements, the $^{14}\text{CO}_2$ produced being trapped in the solution until released by acid. Dainton and Peterson and Dainton and Watt²¹ have shown that there appears to be no change in the yields of the primary products from the radiolysis of water between pH 3 and 11. Rabani and Matheson²² have determined the pK for $\cdot\text{OH}$ ionization to be 11.9. During irradiation the pH of benzoate solutions, initially 10.8, decreased to 10.2 (we have no explanation for the magnitude of this decrease). This means that over 95% of the hydroxyl radical is present in the unionized form. Measurement at pH ~ 7 gave the same relative reaction rate constants.

An attempt was made to measure the relative rate constant for hydroxyl–nitrite reaction but the scatter of points was too great to enable conclusions to be drawn. In this case we think that other reactions may occur and the system cannot be used for measuring this relative rate constant.

Comparison with Other Authors. In Table IV the relative rate constants determined by this method are compared with those found by other authors. Since these are relative values, their relationship is not affected by multiplying by the same factor. It is found that good correspondence is obtained if the values given in Table IV of the paper by Rabani and Stein⁷ are multiplied by 0.0272, those of Adams and Boag⁸ by 0.096, those of Kraljic and Trumbore⁹ by 0.0216, and those of Merz and Waters²³ by 0.073.

The good agreement among these results confirms that it is the hydroxyl radical which brings about the decarboxylation and that the benzoate system can be used to measure relative rate constants for hydroxyl radical reactions. It should be noted that in each case what is measured is the sum of the rate constants of all the reactions between the competitor and radical relative to the sum for benzoate and radical regardless of what the products are.²⁰ For this reason we have not attempted to compare our results with those measured by other authors for solute–radical reactions giving a particular product. The values compared in Table IV are for total reaction rates in all cases.

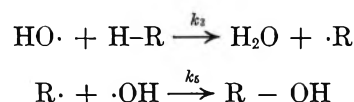
The mechanism used by Merz and Waters²³ in their derivation of the kinetic equations for nonchain re-

Table IV: Comparison with Published Values for OH Relative Reaction Rates

	This work pH 10	Merz and Waters ^a pH 1	Rabani and Stein ^b pH 2.5–10.5	Adams and Boag ^c pH 11	Kraljic and Trumbore ^d pH 9
Iodide	2.4				2.5
Ferro- cyanide	2.1		2.3		2.2
Benzene	1.2	0.23 (—)			
Benzoate	1.0	0.5 (1.0)			
Formate	0.62		0.6		
Nitroben- zene	0.39	0.21 (0.42)			
Ethanol	0.28	0.28	0.26	0.27	0.32
Bromide	0.21			0.16	0.19
Methanol	0.17	0.17			0.19
Carbonate	~ 0.08			0.10	
Acetate	~ 0.016				0.015
Chloride	Very low				< 0.0002

^a See ref. 23. Values multiplied by 0.073. Figures in parentheses are adjusted values. ^b See ref. 7. Values multiplied by 0.0272. ^c See ref. 8. Values multiplied by 0.096. ^d See ref. 9. Values multiplied by 0.0216.

actions included their eq. 3 and 5. The reaction



between $\cdot\text{OH}$ and an aromatic solute is addition⁴ to form H-R-OH rather than the hydrogen abstraction of eq. 3. This does not affect the validity of the equations they derive. However, it is doubtful if the reaction represented by eq. 5 proceeds to any extent with aromatic compounds. RH is present in high concentration compared with HR-OH which is removed mainly by second-order reactions, *e.g.*, dimerization or disproportionation in deaerated solution and reaction with oxygen in aerated solution giving a low steady-state concentration. Since k_3 is of the order of $3 \times 10^9 \text{ M}^{-1} \text{ sec}^{-1}$,²⁴ most of the $\cdot\text{OH}$ will be removed by reaction with ferrous ion or with the solute. The kinetic equations derived by omitting eq. 5 lead to a value of the rate constant relative to the $\text{Fe}^{+2}\cdot\text{OH}$

(21) F. S. Dainton and D. B. Peterson, *Proc. Roy. Soc. (London)*, **A267**, 443 (1962); F. S. Dainton and W. S. Watt, *Nature*, **195**, 1294 (1962); *Proc. Roy. Soc. (London)*, **A275**, 447 (1963).

(22) J. Rabani and M. S. Matheson, *J. Am. Chem. Soc.*, **86**, 3175 (1964).

(23) J. H. Merz and W. A. Waters, *J. Chem. Soc.*, S20 (1949); 2427 (1949).

(24) L. M. Dorfman, I. A. Taub, and D. A. Harter, *J. Chem. Phys.*, **41**, 2954 (1964).

reaction rate twice that given in Table I of their second paper (see Appendix).

When this correction is applied to the aromatic compounds (values in parentheses in Table IV) there is excellent agreement between the values except in the case of benzene. Since Merz and Waters do not appear to have taken any precautions to prevent the volatilization of benzene from the solution, this could account for that difference. The rate calculated does, in fact, agree with that found by us in early experiments with stoppered tubes with considerable air space. There are doubts concerning the reactions between Fenton's reagent and ethanol and more experimental work is required to elucidate these. From the comparisons in Table IV there appears to be no distinction between the $\cdot\text{OH}$ of Fenton's reagents and that of aqueous radiolysis (compare ref. 6).

When the values found are compared with those given by Ferradini,⁵ other disparities emerge. Acrylamide is by no means as efficient a hydroxyl radical scavenger as would be indicated by the figure she has quoted. Phenol in its acid form has been reported to react slowly with hydroxyl radical in acid solution. We have found that in neutral solution it reacts at much the same rate as does benzene. The anion, phenate, reacts more readily. In this case there may be some electron transfer from the O^- group contributing to the total rate as well as or in place of the hydroxyl ring addition.

Comparison between Classes of Compounds. The values for iodide- $\cdot\text{OH}$ and ferrocyanide- $\cdot\text{OH}$ were the highest (2.4 and 2.1) and these reactions must approach being diffusion controlled, reaction occurring at nearly every encounter. The chloride- $\cdot\text{OH}$ rate is very low at pH 10.

All aromatics tested were found to react with hydroxyl radical readily and at much the same rate in contrast to the markedly different rates for the same series of aromatic compounds undergoing an ionic reaction. The values found lie between 1.62 for phenate- $\cdot\text{OH}$ and 0.39 for nitrobenzene- $\cdot\text{OH}$. These are usually considered to be the two extremes for ring activation and deactivation by a single substituent. The relative rate found for ethanol at pH 10.5 is the same as that at pH 3. The reference solute is present as benzoate anion and benzoic acid, respectively, at these two pH values. Since the form of the competitor does not change, its specific rate constant does not change. Therefore benzoate anion and benzoic acid have the same total specific reaction rate. We are continuing to investigate the reactions between aromatic compounds and the hydroxyl radical.

Where the predominant reaction is hydrogen ab-

straction rather than charge transfer or hydroxyl addition, the rates are slower. Methanol is less reactive than is ethanol, showing that it is more difficult to remove H from a CH_3 group than from a CH_2 group α to $-\text{OH}$.²⁵ The influence of the NH_2 group can be seen when the rate for glycine is compared with that for acetate, although the pH is too close to the pK_a of glycine to enable quantitative conclusions to be drawn. The rates for acetone and acetate are low and beyond the range of applicability of the system; small quantities of impurities could affect the values. These are representative of the three classes of hydroxyl radical reactions: electron transfer, double bond addition, and hydrogen abstraction.

Advantages of This Method. For the determination of relative rate constants, the labeled benzoate decarboxylation system has advantages similar in some degree to most other systems used in determining relative rate constants. Providing a linear relationship is obtained, the total reaction rates can be compared without having a detailed knowledge of all of the radiation chemical reactions of reference solute or of any of the radiation chemical reactions of the competitor. The exact dose of ionizing radiation given to the solution does not have to be known provided all samples are given the same dose and it is less than 50,000 rads.

There are in addition some advantages specific to the method. There are no doubts concerning the origin and nature of the product measured; it must arise from the carboxyl group of the benzoate present and must be carbon dioxide. There is no interference from a similar or chemically identical product arising from an added competitor as sometimes occurs in methods based on spectrophotometric measurements. Furthermore, there is little possibility of the $^{14}\text{CO}_2$ reacting with the competitor or its product giving a compound which does not liberate carbon dioxide on reaction with acid.

The chief disadvantages are the presence of the post-irradiation reactions for which due allowance must be made and the fact that the method is more time-consuming than, say, taking a direct spectrophotometric measurement. Further, it is necessary to have available an accurate and precise method of counting $^{14}\text{CO}_2$. Competitors which react with benzoate, e.g., to give $^{14}\text{CO}_2$ or an insoluble precipitate cannot be studied.

The system has possibilities for further development at low doses, since analysis for $^{14}\text{CO}_2$ can be made extremely sensitive,² and over a wider range of concentration, pH, and temperature.

(25) W. T. Dixon and R. O. C. Norman, *J. Chem. Soc.*, 3119 (1963).

Intercomparison of relative rate constants found by reference to different systems is valuable not only in establishing the validity of these systems and of the values obtained but also in revealing disparities. Such a disparity indicates that a complexity exists in the reactions between the competitor and the reference system and this complexity may merit further investigation.

Absolute Rate Constants. Some of the recently published values of absolute rate constants for hydroxyl radical reactions are given in Table V. Since the phenol yield from irradiated aqueous benzene approaches 100% of the hydroxyl radical yield, this suggests that the transient species hydroxyl cyclohexadienyl radical measured at 313 m μ is the only primary product of the attack of hydroxyl radical on benzene in dilute aqueous solution. It follows that the rate of its appearance should be the total (benzene-hydroxyl radical) reaction rate and may be directly compared with our values. In the case of benzoic acid, it has not been established that the transient at 340 m μ represents all of the (benzoic acid-hydroxyl radical) reaction. However, the ratio between the absolute values for the benzoic acid and the benzene rate constants given by Dorfman, Taub, and Harter²⁴ agree within the experimental errors with our relative values.

Table V: Comparison with Published Values for OH Absolute Reaction Rates

	This work	Absolute values $\times 10^{-9} M^{-1} \text{sec.}^{-1}$	Ratio $\times 10^{-9}$
Ferrocyanide	2.1	11 ± 2^a	5.3
Benzene	1.2	3.3 ± 0.8^b	2.7
Benzoic acid	1.0	2.1 ± 0.3^b	2.1

^a See ref. 22. ^b See ref. 24.

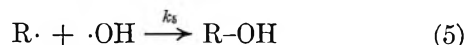
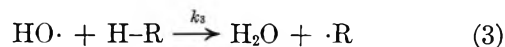
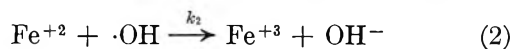
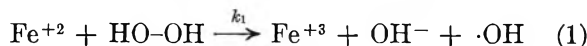
The absolute value given by Rabani and Matheson²² has also been shown to represent the over-all reaction between ferrocyanide and hydroxyl radical. Yet, it can be seen from the last column of Table V that the relative values we have determined do not agree with the ratio of the two independent absolute rate constant determinations which have been made on these compounds. The reason for this is not obvious.

Aside from measurement errors, it can be due to errors of interpretation, there being reactions occurring in the systems in addition to those already postulated. Until this has been resolved, we cannot suggest the factor by which the values in Table III must be multiplied to convert to absolute rate constants.

Acknowledgments. The authors wish to thank Mr. B. O'Leary for irradiating the samples, Mr. D. Davy for his help with instrumentation for liquid scintillation counting, and Mr. D. O'Regan for technical assistance.

Appendix

Merz and Waters²³ give the following equations representing the chemical reactions which take place when Fenton's reagent reacts with a solute that does not participate in a chain reaction. Their equation numbering has been followed and their eq. 4 which applies only to chain oxidations has been omitted.



and derive the relationships

$$\frac{-d[\text{H}_2\text{O}_2]}{-d[\text{R-H}]} = 2 + \frac{k_2}{k_3} \times \frac{[\text{Fe}^{+2}]}{[\text{R-H}]} \quad (\text{G})$$

$$\frac{[\Delta\text{H}_2\text{O}_2]}{[\Delta\text{R-H}]} = \frac{[\Delta\text{H}_2\text{O}_2]}{[\Delta\text{H}_2\text{O}_2 - \Delta\text{Fe}^{+2}]} \quad (\text{as equivalents})$$

The graph of $\Delta\text{H}_2\text{O}_2$ against $\Delta\text{H}_2\text{O}_2 - \Delta\text{Fe}^{+2}$ was found to be a straight line with intercept 2 and slope k_2/k_3 . If eq. 5 is omitted, the relationships become

$$\frac{-d[\text{H}_2\text{O}_2]}{-d[\text{R-H}]} = 1 + \frac{k_2}{k_3} \times \frac{[\text{Fe}^{+2}]}{[\text{RH}]} \quad (\text{G}')$$

$$\frac{[\Delta\text{H}_2\text{O}_2]}{[\Delta\text{R-H}]} = \frac{[\Delta\text{H}_2\text{O}_2]}{1/2[\Delta\text{H}_2\text{O}_2 - \Delta\text{Fe}^{+2}]} \quad (\text{as equivalents})$$

and the graph of $\Delta\text{H}_2\text{O}_2$ against $\Delta\text{H}_2\text{O}_2 - \Delta\text{Fe}^{+2}$ would once again be a straight line with intercept 2 but with slope $2k_2/k_3$. Hence their values of k_3/k_2 for aromatic compounds and nonchain oxidations should be multiplied by 2 to give the correct values.

Carbon-13 Chemical Shifts of Vinyl Carbons

by Gary E. Maciel

Department of Chemistry, University of California, Davis, California (Received December 14, 1964)

The C^{13} chemical shifts $\delta_{C\alpha}$ and $\delta_{C\beta}$ were determined for 17 vinyl compounds $C_{\beta}H_2=C_{\alpha}H-X$ with a wide variety of substituents X. The chemical shifts of the α -carbon atom were found to cover a range of 67.5 p.p.m., while the span of $\delta_{C\beta}$ was found to be 57.5 p.p.m. No simple relationships between these carbon shifts and the corresponding proton shifts were evident. Rough linear relationships were demonstrated between $\delta_{C\alpha}$ and the corresponding C^{13} shifts of the substituted carbon atom in phenyl compounds, and between $\delta_{C\beta}$ and the *ortho* carbon shifts in phenyl compounds. These correlations are interpreted as due to similar inductive, resonance, and neighbor effects in both sets of compounds as a result of similar electronic structures and molecular geometries. A linear correlation was not found between $\delta_{C\alpha}$ and the carbon C^{13} shifts in corresponding acetyl compounds.

Introduction

The many investigations of C^{13} magnetic resonance spectroscopy of the past few years¹⁻²⁶ have included systematic studies of the relationships between C^{13} chemical shifts and structural details in alkanes¹⁻⁴ and substituted alkanes,⁵⁻⁷ aromatic hydrocarbons,⁸⁻¹⁰ substituted benzenes,^{9,11-19} carbonyl compounds,^{7,13,20-24} and alkynes.^{4,22,24} The trends observed in these studies have led to correlations of interest from both a theoretical and practical point of view, and have pointed the way to promising avenues of future research.

Carbon-13 shifts have been reported for several olefinic compounds,^{4,24-26} but data on an extensive and related series of similarly substituted ethylenes have not been available. The absence of such data has contributed to the difficulty of satisfactorily interpreting C^{13} chemical shifts in other classes of compounds in which the carbon hybridization is the sp^2 type. In this paper we report the C^{13} shifts of 17 vinyl compounds $C_{\beta}H_2=C_{\alpha}H-X$ and compare the shifts with those in analogously substituted phenyl and acetyl compounds.

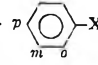
Experimental

Carbon-13 Magnetic Resonance Measurements. The C^{13} n.m.r. spectra were obtained at a frequency of 15.085 Mc./sec. by measuring the resonance of C^{13} in natural abundance, using Varian equipment and the rapid passage, dispersion mode technique described previously by Lauterbur.⁸ For most of the spectra, the

sample container was similar to that described by Spiesscke and Schneider⁶ except that no provision was

- (1) E. G. Paul and D. M. Grant, *J. Am. Chem. Soc.*, **86**, 2977 (1964).
- (2) D. M. Grant and E. G. Paul, *ibid.*, **86**, 2984 (1964).
- (3) J. J. Burke and P. C. Lauterbur, *ibid.*, **86**, 1870 (1964).
- (4) R. A. Friedel and H. L. Reichofsky, *ibid.*, **85**, 1300 (1963).
- (5) G. B. Savitsky and K. Namikawa, *J. Phys. Chem.*, **67**, 2430 (1963).
- (6) H. Spiesscke and W. G. Schneider, *J. Chem. Phys.*, **35**, 722 (1961).
- (7) P. C. Lauterbur, *Ann. N. Y. Acad. Sci.*, **70**, 841 (1958).
- (8) P. C. Lauterbur, *J. Am. Chem. Soc.*, **83**, 1838 (1961).
- (9) P. C. Lauterbur, *Tetrahedron Letters*, **8**, 274 (1961).
- (10) H. Spiesscke and W. G. Schneider, *ibid.*, **14**, 468 (1961).
- (11) G. B. Savitsky, *J. Phys. Chem.*, **67**, 2723 (1963).
- (12) C. P. Nash and G. E. Maciel, *ibid.*, **68**, 832 (1964).
- (13) G. E. Maciel and J. J. Natterstad, *J. Chem. Phys.*, in press.
- (14) P. C. Lauterbur, *ibid.*, **38**, 1406 (1963).
- (15) P. C. Lauterbur, *ibid.*, **38**, 1415 (1963).
- (16) P. C. Lauterbur, *ibid.*, **38**, 1432 (1963).
- (17) H. Spiesscke and W. G. Schneider, *ibid.*, **35**, 731 (1961).
- (18) G. E. Maciel and R. V. James, *J. Am. Chem. Soc.*, **86**, 3893 (1964).
- (19) P. C. Lauterbur, *ibid.*, **83**, 1846 (1961).
- (20) G. E. Maciel and G. C. Ruben, *ibid.*, **85**, 3903 (1963).
- (21) G. E. Maciel and G. B. Savitsky, *J. Phys. Chem.*, **68**, 437 (1964).
- (22) D. D. Traficante and G. E. Maciel, *ibid.*, **69**, 1348 (1965).
- (23) J. B. Stothers and P. C. Lauterbur, *Can. J. Chem.*, **42**, 1563 (1964).
- (24) P. C. Lauterbur in "Determination of Organic Structures by Physical Methods," F. C. Nachod and W. D. Phillips, Ed., Academic Press, New York, N. Y., 1962, Chapter 7.
- (25) G. B. Savitsky and K. Namikawa, *J. Phys. Chem.*, **67**, 2754 (1963).

Table I: C^{13} Chemical Shifts in Vinyl, Phenyl, and Acetyl Compounds, in P.p.m. with Respect to Benzene

Substituent, X	$C_{\beta}H_2=C_{\alpha}H-X$						CH_3COX δ_{CO}^c
	δC_{α}^a	δC_{β}^a	δC_X^b	δC_o^b	δC_m^b	δC_p^b	
I	43.3	-1.8	32.3	-9.9	-2.6	0.4	-29.3
Br	13.1	6.6	5.4	-3.3	-2.2	1.0	-40.9
Cl	2.6	11.3	-6.4	-0.2	-1.0	2.0	-41.9
$CO_2C_2H_5$	-1.1	-1.8	-3.6 ^e	-1.3 ^a	-1.3 ^a	-5.1 ^a	-64.1
$NCO(CH_2)_3$	-1.3	34.4	-11.1 ^e	9.9 ^e	-0.2 ^e	5.6 ^e	
$SiCl_3$	-3.1	-10.0					
CH_2Br	-4.5 ^f	11.0 ^f	-5.0 ^a	0.3 ^a	0.3 ^a	(0.3) ^a	
CH_2Cl	-5.0 ^f	11.2 ^f					-71.9
$Si(CH=CH_2)_3$	-5.8	-6.8					
$SnCl_2CH=CH_2$	-6.5	-11.9					
$CH_2OC_2H_5$	-7.1	14.0	-10.8 ^a	0.6 ^a	0.6 ^a	(0.6) ^a	
$CH_2OCH_2CH=CH_2$	-7.1	12.6					
$Sn(CH=CH_2)_3$	-7.5	-7.9					
$SO_2CH=CH_2$	-9.1	-2.7					
CH_3CO	-9.8	-0.6	-9.3	-0.2	-0.2	-4.2	-69.8
$OCOCH_3$	-13.0	32.3	-23.0	6.4	-1.3	2.3	-37.3
$Pb(CH=CH_2)_3$	-16.7	-6.4					
$C(CH_3)_3$	-20.5 ^d	19.5 ^d	-22.4 ^a	3.2 ^a	0.2 ^a		-83.1
$O-n-C_4H_9$	-22.9	45.6					
OCH_3	-24.2	44.1	-30.2	14.7	-0.9	8.1	-42.0

^a Data from present work (except as noted otherwise). ^b Data from ref. 13 (except as noted otherwise). ^c Data from ref. 22 and 23. ^d Shifts from ref. 4. ^e Data for acetanilide rather than N-phenylpyrrolidone. ^f Data kindly provided by G. B. Savitsky and K. Namikawa.

made for spinning the sample; it consisted of two concentric, thin-walled spherical bulbs about 0.2 and 1.4 cc. in volume, a geometry which obviates the need for bulk susceptibility corrections in these results. The small inner bulb contained a reference for calibration of the resonance lines. Most of the present data were obtained using a reference consisting of a saturated aqueous solution of sodium acetate enriched to about 28% C^{13} at both carbon positions. A calibration experiment with benzene and with this reference using the side-band technique showed the center of the benzene doublet to be 53.1 p.p.m. to higher field than the carbonyl resonance, and the separation between the carbonyl resonance and the center of the methyl quartet of the reference to be 156.3 ± 0.2 p.p.m. These separations were used to calibrate the spectra with respect to the chemical shift of benzene. The spectra of vinyl bromide (in cyclohexane solution), vinyl iodide, divinyltin dichloride, vinylsilicon trichloride, allyl ethyl ether and diallyl ether were obtained using a previously described reference in the center bulb.¹² The C^{13} spectra of vinyl chloride and vinyl methyl ether were obtained on solutions in dimethyl carbonate, saturated and sealed at 0° , using the dimethyl carbonate as both

solvent and internal reference. The C^{13} chemical shifts of dimethyl carbonate have been found previously to be insensitive to most adulterants¹³; the shift of the carbonyl carbon is about 28.0 p.p.m. to lower field than that of benzene, and the separation between the carbonyl resonance line and the center of the methyl quartet is about 102.7 p.p.m. Considering the use of different references and calibration procedures, the shifts of the vinyl carbons presented in Table I with respect to benzene can be considered reproducible to about ± 0.8 p.p.m. The C^{13} shifts of the monosubstituted benzenes obtained in this study were measured with respect to an external reference previously described,¹² and can be considered precise to about ± 0.5 p.p.m.

Materials. Vinyl iodide was prepared by the reaction of iodine with tetravinyltin according to a modification of Seyferth's procedure.²⁷ The C^{13} spectrum was obtained on a sample which had b.p. $55-57^\circ$ [lit.²⁸ $56-56.5^\circ$].

(26) G. B. Savitsky and K. Namikawa, *J. Phys. Chem.*, **68**, 1956 (1964).

(27) D. Seyferth, *J. Am. Chem. Soc.*, **79**, 2133 (1957).

(28) J. Spence, *ibid.*, **55**, 1290 (1933).

The spectra of the other compounds were obtained on neat liquids as they are available from commercial sources. Allyl chloride, allyl ethyl ether, diallyl ether, ethyl benzoate, and benzyl ethyl ether were Eastman White Label reagents. Vinyl bromide, vinyltrichlorosilane, tetravinylsilane, divinylsulfone, and tetravinyllead were from Columbia Organic Chemicals. Vinyl chloride and vinyl ethyl ether were from the Matheson Co. Ethyl acrylate, allyl bromide, and vinyl acetate were Eastman Practical materials. N-Vinylpyrrolidone and *t*-butyl benzene (Puriss) were from Aldrich Chemical Co. Divinyltin dichloride, tetravinyltin, 1-butene-3-one, and vinyl *n*-butyl ether were from K and K Laboratories.

Results and Discussion

Carbon-13 magnetic resonance spectra were obtained on 17 vinyl compounds $C_\beta H_2=C_\alpha H-X$ with a wide variety of substituents X. In each case the spectrum consisted of several peaks: one or more lines due to the reference; a signal due to the α -carbon resonance, split into a doublet by the α -hydrogen atom; a resonance due to the β -carbon, split into a triplet by the β -hydrogens; and peaks due to carbon atoms (if any) in the substituent X. Illustrative examples are the spectra of vinyl iodide and tetravinyltin shown in Figures 1 and 2, respectively. In some cases five distinct lines traceable to vinyl carbons were not observed, but consistent and reasonable assignments could be made on the assumption of peak overlap and C^{13} -H splittings on the order of about 150 c.p.s.; Figure 3, which shows the spectrum of divinyl sulfone, is an example. The data are collected in Table I.

The C^{13} chemical shifts of the α -carbon atom, (δ_{C_α} in Table I) cover a range of 67.5 p.p.m. This is considerably smaller than the corresponding range of C^{13} shifts of the α -carbon in 1-substituted-1-hexynes,²² and about the same as the range of α -carbon shifts in substituted ethanes.⁶ It is slightly larger than the range of shifts of the substituted carbon atom of monosubstituted benzenes^{13,17} (δ_{C_X} in Table I), and is somewhat larger than the corresponding range of carbonyl C^{13} shifts in acetyl compounds (δ_{CO} in Table I).^{23,24}

The shifts in Table I of the β -carbon atom, δ_{C_β} , cover a range of 57.5 p.p.m., which is considerably larger than the ranges of C^{13} shifts for the β -carbons in substituted ethanes⁶ or of 1-substituted-1-hexynes,²² or of the *ortho* carbons in monosubstituted benzenes^{13,17} (δ_{C_o} in Table I).

Comparison of the vinyl C^{13} chemical shifts of Table I with the comprehensive proton chemical shift data published by Brügel, Ankel, and Krückeberg²⁹ for the vinyl group revealed no apparent correlations. This is

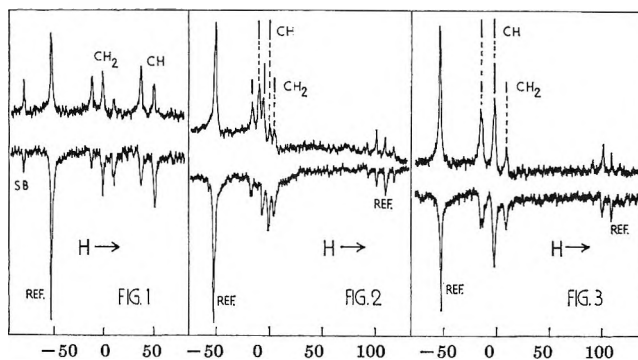


Figure 1. Carbon-13 n.m.r. spectrum of vinyl iodide with $CH_3C^{13}O_2Na$ reference (Ref.) and side band (SB), increasing field sweep (upper), and image of decreasing field sweep (lower) in p.p.m. with respect to benzene.

Figure 2. Carbon-13 n.m.r. spectrum of tetravinyltin with $C^{13}H_3CO_2Na$ and $CH_3C^{13}O_2Na$ reference, increasing field sweep (upper), and image of decreasing field sweep (lower) in p.p.m. with respect to benzene.

Figure 3. Carbon-13 n.m.r. spectrum of divinylsulfone with $C^{13}H_3CO_2Na$ and $CH_3C^{13}O_2Na$ reference, increasing field sweep (upper), and image of decreasing field sweep (lower) in p.p.m. with respect to benzene.

not surprising in view of the considerably different geometrical orientation of carbon and hydrogen atoms at the α - and β -positions with respect to the substituent, thus giving rise to profound differences in neighbor effects due to "neighbor anisotropy"⁶ or intramolecular dispersion forces.³⁰ It is also consistent with the apparent lack of a direct correlation between the corresponding proton and carbon shifts in substituted ethanes and at the *ortho* position in substituted benzenes in the work of Spiess and Schneider.^{6,17}

The very geometrical factors which appear to preclude a direct correlation between proton and carbon chemical shifts in vinyl as well as other groups would seem to set the stage for simple relationships between δ_{C_α} in vinyl compounds and δ_{C_X} in phenyl compounds or δ_{CO} in carbonyl compounds, and between δ_{C_β} in vinyl compounds and δ_{C_o} in phenyl compounds. Each of the carbon atoms in these categories employs sp^2 hybrid orbitals in σ -bonds to three adjacent atoms and contributes a p-orbital to a π -bond. Furthermore, in each of these three pairs the geometrical relationship to the substituent should be nearly the same. Thus, within each pair of categories the neighbor anisotropy and intramolecular dispersion effects exerted by the substituents should be comparable and will not be ex-

(29) W. Brügel, T. Ankel, and F. Krückeberg, *Z. Elektrochem.*, **64**, 1211 (1960).

(30) T. Schaefer, W. F. Reynolds, and T. Yonemoto, *Can. J. Chem.*, **41**, 2969 (1963).

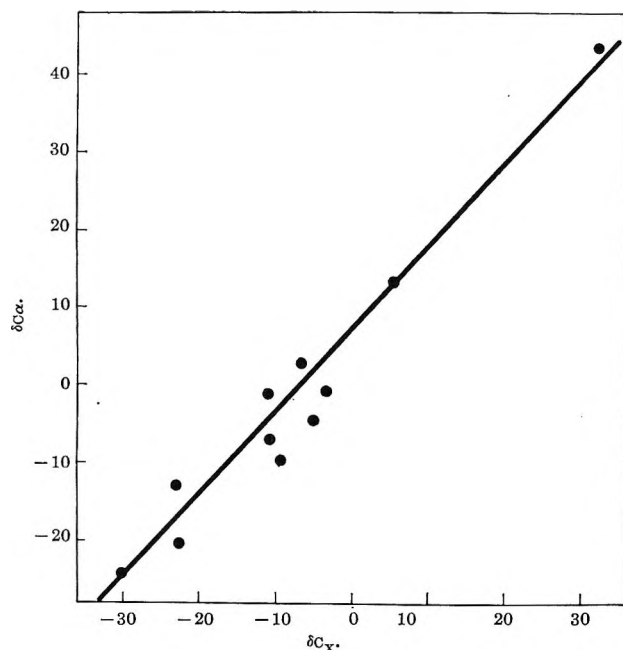


Figure 4. Plot of δ_{C_α} for vinyl compounds vs. δ_{C_X} for the corresponding phenyl compounds.

pected to obscure any correlations of C^{13} shifts due to similar inductive and resonance influences of the substituents on the molecular electronic configurations. This type of consideration previously has been used successfully to relate the C^{13} shifts of carbonyl carbons and of the ethylenic carbons of symmetrical disubstituted ethylenes to carbonyl π -bond polarity.¹³ It also may be responsible for the relatively consistent success of the constitutive relations developed by Savitsky and Namikawa.^{5,26}

In order to test these ideas, we have plotted δ_{C_α} for vinyl compounds vs. δ_{C_X} in phenyl compounds and vs. $\delta_{C=O}$ in acetyl compounds in Figures 4 and 5, respectively, and δ_{C_β} for vinyl compounds vs. $\delta_{C=O}$ for phenyl compounds in Figure 6. Rough linear relationships of the expected type are apparent in Figures 4 and 6.

While the scatter in Figure 4 is quite appreciable, the general trend lends support to the view expressed above that substituent effects should be similar in these closely related cases. The fact that the slope is nearly 1 indicates further that each type of electronic influence may be exerted to about the same degree in these two similar structural situations.

The rough linear correlation displayed in Figure 6 is further evidence for the validity of the above assumptions. However, this plot differs from Figure 4 in two fundamental ways: the slope is nearly 2, rather than 1; and two points, those corresponding to the acetyl and carboethoxy substituents, deviate widely from the

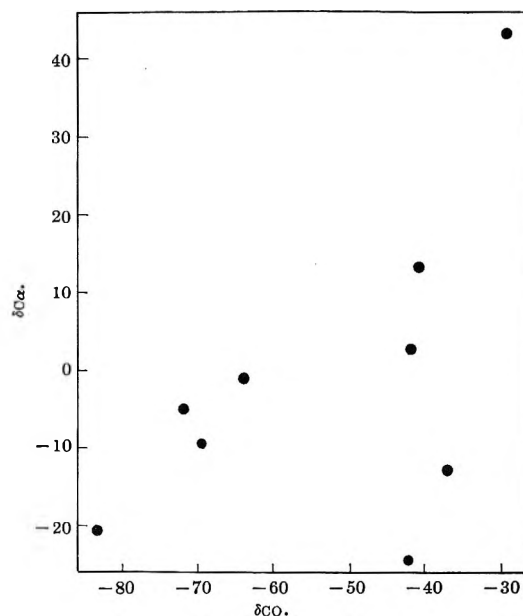


Figure 5. Plot of δ_{C_α} for vinyl compounds vs. $\delta_{C=O}$ for the corresponding acetyl compounds.

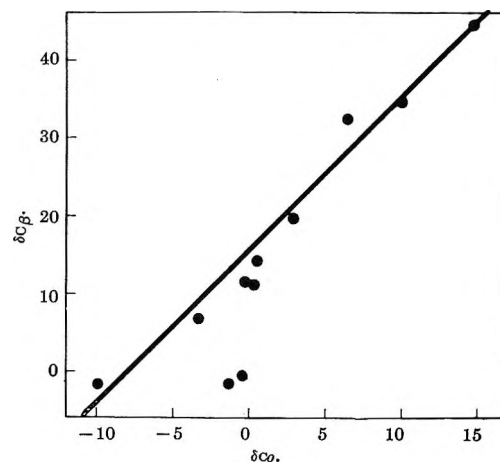
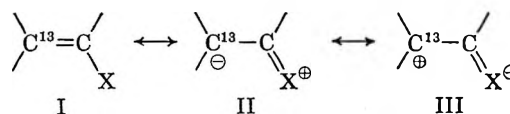


Figure 6. Plot of δ_{C_β} for vinyl compounds vs. $\delta_{C=O}$ for the corresponding phenyl compounds.

correlation line. These departures may be related to differences in the importance of resonance interaction between the substituent and the β -carbon in a vinyl compound in one case, and between the substituent and



the *ortho* carbon in a phenyl compound in the other case. In vinyl compounds, the excess positive or negative charge due to contributions of canonical structures III or II must reside entirely on the β -carbon, whereas in phenyl compounds it may be distributed to both *ortho* carbons as well as to the *para* position. This situation might tend to make a β -carbon more sensitive than an *ortho* carbon to the resonance effect of a substituent, and might account for the twofold greater sensitivity of $\delta_{C\beta}$ than δ_{C_o} to variations of the substituent. Furthermore, the conspicuous deviation of the acetyl and carboethoxy points in Figure 6 may be due to the fact that these substituents are the only -R groups on the graph and, hence, the only cases where structure III might be of importance.

In stark contrast to the rough linear relations dis-

played in Figures 4 and 6, Figure 5 demonstrates that δ_{C_α} is not so related to the carbonyl C^{13} chemical shifts of corresponding acetyl compounds. Since both classes of carbon atoms in question are the sp^2 type, this difference in behavior is most likely not due to differences in C-X bond lengths between these classes of compounds. More likely it is related to the different inductive and resonance effects of the =O fragment as compared to =CH₂, and the influence of the carbonyl bond polarity. Figures 4 and 6 may also reflect a closer relationship between the excited electronic states of vinyl and phenyl compounds than between vinyl and acetyl compounds, as these states are responsible for the large paramagnetic contributions to C^{13} shifts.

Acknowledgment. The author is grateful to Professor George B. Savitsky for helpful discussions.

Unimolecular Decomposition of Product Olefins in Methylene Chemical Activation Systems¹

by F. H. Dorer² and B. S. Rabinovitch

Department of Chemistry, University of Washington, Seattle, Washington 98105 (Received December 28, 1964)

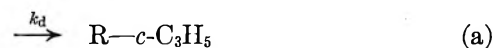
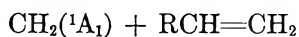
Dilute mixtures of diazomethane in propene, butene-1, and pentene-1 were photolyzed with 4300-Å. radiation at room temperature. The proportions of products were measured for the primary unimolecular isomerizations of the chemically activated alkylcyclopropanes that arise. The quantitative aspects of the data are complicated by an apparent variability of the methylene radical [insertion/addition] ratios with pressure (at higher pressures) and reminiscent of earlier results which could be explained by the occurrence of some triplet methylene along with the singlet methylene. At low pressures, particularly, olefin decomposition is marked. Rate constants for the decomposition by allylic bond rupture of the vibrationally excited alkenes, butene-1, pentene-1, hexene-1, pentene-2, hexene-2, 2-methylbutene-1, and 2-methylpentene-1, have been obtained. The alkene data comprise one of the few homologous series for which microscopic unimolecular rate constants have been measured. Comparison of calculated and experimental decomposition rate constants indicates that the entropy of activation for olefin decomposition seems considerably less than that conventionally assumed for alkane decomposition by C-C rupture. The results also support a low value for the allylic resonance energy.

Introduction

This paper deals with the measurement of rates of some of the primary and secondary decomposition processes of vibrationally excited olefins and cyclopropanes. Several homologous systems have been investigated by reaction of methylene with either propene, butene-1, or pentene-1 in the gas phase. This technique was first used by Kistiakowsky and co-workers to produce various vibrationally excited, ground electronic state cyclopropanes.³ The subsequent reaction of hot product olefins is of particular interest here.

The addition of methylene to an olefin forms a vibrationally "hot" cyclopropane molecule having a minimum energy of approximately 100–110 kcal. mole⁻¹, depending on the source of the methylene.⁴ The formed cyclopropanes may undergo structural isomerization to olefins above a critical energy, E_0 , around 61 kcal, or be stabilized by collisions with the bath molecules.⁵ The olefins produced either by hot cyclopropane isomerization or, in the first instance, by methylene insertion across C-H bonds of the reactant olefin possess approximately 108–118 kcal. of

minimum energy.^{3d} These excited olefins may undergo chemical reaction before collisional stabilization according to the general scheme⁶



(1) Work supported by the National Science Foundation.

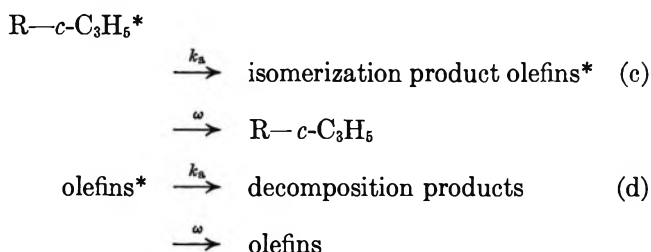
(2) National Science Foundation Predoctoral Fellow.

(3) (a) G. B. Kistiakowsky and W. L. Marshall, *J. Am. Chem. Soc.*, **74**, 88 (1952); (b) G. B. Kistiakowsky and K. Sauer, *ibid.*, **78**, 5699 (1956); (c) H. M. Frey and G. B. Kistiakowsky, *ibid.*, **79**, 6373 (1957); (d) J. N. Butler and G. B. Kistiakowsky, *ibid.*, **82**, 759 (1960); (e) H. M. Frey, *Progr. Reaction Kinetics*, **2**, 131 (1964).

(4) D. W. Setser and B. S. Rabinovitch, *Can. J. Chem.*, **40**, 1425 (1962).

(5) (a) D. W. Setser, B. S. Rabinovitch, and J. W. Simons, *J. Chem. Phys.*, **40**, 1751 (1964); (b) J. W. Simons, B. S. Rabinovitch, and D. W. Setser, *ibid.*, **41**, 800 (1964).

(6) B. S. Rabinovitch and M. C. Flowers, *Quart. Rev. (London)*, **18**, 122 (1964).



where most "insertion" and "isomerization" products are the same species but not necessarily so. Apart from propylene where allylic C-H rupture can occur,^{5b} the principal mode of decomposition of α -olefins is by allylic C-C rupture; butene-2 decomposition occurs mainly by allylic C-H rupture, but pentene-2 and hexene-2 can decompose by allylic C-C rupture. Olefin decomposition by allylic C-C rupture involves a bond dissociation energy above⁷⁻⁹ 65 kcal. mole⁻¹, while allylic C-H rupture requires^{8,9} ≥ 81 kcal. mole⁻¹; the exact values vary with the bond site and are discussed later.

The study of the isomerization of $\text{R}-c\text{-C}_3\text{H}_5^*$, reaction c, is complicated by olefin product decomposition. Direct counting of the apparent amount of isomerization products offers incomplete information if olefin decomposition is important and if total isomerization and stabilization are not otherwise known. However, this information when coupled with known values of the unimolecular rate constants for the cyclopropane isomerization obtained by other methods¹⁰ yields the unimolecular rate constants for decomposition of the individual olefin products.

To our knowledge, the present study provides the first quantitative rate information on the elementary primary process of decomposition of a number of homologous higher olefins.

Experimental

Materials. Diazomethane was prepared by the reaction of KOH with N,N-nitrosomethylurea. It was degassed by pumping at -160° in order to remove ethane and ethylene impurities and was then dissolved in butyl phthalate and stored at -196° . The olefin reactants were Phillips research grade and were further purified by gas chromatography where necessary.

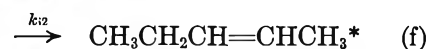
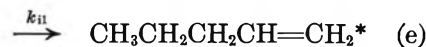
Apparatus and Procedure. All gas handling was performed in a conventional vacuum system. Pyrex reactors in sizes ranging from 1 ml. to 5 l. were pumped down to 10^{-5} mm. before being loaded with reactants. Approximately 1:10 mixtures of diazomethane in olefin were photolyzed with a GE AH-6 high pressure mercury lamp for 1 to 2 hr. Dow Corning No. 5543 and No. 3389 filters provided an average wave length of radiation absorbed by the diazomethane at 4358

\AA . The frequency distribution of the radiation absorbed by the diazomethane has been described elsewhere.^{4,5a}

Analysis. All products condensable at -196° were analyzed by gas chromatography. The methylene-propene and -butene-1 systems were analyzed with 6.09 m. of 40% silver nitrate-ethylene glycol on firebrick followed by 2.74 m. of 40% 2,4-dimethylsulfolane on firebrick. The methylene-pentene-1 product analysis was done on a 91.4-m. squalane capillary column with an argon-type detector. Later methylene-butene-1 runs were also analyzed in this way.

Results

Butene-1 Reactant. This system was studied the most thoroughly. The principal insertion and addition reactions are



Data on the relative rates, k_{ij}/k_{d1} , will be considered in the discussion since there is a difference between the observed high pressure relative rates and those deduced from lower pressure data.

The principal isomerization reactions are



Of the olefin products, 3-methylbutene-1 is formed uniquely by insertion. Figure 1 shows the pressure dependence of the percentage of each of six C_5H_{10} hydrocarbon products produced in a series of methylene-butene-1 runs over the pressure range 0.1-990 mm.

(7) M. J. Molera and F. J. Stubbs, *J. Chem. Soc.*, 381 (1952); W. A. Bryce and P. Kebarle, *Trans. Faraday Soc.*, 54, 1660 (1958).

(8) C. A. McDowell, F. P. Lossing, I. H. S. Henderson, and J. B. Farmer, *Can. J. Chem.*, 34, 345 (1956); H. M. Frey and D. C. Marshall, *J. Chem. Soc.*, 3981 (1962); S. W. Benson, A. N. Bose, and P. Nangia, *J. Am. Chem. Soc.*, 85, 1388 (1963).

(9) A. F. Trotman-Dickenson, "Gas Kinetics," Butterworth and Co. Ltd., London, 1955.

(10) F. H. Dorer and B. S. Rabinovitch, *J. Phys. Chem.*, 69, 1973 (1965).

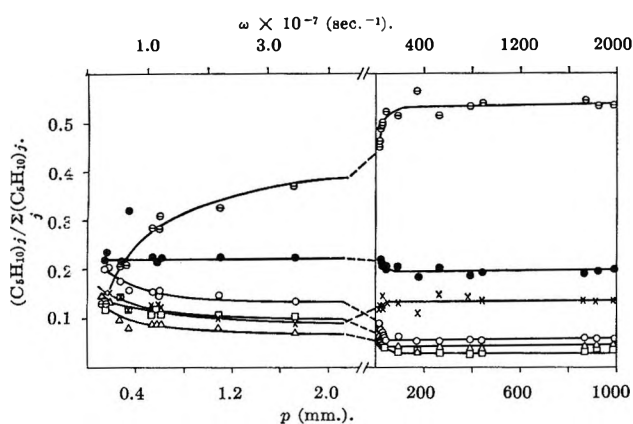
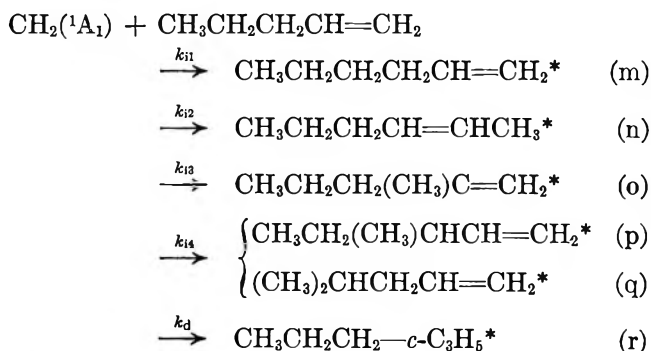


Figure 1. Variation of C_6H_{10} product composition with pressure: ethylcyclopropane, \ominus ; pentene-1, \bullet ; 3-methylbutene-1, \times ; 2-methylbutene-1, Δ ; *trans*-pentene-2, \circ ; *cis*-pentene-2, \square .

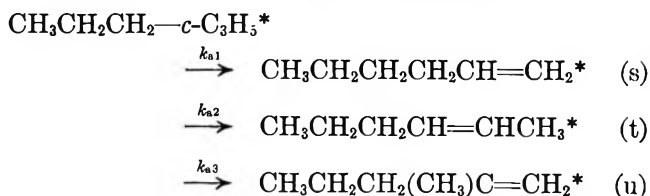
At lower pressures there is a significant number of other hydrocarbon products although these virtually disappear at high pressures. Detailed analysis of low pressure (0.33 mm.) runs on the 91.4-m. squalane capillary column revealed as many as 28 additional "side products," C_6 through C_8 . The six principal C_6H_{10} products constituted approximately 50% of these 34 products. Roughly 20% of the side products were hexene isomers. Addition of 7% of oxygen to the reaction mixture at low pressure virtually eliminated all 28 side products and produced several polar type peaks on the chromatogram instead.

Pentene-1 Reactant. The principal insertion and addition reactions are



For the reasons mentioned earlier, consideration of data for the relative rates, k_{ij}/k_d , will be delayed to the Discussion.

The principal isomerization reactions are



The 3-methylpentene-1 and 4-methylpentene-1 are formed uniquely by insertion. Figure 2 illustrates product variation for the methylene-pentene-1 system over the pressure range 10^{-2} to 46 mm. The 3-methylpentene-1 and 4-methylpentene-1 peaks were only slightly separated on the squalane column, and only their combined total amount is known. The number and relative amounts of side products increased as the total pressure of the system decreased until, at the lowest pressure runs, the above seven C_6H_{12} products comprised only 60% of the more than 20 products detected from C_6 into the C_8 region. A major

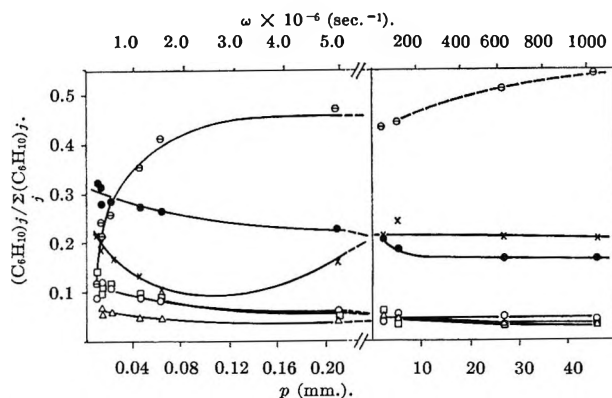
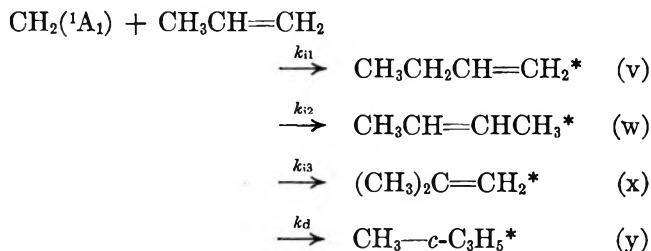


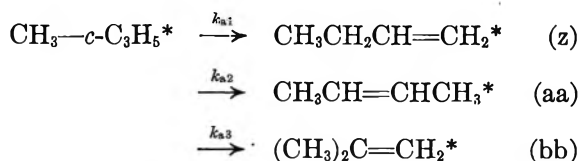
Figure 2. Variation of the C_6H_{12} product yield with pressure: propylcyclopropane, \ominus ; hexene-1, \bullet ; 3-methylpentene-1 + 4-methylpentene-1, \times ; 2-methylpentene-1, Δ ; *trans*-hexene-2, \circ ; *cis*-hexene-2, \square .

side product common to both this system and the butene-1 system had the retention time of 1,5-hexadiene. In the pentene-1 system this product was detected at pressures as great as 0.6 mm. although it was absent at 2 mm.

Propene Reactant. The principal insertion and addition reactions are



The principal isomerization reactions of methylcyclopropane are^{3c}



None of the insertion or isomerization products are uniquely formed in only one way. Only a limited study was conducted. The ratio [butene products/methylcyclopropane] was determined at pressures from 0.23 to 63 cm.

Rates of Decomposition of Cyclopropanes. Figures 3-5 are plots of (Σ olefin/cyclopropane) vs. ω^{-1} for the three systems, where only those olefins that can arise by isomerization as well as by insertion are relevant and are included in the numerator. The quantity ω is the specific collision frequency. The slopes of the lines in the plots are proportional to the total rate constants, k_a , for the alkylcyclopropane isomerization to olefins if subsequent olefin decomposition is unimportant^{3d}; otherwise the slopes are too small. k_a is defined as $\omega D/S$, where D is the total isomerization amount of the hot cyclopropane and S is the collisionally stabilized portion.

Discussion

Thermochemistry and Reaction Parameters. The basis of the following remarks is given in Table I. The heat of addition of methylene to propene is 2.8 kcal. mole⁻¹ less than for ethylene, at 0°K. The heats of methylene addition to propene, butene-1, and pentene-1 are the same at 0°K. Since cyclopropane formed at 300°K. by 4300-Å. photolysis of diazomethane in ethylene is estimated to have an average internal energy, $\langle E \rangle$, around 110 kcal. mole⁻¹,^{4,5} the formed methyl-, ethyl-, and propylcyclopropanes

Table I: Gaseous Heats of Formation at 0°K. (kcal. mole⁻¹)^a

Molecule	ΔH_f°	Molecule	ΔH_f°
Ethylene	14.5	<i>cis</i> -Pentene-2	-0.2
Cyclopropane	16.7 ^b	<i>trans</i> -Pentene-2	-1.3
Propene	8.5	3-Methylbutene-1	-0.7
Methylcyclopropane	13.6 ^c	2-Methylbutene-1	-2.3
Butene-1	5.0	Propylcyclopropane	6.3 ^c
<i>cis</i> -Butene-2	3.5	Hexene-1	-2.5
<i>trans</i> -Butene-2	2.2	<i>cis</i> -Hexene-2	-3.9
Isobutene	1.0	<i>trans</i> -Hexene-2	-5.1
Ethylcyclopropane	10.0 ^d	2-Methylpentene-1	-6.0
Pentene-1	1.1	3-Methylpentene-1	-3.5
		4-Methylpentene-1	-3.5

^a All quantities are from ref. 15 unless otherwise specified.

^b The 298°K. value [J. W. Knowlton and F. D. Rossini, *J. Res. Natl. Bur. Std.*, **43**, 113 (1949)] has been converted to 0°K.; the value given in ref. 4 is slightly in error. ^c Estimated from 0°K. value for ethylcyclopropane by using a value for $\Delta(\Delta H_f^\circ)$ owing to addition or subtraction of a CH₂ group as determined by comparison with related molecules. ^d Obtained from the liquid (25°) heat of combustion value [private communication by E. J. Prosen to P. J. C. Fierens and J. Nasielski, *Bull. soc. chim. Belges*, **71**, 187 (1962)], with an estimated ΔH_{vap} , and converted to 0°K.

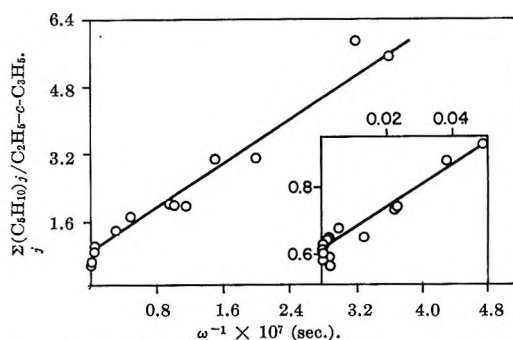


Figure 3. Variation of the [pentene/ethylcyclopropane] ratio with ω^{-1} , where only those pentenes that arise by both insertion and ethylcyclopropane structural isomerization are included.

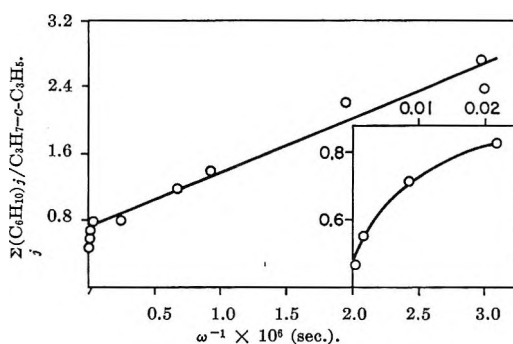


Figure 4. Variation of the [hexene/propylcyclopropane] ratio with ω^{-1} , where only those hexenes that arise by both insertion and propylcyclopropane structural isomerization are included.

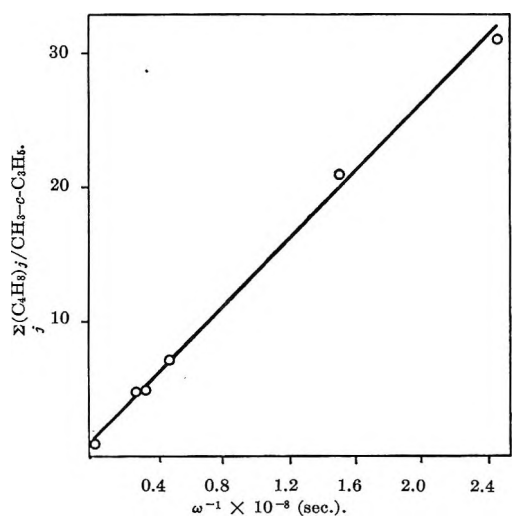


Figure 5. Variation of the [butene/methylcyclopropane] ratio with ω^{-1} . The isobutene product amount has been estimated from the data of Butler and Kistiakowsky.^{3d}

here have values of $\langle E \rangle$ of 107.9, 108.6, and 109.6 kcal. mole⁻¹, respectively; the exact amount for each species depends also on the contributions of ther-

mal energy. The excess energies, $\langle E^+ \rangle = \langle E \rangle - E_0$, with respect to isomerization to olefins are just under³ 50 kcal. mole⁻¹.

Since structural isomerization of cyclopropanes to their respective olefins is exothermic at 0°K. by ≥ 8 kcal. mole⁻¹, the exact amount depending on the particular olefin formed, the excited olefins are formed with $\langle E \rangle \geq 116$ kcal. mole⁻¹. The excitation level of each olefin is independent of its route of formation in the approximation that there is no difference in the energies of the methylenes which react by insertion or addition. The critical energy E_0 for primary-secondary allylic C-C bond rupture in butene-1 is about 70 kcal. mole⁻¹, the exact value varying with the estimate of the allylic resonance energy.⁷⁻⁹ Substitution of C for H on the terminal carbon atom lowers its dissociation energy by 1-2 kcal. mole⁻¹ per attached C atom⁹: E_0 decreases in the order primary-secondary > secondary-secondary > secondary-tertiary, etc. Specific examples are the dissociation energies of the allylic C-C bonds of the pentenes, which decrease as pentene-2 \sim 2-methylbutene-1 > pentene-1 \gtrsim 3-methylbutene-1, the energies ranging above 65 kcal. mole⁻¹. The olefins in these systems thus have excess energy for allylic C-C rupture, $\langle E^+ \rangle \simeq 46$ -55 kcal. Relative to the alkylcyclopropanes,⁹ the quasi-constancy of $\langle E^+ \rangle$ and the increase of the other parameter, $\langle E \rangle$, will cause a decrease in the relative olefin decomposition rate. However, the frequency factors for decomposition by C-C bond rupture of alkanes are often given as $\gtrsim 10^{17}$ sec.⁻¹,^{9,11} a factor $\sim 10^2$ greater than those for the structural isomerization of the cyclopropanes.¹² One might therefore expect that the rate constants for alkene decomposition by allylic C-C bond rupture should be greater in general than those for alkylcyclopropane isomerization.

The above discussion offers the most apparent factors related to the estimate of energetic parameters. Later, we shall have occasion to note several other factors that may modify the thermochemistry. We shall wish to take account of possible changes in the estimate of allylic resonance energy, of a possible small barrier to radical recombination and hence an increase for E_0 for decomposition, of other assumptions regarding the average energy of methylenes as affected by their mode of reaction, and of collisional de-energization of cyclopropanes that isomerize.

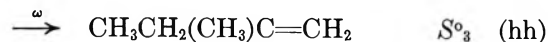
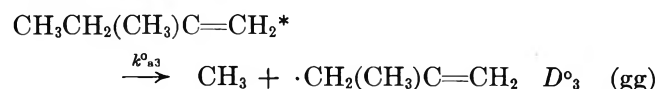
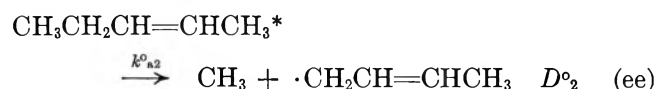
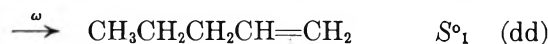
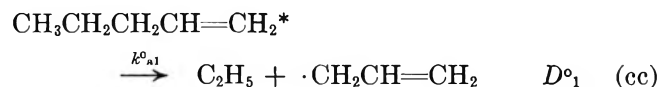
Cyclopropane Isomerization and Olefin Disappearance.

A. *Methylene-Propene System; k_a .* The total rate constant, k_a , for the disappearance of methylcyclopropane, given by the slope of the line in Figure 5, is 6.0×10^8 sec.⁻¹. This value is less by a factor of 1.6 than that obtained by a different technique that was

independent of the measurement of D .¹⁰ Since decomposition by allylic C-H bond rupture has a much greater activation energy than the activation energy for decomposition by allylic C-C bond rupture,⁹ the low value of k_a obtained from Figure 5 is due primarily to loss of butene-1 by the process $\text{CH}_3\text{CH}_2\text{CH}=\text{CH}_2 \rightarrow \text{CH}_3\cdot + \cdot\text{CH}_2\text{CH}=\text{CH}_2$.

B. *Methylene-Butene-1 System; k_a .* The thermal isomerization of ethylcyclopropane produces pentene-1 and pentene-2 in equal amounts.^{12a} Figure 1 indicates that there is considerably greater decomposition of pentene-1 relative to pentene-2 since the former scarcely increases in amount at lower pressures. Pentene-2 decomposition involves primary-secondary allylic C-C bond rupture (reaction ee) and is expected to decompose more slowly than would pentene-1 by secondary-secondary allylic C-C rupture (reaction cc). In fact, addition of 5 to 10% of oxygen (which scavenges free radicals which otherwise can recombine) to a methylene-butene-1 system selectively reduces the percentage of pentene-1 at low pressure to below its high pressure limiting value.¹³

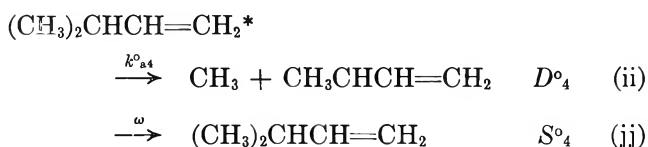
That the other pentene products do actually decompose by allylic C-C bond rupture is indicated by the fact that there are large amounts of 2-methylpentene-1, 3-methylpentene-1, and hexene-2 produced at low pressure. These can arise by combination of ethyl radicals with the various possible methallyl radicals produced by pentene-2, 2-methylbutene-1, and 3-methylbutene-1 decomposition by allylic C-C bond rupture (reactions ee, gg, and ii)



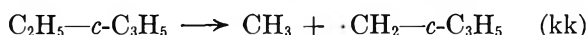
(11) B. S. Rabinovitch and D. W. Setser, *Advan. Photochem.*, **3**, 1 (1964). The absolute rate constants in Table XIII of this reference should be multiplied by 2.

(12) (a) M. L. Halberstadt and J. P. Chesick, private communication; (b) D. W. Setser and B. S. Rabinovitch, *J. Am. Chem. Soc.*, **86**, 564 (1964); J. P. Chesick, *ibid.*, **82**, 3277 (1960).

(13) F. H. Dorer and B. S. Rabinovitch, *J. Phys. Chem.*, **69**, 1964 (1965).



The superscript stands for olefin reaction. The absence of propylcyclopropane and 1-butenylcyclopropane at low pressures indicates that the process

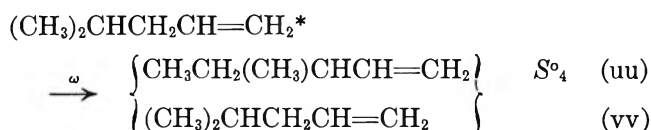
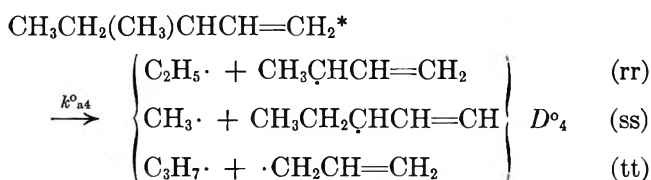
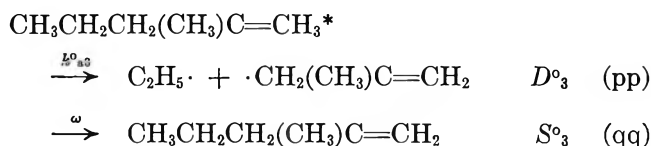
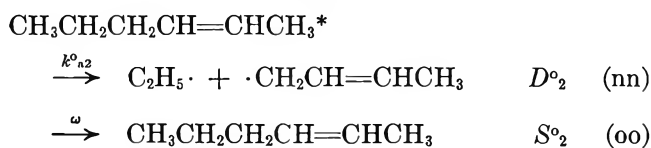
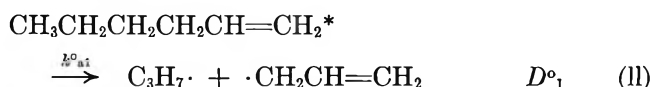


does not occur. The rate constant, k_a , calculated from the slope and intercept of the line in Figure 3 (in which the amounts of pentenes which were actually isolated were used as a measure of D), is $0.8 \times 10^7 \text{ sec.}^{-1}$ and is smaller by a factor of 2.9 than the value measured by other techniques¹⁰; this is indicative of the extensive amount of olefin disappearance.

That pentene decomposition by allylic C-C bond rupture is not the entire explanation of product disappearance or appearance in this system, however, is indicated by the behavior found for 3-methylbutene-1. Decomposition of this molecule involves rupture of a primary-tertiary allylic C-C bond, with a critical energy possibly lower than that for pentene-1 decomposition, together with a reaction path degeneracy of 2. Figure 1 indicates that, at intermediate pressures, only 3-methylbutene-1 shows a decline in amount with reduction of pressure. This is due, at least in part, to the fact that, unlike the other insertion products, it is not replenished by the cyclopropane isomerization. At still lower pressures, nonetheless, there is onset of an increase in this product. This could obviously be due to recombination of methyl and methyl radicals which arise from other sources, e.g., pentene-2 decomposition. However, addition of 5-10% of oxygen did¹³ not completely inhibit all of its increase, and a nonradical olefin isomerization reaction which produces 3-methylbutene-1 must also occur. Isomerization reactions between 2-methylbutene-2, 2-methylbutene-1, and 3-methylbutene-1 are known.¹⁴ However, thermodynamic considerations argue against formation of 3-methylbutene-1 from 2-methylbutene-1 in this system,¹⁵ while 2-methylbutene-2 constituted, at most, only 1% of the total C_5H_{10} products at low pressures. The equilibrium constants for formation of 3-methylbutene-1 from pentene-1 and pentene-2 are 0.69 and 0.68, respectively, at 1500°K.¹⁵ (an approximate lower limit to the "temperature" of these species). The actual concentration ratios at the lowest pressure measurements [3-methylbutene-1/pentene-1] and [3-methylbutene-1/pentene-2] are about 0.6 and 0.4 indicating a possibility that these two olefins isomerize to 3-methylbutene-1 in this system somewhat.

The rate constants k_{aj}° , then, are unimolecular rate constants for olefin disappearance, the primary mode of which is most probably allylic C-C bond rupture but which may include a contribution from isomerization reactions between the pentene isomers that could effectively increase or decrease their net apparent rate of decomposition.

C. Methylene-Pentene-1 System. The product pressure dependence shown in Figure 2 may be explained by arguments analogous to those given for the butene system. In this system, however, no primary-secondary allylic C-C bonds are involved, only weaker ones; the critical energies for bond rupture of some of the hexenes are lower than for the pentenes,⁹ thereby making decomposition relatively more important.



An indication of the importance of olefin decomposition in this system is that the constant k_a for propylcyclopropane isomerization, as calculated from Figure 4 and ignoring olefin product disappearance, is $0.4 \times 10^6 \text{ sec.}^{-1}$; this is a factor of 3.8 less than that measured by a method that does not employ a count of the product olefins.¹⁰

(14) (a) M. C. Flowers and H. M. Frey, *J. Chem. Soc.*, 1157 (1962); (b) M. C. Flowers and H. M. Frey, *ibid.*, 3953 (1959).

(15) F. D. Rossini, "Selected Values of Physical and Thermodynamic Properties of Hydrocarbons and Related Compounds," American Petroleum Institute, 1953.

There is first a marked decrease with lowering of pressure and then an increase in the sum of the 3-methylpentene-1 and the 4-methylpentene-1, which is analogous to the behavior noted earlier for 3-methylbutene-1. Although no low pressure oxygen studies were done in this system, presumably processes analogous to those that governed 3-methylbutene-1 behavior also occur here.

Measurements of k_a° for Olefin Disappearance. Some Experimental Complications. Two different complications were encountered in different pressure regions. (a) The "high pressure" region, in which hot cyclopropanes and olefins are largely quenched by collision before they can react,¹⁶ should provide, in principle, a clear experimental basis for the determination of the relative amounts of methylene addition to the double bond and of insertion into the various C-H positions of the olefin substrate. Instead, it was found that the ratios of [addition/insertion] and also the relative amounts of insertion into various C-H bond types were a function of the total pressure (mixture composition remaining constant) within the high pressure region, at least up to 100 mm. The following discussion will consider this matter more explicitly. However, it may contribute to the clarity of the presentation to describe the most important conclusions. Namely, the data obtained in the region just below 10 mm., *i.e.*, in an "intermediate pressure" region, are the most reliable and accurate. The insertion ratios deduced from the intermediate region are virtually statistical in relative magnitude, while the high pressure values discriminate somewhat against insertion, particularly into the vinyl C-H bond. (b) In a "low pressure" region, below the intermediate region, it was found that the observed rate constants deduced for olefin decomposition, k_{aj}° , tended to decline markedly. This is attributed to the fact that in the low pressure region, where decomposition was quite extensive, reverse recombination of radicals, which is not allowed for in a naive calculational scheme, becomes significant; *cf.* reactions ee, gg, and ii described earlier.

These complications, together with olefin isomerization mentioned earlier, limit the accuracy of these experimental measurements of k_{aj}° and give rise to drift with pressure, in some cases. The values deduced below should not be considered accurate to better than a factor of 2.

Rate Formulation. If the only modes of formation of a vibrationally excited olefin is methylene insertion and cyclopropane isomerization, the steady-stage assumption applied to the concentrations of each of the hot species leads to (compare eq. 2 of ref. 13)

$$k_{aj}^\circ = \frac{S}{S_j^\circ} \left\{ \frac{k_{ij}}{k_d} (k_a + \omega) + k_{aj} \right\} - \omega \quad (1)$$

If a particular hot olefin is formed only by insertion, eq. 1 becomes

$$k_{aj}^\circ = \frac{S}{S_j^\circ} \left\{ \frac{k_{ij}}{k_d} (k_a + \omega) \right\} - \omega \quad (2)$$

From known values for k_a , k_{ij}/k_d , k_{aj}/k_a measurements of S/S_j° as a function of ω yield the rate constants k_{aj}° . As mentioned earlier, the total rate constants, k_a , have been measured independently for methylcyclopropane, ethylcyclopropane, and propylcyclopropane.¹⁰ The details of the measurement and assignment of values for the other two parameters, k_{aj} and k_{ij}/k_d , are now discussed.

The Parameter k_{aj} . The pentene isomer distribution produced by the thermal isomerization of ethylcyclopropane is the same as the analogous butene isomer distribution produced by the thermal isomerization of methylcyclopropane.¹² Thus, the relative values of k_{aj}/k_a for chemically activated ethylcyclopropane may be assumed to be the same as for chemically activated methylcyclopropane measured by Butler and Kistiakowsky (as determined in a pressure region where subsequent olefin decomposition was not important).^{3d}

The Ratio k_{ij}/k_d . The determination of the ratio [insertion/addition] requires a more detailed examination of the high pressure region in these systems. Our methylene-propene work does not offer new information, but the other two systems are more useful. It was found that the [total olefin/cyclopropane] ratios decrease at a faster rate with increasing ω (insets, Figures 3 and 4) than the known rate constants¹⁰ for the respective alkylcyclopropane isomerizations permit. That is to say, the [olefin/alkylcyclopropane] ratios for these systems, even when corrected for any very minor occurrence of olefin decomposition or cyclopropane isomerization, in the high pressure region are all pressure dependent and decrease with increasing ω . The values obtained at lower pressure, in the intermediate region, are the more reliable; Table II gives the measured butene-1 system and pentene-1 system ratios for [insertion/addition] as determined in both the intermediate and high pressure regions. The relative rates of insertion measured at lesser pressure are obviously closer to statistical than the values found at pressure 10- to 100-fold higher.

Similar behavior has previously been observed by

(16) The value of S/D for ethylcyclopropane at $p = 10$ mm. ($\omega = 20 \times 10^7$ sec.⁻¹) is 10. The value of S/D for propylcyclopropane at $p = 2$ mm. ($\omega = 46.6 \times 10^7$ sec.⁻¹) is 31.1.

Table II: The Relative Rates of Methylene Insertion to Double-Bond Addition for the Methylene-Butene-1 and Methylene-Pentene Systems

Product molecule	k_{ij}/k_d		C-H bond type
	Intermed. press. ^a	High press. ^b	
Pentene-1	0.47 (0.16) ^c	0.36 (0.12)	Primary
Pentene-2	0.33 (0.16)	0.16 (0.08)	Vinylc
2-Methylbutene-1	0.12 (0.12)	0.08 (0.08)	Vinylc
3-Methylbutene-1	0.33 (0.16)	0.26 (0.13)	Allylic
Hexene-1	0.45 (0.15)	0.29 (0.10)	Primary
Hexene-2	0.22 (0.11)	0.12 (0.06)	Vinylc
2-Methylpentene-1	0.11 (0.11)	0.05 (0.05)	Vinylc
3-Methylpentene-1 + 4-Methylpentene-1	0.54 (0.14)	0.38 (0.10)	Allylic and secondary

^a Butene system ratios obtained at 10 mm.; pentene system ratios are averages for 2 and 5 mm. ^b Butene system ratios are averages of measurements in the 200 to 1000 mm. range; pentene ratios are from runs at 46 mm. ^c Numbers in parentheses are ratios per C-H bond.

Frey¹⁷ in diazomethane photolysis systems (although the above interpretation was not applied). Also, similar pressure dependence of methylene insertion into the C-H bonds of butane relative to double-bond addition has been observed in this laboratory when diazomethane is photolyzed in butene-1 plus *n*-butane mixtures.¹⁰ These various examples of increase of the [insertion/addition] ratios with decreasing pressure are in the same direction as the change produced in the present work by addition of 5 to 10% of oxygen to a diazomethane-butene system at fixed (high) pressure although the magnitude of the oxygen effect is somewhat less. An increasing importance of insertion in ketene-butene-2 photolysis systems with added oxygen has previously been attributed to the presence at high pressures of approximately 29% of triplet methylene.¹⁸ The presence of 10 to 20% of *trans*-dimethylcyclopropane of the total addition product when diazomethane was photolyzed¹⁹ in admixture with *cis*-butene-2 at total pressures greater than 500 mm. could also be attributed to 20 to 35% of triplet methylene, as based on known ratios of these isomers formed by triplet methylene reaction with *cis*-butene-2.²⁰

The above facts and arguments suggest that the pressure dependence of the [insertion/addition] ratio found in the systems under consideration here may be due, in part at least, to an increasing percentage of triplet methylene at the higher pressures.¹⁸ It is also important to note that both the insertion ratio effects and the geometric stereochemical nonspecificity of addition¹⁸ alter in parallel fashion at higher pressures.

Summary of the Experimental Values of the k_{ij}^o .

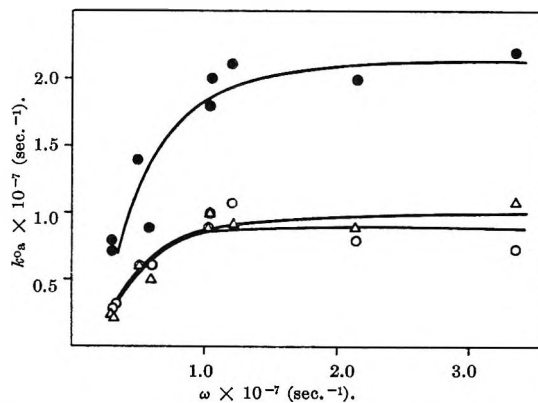


Figure 6. Variation of k_a^o with ω for the pentenes: pentene-1, ●; pentene-2, ○; 2-methylbutene-1, △.

The rate constants k_{a1}^o , k_{a2}^o , and k_{a3}^o for the pentenes are illustrated in Figure 6 as a function of ω . Their extreme pressure dependence for values of $\omega < 10^7$ sec.⁻¹ ($p < 0.53$ mm.) is attributed to the low pressure complication of re-formation of the pentenes by radical recombination at low pressures. The magnitudes of k_{a1}^o , k_{a2}^o , and k_{a3}^o reported for this system in Table III are averages of measurements with $\omega > 10^7$ sec.⁻¹. The value of k_{a4}^o for 3-methylbutene-1 decomposition is too inaccurate to describe quantitatively. It is estimated to be $> 5 \times 10^7$ sec.⁻¹.

Table III: The Rate Constants for Chemically Activated Olefin Decomposition by Allylic C-C Bond Rupture

Olefin	k_a^o , sec. ⁻¹
Butene-1 ^a	1.5×10^8
Pentene-1 ^b	2.0×10^7
Hexene-1 ^c	2.5×10^6
Pentene-2 ^b	9.0×10^6
Hexene-2 ^c	3.7×10^6
2-Methylbutene-1 ^b	1.0×10^7
2-Methylpentene-1 ^c	5.8×10^6
3-Methylbutene-1	$> 5 \times 10^7$

^a Average of measurements with $\omega > 2.1 \times 10^8$ sec.⁻¹ (> 11.8 mm.). ^b Average of measurements with $\omega > 10^7$ sec.⁻¹ (> 0.53 mm.). ^c Quantities obtained by extrapolation to $\omega = 5 \times 10^6$ sec.⁻¹ (0.21 mm.).

(17) H. M. Frey, *Proc. Roy. Soc. (London)*, **A250**, 409 (1959)

(18) J. W. Simons and B. S. Rabinovitch, *J. Phys. Chem.*, **68**, 1322 (1964); a similar collision-induced, pressure-dependent mode of formation of triplets, described in this reference, may apply here.

(19) (a) H. M. Frey, *Proc. Roy. Soc. (London)*, **A251**, 575 (1959); (b) D. W. Setser, F. H. Dorer, and B. S. Rabinovitch, unpublished results.

(20) F. J. Duncan and R. J. Cvetanović, *J. Am. Chem. Soc.*, **84**, 3593 (1962).

The rate constants for hexene-1, hexene-2, and 2-methylpentene-1 decomposition are pressure dependent over most of the range (mainly in the low pressure region) of these measurements (Figure 7); *i.e.*, radical recombination at low pressures again causes fall of the apparent $k_{a_j}^0$. The values reported in Table III were obtained from the highest pressure values which enter the intermediate pressure region ($\omega = 5 \times 10^6$ sec.⁻¹, $p = 0.21$ mm.). The values for hexene-1 disappearance (k_{a1}^0) have been corroborated (Figure 7) by work¹³ involving methylene reaction with pentene-1 and 5,5,5-trifluoropentene-1 mixtures.

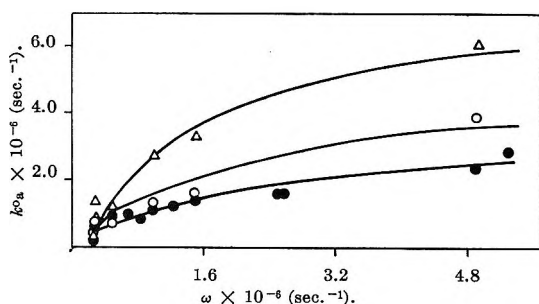


Figure 7. Variation of k_a^0 with ω for the hexenes: hexene-1, ●; hexene-2, ○; 2-methylpentene-1, △. Additional results for k_{a1}^0 were provided by the internal comparison measurements of ref. 10.

The value of k_{a1}^0 for the sum of the disappearance of 3-methylpentene-1 and the 4-methylpentene-1 was again too inaccurate to estimate quantitatively. It is simply estimated to be $>5 \times 10^6$ sec.⁻¹.

The rate constants k_{a1}^0 for butene-1 decomposition (Figure 8) decrease at the lowest pressure measurements (where S/D for butene-1 is ~ 0.3). Such pressure dependence is due to radical recombination at lower pressures. Butene-2 decomposition was not significant at pressures where decomposition of butene-1 was already quite noticeable. A value of k_{a1}^0 for butene-1 decomposition is included in Table III.

Comparison of Calculated and Experimental Rate Constants. Even though the experimental data are not highly accurate, they are still adequate for comparison with theoretical rate constants and can provide insights into the nature of these olefin decomposition processes.

Since for these methylene-olefin systems the distribution function for the formed olefin species is quite narrow relative to $\langle E^+ \rangle$,^{4,5} the experimental rate constant may be closely approximated by $k_{(E)}$, the specific rate constant at the average energy. The average energy of the formed species is determined by the (known) thermal energy of the reactants systems^{4,5} and the thermochemistry of the various species involved

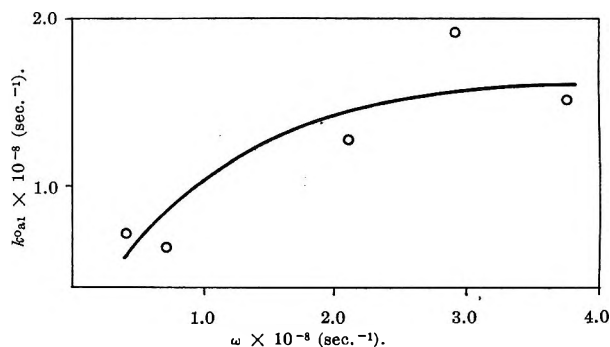


Figure 8. Variation of k_{a1}^0 with ω for butene-1 decomposition.

(Table I). For butene-1, pentene-1, and hexene-1, $\langle E \rangle = 116.5, 117.2,$ and 118.2 kcal. mole⁻¹, respectively.¹⁰

We consider now several prior assertions that affect both $\langle E \rangle$ and E_0 . The assumption that the excitation level of each olefin is independent of whether it is formed directly by insertion or by isomerization of the hot cyclopropane formed on addition is believed reasonable. Since the reactivity of methylene with olefin double bonds is of the order of the collision rate,^{3e} the scavenging effect of the double bonds should cause any energy fractionation of the methylenes reacting by the two paths to be negligible.

Another matter that affects the estimate of $\langle E \rangle$ is the question of whether the average energy of the olefins formed by isomerization is lowered because the alkylcyclopropanes may undergo stepwise collisional deactivation. Since the deactivation step sizes in diazomethane-olefin systems are quite large⁶ and, moreover, only a fraction of the olefins arise by the isomerization pathway, $\langle E \rangle$ for the formed olefins would at most be lowered by, say, 2 kcal. mole⁻¹. This places lower limits on $\langle E \rangle$ of 114.5, 115.2, and 116.2 kcal. mole⁻¹ for butene-1, pentene-1, and hexene-1, respectively.

Recent estimates of the allylic resonance energy⁸ (~ 12 kcal. mole⁻¹) suggest that the critical energy E_0 for decomposition of butene-1 by allylic C-C bond rupture may be as high as 72 kcal. mole⁻¹. In addition, if we seek an upper limit, a small barrier for allyl radical recombination is plausible. We may consider that this establishes a reasonable upper limit: for butene-1 decomposition, $E_0 = 74$ kcal. mole⁻¹. Pentene-1 and hexene-1 would have correspondingly altered (although lower) critical energies for allylic C-C rupture.

The RRKM formulation for k_E , the specific unimolecular rate constant at the energy E , is

$$k_E = \frac{P^+ \Sigma P(E^+_{vr})}{hP^*_1 N(E^*_{vr})} \quad (3)$$

Table IV: Molecular Vibration Models for Butene-1 Decomposition

Motion	Molecule ^a	Activated complex models ^b			
		1	2	3	4 ^c
CH str.	3080, 3000 (2), 2968, 2965 2917, <u>2882</u> , 2860				3140, 2985 (2)
C=C str.	1642	1400	1400	1400	1500
C—C str.	1055, 845	0, 1200	0, 1200	0, 1200	0, 1115
CH bend.	1295, 635				1295, 785
CH ₂ def.	1415, 910				1425, 880
CH ₂ wag	1325, 1165				1190, 1085
CH ₂ bend	1450				1425
CH ₂ twist	1275				1040
CH ₂ rock	765	190	125	190	Free rot.
CH ₃ wag	1165	290	195	290	Free rot.
CH ₃ rock	960	240	160	240	Free rot.
CH ₃ def.	1465 (2), 1380				1420 (2), 950
C=C torsion	995	600	600	600	550
C—C torsion	225, 102	56, 250	38, 250	Free rot., 250	Free rot., 350
Skeletal bend	435, 271	375, 70	375, 45	375, 70	415, free rot.

^a The molecule frequency assignment is that of ref. 22. ^b Only the frequency changes made in forming the activated complexes are indicated. Those CH stretching frequencies changed from the molecule assignment to form the CH stretching frequencies for the planar methyl of complex 4 are underlined. ^c Model 4 contains the vibrational frequencies for a planar methyl radical and an allyl radical. The methyl radical frequency assignment is that of ref. 11 and J. B. Howard, *J. Chem. Phys.*, **3**, 207 (1935). For allyl, $\sigma = 2$ and skeletal angle of 120° were used.

Table V: The Molecular Vibration Models for Pentene-1 Decomposition

Motion	Molecule ^{a,b}	Activated complex models	
		1	2
CH str.	3080, 3000 (2), 2965 (2), 2928, 2916, <u>2885</u> , 2862, 2852		
C=C str.	<u>1642</u>	1400	1400
C—C str.	1035, <u>926</u> , 845	0, 1200	0, 1200
CH bend	1295, 635		
CH ₂ def.	1415, 910		
CH ₂ wag	1391, 1258, 1165		
CH ₂ bend	1460, 1444		
CH ₂ twist	1292, 1249		
CH ₂ rock	<u>845</u> , <u>725</u>	210, 180	140, 120
CH ₃ wag	1165		
CH ₃ rock	1005		
CH ₃ def.	1468, 1461, 1370		
C=C torsion	995	600	600
C—C torsion	<u>215</u> , <u>102</u> , 88	180, 25, ^c 250	180, 17, ^c 215
Skeletal bend	<u>435</u> , <u>401</u> , <u>188</u>	375, 100, 47	375, 67, 30

^a The molecule assignment is that of ref. 22. ^b The molecule frequencies changed in forming the activated complex are underlined. Only the frequency changes made in forming the complexes are tabulated. ^c See footnote c, Table VI.

where P^+_1/P^*_1 is the ratio of the partition functions of adiabatic degrees of freedom, $\Sigma P(E^+_{vr})$ is the sum over all vibrational-internal rotational energy eigenstates of the activated complex, and $N(E^*_{vr})$ is the density of the vibrational-internal rotational energy eigenstates for the activated molecule. This expression

has been discussed in detail in earlier presentations.^{4,18,21}

Calculations are made here for butene-1, pentene-1, and hexene-1 decomposition by allylic C—C rupture on

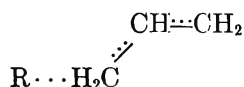
(21) B. S. Rabinovitch, R. F. Kubin, and R. E. Harrington, *J. Chem. Phys.*, **38**, 405 (1963).

Table VI: Molecular Vibration Models for Hexene-1 Decomposition

Motion	Molecule ^{a,b}	Activated complex models	
		1	2
CH str.	3080, 3000 (2), 2965 (2), 2929, 2919, 2915, 2882, 2862, 2856, 2852		
C=C str.	1642	1400	1400
C—C str.	1065, 1035, <u>935</u> , <u>845</u>	0, 1200	0, 1200
CH bend	1295, 635		
CH ₂ def.	1415, 910		
CH ₂ wag	1356, 1303, 1242, 1165		
CH ₂ bend	1463, 1453, 1444		
CH ₂ twist	1303, 1277, 1236		
CH ₂ rock	1038, <u>740</u> , <u>723</u>	185, 180	123, 120
CH ₃ wag	1085		
CH ₃ rock	1005		
CH ₃ def.	1472, 1462, 1370		
C=C torsion	995	600	600
C—C torsion	208, 125, 94, 61	102, 250, 15 ^c	102, 250, 10 ^c
Skeletal bend	435, 370, <u>303</u> , <u>139</u>	375, 76, 45	375, 50, 23

^a The molecule frequency assignment is that of ref. 22. ^b Those molecule frequencies changed in forming the complexes are underlined. Only the frequency changes made in forming the complexes are tabulated. ^c Such a low libration frequency is a formal consequence of the method of assigning the complex frequencies; it provides a rate comparison with more physically realistic models using higher values (or free rotation about the C—C bond, as for butene).

the assumption that all internal degrees of freedom are active, while over-all rotations are effectively adiabatic. The vibrational-internal rotational frequency assignment for these molecules is that used earlier.²² The activated complexes correspond pictorially to



The reaction coordinate is taken to be a C—C stretch. There is some frequency tightening in the allylic fragment owing to allylic resonance. For butene-1, two methyl motions, one CH₂ wag, the CH₃ torsion, and one skeletal bend were lowered. The corresponding pentene-1 and hexene-1 complexes were formed in the same manner except that a CH₂ motion and a skeletal bend and torsion are lowered in the complex instead of methyl motions. The molecule and complex models are tabulated in Tables IV–VI. The sum and density terms were evaluated on an IBM 7094 using programs written by Mr. G. Z. Whitten.

The calculations for butene-1 decomposition are the most extensive, and, consequently, they will be discussed first. Values are presented here for four different butene-1-activated complex models. In Table VII are tabulated the calculational results for these complex models for various combinations of the possible energy parameters. Model 1 corresponds to a semiloose activated complex in that the modes that would go over to free rotations in a "loose" complex

Table VII: Calculational Results for $k_{(E)}$ (sec.⁻¹) for Various Butene-1 Activated Complex Models^a

$(E)^b$	Activated complex model				E_0^b
	1 ^c	2 ^d	3 ^e	4 ^f	
116.5	5.8×10^9	3.7×10^{10}			65
116.5	3.2×10^9	2.0×10^{10}			67
116.5				0.9×10^{11}	70
114.5				0.65×10^{11}	70
116.5	6.4×10^8	4.0×10^9	2.5×10^8	4.7×10^{10}	72
114.5	4.5×10^8	2.2×10^9	1.7×10^8	3.6×10^{10}	72
116.5	3.2×10^8	2.0×10^9	1.3×10^8	2.6×10^{10}	74
114.5	2.3×10^8	1.5×10^9		1.9×10^{10}	74
Exptl.	1.5×10^8				

^a The calculated rate constants include the ratio of the partition functions for the over-all rotational degrees of freedom; a factor of ~ 1.6 for models 1, 2, and 3 and a factor of ~ 5.2 for model 4. ^b Energy units are kcal. mole⁻¹. ^c The calculated ART frequency factor for this model is 2.0×10^{16} sec.⁻¹ at 750°K. The corresponding Arrhenius frequency factor for footnotes c, d, e, and f would be 11.5, 15.0, 7.5, and 2.5 times larger, respectively. ^d The calculated ART frequency factor for this model is 1.3×10^{16} sec.⁻¹ at 750°K. ^e The calculated ART frequency factor for this model is 9.3×10^{14} sec.⁻¹ at 750°K. ^f The calculated ART frequency factor for this model is 4.4×10^{17} sec.⁻¹ at 750°K. Ref. 26 contains an error of a factor of 2.

are lowered to only one-quarter of their magnitude in the molecule. The C···C distance²³ corresponds to

(22) M. J. Pearson and B. S. Rabinovitch, *J. Chem. Phys.*, **42**, 1624 (1965).

(23) D. R. Herschbach and V. W. Laurie, *ibid.*, **35**, 458 (1961).

Table VIII: Calculational Results for $k_{(E)}$ (sec.⁻¹) for Pentene-1 and Hexene-1 Decomposition

Pentene-1				Hexene-1			
E^a	1	2	E_0^a	E^a	1	2	E_0^a
117.2	3.1×10^8	2.5×10^9	65	118.2	6.0×10^6	6.1×10^7	68
115.2	2.2×10^8	1.8×10^9	65	116.2	4.0×10^6	4.1×10^7	68
117.2	1.1×10^8	8.8×10^8	68	118.2	2.5×10^6	2.6×10^7	70
115.2	7.5×10^7	6.3×10^8	68	116.2	1.7×10^6	1.8×10^7	70
117.2	2.0×10^7	1.7×10^8	72 ^b	118.2	1.1×10^6	1.1×10^7	72 ^b
115.2	1.4×10^7	1.1×10^8	72	116.2	7.4×10^5	7.5×10^6	72
Exptl.	2.0×10^7			Exptl.	2.5×10^6		

^a Energy units are kcal. mole⁻¹. The calculations for lower values of E_0 are given for illustrative purpose. ^b Corresponds to the value $E_0 = 74$ for butene-1 with the assumption of a lowering of 2 kcal. in $D(C-C)$ for this molecule.

2.1 Å. (and lower moments of inertia) relative to the very large values (5–6 Å.) that accompany an assertion of free rotation in a loose model.¹¹ This model anticipates a small barrier for methyl-allyl radical recombination and consequently a lower entropy of activation. Model 2 illustrates the effect of lowering the bendings and internal libration to one-sixth of their values with further extension of $r(C \cdots C)$ to 2.3 Å. Model 3 illustrates the effect on the sum term of substituting a free internal rotation for a low frequency libration. One notes that free rotation may actually decrease the magnitude of the sum under the conditions of these calculations. Model 4 represents a completely "loose" model of the Gorin type²⁴ in which the methyl and allyl groups are allowed to tumble freely against each other. Such a model may be tolerated for ethane,²⁵ but is not valid, in general, as pointed out by Johnston and Goldfinger.^{11,24} Calculational details and other models are contained in ref. 26.

The striking result of the calculations (Table VII) is that a loose model 4, or a highly semiloose equivalent model, is incompatible with the experimental data (Table III) even for the most favorable limiting values for the energy parameters. The tighter model 1 is in better agreement with the experimental results, which indicates that alkene decomposition by allylic C–C rupture has a substantially lower entropy of activation than that for ethane decomposition by C–C rupture.²⁷ Model 1, with use of a spin factor of $1/4$ and a reaction path degeneracy of 2, corresponds to a collision efficiency factor for recombination of 5.0×10^{-3} . This is similar to H atom addition to olefins. For model 2, this would rise to 3.0×10^{-2} . The calculations for pentene-1 and hexene-1 decomposition (Table VIII) also compare favorably with the experimental results for a moderate semiloose activated complex (model 1). Furthermore, even for this model, a relatively high value for E_0 of around 72–74 kcal. mole⁻¹ is needed to repro-

duce the experimental rates for butene-1, pentene-1, and hexene-1 decomposition. These data thus suggest that the allylic resonance energy is $\lesssim 12$ kcal. mole⁻¹, which is in agreement with the latest estimates.⁸

It is hoped that other workers will be led to make independent measurements of these decomposition rates. We believe that our values are essentially correct, but, in view of their important implications, they should be further checked.

Unfortunately, the inaccuracy of the experimental results and the uncertainties in the energetics obscure the details of the dependence of the rate on molecular complexity for the homologous series butene-1, pentene-1, and hexene-1. However, the gross effects are obvious, and the comparison with the theory is good (Tables VII and VIII). The experimentally measured decrease in k_a per methylene group is a factor of ~ 8 . The calculated factors (for the highest E_0 parameters, Tables VII and VIII) are somewhat higher, but not unsatisfactory in the light of both experimental inaccuracy and the uncertainty in thermochemical parameters. In view of this, however, it did not seem useful to make calculations for the other olefins of Table III since insertion of appropriate changes of bond dissociation energies into model 1 types of complexes is bound to give order of magnitude agreement for these olefins also.

(24) H. S. Johnston and P. Goldfinger, *J. Chem. Phys.*, **37**, 700 (1962).

(25) There is an interesting relation between the calculated rates obtained with semiloose models which invoke lowered skeletal bendings and those obtained from loose models: the latter models give rates of decomposition for large or asymmetric molecules which are matched in magnitude on a semiloose model only when very low frequency bendings are employed; by contrast, for the symmetrical ethane molecule matching of rates predicted by the loose model is obtained¹¹ with more modest lowering of the bending modes.

(26) F. H. Dorer, Ph.D. Thesis, University of Washington, 1965.

(27) D. W. Setser and B. S. Rabinovitch, *J. Chem. Phys.*, **40**, 2427 (1964).

Unimolecular Reactions of Chemically Activated Species Produced in Systems of Methylene with Propene, Butene-1, 3,3,3-Trifluoropropene, and 4,4,4-Trifluorobutene-1¹

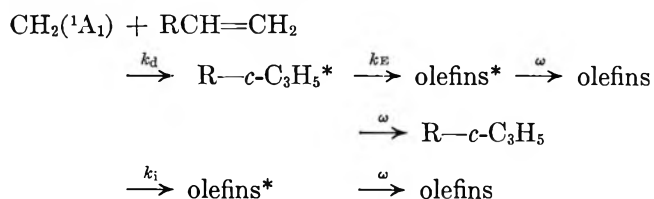
by F. H. Dorer² and B. S. Rabinovitch

Department of Chemistry, University of Washington, Seattle, Washington 98105 (Received December 28, 1964)

Dilute mixtures of ketene in propene, in butene-1, in 3,3,3-trifluoropropene, and in 4,4,4-trifluorobutene-1 were photolyzed at 3200 Å. and 25°. The rates were measured for some isomerization processes of the chemically activated alkyl cyclopropanes that arise. Experiments were performed both in the presence and absence of 3–8% added oxygen. The effect of oxygen on product composition is explained in terms of an earlier suggestion that the proportion of triplet methylene reaction is pressure dependent and that there is approximately 29% triplet methylene in these systems at higher pressures. Some mechanistic effects of the trifluoromethyl group on the relative rates of methylene reaction with olefins, and on various competitive rates connected with alternative modes of hot alkylcyclopropane isomerization, are noted.

Introduction

The preceding paper^{3a} described the decomposition of chemically activated alkene products formed in methylene systems by photolysis of diazomethane-alkene mixtures. The present paper compares the rates of some primary and secondary processes that occur after methylene produced by ketene photolysis has reacted with propene, butene-1, 3,3,3-trifluoropropene, and 4,4,4-trifluorobutene-1. The systems ostensibly follow the scheme



where R is CH₃, C₂H₅, CF₃, and CF₃CH₂. The vibrationally excited cyclopropanes are formed with 100–105 kcal. mole⁻¹ of energy and can undergo structural isomerization to excited olefins with a critical energy $E_0 \sim 61$ kcal. mole⁻¹.⁴ The vibrationally excited olefins, whether formed by isomerization or insertion (some are formed uniquely by insertion), have approxi-

mately 8 kcal. mole⁻¹ more energy than the cyclopropanes; unless collisionally stabilized, they may undergo decomposition by allylic C–C bond rupture with critical energy of approximately 70 kcal. mole⁻¹.³ The relative amounts of the olefin and cyclopropane products have been measured over a range of pressures in each system, both in the presence and in the absence of 3 to 8% added oxygen.

Experimental

Materials. Ketene was purified by gas chromatography at –78° with a Fluoropak column.^{4b} The hydrocarbons were Phillips research grade and were further purified by gas chromatography when necessary.

The 3,3,3-trifluoropropene was prepared by two methods. First,⁵ an equimolar gaseous mixture of

- (1) Work supported by the National Science Foundation.
- (2) National Science Foundation Predoctoral Fellow, 1962–1964.
- (3) (a) F. H. Dorer and B. S. Rabinovitch, *J. Phys. Chem.*, **69**, 1952 (1965); (b) F. H. Dorer, Ph.D. Thesis, University of Washington.
- (4) (a) D. W. Setser and B. S. Rabinovitch, *Can. J. Chem.*, **40**, 1425 (1962); (b) J. W. Simons and B. S. Rabinovitch, *J. Phys. Chem.*, **68**, 1322 (1964); (c) J. W. Simons, B. S. Rabinovitch, and D. W. Setser, *J. Chem. Phys.*, **41**, 800 (1964).
- (5) R. N. Haszeldine, *J. Chem. Soc.*, 2856 (1949).

trifluoromethyl iodide and ethylene was photolyzed with a G.E. AH-6 high pressure lamp in a Pyrex reactor having a bottom collection tip at 0° which was shielded from radiation. The product was dehydroiodated with solid KOH. The propene was also synthesized by the reaction of SF₄ with acrylic acid in a stainless steel vessel at approximately 20 atm. and 100°. After purification by gas chromatography, the principal product from both methods had the same infrared spectra and a mass spectral pattern with a parent peak at mass 96.

4,4-Trifluorobutene-1 was prepared by SF₄ reaction with 1-butenic acid. Yields were approximately 50% of the starting acid. The gaseous product was purified by gas chromatography. Its infrared spectra showed the vinylic CH stretch and C=C double bond stretch frequencies reported by Haszeldine.⁷ The product had a mass spectral parent peak at mass 110.

Apparatus and Procedures. Pyrex reactors, ranging in sizes from 1 to 5000 cm.³, were pumped to at least 10⁻⁴ mm. on a conventional vacuum apparatus before being loaded with a 1:10 ketene-olefin mixture. Reactants were photolyzed for 1 to 2 hr. with an AH-6 lamp fitted with a quartz water jacket and a filter of a NiSO₄·CoSO₄·7H₂O solution circulating through a Corex D glass envelope. The average wave length absorbed by the ketene was 3200 Å.^{4b}

Product Analysis. Condensable products were analyzed by gas chromatography. The methylene-propene products were separated on a column of silver nitrate-ethylene glycol on firebrick. This column did not separate isobutene from the propene so that aliquots of the products were also run on a hexamethylphosphoramide firebrick column. The methylene-butene-1 products were analyzed with the silver nitrate-ethylene glycol column followed by a 2,4-dimethylsulfolane firebrick column. The fluorocarbon systems were analyzed on the 2,4-dimethylsulfolane column followed by a dibutyl phthalate column. The hydrocarbon analyses were calibrated with known samples of each product. Peak area calibrations for several compounds were used as the basis of the measurement of the amounts of fluorocarbons.

Results

Ketene-Propene Systems. The isomerization of chemically activated methylcyclopropane in oxygen-free systems has previously been studied by Butler and Kistiakowsky⁸ (BK). The present results for the 3200-Å. photolysis of ketene in propene, with and without 3 to 8% added oxygen, are illustrated in Figure 1.

The mechanism and notation of the preceding paper

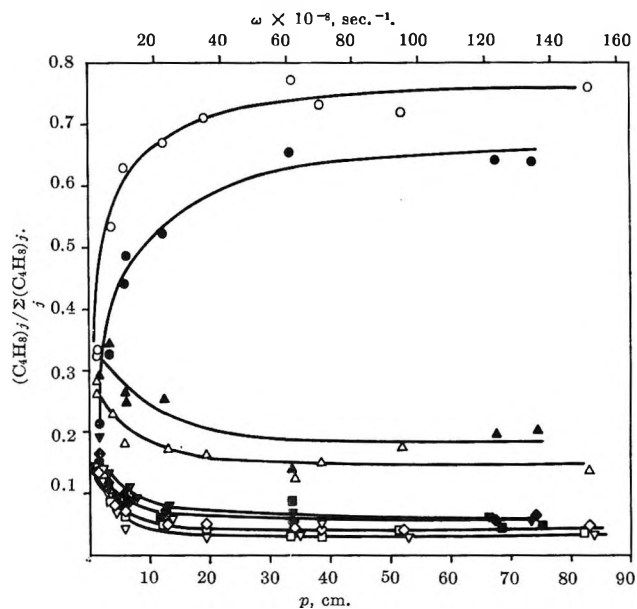


Figure 1. The variation of the C₄H₈ product composition with total pressure for the ketene-propene photolysis system. Open points are pure system results and filled points are results for 5 to 10% oxygen added to the photolysis mixture: methylcyclopropane, O; butene-1, Δ; *trans*-butene-2, ◇; *cis*-butene-2, □; isobutene, ▽.

are used. If olefin decomposition were unimportant, the steady-state assumption applied to the hot species would lead to

$$\frac{\text{total butenes}}{\text{methylcyclopropane}} = \frac{k_a}{\omega} \left(1 + \frac{k_i}{k_d} \right) + \frac{k_i}{k_d} \quad (1)$$

$$\frac{(\text{butene})_j}{\text{methylcyclopropane}} = \frac{k_a}{\omega} \left(\frac{k_{aj}}{k_a} + \frac{k_{ij}}{k_d} \right) + \frac{k_{ij}}{k_d} \quad (2)$$

Here k_{ij}/k_d is the rate of each type of CH insertion relative to double bond addition by the methylene, and $k_i = \sum_{j=1}^3 k_{ij}$. The ratio k_{aj}/k_a represents the fractional rates of formation of the butene isomers by methyl cyclopropane isomerization, and $k_a = \sum_{j=1}^3 k_{aj}$. The same olefins are formed by both insertion and isomerization: butene-1, butene-2, and isobutene ($j = 1, 2, 3$, respectively). Figure 2 presents plots of [total butenes/methylcyclopropane] vs. ω^{-1} for both the pure and oxygen systems. From eq. 1, the slopes of these lines

(6) The sulfur tetrafluoride and some helpful literature were generously supplied by the DuPont Chemical Co.; W. C. Smith, *Angew. Chem. Intern. Ed. Engl.*, **1**, 467 (1962); W. R. Hasek, W. C. Smith, and V. A. Engelhardt, *J. Am. Chem. Soc.*, **82**, 543 (1960).

(7) R. N. Haszeldine, *J. Chem. Soc.*, 2040 (1954).

(8) J. N. Butler and G. B. Kistiakowsky, *J. Am. Chem. Soc.*, **82**, 759 (1960).

Table I: The Rate Constants and Rate Ratios for the Ketene-Propene System

	$k_a, \text{sec.}^{-1}$	Isomerization ^a			Insertion ^b		
		k_{a1}/k_a	k_{a2}/k_a	k_{a3}/k_a	k_{i1}/k_d	k_{i2}/k_d	k_{i3}/k_d
Pure system	3.4×10^{10c}	0.30	0.47	0.23	0.063	0.039	0.035
Pure system (BK)	8.2×10^{10d}	0.53	0.45	0.18	0.060	0.035	0.029
Oxygen system	7.2×10^{10c}	0.27	0.46	0.28	0.097	0.070	0.070

^a Results of least-squares analysis of [(butene)_j/methylcyclopropane] vs. ω^{-1} curves.^{3b} Low pressure scatter of the oxygen data introduces an estimated uncertainty of $\pm 25\%$ in those results. ^b Experimentally measured (per bond) ratios at high pressure. ^c k_a calculated by setting butene-1 equal to the measured butene-2 from isomerization; the change incurred, relative to value based on the measured butene-1, averaged $+5\%$. ^d Value of BK has been converted to the collision diameters used here.

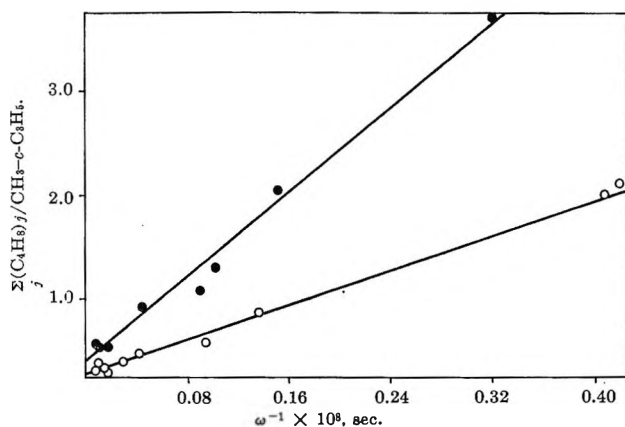


Figure 2. The variation of the butene/methylcyclopropane ratio with ω^{-1} for ketene photolysis in propene. The open circles are pure system results; the closed circles are results for 5 to 10% oxygen added.

are proportional to k_a . Table I tabulates the results obtained from Figure 2 and plots of [(butene)_j/methylcyclopropane] vs. ω^{-1} plots^{3b} (not shown). The results obtained by BK from the 3100-Å. photolysis of ketene in propene are included for comparison.

The disagreement between the total k_a values found here and by BK for the pure system cannot be reconciled by the difference in photolysis energy. (It may be noted that the present value at 3200 Å. accords better with the k_a value determined at 2600 Å. by BK than does their value at 3100 Å.) However, the discrepancy between the two measurements of k_{a1}/k_a is due at least in part to the process



Butene-1 and butene-2 should probably arise in nearly equal amounts from methylcyclopropane, as suggested by the thermal isomerization.⁹ The present measurements included lower pressures than BK, and some butene-1 decomposition occurs. The observed rate of isomerization to butene-1, k_{a1} , compared to butene-2, k_{a2} (Table I), may reflect preferential loss of butene-1.

The rate constant, k_a , included in Table I was calculated by correcting the butene-1 count for the amount that has decomposed, assuming that $k_{a1}/k_a = k_{a2}/k_a$.

The oxygen results for the k_{a3}/k_a are reliable only to $\pm 25\%$, due to the excessive scatter and sparsity of the data for [(butene)_j/methylcyclopropane] ratios below 60 mm. The relative amount of insertion to addition at higher pressures was found to change upon the addition of oxygen (Table I). Similar behavior has been noted previously at higher pressures in a *cis*-butene-2-ketene system^{4b}; the effect of added oxygen in that system was attributed to the presence of 29% triplet methylene.

Ketene-Butene-1 Systems. Figure 3 gives the pressure dependence of the percentage of each of the principal

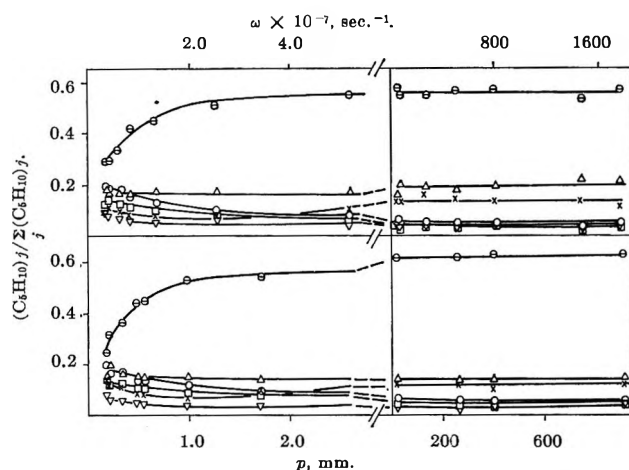


Figure 3. The variation of the C_5H_{10} product composition with total pressure for the ketene-butene-1 photolysis system. Bottom figure gives the pure system results and the top figure gives the results for 5 to 10% oxygen added to the photolysis mixture: ethylcyclopropane, Θ ; pentene-1, Δ ; *trans*-pentene-2, O ; *cis*-pentene-2, \square ; 3-methylbutene-1, X ; 2-methylbutene-1, ∇ .

(9) (a) D. W. Setser and B. S. Rabinovitch, *J. Am. Chem. Soc.*, **86**, 564 (1964); (b) J. P. Chesick, *ibid.*, **82**, 3277 (1960).

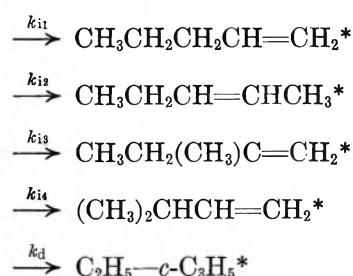
Table II: The Rate Constants and Rate Ratios for the Ketene-Butene-1 System

	k_a , sec. ^{-1a}	k_a , sec. ^{-1b}	Isomerization ^c			Insertion ^d			
			k_{a1}/k_a	k_{a2}/k_a	k_{a3}/k_a	k_{i1}/k_d	k_{i2}/k_d	k_{i3}/k_d	k_{i4}/k_d
Pure system	4.1×10^6	5.8×10^6	0.13	0.70	0.15	0.077	0.075	0.045	0.095
Oxygen system	3.6×10^6	6.4×10^6	0.00	0.85	0.15	0.120	0.070	0.070	0.125

^a Rate constants from least-squares analysis of the curves of Figure 4 which ignores all olefin decomposition. ^b Rate constants based on the most stable olefin, pentene-2, and calculated from the [pentene-2/ethylcyclopropane] vs. ω^{-1} curve.^{3b} This estimate of k_a can still be as much as a factor of 1.6 too low because of pentene-2 decomposition. ^c These results are from least-squares analysis of the [(pentene)_j/ethylcyclopropane] vs. ω^{-1} curves.^{3b} These numerical results serve to indicate that there is extensive olefin decomposition in this system; they do not reflect the true relative rates for olefin formation by ethylcyclopropane isomerization. ^d These are experimentally measured (per bond) quantities at high pressure.

C₅H₁₀ products of the total C₅H₁₀ products for the oxygen-free system, and for the system with 4 to 8% oxygen added. It reveals that at low pressures olefin decomposition and isomerization also occur in ketene systems. This behavior is shifted to lower pressures than for diazomethane,³ corresponding to the lower energy of methylene as produced by ketene photolysis.⁴ At high pressure, oxygen again has the effect (Table II) of altering the [insertion/addition] ratios from the pure system values. A more detailed analysis of the effect of oxygen in the propene and butene-1 systems is postponed to the Discussion.

The general mechanism of the reaction of methylene with butene-1 has been outlined in the preceding paper³; the same notation is continued here



The products of hot ethylcyclopropane isomerization are

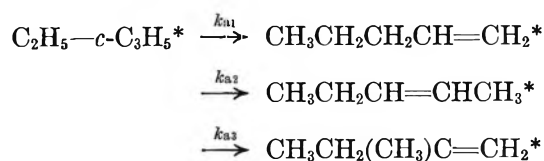


Figure 3 shows that although the pentene-2 qualitatively conforms to the simple mechanism, the pentene-1 appears to be decomposing as fast as it is formed at low pressures. The increase of 3-methylbutene-1 at low pressures in the pure system, as well as the (reduced) increase in the oxygen system, indicates that it

is being formed by some reaction in addition to free radical processes. Similar behavior was displayed by these products in the diazomethane-butene-1 system.³

Unfortunately, explicit values of k_{aj}^o could not be obtained from the data.

The [total pentene/ethylcyclopropane] vs. ω^{-1} curve (Figure 4) is roughly linear throughout the pressure region of the measurements in both the pure and oxygen systems. Only those olefins that can arise from both the insertion reaction and the isomerization of ethylcyclopropane are (or need be) included in the figure. The slopes of the curves in Figure 4 are naive measures of k_a (eq. 1), which neglect the complication of olefin decomposition; *i.e.*, they yield an apparent (too low) k_a value.

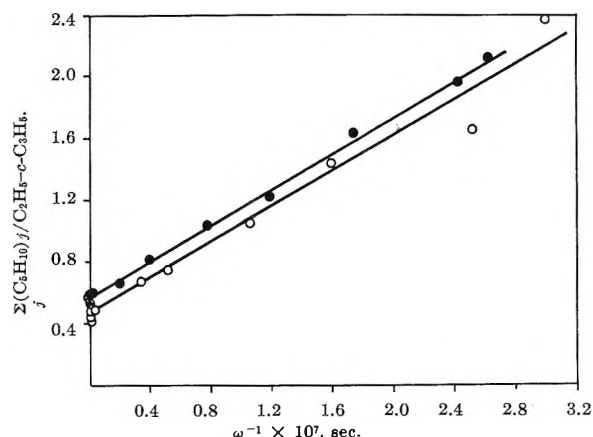


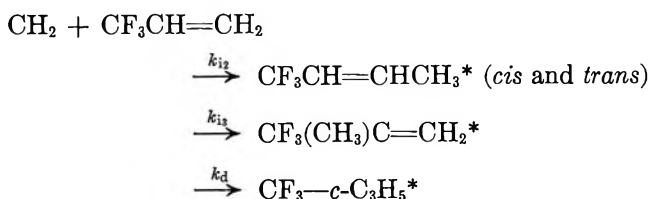
Figure 4. The variation of the pentene/ethylcyclopropane ratio with ω^{-1} where only those pentenes that arise by both insertion and ethylcyclopropane structural isomerization are included. The open circles are pure system results and the closed circles are results for 5 to 10% oxygen added.

The experimentally determined rate constants and rate ratios from these data are tabulated in Table II. Since pentene-2 decomposes more slowly than the other pentene products,³ a rate constant, k_a , was calculated

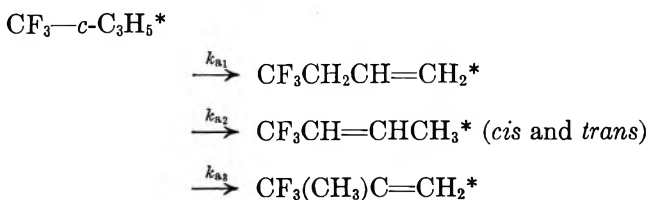
from the [pentene-2/ethylcyclopropane] pressure dependence assuming that the pentene-2 is produced by the ethylcyclopropane in the same ratio as the butene-2 is produced by chemically activated methylcyclopropane isomerization.⁸ This value is also included in Table II for both systems. It is a lower limit to the true rate.

Ketene-3,3,3-Trifluoropropene Systems. Figure 5 shows the pressure dependence of the five major products of the two series of runs over the pressure range 0.4 to 360 mm.

The principal insertion reactions of methylene on trifluoropropene are simplified in that methylene apparently does not insert across CF bonds,¹⁰ an observation that was confirmed here. The insertion and addition reactions are



The isomerization reactions of the trifluoromethylcyclopropane are



Each of the five products gave a mass spectral parent peak at mass 110. The 2-trifluoromethylpropene and 4,4,4-trifluorobutene-1 were further identified by comparison of their g.l.p.c. retention times with known samples. The major product at high pressure was unaffected by bromine (in contrast to the other products) and was identified as trifluoromethylcyclopropane. The two remaining unidentified products, the butene-2 pair, could be isomerized to each other by the technique¹¹ of addition of $\sim 1\%$ H_2S and heating to 450° for 3 min. Their identity as the butene-2 isomers was confirmed by comparison of their g.l.p.c. retention times with those of the gaseous products resulting from dehydroiodation of the liquid produced by trifluoromethylidide photolysis in propene. The pyrolysis of trifluoromethylcyclopropane supported the above product assignment.¹²

The reaction of methylene with trifluoropropene appeared very clean at all pressures. Only one extra product in the C_4 to C_6 hydrocarbon range was ob-

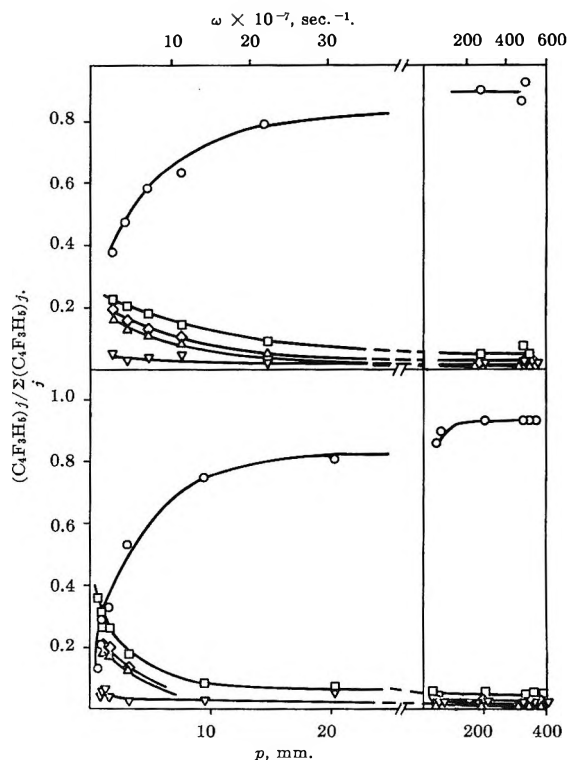


Figure 5. Variation of the $\text{C}_4\text{F}_3\text{H}_5$ product composition with total pressure in the ketene-3,3,3-trifluoropropene system. The bottom figure gives the pure system results where, for several runs, only the total of the butene-1 and *trans*-butene-2 were measured; the top figure gives the results for 5 to 10% oxygen added: trifluoromethylcyclopropane, O; trifluorobutene-1, Δ ; *trans*-trifluorobutene-2, \diamond ; *cis*-trifluorobutene-2, \square ; 2-trifluoromethylpropene, ∇ .

served and at most it amounted to only 3% of the olefin products. No C_2F_6 was observed at any pressure. Olefin decomposition is therefore not important for this system in the pressure region of these measurements.

Figure 6 presents the [total butene/trifluoromethylcyclopropane] vs. ω^{-1} curve for the two systems; the measurements in the oxygen-free system extend to lower pressures. Data obtained by least-squares analysis of these and the [(butene)₃/cyclopropane] vs. ω^{-1} plots^{3b} (not shown) are tabulated in Table III. The sparsity of the data limit the accuracy of the k_{a3}/k_a value for the pure system. The effect of oxygen, as measured at high pressure, was again to increase the relative importance of the insertion reaction a little, although it had little effect on the k_a values here be-

(10) B. A. Grzybowska, J. H. Knox, and A. F. Trotman-Dickenson, *J. Chem. Soc.*, 746 (1963).

(11) F. S. Looney and B. S. Rabinovitch, unpublished work.

(12) D. W. Placzeck and B. S. Rabinovitch, *J. Phys. Chem.*, in press.

Table III: Rate Constants and Rate Ratios for the Ketene-Trifluoropropene System

	k_a , sec. ⁻¹	k_{a1}/k_a	k_{a2}/k_a	k_{a3}/k_a	k_{i1}/k_d^a	k_{i2}/k_d^a	k_{i3}/k_d^a
Pure system	3.6×10^7	0.26	0.57	0.05	0.00	0.026	0.015
Oxygen system	4.1×10^7	0.28	0.68	0.03	0.00	0.033	0.030

^a These are high pressure measured ratios per CH bond.

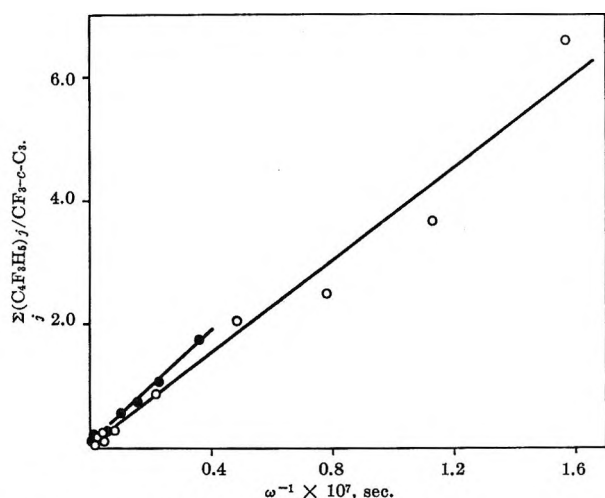
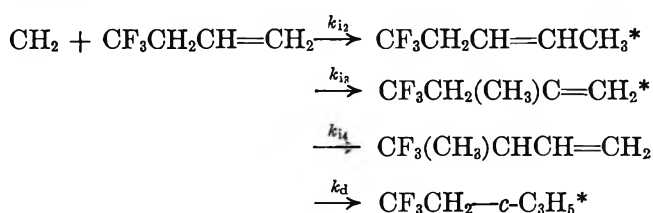


Figure 6. Variation of the trifluorobutene/trifluoromethylcyclopropane ratio with ω^{-1} for the ketene-trifluoropropene photolysis system. Open circles are pure system results and closed circles are results for 5 to 10% oxygen added.

cause of the relatively small amounts of insertion that occur in these systems in any case.

Ketene-4,4,4-Trifluorobutene-1 Systems. Figure 7 illustrates the pressure dependence of the principal products produced in both the oxygen and oxygen-free systems. Only the total of trifluoropentene-1 and 2-methyltrifluorobutene-1 was determined.

The principal addition and insertion products of methylene here are



The isomerization reactions of the trifluoroethylcyclopropane are

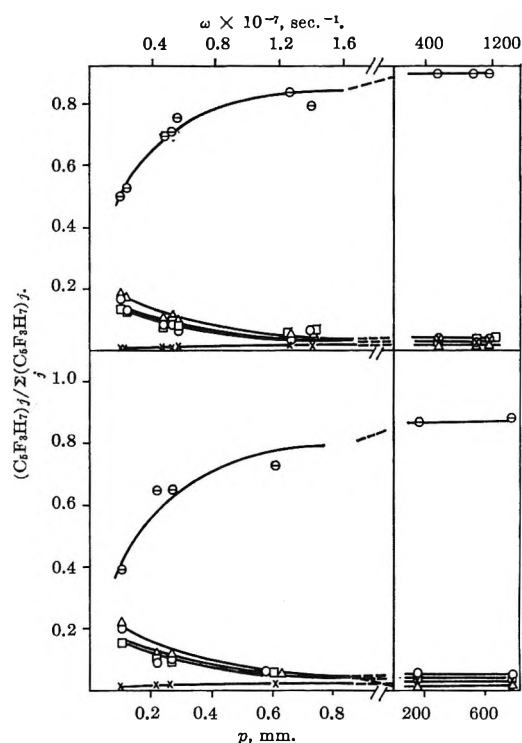
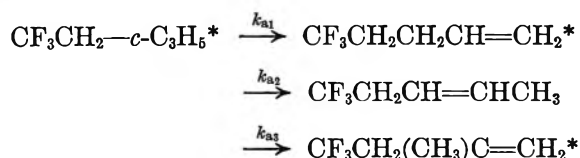


Figure 7. Variation of the $\text{C}_6\text{F}_3\text{H}_7$ composition with pressure in the ketene-4,4,4-trifluorobutene-1 photolysis system. The top figure gives the pure system results and the bottom figure gives results for 5 to 10% oxygen added: trifluoroethylcyclopropane, \ominus ; 5,5,5-trifluoropentene-1 + 2-methyl-4,4,4-trifluorobutene-1, Δ ; *trans*-5,5,5-trifluoropentene-2, \circ ; *cis*-5,5,5-trifluoropentene-2, \square ; 3-methyl-4,4,4-trifluorobutene-1, \times .

Identification of the principal products was made by comparison of g.l.p.c. retention times of similar and known compounds, their mass spectra, and their behavior with bromine.

Hot olefin decomposition does occur in these systems although not as extensively as in the analogous hydrocarbon systems. A run at 0.28 mm. with diazomethane as the methylene source (S/D for trifluoroethylcyclopropane was ~ 1),¹³ and analyzed on a 91.5-m. squalane capillary column, revealed ten products besides the principal products in the C_4 to C_6 hydrocarbon range,

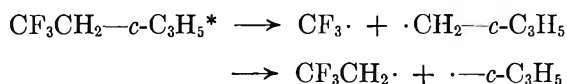
(13) F. H. Dorer and B. S. Rabinovitch, *J. Phys. Chem.*, **69**, 1973 (1965).

Table IV: Rate Constants and Rate Ratios for the Ketene-Trifluorobutene-1 System

	k_a , sec. ^{-1a}	$(k_{a1} + k_{a3})/k_a^b$	k_{a2}/k_a^b	k_{i1}/k_d^c	k_{i2}/k_d^c	k_{i3}/k_d^c	k_{i4}/k_d^c
Pure system	1.5×10^6	0.46	0.52	0.00	0.040	0.016	0.013
Oxygen system	2.0×10^6	0.44	0.50	0.00	0.050	0.023	0.015

^a These values are too low by ~20% due to neglect of olefin decomposition. ^b These ratios are from the respective [(trifluoropentene)_i/trifluoroethylcyclopropane] vs. ω^{-1} curves.^{3b} Their numerical values are only of qualitative significance because of olefin decomposition. ^c These are ratios per CH bond measured at high pressure.

and no other side products through C₇. The primary products of interest constituted 70–80% of the total products. This is in contrast to the 28 extra (higher) products that constituted 50% of the total in the diazomethane-butene-1 system at these pressures at which olefin decomposition was extensive³; side reaction went essentially to zero at high pressures. Butene-1 plus butadiene (not separated by analysis) was the major side product in this fluorocarbon system and it constituted up to 7% of the total products. Hexafluoroethane, trifluoropropene, and a small amount of a product suspected of being hexafluorobutane (CF₃CH₂CH₂CF₃) were observed. It is difficult to ascertain if the processes



take place at all.

Figure 8 shows the [total olefin/cyclopropane] vs. ω^{-1} plots for these systems. Detailed plots of [(olefin)_i/cyclopropane] are given elsewhere.^{3b} The data obtained from these plots using the measured high pressure limits are recorded in Table IV for both the pure and oxygen systems. These k_a values are probably low by a factor of ~1.2 due to olefin decomposition.

Discussion

Effect of Oxygen. In all systems studied here, the relative rate of insertion to addition by the methylene generally increased (the exact amount depending on the bond type) when 5–10% oxygen was added to a reaction mixture (Tables I to IV). The effect of oxygen on the high pressure product composition in the ketene-*cis*-butene-2 and ketene-*cis*-butene-2-*d*₈ systems has been attributed earlier to the presence of ~29% triplet methylene.^{4b} The high pressure product composition resulting from triplet methylene (produced by mercury-photosensitization of ketene) reaction with butene-1¹⁴ is compared in Table V to the measured high pressure ($p > 170$ mm.) product composition of the ketene-butene-1 (3200 Å.) photolysis

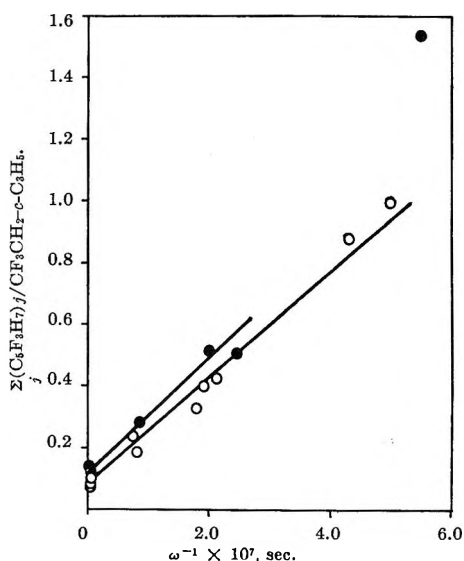


Figure 8. Variation of the trifluoropentene/trifluoroethylcyclopropane ratio with ω^{-1} where only those trifluoropentenes that arise by both insertion and trifluoroethylcyclopropane structural isomerization are included. Open circles are pure system results, closed circles are results for 5 to 10% oxygen added.

system. Not unlike an earlier comparison for ketene-*cis*-butene-2 systems,^{4b} agreement here between the oxygen results and the pure system results as corrected for the presence of ~29% triplet methylene is striking (even to the extent that although over-all insertion becomes more important in a pure singlet system, the percentage of pentene-2 product decreases).

Earlier, we suggested³ that since the percentage of apparent "insertion" products decrease in the triplet methylene-olefin systems,^{14–16} at least part of the pressure dependence of the insertion/addition ratio found in the diazomethane-olefin photolysis systems is due to an increasing concentration of triplet methylene with increase of pressure at high pressures. Indications are

(14) F. J. Duncan and R. J. Cvetanović, *J. Am. Chem. Soc.*, **84**, 3593 (1962).

(15) F. J. Duncan and R. J. Cvetanović, private communication.

(16) H. M. Frey, *J. Am. Chem. Soc.*, **82**, 5947 (1960).

Table V: Product Composition (%) for Reaction of Singlet and Triplet Methylene Radicals with Butene-1

	Triplet ^a	Exptl. ^b	Corrected ^c singlet	O ₂ results ^d
Ethylcyclopropane	79.2	61.3	54.5	54.8
Pentene-1	4.8	14.0	18.0	19.7
<i>cis</i> -Pentene-2	4.1	3.4	3.1	2.7
<i>trans</i> -Pentene-2	7.3	5.6	5.0	4.8
2-Methylbutene-1	...	3.2	4.6	4.0
3-Methylbutene-1	4.8	11.8	14.8	13.7

^a Triplet methylene reaction with butene-1 data is from the mercury-photosensitization of ketene in butene-1 (ref. 14 and private communication). ^b Experimental results measured for the pure system at high pressures. ^c Data for pure system corrected assuming the presence of 29% triplet methylene by using column 1. ^d Experimental results from this work for system with 5–10% oxygen added.

that the proportion of triplet methylene is pressure dependent in the ketene-*cis*-butene-2 systems also^{4b}; similar dependence, although not unexpected, could not be demonstrated as explicitly in the present systems because of the uncertainty in the true values of the relevant k_a and k_a° quantities.

Another manifestation of the pressure dependence of a triplet methylene component is that the rate constants for structural isomerization of cyclopropane,¹⁷ and of methylcyclopropane studied here, are enhanced by a factor of at least 2 when 5 to 10% oxygen is added to the system. These systems exhibit relatively high k_a values and were studied at pressures above 10 mm. in general. By contrast, the k_a values for the slower structural isomerization reactions of trifluoromethylcyclopropane and of dimethylcyclopropane,^{4b} and studied below 10 mm., are unaffected (or even decreased by ~30%) by the presence of oxygen. Thus, in the lower pressure region triplet methylene effects seem again to be substantially decreased.

The quantum yield of photolytic decomposition of pure ketene is pressure dependent even at 3130 Å.^{18,19}; this suggests that *some* of the present behavior could conceivably be due to changing average energy of the formed methylene with total pressure of the system due to collisional vibrational deactivation of excited singlet ketene.¹⁹ However, the pressure effects in our systems cannot be adequately explained by a possible variation of the average energy of the reacting methylene and therefore these results support the possibility of a collision-induced singlet-triplet transition of the excited ketene followed by triplet methylene formation, as suggested earlier.^{4b}

Trifluoromethyl Influence on Insertion/Addition Ratios. It has been reported that fluorine substitution

in ethylene makes the double bond and the remaining CH bonds less susceptible to reaction with methylene.²⁰ The data of ref. 13 have shown that a trifluoromethyl group adjacent to a double bond does not cause a decreased rate of methylene addition. However, the present data (Tables I to IV) reveal that the presence of a trifluoromethyl group *does* decrease the rate of methylene insertion into CH bonds *relative* to double bond addition. The extent of deactivation of the CH bond depends on its proximity to the trifluoromethyl group. The closer it is to the trifluoromethyl group the greater is its deactivation; this becomes as great as a factor of 7 to 8 in the pure and oxygen systems for the relative rate of allylic CH insertion to addition for trifluorobutene-1, as compared to the allylic CH insertion to addition ratio for butene-1, *i.e.*, $(k_{i4}/k_a)_H/(k_{i4}/k_a)_F \simeq 7-8$. Such deactivation is plausible in terms of the electrophilicity of methylene.

The Relative Rates of Olefin Formation by Alkyl Cyclopropane Isomerization. Table VI gives the ratios for the relative rates of olefin formation by methylcyclopropane and trifluoromethylcyclopropane. Due to the sparsity of the data in several cases and the experimental complications, these results are only of a semiquantitative nature. They do indicate, however, that the relative probability for formation of 2-trifluoromethylpropene by trifluoromethylcyclopropane isomerization is less than the relative probability of isobutene formation by methylcyclopropane, *i.e.*, $(k_{a3}/k_a)_H/(k_{a3}/k_a)_F = \sim 4-8$ for pure and oxygen systems. The activation energy for isobutene formation from methylcyclopropane isomerization is greater than that for the formation of the other butene isomers⁹ and these data suggest that the activation energy difference is greater yet for trifluoromethylcyclopropane isomerization.

Table VI: Comparison of the Relative Rates of Olefin Formation by Methyl Cyclopropane^a and Trifluoromethylcyclopropane

	$\frac{(k_{a1}/k_a)_H}{(k_{a1}/k_a)_F}$	$\frac{(k_{a2}/k_a)_H}{(k_{a2}/k_a)_F}$	$\frac{(k_{a3}/k_a)_H}{(k_{a3}/k_a)_F}$
Pure system	1.5	0.7	4
Oxygen system	1.4	0.6	8

^a Corrected for butene-1 decomposition.

- (17) J. W. Simons, Ph.D. Thesis, University of Washington, 1964.
 (18) B. T. Connelly and G. B. Porter, *Can. J. Chem.*, **36**, 1640 (1958).
 (19) G. B. Porter and B. T. Connelly, *J. Chem. Phys.*, **33**, 81 (1960).
 (20) A. F. Trotman-Dickenson, *Proc. Chem. Soc.*, 249 (1964).

The data of Table III show that the probability of formation of the trifluorobutene-2 is more than twice as great as the formation of trifluorobutene-1, *i.e.*, $(k_{a2}/k_{a1})_F \sim 2$. This reflects a tendency for H atoms to transfer to the C atom farthest from the trifluoromethyl group (both butene isomers arise by rupture of the same C-C bonds and involve H transfer to different C atoms with the same reaction path degeneracy). The corresponding ratio is unity⁸ for methylcyclopropane.

Decomposition of the pentene products makes a comparison like that shown in Table VI impossible for the ethylcyclopropane and trifluoroethylcyclopropane systems. However, the ratios k_{aj}/k_{a1} , in the trifluoroethylcyclopropane system (Table IV), even though uncorrected for olefin decomposition, still show that the relative rate of formation of the trifluoropentenes by the isomerization reaction is more statistical (the statistical ratio $(k_{a1} + k_{a3})/k_{a2}$ is 1.5, experimental is 0.9) than the analogous trifluorobutene isomer formation by trifluoromethylcyclopropane isomerization for which $(k_{a1} + k_{a3})/k_{a2} = 0.5$ (Table III). Removal of the trifluoromethyl from the reaction site by one $-\text{CH}_2$ group thus reduces its mechanistic influence by a factor of almost 2.

Total Cyclopropane Structural Isomerization Rate Constants. Unfortunately, the use of a naive measure of olefin formation (D) in order to obtain the total rate constant, k_a , does not yield quantitative results for molecules larger than the methylcyclopropanes because of the "hot" olefin decomposition. Other methods that do not depend on a direct count of D have been used to obtain the k_a quantities for the larger cyclopropanes and are reported in a later paper.¹³

Since butene-1 decomposition is small and can be corrected in the methylcyclopropane system, while fluorobutene decomposition is negligible in the pressure region of the measurements for trifluoromethylcyclopropane, their measured rate constants, k_{aH} and k_{aF} , are fairly reliable. The rate constants measured here for these two systems (without oxygen) are a factor of ~ 3 lower than those obtained for these molecules when diazomethane is the methylene precursor¹³; this is about the difference expected due to the difference in the methylene energy for the two sources.⁴ A more quantitative experimental investigation and a theoretical treatment of the rate constants for alkyl and trifluoroalkylcyclopropane structural isomerization reactions is given in the following paper.¹³

An Experimental Generalization of Quantum Statistical Weight Effects in Nonequilibrium Unimolecular Reactions¹

by F. H. Dorer² and B. S. Rabinovitch

Department of Chemistry, University of Washington, Seattle, Washington 98106 (Received December 28, 1964)

The unimolecular rate constants for the structural isomerization of a series of vibrationally excited alkylcyclopropanes and for their trifluoro analogs have been measured. The compounds $\text{CH}_3(\text{CH}_2)_n\text{-}c\text{-C}_3\text{H}_5$ ($n = 0, 1, 2$) and $\text{CF}_3(\text{CH}_2)_n\text{-}c\text{-C}_3\text{H}_5$ ($n = 0, 1, 2$) were studied by an internal comparison chemical activation technique. Confirmation of the internal comparison technique was obtained by measurement of the rate constants for a member of the series, ethylcyclopropane, by an alternative butane monitor technique. These series of molecules provide two different types of examples and tests of the variation of microscopic elementary rate constants that occur when systematic variation of molecular structure, and hence of molecular vibrational-rotational frequency patterns, is made: first, successive methylene group structural increments, and second, the simpler F atom substitution for H atom. With regard to the first, the isomerizations of the homologous series of molecules $c\text{-C}_3\text{H}_6$, $\text{CH}_3\text{-}c\text{-C}_3\text{H}_5$, $\text{C}_2\text{H}_5\text{-}c\text{-C}_3\text{H}_5$, and $n\text{-C}_3\text{H}_7\text{-}c\text{-C}_3\text{H}_5$ and of a shorter second series $\text{CF}_3\text{-}c\text{-C}_3\text{H}_5$, $\text{CF}_3\text{CH}_2\text{-}c\text{-C}_3\text{H}_5$, and $\text{CF}_3\text{CH}_2\text{CH}_2\text{-}c\text{-C}_3\text{H}_5$ provide two more new examples and tests of the relation between rate and structure within homologous series. With regard to the second, comparison between the two series provides an effect owing to the replacement of three H by three F atoms; it yields an experimental quantum statistical effect of 1.69 per F atom, which is in excellent agreement with the theoretical RRKM calculations for these systems in which all internal degrees of freedom are taken as active and efficient intramolecular energy relaxation occurs. Agreement between the calculated and experimental rate constants for members of the two homologous series is also good.

Introduction

Experimental investigation of quantum statistical weight effects³ in nonequilibrium unimolecular reactions has so far been limited to the study of intermolecular secondary isotope effects.⁴⁻⁷ Depending upon the mode of activation of the molecules, both *normal*⁴ and *inverse*⁵ secondary isotope effects may arise. Chemical activation has been used to investigate the magnitudes of normal secondary isotope effects with respect to extent of isotopic substitution and energetic parameters.⁶ Theoretical formulation³ of these systems in terms of the RRKM theory⁸ has been given. Agreement between theory and experiment is good.

A requirement for a "pure" secondary normal isotope effect is that substitution involves normal coordinates which are orthogonal to the reaction coordinate. Thus, substitution of D for H decreases the

ratio of the accessible volumes of phase space of activated complex to the energized species without altering the details of the potential energy surface for reaction.

(1) Supported by the National Science Foundation.

(2) National Science Foundation Predoctoral Fellow, 1962-1964.

(3) B. S. Rabinovitch, D. W. Setser, and F. W. Schneider, *Can. J. Chem.*, **39**, 2609 (1961); B. S. Rabinovitch and J. H. Current, *ibid.*, **40**, 557 (1962).

(4) B. S. Rabinovitch and L. W. Setser, *J. Am. Chem. Soc.*, **84**, 1765 (1962); J. H. Current and B. S. Rabinovitch, *J. Chem. Phys.*, **38**, 1967 (1963).

(5) F. W. Schneider and B. S. Rabinovitch, *J. Am. Chem. Soc.*, **85**, 2365 (1963).

(6) J. W. Simons, B. S. Rabinovitch, and R. F. Kubin, *J. Chem. Phys.*, **40**, 3343 (1963).

(7) J. W. Simons and B. S. Rabinovitch, *J. Phys. Chem.*, **68**, 1322 (1964).

(8) R. A. Marcus and O. K. Rice, *J. Phys. Colloid Chem.*, **55**, 894 (1951); R. A. Marcus, *J. Chem. Phys.*, **20**, 359 (1952).

This condition allows experimental generalization of the investigation of quantum statistical effects by the substitution of atoms of different chemical type (rather than D) for H. Specifically, we have substituted F for H, thereby obtaining a more general experimental characterization of the dependence of quantum statistical effects on molecular vibrational frequency patterns, and this work is reported here.

General quantum statistical weight effects cannot be studied in thermal systems at (or near) the high pressure limit. The effects in question have been shown to largely cancel under equilibrium conditions, so that the microscopic rate constants for decomposition, k_E , which reflect the effects of variation of structural parameters, are not obtained.³ Low pressure, nonequilibrium thermal conditions could, in principle, be used to yield useful quantitative data of the type desired, but such information does not yet exist. Nonequilibrium data are, in fact, more readily obtained by the chemical activation method employed here.

Previously, it was shown⁷ that, even for species with high excess energy E^+ above the critical energy E_0 , secondary isotope effects may be large if E_0 is large. Ketene photolysis by 3200-Å. radiation when carried out in the presence of *cis*-butene-2 or of *cis*-butene-2-*d*₃, at 300°K., produces the respective vibrationally excited *cis*-1,2-dimethylcyclopropanes. The average energy of these hot molecules is $\langle E \rangle \sim 106$ kcal. mole⁻¹, and $\langle E^+ \rangle \sim 46$ kcal. mole⁻¹. The secondary intermolecular isotope effect for structural isomerization of these alkylcyclopropanes to olefins is 4.3.⁷ The rate constants, k_a , for structural isomerization of chemically activated $\text{CH}_3(\text{CH}_2)_n\text{-c-C}_3\text{H}_5$ ($n = 0, 1, 2$) and $\text{CF}_3(\text{CH}_2)_n\text{-c-C}_3\text{H}_5$ ($n = 0, 1, 2$) have now been measured by an internal comparison technique that does not require a direct count of the amount of decomposition. Affirmation of the results of this technique has also been made by an independent measurement of the rate constants for one of the molecules in the series by an alternate method using a butane monitor.

Activation by methylene addition to olefins at room temperature offers the advantage that the distribution function of the formed species is quite narrow⁹; *i.e.* $f(E) \sim \delta(E)$, so that $k_a \sim k_{\langle E \rangle}$, where k_a is the experimental rate constant, and $k_{\langle E \rangle}$ is the specific rate constant at the average energy $\langle E \rangle$. The exact value of $\langle E \rangle$ is a function of the exothermicity of the addition reaction and of the average thermal energy of the reactants. The normal quantum statistical weight effect is then given by

$$\frac{k_{aH}}{k_{aF}} \sim \frac{k_{\langle E \rangle H}}{k_{\langle E \rangle F}} = \frac{I_{rH}}{I_{rF}} \times \frac{\sum_0^{E^+} P(E^+_{vr})_H}{\sum_0^{E^+} P(E^+_{vr})_F} \times \frac{N^*(E)_F}{N^*(E)_H} \quad (1)$$

where I_{rH}/I_{rF} is the ratio of the partition functions for the adiabatic degrees of freedom, $P(E^+_{vr})$ is the sum of the vibration-rotation energy eigenstates at the energy E^+_{vr} for the activated complexes, and the $N^*(E)$ are the densities of vibration-rotation energy eigenstates at the energy E for the activated molecules.

The results obtained in the present work also provide microscopic rate constants for two homologous series of molecules, *c*-C₃H₆ through CH₃(CH₂)₂-*c*-C₃H₅ and CF₃-*c*-C₃H₅ through CF₃(CH₂)₂-*c*-C₃H₅, at a much greater level of total energy and of critical energy than the alkyl radical series¹⁰ recently reported.

Experimental

Materials. Diazomethane was prepared and then stored at -196° as described previously.¹¹ The olefins were Phillips research grade materials that were further purified by gas chromatography where necessary. The 3,3,3-trifluoropropene and 4,4,4-trifluorobutene-1 preparations have been described.¹² The 5,5,5-trifluoropentene-1 was prepared in small (3%) yields, based on the starting acid, by the sulfur tetrafluoride reaction with 5-pentenoic acid under conditions similar to those used for the trifluorobutene-1 preparation.¹²

Apparatus and Procedures. Photolysis of olefin-trifluoro olefin mixtures containing 10% diazomethane was carried out at room temperature for 1 to 2 hr. with 4358-Å. radiation by similar procedures and with the same apparatus as those used for the diazomethane-olefin photolysis experiments.¹¹ The fluoro olefin: olefin relative concentrations used for these runs were trifluoropropene:propene = 0.551, trifluorobutene-1:butene-1 = 0.840, trifluoropentene-1:pentene-1 = 0.699; for standard mixtures, not even their composition need be known accurately with this technique. The Pyrex reactors were pumped to 10⁻⁵ mm. before being loaded with reactants. After photolysis, the product mixtures were run through a short silver nitrate-glycerol on firebrick column to decompose any unreacted diazomethane.

(9) D. W. Setser and B. S. Rabinovitch, and J. W. Simons, *J. Chem. Phys.*, **40**, 1751 (1964); D. W. Setser and B. S. Rabinovitch, *Can. J. Chem.*, **40**, 1425 (1962).

(10) M. J. Pearson and B. S. Rabinovitch, *J. Chem. Phys.*, **41**, 280 (1964); see M. J. Pearson, B. S. Rabinovitch, and G. Z. Whitten, *ibid.*, submitted, for the deuterioalkyl series.

(11) F. H. Dorer and B. S. Rabinovitch, *J. Phys. Chem.*, **69**, 1952 (1965).

(12) F. H. Dorer and B. S. Rabinovitch, *ibid.*, **69**, 1964 (1965).

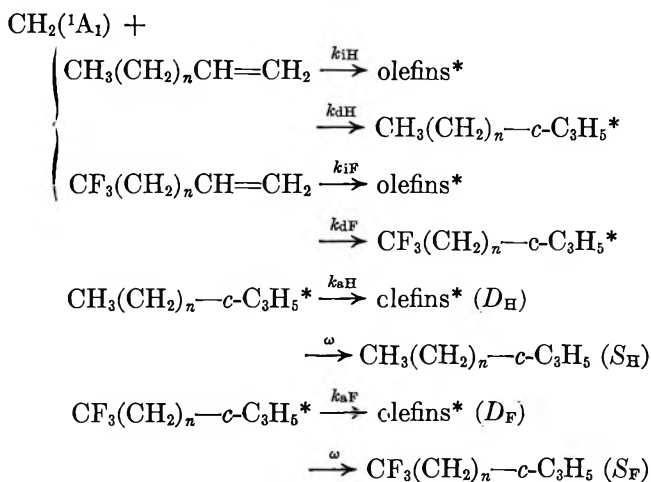
Experiments were also performed with butene-1-butane mixtures which were photolyzed with diazomethane. The butene-1 : *n*-butane ratio was 1.15.

Analysis. (a) *Propene-Trifluoropropene System.* The products of the photolysis were analyzed on a combination of a 40% silver nitrate-ethylene glycol on firebrick column followed by a short dibutylphthalate or by a dimethylsulfolane column. Two analyses were necessary with these columns in order to obtain the trifluoromethylcyclopropane:methylcyclopropane ratio. Calibrated peak areas were used to determine these product ratios although, in general, absolute product sensitivities were not actually required by this experimental technique.

(b) All other systems were analyzed on a 109.4-m. squalane capillary column with an argon-type detector. Although in several cases not all of the products were completely separated by this column, the relative amounts of the primary stabilization products of interest were always isolated for each of the systems.

Results

Internal Comparison Method. Methylene was produced by photolysis and allowed to react with mixtures of olefins and trifluoro olefins at room temperature



The rate constants, k_a , for structural isomerization are defined as $\omega \times (D/S)$, where ω is the specific collision frequency of the energized species. If the decomposition and stabilization events following activation are both of random nature, then

$$\frac{\omega_{\text{H}} R_{\text{H}}}{k_{a\text{H}} + \omega_{\text{H}}} = S_{\text{H}} \quad (2)$$

$$\frac{\omega_{\text{F}} R_{\text{F}}}{k_{a\text{F}} + \omega_{\text{F}}} = S_{\text{F}} \quad (3)$$

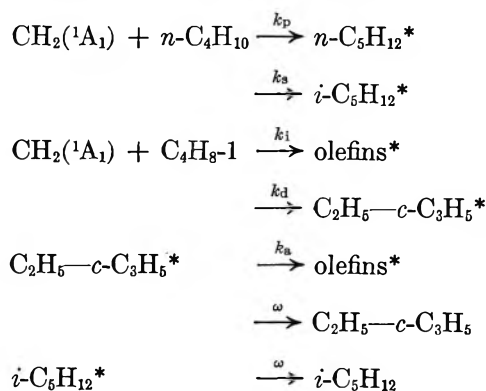
where R_{F} is the total amount of $\text{CH}_3(\text{CH}_2)_n\text{-c-C}_3\text{H}_5^*$ formed, and similarly for R_{H} . Division of (2) by (3)

with rearrangement yields

$$k_{a\text{F}} = \frac{\omega_{\text{F}} R_{\text{F}}}{\omega_{\text{H}} R_{\text{H}}} \left[\frac{S_{\text{H}}}{S_{\text{F}}} (k_{a\text{H}} + \omega_{\text{H}}) \right] - \omega_{\text{F}} \quad (4)$$

The ratio $[R_{\text{F}}/R_{\text{H}}]$ depends on the relative rate of addition of methylene to the two reactant olefins, $k_{d\text{F}}/k_{d\text{H}}$, and can, in principle, be measured at pressures high enough so that no decomposition of the formed cyclopropanes occurs. Measurement of the ratio $S_{\text{H}}/S_{\text{F}}$ at any two lower pressures where decomposition occurs leads to the determination of the two unknowns $k_{a\text{H}}$ and $k_{a\text{F}}$ through eq. 4. Alternatively, three measurements of $S_{\text{H}}/S_{\text{F}}$ in the low pressure region may be used to calculate the three unknowns $k_{a\text{F}}$, $k_{a\text{H}}$, and $k_{d\text{F}}/k_{d\text{H}}$ by eq. 4.

Butane Monitor Method. An independent check of the above method was made by measurement of k_a for ethylcyclopropane isomerization by the procedure of treating methylene with an *n*-butane-butene-1 mixture. Experiments on methylene reaction with pure *n*-butane revealed that, although the apparent primary-secondary C-H insertion ratio is pressure dependent, the formed vibrationally excited *n*-pentane and isopentane did not decompose appreciably (<10%) even at the lowest pressure (0.3 mm.). Therefore, from the known, measured relative rates of methylene reaction with butene-1 and *n*-butane, either of these pentane products could be used to monitor the disappearance of ethylcyclopropane even in its low pressure region. In these experiments, isopentane was actually used as standard for analytical reasons. The following scheme illustrates the principal processes



Equation 5 may be derived for this system by application of the steady-state assumption to the concentrations of the excited species

$$\frac{i\text{-C}_5\text{H}_{12}}{\text{C}_2\text{H}_5\text{-c-C}_3\text{H}_5} = \frac{1}{\omega} \left[\frac{k_{\text{a}} \times \text{C}_4\text{H}_{10}}{\text{C}_4\text{H}_8\text{-1}} \times \frac{k_{\text{a}}}{k_{\text{d}}} \right] + \frac{k_{\text{a}}}{k_{\text{d}}} \times \frac{\text{C}_4\text{H}_{10}}{\text{C}_4\text{H}_8\text{-1}} \quad (5)$$

Here C_4H_{10}/C_4H_8-1 is the ratio of the concentrations of the reactant hydrocarbons. A plot of $[i-C_5H_{12}/C_2H_5-c-C_3H_6]$ vs. ω^{-1} should then be a straight line; its slope and intercept yield k_a and k_s/k_a .

Internal Comparison Measurements. Figure 1 illustrates the experimental results in the form of S_H/S_F ratios as a function of ω^{-1} for the three pairs of molecules studied. Within experimental error there was no difference in the relative rate of methylene addition to the double bonds of the two propenes. By contrast, fluorine substitution directly on the double bond in ethylene decreases the rate of addition to the double bond.¹³ It was then assumed that there was no difference in the relative rate of addition to the two butene-1 and the two pentene-1 molecules. Any error in this assertion has absolutely no consequence for the determination of k_{aH} and k_{aF} from eq. 4. It was

found for each mixture that the high pressure limiting values of double bond addition, as calculated by use of eq. 4 with the lower pressure data, agreed with the measured high pressure ratios. There was, thus, no pressure dependence of the relative rate of methylene addition to the two olefins, in contrast to pressure dependence of the *internal* insertion: addition ratios reported earlier for butene-1.¹¹

The data for the trifluoromethylcyclopropane: methylcyclopropane ratio were less precise since two analyses per run were necessary; the closeness on the pressure scale of some of the measurements accentuated the experimental error. Consequently, eq. 4 was applied only to measurements not adjacent in pressure in order to minimize the experimental error on k_{aH} and k_{aF} .

For the remaining two systems, eq. 4 was applied to all possible pairs of low pressure runs to obtain average values of k_{aH} and k_{aF} . The experimental results for these systems by this method may be found in Table I.

***n*-Butane Monitor Measurements.** The isopentane: ethylcyclopropane ratio is illustrated as a function of ω^{-1} in Figure 2. Least-squares analysis of all the runs gives $k_a = 2.4 \times 10^7 \text{ sec.}^{-1}$ for ethylcyclopropane isomerization. However, insertion: addition ratios in diazomethane-hydrocarbon systems are known to be pressure dependent,¹¹ and a better evaluation of the rate is made by considering only the low pressure measurements (here $p \leq 3.2 \text{ mm.}$). The five low pressure results give $k_a = 1.9 \times 10^7 \text{ sec.}^{-1}$, in good agreement with the value reported in Table I.

Further evidence of the pressure dependence of the insertion: addition ratio is provided by these runs. The extrapolated value for k_s/k_a (per secondary C-H

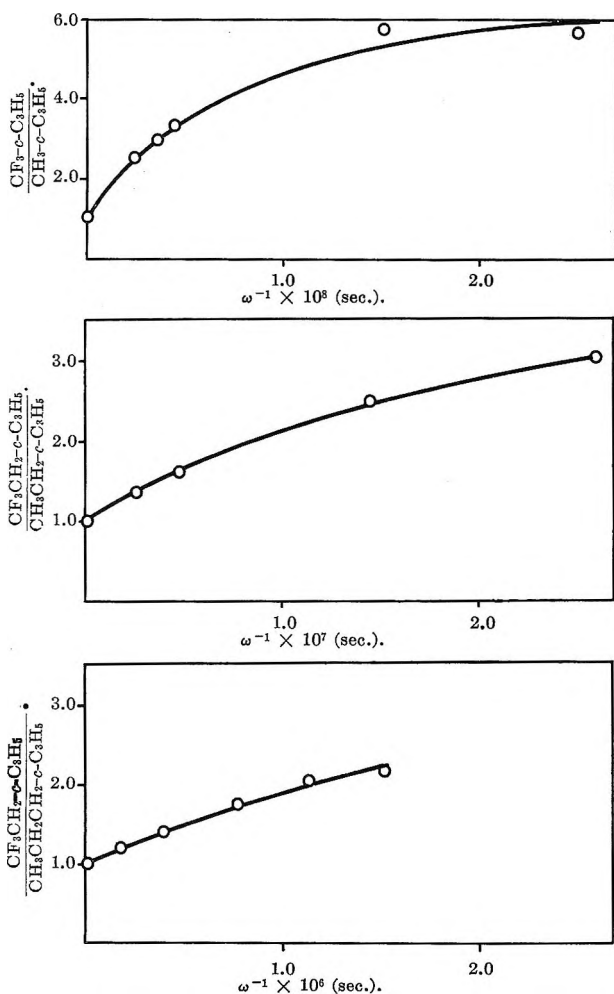


Figure 1. Plots of relative amounts of stabilization products vs. ω^{-1} for the several internal comparison systems at 25°. The data are normalized to a 1:1 mixture ratio of the reactant olefins.

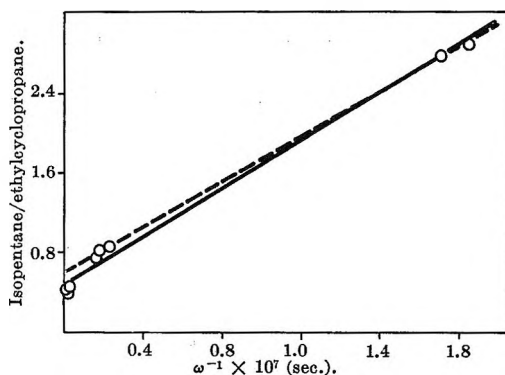


Figure 2. Plot of the isopentane:ethylcyclopropane ratio vs. ω^{-1} for diazomethane photolysis in a butene-1 and *n*-butane mixture at 25°. The butene-1:*n*-butane ratio was 1.15.

(13) A. F. Trotman-Dickenson, *Proc. Chem. Soc.*, 249 (1964).

Table I: Summary of Calculated and Experimental Rate Constants

System	$\langle \bar{\nu} \rangle$, kcal. mole ⁻¹	E_0 , kcal. mole ⁻¹	$k_{(E)}$, sec. ⁻¹	k_a (exptl.), sec. ⁻¹	$\frac{\langle k_{(E)} \rangle_H}{\langle k_{(E)} \rangle_F}$	$\frac{\langle k_a \rangle_H}{\langle k_a \rangle_F}$
c-C ₃ H ₆ ^a	113.0	62.7	(4.5 × 10 ¹⁰)	4.5 × 10 ¹⁰		
CH ₃ -c-C ₃ H ₅	107.9	61.4	3.98 × 10 ⁹	9.7 × 10 ⁸	9.7 ^b	8.1
C ₂ H ₅ -c-C ₃ H ₅	108.6	61.4	1.79 × 10 ⁷	2.0 × 10 ⁷	4.6	4.5
		60.4	2.36 × 10 ^{7c}		6.1 ^c	
C ₃ H ₇ -c-C ₃ H ₅	109.6	61.4	1.27 × 10 ⁸	1.4 × 10 ⁸	4.5	4.8
		60.4	1.68 × 10 ^{8c}		6.0 ^c	
CF ₃ -c-C ₃ H ₅	109.0	64.0	4.10 × 10 ⁷	1.2 × 10 ⁸		
CF ₃ CH ₂ -c-C ₃ H ₅	109.7	61.4	3.88 × 10 ⁶	4.4 × 10 ⁶		
CF ₃ CH ₂ CH ₂ -c-C ₃ H ₅	110.6	61.4	2.80 × 10 ⁶	2.9 × 10 ⁶		

^a Data of ref. 7. ^b Calculated for ΔE_a (i.e., $E_{aF} - E_{aH}$) = 2.6 kcal. mole⁻¹ for this pair. ^c Calculated with the possible assertion ΔE_a (i.e., $E_{aF} - E_{aH}$) = 1 kcal. for this pair; the boldface value, for $\Delta E = 0$, is considered more correct for the propyl ratio and may be more correct for the ethyl ratio.

bond) from the low pressure runs ($p \leq 3.2$ mm.) is 0.17, and the value measured at high pressure (160 mm. $< p < 1000$ mm.) is 0.12.

Discussion

Calculational Results. Comparison with Experiment. The pertinent energy parameters for a diazomethane source of methylene are presented in Table I and are discussed in Appendix I. The level of excitation is increased somewhat relative to a ketene source. The rate ratio $k_{(E)H}/k_{(E)F}$ is given by eq. 1. In the calculations, all vibrational and internal rotational modes have been taken as active for both the energized molecules and their respective activated complexes. For both the alkyl- and trifluoroalkylcyclopropanes it is more instructive at this time to consider a general model for the isomerization complexes that is rational for all of the cyclopropanes (with appropriate alterations for each specific species) rather than to attempt, in each case, to fit the existing thermal data which display some difficulty interpretable, if minor, vagaries. The details of the calculations including frequency assignments are given in Appendix II.

A. Quantum Statistical Weight Effect Produced by F Atom Substitution for H (k_{aH}/k_{aF}). Table I gives both the experimental and calculated rate ratios. Their agreement is remarkably good. One certainly expects, as indeed thermal activation energy measurements show (Appendix I), that the trifluoromethyl group exerts a mechanistic effect on trifluoromethylcyclopropane structural isomerization. However, the activation energy measurements also show that these mechanistic effects are quite small for trifluoroethylcyclopropane,^{14,15} and one is reasonably confident that they are negligible for the trifluoropropylcyclopropane,

so that at least the rate ratio k_{aH}/k_{aF} for the propyl-cyclopropane pair represents essentially a pure quantum statistical weight effect. These experiments, thus, provide the first¹¹ illustration that experimental investigation of atomic substitution may be extended to substitution of one type of atom by others of different chemical type and need not be limited to isotopic substitution.

The ratio of the total rates of propyl and trifluoropropylcyclopropane isomerization is 4.8. This statistical weight effect of ~ 1.69 per F atom is considerably greater than the value of ~ 1.2 per D measured in a similar cyclopropane system with approximately the same energetic parameters.⁷ F atom substitution for H in systems having lower relative values of $\langle E^+ \rangle$ should cause an even more pronounced effect on rates.

B. Rates in Homologous Series. The present data and calculations provide still another manifestation of the effect of molecular vibrational-internal rotational frequency patterns on microscopic rate constants, k_E , namely, a more complex but interesting comparison of members of a homologous series. For a particular mode of activation, addition of a methylene group to the side chain causes an increase in both $N^*(E)$ and $\Sigma P(E^+_{vr})$ in eq. 1, while altering the potential energy surface for the reaction little or not at all. The alkyl and deuterioalkyl radical series¹⁰ have so far provided the only examples of quantitative experimental investigations of this effect. The observed decrease in $k_{a\infty}$ per added methylene group for (2-butyl to 2-octyl) radical decomposition was a factor of ~ 5 (al-

(14) F. H. Dorer, B. S. Rabinovitch, and D. W. Placzek, *J. Chem. Phys.*, **41**, 3995 (1964).

(15) D. W. Placzek, *J. Phys. Chem.*, **69**, 1782 (1965).

though the intrinsic factor would be ~ 8 if excitation energy were constant in the series, rather than rising a little as it did); in those systems $\langle E \rangle$ was ~ 44 to 48 kcal. mole $^{-1}$ and E_0 was ~ 31 – 33 kcal. mole $^{-1}$. In the present studies, the alkyl- and trifluoroalkylcyclopropanes provide two further examples of such reaction series, but at a much higher level of total energy, critical energy, and excess energy. They, therefore, provide an illustration of the effect on $k_{(E)}$ produced by this type of vibrational-rotational frequency pattern change at a different level of these energy parameters. In a preceding paper,¹¹ data were presented for a fifth reaction series, the decomposition of homologous alkenes.

Cyclopropane may be compared as a member of one series (Table I) along with methyl-, ethyl-, and propylcyclopropanes; this is permissible because the difference in E_0 for cyclopropane relative to the other members is only 2 kcal. relative to the very large values of both $\langle E \rangle$ and $\langle E^+ \rangle$, which tends to minimize the effect of small "mechanistic" differences. Again, as with the alkyl radical series, agreement between theory and experiment is fairly good, particularly for the larger molecules. The principal disagreement between calculation and experiment for the alkylcyclopropanes is those comparisons involving methylcyclopropane. The error here may be due in part to uncertainties in the energy parameters. The decrement in $k_{(E)}$ per additional methylene group is considerably greater than that measured in the alkyl radical series. This change in the increment per methylene group with change of energy parameters reflects the nature of the changes in the sum and density terms in eq. 1 between the different reaction series.

C. Absolute Rate Constant Comparisons. Various assumptions about the energetics, activated complexes, etc. tend to cancel, partially or completely, for comparison of rate ratios. A more stringent test of the theory is the comparison of the calculated and measured rate constants for a particular species where these assumptions do not cancel. Agreement here between $k_{(E)}$ and k_a is good, especially for the larger molecules. In fact, in view of the uncertainties in energetics and assumptions involved for the activated complex, the agreement is even better than expected. For the hydrocarbon series, the agreement extends over a range of absolute rates that vary by a factor which is $>3 \times 10^4$ from cyclopropane to propylcyclopropane.

Appendix I. Thermochemistry

$\langle E \rangle$. The heat of formation at 0°K. of ethylcyclopropane calculated from the heat of combustion data

dictates that the exothermicity of the addition of methylene to butene-1 is 2.8 kcal. mole $^{-1}$ less than that of its addition to ethylene.¹⁶ Estimates of ΔH_f° of methylcyclopropane and propylcyclopropane indicate that the heats of addition of methylene to propene, butene-1, and pentene-1 are the same at 0°K. Since for cyclopropane produced under these experimental conditions $\langle E \rangle = 110$ kcal. mole $^{-1}$,⁹ the formed alkylcyclopropanes should have $\langle E \rangle$ correspondingly lowered by 2.8 kcal. mole $^{-1}$; however, the contribution of the thermal energy of the reactants either partially or completely (depending on the complexity of the formed species) offsets the change.

It has been assumed, for lack of thermochemical data, that the exothermicity of the addition of methylene to the fluoro olefins is the same as for addition to the corresponding olefin. The validity of this assumption improves along the two homologous series.

E_0 . The following measured thermal activation energies, E_a , are relevant (kcal. mole $^{-1}$): CH₃-c-C₃H₆, 63.2 (ref. 17); C₂H₅-c-C₃H₅, 61.6 (ref. 18); (CH₃)₂-c-C₃H₄, 63.2 (ref. 19); *trans*-CH₃-c-C₃H₄CH₃, 63.3 (ref. 20); CF₃-c-C₃H₅, 65.6 (ref. 15); CF₃CH₂-c-C₃H₅, 63.6 (ref. 15). From the value of E_a for methylcyclopropane, the calculated²¹ value of E_0 is 61.4 kcal. Some uncertainties regarding the pyrolysis mechanism of ethylcyclopropane suggest that the measured E_a for this molecule is not precisely established. Inspection of the E_a values for the dimethyl molecules similar to ethylcyclopropane offers no support for a low value of 61.6 kcal., and for the purposes of these calculations a composite value of 63.2 kcal. mole $^{-1}$ was also chosen from which, again, E_0 is 61.4 kcal. mole $^{-1}$. The same value is reasonably assumed also to apply for propylcyclopropane. Computational results for some lower values of E_0 for ethyl- and propylcyclopropane are also included in Table I but are less compatible with the experimental results.

The trifluoromethyl group causes an increase in E_a for ring rupture. The magnitude of the effect depends upon the proximity of the trifluoromethyl to the ring. Since the activation energy increase for trifluoroethylcyclopropane relative to the hydrogen analog is quite

(16) Relevant heat of formation data and explanation of their origin are contained in ref. 11.

(17) (a) D. W. Setser and B. S. Rabinovitch, *J. Am. Chem. Soc.*, **86**, 564 (1964); (b) J. P. Chesick, *ibid.*, **82**, 3277 (1960).

(18) M. L. Halberstadt and J. P. Chesick, private communication.

(19) M. C. Flowers and H. M. Frey, *J. Chem. Soc.*, 1157 (1962).

(20) M. C. Flowers and H. M. Frey, *Proc. Roy. Soc. (London)*, **A260**, 424 (1961).

(21) S. Glasstone, K. J. Laidler, and H. Eyring, "The Theory of the Rate Processes," McGraw-Hill Book Co., New York, N. Y., 1941, p. 194.

Table II: Frequency Assignments for the Alkylcyclopropanes^a

Motion	CH ₃ -c-C ₃ H ₅ ^b	C ₂ H ₅ -c-C ₃ H ₅ ^b	C ₃ H ₇ -c-C ₃ H ₅ ^b
Skeletal bending	291, 349	290, 570 441	290, 370 441, 155
Torsion	225	225, 150	225, 100 88
HCC ring ^c	<i>756, 804</i> 810, 911 983, 1016 1111, 1387	<i>747, 768</i> 817, 918 957, 1012 1107, 1329	<i>747, 768</i> 817, 918 957, 1012 1107, 1329
HCH ring	1419, 1488	1427, 1460	1427, 1460
Ring deformation	<i>889, 1047</i> <i>1202</i>	<i>890, 1029</i> <i>1198</i>	<i>890, 1029</i> <i>1198</i>
C-C stretch	968	983, 1088	983, 1088(2)
HCC methyl	1021, 1072	941, 1041	941, 1041
HCH methyl	1380, 1465 1474	1383, 1460(2)	1383, 1460(2)
HCC methylene CH ₂ -CCH methyl- ene		1273, 1310 768	1273(2), 1310(2) 768(2)
HCH methylene		1444	1444(2)
CH stretch-ring	3017(2), 3055 3079, <i>3100</i>	3006(2), 3069(2) <i>3080</i>	3006(2), 3069(2) <i>3080</i>
CH stretch methyl CH stretch meth- ylene	2898, 2976(2)	2909, 2965(2)	2909, 2965(2)
		2936, 2965	2936(2), 2965(2)

^a Frequencies are in units of cm.⁻¹. ^b The italic frequencies were changed to the following values in constructing the activated complexes: HCC ring, 670 and 680; ring deformations, 640, 930, and 1300; CH stretch-ring, 0. The remaining frequencies were not changed. ^c The nomenclature in this column is that of ref. 22a.

small (<1 kcal. mole⁻¹), the activation energy difference for the propylcyclopropane pair may be assumed to be negligible. Correspondingly, the critical energy differences between the light and the trifluoropropylcyclopropanes are close to zero.

Appendix II. Computational Details

Molecular Vibration Models. (a) *Alkylcyclopropanes.* The molecular vibrational frequency assignments for methyl- and ethylcyclopropane^{22a} were extended, by addition of the nine frequencies associated with another methylene group, to include propylcyclopropane. Calculations were made in which the methyl torsion was taken either as a free rotation or as a libration in both the activated complex and the excited molecules; the former treatment raises the values of k_a by only 20%. All other internal rotations were assigned as low librational frequencies.^{10, 22b}

The activated complexes were geometrically similar to the cyclopropane model for isomerization to propylene.¹⁴ However, there are three different activated complexes⁷ corresponding to formation of these different olefin isomers by each alkylcyclopropane molecule. An over-all complex was constructed for each alkylcyclopropane from a weighted average of the three different complexes. The frequency assignments fit

the measured thermal data for methylcyclopropane structural isomerization.^{17a}

(b) *Trifluoroalkylcyclopropanes.* The molecule frequency assignments were made by appropriate alteration of their hydrocarbon analogs. The trifluoromethyl frequency assignments were guided by the available assignments for 1,1,1-trifluoroethane²³ and hexafluoropropene.²⁴ Bending frequencies were constructed by analogy with the *n*-propyl halide²⁵ and isopropyl halide skeletal motions.²⁶ Mass effects on the ring frequencies were deduced by extension of the alteration produced in cyclopropane by addition of a methyl, ethyl, or propyl group to a trifluoromethyl, trifluoroethyl, and trifluoropropyl group.

The activated complexes were assigned the same geometrical configuration as their hydrocarbon analogs.

Table III: Frequency Assignments for the Trifluoroalkylcyclopropanes^a

Motion	CF ₃ -c-C ₃ H ₅ ^b	CF ₃ CH ₂ -c-C ₃ H ₅ ^b	CF ₃ CH ₂ CH ₂ -c-C ₃ H ₅ ^b
Skeletal bending	200, 300	200, 320 335	150, 290 325, 335
Torsion	90	90, 80	90, 80, 60
HCC ring ^c	<i>630, 750</i> 810, 870 920, 1000 1100, 1170	<i>620, 750</i> 817, 847 920, 1000 1100, 1120	<i>620, 747</i> 817, 847 920, 1000 1100, 1120
HCH ring	1419, 1450	1427, 1430	1427, 1430
Ring deformation	<i>700, 1036</i> <i>1202</i>	<i>700, 1020</i> <i>1198</i>	<i>700, 1020</i> <i>1198</i>
C-C stretch	700	800, 820	800, 900 983
FCC methyl	365(2)	365(2)	365(2)
FCF methyl	541, 361 605	541, 361 605	541, 561 605
HCC methylene CH ₂ -CCH methyl- ene		1170, 1250 768	1273(2), 1310(2) 768(2)
HCH methylene		1444	1444(2)
CH stretch-ring	3017(2), 3055 3079, 3100	3006(2), 3069(2) 3080	3006(2), 3069(2) 3080
CF stretch methyl CH stretch meth- ylene	1233(2), 1280	1233(2), 1280	1233(2), 1280
		2936, 2965	2936(2), 2965(2)

^a Frequencies are in units of cm.⁻¹. ^b The italic frequencies were changed to the following values in constructing the activated complexes: HCC ring, 600 and 620; ring deformations, 575, 930, and 1300; CH stretch-ring, 0. The remaining frequencies were not changed. ^c See footnote c, Table II.

(22) (a) L. M. Sverdlov and E. P. Kraynov, *Opt. i Spektroskopiya*, **7**, 460 (1959); (b) B. S. Rabinovitch and D. W. Setser, *Advan. Photochem.*, **3**, 1 (1963).

(23) J. R. Nielsen and H. H. Claassen, *J. Chem. Phys.*, **18**, 1471 (1950).

(24) J. R. Nielsen, H. H. Claassen, and D. C. Smith, *ibid.*, **20**, 1916 (1952).

(25) J. K. Brown and N. Sheppard, *Trans. Faraday Soc.*, **50**, 1164 (1954).

(26) N. Sheppard, *ibid.*, **46**, 533 (1950).

There was some frequency lowering for increased mass effects. All internal rotations were assigned as low librational frequencies. The fit of k_∞ given by these models as compared with the thermal isomerization data¹⁶ was good for trifluoromethylcyclopropane (within ~50%) and fair for trifluoroethylcyclopropane (within a factor of 3). The frequency assignments are tabulated in Tables II and III.

Further computational details and results of calculations for various models may be found elsewhere.²⁷

Computations. The I_r ratio in eq. 1 reduces to the

product of the ratio of the principal moment of inertia ratio of the complex and molecule and the reaction path degeneracy. The moment of inertia ratio is ~1.1, and the reaction path degeneracy is 10.

Acknowledgment. The evaluation of the vibrational-rotational energy eigenstate sums and density terms was done on an IBM 709 computer using a program written by Mr. G. Z. Whitten.

(27) F. H. Dorer, Ph.D. Thesis, University of Washington, 1965.

The Solution Thermochemistry of Polyvalent Electrolytes. III.

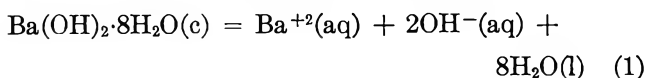
Barium Hydroxide Octahydrate

by Harry P. Hopkins, Jr., and Claus A. Wulff¹

Department of Chemistry, Carnegie Institute of Technology, Pittsburgh, Pennsylvania 15213
(Received December 28, 1964)

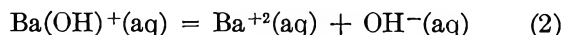
The solution thermochemistry of $\text{Ba}(\text{OH})_2 \cdot 8\text{H}_2\text{O}$ has been investigated using a newly determined enthalpy of solution with data from the literature. The major problem besetting this system is the value of the ionization constant for $\text{Ba}(\text{OH})^+$. Evidence is presented favoring a value of $K_2 = 0.006$ rather than the commonly accepted value of 0.23. For dissolution of the octahydrate, we compute $\Delta G^\circ = 4.9 \pm 0.2$ and $\Delta H^\circ = 13.7 \pm 0.1$ kcal./mole, and for the standard partial molal entropy of $\text{Ba}(\text{OH})^+$, 14 cal./(mole °K.).

As part of a continuing investigation of the solution thermochemistry of polyvalent electrolytes, we have determined the enthalpy of solution of barium hydroxide octahydrate in water, *i.e.*, ΔH_1° for eq. 1. A previous



paper in this series² supported the conclusion that calcium hydroxide is a "weak" base in its second ionization. Data in the literature³⁻⁶ indicate similar behavior for barium hydroxide but show considerable discord with respect to the value for the second ionization constant. Davies,^{3a} and Gimblett and Monk,^{3b}

using the data of Harned and Mason^{4,5} report $K_2 = 0.23$ for



Kruger and Thilo,⁶ however, report $K_2 = 0.006$ at 20°.

(1) To whom inquiries should be addressed.

(2) H. P. Hopkins, Jr., and C. A. Wulff, *J. Phys. Chem.*, **69**, 6 (1965).

(3) (a) C. W. Davies, *J. Chem. Soc.*, 349 (1939); (b) G. R. Gimblett and C. B. Monk, *Trans. Faraday Soc.*, **50**, 965 (1954).

(4) H. S. Harned and C. M. Mason, *J. Am. Chem. Soc.*, **54**, 1439 (1932).

(5) H. S. Harned and C. M. Mason, *ibid.*, **54**, 3112 (1932).

(6) G. Kruger and E. Thilo, *Z. anorg. allgem. Chem.*, **308**, 242 (1961).

(Temperature coefficients for such changes in state are sufficiently small that no error is introduced by taking the latter value to be 0.006 at 25° also.) Both sets of data are based upon e.m.f. studies and could be in error because of carbon dioxide in the solutions. Harned and Mason^{4,5} utilized the cells H_2 -Ba(OH)₂(*m*), BaCl₂(*m'*)-AgCl-Ag, and H_2 -Ba(OH)₂(*m*)-Ba₂Hg-Ba(OH)₂(*m'*)-H₂, whereas the results of Kruger and Thilo⁶ were based upon the cell H_2 -Ba(OH)₂(*m*)-saturated calomel. Harned and Mason, themselves, point out the difficulties involved in the use of the barium amalgam, and the AgCl-Ag couple is less reliable in basic than in acidic media.

Robinson and Stokes⁷ compute the Bjerrum distance of closest approach for the Ba(OH)⁺ and Ca(OH)⁺ species (using $K_2 = 0.23$ for barium) and compare these with the sums of the crystallographic radii. For calcium the agreement is excellent, while the Bjerrum value for barium is almost twice the sum of the radii. Substitution of $K_2 = 0.006$ into the Bjerrum relations⁷ gives a distance of closest approach (2.7 Å.) quite close to the sum of the radii (2.9 Å.). In view of the lack of an *a priori* choice between the two values for K_2 , we have investigated the thermodynamics of eq. 1 and 2 in an attempt to resolve the discord.

The standard Gibbs free energy of solution of the octahydrate, ΔG_1° , is given by

$$\Delta G_1^\circ = -RT \ln m_{Ba^{2+}} m_{OH^-}^{-2} \gamma_{Ba^{2+}} \gamma_{OH^-}^{-2} a_{H_2O}^8 \quad (3)$$

The activity of water in the saturated solution ($m = 0.274^8$) may be approximated by using the osmotic coefficient for CaCl₂⁷—and is close to unity in any case. The concentrations and activity coefficients are solutions to the following set of equations.

$$\log \gamma_i = -0.505 z_i^2 I^{1/2} / (1 + I^{1/2}) + 0.15I \quad (4)$$

$$I = m(1 + 2\alpha) \quad (5)$$

$$K_2 = (m_{Ba^{2+}} m_{OH^-} / m_{BaOH^+}) (\gamma_{Ba^{2+}} \gamma_{OH^-} / \gamma_{BaOH^+}) \quad (6)$$

Equation 4 is an extended Debye-Hückel relation of the type introduced by Davies,⁹ where the constant 0.15 has been chosen to reproduce the measured activity coefficients of BaCl₂ and BaBr₂. The parameter α is the degree of second ionization defined by $\alpha = m_{Ba^{2+}} / (m_{Ba^{2+}} + m_{BaOH^+})$. These equations have been solved by an iterative process to give $\Delta G_1^\circ = 3.2$ or 4.9 kcal./mole, reflecting the choice of $K_2 = 0.23$ or $K_2 = 0.006$, respectively.

The entropy of the octahydrate has not been determined calorimetrically but may be estimated from the data for BaO, CaO, and Ca(OH)₂¹⁰ and from Latimer's rules¹¹ as 102 cal./(mole °K.). The entropy increment for eq. 1, ΔS_1° , may be estimated from this

datum and the tabulated standard entropies¹⁰ as 29 ± 3 cal./(mole °K.). The standard enthalpy of solution, ΔH_1° , is then either 11.8 ± 1.0 or 13.5 ± 1.0 kcal./mole—the two values again reflecting a choice of $K_2 = 0.23$ or $K_2 = 0.006$, respectively. Literature data for this quantity are 14.5 (de Forcrand¹²), 15.2 (Thomsen¹³), 16.2 (Sill¹⁴) and 19.8 (calculated from the temperature dependence of the solubility⁸) kcal./mole. The work of de Forcrand and Thomsen¹³ was done in "dilute solution," presumably at about 18°, that of Sill in saturated solution, and that from the solubility relation is inherently dubious. From the preceding it is obvious that an accurate determination of the enthalpy of solution of the octahydrate is a necessary datum in the resolution of the thermodynamics of this system.

Experimental

Fisher Certified Reagent grade barium hydroxide was used without further purification in all calorimetric determinations. Titration with standard HCl indicated a purity of $99.7 \pm 0.2\%$. Calorimetric measurements were carried out in a solution calorimeter, similar to one already described,¹⁵ in which a laboratory wound, nickel coil resistance thermometer was used as the temperature-sensing device. All measurements were made into 950 ml. of freshly boiled distilled water. A gram formula mass of 315.50 was used to convert the observed heats to enthalpies of solution. In the concentration range $m = 0.002$ to 0.007, the data were fitted, by least squares, to the straight line

$$\Delta H_{\text{obsd}} = 13.72 + 7.13m^{1/2} \pm 0.035 \text{ kcal./mole} \quad (7)$$

where the uncertainty is the standard deviation.

Discussion

The concentration dependence of ΔH_{obsd} in eq. 7 is three times as steep as that of a typical completely dissociated 2-1 electrolyte.^{16,17} From this observa-

(7) R. A. Robinson and R. H. Stokes, "Electrolyte Solutions," Butterworths Scientific Publications, London, 1959, p. 410.

(8) E. Terres and K. Bruchner, *Z. Elektrochem.*, **26**, 1 (1920).

(9) C. W. Davies, *J. Chem. Soc.*, 2093 (1938).

(10) K. K. Kelley and E. G. King, "Contributions to the Data on Theoretical Metallurgy. XV. Entropies of the Elements and Inorganic Compounds," U. S. Government Printing Office, Washington, D. C., 1961.

(11) W. M. Latimer, "Oxidation Potentials," Prentice Hall, Inc., New York, N. Y., 1952, p. 359.

(12) R. de Forcrand, *Compt. rend.*, **130**, 834 (1900).

(13) J. Thomsen, "Thermochemische Untersuchungen," Johann Ambrosius Barth Verlag, Leipzig, 1883.

(14) H. F. Sill, *J. Am. Chem. Soc.*, **38**, 2632 (1916).

(15) C. Wu, M. M. Birky, and L. G. Hepler, *J. Phys. Chem.*, **67**, 1202 (1963).

tion we can conclude that our measurements encompass the heat effects of a secondary process as well as those of solution. The observed enthalpy of solution can be expressed in the form

$$\Delta H_{\text{obsd}} - \phi_L = \Delta H_1^\circ - (1 - \alpha)\Delta H_2^\circ \quad (8)$$

where ϕ_L is the concentration-dependent, relative, apparent heat content of the solution (estimated from the known quantities for completely dissociated 2-1 electrolytes¹⁷), ΔH_1° and ΔH_2° are the standard enthalpy increments for eq. 1 and 2, respectively, and α is as defined before. Table I contains representative values for α and ϕ_L , at various concentrations for both values of K_2 . Equation 8 was fitted, by least squares, to the straight lines

$$\Delta H_{\text{obsd}} - \phi_L = 13.81 + (1 - \alpha)9.6 \quad (K_2 = 0.23) \quad (9a)$$

$$\Delta H_{\text{obsd}} - \phi_L = 13.61 + (1 - \alpha)1.1 \quad (K_2 = 0.006) \quad (9b)$$

Table I: Enthalpies of Solution and Dilution^a

m	α	ΔH_{obsd}	ϕ_L
$K_2 = 0.23$			
0.002	0.988	14.041	0.095
0.007	0.967	14.319	0.171
$K_2 = 0.006$			
0.002	0.70	14.041	0.090
0.004	0.58	14.169	0.120
0.006	0.52	14.226	0.130
0.007	0.49	14.319	0.150

^a Units: kcal./mole.

The value of ΔH_2° , -9.6 kcal./mole, from the assumption that $K_2 = 0.23$ is very uncertain in view of the small variation of α over the concentration range studied. A better estimate of this quantity can be obtained from the value of ΔH_{obsd} in saturated solution¹⁴ and estimates of ϕ_L from those for BaCl_2 and BaBr_2 .¹⁸ These data lead to $\Delta H_2^\circ = -8.3$ kcal./mole.

We are now in a position to compute the standard entropy increment for eq. 2, ΔS_2° , and the standard partial molal entropy, S° , for $\text{Ba}(\text{OH})^+(\text{aq})$. For $K_2 = 0.23$, $\Delta G_2^\circ = -1364 \log 0.23 = 0.9$ kcal./mole, and for $K_2 = 0.006$, $\Delta G_2^\circ = 3.0$ kcal./mole. The corresponding values of ΔS_2° are then $(-8.3 - 0.9)/0.298 = -31$ and $(-1.1 - 3.0)/0.298 = -14$ cal./(mole °K.). Comparison with the corresponding entropy increment

for $\text{Ca}(\text{OH})^+$, -12 cal./(mole °K.),² indicates that the latter value is to be preferred for $\text{Ba}(\text{OH})^+$. From the tabulated standard entropies¹⁰ we compute $S^\circ = 14$ cal./(mole °K.) for $\text{Ba}(\text{OH})^+$.

Gimblett and Monk^{3b} have estimated ΔH_2° from the temperature dependence of K_2 as -1.75 kcal./mole. In view of the data leading to that value, it is difficult to justify their implied precision since a reasonable estimate of the uncertainty is 0.8 kcal./mole. Even so, this datum can be considered to accord with our derived value (eq. 9b) of -1.1 kcal./mole, based, however, on $K_2 = 0.006$. Such a coincidence might indicate an unnoticed systematic error in the e.m.f. work leading to $K_2 = 0.23$.

Our derived value for ΔH_1° can be compared with the estimates made previously from the free energies and entropy of solution. Such a comparison indicates the schema utilizing $K_2 = 0.006$ to be preferable. However, the uncertainties in the computed values of ΔH_1° are large, owing to the estimated entropy of the octahydrate.

We can now make a choice between the two literature values for K_2 . If the smaller value, 0.006 , is assumed then (a) calculated and observed values of ΔH_1° agree and (b) the values of ϕ_L and ΔS_2° (which are not independent in our derivation) are consistent with those of similar systems. If, on the other hand, we adopt $K_2 = 0.23$, the accord between calculated and observed values of ΔH_1° is poorer, and the concentration dependence of ϕ_L and/or ΔS_2° must be assumed to be substantially different from those for similar substances.

We conclude that $K_2 = 0.006$ is to be preferred and on that basis calculate the following values for the thermodynamic state function increments for the solution of $\text{Ba}(\text{OH})_2 \cdot 8\text{H}_2\text{O}(\text{c})$: $\Delta G_1^\circ = 4.9 \pm 0.2$ kcal./mole; $\Delta H_1^\circ = 13.7 \pm 0.1$ kcal./mole; $\Delta S_1^\circ = 29$ cal./(mole °K.).

Acknowledgment. The authors are grateful to Professor Loren G. Hepler for his discussion of the problem and for the use of his laboratory facilities. The assistance of Dr. Gary Bertrand in compiling the data is gratefully acknowledged, as is the partial financial support of the National Science Foundation.

(16) C. W. Davies, *Endeavour*, 4, 114 (1945).

(17) H. S. Harned and B. B. Owen, "The Physical Chemistry of Electrolytic Solutions," Reinhold Publishing Corp., New York, N. Y., 1958.

(18) F. D. Rossini, D. D. Wagman, W. H. Evans, S. Levine, and I. Jaffe, "Selected Values of Chemical Thermodynamic Properties," National Bureau of Standards Circular 500, U. S. Government Printing Office, Washington, D. C., 1952.

Glutaronitrile. Calorimetrically Determined Thermal Properties from 5 to 350°K. and Statistical Gaseous Entropy^{1a}

by H. Lawrence Clever, Claus A. Wulff, and Edgar F. Westrum, Jr.^{1b}

Department of Chemistry, University of Michigan, Ann Arbor, Michigan (Received February 8, 1965)

Heat capacities of solid and liquid glutaronitrile and the enthalpy of fusion have been determined by adiabatic calorimetry. The entropy of fusion at the triple point, 244.21°K., is 12.32 cal./mole °K. This entropy of fusion and the absence of an enantiomorphic transition indicate that this substance does not possess a plastic crystal phase. Values of the heat capacity (C_p), entropy (S°), enthalpy function $[(H^\circ - H^\circ_0)/T]$, and Gibbs energy function $[(G^\circ - H^\circ_0)/T]$ are 43.80, 57.23, 32.44, and -24.79 cal./mole °K., respectively, for the liquid at 298°K. For the ideal gas, the entropy at this temperature is 88.1 cal./mole °K. from thermal data. The close accord of this datum with the calculated value, 88.1, evidences lack of residual disorder in the solid at low temperatures.

Introduction

Though lacking the high molecular symmetry usually associated with plastic crystals, succinonitrile has been shown to possess most of the macroscopic properties characteristic of this state.² The entropy of transition from normal to plastically crystalline succinonitrile can be quantitatively accounted for in terms of changes in molecular and crystalline symmetry, the onset of hindered internal rotation, and the concomitant volume increment. van de Vloed³ has shown that the homolog, glutaronitrile (GN), on fast cooling goes to a metastable form. Matsubara's^{4,5} infrared studies indicate that the metastable solid (crystal II) and the stable solid (crystal I) contain different rotational isomers. This paper reports a study of glutaronitrile in the stable solid and liquid phases; the metastable phase was not formed in the cryostat. Because of the reported phase complexity and the desirability of verifying the absence of residual disorder in the GN crystal phase on which our measurements were performed (presumably the crystal I phase of Matsubara) the entropy of the ideal gaseous state is calculated from spectroscopic data and compared with the experimental value.

Experimental

Glutaronitrile Sample. The center cut of a GN sample (Eastman Kodak Co.) that had been subjected to

three successive vacuum distillations in a Podbielniak fractionating column was degassed by repeated freezing, evacuation, and melting cycles and was transferred as a liquid into the evacuated calorimeter. Vapor-liquid partition chromatography indicated that the distillation procedure virtually eliminated the only detected contaminant. The sample was further characterized by infrared spectroscopy and by fractional fusion as will be discussed later.

Anal. Calcd.: C, 63.81; H, 6.42; N, 29.76. Found: C, 63.84; H, 6.43; N, 29.74.

Cryostat and Calorimeter. Measurements were made by employing a gold-plated copper calorimeter W-24⁶ sealed with a gold-gasketed, demountable valve in the Mark III cryostat.⁷ The quasi-adiabatic technique⁸ was used. The scale of the capsule-type platinum resistance thermometer (laboratory designation A-3) is considered to accord with the thermodynamic tem-

(1) (a) This work was supported in part by the U. S. Atomic Energy Commission; (b) to whom communications should be addressed.

(2) C. A. Wulff and E. F. Westrum, Jr., *J. Phys. Chem.*, **67**, 2376 (1963).

(3) A. van de Vloed, *Bull. soc. chim. Belges*, **48**, 229 (1939).

(4) I. Matsubara, *J. Chem. Phys.*, **35**, 373 (1961).

(5) I. Matsubara, *Bull. Chem. Soc. Japan*, **34**, 1719 (1961).

(6) E. T. Chang and E. F. Westrum, Jr., *J. Phys. Chem.*, in press

(7) E. F. Westrum, Jr., *J. Chem. Educ.*, **39**, 443 (1962).

(8) E. F. Westrum, Jr., J. B. Hatcher, and D. W. Osborne, *J. Chem. Phys.*, **21**, 419 (1953).

perature scale within 0.03°K. from 10 to 90°K. and within 0.04°K. from 90 to 350°K. The heat capacity of the calorimeter–heater–thermometer assembly was determined by a separate series of measurements with small adjustments applied as needed for slight differences in the quantities of helium and thermal-conductivity grease between the runs with sample and without. Manual shield control was used below 80°K. Above this temperature three separate channels of recording electronic circuitry provided with proportional, rate, and reset control actions maintained the adiabatic shield within approximately a millidegree of the calorimeter temperature. Thus the energy exchange between calorimeter and surroundings was reduced so that it was negligible in comparison with other sources of error. All measurements of temperature, time, potential, resistance, and mass were referred to standardizations or calibrations of the National Bureau of Standards.

The degassed sample of glutaronitrile was transferred as a liquid into the calorimeter and 399 torr of helium gas was added to the 8-cc. vapor space to enhance thermal equilibration. The sample had a mass of 67.923 g. *in vacuo*. Its heat capacity was at minimum 64% of the total (*i.e.*, of sample, calorimeter, heater, and thermometer).

Results and Discussion

Heat Capacity. The experimental heat capacity measurements are presented in Table I in chronological order so that temperature increments across individual runs in a series may be estimated from adjacent mean temperatures and are shown in Figure 1 as a function of temperature. The data are stated in terms of the defined thermochemical calorie exactly equal to 4.1840 J., an ice point of 273.15°K., and a gram formula mass of 94.117 g. An analytically determined curvature correction has been applied to the measured values of $\Delta H/\Delta T$. These data are considered to be characterized by a probable error of about 4% near 10°K., decreasing to 1% at 15°K. and to less than 0.1% above 25°K.

Heat Capacity of the Liquid. The vapor pressure is sufficiently low,⁹ 13 μ at 303°K., to preclude the need for a vaporization correction. Three heat-capacity determinations in series XII were made on the undercooled liquid. These and the heat capacity of the normal liquid are fitted by the least-squares line $C_p = 0.03170T + 34.25 \pm 0.06\%$.

Thermodynamic Functions for the Condensed States. The molal values of the heat capacity, entropy, enthalpy increment, and Gibbs energy function are listed in Table II at selected temperatures. Derived thermal

Table I: Heat Capacity of Glutaronitrile^a

T	C _p	T	C _p	T	C _p
—Series I—					
196.74	25.94	15.45	1.335	243.69	3850
203.44	26.56	17.19	1.738	243.79	6394
212.04	27.85	19.10	2.214	254.79	108.0
221.23	30.54	21.15	2.765	270.61	42.83
230.37	34.74	23.41	3.401	278.77	43.03
237.83	61.29	26.12	4.181	286.85	43.36
241.68	218.1	—Series VII—			
242.98	708.4	24.85	3.816	302.58	43.94
243.44	1672.5	29.76	5.219	310.32	44.32
243.64	3187	33.32	6.217	318.00	44.66
243.76	4736	37.03	7.214	325.63	44.94
243.86	4985	40.94	8.171	333.15	45.21
246.79	64.73	45.22	9.151	340.62	45.60
—Series II—					
144.09	21.46	49.99	10.16	346.82	45.86
151.96	22.22	55.46	11.20	—Series XII—	
161.22	22.98	—Series VIII—			
165.18	23.30	57.30	11.53	234.72	41.72 ^b
174.29	24.10	64.28	12.72	238.51	41.81 ^b
183.19	24.86	70.97	13.68	241.97	41.95 ^b
192.29	25.62	78.29	14.69	245.41	42.00
201.45	26.43	86.37	15.88	248.84	42.06
210.43	27.57	93.86	16.64	—Series XIII—	
—Series III—					
230.12	34.44	101.97	17.46	233.16	37.16
ΔHm Run A					
—Series IV—					
ΔHm Run B					
—Series V—					
5.55	0.0449	120.67	19.33	ΔHm Runs D	
5.88	0.0643	—Series IX—			
6.82	0.1096	92.37	16.46	—Series XIV—	
7.75	0.1731	102.32	17.50	ΔHm Runs E	
—Series VI—					
6.39	0.0883	111.33	18.42	—Series XV—	
7.19	0.1327	120.38	19.31	209.40	27.40
8.08	0.2012	—Series X—			
9.01	0.2903	130.83	20.29	218.03	29.42
10.08	0.4235	139.76	21.11	226.26	31.10
11.21	0.5615	148.67	21.99	233.76	37.96
12.50	0.7517	157.72	22.77	239.25	74.51
13.90	1.013	166.76	23.55	241.96	235.3
—Series VII—					
ΔHm Run F					
—Series XI—					
Enthalpy Run G					
—Series XVI—					
ΔHm Run F					
6.39	0.0883	179.97	24.62	251.15	42.23
7.19	0.1327	206.86	27.90	257.56	42.43
8.08	0.2012	ΔHm Runs C			
9.01	0.2903	232.08	36.85	263.95	42.65
10.08	0.4235	239.06	80.65	270.31	42.83
11.21	0.5615	242.27	346.0	276.63	43.02
12.50	0.7517	243.18	1081	329.20	45.07
13.90	1.013	243.51	2174	336.61	45.39
				343.97	45.72

^a Units are calories, moles, and degrees Kelvin. ^b Data on undercooled liquid.

property values have been calculated with a high-speed digital computer by integration of a least-squares polynomial fitted through the data points. Below 5°K.

(9) A. L. Woodman, W. J. Murbach, and M. H. Kaufman, *J. Phys. Chem.*, **64**, 658 (1960).

the heat capacity data were extrapolated by means of the Debye T^3 limiting law. Nuclear spin and isotopic mixing contributions have not been included in the entropy and Gibbs energy functions. Estimated probable errors in the thermodynamic functions are less than 0.1% above 100°K.

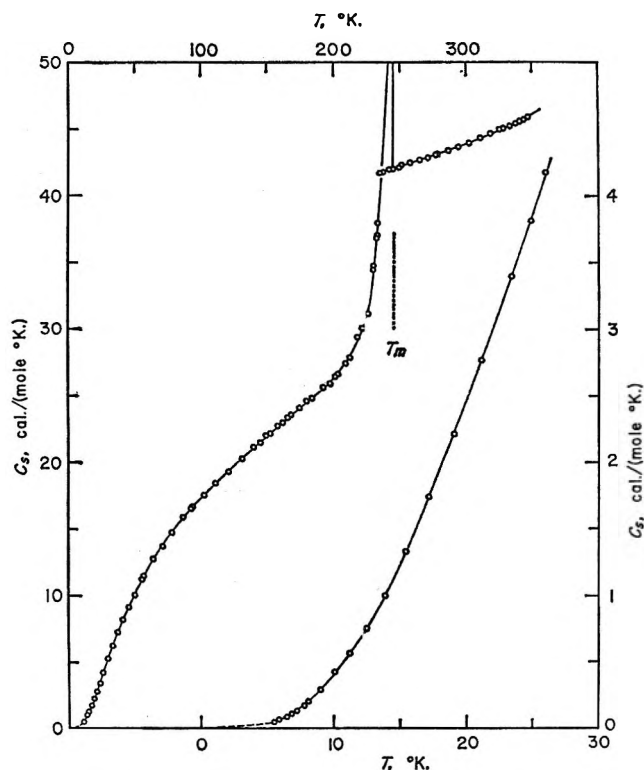


Figure 1. The heat capacity of glutaronitrile.

Melting. In the course of heat capacity measurements seven sets of runs (*cf.* Table III) were made through the melting region; two of these, series I and series XV, define purity and melting point. The average enthalpy of melting, 3008 ± 1 cal./mole, corresponds to an entropy of melting of 12.32 cal./mole °K. The GN crystalline phase characterized by these measurements is, therefore, obviously not plastically crystalline. Melting points were taken during runs C and D to confirm that the same crystal phase was present.

The amount of liquid-soluble solid-insoluble impurity can be estimated from a plot of the apparent melting temperature, T , against the fraction melted, $1/F$. The temperature (243.87°K.) corresponding to $1/F = 1$ is the triple point, T_1 , of the calorimetric sample. That (244.21°K.) corresponding to $1/F = 0$ is the triple point, T_0 , of the pure sample. The mole fraction of impurity, N_2 , is given by

$$N_2 = \frac{\Delta H_m(T_0 - T_1)}{RT_0^2} = 0.0086$$

The melting point has previously^{3,10} been reported as -29.45° (243.70°K.).

Attempts to Obtain a Metastable Solid. Matsubara^{4,5} reported that the metastable solid is obtained by cooling the liquid rapidly to about 213°K. Two such rapid

Table II: Thermodynamic Properties of Glutaronitrile^a

T	C_p	S°	$H^\circ - H_0^\circ$	$-(G^\circ - H_0^\circ)/T$
5	0.033	0.011	0.042	0.003
10	0.399	0.118	0.916	0.027
15	1.236	0.423	4.818	0.102
20	2.45	0.938	13.92	0.243
25	3.86	1.636	29.67	0.449
30	5.29	2.466	52.56	0.714
35	6.67	3.387	82.50	1.029
40	7.94	4.362	119.1	1.385
45	9.11	5.362	161.8	1.771
50	10.16	6.381	210.0	2.181
60	12.00	8.401	321.1	3.050
70	13.57	10.37	449.1	3.956
80	14.95	12.28	591.9	4.878
90	16.18	14.11	747.7	5.802
100	17.30	15.87	915.2	6.722
110	18.32	17.57	1,093	7.632
120	19.28	19.21	1,281	8.528
130	20.22	20.79	1,479	9.411
140	21.14	22.32	1,686	10.28
150	22.06	23.81	1,902	11.13
160	22.95	25.26	2,127	11.97
170	23.80	26.68	2,361	12.79
180	24.60	28.06	2,603	13.60
190	25.38	29.41	2,853	14.40
200	26.27	30.74	3,111	15.18
244.21	...	36.37	4,354	18.54
Liquid				
244.21	...	48.69	7,362	18.54
250	42.16	49.67	7,605	19.25
260	42.46	51.33	8,028	20.45
270	42.79	52.94	8,455	21.63
280	43.13	54.50	8,884	22.77
290	43.49	56.02	9,317	23.89
300	43.87	57.50	9,754	24.99
310	44.26	58.95	10,195	26.06
320	44.67	60.36	10,639	27.11
330	45.10	61.74	11,088	28.14
340	45.54	63.09	11,541	29.15
350	46.00	64.42	11,999	30.14
273.15	42.90	53.44	8,590	21.99
298.15	43.80	57.23	9,673	24.79

^a Units are calories, moles, and degrees Kelvin.

(10) J. Timmermans and J. Naveau, *Bull. soc. chim. Belges*, 67, 560 (1958).

Table III: Enthalpy of Melting of Glutaronitrile^a

Designation	Number of runs	($H_{230} - H_{200}$)	Excess ($H_{230} - H_{200}$) ^b	ΔH_m
Series I	9	3624	2962	3009
ΔH_m Run A	1	3624.0	2961	3008
ΔH_m Run B	1	3623.7	2961	3008
ΔH_m Runs C	2	3623.9	2961	3008
Series XV	8	3623	2960	3007
ΔH_m Runs D	2	3625.7	2963	3010
ΔH_m Run E	1	3625.3	2962	3009
			Av.	3008 \pm 1

^a Units are calories, moles, and degrees Kelvin. ^b *I.e.*, enthalpy above the extrapolated normal lattice curve. The excess ($H_{230} - H_{200}$) is 47 cal./mole for each set of runs.

cooling experiments were tried in which the sample was cooled from 315 to 225°K. at rates of $1.7 \pm 0.1^\circ\text{K./min.}$ This is the maximum cooling rate obtainable even with exchange gas in the cryostat. Heat capacity determinations and equilibrium melting temperatures at the same fraction melted on the rapidly cooled samples (series XIV and XV) did not differ from values found for the more slowly cooled solid. The presence (or absence) of certain impurities or inadequate quenching rates may account for failure to obtain the metastable solid phase.

Entropy of the Gas

In view of the phase behavior recorded previously for glutaronitrile, it is desirable to verify that the sample used for heat capacity measurements contains no residual disorder. The thermodynamic state function most applicable to this end is the entropy, which is capable both of elucidating the existence of disorder and of providing a quantitative estimate of its extent. The usual schema, to be applied here, is a comparison of the measured thermal entropy (invoking the third law postulate) with an entropy computed from the energetics of the system as derived from structural and spectroscopic data. However, the computational difficulties involved limit such a comparison to the ideal gas standard state.

Experimental Entropy of the Gas. The low temperature thermal data on the condensed phases augmented by vapor pressure data of Woodman, *et al.*,⁹ on liquid GN permit an estimate of the entropy of ideal gaseous glutaronitrile. Details of the calculation are shown in Table IV.

Calculated Entropy of the Gas. Description of the position, spatial alignment, and internuclear separations of an n -atom molecule requires specification of positional coordinates for the $3n$ degrees of freedom.

Table IV: The Thermal Entropy of GN (Ideal Gas) at 298.15°K.^a

Temp., °K.		ΔS
0-5	Debye T^3 extrapolation	0.01
5- T_m	Numerical integration of $C_p dT/T$	36.36
243.87	$\Delta H_m/T_m$, melting	12.32
T_m -298.15	Numerical integration of $C_p dT/T$	8.54
298.15	$\Delta H_v/298.15$, vaporization ^b	53.6
	$R \ln p$, compression to 1 atm. ^b	-22.7
	Ideal gas correction ^c	0.00
	Thermal entropy of GN (ideal gas)	88.1

^a Units are calories, moles, and degrees Kelvin. ^b See ref. 9. ^c Negligible since vapor pressure of GN is only 1.075×10^{-6} atm. at 298°K.

After delineation of the translational and rotational coordinates, the remaining ($3n - 6$) degrees of freedom 1:1 are assigned to correspondence with the ($3n - 6$) fundamental vibrations deduced by normal coordinate analysis. Upon the assumption of (a) separability of the $3n$ degrees of freedom, (b) rigid rotation about the center of mass, and (c) harmonic oscillator behavior for the ($3n - 6$) normal vibrations, high-temperature limits for the $3n$ partition functions in terms of the molecular mass, equilibrium internuclear separations, and the normal vibrational frequencies and resultant thermodynamic state functions may be evaluated. However, calculation is complicated by the necessity for using two of the normal vibrational degrees of freedom to describe the internal rotational degrees of freedom and by the concomitant rotational isomerism. Internal rotation results in nine configurations grouped into four enantiomorphic pairs¹¹ (TG , GT , GG , and GG') and one unpaired configuration¹¹ (TT). The entropy calculation is simplified in the manner adopted for succinonitrile,² *i.e.*, an entropy is computed for each conformation that exists in GN vapor; these contributions together with the entropy of isomer mixing are summed to obtain the molal entropy, S° , of GN (ideal gas).

$$S^\circ = \sum_{i=1}^9 X_i \left(\sum_{j=1}^{3n} S_j \right) - R \sum_{i=1}^9 X_i \ln X_i$$

A. *Translation.* The high-temperature, limiting, translational, partition function is dependent only on the molecular mass and is, therefore, identical for all rotational isomers. Taking the gram formula mass to be 94.117, the entropy of translation is given by¹²

(11) For the nomenclature of rotational isomerism see S. Mizushima, "Structure of Molecules and Internal Rotation," Academic Press, Inc., New York, N. Y., 1954.

$$S_{\text{tr}}^{\circ} = R(3/2 \ln M + 5/2 \ln T) - 2.315 = 39.541 \text{ cal./mole } ^{\circ}\text{K.}$$

B. Over-all Rotation. The high-temperature rigid-rotor limit of the partition function is dependent on the value of the moment of inertia determinant, D , and upon the rotational symmetry number, σ . Of the rotational conformations listed previously the GG' is absent in GN,⁵ and the TG and GT are spectroscopically and rotationally equivalent. For C—C, C=N, and C—H bond lengths of 1.542, 1.149, and 1.071 Å., and for C, N, and H atomic masses of 12.01, 14.008, and 1.008, respectively, the evaluation of the moment of inertia determinants yields the values given in Table V. Values of σ and of the rotational entropy, S_r° ,¹² which is given by

$$S_r^{\circ} = R[1/2 \ln (D \times 10^{117}) + 3/2 \ln T - \ln \sigma]$$

also are presented in the same table.

Table V: Rotational, Vibrational, and Conformational Entropy Contributions for GN^a

Contribution or quantity	Conformations		
	<i>TT</i>	<i>TG,GT</i>	<i>GG</i>
Inertial determinant, $D \times 10^{113}$, g. ³ cm. ⁶	3.28	6.21	5.01
Symmetry number, σ	2	1	2
S_r°	26.555	27.923	26.331
S_v°	11.156	10.234	9.939
Mole fractions	0.43	0.50	0.07
Configurations	1	4	2
S_{298-15}°	84.71	85.16	83.27

^a Entropies are in calories per mole degree Kelvin.

C. Vibration. Of the $3n = 39$ degrees of freedom for the molecule we have assigned 6 for translation and over-all rotation and 2 for the internal rotations. The remaining 31 degrees of freedom correspond to the fundamental vibrations of the molecule and differ for the spectroscopically distinguishable conformations. An analysis of the infrared spectrum of GN between 4000 and 400 cm.⁻¹ has been reported by Matsubara⁴ and a complete set of fundamental, skeletal vibrations based upon force constants derived from the observed spectrum has been given for each conformation existent in GN. Summations of the entropy contributions for each set of 31 frequencies are made by utilizing tabulated harmonic oscillator functions.¹³ These sums are in Table V also.

D. Internal Rotation. The potential energy function describing the hindered internal rotation in GN is a function of two angles which can be thought of

naïvely as rotations about the two C—C bonds. An exact treatment involving the calculation of appropriate energy levels is prohibitively difficult, necessitating the adoption of some approximate treatment. As has been indicated,¹⁴ since the entropy is not very sensitive to assumed potential energy function, even a severely strained potential model might provide a suitable value for this entropy contribution.

One approximate treatment is provided by the entropy tabulations of Pitzer and Gwinn¹⁵ for hindered rotation of groups attached to a rigid framework. If the central methylene group in GN is considered as the rigid framework, the reduced moment of inertia, I_r , 6.83×10^{-40} g. cm.², is computed using the atomic masses and bond lengths given previously. A cosine potential of the form $V = 1/2 V_0(1 - \cos \phi)$ is assumed with V_0 , the maximum barrier height, ranging between 3000 and 3600 cal./mole, these values being consistent with those for a number of substituted alkanes. The internal rotation symmetry number, n , is taken as 3 and will be discussed later. The high-temperature limit of the partition function¹² is $2.7935(10^{38} I_r T)^{1/2} / n = 4.203$. The entropy contribution consists of three terms and is for *both* internal rotators.

$$S_{\text{ir}}^{\circ} = 2R(1/2 + \ln 4.203) - 2(S_t - S) + R \ln g$$

The first of these terms is the contribution calculated on the basis of free internal rotation, *i.e.*, $V_0 = 0$. The second is the effect of the nonzero V_0 and can be evaluated using the tables of Pitzer and Gwinn¹⁵ where $(S_t - S)$ is tabulated as a function of I_r and V_0 . The third term is related to the rotational symmetry number n . The parameter g is the number of distinct conformations produced by complete rotations about the two axes of internal rotation. As stated above, nine configurations are grouped into five distinct conformations. Since only four of these contribute to the partition functions of GN, $g = 4$ and the entropy contribution is $R \ln 4$. An alternate approach to evaluating the effect of rotational isomerism involves inclusion of all five conformations in g , but restriction of the integration of the potential energy to regions that do not include the GG' configurations. For the analogous, but simpler, system—succinonitrile—both methods were employed and gave results which differed in entropy

(12) G. N. Lewis and M. Randall, "Thermodynamics," 2nd Ed., revised by K. S. Pitzer and L. Brewer, McGraw-Hill Book Co., Inc., New York, N. Y., 1961.

(13) J. Hilsenrath and G. G. Ziegler, "Tables of Einstein Functions," U. S. National Bureau of Standards, Monograph 59, U. S. Government Printing Office, Washington, D. C., 1962.

(14) C. A. Wulff, *J. Chem. Phys.*, **39**, 1227 (1963).

(15) K. S. Pitzer and W. D. Gwinn, *ibid.*, **10**, 428 (1942).

by 0.15 cal./mole °K. Because of the approximations already made here, use of the alternate method was not warranted. The entropy is computed as

$$S^{\circ}_{ir} = 2R(\frac{1}{2} + \ln 4.203) - 2(1.49 \pm 0.12) + \\ R \ln 4 = 7.46 \pm 0.25 \text{ cal./mole } ^{\circ}\text{K.}$$

and the precision index is determined by the range of V_0 .

A second route is available to the evaluation of $(S_f - S)$ through the work of Scott and McCullough,¹⁶ who considered the effect of rotational isomerism upon thermodynamic functions. Their tabulations of $(S_f - S)$ are dependent on two barrier heights that characterize a synthesized potential energy function. Assigning values of $V_2 = 1000 \pm 200$ cal./mole and $V_1 = 2000 \pm 200$ cal./mole (notation of Scott and McCullough) a value of 7.84 ± 0.25 cal./mole °K. is obtained for S°_{ir} . The numerical values assigned to the two barrier heights are those used for succinonitrile² and are consistent with barriers observed in substituted alkanes. A mean value of 7.83 ± 0.40 cal./mole °K. has been adopted for S°_{ir} and is the same for each of the conformations.

E. Entropy of Mixing. No data exist for the vapor phase energy separations of the configurations contributing to GN. A conformeric distribution is available for the symmetrically substituted analog, *n*-

pentane.¹⁷ This differs little from that for similar compounds¹⁷ and has been adopted for GN. Mole fractions of $X_{TT} = 0.43$, $X_{TG,GT} = 0.50$, and $X_{GG} = 0.07$ yield an entropy of mixing of 3.30 cal./mole °K.

F. Entropy of GN (Ideal Gas) at 298.15°K. From the composition and the conformational entropies summarized in Table V the entropy of GN (ideal gas) is 88.1 ± 0.6 cal./mole °K.

Comparison of Calculated and Thermal Entropies. The agreement between the thermal (88.1 ± 0.1 cal./mole °K.) and calculated (88.1 ± 0.6 cal./mole °K.) values for the entropy of GN (ideal gas) indicates a lack of residual disorder at low temperatures in the crystalline phase characterized by these thermal measurements. However, because of the assumptions made in obtaining the calculated value, the thermal value is preferred for chemical thermodynamic use.

Acknowledgment. C. A. W. thanks the Institute of Science and Technology of the University of Michigan for assistance in the form of a postdoctoral fellowship. The partial financial support of the U. S. Atomic Energy Commission is greatly appreciated.

(16) D. W. Scott and J. P. McCullough, Bureau of Mines Report of Investigation RI 5930, U. S. Government Printing Office, Washington, D. C., 1962.

(17) F. A. Momany, R. A. Bonham, and W. H. McCoy, *J. Am. Chem. Soc.*, **85**, 3077 (1963).

The Critical Temperature and Coexistence Curve for Bismuth Bromide

by J. W. Johnson, D. Cubicciotti, and W. J. Silva

Stanford Research Institute, Menlo Park, California (Received December 25, 1964)

The critical temperature of BiBr_3 has been found to be $1220 \pm 5^\circ\text{K}$. and the critical density to be 1.487 ± 0.015 g./cc. The coexistence curve for liquid and vapor has been fitted by the equations: $\rho = 1.487 + 1.486[(1220 - T)/1220] \pm 2.819[(1220 - T)/1220]^{1/3}$ (+ for liquid phase; - for vapor phase). These equations are of the same form as those developed by Guggenheim for argon, nitrogen, oxygen, methane, and carbon monoxide.

Introduction

In a previous paper¹ it was shown that some of the empirical relationships developed to describe the liquid-vapor coexistence curve for molecular fluids were also applicable to the liquid-vapor coexistence curve for ionic bismuth chloride. To determine if the relationships could be applied to other bismuth halides, the critical temperature and orthobaric densities of bismuth bromide were determined. This paper is a report of the results of that investigation.

Experimental

The apparatus and methods used for determining the critical temperature and orthobaric densities of bismuth chloride¹ were employed in this work.

Bismuth bromide, purified by three distillations under a dry oxygen atmosphere, was distilled into quartz tubes of various dimensions under dry oxygen at a pressure of 100 mm. The tubes were evacuated to remove residual gas and sealed off under vacuum. The oxygen atmosphere served to oxidize any reduced bismuth to bismuth oxide, which has a negligible vapor pressure and is insoluble in bismuth bromide at the temperature used for distillation.

The tubes intended for use in the critical temperature determinations were constructed of 2-mm. bore by 6-mm. o.d. quartz tubing 6 cm. long. These were filled to approximately one-third the total internal volume with molten bismuth bromide at 300° . The tubes used in the liquid and vapor density determinations were 3-mm. bore by 6-mm. o.d. with a few of the low temperature density determinations being made with 4-mm. bore by 6-mm. o.d. tubes. The quartz floats of predetermined density were placed in the empty tubes, which were sealed to the quartz manifold,

and then the required amount of bismuth bromide was distilled into them. The vapor density determinations were made by observing the temperature of the disappearance of the last trace of liquid in the bottom of the tube. The weight of bismuth bromide and the internal volume of the tube were determined after the run from which the vapor density could be calculated.

In the critical temperature determinations, continuous visual observation of the meniscus as it approached the critical temperature from below was not practical owing to the high radiation losses occurring at the critical temperature of bismuth bromide. These radiation losses set up large temperature gradients between the sample and the nickel block. The procedure adopted was to keep the nickel block rotated so that the sample was not exposed to the observation slit until it had reached the desired temperature. Visual observation was made by rotating the nickel block until the sample became visible and the presence or absence of a meniscus was determined. Through careful adjustment of the temperature it was possible to reduce the difference between the presence or absence of the meniscus to an interval of $3\text{--}4^\circ$ and in some instances less. The practice of keeping the sample tube shielded until ready to make an observation reduced the temperature gradient between the sample position and the block to less than 1° .

Results and Discussion

The method of observing the presence or absence of a liquid-vapor interface at a definite temperature precluded observation of the sample as it approached,

(1) J. W. Johnson and D. Cubicciotti, *J. Phys. Chem.*, **68**, 2235 (1964).

reached, and exceeded the critical temperature. The temperatures at which the absence or presence of a meniscus was determined are listed in Table I. When

Table I: Critical Temperature Data for Bismuth Bromide

Tube no.	Temp., °C., meniscus		Av. density, g./cc.
	Absent	Present	
1	948.1	944.6	1.416
	946.9	945.5	
	946.0	945.6	
2	944.9	943.5	1.732
	945.1	943.6	
	945.7	944.0	
3	948.5	944.0	1.630
	947.9	944.6	
	947.0	944.9	
Accepted value		945 ± 5°.	

the meniscus was absent, visual observation was continued until the sample had cooled sufficiently for the meniscus to appear in the interior of the tube. This ensured that the loading was sufficient for both a liquid and vapor phase to be present just below the critical temperature. In view of the spread of temperatures in Table I, the critical temperature was taken as 945 ± 5°. The three tubes used for the critical temperature experiments were opened, and the weight of charge and internal volume of the tube determined. From these quantities the average density of the sample was calculated and appears in Table I. The density interval (1.416 to 1.732 g./cc.) in which the critical transition can be observed is surprisingly large, amounting to 20% of the critical density. However, the critical transition has been observed in ethane² over an interval amounting to 15% of the critical density. This flat top character is somewhat arbitrary since the temperature range is ±5°K.

The experimental densities of bismuth bromide liquid and vapor at various temperatures are presented in Table II, and the coexistence curve is shown in Figure 1. All the liquid densities, except for the critical transition experiments, were determined with quartz "floats," while the vapor densities were all determined by volume (see ref. 1). An uncertainty of ±3° is assigned to all temperatures listed in Table II.

The empirical equation developed by Guggenheim³ for the coexistence curves of the inert gases has the form

$$\rho/\rho_{\text{crit}} = 1 + a\left(\frac{T_c - T}{T_c}\right) \pm b\left(\frac{T_c - T}{T_c}\right)^{1/2} \quad (1)$$

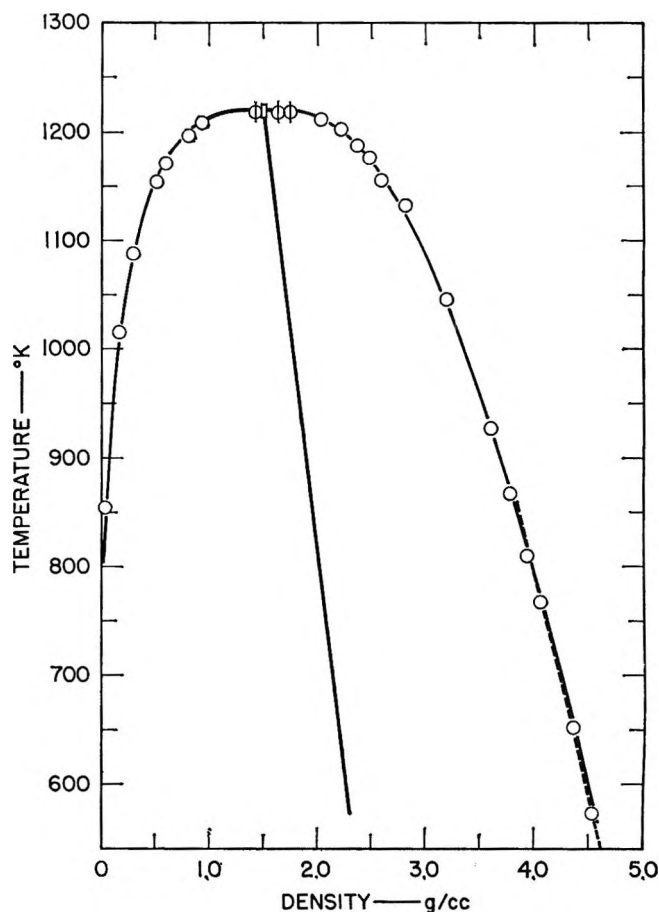


Figure 1. Coexistence curve for bismuth bromide. Dashed line from ref. 4.

where ρ_{crit} is the critical density, T_c is the critical temperature, a and b are constants, the positive sign is used for the liquid phase, and the negative sign is used for the vapor phase.

This equation was found to apply to bismuth chloride and so was used to fit the data for bismuth bromide. It was determined, by trial and error, that the data could be fitted by

$$\rho = 1.487 + 1.486\left(\frac{1220 - T}{1220}\right) \pm 2.819\left(\frac{1220 - T}{1220}\right)^{1/2} \quad (2)$$

where the critical density is 1.487 g./cc. and the critical temperature T_c is 1220°K. This value of the critical temperature is higher than the value 1218°K. given in Table I but is still within the estimated limits of

(2) J. G. Mason, S. N. Naldreth, and O. Maass, *Can. J. Res.*, **18B**, 103 (1940).

(3) E. A. Guggenheim, *J. Chem. Phys.*, **13**, 253 (1945).

error. The equation fits the experimental data for the liquid phase with an average deviation of ± 0.015 g./cc. and the vapor phase data with an average deviation of ± 0.014 g./cc. The solid line in Figure 1 was calculated by means of eq. 2.

Rearranging eq. 2 to give an equation for the average density of coexisting liquid and vapor results in

$$\frac{\rho_{\text{liq}} + \rho_{\text{vap}}}{2} = 1.487 + 1.218 \times 10^{-3}(1220 - T) \quad (3)$$

Keneshea and Cubicciotti⁴ determined the density of bismuth bromide from the melting point to the boiling point. Assuming a negligible vapor density in this temperature range, their data give an average density equation

$$\frac{\rho_{\text{liq}} + \rho_{\text{vap}}}{2} = 1.488 + 1.20 \times 10^{-3}(1220 - T) \quad (4)$$

The excellent agreement between (3) and (4) is somewhat fortuitous since the average deviation of the experimental liquid and vapor densities from values calculated by (2) is ± 0.015 and the critical temperature is uncertain by $\pm 5^\circ\text{K}$. This confirms the observation made in the case of bismuth chloride that a good approximation to the critical density can be obtained

Table II: Orthobaric Densities of Bismuth Bromide

Temp., °C.	Temp., °K.	Density, g./cc.		Dev., g./cc.
		Obsd.	Calcd.	
Liquid				
300	573	4.525	4.558	0.033
379	652	4.344	4.365	0.021
494	767	4.051	4.066	0.015
537	810	3.924	3.947	0.023
594	867	3.772	3.782	0.010
654	927	3.590	3.597	0.007
773	1046	3.182	3.172	-0.010
859	1132	2.802	2.768	-0.035
883	1156	2.586	2.621	0.035
903	1176	2.468	2.473	0.005
915	1188	2.360	2.364	0.004
929	1202	2.207	2.201	-0.006
939	1212	2.024	2.025	0.001
				Av. ± 0.015
Vapor				
581	854	0.035	0.045	0.010
743	1016	0.160	0.181	0.021
815	1088	0.290	0.304	0.014
881	1154	0.503	0.501	-0.002
898	1171	0.593	0.581	-0.012
924	1197	0.800	0.765	-0.035
936	1209	0.920	0.913	-0.007
				Av. ± 0.014

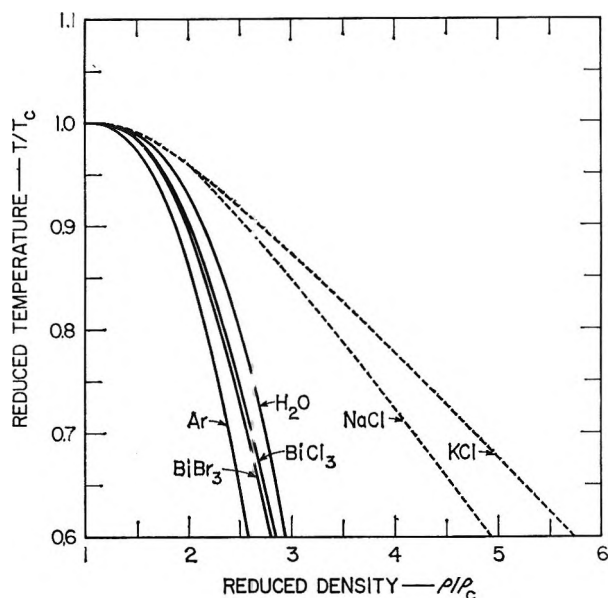


Figure 2. Comparison of reduced liquid densities.

by a linear extrapolation of half the density of the liquid below the boiling point to the critical temperature of these salts.

Figure 2 gives the reduced densities for the liquid state of BiBr_3 and BiCl_3 as a function of reduced temperature compared with the values for argon and water given by Landolt-Bornstein.⁵ The curves, estimated by Kirschenbaum, *et al.*,⁶ for NaCl and KCl are also shown. The reduced density curves for the bismuth halides fall between those for Ar and H_2O , as do the many molecular fluids such as Al_2Br_6 , SnCl_4 , CO_2 , SO_2 , and HCl .⁵ If similarity of position on the reduced density scale is indicative of a similarity in the nature of liquid forces, the bismuth halides should then be classed as molecular fluids in spite of the relatively high electrical conductivities of their liquids.

The critical parameters for normal molecular fluids have been related to their vapor pressures and liquid densities by Riedel. A convenient scheme for estimating the critical parameters based on the Riedel relationship has been given by Pitzer and co-workers.⁷ This method was applied to bismuth bromide. The data used were the normal boiling point (735°K),⁸ the 100-mm. boiling point (633°K),⁸ and the density of the liquid (4.343 g./cc. at 650°K).⁴ The critical

(4) F. J. Keneshea and D. Cubicciotti, *J. Phys. Chem.*, **63**, 112 (1959).

(5) "Landolt-Bornstein Tabellen," 5th Ed.

(6) A. D. Kirschenbaum, J. A. Cahill, P. J. McGonigal, and A. V. Grosse, *J. Inorg. Nucl. Chem.*, **24**, 1287 (1962).

(7) See K. S. Pitzer and I. Brewer, revision of "Thermodynamics" by Lewis and Randall, McGraw-Hill Book Co., Inc., New York, N. Y., 1961, Appendix 1.

(8) D. Cubicciotti and F. J. Keneshea, *J. Phys. Chem.*, **62**, 999 (1958).

parameters estimated by the method of Pitzer were $T_c = 1185^\circ\text{K}$., $P_c = 83$ atm., $V_c = 310$ cc. (and acentric factor = 0.32). These compare with the experimental values reported above: $T_c = 1220^\circ\text{K}$. and $V_c = 302$ cc.

The agreement of the estimated T_c and V_c with the experimental values is good. This indicates that the correspondence between critical constants (T_c and V_c) and liquid density and vapor pressures observed for many molecular fluids by Riedel also obtains for bismuth bromide (as for bismuth chloride). Pitzer⁷ indicates that a more stringent test of a normal fluid can be made with the surface tension. Using the measured T_c and V_c , we calculated from Pitzer's eq.⁷ A 1-20 a value for σ_0 of 148 dynes/cm. and from his eq. A 1-19 and the measured values of T_c and

density a value of 75 dynes/cm. for the surface tension of the liquid at 250° . An experimental value of 66.5 dynes/cm. was given by Jaeger.⁹ Pitzer⁷ indicates that a deviation of the calculated surface tension of more than 5% from the estimated value indicates significant deviation from normal behavior. Therefore, although bismuth bromide behaves like a molecular fluid with regard to its critical volume and temperature, it may be expected to deviate from "normal" behavior in some of its other properties.

Acknowledgment. This work was supported jointly by the Research Division of the U. S. Atomic Energy Commission under Contract No. AT(04-3)-106 and Stanford Research Institute.

(9) F. M. Jaeger, *Z. anorg. allgem. Chem.*, **101**, 176 (1914).

The Radiation-Induced Oxidation of *p*-Xylene Sensitized by Organic Bromine Compounds

by D. Verdin, S. M. Hyde, and F. Neighbour

Wantage Research Laboratory, United Kingdom Atomic Energy Authority, Wantage, Berkshire, England
(Received December 29, 1964)

The oxidation of *p*-xylene at 25° induced by ^{60}Co γ -radiation is accelerated by the addition of organic bromine compounds. CBr_4 is the most efficient sensitizer, and the rate of absorption of oxygen accelerates to a maximum at about 2% oxidation and then decreases. The observed kinetics are consistent with a mechanism in which the autoretardation and the postirradiation oxidation result from the reaction, $\text{ROOH} + \text{HBr} \rightarrow \text{RO}\cdot + \text{H}_2\text{O} + \text{Br}\cdot$, between the hydroperoxide and hydrogen bromide formed as intermediates.

Introduction

The oxidation of *p*-xylene to terephthalic acid is normally carried out in organic acid solution in the presence of metal bromides at temperatures above 120° .¹ The metal ion catalyzes the conversion of the transient peroxy radicals to an aldehyde, and the bromine atoms formed abstract a hydrogen atom from

the methyl group in the intermediate *p*-toluic acid much more readily than peroxy radicals are able to do.²

In an attempt to increase the rate of oxidation of *p*-xylene Imamura and Ohta³ investigated the influence

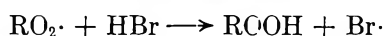
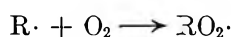
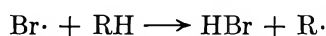
(1) G. H. Whitfield, British Patent 837,321 (1960).

(2) D. A. S. Ravens, *Trans. Faraday Soc.*, **55**, 1768 (1959).

of ^{60}Co γ -radiation on the reaction. At 80° no acceleration of the reaction occurred on irradiating, but at 135° irradiation doubled the rate of hydroperoxide formation and increased the production of acids. However, no terephthalic acid was obtained, and the conversion did not exceed 5 mole % owing to the production of an inhibitor. Irradiation of the much faster cobalt naphthenate catalyzed oxidations of *p*-xylene or *p*-toluic acid caused negligible changes.

Costea, *et al.*,⁴ oxidized *p*-xylene at temperatures from 60 to 130° using reactor irradiation, but even at the higher temperature they found that conversion to peroxide and *p*-toluic acid was less than 2% after 40 hr. However, with 1% cobalt naphthenate catalyst, these authors found that irradiation gave a yield of 20% *p*-toluic acid in 8 hr. under conditions where negligible reaction occurred in the absence of radiation.

Bakh⁵ found that the radiation-induced oxidation of toluene at 25° gave a low yield of peroxides, the total *G* value being 1.8. Peroxy radicals do not readily abstract primary hydrogen atoms from alkyl benzenes⁶ so that a similar nonchain mechanism is expected for the radiation-induced oxidation of pure *p*-xylene at 25° . However, bromine atoms have a low activation energy for such abstractions⁷ and may be able to induce a chain oxidation at room temperature, similar to that observed in gas phase oxidations catalyzed by HBr, in which the following propagating sequence occurs.⁸



We have therefore examined the ^{60}Co γ -radiation-induced oxidation of *p*-xylene containing organic bromine compounds at 25° . The radiolysis of the additive should produce a steady supply of bromine atoms which could possibly maintain the oxidation sequence to high conversions of the *p*-xylene.

Experimental

Materials. *p*-Xylene (Phillips Petroleum Co., pure grade) was repeatedly shaken with concentrated H_2SO_4 until the acid layer was colorless. It was then washed with 10% Na_2CO_3 solution and several times with distilled water, then dried with anhydrous CaSO_4 . After repeated shaking with mercury until tarnishing was insignificant, it was fractionally distilled in a nitrogen atmosphere through a 72-theoretical-plate column. The distillate was passed through a 12-cm. column of chromatographic alumina, collected in a

blackened flask, and stored under nitrogen in a grease-free automatic buret. The boiling point range $138.36 \pm 0.03^\circ$ (corrected to 760 mm.) agreed with the literature value,⁹ and gas-liquid chromatographic analysis revealed no detectable impurities. The rate of the radiation-induced oxidation of the above *p*-xylene was unchanged after three recrystallizations.

Oxygen from a cylinder was passed through columns of silica gel and KOH and then through a trap at -78° .

Carbon tetrabromide (Hopkin and Williams Ltd.) was recrystallized twice from ethanol and twice from petroleum ether (b.p. 40 – 60°) and then sublimed according to the procedure of Bradley and Drury.¹⁰ The absorption spectrum of the purified material was unchanged on further sublimation and had a maximum at $229 \text{ m}\mu$ with a molar extinction coefficient of 4.66×10^3 in Spectrosol hexane at 20.0° .

Bromobenzene, bromoform, ethyl bromide (treated to remove alcohol and water⁹), carbon tetrachloride, and bromotrichloromethane were fractionally distilled in a nitrogen atmosphere in a 35-plate all-glass column shielded from light. Small middle fractions were collected at boiling points agreeing with published values.⁹ Immediately after distillation the required amounts of the liquids were degassed in small ampoules with break-seals and stored in the dark until used.

Hydrogen bromide (Matheson Co., Inc., anhydrous) was degassed by freezing and thawing cycles and then stored in a blackened bulb until used. A calibrated bulb was filled at 20.0° to pressures measured with a mercury manometer, and the known amounts of HBr were condensed into the reaction vessel. Similar condensation of the HBr into excess alkali, followed by titration, confirmed its purity as 99.9%.

Benzyl alcohol and cobalt naphthenate (Hopkin and Williams Ltd.) and D_2O (L. Light and Co. Ltd., 99.5%) were used as supplied.

Measurement of Oxygen Absorption. The rates of oxygen absorption at selected pressures were measured

(3) J. Imamura and N. Ohta, *Tokyo Kogyo Shikensho Hokoku*, **55**, 346 (1960).

(4) T. Costea, C. Mantescio, and I. Negoescu, *Intern. J. Appl. Radiation Isotopes*, **13**, 306 (1962).

(5) N. A. Bakh, Symposium on Radiation Chemistry, Academy of Sciences of the U.S.S.R., English Translation, Consultants Bureau, New York, N. Y., 1956, p. 119.

(6) G. A. Russell, *J. Am. Chem. Soc.*, **78**, 1047 (1956).

(7) H. R. Anderson, H. A. Scheraga, and E. R. Van Artsdalen, *J. Chem. Phys.*, **21**, 1258 (1953).

(8) F. F. Rust and W. E. Vaughan, *Ind. Eng. Chem.*, **41**, 2595 (1949).

(9) A. Weissberger, *et al.*, "Technique of Organic Chemistry," Vol. VII, Interscience Publishers, Inc., New York, N. Y., 1955.

(10) R. S. Bradley and T. Drury, *Trans. Faraday Soc.*, **55**, 1844 (1959).

automatically in a constant pressure apparatus.¹¹ Oxidations were performed in cylindrical glass reaction vessels of 30-mm. internal diameter and 10-mm. internal thickness, and having a 7-mm.-diameter side tube incorporating a diaphragm break-seal and a narrow bore side arm. Measured amounts of previously degassed *p*-xylene and additives were distilled or sublimed under vacuum into the reaction vessel through the side arm, which was then sealed off. The reaction vessel was immersed in a thermostat controlled to $\pm 0.02^\circ$ and clamped to a bar at reproducible positions with respect to a 230-curie ⁶⁰Co source¹² which was also immersed in the thermostat. To keep the solutions saturated with oxygen the reaction vessel was continuously shaken at measured rates by means of a motor driving a Kopp Variator (Allspeeds Ltd.) connected, by an eccentrically mounted rod, to the bar supporting the reaction vessel. The latter was connected to the oxygen absorption apparatus *via* a flexible glass spiral. After evacuating the system and filling with oxygen to the required pressure, the break-seal was fractured by a glass-covered magnet, and the apparatus controls were set before introducing the ⁶⁰Co source to start the reaction. The rate of oxygen absorption was independent of the shaking speed from 188 to 655 c./min.; measurements were normally made at a rate of about 540 c./min.

Dosimetry. The rates of energy absorption in the *p*-xylene solutions were calculated on the basis of electron densities from measurements made in the reaction vessels with the ferrous sulfate dosimeter, taking $G_{\text{Fe}^{3+}} = 15.5$,¹³ and correcting for ⁶⁰Co decay.

Analysis. The formation of reaction products was investigated in the reaction vessels used for the oxygen absorption runs, but having a stoppered side arm added for sample withdrawal, the oxygen pressure being maintained at about 850 mm.

Hydroperoxides were measured by the iodometric method of Wibaut, *et al.*,¹⁴ and it was shown that CBr₄ and benzyl alcohol present in the amounts used in this work did not affect the results of analyses using pure *t*-butyl hydroperoxide. Samples were analyzed immediately after removal from the radiation source.

Infrared spectra of the reaction products were measured after removing *p*-xylene and volatile products by vacuum distillation.

Results

Irradiation of *p*-xylene at a dose rate of 1.93×10^{18} e.v. l.⁻¹ sec.⁻¹ in the presence of oxygen at 25° resulted in oxygen being absorbed at a rate of 8.65×10^{-8} mole l.⁻¹ sec.⁻¹ (mean of four runs) which was constant to an absorbed dose of at least 1.04×10^{24} e.v. l.⁻¹.

This rate corresponds to an observed G value for oxygen absorption of 2.70. However, the value must be corrected for the radiolytic formation of H₂ and CH₄ which occurs in the presence of O₂ and amounts to $G_{\text{H}_2} + G_{\text{CH}_4} = 0.22$ ¹⁵ under the irradiation conditions used here, so that the true rate of oxygen absorption is $G_{(-\text{O}_2)} = 2.92$.

To determine the relative influence of a range of halogen-containing additives, oxidations were carried out at 25° and approximately the same dose rate. The additives were all present at the same electron fraction of the solutions, so that the proportion of the radiation energy absorbed in them should be the same, and the oxidation rates should be determined by their radical yields and the efficiency of these radicals in establishing oxidation chains. Plots of O₂ absorbed as a function of time (radiation dose) for some of the additives are compared with that for *p*-xylene in Figure 1. The corresponding plot for CHBr₃ resembled those of CBr₄ and CCl₃Br in showing an initial period of accelerating rate, while those for C₂H₅Br, C₆H₅Br, and CCl₄ all showed an initial oxidation rate which started to decrease in the region 0.5–1% oxidation. The maximum rates of oxygen absorption are summarized in Table I.

Table I: Maximum Oxidation Rates of *p*-Xylene Solutions of Halogen Compounds at 25.0° (electron fraction of additives = 0.0420)

Additive	Dose rate, e.v. l. ⁻¹ sec. ⁻¹ $\times 10^{-18}$	$-\frac{d(\text{O}_2)}{dt}$, moles l. ⁻¹ sec. ⁻¹ $\times 10^7$	Maximum $G_{(-\text{O}_2)}$ ^a
None	1.93	0.865	2.92
C ₂ H ₅ Br	1.88	4.59	14.9
C ₆ H ₅ Br	2.00	8.81	26.8
CHBr ₃	1.91	9.27	29.5
CCl ₄	1.99	3.41	10.5
CCl ₃ Br	1.92	12.3	38.6
CBr ₄	1.96	20.3	62.6

^a Corrected for H₂ and CH₄ production.

Sensitization by CBr₄. It is seen that CBr₄ is the most effective additive for increasing the oxidation rate, and the kinetics of this system were therefore studied in more detail, the rate of oxidation always

(11) F. Neighbour and D. Verdin, *J. Sci. Instr.*, **41**, 219 (1964).

(12) G. S. Murray, R. Roberts, and D. Dove, *Radioisotopes in Scientific Research, Proceedings of the 1st International Conference, Paris, Sept. 1957, Vol. 1, Pergamon Press Ltd., London, 1958, p. 139.*

(13) R. H. Schuler and A. O. Allen, *J. Chem. Phys.*, **24**, 56 (1956).

(14) J. P. Wibaut, H. B. van Leeuwen, and B. van der Wal, *Rec. trav. chim.*, **73**, 1033 (1954).

(15) D. Verdin, *J. Phys. Chem.*, **67**, 1263 (1963).

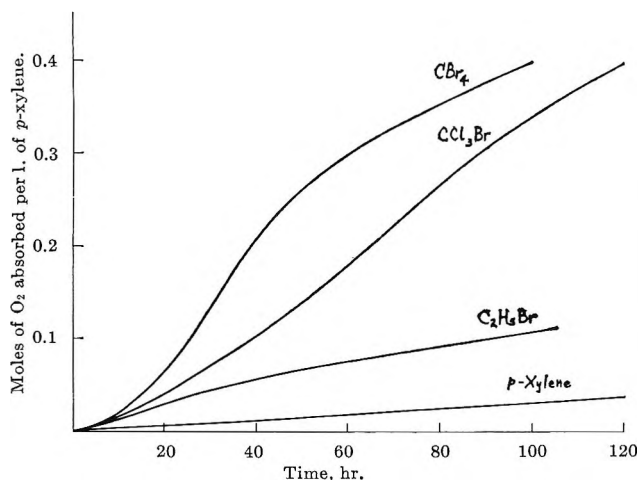


Figure 1. Absorption of O_2 by *p*-xylene solutions at 25.0° ; dose rate = $1.92 \pm 0.04 \times 10^{18}$ e.v. l. $^{-1}$ sec. $^{-1}$, electron fraction of additives = 0.0420.

being measured as the maximum slope of the oxygen absorption curve.

The maximum rate of oxidation at 25° was independent of the oxygen pressure above the solution over the range 411–1077 mm., the rates being measured at a dose rate of 1.05×10^{18} e.v. l. $^{-1}$ sec. $^{-1}$ and a CBr_4 concentration of 0.141 *M*. Oxidation rates were normally measured at pressures of about 850 mm.

The rate of oxygen absorption increased linearly with the radiation dose rate (Figure 2) over the range 8.41×10^{16} to 2.08×10^{18} e.v. l. $^{-1}$ sec. $^{-1}$ at 25.0° , and extrapolation of this plot to zero dose rate gave a finite rate of oxygen absorption (R_0). The manner in which the reaction rate depended on the concentration of CBr_4 is shown in Figure 3. The highest concentration employed corresponds to an electron fraction of CBr_4 in the solution of 0.154. A logarithmic plot of the data leads to the expression

$$\frac{-d(O_2)}{dt_{max}} = k_{obsd}(CBr_4)^{0.26}I + R_0$$

for the maximum rate of oxygen absorption, where I is the dose rate.

The variation of reaction rate with temperature was determined from measurements of the rate of oxygen absorption at three dose rates at each temperature. The linearity of reaction rate with dose rate persisted to the highest temperature used, and the intercept at zero dose rate increased with temperature (Figure 2). The runs were all performed at a CBr_4 concentration of 0.141 *M*, and the slopes of the plots of $-d(O_2)/dt$ against I were divided by $(CBr_4)^{0.26}$ to obtain k_{obsd} . An Arrhenius plot of the values of k_{obsd} summarized

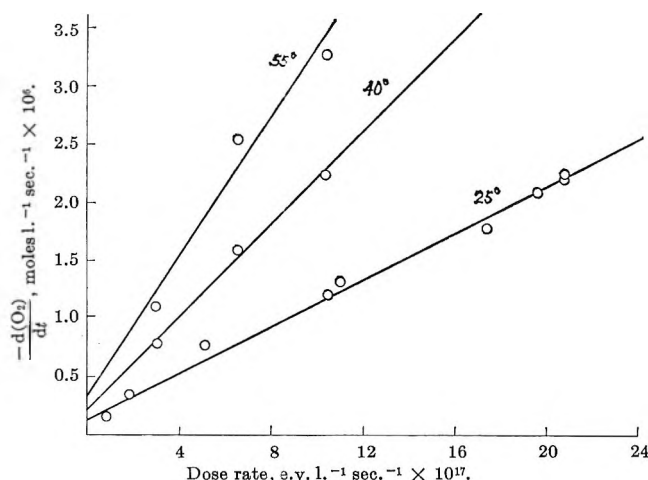


Figure 2. Variation of maximum rate of oxidation of 0.141 *M* CBr_4 solutions in *p*-xylene with dose rate and temperature.

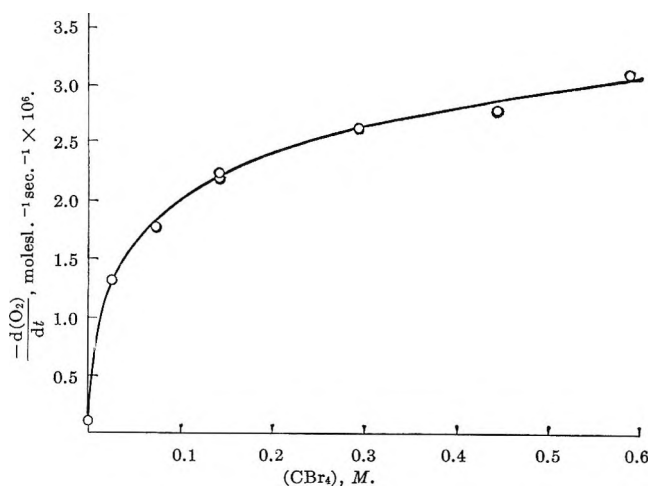


Figure 3. Effect of CBr_4 concentration on oxidation rate at 25.0° ; dose rate = 2.08×10^{18} e.v. l. $^{-1}$ sec. $^{-1}$.

in Table II leads to an over-all activation energy of 8.1 kcal./mole for the maximum rate of oxidation.

The formation of hydroperoxides during the oxidation is compared with the absorption of oxygen under identical conditions in Figure 4. Infrared spectra of the nonvolatile reaction products, which were yellow colored, after 22- and 70-hr. irradiation closely resembled

Table II: Temperature Dependence of Rate Constant for Maximum Rate of Oxygen Absorption

Temp., $^\circ C.$	$k_{obsd} \times 10^{24}$, mole $^{0.74}$ l. $^{0.26}$ e.v. $^{-1}$
25.0	1.63
40.0	3.23
55.0	4.94
70.0	9.90

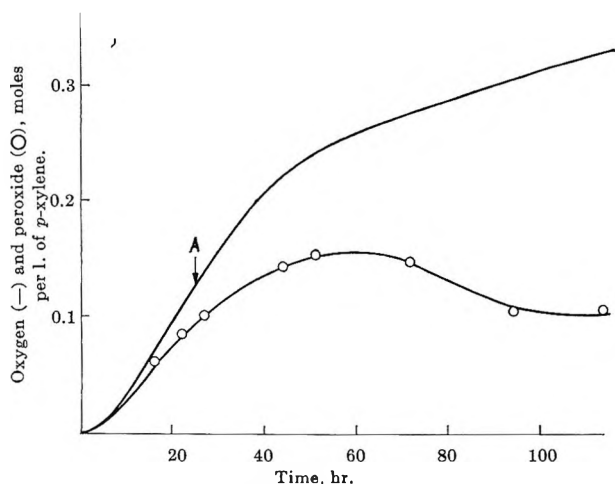


Figure 4. Comparison of O_2 absorption and hydroperoxide formation in the oxidation of $0.141 M CBr_4$ in *p*-xylene at 25.0° ; dose rate = 1.74×10^{18} e.v. l.⁻¹ sec.⁻¹, point A = 1.57% oxidation.

that of benzyl alcohol, including a strong band at 3500 cm.^{-1} , which confirms the appearance of OOH and/or OH groups¹⁶ in one of the methyl groups of *p*-xylene. The ultraviolet absorption spectrum of the oxidate after 25-hr. irradiation showed a peak at 229μ due to CBr_4 , but no quantitative measure of the CBr_4 concentration was possible owing to the high absorption of *p*-xylene in this region.

Postirradiation Oxidation. Removal of the radiation source during the course of an oxidation resulted in a marked decrease in the rate of oxygen absorption. Subsequent reintroduction of the source did not immediately restore the reaction rate to its value prior to removal of the source, but there was a gradual acceleration in rate. The postirradiation rate depended on the degree of oxidation at which the irradiation was stopped in the manner shown in Figure 5, and at each conversion the rate decreased with time and eventually became zero. The postirradiation rate attained its highest values in the same conversion range as the maximum rate of oxidation occurred, that is, between 1.0 and 2.5% oxidation, and at conversions exceeding 3.6% oxidation there was no posteffect.

The reaction product has been found to contain hydroperoxide, and to determine whether this could give rise to the postirradiation oxidation, a $2.6 \times 10^{-3} M$ solution of pure *t*-butyl hydroperoxide in *p*-xylene was shaken with O_2 ; however, the solution absorbed no O_2 in 41 hr. at 25° . HBr is a probable intermediate in the reaction and also might cause the postirradiation effect. To examine this, reaction vessels were employed in which *p*-xylene was saturated with O_2 before breaking the seal of a compartment into which

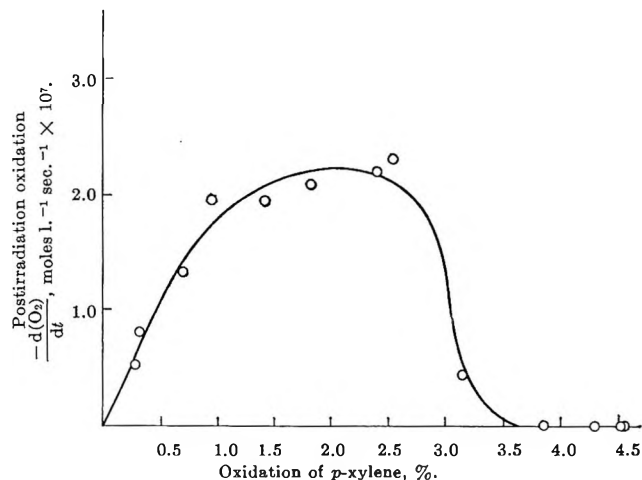


Figure 5. Postirradiation oxidation of $0.141 M CBr_4$ in *p*-xylene after radiation-induced oxidation to various conversions at 25° ; dose rate = 1.89×10^{18} e.v. l.⁻¹ sec.⁻¹.

HBr had been distilled. These solutions, which were $0.087 M$ with respect to HBr, absorbed O_2 very rapidly at 25° (at initial rates of approximately 5×10^{-5} mole l.⁻¹ sec.⁻¹), after an induction period of about 3.5 hr. The reaction rate decreased rapidly and was zero after 1.8% oxidation. The induction period was reduced to less than 5 min. by irradiating the solutions at a dose rate of 6.8×10^{17} e.v. l.⁻¹ sec.⁻¹, and after the reaction had started removal and reintroduction of the radiation source had no effect on the oxidation rate. Moreover, if the reaction was allowed to go to completion in the absence of radiation, there was no further absorption of O_2 on irradiating or introducing more HBr.

If HBr was added in the above manner (to give a concentration of $0.073 M$) to a $2.6 \times 10^{-3} M$ solution of *t*-butyl hydroperoxide in *p*-xylene, a similar rapid absorption of O_2 occurred with no induction period and at initial rates of approximately 1.6×10^{-4} mole l.⁻¹ sec.⁻¹. The reaction rate decreased as the reaction proceeded and became zero after 1.0% oxidation. If solutions of these concentrations of HBr and hydroperoxide were mixed in the reaction vessel and left for 24 hr. before admitting O_2 , there was an induction period of 14 hr. before O_2 was absorbed at an initial rate of 2.0×10^{-6} mole l.⁻¹ sec.⁻¹, which fell to zero after 0.59% oxidation. The initial rate of the reaction and the final extent of oxidation both increase as the initial concentrations of HBr and hydroperoxide are increased, e.g., with HBr = $0.26 M$ and hydroperoxide = $5.4 \times 10^{-3} M$ the initial rate of O_2 absorption exceeded 3.8×10^{-4} mole l.⁻¹ sec.⁻¹, and the reaction

(16) G. J. Minkoff, *Proc. Roy. Soc. (London)*, A224, 176 (1954).

had almost stopped absorbing O_2 after 10 hr. when 3.9% oxidation had occurred. The initial rates of O_2 absorption in these solutions were insufficiently reproducible to permit kinetic study of the system, probably owing to the reaction rate being comparable to the rate of diffusion of O_2 into the liquid phase, and distribution of HBr between the two phases may also contribute in this way.

It was observed that the addition of *t*-butyl hydroperoxide (to give a concentration of 0.06 *M*) to a 0.141 *M* solution of CBr_4 in *p*-xylene resulted in the absorption of oxygen. However, the rate was negligible compared with the postirradiation oxidation which occurs at conversions corresponding to this hydroperoxide content in the radiation-induced oxidation of *p*-xylene containing the same concentration of CBr_4 .

The above experiments demonstrate that a reaction capable of initiating oxidation occurs between HBr and *t*-butyl hydroperoxide or the hydroperoxide produced when *p*-xylene containing O_2 and HBr is irradiated. Moreover, the reaction forms a product which acts as an oxidation inhibitor. The production of inhibitors in the CBr_4 sensitized oxidation was confirmed by oxidizing *p*-xylene containing 0.141 *M* CBr_4 until it reached 3.9% conversion and then adding a fresh portion of CBr_4 and continuing the oxidation. The maximum rate of O_2 absorption in this second stage was less than 30% of the maximum rate of the original oxidation.

Retardation of Oxidation. One of the probable reaction products is *p*-methyl benzyl alcohol and it is desirable to know to what extent it can retard the oxidation. Benzyl alcohol should exhibit a very similar degree of retardation and it was used for this test in view of its commercial availability. The oxidation rate as a function of the concentration of benzyl alcohol added at the beginning of the runs is shown in Figure 6. The slight increase in oxidation rate after the rapid initial fall is probably due to direct oxidation of the benzyl alcohol at the higher concentrations absorbing an appreciable amount of oxygen.

Water also exhibits a retarding effect on the oxidation and this is illustrated in Figure 6. The saturation solubility of water in xylene at 25° is 0.02 *M*,¹⁷ so that after a relatively small amount of a second phase has been formed (approximately 10 times the solubility, *i.e.*, 0.02 ml. of water in samples containing 5 ml. of *p*-xylene), the addition of more water causes negligible further decrease in oxidation rate. To provide information on the mechanism by which water retards the oxidation its influence was compared with that of similar amounts of D_2O , and these results are included on the same graph. It is seen that within experi-

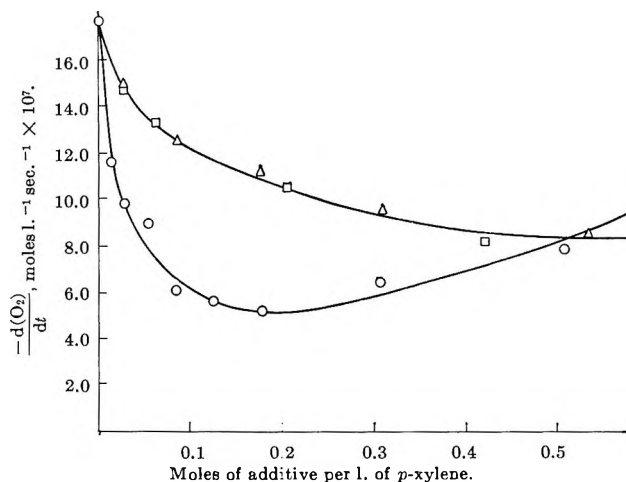


Figure 6. Effect of benzyl alcohol (O), water (Δ), and D_2O (\square) on the maximum rate of oxidation of 0.141 *M* CBr_4 in *p*-xylene at 25.0°; dose rate = 1.71×10^{18} e.v. $l.^{-1} sec.^{-1}$.

mental error the behavior of water and D_2O is identical. It is significant to note that the addition of excess water to a 2.6×10^{-3} *M* solution of *t*-butyl hydroperoxide in *p*-xylene before the addition of HBr (to give a 0.073 *M* solution) entirely prevented the absorption of O_2 by this system, which would otherwise have undergone a rapid oxidation.

The addition of cobalt naphthenate (1.77% by weight) to an oxidation which was performed under identical conditions with that illustrated in Figure 4 gave a maximum rate of oxygen absorption of 9.81×10^{-7} mole $l.^{-1} sec.^{-1}$, which is approximately half of that in the absence of cobalt naphthenate. This rate was attained after a period of 85 hr. during which the oxidation slowly accelerated, and at the end of the run the vessel contained a precipitate of a bromine compound of cobalt. Cobalt naphthenate therefore does not function as a catalyst under the conditions used in this system.

Discussion

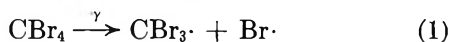
The low *G* value of 2.92 for oxygen absorption by *p*-xylene in the absence of additives and the *G* values for radical production from alkylbenzenes¹⁸ indicate that a nonchain oxidation is occurring, as would be expected at 25° from the low reactivity of the methyl hydrogen atoms toward peroxy radicals.⁶ Our result is consistent with that of Bakh,⁵ who found a total yield of peroxides of $G = 1.8$ in the radiation-induced oxidation of

(17) A. Seidell, "Solubilities of Organic Compounds," Vol. II, D. Van Nostrand Co., Inc., New York, N. Y., 1941, p. 607.

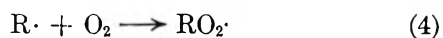
(18) E. N. Weber, P. F. Fosyth, and R. H. Schuler, *Radiation Res.*, 3, 68 (1955).

toluene at a dose rate of 4.8×10^{18} e.v. l.⁻¹ sec.⁻¹ at 25°.

The G values for the absorption of O₂ in the presence of various sensitizers (Table I) indicate that the oxidation occurs by a chain mechanism, but that the chain lengths are short. There are insufficient published data on radical yields to enable predictions to be made on the relative oxidation rates induced by these compounds, but the $G_{(-O_2)}$ values for C₂H₅Br and C₆H₅Br indicate the effectiveness of Br atoms for inducing oxidation. It is improbable that the radical yield from CCl₃Br will exceed that from CCl₄ by a factor of 4, so that the fourfold higher oxidation rate (Table I) of *p*-xylene in the presence of CCl₃Br must result from the oxidation chains established by the Br atom. However the fact that CCl₄ does accelerate the oxidation of *p*-xylene implies that the CCl₃· fragment from CCl₃Br contributes to the $G_{(-O_2)}$ value observed with this sensitizer. Consequently the difference in behavior between CCl₃Br and CBr₄ would require the latter to have about twice the Br atom yield of CCl₃Br if CBr₃· radicals did not initiate oxidation chains. In view of the equality of C-Br bond dissociation energies in these two molecules, and the fact that dissociation energies for C-Cl bonds in such molecules are much greater than for C-Br bonds,¹⁹ it is unlikely that the Br atom yields differ by a factor of 2, and it is suggested that when CBr₄ is used as a sensitizer both the Br· and CBr₃· species initiate oxidation chains. The initiation steps in the oxidation may be represented by the equations



Reaction 3 occurs in the side-chain bromination of toluene in the gas phase and has an activation energy of 7.2 kcal./mole.⁷ The oxidation rate is independent of the oxygen pressure so that all the *p*-xylyl (R·) radicals must react rapidly with oxygen.



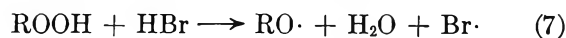
The activation energy for attack of peroxy radicals on *p*-xylene should exceed the value of 10.5 kcal./mole for *p*-cymene²⁰ so that the peroxy radicals will not compete with reaction 3 but will take part in the following propagating steps.



Reactions 3, 4, and 6 are those invoked to explain the

catalytic effect of HBr in the gas phase oxidation of hydrocarbons.^{8,21}

The lifetimes of the transient radicals in the above reactions will be short, so that the postirradiation oxidation must arise from reactions between intermediate products. We have found that the reaction of HBr with a hydroperoxide can initiate the oxidation of *p*-xylene, and we therefore include reaction 7 in the scheme to provide a source of bromine atoms to initiate the postirradiation oxidation. It has been proposed that

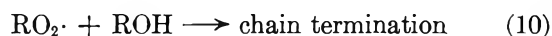


this reaction causes chain branching in the HBr-catalyzed oxidation of isobutene in the gas phase.²¹

The linear dependence of oxidation rate on radiation intensity indicates that the termination reactions do not involve bimolecular interaction of chain-carrying species. The retardation of the reaction at low conversions, and the complete cessation at equally low conversions of oxidations initiated by mixtures of HBr and hydroperoxide, implies that reaction 7 gives rise to this autoretardation. The infrared spectrum of the product is consistent with the presence of a benzyl-type alcohol, and we found that benzyl alcohol added to the reaction mixture strongly retards the oxidation. The RO radicals produced in reaction 7 must therefore form *p*-methyl benzyl alcohol (ROH), probably by reactions 8 and 9, and the resulting alcohol will compete



with reactions 5 and 6 for peroxy radicals and so retard the oxidation. We therefore include reaction 10, and it may be noted that benzyl alcohol is an effective inhibitor of the HBr-catalyzed oxidation of benzyl bromide²² in the liquid phase at temperatures exceeding 194°.



Addition of water at the beginning of the oxidation markedly reduces the rate, but it is a less effective retarder than benzyl alcohol. In view of the high O-H bond dissociation energy in H₂O it seems improbable that H-atom abstraction is involved in the retardation, and it is proposed that it functions by converting HBr into the ionized form, in which it will no longer take

(19) N. N. Semenov, "Some Problems of Chemical Kinetics and Reactivity," Vol. I, Pergamon Press Ltd., London, 1958, p. 19.

(20) H. Boardman, *J. Am. Chem. Soc.*, **84**, 1376 (1962).

(21) P. Hurst, G. Skirrow, and C. F. H. Tipper, *Proc. Roy. Soc. (London)*, **A268**, 405 (1962).

(22) R. Barnett, E. R. Bell, F. H. Dickey, F. F. Rust, and W. E. Vaughan, *Ind. Eng. Chem.*, **41**, 2612 (1949).

part in reaction 6 or 7. When the solubility of H₂O in *p*-xylene is exceeded the distribution coefficient for HBr will greatly favor its transfer to the aqueous phase when only a small amount is present.



The identical behavior of D₂O and water implies that the retardation does not involve bond breakage in the water molecule and supports the proposal that ionization of the HBr causes the retardation, since no primary isotope effect in the water molecule is involved and water and D₂O should have similar efficiencies in bringing about reaction 11.

When only a small amount of the aqueous phase has appeared the addition of more water causes no further decrease in oxidation rate, and we also found that excess water completely inhibits oxidations initiated by the reaction between HBr and a hydroperoxide. However, in the irradiated CBr₄ system, excess water reduces the oxidation rate to only half of that in the absence of added water. This is consistent with the proposed mechanism since water will not affect the oxidation chain (reactions 2, 4, and 5) initiated by CBr₃ radicals, and the result implies that the sequence accounts for approximately half of the oxidation occurring. Benzyl alcohol is able to reduce the oxidation rate below that caused by the presence of excess water since it acts by scavenging peroxy radicals and thus retards the oxidation chains initiated by both Br atoms and CBr₃ radicals.

Although reaction 11 removes bromine from the oxidation sequence, some bromine must be removed by another process which will give rise to the product causing the yellow color of the oxidate. The low volatility of the colored product shows that it is not molecular bromine, and it may be derived from the CBr₃ radical; however, the identity of the colored product was not established.

If the termination reactions are first order with respect to the chain-carrying species, then the reaction rate will be proportional to the initiation rate and the observed linear dependence on dose rate is consistent with reaction 1 being the main process for initiation. It might be expected that the oxidation rate would be proportional to the CBr₄ concentration; however, the observed dependence (Figure 3) probably reflects the occurrence of energy transfer from *p*-xylene to the CBr₄, or the reaction of CBr₄ with electrons by dissociative capture to produce CBr₃ radicals and Br⁻ ions which are subsequently neutralized. Analogous behavior was reported²³ for some organic halogen compounds as sensitizers of the radiation-induced polymerization of styrene. *p*-Xylene and CBr₄ form a donor-acceptor

complex due to the interaction of the Br atoms with π -electrons of the aromatic ring²⁴ and this could enhance the probability of energy transfer in this system. On irradiating CCl₄ solutions in benzene, Oster and Kallmann²⁵ found that the transfer of energy from benzene to CCl₄ leads to the production of radicals at a rate which depends on the concentration of CCl₄ in a similar manner to Figure 3 in the same range of concentrations of the halogen compound. If the *G* value for loss of CBr₄ is taken as 10 and it is assumed that all the energy absorbed in the solution leads to decomposition of CBr₄, then, for the oxidation represented in Figure 4, 36.9% of the initial CBr₄ would be decomposed after 50-hr. irradiation, so that loss of CBr₄ by radiolysis does not contribute significantly to the falloff in oxidation rate.

By assuming stationary concentrations of all the radical species involved, the instantaneous oxidation rate may be expressed in terms of the concentrations of the reaction intermediates and products by the equation

$$\frac{-d(\text{O}_2)}{dt} = \left[\frac{2G_{(-\text{CBr}_4)}}{100N} (\text{CBr}_4)^\alpha I + 2k_7(\text{ROOH})(\text{HBr}) \right] \times \left[1 + \frac{k_5(\text{CHBr}_3) + k_6(\text{HBr})}{k_{10}(\text{ROH})} \right]$$

where *N* is Avogadro's number and the index α allows for energy transfer to CBr₄.

The reaction sequence predicts that the concentration of HBr in the *p*-xylene will pass through a maximum, and in the region where this occurs the oxidation rate should also be a maximum. The above rate equation indicates that this maximum rate will vary linearly with the dose rate and that the graph will extrapolate to a finite intercept at zero dose rate, and this intercept should increase with temperature because of the activation energies of the rate constants involved. Figure 2 shows that the system does behave in this way. As appreciable amounts of a separate aqueous phase form, removal of HBr progressively reduces the terms involving (HBr) and the rate of oxidation falls. Further reduction in the rate of oxygen absorption occurs as the concentration of the alcohol increases; however, when its concentration becomes sufficiently high, the direct radiation-induced oxidation of the alcohol²⁶

(23) D. W. Brown and L. A. Wall, *J. Polymer Sci.*, **44**, 325 (1960).

(24) F. J. Strieter and D. H. Templeton, *J. Chem. Phys.*, **37**, 161 (1962).

(25) G. K. Oster and H. D. Kallmann, *Nature*, **194**, 1033 (1962).

(26) N. A. Bakh, Proceedings of the International Conference on the Peaceful Uses of Atomic Energy, Geneva, 1955, Vol. 7, Columbia University Press, New York, N. Y., 1956, p. 538.

will compensate for the decrease in rate of oxygen absorption. When sufficient water has been produced to eliminate the chain involving HBr, the CBr₃ oxidation chain should continue to increase the hydroperoxide concentration. The observation that the hydroperoxide concentration falls to a lower level may be due to energy transfer from *p*-xylene to the hydroperoxide resulting in its decomposition. Such transfer can lead to high *G* values for peroxide decomposition when both the peroxide and the solvent are aromatic.²⁷ The postirradiation oxidation is consistent with the above equation, which indicates that its rate will follow the HBr and hydroperoxide concentrations and will be zero when there is sufficient water to remove all the HBr. The over-all activation energy of the oxidation in terms of the activation energies of the individual steps in the oxidation scheme would involve too many unknown values to permit any comparison between the calculated and experimental values. The reaction may involve additional steps such as further reactions of the CBr₃ radicals or hydroperoxide mole-

cule; however, the above mechanism explains the essential features of the system.

Hendry and Russell²⁸ have recently observed that the liquid phase oxidation of cumene containing traces of HBr proceeds extremely rapidly initially but soon inhibits itself, which they assumed to be due to the formation of phenol by an acid-catalyzed decomposition of cumene hydroperoxide. However, in cumene solution the HBr would be in the covalent form, and on the basis of the present work it would be expected to react with the hydroperoxide to produce dimethylphenylcarbinol and water which would inhibit the oxidation. HBr is also known²² to catalyze the liquid phase oxidation of benzyl bromide and mesitylene at temperatures in the region of 200°, where the water produced would be removed in the O₂ gas stream and so permit extensive oxidation.

(27) V. A. Krongauz and Kh. S. Bagdasaryan, *Zh. Fiz. Khim.*, **32**, 717 (1958).

(28) D. G. Hendry and G. A. Russell, *J. Am. Chem. Soc.*, **86**, 2371 (1964).

The Effect of Ions on the Self-Diffusion of Water. I.

Concentration Dependence

by David W. McCall and Dean C. Douglass

Bell Telephone Laboratories, Incorporated, Murray Hill, New Jersey (Received January 4, 1965)

The self-diffusion coefficient of water has been measured as a function of concentration for several ionic solutions at 23°. Most ions tend to reduce the water diffusion rate but a few increase the diffusion rate. The observed concentration dependences for self-diffusion are closely correlated with concentration dependences for the fluidity. The data are presented in relation to other experimental quantities and certain theoretical models. Hydration numbers are deduced and discussed. An attempt is made to adapt Kirkwood's statistical results to water in a semiempirical manner.

I. Introduction

This paper presents the results of an investigation of the self-diffusion of water. Despite the great interest that the study of aqueous solutions has sustained over many decades,¹⁻³ relatively few self-diffusion experiments for water in solutions have been reported. Therefore, we have made concentration dependence measurements for 29 electrolyte systems, salts, bases, and acids, in order to obtain a general picture. The nuclear magnetic resonance spin-echo method was employed,⁴⁻⁷ and the measurements were carried out at room temperature.

The self-diffusion coefficient for pure water has been the subject of many experimental studies.⁸⁻¹¹ Unfortunately, the spread within the reported data is great, much greater than the estimated errors that have been published. Although the absolute value of the self-diffusion coefficient for water is not our principal concern in this paper, our method is absolute and we shall make our contribution to the body of data. In general, the resonance method is in satisfactory agreement with tracer methods.

For the purpose of discussing the effect of ionic solutes on the self-diffusion coefficient of water, we shall define a parameter Δ_1 , the relative change of the diffusion coefficient of water between 0 and 1 *M*. This quantity is moderately useful since the observed concentration dependences are approximately linear in many cases. We will show that the Δ_1 terms can be approximately decomposed into individual ionic terms. These ionic Δ_1 terms can be used to predict concentra-

tion dependences for many substances that have not been measured. In addition, the Δ_1 terms will be shown to be correlated with a similar concentration dependence parameter based on fluidity¹² (*i.e.*, reciprocal viscosity) data. This relationship is so striking that empirical estimates of the concentration dependences of the water self-diffusion could also be based on viscosity data.

One of the chief aims of this study concerns the relationship between self-diffusion and structural properties. With some ions, definite hydrates are formed that are known to persist for many hours. With other ions the lifetimes for hydrate complexes may be so short as to be of little interest in relation to some experiments. The implication of the hydrate concept,

(1) H. S. Harned and B. B. Owen, "The Physical Chemistry of Electrolytic Solutions," 3rd Ed., Reinhold Publishing Co., New York, N. Y., 1958.

(2) R. A. Robinson and R. H. Stokes, "Electrolyte Solutions," Butterworth and Co. Ltd., London, 1959.

(3) R. W. Gurney, "Ionic Processes in Solution," McGraw-Hill Book Co., Inc., New York, N. Y., 1953.

(4) E. L. Hahn, *Phys. Rev.*, **80**, 580 (1950).

(5) H. Y. Carr and E. M. Purcell, *ibid.*, **94**, 630 (1954).

(6) D. C. Douglass and D. W. McCall, *J. Phys. Chem.*, **62**, 1102 (1958).

(7) D. W. McCall, D. C. Douglass, and E. W. Anderson, *Z. Elektrochem.*, **67**, 336 (1963).

(8) See ref. 2, p. 328.

(9) J. H. Simpson and H. Y. Carr, *Phys. Rev.*, **111**, 1201 (1958).

(10) L. Devell, *Acta Chem. Scand.*, **16**, 2177 (1962).

(11) P. A. Johnson and A. L. Babb, *Chem. Rev.*, **56**, 387 (1956).

(12) E. C. Bingham, *J. Phys. Chem.*, **45**, 885 (1941).

that is that a definite number of water molecules are influenced by a given ion while the other water molecules and ions are not, is obviously an oversimplification, particularly in the concentrated solutions under discussion here. Nevertheless, the hydrate concept is useful so long as we keep in mind that lifetime and geometry are important characteristics. Another structural phenomenon relevant here is "structure breaking." Water is known to have a significant amount of (pseudo-crystalline) structure above the melting point and certain ions tend to disrupt this structure. The concept is quite reasonable but it is unfortunate that a quantitative definition has not been developed. Of course, the concentration dependence of any quantity in aqueous solutions can be qualitatively explained by a judicious mixture of structure breaking and complex formation. We shall attempt to carry the discussion somewhat beyond this point.

The ionic solutes chosen for the present study yield ions that form relatively short-lived hydrates. Over the time interval required for making a self-diffusion measurement by the spin-echo method, say about 0.1 sec., we expect the hydrate water molecule to exchange many times with the bulk water. (Aqueous solutions of Al^{+3} may be an exception to this expectation at high concentrations.) Thus, we measure an average diffusion coefficient, the average representing all the various states of the water in the solution. Because of the enormous difference between the experiment time and the times associated with elementary molecular processes, *e.g.*, oscillation, jumping, and perhaps exchange, we shall not emphasize structural characteristics deduced from self-diffusion data alone. Rather, we shall consider these data in the light of deductions made on the basis of other physical properties.

II. Experimental

The proton magnetic resonance spin-echo method, suggested by Hahn⁴ and worked out by Carr and Purcell,⁵ has been employed in this work. Specific details of the method as used in our laboratory have been published.⁶ It is important to recall that the method involves measurement of relaxation in the presence of a macroscopic magnetic field gradient in comparison with relaxation in the absence of such a gradient. Thus, the method yields a true macroscopic diffusion coefficient and should be directly comparable with tracer results. In the systems that have been studied by both resonance and tracer methods satisfactory agreement exists.¹³

Relaxation of the entire proton magnetization is followed, but owing to the rapid exchange there will be only one type of proton present on the average.

This is not true in the case of potassium acetate, but the water protons are much more abundant than the methyl protons over most of the concentration range. Long-lived hydrate complexes could lead to minor complications in the relaxation behavior, but the average water diffusion coefficient obtained by our method would represent a suitable average coefficient for bound and unbound water.

The absolute accuracy of the self-diffusion coefficients is estimated to be about 5%. Relative values are probably known to within 1 or 2%. Pure water was measured with each solute concentration dependence series and the relative accuracy applies to the concentration dependences.

The solutions were prepared from reagent grade materials and distilled water. In most cases the most concentrated solution was subsequently analyzed by standard chemical techniques.¹⁴ No appreciable inaccuracies were found. The concentration accuracy is probably about 1%. It was necessary to acidify some of the ZnCl_2 solutions slightly with HCl in order to render the salt soluble.

Viscosity data were drawn from the "International Critical Tables,"¹⁵ as were density data necessary for making the conversions between molality and molarity. In some cases viscosity data were lacking, or, in one case (NaBr), they were suspicious. Supplementary viscosity measurements were made in these cases. A Cannon-Fenske type viscometer was used in this connection. No attempt was made to obtain great accuracy but the measurements are probably good to 1 or 2%. In the case of NaBr, it appears that the "International Critical Tables" are incorrect. All measurements were made at 22 or 23° and the temperature was held to within 1° of the nominal.

III. Experimental Results

Pure water was measured during each series in an effort to minimize the error. This gave over 25 separate determinations collected over a period of several months. All of the data for pure water (except as noted below) at 23° are found to lie between 2.38×10^{-5} and 2.52×10^{-5} cm.²/sec. and part of this range can be attributed to the $\pm 1^\circ$ temperature variation. The average is 2.45×10^{-5} cm.²/sec. This figure agrees very well with the figure Robinson and Stokes⁸ arrived at on the basis of a critical study of the earlier evidence, mainly tracer work, 2.44×10^{-5}

(13) D. C. Douglass and D. W. McCall, unpublished results.

(14) We are indebted to Mr. L. D. Blitzer for carrying out the analyses.

(15) "International Critical Tables," McGraw-Hill Book Co., Inc., New York, N. Y., 1927.

Table I: Self-Diffusion Coefficients for Water (23°)

Solute	c_i M	$10^5 D$	D/D_0	Solute	c_i M	$10^5 D$	D/D_0	Solute	c_i M	$10^5 D$	D/D_0	Solute	c_i M	$10^5 D$	D/D_0
HCl	0	2.47	1.00	HI	0	2.52	1.00	CaCl ₂	0	2.43	1.00	MgCl ₂	0	2.47	1.00
	0.75	2.44	0.99		0.75	2.52	1.00		0.43	2.34	0.96		0.19	2.32	0.94
	1.50	2.45	0.99		1.25	2.52	1.00		0.81	2.12	0.87		0.38	2.19	0.89
	3.00	2.21	0.89 ₅		2.14	2.52	1.00		1.36	1.81	0.75		0.75	1.96	0.79
	6.00	1.89	0.76 ₅		3.75	2.45	0.98		2.38	1.33	0.55		1.50	1.48	0.60
	12.0	1.21	0.49		7.49	1.88	0.77		4.76	0.42	0.17		3.00	0.80	0.32
H ₂ SO ₄	0	2.44	1.00	CH ₃ COOK	0	2.43	1.00	ZnCl ₂	0	2.40	1.00	NaCl	0	2.47	1.00
	0.78	2.22	0.91		0.50	2.30	0.95		0.79	2.04	0.85		0.22	2.36	0.95
	1.34	2.03	0.83 ₅		1.43	2.00	0.82		1.44	1.87	0.78		0.44	2.40	0.97
	3.11	1.64	0.67 ₄		2.45	1.64	0.67		2.47	1.66	0.69		0.87	2.29	0.93
	4.68	1.16	0.48		4.29	1.07	0.44		4.31	1.12	0.47		1.75	2.14	0.87
	10.1	0.47	0.19 ₄		8.58	0.29	0.12		8.64	0.24	0.10		3.49	1.80	0.73
	18.2	0.15	0.06												
NaOH	0	2.44	1.00	NaBr	0	2.44	1.00	NaI	0	2.44	1.00	LiOH	0	2.44	1.00
	0.68	2.12	0.87		0.67	2.39	0.98		0.43	2.45	1.00		0.43	2.28	0.93
	1.13	2.02	0.83		1.68	2.26	0.93		0.87	2.38	0.98		0.85	2.03	0.83
	1.70	1.82	0.74		3.35	1.93	0.79		1.73	2.38	0.98		1.70	1.78	0.73
	3.40	1.20	0.49		6.71	1.24	0.51		3.46	1.98	0.81		3.41	1.14	0.47
KNO ₃	0	2.38	1.00	KBr	0	2.45	1.00	LiBr	0	2.46	1.00	LiCl	0	2.46	1.00
	0.42	2.51	1.05		0.43	2.55	1.04		0.46	2.45	1.00		0.56	2.27	0.93
	0.71	2.55	1.07		0.87	2.70	1.10		0.92	2.30	0.94		1.12	2.18	0.89
	1.25	2.58	1.08		1.73	2.68	1.09		2.30	1.92	0.78		2.80	1.75	0.71
	2.50	2.58	1.08		3.46	2.71	1.11		4.60	1.50	0.61		5.60	1.13	0.46
									9.21	0.58	0.24		11.2	0.31	0.13
KOH	0	2.41	1.00	K ₂ CO ₃	0	2.47	1.00	BaCl ₂	0	2.50	1.00	CsI	0	2.47	1.00
	0.19	2.42	1.00		0.47	2.23	0.90		0.50	2.32	0.93		0.20	2.43	0.99
	0.39	2.36	0.98		0.85	2.07	0.84		1.00	2.07	0.87		0.40	2.46	1.00
	0.74	2.25	0.93		1.46	1.77	0.72		1.46	1.87	0.75		0.80	2.61	1.06
	1.49	2.10	0.87		2.55	1.31	0.53						1.60	2.71	1.10
	2.97	1.72	0.71		5.10	0.52	0.21								
KF	0	2.45	1.00	HNO ₃	0	2.47	1.00	AlCl ₃	0	2.45	1.00	Be(ClO ₄) ₂	0	2.20	1.00
	0.53	2.30	0.94		0.53	2.43	0.98		0.39	2.04	0.83		0.29	2.13	0.97
	1.01	2.14	0.87		1.02	2.44	0.99		0.66	1.79	0.73		0.58	1.00	0.90
	1.85	1.99	0.81		2.72	2.29	0.93		1.16	1.35	0.55		0.96	1.73	0.79
	3.15	1.72	0.70		4.65	2.05	0.83		1.54	0.94	0.38		1.92	1.12	0.51
	5.55	1.23	0.50		8.15	1.64	0.67		2.31	0.57	0.23				
	11.10	0.63	0.26		16.3	1.09	0.44								
K ₂ SO ₄	0	2.42	1.00	HClO ₄	0	2.16	1.00	Th(ClO ₄) ₄	0	2.20	1.00				
	0.25	2.41	1.00		1.0	2.22	1.03		0.27	1.92	0.87				
	0.49	2.28	0.94		11.7	0.59	0.27		0.54	1.55	0.71				
									0.82	1.22	0.56				
									1.32	0.64	0.29				
KCl	0	2.47	1.00	KI	0	2.47	1.00								
	0.22	2.48	1.00		0.22	2.51	1.02								
	0.43	2.49	1.01		0.43	2.59	1.05								
	0.86	2.40	0.97		0.85	2.57	1.04								
	1.73	2.44	0.99		1.70	2.80	1.13								
	3.45	2.38	0.96		3.40	2.73	1.10								

cm.²/sec. at 25°. Bear in mind that the spin-echo method is absolute and no empirical adjustments have been made.

On the other hand, there are reasons for believing that the diffusion coefficient for pure water at room temperature is appreciably lower than 2.45×10^{-5} cm.²/sec. In our own work, the perchlorate solutions and associated pure water samples were measured several years ago and the values appear low when compared with our other data. We have not included these data in the above average. We feel that this is a calibration matter as our gradient coils have been altered from time to time. (Relative diffusion coefficients would not be affected.) Earlier,

we found $D_0 \cong 2.2 \times 10^{-5}$ cm.²/sec. We tend to favor our recent calibration, leading to the higher figure, but we know of no reason for excluding the former calibration.

Simpson and Carr⁹ have reported self-diffusion results obtained by the spin-echo method and, although their experiment differs in minor detail from ours, their results should be directly comparable with ours. For pure water these authors found $D_0 = 2.13 \times 10^{-5}$ cm.²/sec. at 25°. Furthermore, Devell¹⁰ in reporting recent tracer work and analyzing the existing literature concludes that $D_0 = 2.25 \times 10^{-5}$ cm.²/sec. at 25°.

It is distressing, considering the large number of

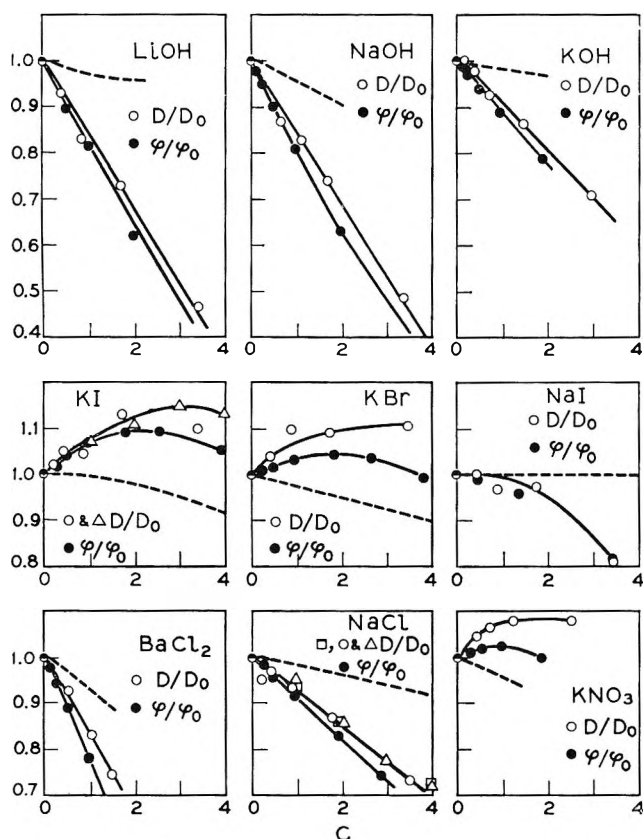


Figure 1. Relative self-diffusion coefficients of water, D/D_0 , plotted against electrolyte concentration. Relative solution fluidities, φ/φ_0 , are included for comparison. The dashed curves are relative Stokes-Einstein radii, $D_0\varphi/D\varphi_0$. The triangles on the plots for KI and NaCl are taken from Wang's paper. The squares represent Devell's results for NaCl.

studies that have been made, that the situation concerning such an elementary quantity should be so tentative. There would probably be little danger in stating that $D_0 = 2.3 \times 10^{-5}$ cm.²/sec. at 25° with an accuracy estimate of about $\pm 10\%$. The matter is deserving of further attention and illumination.

Table I lists the experimental self-diffusion data showing the effects of the various solutes. These data are plotted in Figures 1-4 as relative water diffusion coefficient, D/D_0 , against molar solute concentration. Table II shows the new viscosity results. These viscosities and similar data taken from the "International Critical Tables" were converted to relative fluidities, $\varphi/\varphi_0 = \eta_0/\eta$, and plotted in Figures 1-4 for comparison. Relative fluidities and diffusion coefficients are seen to behave similarly.

The concentration dependence parameter, Δ_1 , is given in Table III. $\Delta_1 \equiv (D_1 - D_0)/D_0$, where D_0 is the self-diffusion coefficient for pure water and D_1 is

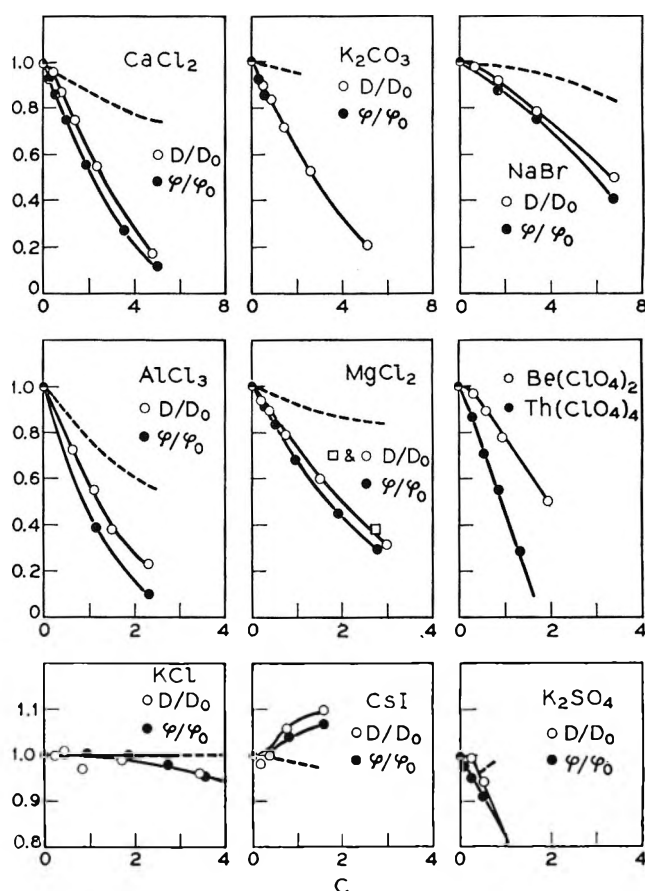


Figure 2. Relative self-diffusion coefficients of water, D/D_0 , plotted against electrolyte concentration. Relative solution fluidities, φ/φ_0 , are included for comparison. The dashed curves are relative Stokes-Einstein radii, $D_0\varphi/D\varphi_0$. Devell's result for $MgCl_2$ is indicated by a square.

the self-diffusion coefficient for water in the 1 M solution. The analogous parameter for fluidity,¹² $\Delta_1^f \equiv (\varphi_1 - \varphi_0)/\varphi_0$, is also included in Table III.

In Figure 1, Wang's tracer data¹⁶ are included in the NaCl and KI graphs. The agreement between Wang's results and the present spin-echo results is excellent. Devell's tracer results¹⁰ are shown for NaCl (Figure 1), $MgCl_2$ (Figure 2), and LiBr (Figure 3), and again excellent agreement is found. These findings support our suggestion that the lack of agreement between the absolute values for D_0 is primarily a calibration matter and relative diffusion coefficients are unaffected.

The concentration dependence of D/D_0 is remarkably linear out to rather high concentrations for most of the solutes investigated. Those substances that increase the water diffusion coefficient, KI, KBr,

(16) J. H. Wang, *J. Phys. Chem.*, 58, 686 (1954).

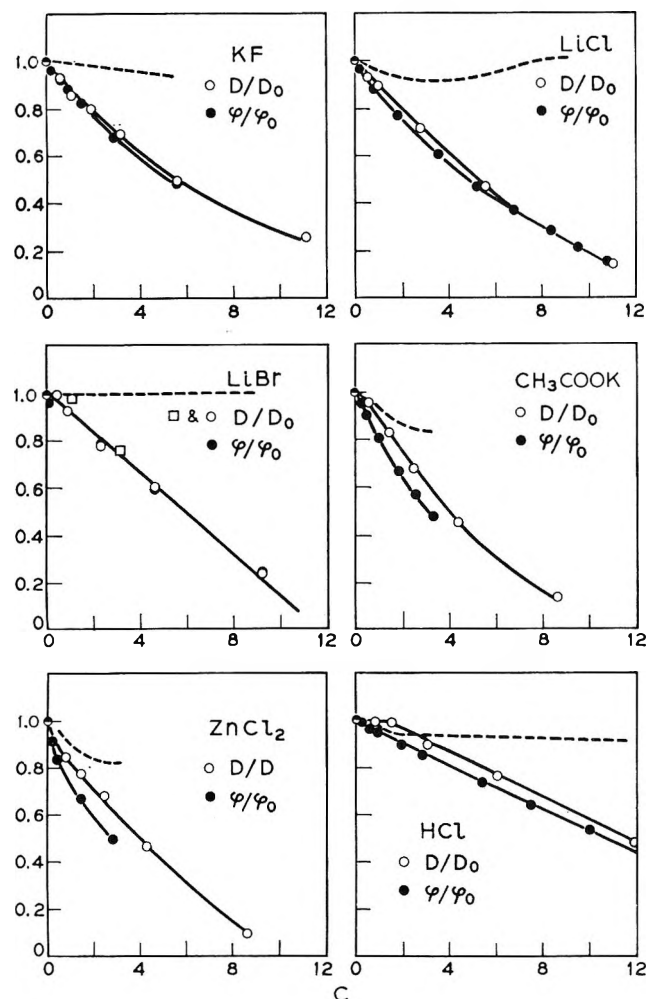


Figure 3. Relative self-diffusion coefficients of water, D/D_0 , plotted against electrolyte concentration. Relative solution fluidities, φ/φ_0 , are included for comparison. The dashed curves are relative Stokes-Einstein radii, $D_0\varphi/D\varphi_0$. Devell's results for LiBr are indicated by squares.

NaI, CsI, and KNO_3 , seem to approach a limiting maximum value. Those substances that decrease the diffusion coefficient usually exhibit linear dependences over a substantial range. LiBr and HNO_3 are linear out to 10 M. H_2SO_4 , HI, CH_3COOK , LiCl, KF, CaCl_2 , K_2CO_3 , NaBr, ZnCl_2 , KCl, LiOH, NaOH, KOH, and NaCl are linear to 3 M or more. The plots for BaCl_2 , AlCl_3 , and $\text{Th}(\text{ClO}_4)_4$ are linear to concentrations at which D/D_0 has fallen substantially. Obviously, D/D_0 cannot fall below zero, so curvature must set in at sufficiently high concentrations and such concentrations are lowest for substances showing the largest effects. The HCl, HClO_4 , $\text{Be}(\text{ClO}_4)_2$, and NaI plots seem to begin with zero slope and then become concave downward. This behavior will be discussed later.

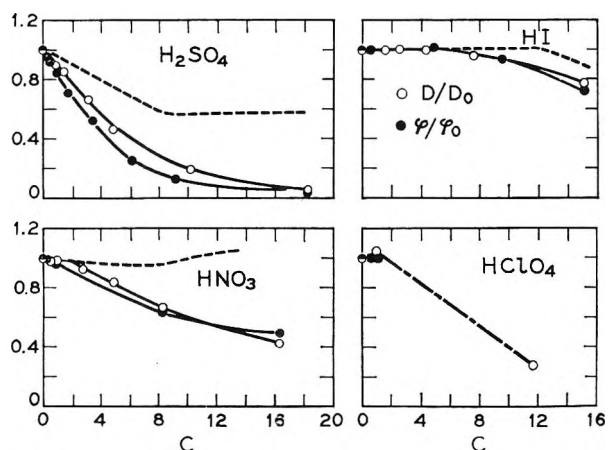


Figure 4. Relative self-diffusion coefficients of water, D/D_0 , plotted against electrolyte concentration. Relative solution fluidities, φ/φ_0 , are included for comparison. The dashed curves are relative Stokes-Einstein radii, $D_0\varphi/D\varphi_0$.

Table II: Viscosities for Solutions (22–23°)

Solute	c, M	$\eta, \text{cp.}$	η_0/η	Solute	c, M	$\eta, \text{cp.}$	η_0/η
AlCl_3	0	0.96	1.00	HNO_3	0	0.96	1.00
	1.15	2.48	0.39		8.1	1.49	0.65
	2.30	9.36	0.10		16.3	1.93	0.50
HI	0	0.96	1.00	NaBr	0	0.95	1.00
	1.18	0.96	1.00		1.68	1.06	0.90
	2.35	0.95	1.01		3.35	1.25	0.76
	4.70	1.03	0.93		6.71	2.30	0.41
	7.49	1.31	0.72				
CsI	0	0.92	1.00	ZnCl_2	0	0.96	1.00
	0.80	0.88	1.04		1.44	1.40	0.685
	1.60	0.86	1.07		2.88	1.89	0.51
LiBr	0	0.94	1.00	H_2SO_4	0	0.96	1.00
	2.30	1.18	0.79		6.1	3.86	0.25
	4.60	1.57	0.60		9.1	7.65	0.13
	9.21	3.76	0.25		18.2	21.9	0.044

Thus, Δ_1 gives a useful indication of the concentration dependence of D/D_0 for all the substances. When $\Delta_1 \geq 0$ or $\Delta_1 < -0.2$ the linear range is apt to be small, say 1–2 M. The solutes studied are expected to be ionized to a high degree and therefore we expect that the Δ_1 's should be such that they can be expressed as a sum of ionic Δ_1 's. For a solute A_mB_n we shall write $\Delta_1 = m\Delta_{1+} + n\Delta_{1-}$. In order to establish the $\Delta_{1\pm}$ terms, at least one ion must arbitrarily be assigned a value. We have chosen $\Delta_{1+} = 0$ for K^+ , and Table IV displays the $\Delta_{1\pm}$ terms deduced therefrom. The choice of K^+ as the reference ion is not intended to be especially significant. Table IV is similar to Bingham's based on fluidity.¹²

Table III: Self-Diffusion and Viscosity Concentration Dependence Parameters

Solute	Δ_1	Δ_1^φ	Solute	Δ_1	Δ_1^φ
LiCl	-0.11	-0.15	CH ₃ COOK	-0.13	-0.20
LiBr	-0.08	-0.08	KNO ₃	0.08	0.03
NaCl	-0.08	-0.09	K ₂ CO ₃	-0.19	-0.22
NaBr	-0.04	-0.06	K ₂ SO ₄	-0.18	-0.18
NaI	-0.01	-0.01	LiOH	-0.16	-0.18
KF	-0.11	-0.12	NaOH	-0.15	-0.19
KCl	0.00	0.00	KOH	-0.09	-0.11
KBr	0.07	0.04	HCl	0.00	-0.06
KI	0.08	0.07	HI	0.00	0.00
CsI	0.07	0.05	HNO ₃	-0.01	-0.03
ZnCl ₂	-0.19	-0.27	H ₂ SO ₄	-0.13	-0.19
MgCl ₂	-0.26	-0.33	HClO ₄	0.03	0.00
CaCl ₂	-0.19	-0.25	Be(ClO ₄) ₂	-0.23	-0.26
BaCl ₂	-0.17	-0.23	Th(ClO ₄) ₄	-0.62	
AlCl ₃	-0.41	-0.55			

Table IV: Ionic Self-Diffusion Concentration Parameters

I ⁻	0.08	H ⁺	0.00	CH ₃ COO ⁻	-0.13	Zn ⁺²	-0.19
NO ₃ ⁻	0.08	Cs ⁺	-0.01	Ba ⁺²	-0.17	Mg ⁺²	-0.26
Br ⁻	0.07	Na ⁺	-0.08	SO ₄ ⁻²	-0.18	Be ⁺²	-0.29
ClO ₄ ⁻	0.03	OH ⁻	-0.09	Ca ⁺²	-0.19	Al ⁺³	-0.41
K ⁺	(0.00)	F ⁻	-0.11	CO ₃ ⁻²	-0.19	Th ⁺⁴	-0.74
Cl ⁻	0.00	Li ⁺	-0.11				

The value of these ionic parameters lies in their use in predicting Δ_1 's for solutes that have not been studied. Devell¹⁰ has published data for MgSO₄ that yield $\Delta_1 \sim -0.4$. From Table IV, $\Delta_1 = -0.26 - 0.18 = -0.44$. Table V shows the computed Δ_1 values based on Table IV compared with the observed Δ_1 values. Only those substances not used in establishing Table IV are included. The predictions are seen to be only approximately correct. HNO₃ is particularly poor. It may develop that a superior set of $\Delta_{1\pm}$ values can be worked out by a combination of theory and further experiments.

IV. Discussion

It is of interest to compare the self-diffusion concentration dependences with concentration dependences

Table V: Comparison of Observed and Computed Values of Δ_1

Solute	Δ_1 (obsd.)	Δ_1 (Table IV)
NaBr	-0.04	-0.01
NaI	-0.01	0.00
LiOH	-0.16	-0.20
HI	0.00	0.00
HNO ₃	-0.01	0.08
H ₂ SO ₄	-0.13	-0.18

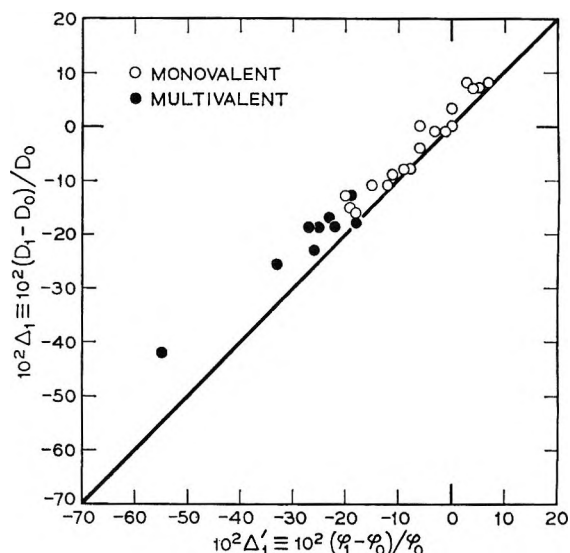


Figure 5. Comparison of Δ_1 with the corresponding fluidity parameter, Δ_1^φ . The solid line indicates equality of Δ_1 and Δ_1^φ .

of other quantities. The most obvious quantity to compare is the fluidity, and this has been shown in Figures 1-4 and indicated in Table III. Figure 5 shows Δ_1 plotted against Δ_1^φ . The line indicates $\Delta_1 = \Delta_1^\varphi$. The correlation is extremely close. For 1-1 electrolytes, near equality is observed. For ions of higher charge, the effect on fluidity becomes appreciably stronger than the effect on self-diffusion.

The Stokes-Einstein relation is often used to obtain a radius for a diffusing particle. This relation can be written $a = kT/6\pi D\eta$, and thus $a/a_0 = D_0\eta_0/D\eta = D_0\varphi/D\varphi_0$. Here a is the Stokes-Einstein radius and the subscript zero indicates pure water. As D and φ tend to vary with concentration in a similar way, a/a_0 tends to remain unchanged. The dashed lines in Figures 1-4 show the concentration dependences of the relative Stokes-Einstein radii. In every case a/a_0 decreases, but the effect is usually less than 10%. This decrease makes it clear that the principal effect cannot be the change in radius of the diffusing molecule. Any hydrate complex must be larger than a water molecule and on this basis the quantity a/a_0 should increase with concentration. We recognize the limitations inherent in the use of the Stokes-Einstein formula. In the present discussion we only want to point out that the Stokes-Einstein radii cannot explain the data.

In Table VI¹⁷ a comparison is shown between ionic and water self-diffusion coefficients and the correspond-

(17) See ref. 1, p. 256, for reference list.

ing concentration dependences. The Δ_1 values for ionic self-diffusion have been obtained from literature data, $\Delta_1 = (D_1 - D_0)/D_0$. The Δ_1 values for ionic self-diffusion do not correlate with Δ_1^ν as well as the water Δ_1 values. The ions diffuse more slowly than water and the smallest ions, Na^+ and Ca^{+2} , have the smallest diffusion coefficients.

Table VI: Self-Diffusion Summary, Ionic and Water (Room Temperature)

	$10^5 D_0$	Δ_1	Δ_1^ν
Na^+	1.32	-0.05	-0.09
Cl^-	1.98	-0.09	
H_2O	2.47	-0.08	
Na^+	1.31	-0.04	-0.01
I^-	1.96	-0.12	
H_2O	2.44	-0.01	
K^+	1.97	+0.03	+0.07
I^-	2.02	-0.04	
H_2O	2.47	+0.08	
Ca^{+2}	0.78	-0.18	-0.25
Cl^-	1.89	-0.18	
H_2O	2.43	-0.19	
Rb^+	2.06	-0.04	}
I^-	2.03	-0.09	
H_2O (estd.)	(2.45)	(+0.08)	
H^+ (estd.)	9.3	...	0.00
I^-	2.01	-0.06	
H_2O	2.52	0.00	
Li^+ (estd.)	1.03	...	-0.08
I^-	2.00	-0.13	
H_2O (estd.)	(2.45)	(-0.03)	

Another quantity that can be compared with Δ_1 is the concentration dependence of the proton magnetic resonance position. The effects of electrolytic solutes on the water resonance have been studied and the proton chemical shift is found to vary approximately linearly with concentration.¹⁸⁻²¹ We have compared the shift between 1 M solutions and pure water with Δ_1 and we find a rough correlation. Those substances that tend to increase the proton shielding of water tend to increase or only slightly decrease the self-diffusion coefficient of water. Those substances that reduce the shielding strongly decrease the water diffusion rate; $\Delta_1 \sim -0.1$ when the chemical shift is zero. This rough correlation is in general accord with the notion that decreased shielding is brought about by solutes that form complexes and increased shielding is caused by structure breakers. The acids are ex-

ceptional as they have $\Delta_1 \sim 0$ and strongly decrease shielding. We found no data for bases.

We expected to find Δ_1 and the molar depression of the dielectric constant of water to be closely related. Both quantities measure the extent of solute influence on molecular mobility, translational and rotational, respectively. However, with the data now available,²²⁻²⁴ the correlation is so rough as to be hardly noticeable. For example, KI and LiCl have about the same effect on the dielectric constant of water but quite different effects on the self-diffusion of water. This finding is disappointing and we have no explanation at present.

Δ_1 and the molar heat of solution are very crudely correlated in the expected way.²⁵ Solutes that increase the water diffusion rate are endothermic on solution. Solutes that are strongly exothermic on solution decrease the diffusion coefficient of water. The data show considerable scatter when ΔH_{sol} is plotted against Δ_1 . The acids HCl and HI stand apart: they are rather strongly exothermic solutes but they do not affect the diffusion rate. On the other hand, K_2SO_4 is endothermic and decreases the diffusion rate strongly.

The ratio of the partial molar volume of solute to the molar volume of the pure solute is another quantity for which the expected correlation with Δ_1 was not found. This kind of comparison is somewhat questionable owing to the fact that the pure solutes are crystalline and an appropriate molar volume is to some extent arbitrary. Volume changes are interesting in themselves and we shall say more about them below.

In Figure 6 the "conventional ionic entropy,"^{26,27} ΣS° , is plotted against Δ_1 . It is seen that quite a good correlation exists. This correlation is intuitively attractive, as those substances that increase the water diffusion coefficient have high entropies in solution and thus fit the accepted "structure-breaking" picture. At the other extreme, the solutes with low entropies

- (18) J. N. Shoolery and B. Alder, *J. Chem. Phys.*, **23**, 805 (1955).
 (19) H. G. Hertz and W. Spalshoff, *Z. Elektrochem.*, **63**, 1096 (1959).
 (20) J. C. Hindman, *J. Chem. Phys.*, **36**, 1000 (1962).
 (21) M. S. Bergquist and E. Forslind, *Acta Chem. Scand.*, **16**, 2069 (1962).
 (22) J. B. Hasted, D. M. Ritson, and C. H. Collie, *J. Chem. Phys.*, **16**, 1 (1948).
 (23) J. B. Hasted and G. W. Roderick, *ibid.*, **29**, 17 (1958).
 (24) F. E. Harris and C. T. O'Konski, *J. Phys. Chem.*, **61**, 310 (1957).
 (25) See J. P. Hunt, "Metal Ions in Aqueous Solution," W. A. Benjamin, Inc., New York, N. Y., 1963, for a convenient tabulation.
 (26) W. M. Latimer, K. S. Pitzer, and C. M. Slansky, *J. Chem. Phys.*, **7**, 108 (1939).
 (27) R. E. Powell and W. M. Latimer, *ibid.*, **19**, 1139 (1951).

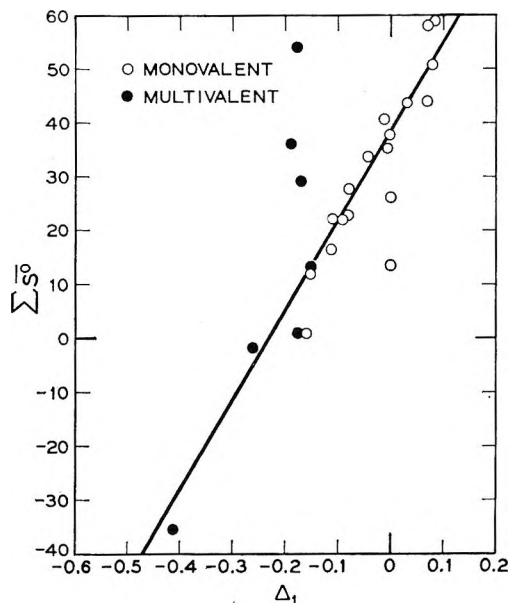


Figure 6. Conventional ionic entropy as a function $(D_1 - D_0)/D_0$.

in solution reduce the diffusion rate. The low entropy suits the general notion of complex or structure formation. Four points deviate very badly from the group, from the top K_2SO_4 , K_2CO_3 , and $BaCl_2$ above the line and HCl below the line. We have no profound explanations for these defections but the following comments may be pertinent. $BaCl_2$ and K_2SO_4 are not very soluble in water and thus Δ_1 may be too coarse a parameter for these materials. HCl has $\Delta_1 \sim 0$ but D/D_0 decreases considerably at higher concentrations.

A theoretical discussion of any property of any liquid is extremely difficult and water is certainly one of the most awkward examples. One approach is to construct simple "model" systems and seek a consistent (small) set of parameters for describing various properties. Another approach is to carry over statistical mechanical results derived for simpler molecular systems to aqueous solutions for which certain of the underlying assumptions are not valid. Neither method is entirely satisfying but both can be of value in correlating data and gaining insight into structural features of importance.

The theory of absolute reaction rates has also been of considerable use in describing diffusion. Various molecular models can be grafted onto this general framework. We shall not use this theory extensively in this paper but it is perhaps worthwhile to point out that self-diffusion in water is unique in terms of the activation parameters. The activation energy at constant pressure, $-R[\partial \ln D/\partial(1/T)]_p$, varies from about 5 kcal./mole near the melting point to about 3

kcal./mole near the boiling point. These are large numbers. The activation volume, $-RT(\partial \ln D/\partial p)$, at room temperature is about zero. Judging from viscosity data, we expect the activation volume to be positive above room temperature and negative below room temperature.²⁸ At room temperature, the activation energies at constant volume and constant pressure are equal.

Let us now consider a "two-state" model.⁷ We suppose that the concentration dependence of the coefficient of self-diffusion is a consequence of the water existing in a hydrate form in addition to the pure water form. The measured diffusion coefficient is a suitably weighted average of the two forms. Let the hydrated ions be characterized by a diffusion coefficient D_i and let h be the number of water molecules bound to a given ion. We assume, for convenience, that only one of the two ions is hydrated, usually the positive ion. In this case

$$D = [(c_w - ch)D_0 + chD_i]/c_w \quad (1)$$

where c is the concentration (moles/liter) of the hydrated ion and c_w is the water concentration. For solutions not too concentrated, $c_w \sim 55$ moles/l. Therefore

$$h = -55\Delta_1 D_0 / (D_0 - D_i) \quad (2)$$

For Ca^{+2} in $CaCl_2$ we have found $\Delta_1 = -0.19$, and $D_i = 0.78 \times 10^{-5}$ cm.²/sec., so $h \cong 15$. Table VII lists h for the various ions obtained in this way. When ion diffusion results were not available D_i was calculated as $2.66 \times 10^{-7} \lambda^0/|z|$, where λ^0 is the limiting equivalent conductance and z is the charge of the ion.

For the chlorides it is probable that the principal hydration occurs at the positive ions. However, in

Table VII: Hydration Numbers

Solute	Ion assumed hydrated	h (eq. 2)	h (eq. 4)
KCl	...	0	0
NaCl	Na^+	9.6	1
LiCl	Li^+	10.4	4-5
$CaCl_2$	Ca^{+2}	15.3	6-7
$ZnCl_2$	Zn^{+2}	14.6	8-9
$MgCl_2$	Mg^{+2}	20.1	8
$BaCl_2$	Ba^{+2}	14.3	6-7
$AlCl_3$ (estd.)	Al^{+3}	28	21
KF	F^-	15.1	1-2
KOH (estd.)	OH^-	12.1	3

(28) P. W. Bridgman, "Physics of High Pressures," G. Ball and Sons, London, 1952.

KF it seems probable that the fluoride ion is hydrated while the potassium ion is not. The hydroxide ion also is likely to be hydrated but in this case the ion diffusion coefficients are not known. In constructing Table VII we guessed the OH^- ion diffusion coefficient to be about the same as for the F^- ion. In addition we estimated the Al^{+3} ion diffusion coefficient to be about 0.45×10^{-5} cm.²/sec.

In all cases studied, ions diffuse more slowly than water molecules. Therefore, the use of eq. 2 leads to negative hydration numbers for those solutes that increase the diffusion rate of water. This feature is unsatisfactory and it is generally believed that a separate mechanism, called "structure breaking," is operative with these ions. Bromide and iodide ions are the simplest examples. Serious consideration of the hydration numbers in Table VII involves the tacit assumption that the chloride ion is large enough that it is not hydrated but small enough that it does not cause appreciable structure breaking. At least, the effects must cancel one another. Qualitatively, the data are consistent with this view.

It can be argued that D_0 and D_i in eq. 1 should be scaled by the relative fluidity

$$D = (\eta_0/\eta)[(c_w - ch)D_0 + chD_i]/c_w \quad (3)$$

On rearrangement, this can be written as

$$h = -55 \frac{(\Delta_1 - \Delta_1^\circ)}{(\Delta_1^\circ + 1)} \frac{D_0}{(D_0 - D_i)} \quad (4)$$

$\Delta_1^\circ \leq \Delta_1$ and $\Delta_1^\circ + 1 > 0$ in all cases that have been studied. Consequently, negative hydration numbers do not arise. Hydration numbers obtained from eq. 4 are listed in Table VII. It is important to keep in mind that $(\Delta_1 - \Delta_1^\circ)$ is usually small and this severely limits the accuracy of the resulting hydration numbers.

Both eq. 1 and 3 show a linear concentration dependence of D in agreement with experiment. The widely used square-root concentration plots would be a useless complication in the concentration range under consideration here. The first model, eq. 1, is a consistent "two-state" model. Equation 3 treats diffusion in the "two-state" manner and viscosity as a uniform quantity. With naïve models such as these, perhaps the best measure of success is consistency of the hydration numbers derived with similar quantities derived from other experiments. Robinson and Stokes² have collected hydration numbers from many sources and the numbers given in Table VII neither agree closely with nor diverge strongly from the earlier work.

Although the meaning of a hydration number is to some extent ambiguous it is possible to distinguish

certain features in a meaningful way. In a dilute solution of a strong electrolyte any ion will have a number of water molecules as near neighbors. These neighbors will be located about $(r_i + r_w)$ from the ion and the number will be determined to a large extent by the size of the ion, *i.e.*, bigger ions have more surface. Highly charged ions will exert strong attractions on the water molecules but, owing to the low compressibility of water, the amount of space available will be the dominant factor. Thus, simply counting the average number of nearest neighbors leads to a hydration number that is governed by ionic size and, to a lesser degree, ionic charge. The strength of the ion-water interaction, on the other hand, will be dominated by the charge but significantly influenced by ionic size. Highly charged and small ions tend to have large hydration energies and form relatively long-lived complexes. Further, highly charged ions influence water molecules more distant than near neighbors. We might expect the viscosity to be particularly sensitive to these intermolecular force factors.

Darmoir²⁹ based a study of hydration on the following argument. If we place one ion in a solution containing N molecules of water, we can use partial molar volumes to write the volume in two forms

$$V = (N - h_+) \bar{v}_w + \bar{v}_{+h} = N\bar{v}_w + \bar{v}_+ \quad (5)$$

where the subscripts w, +h, and + refer to water, hydrated ion, and bare ion, respectively. Thus

$$h_+ = (\bar{v}_{+h} - \bar{v}_+)/\bar{v}_w \quad (6)$$

This approach has been used by Bernal and Fowler³⁰ and by Darmoir,²⁹ although their developments differ in detail. Bernal and Fowler emphasized the approximate consistency of known coordination numbers taken from hydrate crystal structures with those deduced from partial ionic volumes and ionic radii from crystallographic data. Darmoir used Stokes' law and ionic equivalent conductance data to establish the hydrate ion radius and thus the volume. Neither of these procedures is above criticism. Stokes' law radii frequently turn out to be smaller than one would expect on the basis of known molecular size. For example, the Stokes' law radius for water itself is only 0.87 Å., leading to a molecular volume of less than 3 Å.³.

Table VIII exhibits a comparison between the results of the present study and earlier studies. Good discussions of the other techniques can be found in the book by Robinson and Stokes.² Only rough magnitudes are worthy of consideration. h_{comp} , de-

(29) E. Darmoir, *J. Phys.*, 2, 2 (1941).

(30) J. D. Bernal and R. F. Fowler, *J. Chem. Phys.*, 1, 515 (1933).

rived from compressibility data, and h_{act} , derived from activity data, were taken from Robinson and Stokes' tabulation.

Table VIII: Comparison of Hydration Numbers

Ion	h (eq. 2)	h (eq. 4)	h (B and F) ^a	h (D) ^b	h_{comp}	h_{act}
K ⁺	0	0	0	...	7	7
Na ⁺	10	1	8	1	7	3.5
Li ⁺	10	4-5	6	2	6	2
Ca ⁺²	15	6-7	6	5
Zn ⁺²	15	8-9	...	6.7
Mg ⁺²	20	8	6	6.6	16	14
Ba ⁺²	14	6-7	6	4	16	8
Al ⁺³	28	21	6	6	31	...
F ⁻	15	1-2	1	0.4	8-9	...
OH ⁻	12	3	1	0

^a See Bernal and Fowler, ref. 30. ^b See Darroir, ref. 29.

The disparities shown indicate that we are still in the policy-making stage of hydration number formulation. However, eq. 4 of this study yields magnitudes that are encouraging when compared with Darroir's or Bernal and Fowler's conclusions. A possible rationale to accompany eq. 4 might run as follows. The two-state model for diffusion holds and suffices to define hydration numbers. It is further hypothesized that the viscosity of the solution is a direct measure of the molecular friction encountered by both the hydrated ions and the unbound water. The resulting numbers indicate the number of water molecules "traveling with" an ion; *i.e.*, to be counted, a water molecule would have to remain with the ion for several diffusion jumps. The minimum time can be estimated to be 10^{-9} to 10^{-10} sec. Water in next-nearest neighbor shells might be strongly enough bound to satisfy this condition with some ions, *e.g.*, Al⁺³.

The statistical mechanical theory of diffusion in liquids was first set forth in a forceful way by Kirkwood.³¹ The Kirkwood equation for the molecular friction factor,^{32,33} $\zeta \equiv kT/D$, is

$$\zeta^2 = (4\pi n m/3) \int_0^\infty g(R) \nabla^2(R) R^2 dR \quad (7)$$

where n is the number of molecules/cm.³, m is the molecular mass, $g(R)$ is the radial distribution function, and $u(R)$ is the intermolecular pair potential. Rice has summarized some of the various sets of assumptions on which the Kirkwood equation can be derived.³³ Aside from our meager knowledge of $g(R)$ and $u(R)$ in experimentally accessible systems, this equation

has some serious assumptions in its derivation and the physics of these assumptions is not obvious. However, this equation can be obtained in a straightforward way by assuming a simple one-parameter, gas-like decay for the velocity correlation function.³⁴ This function is then completely specified by the mean-square force on the center of mass of a molecule. In addition, one usually assumes that the molecules interact through central forces only. It is probably fair to say that these assumptions are involved, either explicitly or implicitly, in other modes of derivation as well. The assumption of central forces is removed if the noncentral forces arise from the interaction of permanent electric multipole moments of the molecules, since the Laplacian of the electrostatic energy is zero. It has been suggested by some authors that the dominant noncentral forces between water molecules arise from their permanent dipole and quadrupole moments.³⁵⁻³⁷ Rough calculations based on eq. 7 yield diffusion coefficients that are too large by a factor of 2 or 3 for ordinary liquids, including water.

Bearing these limitations in mind, we feel that it is interesting to determine whether the analog of eq. 7 for ionic solutions contains, even in principle, the information that would allow the theoretical study of concentration effects exhibited by the data of this paper.

The analog of eq. 7 for ionic solutions is obtained by writing down the mean square force on the center of gravity of a water molecule, and with the assumptions cited above one obtains

$$\zeta_w^2 = (4\pi m_w/3) \{ n_w \int g_{ww} \nabla^2 u_{ww} R^2 dR + n_+ \int g_{w+} \nabla^2 u_{w+} R^2 dR + n_- \int g_{w-} \nabla^2 u_{w-} R^2 dR \} \quad (8)$$

where m_w is the mass of the water molecule, u_{ww} is the pair potential between two water molecules, and g_{ww} is the radial distribution function for water molecules about a central water molecule. n_w , n_+ , and n_- are the number densities. g_{w+} and g_{w-} are the radial distribution functions for ions about the central water molecule and u_{w+} and u_{w-} are the pair potentials between the ions and a water molecule.

Inasmuch as we wish to test the content of eq. 8 rather than our knowledge and intuition regarding $g(R)$ and $u(R)$, it is undesirable to calculate the in-

(31) J. G. Kirkwood, F. P. Buff, and M. S. Green, *J. Chem. Phys.*, **17**, 988 (1949).

(32) D. C. Douglass, D. W. McCall, and E. W. Anderson, *ibid.*, **34**, 152 (1961).

(33) S. A. Rice, *ibid.*, **33**, 1376 (1960).

(34) D. C. Douglass, *ibid.*, **35**, 81 (1961).

(35) J. A. Pople, *Proc. Roy. Soc. (London)*, **A205**, 163 (1951).

(36) A. D. Buckingham, *Discussions Faraday Soc.*, **24**, 151 (1957).

(37) J. S. Rowlinson, *Trans. Faraday Soc.*, **47**, 120 (1951).

tegrals. Instead, one notes that in dilute solutions one can identify the integrals with the mean-square force on the ions and thus obtain the relation

$$\zeta_w^2 = n_w \zeta_{w_0}^2 / n_{w_0} + n_+ m_w \zeta_{+0}^2 / n_w m_+ + n_- m_w \zeta_{-0}^2 / n_w m_- \quad (9)$$

Using $n_w \bar{v}_w + n_+ \bar{v}_+ + n_- \bar{v}_- = 1$, and making approximations valid at low concentrations (*i.e.*, $n_+ < n_w/10$), we can write

$$\zeta_w^2 \cong \zeta_{w_0}^2 + (n_+/n_w) [(m_w/m_+) \zeta_{+c}^2 - (\bar{v}_+/\bar{v}_w) \zeta_{w_0}^2] + (n_-/n_w) [(m_w/m_-) \zeta_{-c}^2 - (\bar{v}_-/\bar{v}_w) \zeta_{w_0}^2] \quad (10)$$

and

$$\Delta_1 \cong -(1/110) \{ (m_w/m_+) (D_0/D_{+0})^2 - (m_w/m_-) (D_0/D_{-0})^2 - (\bar{v}_-/\bar{v}_w) \} \quad (11)$$

This applies to 1:1 electrolytes, but the generalization to other cases is obvious.

Values of Δ_1 computed according to eq. 11 (using ionic diffusion coefficients calculated from limiting conductance data) are compared with experimental results in Table IX. Considering that no adjustment has been made, we feel cautiously encouraged. The sign of the effect and qualitative trends in the data are correctly predicted. As mentioned, eq. 7 leads to friction factors that are too small, owing to the use of a gas-like velocity correlation function. It can be convincingly argued that a more realistic liquid velocity correlation function would increase the magnitude of both the calculated friction and the calculated concentration dependence. A detailed discussion of these points is beyond the scope of the present paper.

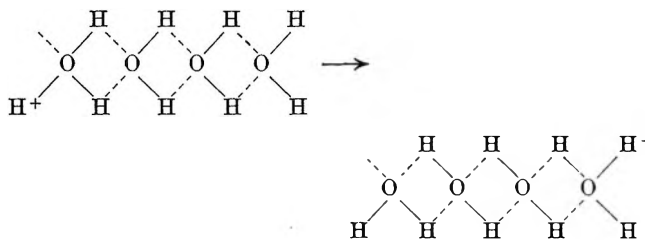
Table IX: Test of Equation 11

Solute	Δ_1 (eq. 11)	Δ_1 (exptl.)	Solute	Δ_1 (eq. 11)	Δ_1 (exptl.)
LiCl	-0.13	-0.11	KI	+0.014	+0.08
LiBr	-0.12	-0.08	CsI	+0.026	+0.07
NaCl	-0.026	-0.08	ZnCl ₂	-0.029	-0.19
NaBr	-0.013	-0.04	MgCl ₂	-0.08	-0.26
NaI	-0.008	-0.01	CaCl ₂	-0.045, -0.08 ^a	-0.17
KF	-0.027	-0.11	BaCl ₂	-0.003	-0.17
KCl	0.000	0.00	HCl	-0.009	0.00
KBr	+0.008	0.07	HI	+0.007	0.00

^a Concentration dependence of ion diffusion included.

Inasmuch as our experimental technique actually measures proton diffusion rather than molecular diffusion, we feel that the relation of "excess" proton mobility to our measurements deserves some discussion. The proton exchange mechanism is well established

for the abnormally high proton mobility in water.^{3,8,9} Briefly, the mechanism involves the migration of a positive charge without molecular translation. For example



The excess proton has moved from left to right by merely exchanging covalent OH bonds for hydrogen bonds. Following molecular rotations, the process can again transfer an excess proton from left to right.

The important point here is that this mechanism only works for ionized hydrogen (hydronium) and does not play a significant role in self-diffusion. Thus, the coefficients of self-diffusion measured by O¹⁸ tracer techniques and proton resonance are the same for water. Direct verification of this is shown by comparison of our data with those of Wang.¹⁶

In acid and base solutions a portion of the protons have the excess mobility. For example, in 1 M HCl about 1% of the protons are available for transfer through the exchange mechanism. Since we measure a weighted average of the proton diffusion, we may expect that the proton diffusion coefficient will be, at most, a few per cent higher than the diffusion coefficient measured by O¹⁸ tracer methods. To our knowledge, the latter measurements have not been made. Our concentration dependence data for HCl and HI reveal that the diffusion coefficient is almost constant from 0 to 2 M while the viscosity increases continuously through this range. One could suggest that the excess proton mobility effect is counterbalanced by the effect of increased viscosity.

Acknowledgments. We are indebted to Drs. L. C. Allen, F. A. Bovey, P. C. Milner, and C. P. Slichter for valuable discussions in the course of this work. Particular thanks are due Dr. W. P. Slichter for his patient counsel and guidance in the development of this paper. Our interest in this area was greatly stimulated by Professor E. Wicke, Dr. H. G. Hertz, and Dr. T. Ackermann, Institute for Physical Chemistry, The University of Münster. Mr. L. Anderson, Cornell University, kindly provided the beryllium and thorium solutions.

(38) S. Meiboom, *J. Chem. Phys.*, **34**, 375 (1961).

(39) E. Grunwald, C. F. Jumper, and S. Meiboom, *J. Am. Chem. Soc.*, **84**, 4664 (1962).

Kinetics of Hydrogen Reduction of Uranium Trioxide

by Victor H. Heiskala¹

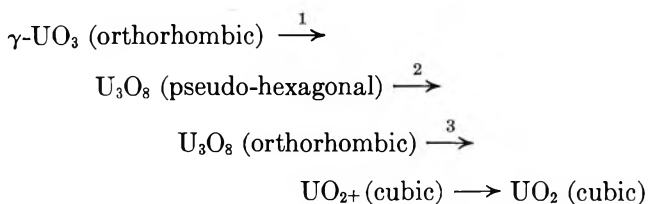
*Department of Nuclear Engineering, Michigan Technological University, Houghton, Michigan
(Received January 4, 1965)*

The reaction between uranium trioxide (UO₃) and pure hydrogen was investigated in the temperature range 575 to 750°. It was determined that, after an induction period in which the reduction rate reached its maximum value, the reaction proceeded at a constant rate which was independent of the thickness of the reduced uranium dioxide (UO₂) layer. The rate-limiting step in the reduction was the reaction at the UO₃-UO₂ interface. Microscopic examination and X-ray powder patterns of samples partly reduced below 750° failed to reveal the presence of oxides intermediate between UO₃ and UO₂ at this interface. The activation energy for the reduction was determined experimentally to be 33.3 ± 0.3 kcal./mole. Absolute reaction rate theory was used to develop an analytical expression for the rate of reduction assuming an immobile adsorbed H₂O layer as part of a (H₂O-UO₂) complex. The rate constants calculated with this model agreed favorably with experimental values when compared on an equivalent basis.

Introduction

The hydrogen reduction of uranium trioxide to form uranium dioxide has been used as an intermediate step in the commercial preparation of uranium tetrafluoride in the United States,² England,^{3a} France,^{3b} and other countries. Over the years, workers have attempted to define the optimum conditions for this process through experimental and theoretical studies of the reaction kinetics.

Several authors contend that the reaction proceeds *via* three-step kinetics with the appearance of the U₃O₈ intermediate oxide phase,^{4,5} thus



However, there is some evidence that the reaction proceeds directly from UO₃ to UO₂ without the appearance of the intermediate U₃O₈ phase.⁶ One author has found the rate-limiting step in the reaction to be the adsorption of hydrogen upon oxygen sites in the reaction surface⁷ while yet another author contends that the reduction of U₃O₈ by hydrogen may involve thermal

decomposition of the oxide accompanied by hydrogen reduction of the liberated oxygen.⁸

The object of this study was to obtain reliable fundamental information regarding the character of the hydrogen-uranium trioxide reaction in the range of temperatures that has been used in commercial reduction processes. Through the use of high-purity samples and by the proper control of incidental variables, this object was realized.

Experimental

Samples. The UO₃ powder used in this kinetic study

- (1) Atomics International, Canoga Park, Calif.
- (2) M. Benedict and T. R. Pigford, "Nuclear Chemical Engineering," McGraw-Hill Book Co., Inc., New York, N. Y., 1957, p. 149.
- (3) (a) L. Grainger, *Proc. Intern. Conf. Peaceful Uses At. Energy, Geneva, 1955*, 8, 149 (1956); (b) B. Goldschmidt and P. Vertes, *ibid.*, 8, 152 (1956).
- (4) K. J. Notz, C. W. Huntington, and W. Burkhardt, "Hydrogen Reduction of Uranium Oxides: A Phase Study," National Lead Co. of Ohio, Cincinnati, Ohio, TID-11146 (1960), p. 10.
- (5) K. J. Notz and M. G. Mendel, *J. Inorg. Nucl. Chem.*, 14, 55 (1960).
- (6) J. J. Katz and E. Rabinowitch, "The Chemistry of Uranium, Part I. The Element, Its Binary and Related Compounds," McGraw-Hill Book Co., Inc., New York, N. Y., 1951, p. 304.
- (7) W. R. DeHollander, "A Kinetic Study of the Reduction of Uranium Oxides with Hydrogen," HW-46685, Hanford Atomic Products Operation, Richland, Wash., 1956, p. 4.
- (8) See ref. 6, p. 306.

was produced at the Argonne National Laboratory by the fluidized-bed denitration technique.⁹ Typical chemical analyses performed by the Argonne National Laboratory are shown in Table I.

Table I: UO₃ Analyses (wt. %)

Sample no.	UO ₃	H ₂ O	NO ₂	SO ₄
1	99.1	0.17	0.40	0.10
2	99.5	0.12	0.35	0.18
3	98.9	0.18	0.58	<0.01
4	99.0	0.14	0.47	0.11
5	99.1	0.20	0.52	0.10
6	99.0	0.14	0.56	<0.01

Iron content = 50 γ /g.

The as-received powder, whose individual particles were yellowish orange, granular, and highly spherical, was screened, and the resulting 60–65 mesh fraction was dried in air at 290° for 24 hr. to drive off absorbed gases. Identification as γ -UO₃ was then made by means of the most intense line for UO₃ which corresponds to an angle of $2\theta = 25.8^\circ$ for Cu K α radiation.¹⁰

Density measurements with a 2-cc. pycnometer gave an average density of 8.0 g./cc. for the 60–65 mesh powder.

Apparatus. The reduction apparatus, which is essentially the same as that used by Hockings,¹¹ is shown schematically in Figure 1. The basis of this apparatus is the gas thermal conductivity cell which can be used to follow the progress of the reaction continuously.

Hydrogen was metered with flowmeter A at 400 cc./min. (STP) to a 2.54-cm. diameter, 0.91-m. long Vycor reaction tube heated by two 30.5-cm. Multiple Unit Hevi Duty electric furnaces B and B'. The sample was positioned at the center of furnace B' by means of a stainless steel rod D. Attached to the rod was a piece of platinum wire which supported a platinum sample boat. The temperature of the sample was measured with a chromel–alumel thermocouple junction C located approximately 1.27 cm. upstream from the boat. A continuous gas sample of 100 cc./min. (STP) was withdrawn by flowmeter A' from the furnace through gas-sampling tube G located 2.54 cm. downstream from the reaction boat. The gas sample passed through the measuring side of a Burrell Model SS Detector No. 340–148 thermal conductivity cell E, through absorber F containing Ascarite, Anhydrone, and phosphorus pentoxide, and finally through the reference side of the thermal conductivity cell. The hot-wire type of thermal conductivity cell consisted of

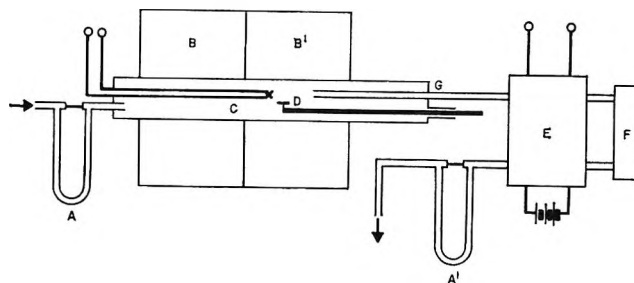


Figure 1. Reduction apparatus.

four tungsten filaments mounted in a 100° thermostated stainless steel block.

The output from the cell, which was operated at a sensitivity of 2.5 mv./% of H₂O, was recorded continuously on a strip-chart recorder with a variable millivolt range adjustment.

Procedure. To perform a reduction test, the furnaces were brought up to the desired reaction temperature while being purged with 100–150 cc. of H₂/min. The UO₃ sample (approximately 50 mg.) was introduced into the sample boat positioned in the cold end of the reaction tube. The H₂ flow to the system was then adjusted to 400 cc./min. and the gas flow rate through the cell to 100 cc./min. After about 10 min. of purging, the thermal conductivity cell was turned on and the current to the cell slowly adjusted to its operating value. The cell and strip-chart recorder were then simultaneously zeroed, and the sample was moved quickly into the hot reaction zone of the furnace by means of the positioning rod. When the recorder pen returned to zero (corresponding to complete reduction), the reduced sample was pulled back to the cold end of the furnace, allowed to cool for several minutes, and then removed.

Reduction Rate Calculation. The rate of reduction of the UO₃ sample is directly proportional to the concentration of water in the product gas stream. Since the voltage output from the thermal conductivity cell, E, is also proportional to the water content of this stream, the rate of reduction dR/dt , can be found from the expression¹²

$$dR/dt = \frac{100MFE}{22,400BW} \quad (1)$$

where $R = \%$ of UO₃ converted to UO₂; $t =$ time, min.;

(9) S. Lawroski, A. A. Jonke, N. Levitz, and E. J. Petkus, *Proc. Intern. Conf. Peaceful Uses At. Energy, Geneva, 2nd*, 17, 488 (1958).

(10) See ref. 6, p. 257.

(11) W. A. Hockings, *Blast Furnace, Coke Oven, Raw Mater. Comm., Proc.*, 19, 171 (1960).

(12) W. A. Hockings, *ibid.*, 19, 172 (1960).

M = molecular weight of UO_3 ; F = hydrogen flow rate, cc./min., at STP; W = weight of UO_3 sample, g.; B = sensitivity of cell, v./% of H_2O ; E = output voltage of cell, v.

Preliminary reduction tests were run to determine qualitatively the nature of the reaction. These tests were characterized by two regions: (1) an initial rapid rise in the reduction rate to a maximum followed by (2) a slow decline of the rate to zero where reduction is complete. Particles from several of the partly reduced samples were sectioned and examined microscopically. All of these particles, which were highly spherical, consisted of a porous layer of UO_2 of a uniform thickness surrounding a core of unreduced UO_3 . The phases, UO_2 and UO_3 , were identified from X-ray powder patterns; these same patterns failed to show any lines which might correspond to a third phase. Microscopic examination of the UO_3 - UO_2 interface at magnifications up to $1300\times$ also failed to show the existence of a third phase. From this it was concluded that, if oxide phases intermediate between UO_2 and UO_3 are present in the reaction, their rate of reduction must be at least as great as that of UO_3 or their presence in the partly reduced samples would be evident, and, because of this lack of intermediate oxides, the reaction at the UO_3 surface must be rate controlling.

For the case of only two predominant phases in the reaction, the degree of reduction, R , can be expressed as

$$R = 100 \frac{V_0 - V}{V_0} \quad (2)$$

where V_0 and V are the volumes of unreduced UO_3 originally and at time t .

Since the reaction proceeds at the UO_3 - UO_2 interface, a rate constant k can be defined as the rate of change in thickness of the UO_3 layer in a direction normal to the UO_3 surface or, equivalently, as the rate of growth in thickness of the UO_2 layer. Thus, after differentiation, eq. 2 can be written

$$\frac{dR}{dt} = \frac{-100}{V_0} \frac{dV}{dt} \quad (3)$$

and, since the UO_3 particles used in these tests can be closely approximated as spheres

$$\frac{dV}{dt} = S \frac{dr}{dt} \quad (4)$$

where S is the surface area at radius r of the unreduced UO_3 particle core at any time. Therefore

$$v = \frac{-dr}{dt} = \frac{V_0}{100} \frac{1}{S} \frac{dR}{dt} = \frac{V_0}{100S_0} \frac{dR/dt}{S/S_0} \quad (5)$$

where S_0 is the surface area of the UO_3 particle at $t = 0$. Whereas

$$\frac{S}{S_0} = \left(\frac{100 - R}{100} \right)^{2/3} \quad (6)$$

and, for a sphere¹³

$$S_0 = (36\pi)^{1/3} V_0^{2/3} \quad (7)$$

Equation 5 can be written

$$v = \left(\frac{V_0}{3600\pi} \right)^{1/3} \left(\frac{1}{100 - R} \right)^{2/3} \frac{dR}{dt} \quad (8)$$

for a single particle or, for a group of identical particles comprising a sample with initial weight W_0 and average density d

$$v = \left(\frac{W_0}{3600\pi d} \right)^{1/3} \frac{dR/dt}{(100 - R)^{2/3}} \quad (9)$$

which is the defining equation for the rate constant as used in this study.

In order for the reaction to be first order in regard to the unreduced surface area, the right-hand side of eq. 9 must be constant during a particular test. The value of this term for varying degrees of reduction was calcu-

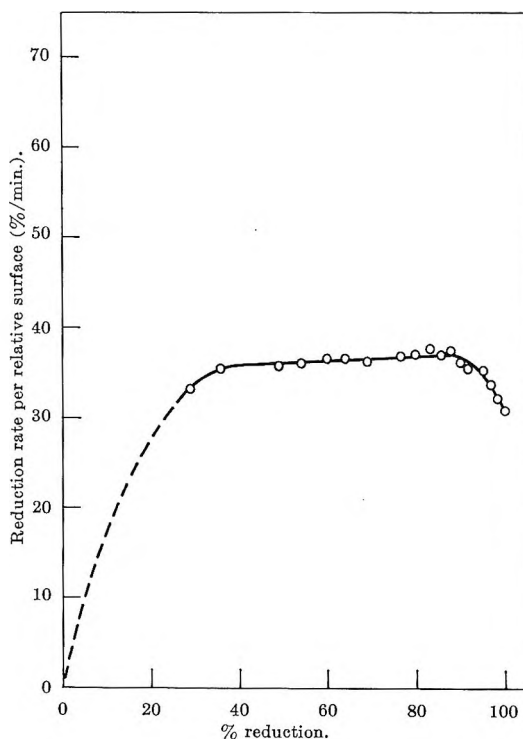


Figure 2. Typical plot, reduction rate per relative surface vs. degree of reduction.

(13) The surface area calculated in this manner is obviously too small; however, this effect will be eliminated in the comparison made later.

lated using eq. 1 and 6 in conjunction with a numerical iteration for each test. A typical plot of this term as a function of the percentage of unreduced UO_3 is shown in Figure 2. After an initial rise, the value remains constant for the major portion of the reduction and then decreases slightly at the end. The early rise in the curve might correspond to an induction period for nucleation growth and/or for heating of the particles. The decrease in the curve near the end of the reduction could be explained as a decrease in the number of smaller particles still undergoing reduction. In any event, during the major portion of the reaction, the rate constant ν appears independent of the thickness of the reduced layer.

After reviewing the calculations for the rate constant for a large number of the reduction tests, it was found that the minimum region of constancy for this value was between 35 and 80% degree of reduction. Accordingly, the calculation of the rate constant for a test was based on the average value of the rate of reduction per relative surface area in this interval.

Results and Discussion

A summary of the calculated rate constants is given in Table II and also in the Arrhenius plot of Figure 3.

Table II: Reduction Rate Constant for 60–65 Mesh UO_3 at Various Temperatures

Temp., °C.	Rate constant, cm. of UO_3 / min. $\times 10^2$	Temp., °C.	Rate constant, cm. of UO_3 / min. $\times 10^2$
582	0.415	554	2.121
582	0.431	554	1.966
621	0.893	554	1.900
621	0.916	554	1.926
621	0.879	557	2.103
635	1.117	566	1.835
635	1.212	568	2.201
635	1.136	571	2.213
635	1.234	571	1.808
638	1.427	571	1.827
638	1.342	588	3.375
638	1.357	596	3.029
641	1.569	704	3.411
643	1.426	710	4.389
644	1.489	713	4.566
646	1.464	738	7.887
646	1.450	741	7.132

The energy of activation for the reduction is $E = 33.3 \pm 0.3$ kcal. mole⁻¹. The pre-exponential (frequency) factor could also be found from Figure 3; however, the value so found would be meaningless because

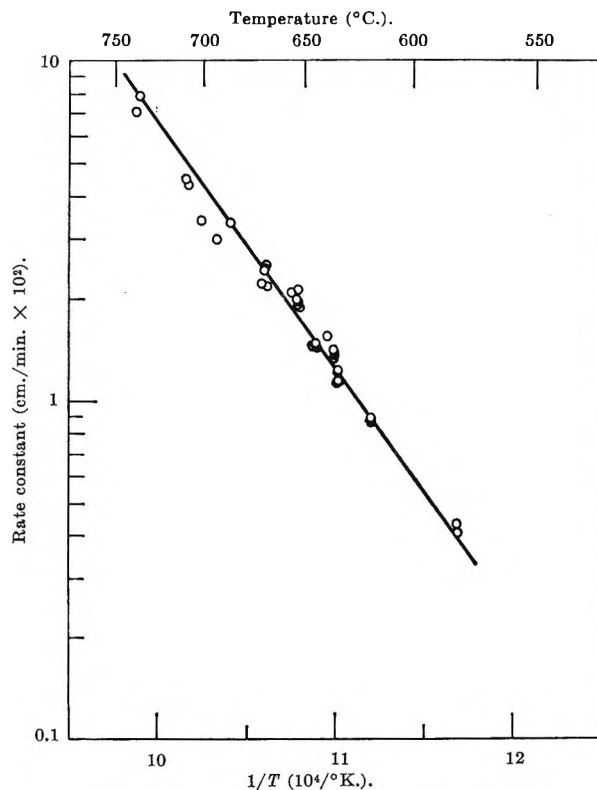


Figure 3. Arrhenius plot for UO_3 reduction.

of the surface area approximation that was made earlier in the derivation of the experimental rate expression.

Absolute reaction rate theory can be used to develop an expression for the rate of reduction for comparison with experiment. Thus, for a reaction between a gaseous molecule of H_2 and an active UO_3 reaction center to form an adsorbed molecule on the UO_3 surface, the equilibrium between the initial and activated states may be written



for which¹⁴

$$\frac{C^*}{C_g C_s} = \frac{f^*}{F_g f_s} e^{-E_0/kT} \quad (10)$$

where C_g is the concentration in the gas phase, molecules per volume; C_s and C^* are the concentrations of the adsorption centers and activated complexes, sites per area; F_g is the partition function per unit volume for the gas phase; f_s and f^* are the complete partition functions for the adsorption centers and activated complexes; and E_0 is the zero-point activation energy per molecule. The reaction rate is then

(14) S. Glasstone, K. J. Laidler, and H. Eyring, "The Theory of Rate Processes," McGraw-Hill Book Co., Inc., New York, N. Y., 1941, p. 373.

$$v = C_g C_s \frac{kT}{h} \frac{f^*}{F_s f_s} e^{-E_0/kT} \quad (11)$$

Treating the activated complex as immobile, its partition function (apart from the symmetry factor, σ^*) may be taken as unity. In addition, the adsorption center, which is transfixed in the parent ceramic, may be considered immobile so that its partition function may also be taken as unity. For the diatomic gas molecule, only the translational and rotational modes of freedom need be considered. Therefore

$$v = C_g C_s \frac{kT}{h} \frac{1/\sigma^*}{\frac{(2\pi mkT)^{3/2}}{h^3} \frac{8\pi^2 IkT}{h^2 \sigma}} e^{-E_0/kT} \quad (12)$$

where σ is the symmetry number, m is the mass, and I is the moment of inertia of the hydrogen molecule. The concentration in the gas phase, C_g , is given as p/kT , where p is the pressure in reduction tube—atmospheric in this case. With this substitution, eq. 12 becomes

$$v = C_s \frac{\sigma}{\sigma^*} \frac{ph^4}{8\pi^2 IkT (2\pi mkT)^{3/2}} e^{-E_0/RT} \frac{\text{molecules of H}_2}{\text{cm.}^2\text{-sec.}} \quad (13)$$

It is assumed that the experimentally determined activation energy can be used for E_0 in lieu of attempting to estimate this value from a potential energy surface. Thus, since the experimental activation energy, E , was found from the equation

$$\frac{d \ln v}{dT} = \frac{E}{RT^2} \quad (14)$$

eq. 13 must be put in the equivalent form to find E_0 . Therefore, for eq. 13

$$\frac{d \ln v}{dT} = -\frac{5}{2T} + \frac{E_0}{RT^2} \quad (15)$$

and

$$\frac{E_0}{RT} = \frac{E}{RT} + \frac{5}{2}R \quad (16)$$

In order to compare eq. 13 with experimentally determined rates, it is necessary to remove the surface area dependence from the calculation. A satisfactory basis for comparing the rates is molecules of $\text{H}_2/\text{g. of UO}_3\text{-sec.}$ Now, the experimental values in Table II can be put on this basis simply by multiplying by $(S_0/V_0)(N_a/M)$, where N_a is Avogadro's number. Also, if it is assumed that the concentration of active adsorption centers is just equal to the number of UO_3 molecules

in the interface at any time, the analytical equation for the rate, eq. 13, can also be put on this basis by replacing C_s by N_a/M . Then

$$v' = \frac{N_a}{M} \frac{\sigma}{\sigma^*} \frac{ph^4}{8\pi^2 IkT (2\pi mkT)^{3/2}} e^{-E_0/RT} \frac{\text{molecules of H}_2}{\text{g. of UO}_3\text{-sec.}} \quad (17)$$

The activated complex is assumed to be very near to H_2O adsorbed on UO_2 so that σ^* has a value 2. Substituting known values¹⁵ into eq. 17 leads to an expression which can be solved to find the reduction rate in molecules of $\text{H}_2/\text{g. of UO}_3\text{-sec.}$ The values so calculated are compared to average experimental values at various temperatures in Table III.

Table III: Comparison of Calculated and Experimental Rate Constants

Temp., °C.	Rate constant (10^{-19} molecules of $\text{H}_2/\text{g. of UO}_3\text{-sec.}$)	
	Av. exptl.	Calcd.
582	0.39	0.31
621	0.82	0.54
635	1.09	0.81
654	1.85	1.14
671	1.79	1.47
696	2.79	2.23
710	4.08	2.80
738	7.26	3.95

The rate constants are seen to agree very favorably when compared in this manner and, on the basis of this comparison, the mechanism proposed in the previous section appears valid. Unfortunately, apparatus were not available to measure the surface area of the powder used in this study, and, for this reason, the rate constant cannot be expressed in the usual manner, *i.e.*, molecules of $\text{H}_2/\text{cm.}^2\text{-sec.}$ However, using surface area measurements reported by DeHollander (0.5 to 5.5 $\text{m.}^2/\text{g.}$) for the same type of powder would lead to rates of the order 10^{14} to 10^{16} molecules of $\text{H}_2/\text{cm.}^2\text{-sec.}$

Acknowledgment. The author is indebted to Dr. R. F. Makens, Department of Nuclear Engineering, Michigan Technological University, and Mr. W. A. Hockings, Institute of Minerals Research, Houghton, Michigan, for their many suggestions and continued interest in this project.

(15) For H_2 , $m = 3.32 \times 10^{-24}$ g., $\sigma = 2$, $I = 4.6 \times 10^{-41}$ g.-cm.², $p = 1.013 \times 10^6$ dynes/cm.²; for UO_3 , $M = 286$ g./mole; $h = 6.625 \times 10^{-27}$ erg-sec., $k = 1.38 \times 10^{-16}$ erg/°K., $R = 1.986$ cal./mole °K.

Mean Amplitudes of Vibration, Bastiansen–Morino Shrinkage Effect, Thermodynamic Functions, and Molecular Polarizability of Sulfur Trioxide¹

by G. Nagarajan, E. R. Lippincott, and J. M. Stutman

Department of Chemistry, University of Maryland, College Park, Maryland (Received January 4, 1965)

Mean-square amplitude quantities, generalized mean-square amplitudes (mean-square parallel amplitudes, mean-square perpendicular amplitudes, and mean cross products), and mean amplitudes of vibration for the bonded and nonbonded distances have been computed for sulfur trioxide by the Cyvin method at the temperatures $T = 0, 298,$ and 500°K . From the generalized mean-square amplitudes, the Bastiansen–Morino shrinkage effect has been calculated at these temperatures. Molar thermodynamic functions for the temperature range $200\text{--}2000^\circ\text{K}$. have been computed on the basis of a rigid rotator, harmonic oscillator model using the revised vibrational assignment. Bond polarizabilities and average molecular polarizability have also been calculated by the Lippincott–Stutman method employing the δ -function potentials.

Introduction

Sulfur trioxide, one of the very simplest molecules and most useful in the industrial process for the manufacture of sulfuric acid, has been subjected to several investigations in determining various thermodynamic quantities, assigning the fundamental frequencies and elucidating the molecular structure. Though the molecule is simple in structure, there are many conflicting reports in ascertaining the lowest bending mode. The Raman spectrum of sulfur trioxide in the liquid and gaseous states was studied by Gerding, Nijveld, and Muller^{2a} and the infrared spectrum of the same in the gaseous state was reported by Gerding and Lecomte.^{2b} Polarization measurements were carried out by Bhagavantam³ and Venkateswaran.⁴ The electron diffraction studies by Palmer⁵ and dielectric measurements by Smits, Moerman, and Pathuis⁶ for this molecule in the vapor phase are in conformity with a planar trigonal symmetrical structure under the symmetry point group D_{3h} . Since the values of the equilibrium constant calculated from the fundamental frequencies² were not in good agreement with those of the experimental ones, several investigators proposed different sets of fundamental frequencies of which the recent set, *i.e.*, ν_1 1069, ν_2 652, ν_3 1333, and ν_4 440 cm^{-1} , given by Khachkuruzov⁷ is the most satisfactory one. One may refer to Khachkuruzov⁷ for a detailed dis-

ussion of the vibrational assignment. It is the aim of the present investigation to calculate the mean amplitudes of vibration and Bastiansen–Morino shrinkage effect at the temperatures $T = 0, 298,$ and 500°K ., the statistical thermodynamic functions on the basis of a rigid rotator, harmonic oscillator model for the temperature range $200\text{--}2000^\circ\text{K}$. and molecular polarizability employing the δ -function model of chemical binding.

Mean Amplitudes of Vibration

A schematic representation of the normal modes of oscillation for a planar symmetrical XY_3 molecule possessing the symmetry point group D_{3h} has already been given by Silver and Shaffer⁸ and Herzberg.⁹

(1) This research was supported in part by a Materials Science Program from the Advanced Research Projects Agency, Department of Defense, and the National Institutes of Health Training Program in Physical Chemistry.

(2) (a) H. Gerding, W. J. Nijveld, and G. J. Muller, *Z. physik. Chem. (Leipzig)*, **B35**, 193 (1937); (b) H. Gerding and J. Lecomte, *Physica*, **6**, 737 (1939).

(3) S. Bhagavantam, *Indian J. Phys.*, **5**, 63 (1930).

(4) S. Venkateswaran, *Phil. Mag.*, **15**, 263 (1933).

(5) K. J. Palmer, *J. Am. Chem. Soc.*, **60**, 2360 (1938).

(6) A. Smits, N. F. Moerman, and J. C. Pathuis, *Z. physik. Chem.*, **B35**, 60 (1937).

(7) G. A. Khachkuruzov, *Opt. Spectry. (USSR)*, **8**, 19 (1960).

(8) S. Silver and W. H. Shaffer, *J. Chem. Phys.*, **9**, 599 (1941).

This molecule gives rise to six vibrational degrees of freedom constituting only four fundamental frequencies which are distributed under the various irreducible representations as follows: $A_1'(R, p) + A_2''(I, \parallel) + 2 E'(R, dp; I, \perp)$ where R, I, p, dp, \parallel , and \perp stand for Raman active, infrared active, polarized, depolarized, parallel, and perpendicular, respectively. ν_1 coming under the symmetry species A_1' is a totally symmetrical stretching vibration, ν_2 coming under the species A_2'' is an out-of-plane vibration, ν_3 and ν_4 coming under the species E' are the asymmetrical stretching and deformation vibrations. ν_1 and ν_2 are the frequencies corresponding to the nondegenerate vibrations while ν_3 and ν_4 to the degenerate vibrations.

A theory for the determination of mean amplitudes of vibration for a molecule of the present study has already been developed by Cyvin.^{10,11} The same method is adopted in the present investigation. The secular equations giving the normal frequencies in terms of the mean-square amplitude quantities were constructed at the temperatures $T = 0, 298, \text{ and } 500^\circ\text{K}$. with help of the Σ and G matrices, vibrational frequencies,⁷ and electron diffraction data.⁵ The symmetrized mean-square amplitude matrices Σ_{11} and Σ_{22} were evaluated directly since the secular equations under the symmetry species A_1' and A_2'' are only singular. But there are three elements with only two equations under the species E' and it is not possible to solve for them uniquely unless some approximations are made. Hence the symmetrized mean-square amplitude matrices Σ_{33} , Σ_{44} , and Σ_{34} were evaluated in the manner described by Cyvin¹⁰ and their values in \AA^2 are given in Table I at the temperatures $T = 0, 298, \text{ and } 500^\circ\text{K}$.

Table I: Symmetrized Mean-Square Amplitude Matrices in \AA^2 for Sulfur Trioxide

Element	Symmetrized mean-square amplitude matrix		
	0°K.	298°K.	500°K.
Σ_{11}	0.0009859	0.0009972	0.0010808
Σ_{22}	0.0131081	0.0132039	0.0164682
Σ_{33}	0.0013876	0.0014478	0.0016327
Σ_{44}	0.0108795	0.0126034	0.0163646
Σ_{34}	0.0009548	0.0003513	-0.0004285

If two arbitrary displacement coordinates designated as ξ_i and ξ_j are given in terms of the symmetry coordinates S_k by $\xi_i = \sum_k A_{ik} S_k$ and $\xi_j = \sum_k A_{jk} S_k$, then the mean-square amplitude quantities may correspondingly be obtained from the following: $\langle \xi_i^2 \rangle = \sum_k \sum_l A_{ik} A_{il} \Sigma_{kl}$ and $\langle \xi_i \xi_j \rangle = \sum_k \sum_l A_{ik} A_{jl} \Sigma_{kl}$ where Σ_{kl} stands for the

elements of Σ matrix. On the basis of the above principle, the mean-square amplitude quantities in terms of the symmetrized mean-square amplitude matrices for the present molecular system were obtained as follows: $\sigma_r = (1/3)\Sigma_{11} + (2/3)\Sigma_{33}$, $\sigma_{rr} = (1/3)\Sigma_{11} - (1/3)\Sigma_{33}$, $\sigma_\theta = (2/3)\Sigma_{44}$, $\sigma_{\theta\theta} = -(1/3)\Sigma_{44}$, $\sigma_\phi = \Sigma_{22}$, $\sigma_{r\theta} = (2/3)\Sigma_{34}$, $\sigma_{r\theta}' = -(1/3)\Sigma_{34}$, $\sigma_d = \Sigma_{11} + (1/2)\Sigma_{33} + (1/6)\Sigma_{44} - (1/\sqrt{3})\Sigma_{34}$, $\sigma_{rd} = (1/\sqrt{3})\Sigma_{11} - (1/\sqrt{3})\Sigma_{33} + (1/3)\Sigma_{34}$, and $\sigma_{rd}' = (1/\sqrt{3})\Sigma_{11} + (1/2\sqrt{3})\Sigma_{33} - (1/6)\Sigma_{34}$.

The mean-square amplitude quantities were calculated with help of the symmetrized mean-square amplitude matrices in \AA^2 given in Table I and their values in \AA^2 are given in Table II at the temperatures $T = 0, 298, \text{ and } 500^\circ\text{K}$. where σ_r is the mean-square amplitude quantity due to the bonded atom pair S-O, σ_θ the quantity due to the bending O-S-O, σ_ϕ the quantity due to the out-of-plane vibration, σ_d the quantity due to the nonbonded atom pair O—O, and σ_{rr} , $\sigma_{\theta\theta}$, $\sigma_{r\theta}$, $\sigma_{r\theta}'$, σ_{rd} , and σ_{rd}' are the respective interaction quantities. Most of the interaction quantities such as σ_{rr} , $\sigma_{r\theta}$, $\sigma_{r\theta}'$, σ_{rd} , and σ_{rd}' are very much smaller than the other quantities. The quantity due to the out-of-plane vibration is greater than that of the O-S-O bending and many times greater than the other quantities. The quantity due to the nonbonded atom pair is, as expected, greater than that of the bonded atom pair.

The generalized mean-square amplitude quantities, namely, mean-square parallel amplitude $\langle \Delta z^2 \rangle$, mean-square perpendicular amplitudes $\langle \Delta x^2 \rangle$ and $\langle \Delta y^2 \rangle$, and mean cross products $\langle \Delta x \Delta y \rangle$, $\langle \Delta y \Delta z \rangle$, and $\langle \Delta z \Delta x \rangle$ were, according to Cyvin,¹¹ calculated for sulfur trioxide from the values of the symmetrized mean-square amplitude matrices in \AA^2 given in Table I and their values in \AA^2 for the bonded as well as nonbonded atom pairs are given in Table III at the temperatures $T = 0, 298, \text{ and } 500^\circ\text{K}$. The mean cross products, namely, $\langle \Delta x \Delta y \rangle$, $\langle \Delta y \Delta z \rangle$, and $\langle \Delta z \Delta x \rangle$ for the bonded and nonbonded atom pairs and the mean-square perpendicular amplitude quantity $\langle \Delta y^2 \rangle$ for the nonbonded atom pair vanish because of the symmetry of the molecular system. The corresponding calculated values of the mean amplitudes of vibration in \AA . at the temperatures $T = 0, 298, \text{ and } 500^\circ\text{K}$. are as follows: 0.0354, 0.0359, and 0.0381 for the bonded atom pair S-O; 0.0542, 0.0602, and 0.0698 for the nonbonded atom pair O—O. The values increase with increasing temperature.

(9) G. Herzberg, "Infrared and Raman Spectra of Polyatomic Molecules," D. Van Nostrand Co., New York, N. Y., 1960.

(10) S. J. Cyvin, *Acta Chem. Scand.*, **13**, 334 (1959).

(11) S. J. Cyvin, *Spectrochim. Acta*, **17**, 1219 (1961).

Table II: Mean-Square Amplitude Quantities in \AA^2 for Sulfur Trioxide

Symbol	Mean-square amplitude quantity		
	0° K.	298° K.	500° K.
σ_r	0.0012537	0.0012916	0.0014487
σ_{rr}	-0.0001339	-0.0001502	-0.0001840
σ_θ	0.0072530	0.0084023	0.0109097
$\sigma_{\theta\theta}$	-0.0036265	-0.0042011	-0.0054549
σ_ϕ	0.0121081	0.0132039	0.0164682
$\sigma_{r\theta}$	0.0006365	0.0002342	-0.0002857
$\sigma_{r\theta}'$	-0.0003183	-0.0001171	0.0001428
σ_d	0.0029417	0.0036189	0.0048720
σ_{rd}	0.0000863	-0.0001430	-0.0004615
σ_{rd}'	0.0008106	0.0009352	0.0011668

According to the equation for the normal frequency, the hyperbolic cotangent differs very little from unity at the room temperature and correspondingly the mean-square amplitude quantity is an independent function of temperature when the fundamental frequency is above 1200 cm^{-1} . On the other hand, when the fundamental frequency is below 200 cm^{-1} , the cotangent function leads only to an approximate value and correspondingly the mean-square amplitude quantity is a dependent function of temperature. Hence, the reliability of the mean-square amplitude quantities depends upon the fundamental frequencies falling from 200 to 1200 cm^{-1} . The fundamental frequencies of the present study are in the above range except the frequency corresponding to the asymmetrical stretching vibration which is actually not too high.

Bastiansen–Morino Shrinkage Effect

The concept of the shrinkages of the chemical bonds was first initiated by Karle and Karle¹² and confirmed by Bastiansen and his co-workers^{13–18} during their electron diffraction studies of gaseous molecules. Because of the importance of such studies in elucidating the structures of various polyatomic molecules, a theory was established by Morino¹⁹ for this effect in terms of the intramolecular motion using the generalized mean-square amplitudes. The theory is based on a power series expansion for the shrinkage effects of linear as well as nonlinear conformations as developed by Morino and his associates.^{20,21} In the case of a linear conformation, the shrinkage is mainly due to the perpendicular displacements of the atom pair. In the case of a nonlinear conformation, two kinds of shrinkages, namely, “natural” and “practical” shrinkages, have been defined and shown to be identical with the first-order approximation. The

anharmonic terms in contrast to the linear conformations are not canceled out in the nonlinear conformations except for highly symmetrical molecules having no totally symmetrical bending modes in the ground state. The name, Bastiansen–Morino shrinkage effect, was introduced later by many investigators to describe this phenomenon.²²

The calculation for the Bastiansen–Morino shrinkage effect needs only the values of the mean-square perpendicular amplitudes and internuclear distances at the equilibrium configuration. Very accurate values of the internuclear distances at the equilibrium position are, however, not required and approximate values from microwave studies, X-ray diffraction studies, or any other experimental investigations, if the results of electron diffraction studies are not available, will quite be sufficient since the second-order term in the basic equation²¹ for the calculation of the shrinkage is only a minor correction term. Using the value of the internuclear distance in \AA . given by Palmer⁵ and the generalized mean-square amplitude quantities in \AA^2 given in Table III, the values of the Bastiansen–Morino shrinkage effect were, according to Meisingseth and Cyvin,²³ calculated for sulfur trioxide and their respective values in \AA . at the temperatures $T = 0, 298, \text{ and } 500^\circ\text{K}$. are given as follows: 0.001884, 0.002055, and 0.002545. Though the value of the Bastiansen–Morino shrinkage effect appears small, it is real. This distance must be added at the appropriate temperature to the observed nonbonded distance from electron diffraction studies in order to obtain the actual nonbonded distance of the molecule.

Thermodynamic Functions

The statistical thermodynamic functions, namely, heat content, free energy, entropy, and heat capacity

- (12) I. Karle and J. Karle, *J. Chem. Phys.*, **17**, 1052 (1949).
- (13) A. Almendingen, O. Bastiansen, and T. Munthe-Kass, *Acta Chem. Scand.*, **10**, 261 (1956).
- (14) A. Almendingen, O. Bastiansen, and M. Traetteberg, *ibid.*, **13**, 1699 (1959).
- (15) O. Bastiansen and M. Traetteberg, *Acta Cryst.*, **13**, 1108 (1960).
- (16) T. Munthe-Kass, Thesis, University of Oslo, 1955.
- (17) H. Breed, O. Bastiansen, and A. Almendingen, *Acta Cryst.*, **13**, 1108 (1960).
- (18) M. Traetteberg, Dissertation, Norges Tekniske Hogskole, Trondheim, Norway, 1960.
- (19) Y. Morino, *Acta Cryst.*, **13**, 1107 (1960).
- (20) Y. Morino, K. Kuchitsu, and T. Oka, *J. Chem. Phys.*, **36**, 1108 (1962).
- (21) Y. Morino, S. J. Cyvin, K. Kuchitsu, and T. Ijima, *ibid.*, **36**, 1109 (1962).
- (22) A complete set of data is given by G. Nagarajan and E. R. Lippincott, *ibid.*, **42**, 1809 (1965).
- (23) E. Meisingseth and S. J. Cyvin, *J. Mol. Spectry.*, **8**, 464 (1962).

Table III: Generalized Mean-Square Amplitude Quantities in Å.² for Sulfur Trioxide

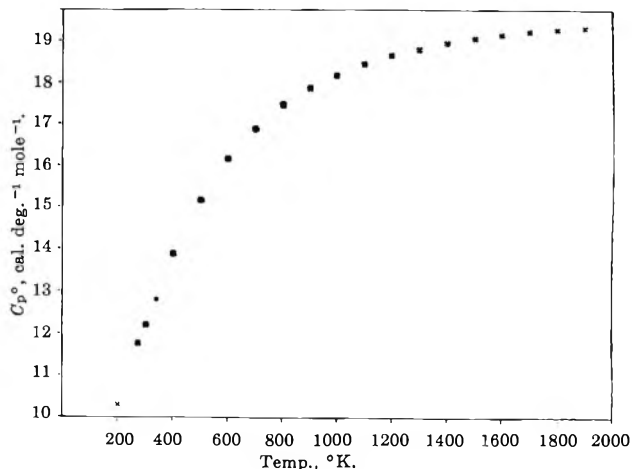
Distance	Symbol	Generalized mean-square amplitude quantity—		
		0°K.	298°K.	500°K.
S—O	$\langle \Delta z^2 \rangle$	0.0012537	0.0012916	0.0014487
	$\langle \Delta x^2 \rangle$	0.0072530	0.0084023	0.0109097
	$\langle \Delta y^2 \rangle$	0.0013453	0.0014671	0.0018298
	$\langle \Delta x \Delta y \rangle$	0	0	0
	$\langle \Delta y \Delta z \rangle$	0	0	0
	$\langle \Delta z \Delta x \rangle$	0	0	0
O—O	$\langle \Delta z^2 \rangle$	0.0029417	0.0036189	0.0048720
	$\langle \Delta x^2 \rangle$	0.0019558	0.0026216	0.0037912
	$\langle \Delta y^2 \rangle$	0	0	0
	$\langle \Delta x \Delta y \rangle$	0	0	0
	$\langle \Delta y \Delta z \rangle$	0	0	0
	$\langle \Delta z \Delta x \rangle$	0	0	0

of the sulfur trioxide molecule were calculated using the vibrational frequencies given by Khachkuruzov⁷ and the structural data given by Palmer⁵ for the temperature range 200–2000°K. A rigid rotator, harmonic oscillator model was assumed and all the quantities were calculated for a gas in the thermodynamic standard gaseous state of unit fugacity (1 atm.) by using the standard formulas and tables of functions for the harmonic oscillator contributions given by Pitzer.²⁴ The calculated values of the principal moments of inertia are given as follows

$$I_{xx} = I_{yy} = 49.0776 \text{ a.m.u. } \text{Å}^2 \text{ (} 81.5243 \times 10^{-40} \text{ g. cm.}^2 \text{)}$$

$$I_{zz} = 98.1552 \text{ a.m.u. } \text{Å}^2 \text{ (} 163.0486 \times 10^{-40} \text{ g. cm.}^2 \text{)}$$

Assumed in the calculations were a symmetry number of 6, singlet ground electronic states, and chemical atomic weights. Neglected in the calculations were the contributions due to the centrifugal distortion, isotopic mixing, and nuclear spins. The calculated values of the thermodynamic functions in calories per degree mole are given in Table IV. A graph is drawn between the heat capacities in calories per degree mole and temperatures in degrees Kelvin (see Figure 1). The nature of the smooth curve connecting all the crosses indicates the correctness in adopting the value for the lowest bending mode as 440 cm.⁻¹ by Khachkuruzov.⁷ Further, the curve due to the results of the present investigation without anharmonicity corrections is far better than the one due to those by Stockmayer, Kavanagh, and Mickley²⁵ with anharmonicity corrections.

**Figure 1.** Heat capacity vs. temperature for sulfur trioxide in the ideal gaseous state.**Table IV:** Heat Content, Free Energy, Entropy, and Heat Capacity of Sulfur Trioxide for the Ideal Gaseous State at 1 Atm. Pressure^a

Temp., °K.	$(H_0 - E_0^\circ)/T$	$-(F_0 - E_0^\circ)/T$	S°	C _p °
200	8.594	48.431	57.025	10.258
273.16	9.244	51.207	60.451	11.743
298.16	9.478	52.028	61.506	12.218
300	9.489	52.083	61.572	12.236
400	10.393	54.942	65.335	13.890
500	11.220	57.342	68.562	15.187
600	11.984	59.477	71.461	16.189
700	12.637	61.371	74.008	16.927
800	13.208	63.091	76.299	17.482
900	13.712	64.685	78.397	17.906
1000	14.142	66.146	80.288	18.225
1100	14.522	67.487	82.009	18.225
1200	14.860	68.770	83.630	18.680
1300	15.167	69.986	85.153	18.847
1400	15.434	71.130	86.564	18.974
1500	15.667	72.089	87.756	19.079
1600	15.876	73.163	89.039	19.170
1700	16.089	74.205	90.294	19.249
1800	16.255	75.108	91.363	19.307
1900	16.430	76.028	92.458	19.368
2000	16.561	76.786	93.347	19.412

^a T is the temperature in degrees Kelvin; the other quantities are in calories per degree mole, and E₀[°] is the energy of 1 mole of perfect gas at absolute zero temperature.

Molecular Polarizability

The molecular polarizability is one of the fundamental electrical properties of a molecular system. From

(24) K. S. Pitzer, "Quantum Chemistry," Prentice-Hall, Inc., New York, N. Y., 1953, p. 457.

(25) W. H. Stockmayer, G. M. Kavanagh, and H. S. Mickley, *J. Chem. Phys.*, 12, 408 (1944).

the experimental viewpoint, one need measure the index of refraction of a substance and one can then deduce the molecular polarizability from the Lorentz-Lorenz equation. One could also measure the dielectric constant of a substance and its temperature dependence and thereby deduce both the polarizability and the average magnitude of the molecular dipole moment. From the molecular point of view, however, an average molecular polarizability may be obtained by averaging the three directional diagonal components of the polarizability tensor; *i.e.*, if

$$\alpha = \begin{bmatrix} \alpha_{xx} & \alpha_{xy} & \alpha_{xz} \\ \alpha_{yx} & \alpha_{yy} & \alpha_{yz} \\ \alpha_{zx} & \alpha_{zy} & \alpha_{zz} \end{bmatrix}$$

then $\alpha_M = (1/3)(\alpha_{xx} + \alpha_{yy} + \alpha_{zz})$. On the basis of the quantum mechanical models, the calculations of atomic and molecular polarizabilities have been, in recent years, developed in many ways. Several investigators calculated the polarizabilities of various molecules and ions by adopting different potential models in order to test how far the polarizability could be useful a criterion for testing the accuracy of the wave functions adopted. Recently Lippincott and Stutman²⁶ have applied δ -function potentials to the calculations of bond and molecular polarizabilities for various diatomic and polyatomic systems. The same method has been applied in the present investigation to calculate the molecular polarizability of sulfur trioxide and one may refer to Lippincott and Stutman²⁶ for the detailed theoretical considerations and calculations.

The δ -function strengths, A , in atomic units, atomic polarizabilities, α , in 10^{-25} cm.³, and c values in atomic units have been adopted for the present investigation from the earlier work²⁶ as follows: $A_S = 0.688$, $A_O = 1.00$, $\alpha_S = 18.20$, $\alpha_O = 5.92$, $c_S = 4.128$, and $c_O = 4.899$. The c value for the sulfur atom is obtained in the manner described by Lippincott and Dayhoff²⁷ for a bond of polyatomic system.

The polarizability contribution to the parallel component from the nonbond-region electrons for sulfur trioxide is given as follows: $\Sigma\alpha_{||n} = \Sigma f_j \alpha_j = (8/3)\alpha_O = 15.787 \times 10^{-25}$ cm.³. Here α_j is the atomic polarizability of the j th atom obtainable from the δ -function strength A_j and f_j the fraction of the electrons in the valence shell of the j th atom not involved in bonding. The polarizability contribution to the parallel component from the bond-region electrons may be calculated

using a linear combination of atomic δ -function wave functions representing the two nuclei in the bond and an analytical expression for it may be given as follows: $\alpha_{||b} = 4nA_{SO}(1/a_0)(\langle x^2 \rangle)^2$ where n is the bond order, A_{SO} the root mean-square δ -function strength of the two nuclei, *i.e.*, $A_{SO} = (A_S A_O)^{1/2}$, and $\langle x^2 \rangle$ the mean-square position of a bonding electron expressed as $\langle x^2 \rangle = (R^2/4) + (1/2)c_S c_O$. Here R is the internuclear distance of S-O at the equilibrium configuration. The bond order for S-O bond was considered as $4/3$ and the computed value for the total parallel bond component contribution is 54.734×10^{-25} cm.³.

A reasonable assumption has been made²⁶ for the average magnitude of the bond perpendicular component as a function of the charge separation. The atomic contributions have been weighted according to their respective electronegativities. This leads to the greater contribution of the bond perpendicular component for the atom having the larger charge distribution in its vicinity. The analytical expression for the sum of the perpendicular components of all the bonds in the molecule is

$$\Sigma 2\alpha_{\perp} = n_{df} \frac{\Sigma X_j^2 \alpha_j}{\Sigma X_j^2}$$

where n_{df} is the number of residual atomic degrees of freedom, X_j the electronegativity of the j th atom, and α_j the atomic polarizability of the j th atom. The number of residual atomic degrees of freedom for sulfur trioxide is seven and one may refer to Lippincott and Stutman²⁶ for a detailed discussion. From the above equation the calculated value of $\Sigma 2\alpha_{\perp}$ for sulfur trioxide is 53.934×10^{-25} cm.³. The average or mean molecular polarizability is

$$\begin{aligned} \alpha_M &= (1/3)(\Sigma\alpha_{||b} + \Sigma\alpha_{||n} + \Sigma 2\alpha_{\perp}) \\ &= (1/3)(54.734 + 15.787 + 53.934) \times 10^{-25} \text{ cm.}^3 \\ &= 41.485 \times 10^{-25} \text{ cm.}^3 \end{aligned}$$

The experimental value of the average molecular polarizability for sulfur trioxide is obtained as 41.805×10^{-25} cm.³ from the measurements of dielectric constant by Smits, Moerman, and Pathuis⁵ and the well-known Lorentz-Lorenz equation. The experimental and calculated values are in good agreement with less than 1% error.

(26) E. R. Lippincott and J. M. Stutman, *J. Phys. Chem.*, **68**, 2926 (1964).

(27) E. R. Lippincott and M. O. Dayhoff, *Spectrochim. Acta*, **16**, 807 (1960).

The Nuclear Magnetic Resonance Spectra of Some 9,10-Bridged 9,10-Dihydroanthracenes¹

by William B. Smith and Ben A. Shoulders

Department of Chemistry, Texas Christian University, Fort Worth, Texas (Received January 4, 1965)

The chemical shifts for a series of arylalkanes have been determined along with the values of $J_{C^{13}-H}$ for the alkyl protons. The observation that the alkyl protons in triptycene are more shielded than that of triphenylmethane led to the determination of the n.m.r. parameters for a series of 9,10-bridged 9,10-dihydroanthracenes. The results of this study are presented.

The chemical shifts of the alkyl protons in the arylalkanes may be considered to be a function of the inductive and resonance effects of the attached aromatic rings as well as the ring current effects exhibited by such rings. The values of the chemical shifts and $J_{C^{13}-H}$ for a related series of arylalkanes are given in Table I. The determination of the contributions which the various possible effects make to the alkyl protons is difficult although presumably one can calculate the ring current effect by the approximate methods of Waugh and Fessenden² or Johnson and Bovey.³

Examination of the alkyl proton shifts in Table I shows that the difference between the pairs toluene-

diphenylmethane, diphenylmethane-triphenylmethane, and *o*-xylene-9,10-dihydroanthracene is remarkably constant (τ 1.58-1.65 per phenyl). In contrast, the chemical shift for the *tertiary* protons in triptycene would seem to be unexpectedly to the high field side by about τ 0.2. This result is not due to some odd solvent effect, for in cyclohexane the values for triphenylmethane and triptycene are τ 4.53 and 4.77, respectively.

The observation of the triptycene alkyl proton as being more shielded than that of triphenylmethane is most curious. The results from the pairs mentioned above suggest that inductive and resonance contributions per phenyl are of a similar magnitude. The *tertiary* protons in triptycene lie in the planes of the three aromatic rings where ring current effects should be to deshield the protons.^{2,3} Dipole moment studies of triphenylmethane indicate that the phenyl rings are tilted about 45° from the alkyl C-H axis.⁴ On the basis of ring current effects, one would expect the alkyl proton in triphenylmethane to be more shielded than those in triptycene.

The values for the alkyl $J_{C^{13}-H}$ are also given in Table I. The additivity rule of Juan and Gutowsky⁵ is followed well by all examples except triptycene.

Table I: Proton Chemical Shifts and $J_{C^{13}-H}$ for Some Arylalkanes

Compound	Ar-H ^a	R-H ^a	$J_{C^{13}-H}$ ^b
Toluene	2.90 ^c	7.66 ^c	126 ^d
Diphenylmethane	2.86 ^c	6.08 ^c	127 ^d
Triphenylmethane	2.83	4.50	132 ± 2
<i>o</i> -Xylene	2.90 ^e	7.75 ^e	126 ± 1
9,10-Dihydroanthracene	2.83	6.10	128 ± 2
Triptycene	2.88	4.70	145 ± 1

^a Chemical shifts in τ -units determined in carbon tetrachloride or deuteriochloroform. ^b Value for alkyl proton(s) in c.p.s. ^c G. V. D. Tiers, "Characteristic Nuclear Magnetic Shielding Values, etc.," Minnesota Mining and Manufacturing Co., St. Paul, Minn., 1958. ^d C. Juan and H. S. Gutowsky, *J. Chem. Phys.*, **37**, 2198 (1962). ^e Varian Catalog of N.m.r. Spectra, Varian Associates, Palo Alto, Calif., 1962, p. 201.

(1) Presented, in part, at the Southwest Regional Meeting of the American Chemical Society, Shreveport, La., Dec. 1964.

(2) J. S. Waugh and R. W. Fessenden, *J. Am. Chem. Soc.*, **79**, 846 (1957).

(3) C. E. Johnson and F. A. Bovey, *J. Chem. Phys.*, **29**, 1012 (1958).

(4) M. Aroney and R. J. W. LeFevre, *J. Chem. Soc.*, 3600 (1960).

(5) See Table I, footnote d.

Matwiyoff and Drago⁶ have recently considered the theoretical bases for the frequently observed linear relation between proton chemical shifts and $J_{C_{13}-H}$. The anomalous value of the *tertiary* proton shift in triptycene is emphasized by the observation that a good linear plot of τ vs. $J_{C_{13}-H}$ is obtained for all entries in Table I except triptycene.

One possible explanation of the anomalous shift of triptycene is offered by the possibility of a ring current effect arising from an "around the barrel" type of flow of the π -electrons in the triptycene aromatic rings (*i.e.*, circular current perpendicular to the face of each ring). No support for this contention was found in the literature. The ultraviolet spectrum of triptycene is only slightly different from that of *o*-xylene, and it has been suggested that at best only a slight perturbation of the π -systems occur owing to interactions between the aromatic rings.⁷ Similar calculations have indicated that there is no ground-state π -electron interaction in bicyclo[2.2.2]octatriene (barrelene).⁸ Nor is any interaction indicated in the n.m.r. spectrum of this substance, for the bridgehead protons in the series bicyclo[2.2.2]octene, bicyclo[2.2.2]octadiene, and bicyclo[2.2.2]octatriene fall in the regular sequence of τ 7.51,⁹ 6.41,⁹ and 5.31,¹⁰ respectively.

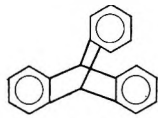
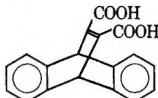
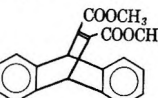
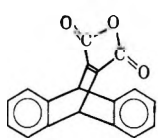
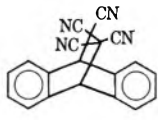
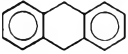
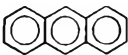
As a consequence of the above results, we were led to an examination of the chemical shifts and coupling constants of the aromatic protons in triptycene. For comparison, 9,10-dihydroanthracene, anthracene, and a series of 9,10-bridged 9,10-dihydroanthracenes were also examined. Acetone was selected as a solvent only because it was the only common solvent in which all of the compounds were sufficiently soluble to enable a detailed spectral analysis.

The ring spectrum of triptycene (Figure 1) is a typical A_2B_2 system and was treated accordingly. The downfield half of the spectrum showed slightly broadened lines suggesting a weak coupling with the bridgehead protons. The coupling constants and chemical shifts are given in Table II, and the calculated spectrum is shown in Figure 1. The spectrum of 9,10-dihydroanthracene (Figure 1) was more difficult to interpret. However, a satisfactory set of parameters was found by conventional means as discussed in the Experimental section. The list of compounds used in this study and the determined n.m.r. parameters are all given in Table II. The values given there for anthracene are in excellent agreement with the literature values.¹¹

Examination of the data in Table II reveals only a slight change in coupling constants in the series anthracene, 9,10-dihydroanthracene, and the 9,10-bridged

9,10-dihydroanthracenes. Jonathan, Gordon, and Dailey¹¹ have found a correlation between coupling constants and π -bond order for a series of polynuclear aromatic hydrocarbons. The variations noted in Table II may reflect such changes. However, little is known of the effect of substituents on π -bond order, and, consequently, no further conclusions are warranted.

Table II: Chemical Shifts and Coupling Constants in Acetone

Compound	τ , A_2B_2	Δ_{AB} , c.p.s.	τ , bridge	J_{AB}	$J_{AB'}$	$J_{AA'}$	$J_{BB'}$
	2.75	28.26	4.40	7.60	1.20	0.00	7.70
	2.72	27.46	3.98	7.60	1.20	0.00	7.70
	2.71	27.06	4.33	7.60	1.20	0.00	7.70
	2.68	30.76	4.21	7.60	1.20	0.00	7.70
	2.33	15.80	4.18	8.30	1.20	0.00	7.50
	2.75	7.14	6.09	7.93	1.47	0.00	7.10
	2.17	33.70	1.52	8.30	1.20	0.00	6.50

The ring proton spectrum of *o*-xylene consists of a single sharp line. However, the ring spectrum of 9,10-dihydroanthracene shows a difference of chemical shifts between the A and B type protons of 7.14 c.p.s.

(6) N. A. Matwiyoff and R. S. Drago, *J. Chem. Phys.*, **38**, 2583 (1963).

(7) C. F. Wilcox, *ibid.*, **33**, 1874 (1960).

(8) C. F. Wilcox, S. Winstein, and W. C. McMillan, *J. Am. Chem. Soc.*, **82**, 5450 (1960).

(9) K. Tori, R. Muneyuki, and H. Tanida, *Can. J. Chem.*, **41**, 3142 (1963).

(10) H. E. Zimmerman and G. L. Grunewald, *J. Am. Chem. Soc.*, **86**, 1434 (1964).

(11) N. Jonathan, S. Gordon, and B. P. Dailey, *J. Chem. Phys.*, **36**, 2443 (1962).

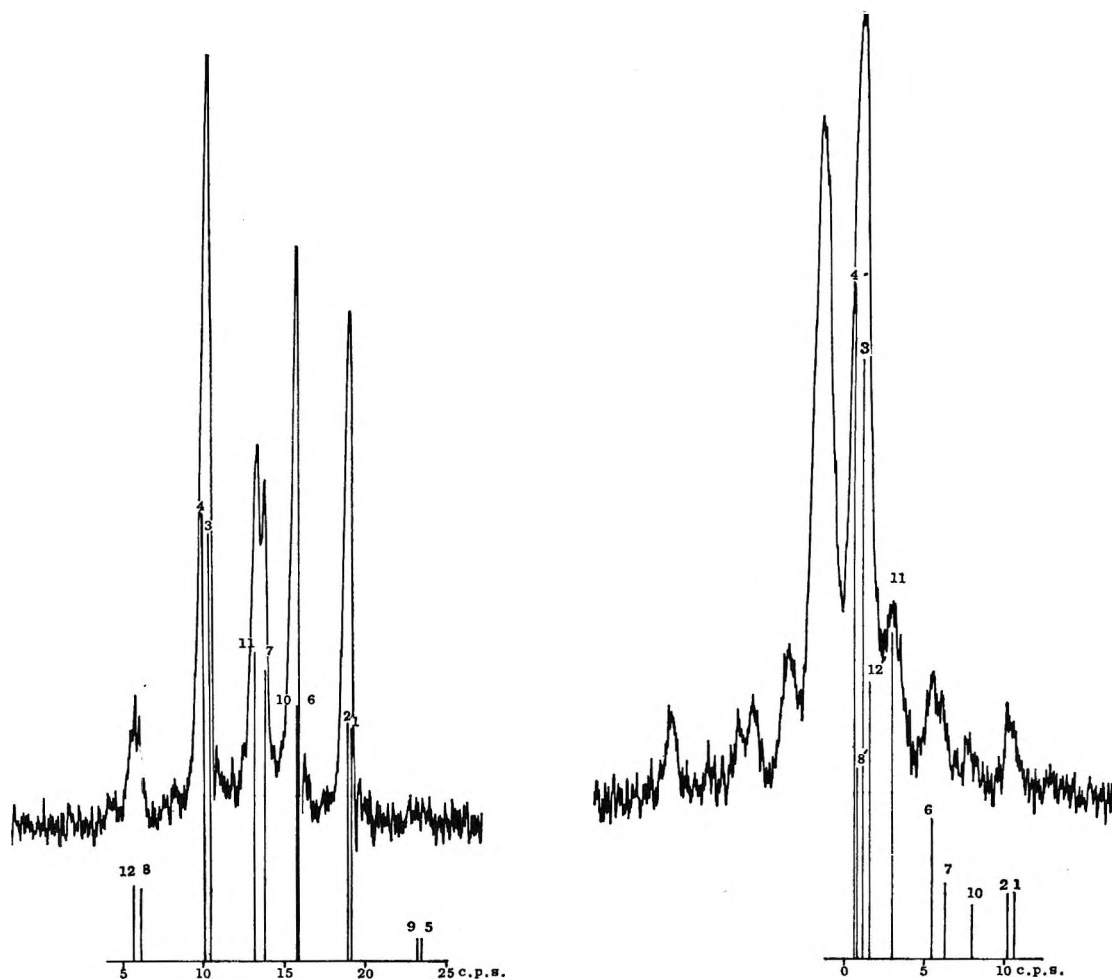


Figure 1. The n.m.r. spectra of the aromatic protons in triptycene (left—only the upfield half shown) and 9,10-dihydroanthracene (right) in acetone.

Presumably, this reflects the ring current effect of one aromatic ring upon the protons in the other ring. Using Dreiding models to measure distances and angles, one calculates a ring current effect of 6.6 c.p.s. by the method of Johnson and Bovey.³ Similar calculations were carried out on the tetracyanoethylene adduct of anthracene. It was assumed that the internal chemical shift between the pairs of aromatic protons in one ring was determined by the ring current effect of the other ring plus the contributions owing to the anisotropy of the two nearest cyano groups.¹² Measurements were again made from Dreiding models. The calculated and experimental values for Δ_{AB} were 12.4 and 15.80 c.p.s., respectively. In view of the variety of assumptions inherent in the calculation of ring current effects and magnetic anisotropies on proton shielding, the calculated results above can be considered in excellent agreement with the experimental values.

Similar calculations, using the Johnson-Bovey method, were made for the ring current effects of the two aromatic rings in triptycene on the chemical shifts of the aromatic protons in the third ring. The calculated value of Δ_{AB} was 12.0 c.p.s., a value considerably below the experimental value of 28.26 c.p.s. In view of the success of the calculations above, this result can be taken as a further indication of the peculiarities of the triptycene molecule.

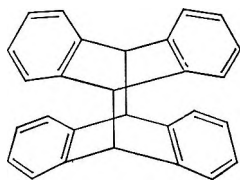
The value of J_{Cl_3-H} for the bridgehead proton in triptycene is similar in magnitude to those observed

(12) McConnell's equation [H. M. McConnell, *J. Chem. Phys.*, **27**, 226 (1957)] was used. The value of $\Delta\chi_{CN}$ of 14.2×10^{-30} cm.³ was used in these calculations. This number was obtained by a back calculation from the chemical shift differences of the β -protons of acrylonitrile using the published data of G. S. Reddy, J. H. Goldstein, and L. M. Mandell, *J. Am. Chem. Soc.*, **83**, 1300 (1961), and is intermediate between the value used by them (13.46×10^{-30} , E. B. Whipple, Ph.D. Thesis, Emory University, 1959) and that derived later by another technique [16.5×10^{-30} , G. S. Reddy and J. H. Goldstein, *J. Chem. Phys.*, **39**, 3509 (1963)].

by Musher¹³ for a series of bicyclo[2.2.1]heptanols and by Tori, *et al.*,¹⁴ for a related series containing the bicyclo[2.2.1]cycloheptyl ring system. The authors consider the large values of J_{C1-H} to reflect enhanced s-character in the *tertiary* C-H bond and resultant π -character in the strained ring systems.¹⁵ Bartlett and Lewis¹⁶ have pointed out that the ring strain at the bridgehead carbons in triptycene more closely resembles that in bicyclo[2.2.1]heptane than bicyclo[2.2.2]octane. While the concepts of π -character or "bent" bonds may serve ultimately to account for the observations recorded here for triptycene, there is presently no way in which quantitative calculations using these concepts can be reasonably applied to this molecule.

Two ancillary experiments carried out during this study merit mention. First, the methylene spectrum of 9,10-dihydroanthracene was observed as a sharp singlet in carbon disulfide solutions down to -60° . While the boat structure of the central ring suggests that the methylene hydrogens should be magnetically nonequivalent, the boat-boat interconversion apparently is very rapid even at this temperature.

Second, the photodimer of anthracene was synthesized.



This interesting molecule was found to be insoluble in all common solvents, but the chemical shift of the bridgehead hydrogens was found to τ 5.75 in a naphthalene solution at 180° . Assuming that the effects of adjacent rings would be the same as in dihydroanthracene, the ring current effect of the nonadjacent rings was calculated. Subject to the assumption that other effects, *i.e.*, C-C bond anisotropy, solvent effects, etc., were negligible, the calculated value of τ 5.81 was obtained. However, the agreement may be fortuitous.

Experimental

Anthracene, dihydroanthracene, and triptycene were commercial products. The adduct of tetracyanoethylene and anthracene was prepared by a procedure similar to that of Middleton, *et al.*¹⁷ The photodimer of anthracene was prepared by the method of Luther and Weigert.¹⁸

The adduct of anthracene and acetylenedicarboxylic acid was obtained by heating equimolar amounts of the two reactants under reflux in xylene. Upon cooling,

a solid was obtained which appeared to be a mixture of the free acid and the corresponding anhydride on the basis of the n.m.r. spectrum. Extraction of the mixture with a concentrated potassium hydroxide solution followed by acidification of the extract gave material (m.p. $215-216^\circ$) which appeared (n.m.r.) to be the free acid. Carbon-hydrogen analyses were unsatisfactory, however. Consequently, the crude reaction product was converted to the corresponding dimethyl ester by heating the mixture under reflux in acidified methanol and to the anhydride by heating the mixture in acetic anhydride. Both the dimethyl ester and the anhydride had melting points in agreement with the literature values.¹⁹

All n.m.r. spectra were determined either in carbon tetrachloride or acetone solutions using a Varian A-60 instrument operating at room temperature. The exception to this statement was the photodimer of anthracene which was determined at 180° in a naphthalene solution. All chemical shifts (Tables I and II) were in dilute solutions (10% or less). Coupling constants and values of J_{C1-H} were determined on somewhat more concentrated solutions. The value of J_{C1-H} for *o*-xylene was determined for the neat liquid.

Spectral Analyses. The n.m.r. spectrum of triptycene in acetone consists of a slightly broadened singlet at τ 4.40 and a nearly symmetrical A_2B_2 pattern centered about τ 2.75. The downfield half of the aromatic proton pattern showed slight broadening owing to a long-range coupling with the bridgehead protons. In the most exact sense, this weak long-coupling effect should be included in the calculation of the ring proton spectrum. However, this would place the analysis beyond the capabilities of our four-spin computer program. Consequently, the upfield half of the spectrum was analyzed as half of a true A_2B_2 system. We have previously used this approximation with good results.²⁰

The details of the analysis of A_2B_2 spectra have been covered elsewhere.²¹ All calculations were carried

(13) J. I. Musher, *Mol. Phys.*, **6**, 94 (1963).

(14) K. Tori, R. Muneyuki, and H. Tanida, *Can. J. Chem.*, **41**, 3142 (1963).

(15) See, however, G. Karabatsos, *J. Am. Chem. Soc.*, **86**, 3574 (1964).

(16) P. D. Bartlett and E. S. Lewis, *ibid.*, **72**, 1005 (1950).

(17) W. J. Middleton, R. E. Heckert, E. L. Little, and C. G. Krespan, *ibid.*, **80**, 2783 (1958).

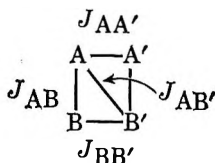
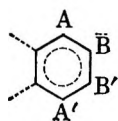
(18) R. Luther and F. Weigert, *Chem. Zentr.*, **75**, 117 (1904).

(19) O. Diels and K. Alder, *Ann.*, **486**, 191 (1931).

(20) W. B. Smith and B. A. Shoulders, *J. Am. Chem. Soc.*, **86**, 3118 (1964).

(21) D. M. Grant, R. C. Hirst, and H. S. Gutowsky, *J. Chem. Phys.*, **38**, 470 (1963), and references therein.

out with the aid of the FREQUENT IV A 1620 program on an IBM 1620 computer. The notations pertinent to the discussion are



$$\begin{aligned} N &= J_{AB} + J_{AB'} \\ L &= J_{AB} - J_{AB'} \\ K &= J_{AA'} + J_{BB'} \\ M &= J_{AA'} - J_{BB'} \\ \Delta_{AB} &= \nu_A - \nu_B \end{aligned}$$

The assignment of the spectral lines and determination of the above parameters followed conventional procedures.²¹ The sum and difference relationships for lines 1 and 3 gave values for both N and Δ_{AB} directly. The near degeneracy of the pairs 8,12; 7,11; 6,10; and 5,9 indicated that K and M are very nearly the same and have a value close to the difference between lines 8,12 and 7,11 or 6,10 and 5,9. The value of L was determined by trial. Both K and L were adjusted so that no line was on error by more than 0.2 c.p.s. The results of this and related cases are given in Table II.

The analysis of the spectrum of 9,10-dihydroanthracene appeared at first to be a formidable task

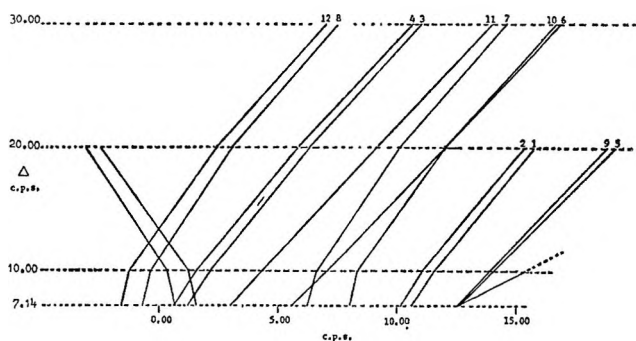


Figure 2. The change in the triptycene spectrum with decreasing values of Δ_{AB} .

since the value of Δ_{AB} is quite small. Since there seemed to be no great variation among the reported coupling constants of *ortho*-disubstituted benzenes, it was assumed that no great change would be observed between the values for triptycene and 9,10-dihydroanthracene. The movement of individual lines was followed using the triptycene coupling constants and progressively smaller values of Δ_{AB} (Figure 2). Once the line assignments were made, the analysis proceeded in a conventional fashion.

Acknowledgment. We wish to acknowledge the generous financial aid of the Robert A. Welch Foundation in support of this work.

Abstraction Reactions of Hydrogen and Deuterium Atoms:

Mercury-Photosensitized Decomposition of Mixtures of Cyclohexane and Cyclohexane- d_{12}

by Robert R. Hentz, Joseph Y. Chang, and Milton Burton

Department of Chemistry and Radiation Laboratory,¹ University of Notre Dame, Notre Dame, Indiana 46556
(Received January 4, 1965)

Hg-photosensitized decomposition of mixtures of cyclohexane and cyclohexane- d_{12} yields information regarding isotope effects in the primary process and in abstraction reactions of H and D atoms acting on C_6H_{12} and C_6D_{12} . At 12° in the gas phase, production of the H atom is ~ 13 times more probable than production of the D atom, and abstraction of the H atom is ~ 16 times as probable as abstraction of the D atom. A defined parameter $f \equiv (\text{HD yield})^2/(\text{H}_2 \text{ yield})(\text{D}_2 \text{ yield})$ is shown to be ≥ 4 in the gas phase, as expected from theoretical consideration of purely atomic abstraction reactions, but < 4 in liquid phase photosensitization and radiolysis. The latter result may be ascribed to some "molecular decomposition" in radiolysis, but a more realistic view with respect to photosensitization is that possible cage effects in the liquid phase (perhaps involving short-lived HgH) so affect the probability of reaction of the H (or D) atom with its sibling radical that a distinction from molecular decomposition is largely semantic.

Introduction

Study of the ratio of yields $H_2:HD:D_2$ from radiolysis of mixtures of pure hydrocarbons and their completely deuterated analogs does, in principle, provide some insight into the elementary decomposition processes.² However, the method requires some calibration. Fortunately, the mercury-photosensitized decomposition of gaseous cyclohexane seems to provide a well-understood and relatively simple case. According to Beck, Kniebes, and Gunning,³ the products (H_2 , cyclohexane, and bicyclohexyl) can be satisfactorily explained on the basis of energy transfer from excited $Hg(6^3P_1)$ to C_6H_{12} , rupture of a C-H bond, H atom abstraction reactions, and disproportionation and combination reactions of cyclohexyl radicals. Ring cleavage of any kind was not observed. Because this system appears to be one of a few in which all hydrogen is produced by abstraction reactions of H atoms, it is possible to establish and to test certain kinetic criteria characteristic of "all-atomic" reaction processes.

The technique here employed is merely to test the

yields of H_2 , HD, and D_2 in the mercury-photosensitized decomposition of $C_6H_{12} + C_6D_{12}$. Earlier data on the activation energies of the reactions involved appear too uncertain⁴ for purposes of prediction in this case. Consequently, a part of the effort has been in setting up the consequences of the relatively simple elements of the kinetics and in testing them for the gaseous decomposition. In a second stage of the work, the method is extended to the liquid mixture, and the results are interpreted.

Experimental

Materials. Eastman Spectro Grade cyclohexane was

(1) The Radiation Laboratory of the University of Notre Dame is operated under contract with the U. S. Atomic Energy Commission. This is A.E.C. Document No. COO-38-374.

(2) S. Gordon and M. Burton, *Discussions Faraday Soc.*, **12**, 88 (1952).

(3) P. W. Beck, D. V. Kniebes, and H. E. Gunning, *J. Chem. Phys.*, **22**, 672 (1954). Cf. also H. E. Gunning and O. P. Strausz, *Advan. Photochem.*, **1**, 209 (1963).

(4) E. W. R. Steacie, "Atomic and Free Radical Reactions," Vol. I, Reinhold Publishing Corp., New York, N. Y., 1954, Section V-25.

purified by passage through a silica gel column and vacuum distillation at ice-water temperature. Cyclohexane- d_{12} was obtained from Merck and Co. of Canada. Mass spectrometric analysis of the latter sample indicated approximately 7.4% of $C_6D_{11}H$ isotopic impurity or a D atom content >99%. Mixtures of C_6H_{12} and C_6D_{12} in small quantities were prepared in the liquid state; their actual compositions were determined by mass spectrometric analysis of the vapor. For the liquid studies, it was assumed, with sufficient accuracy, that the vapor pressures of the two compounds are equal and that compositions of the vapor and liquid phases are identical.

Light Source and Procedures. The mercury lamp used in this work was a Hanovia SC 2537 helical grid type. A quartz tube of 25-mm. diameter with an inlet and outlet for water, fitted into the central space of the helical coil of the lamp, served as a constant-temperature jacket. Temperature was read with a thermometer fitted through a rubber stopper at the bottom end. During irradiation the cell was fitted in from the top end of the water jacket and immersed in running water of constant temperature.

The irradiation cell, made of Vycor, with a 4–5-mm. i.d., 8-cm. length, and a total volume of ~ 1.5 cc., was connected through a graded seal to a Pyrex vessel with a total vapor space of approximately 250 cc. The large ratio, ~ 170 , of total vapor space to volume of the irradiation cell served to eliminate experimental difficulties connected with secondary reactions.

Mixtures of cyclohexane vapors were irradiated at saturation pressure at 12° . Small amounts (0.15–0.2 ml.) of liquid mixtures were transferred into the cell containing some droplets of clean Hg and were degassed by the conventional freezing-out technique. During irradiation, the excess liquid was trapped in the Pyrex vessel by a cold finger with cooling water at 12° . No measurement of absolute intensities was made.

Preliminary experiments were performed to determine the effect of products on the composition of hydrogen formed by irradiation. In one experiment a cyclohexane mixture was irradiated for intermittent intervals. After each period of irradiation, gases non-condensable at -196° were collected and analyzed; then the unreacted cyclohexanes with condensable products was again irradiated. The rate of total hydrogen production was found to decrease slightly as accumulated exposure increased, a result similar to that found in experiments in which only C_6H_{12} was irradiated. (Beck, Kniebes, and Gunning³ have attributed this effect to accumulation of cyclohexene.) However, the composition of the hydrogen mixture remained invariant with increase in accumulated exposure

within the experimental accuracy. Similar results were obtained with separate samples of a given cyclohexane composition which were irradiated for different periods of time. In another experiment an amount of H_2 comparable to that expected in the irradiation was added to a cyclohexane mixture. Subtraction of this amount of added H_2 after irradiation gave the same hydrogen composition as was obtained on irradiation of the same mixture without added H_2 . Thus, the hydrogen products do not enter into the kinetics of hydrogen formation. Nevertheless, in order to avoid complications, it was considered important to keep the partial pressures of products as low as possible. The irradiation time was kept short, varying from 3 to 30 min.; in this period, sufficiently large amounts of products (1–4 μ -moles) were produced for accurate mass spectrometric analysis. With all other factors unchanged, the light absorbed by the cyclohexane vapor is proportional to the volume of the irradiation cell, and the concentration of the products is inversely proportional to the volume of the total vapor space. Thus, increase of the volume of the vapor phase very effectively decreased the product:reactant concentration ratio. Under the conditions employed this ratio was smaller than 10^{-3} .

For comparison with gas phase results, some preliminary liquid phase experiments were performed with three samples containing 0.25, 0.50, and 0.77 mole fraction of deuterated cyclohexane. Samples, of ~ 1.6 cc. volume, with added droplets of mercury were introduced into a Vycor cell attached to a small Pyrex condenser through a graded seal. The condenser, fitted with a breakoff seal, was attached to the vacuum line, and samples were degassed by repetitions of the standard freeze, pump, and thaw technique. The cell was then sealed off above the condenser and inserted inside the helical coils of the Hanovia lamp which, in turn, was enclosed in a box. Compressed air, cooled by a large ice bath, was blown through the box, and cooling water was circulated through the condenser which surmounted the Vycor cell. In the 1-hr. irradiations, 5–10 min. was required for the cell to reach the steady-state temperature of $48 \pm 2^\circ$. One liquid phase experiment was performed with 0.77 mole fraction of deuterated cyclohexane at 15° in the same system used for gas phase experiments.

H_2 , HD, and D_2 , the only products of present interest, were determined mass spectrometrically. No other gaseous products were observed. Cyclohexene and bicyclohexyl are the only other known products. Because these were not pertinent to our study and because the isotopic compositions of these compounds in micromole quantities could not be determined conveniently, no effort was made to examine them. In

preliminary experiments, however, bicyclohexyl was found by gas chromatographic technique to be approximately 70% of the total hydrocarbon products, in agreement with the results of Beck, Kriebes, and Gunning.³

Results

The main body of experimental results was obtained at 12°; the percentages of isotopic hydrogen products obtained at this temperature are given in Figure 1 as a function of mole fraction of C₆D₁₂. Many of the single points represent average values for several experiments at the given mole fraction. Less extensive results obtained at higher temperatures are not shown in Figure 1, but they are considered in the Discussion.

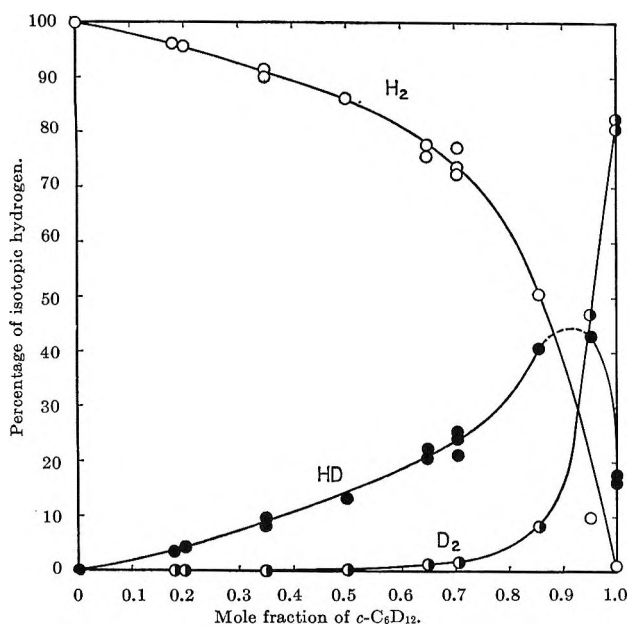
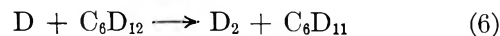
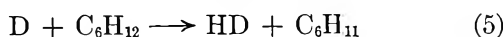
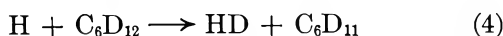
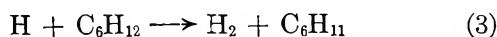
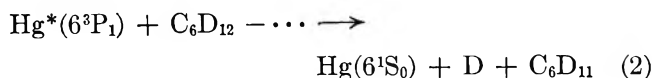
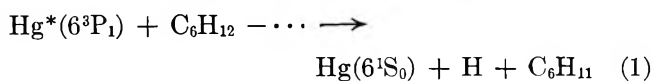


Figure 1. Percentages of isotopic hydrogens produced in vapor mixtures of *c*-C₆H₁₂ and *c*-C₆D₁₂ at 12°.

Discussion

Kinetic Considerations. If we neglect reactions between products, a simplified mechanism for hydrogen production in the photosensitized decomposition of gaseous C₆H₁₂ + C₆D₁₂ mixtures can be written as



The rates of production of H₂ and D₂ in any system, pure or mixed, are

$$\frac{d(\text{H}_2)}{dt} = k_3[\text{H}][\text{C}_6\text{H}_{12}]; \quad \frac{d(\text{D}_2)}{dt} = k_6[\text{D}][\text{C}_6\text{D}_{12}]$$

(where concentrations of the reactants are expressed in mole fraction), so that

$$\frac{d(\text{HD})}{dt} = k_4[\text{H}][\text{C}_6\text{D}_{12}] + k_5[\text{D}][\text{C}_6\text{H}_{12}] = \frac{k_4[\text{C}_6\text{D}_{12}]}{k_3[\text{C}_6\text{H}_{12}]} \frac{d(\text{H}_2)}{dt} + \frac{k_5[\text{C}_6\text{H}_{12}]}{k_6[\text{C}_6\text{D}_{12}]} \frac{d(\text{D}_2)}{dt}$$

Consequently, one may write the relationship

$$\frac{k_4[\text{C}_6\text{D}_{12}]}{k_3[\text{C}_6\text{H}_{12}]} \frac{\Phi(\text{H}_2)}{\Phi(\text{HD})} + \frac{k_5[\text{C}_6\text{H}_{12}]}{k_6[\text{C}_6\text{D}_{12}]} \frac{\Phi(\text{D}_2)}{\Phi(\text{HD})} = 1 \quad (7)$$

Thus, a plot of $[\text{C}_6\text{D}_{12}]\Phi(\text{H}_2)/[\text{C}_6\text{H}_{12}]\Phi(\text{HD})$ as ordinate vs. $[\text{C}_6\text{H}_{12}]\Phi(\text{D}_2)/[\text{C}_6\text{D}_{12}]\Phi(\text{HD})$ as abscissa should give a straight line with values of k_4/k_3 and k_5/k_6 determinable from the intercepts on ordinate and abscissa, respectively. Figure 2 shows such plots for data obtained in exposures at 12, 30, and 77°. In spite of scattering, linear relationships at each of the temperatures are apparent. The scattering is only partly attributable to lack of elaborate temperature control; it is mainly the result of extreme sensitivity to the parameters employed.⁵ The solid lines shown are least-square plots. Table I gives the values of k_3/k_4 and k_5/k_6 obtained; the results at the different tempera-

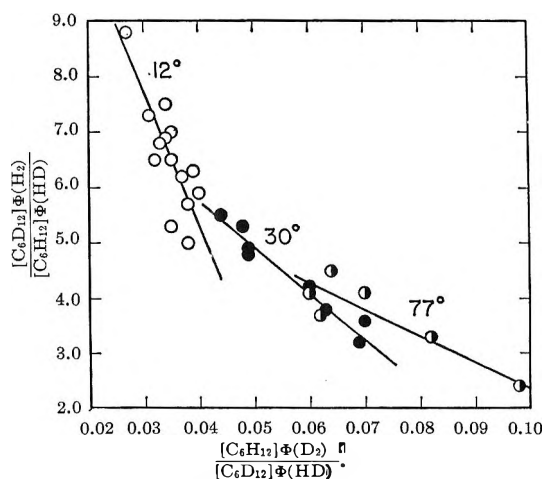


Figure 2. Analysis of hydrogen composition data.

(5) For example, at $[\text{C}_6\text{D}_{12}] < 0.5$ the D_2 fraction in the product is so small (cf. Figure 1) that the abscissa in Figure 2 could be as much as 30% in error. This statement is true also of the f values in Figure 4.

tures are not sufficiently precise to justify experimental evaluation of the corresponding differences in activation energy in this way.

Table I: Ratios of Atomic Abstraction Rate Constants^a Obtained from Plots in Figure 2

Temp., °C.	k_3/k_4	k_5/k_6
12 ± 0.4	15	16
30 ± 1	9	9
77 ± 3	7	7

^a Cf. Appendix.

The more extensive data obtained at 12° may be considered more reliable *in toto* than those reported for higher temperatures. Simple computations from collision theory for that temperature give the relationship between activation energies, $E_4 - E_3 \simeq E_6 - E_5 \simeq 1.6$ kcal. There are not many recent experimental results available on such isotopic abstraction reactions for comparison with our data. However, McNesby⁶ has reported results on isotopic effect in abstraction reactions of methyl radicals with ethane, ethane-*d*₆, and ethane-1,1,1-*d*₃. His results seem to be in qualitative agreement with ours. For a reaction pair such as



he reported $k_{\text{H}}/k_{\text{D}} = k_7/k_8 = \exp(1500/RT)$. At 12°, $k_7/k_8 = 14$. McNesby also concluded that the same relationship applies to similar abstraction reactions of methyl radicals in a number of systems. For a different type of hydrocarbon, C₆H₅CHDCH₃, Herk and Szwarc⁷ reported $\Delta E = 1.56$ kcal. for the abstraction of H and D atoms by CH₃ radicals and 1.1 to 1.7 kcal. in a few other systems.

The value of k_1/k_2 may be calculated from

$$\frac{k_1}{k_2} = \frac{\Phi(\text{H}_2) [\text{C}_6\text{D}_{12}] 1 + k_4[\text{C}_6\text{D}_{12}]/k_3[\text{C}_6\text{H}_{12}]}{\Phi(\text{D}_2) [\text{C}_6\text{H}_{12}] 1 + k_5[\text{C}_6\text{H}_{12}]/k_6[\text{C}_6\text{D}_{12}]} \quad (\text{II})$$

Substitution of $k_3/k_4 = 15$ and $k_5/k_6 = 16$ gives $k_1/k_2 = 13$ at 12° (average of values calculated at four mole fractions of C₆D₁₂: 0.50, 0.65, 0.706, 0.857).

Similar isotope effects have been reported by Dorfman and co-workers⁸ for Hg-photosensitized decomposition of C₄H₁₀-C₄D₁₀ mixtures. It was found that for the reactions in butane, analogous to our reactions 1-6, $k_1/k_2 \approx k_3/k_4 \approx k_5/k_6 \approx 20$. Those authors speculate that the value of k_1/k_2 may indicate a mechanism involving abstraction by excited mercury to form HgH

and HgD in the primary process. Gunning and his co-workers⁹ have reported isotope effects in quenching of Hg*(6³P₁) by a large number of substances and give a value of 14.3 at 25° for C₆H₁₂ relative to C₆D₁₂. They relate the efficiency of energy transfer to the chemical nature of Hg*(6³P₁).¹⁰ For saturated hydrocarbons good agreement is obtained between measured isotope effects in quenching and those calculated from absolute rate theory, assuming a linear transition state (C-H-Hg) for quenching that would also be applicable to an abstraction reaction.

We have not been able to obtain ratios such as k_3/k_5 from our data.

The accuracy of the calculated rate constant ratios depends on the extent to which processes other than those assumed (*e.g.*, combination at the walls or disproportionation of hydrogen atoms with cyclohexyl radicals) contribute to hydrogen formation. By examination of the kinetics of the possible competing processes, choosing plausible values for the various kinetic parameters, it is possible to argue that hydrogen formation by such other processes would not be sufficient to affect the calculated rate constant ratios appreciably. In view of the numerous uncertainties involved, such detailed and extensive examination does not seem justified. A high order of accuracy is not claimed for the rate constant ratios. Nevertheless, agreement with comparable published values (in some cases for quite different experimental conditions; *cf.* ref. 8) is reasonably good. In the next section, the behavior of *f* values is shown to conform with that expected on the basis of the calculated rate constant ratios.

Distribution Parameter f. We define a parameter

$$f \equiv \frac{(\text{HD})^2}{(\text{H}_2)(\text{D}_2)} \quad (\text{III})$$

where the quantities in parentheses signify yields in any arbitrary units in any single experiment. It can be shown from the expressions for rates of H₂, D₂, and HD production that for relatively small production of those compounds

$$f = \frac{1}{k_3k_6} \left(2k_4k_5 + k_4^2Y + k_5^2 \frac{1}{Y} \right) \quad (\text{IV})^{11}$$

(6) J. R. McNesby, *J. Phys. Chem.*, **64**, 1671 (1960).

(7) L. Herk and M. Szwarc, *J. Am. Chem. Soc.*, **82**, 3558 (1960).

(8) E. G. Spittler, P. Jordon, L. M. Dorfman, and M. C. Sauer, Jr., *J. Phys. Chem.*, **67**, 2235 (1963).

(9) M. G. Bellas, Y. Rousseau, O. P. Strausz, and H. E. Gunning, *J. Chem. Phys.*, **41**, 768 (1964).

(10) Y. Rousseau, O. P. Strausz, and H. E. Gunning, *ibid.*, **39**, 962 (1963).

(11) This is a general equation applicable in any similar case where H₂, HD, and D₂ are formed exclusively by atom abstraction reactions (or their equivalent) and where all C-H bonds in the hydrocarbon (as well as all C-D bonds in the deuteriocarbon) are equivalent.

where

$$Y = \frac{k_1 k_5 + (k_6 - k_5)N_D}{k_2 k_3 + (k_4 - k_3)N_D} \quad (\text{V})$$

in which N_D is the mole fraction (of hydrocarbon) which is completely deuterated.¹²

When scavenger S (such as cyclohexene, which is a product) is present and scavenging reactions such as



must also be considered, f has the same form as in (IV), except that reactions 9 and 10 must be specifically considered. For $[\text{S}] \ll [\text{C}_6\text{H}_{12} + \text{C}_6\text{D}_{12}]$, Y has the form

$$Y = Y_S \approx \frac{k_1 k_5 + (k_6 - k_5)N_D + k_{10}N_S}{k_2 k_3 + (k_4 - k_3)N_D + k_9 N_S} \quad (\text{VI})$$

where N_S is the mole fraction of scavenger.

In the present case, eq. V is an adequate description of Y . Nevertheless, the behavior of f can be complicated. For the condition $k_2/k_4 = k_5/k_6$, $Y = k_1 k_6 / k_2 k_4$ so that (irrespective of concentrations) f has the constant value

$$f = 2 + \frac{k_1/k_2}{k_3/k_4} + \frac{k_3/k_4}{k_1/k_2}; \quad k_3/k_4 = k_5/k_6$$

The value of the constant depends on k_1/k_2 . Its minimum value (when $k_1/k_2 = k_3/k_4$) is 4.

Successive differentiation of eq. IV with detailed examination of the meaning of the results yields precise notions as to the allowed values of k_1/k_2 , k_3/k_4 , and k_5/k_6 . Thus, it can be shown that the complete curve of f vs. N_D (extending into the experimentally unrealizable regions where $N_D < 0$ and $N_D > 1$) has both a maximum and a minimum. Irrespective of the actual k values, the b values rather surprisingly are

$$f_{\max} = 0$$

$$f_{\min} = 4k_4k_5/k_3k_6$$

It appears that the location of the maximum is without experimental significance but that the value of the minimum is a criterion of mechanism and that its location reveals much regarding isotope effects. The treatment, of course, considers only cases in which the k values are positive.

The location of f_{\max} is worthy of note. Figure 3 shows a curve in which the values taken are $k_1/k_2 = 13$ (note use of eq. II), $k_5/k_6 = 16$, and $k_3/k_4 = 15$. The maximum occurs between discontinuities at $N_D = k_5/(k_5 - k_6)$ and $k_3/(k_3 - k_4)$, *i.e.*, in the case shown between the unrealizable 16/15 and 15/14.

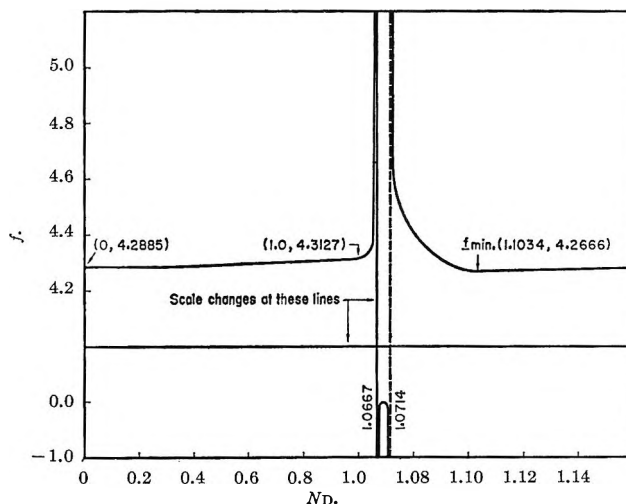


Figure 3. Illustration of the predicted dependence of distribution parameter f on mole fraction of $c\text{-C}_6\text{D}_{12}$ for $k_1/k_2 = 13$, $k_3/k_4 = 15$, and $k_5/k_6 = 16$; $f \rightarrow 4.2872$ as $N_D \rightarrow \pm\infty$.

By contrast, f_{\min} is under certain conditions experimentally observable, and its location has mechanistic and quantitative implications. We define a new quantity, f_{least} , the lowest experimentally observable value (*i.e.*, in the range $0 < N_D < 1$); $f_{\text{least}} \geq f_{\min}$.

For the results of kinetic analysis at 12° shown in Table I, $f_{\min} = 4.267$ (theoretical). The location of f_{\min} depends on the value of k_1/k_2 . With $k_5/k_6 > k_3/k_4$, there are three cases to consider.

Case 1: $k_1/k_2 < k_3/k_4$. In this case, f_{\min} lies outside the realizable range of N_D , and f increases as N_D increases from 0 to 1.

Case 2: $k_3/k_4 \leq k_1/k_2 \leq k_5/k_6$. In this case, f_{\min} falls within the realizable range and shifts from location at $N_D = 0$ for $k_1/k_2 = k_5/k_4$ to location at $N_D = 1$ for $k_1/k_2 = k_5/k_6$.

Case 3: $k_1/k_2 > k_5/k_6$. In this case, f_{\min} lies in the unrealizable range between $N_D = 1$ and $N_D = k_5/(k_5 - k_6)$. The function f decreases as N_D increases from 0 to 1.

Unfortunately, f is very insensitive to change in N_D within the experimentally realizable range for $k_3/k_4 \approx k_5/k_6$. Values of f calculated from the experimental data at 12° are plotted in Figure 4. The dotted line represents the theoretical curve of Figure 3. Although there is considerable scatter in the experimental points, the data plot of Figure 4 does confirm an all-atomic mechanism with near equality of k_5/k_6 and k_3/k_4 but

(12) It is assumed in eq. V that the mole volume of the hydrocarbon is practically independent of the hydrogen-deuterium ratio; *e.g.*, it has the same value for both C_6H_{12} and C_6D_{12} .

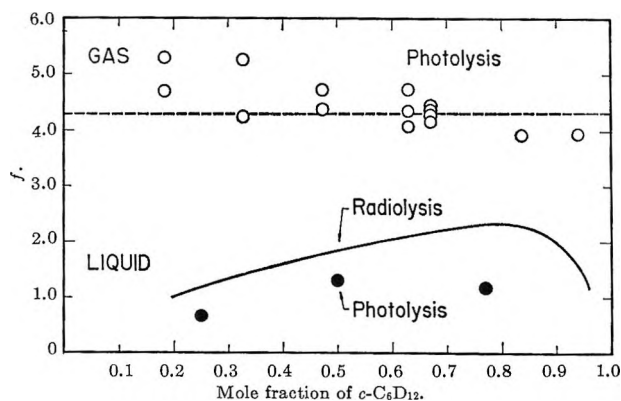
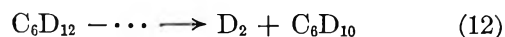
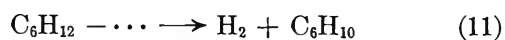


Figure 4. Distribution parameter f in mixtures of $c\text{-C}_6\text{H}_{12}$ and $c\text{-C}_6\text{D}_{12}$.

does not permit any precise confirmation of the value of k_1/k_2 .

Comparison with Radiolysis and Photosensitized Decomposition of Liquid. The f values for photosensitized decomposition of the vapor mixtures contrast sharply with f values obtained from liquid phase data on radiolysis and photosensitized decomposition; cf. Figure 4. The solid curve represents unpublished results obtained by irradiation with high-energy radiations. Data points are presented for three results of the Hg-photosensitized decomposition of the liquid at 48° ; in a single experiment at 15° a value of $f = 1.73$ was obtained at $N_D = 0.77$. Any possible temperature effect is outside present interest. It is sufficient to note that k_3/k_4 is approximately equal to k_5/k_6 in the range 12 to 77° in gas phase experiments (cf. Table I); therefore, the criterion of an all-atomic mechanism remains $f_{\min} \cong 4$ over this temperature range. Note also that all four f values obtained in liquid-phase Hg photosensitization lie below the f values obtained in room temperature radiolyses for the same values of N_D .

The occurrence of processes which yield H_2 and D_2 in a single decomposition act (so-called "molecular" processes), e.g.



in addition to reactions 3-6, can explain such data.¹³ If F_H and F_D represent the fractions of C_6H_{12} and C_6D_{12} decompositions, respectively, that form hydrogen *via* an atomic mechanism (i.e., reactions 3-6) then

$$f = \frac{2k_4k_5F_HF_D + k_4^2YF_H^2 + (k_5^2/Y)F_D^2}{k_3k_6(1 + \beta)} \quad (VII)$$

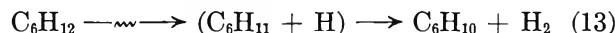
where

$$\beta = \frac{k_5(1 - N_D)(1 - F_D)}{k_6N_D} + \frac{k_4N_D(1 - F_H)}{k_3(1 - N_D)} + \frac{k_4k_5(1 - F_H)(1 - F_D)}{k_3k_6} \quad (VIII)$$

Clearly, $f = 0$ at $N_D = 0$ and $N_D = 1$; therefore, there must be a maximum within the experimentally realizable range of N_D , as is seen to be the case in Figure 4. It is possible by successive differentiation of f in eq. VII with respect to N_D to obtain a relationship between N_D at the maximum and the ratio $(1 - F_H)/(1 - F_D)$, which would permit an estimate of the relative contributions of "molecular" processes for comparison with measurements in radiolytic studies at the extremes of the N_D range¹³; however, the accuracy with which the maximum is in this case located does not appear adequate to warrant such an analysis.

Examination of eq. VII shows that, for any value of N_D , as F_H or F_D or both become smaller (i.e., as "molecular" processes contribute more), f decreases.

In radiation chemistry one can account for processes like (11) and (12) as representing both some decomposition directly into molecules¹⁴ and reactions of sibling atoms and radicals while they are still within the spur¹⁵; i.e., for example



The distinction between the two processes may be purely semantic. The evident increased importance of the apparently "molecular" process in the case of Hg photosensitization may be rationalized in straightforward fashion. Results have been presented^{13,16} which indicate that most of the hydrogen in radiolysis of cyclohexane is formed, in reactions 3-6, *via* "hot" hydrogen atoms and but little by thermal hydrogen atoms. Such "hot" hydrogen atoms would conform to the atomic mechanism with little or no isotope effect, and f would always exceed 4. Therefore, only the small truly molecular yield and the small yield of thermal hydrogen atoms reacting in the spur, as in reaction 13, contribute to the "molecular" yield in radiolysis. In the Hg-photosensitized decomposition a transient HgH may be formed with considerably lower probability of escape from the sibling radical than that of

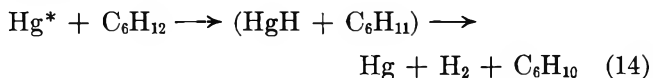
(13) This conclusion was reached independently by P. J. Dyne and W. M. Jenkinson, *Can. J. Chem.*, **39**, 2163 (1961), and by J. Y. Chang and M. Burton in unpublished work; cf. paper presented at 137th National Meeting of the American Chemical Society, Cleveland, Ohio, April 1960; also J. Y. Chang, Ph.D. Thesis, University of Notre Dame, June 1958.

(14) P. J. Dyne, *J. Phys. Chem.*, **66**, 767 (1962).

(15) J. W. Falconer and M. Burton, *ibid.*, **67**, 1743 (1963).

(16) S. Z. Toma and W. H. Hamill, *J. Am. Chem. Soc.*, **86**, 1478 (1964).

any hydrogen atom. Thus, the important "molecular" mechanism in mercury photosensitization would be in this case



and a similar reaction for C_6D_{12} . Kuntz and Mains have presented evidence for HgH in Hg-photosensitized decomposition of liquid hydrocarbons.¹⁷

As mentioned in the discussion following eq. VI, f has a minimum value when $k_1/k_2 = k_3/k_4 = k_5/k_6$. Because the primary isotope effect in radiolysis (equivalent to k_1/k_2) would be appreciably smaller¹³ than that for mercury photosensitization, the value of f in radiolysis for any particular mixture and for any particular values of F_{H} and of F_{D} must be greater than in photolysis. Thus, the relationship of the two lower curves in Figure 4 is what may be expected on such basis alone. It is not possible with the data at hand to make a direct comparison of F_{H} and F_{D} in those cases.

Acknowledgment. We are greatly indebted to Dr. J. W. Falconer for helpful criticism during the preparation of this paper for publication.

Appendix

The C_6D_{12} sample used in this work contained 7.4% of $\text{C}_6\text{D}_{11}\text{H}$ as isotopic impurity. Photosensitized de-

composition of such samples by Hg vapor produces isotopic hydrogens containing 1.1% of H_2 and 17.1% of HD; *i.e.*, there is a very large isotopic effect. We have in other (unreported) cases corrected for similar effects attributable to such isotopic impurities. Qualitative calculations performed in the present case showed that the effect of the $\text{C}_6\text{D}_{11}\text{H}$ impurity is important only at very small concentration of C_6H_{12} (*i.e.*, <5%). This result is not unexpected on the basis of the observed very large isotopic abstraction ratio (*cf.* k_3/k_4 and k_5/k_6) and the large ratio of primary decomposition constants, k_1/k_2 . In mixtures containing more than 5% of C_6H_{12} , the production of H atoms from $\text{C}_6\text{D}_{11}\text{H}$ is extremely small compared with that from reaction 1. A similar argument applies in consideration of secondary abstraction reactions. Because in all but one mixture used in this work the C_6H_{12} content is greater than 10 mole %, corrections for the effect of isotopic impurities are not expected to change the numerical results reported.

Repeated irradiation of a C_6D_{12} sample gave hydrogen products of decreasing H content, consistent with the large isotope effects observed. Such a procedure, followed by purification of the irradiated sample, could be utilized to minimize the H content of perdeuterated hydrocarbons.

(17) R. R. Kuntz and G. J. Mains, *J. Am. Chem. Soc.*, **85**, 2219 (1963).

Radiolysis of Benzene and Benzene-Cyclohexane Mixtures in the Presence of Nickel Tetracarbonyl

by Helmut F. Barzynski, Robert R. Hentz, and Milton Burton

Department of Chemistry and the Radiation Laboratory,¹ University of Notre Dame, Notre Dame, Indiana 46556
(Received January 9, 1965)

G values of hydrogen and biphenyl formation in γ -irradiated mixtures of benzene and nickel tetracarbonyl show that some excited benzene species are protected against decomposition by nickel tetracarbonyl. It is argued that two kinds of primary process contribute to the hydrogen yield: (1) a rapid unimolecular elimination of molecular hydrogen that is not quenched by carbonyl; (2) a process giving a second-order hydrogen yield that is associated with biphenyl formation and is quenched by carbonyl. Yields were determined for the major radiolysis products from benzene-cyclohexane mixtures containing nickel tetracarbonyl at fixed electron fraction (ϵ 0.68) at different electron fractions of each hydrocarbon in the range ϵ 0 to 0.32. At ϵ (nickel tetracarbonyl) 0.68 most of the cyclohexane decomposition is inhibited; the residual decomposition of the cyclohexane is to a major extent by rearrangement to ultimate molecules and to a minor extent by rupture into free radicals and atoms. These residual decomposition processes are not appreciably quenched by further addition of either protective agent. The suppression of products by benzene, in this case, represents actual scavenging of free radicals and atoms.

Introduction

Nickel tetracarbonyl seems to possess remarkable resistance to decomposition by ultraviolet light² and γ -radiation.³ Flash photolysis studies indicate that this appearance of resistivity is the result of a rapid back reaction between the primary decomposition products, nickel tricarbonyl and carbon monoxide.⁴ The fact that nickel tetracarbonyl has an electron-impact ionization potential of 8.64 e.v.,⁵ below that of either benzene or cyclohexane, suggests that it can act as a chemically inert energy sink and thus, by its presence, protect other substances from radiolysis. A study of the radiolysis of mixtures of cyclohexane and nickel tetracarbonyl has indeed shown that the latter protects cyclohexane very effectively.⁶ The possibility that it might likewise truly protect a protective agent like benzene is intriguing. Accordingly, this paper reports a limited study of the radiolysis process in solutions of nickel tetracarbonyl containing benzene and benzene plus cyclohexane.

Experimental

Phillips Spectrograde cyclohexane was purified by successive steps of distillation through a spinning-band column and by preparative vapor-phase chromatography with a silicone grease column (Aerograph Autoprep Model 700). Benzene was purified by crystallization. K and K nickel tetracarbonyl was used without further purification.

Five-milliliter samples, in glass ampoules fitted with breakseals, were degassed by repeated freeze-thaw cycles on a vacuum line prior to seal-off and then

(1) The Radiation Laboratory of the University of Notre Dame is operated under contract with the Atomic Energy Commission. This is A.E.C. document no. COO-38-368.

(2) A. P. Garratt and H. W. Thompson, *J. Chem. Soc.*, 1817 (1934).

(3) H. Barzynski and D. Hummel, *Z. physik. Chem.* (Frankfurt), **38**, 103 (1963).

(4) A. B. Callear, *Proc. Roy. Soc. (London)*, **A265**, 71 (1961).

(5) R. E. Winters and R. W. Kiser, *Inorg. Chem.*, **3**, 699 (1964).

(6) H. Barzynski and D. Hummel, *Z. physik. Chem.* (Frankfurt), **39**, 148 (1963).

irradiated in a 10-ke. ^{60}Co source at a dose rate of $\sim 2 \times 10^{18}$ e.v. $\text{g}^{-1} \text{min}^{-1}$ depending on the electron density of the solution. For solutions of nickel tetracarbonyl in benzene doses up to 3.6×10^{20} e.v. g^{-1} were used, and for solutions in benzene plus cyclohexane doses up to $\sim 2 \times 10^{21}$ e.v. g^{-1} were used. Dosage was established by Fricke dosimetry using $G(\text{Fe}^{+3}) = 15.6$ and a correction factor equal to the electron density of the particular solution relative to that of the dosimeter. A small amount of carbon monoxide is formed in unirradiated samples as the result of thermal decomposition; it was found that such an amount was without effect on the radiolysis of the pure hydrocarbons. The amount of carbon monoxide in irradiated samples was not measurably different from that in unirradiated samples and was independent of dose.

Mass spectrometric analysis of gas noncondensable at -196° gave the hydrogen yields. Liquid products were determined by liquid-vapor chromatography. No products related to nickel tetracarbonyl could be detected.

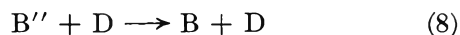
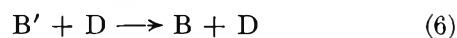
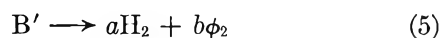
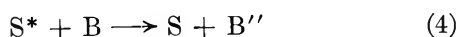
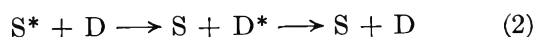
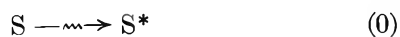
Results

Figure 1 shows plots of G values (100-e.v. yields) of hydrogen and biphenyl as a function of electron fraction, ϵ , of $\text{Ni}(\text{CO})_4$ dissolved in benzene. Chromatographic peaks corresponding to hydrogenated biphenyls were observed, but positive identifications were not made. $\text{Ni}(\text{CO})_4$ reduced the hydrogenated biphenyl areas much more than the biphenyl areas. At $\epsilon[\text{Ni}(\text{CO})_4] < \sim 0.20$, irradiation caused the samples to become yellow. Addition of irradiated benzene to unirradiated $\text{Ni}(\text{CO})_4$ did not yield a yellow color.

Figures 2 and 3 show G values for the major radiolysis products in solutions of $\text{Ni}(\text{CO})_4$ in benzene plus cyclohexane. In this portion of the work the $\text{Ni}(\text{CO})_4$ electron fraction was fixed at ~ 0.68 ; the electron fraction of each hydrocarbon was varied from zero to ~ 0.32 . The abscissas show the electron fraction of benzene relative to that of total hydrocarbon in the solution.

Discussion

Nickel Tetracarbonyl and Benzene. With the objective of generality, we present the equations



Reaction 0 represents energy deposition in the system S to give some unspecified state (or compendium of states) S^* . Reaction 1 represents all internal conversion processes of S^* which do not yield product. Reaction 2 represents quenching of the excited system (*i.e.*, unproductive dissipation of the energy of the system)

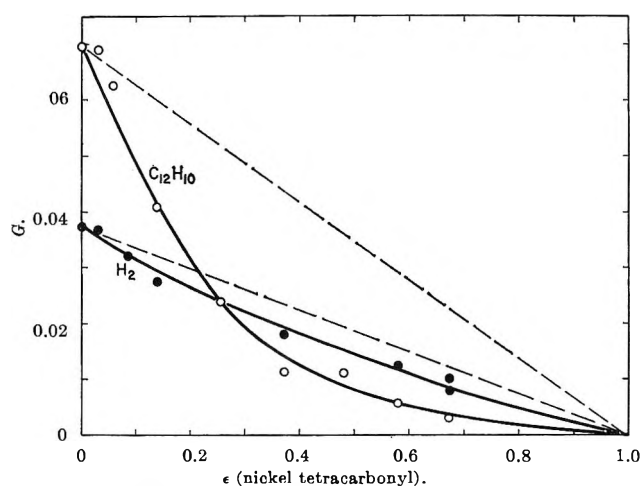


Figure 1. Hydrogen and biphenyl yields in mixtures of benzene and nickel tetracarbonyl.

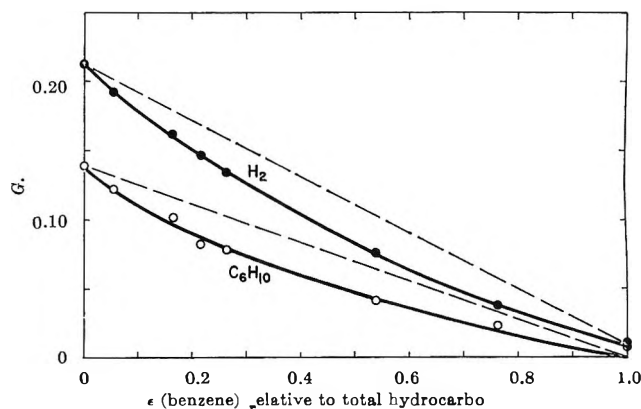


Figure 2. Hydrogen and cyclohexene yields in mixtures of benzene, cyclohexane, and nickel tetracarbonyl with carbonyl electron fraction equal to 0.68 in all mixtures.

(7) No special significance is attached to the use of electron fraction as a measure of relative concentration. It is selected entirely as a convenience because so much other work has been reported on this basis. Certainly, in this case, its use appears without special theoretical significance. Cf. A. G. Maddock, *Discussions Faraday Soc.*, 12, 118 (1952); M. Burton, *ibid.*, 36, 7 (1963).

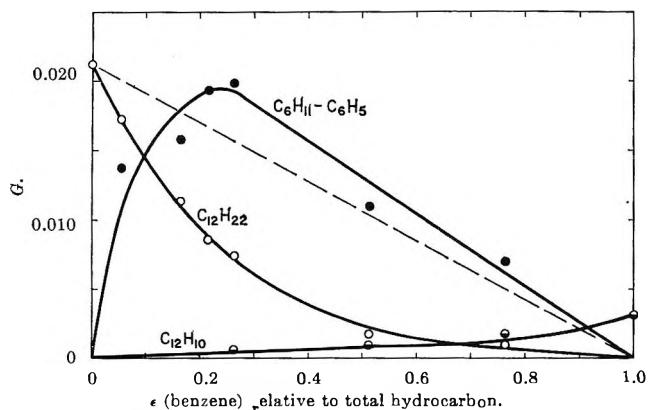
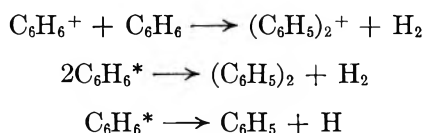


Figure 3. Bicyclohexyl, biphenyl, and phenylcyclohexane yields in mixtures of benzene, cyclohexane, and nickel tetracarbonyl with carbonyl electron fraction equal to 0.68 in all mixtures.

by localization of energy on molecules of the protective agent D, in this case $\text{Ni}(\text{CO})_4$. Reactions 3 and 4 are processes in which energy of the excited system is localized on molecules of B (*i.e.*, benzene) to yield two excited states of the latter. The fraction of deposited energy localized on B is determined by some unspecified function of $\text{Ni}(\text{CO})_4$ concentration, $f_c([\text{D}])$.

Figure 1 shows that biphenyl yields are reduced by added carbonyl to a considerably greater extent than are hydrogen yields. Consider that some function of $\text{Ni}(\text{CO})_4$ concentration, $f([\text{D}])$, other than electron fraction, exists and may be chosen as abscissa in Figure 1 so that each point on the hydrogen curve would be translated horizontally to the dashed hydrogen line. Then each corresponding point on the biphenyl curve would be translated an equal number of units along the abscissa. Cursory examination of Figure 1 shows that the biphenyl curve would still fall well below the dashed biphenyl line. Thus, even if $f([\text{D}])$ were identical with $f_c([\text{D}])$,⁸ the conclusion would be that there must be a process involving localization of excitation in benzene molecules which thereupon yield biphenyl and that such excited benzene molecules are quenched by $\text{Ni}(\text{CO})_4$. This reaction (6) is not to be confused with reaction 2.

According to Dyne and Jenkinson,⁹ $G(\text{H}_2) = 0.038$ from benzene can be separated into a first-order $G_1 = 0.02$ and a second-order $G_2 = 0.018$. It seems likely that any second-order process which gives hydrogen would be associated with biphenyl formation, for example



The effect of suppression of such reactions by $\text{Ni}(\text{CO})_4$ would be corresponding reductions of hydrogen and biphenyl yields. The actual amounts of reduction would depend on the competing processes by which the free radicals and atoms might otherwise disappear. Further, it seems reasonable that G_1 would correspond to a process not associated with biphenyl formation (*e.g.*, $\text{C}_6\text{H}_6^* \rightarrow \text{C}_6\text{H}_4 + \text{H}_2$). A logical inference is that $f([\text{D}]) \cong f_c([\text{D}])$ and that to some degree, after localization of energy on benzene, nickel carbonyl suppresses a second-order hydrogen yield associated with biphenyl formation. Thus, excited benzene may decompose in two processes to yield both H_2 and Φ_2 in one reaction (5) or just H_2 in the other (7). The processes 6 and 8 are quenching (*i.e.*, protective) processes; it is assumed consistently with the small effect of $\text{Ni}(\text{CO})_4$ on H_2 yield that the rate $r_8 = 0$.

In benzene, neither radiosensitized decomposition of metal perphenyls¹⁰ nor radiosensitized luminescence of scintillators¹¹ affects product yields from the benzene itself. Such results tend to confirm the notion that decomposition in irradiated benzene occurs very rapidly either before neutralization of the parent ion or from a highly excited molecule. Thus, interference with such decomposition processes requires the presence of a sufficiently high concentration of additive either to compete with localization of energy on benzene and thus to prevent formation of the labile species or to compete by energy transfer with the rapid decomposition of the labile species after localization. The states involved in decomposition of benzene are clearly not those involved in luminescence studies; for the latter, a long lifetime exceeding 15 nsec. has been measured.^{10,12}

Appearance of a yellow color at low concentrations of carbonyl suggests some reaction of carbonyl with a benzene species, formation of which is suppressed at higher carbonyl concentrations.

Nickel Tetracarbonyl and Benzene Plus Cyclohexane. In cyclohexane at 0.01 electron fraction of carbonyl, the value of $G(\text{C}_6\text{H}_{10})/G(\text{C}_{12}\text{H}_{22})$ remains essentially the same as in pure cyclohexane, 1.7, but the G values are reduced by 75%.⁶ Such a result suggests a com-

(8) Note that $f([\text{D}])$ would then correspond to a relative cross section for localization of deposited energy on benzene less than that corresponding to the use of electron fraction; use of electron fraction corresponds to a relative cross section that is one-half of that corresponding to the use of mole fraction.

(9) P. J. Dyne and W. M. Jenkinson, *Can. J. Chem.*, **40**, 1746 (1962).

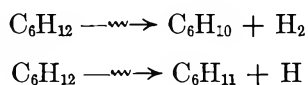
(10) D. B. Peterson, T. Arakawa, D. A. G. Walmsley, and M. Burton, to be published. For sensitized decomposition of metal perphenyls, $G \approx 1$ at concentrations of ≈ 1 mole %.

(11) M. Burton and W. N. Patrick, *J. Chem. Phys.*, **22**, 1150 (1954); C. Reid, *ibid.*, **22**, 1947 (1954).

(12) Recent results of M. A. Dillon from this laboratory.

mon precursor for most of these products.¹³ However, at 0.68 electron fraction of Ni(CO)₄, $G(\text{C}_6\text{H}_{10})/G(\text{C}_{12}\text{H}_{22})$ becomes 6.4 (*cf.* Figures 2 and 3). It appears that processes of energy deposition and localization, as well as the nature of the species involved in decomposition and energy-transfer processes, may be quite different at very high carbonyl concentrations.

Figures 2 and 3 show that reduction of bicyclohexyl yield relative to that of cyclohexene is accentuated by the addition of benzene. Such results suggest the existence, at 0.68 electron fraction of Ni(CO)₄ in cyclohexane, of two residual cyclohexane decomposition processes not readily quenched by further addition of any protective agent



The "molecular" reaction is apparently predominant.

The suppression of all yields and formation of C₆H₁₁-C₆H₅ is then understandable in terms of scavenging of H and C₆H₁₁ by benzene; the small reduction of cyclohexene yield is consistent with a disproportionation to combination ratio of 1.3–1.5.¹⁴ The curves of dimer yields are similar to those in benzene-cyclohexane mixtures without additive.¹⁵ However, the maximum $G(\text{C}_6\text{H}_{11}\text{C}_6\text{H}_5)$ occurs at 0.25 electron fraction of benzene in excess carbonyl as compared to 0.12 in the system with no additive.¹⁵ This result is consistent with considerably greater excitation localization on benzene in the mixtures free of carbonyl as compared to mixtures in which carbonyl completely quenches states of cyclohexane responsible for most of the product yields.

(13) S. Z. Toma and W. H. Hamill, *J. Am. Chem. Soc.*, **86**, 1478 (1964).

(14) J. W. Falconer and M. Burton, *J. Phys. Chem.*, **67**, 1743 (1963); C. E. Klots and R. H. Johnsen, *Can. J. Chem.*, **41**, 2702 (1963).

(15) T. Gaeumann, *Helv. Chim. Acta*, **44**, 1337 (1961).

Mechanism of the Oxidation of Reducing Sugars (Hexoses) by Hexacyanoferrate(III) in Alkaline Medium and Lobry de Bruyn Transformation

by Narendra Nath and M. P. Singh

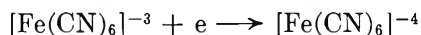
Department of Chemistry, University of Allahabad, Allahabad, India (Received January 6, 1965)

A general mechanism for the oxidation of reducing sugars (aldo- and ketohexoses) by alkaline potassium ferricyanide has been proposed. The rate equation has been derived as $-d[\text{Fe}(\text{CN})_6^{-3}]/dt = k[\text{S}][\text{OH}^-]$ where $[\text{S}]$ is the concentration of reducing sugar. Further, a single scheme governing the oxidation, as well as the interconversion of reducing sugars through a common intermediate, 1,2-enediol, has been advanced, which further suggests that the rates of oxidation of aldo and keto sugars are their corresponding rates of enolization.

Introduction

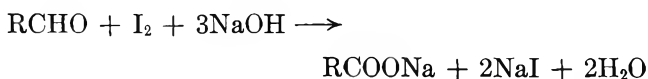
In recent years several oxidizing agents, specific and selective to varying degrees, have been added to the literature of organic chemistry. Selenium dioxide, aluminum alkoxide, osmium tetroxide, organic peracids, and potassium ferricyanide have greatly enhanced the skill of the organic chemist in introducing and attacking particular groups in simple or large molecules.

Potassium ferricyanide falls into the class of oxidizing agents comprising ceric sulfate, ammoniacal silver nitrate, and Fehling's solution, in all of which the oxidizing species is a complex electron-abstracting ion.



Consequently, ferricyanide has been used in systems obviously favored for oxidation in this manner, that is, extraction of an electron from an electron-rich site.

Most of the works in connection with the kinetics of oxidation of reducing sugars have been done by using halogens^{1,2} in alkaline and acidic media as oxidizing agents. In these oxidations the aldo sugars are oxidized directly to their corresponding aldonic acids as shown



Ingels and Israel³ have studied the kinetics of oxidation of simple monosaccharides as well as disaccharides

by alkaline hypiodide. Isbell and co-workers,^{4,5} while studying the kinetics of oxidation of different anomeric pairs of aldoses with aqueous bromine, found in general that β -forms react faster. Ingels and Israel³ have also reported that under certain conditions (pH about 9.2), the β -D-form is oxidized approximately 28 times faster than the α -D-anomer. However, Reeve⁶ has reported that the rate of mutarotation of the free sugars is greatly enhanced in alkaline solutions and, beyond the pH range of 11.8, becomes much faster than oxidation, the result being that under these circumstances both forms are oxidized at identical rates.

Further, the systematic studies of the kinetics of oxidation of D-glucose, D-galactose, D-fructose, L-arabinose, and D-xylose by cupric tartrate and cupric citrate in presence of sodium hydroxide were made in this laboratory by Singh, Krishna, and Ghosh.^{7,8} They have reported that the reaction is first order both with respect to the reducing sugar and hydroxyl ion and zero order with respect to the cupric complex. They have further

- (1) J. W. Green, *Advan. Carbohydrate Chem.*, **3**, 129 (1948).
- (2) F. Shafizadeh, *ibid.*, **13**, 9 (1958).
- (3) O. G. Ingels and E. C. Israel, *J. Chem. Soc.*, 810 (1948).
- (4) H. S. Isbell and W. W. Pigman, *J. Res. Natl. Bur. Std.*, **10**, 337 (1933).
- (5) H. S. Isbell and W. W. Pigman, *ibid.*, **18**, 141 (1937).
- (6) K. D. Reeve, *J. Chem. Soc.*, 172 (1951).
- (7) M. P. Singh, B. Krishna, and S. Ghosh, *Proc. Natl. Acad. Sci., India*, **A28**, 21, 39 (1959).
- (8) M. P. Singh, B. Krishna, and S. Ghosh, *Z. physik. Chem.*, **204**, 1 (1955); **205**, 285 (1956); **208**, 265 (1958).

observed that the reaction rate has an induction period and there is an autocatalysis due to the cuprous oxide produced in the system.

Marshall and Waters⁹ have studied the kinetics of D-glucose and acetoin oxidation by bivalent copper complexed with sodium and potassium tartrates, sodium citrate, and picolinic acid in presence of sodium hydroxide and sodium carbonate and have confirmed the results of Singh, Krishna, and Ghosh in case of D-glucose.

Experimental

The mixture of potassium ferricyanide and alkali was kept in a black-coated Jena bottle maintained at constant temperature within the limits of $\pm 0.1^\circ$ by an electrically operated thermostat, and the fresh solution of reducing sugar was also kept separately in the same bath to attain the temperature of the bath. The reaction was started by adding the quantity of sugar, and the time was measured with the stopwatch. Immediately, 10 ml. of the aliquot was taken out and poured into a beaker containing 5 ml. of 2 N sulfuric acid (Analar) to check the reaction. Then the remaining ferricyanide was titrated iodometrically. All the reducing sugars were of E. Merck grade except D-glucose which was of B.D.H. (Analar) grade. Also the potassium ferricyanide and sodium hydroxide used were of B.D.H. (Analar) grade. The number of equivalents of potassium ferricyanide required by one equivalent of D-glucose and D-fructose was found to be four. The experimental procedure has already been published.¹⁰

Results and Discussion

(a) *Kinetics of Oxidation of Reducing Sugars by Alkaline Ferricyanide.* The present authors¹⁰⁻¹² have studied the kinetics of oxidation of three aldohexoses (D-glucose, D-galactose, and D-mannose) and two ketohexoses (D-fructose and L-sorbose) by ferricyanide in presence of sodium hydroxide. It has been observed that the order of the reaction is zero with respect to the ferricyanide ion and first order both with respect to the reducing sugar and the hydroxyl ion. The reaction has also a small induction period which practically disappears by carrying out the reactions in an atmosphere of nitrogen. Hence, it has been concluded that this small induction period is due to the presence of oxygen, which partly oxidizes the ferrocyanide initially produced to ferricyanide.

The summarized tables (I-III) justify the preceding experimental results.

In all the sugars studied so far, the kinetics of the

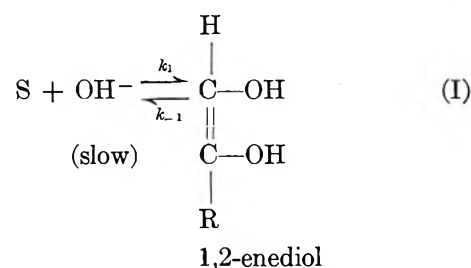
Table I: Effect of Varying the Ferricyanide Ion Concentration^a

Temp., °C.	Over-all concn. of sugar and alkali	Over-all concn. of ferricyanide $\times 10^4, M$	Mean zero-order $k_2 \times 10^4, M^{-1} \text{ min.}^{-1}$
30	D-Glucose 0.01 M	20.00	24.39
	NaOH 0.01 N	25.00	25.63
		33.00	24.58
30	D-Galactose 0.01 M	20.00	32.90
	NaOH 0.025 N	25.00	31.60
		33.00	31.40
30		50.00	31.50
	D-Mannose 0.005 M	20.00	33.80
	NaOH 0.05 N	25.00	32.09
30		33.00	32.02
	D-Fructose 0.005 M	20.00	38.40
	NaOH 0.0066 N	25.00	39.60
25		33.00	34.10
	L-Sorbose 0.005 M	20.00	34.84
	NaOH 0.0125 N	25.00	37.44
		33.00	37.00

^a Total volume of reaction mixture 200 ml. A perusal of the table shows that the reaction rates are independent of ferricyanide ion concentration.

reaction is so similar that the present authors are forced to formulate a single and simple mechanism.

Since the order of the reaction is zero with respect to the ferricyanide ion and first order both with respect to the hydroxyl ion and the reducing sugar in all the cases, it appears that the first step involves the reaction between the hydroxyl ion and the reducing sugar leading to the formation of an intermediate enediol which is subsequently oxidized by ferricyanide, the latter being a comparatively faster process, so that the reaction becomes zero order with respect to ferricyanide ion. Accordingly, the first step is the slow transformation of the sugar into the intermediate enediol as



(9) B. A. Marshall and W. A. Waters, *J. Chem. Soc.*, 2392 (1960).

(10) N. Nath and M. P. Singh, *Z. physik. Chem.*, **221**, 204 (1962).

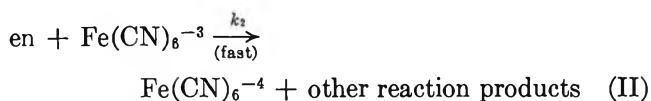
(11) N. Nath and M. P. Singh, *ibid.*, **224**, 419 (1963).

(12) N. Nath and M. P. Singh, *ibid.*, in press.

Table II: Effect of Varying the Sugar Concentration^a

Temp., °C.	Over-all concn. of NaOH, <i>N</i>	Over-all concn. of sugar × 10 ³ , <i>M</i>	<i>k</i> ₂ × 10 ⁶ , <i>M</i> ⁻¹ min. ⁻¹	$\frac{k_2}{[\text{sugar}]} \times 10^3$
D-Glucose				
30	0.01	20.00	44.26	2.21
		10.00	25.63	2.56
		5.00	12.69	2.53
D-Galactose				
30	0.0166	20.00	41.07	2.05
		10.00	23.53	2.35
		5.00	12.12	2.42
D-Mannose				
35	0.0125	10.00	27.34	2.73
		6.66	20.09	3.01
		5.00	14.65	2.93
D-Fructose				
25	0.0062	10.00	38.85	3.88
		5.00	19.65	3.93
L-Sorbose				
25	0.01	10.00	53.81	5.38
		6.66	41.07	6.16
		5.00	29.92	5.98

^a Total volume 200 ml.; over-all concentration of K₃Fe(CN)₆ is 0.0025 *M*. From the table it is obvious that the reaction rates are directly proportional to the reducing concentration.



where S and en represent the reducing sugar and intermediate enediol, respectively. Involving steps I and II

$$\frac{d(\text{en})}{dt} = 0 = k_1(\text{S})(\text{OH}^-) - k_{-1}(\text{en}) - k_2(\text{en})(\text{F}^{-3}) \quad (1)$$

at steady state.

$$-\frac{d(\text{F}^{-3})}{dt} = k_2(\text{en})(\text{F}^{-3}) \quad (2)$$

However, from (1)

$$k_2(\text{en})(\text{F}^{-3}) = k_1(\text{S})(\text{OH}^-) - k_{-1}(\text{en}) \quad (3)$$

Substituting (3) into (2) gives

$$-\frac{d(\text{F}^{-3})}{dt} = k_1(\text{S})(\text{OH}^-) - k_{-1}(\text{en}) \quad (4)$$

(F⁻³) does not appear on the right-hand side. Further, *k*₁ and *k*₋₁ may be of about the same order of magnitude,

Table III: Effect of Variation of Hydroxyl Ion Concentration

Temp., °C.	Over-all concn. of sugar, <i>M</i>	Over-all concn. of NaOH × 10 ³ , <i>N</i>	<i>k</i> ₂ × 10 ⁶ , <i>M</i> ⁻¹ min. ⁻¹	$\frac{k_2}{[\text{NaOH}]} \times 10^3$
D-Glucose				
30	0.01	25.00	54.80	2.19
		12.50	31.10	2.48
		10.00	23.30	2.33
D-Galactose				
30	0.01	25.00	32.04	1.28
		16.60	24.06	1.44
		12.50	17.50	1.40
D-Mannose				
35	0.01	10.00	13.01	1.30
		8.30	11.13	1.34
		25.00	40.42	1.61
D-Fructose				
35	0.01	16.60	30.02	1.80
		10.00	20.23	2.02
		8.30	16.80	2.02
L-Sorbose				
30	0.005	10.00	52.19	5.22
		8.30	47.19	5.68
		16.60	51.02	3.07
25	0.005	12.50	37.44	2.99
		10.00	29.92	2.99
		8.30	25.81	3.10
		6.66	22.98	3.45

^a Total volume 200 ml.; over-all concentration of K₃Fe(CN)₆ is 0.0025 *M*. From the results given in the table it is evident that the reaction rates are also directly proportional to hydroxyl ion concentration.

but (en) ≪ (S)(OH⁻) during most of the reaction because the over-all rate *k*₋₁ + *k*₂, which uses up en, is much larger than the rate *k*₁, which produces en. Therefore

$$k_1(\text{S})(\text{OH}^-) \gg k_{-1}(\text{en})$$

and

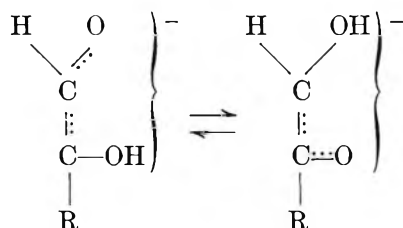
$$-\frac{d(\text{F}^{-3})}{dt} \cong k_1(\text{S})(\text{OH}^-)$$

This explains the direct proportionality of the reaction rate with respect to the reducing sugar and hydroxyl ion concentration and independence of the velocity of the reaction on the concentration of the ferricyanide ion.

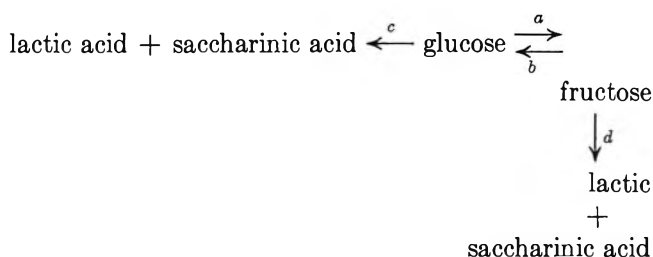
Evidence of an enediol form of sugars in alkaline solution is afforded by the ability of alkaline sugar solu-

tions to take up large quantities of iodine¹³ by the observation that sugars are oxidized with cleavage between C₁ and C₂ in alkaline solutions^{14,15} and by the studies of the ultraviolet absorption spectra (which show a maximum, characteristic of dicarbonyl compounds attributed¹⁶ to an enediol). Further evidence for the formation of an enediol is furnished by the observed ability of alkaline solutions of carbohydrates to decolorize solutions of 2,6-dichlorophenolindophenol.¹⁷

(b) *Lobry de Bruyn Transformation*. The classical transformation of Lobry de Bruyn and Alberda van Ekenstein¹⁸ is a base-catalyzed enolization giving an enediol which may either revert to the starting aldose or be converted to epimers of the original aldose. Nearly all of the investigations of the kinetics of this transformation have failed because of the complications imposed by side reactions (aldolization, degradation, etc.). The most commendable work is of Nef,¹⁴ Wolfrom and Lewis,^{13a} Sowden and Schaffer,¹⁹ and Bamford and Collins.²⁰ Bamford and Collins have studied the kinetics of interconversion and also degradation of glucose and fructose in strongly alkaline solution. They have suggested the existence of two enolate ions, considered to be in tautomeric equilibrium, instead of intermediate enediol.



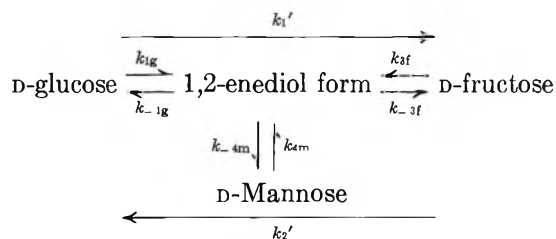
They have further calculated the forward and backward velocity constants in 1 *N* potassium hydroxide on the following scheme at 25 and 45°.



where *c* and *d* are the rate constants of degradation and *a* and *b* are the forward and backward rate constants for interconversion given as follows: *a* = 0.043 and 0.90 hr.⁻¹ at 25 and 45°, respectively; *b* = 0.045 and 0.82 hr.⁻¹ at 25 and 45°, respectively.

Now, if the rate of enolization is the rate of oxidation of reducing sugars, then the entire equilibrium between

D-glucose, D-fructose, and D-mannose may be represented as



where *k*₁' and *k*₂' are the forward and backward rate constants in the interconversion which are equivalent to *a* and *b* in the data of Bamford and Collins. *k*_{1g}, *k*_{3f}, and *k*_{4m} are the specific rate constants of the oxidation of D-glucose, D-fructose, and D-mannose, respectively.

In support of the above mechanism, the following experiments were performed by previously treating the reducing sugars with alkali for different intervals of time, and then the kinetics of oxidation of the mixture of the sugars was followed as described below.

A 100-ml. aliquot of the reactants containing sodium hydroxide and reducing sugar was kept in the thermostat for certain hours as mentioned in the tables given below, and then another sample containing 100 ml. of ferricyanide previously kept in the thermostat was added to study the course of the reaction. From the experiment it is evident that during treatment the sugar concentration as well as the alkali concentration are twice the final concentration while studying the course of the reaction. The experimental results are given in the Table IV.

A perusal of Table IV shows that, while previously treating D-glucose and D-fructose with alkali, the values of *k*_a are in increasing and decreasing order, respectively, with increasing time intervals of treatment. This is due to the fact that, during previous treatment of D-glucose with alkali, D-fructose is the main product which has higher rate of oxidation than D-glucose, and the reverse is the case during previous treatment of D-fructose with alkali.

(13) (a) M. L. Wolfrom and W. L. Lewis, *J. Am. Chem. Soc.*, **50**, 837 (1928); (b) J. H. Simons and H. C. Struck, *ibid.*, **56**, 1947 (1934).

(14) J. U. Nef, *Ann.*, **403**, 204 (1914); **357**, 214 (1907).

(15) O. Spengler and A. Pfannensteil, *Z. Ver. deut. Zucker-Ind.*, **85**, 546 (1933).

(16) F. Petuely and N. Meixner, *Chem. Ber.*, **86**, 1255 (1953).

(17) P. Hirsch and R. Schlags, *Z. physik. Chem. (Leipzig)*, **A141**, 387 (1929).

(18) (a) C. A. Lobry de Bruyn and W. Alberda van Ekenstein, *Rec. trav. chim.*, **16**, 262 (1897); (b) J. C. Speck, Jr., *Advan. Carbohydrate Chem.*, **13**, 63 (1958).

(19) J. C. Sowden and R. Schaffer, *J. Am. Chem. Soc.*, **74**, 499 (1952); **74**, 505 (1952).

(20) C. H. Bamford and J. R. Collins, *Proc. Roy. Soc. (London)*, **A204**, 62 (1950); **A204**, 85 (1950); **A228**, 100 (1955).

Table IV^a

Over-all concn. of sugar and alkali	Time of treatment, hr.	Mean zero-order $k_s \times 10^6$, $M^{-1} \text{ min.}^{-1}$	$k_s' \times 10^3 = \frac{k_s}{k_a} / [\text{OH}^-] \times 10^3$
25°			
D-Glucose 0.01 M	0	12.88	...
	2	15.68	1.568
NaOH 0.01 N	4	18.63	1.863
	6	19.77	1.977
D-Fructose 0.005 M	0	44.70	...
	3.5	41.50	2.500
NaOH 0.0166 N	5.0	38.77	2.335
	45°		
D-Glucose 0.005 M	0	75.69	...
	2	156.30	18.76
NaOH 0.00833 N	4	163.60	19.64
	D-Fructose 0.005 M	0	216.50
0.5		177.20	26.60
NaOH 0.00666 N	1.0	160.20	24.05
	1.5	146.60	22.01
	2.5	133.60	20.06

^a Total volume 200 ml.; over-all concentration of $\text{K}_3\text{Fe}(\text{CN})_6$ is 0.0025 M.

Now as it follows, the attempt has been made to calculate the amount of D-fructose and D-glucose produced during interconversion of D-glucose and D-fructose, respectively, from our kinetic data.

The zero-order velocity constant that has been measured in the case of treatment of D-glucose, D-fructose, and D-mannose (*i.e.*, allowing these sugars for their interconversion for a known interval of time) will be given by

$$-\frac{d[\text{Fe}(\text{CN})_6^{-3}]}{dt} = k_s' = k_{1g}c_g + k_{3f}c_f + k_{4m}c_m \quad (5)$$

where k_s' is the standard, mean zero-order velocity constant that has been calculated for 1 N NaOH concentration in case of mixtures of sugars produced after previous alkali treatment. In the interconversion of D-glucose and D-fructose the equilibrium concentration of D-mannose is very small (2.4%), given by Wolfrom and Lewis,^{13a} so it can be neglected. Hence eq. 5 reduces to

$$k_s' = k_{1g}c_g + k_{3f}c_f \quad (6)$$

From Table IV at 25°

$$k_{1g} = \frac{k_a}{c_g c_{\text{OH}^-}} = \frac{12.88 \times 10^{-6}}{0.01 \times 0.01} = 0.1288 \text{ l. } M^{-1} \text{ min.}^{-1}$$

and

$$k_{3f} = \frac{k_s}{c_f c_{\text{OH}^-}} = \frac{44.70 \times 10^{-6}}{0.0166 \times 0.005} = 0.5385 \text{ l. } M^{-1} \text{ min.}^{-1}$$

If c is taken as the initial concentration of D-glucose during kinetic measurements then

$$c = c_g + c_f \quad (7)$$

where c_g and c_f are the concentrations of respective sugars in the mixture. Therefore, during treatment

$$2c = 2c_g + 2c_f \quad (8)$$

Substituting the value of c_g from (7) into (8)

$$k_s' = k_{1g}(c - c_f) + k_{3f}c_f \quad (9)$$

The value of k_s' for 2 hr. at 1 N NaOH from Table IV at 25° is 1.568×10^{-3} . Therefore, substituting the values of k_s' , c , k_g , and k_f into (9) yields $0.001568 = 0.1288(0.01 - c_f) + 0.5385c_f$, from which the value of c_f comes out to be $6.8 \times 10^{-4} M$. Hence, the concentration of D-fructose produced in a 2-hr. treatment from D-glucose will be $2 \times 6.8 \times 10^{-4} M = 13.60 \times 10^{-4} M$.

Similarly, the amount of D-glucose c_g from the interconversion of D-fructose can be calculated with the help of

$$k_s' = k_{1g}c_g + k_{3f}(c - c_g) \quad (10)$$

Now the above value for D-fructose produced in a 2-hr. treatment from D-glucose can be calculated theoretically as follows from the values of forward and backward velocity constants k_1' and k_2' at 25° for 1 N alkali given by Bamford and Collins mentioned previously.

For a reversible reaction

$$k_1' + k_2' = \frac{2.303}{t} \log \frac{c_{fe}}{c_{fe} - c_f} \quad (11)$$

where c_f is the concentration of D-fructose produced after a time of t hr. and c_{fe} is its equilibrium concentration whose value can be calculated as

$$\frac{k_1'}{k_2'} = \frac{c_{fe}}{c_{ge}} \quad (12)$$

where

$$c_{ge} = 2c - c_{fe} \quad (13)$$

At 25°, $k_1' + k_2' = 0.088$ and the value of c_{fe} calculated with the help of eq. 12 and 13 is 0.00977 M.

Thus, for $t = 2$ hr., substituting the above values into eq. 11, the theoretical value of c_f comes out to be $15.77 \times 10^{-4} M$.

Similarly, the values of D-glucose produced from D-fructose can be calculated theoretically with the help of the equation

$$k_1' + k_2' = \frac{2.303}{t} \lg \frac{c_{ge}}{c_{ge} - c_g} \quad (14)$$

Now the tables given below show the experimental and theoretical values for D-fructose and D-glucose produced

Table V^a

Temp., °C.	Time of treatment, hr.	—D-Fructose concn. × 10 ⁴ M—	
		Exptl.	Theoret.
2 × 0.01 M D-glucose			
25	2	13.67	15.77
	4	28.08	28.99
	6	33.64	39.15
2 × 0.005 M D-glucose			
45	2	41.36	50.64
	4	45.14	52.28
—D-Glucose concn. × 10 ⁴ M—			
Exptl. Theoret.			
2 × 0.005 M D-fructose			
25	3.5	13.55	9.37
	5.0	17.42	18.20
45	0.5	25.32	27.51
	1.0	36.24	39.13
	1.5	44.96	44.07
	2.5	53.34	47.02

^a NaOH concentration is 1 N.

during interconversion of D-glucose and D-fructose, respectively, at 25 and 45° on the basis of preceding calculations.

A perusal of the preceding results shows good agreement between experimental and theoretical values. One, however, may point out that the velocities of interconversion given by Bamford and Collins have been determined in presence of potassium hydroxide. But this point ceases to be valid because they themselves²⁰ have reported that the rates of interconversion exhibited no observable change on substituting NaOH for KOH. Further, the experimental values may be considered to be more accurate because the interconversion and the rate determinations were carried at low alkali concentrations. Under this condition no degradation is possible. The only slight error in the values may be due to saccharinic acid formation and polymerization.

The theory outlined in the previous pages clearly suggests that the single scheme proposed through a common intermediate, 1,2-enediol, is completely valid for the interconversion as well as for the oxidation of reducing sugars. Further, the rates of oxidation of aldo and keto sugars are their corresponding rates of enolization.

Acknowledgment. N. N. wishes to thank the Council of Scientific and Industrial Research (C.S.I.R.), Government of India, for financing the project.

The Effect of Solvent on the Acid-Base Kinetics of the Excited State of β -Naphthol¹

by Norman M. Trieff and Benson R. Sundheim

Department of Chemistry, New York University, Washington Square, New York, New York 10003
(Received January 8, 1964)

The methods developed by Förster and Weller for using fluorescence intensity measurements to follow the kinetics of excited-state reactions were applied to β -naphthol in mixed aqueous solvents, *e.g.*, methanol-water and glycerol-water mixtures. Steady-state rate and equilibrium constants were obtained in different solvents for the excited-state proton-transfer reactions where water and acetate ion are the proton acceptors. The forward rate constant for both reactions decreased progressively with the addition of organic solvents to water, each having a different effect on a molar basis, while the variation of the backward rate constant with solvent was more complex. The quenching reaction between β -naphtholate* and iodate was taken as a standard diffusion-controlled reaction in order to reveal features in the acid-base reaction which are peculiar to the proton transfer. It was found that only in the case of the β -naphtholate*-hydronium ion reaction in glycerol solutions did the rate constants vary with solvent in a fashion markedly different from the standard reaction. The rate constants for the (activation-controlled) reaction of β -naphthol* with water were also obtained in the methanol-water and glycerol-water systems. The results could be rationalized in terms of a model involving preliminary ionization of the weak acid.

Introduction

It has been shown by Förster^{2a} that when some organic molecules capable of fluorescence are excited by light of suitable energy, they display an acidity in the excited singlet state markedly different from that in the ground state. The excitation causes a change in the electronic distribution³ which leads to inhibition or enhancement of proton removal (or addition). In many cases a pK_a shift of as much as 6-7 pH units has been observed. In some cases an acid-base equilibrium in the excited state, completely independent of that in the ground state, is achieved. This shift in equilibrium position between the ground and excited states is reflected in the differing dependence of the absorption and the fluorescence spectra of both the acidic and basic forms of the molecule. Just as the absorbances of the acid and basic forms of an acid-base system provide information concerning the extent of dissociation of the unexcited molecules, so do the fluorescence intensities of the acidic and basic forms reflect the extent of dissociation of the excited molecules.

The fluorescence, in comparison to absorbance, is thus a gauge by which the change in acidity upon excitation can be detected. Such a change is detectable only if the rate constant for proton transfer in the excited state is comparable to or greater than the rate of decomposition of fluorescence. In this case, the absorption spectra exhibits a pH dependence different from that of the fluorescence spectra so that the ground and excited states may be characterized by different pK_a values. If there is no proton transfer in the excited state, the fluorescence spectral transition occurs at the same pH as the absorption spectral transition so that the pK_a values in the ground and excited states are identical.

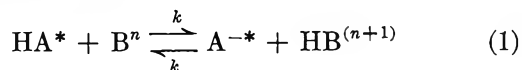
In a series of papers, Weller⁴ reported investigations of the kinetics of proton-transfer reactions in the

(1) Abstracted in part from a doctoral dissertation of N. M. Trieff.

(2) (a) T. Förster, *Naturwiss.*, **36**, 186 (1949); (b) T. Förster, *Z. Elektrochem.*, **54**, 42, 531 (1950).

(3) H. H. Jaffé and M. Orchin, "Theory and Application of Ultra violet Spectroscopy," John Wiley and Sons, Inc., New York, N. Y. 1962, pp. 147-157.

excited state by means of fluorescence measurements.^{5,6} He was able to determine the forward and backward rate constants for the reaction



where HA^* and A^{-*} are the acidic and basic forms of the fluorescent compound concerned, B^n is the proton acceptor (n is the charge) which may be water, acetate, hydroxide ion, etc. A detailed mechanism was also proposed.

It is of considerable interest to determine the role of solvent in reactions of type 1. A knowledge of the effects of changing solvent properties such as viscosity, dielectric constant, and concentration of water, for example, would help to elucidate some details of the acid-base reaction (1). In addition, the measurement of solvent effects would provide a basis for testing the mechanism proposed by Weller. Therefore, we undertook a study of the fluorescences of the acidic and basic forms of β -naphthol as a function of proton acceptor (or conjugate) and for mixed aqueous solvents of varying composition. The proton acceptors employed were water and acetate ion. The rate constants for each solvent determined from fluorescence data are related in a simple manner to the equilibrium constant in the excited state. Equilibrium constants were determined as a function of solvent and compared with ground-state equilibrium constants determined from titration and absorption spectral data. Also, in connection with the interpretation of the results, the rate constants for proton transfer in various solvents were compared with those for the quenching reaction between β -naphtholate and iodate in the respective solvents.

Experimental

A. Reagents, Solvents, and Buffers. Fisher Certified reagent grade β -naphthol was purified by vacuum sublimation at about 150° ; the sublimed colorless needles were oven-dried and stored in a dark bottle in a desiccator. The melting point was 126 – 129° for the unpurified material and 123 – 125° for the sublimed material. Additional criteria of purification—infra-red absorption spectra and ultraviolet absorption spectra—indicated essentially no change in composition of the β -naphthol upon sublimation. Because of the decomposition which β -naphthol undergoes, particularly in strong alkaline and very strong acid solutions, fresh $10^{-3} M$ β -naphthol stock solutions were made up in water (heating to 70 – 80° being necessary to effect solution), every 2 weeks. Directly before making all measurements, the appropriate solu-

tions were made up with regard to proper pH, concentration of β -naphthol, and solvent mixture. No attempt was made to eliminate oxygen from the solutions, since according to Förster,⁷ the fluorescence of β -naphthol is not quenched appreciably by oxygen.

Methanol and glycerol were ACS reagent grade and used without further purification. Reagent grade dioxane was distilled with sodium ribbon under nitrogen and stored in the same way. The observed boiling point was 97 – 99° and distilled dioxane diluted with an equal volume of distilled water had a pH of about 6.

Reagent grades of perchloric acid and sulfuric acid were used without further purification. Stock solutions of approximately $1 M$ HClO_4 and $0.5 M$ H_2SO_4 were prepared and standardized with standard NaOH . Further dilutions were made from these stock solutions.

An acetate buffer stock solution, $0.2 M$ in NaOAc and $0.02 M$ in HOAc was made up from reagent grade materials and found to have a pH (glass electrode) of 5.59 at 25° . Appropriate dilutions of this buffer for study of proton transfer to acetate ion were performed directly before use. Acetate buffers of higher ionic strength were prepared by suitable dilution from $0.5 M$ NaOAc and $0.2 M$ HOAc .

A universal buffer system proposed by Davies⁸ was used to adjust the pH for the spectrophotometric determination of the pK_a of β -naphthol in water and 0.05 mole fraction glycerol-water while assorted phosphate and borate buffers were used for the pK_a determinations in other solvent mixtures.

B. Titration Studies. Titration curves of acetic acid and β -naphthol in various methanol-water, glycerol-water, and dioxane-water mixtures were made using an SBR₂ titrator, SBULa syringe buret, TTT 1 titrator, and TTT 2 titrator assembly manufactured by Radiometer, Copenhagen, Denmark.

The pK_a values of the acids were determined by noting the pH at 50% titration and correcting the pH for the ionic strength and primary medium effect as described by Van Uitert, *et al.*^{9,10}

C. Absorption Spectra. Absorption spectra were

(4) The extensive work of Weller in this field is reviewed together with a complete bibliography in "Fast Reactions of Excited Molecules," by A. Weller in "Progress in Reaction Kinetics," Vol. I, G. Porter, Ed., Pergamon Press, New York, N. Y., 1961.

(5) (a) A. Weller, *Z. Elektrochem.*, **56**, 662 (1952); (b) *ibid.*, **58**, 849 (1954).

(6) A. Weller, *Z. Physik. Chem. (Frankfurt)*, **3**, 238 (1955).

(7) T. Förster, personal communication.

(8) M. T. Davies, *Analyst*, **84**, 248 (1959).

(9) L. G. Van Uitert and C. G. Haas, *J. Am. Chem. Soc.*, **75**, 451 (1953).

(10) L. G. Van Uitert, C. G. Haas, W. C. Fernelius, and B. E. Douglas, *ibid.*, **75**, 455 (1953).

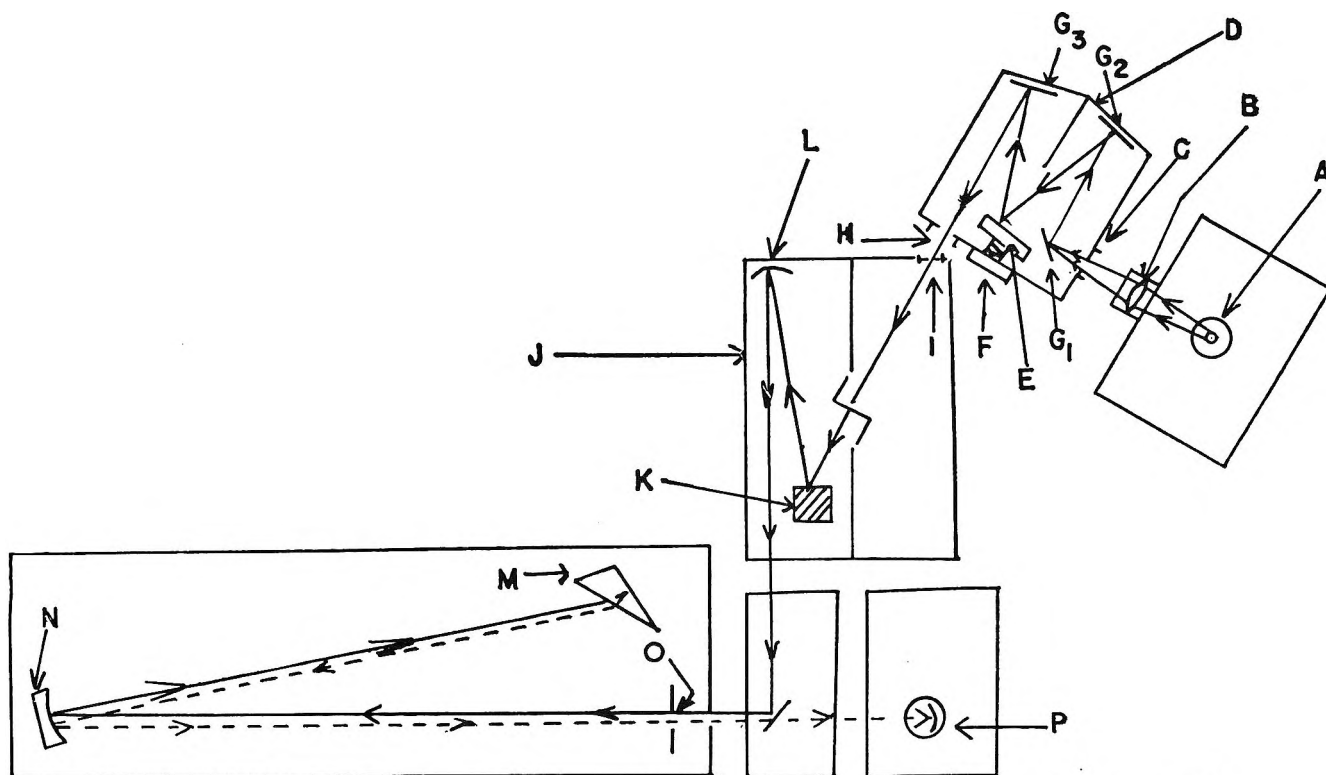


Figure 1. Optical diagram of Beckman fluorescence assembly: A, high pressure d.c. xenon compact arc lamp (Hanovia) in housing; B, condensing lens; C, entrance slit; D, Farrand ultraviolet grating monochromator; E, grating; F, calibrated wave length dial; G₁, G₂, and G₃, plane mirrors; H, exit slit of monochromator; I, aperture; J, Beckman fluorescence attachment; K, quartz cuvette containing fluorescent sample; L, condensing mirror; M, prism; N, collimating mirror; O, slit; P, phototube.

determined (Cary Model 14 and Beckman Model DU) as a function of pH and solvent composition.

D. Fluorescence Measurements. Most fluorescent measurements were performed on the spectrofluorophotometer shown in Figure 1. It consists of a d.c. xenon compact arc lamp in a Farrand ultraviolet grating monochromator for the exciting light; a Beckman fluorescence attachment which holds the fluorescent sample in a 1-cm. quartz cuvette inserted such that the incident light strikes a transparent face; the prism monochromator of the Beckman DU to disperse the fluorescent light; a suitable phototube mounted on the Beckman face plate; and an Aminco multiplier photometer. The optics are indicated in the figure.

The Farrand monochromator (calibrated against the Beckman monochromator) was used to transmit mainly 313-m μ light onto the sample. This wave length is short enough so that the acid form of β -naphthol can be excited. The fluorescence intensities were measured in all cases at 357 and 416 m μ , the fluorescence maxima of the acidic and basic forms of β -naphthol in water. It was found experimentally that the acid maximum undergoes essentially no shift

with solvent, while there is a very slight solvent shift of the basic maximum, but it is too slight to affect results. A slit width of 2 mm. on the Beckman DU and appropriate settings on the Aminco photometer were used to give suitable sensitivity.

For each solvent studied, a series of solutions was prepared containing $2 \times 10^{-4} M$ β -naphthol and varying concentrations of perchloric acid or acetate. Also, for each solvent run there were prepared a "primary reference" solution consisting of $2 \times 10^{-4} M$ β -naphthol in aqueous 0.0483 M H_2SO_4 , an "acid reference" consisting of $3.04 \times 10^{-4} M$ β -naphthol in 0.2 M NaOH in the same solvent. (The higher concentration of β -naphthol in the "basic reference" is due to the lower extinction coefficient of the basic form compared to the acid at 313 m μ . The concentration of the "basic reference" is chosen to make the absorbances of β -naphthol the same in all solutions.)

Samples were brought to 25° by a constant temperature bath just before being studied. First, the fluorescence intensity of the "primary standard" was taken at 357 m μ (on the Beckman DU monochromator) by adjusting it with the settings on the Aminco photometer to an arbitrary value on the par-

ticular scale. Without any change in these settings, fluorescence intensity readings for all the other samples, including the acidic and basic references, were taken at 357 and 426 $m\mu$. The reading for the "primary reference" at 357 $m\mu$ was repeated after every three samples during the run in order to account for fluctuations in lamp intensity. The rather small intensities of distilled water at 357 and 426 $m\mu$ due to scattering were subtracted from the observed intensity readings and these net readings were multiplied in each case by a correction factor. This same correction factor by which the respective "primary reference" reading must be multiplied in order to keep the "primary reference" readings constant from the start of the run.

In some cases, the fluorescence attachment to the Cary Model 14 spectrophotometer was used in place of the Beckman monochromator.

E. Fluorescence Lifetime Measurements. The fluorescence lifetimes of the acidic and basic forms were studied as a function of solvent by Professor A. Schmilen of the Institute of Physics at the University of Giessen by means of an ultrasonic cell fluorometer.¹¹

Results and Discussion

A. Absorption Spectral Data. The absorption spectra of β -naphthol in water as a function of pH are shown in Figure 2a. With an increase in pH, the absorption peaks move to longer wave lengths (red shift) due to the shifts in the ground state acid-base equilibrium for β -naphthol



Absorption spectra were also determined as a function of pH in a 0.05 mole fraction glycerol-water mixture. These spectra are identical within experimental error with the spectra in water. The absorption maxima found in water were 327.3 ± 0.2 and $345.0 \pm 0.2 m\mu$ for the acidic and basic forms, respectively, which are in good agreement with the values in the literature.

Graphical determination of the pK_a of β -naphthol in water and 0.05 mole fraction glycerol were performed using the Henderson-Hasselbach equation and pertinent absorption spectral data following the general method discussed in the literature.¹² The pK_a for β -naphthol in water was found to be 9.57 ± 0.04 at 25° to be compared with Weller's^{5a} value of 9.49 at 25°. A value for the pK_a in a 0.05 mole fraction glycerol of 9.61 was also obtained spectrophotometrically.

B. Titration Data for β -Naphthol and Acetic Acid in Different Solvents. The pK_a values for β -naphthol and acetic acid calculated from titration data are

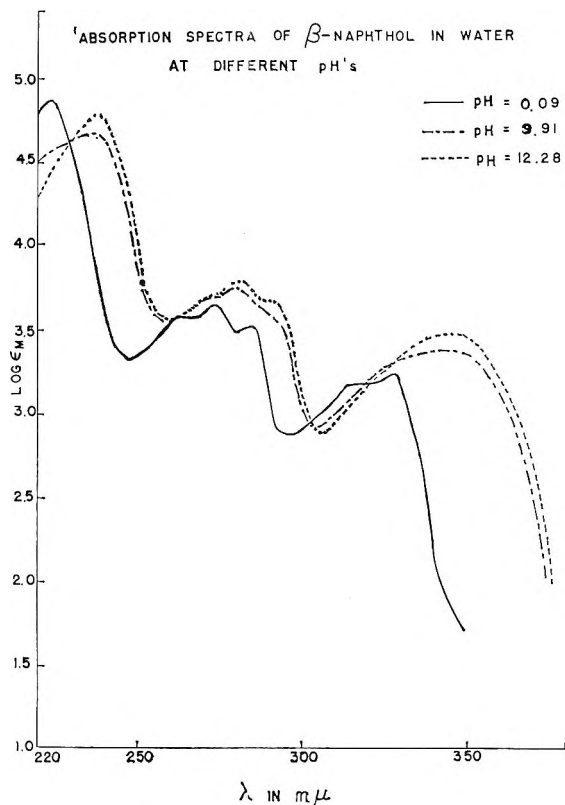


Figure 2a. Absorption and fluorescence spectra of β -naphthol in water at different pH values. Absorption spectra of $1 \times 10^{-4} M$ β -naphthol solutions at room temperature (Beckman DU spectrophotometer).

plotted as a function of weight per cent nonaqueous solvent in Figure 3, along with values for the excited state of β -naphthol which were calculated from fluorescence data. In each of the three cases, for a given weight per cent of nonaqueous solvent, the pK_a is highest in methanol-water mixtures and lowest in glycerol-water mixtures. It is clear from the data that β -naphthol in the excited state is a somewhat stronger acid than acetic acid which in turn is considerably stronger than β -naphthol in the ground state.

C. Fluorescence Investigation of β -Naphthol-Water Reaction.* Fluorescence spectra for β -naphthol in aqueous 0.2 M HClO_4 and 0.2 M NaOH are plotted in Figure 2b. The respective maxima are 357 and 417.5 $m\mu$.

The relative quantum yields for acidic and basic fluorescence, η/η_0 and η'/η'_0 , were determined experimentally from fluorescence measurements using a modification (cf. thesis of Trieff, ref. 1) of the method of Weller¹³ which corrects for overlap of fluorescence

(11) A. Schmilen, *Z. Physik*, **135**, 294 (1953).

(12) H. H. Jaffé and M. Orchin, ref. 3, pp. 556, 567.

(13) A. Weller, *Z. physik. Chem.* (Frankfurt), **17**, 224 (1958).

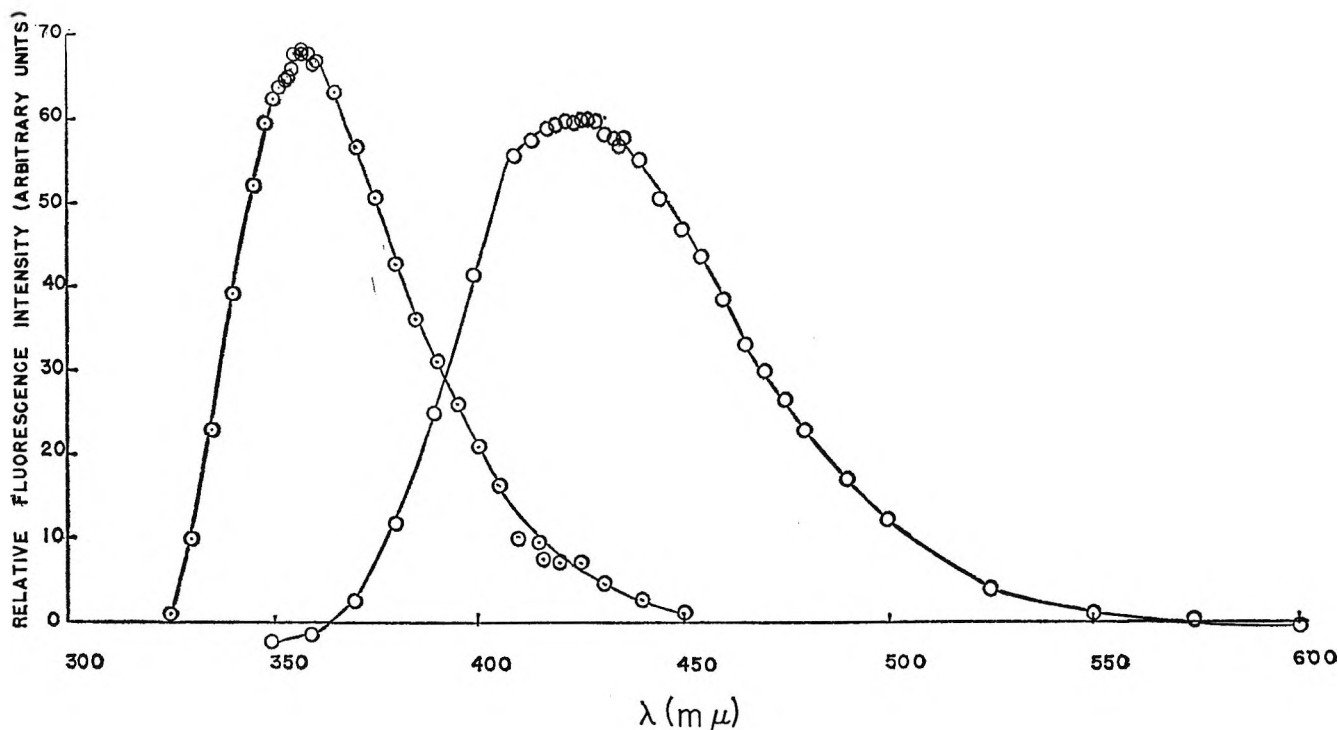


Figure 2b. Fluorescence spectra of β -naphthol in water, using 313-m μ exciting light on 2×10^{-4} M solution (Beckman fluorescence assembly): O, in 0.2 M HClO₄; ●, in 0.2 M NaOH.

(i.e., the contribution of pure acid form to basic fluorescence and *vice versa*), as well as for quenching in strongly acid solution. For a given solvent, the fluorescence intensity measurements (arbitrary units) are obtained at 357 m μ (acidic fluorescence, I) and 426 m μ (basic fluorescence, I') at pH values varying from the strongly acid to strongly basic solutions, all solutions possessing the same absorbance for the exciting light. Using the equations of Weller¹³

$$\eta/\eta_0 = I/I_0 - p'\eta'/\eta_0' \quad (\text{A})$$

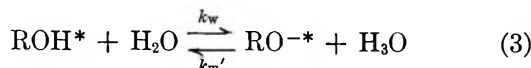
$$\eta'/\eta_0' = I/I_0 - p\eta/\eta_0 \quad (\text{B})$$

$$\eta/\eta_0 + \eta'/\eta_0' = 1 \quad (\text{C})$$

where I_0 is the theoretical fluorescence intensity at the acid maximum in strongly acid solution in the absence of quenching, I_0' is the same for the basic maximum in strongly basic solution, p and p' are the fluorescence overlap corrections which were found experimentally (*cf.* thesis of Trieff, ref. 1) to have the values, 0.087 and 0. Combination of eq. A–C results in a linear expression relating I , I' , I_0 , and I_0' . The use of data at all pH values and subsequent least-mean-square treatment of the data results in values for I_0 and I_0' which best fit all of the data. Then, with these values for I_0 and I_0' , eq. A and B are used for the calculation of η/η_0 and η'/η_0' . This method of calculation of I_0

and I_0' does not put entire reliance on measurements in the strong acidic and basic regions as well as one intermediate pH as does Weller, but considers the entire pH region.

In Figure 4, the relative quantum yields η/η_0 and η'/η_0' are plotted as a function of experimental pH and volume per cent of methanol. An examination of the curve obtained for water (0% methanol), which agrees well with the data of Förster^{2b} and Weller,^{5a} shows that the η/η_0 curve starts at 1.0 in strong acid, gradually descending as the pH is increased until a plateau value of 0.695 is attained at a pH of about 4. Throughout this same pH range, the η'/η_0' curve starts at approximately zero in strong acid and with increasing pH rises until a plateau value of 0.330 is reached at about pH 4.5. (It should be noted that, if only proton-transfer reaction occurs in the excited state, then $\eta/\eta_0 + \eta'/\eta_0' = 1$. If some other reaction is competitive, *e.g.*, a quenching reaction, $\eta/\eta_0 + \eta'/\eta_0' < 1$.) These acidic and basic plateau values are to be compared with those of Weller^{5a}: 0.731 and 0.280. The shape of this curve may be understood on the basis of the following reaction occurring in the excited state



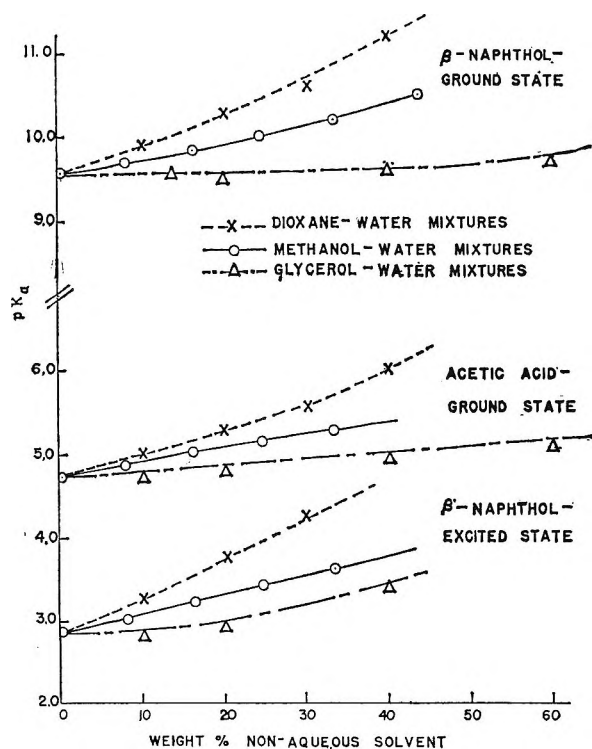


Figure 3. pK_a values of β -naphthol in ground and excited states and of acetic acid as a function of solvent composition at $25 \pm 1^\circ$.

In the plateau region (pH 3-7) fluorescence is emitted from excited naphthol (ultraviolet) and naphtholate (blue). The presence of an appreciable concentration of excited naphtholate ion at pH 3-7 clearly indicates that it must have arisen from some excited state reaction, since RO^- is virtually nonexistent in the ground state at more than 2-3 pH units to the acid side of the pK_a of 9.5. The proton acceptor in this region cannot be OH^- since the concentration of OH^- is very low in this region and the rate does not depend on $[OH^-]$. The most likely proton acceptor is water. In the plateau region the backward reaction must occur only to a negligible extent; otherwise, there would be a pH dependency. With further increase of $[H_3O^+]$ a rise in η/η_0 and fall η'/η_0' occurs due to the marked acceleration of the backward reaction, until at $[H_3O^+] = 0.1$, only the ultraviolet fluorescence arises. At pH 7-8, although this is not shown, there is an abrupt drop in η/η_0 and rise in η'/η_0' with increasing pH. This is due to the ground-state equilibrium reaction, eq. 2, being shifted significantly to the right in the region of the pK_a of β -naphthol. The consequent decrease in ROH leads, in turn, to a decrease in $[ROH^*]$. Simultaneously, the $[RO^-]$ and $[RO^{*-}]$ increase.

In Figure 4, it should be noted that the η/η_0 curves descend less sharply as the concentration of methanol increases, the position of the plateaus rising toward 1.0. Simultaneously, the η'/η_0' curves rise less steeply and the plateaus of this curve fall toward zero. Thus, with increasing concentrations of methanol, the net amount of proton transfer between the initially ex-

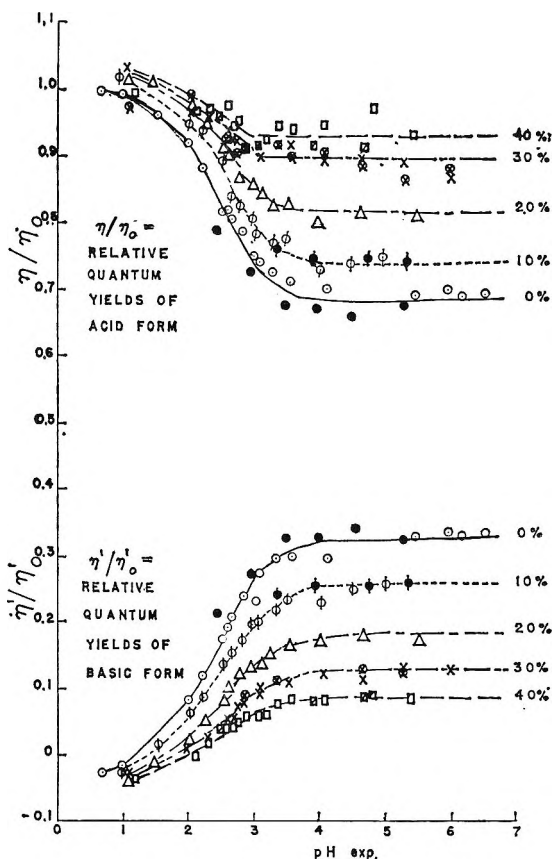
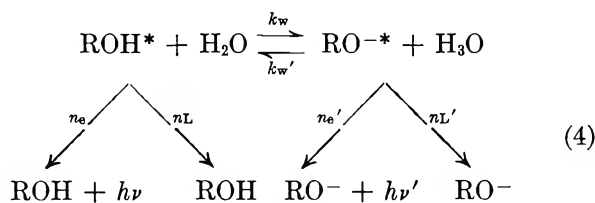


Figure 4. Relative quantum yields vs. experimental pH for β -naphthol as a function of methanol concentration (volume %): exciting light was at 313 μ . For most solvent mixtures, two sets of measurements were taken either on the Beckman DU (B) alone or the Beckman DU and Cary-14 (C). Key: 0%: O, B; \bullet , C; 10%: ϕ , B; \blacklozenge , C; 20%: Δ , B; 30%: \times , B; \otimes , C; 40%: \square , B; \oslash , C.

cited naphthol molecules and water molecules is diminished and fewer excited naphtholate ions are formed. Similar experiments were performed for various glycerol-water and dioxane-water mixtures. Although these curves are not shown, essentially the same effect was observed for glycerol and dioxane as well.

D. Determination of Rate Constants for β -Naphthol*-Water Reactions. The reaction scheme may be written⁴



where n_e and n_L are the rate constants for light emission and for radiationless deactivation of the excited naphthol molecule, while k_w is the velocity constant for proton transfer from the excited naphthol molecule. The primed values are the analogous terms for the excited naphtholate ion.

By conventional analysis of this expression for this rate scheme one may relate^{5a,6,13,14} the forward and backward rate constants, k_w and k_w' , to measurable quantities. The exact expression is

$$W_{\text{H}^+} \times \frac{\eta/\eta_0}{\eta'/\eta_0'} - (1 - W_{\text{H}^+}) = \frac{1}{k_w\tau_0} + \frac{k_w'\tau_0'}{k_w\tau_0} \times F \times [\text{H}_3\text{O}^+] \quad (5)$$

A graph of the left-hand side of the equation vs. $F \times [\text{H}_3\text{O}^+]$ is a straight line with intercept equal to $1/k_w\tau_0$ and slope equal to $k_w'\tau_0'/k_w\tau_0$. From these, the rate constants k_w and k_w' may be determined providing that experimental values of the fluorescence lifetimes for acidic and basic fluorescence, τ_0 and τ_0' are known. Equation 5 treats only the steady-state reaction in the excited state. The factor W_{H^+} , used to correct the effect of transient or starting reaction, is equal to the fraction of excited naphtholate ions which do not have H_3O^+ ions in their diffusion volume, V_D , and therefore are involved only in the steady-state reaction. The remaining fraction $(1 - W_{\text{H}^+})$ are involved in the transient reaction. That is, these molecules upon excitation find an H_3O^+ in their diffusion volume and can react essentially instantaneously with it. W_{H^+} is given⁶ by

$$W_{\text{H}^+} = \exp\left(-\frac{V_D \times N \times [\text{H}_3\text{O}^+]}{1000}\right) \quad (6)$$

where N is Avogadro's number and V_D is defined by

$$V = 4\pi(\gamma R_0)^2 \sqrt{D\tau'} B \sqrt{D\tau_0'} / [(1 - \gamma)R_0 + B\sqrt{D\tau_0'}] \quad (7)$$

where γ is the efficiency factor for the reaction between RO^{*-} and H_3O^+ ; R_0 is the encounter distance between RO^{*-} and H_3O^+ ions taken as 5.5 Å. for all calculations.¹⁵ D is the relative diffusion coefficient between RO^{*-} and H_3O^+ ions, τ_0' and τ' are fluorescence lifetimes of naphtholate ion in strong base at the exist-

ing $[\text{H}_3\text{O}^+]$, respectively, and B is an electrostatic factor depending upon the charges of the reacting species, dielectric constant, temperature, etc. In eq. 5, F is the kinetic activity factor of Brønsted,¹⁶ which is introduced to consider the effect of ionic strength on the rate of reaction between RO^{*-} and H_3O^+ ions. For the RO^{*-} - H_3O^+ reaction

$$F = (f_{\pm})^2 \quad (8)$$

where f_{\pm} is the mean activity coefficient of a univalent electrolyte for the given ionic strength (concentration of HClO_4) and may be determined either from values in the literature or the Debye-Hückel equation¹⁷

$$\log f_{\pm} = \frac{-P\sqrt{\mu}}{1 + Qa'\sqrt{\mu}} \quad (9)$$

where μ is the ionic strength, a' is taken to be 5.5×10^{-8} cm., and P and Q are parameters which are defined in the reference cited. Based on their dependency with regard to dielectric constants, P and Q may be calculated simply for solvents other than water. Values for P and Q along with other properties of the solvents concerned are listed in Table I.

The procedure for determination of k_w and k_w' involves a method of successive approximations. A graph of (5) is first made with $W_{\text{H}^+} = 1$ (cf. Figure 5). This gives the first approximation values of k_w and k_w' . A first approximation value for the efficiency factor γ is obtained from the definition

$$\gamma = \frac{k_w'}{k_D} \quad (10)$$

where k_w' is the experimentally determined value of the backward rate constant and k_D is the diffusion rate constant for the encounter of naphtholate and hydronium ions given by the equation of Debye.^{18,19} Using this value for and other required parameters, V_D is obtained for each solution using (6). For each solvent, eq. 5 is replotted and second approximation values are obtained for k_w , k_w' , and γ . If there was a difference between the successive approximations of more than 5%, a third cycle of approximation was performed.

(14) A. Weller, *Z. physik. Chem. (Frankfurt)*, **15** (Bonhoeffer-Gedenkband), 438 (1958).

(15) E. Wicke, M. Eigen, and T. Ackermann, *ibid.*, **1**, 340 (1954).

(16) A. J. Rutgers, "Physical Chemistry," Interscience Publishers, Inc., New York, N. Y., 1954, pp. 665-672.

(17) J. T. Edsall and F. Wyman, "Biophysical Chemistry," Vol. I, Academic Press, New York, N. Y., 1958, pp. 290, 291.

(18) P. Debye, *Trans. Electrochem. Soc.*, **82**, 265 (1942).

(19) A. Weller, *Z. physik. Chem. (Frankfurt)*, **13**, 335 (1957).

Table 1: Properties of Solvent Mixtures

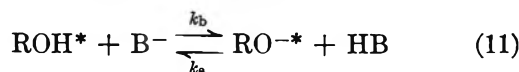
Solvent ^a	Wt. % non-aqueous solvent ^b	Mole fraction ^b	ρ , ^c g./ml.	η , ^d poises $\times 10^3$	ϵ	Debye-Hückel constants		
						P	$Q \times 10^{-7}$	Qa' ($a' = 5.5 \text{ \AA}$)
Water	0		0.9971	8.93	78.54	0.509166	3.2867	1.80768
10 M	8.005	0.04665	0.9826	11.2	75.00	0.545638	3.36338	1.84986
20 M	16.205	0.09809	0.9708	13.2	71.40	0.587388	3.44706	1.89588
30 M	24.614	0.1551	0.9587	14.8	67.66	0.636708	3.54096	1.94753
40 M	33.27	0.2190	0.9456	16.0	63.90	0.693776	3.64373	2.00405
10 G	10.00	0.02198	1.0221	11.53	75.50	0.541294	3.3544	1.84492
20 G	20.00	0.04670	1.0470	15.42	72.90	0.569299	3.4113	1.87622
40 G	40.00	0.1155	1.0995	31.81	67.10	0.644808	3.5559	1.95574
60 G	60.00	0.2269	1.1533	88.23	60.00	0.762527	3.7603	2.06816

^a In this and all subsequent tables, the following code is used for solvent mixtures: M = methanol (volume %); G = glycerol (weight %). ^b Determined by method of successive approximations for methanol assuming first that vol. % = wt. %. ^c Methanol mixtures: N. A. Lange, "Handbook of Chemistry," 9th Ed., Handbook Publishers, Sandusky, Ohio, pp. 1182-1185 (ρ values are for 20°; no correction was made for temperature change to 25°); glycerol mixtures: "Handbook of Chemistry and Physics," 35th Ed., Chemical Rubber Publishing Co., Cleveland, Ohio, 1953, pp. 1834, 1835. ^d Methanol mixtures: A. R. Tourky and S. Z. Mikhail, *Egypt. J. Chem.*, 1, 1 (1958); glycerol mixtures: "Handbook of Chemistry and Physics," 35th Ed., Chemical Rubber Publishing Co., Cleveland, Ohio, 1953, p. 2006. ^e Methanol mixtures: B. Conway, "Electrochemical Data," Elsevier Publishing Co., New York, N. Y., 1952, Table 10, p. 11; glycerol mixtures: H. S. Harned and B. B. Owen, "Physical Chemistry of Electrolytic Solutions," 2nd Ed., Reinhold Publishing Co., New York, N. Y., 1950, p. 118.

E. Fluorescence Investigation of β -Naphthol-Acetate Reaction.* The reaction of excited naphthols with acetate, sulfate, formate, propionate, and butyrate ions were studied recently by Weller.^{6b,13} The experimental procedure used^{5b} required that a constant pH of 5.7 (the plateau region for the β -naphthol*-H₂O reaction) be maintained throughout the investigation, the total concentration of acetate being the only variable. It was shown that in water, for a given pH, the fluorescence of ROH* is reduced with increasing acetate concentration while that of RO^{-*} increases. Analogous results were obtained for other base catalytic buffers.

In this investigation the study is extended to the other solvents already mentioned. Figure 6 shows the relative quantum yields of β -naphthol in 1:10 HOAc-NaOAc buffer vs. concentration of NaOAc as a function of glycerol concentration. It is seen that for any given acetate ion concentration, η/η_0 is displaced upward by the addition of glycerol, while simultaneously η'/η_0' is displaced downward. This indicates that the addition of glycerol to a β -naphthol solution of given pH and acetate ion concentration suppresses the rate of proton transfer which occurs between excited β -naphthol as donor and water or acetate as acceptor. The same was shown to hold true qualitatively for methanol.

F. Determination of Rate Constants of β -Naphthol-Acetate Reactions.* By considering reaction scheme 4 and the additional proton transfer to acetate ion



Weller has derived^{13,14} the following equations which consider only stationary-state reactions in the excited state and are similar to those already listed for the β -naphthol*-water reaction

$$W_B \frac{\eta'/\eta_0'}{\eta/\eta_0} - (1 - W_B) = k_w \tau_0 + k_b \tau_0 C_{B^-} \quad (12)$$

Here W_B is the probability that an excited β -naphthol molecule contains no acetate ion in the diffusion volume V_D and is given by

$$W_B = \exp \left[\frac{(-V_D N C_{B^-})}{1000} \right] \quad (13)$$

where

$$V_D = \frac{4\pi\gamma^2(R_0)^2 B \sqrt{D\tau} \times \sqrt{D\tau_0}}{(1-\gamma)R_0 + B\sqrt{D\tau_0}} \quad (14)$$

The terms in eq. 14 are quite analogous to those in eq. 7. Here γ is given by

$$\gamma = k_b/k_D \quad (15)$$

k_D is the Debye rate constant for encounter by diffusion between ROH and B⁻, R_0 is again taken as 5.5 Å., and D is the relative diffusion coefficient between ROH and B⁻.

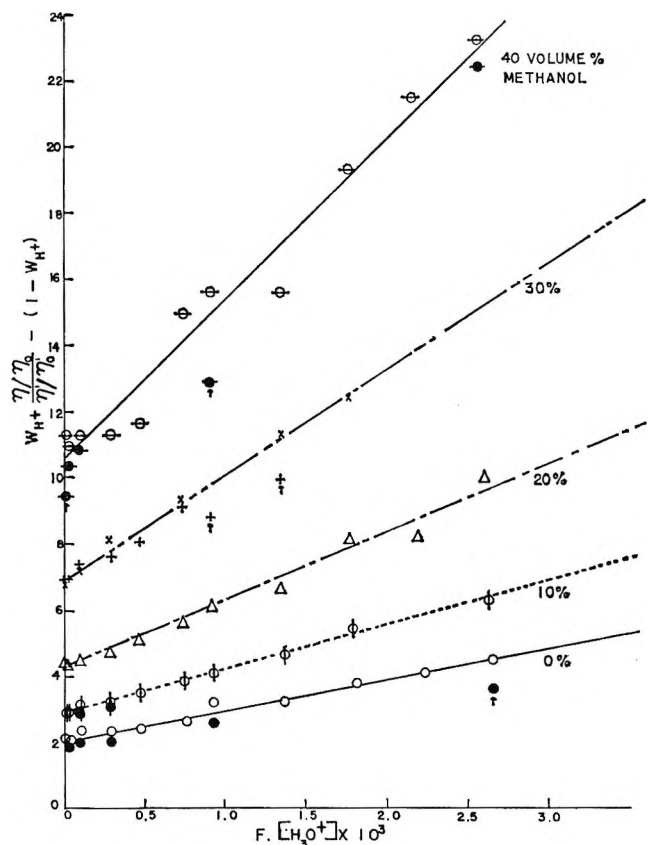


Figure 5. Graphs for determination of rate constants of β -naphthol*-water reaction in various methanol-water mixtures. Note: points designated by arrows are not included in least-mean-square determinations. Key: 0%: O, B; \bullet , C; 10%: ϕ , B; \blacklozenge , C; 20%: Δ , B; 30%: \times , B; +, B; 40%: \ominus , B; \blacklozenge , C.

A graph of $W_B[(\eta'/\eta_0')/(\eta/\eta_0)] - (1 - W_B)$ vs. C_B^- , the concentration of acetate ion as in eq. 12, results in a straight line with intercept equal to $k_w\tau_0$ and slope equal to $k_b\tau_0$. In this manner second approximations of k_w and k_b may be evaluated. The first approximation of k_t , determined by setting W_B in eq. 12 equal to 1, is used to evaluate γ by (15) so that values of V_D and W_B may be calculated from (14) and (13), respectively. Such graphs for various glycerol-water mixtures appear in Figure 7.

With regard to the calculation of k_a , the over-all backward rate constant for reaction 11, it may be shown that

$$k_a = k_b \times 10^{(pK_{ROH^*} - pK_{HB})} \quad (16)$$

where K_{ROH^*} is the dissociation constant for β -naphthol in the excited state and is given by

$$K_{ROH^*} = k_w/k_w' \quad (17)$$

while K_{HB} is the dissociation for acetic acid in the

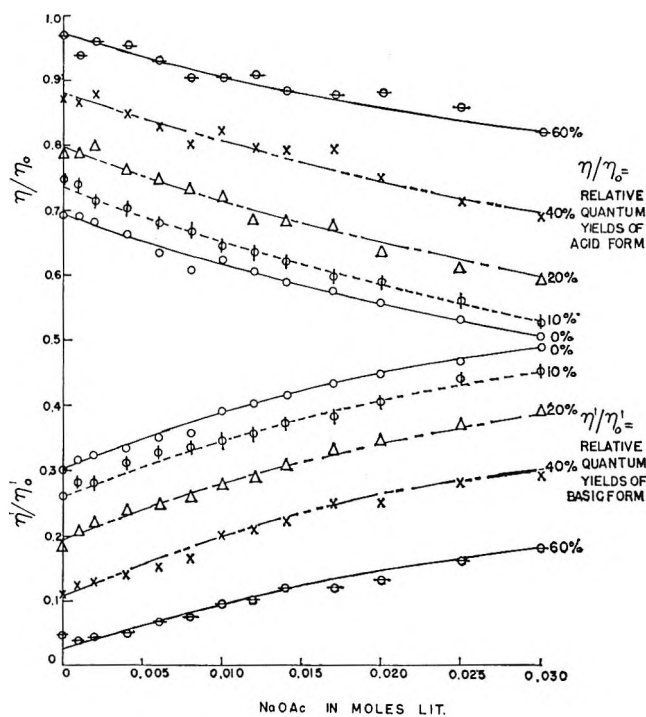


Figure 6. Relative quantum yields of β -naphthol in 1:10 acetic acid-sodium acetate buffer vs. concentration of sodium acetate as a function of glycerol concentration (wt. %); $T = 25 \pm 1^\circ$; concentration of β -naphthol = $2 \times 10^{-4} M$; exciting light at 313 μ . The pH of most solutions (glass electrode) was close to 5.7 except at the highest concentrations.

ground state and is determined for the various solvent mixtures by titration as already noted.

G. Rate Constants as a Function of Solvent. The successive approximations of k_w and k_w' obtained from the plots of eq. 5 appear in Table II along with values of k_w obtained from the plots of eq. 12 and values of pK_{ROH^*} obtained by means of eq. 17. The value of k_w for each solvent system should be the same regardless of whether it is determined from data for the β -naphthol*-water or β -naphthol*-acetate reaction. The agreement is, in fact, in most cases better than 10%. The limits of error given are 95% limits of confidence for the mean determined by the computation of variance for slopes of least-mean-square lines.^{20,21}

Graphs of k_w as a function of solvent appear in Figure 8, and it is seen that for both solvent systems k_w decreases with increasing mole fraction of each solvent. For a given mole fraction of solvent, the rate constant k_w will be highest for methanol. The effect

(20) W. J. Youden, "Statistical Methods for Chemists," John Wiley and Sons, Inc., New York, N. Y., 1951, pp. 42-44.

(21) E. B. Wilson, Jr., "An Introduction to Scientific Research," McGraw-Hill Book Co., Inc., New York, N. Y., 1952, pp. 272, 273.

Table II: Rate and Equilibrium Constants for β -Naphthol*-Water Reaction as a Function of Solvent at $25 \pm 1^\circ$ ($R_0 = 5.5 \text{ \AA}$.)

Solvent ^a	$k_w \times 10^{-7}, \text{sec.}^{-1} (\text{ROH}^*-\text{H}_2\text{O})$			$k_w' \times 10^{-11}, \text{l. mole}^{-1} \text{sec.}^{-1}$			$k_w \times 10^{-7}, \text{sec.}^{-1}$ ($\text{ROH}^*-\text{OAc}^-$)	pK_{ROH^*} (av. k_w used)
	First	Second	Third	First	Second	Third		
Water	6.30	6.59 \pm 0.48		4.66	4.93 \pm 0.57		5.82 \pm 0.31	2.90 \pm 0.13
10 M	4.63	4.68 \pm 0.26		4.96	4.94 \pm 0.29		4.23 \pm 0.42	3.04 \pm 0.10
20 M	3.01	3.00 \pm 0.22		5.19	5.03 \pm 0.54		2.99 \pm 0.19	3.22 \pm 0.13
30 M	1.82	1.82 \pm 0.10		4.90	4.83 \pm 0.35		1.75 \pm 0.12	3.43 \pm 0.09
40 M	1.14	1.14 \pm 0.08		4.75	4.60 \pm 0.49		0.945 \pm 0.059	3.65 \pm 0.13
10 G	5.30	5.32 \pm 0.32		3.92	4.00 \pm 0.24		4.75 \pm 0.26	2.90 \pm 0.08
20 G	3.80	3.74 \pm 0.25		3.86	3.46 \pm 0.39		3.15 \pm 0.17	3.00 \pm 0.13
40 G	1.71	1.74	1.75 \pm 0.18	5.74	5.05	5.23 \pm 0.96	1.48 \pm 0.10	3.51 \pm 0.20
60 G							0.408 \pm 0.071	

^a M = methanol (volume %); G = glycerol (weight %).

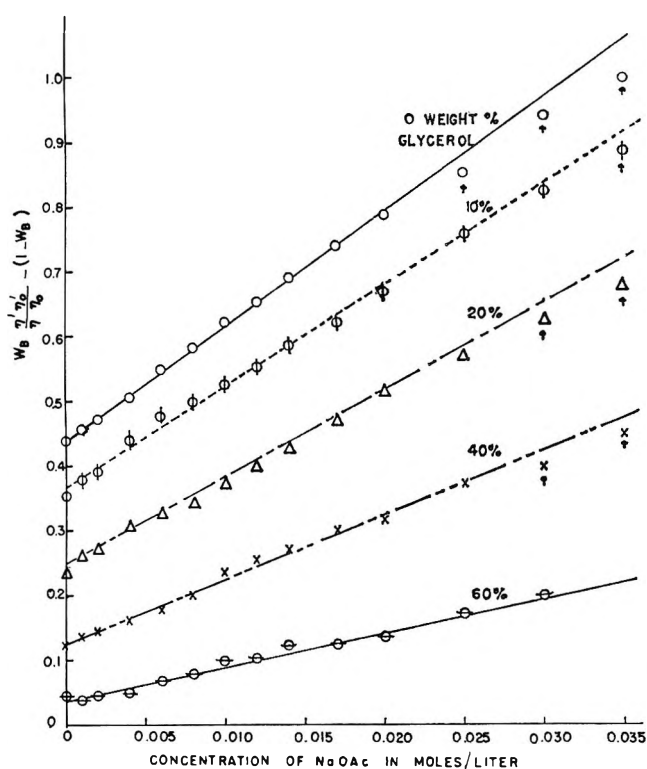


Figure 7. Graph for the determination of rate constants of β -naphthol*-acetate reaction in glycerol-water mixtures containing 1:10 acetic acid-sodium acetate buffers; $T = 25^\circ$, concentration of β -naphthol = $2 \times 10^{-4} M$. Note: points designated by arrows were not included in least-mean-square calculations.

of mole fraction of solvent on k_w' is more complex as shown in Figure 9. Here, k_w' is virtually constant for varying concentrations of methanol, and for glycerol addition there is first a slight decrease, then an increase in k_w' .

Values of k_b and k_a for different solvents appear in Table III, the 95% confidence limits for k_a being cal-

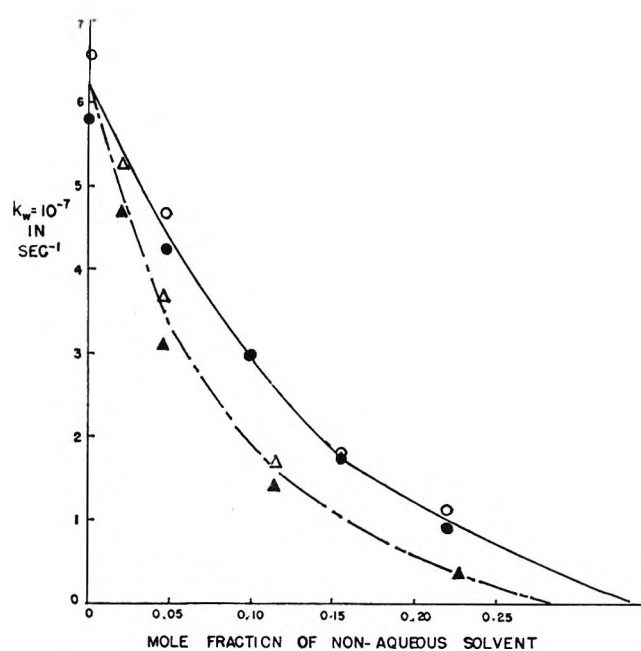


Figure 8. Pseudo-first-order forward rate constants, k_w , for β -naphthol*-water reaction as a function of solvent composition at $25 \pm 1^\circ$. From β -naphthol*-water reaction: O, methanol-water; Δ , glycerol-water. From β -naphthol*-acetate reaction: \bullet , methanol-water; \blacktriangle , glycerol-water.

culated by the method of total differentials²² which tends to overestimate the random error. The graphs of k_b and k_a vs. mole fraction of nonaqueous solvent appear in Figures 10 and 11. In Figure 10, k_b decreases with increasing mole fraction for both solvents. The glycerol curve descends being curved markedly. The methanol graph decreases linearly but with much

(22) H. S. Mickley, T. K. Sherwood, and C. E. Reed, "Applied Mathematics in Chemical Engineering," 2nd Ed., McGraw-Hill Book Co., Inc., New York, N. Y., 1957, pp. 53-55.

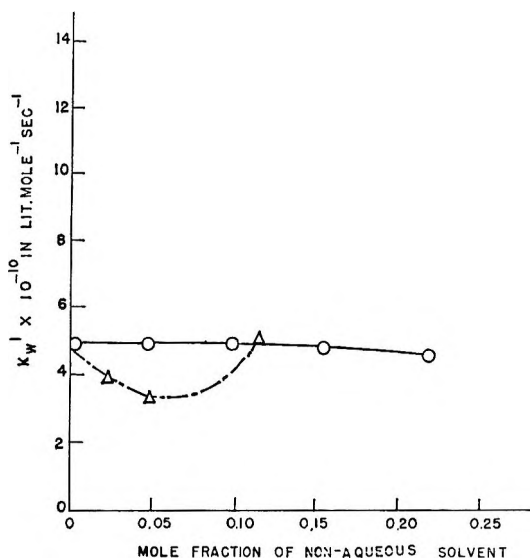


Figure 9. Backward rate constant, k_w' , for β -naphthol*-water reaction as a function of solvent composition at $25 \pm 1^\circ$: O, methanol-water; Δ , glycerol-water.

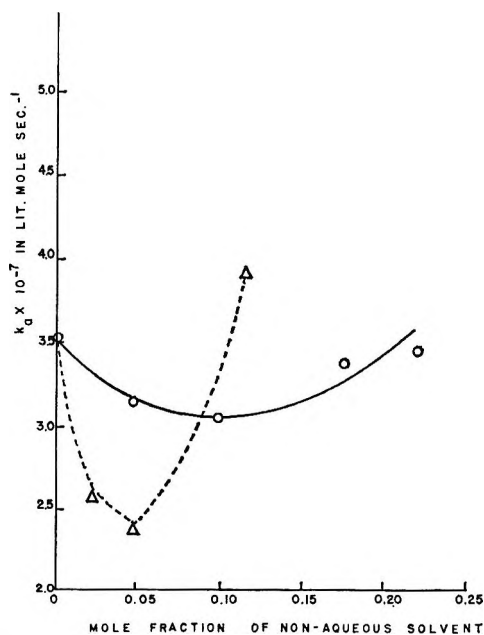


Figure 10. Backward rate constant, k_b , for β -naphthol*-acetate reaction as a function of solvent at $25 \pm 1^\circ$: O, methanol-water; Δ , glycerol-water.

lower slope. With regard to the k_b graphs in Figure 11, they are quite similar to those for k_w' , except for the fact that there is a larger dip for the glycerol graph and for methanol the curve here appears to go through a slight minimum while it is virtually horizontal for k_w' .

H. Discussion. This study deals, in part, with the effect of changing solvent on the reaction between

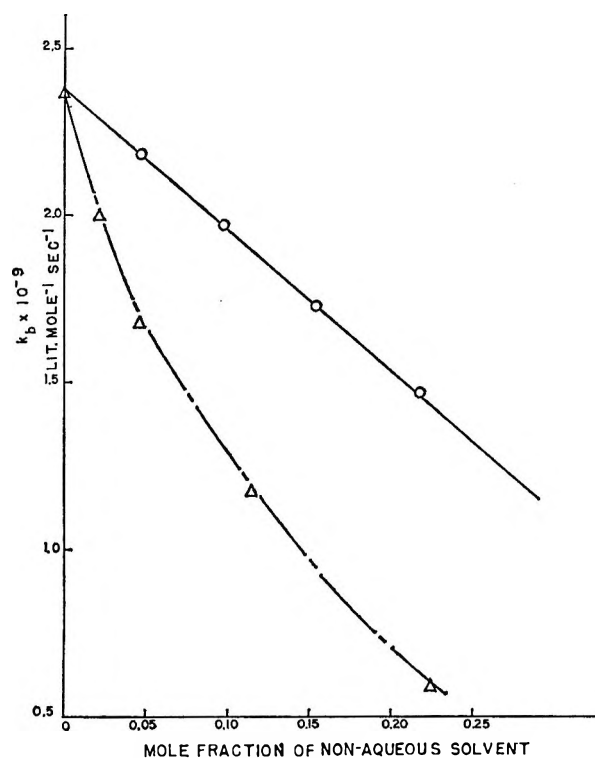


Figure 11. Forward rate constant, k_b , for β -naphthol*-acetate reaction as a function of solvent at $25 \pm 1^\circ$: O, methanol; Δ , glycerol.

Table III: Rate and Equilibrium Constants for β -Naphthol*-Acetate Reaction as a Function of Solvent Composition at $25 \pm 1^\circ$ ($R_0 = 5.5 \text{ \AA}$.)

Solvent ^a	$k_b \times 10^{-9}, \text{l. mole}^{-1} \text{sec.}^{-1}$		$10(\text{p}K_{\text{ROH}^*} - \text{p}K_{\text{HOAc}}) \times 10^2$	$k_a \times 10^{-7}, \text{l. mole}^{-1} \text{sec.}^{-1}$
	First	Second		
Water	2.53	2.38 ± 0.13	1.479	3.52 ± 0.79
10 M	2.20	2.18 ± 0.23	1.445	3.15 ± 0.77
20 M	2.18	1.97 ± 0.13	1.549	3.05 ± 0.72
30 M	1.81	1.73 ± 0.12	1.950	3.37 ± 0.67
40 M	1.60	1.47 ± 0.07	2.344	3.45 ± 0.75
10 G	2.13	2.01 ± 0.12	1.288	2.59 ± 0.47
20 G	1.79	1.69 ± 0.10	1.413	2.39 ± 0.55
40 G	1.16	1.19 ± 0.08	3.311	3.94 ± 1.21
60 G	0.68	0.61 ± 0.05		

^a M = methanol (volume %); G = glycerol (weight %).

the naphtholate ion in the excited state (RO^*) and the hydronium ion. A thorough examination of this reaction in water has been carried out by Weller.⁴ He calculated the limiting rate constant expected for this reaction on the hypothesis that it is diffusion-controlled as follows: the encounter rate is multiplied by three factors. The first is an electrostatic factor $\delta/(\epsilon\delta - 1)$ to allow for the effect of ionic charges.

Table IV: Calculated and Experimental Results for the β -Naphthol*-Water Reaction in Different Solvents at 25°

Solvent ^a	$(K_{ROH^*})^{-1}$	k_w (exptl.) $\times 10^{-7}$, sec. ⁻¹	$k_w' \times 10^{-10}$, l. mole ⁻¹ sec. ⁻¹			γ (7.5 Å.) for RO ^{-*} -H ₃ O ⁺		
			Exptl.	Calcd. (Weller)	Calcd. (La Mer)	Exptl.	Calcd. (Weller)	Calcd. (La Mer)
Water	795	6.2 \pm 0.4	4.9 \pm 0.6	4.5	4.9	0.55 \pm 0.08	0.50	0.55
10 M	1110	4.5 \pm 0.3	4.9 \pm 0.3	3.7	4.1	0.67 \pm 0.04	0.50	0.55
20 M	1680	3.0 \pm 0.2	5.0 \pm 0.5	3.2	3.8	0.79 \pm 0.08	0.50	0.59
30 M	2710	1.8 \pm 0.1	4.8 \pm 0.4	2.8	3.5	0.88 \pm 0.06	0.50	0.63
40 M	4420	1.0 \pm 0.1	4.6 \pm 0.5	2.4	3.1	0.96 \pm 0.10	0.50	0.64
10 G	790	5.0 \pm 0.3	4.0 \pm 0.2	3.7	4.3	0.53 \pm 0.03	0.50	0.55
20 G	1010	3.4 \pm 0.2	3.5 \pm 0.4	3.0	3.7	0.57 \pm 0.06	0.50	0.56
40 G	3250	1.6 \pm 0.1	5.2 \pm 1.0	1.5	2.2	1.7 \pm 3 ^b	0.50	0.62
60 G		0.41 \pm 0.07				b	0.50	0.79

^a M = methanol (volume %); G = glycerol (weight %). ^b These efficiency factors may be considered equal to 1 in the comparisons with the calculated values.

Table V: Experimental and Calculated Parameters for the β -Naphthol*-Acetate Reaction in Different Solvents at 25° ($R_0 = 6.5$ Å.)

Solvent ^a	$k_b \times 10^{-9}$, l. mole ⁻¹ sec. ⁻¹		$k_a \times 10^{-7}$, l. mole ⁻¹ sec. ⁻¹		K^*_{exptl}	γ^b		
	Exptl.	Calcd.	Exptl.	Calcd.		Exptl.	Calcd. (Weller)	Calcd. (La Mer)
Water	2.4 \pm 0.1	2.7	3.5 \pm 0.8	3.9	68	0.22 \pm 0.01	0.24	0.22
10 M	2.2 \pm 0.2	2.1	3.2 \pm 0.8	3.1	69	0.25 \pm 0.03	0.24	0.23
20 M	2.0 \pm 0.1	1.8	3.0 \pm 0.7	2.8	65	0.27 \pm 0.02	0.24	0.25
30 M	1.7 \pm 0.1	1.6	3.4 \pm 0.7	3.1	51	0.26 \pm 0.02	0.24	0.28
40 M	1.5 \pm 0.1	1.5	3.4 \pm 0.8	3.4	43	0.24 \pm 0.01	0.24	0.29
10 G	2.0 \pm 0.1	1.9	2.6 \pm 0.5	2.7	78	0.24 \pm 0.01	0.24	0.22
20 G	1.7 \pm 0.1	1.5	2.4 \pm 0.6	2.2	71	0.26 \pm 0.02	0.24	0.23
40 G	1.2 \pm 0.1	0.72	3.9 \pm 1.2	2.4	30	0.39 \pm 0.03	0.23	0.27
60 G	0.61 \pm 0.1	0.25		1.2		0.55 \pm 0.5	0.23	0.46

^a M = methanol (volume %); G = glycerol (weight %).

The second, σ , allows for the probability of achieving the proper relative configuration of the reactants; values recommended for the proton-transfer reaction are given by Weller.^{6,23} The third factor, p , is the probability of the encounter complex dissociating in the forward direction. It depends upon steric factors, the experimental value of the equilibrium coefficient, the diffusion coefficients of the reactants, and the products and the electrostatic factors of both. Values for the various rate constants calculated in this manner are compared with the experimental results in Tables IV and V. Equilibrium constants and comparisons with previously determined values are also given in these tables.

The quantity γ is defined as the ratio of the experimental rate constant, corrected for the transient reaction, to k_D .

$$\gamma = k_w'/k_D$$

$$k_D = 4\pi R_0 N' D \delta / (e^\delta - 1)$$

$$\delta = z_1 z_2 e_0^2 / \epsilon k T R_0$$

In this expression, R_0 is the encounter distance, D is the relative diffusion coefficient between the reactants, N' is Avogadro's number divided by 1000, ϵ is the dielectric constant, and k is the Boltzmann constant. D is directly proportional to the ionic mobilities which often are to be found in the literature. When the ion is relatively large, as in the case of naphtholate or acetate, it is reasonable to assume that Walden's rule may be applied, *i.e.*, that the ionic mobility is inversely proportional to the viscosity of the solvent.

(23) A. Weller, *Discussions Faraday Soc.*, 27, 28 (1959).

The mobility of H_3O^+ is anomalous, however, because of the proton-jump mechanism²⁴ leading to abnormally high values. Therefore, for H_3O^+ the mobilities were obtained directly from the literature or by use of transference numbers and the additivity of ionic conductances. A value of 7.5 Å. was selected for R_0 .²³ The efficiency factors, γ , calculated on this basis are also given in Tables IV and V. The general similarity in magnitude between the encounter rate and the rate of the reaction indicates (as was previously concluded by Weller) that the reactions studied here are not limited by the proton-transfer step itself.

In this formation all errors due to inadequacies of the model or the means of mathematically treating the model appear in values of γ . The fact that the values of γ vary considerably with the solvent composition and, in some cases, rise well above the theoretical limit of unity shows that further analysis is needed. Presumably we must deal with the questions of homogeneity of solvent distribution, local viscosity, local dielectric constant, local hydrogen bond structure, etc. In the present study we avoid detailed consideration of some of these problems by the device of comparing one reaction with another.

Thus, most of the complications introduced in the estimate of the encounter rate upon variation of the solvent can be taken into account by comparing the rate with that of another diffusion-controlled reaction. The quenching of the fluorescence of the β -naphtholate ion by iodate ion was employed for this purpose. This is presumably a diffusion-controlled reaction with a reasonably high quenching efficiency and may be expected to give a useful measure of the actual encounter rate in the various solutions.

The observed quenching constants for this reaction are given as functions of solvent compositions in Table VI for the glycerol-water and the methanol-water systems. We note that the quenching constants vary from 34.2 for pure water down to 9.36 for 60% glycerol. The magnitude of the quenching constant in water is about the same as that observed for the quenching of uranin by aniline^{25a} or of fluorescein by iodide ion in acid medium.^{25b} There is a strong dependence of the quenching constant on viscosity as shown by the fact that a given mole fraction of glycerol suppresses the quenching reaction much more than the same concentration of methanol. The curve in Figure 12, showing the quenching constants as function of the reciprocal of the viscosity, is very similar to those obtained by Svshnikov²⁶ for the effect of viscosity on the quenching of fluorescein by iodide and aniline. Positive deviations from the ideal linear relation are generally considered to be a result of the cage effect.

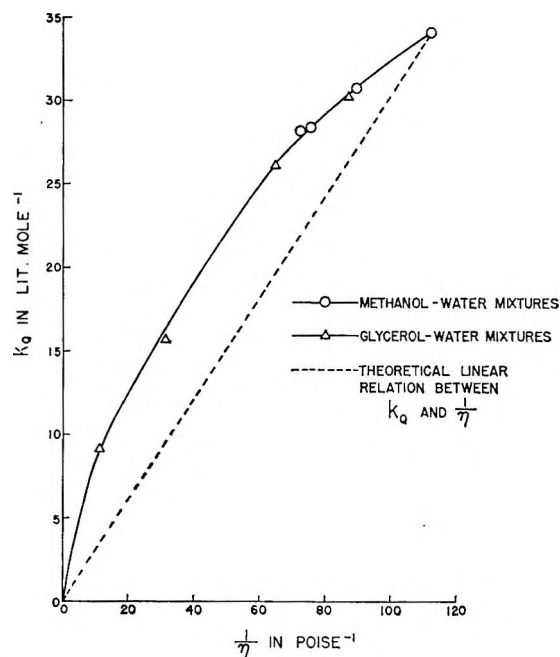


Figure 12. Quenching constant, k_q , for β -naphtholate*-iodate quenching reaction as a function of the fluidity (η^{-1}) of the solutions at $25 \pm 1^\circ$.

Because of the increased number of collisions in more viscous media, the chances for quenching in each encounter are enhanced. This means effectively that the efficiency factor, γ , for the quenching reaction should increase with the viscosity; such a variation is indeed found here. In the present reaction, the magnitude of γ for pure water, 0.34, is close to that estimated for the uranin-aniline reaction (0.53) and for the fluorescein-iodide reaction (approximately 0.25).²⁷

In the present work, no corrections were made for the effect of ionic strength on the quenching reaction ($F = 1$ here) or for the effects of reabsorption. Corrections for the transient reaction were made by the method of successive approximations used above.

In the calculation of k_D , it is necessary to assume a value for R_0 , the effective encounter distance. A value of 10 Å. was estimated as the sum of the radii of hydrated naphtholate and hydrated iodate ions. With this value, the efficiency factor for 60% glycerol is greater than 1 (1.12) and would further increase if R_0 were decreased, for example, to 7.5 Å. (2.21). For

(24) R. W. Gurney, "Ionic Processes in Solution," McGraw-Hill Book Co., Inc., New York, N. Y., 1953, pp. 73-79.

(25) (a) B. Williamson and V. K. La Mer, *J. Am. Chem. Soc.*, **70**, 717 (1948); (b) R. W. Stoughton and G. K. Rollefson, *ibid.*, **61**, 2634 (1939).

(26) B. Svshnikov, *Zh. Fiz. Khim.*, **4**, 453 (1936); **7**, 755 (1937).

(27) J. Q. Umberger and V. K. La Mer, *J. Am. Chem. Soc.*, **67**, 1099 (1945).

Table VI: Experimental Values for β -Naphtholate*-Iodate Quenching Reaction at $25 \pm 1^\circ$

Solvent ^a	k_Q , l. mole ⁻¹ (Second approx.)		$n_Q \times 10^{-9}$, l. mole ⁻¹ sec. ⁻¹ (Second approx.)		$k_D \times 10^{-9}$, l. mole ⁻¹ sec. ⁻¹		γ (Second approx.)		$V_D' \times 10^{20}$, cm. ³ (First approx.)	
	$R_0 = 10 \text{ \AA.}$	$R_0 = 7.5 \text{ \AA.}$	$R_0 = 10 \text{ \AA.}$	$R_0 = 7.5 \text{ \AA.}$	$R_0 = 10 \text{ \AA.}$	$R_0 = 7.5 \text{ \AA.}$	$R_0 = 10 \text{ \AA.}$	$R_0 = 7.5 \text{ \AA.}$	$R_0 = 10 \text{ \AA.}$	$R_0 = 7.5 \text{ \AA.}$
Water	34.2	34.0	3.57	3.55	10.53	7.041	0.339	0.504	0.687	0.907
10 M	30.8	30.6	3.24	3.22	8.238	5.480	0.394	0.587	0.768	1.03
20 M	28.5	28.1	3.00	2.96	6.850	4.521	0.438	0.654	1.09	1.50
25 M	28.3	28.0	2.95	2.92	6.372	4.196	0.463	0.695	1.10	1.52
10 G	30.6	30.4	3.19	3.16	8.029	5.340	0.398	0.592	0.831	1.12
20 G	26.4	26.0	2.75	2.71	5.906	3.917	0.465	0.692	1.07	1.46
40 G	15.9	18.1	1.71	1.95	2.762	1.805	0.620	1.08	1.02	1.63 ^b
60 G	9.36	11.8	1.06	1.34	0.942	0.604	1.12	2.21	1.69 ^b	0.953 ^b

^a M = methanol (volume %); G = glycerol (weight %). ^b In these three cases γ has been assumed equal to one in the calculation of V_D' .

the sake of comparison, the values of γ were also calculated under the assumption that R_0 is 7.5 \AA . It should be noted that the values for k_Q and n_Q change only slightly with such changes in R_0 . Furthermore, one may take R_0 as independent of solvent composition so that the general shape of the graph of γ as a function of solvent composition is unaffected.

On the basis of these results, it is assumed that the quenching of naphtholate by iodate may be used as a standard diffusion-controlled reaction for comparison with the naphtholate-hydronium ion reaction.

The ratio of the efficiency factors for the reaction of excited naphtholate ions with hydronium ions to that for excited naphtholate with iodate is shown in Figure 13, for the methanol-water and glycerol-water systems. For the methanol system, we note that this ratio is nearly constant, suggesting that the proton-transfer reactions here contains no special features not met in the quenching reaction. The fact that the ratio of efficiency factors is not unity may be due to slightly different effective radii or to somewhat different geometrical requirements of the two reactions. On the other hand, the same pair of reactions, when compared in the glycerol-water systems, differ considerably in their dependence on the solvent composition.

In order to gain further insights into this situation, the reaction of excited naphthol with acetate ion was studied in the same way and similarly compared with the quenching reaction (Figure 13). Here it is seen that both the methanol-water and the glycerol-water systems give more or less straight lines with small (negative) slopes as a function of solvent composition. The slow falling off of the relative efficiency factors with decreasing mole fraction of water (*i.e.*, the increasing relative efficiency of the quenching reaction) is in the opposite direction to that expected for a dielectric constant effect. In these two cases as well as

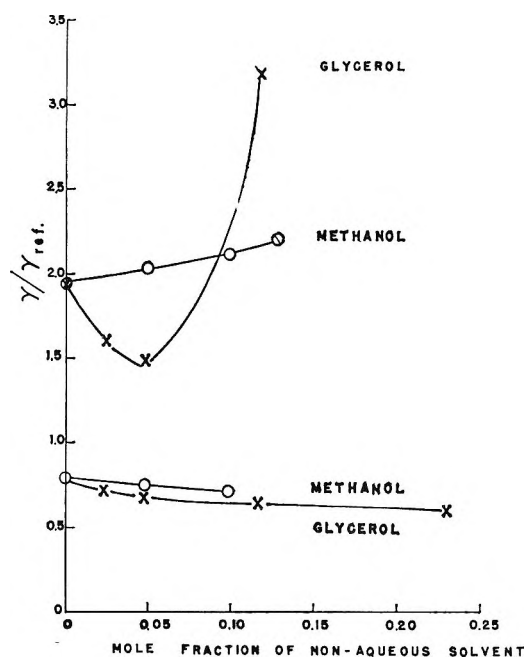


Figure 13. Efficiencies relative to the β -naphtholate*-iodate quenching reaction as a function of solvent: upper two curves, β -naphtholate*-water; lower two curves, β -naphthol*-acetate.

in the case of the naphtholate-hydronium ion reaction in methanol, the reduced relative efficiencies do not seem to fall outside of the accumulated uncertainties in the model. The behavior of the naphtholate-hydronium ion reaction in glycerol, however, appears to need special explanation. We may speculate that this is a consequence primarily of the effect on the local hydrogen bond structure. The methanol bond substitutes more or less for that of water slowly and steadily disrupting the structure. However, the glycerol, because of its internal hydrogen bond structure, provides for the proton a highly organized hydrogen

bond structure which may facilitate the proton-transfer step.

The effect of changing the solvents on the kinetics of fast reactions has also been discussed from the point of view of the energy of activation for diffusion. For example, Williamson and La Mer^{25a} equated the efficiency factor, γ , to the ratio of the probability of reaction per collision to the sum of the probability of reaction per collision and the probability of diffusion out of the encounter by either reactant between collisions; thus

$$\gamma = \frac{P \exp(-E_a/RT)}{P \exp(-E_a/RT) + c' \exp(-E_{diff}/RT)}$$

where P is the steric factor for the reaction, c' is a parameter containing orientation and other factors which influence the diffusion of a molecule out of an encounter, E_a is the chemical energy of activation, and E_{diff} is the energy of activation for diffusion in a particular solvent by either reactant.

The values of E_{diff} vary considerably from solvent to solvent. The lower the value, the more likely an encounter is to be broken off by diffusion between collisions and the lower the efficiency factor will be. Values of E_{diff} in various glycerol and methanol mixtures with water, which were reported by Hodges and La Mer,²⁸ were used to calculate γ in glycerol and methanol-water mixtures. It was assumed by Hodges and La Mer and also in the present investigation that E_{diff} is a function of the solvent rather than of the solute and is the same regardless of which encounter reaction is considered. On the other hand, the solvent was assumed to have no effect on the value of E_a . Here we took E_a as 4.4 kcal./mole.^{5b} The steric factor for the reaction, P , was taken as equal to the value of σ given by Weller for this reaction, namely, $1/4$. P was assumed to remain constant in all solvents, although in fact changes in the solvation of the reactants may affect P . Not enough molecular parameters were available to evaluate c' in different solvents. According to Williamson and La Mer,^{25a} c' is a small number approximately equal to unity for nearly spherical molecules. To simplify the calculations, it was assumed that c' is constant in all solvents. The experimental value of γ in water for the naphthol-acetate reaction, 0.22, was used in conjunction with the values of the other parameters to arrive at an estimate of $c' = 0.4545$. This value was used in the other solvents together with the appropriate values of E_{diff} to calculate the various values of γ appearing in the last columns of Tables IV and V. It is to be seen that this mode of correction of γ in comparison with that of Weller improves the agreement between experimental and theoretical values

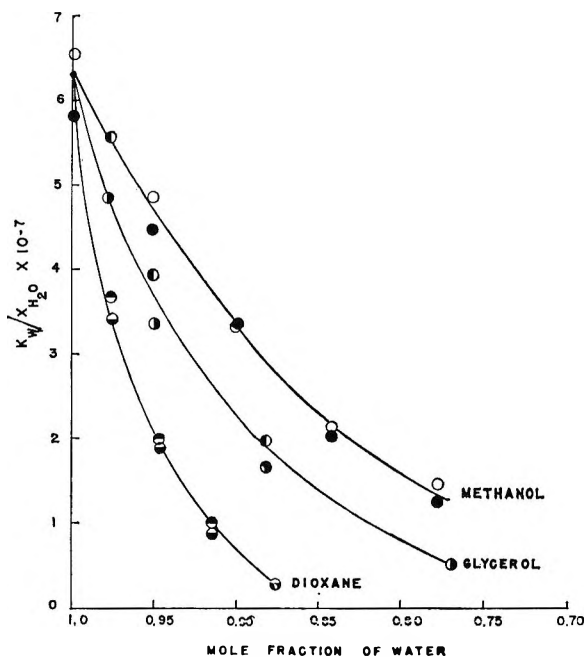


Figure 14. Second-order constants, k_w/X_{H_2O} , for the reaction β -naphthol*-water as a function of solvent composition: O, ●, ◐, points from β -naphthol*-water reaction; ●, ◐, ◑, points calculated from β -naphthol*-acetate reaction. Compare with Figure 8.

somewhat for the methanol solution but does not remove the great difference in behavior in glycerol solutions.

We now turn our attention to the reaction between β -naphthol in the excited state and water. The rate constant for this reaction can be obtained in the analysis of the naphtholate-hydronium ion reaction and also in the naphthol-acetate reaction. The pseudo-first-order rate constants are shown as functions of the solvent composition in Figure 8. We note that the reaction, which is not diffusion controlled, proceeds more slowly as the mole fraction of nonaqueous solvent is increased. The qualitative behavior is similar, but the quantitative variation of k_w with mole fraction of water is different in the methanol-water and glycerol-water systems. Dividing k_w by the mole fraction of water in order to obtain a formal second-order rate constant, Figure 14, tends to straighten out the curves but fails to remove their pronounced dependence on the mole fraction of water and does not remove the differences in the curves belonging to the two different solvent systems.

In the simplest terms we might remark that the rate appears to depend on the mole fraction of water to a power considerably higher than the first. If the re-

(28) K. C. Hodges and V. K. La Mer, *J. Am. Chem. Soc.*, **70**, 722 (1948).

action entails a preliminary ionization followed by reaction of the ions with water and a transfer of the proton away from the reaction zone, then the dielectric constant might well be a significant feature of the solvent. In order to test this hypothesis, the experiments were extended to the dioxane-water system with results as shown in Figure 14. It is seen that the general shape of the curve resembles those found for methanol-water and glycerol-water, but falls distinctly

below them, supporting the idea that the dielectric constant plays an important role in this system.

Acknowledgments. The authors are most grateful to Professor A. Schmillen of the Institute of Physics, University of Giessen, Germany, for having performed the fluorescence lifetime measurements. It is a pleasure to acknowledge assistance from the National Science Foundation.

Radiation Chemistry of Perfluorocyclohexane and Perfluorocyclobutane.

Mass Spectroscopic Identification of Products

by Michael B. Fallgatter and Robert J. Hanrahan

Chemistry Department, University of Florida, Gainesville, Florida (Received January 11, 1965)

Dimeric hydrocarbons appear to be the predominant products of the γ -radiolysis of pure perfluorocyclohexane at low doses. They have been separated and measured by gas chromatography and identified by mass spectrometry. Yields are dose dependent; initial G values are 2.2, 0.66, and 0.22 for perfluorobicyclohexyl, perfluorocyclohexylhexene, and perfluorocyclohexylhexane, respectively. Minor yields of low-boiling products were observed, as well as compounds in the C_7 - C_{11} range at higher doses. No perfluorocyclohexene was found. Perfluorocyclobutane was investigated qualitatively and gave considerable yields of C_6 , C_8 , and C_8 (dimer) compounds, as well as perfluoroethylene and perfluorocyclopropane. These results are compared with earlier work on fluorocarbons and other related systems. The mass spectra of several of the radiolysis products are reported.

Introduction

Although the radiation chemistry of hydrocarbons has been studied extensively, there is relatively little published information on the effects of ionizing radiation on their partially or wholly fluorinated analogs. The papers published to date¹⁻⁷ have largely dealt with fluorocarbons irradiated to high doses so that the questions of initial products and initial product yields are left open. There have also been some studies of the effect of electron impact on fluorocarbons at low pressures.⁸⁻¹⁰ In general, these and the previously mentioned studies have indicated that, despite the remark-

able thermal stability of many fluorocarbons, their radiation stabilities are not notably greater than those

(1) R. E. Florin, L. A. Wal, and D. W. Brown, *J. Res. Natl. Bur. Std.*, **64A**, 269 (1960).

(2) J. H. Simmons and E. H. Taylor, *J. Phys. Chem.*, **63**, 636 (1959).

(3) R. F. Heine, *ibid.*, **66**, 2116 (1962).

(4) P. Y. Feng, *Proc. 2nd. Intern. Conf. Peaceful Uses At. Energy*, **29**, 166 (1958).

(5) L. Kevan and P. Hamlet, Paper No. 126, Division of Physical Chemistry, 148th National Meeting of the American Chemical Society, Chicago, Ill., Sept. 4, 1964.

(6) D. R. MacKenzie, F. W. Bloch, and R. H. Wiswall, Jr., to be published.

of the corresponding hydrocarbons. In addition, the thermodynamics of various possible reactions involving free radical or ionic species which are postulated to occur in hydrocarbon radiolyses are unfavorable in fluorocarbon systems so that a comparison of perfluorocarbons with their hydrocarbon analogs may provide added insight into the nature of the processes occurring in both sorts of systems. Perfluorocyclohexane is particularly interesting in this respect since so much information is available on the radiolysis of ordinary cyclohexane. This report is primarily concerned with initial radiolysis products and product yields in F-cyclohexane,¹¹ quantities which have been determined as part of studies currently being undertaken of the radiation chemistry of F-cyclohexane-cyclohexane mixtures. Some preliminary qualitative work on F-cyclobutane is also reported.

Experimental

Sample Preparation and Irradiation. The F-cyclohexane used in these studies was obtained from Imperial Smelting Ltd., Avonmouth, England. The material as received was only about 95% pure and was repurified using preparative scale gas-liquid chromatography. The column used was 5 m. long, 1.9 cm. in diameter, packed with 15 g. of silicone gum rubber/100 cc. of 30-60 mesh crushed firebrick, and operated at 40°. F-Cyclobutane for the preliminary studies reported here was used as received from E. I. du Pont de Nemours and Co., Inc. The F-bicyclohexyl, which was used as received as a chromatographic standard, was obtained from Imperial Smelting Ltd.

Samples for radiolysis were degassed on a vacuum line, dried by passage of the vapors through P₂O₅, and sealed in Pyrex ampoules with a volume of about 0.2 cc. Samples of 0.15-cc. volume were irradiated for quantitative experiments; they were metered out as gases using PVT procedures on the vacuum line. All irradiations were done in a "Wisconsin" type Co⁶⁰ γ -irradiator which has been described previously.¹² Dose rates were measured relative to $G(\text{Fe}^{+3})$ of 15.5 for the Fricke dosimeter and corrected to dose absorbed in the fluorocarbon using relative electron densities. For F-cyclohexane, the absorbed dose rate was about 0.9×10^{18} e.v./ml. min. Doses used for F-cyclohexane ranged from 0.2 to 8 Mrads. Qualitative observations made on F-cyclobutane were done with samples irradiated to about 8 Mrads. To keep F-cyclohexane in the liquid state, it was irradiated at $64 \pm 1^\circ$ using an oil thermostat bath.

Glass irradiation vessels were used to facilitate sample preparation and handling. It has been stated⁶ that this leads to the production of SiF₄ from reaction of

fluorine with the walls. However, the same workers⁶ have reported that there is no net formation of F₂ in this system, even in prefluorinated nickel vessels. Relatively slow diffusion in the liquid state should minimize reaction with the walls for small amounts of fluorine possibly present in the steady state during radiolysis. Finally, we have observed no etching of the walls even after doses of 8 Mrads and no fuming when the cell contents were exposed to air.

Sample Analysis. Qualitative analyses of the radiolysis products of F-cyclohexane and F-cyclobutane were made using a combination of gas-liquid chromatography and mass spectrometry (Figure 1). The effluent from the chromatograph column passed a stream-splitting needle valve (A) through which a portion of the column output could be diverted into the mass spectrometer, a Bendix Model 14 time-of-flight instrument, equipped with an extra long flight tube giving unit resolution to mass 300. (For fluorocarbons, where the more likely mass peaks occur a minimum of five mass units apart, the instrument permits

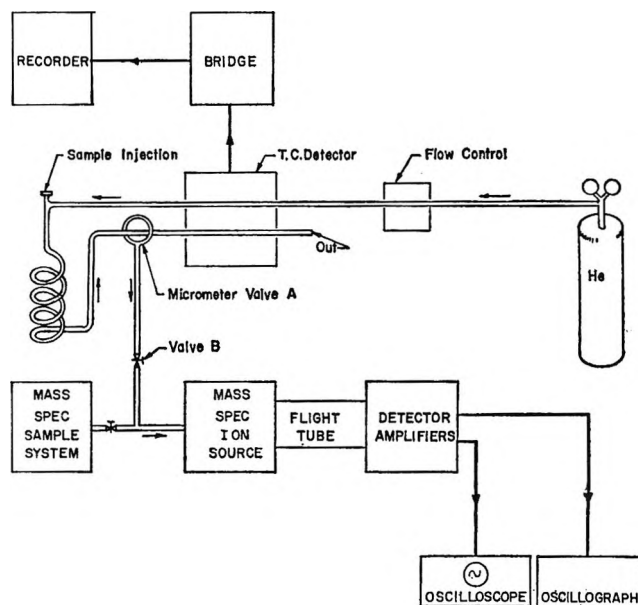


Figure 1. Block diagram of gas chromatograph-mass spectrometer combination.

- (7) V. A. Khranchenkov, *Soviet J. At. Energy*, 17, 53 (1964).
- (8) P. Natalis, *Bull. Soc. Roy. Sci. Liege*, 29, 94 (1960).
- (9) J. R. Majer, "Advances in Fluorine Chemistry," Vol. 2, Butterworth, Inc., Washington, D. C., 1961, p. 55.
- (10) G. A. W. Derwish, A. Galli, A. Giardini-Guidoni, and G. G. Volpi, *J. Am. Chem. Soc.*, 86, 4563 (1964).
- (11) For convenience, any completely fluorinated organic compound will be labeled with the prefix F- rather than the prefix perfluoro-.
- (12) R. J. Hanrahan, *Intern. J. Appl. Radiation Isotopes*, 13, 254 (1962).

identification of mass peaks out to at least mass 700.) With large chromatograph peaks, it was possible to take the mass spectrum as the peak was being eluted, but small peaks had to be treated somewhat differently. In these cases a second valve (B) on the sample manifold of the spectrometer was closed as the peak of interest was eluted so that a sample of the column effluent accumulated in the section of tubing between valves A and B. Valve A was then closed and a segment of the intermediate tubing was cooled with liquid nitrogen, freezing out the sample of interest. The helium carrier gas was then bled out through the mass spectrometer and the cooled section of tubing was allowed to warm to room temperature. The sample of interest was then admitted to the mass spectrometer, using valve B as a controlled leak. It was not possible to keep the source pressure absolutely constant while the mass spectrum was being taken in this manner, but mass spectra of F-bicyclohexyl taken using this technique were nearly identical with those taken using the normal method of sample admission to the mass spectrometer through a pinhole molecular leak. For qualitative analysis of the radiolysis products of F-cyclobutane, a silica gel column 1 m. long, 5 mm. in diameter, and temperature programmed from room temperature to 150° at 5.6°/min. was used. Qualitative and quantitative analyses of the initial C₁₂ radiolysis products of F-cyclohexane were made by gas-liquid chromatography, using a 1.9-m. column, 5 mm. in diameter, packed with 15 g. of silicone gum rubber/100 cc. of Chromosorb W and operated at 40°. For analysis of F-bicyclohexyl, a standard solution was used to determine the sensitivity of the gas chromatograph, injections of the standard solution being made before and after analysis of a radiolyzed sample. Standards were not available for the other C₁₂ radiolysis products of F-cyclohexane, so the chromatographic sensitivities to these products were assumed to be the same as to F-bicyclohexyl. Ampoules of radiolyzed sample were broken in the chromatograph inlet system, which included a short side arm consisting of an 18/9 ball and socket joint into which the ampoules were loaded. The thin stems of the ampoules could then be broken by twisting the joint. Most of the quantitative analyses were done using an Aerograph flame ionization detector, but a few analyses done using a Gow-Mac thermal conductivity cell with W-2 filaments agreed well with those done using flame ionization detection.

Results

F-Cyclohexane. In previously published work on F-cyclohexane by MacKenzie, *et al.*,⁶ numerous radiolysis products were found, not all of which were identified.

In particular, products in the C₁-C₄ range were formed with a total *G* value of 0.204, C₄-C₆ products were found by them to be formed with a *G* value of 0.09, and other products having molecular weights greater than that of F-cyclohexane starting material were formed with a total *G* value of 2.1, reported in terms of loss of starting material. Our studies were made at much lower doses than those of MacKenzie, *et al.*,⁶ and thus we have observed a somewhat different distribution of products. At the doses used in our studies, the yields of C₁-C₆ products were too low to measure accurately, and we estimate the maximum total *G* value for these compounds to be 0.3. At low doses, chromatograms of compounds less volatile than F-cyclohexane showed only three prominent peaks, closely spaced but well resolved, with area ratios roughly 1:3:8. We will temporarily designate these products as compounds A, B, and C, respectively. The mass spectra of these compounds are given in Table I, which lists all ions contributing more than 1% of the total, plus others of special structural significance.

Table I: Mass Spectra of C₁₂ Radiolysis Products of F-Cyclohexane

<i>m/e</i>	Species	Relative intensities		
		A (Cyclohexylhexane)	B (Cyclohexylhexene)	C (Bicyclohexyl)
581	C ₁₂ F ₂₃	0.74		
562	C ₁₂ F ₂₂		0.02	
543	C ₁₂ F ₂₁		1.2	2.0
393	C ₉ F ₁₅	0.10	0.21	6.5
331	C ₇ F ₁₃	1.2	0.56	
319	C ₆ F ₁₃	0.57		
281	C ₆ F ₁₁	2.3	6.7	1.4
269	C ₆ F ₁₁	1.1		0.07
231	C ₆ F ₉	1.0	1.8	1.7
219	C ₄ F ₉	1.8		0.23
193	C ₅ F ₇	1.0	1.8	1.9
181	C ₄ F ₇	3.0	2.6	3.6
169	C ₃ F ₇	3.2	0.59	1.4
162	C ₄ F ₆	1.3	2.4	2.4
143	C ₄ F ₆	0.89	1.6	1.7
131	C ₃ F ₅	12.5	21.0	20.3
119	C ₂ F ₅	8.9	3.8	3.3
100	C ₂ F ₄	6.1	7.4	7.0
93	C ₃ F ₃	2.6	4.4	3.3
69	CF ₃	45.6	34.4	26.1
31	CF	2.3	3.3	1.9

Compound C is identified as F-bicyclohexyl, since both its mass spectrum and chromatographic retention time were identical with those of our standard sample of F-bicyclohexyl. It is clear from Table I that compounds A and B are both C₁₂ compounds and also that

they must bear some structural similarity to F-bicyclohexyl, since all three fragmentation patterns are rather similar. In considering these mass spectra, it is important to recall that saturated perfluorocarbons frequently do not give a parent positive ion but do give an ion lacking one fluorine atom, and that perfluoroolefins often do give the parent ion, but in small abundance. In the mass spectrum of compound A, the highest peak observed is at mass 581, corresponding to the fragment $C_{12}F_{23}$. This indicates that the formula of the compound is probably $C_{12}F_{24}$ (molecular weight 600) which presumably could be either a noncyclic monoolefin or an alkyl cyclohexane. Since no parent ion peak at mass 600 could be found, we conclude that compound A is F-cyclohexylhexane. The highest prominent peak in the spectrum of compound B is 543, corresponding to the grouping $C_{12}F_{21}$ and suggesting that the formula of the compound is $C_{12}F_{22}$. This could either be an unsaturated alkyl cyclohexane or a bicyclic compound. Since an examination of the mass spectrum at high sensitivity showed the presence of a weak ion peak at mass 562, and since compound C has already been shown to be bicyclohexyl, we identify compound B as F-cyclohexylhexene. Furthermore, a more detailed examination of Table I strongly suggests that compound B has its double bond at the end of the side chain since the mass peaks at 69 (CF_3^+) and 119 ($C_2F_5^+$) are smaller for compound B than for compound A. These would have to be rearrangement products if B is a terminal olefin.

Figure 2 shows the yields of the three C_{12} products with dose. The initial G values are given in Table II.

Table II: Yields of Radiolysis Products of F-Cyclohexane

Products	Yields (G values)	
	This study	MacKenzie, <i>et al.</i> ⁶
C_1-C_6	0.3 (estimated)	0.3 ^a
$>C_6$	3.1 ^b	2.1 ^c
F-Bicyclohexyl	2.2 ^d	0.36
F-Cyclohexylhexene	0.66 ^d	...
F-Cyclohexylhexane	0.22 ^d	...

^a Consisting of $G(CF_4) = 0.07$, $G(C_2F_6) = 0.065$, $G(C_3F_8) = 0.035$, and $G(C_4F_{10}) = 0.034$. ^b Sum of the C_{12} products listed below. ^c Reported as loss of F-cyclohexane. ^d Initial G values taken from slopes of straight lines in Figure 2.

The G value for F-bicyclohexyl by MacKenzie, *et al.*,⁶ is not necessarily in disagreement with our value since their measurements were made at higher doses at which the yield of F-bicyclohexyl decreases, as is seen in Figure 2.

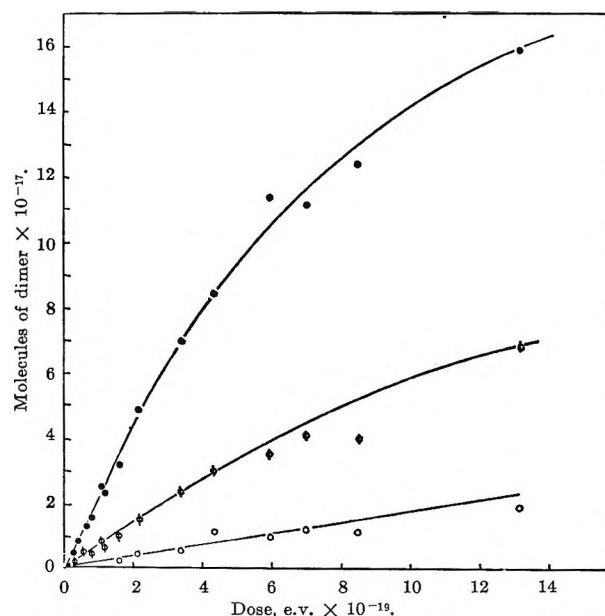


Figure 2. Dimeric products in the γ -radiolysis of F-cyclohexane at 64°: ●, F-bicyclohexyl; ○, F-cyclohexylhexene; ○, F-cyclohexylhexane. The indicated doses were delivered to 0.15-ml. samples.

At higher doses, additional products between C_6 and C_{12} are formed. Of these products, two have been identified from their mass spectra as F-methylcyclohexane and F-ethylcyclohexane. These and other C_6-C_{12} products, presumably F-alkylcyclohexanes of various chain lengths, were formed in very small amounts and no quantitative determinations were made of their yields. Similarly, although small amounts of CF_4 , C_2F_6 , and C_3F_8 are formed, the initial yields are at least one order of magnitude lower than those of the C_{12} products and detailed yield measurements were not made. We estimate that the total G value for these compounds is less than 0.3.

One of the major products in the radiolysis of cyclohexane is cyclohexene and it seems a question of some interest if F-cyclohexene is formed during F-cyclohexane radiolysis. We were not able to identify any chromatograph peak as F-cyclohexene, but the possibility existed that our chromatograph column was not separating F-cyclohexene and F-cyclohexane. To test this possibility, the ability of the Bendix time-of-flight mass spectrometer to scan several mass peaks simultaneously was used. One scanner was set on mass 131, the highest intensity peak in the mass spectrum of F-cyclohexane, and a second scanner was set on mass 162, which is the highest intensity peak in the mass spectrum of F-cyclohexene,⁹ but which in the spectrum of F-cyclohexane is only 4% as intense as the 131 peak.

The F-cyclohexane chromatograph peak in a sample irradiated to about 2×10^{21} e.v./g. was then monitored for these two masses. The ratio of the two mass peaks did not change throughout the course of the experiment, indicating that little if any F-cyclohexane was present. We estimate that formation of F-cyclohexane with a G value of 0.1 or greater would have produced enough of the material to cause an easily observable change in the 162:131 ratio during the passage of the chromatographic peak.

Another problem in accounting for the distribution of radiolysis products in F-cyclohexane is that of fluorine balance. The fluorine which must be accounted for as a result of formation of F-bicyclohexyl and F-cyclohexylhexene amounts to $G(\text{F}) = 6$. Although formation of saturated straight chain and alkylcyclohexyl products can account for a portion of this fluorine, no more than perhaps 10% can be accounted for in this manner. MacKenzie, *et al.*,⁶ report no F_2 production in the radiolysis of F-cyclohexane. It would appear then that there must be other radiolysis products which have so far been unidentified. Perhaps the most likely possibility for such a product is F-*n*-hexane which might not have been separated from the F-cyclohexane parent by our chromatographic columns. Experiments are in progress to determine if this is the case.

F-Cyclobutane. Chromatography on a silica gel column of irradiated F-cyclobutane gave three small chromatographic peaks (I, II, III) of shorter retention time than the parent and three much larger peaks (IV, V, VI), at longer retention times. Peak I is taken to be F-ethylene, since its retention time agreed with a known sample. Peak II is identified as CHF_3 since its mass spectrum is in good agreement with that of a known sample of this substance. The base peak in each case is at m/e 51, corresponding to CHF_2^+ . (Our fragmentation pattern disagrees with that reported by Majer,⁹ which shows 69 rather than 51 as the most intense peak.)

Peak III is identified as F-cyclopropane from its mass spectrum, which is given in Table III. This fragmentation pattern is unlike that of either F-propylene (also listed in Table III for comparison) or F-propane as given by Majer.⁹ However, it is essentially identical with the cracking pattern of a product obtained in the mercury-sensitized photolysis of F-ethylene (done in a corollary experiment) which has been reported to be F-cyclopropane.¹³ If F-cyclopropane is a radiolysis product it would seem reasonable to expect some F-propylene as well, since any mechanism which would lead to the former might be expected to give at least some of the latter as a by-product. No evidence of a chromatograph peak which could correspond to F-

Table III: Mass Spectra of Some C_3 Fluorocarbons

m/e	Species	Relative abundance	
		Radiolysis product (F-cyclopropane)	F-Propylene (ref. 9)
150	C_3F_6	2.52	28.6
131	C_3F_5	15.59	72.0
100	C_2F_4	58.46	36.1
93	C_3F_3	1.79	5.87
81	C_2F_3	11.12	14.2
69	CF_3	74.02	77.1
50	CF_2	35.97	12.1
43	C_2F	12.2	4.06
31	CF	100.0	100.0

propylene was actually found. However, the F-cyclopropane peak is eluted just before the large peak for the parent F-cyclobutane, which could have obscured a peak for F-propylene. The latter compound is reported to elute between F-cyclopropane and F-cyclobutane on a silica gel column.⁶

The major post-parent chromatograph peaks were apparently mixtures of unresolved C_5 , C_6 , and C_8 fluorocarbons, since mass spectra of the chromatograph peaks taken using samples irradiated to different doses gave different cracking patterns. The highest mass peaks observed in the cases of the C_5 and C_6 chromatograph peaks corresponded to saturated, noncyclic species, C_5F_{12} and C_6F_{14} . However, these spectra also had very high intensities at m/e 100 (corresponding to C_2F_4^+), which is characteristic of an F-cyclobutane ring. We conclude, therefore, that these products are mainly F-methylcyclobutane and F-ethylcyclobutane, respectively, with smaller amounts of F-pentane and F-hexane also present. The absence of an appreciable C_7 chromatograph peak is curious; since this corresponds to a C_3 fragment plus butane, it may be related to the presence of cyclopropane as a radiolysis product.

The largest value of m/e observed in the mass spectrum of the C_8 chromatograph peak was 381, corresponding to the fragment $\text{C}_8\text{F}_{16}^+$ and indicating the parent molecule C_8F_{16} . Again there was a very high intensity at m/e 100, indicating F-cyclobutane rings. We postulate that this peak consists of F-butylicyclobutane and probably also F-bicyclobutyl (by analogy with the case of F-cyclohexane) with little if any saturated F-octane formed.

It should be noted that, during the analysis of all three of the post-parent chromatograph peaks, the mass spectrometer showed a weak peak at m/e 51 (CHF_2^+), indicating that small amounts of hydrogen-

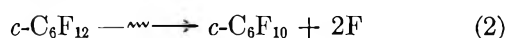
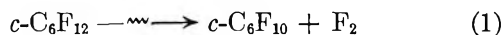
(13) B. Atkinson, *J. Chem. Soc.*, 2684 (1952).

containing materials were being eluted along with the perfluorocarbons listed above. The production of CHF_3 was also noted earlier. It is apparent that the F-cyclobutane sample which we used contained some partially hydrogenated materials. Although quantitative work was not undertaken pending the further purification of the sample, we believe that the qualitative observations described above are valid.

Discussion

Although extended speculation about mechanism is premature, some generalizations may be pertinent. Among the major differences between the perfluorocarbons and the hydrocarbons are the great strength of the C-F bond compared to the C-H bond, and the weakness of the F-F bond compared to the H-H bond. The former is clearly no deterrent to C-F bond rupture during radiolysis; more than 80% of the observed bond rupture in the radiolysis of liquid F-cyclohexane involves C-F rather than C-C bonds. It is true that F-cyclohexane is probably not a typical compound, since ordinary cyclohexane shows far less C-C bond rupture than hydrocarbons in general. Nevertheless, implications that the radiation chemistry of perfluorocarbons is centered in C-C rather than C-F bonds should be avoided.

The weakness of the F-F bond is important since it must mean that abstraction from fluorocarbon substrate by F atoms to make F_2 is essentially impossible. This factor alone would be enough to make the radiation chemistry of fluorocarbons much different from that of hydrocarbons. It may also be related to the apparent lack of F-cyclohexene among the radiolysis products. In the case of cyclohexane radiolysis, most mechanisms proposed for cyclohexene production involve either molecular elimination of H_2 or the elimination of two (possibly hot) hydrogen atoms. The corresponding reactions in F-cyclohexane are both quite unfavorable thermodynamically

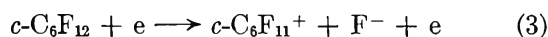


The first is endothermic by about 150 kcal./mole; the second is about 40 to 50 kcal./mole more endothermic than in the case of ordinary cyclohexane. Furthermore, in both cases the products would be subject to caged recombination (unlike the case of the hydrocarbons where H_2 is presumably nearly inert). The abstraction of fluorine from the substrate is so endothermic (82 kcal./mole) that it is dubious even as a "hot" process.

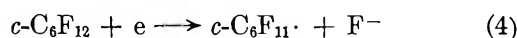
The role of fluorine in the radiolysis, whether as F

or F_2 , remains to be further elucidated. It can be pointed out that in the case of ordinary cyclohexane, a large part of the total hydrogen gas yield (G of about 5.5) is balanced by the production of cyclohexene (G of about 3). Since F-cyclohexene apparently is not formed, the maximum yield of F_2 which might be expected would be less than the corresponding H_2 yield from cyclohexane. As we have noted above, the present results show a deficit of molecular fluorine with a G value of about 3, or 6 for fluorine atoms. Although this deficit could be attributed to the use of glass vessels, the same general problem seems to occur in studies using metal vessels, in which no fluorine was found.⁶

With respect to possible ionic aspects of the mechanism, consideration may be given to mass spectroscopic evidence. One common aspect of fluorocarbon mass spectra, true of F-cyclohexane, is the near zero abundance of the parent positive ion. Field and Franklin¹⁴ point out that the most probable ionization process for fluorocarbons may involve loss of F^- , presumably



The rather similar electron capture process would give F-cyclohexyl radical as one of the products



In spite of the high electron affinity of fluorine, this reaction cannot occur with thermalized electrons because the C-F bond strength greatly exceeds the electron affinity. These processes, if they occur, would modify the nature of the neutralization process, as well as providing a mechanism for C-F bond rupture. Unfortunately, the general pertinence of the 70-v. mass spectrum is even more dubious here than in the case of hydrocarbons. The most intense peaks in the cracking pattern of F-cyclohexane are m/e 131 (C_3F_5^+) and 69 (CF_3^+); corresponding radiolysis products do not occur in significant yield. The radical ion $\text{C}_6\text{F}_{11}^+$ occurs with an abundance of only 3.43% in contrast to the preponderance of C_6F_{11} fragments under radiolysis.

It seems simplest and most reasonable to attribute the formation of F-bicyclohexyl to radical recombination. The experimental results indicate that the production of F-cyclohexylhexene and F-cyclohexylhexane are not coupled to that of F-bicyclohexyl, since the former two increase nearly linearly with dose while the production of the latter falls off markedly. Hence there is a temptation to write a different sort of mechanism—possibly an ionic one—for the first two com-

(14) F. H. Field and J. L. Franklin, "Electron Impact Phenomena," Academic Press, New York, N. Y., 1957, p. 179.

pounds. Although a plausible ion-molecule sequence can be written leading to these products, there is no supporting evidence for the reactions involved. No data on ion-molecule reactions in saturated fluorocarbons have been published, although a paper on the high-pressure mass spectrum of F-ethylene appeared recently.¹⁰

The qualitative data on F-cyclobutane seem to fit the same general pattern as F-cyclohexane and will not be discussed in detail. The greater amount of fragmentation in this case can be attributed to greater ring strain.

In the above discussion we have stressed comparison of F-cyclohexane with hydrocarbon systems. In many ways the radiation chemistry of CCl_4 may be more pertinent. Points of comparison include great sensitivity to impurities, rather low net yields, high

electronegativity of the halogen involved, and implausibility of abstraction reactions. Radiolysis of hydrogen-containing substances in the two media have some analogous aspects as well; work in this direction is currently in progress in our laboratories.

Acknowledgment. This work was supported by AEC Contract AT-(40-1)-3106 and by the University of Florida Nuclear Sciences Program. We wish to thank E. C. Stump of Peninsular ChemResearch, Gainesville, Fla., D. R. MacKenzie of Brookhaven National Laboratory, D. G. Hummel of DuPont Co., and T. M. Reed of the University of Florida for providing various fluorocarbon samples. This work was described in part in paper no. 127, Division of Physical Chemistry, 148th National Meeting of the American Chemical Society, Chicago, Ill., Sept. 4, 1964.

The Volatilization of Molybdenum in the Presence of Water Vapor

by G. R. Belton and A. S. Jordan

Department of Metallurgy, University of Pennsylvania, Philadelphia 4, Pennsylvania (Received March 15, 1966)

A study has been made, using the transpiration technique, of the enhanced volatility of molybdenum in mixtures of water vapor, hydrogen, and argon. The major volatilization is shown to occur by the reaction $\text{Mo(s)} + 4\text{H}_2\text{O(g)} = \text{MoO}_3\text{H}_2\text{O(g)} + 3\text{H}_2\text{(g)}$. The standard free energy change for the reaction between 1200 and 1500° is given by $\Delta F^\circ = 40,410 - 7.10T$. The standard free energy changes for the reactions $\text{Mo(s)} + 3\text{H}_2\text{O(g)} = \text{MoO}_3\text{(g)} + 3\text{H}_2\text{(g)}$ and $\text{Mo(s)} + 2\text{H}_2\text{O(g)} = \text{MoO}_2\text{(g)} + 2\text{H}_2\text{(g)}$, obtained by combination of this work with mass spectrometric studies from the literature, are given by $\Delta F^\circ = 100,120 - 33.99T$ and $\Delta F^\circ = 119,900 - 41.04T$, respectively.

Introduction

In a recent paper¹ the enhanced volatility of metallic tungsten in the presence of water vapor at elevated temperatures was shown to be due to the formation of the gaseous hydrated compound $\text{WO}_3\text{H}_2\text{O}$. The present paper describes a similar study of the effect of water vapor on the volatility of molybdenum.

Millner and Neugebauer² were the first to note that

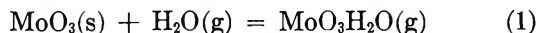
the volatility of molybdenum trioxide at 600 and 700° was increased by the presence of water vapor. Later, Brewer and Elliott³ extended this work by measuring

(1) G. R. Belton and R. L. McCarron, *J. Phys. Chem.*, **68**, 1852 (1964).

(2) T. Millner and J. Neugebauer, *Nature*, **163**, 601 (1949).

(3) L. Brewer and G. R. B. Elliott, University of California, Radiation Laboratory Report 1831, 1952.

the amount of MoO_3 which could be volatilized in sealed silica tubes in the presence of various amounts of water at 560° . These authors concluded that the volatility was a linear function of the water pressure and that the volatilization occurred by the reaction



Glemser and Haeseler⁴ have since carried out more precise transpiration experiments on the volatility of the oxide in water vapor + oxygen mixtures from 600 to 690° . This work, together with the measurements of Wendlandt and Glemser⁵ on the volatility of MoO_3 in steam at elevated pressures and at 500° , supported the linear dependence necessary for reaction 1. However, the possibility of more than one MoO_3 unit in the volatile species cannot be ruled out by the above results although the simple species would be expected by analogy with the behavior of tungsten.

The purpose of the present investigation has been to prove conclusively the formula of the volatile compound and to obtain thermodynamic data for the formation of the compound directly from the metal and over a substantial temperature range. This has been achieved by using the transpiration technique to measure the apparent vapor pressure of molybdenum in the presence of water vapor + hydrogen + argon mixtures insufficiently oxidizing to permit formation of the condensed oxide. The contribution of the gaseous oxide to the volatility has been derived by taking advantage of the dependence of the oxide pressure on the water vapor-hydrogen ratio alone.

Experimental

The transpiration apparatus and experimental procedure were substantially the same as were used in the earlier work¹ and described in some detail by Belton and Richardson.⁶ A change in procedure was introduced, however, by the desire to vary the pressure of water vapor independently of the water vapor-hydrogen ratio. This was achieved by saturating several argon + hydrogen mixtures as well as pure hydrogen.

Materials. High purity molybdenum wire (Fansteel Metallurgical Corp.) approximately 0.25 mm. in diameter and with a minimum molybdenum content of 99.95% was used in the experiments. Experimental specimens which were approximately 25 mm. long by 4 mm. in diameter were constructed of two concentric coils of the wire.

Apart from pure hydrogen, three commercially prepared high purity argon-hydrogen gas mixtures were used. Their hydrogen contents in volume per cent were 33.3 ± 0.1 , 14.9 ± 0.1 , and 4.56 ± 0.01 .

The maximum impurity contents were $\text{N}_2 < 250$ p.p.m., $\text{O}_2 < 10$ p.p.m., and hydrocarbons < 20 p.p.m.

Results

The experimental results are shown in Figures 1 and 2, where the apparent vapor pressure of molybdenum is shown plotted against the flow rate (STP) of the equilibrium gas. Two additional sets of data obtained at 1500° and with a water vapor-hydrogen ratio of 1.00 are not shown; however, these data showed experimental scatter similar to those illustrated.

The equilibrium pressures were taken as the "plateau" values, *i.e.*, the regions where the apparent vapor pressure is independent of flow rate. These values, together with the experimental conditions, are presented in Table I. The average value of the mean deviations from the equilibrium results, listed in Table I, is approximately 3%. As the vapor pressure of molybdenum⁷ is negligible at the temperatures of the experiments, the listed equilibrium pressures are directly ascribable to the one or more gaseous compounds stable under the conditions of the experiments.

Table I: The Volatility of Molybdenum in the Presence of Water Vapor

Temp., °C.	$p_{\text{H}_2\text{O}}/p_{\text{H}_2}$	$p_{\text{H}_2\text{O}}$, mm.	Total apparent vapor press., atm. $\times 10^6$
1500	1.00	99.1	62.60
1500	1.00	33.1	29.50
1479	1.00	33.1	22.72
1479	1.00	99.1	56.38
1479	1.00	190.5	91.77
1479	0.82	27.2	12.99
1479	0.82	82.1	26.20
1479	0.82	162.3	45.80
1479	0.82	340.0	90.92
1383	1.40	45.6	31.33
1383	1.40	241.8	133.80
1283	1.00	33.1	3.08
1283	1.00	190.5	16.16
1200	1.00	33.1	1.67
1200	1.00	99.1	5.30
1200	1.00	381.8	19.34
1200	0.87	353.8	11.55

(4) O. Glemser and R. Haeseler, *Z. anorg. allgem. Chem.*, **316**, 168 (1962).

(5) H. G. Wendlandt and O. Glemser, *Angew. Chem.*, **75**, 949 (1963).

(6) G. R. Belton and F. D. Richardson, *Trans. Faraday Soc.*, **58**, 1562 (1962).

(7) J. W. Edwards, H. L. Johnston, and P. E. Blackburn, *J. Am. Chem. Soc.*, **74**, 1534 (1952).

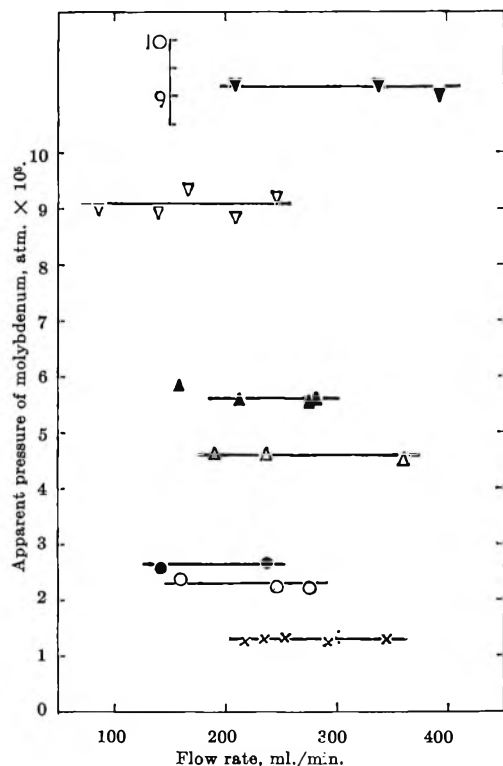
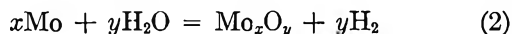


Figure 1. Results obtained from transpiration experiments at 1479°. Values of p_{H_2O}/p_{H_2} and p_{H_2O} (mm.), respectively, are: ∇ , 1.00, 190.5; ∇ , 0.82, 340.0; \blacktriangle , 1.00, 99.1; \triangle , 0.82, 162.3; \bullet , 0.82, 82.1; \circ , 1.00; 33.1; \times , 0.82, 27.2.

Each pressure may then be separated into an oxide contribution and the hydrated species contribution by taking advantage of the pressure dependence on gas composition. If a general reaction for the formation of a gaseous oxide is formulated



it follows that the apparent pressure of the oxide is directly proportional to $(p_{H_2O}/p_{H_2})^y$. Hence, for any set of data taken with a constant water vapor-hydrogen ratio, the contribution which is independent of water pressure must be due to the volatile oxide or oxides.

In Figures 3 and 4 the apparent pressures of Mo are shown plotted against the partial pressure of water vapor at constant water vapor-hydrogen ratios. The values of the intercepts at zero water pressure represent the pressures of the gaseous oxides. A linear dependence of the pressure of molybdenum on the pressure of water is clearly shown by the data at 1479 and 1200°. Hence, the data were analyzed by the method of least mean squares to determine the best values for the intercepts (oxide contribution) and slopes (hydrated species contribution) of the straight line. Each separate measurement was given equal weight in these

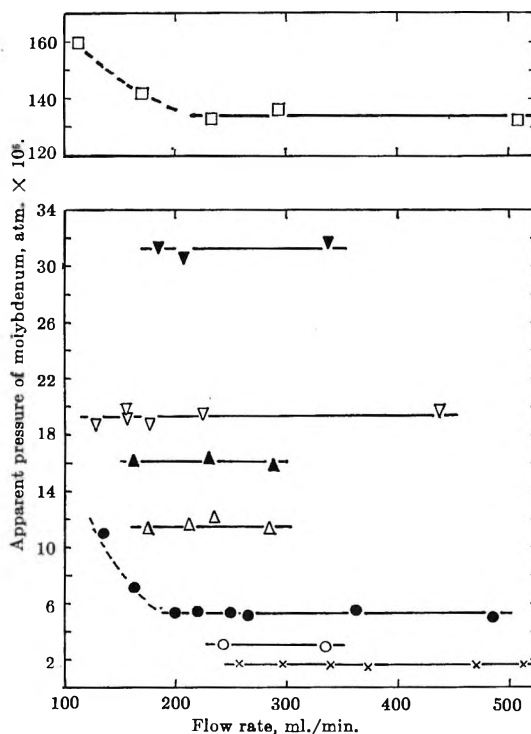


Figure 2. Results obtained from transpiration experiments at 1200 to 1383°. Values of p_{H_2O}/p_{H_2} , p_{H_2O} (mm.), and temperature (°C.), respectively, are: \square , 1.40, 241.8, 1383°; \blacktriangle , 1.40, 45.6, 1383°; ∇ , 1.00, 381.8, 1200°; \blacktriangle , 1.00, 190.5, 1283°; \triangle , 0.87, 353.8, 1200°; \bullet , 1.00, 99.1, 1200°; \circ , 1.00, 33.1, 1283°; \times , 1.00, 33.1, 1200°.

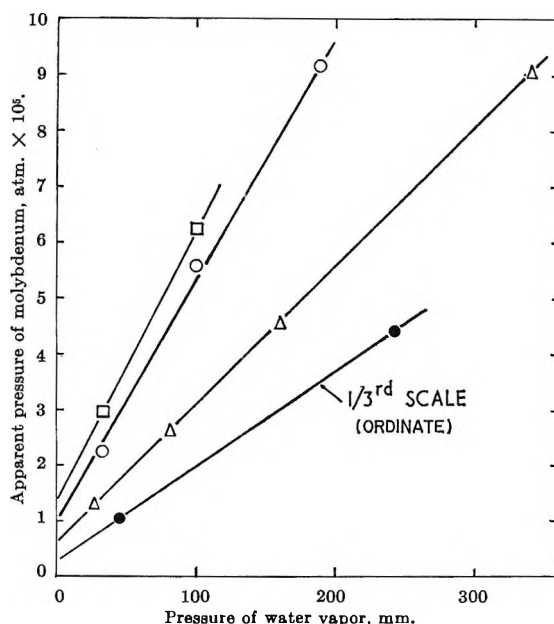


Figure 3. Dependence of apparent volatility of Mo on the pressure of water vapor at constant p_{H_2O}/p_{H_2} ratios. Values of p_{H_2O}/p_{H_2} and temperature (°C.), respectively, are: \square , 1.00, 1500°; \circ , 1.00, 1479°; \triangle , 0.82, 1479°; \bullet , 1.40, 1383°.

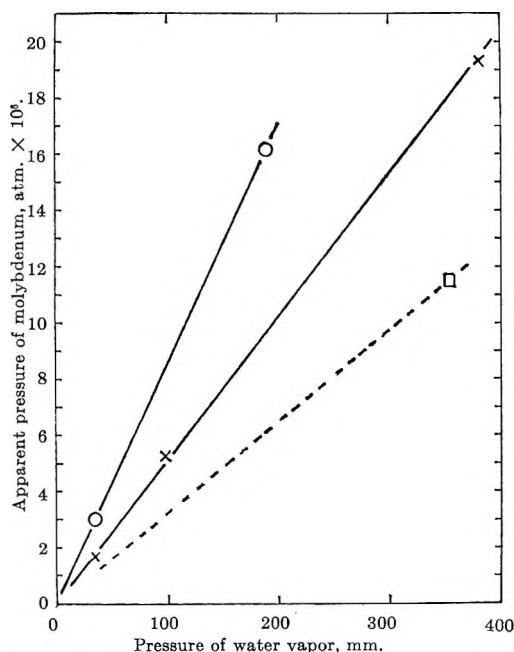


Figure 4. Dependence of apparent volatility of Mo on the pressure of water vapor at constant $p_{\text{H}_2\text{O}}/p_{\text{H}_2}$ ratio at the lower temperatures. Values of $p_{\text{H}_2\text{O}}/p_{\text{H}_2}$ and temperature ($^{\circ}\text{C}.$), respectively, are: \circ , 1.00, 1283 $^{\circ}$; \times , 1.00, 1200 $^{\circ}$; \square , 0.87, 1200 $^{\circ}$.

calculations in order to give meaningful probable errors. The resulting pressures of the oxides and of the hydrated species are presented in Table II. The data at 1283 and 1200 $^{\circ}$ gave zero intercepts within the probable errors of the experiments and were interpreted accordingly.

Table II: Derived Partial Pressures of Hydrated and Unhydrated Species

Temp., $^{\circ}\text{C}.$	$p_{\text{H}_2\text{O}}/p_{\text{H}_2}$	Press. of hydrated species/atm. of H_2O , atm. $\times 10^6$	Total press. of oxide species, atm. $\times 10^6$
1500	1.00	380.4 \pm 6.7	13.00 \pm 1.1
1479	1.00	330.5 \pm 6.8	10.48 \pm 1.20
1479	0.82	189.2 \pm 1.5	5.92 \pm 0.39
1383	1.40	404.2 \pm 6.7	7.11 \pm 1.54
1283	1.00	67.6 \pm 2.1	...
1200	1.00	38.2 \pm 1.1	...
1200	0.87	24.7 \pm 0.6	...

Discussion

Errors. In the similar study¹ on tungsten the maximum uncertainty in the derived vapor pressures was

shown to be about $\pm 6.5\%$. An additional small error arises in the present work because of the uncertainty in the composition of the argon and hydrogen gas mixtures. If this is taken into account, the uncertainty in the derived pressures in the present work is approximately $\pm 7\%$. The calculated probable errors in the slopes of the straight lines (column 3 in Table II), being derived from several such data, are consistent with this uncertainty.

Several specimens with a combined weight of approximately 5 g. were used in the experiments. The combined weight loss was about 0.15 g. or 3%. The specified maximum impurity content of the molybdenum was 0.05%; hence, it is concluded that the impurities present in the molybdenum could not significantly affect the results.

Confirmation and Thermodynamic Properties of the Gaseous Species $\text{MoO}_3\text{H}_2\text{O}$. At constant temperature and constant water vapor-hydrogen ratio, the pressure of the hydrated compound has been shown to be a linear function of the water pressure. This means that the compound must stoichiometrically contain one molecule of H_2O which is in agreement with the previously cited work³⁻⁵ on the volatility of MoO_3 . The manner in which the apparent pressure varies with the ratio of water vapor to hydrogen may then be used to determine the additional number of oxygen atoms in the gaseous compound. Table III summarizes the calculations on the three species which most nearly satisfy the measurements. Column 2 shows the apparent pressure *per atmosphere* of water vapor calculated for the condition when $p_{\text{H}_2\text{O}}/p_{\text{H}_2}$ is equal to 0.82 at 1479 $^{\circ}$ from the results obtained at this temperature when $p_{\text{H}_2\text{O}}/p_{\text{H}_2}$ was equal to 1.00. The observed value is shown at the bottom of this column. Column 3 shows the results calculated for a ratio of 0.87 from the results at a ratio of 1.00 at 1200 $^{\circ}$.

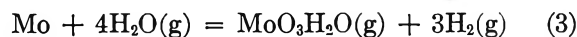
Table III: Results of Calculations on the Choice of Volatile Species from $\text{Mo} + \text{H}_2\text{O} + \text{H}_2 + \text{A Experiments}$

Supposed species	Calcd. vapor press./atm. of water vapor, atm. $\times 10^6$	
	1479 $^{\circ}$, $p_{\text{H}_2\text{O}}/p_{\text{H}_2} = 0.82$ Calcd. ^a	1200 $^{\circ}$, $p_{\text{H}_2\text{O}}/p_{\text{H}_2} = 0.87$ Calcd. ^b
$\text{MoO}_2\text{H}_2\text{O}$	222.1 \pm 11.1	28.7 \pm 1.4
$\text{MoO}_3\text{H}_2\text{O}$	181.8 \pm 10.9	25.1 \pm 1.5
$\text{MoO}_4\text{H}_2\text{O}$	149.1 \pm 10.4	21.9 \pm 1.5
	Obsd.	Obsd.
	189.2 \pm 1.5	24.7 \pm 0.6

^a From results at 1479 $^{\circ}$ and $p_{\text{H}_2\text{O}}/p_{\text{H}_2} = 1.00$. ^b From results at 1200 $^{\circ}$ and $p_{\text{H}_2\text{O}}/p_{\text{H}_2} = 1.00$.

The uncertainties listed for the calculated values were derived by combining the probable errors listed in Table II with the uncertainty in the water vapor-hydrogen ratio. The species $\text{MoO}_3\text{H}_2\text{O}$ fully satisfies the calculations, but the remaining two species must be considered as possibilities. Species requiring either higher or lower dependences than those listed are clearly ruled out.

If the species $\text{MoO}_3\text{H}_2\text{O}$ is considered, the reaction in the presence of H_2 and H_2O would be



for which

$$K = (p_{\text{MoO}_3\text{H}_2\text{O}})(p_{\text{H}_2})^3 / (p_{\text{H}_2\text{O}})^4 \quad (4)$$

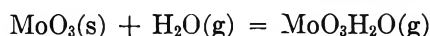
Values of $\log K$ derived from the values of $p_{\text{MoO}_3\text{H}_2\text{O}}/p_{\text{H}_2\text{O}}$ listed in Table II are shown plotted against $1/T$ ($^\circ\text{K}.$) in Figure 5. The best straight line calculated by the method of least squares is

$$\log K = -\frac{8830 (\pm 200)}{T} + 1.55 (\pm 0.12) \quad (5)$$

The standard free energy change for reaction 3 would then be

$$\Delta F^\circ = 40,410 - 7.10T \quad (6)$$

The standard free energy change for the reaction



may then be calculated by appropriate combination of eq. 6 with the standard free energies of formation of H_2O ⁸ and MoO_3 .⁹ At $900^\circ\text{K}.$ the value is $+15,870$ cal.

From this, one can readily calculate that, at $900^\circ\text{K}.$, unit activity of MoO_3 , and 760 mm. of H_2O , $p_{\text{MoO}_3\text{H}_2\text{O}} = 0.106$ mm. This is subject to a factor of error of approximately 2 if account is taken of the probable errors in slope and intercept of eq. 5. The measured value of Glemser and Haeseler under approximately these conditions ($903^\circ\text{K}.$ and 744 mm.) is 0.6 mm. This is in surprisingly good agreement when the long extrapolation of 600° is considered. If similar calculations are carried out for the remaining species in Table III or for all three species when assumed to contain more than one atom of molybdenum, the results are several orders of magnitude away from the measured value and they are effectively ruled out.

Thus, there is conclusive evidence that the major hydrated gaseous species is stoichiometrically $\text{MoO}_3\text{H}_2\text{O}$ and that the vaporization reaction in the presence of water vapor is as given by eq. 3. The most probable values for the standard free energy change of this re-

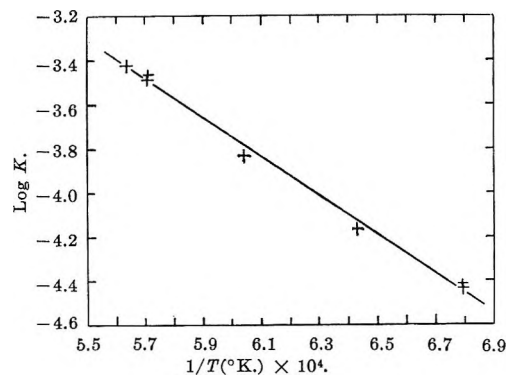


Figure 5. Temperature dependence of equilibrium constant for the reaction $\text{Mo} + 4\text{H}_2\text{O} = \text{MoO}_3\text{H}_2\text{O} + 3\text{H}_2$.

action are given by the equation $\Delta F^\circ = 40,410 - 7.10T$ (± 450 cal.).

The entropy of the gaseous species may be calculated by combination of the entropy change of reaction 3 with the well-established entropies of Mo , H_2O , and H_2 taken from the literature.¹⁰ The most probable value at $1600^\circ\text{K}.$ is $S^\circ = 137.9 \pm 0.55$ e.u.

The molecule $\text{WO}_3\text{H}_2\text{O}$, which is probably isostructural with the molybdenum species, was previously found¹ to have an entropy at this temperature of 136.7 ± 1.05 e.u. This similarity in entropy values is surprising in view of the difference in molecular weight between the two species but is not unreasonable when compared with the difference in entropies of the hexafluorides, the only other seven-atom gas molecules of Mo and W for which data are available. At $1600^\circ\text{K}.$ the entropy of MoF_6 is 138.07 ± 1 e.u.,¹⁰ and that of WF_6 is 139.49 e.u.,¹¹ both these values being based upon spectroscopic studies.

The Volatile Oxides. As pointed out earlier in this paper, the pressures listed in column 4 of Table II represent the total pressures of the volatile oxides under the conditions of the experiments. If the data taken at 1479° with $p_{\text{H}_2\text{O}}/p_{\text{H}_2}$ ratios of 1.00 and 0.82 are considered, the species MoO_2 and MoO_3 would both satisfy calculations of the type carried out for the hydrated species. However, the mass spectrometric investigation of the sublimation of $\text{MoO}_2 + \text{Mo}$ at

(8) "Selected Values of Chemical Thermodynamic Properties," Series III, Vol. 1, National Bureau of Standards, Washington 25, D. C.

(9) E. G. King, W. W. Weller, and A. U. Christensen, U. S. Department of the Interior, Bureau of Mines, Report of Investigations 5664, 1960.

(10) K. K. Kelley, U. S. Bureau of Mines Bulletin 584, U. S. Government Printing Office, Washington, D. C., 1960; K. K. Kelley and E. G. King, U. S. Bureau of Mines Bulletin 592, U. S. Government Printing Office, Washington, D. C., 1961.

(11) "JANAF Thermochemical Tables," The Dow Chemical Co., Midland, Mich., 1963.

1500–1780°K. of Burns, *et al.*,¹² has shown that there are several species which, in decreasing order of importance, are MoO₃, (MoO₃)₂, MoO₂, and (MoO₃)₃.

The expected pressures of MoO₃ under the conditions of the present experiments may be calculated from the standard free energy change of the reaction



derived by appropriate combination of the pressure data of Burns, *et al.*, with the data for H₂O(g)⁸ and MoO₂(s). Taking the standard free energy of formation of MoO₂(s) to be that reported by King, *et al.*,⁹ corrected by -500 cal. in view of the later work of Rapp,¹³ the resulting pressures are as shown in column 3 of Table IV. These are substantially lower than the total apparent pressures determined in *this* work, shown in column 4 of the same table.

Table IV: Derived Pressures of the Volatile Oxides MoO₃ and MoO₂

Temp., °C.	$p_{\text{H}_2\text{O}}/p_{\text{H}_2}$	Calcd. ^a press. of MoO ₃ , atm. × 10 ⁶	Total oxide press. from expt., atm. × 10 ⁶	Press. attributed to MoO ₃ , atm. × 10 ⁶	Press. attributed to MoO ₂ , atm. × 10 ⁶
1500	1.00	2.21	13.00	10.41	1.47
1479	1.00	1.57	10.48	8.43	1.12
1479	0.82	0.87	5.92	4.98	0.81
1383	1.40	0.83	7.11	4.96	0.23

^a From data of Burns, DeMaria, Drowart, and Grimley.

The data of Burns, *et al.*, were used therefore only to calculate the expected proportions of the various oxide species in the gas phase for each experimental condition. The pressures attributable to MoO₃ and MoO₂, the major oxide species, under the existing conditions, were then derived from the measured pressures.¹⁴ These are shown in column 5 and 6 of Table IV.

Derived values of log *K* for reaction 7, where

$$K = (p_{\text{MoO}_3})(p_{\text{H}_2})^3/(p_{\text{H}_2\text{O}})^3 \quad (8)$$

are shown plotted against 1/*T* (°K.) in Figure 6.

Since the temperature range of the experiments is small, the enthalpy change of reaction 7 is taken as that given by the combination of the data of Burns, *et al.*, with the calorimetrically determined heat of formation of MoO₂(s)⁹ and the selected value for H₂O(g).⁸ This yields for the straight line shown in Figure 6.

$$\log K = -\frac{21,900}{T} + 7.43 (\pm 0.05) \quad (9)$$

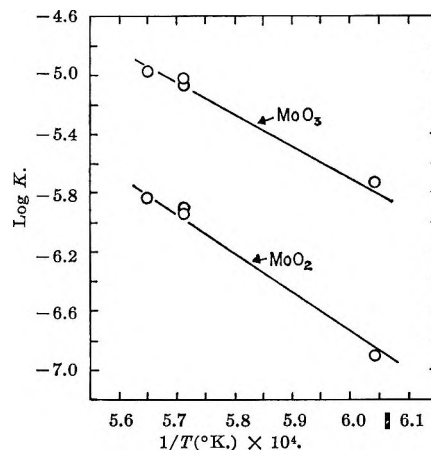


Figure 6. Temperature dependence of equilibrium constants for the reactions $\text{Mo} + 2\text{H}_2\text{O} = \text{MoO}_2 + 2\text{H}_2$ and $\text{Mo} + 3\text{H}_2\text{O} = \text{MoO}_3 + 3\text{H}_2$.

Hence, the standard free energy change for reaction 7 would be given by

$$\Delta F^\circ = 100,120 - 33.99T \quad (10)$$

Derived values of log *K* for the reaction



calculated by the same method, are also shown in Figure 6. The straight line equation is

$$\log K = -\frac{26,210}{T} + 8.97 (\pm 0.05) \quad (12)$$

giving for the standard free energy change of reaction 11

$$\Delta F^\circ = 119,900 - 41.04T \quad (13)$$

The pressures of the oxides derived in this work are higher by a factor of about 5.4 than the expected pressures derived from the data of Burns, *et al.* This factor is subject to an error of approximately $\pm 10\%$ if account is taken of the probable errors listed in Table II. The earlier Knudsen cell measurements of Blackburn and his co-workers¹⁵ on the Mo + MoO₂ system also gave higher apparent pressures. If the mass spectrometric data are used to calculate the proportions of the species present at 1818°K. (the lowest temperature of Blackburn) and the pressures re-determined from the weight loss of the Knudsen cell,

(12) R. P. Burns, G. DeMaria, J. Drowart, and R. T. Grimley, *J. Chem. Phys.*, **32**, 1363 (1960).

(13) R. A. Rapp, *Trans. AIME*, **227**, 371 (1963).

(14) Within experimental error, the variation of the total oxide pressure with the H₂O/H₂ ratio at 1479° is in agreement with the mass spectrometric proportions of MoO₂ and MoO₃.

(15) P. E. Blackburn, M. Hoch, and H. L. Johnston, *J. Phys. Chem.*, **62**, 769 (1958).

the pressure of MoO_3 is again higher than that extrapolated from Burn's equation by a factor of 5.5, in good agreement with this work.

Inghram and Drowart¹⁶ have suggested that pressures derived from mass spectrometer studies of this type are subject to a maximum error of $\times 2$. However, evidence has been accumulated recently that the principle of additivity of relative ionization cross sections¹⁷ used in the calculation of results is in error. For example, the work of Goldfinger and Jeunehomme¹⁸ has shown that the ratio of cross sections for certain homonuclear diatomic molecules compared to the atoms is about 1.5. Berkowitz and his co-workers¹⁹ have obtained values of 1 to 1.4 for the dimer/monomer cross-section ratios of the lithium halides. This type of error would lead to a too low pressure. In addition, as the ionization cross sections normally refer to energies at the maxima of the ionization efficiency curves, it is usual¹⁶ to correct the cross sections to the ionizing energies used. This was not done by Burns, *et al.*, and could be responsible for serious error.

Derivation of eq. 9 and 12 involved the assumption

that the mass spectrometric work gave the correct relative proportions of the oxide species; *i.e.*, the ionization cross sections used were in error only with respect to silver, the calibrating substance. Any other relative errors among the cross sections must lead to errors in these equations. For these reasons, equations involving $(\text{MoO}_3)_2$ and $(\text{MoO}_3)_3$, the more complex and lower pressure species, are not presented.

Acknowledgment. This study, a contribution from the Laboratory for Research on the Structure of Matter, University of Pennsylvania, was supported by the Advanced Research Projects Agency, Office of the Secretary of Defense.

(16) M. G. Inghram and J. Drowart, Proceedings of the International Symposium on High Temperature Technology, McGraw-Hill Book Co., Inc., New York, N. Y., 1960, p. 219.

(17) J. W. Otvos and D. P. Stevenson, *J. Am. Chem. Soc.*, **78**, 546 (1956).

(18) P. Goldfinger and M. Jeunehomme, *Trans. Faraday Soc.*, **59**, 2851 (1963).

(19) J. Berkowitz, H. A. Tasman, and W. A. Chupka, *J. Chem. Phys.*, **36**, 2170 (1962).

Radiolytic Stress Relaxation of an Ethylene-Propylene Copolymer¹

by Hyuk Yu and Leo A. Wall

National Bureau of Standards, Washington, D. C. (Received January 14, 1965)

The kinetics of network chain scission induced by γ -rays has been studied by stress relaxation at constant elongation under vacuum and in air. The rate of chain scission of a 1:1 ethylene-propylene copolymer was found to be independent of initial network chain density, and the initial rates were roughly the same in air and under vacuum. Parameters for cross linking induced by γ -rays were obtained by sol extraction and by measurement of elastic properties of the resulting networks. G values for scission and cross linking and gel dose, obtained by stress relaxation, by elastic properties, and by sol extraction, were found to be in agreement with each other.

Introduction

It has been well established that some vinyl polymers undergo simultaneous cross linking and chain scission under high energy irradiation.²⁻³ However, a clean-cut separation of the two competing processes is not readily effected by the usual sol-gel partitioning method commonly employed in investigations of radiation effects on polymers. This method was first advanced by Charlesby and Pinner⁴ as an extension of the theory of gelation proposed by Flory⁵ and Stockmayer⁶ and was recently generalized by Inokuti and Dole.^{7,8} The method requires a knowledge of the molecular weight distribution and makes the assumption that cross linking and chain scission processes occur linearly with respect to the radiation dose. Even so, this method does not directly provide one with a knowledge on the radiation yield for chain scission. It is obtained only indirectly from the relative radiation yield of the two processes and the measured cross-linking efficiency. We have sought a more direct method for the problems of chain scission and cross linking in polymers by high energy radiation. This method, which is based on the stress relaxation of a polymeric network at constant elongation, was originally devised by Tobolsky and his co-workers,⁹ and, subsequently, it was demonstrated to be a fruitful tool for the kinetic investigation of chain scissions in amorphous polymers.¹⁰

In this paper we report that stress relaxation measurements can provide answers to important questions connected with radiolytic chain scission of amorphous polymers and that the elasticity measurements of

resulting networks can yield the efficiency of cross linking as well as the dose of incipient gelation without a knowledge of the molecular weight distribution. Moreover, we show that the scission event is random along a polymer chain and that the scission and cross-linking processes are linear with respect to the radiation dose.

Essential to the interpretation of stress relaxation data at constant elongation is the fact that the stress at any time t is directly proportional to the remaining number of elastically active network chains present in the unstrained condition and receives no contributions from the network chains formed under the strained condition. Thus, the decay of stress is a direct measure of chain scissions within a network and is not connected in any way with the concurrent chain cross-linking

(1) Based on research supported by the National Aeronautics and Space Administration.

(2) (a) A. Charlesby, "Atomic Radiation and Polymers," Pergamon Press, New York, N. Y., 1960, Chapter 11; (b) A. Chapiro, "Radiation Chemistry of Polymeric Systems," John Wiley and Sons, Inc., New York, N. Y., 1962, Chapter 3.

(3) L. A. Wall and J. H. Flynn, *Rubber Chem. Technol.*, **35**, 1157 (1962).

(4) A. Charlesby and S. H. Pinner, *Proc. Roy. Soc. (London)*, **A249**, 367 (1959).

(5) P. J. Flory, *J. Am. Chem. Soc.*, **63**, 3097 (1941).

(6) W. H. Stockmayer, *J. Chem. Phys.*, **12**, 125 (1944).

(7) M. Inokuti, *ibid.*, **38**, 2999 (1963).

(8) M. Inokuti and M. Dole, *ibid.*, **38**, 3006 (1963).

(9) A. V. Tobolsky, I. B. Pretyman, and J. H. Dillon, *J. Appl. Phys.*, **15**, 380 (1944).

(10) A. V. Tobolsky, "Structure and Properties of Polymers," John Wiley and Sons, Inc., New York, N. Y., 1960, Chapter 5.

process. Since the initial statement of this hypothesis by Andrews, Tobolsky, and Hanson¹¹ it has received a considerable amount of substantiation, criticism, and refinement.¹²⁻¹⁵ We shall assume in this paper the "two-network" hypothesis¹² of Andrews, Tobolsky, and Hanson and neglect fine corrections which we feel inconsequential with regard to the main points we now wish to make.

We start with the elastic equation of state for simple elongation

$$f = \Phi \nu k T (\alpha - \alpha^{-2}) \quad (1)$$

where f is the tensile stress in terms of the cross-sectional area in the unstrained state, Φ is the "front factor," ν is the number of network chains per unit volume, k is Boltzmann's constant, T is the absolute temperature, and α is the length ratio; *i.e.*, $\alpha = l_t/l_0$, l_t being the final length of the elongated sample and l_0 the original length. Under an isothermal condition with a constant elongation, we see that the tensile stress f is directly proportional to ν if the front factor Φ remains constant during the process of cross linking and scission. Inasmuch as Φ is generally regarded as a parameter for a type of cross-linking process^{16,17} within the network, it is reasonable to assume Φ constant throughout the course of a given type of cross linking and scission.

From the observed tensile stress decay one can deduce the number of chain scissions occurring randomly along the polymer chain under different chain length distributions. For a case of uniform chain length distribution, the relationship between the observed stress and the number of scissions was formulated by Tobolsky, Metz, and Mesrobian¹⁸ as

$$q(t) = -\nu_0 \ln \frac{f(t)}{f(0)} \quad (2)$$

where $q(t)$ is the total number of scissions which have occurred up to time t per unit volume of the network, ν_0 the original number of network chains, $f(t)$ the tensile stress at time t , and $f(0)$ the stress at time zero. Starting with the most probable distribution of chain length, one finds that there are two different ways of counting the number of scissions from the stress decay, depending upon the assumption introduced into the formulations.¹⁹⁻²¹ The two methods, however, reduce to the same formula in the limit for a number-average chain length longer than 100. The limiting formula²¹ appears as

$$q(t) = \nu_0 \left(\frac{f(0)}{f(t)} - 1 \right) \quad (3)$$

where all notations have the same definition as in eq. 2. The difference between eq. 2 and 3 becomes ap-

preciable as the average chain length increases. In this paper, our preference for eq. 3 over eq. 2 is a natural one, particularly in the light of the random cross linking by radiation. Although there is no way that one can test experimentally how chain lengths are distributed within a network, it seems that the most probable distribution is close to the actual situation. It should be pointed out, however, that *a priori* choice of one distribution over the other for the interpretation of stress relaxation is a matter of judgment.²² The network chain density ν_0 , with which we deal in this paper, is well within the range of an average chain length above 100 units. Consequently, the number of scissions is calculated from the observed stress data according to eq. 3.

Experimental

We have chosen the 1:1 ethylene-propylene copolymer for study because it has the simplest hydrocarbon structure that is amorphous in the temperature range of interest (room temperature up to 120°). Thin films of a copolymer composition of 50 ± 5% propylene content, 0.0254 cm. thick, free of antioxidant, were kindly supplied to us by the Synthetic Rubber Research Division of the Goodyear Tire and Rubber Co.

The film was cut into strips of 0.64 cm., placed inside glass tubing, and evacuated at *ca.* 1 μ pressure for 48 hr. at room temperature. The tubes were then sealed under vacuum. The films were irradiated using a Co⁶⁰ source of approximately 50,000 curies in a water pool arrangement, and dose rates at different geometries were calibrated by commercial cobalt glass dosimeters. Irradiation of films for the formation of networks was carried out at a dose rate of 1.29–1.33 × 10²⁰ e.v./hr. (2.13–2.22 Mrads/hr., and 1 roentgen = 0.968 rad for this polymer). After the required dose the sample films were removed from the glass tubes and various measurements performed.

(11) R. D. Andrews, A. V. Tobolsky, and E. E. Hanson, *J. Appl. Phys.*, **17**, 352 (1946).

(12) J. P. Berry, J. Scanlan, and W. F. Watson, *Trans. Faraday Soc.*, **52**, 1137 (1956).

(13) J. Scanlan and W. F. Watson, *ibid.*, **54**, 740 (1958).

(14) P. J. Flory, *ibid.*, **56**, 722 (1960).

(15) J. Scanlan, *ibid.*, **57**, 839 (1961).

(16) A. Ciferri, C. A. J. Hoeve, and P. J. Flory, *J. Am. Chem. Soc.*, **83**, 1015 (1961).

(17) A. V. Tobolsky, D. W. Carlson, and N. Indictor, *J. Polymer Sci.*, **54**, 175 (1961).

(18) A. V. Tobolsky, D. J. Metz, and R. B. Mesrobian, *J. Am. Chem. Soc.*, **72**, 1942 (1950).

(19) A. M. Bueche, *J. Chem. Phys.*, **21**, 614 (1953).

(20) J. P. Berry and W. F. Watson, *J. Polymer Sci.*, **18**, 201 (1955).

(21) H. Yu, *ibid.*, **B2**, 631 (1964).

(22) A. V. Tobolsky, *ibid.*, **B2**, 637 (1964).

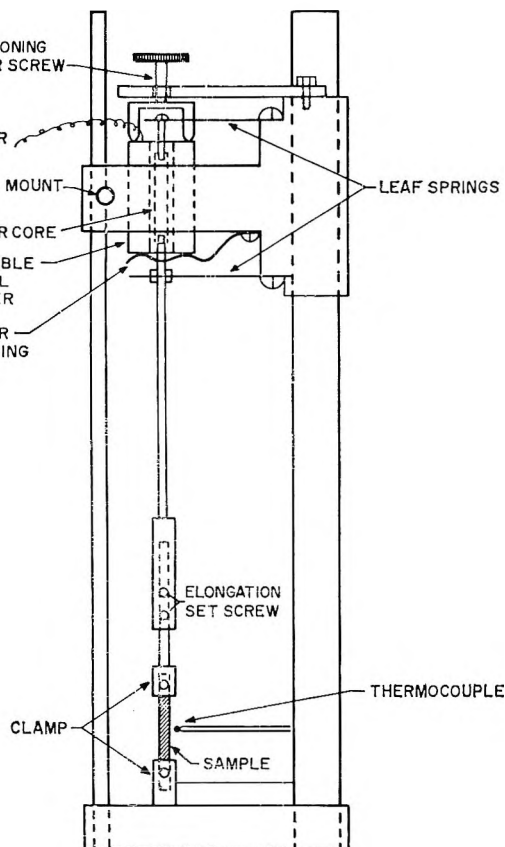


Figure 1. A schematic illustration of stress relaxometer.

Equilibrium stresses of the resulting networks at different temperatures were measured *in vacuo* by a relaxometer, shown in Figure 1, consisting of a linear variable transformer (Schaevitz Engineering Co., 060SS-L, 8-kHz excitation frequency), a pair of cantilever springs supporting the transformer core, and a sample clamp. The relaxometer was placed inside a glass envelope, and the six leads from the transformer were connected across a glass seal to six Ni-W-Cu lead wires (A and S Lead Wire Corp.). A Transducer amplifier-indicator (Daytronic Corp., Model 300C) was used for the signal input and output amplification, and the final output signal was continuously recorded (Leeds and Northrop Speedomax Type G recorder, Model S 60000). Elongation of the film was determined by measuring the distance between the flat edges of the upper and lower clamp with a cathetometer. After the sample was stretched to a desired elongation (30–45%), the relaxometer was placed inside the cell and the stress monitored continually while the cell was evacuated. When the pressure reached *ca.* 1μ , the temperature of the sample was raised with an external heater. Sample temperature was determined by a thermocouple wrapped with a piece of the same

sample and placed close to the stretched film. The reason for measuring the stress *in vacuo* was to avoid possible oxidative degradation at high temperatures during the experiment. After the stress attained a sensibly constant value (16–24 hr.) at the highest temperature under investigation, the sample temperature was lowered by intervals and the corresponding stress recorded. A similar procedure was repeated for ascending temperature intervals when the sample reached room temperature. A typical stress-temperature measurement of a radiation-induced network is shown in Figure 2. From the equilibrium stress found by this procedure, the network chain density is calculated according to eq. 1, and the results are shown in Table I and Figure 3. Sol fractions of the networks produced by various radiation doses are also included in Table I.

Densities of cross-linked, unextracted samples determined by hydrostatic weighing with methanol at room temperature showed that only a slight increase ($\sim 2\%$) was associated with the cross linking. Thus, the density of 0.85 g./cc. was used in calculating ν_0

Table I

Sample	Dose, ^a τ , e.v./g. $\times 10^{-20}$	Reduced dose, ^b τ_g/τ	Network chain density, ν_0 (chain/cc.) $\times 10^{-19}$	Sol fraction, <i>S</i>
1	7.25	0.625	0.84	0.62
2	13.9	0.325	1.9	0.44
3	20.9	0.217	3.4	0.26
4	31.6	0.143	4.5	0.16
5	46.6	0.098	5.6	0.12

^a Conversion factor: 1 Mr. = 6.05×10^{19} e.v./g. ^b τ_g (gel dose) = 4.55×10^{20} e.v./g.

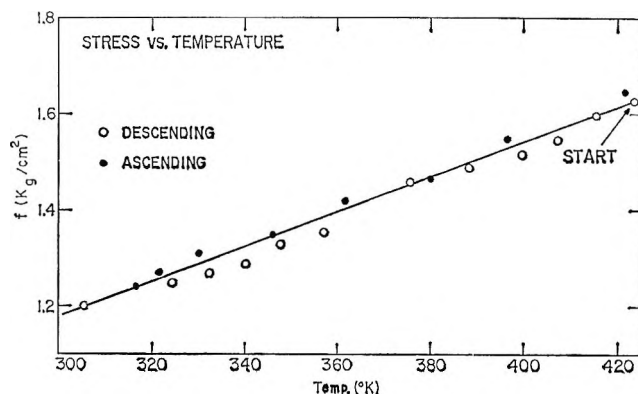


Figure 2. A typical stress temperature measurement of a radiation-induced 1:1 ethylene-propylene copolymer network. Network chain density ν_0 of 3.38×10^{19} chains/cc. is determined from the observed equilibrium stress using the rubber elasticity equation.

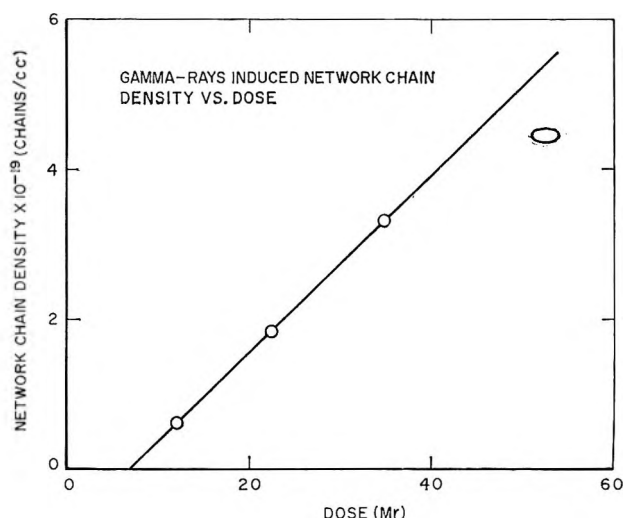


Figure 3. Network chain density of the radiation-cross-linked 1:1 ethylene-propylene copolymer vs. dose. The point for the largest dose is drawn to scale the range of errors in the measurement.

for all the samples without introducing any significant error.

Stress relaxation of networks was carried out in air, under vacuum, and in He with the films cross linked in a manner previously described. The dose rate was $1.33\text{--}1.39 \times 10^{20}$ e.v./g. hr. (2.2–2.3 Mr./hr.), and the temperature range was between the pool temperature (25°) and 120° . Before the relaxometer cell was placed in the source, the usual stress relaxation of a network to an equilibrium value was allowed to proceed for 24–48 hr. at room temperature. For the runs under vacuum, the elongated samples were evacuated at 100° for 30–48 hr. until the pressure in the cell reached a few microns. Then the cell was sealed. At the conclusion of a run the seal was broken, the relaxometer removed from the cell, and the sample cut off from the clamp. This removed any residual stress and enabled us to ascertain if the signal output had returned to the original null position at zero elongation in the electronic system. Drifting of the zero stress signal output was found to be insignificant (0.5–1%) after 16–40 hr. of continuous measurement in the Co^{60} source, indicating the stability of the measurement system.

The extraction of sol from the cross-linked samples was carried out with toluene at room temperature. Samples (0.5 g.) were repeatedly swelled and dried *in vacuo* until the weight of the remaining gel was maintained between consecutive swelling and drying. Fractional weight loss was regarded as the sol fraction; this is also tabulated in Table I.

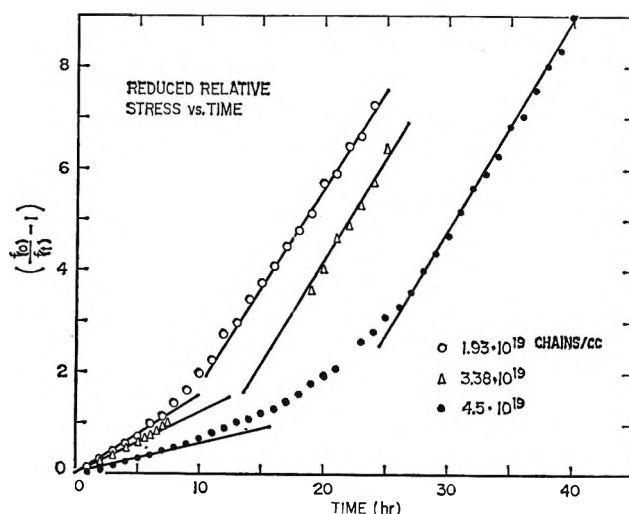


Figure 4. Stress relaxation of 1:1 ethylene-propylene copolymer for various network chain densities in air at dose rate of 1.33×10^{20} e.v./g. hr. (2.2 Mr./hr.).

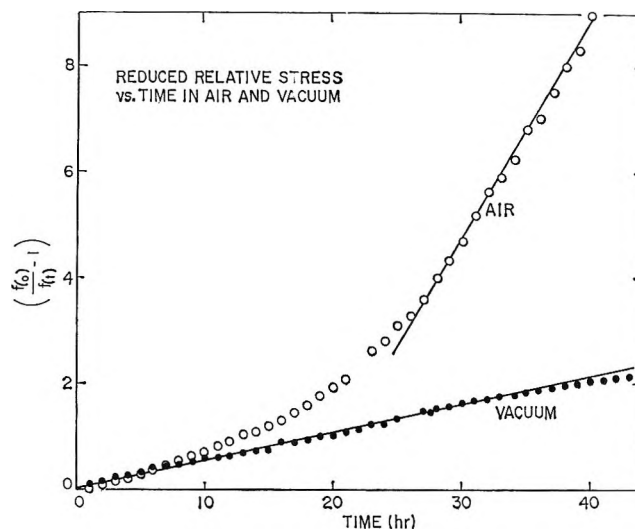


Figure 5. Comparison of stress relaxation of a 1:1 ethylene-propylene copolymer network (4.5×10^{19} chains/cc.) in air and under vacuum at room temperature. Dose rate: 1.33×10^{20} e.v./g. hr.

Results and Discussion

The results of stress relaxation experiments in air are shown in Figure 4 by plotting $\{ [f(0)/f(t)] - 1 \}$ against time, with the samples of different network chain densities. The result of the stress relaxation of a network in air is compared with that under vacuum in Figure 5. The shape of the curves in Figure 4 indicates that scission is taking place randomly along the network chains during the first stage of relaxation; the slopes of the straight lines drawn over the first linear portion of the experimental points are inversely proportional to the

original network chain density ν_0 , consistent with the scheme of random scission of eq. 3. We note in Figure 5 that the rate of the stress relaxation at the first stage in air is the same as under vacuum. The equal rate means that the cleavage of the chain backbone carbon-carbon bond in air is a primary process induced by γ -rays and not an oxidative process. These findings are summarized in Table II, where the rate of chain scission in air is determined according to eq. 3, with the slope of straight lines drawn over the first linear portion of the relaxation data in Figure 4 (up to 9 Mr.). The scission rates under vacuum are calculated in a similar manner. It is evident from Table II that all scission rates are practically identical irrespective of the initial number of cross links per chain in agreement with the scheme of random scission. We note at this point that the comparison of the stress relaxation results in air with those under vacuum affords us a means of resolving the uncertainty as to when the oxidative degradation of a polymer sets in during the irradiation.²³ For the ethylene-propylene copolymer under study, we find that at about 9 Mr. the oxidative process begins to be appreciable.

The linearity of the chain scission process with respect to radiation dose up to 80 Mr. is clearly illustrated, at least under vacuum, in Figure 5, and this is the first instance of the direct confirmation, we believe, of the linearity assumption commonly invoked in the sol-gel extraction method.^{2,4,7,8} We should also point out that the method employed here is a direct way of determining radiation yield of chain scission which is cleanly separable from that of cross linking. From the rate of chain scission in Table II, a G value for scission, 2.11 ± 0.36 cuts/100 e.v., is estimated; a conversion factor 1 roentgen = 0.968 rad and density of polymer 0.85 g./cc. are used in the estimate. It is of interest to note that this value is very similar to the result of Chapiro²⁴ for radiation yield of C-C cleavage in normal alkane ($G = 1-2$) deduced from possible primary free-radical processes. We can surmise then that alkyl substituents on a hydrocarbon chain do not affect the rate of radiolytic backbone C-C bond cleavage appreciably. We wish to pursue this point further by studying the effects of other substituents, *i.e.*, halogens, aryl, etc., on the hydrocarbon backbone scission.

Table II: Rate of Chain Scission of 50:50 Ethylene-Propylene Copolymer Induced by γ -Rays at Room Temperature

Sample	Network chain density, (chains/cc.) $\times 10^{-19}$	dq/dt , (cuts/cc. hr.) $\times 10^{-18}$		dq/dr , (cuts/cc. e.v.) $\times 10^2$	
		Air	Vacuum	Air	Vacuum
2	1.9	2.94	...	2.48	...
4	4.5	2.92	2.43	2.6	2.14
5	5.6	2.52	1.85	2.24	1.75
		Av.		2.11 ± 0.36	

That the second portion of relaxation data in air (Figure 4) is not due to a random chain scission process can easily be seen by observing the parallel slope for all three runs. We suspect that a mechanism possibly responsible for this portion of relaxation is a radiolytic cleavage of tertiary hydroperoxide formed on cross-link sites during the irradiation, which in turn induces the rupture of cross links. Although we have not as yet confirmed this point conclusively, the observed equal rate of stress relaxation for the networks of different cross-link density is certainly inconsistent with the random chain scission scheme. Further study of radiolytic stress relaxation in air to determine the exact nature of cross-link rupture for this polymer is in progress.

The relaxation measurements at a higher temperature under vacuum (120°) and in He (115°) show that the scission rates are practically identical with those of room temperature runs, as shown in Figure 6. The absence of a temperature coefficient for chain scission in the range of temperatures studied and the fact that no postirradiation relaxation of the stress was observed when the relaxometer cell was removed from the source support the claim of a direct cleavage of backbone C-C bonds that involves no long-lived chemical intermediates nor any chain reactions. It is noteworthy to recall a recent result of Kitamaru and Mandelkern²⁵ in this respect. They also found no temperature coefficient of cross-linking efficiency for polyethylene in the amorphous state, whereas in the crystalline state the cross-linking efficiency increases with temperature.

Since radiation-induced cross-linking and scission processes are concurrently occurring in a polymer sample, what one observes in the elastic properties of a sample, after a certain dose of radiation in the unstretched state, is the net effect of these two processes. We have shown in Figure 3 this over-all effect by plotting against dose the resulting network chain density ν_0 calculated through eq. 1. A reasonable linearity between ν_0 and dose up to 40 Mr. assures us that the cross-linking rate is also constant since we have estab-

(23) See ref. 2b, p. 429.

(24) See ref. 2b, p. 108.

(25) R. Kitamaru and L. Mandelkern, *J. Am. Chem. Soc.*, **86**, 3529 (1964).

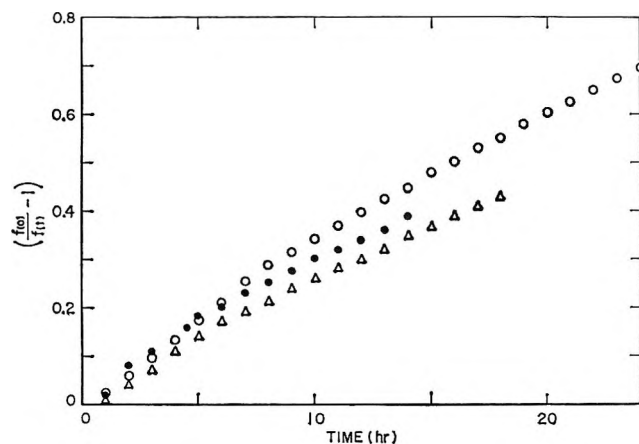


Figure 6. Stress relaxation of a 1:1 ethylene-propylene copolymer network (5.6×10^{19} chains/cc.): O, under vacuum at 120°; ●, in He at 115°; Δ, under vacuum at room temperature.

lished chain scission to be linear with dose. The slope of the line drawn through the data in Figure 3 is therefore taken as the difference between the rates of cross linking and scission, and the intercept with the abscissa is taken as the gel dose. Subsequently, we estimate from the slope the net number of chains formed per cc. to be 2.59/100 e.v. If we assume that each cross-linking event adds one chain to the network while each scission process removes one, the over-all cross-linking efficiency/100 e.v., *i.e.*, the G value of cross linking, will be $2.11 + 2.59 = 4.70$. The corresponding ratio, $\lambda = G(s)/G(x)$, of two G values then appears as 0.45. The gel dose from the intercept with the abscissa in Figure 3 is determined to be 7.5 Mr.

From the result of a sol extraction experiment we find 0.4 for λ by extrapolating, to infinite dose, the plot of the Charlesby-Pinner function, $s + \sqrt{s}$, against inverse dose. Here s is the sol fraction. This is in fair agreement with the same quantity obtained quite differently from the measurements of the elastic parameter and the stress relaxation, as cited above. We have collected in Table III the values of λ for polyethylene and polypropylene in the literature for a comparison with our result. It appears that the 1:1 ethylene-propylene copolymer is similar to polyethylene in its radiolytic behavior. Just how real the difference is between Inokuti and Dole's atactic polypropylene result and ours will be tested with their sample by our method.

In order to make contact with the recent theory of Inokuti, we have plotted, in Figure 7, the observed $s + \sqrt{s}$ against a reduced dose r_g/r , where r_g is the gel dose and r is any dose beyond the gel point. The solid curve is drawn according to Inokuti's numerical computation of the gel fraction at the relative cross-link density

Table III

Polymer	$G(\text{scission})/G(\text{cross links})^a$	Method ^b	Ref.
Atactic polypropylene	0.8	A	c
Isotactic polypropylene	1.4	A	c
Polyethylene	0.36-0.40	A	d
	0.56-0.68	A	e
	0.44	A	f
50:50 ethylene-propylene copolymer	0.4	A	Our work
	0.46	B	Our work

^a This is $\lambda = G(\text{scission})/G(\text{cross links})$ in Inokuti's notation and corresponds to Charlesby and Pinner's $2P_0/q_0$. ^b A, sol extraction; B, stress relaxation. ^c See ref. 8. ^d A. C. Baskett and C. W. Miller, *Nature*, 174, 364 (1954). ^e See ref. 4. ^f Y. Okada, *J. Appl. Polymer Sci.*, 8, 467 (1964).

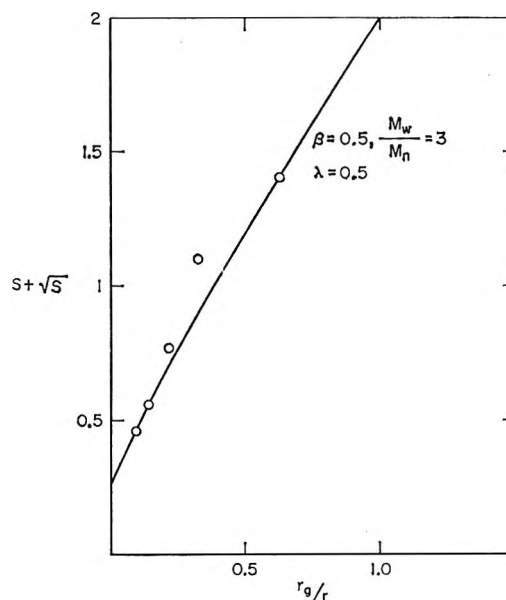


Figure 7. Charlesby-Pinner function $s + \sqrt{s}$ vs. reduced dose r_g/r for 1:1 ethylene-propylene copolymer. Solid curve is according to the result of Inokuti⁷ where $M_w/M_n = 3$ and $\lambda = G(s)/G(x) = 0.5$.

y_g/y_n , where y_g is the number of cross links per initial number-average molecule at the gel point and y_n denotes the corresponding value at a dose which yields the fractional gel fraction, $g = (n/10)g_{\text{max}}$, where $0 \leq n \leq 10$. The maximum gel fraction g_{max} is given by

$$g_{\text{max}} = \frac{1}{2}[1 - \lambda + (1 + \lambda)^{1/2}] \quad (4)$$

Since we have already established that the cross linking is linear with dose, it is permissible to equate our r_g/r to Inokuti's y_g/y_n . In drawing the solid curve we have used a λ value of 0.5, which is reasonably close to

our observed value of 0.45. Also, the molecular weight distribution parameter $\beta = [(M_w/M_n) - 1]^{-1}$ of 0.5 was chosen since it gave the best fit. The agreement between our experimental points and the calculated curve with the exception of one point implies that the sample under study has a heterogeneity index, M_w/M_n , of 3. It may also be added that one can calculate the value of β in principle from

$$[4/(\lambda^2 y_g)] \{ \lambda y_g - 1 + [1 + (\lambda y_g / \beta)]^{-\beta} \} = 1 \quad (5)$$

by knowing λ and y_g . This is eq. 19 of Inokuti.⁷ As we have already shown, the value of λ is available from the stress relaxation and the elasticity measurements. However, one has to know at least the number-average molecular weight and the gel dose to find y_g . Thus, with the aid of eq. 5, we can, in principle, find a measure of molecular weight distribution of a polymer sample from the stress relaxation and equilibrium stress of a radiation-induced network together with the gel dose and the number-average molecular weight.

In conclusion, then, we can state that the method

described in this paper is capable not only of making direct measurements of the G values for scission and cross linking but also of giving a measure of the molecular weight distribution, either from a knowledge of M_n and the gel dose or from a knowledge of the sol fraction.

Previous estimates of scission and cross links produced in polymers by high energy radiation have been from the measurements made some time after irradiation and through theories based on the assumption that the number of scission and cross-linking acts increase linearly with dose. Hence, we have demonstrated for the ethylene-propylene copolymer that (1) the linearity of scission and cross-linking processes with dose and (2) the previously measured scission rates are primary acts.

Acknowledgment. The authors wish to thank Mr. Robert M. Pierson and Dr. Robert E. Cunningham of the Synthetic Rubber Research Division of the Good-year Tire and Rubber Co. for the sample of the ethylene-propylene copolymer.

Specific Heat of Polyethylene Single Crystals

by Bernhard Wunderlich

Department of Chemistry, Rensselaer Polytechnic Institute, Troy, New York (Received January 8, 1965)

The specific heat of extended molecular chain single crystals of polyethylene has been measured with a differential scanning calorimeter. The range from 180 to 410°K. was covered with a standard deviation of $\pm 2\%$. Previous extrapolations from data of less than perfect crystallinity and paraffins were found fairly correct. The data from 230 to 400°K. fit the theoretical specific heats from vibrational spectra within the experimental error. At lower temperature a small deviation remains, indicating the necessity of improvement of the frequency spectrum.

I. Introduction

During the past 3 years it has become possible to grow in our laboratory single crystals of polyethylene with extended molecular chains.¹ These single crystals still contain a broad range of chain

length, but all crystals are made up of molecules in the extended-chain conformation. No folded-chain crys-

(1) T. Arakawa, Thesis, Cornell University, Department of Chemistry, 1964; B. Wunderlich and T. Arakawa, *J. Polymer Sci.*, **2A**, 3697 (1964).

tals could be discovered on inspection of bulk fracture surface replicas with the electron microscope.² The density at 298°K. of the bulk material which was crystallized at 500°K. and 4350 atm. of hydrostatic pressure is 0.997 g. cm.⁻³, almost that calculated from the unit-cell parameters.

To arrive at the specific heat of such single-crystalline polyethylene, two paths had been chosen in the past few years. Paraffin data have been extrapolated to infinite chain length,³ and polyethylene data of different degrees of crystallinity have been extrapolated to 100% perfection.⁴

In this paper measurements on actual single crystals between 180 and 400°K. are described and compared with the previous extrapolations.

For the measurement, a Perkin-Elmer Corp. (Norwalk, Conn.) differential scanning calorimeter was used to enable measurements on the small quantities of single crystals available. The experimental data will be compared with the vibrational frequency spectrum derived earlier.⁵

II. Experimental

A. Specific Heats. A detailed discussion of the Perkin-Elmer differential scanning calorimeter has been published by the people involved in the design of this instrument.⁶ Basically, two miniature sample holders are kept at constant temperature by supplying different electrical power to each sample holder. The differential power input is recorded alongside time and temperature signals.

Samples, as well as reference, are enclosed in 21.5 ± 0.2 mg. aluminum capsules before putting them into the sample holders. Approximately 30 mm.³ of sample could be accommodated in the aluminum capsules, giving a maximum of about 30 mg. of polymer or 100 mg. of sapphire sample weights. The sapphire was used for calibration.

The mode of operation was as follows. Preliminary calibration adjusted all controls, so that over the whole temperature range of 180 to 480°K. the power recording remained on scale. The most sensitive scale (2×, about 5 mcal. sec.⁻¹ full scale deflection) was found to be nonlinear, and accordingly only the 4× scale (about 13 mcal. sec.⁻¹ for full scale (12.7-cm.) deflection) was used. The heating rate was chosen as 5°K. min.⁻¹. At rates above 10°K. min.⁻¹ a measurable lag of temperature sensing was established while slower rates were excluded because of reduction of sensitivity. The mode of heating consisted of cooling to 180°K. with liquid nitrogen, which was used as coolant throughout the whole temperature range. After establishing a base line of differential power in-

put into sample and reference for constant temperature, heating was started at a rate of 5°K. min.⁻¹ for 4 min. After this again a new base line was established. In this fashion the whole temperature range was covered in 20°K. steps. About 1 to 1.5 min. (5 to 7°K. temperature rise on heating) was the time required to reach steady-state power input or to settle on the new base line after stopping the heating. Planimeter traces under the differential power-time recording gave identical readings as steady-state amplitudes multiplied with the appropriate time constant, so that only the latter method was used to evaluate specific heats. The amplitudes were read from the recording chart with the help of an engine-divided ruler calibrated in 0.02 in. and read to 0.005 in.

The following four series of measurements were performed. First, the empty reference aluminum capsule was run against another empty capsule of determined weight to establish the asymmetry of the system as a function of temperature. This procedure was repeated five times over a period of 2 months to check on the long-term stability. All data fell on the same curve with an average maximum spread of 0.06 mcal. sec.⁻¹. The asymmetry increased smoothly from 0.60 to 0.65 mcal. sec.⁻¹ between the limits of 180 and 480°K. All amplitudes measured were corrected by subtracting the appropriate asymmetry value.

The second series of measurements involved the power calibration with Al₂O₃. Sapphire similar to that of Ginnings and Furukawa⁷ was used. Again, a total of five runs was completed to achieve statistically significant averages. Two weights, 75.23 and 40.11 mg. of Al₂O₃, were used. The length of time over which these measurements were carried out was also about 2 months, and again all points could be combined on one graph. The standard deviation was ±0.0006 mcal. sec.⁻¹ mg.⁻¹. Using Ginnings and Furukawa's values on specific heats of Al₂O₃, which are believed accurate to ±0.2%, a calibration curve was established. For the chosen conditions (4× scale and 5°K. min.⁻¹ heating) the conversion factor to change 0.02-in. deflection from the base line to mcal. °K.⁻¹ varied smoothly from 0.075 to 0.052 for the temperature range 180 to 480°K.^{7a}

(2) P. H. Geil, F. R. Anderson, B. Wunderlich, and T. Arakawa, *J. Polymer Sci.*, **2A**, 3707 (1964).

(3) M. G. Broadhurst, *J. Res. Natl. Bur. Std.*, **67A**, 233 (1963).

(4) B. Wunderlich, *J. Chem. Phys.*, **37**, 1203 (1962).

(5) B. Wunderlich, *ibid.*, **37**, 1207 (1962).

(6) M. J. O'Neill, *Anal. Chem.*, **36**, 1238 (1964); E. S. Watson, M. J. O'Neill, J. Justin, and N. Brenner, *ibid.*, **36**, 1233 (1964).

(7) D. C. Ginnings and G. T. Furukawa, *J. Am. Chem. Soc.*, **75**, 522 (1953).

The third series consisted of five runs on extended-chain crystallized polyethylene. The weights varied between 25 and 35 mg. The first run was unannealed and showed small but definite signs of recrystallization above 340°K. Subsequent samples were annealed by heating to 410°K. for 5 min. and cooling at 0.625°K. min.⁻¹ to room temperature inside the calorimeter. This procedure melts only a minute fraction of the polymer; however, it leads to a thermally quite stable material as the results show. The recrystallized material as judged from the calorimeter trace is so small that no measurable density change results from this annealing. Except for the unannealed run, measurements were taken up to 410°K. The average maximum spread of measured points up to 370°K. was 0.0029 mcal. sec.⁻¹ mg.⁻¹. About 0.0292 mcal. sec.⁻¹ mg.⁻¹ was added in this temperature region to heat the polymer. This makes the maximum error less than $\pm 5\%$. The standard deviation of the averages of the five runs from a smooth curve is $\pm 2\%$.

The fourth series of measurements consisted of two runs of polymethylene run identically to the third series.

Small discrepancies in the weight of the aluminum were corrected using known specific heats. The platinum temperature scale of the calorimeter was corrected by calibration at 20 points with standard melting point substances. Deviations from a linear resistance-temperature relationship lie on a parabolic curve with deviations going from +6.0°K. at 150°K. to a minimum of -1.5°K. at 350°K. and finally to +7°K. at 550°K. Quoted temperatures are thought to be reliable to $\pm 0.5^\circ\text{K}$.

B. Materials. The linear polyethylene was of the Marlex 50 type. Its molecular weight distribution was checked by gel permeation chromatography.⁸ Full credit for this characterization goes to Dr. B. A. Denenberg of Waters Associates, Inc. Further detail is published in the thesis of ref. 1. The number-average molecular weight was 9800, while the weight-average was 130,000. The crystallization at elevated pressure was carried out by heating to 500°K. at atmospheric pressure, followed by pressurization to 4350 atm. at constant temperature. These conditions of temperature and pressure correspond to about 2°K. supercooling. After 20 hr. of crystallization time, the sample was cooled to room temperature at a constant pressure of 4350 atm. at a rate of 1.6°K. hr.⁻¹. At room temperature the pressure was released and the sample analyzed. A full report about the crystal morphology and pressure crystallization technique has been published elsewhere.^{1,2} The specific volume of the sample at 298°K. was 1.003 ml. as determined by density

gradient column, which corresponds to 99% crystallinity. The extrapolated amorphous specific volume at 298°K. is 1.173 ml. g.⁻¹, and the X-ray unit cell specific volume at 298°K. is 1.001 ml. g.⁻¹.⁹

A commercially available sample of polymethylene made from diazomethane was used. The molecular weight of the sample is estimated to be above 10⁷. The mode of crystallization was identical with that of polyethylene. The maximum temperature and pressure were 500°K. and 4760 atm., respectively. The specific volume of the polymethylene after pressure crystallization was 1.005 ml. g.⁻¹ or 98% crystallinity.

Experimental maximum melting points on slow heating by dilatometry on the polyethylene and polymethylene were 411.9 and 414.6°K., respectively.

III. Results

Table I contains the smoothed values of the specific heat at constant pressure in cal. deg.⁻¹ g.⁻¹, along with

Table I: Specific Heat, c_p , of Polyethylene (cal. deg.⁻¹ g.⁻¹)

Temp., °K.	Exptl. c_p	Calcd. ⁵		Extrapolated c_p	
		c_p	Dev. (%)	From paraffins ⁴	From crys- tallinity ⁴
180	0.265	0.241	-10	0.248 (0.242)	0.255
190	0.275	0.250	-10	0.260 (0.251)	0.266
200	0.285	0.260	-10	0.275 (0.262)	0.276
210	0.295	0.271	-9	0.288 (0.272)	0.286
220	0.300	0.281	-7	0.301 (0.282)	0.295
230	0.305	0.291	-5	0.314 (0.289)	0.303
240	0.310	0.302	-3	0.328 (0.296)	0.309
250	0.320	0.314	-2	0.342 (0.308)	0.315
260	0.325	0.325	± 0	0.356 ...	0.330
270	0.335	0.338	+1	0.370 ...	0.354
280	0.350	0.352	+1	0.384 ...	0.368
290	0.360	0.365	+1	0.398 ...	0.392
300	0.375	0.379	+1	0.413 ...	0.418
310	0.385	0.394	+2	0.427 ...	0.435
320	0.400	0.408	+2	0.441 ...	0.459
330	0.420	0.425	+1	0.455 ...	0.477
340	0.435	0.441	+1	0.469 ...	0.495
350	0.455	0.458	+1	0.483 ...	0.513
360	0.475	0.476	+1	0.496 ...	0.531
370	0.500	0.495	-1	0.510 ...	0.549
380	0.525	0.516	-2	0.523 ...	0.567
390	0.550	0.536	-3	0.537 ...	0.585
400	0.580	0.559	-4	0.550 ...	0.604
410	0.615	0.586	-5	0.563 ...	0.622

(7a) NOTE ADDED IN PROOF. This varying conversion factor does not necessarily indicate a nonlinearity of the measuring circuit. A large portion of it is coupled with the nonlinearity of the Pt temperature-resistance curve.

(8) J. C. Moore, *J. Polymer Sci.*, **2A**, 835 (1964).

(9) P. R. Swan, *ibid.*, **56**, 403 (1962); M. G. Gubler and A. J. Kovacs, *ibid.*, **34**, 551 (1959); L. E. Nielsen, *J. Appl. Phys.*, **25**, 1209 (1954).

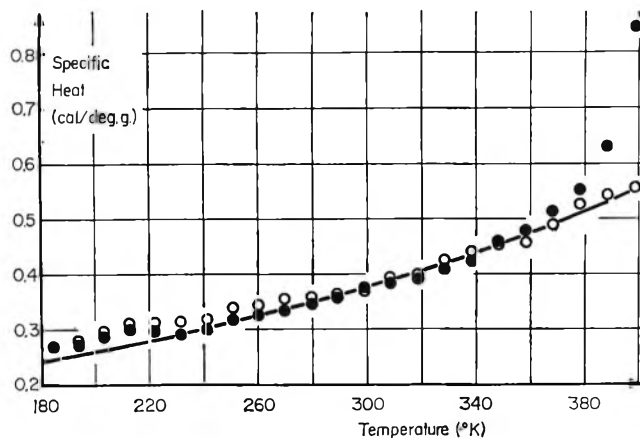


Figure 1. Specific heat of polyethylene in cal./deg. g.: drawn-out curve, calculated from the vibrational spectrum; open circles, polymethylene; filled circles, polyethylene.

the extrapolated data as given in the respective ref. 3 and 4, and the calculated values from the frequency spectrum⁵ and the discrepancy percentage. Figure 1 shows the measured points of polyethylene and -methylene and the calculated curve from the best frequency spectrum.⁵ The calculated data were changed from values at constant volume⁵ to constant pressure using the relationship $c_p - c_v = 6.87 \times 10^{-4} \times c_p^2 T$. This expression was given previously⁴; c_p and c_v are expressed in cal. deg.⁻¹ g.⁻¹; T is the absolute temperature in °K.

IV. Discussion

The temperature region of 180 to 400°K. is characterized by the almost full excitation of the acoustical modes of vibration and the start of the excitation of the low-frequency optical modes of vibration.⁵ The experimental data show clearly the specific heat leveling off between 180 and 240°K. at a value of about 0.3 cal. deg.⁻¹ g.⁻¹ which corresponds to a C_v of approximately $2R$ per degree and mole of CH_2 . The increase visible at about 250°K. comes from the low optical vibration and at 400°K. is completed to only $1.5R$ out of a total of $5R$. The two high optical vibrations (CH_2 stretching) are of little importance even at 400°K. At this temperature they make up no more than 2% of the total specific heat.⁴

The new measurements presented here show that the extrapolations from samples of different crystallinity⁴ were virtually correct up to 300°K. Above this temperature the new data are somewhat lower and are in better agreement with the calculated c_p from the vibrational spectrum. In this range c_p was previously estimated from the change in crystallinity with temperature.¹⁰ Extrapolation of c_p was at that time⁴ impossible because of the onset of melting somewhat above the glass transition (237°K.) of the only partially crystalline polymers.^{11,12} In fact, it can be seen from Figure 1 that the polyethylene, which contains still a certain amount of low molecular weight polymer, starts deviating from the purely vibrational specific heat at about 370°K., while the polymethylene with no low molecular weight components, but with a slightly lower crystallinity, shows no indication of melting up to 400°K.

The extrapolation from paraffins³ also agrees well, when corrected for the low optical vibrations which are not excited at the temperatures at which most paraffins used in the analysis are solid. The correction was made using an Einstein function fitted to give the proper melting equilibrium.³

It can be concluded that the specific heat from at least 230 to 410°K. is in agreement with the frequency spectrum as given in ref. 5. In the range 150 to 220°K. the specific heat shows a 10% discrepancy which is beyond the experimental error limit. The origin of this deviation is expected to lie in the insufficient accuracy of the upper end of the acoustical vibrations or the lower end of the optical vibrations.

With respect to the previous extrapolations, it remains to be remarked that the changes in composition (branching) or morphology (folding distances) which were necessary to reach different crystallinities had little or no influence on the final extrapolated specific heat data for 100% crystallinity.

Acknowledgment. Financial support from the National Aeronautics and Space Administration is gratefully acknowledged.

(10) B. Wunderlich and M. Dole, *J. Polymer Sci.*, **24**, 201 (1957).

(11) B. Wunderlich, *J. Chem. Phys.*, **37**, 2429 (1962).

(12) B. Wunderlich, P. Sullivan, T. Arakawa, A. DiCyan, and J. Flood, *J. Polymer Sci.*, **1A**, 3581 (1963).

Electromotive Force Studies of Cadmium Chloride in Water, Water-Ethanol, and Ethanol Solutions¹

by Jack D. Hefley and Edward S. Amis

Chemistry Department, University of Arkansas, Fayetteville, Arkansas (Received January 18, 1965)

The electromotive force of the cell $\text{Cd}-\text{Cd}_x\text{Hg}(11\%)\text{CdCl}_2(m)\text{AgCl}-\text{Ag}$ was measured at 25, 30, 35°, in water, water-ethanol, and ethanol solvents over a concentration range of cadmium chloride of 0.00050–0.010 *m*. The standard potential of the cell for each solvent at each temperature was calculated using only one method of ionization and simultaneously varying the value of the ionization equilibrium constant at a fixed distance of closest approach of the ions as the solvent composition was varied. The equilibrium constants decreased as the dielectric constants of the solvents decreased according to Bjerrum's theory of ionic association. The standard potentials were used to calculate the mean activity coefficients of cadmium chloride in the various solvents. The activity coefficients of cadmium chloride in the different solvents are similar to those determined by other investigators in mixed and nonaqueous solvent systems.

Measurements of the electromotive force of the cell $\text{Cd}-\text{Cd}_x\text{Hg}(11\%)\text{CdCl}_2(m)\text{AgCl}-\text{Ag}$ have been made at 25, 30, and 35° throughout a cadmium chloride concentration range of 0.0005–0.01 *m* and over the complete solvent range for the water-ethanol systems. From the results, the standard potential, E_0 , of the cells and the activity coefficients of cadmium chloride in the various solvent systems have been computed.

Experimental

The silver-silver chloride electrodes of the kind designated by Harned^{2a} as type 2 were used. The cadmium amalgam was prepared from distilled mercury and high purity cadmium metal supplied at special request by the E. H. Sargent Co. The amalgam electrodes containing 11% total cadmium were made individually in each cell vessel according to the method of Harned and Fitzgerald.^{2b}

A standard concentrated stock solution was made from Baker Analytical Reagent cadmium chloride and conductivity water. Its strength was found by gravimetric determination of its chloride content. More dilute solutions were prepared by adding weighed amounts of the standard solution to known weights of water. This same procedure was used in mixed solvents.

In order to prepare solutions in pure nonaqueous solvents, a known weight of the standard concentrated aqueous stock solutions mentioned above was evaporated and dried at 150° for 24 hr., then dissolved in the ethanol which had been purified according to the procedure of Smith.³ More dilute solutions in the nonaqueous solvent were then prepared in a manner similar to that for aqueous and mixed solvents.

Oxygen was removed from each cell by purging it with argon saturated with vapor whose composition and temperature were the same as the solvent in the individual cell. The cells came to equilibrium in 1–2 hr. after preparation. The temperature control was within $\pm 0.01^\circ$.

The electromotive force of each cell was measured seven times with a Leeds and Northrup Type K-3 universal potentiometer and each observed e.m.f. value which is recorded in this work is the average of these seven measurements.

(1) This communication is based on a dissertation presented to the Graduate Faculty at the University of Arkansas by J. D. H. in partial fulfillment of the requirements for the degree of Doctor of Philosophy.

(2) (a) H. S. Harned, *J. Am. Chem. Soc.*, **51**, 416 (1929); (b) H. S. Harned and M. E. Fitzgerald, *ibid.*, **58**, 2624 (1936).

(3) E. L. Smith, *J. Chem. Soc.*, 1288 (1927).

Results

When the electromotive force was measured on cadmium chloride in water solutions at different molality values, the values in Table I were obtained. A graphical presentation is shown in Figure 1, where the observed electromotive force is plotted against the molality. It can be seen from Figure 1 that the data of this work are in very good agreement with the data of Harned and Fitzgerald.^{2b}

Table I: Electromotive Force Measurements of Cadmium Chloride in Water Solutions at 25°

Sample no. ^a	Concn., <i>m</i>	<i>E</i>
R1	0.00050	0.85390
R2	0.00100	0.82997
R3	0.00200	0.80701
R4	0.00500	0.77851
R5	0.00700	0.76862
R6	0.01000	0.75846
R7	0.02000	0.73976
R8	0.05000	0.71739
R9	0.10000	0.70175
1	0.00086	0.83447
2	0.00288	0.79710
3	0.00653	0.77074
4	0.01030	0.75690
5	0.01620	0.74657

^a R indicates the values according to Harned and Fitzgerald.^{2b}

The electromotive force measurements of cadmium chloride in water-ethanol and ethanol solutions are shown in Table II. The graphical presentation of these data are shown in Figure 2. Only those data for 25° are shown graphically due to the small temperature coefficient. It can be seen from Figure 2 that the

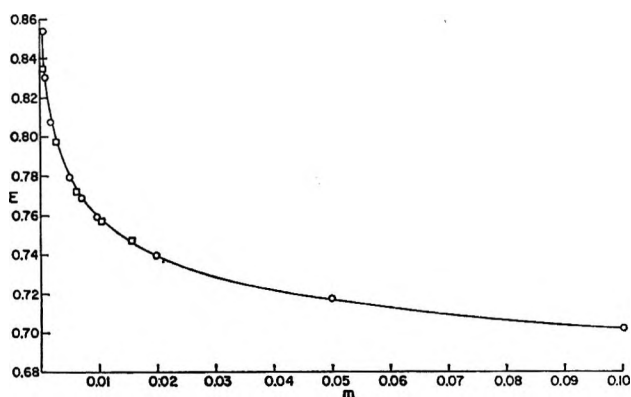


Figure 1. Electromotive force of cadmium chloride in water at 25° plotted against the cadmium chloride molality: O, data of Harned and Fitzgerald^{2b}; □, data of this work.

electromotive force data in the various ethanol solutions are a smooth function of the molality.

Table II: Electromotive Force Measurements of Cadmium Chloride in Ethanol-Water Solvents

Sample no.	Concn., <i>m</i>	E.m.f.		
		25°	30°	35°
30% Ethanol				
6	0.000482	0.81115	0.81396	0.81632
7	0.00125	0.78343	0.78538	0.78761
8	0.00221	0.76346	0.76620	0.76864
9	0.00390	0.75106	0.75272	0.75397
10	0.00649	0.73639	0.73816	0.73993
11	0.0110	0.72182	0.72312	0.72481
12	0.0171	0.71243	0.71386	0.71500
13	0.0379	0.69486	0.69640	0.69764
14	0.0838	0.68000	0.68105	0.68185
60% Ethanol				
15	0.000659	0.75073	0.75169	0.75305
16	0.00145	0.73269	0.73564	0.73765
17	0.00249	0.72286	0.72361	0.72452
18	0.00439	0.70990	0.71096	0.71178
19	0.00724	0.69941	0.70045	0.70125
20	0.0140	0.68585	0.68661	0.68730
21	0.0187	0.68101	0.68175	0.68241
22	0.0474	0.66561	0.66630	0.66685
23	0.0978	0.65538	0.65627	0.65695
90% Ethanol				
24	0.000699	0.68158	0.68205	0.68244
25	0.00162	0.67154	0.67199	0.67233
26	0.00257	0.66478	0.66529	0.66548
27	0.00439	0.65883	0.65922	0.65965
28	0.00656	0.65428	0.65452	0.65500
29	0.0113	0.64817	0.64861	0.64891
30	0.0206	0.64016	0.64074	0.64086
31	0.0422	0.63381	0.63388	0.63396
32	0.0612	0.63094	0.63098	0.63101
33	0.0973	0.62657	0.62663	0.62671
100% Ethanol				
34	0.000824	0.64743	0.64764	0.64777
35	0.00154	0.63724	0.63734	0.63745
36	0.00222	0.63691	0.63711	0.63733
37	0.00236	0.63575	0.63597	0.63619
38	0.00454	0.62832	0.62844	0.62868
39	0.00797	0.62005	0.62009	0.62020
40	0.0158	0.61693	0.61704	0.61717
41	0.0291	0.61570	0.61581	0.61591
42	0.0581	0.61198	0.61208	0.61216

The experimental accuracy in aqueous solutions was in general of the order of 0.02 mv. In the alcoholic solutions the accuracy was somewhat less. Due to the nature of the calculations, the accuracy of the values of the standard potentials discussed below is believed to be at least ± 2.0 mv.

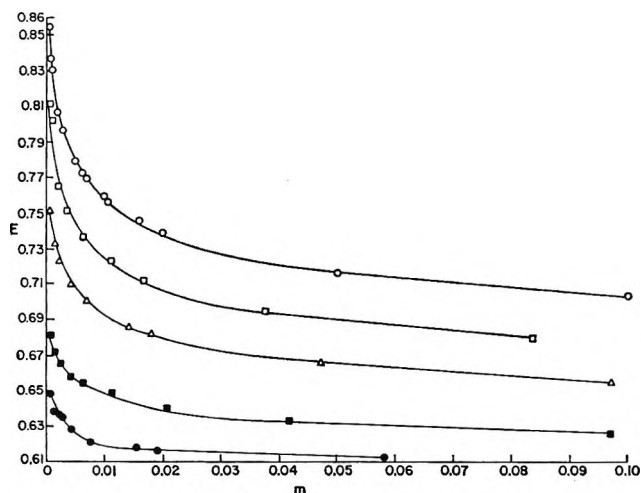


Figure 2. Electromotive force of cadmium chloride in water, water-ethanol, and ethanol at 25°: O, H₂O; □, 30% EtOH; △, 60% EtOH; ■, 90% EtOH; ●, 100% EtOH.

Evaluation of the Standard Potentials

The determination of the standard potentials of cadmium chloride in the different solvent systems was based on the method used by Harned and Fitzgerald^{2b} to determine the standard potential of cadmium in an aqueous solution. In their work they assumed that cadmium chloride is an incompletely dissociated electrolyte and then corrected for the degree of dissociation, α , from the equilibrium constant, K , and the activity coefficient of barium chloride by using the law of mass action and the Debye-Hückel theory.

In this work it was necessary to modify the method of Harned and Fitzgerald^{2b} in two ways. These two modifications will be discussed below.

The electromotive force of the cell may be represented by eq. 1, where E_0 is the standard potential, m

$$E = E_0 - k \log 3m^3\gamma_{\pm}^3 \quad (1)$$

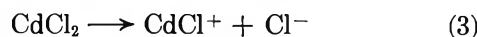
is the molality, γ_{\pm} is the mean ionic activity coefficient, and k equals $2.303RT/2\mathfrak{F}$. By replacing $\log \gamma_{\pm}$ by $(-S'_{(t)}\sqrt{m} + B'm)$ where $S'_{(t)}$ is the limiting slope of the Debye-Hückel theory, one obtains eq. 2.

$$E + k \log 4m^3 - 3kS'_{(t)}\sqrt{m} = E_0 - 3kB'm = E_H \quad (2)$$

According to eq. 2, if cadmium chloride were a completely dissociated electrolyte, a plot of $E + k \log 4m^3 - 3kS'_{(t)}\sqrt{m}$ should be linear with m in dilute solutions. This is not the case and confirms the conductance data which indicate that cadmium chloride is incompletely dissociated.

The dissociation mechanism which appears to be most suitable from the character of the data is that of

eq. 3 and 4. According to these equations cadmium



chloride is completely dissociated while the ion CdCl^+ is partially dissociated. It is probable that both cadmium chloride and CdCl^+ are incompletely dissociated. The above assumption neglects the first association as having a negligible effect compared to the second in dilute solutions.

Now if $\gamma_{\text{Cd}^{2+}} = \gamma_{\text{aM}} = \gamma_{\text{ax}}$ ⁴, the equilibrium constant of eq. 4 is

$$K = \frac{(\alpha m \gamma_{\text{aM}})(1 + \alpha)\gamma_{\text{ax}}m}{m(1 - \alpha)\gamma_{\text{ax}}} = \frac{m\gamma_{\text{aM}}\alpha(1 + \alpha)}{1 - \alpha} \quad (5)$$

where α is the degree of dissociation. Solving for α gives

$$\alpha = \frac{1}{2} \left[- \left(1 + \frac{K}{m\gamma_{\text{aM}}} \right) + \sqrt{\left(1 + \frac{K}{m\gamma_{\text{aM}}} \right)^2 + \frac{4K}{m\gamma_{\text{aM}}}} \right] \quad (6)$$

Using the reiterative procedure of Harned and Fitzgerald^{2b} and of Harned and Owen,^{4a} the equilibrium constant for the dissociation constant, K , and the degree of dissociation, α , for the process represented in eq. 4 were found, as were γ_{aM} , the activity coefficient of the M^{2+} ions; μ' , the real ionic strength; and γ_{a} , the real mean activity coefficient of cadmium chloride.

Harned and Fitzgerald^{2b} in their work on cadmium chloride in aqueous solution used the activity coefficient of barium chloride obtained by Tippetts and Newton^{4b} for the real activity coefficient of cadmium chloride. In this work, data on cadmium chloride in aqueous solution were taken initially to check the experimental procedure for reproducibility. Since these data compared favorably with the data of Harned and Fitzgerald the two sets of data were listed together and treated according to the theory of Harned and Fitzgerald^{2b,4a} with the aid of an IBM 7074 computer. The value of E° obtained from the mixed data was 0.57340 v. compared to the value of E° of 0.57300 v. found by Harned and Fitzgerald.

The next step in the treatment of the data was to replace the activity coefficient of barium chloride by $\gamma_{\text{aM}}^{1/2}$ or γ_{a} , the mean activity coefficient for cad-

(4) (a) H. S. Harned and B. B. Owen, "The Physical Chemistry of Electrolytic Solutions," 3rd Ed., Reinhold Publishing Corp., New York, N. Y., 1958, pp. 551-560; (b) E. A. Tippetts and R. F. Newton, *J. Am. Chem. Soc.*, 56, 1675 (1934).

mium chloride from which the best value of α was computed using the reiterative procedure described above. This procedure gave in this case 0.57162 v. for E° . Since this treatment of the data gave a value within 1.4 mv. of the value determined by Harned and Fitzgerald, it was decided to write a program for the IBM 7074 computer which was similar to the treatment of Harned and Fitzgerald except for two changes listed below.

The first change was that $\gamma_a = \gamma_{aM}^{1/2}$ for cadmium chloride was used instead of γ_a for barium chloride.

The second change was that curves corresponding to the equations for $E^{\circ'}$ and $E^{\circ'} - E^\circ$ were not considered separately, but rather their difference was computed since the difference was E° . The two pertinent equations are

$$E^{\circ'} = E + \frac{3 \times 2.303RT}{2\mathfrak{F}} \log m - \frac{3 \times 2.303RT}{2\mathfrak{F}} S'_{(t)} \sqrt{m} + \frac{2.303RT}{2\mathfrak{F}} \log 4 \quad (7)$$

$$E^{\circ'} - E^\circ = \frac{2.303RT}{2\mathfrak{F}} \log 4 - \frac{2.303RT}{2\mathfrak{F}} \log \alpha (1 + \alpha)^2 - \frac{3 \times 2.303RT}{2\mathfrak{F}} \log \gamma_a - \frac{3\sqrt{2} \times 2.303RT}{2\mathfrak{F}} S_{(t)} \sqrt{\mu} \quad (8)$$

Subtracting eq. 8 from eq. 7 one obtains

$$E^\circ = E + \frac{3 \times 2.303RT}{2\mathfrak{F}} \log m + \frac{3 \times 2.303RT}{2\mathfrak{F}} \log \gamma_a - \frac{3 \times 2.303RT}{2\mathfrak{F}} S'_{(t)} \sqrt{m} + \frac{3\sqrt{2} \times 2.303RT}{2\mathfrak{F}} S_{(t)} \sqrt{\mu} + \frac{2.303RT}{2\mathfrak{F}} \log \alpha (1 + \alpha)^2 \quad (9)$$

This was the final form which was used to evaluate E° for each observed value of E at a given molality. The values of E° computed from this equation for each value of E and m were averaged. The IBM 7074 computer program was stated so that different values of K and a selected value of \bar{d} were tried until the correct combination gave an average E° value with an average deviation of 1.5 mv. or less. This amounts to the difference between the curves from eq. 7 and 8 being a straight line with a slope of zero within about 1.5 mv. In the higher alcohol solutions the average minimum deviation of E° was somewhat higher. While Harned

and Fitzgerald did not list their deviations, the points on the horizontal lines from which E° values were determined showed deviations comparable to the ones listed in Table III.

In Table III are listed the calculated values of E° together with the values of the equilibrium constants and the mean distance of approach of the ions which were used in order for the E° values to show a suitable minimum deviation. The dielectric constants of the solvents and the thermodynamic functions ΔF° , ΔH° , and ΔS° for the cell process are presented in the table.

The values of ΔF° were obtained from

$$\Delta F^\circ = -n\mathfrak{F}E^\circ \quad (10)$$

those of ΔH° were calculated from

$$\Delta H^\circ = \frac{\Delta \left(\frac{\Delta F^\circ}{T} \right)}{\Delta \left(\frac{1}{T} \right)} \quad (11)$$

and those of ΔS° from

$$\Delta S^\circ = \frac{\Delta H^\circ - \Delta F^\circ}{T} \quad (12)$$

In the above equations ΔF° , ΔH° , and ΔS° are the changes of free energy, enthalpy, and entropy, respectively, for the cell process when the reactant and product species are at unit activity, n is the number of electrons transferred in the reaction, and \mathfrak{F} is the faraday (96,512 international coulombs, since E° is in international volts).

In order for E° to reach this minimum it was not necessary to change the value of \bar{d} as the solvent was varied from water to 100% ethanol. Oiwa⁵ found a trend for \bar{d} when HCl was studied in water-methanol solutions, although the range of variation in \bar{d} for HCl was not large. He indicated that this was due to a preferential solvation effect of the ions. Present work in these laboratories on cadmium chloride in water-methanol solvents indicates a constancy in \bar{d} .

In Figure 3 the E° values listed in Table III are plotted against the reciprocal of the dielectric constant of the medium in which each E° value was determined. The resulting lines are almost straight. The data taken by Corsaro⁶ on zinc chloride in water-alcohol solutions gave straight lines for such plots. He found that the E° value of the salt varied linearly with the reciprocal of the dielectric constant of the medium in which the

(5) I. T. Oiwa, *J. Phys. Chem.*, **60**, 754 (1956).

(6) C. Corsaro and H. L. Stephens, *J. Electrochem. Soc.*, **104**, 512 (1957).

Table III: Tabulated Values of Derived Quantities in Different Solvents and at Different Temperatures

Solvent	Temp., °K.	D	K	d , Å.	E° , v. ^a	Deviation in E°	$-\Delta F^\circ$, cal./mole	$-\Delta H^\circ$, cal./mole	$-\Delta S^\circ$, e.u.
H ₂ O	298.16	78.5	0.07	5	0.57162	0.00130	26,363		
H ₂ O	303.16	76.8	0.07	5	0.56890 ^b		26,238	33,800	24.9
H ₂ O	308.16	75.0	0.07	5	0.56670 ^b		23,136	32,400	20.3
30% EtOH	298.16	61.1	0.04	5	0.52742	0.00106	24,325		
30% EtOH	303.16	59.7	0.04	5	0.52544	0.00095	24,233	29,800	18.4
30% EtOH	308.16	58.2	0.04	5	0.52308	0.00093	23,124	30,800	21.7
60% EtOH	298.16	43.4	0.005	5	0.46930	0.00167	21,644		
60% EtOH	303.16	42.3	0.005	5	0.46554	0.00188	21,466	32,300	35.8
60% EtOH	308.16	41.1	0.005	5	0.46055	0.00183	21,240	35,200	45.3
90% EtOH	298.16	28.1	0.0007	5	0.37498	0.00175	17,294		
90% EtOH	303.16	27.4	0.0007	5	0.37069	0.00190	17,096	29,100	39.6
90% EtOH	308.16	26.5	0.0007	5	0.36399	0.00192	16,787	35,800	61.7
100% EtOH	298.16	24.3	0.0006	5	0.33711	0.00124	15,547		
100% EtOH	303.16	23.7	0.0006	5	0.33183	0.00144	15,304	30,000	48.5
100% EtOH	308.16	23.0	0.0006	5	0.32430	0.00160	14,957	36,400	67.9

^a International volts. ^b Extrapolated from temperature coefficient.

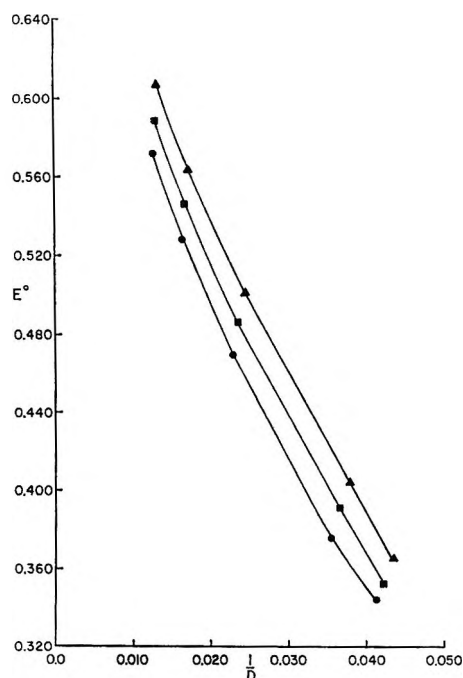


Figure 3. Standard potentials of cadmium chloride plotted against $1/D$ using ethanol solutions: ●, EtOH solutions at 25°; ■, EtOH solutions at 30° +0.02000 v.; ▲, EtOH solutions at 35° +0.04000 v.

E° was determined, when alcohol and water-alcohol solutions were used. Harned and Owen⁷ have discussed this dependence of E° on $1/D$ theoretically on the basis of the work necessary to separate the ions of the salt against the attractive coulombic forces. These authors used the activity coefficient in their derivation and thus introduced the thermal energy, kT , in their final equation. Amis⁸ using a purely electrostatic approach has derived an equation for a linear relation between E° and $1/D$ which does not involve the thermal energy. Amis explains the reason for deviation from a straight line as due to selective solvation of the ions.

The method of treating the raw data in this work has yielded satisfactory values of E° in the various solvent compositions. However, the variation in the parameter K in the different solvent systems needs to be justified.

The variation in the dissociation constant, K , is not at all unusual when one considers Bjerrum's⁹

(7) H. S. Harned and B. B. Owen, "The Physical Chemistry of Electrolytic Solutions," Reinhold Publishing Corp., New York, N. Y., 1950, pp. 336-340.

(8) E. S. Amis, *J. Electroanal. Chem.*, **8**, 413 (1964).

theory of ionic association in media other than water. This theory states that the ions of all electrolytes tend to associate more and more as the dielectric constants of the solvent media decrease. This phenomenon is attributed to the fact that when electrolytes are dissolved in solvents of low dielectric constants, the simple coulombic forces are sufficient to cause ionic association. Experimental verification of Bjerrum's theory has been presented by Fuoss and Kraus.¹⁰ They found from conductance data on tetraisoamylammonium nitrate in dioxane-water solutions that a threefold decrease in the dielectric constant of the solvent caused the dissociation constant to decrease by a factor of 10^{-3} . The same trends were observed in this work. When an approximate threefold decrease in the dielectric constant of the solvent was made, the dissociation constant was decreased by a factor of 10^{-2} . In view of these same qualitative trends, it is felt that the variation of the dissociation constants for cadmium chloride in the different solvents is reasonable.

As seen from Table III, the standard free energy change of the cell process increases (becomes continually less negative) as the percentage of ethyl alcohol in the solvent increases. This means that the process is less spontaneous at unit activity of reactants as the nonaqueous component of the solvent increases. The increase of standard free energy with decrease of the dielectric constant of the solvent might be due, among other things, to the difference in the nature and extent of solvation, change in structure of the solvent, and increased energy necessary to prevent association of the ions. Perhaps the greatest cause of the decrease in spontaneity, in fact the cause which probably predominates, is the greater energy requirement to prevent association of the ions in lower dielectric constant media. That this is the predominant cause of decrease in spontaneity is shown by the practically linear relationship between E° and $1/D$.⁸ In general the spontaneity decreases with increase in temperature again perhaps because the dielectric constants of the solvents decrease at higher temperatures.

Since ΔH° and ΔS° values depend on differences in ΔF° , the errors in these functions are no doubt much greater than in the ΔF° values. The small differences in large numbers retain the same magnitude of errors, and hence much larger percentage errors than do the original large numbers. Thus ΔH° and ΔS° values have been rounded off to three significant numbers and their trends are not nearly so regular or amenable to interpretations as are the values of ΔF° . Nevertheless these values are presented so that they may be available for comparison with future data. The reaction is exothermic throughout and shows a negative

entropy increment in all solvents. The exothermicity and negative entropy increments are greater in the higher than in the lower temperature range except in pure water as a solvent.

The decreases in entropy of the process indicate an ordering effect which, except for water, is greater at higher temperature ranges than at lower ranges. The greater decreases in entropy and hence greater order at higher temperature ranges might be due to reduced dielectric constant so that solvation or other effects of ethyl alcohol may cause the number of accessible states of order to increase with increase in temperature. The opposite trend in water might be due to the decreased hydrogen bonding at the higher temperature, reducing the possibility of longer chains being orientated by the ions. The greater negative values of entropy in pure alcohol indicate a greater ordering effect in this solvent, perhaps arising from the fact that for the same number of molecules ordered in this media as contrasted with water, greater weight and volume fractions of the solvent are ordered.

Activity Coefficients

After the E° values were determined for each solvent composition, the activity coefficients were calculated from eq. 1.

The logarithms of the activity coefficients which were determined in this manner are listed in Tables IV and V. A graphical representation of these data

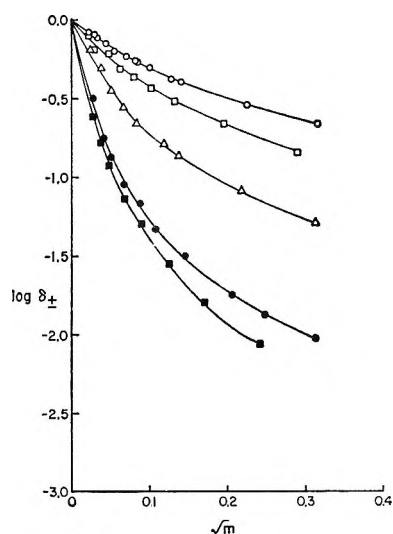


Figure 4. Activity coefficients of cadmium chloride in the water-ethanol system at 25°C: O, H₂O; □, 30% EtOH; △, 60% EtOH; ●, 90% EtOH; ■, 100% EtOH.

(9) N. Bjerrum, *Kgl. Danske Videnskab. Selskab*, 7, No. 9 (1926).

(10) R. M. Fuoss and C. A. Kraus, *J. Am. Chem. Soc.*, 55, 1019 (1933).

Table IV: Activity Coefficients of Cadmium Chloride in Water at 25°

m	\sqrt{m}	$-\log \gamma_{\pm}$
0.000500	0.0224	0.0803
0.000861	0.0293	0.0974
0.00100	0.0316	0.1117
0.00200	0.0447	0.1540
0.00288	0.0537	0.2007
0.00500	0.0707	0.2308
0.00653	0.0808	0.2595
0.00700	0.0837	0.2655
0.0100	0.100	0.3062
0.0103	0.101	0.3014
0.0162	0.127	0.3817
0.0200	0.141	0.3965
0.0500	0.224	0.5423
0.100	0.316	0.6671

in which $\log \gamma_{\pm}$ is plotted against \sqrt{m} is shown in Figure 4. Only those data for 25° are shown graphically due to the small temperature coefficient.

The variation of the activity coefficients of cadmium chloride with the dielectric constant (or solvent composition), as shown in the figures, follows the same general trends which Harned and Morrison^{11,12} observed for hydrochloric acid in water-dioxane solvents. This trend, of course, is a deviation from the straight line limiting slope of the Debye-Hückel theory at a lower value of the molality as the dielectric is decreased.

Summary

The electromotive force of cadmium chloride was determined in water, water-ethanol, and ethanol solvents over a concentration range of 0.00050–0.010 m . The measurements were made using a Leeds and Northrup Type K-3 potentiometer and an amalgam cell without transference.

In order to determine the standard potential of cadmium chloride in the various solvents it was necessary to extrapolate the molality to zero by a suitable linear function of the observed electromotive force. Satisfactory values of the standard potential were determined over the entire solvent, temperature, and concentration ranges by assuming only one method of ionization and simultaneously varying the equilibrium constant at a fixed distance of closest approach of the ions as the solvent composition was varied.

The justification for decreasing the dissociation constant as the dielectric constant was decreased was based on Bjerrum's theory of ionic association in media other than water.

The laborious calculations involved in the determination of the standard potentials were accomplished by using an IBM 7074 computer.

Table V: Activity Coefficients of Cadmium Chloride in Ethanol-Water Solvents

m	\sqrt{m}	$-\log \gamma_{\pm}$		
		25°	30°	35°
30% Ethanol				
0.000482	0.02195	0.0811	0.0810	0.0809
0.001250	0.03536	0.183	0.178	0.182
0.00221	0.04701	0.205	0.213	0.222
0.00390	0.06245	0.312	0.309	0.309
0.00649	0.08056	0.368	0.370	0.377
0.0110	0.10488	0.433	0.433	0.441
0.0171	0.13076	0.519	0.522	0.526
0.0379	0.19467	0.666	0.674	0.683
0.0838	0.28949	0.843	0.848	0.855
60% Ethanol				
0.000659	0.02567	0.191	0.191	0.209
0.00145	0.03808	0.330	0.355	0.383
0.00249	0.04990	0.454	0.457	0.475
0.00439	0.06626	0.554	0.563	0.582
0.00724	0.08509	0.654	0.664	0.685
0.0140	0.11832	0.787	0.797	0.819
0.0187	0.13675	0.858	0.868	0.891
0.0474	0.21772	1.089	1.101	1.126
0.0978	0.31272	1.288	1.305	1.332
90% Ethanol				
0.000699	0.02642	0.500	0.496	0.517
0.00162	0.04025	0.752	0.749	0.772
0.00257	0.05069	0.876	0.875	0.898
0.00439	0.06626	1.042	1.041	1.067
0.00656	0.08809	1.165	1.163	1.190
0.0113	0.10630	1.332	1.334	1.360
0.0206	0.14353	1.502	1.507	1.533
0.0422	0.20453	1.743	1.743	1.769
0.0612	0.24739	1.872	1.872	1.899
0.0973	0.31193	2.024	2.025	2.053
100% Ethanol				
0.000824	0.02871	0.614	0.616	0.643
0.00154	0.03924	0.770	0.774	0.802
0.00222	0.04712	0.925	0.930	0.960
0.00236	0.04858	0.939	0.944	0.974
0.00454	0.06738	1.139	1.145	1.176
0.00797	0.08927	1.291	1.297	1.328
0.0158	0.12569	1.553	1.560	1.592
0.0291	0.17059	1.804	1.812	1.844
0.0581	0.24104	2.062	2.070	2.103

The standard potentials which were determined were used to calculate the mean ionic activity coefficients of cadmium chloride in the various solvents. The calculations were made by using the form of the Nernst equation which is applicable to a 2-1 electrolyte.

The activity coefficients of cadmium chloride in the

(11) H. S. Harned and J. O. Morrison, *Am. J. Sci.*, **33**, 161 (1937).

(12) H. S. Harned and J. O. Morrison, *J. Am. Chem. Soc.*, **58**, 1908 (1936).

various solvent systems are similar to those determined by other investigators for electrolytes in mixed and nonaqueous solvents. The general behavior is that deviations from the Debye-Hückel theory occur at lower concentrations as the dielectric constant of the solvent is decreased.

Acknowledgment. The authors wish to thank the U. S. Atomic Energy Commission, which supported this work financially under contract AT-(40-1)-2069. Thanks are also due Union Carbide Chemicals Company for use of its IBM 7074 computer in calculating the values of E° .

Fluorine Bomb Calorimetry. X. The Enthalpies of Formation of Niobium and Tantalum Pentafluorides^{1,2}

by Elliott Greenberg, Carol A. Natke, and Ward N. Hubbard

Chemical Engineering Division, Argonne National Laboratory, Argonne, Illinois (Received January 18, 1965)

The energies of formation of niobium and tantalum pentafluorides were measured by direct combination of the elements in a bomb calorimeter. From these measurements the standard enthalpies of formation, $\Delta H_f^\circ_{298.15}$, of niobium and tantalum pentafluorides were calculated to be -433.50 ± 0.15 and -454.97 ± 0.19 kcal. mole⁻¹, respectively.

Introduction

The determination of the heats of formation of the pentafluorides of niobium and tantalum is part of a continuing program³ to obtain precise thermochemical data by fluorine bomb calorimetry.

Experimental

Calorimetric System. The calorimeter, laboratory designation ANL-R1, and combustion bomb, laboratory designation Ni-T, have already been described.^{3,4} Twelve calibration experiments were carried out with benzoic acid (National Bureau of Standards Sample 39i), some preceding and some following the fluorine combustions. The certified energy of combustion for this sample was 26.434 ± 0.003 abs. kjoule g.⁻¹. ε (calor.), the energy equivalent of the calorimetric system, was 3566.30 cal. deg.⁻¹ for the niobium experiments and 3566.24 for the tantalum experiments. In each case the standard deviation of the mean was ± 0.2 cal. deg.⁻¹, or 0.005%.

Materials. Samples of niobium and tantalum were

obtained from the Wah Chang Corp. and the National Research Corp., respectively, in the form of 0.317-cm. diameter rod, 0.0127-cm. foil, and 0.0254-cm. diameter wire. The outer portion of the rods was removed by taking surface cuts with a small lathe, using a tungsten carbide tool bit and keeping the sample flooded with Chlorothene (inhibited 1,1,1-trichloroethane). The machined samples were then stored under vacuum to minimize any possible surface oxidation. Samples for the combustion experiments and analyses were cut at appropriate positions along the length of a single rod. The impurities found in these samples are summarized in Table I. No other metallic impurities were de-

(1) This work was performed under the auspices of the U. S. Atomic Energy Commission.

(2) Presented in part at the 18th Calorimetry Conference in Bartlesville, Okla., Oct. 1963.

(3) E. Greenberg, J. L. Settle, H. M. Feder, and W. N. Hubbard, *J. Phys. Chem.*, **65**, 1168 (1961). See also succeeding papers in this series.

(4) E. Greenberg, J. L. Settle, and W. N. Hubbard, *ibid.*, **66**, 1345 (1962).

tected. The chemical states of the impurities are unknown, but the assumed states of combination are indicated in the table. In each case, the foil and wire samples were of comparable quality to the rod samples and, because these items constituted only a small fraction of the total sample, it was not considered necessary to analyze them for their specific impurity contents.

Table I: Impurities in the Samples

Impurity	P.p.m.		Assumed form of impurity
	Nb	Ta	
C ^a	38	22	MC ^b
O ^a	83	68	M ₂ O ₆ ^b
H ^a	3	0.2	Solid soln.
N ^a	50	16	MN ^b
Ti	94	...	Ti
W	60	8	W
Fe	..	51	Fe
Zr	50	...	Zr
Nb	..	16	Nb
Si	..	11	Si
Al	..	11	Al
Ca	..	9	Ca
Na	..	9	Na
Mg	..	7	Mg
Mo	7	...	Mo
Ta	5	...	Ta
Cu	5	...	Cu
Hf	3	...	Hf

^a Average of chemical analyses by manufacturer and Chemical Research Services, Inc., Addison, Ill.; all others are spectrochemical data provided by manufacturer and J. Goleb, Argonne National Laboratory. ^b M represents either niobium or tantalum.

Purified fluorine (99.97%) was prepared by distillation of commercial fluorine in a low temperature still.^{3,5}

Combustion Technique. The sample arrangement and combustion technique were similar to those described³ for the combustion of zirconium in fluorine. Preliminary combustion experiments indicated a tendency for preferential attack of the sample at the point of contact between it and the nickel support. This attack, which often cut through the sample near its base before the end of the combustion, was greater at higher fluorine pressures. Satisfactory combustions were obtained with fluorine pressures of 1500 mm. in the niobium experiments and 2000 mm. in the tantalum experiments. No inert diluent gas was necessary because of the high melting point of these metals. Under these conditions it was satisfactory to machine the lower end of the niobium sample rods to a diameter of 0.089 cm. but it was necessary to increase this dimension to 0.14 cm. for tantalum in order to prevent burning through near the

base of the sample. The assembled bomb was always pretreated with fluorine at operating pressure for a few minutes before final evacuation and charging. The calorimetric measurements were made in the usual manner.

Surface Fluorination Experiments. Trial exposures of weighed samples to fluorine indicated a definite spontaneous surface reaction. Since this reaction occurs before intentional ignition of the sample, the associated thermal effect represents heat evolved which is not detected during the calorimetric experiment, thereby necessitating a correction. Therefore, in carrying out the calorimetric experiments a special effort was made to reproduce as closely as possible the elapsed time between first exposure of the sample to fluorine and the initiation of the combustion reaction in the calorimeter. After the calorimetric combustions were completed, a series of blank experiments was run with each metal in which typical weighed samples were loaded and treated in a manner identical with the procedure employed for the calorimetric runs. After exposure of the sample to fluorine for the appropriate time interval, the bomb was evacuated, flushed with argon, and the sample recovered and reweighed. The reweighing was performed in an inert-atmosphere glove box in order to avoid reaction between atmospheric moisture and the metal fluoride on the sample surface. From the gain in weight of the sample (about 0.4 ± 0.1 mg., assumed to be due to the formation of the corresponding pentafluoride) an appropriate thermal correction was calculated for the prefluorination of the sample.

Analysis of Combustion Products. After the completion of each calorimetric measurement, the bomb was discharged and the unburned metal was quickly recovered, flooded with water, dried under vacuum, and weighed.

The white, solid, combustion products recovered from the bomb exhibited the characteristic physical properties of NbF₅ and TaF₅, respectively, and yielded X-ray diffraction patterns which were quite spotty, possibly owing to the coarseness of the crystallites. After these products were ground in an inert-atmosphere glove box, satisfactory X-ray patterns were obtained, provided the inert atmosphere was sufficiently pure to be unreactive. The patterns agreed with those obtained by Edwards⁶ for NbF₅ and TaF₅.

In some of the combustion experiments the small amount of gas remaining in the bomb after combustion

(5) L. Stein, E. Rudzitis, and J. L. Settle, "Purification of Fluorine by Distillation," Argonne National Laboratory, ANL-6364 (1961). (Available from Office of Technical Services, U. S. Department of Commerce, Washington 25, D. C.)

(6) A. J. Edwards, *J. Chem. Soc.*, 3714 (1964).

Table II: Results of Niobium Combustions

	Combustion no.					
	1	2	3	4	5	6
(1) Mass, g.	1.05270	1.05769	1.04740	1.04976	1.04358	1.04506
(2) Δt_c , deg.	1.36953	1.37599	1.36254	1.36601	1.35739	1.35935
(3) $\varepsilon(\text{calor.})(-\Delta t_c)$, cal.	-4884.15	-4907.19	-4859.23	-4871.60	-4840.86	-4847.86
(4) $\Delta E_{\text{contents}}$, cal. ^{a,b}	-9.81	-9.88	-9.81	-9.82	-9.75	-9.81
(5) $\Delta E_{\text{ignition}}$, cal.	0.61	0.77	0.84	0.92	1.14	0.88
(6) ΔE_{gas} , cal. ^c	-0.10	-0.10	-0.10	-0.10	-0.10	-0.10
(7) $\Delta E_{\text{prefluorination}}$, cal.	-1.73	-1.73	-1.73	-1.73	-1.73	-1.73
(8) $\Delta E_{\text{impurities}}$, cal.	-0.35	-0.35	-0.35	-0.35	-0.34	-0.34
(9) $\Delta Ec^\circ/M$, cal. g. ⁻¹	-4650.45	-4650.21	-4649.97	-4651.23	-4649.04	-4649.46
					Mean $\Delta Ec^\circ/M = -4650.1$ cal. g. ⁻¹	
					Std. dev. of mean = ± 0.3 cal. g. ⁻¹	

^a $\Delta E_{\text{contents}} = \varepsilon^i(\text{cont.})(t_i - 25) + \varepsilon^f(\text{cont.})(25 - t_f + \Delta t_{\text{corr}})$ in which t_i varied from 22.9 to 23.3°. ^b The bomb contents included about 65.2 g. of nickel and 0.08 g. of Teflon. ^c $\Delta E_{\text{gas}} = \Delta E^i(\text{gas})]_0^{P_i(\text{gas})} + \Delta E^f(\text{gas})]_0^{P_f(\text{gas})}$.

Table III: Results of Tantalum Combustions^a

	Combustion no. ^b						
	8	9	11	12	13	14	15
(1) Mass, g.	2.72870	2.74600	2.72486	2.72652	2.72309	2.67219	2.73363
(2) Δt_c , deg.	1.91390	1.92466	1.91106	1.91167	1.90853	1.87522	1.91716
(3) $\varepsilon(\text{calor.})(-\Delta t_c)$, cal.	-6825.43	-6863.80	-6815.30	-6817.47	-6806.28	-6687.48	-6837.05
(4) $\Delta E_{\text{contents}}$, cal. ^{c,d}	-13.91	-13.97	-13.91	-13.90	-13.88	-13.59	-13.89
(5) $\Delta E_{\text{ignition}}$, cal.	1.19	0.67	0.68	0.60	0.90	0.92	0.68
(6) ΔE_{gas} , cal. ^e	-0.18	-0.18	-0.18	-0.18	-0.18	-0.18	-0.18
(7) $\Delta E_{\text{prefluorination}}$, cal.	-1.72	-1.72	-1.72	-1.72	-1.72	-1.72	-1.72
(8) $\Delta E_{\text{impurities}}$, cal.	0.25	0.25	0.25	0.25	0.25	0.24	0.25
(9) $\Delta Ec^\circ/M$ cal. g. ⁻¹	-2506.61	-2505.01	-2506.62	-2505.91	-2504.84	-2507.98	-2506.52
						Mean $\Delta Ec^\circ/M = -2506.2$ cal. g. ⁻¹	
						Std. dev. of mean = ± 0.4 cal. g. ⁻¹	

^a An earlier series of combustion experiments gave somewhat less precise results because of minor experimental difficulties, and, for this reason, the data are not included in the final tabulation. However, the mean $\Delta Ec^\circ/M$ value for the first series does not differ significantly from that reported herein. ^b No data were obtained for run 10 because the calorimeter stirrer failed during the reaction period. ^c $\Delta E_{\text{contents}} = \varepsilon^i(\text{cont.})(t_i - 25) + \varepsilon^f(\text{cont.})(25 - t_f + \Delta t_{\text{corr}})$ in which t_i was approximately 22.77°. ^d The bomb contents included about 65.0 g. of nickel and 0.09 g. of Teflon. ^e $\Delta E_{\text{gas}} = \Delta E^i(\text{gas})]_0^{P_i(\text{gas})} + \Delta E^f(\text{gas})]_0^{P_f(\text{gas})}$.

was transferred to an infrared cell for analysis. The analyses confirmed that the carbon and silicon impurities in the samples were burned to their respective tetrafluorides.

Results

Experimental Results. The results of the niobium and tantalum combustion experiments, expressed in terms of the defined calorie equal to (exactly) 4.184 absolute joules, are summarized in Tables II and III. The corrections to standard states were applied in accordance with the procedure illustrated for the combustion of molybdenum in fluorine.⁷ The entries in the tables are (1) the mass *in vacuo* of the sample burned, which was determined by subtracting the mass of un-

burned metal recovered after combustion from the mass of sample originally introduced into the bomb; (2) the observed increase in the calorimeter temperature, corrected for heat exchanged between the calorimeter and its surroundings, $\Delta t_c = t_f - t_i - \Delta t_{\text{corr}}$; (3) the energy equivalent of the calorimetric system minus the contents of the bomb, multiplied by $-\Delta t_c$; (4) the energy equivalents of the initial and final contents of the bomb, each multiplied by its appropriate portion of $-\Delta t_c$ to correct the results to the energy of the hypothetical isothermal process at 25°; (5) the

(7) W. N. Hubbard, "Experimental Thermochemistry," Vol. II, H. A. Skinner, Ed., Interscience Publishers Ltd., London, 1962, Chapter 6.

measured electrical energy input for ignition of the fuse; (6) the net correction for reducing the pressure of the bomb gas to standard-state conditions; (7) the correction for the spontaneous surface reaction of the sample with fluorine before intentional ignition of the sample; (8) the net correction for impurities in the sample; (9) the energy change per gram of metal for the reaction



where M represents either niobium or tantalum.

For calculation of item 4 the following values were used: heat capacities at constant pressure—0.106₁, 0.28, 0.0633, 0.0335, 0.1715, and 0.118 cal. deg.⁻¹ g.⁻¹ for Ni,⁸ Teflon,⁹ Nb,¹⁰ Ta,¹⁰ NbF₅,¹¹ and TaF₅,¹² respectively; heat capacity at constant volume—5.50 cal. deg.⁻¹ mole⁻¹ for fluorine.¹³

The coefficients $(\partial E/\partial P)_T$ and μ (in the equation $PV = nRT(1 - \mu P)$), which were required for calculation of item 6, were estimated by the method of Hirschfelder, *et al.*,¹⁴ from the force constants for fluorine.¹⁵ The coefficients at 25° were 0.000803 atm.⁻¹ and -1.781 cal. atm.⁻¹ mole⁻¹ for μ and $(\partial E/\partial P)_T$, respectively. For estimation of the internal volume of the bomb in the initial and final states, the densities used were 8.907, 2.24, 8.53, 16.626, 3.54, and 5.19 g. cc.⁻¹ for Ni,¹⁶ Teflon,⁹ Nb,¹⁷ Ta,¹⁶ NbF₅,⁶ and TaF₅,⁶ respectively. The internal volume of the empty bomb was 0.358 l.

For calculation of item 8 the assumptions indicated in Table I were made regarding the states of combination of the impurities. After the combustion, carbon, oxygen, hydrogen, and nitrogen were assumed to be present as CF₄, O₂, HF, and N₂, respectively. The remaining impurities were assumed to form their most stable fluorides during combustion. For the small silicon impurity in the tantalum sample there is no significant change in the correction if the silicon is assumed to be combined. The required enthalpies of formation were taken from the indicated sources: NbC,^{18,19} TaC,^{18,20} Nb₂O₅ and Ta₂O₅,²¹ Nb-H system,²² NbN and TaN,²³ CF₄,²⁴ HF,²⁵ TiF₄,⁴ WF₆,²⁶ SiF₄,²⁷ AlF₃,²⁸ FeF₃,²⁹ MgF₂,³⁰ CaF₂,³¹ and NaF.³¹

The approximate corrections to the measured heat for the niobium sample were: oxygen, -0.018%; carbon, +0.009%; nitrogen, -0.009%; hydrogen, +0.008%; titanium, +0.007%; tungsten, -0.003%. Corrections for the tantalum sample were: oxygen, -0.023%; carbon, +0.011%; silicon and aluminum, +0.005% each; nitrogen, -0.004%; iron, +0.004%; calcium and magnesium, +0.002% each; niobium and sodium, +0.001% each; other impurity corrections were negligible. The net correction made for all impurities (item 8) was $(-0.007 \pm 0.014)\%$ for the niobium

sample and $(0.004 \pm 0.019)\%$ for the tantalum sample. In each case the uncertainty attached to the net impurity correction is relatively large as compared to the actual correction owing to fortuitous partial cancellation of the individual corrections. These uncertainties include a generous allowance for analytical uncertainties and for the possibility that the impurities existed in states of combination other than those assumed.

All other corrections to standard states were neg-

(8) R. H. Busey and W. F. Giaque, *J. Am. Chem. Soc.*, **74**, 3157 (1952).

(9) W. D. Good, D. W. Scott, and G. Waddington, *J. Phys. Chem.*, **60**, 1080 (1956).

(10) R. Hultgren, R. L. Orr, P. D. Anderson, and K. K. Kelley, "Selected Values of Thermodynamic Properties of Metals and Alloys," John Wiley and Sons, Inc., New York, N. Y., 1963, pp. 189, 272.

(11) A. P. Brady, O. E. Myers, and J. K. Clauss, *J. Phys. Chem.*, **64**, 588 (1960).

(12) Estimated.

(13) W. H. Evans, T. R. Munson, and D. D. Wagman, *J. Res. Natl. Bur. Std.*, **55**, 147 (1955).

(14) J. O. Hirschfelder, C. F. Curtiss, and R. B. Bird, "Molecular Theory of Gases and Liquids," John Wiley and Sons, Inc., New York, N. Y., 1954.

(15) D. White, J. H. Hu, and H. L. Johnston, *J. Chem. Phys.*, **21**, 1149 (1953).

(16) H. E. Swanson and E. Tatge, "Standard X-ray Diffraction Powder Patterns," Vol. I, National Bureau of Standards Circular 539, U. S. Government Printing Office, Washington, D. C., 1953, pp. 13, 31.

(17) M. R. Nadler and C. P. Kempter, *Anal. Chem.*, **31**, 1922 (1959).

(18) A. N. Kornilov, V. Ya. Leonidov, and S. M. Skuratov, *Vestn. Mosk. Univ. Ser II: Khim.*, **17**, No. 6, 48 (1962).

(19) E. J. Huber, Jr., E. L. Head, C. E. Holley, Jr., E. K. Storms, and N. H. Krikorian, *J. Phys. Chem.*, **65**, 1846 (1961).

(20) E. J. Huber, Jr., E. L. Head, C. E. Holley, Jr., and A. L. Bowman, *ibid.*, **67**, 793 (1963).

(21) A. N. Kornilov, V. Ya. Leonidov, and S. M. Skuratov, *Dokl. Akad. Nauk SSSR*, **144**, 355 (1962).

(22) E. Veleckis, Ph.D. Thesis, Illinois Institute of Technology, 1960.

(23) A. D. Mah and N. L. Gellert, *J. Am. Chem. Soc.*, **78**, 3261 (1956).

(24) D. W. Scott, W. D. Good, and G. Waddington, *ibid.*, **77**, 245 (1955).

(25) The value of -64.8 kcal. mole⁻¹ for the standard enthalpy of formation of HF(g) has been tentatively adopted by W. H. Evans, National Bureau of Standards, Washington, D. C., for the revised edition of N.B.S. Circular 500 (private communication, 1963).

(26) O. E. Myers and A. P. Brady, *J. Phys. Chem.*, **64**, 591 (1960).

(27) S. S. Wise, J. L. Margrave, H. M. Feder, and W. N. Hubbard, *ibid.*, **67**, 815 (1963).

(28) "Janaf Thermochemical Tables," The Dow Chemical Co., Midland, Mich., Sept. 1963.

(29) L. Brewer, L. A. Bromley, P. L. Gilles, and N. L. Lofgren, "The Chemistry and Metallurgy of Miscellaneous Materials: Thermodynamics," L. L. Quill, Ed., McGraw-Hill Book Co., Inc., New York, N. Y., 1950, pp. 76-192.

(30) E. Rudzitis, H. M. Feder, and W. N. Hubbard, *J. Phys. Chem.*, **68**, 2978 (1964).

(31) "Selected Values of Chemical Thermodynamic Properties," National Bureau of Standards Circular 500, U. S. Government Printing Office, Washington, D. C., 1952.

ligible. $\Delta Ec^\circ/M$ is just the sum of items 3 through 8 divided by the mass of sample reacted.

Derived Data. Table IV presents derived standard thermal data for the formation of niobium and tantalum pentafluorides at 25° as shown by reaction 1. The atomic weights³² of niobium and tantalum were taken as 92.906 and 180.948 g. (g.-atom)⁻¹, respectively. The entropies, S° , at 25°, of Nb(c),¹⁰ Ta(c),¹⁰ NbF₅(c),¹¹ TaF₅(c),³³ and F₂(g)¹³ were taken as 8.70, 9.92, 38.3, 40.6, and 48.45 cal. deg.⁻¹ mole⁻¹, respectively. The uncertainties given are uncertainty intervals³⁴ equal to twice the combined standard deviations arising from known sources.

Table IV: Derived Data at 25°

	NbF ₅ (c)	TaF ₅ (c)
Energy of formation, $\Delta Ef^\circ = \Delta Ec^\circ$, kcal. mole ⁻¹	-432.02 ± 0.15	-453.49 ± 0.19
Enthalpy of formation, ΔHf° , kcal. mole ⁻¹	-433.50 ± 0.15	-454.97 ± 0.19
Entropy of formation, ΔSf° , cal. deg. ⁻¹ mole ⁻¹	-91.5	-90.4
Gibbs energy of formation, $\Delta Gf^\circ = \Delta Hf^\circ - T\Delta Sf^\circ$, kcal. mole ⁻¹	-406.22 ± 0.15	-428.02 ± 0.19

Conclusion

The standard enthalpies of formation of crystalline niobium and tantalum pentafluorides have been deter-

mined to be -433.50 ± 0.15 and -454.97 ± 0.19 kcal. mole⁻¹, respectively, by direct combination of the elements in a combustion bomb calorimeter. The only previous thermochemical study reported is that by Myers and Brady²⁶ for niobium pentafluoride. They carried out three different heat of solution measurements, with each of the thermochemical cycles involving estimation of unknown auxiliary data. Their values were -439 ± 8 , -423 ± 10 , and -435 ± 8 , with the average reported as -432 kcal. mole⁻¹. Considering the uncertainties involved in their work, their value is in surprisingly good agreement with the value reported herein. Glassner³⁵ and Amosov³³ estimated -342 and -370 ± 30 kcal. mole⁻¹, respectively, for NbF₅, and -360 and -380 ± 20 kcal. mole⁻¹, respectively, for TaF₅, while Brewer, *et al.*,²⁹ estimated -300 kcal. mole⁻¹ for TaF₅. These estimates, in common with a number of others for metal fluorides, were very wide of the mark.

Acknowledgment. We wish to thank R. V. Schablaske for the X-ray diffraction analyses required in this work.

(32) A. E. Cameron and E. Wichers, *J. Am. Chem. Soc.*, **84**, 4175 (1962).

(33) V. M. Amosov, *Izv. Vysshikh Uchebn. Zavedenii, Tsvetn. Met.*, **6**, No. 2, 103 (1963).

(34) F. D. Rossini, "Experimental Thermochemistry," F. D. Rossini, Ed., Interscience Publishers, Inc., New York, N. Y., 1956, Chapter 14.

(35) A. Glassner, "The Thermochemical Properties of the Oxides, Fluorides, and Chlorides to 2500°K.," Argonne National Laboratory, ANL-5750 (1957). (Available from the U. S. Government Printing Office, Washington 25, D. C.)

Thermodynamic Properties of *n*-Propyl-, *n*-Butyl-, and *n*-Decyl-Substituted Cyclohexane from 10 to 370°K.

by Herman L. Finke, John F. Messerly, and Samuel S. Todd

Contribution No. 139 from the Thermodynamics Laboratory of the Bartlesville Petroleum Research Center, Bureau of Mines, U. S. Department of the Interior, Bartlesville, Oklahoma (Received January 19, 1965)

Heat capacities from 12 to 370°K., heats of fusion, triple points, and purities of *n*-propylcyclohexane, *n*-butylcyclohexane, and *n*-decylcyclohexane were determined by adiabatic calorimetry, and the data were used to calculate the thermodynamic functions $(G_s - H^{\circ}_0)/T$, $(H_s - H^{\circ}_0)/T$, $H_s - H^{\circ}_0$, S_s , and C_s , for the solid and liquid states at selected temperatures in the range 10 to 370°K. From the Clapeyron equation and Cox equations fitted to vapor pressure data from the literature, the entropies of these compounds in the ideal gas state at 298.15°K. were calculated. The average entropy increments per methylene group between *n*-butyl- and *n*-decylcyclohexane in the liquid and ideal gas states were found to be 7.78 ± 0.03 and 9.35 ± 0.04 cal. deg.⁻¹ mole⁻¹, respectively. These values agree well within experimental error with the constant values for the corresponding higher members of the *n*-alkane series of hydrocarbons and with the average value obtained from *n*-butyl- and *n*-decylcyclopentanes.

Introduction

As a part of the continuing program of the Bureau of Mines to provide thermodynamic data on materials either in or derivable from petroleum, measurements of the heat capacities of the condensed phases, heats of fusion, and triple points of *n*-propyl-, *n*-butyl-, and *n*-decyl-substituted cyclohexane were made. As mentioned in a previous publication¹ from this laboratory, the utilization of the same apparatus and method in all measurements will tend to minimize the effects of systematic errors with the result that greater precision will be obtained for the incremental values of the thermodynamic functions per methylene group than from the results of a number of different investigators.

Measurements of the low-temperature thermodynamic properties of the nine *n*-paraffin hydrocarbons, *n*-octane through *n*-hexadecane, by Finke, *et al.*,² together with like measurements of *n*-pentane,³ *n*-hexane,⁴ *n*-heptane,⁵ *n*-heptadecane,³ and *n*-octadecane,³ have shown that the entropy increment per methylene group for the liquid at 298.15°K. is essentially constant within the precision of the measurements in this laboratory. Person and Pimentel⁶ have shown that the entropy increment per methylene group for the *n*-alkanes,

n-octane through *n*-hexadecane, in the ideal gas state at 298.15°K. is also constant. Unpublished results from this laboratory show that this constancy of the methylene increment also holds from C₅ through C₁₈ in the ideal gas state at 298.15°K. Messerly, *et al.*,¹ have shown that the average entropy increment per methylene group in both the liquid and ideal gas states for *n*-butyl- through *n*-decylcyclopentane is similar to that for the *n*-alkanes within the limits of the precision of the measurements. The measurements reported in this paper were undertaken to determine whether this entropy increment would hold for *n*-propyl-, *n*-butyl-, and *n*-decyl-substituted cyclohexane.

None of the three *n*-alkyl-substituted cyclohexanes

(1) J. F. Messerly, S. S. Todd, and H. L. Finke, *J. Phys. Chem.*, **69**, 353 (1965).

(2) H. L. Finke, M. E. Gross, G. Waddington, and H. M. Huffman, *J. Am. Chem. Soc.*, **76**, 333 (1954).

(3) Unpublished results, this laboratory.

(4) D. R. Douslin and H. M. Huffman, *J. Am. Chem. Soc.*, **68**, 1704 (1946).

(5) J. P. McCullough and J. F. Messerly, U. S. Bureau of Mines Bulletin 596, U. S. Government Printing Office, Washington, D. C., 1961.

(6) W. B. Person and G. C. Pimentel, *J. Am. Chem. Soc.*, **75**, 532 (1953).

reported here have been investigated by any other laboratories, and, as far as the authors are aware, the only other low-temperature thermodynamic studies of longer chain *n*-alkyl-substituted cyclohexane are those by Parks, *et al.*,⁷ on *n*-heptyl- and *n*-dodecylcyclohexane. The latter measurements were made in an apparatus of lower precision on samples whose impurities were at least an order of magnitude greater than those reported here.

Experimental

Materials. The samples used in these investigations were all API Research hydrocarbons.⁸ The materials were checked for dryness by cooling each in its breakoff-tip ampoule, as received, to a temperature just above the melting point and observing the absence or presence of "floaters." As no evidence of water was noted, each sample was transferred *in vacuo* to the calorimeter, in turn, to preserve the purity of the sample. An estimate of the purity of each sample is given in a later section.

Apparatus and Physical Constants. Measurements were made in the low-temperature adiabatic cryostat described by Ruehrwein and Huffman.⁹ The sample (*ca.* 0.5 mole) was sealed in a copper calorimeter equipped with horizontal, perforated heat-distributing disks of copper. A small amount of helium (*ca.* 40 mm. pressure) was left in the calorimeter to promote thermal equilibration at low temperatures. The 1951 International Atomic Weights¹⁰ and values of the fundamental physical constants¹¹ were used. Measurements of the electrical energy supplied to the calorimeter heater and the resistance of the platinum resistance thermometer were made on a White double potentiometer. Measurements of potential were in terms of a bank of six saturated cadmium cells calibrated at the National Bureau of Standards. The electrical stopclock used for time measurements was driven by a constant-frequency ($\pm 0.002\%$) a.c. power source; the estimated uncertainty in time measurements was less than 0.01%. Temperature measurements were made with platinum resistance thermometers calibrated in terms of the International Temperature Scale of 1948¹² from 90 to 400°K. and in terms of the provisional scale of the National Bureau of Standards¹³ from 11 to 90°K. Celsius temperatures were converted to Kelvin temperatures by the addition of 273.15°.¹⁴ Energy was measured in joules and converted to calories by the relation 1 cal. = 4.184 (exactly) joules.

Results

Heat Capacity Measurements. The observed heat capacities at saturation pressure, C_s , of solid and liquid

n-propyl-, *n*-butyl-, and *n*-decyl-substituted cyclohexane are presented in Table I. Under the conditions of the measurements the quantity C_s differs from C_p by less than 0.04% at the highest temperature for the most volatile material, *n*-propylcyclohexane. At all other temperatures the difference between C_s and C_p is barely significant. The temperature increments used in the experiments were small enough that corrections for nonlinear variation of C_s with T were unnecessary (the increments employed were approximately 10% of the absolute temperature below 50°K., 5 to 8° from 50 to 150°K., and 8 to 10° above 150°K.). The precision of the heat capacity measurements was usually better than 0.1%; above 30°K. the accuracy uncertainty of the values of C_s should not exceed 0.2%, except in regions near phase transformations. The values of the heat capacities determined near phase changes may be of lower precision and accuracy because of rapid changes in C_s with T , slow equilibration, or uncertainties caused by the presence of impurities.

Empirical equations were calculated to represent the heat capacity of each compound in the liquid state. The constants for these equations are listed in Table II, together with the values of the deviations from observed data as an estimate of the reliability of the results.

Solid State Phase Transformations. No solid-solid phase transitions were observed in the *n*-alkylcyclohexanes. Two rather interesting phenomena were observed in the *n*-decylcyclohexane measurements. Near 41°K., a small cusp-like irregularity was observed in the heat capacity. This irregularity was observed in two separate series of runs through this region but was quite small and involved only about 0.002 cal. deg.⁻¹ mole⁻¹ of entropy. In neither case were abnormal equilibrations of the compound observed. The second phenomenon was the existence of a nonreproducible area in the heat capacity curve starting about 50°

(7) G. S. Parks, G. E. Moore, M. L. Renquist, B. F. Naylor, L. A. McClaine, P. S. Fujii, and J. A. Hatton, *J. Am. Chem. Soc.*, **71**, 3386 (1949).

(8) These samples of API Research hydrocarbons were made available through the American Petroleum Institute Research Project 44 on the "Collection, Analysis and Calculation of Data on Properties of Hydrocarbons" and were purified by the American Petroleum Institute Research Project 6 on the "Analysis, Purification and Properties of Hydrocarbons."

(9) R. A. Ruehrwein and H. M. Huffman, *J. Am. Chem. Soc.*, **65**, 1620 (1943).

(10) E. Wichers, *ibid.*, **74**, 2447 (1952).

(11) F. D. Rossini, F. T. Gucker, Jr., H. L. Johnston, L. Pauling, and G. W. Vinal, *ibid.*, **74**, 269c (1952).

(12) H. F. Stimson, *J. Res. Natl. Bur. Std.*, **42**, 209 (1949).

(13) H. J. Hoge and F. G. Brickwedde, *ibid.*, **22**, 351 (1939).

(14) H. F. Stimson, *Am. J. Phys.*, **23**, 614 (1955).

Table I: Heat Capacity

C_s , cal. mole ⁻¹ °K. ^{-1b}		C_s , cal. mole ⁻¹ °K. ^{-1b}		C_s , cal. mole ⁻¹ °K. ^{-1b}		C_s , cal. mole ⁻¹ °K. ^{-1b}		C_s , cal. mole ⁻¹ °K. ^{-1b}		C_s , cal. mole ⁻¹ °K. ^{-1b}	
T , °K. ^a		T , °K. ^a		T , °K. ^a		T , °K. ^a		T , °K. ^a		T , °K. ^a	
<i>n</i> -Propylcyclohexane						<i>n</i> -Decylcyclohexane					
Crystal						Crystal					
11.36	0.835	28.21	5.930	103.34	21.419	11.54	1.288	73.88	28.634	235.11 ^e	68.662
12.56	1.127	31.23	6.896	107.77	22.118	12.11	1.477	79.00	30.332	235.47 ^f	68.822
13.35	1.332	34.66	7.919	108.64	22.246	12.76	1.726	79.95	30.652	236.64 ^g	69.157
13.84	1.468	40.57	9.529	113.75	23.042	13.56	2.011	85.39	32.413	239.03 ^h	69.792
14.46	1.629	44.74	10.580	119.16	23.894	14.22	2.287	92.15	34.359	239.55 ⁱ	69.906
15.13	1.829	49.45	11.682	124.87	24.785	15.11	2.649	98.07	35.970	242.45 ^e	70.711
15.73	1.994	54.57	12.763	130.39	25.648	16.01	3.019	99.29	36.264	242.67 ^f	70.345
16.59	2.252	55.67	13.038	136.17	26.558	16.99	3.455	105.09	37.808	243.09 ^k	70.949
17.20	2.427	59.61	13.841	142.19	27.534	18.07	3.936	106.92	38.273	243.22 ^l	70.939
18.40	2.818	60.21	13.972	142.84	27.669	19.31	4.529	112.11	39.610	244.72 ^o	71.538
18.75	2.924	65.12	14.958	147.66	28.505	20.31	5.008	115.34	40.390	246.06 ^m	71.894
20.44	3.491	70.30	15.892	148.03	28.527	22.01	5.860	124.03	42.496	246.09 ⁿ	71.997
20.57	3.521	75.39	16.799	148.49	28.649	22.78	6.268	132.32	44.432	246.65 ^j	72.069
22.75	4.238	80.62	17.751	154.27	29.699 ^c	23.21	6.469	140.27	46.250	247.38 ^e	72.353
22.84	4.266	86.00	18.709	160.66	30.936 ^c	24.96	7.368	148.45	48.082	248.52 ^k	72.673
25.36	5.080	91.49	19.600	165.83	31.987 ^c	25.83	7.812	156.88	49.941	248.65 ^l	72.549
25.44	5.105	97.14	20.479	166.83	32.247 ^c	25.91	7.848	163.85	51.505	249.41 ^m	73.262
28.15	5.956	102.53	21.312			28.13	9.014	165.03	51.753	250.00 ^j	73.484
Liquid						Liquid					
185.51	46.473	236.47	50.809	302.40	58.394	28.74	9.304	171.75	53.250	252.18 ^e	74.971
188.07	46.669	246.28	51.811	311.78	59.601	29.39	9.686	172.93	53.509	252.57 ^o	74.548
192.89	47.009	255.92	52.858	321.76	60.887	31.44	10.765	179.89	55.042	252.70 ^m	75.028
197.79	47.374	265.81	53.963	332.30	62.283	32.89	11.544	180.60	55.212	252.73 ^k	74.150
202.61	47.757	275.94	55.148	342.63	63.649	34.90	12.639	188.52	57.019	252.78 ^l	73.825
207.36	48.133	285.87	56.340	352.78	65.042	35.63	13.031	196.68	58.909	252.95 ^h	74.733
216.76	48.942	295.28	57.494	362.74	66.362	37.83	14.208	204.61	60.819	253.28 ^j	75.141
226.47	49.836	295.62	57.546	373.20	67.724	38.64	14.668	208.21	61.687	255.96 ^m	74.955
<i>n</i> -Butylcyclohexane						<i>n</i> -Decylcyclohexane					
Crystal						Crystal					
11.57	0.922	29.42	6.726	101.62	23.578	39.81	15.344	209.86	62.033	256.12 ^k	74.671
11.60	0.941	32.43	7.739	107.68	24.611	41.64	16.423	212.75	62.833	256.26 ^j	75.121
12.80	1.249	35.85	8.835	113.72	25.620	42.87	16.800	214.79	63.267	257.32 ^l	74.837
12.80	1.252	39.63	9.992	120.23	26.683	43.51	17.084	216.05	63.587	257.37 ^e	75.926
14.11	1.614	43.65	11.162	126.97	27.779	45.77	17.817	216.53	63.752	259.20 ^m	76.055
14.21	1.651	47.85	12.319	133.91	28.862	47.71	18.633	217.05	63.896	259.22 ^j	76.179
15.54	2.047	52.39	13.486	141.07	29.972	49.29	19.309	221.08	64.934	259.35 ^k	75.714
15.81	2.119	55.88	14.361	147.93	31.015	49.29	19.309	223.05	65.425	259.64 ^h	76.577
17.12	2.541	57.35	14.703	148.05	31.062	52.48	20.610	224.99	65.920	260.18 ^g	76.835
17.65	2.707	60.52	15.464	154.88	32.138	53.08	20.889	225.63	66.132	262.39 ^m	77.547
18.78	3.081	65.54	16.621	155.85	32.276	54.30	21.369	226.19 ^f	66.256	262.41 ^j	77.697
19.69	3.390	70.80	17.727	158.00	32.624	56.23	22.149	227.63 ⁱ	66.447	262.47 ^e	78.265
20.46	3.661	75.97	18.780	161.51	33.168	59.94	23.631	229.38 ^o	67.092	262.50 ^l	76.902
21.87	4.148	81.27	19.880	163.50	33.473	62.01	24.395	231.25 ^h	67.521	262.82 ^k	77.057
22.26	4.288	86.71	20.990	164.03	33.567	66.06	25.949	233.40 ⁱ	68.140	265.51 ^m	80.438
24.17	4.942	90.26	21.620	170.43	34.583 ^d	67.89	26.599	234.60 ^l	68.528	265.53 ^j	80.191
24.39	5.023	91.87	21.915	176.68	35.602 ^d	72.51	28.164	234.98 ^k	68.641	265.65 ^h	81.481
26.70	5.811	95.67	22.552	182.77	36.795 ^d						
28.27	6.334										
Liquid						Liquid					
207.52	54.375	249.95	58.657	305.97	65.862	274.26	104.028	283.33	105.479	293.33	107.234
209.98	54.570	260.05	59.837	315.81	67.247	278.44	104.678	286.10	105.964	296.47	107.792
214.21	54.979	270.40	61.105	325.86	68.679	280.27	105.004	289.38	106.516	300.48	108.514
219.87	55.482	280.56	62.402	335.73	70.077						
221.77	55.663	286.74	63.227	345.43	71.475						
230.07	56.491	290.54	63.727	355.31	72.924						
240.10	57.560	296.36	64.528	365.38	74.392						

^a T is the mean temperature of each heat capacity measurement. ^b C_s is the heat capacity of the condensed phase at saturation pressure. Values of C_s for crystals are *not* corrected for premelting caused by impurities. ^{c,d} The temperature increments of these measurements are in order of increasing T , °K.: (c) 6.498, 6.281, 5.079, 6.070; (d) 6.326, 6.173, 6.007. ^{e-m} Denote separate series of measurements.

Table II: Equations for Heat Capacity of Liquid

$$C_p = A + BT + CT^2 + DT^3, \text{ cal. deg.}^{-1} \text{ mole}^{-1}$$

Compd.	A	B	C × 10 ⁴	D × 10 ⁷	Range, °K.	Av. dev., cal.	Max. dev., cal.
<i>n</i> -Propylcyclohexane	51.742	-0.14864	7.8247	-7.2145	185-375	0.01	0.03
<i>n</i> -Butylcyclohexane	67.440	-0.25653	11.698	-11.376	207-365	0.01	0.04
<i>n</i> -Decylcyclohexane	97.940	-0.1150	5.000	...	274-300	0.01	0.02

below the melting point. Numerous runs in which various crystallization and cooling rates were used were made through this region. No correlation could be found between the deviations and either the history of cooling or mode of heating. From 230 to 270°K. thermal equilibration was extremely slow, necessitating abnormally large corrections. As these abnormalities in behavior were primarily in the pre-melting region, it is felt that they are the result of impurities. Efforts were made to promote any transition that may have been supercooled, but with no success. The results reported in Table I are uncorrected for any effect of premelting caused by impurities. (Table V lists values at selected temperatures determined from the best smooth curve drawn through all the data from Table I after appropriate corrections for premelting have been made.)

Heats of Fusion, Triple Point Temperatures, and Purity of Samples. The heats of fusion, ΔH_m , were determined from the heat capacity data and enthalpy measurements made over finite temperature intervals that included the triple point temperature. The average of two or more measurements for each compound is listed in Table III.

Table III: Triple Point Temperatures, Heats of Fusion, and Cryoscopic Constants

Compd.	T_{tp} , °K.	ΔH_m , cal. mole ⁻¹	A, deg. ⁻¹	B, deg. ⁻¹
<i>n</i> -Propylcyclohexane	178.25	2479 ± 1 ^a	0.03926	0.00323
<i>n</i> -Butylcyclohexane	198.42	3384 ± 2 ^a	0.04324	0.00287
<i>n</i> -Decylcyclohexane	271.43	9225 ± 6 ^a	0.06350	0.00238

^a Maximum deviation from mean.

The triple point temperature and sample purity for each compound were determined from studies of the equilibrium melting temperature as a function of the fraction of sample melted.¹⁵ The resulting melting point summaries are given for the three compounds in Table IV. In all cases the equilibrium temperatures, T_F , were plotted as functions of $1/F$, the reciprocal of the fraction of the total sample in the liquid

state. The triple point temperatures, T_{tp} , were determined by linear extrapolations to the zero value of $1/F$. If the impurities form ideal solutions in the liquid phase and are insoluble in the solid phase, the relation between mole fraction of total impurity, N_2^* , and melting point depression, $\Delta T = T_{tp} - T_F$, is¹⁶

$$-\ln(1 - N_2) = A\Delta T(1 + B\Delta T + \dots) \quad (1)$$

where $N_2 = N_2^*/F$. The cryoscopic constants, $A = \Delta H_m/RT_{tp}^2$ and $B = 1/T_{tp} - \Delta C_m/2\Delta H_m$, were

Table IV: Melting Point Summaries

F	1/F	T_F , °K.	$T_{calcd.}$, °K.
<i>n</i> -Propylcyclohexane (impurity = 0.04 mole %)			
0.0981	10.196	178.1861	178.1386
0.2646	3.779	178.2140	178.2064
0.5030	1.988	178.2263	178.2253
0.6937	1.442	178.2311 ^a	178.2311
0.9083	1.101	178.2347 ^a	178.2347
1.0000	1.000		178.2358
Pure	0		178.2463
<i>n</i> -Butylcyclohexane (impurity = 0.03 mole %)			
0.1031	9.699	198.3776	198.3557
0.2538	3.940	198.3989	198.3932
0.5107	1.958	198.4067	198.4061
0.7070	1.414	198.4096 ^a	198.4096
0.9032	1.107	198.4116 ^a	198.4116
1.0000	1.000		198.4123
Pure	0		198.4188
<i>n</i> -Decylcyclohexane (impurity = 0.09 mole %)			
0.0929	10.76	271.2967	271.2752
0.2355	4.246	271.3726	271.3698
0.4809	2.079	271.4014 ^a	271.4014
0.6957	1.437	271.4110	271.4107
0.9001	1.1110	271.4155 ^a	271.4155
1.0000	1.0000		271.4171
Pure	0		271.4316

^a Straight line through these points extrapolated to $1/F = 0$ to calculate triple point temperature.

(15) J. P. McCullough and G. Waddington, *Anal. chim. Acta*, **17**, 80 (1957).

(16) A. R. Glasgow, Jr., A. J. Streiff, and F. D. Rossini, *J. Res. Natl. Bur. Std.*, **35**, 355 (1945).

Table V: Thermodynamic Functions for Condensed Phases^a

T, °K.	$-(G_s - H^\circ_s)/T,$	$(H_s - H^\circ_s)/T,$	$H_s - H^\circ_s,$	$S_s,$	$C_s,$	T, °K.	$-(G_s - H^\circ_s)/T,$	$(H_s - H^\circ_s)/T,$	$H_s - H^\circ_s,$	$S_s,$	$C_s,$
	cal. mole ⁻¹ °K. ⁻¹	cal. mole ⁻¹ °K. ⁻¹		cal. mole ⁻¹ °K. ⁻¹	cal. mole ⁻¹ °K. ⁻¹		cal. mole ⁻¹ °K. ⁻¹	cal. mole ⁻¹ °K. ⁻¹		cal. mole ⁻¹ °K. ⁻¹	cal. mole ⁻¹ °K. ⁻¹
<i>n</i> -Propylcyclohexane						<i>n</i> -Butylcyclohexane					
Crystal						Crystal					
10	0.048	0.146	1.457	0.194	0.579	10	0.052	0.156	1.562	0.208	0.620
15	0.162	0.471	7.069	0.633	1.780	15	0.172	0.498	7.466	0.670	1.876
20	0.365	0.986	19.726	1.351	3.333	20	0.386	1.039	20.779	1.425	3.497
25	0.651	1.620	40.49	2.271	4.961	25	0.687	1.704	42.59	2.391	5.221
30	1.007	2.308	69.24	3.315	6.519	30	1.062	2.431	72.94	3.493	6.913
35	1.415	3.017	105.58	4.432	8.013	35	1.493	3.190	111.66	4.683	8.550
40	1.865	3.728	149.10	5.593	9.378	40	1.970	3.957	158.29	5.927	10.087
45	2.344	4.427	199.20	6.771	10.642	45	2.480	4.720	212.41	7.200	11.526
50	2.846	5.107	255.33	7.953	11.802	50	3.015	5.469	273.44	8.484	12.864
60	3.893	6.403	384.1	10.296	13.929	60	4.142	6.912	414.7	11.054	15.336
70	4.973	7.619	533.3	12.592	15.838	70	5.310	8.279	579.5	13.589	17.553
80	6.065	8.758	700.6	14.823	17.640	80	6.501	9.566	765.2	16.067	19.601
90	7.160	9.843	885.8	17.003	19.362	90	7.699	10.795	971.5	18.494	21.584
100	8.250	10.873	1,087.3	19.123	20.920	100	8.897	11.959	1,195.9	20.856	23.278
110	9.333	11.856	1,304.1	21.189	22.460	110	10.089	13.066	1,437.2	23.155	24.995
120	10.405	12.805	1,536.5	23.210	24.021	120	11.272	14.129	1,695.5	25.401	26.647
130	11.467	13.728	1,784.6	25.195	25.591	130	12.444	15.154	1,970.0	27.598	28.241
140	12.518	14.631	2,048.3	27.149	27.173	140	13.604	16.145	2,260.3	29.749	29.805
150	13.558	15.524	2,328.6	29.082	28.898	150	14.74	17.107	2,566.1	31.85	31.34
160	14.588	16.416	2,626.5	31.004	30.716	160	15.88	18.047	2,887.4	33.93	32.92
170	15.610	17.313	2,943.2	32.923	32.617	170	17.00	18.968	3,224	35.97	34.48
178.25	16.450	18.058	3,219.1	34.508	34.200	180	18.11	19.873	3,577	37.98	36.06
						190	19.21	20.767	3,945	39.98	37.63
						198.42	20.13	21.511	4,268	41.64	38.94
Liquid						Liquid					
178.25	16.450	31.965	5,698.1	48.415	45.983	198.42	20.13	38.56	7,652	58.69	53.60
180	16.76	32.10	5,778	48.86	46.10	200	20.43	38.68	7,736	59.11	53.73
190	18.52	32.85	6,242	51.37	46.79	210	22.34	39.42	8,278	61.76	54.58
200	20.22	33.57	6,714	53.79	47.54	220	24.19	40.13	8,828	64.32	55.49
210	21.88	34.25	7,193	56.13	48.36	230	25.99	40.81	9,388	66.80	56.47
220	23.49	34.91	7,681	58.40	49.23	240	27.74	41.49	9,958	69.23	57.54
230	25.05	35.56	8,178	60.61	50.17	250	29.45	42.16	10,539	71.61	58.66
240	26.57	36.19	8,685	62.76	51.16	260	31.11	42.81	11,131	73.92	59.82
250	28.06	36.81	9,202	64.87	52.21	270	32.74	43.47	11,735	76.21	61.04
260	29.52	37.42	9,729	66.94	53.31	273.15	33.25	43.67	11,929	76.92	61.45
270	30.94	38.03	10,268	68.97	54.45	280	34.34	44.11	12,352	78.45	62.34
273.15	31.39	38.22	10,441	69.61	54.82	290	35.90	44.76	12,982	80.66	63.66
280	32.34	38.64	10,819	70.98	55.63	298.15	37.15	45.30	13,506	82.45	64.78
290	33.71	39.24	11,381	72.95	56.84	300	37.42	45.42	13,626	82.84	65.03
298.15	34.80	39.74	11,849	74.54	57.85	310	38.93	46.07	14,283	85.00	66.42
300	35.05	39.85	11,956	74.90	58.08	320	40.40	46.73	14,954	87.13	67.83
310	36.36	40.46	12,543	76.82	59.36	330	41.85	47.39	15,640	89.24	69.25
320	37.66	41.07	13,143	78.73	60.65	340	43.27	48.06	16,340	91.33	70.69
330	38.93	41.68	13,756	80.61	61.98	350	44.67	48.73	17,054	93.40	72.14
340	40.18	42.30	14,383	82.48	63.31	360	46.05	49.40	17,783	95.45	73.59
350	41.42	42.92	15,022	84.34	64.64	370	47.41	50.07	18,526	97.48	75.06
360	42.64	43.54	15,676	86.18	65.98						
370	43.84	44.16	16,342	88.00	67.31						
380	45.03	44.79	17,022	89.82	68.64						

Table V (Continued)

$T, ^\circ\text{K.}$	$-(G_s - H^\circ_s)/T,$ cal. mole ⁻¹ °K. ⁻¹	$(H_s - H^\circ_s)/T,$ cal. mole ⁻¹ °K. ⁻¹	$H_s - H^\circ_s,$ cal. mole ⁻¹	$S_s,$ cal. mole ⁻¹ °K. ⁻¹	$C_s,$ cal. mole ⁻¹ °K. ⁻¹
<i>n</i> -Decylcyclohexane					
Crystal					
10	0.072	0.215	2.149	0.287	0.854
15	0.240	0.694	10.417	0.934	2.580
20	0.536	1.442	28.834	1.978	4.840
25	0.956	2.374	59.36	3.330	7.385
30	1.480	3.425	102.75	4.905	10.010
35	2.092	4.558	159.54	6.650	12.690
40	2.777	5.744	229.75	8.521	15.445
45	3.525	6.953	312.9	10.478	17.533
50	4.318	8.112	405.6	12.430	19.615
60	5.997	10.368	622.1	16.365	23.650
70	7.760	12.535	877.5	20.295	27.320
80	9.568	14.594	1,167.5	24.162	30.67
90	11.403	16.557	1,490.2	27.960	33.77
100	13.24	18.415	1,841.5	31.66	36.46
110	15.09	20.174	2,219.2	35.26	39.05
120	16.91	21.851	2,622.1	38.76	41.52
130	18.72	23.456	3,049.2	42.18	43.90
140	20.52	24.998	3,500	45.52	46.18
150	22.30	26.485	3,973	48.78	48.41
160	24.05	27.925	4,468	51.97	50.64
170	25.78	29.327	4,986	55.11	52.86
180	27.49	30.70	5,525	58.19	55.08
190	29.19	32.04	6,087	61.23	57.34
200	30.87	33.36	6,672	64.23	59.68
210	32.53	34.67	7,281	67.20	62.06
220	34.18	35.97	7,914	70.15	64.56
230	35.80	37.27	8,573	73.07	67.19
240	37.41	38.58	9,258	75.99	69.91
250	39.02	39.89	9,973	78.91	73.34
260	40.61	41.24	10,722	81.85	75.80
270	42.19	42.57	11,495	84.76	79.03
271.43	42.42	42.77	11,609	85.19	79.54
Liquid					
271.43	42.42	76.75	20,834	119.17	103.61
273.15	42.90	76.92	21,012	119.82	103.86
280	44.82	77.59	21,726	122.41	104.93
290	47.56	78.56	22,784	126.12	106.63
298.15	49.75	79.35	23,660	129.10	108.09
300	50.23	79.53	23,859	129.76	108.42
310	52.86	80.49	24,953	133.35	110.23

^a The values tabulated are the Gibbs energy function, enthalpy function, enthalpy, entropy, and heat capacity of the condensed phases at saturation pressure.

calculated from the values of ΔH_m and \bar{T}_{tp} in Table V and values of ΔC_m , the difference between the heat capacities of the compound in the solid and liquid states at the triple point, obtained from data in Table V (discussed in the following section). Values of A and B are included in Table III. Impurity values given in Table IV were calculated using eq. 1 in its simplified form (for $N_2^* \ll 1$), $N_2^* = A_F \Delta T$.

The impurity values reported for the three *n*-alkyl-substituted cyclohexanes as supplied by the American Petroleum Institute Research Project 44 were: *n*-propyl-, 0.06 mole %; *n*-butyl-, 0.04 mole %; *n*-decyl-, 0.12 mole %. These values are to be compared with those found in these studies and given in Table IV, viz., 0.04, 0.03, and 0.09, respectively.

Chemical Thermodynamic Properties in the Solid and Liquid States. The low temperature data for *n*-propylcyclohexane, *n*-butylcyclohexane, and *n*-decylcyclohexane were used in calculating values of the Gibbs energy function, enthalpy function, enthalpy, entropy, and heat capacity for the compounds in the solid and liquid states at selected temperatures from 10 to 370°K. The values at 10°K. were calculated from Debye functions, the parameters of which were evaluated from the heat capacity data between 11 and 20°K.¹⁷ Thermodynamic properties above 10°K. were calculated from values of heat and temperature of phase changes and from appropriate integration of smoothed values of C_s at regular intervals. The results are in Table V. Corrections for the effects of premelting were applied as necessary in computing the "smoothed" data in Table V.

Vapor Pressures and Calculation of Heats and Entropies of Vaporization. In order to calculate the entropy and enthalpy of the compounds in the ideal gas state at 298.15°K., values of the heat of vaporization and vapor pressure were required for each compound. For *n*-propylcyclohexane the value of Osborne and Ginnings¹⁸ was used. For the other two compounds studied, experimentally determined heats of vaporization were not available. To obtain more reliable heats of vaporization, Cox equations were fitted to the experimentally determined vapor pressures from the literature. Unpublished results from this laboratory have shown that the Cox equation can be fitted to the experimental data and extrapolated with more precision than the Antoine equation as

(17) The number of degrees of freedom used and the characteristic Debye temperature, respectively, were determined for the following compounds: *n*-propylcyclohexane, 6.0 and 116.7°; *n*-butylcyclohexane, 6.0 and 114.0°; and *n*-decylcyclohexane, 8.5 and 115.1°.

(18) N. S. Osborne and D. C. Ginnings, *J. Res. Natl. Bur. Std.*, 39, 468 (1947).

Table VI: Vapor Pressure Expressed by the Cox Equation^a

Compd.	B, °K.	a	b × 10 ²	c × 10 ⁵	Dev. from obsd. data, mm.		Range, mm.
					Av.	Max.	
<i>n</i> -Propylcyclohexane	429.874	0.870924	-0.741755	0.661792	0.03	0.09	48-780
<i>n</i> -Butylcyclohexane	454.097	0.891970	-0.757619	0.644674	0.02	0.05	48-780
<i>n</i> -Decylcyclohexane	570.715	0.976863	-0.748865	0.498379	0.10	0.58	52-759

^a Log $p(\text{mm.}) = A(1 - B/T)$ where B is n.b.p. in °K. and A is defined by $\log A = a + bT + cT^2$; T in °K.

used by Rossini and co-workers.¹⁹ From the Clapeyron equation and the value of dp/dT determined from the Cox equation fitted to the data of Rossini and co-workers,¹⁹ the heats and entropies of vaporization were calculated. Corrections for effects of gas imperfection were negligible and omitted. The constants for the Cox equation and maximum and average deviations from the experimentally observed data are given for the three compounds in Table VI. The heats of vaporization at 298.15°K. calculated for the compounds, together with the experimentally determined value of Osborne and Ginnings,¹⁸ are given in Table VII.

Table VII: Heats and Entropies of Vaporization at 298.15°K.

Compd.	Calcd.		Lit. ΔH_{vap} , cal. mole ⁻¹
	ΔH_{vap} , cal. mole ⁻¹	ΔS_{vap} , cal. mole ⁻¹ °K. ⁻¹	
<i>n</i> -Propylcyclohexane	10,790	36.19	10,776 ¹⁷
<i>n</i> -Butylcyclohexane	11,957	40.10	
<i>n</i> -Decylcyclohexane	18,825	63.14	

Discussion

The entropies in the ideal gas state for the three compounds studied were obtained from the values of the entropy in the liquid state as listed in Table V, together with the entropy of vaporization listed in Table VII and the entropy of compression calculated from the vapor pressures listed in Table VI. The resulting entropy values obtained are presented in Table VIII, together with the entropy values for the liquid and the average entropy increment per methylene group, $\Delta S/\text{CH}_2$.

The entropy increment for the liquid state at

298.15°K. between *n*-propyl- and *n*-butylcyclohexane, 7.91 cal. deg.⁻¹ mole⁻¹, is slightly greater than the average increment calculated between *n*-butyl- and *n*-decylcyclohexane, 7.78 cal. deg.⁻¹ mole⁻¹. The latter value is in very good agreement with the values of

Table VIII: Entropies at 298.15°K. (cal. mole⁻¹ °K.⁻¹)

Compd.	Liquid		Ideal gas	
	S°	$\Delta S/\text{CH}_2$	S°	$\Delta S/\text{CH}_2$
<i>n</i> -Propylcyclohexane	74.54		100.35	
		7.91		9.54
<i>n</i> -Butylcyclohexane	82.45		109.89	
		7.78		9.35
<i>n</i> -Decylcyclohexane	129.10		165.97	

7.74 and 7.76 cal. deg.⁻¹ mole⁻¹ found for the liquid normal paraffins from C₅ through C₁₈ and liquid *n*-alkylcyclopentanes,¹ respectively. For the ideal gas state the methylene increment between *n*-butyl- and *n*-decylcyclopentane was found to be 9.35 cal. deg.⁻¹ mole⁻¹, again in close agreement with the values of 9.31 and 9.33 cal. deg.⁻¹ mole⁻¹ found for the *n*-paraffin hydrocarbons from C₈ through C₁₆ by Person and Pimentel⁶ and the *n*-alkylcyclopentanes.¹ For the *n*-alkylcyclohexanes lower than *n*-butyl, the entropy differences per methylene group for both the liquid and ideal gas states at 298.15°K. are irregular.

Acknowledgments. The assistance of Dr. J. P. McCullough, Mrs. M. E. Gross, and Mrs. T. C. Kincheloe with part of the measurements and calculations is gratefully acknowledged.

(19) (a) *n*-Propylcyclohexane and *n*-butylcyclohexane: A. F. Forziati, W. R. Norris, and F. D. Rossini, *J. Res. Natl. Bur. Std.* **43**, 555 (1949); (b) *n*-decylcyclohexane: D. L. Camin, A. F. Forziati, and F. D. Rossini, *J. Phys. Chem.*, **58**, 440 (1954).

Pure Quadrupole Resonance of Halogens in Potassium

Hexahalorhenates(IV) and Hexachlorotungstate(IV)¹

by Ryuichi Ikeda, Daiyu Nakamura, and Masaji Kubo

Department of Chemistry, Nagoya University, Chikusa, Nagoya, Japan (Received January 25, 1965)

The pure quadrupole resonance of halogens in potassium hexahalorhenates(IV) and hexachlorotungstate(IV) was observed at various temperatures. The hexachloro- and hexabromorhenates(IV) showed a single resonance line at room temperature in agreement with the potassium hexachloroplatinate(IV) structure of these complexes. At lower temperatures, they gave rise to multiplet resonance lines, indicating that the symmetry of the crystals is lower than cubic symmetry. Potassium hexaiodorhenate(IV) yielded a triplet structure of resonance lines at all temperatures between room and liquid nitrogen temperatures. For potassium hexachlorotungstate(IV), a single line was observed only at room temperature. The unusual positive temperature coefficient of resonance frequencies observed for the cubic crystals can be explained in terms of the partial $d\pi$ - $p\pi$ -bond character of metal-ligand bonds.

Introduction

We already have observed the pure quadrupole resonance of chlorine in potassium hexachloroiridate(IV) and hexachloroosmate(IV) and pointed out the importance of π -bond character in discussing the nature of metal-ligand bonds in these complexes.² It was shown that the ionic character of metal-halogen bonds $M-X$ in potassium hexahaloplatinates(IV), hexahalopalladates(IV), hexachloroiridate(IV), and hexachloroosmate(IV) is in linear relation to the difference, $\chi_X - \chi_M$, between the electronegativities of atoms involved in the bonds and that the net charge on the central metal ion is a positive fraction of the electronic charge throughout this series of complexes. On the other hand, if the π -bond character is disregarded, the data on iridium and osmium complexes deviate from the linear relation to a considerable extent, and the net charges on the iridium and osmium ions are increased in contradiction to Pauling's electroneutrality principle.

Whereas iridium(IV) and osmium(IV) ions have one and two electronic vacancies, respectively, in their d orbitals, rhenium(IV) and tungsten(IV) ions have three and four holes, respectively. Accordingly, it is expected that the effect of partial π -bond character of metal-ligand bonds in rhenium and tungsten complexes

is more marked than in other complexes. The present investigation of potassium hexahalorhenates(IV) and hexachlorotungstate(IV) has been undertaken in order to examine the nature of metal-ligand bonds in these paramagnetic complexes.

Experimental

Apparatus. A Deaer-type, self-quenching, super-regenerative spectrometer already described³ was used for the observation of quadrupole resonance frequencies of chlorine isotopes. For detecting the resonance absorptions of bromine and iodine isotopes, a self-quenching, super-regenerative spectrometer³ equipped with Lecher lines was employed. Resonance frequencies were determined at room, Dry Ice, and liquid nitrogen temperatures. Since the data for potassium hexabromorhenate(IV) at these temperatures suggested the existence of transition points, measurements were performed also between Dry Ice temperature and room temperature. For potassium hexaiodorhenate(IV), frequency determination was extended up to 200° in

(1) Presented before the 8th International Conference on Coordination Chemistry held in Vienna on Sept. 7-11, 1964.

(2) K. Ito, D. Nakamura, K. Ito, and M. Kubo, *Inorg. Chem.*, **2**, 690 (1963).

(3) D. Nakamura, Y. Kurita, K. Ito, and M. Kubo, *J. Am. Chem. Soc.*, **82**, 5783 (1960).

order to locate a possible transition to a cubic structure. The unusual positive temperature coefficients of resonance frequencies of potassium hexachlororhenate(IV), hexabromorhenate(IV), and hexachlorotungstate(IV) were checked by extending measurements up to 30, 180, and 35°, respectively.

Materials. Potassium hexachlororhenate(IV) and hexabromorhenate(IV) were prepared by reducing potassium perrhenate(VII) dissolved in concentrated hydrochloric acid and hydrobromic acid, respectively, with hypophosphorous acid.^{4,5} *Anal.* Calcd. for K_2ReCl_6 : Cl, 44.6. Found: Cl, 44.3. Calcd. for K_2ReBr_6 : Br, 64.4. Found: Br, 64.3. Potassium hexaiodorhenate(IV) was synthesized in a similar manner using potassium iodide in place of hypophosphorous acid as a reducing agent.⁶ *Anal.* Calcd. for K_2ReI_6 : I, 74.2. Found: I, 74.1. For the preparation of potassium hexachlorotungstate(IV), a mixture of excess tungsten(VI) hexachloride and finely pulverized dry potassium iodide was heated in a sealed glass tube in the absence of air for several days at 130°. The excess of tungsten(VI) hexachloride as well as iodine formed during the reaction was removed under high vacuum. *Anal.* Calcd. for K_2WCl_6 : Cl, 44.9. Found: Cl, 43.8. The X-ray powder patterns of this sample indicated that the complex formed crystals of the potassium hexachloroplatinate(IV) structure with its lattice constant $a = 9.89 \text{ \AA}$. in agreement with data found in the literature⁷ within experimental errors.

Results

The resonance frequencies of chlorine isotopes, ^{35}Cl and ^{37}Cl , were observed for potassium hexachlororhenate(IV) and hexachlorotungstate(IV) and yielded the isotope frequency ratio equal to 1.270, in good agreement with the known value. Similarly, potassium hexabromorhenate(IV) gave both ^{79}Br and ^{81}Br resonance lines at room temperature, the isotope frequency ratio being 1.197, in agreement with data found in the literature. At low temperatures, the intensity of the ^{81}Br resonance line was weak and escaped detection, partly because the sensitivity of available spectrometers was low in this wave length range. For potassium hexaiodorhenate(IV), three pairs of lines showing a frequency ratio approximately equal to 1:2 were observed. Although ^{185}Re and ^{187}Re also have a nuclear spin equal to $5/2$, the observed signals can be attributed unequivocally to ^{127}I . This is because the quadrupole coupling constant eQq of ^{187}Re in ReO_3F is reported⁸ to be equal to 48.4 Mc./sec., corresponding to $\nu_2 = 14.5$ Mc./sec. A rhenium nucleus in potassium hexaiodorhenate(IV) located at the center of a complex anion essentially having an O_h symmetry must experience a

field gradient much smaller than that at a rhenium nucleus in ReO_3F . Accordingly, ν_2 is expected to appear at a frequency much lower than 14.5 Mc./sec. in contradiction to the observed values. The resonance frequencies of ^{35}Cl , ^{79}Br , and ^{127}I observed at various temperatures are listed in Table I.

Table I: Pure Quadrupole Resonance Frequencies of ^{35}Cl , ^{79}Br , and ^{127}I in Potassium Hexahalorhenates(IV) and Hexachlorotungstate(IV)

Compound	Temp., °C.	Freq., Mc./sec.	Multiplet component	
K_2ReCl_6	23.0	13.887 ± 0.001		
	-76	13.875 ± 0.001		
K_2ReBr_6	Liquid N ₂	13.986 ± 0.005		
		13.966 ± 0.005		
	18.0	112.70 ± 0.05		
	-78	114.23 ± 0.08		
		115.04 ± 0.08		
	K_2ReI_6	Liquid N ₂	115.09 ± 0.05	
115.86 ± 0.05				
ν_1		21.0	116.06 ± 0.05	
			121.91 ± 0.05	I
		-77	122.99 ± 0.05	II
			123.13 ± 0.05	III
			122.52 ± 0.05	I
			123.43 ± 0.05	II
			123.89 ± 0.05	III
			122.92 ± 0.05	I
		Liquid N ₂	123.73 ± 0.05	II
			124.58 ± 0.05	III
ν_2	20.6	243.68 ± 0.07	I	
		245.16 ± 0.07	II	
	-76	245.34 ± 0.07	III	
		244.84 ± 0.07	I	
		245.98 ± 0.07	II	
		246.49 ± 0.07	III	
		245.52 ± 0.07	I	
		246.55 ± 0.07	II	
	Liquid N ₂	247.45 ± 0.07	III	
	K_2WCl_6	22.5	10.22 ± 0.01	

A single resonance line was observed for each isotope of chlorine in potassium hexachlororhenate(IV) at room and Dry Ice temperatures, indicating that all chlorine atoms are crystallographically equivalent, in agreement with the results of X-ray crystal analysis that this compound crystallizes in the potassium hexa-

(4) G. W. Watt and R. J. Thompson, *Inorg. Syn.*, **7**, 189 (1963).

(5) C. L. Rulfs and R. J. Meyer, *J. Am. Chem. Soc.*, **77**, 4505 (1955).

(6) H. V. A. Briscoe, P. L. Robinson, and A. J. Rudge, *J. Chem. Soc.* 3218 (1931).

(7) C. D. Kennedy and R. D. Peacock, *ibid.*, 3392 (1963).

(8) J. F. Lotspeich, A. Javan, and A. Engelbrecht, *J. Chem. Phys.*, **31**, 633 (1959).

chloroplatinate(IV) structure.^{9,10} The resonance frequency observed at room temperature is higher than that at Dry Ice temperature. In other words, the temperature coefficient of the resonance frequency is positive for this cubic structure as confirmed further by measurement at 30°. At liquid nitrogen temperature, a closely spaced doublet was observed. The multiplet component of higher frequency is more intense than its counterpart, the intensity ratio being about 2:1. Therefore, it is concluded that two kinds of crystallographically nonequivalent chlorine atoms exist in this compound at liquid nitrogen temperature and that at least one transition point exists between liquid nitrogen temperature and Dry Ice temperature. In fact, Busey, *et al.*,¹¹ have carried out heat capacity measurements and found that second-order transitions take place at 76, 103, and 111°K.

Potassium hexabromorhenate(IV) gives rise to a single resonance line at room temperature in agreement with the potassium hexachloroplatinate(IV) structure of this crystal.¹² At Dry Ice and liquid nitrogen temperatures, two and three resonance lines were observed, respectively. In order to locate transition points, the temperature dependence of resonance frequencies was traced between room and Dry Ice temperatures. The results are shown in Figure 1. A single line was observed in a temperature range from -5.5 to 180°. The curve is almost linear with a positive temperature coefficient. Below -5.5°, two resonance lines of equal intensity were observed. The low frequency line gradually became less intense from about -10° and disappeared at about -15°. Below this temperature, a new line of slightly higher frequency appeared with a different temperature coefficient. The line became weak at about -24° and completely disappeared at -27°, below which a new line appeared on the high frequency side. This line showed a continuous change of frequency and no appreciable change in intensity until Dry Ice temperature was reached. On the other hand, the high frequency resonance line exhibited no discontinuity in its frequency down to -27° and no change in its intensity down to -17°. Below -17°, the intensity became weaker. At the same time, a new line of equal intensity appeared on the high frequency side. These two resonance lines disappeared at -27°, and a new line appeared below this temperature. This line showed no change in its intensity and no discontinuity of its frequency down to Dry Ice temperature. When the temperature was increased from Dry Ice temperature, the reverse process could be followed, the transition points being located at -4, -16, and -27°. The transition at -4° is presumed to correspond to a structural change from the cubic structure to a less

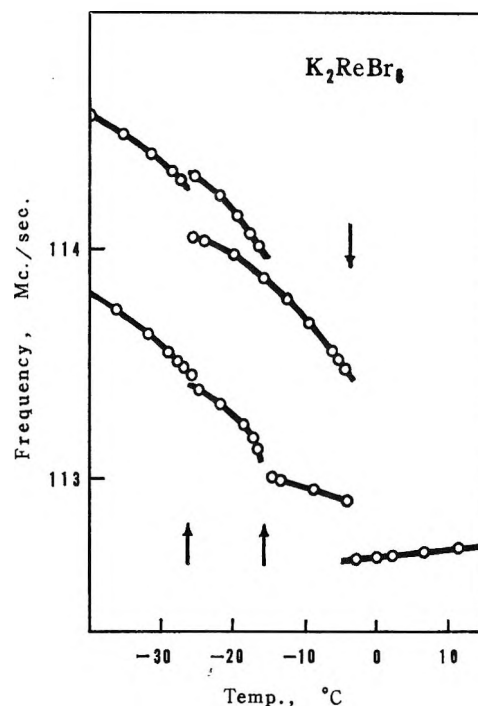


Figure 1. Temperature dependence of pure quadrupole resonance frequencies of ^{79}Br in potassium hexabromorhenate(IV) showing the existence of three transition points at -4 , -16 , and -27° .

symmetric one. It is noteworthy that one of the multiplet components is insensitive to the transition at -16° . Possibly, some but not all of the bromine atoms in the crystal suffer no change in field gradient when the rotation of complex anions takes place about their respective Re-Br axes.¹³ Phase transitions of similar nature have been observed for potassium hexabromoselenate(IV)¹⁴ and rubidium hexaiodotellurate(IV)¹⁵ also. Busey and Sonder¹⁶ have measured the heat capacity of this compound and observed two transition points at -28 and -48° . The former transition point agrees excellently with -27° of the present investigation, whereas the latter was not detected by quadrupole resonance spectroscopy.

(9) B. Aminoff, *Z. Krist.*, **A94**, 246 (1936).

(10) J. Dalziel, N. S. Gill, E. S. Nyholm, and R. D. Peacock, *J. Chem. Soc.*, 4012 (1958).

(11) R. H. Busey, H. H. Dearman, and R. B. Bevan, Jr., *J. Phys. Chem.*, **66**, 82 (1962).

(12) D. H. Templeton and C. H. Dauben, *J. Am. Chem. Soc.*, **73**, 4492 (1951).

(13) R. G. S. Morfee, L. A. K. Staveley, S. T. Walters, and D. L. Wigley, *Phys. Chem. Solids*, **13**, 132 (1960).

(14) D. Nakamura, K. Ito, and M. Kubo, *Inorg. Chem.*, **2**, 61 (1963).

(15) D. Nakamura and M. Kubo, *J. Phys. Chem.*, **68**, 2986 (1964).

(16) R. H. Busey and E. Sonder, *J. Chem. Phys.*, **36**, 93 (1962).

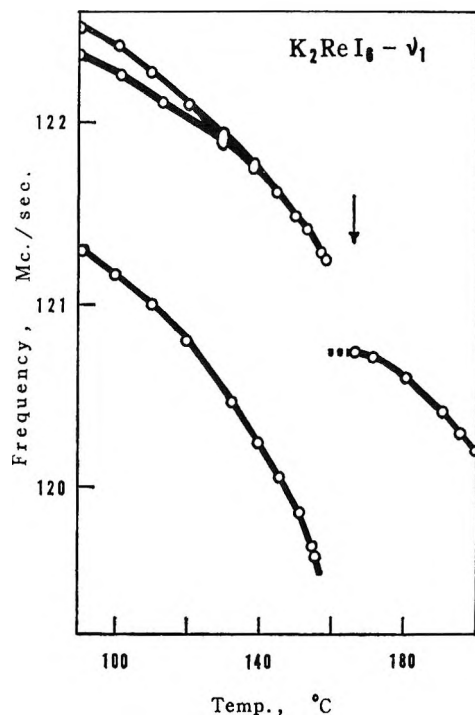


Figure 2. Temperature dependence of pure quadrupole ν_1 resonance frequencies of ^{127}I in potassium hexaiodorhenate(IV).

Both ν_1 and ν_2 resonance frequencies of potassium hexaiodorhenate(IV) showed triplet structure at all temperatures below room temperature, indicating the existence of at least three kinds of crystallographically nonequivalent iodine atoms in crystals. The crystal symmetry of this complex is known to be orthorhombic^{10,17} although detailed X-ray crystal analysis has not been carried out as yet. The correspondence of multiplet components has been made as shown in the last column of Table I by taking into account the requirement that $2\nu_1 \geq \nu_2$ and by measuring the temperature variation of the resonance frequencies between room and Dry Ice temperatures. Figure 2 illustrates the temperature dependence of ν_1 resonance frequencies above room temperature. The ν_2 frequencies show an analogous temperature variation. With increasing temperature, the separation between two high-frequency multiplet components decreased, until at about 130° they coalesced into a single line, which became weaker and disappeared at about 159°. The low-frequency component of the triplet also became less intense with increasing temperature and disappeared at about 155°. At 166°, a new, fairly intense line appeared. On lowering the temperature from 200°, the single line disappeared at about 160°. As contrasted with the case of other hexahalorhenates(IV), the tem-

perature coefficient of the single resonance line is negative. However, there are good reasons for believing that although only a single resonance line was observed, the structure of this crystal phase is not cubic. Firstly, the asymmetry parameter observed at 179° is fairly large ($\eta = 0.05$). Secondly, the Norelco X-ray powder patterns clearly indicate a lower than cubic symmetry. Lastly, the transition bears striking resemblance, regarding changes in the frequency and intensity of resonance lines, with temperature to that of rubidium hexaiodotellurate(IV)¹⁵ at -16° , above which it forms crystals of lower than cubic symmetry.

The existence of a transition at about 166° was confirmed by differential thermal analysis also. A peak of heat capacity appeared at 170.5° descending with a gradual slope on the low temperature side to about 155°.

For potassium hexachlorotungstate(IV), a single line was observed at room temperature as expected from the potassium hexachloroplatinate(IV) structure of this crystal.⁷ The line was very weak and difficult to observe between about 10° and Dry Ice temperature. At liquid nitrogen temperature, multiplet lines were barely detectable, but it was not feasible to determine the frequencies accurately owing to low intensity.

Discussion

Quadrupole Coupling Constants and Asymmetry Parameters. From the resonance frequencies observed at liquid nitrogen temperature, the quadrupole coupling constants eQq of chlorine and bromine isotopes were evaluated assuming that the asymmetry parameter η is negligibly small. The assumption is plausible since the complex anions in question have O_h symmetry as has been confirmed by X-ray analysis on potassium hexachlororhenate(IV),^{9,10} hexabromorhenate(IV),¹² and hexachlorotungstate(IV).⁷ For ^{127}I with its nuclear spin equal to $5/2$, the quadrupole coupling constant and asymmetry parameter can be calculated from the two observed frequencies, ν_1 and ν_2 , with the aid of Livingston and Zeldes' table.¹⁸ The results are shown in Table II.

Multiplet component I of the triplet resonance absorption of iodine in potassium hexaiodorhenate(IV) yields a smaller quadrupole coupling constant and a smaller asymmetry parameter than the other multiplet components, II and III, at all temperatures investigated. At room temperature, the quadrupole coupling constant and the asymmetry parameter for multiplet com-

(17) J. C. Morrow, *J. Phys. Chem.*, **60**, 19 (1956).

(18) R. Livingston and H. Zeldes, "Table of Eigenvalues for Pure Quadrupole Spectra, Spin $5/2$," ONRL Report 1913, Oak Ridge National Laboratory, Oak Ridge, Tenn., 1955.

Table II: Quadrupole Coupling Constants and Asymmetry Parameters of Halogens in Potassium Hexahalorhenates(IV) and Hexachlorotungstate(IV)

Compound	Temp., °C.	eQq , Mc./sec.	η
K_2ReCl_6	Liquid N_2	27.932	0
		27.972	0
		27.952 (av.)	
K_2ReBr_6	Liquid N_2	230.18	0
		231.72	0
		232.12	0
		231.34 (av.)	
		812.35 \pm 0.09	0.021 \pm 0.015
K_2ReI_6	21.0	817.59 \pm 0.16	0.051 \pm 0.006
		818.27 \pm 0.15	0.054 \pm 0.005
	-77	816.26 \pm 0.13	0.025 \pm 0.012
		820.41 \pm 0.14	0.053 \pm 0.005
		822.26 \pm 0.13	0.064 \pm 0.005
	Liquid N_2	818.54 \pm 0.13	0.032 \pm 0.008
	822.34 \pm 0.13	0.053 \pm 0.005	
	825.74 \pm 0.19	0.073 \pm 0.004	
	822.21 (av.)		
K_2WCl_6	22.5	20.44	0

ponent II are practically equal to those for multiplet component III. These facts can be explained on the basis of the crystal structure of this complex. It is known that at room temperature this complex forms orthorhombic crystals with one lattice constant greater than two others of almost equal length.^{10,17} In other words, the lattice symmetry may well be approximated with a tetragonal symmetry. For the tetragonal symmetry, one can expect a vanishing asymmetry parameter for iodine nuclei located on the fourfold symmetry axis and a finite asymmetry parameter for all other iodine nuclei. For a potassium hexachloroplatinate(IV) structure elongated in the direction of the fourfold symmetry axis, the field gradient at an iodine nucleus along the fourfold symmetry axis is smaller than that along the perpendicular directions, and, hence, the quadrupole coupling constant for iodine nuclei in the axial direction is smaller than that for iodine nuclei in the perpendicular directions, in qualitative agreement with experiments. Potassium hexaiodoplatinate(IV), which is isomorphous with potassium hexaiodorhenate(IV), shows a similar behavior with regard to the quadrupole coupling constant and the asymmetry parameter of the triplet lines.³

Nature of Metal-Ligand Bonds. We already have extended² the Townes-Dailey equation^{19,20} relating the observed quadrupole coupling constant eQq with the ionic character i of metal-halogen bonds as

$$eQq = [(1 - s)(1 - i - \pi) - \pi/2](eQq)_{atom} \quad (1)$$

when $d\pi$ - $p\pi$ -bond character is involved in the bonds.

Here, s denotes the extent of s-character in the sp-hybridized bonding σ -orbitals of halogens; π stands for the extent of the π -character of the bonds; and $(eQq)_{atom}$ is the atomic quadrupole coupling constant. As in a previous paper,² s was assumed to amount to 15%²⁰⁻²² and π was estimated on the basis of the results of electron spin resonance experiments carried out by Griffiths, *et al.*, on hexachloro- and hexabromoiridates(IV)²³⁻²⁶ ($\pi = 5.4\%$) with an additional assumption that the number of electrons migrating from a halogen ion to the central metal ion through π -bonding is proportional to the number of electronic vacancies in the $d\epsilon$ orbitals of the central metal ion. Since the atomic quadrupole coupling constant $(eQq)_{atom}$ is known,²⁷⁻²⁹ the extent of ionic character i and the covalent σ -bond character, $\sigma = 1 - i - \pi$, of the metal-ligand bonds can be calculated from the quadrupole coupling constants (observed at liquid nitrogen temperature except for potassium hexachlorotungstate(IV), for which the resonance frequency was observed only at room temperature) along with the net charge, $\rho = 4 - 6(1 - i)$ (in electronic units), on the central metal ion as shown in Table III.

Table III: The Bond Character of Metal-Ligand Bonds and the Net Charge on the Central Metal Atom in Potassium Hexahalorhenates(IV) and Hexachlorotungstate(IV)

Compound	Ionic character, i	σ -Bond character, σ	π -Bond character, π	Net charge, ρ
K_2ReCl_6	0.45	0.39	0.16	0.70
K_2ReBr_6	0.39	0.45	0.16	0.34
K_2ReI_6	0.32	0.52	0.16	-0.08
K_2WCl_6	0.43	0.35	0.22	0.58

The ionic character of metal-ligand bonds in hexachlororhenate(IV) and hexachlorotungstate(IV) (0.45, 0.43) is nearly the same as that in hexachloroplatinate-

- (19) C. H. Townes and B. P. Dailey, *J. Chem. Phys.*, **17**, 782 (1949).
- (20) B. P. Dailey and C. H. Townes, *ibid.*, **23**, 118 (1955).
- (21) B. P. Dailey, *ibid.*, **33**, 1641 (1960).
- (22) M. A. Whitehead and H. H. Jaffé, *Trans. Faraday Soc.*, **57**, 1854 (1961).
- (23) J. H. E. Griffiths, J. Owen, and I. M. Ward, *Proc. Roy. Soc. (London)*, **A219**, 526 (1953).
- (24) J. H. E. Griffiths and J. Owen, *ibid.*, **A226**, 96 (1954).
- (25) J. Owen, *Discussions Faraday Soc.*, **19**, 127 (1955).
- (26) E. Cipollini, J. Owen, J. H. M. Thornley, and C. Windsor, *Proc. Phys. Soc.*, **79**, 1083 (1962).
- (27) V. Jaccarino and J. G. King, *Phys. Rev.*, **83**, 471 (1951).
- (28) J. G. King and V. Jaccarino, *ibid.*, **91**, 209 (1953).
- (29) V. Jaccarino, J. G. King, R. A. Satten, and H. H. Stroke, *ibid.*, **94**, 1798 (1954).

(IV), hexachloroiridate(IV), and hexachloroosmate(IV)² (0.44, 0.47, 0.47). As a result, the net charge on each central metal ion is a positive fraction of the electronic charge as in the hexahalo complexes of the platinum series. In previous papers,^{2,14,30} we have shown that the covalent character, $1 - i$, of metal-halogen bonds M-X in hexahaloplatinates(IV), hexahalopalladates(IV), hexachloroiridate(IV), and hexachloroosmate(IV) plotted against the difference, $\chi_X - \chi_M$, between the electronegativities of atoms involved in the bonds gives a straight line within the reliability of the electronegativity values. The electronegativities of rhenium and tungsten are reported as 1.9–2.1 and 1.6–1.8, respectively.^{8,31–34} It is rather surprising to find that the data of ionic character observed for potassium hexahalorhenates(IV) conform to the aforementioned linear relation in the plot against the electronegativity difference for the complexes of the platinum series.

Positive Temperature Coefficient of Resonance Frequencies. The temperature coefficient of pure quadrupole resonance frequencies is normally negative.³⁵ However, we have found positive temperature coefficients for potassium hexachlororhenate(IV), hexabromorhenate(IV), and hexachlorotungstate(IV) in the temperature range in which these complexes show a single resonance line; *i.e.*, they form cubic crystals having the potassium hexachloroplatinate(IV) structure. (Potassium hexaiodorhenate(IV) did not crystallize in a cubic structure at any temperature studied. No positive temperature coefficient was observed in the temperature range.) This is the first instance of complex compounds ever reported to show a positive temperature coefficient although a few simple inorganic compounds such as tungsten hexachloride,³⁶ titanium tetrabromide,³⁷ and thorium tetrachloride³⁸ have been reported to exhibit such temperature dependence. The change of resonance frequencies with temperature is almost linear in the temperature range of the cubic crystal structure. Table IV shows the quadrupole resonance frequency ν and its temperature coefficient $d\nu/dT$ of the rhenium and tungsten complexes at 20° along with those of related complexes.

It is seen from Table IV that the resonance frequency of the hexachloro complexes decreases while the temperature coefficient increases progressively with decreasing atomic number of the central metal atoms or with increasing electron deficiency in the $d\epsilon$ orbitals. This regularity suggests that the frequency decrease and the positive temperature coefficient are closely related to the vacancy in the $d\epsilon$ orbitals or the partial $d\pi$ - $p\pi$ -bond character of the metal-ligand bonds.

Table IV: The Temperature Coefficient of the Pure Quadrupole Resonance Frequencies of Potassium Hexahalorhenates(IV), Hexachlorotungstate(IV), and Related Complexes at 20°

Compound	ν , Mc./sec.	$d\nu/dT$, kc./deg.	Temp. range, °C.
K ₂ PtCl ₆	25.82	-1.00	-75.0-23.5
K ₂ IrCl ₆	20.73	-0.54	-69.0-24.2
K ₂ OsCl ₆	16.84	-0.22	-70.0-26.0
K ₂ ReCl ₆	13.89	+0.13	-76.0-21.2
K ₂ WCl ₆	10.22	+0.44	10.5-35.0
K ₂ ReBr ₆	112.71	+2.8	-3.0-181.0

With increasing π -bond character, electrons in the p_z and p_y orbitals of chlorine migrate toward the central metal ion, where the z -axis is taken along the metal-ligand bond. The resulting electron deficiency leads to the decrease in the quadrupole resonance frequency of chlorine, in agreement with experimental observation.

As regards the dependence of the resonance frequency on temperature, a simple thermodynamical calculation yields^{39,40}

$$(\partial\nu/\partial T)_p = (\partial\nu/\partial T)_v + (\partial\nu/\partial V)_T(\partial V/\partial T)_p \quad (2)$$

The thermal expansion $(\partial V/\partial T)_p$ is positive. In the case of potassium hexachloroplatinate(IV) type crystals, $(\partial\nu/\partial V)_T$ is also positive for the following reason. Since the field gradient q is the sum of $q_{e.i.}$, originating from charges within the complex ion except for the halogen nucleus, and $q_{n.i.}$, the field gradient owing to all neighboring ions, one has

$$\nu = 1/2 |eQq| = 1/2 |eQ| (q_{e.i.} + q_{n.i.}) \quad (3)$$

for nuclei having $I = 3/2$. Now, $q_{e.i.}$ is positive because the halogen atom has partial vacancy in the p_z orbital whereas both the p_x and p_y orbitals are filled. The second term, $q_{n.i.}$, which depends directly on the

(30) D. Nakamura, *Bull. Chem. Soc. Japan*, **36**, 1662 (1963).

(31) W. Gordy and W. J. O. Thomas, *J. Chem. Phys.*, **24**, 439 (1956).

(32) J. F. Lotspeich, *ibid.*, **31**, 643 (1959).

(33) L. Pauling, "The Nature of the Chemical Bond," 3rd Ed., Cornell University Press, Ithaca, N. Y., 1960, p. 93.

(34) M. Haïssinsky, *J. phys. radium*, **7**, 7 (1946).

(35) H. Bayer, *Z. Physik*, **130**, 227 (1951).

(36) R. P. Hamlen and W. S. Koski, *J. Chem. Phys.*, **25**, 360 (1956).

(37) R. G. Barnes and R. D. Engardt, *ibid.*, **29**, 248 (1958).

(38) A. H. Reddoch, *ibid.*, **35**, 1085 (1961).

(39) T. Kushida, G. B. Benedek, and N. Bloembergen, *Phys. Rev.*, **104**, 1364 (1956).

(40) H. S. Gutowsky and G. A. Williams, *ibid.*, **105**, 464 (1957).

lattice constant, has been calculated¹⁵ for a point-charge model. For crystals having the potassium hexachloroplatinate(IV) structure, it is negative and is one or two orders of magnitude smaller than the first term, the absolute value decreasing with increasing lattice constant. Accordingly, $(\partial\nu/\partial V)_T$ is positive. This theoretical conclusion is supported by our experimental observation that at a constant temperature the resonance frequency of chlorine or bromine in hexahaloplatinates(IV) having various cations increases with increasing lattice constant.¹⁵

The fact that the observed temperature coefficient $(\partial\nu/\partial T)_p$ is normally negative implies that the major term $(\partial\nu/\partial T)_V$ is negative. Although this quantity is not accessible to direct measurements, it has an advantage for theoretical discussion that it takes into account the thermal vibration of complex anions but is free from the effect of the thermal expansion of the lattice.^{35,41} With increasing thermal vibration of the complex ion, especially bending vibrations, the overlap of the σ orbital of the central metal ion with the p_z orbital of chlorine decreases leading to decreased covalent character of the metal-ligand bond. Accordingly, the field gradient q and, hence, the quadru-

pole resonance frequency, also, decrease with increasing temperature.

The foregoing discussion applies to complexes involving no bonds having π -bond character. However, when $d\pi$ - $p\pi$ -bonds are involved, as in paramagnetic complexes, the decrease of overlap owing to thermal vibration leads to the decrease of π -bond character. This means that electrons in the p_x and p_y orbitals of a halogen atom migrate toward the $d\pi$ -orbitals to a smaller extent, and hence the field gradient increases with increasing temperature. The positive temperature coefficient of quadrupole resonance frequencies results when this effect along with the second term of the right-hand side of eq. 2 predominates over the normal negative temperature coefficient. This is the case with hexahalorhenates(IV) and hexachlorotungstate(IV) of the cubic structure involving metal-ligand bonds of high π -bond character.

Acknowledgment. The authors wish to thank Dr. H. Chihara and Mr. N. Nakamura of Osaka University for carrying out differential thermal analysis on potassium hexaiodorrhenate(IV).

(41) H. G. Dehmelt and H. Ktger, *Z. Physik*, **129**, 401 (1951).

Studies on the Anion Radicals of the Thianthrene Oxides^{1,2}

by E. T. Kaiser and D. H. Eargle, Jr.

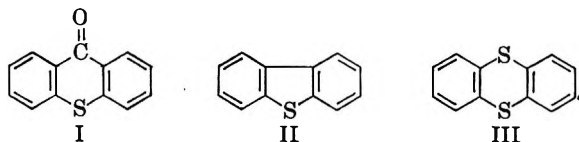
Department of Chemistry, University of Chicago, Chicago, Illinois 60637, and the Department of Chemistry, The George Washington University, Washington, D. C. (Received January 25, 1965)

The electron spin resonance spectra of the anion radicals of thianthrene 5-oxide (IV), *trans*-thianthrene 5,10-dioxide (V), *cis*-thianthrene 5,10-dioxide (VI), thianthrene 5-dioxide (VII), thianthrene 5,10-trioxide (VIII), and thianthrene 5,10-tetroxide (IX) have been determined. The spectral behavior of the radicals is markedly influenced by the orientation of their sulfur-oxygen bonds. Furthermore, as the oxidation state of the sulfur-containing groups in the series IV-VII is increased, a trend is observed toward the narrowing of the total widths of the spectra. However, when at least one sulfone group is present, as in VII-IX, no further changes in the spectral widths of the radicals are found.

Introduction

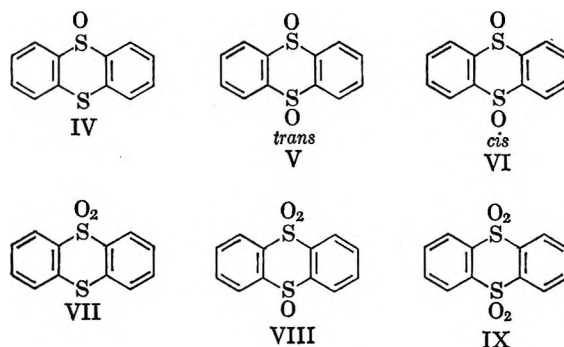
We have been engaged in an extensive investigation by means of electron spin resonance (e.s.r.) techniques of the effects of changes in the oxidation state of sulfur and in the geometry of sulfur-oxygen bonds upon the properties of sulfur-containing aromatic anion radicals.^{3a}

In our studies of the anion radicals formed by the reduction of thioxanthone (I), dibenzothiophene (II), and their oxides we have noted the following trend: the higher the oxidation state of the sulfur group, the narrower the total widths of the e.s.r. spectra which are observed. We have now prepared the anion radicals of all six oxides of the thianthrene ring system (III), and their preparation permits us to examine in more detail this and other trends.



Results and Discussion

In order to avoid decomposition and/or lowered electron affinity at higher temperatures, the radicals of the thianthrene oxides IV-IX were formed by potassium reduction using 1,2-dimethoxyethane as the solvent at temperatures near -60° . The spectra were usually best resolved at -70 to -80° . When the temperature was raised the e.s.r. signals for most of the radicals gradually disappeared, and this disappearance was accompanied by darkening of the reaction solutions.



We were unsuccessful in preparing a reduction product which gave a discernible e.s.r. spectrum only in the case of thianthrene. At -70° no noticeable color change occurred in short times when a solution of thianthrene in 1,2-dimethoxyethane was shaken over a potassium mirror nor was an e.s.r. signal observed. Over longer periods of time and at higher temperatures a yellow color developed, but no appreciable resonance signal could be detected. At -30° after a few minutes reaction a strong thiophenol-like odor was noticed when the sample tube was broken open, and this suggests that the yellow color may be due to decompo-

(1) Grateful acknowledgment is made to the Donors of the Petroleum Research Fund for support of this research.

(2) Paper IV in the series on "Conjugative Effects of Sulfur in Aromatic Anion Radicals." Initial phases of this work were carried out while both authors were in the Department of Chemistry, Washington University, St. Louis, Mo.

(3) (a) E. T. Kaiser and D. H. Eargle, Jr., *J. Am. Chem. Soc.*, **85**, 1821 (1963); (b) *J. Chem. Phys.*, **39**, 1353 (1963); (c) D. H. Eargle, Jr., and E. T. Kaiser, *Proc. Chem. Soc.*, 22 (1964).

sition products formed by cleavage of the thianthrene ring.

Although thianthrene 5-oxide (IV) was reduced with some difficulty,⁴ perhaps because it has a relatively low electron affinity, we were still able to prepare its anion radical and to determine the resulting e.s.r. spectrum. This spectrum was 17 gauss wide and consisted of at least 40 evenly spaced lines. When the *trans* dioxide V was reduced, a similar e.s.r. spectrum with about 40 lines was observed again. When the modulation was increased, effectively removing the hyperfine detail of the spectrum, three strong lines remained. The primary splitting then appears to be due to the interaction of the odd electron with two equivalent protons. There is one rather notable difference from the spectrum for the anion radical of IV. The spectrum of the anion radical of V is 15.4 gauss wide, and thus it is narrower than that found with reduced IV. A reasonable explanation for this observation is that the odd-electron density in the aromatic rings of reduced V is lower than in those of reduced IV and, correspondingly, the concentration of the odd-electron density on the sulfur-containing groups of V is greater than on the related groups of IV.⁵

As has been reported before in a preliminary note,^{3b} the anion radical of the *cis* dioxide VI has an e.s.r. spectrum which differs a great deal from that of the *trans* dioxide radical, both in the number of lines found as well as in the total width. The spectrum of the *cis* radical contains five major groups of lines with five hyperfine lines per group, and its total width is 9.5 gauss. From this decreased spectral width as compared to that of the anion radical of the *trans* dioxide it can be concluded that the sulfoxide groups of the *cis* radical exhibit an enhanced ability to withdraw odd-electron⁵ density from the outer aromatic rings. Furthermore, the observation that the anion radicals of the *cis* and *trans* dioxides are discrete entities and do not interconvert readily indicates that the geometry of the sulfur-oxygen bonds in these compounds must be substantially retained on reduction. This geometry is illustrated in Figure 1, which gives a stereochemical representation of the central heterocyclic rings of V and VI.⁶

Even narrower spectra are exhibited by the anion radicals of the sulfones VII-IX. In all three of these cases five lines are observed with a splitting of 2.1 gauss. The total spectral widths are essentially identical, 8.9 gauss. Considerable differences exist, however, with respect to the ease of formation,⁴ the color, and the stability of the radicals. Thus, the ease of reduction⁴ in the series thianthrene 5-dioxide, thianthrene 5,10-trioxide, and thianthrene 5,10-tetroxide

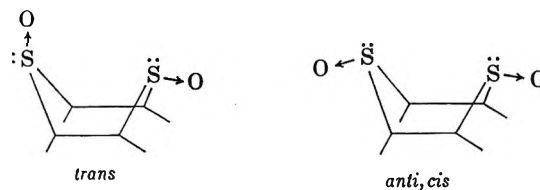


Figure 1.

shows a progressive increase as the oxidation state of the sulfur-containing groups in the thianthrene nucleus becomes greater. The increase can probably be ascribed to the greater electron affinity of the heterocyclic ring system as the oxidation state of its sulfur atoms increases.

The colors of the 1,2-dimethoxyethane solutions containing the radicals also contrast strongly. A solution of the anion radical of thianthrene 5-dioxide (VII) is yellow, that of the anion radical of the thianthrene 5,10-trioxide (VIII) is brown, and finally, that of the anion radical of thianthrene 5,10-tetroxide (IX) is blue. The variation in the stabilities of the anion radicals is just as striking. Whereas the radicals of VII and VIII are relatively stable only at low temperatures for long periods of time, the anion radical of the tetroxide IX is remarkably stable even at room temperature, lasting for several months and furnishing an excellent standard through its strong and simple spectrum.

From a study of the anion radical of 2,7-dimethylthianthrene 5,10-tetroxide we have determined that the spin density in the aromatic rings is concentrated at the β -positions with very little at the α -positions.^{3a} Hence, the five major lines in the e.s.r. spectrum of the anion radical of thianthrene 5,10-tetroxide are ascribed to splitting by the four β -protons. By analogy, the five lines found for the reduction products of VII and VIII are probably due to the magnetic interaction of the odd electron with the four protons situated in the β -positions of the aromatic rings of these compounds. Also, on this basis the assignment of the five major groups of lines in the spectrum of the anion radical of the *cis* dioxide to strong splittings by the β -protons and of the five hyperfine lines per group to weaker splittings

(4) Ease of formation or ease of reduction as used in this work are relative terms which refer to the length of time the cold solution of unreduced material was in contact with the potassium mirror before a strong e.s.r. signal was produced. The more difficultly reduced materials required some agitation and as long as 20 min. reaction time before any evidence of reduction was detected. In contrast, the tetroxide IX was fully reduced in less than 1 min.

(5) Although the explanation given is a reasonable one, other possible explanations cannot be ruled out at present. Experiments which are designed to bear directly on this point are being planned.

(6) (a) S. Hosoya and R. G. Wood, *Chem. Ind. (London)*, 1042 (1957); (b) S. Hosoya, *ibid.*, 980 (1958).

by the α -protons seems reasonable. Detailed analysis of the spectra of the radicals from thianthrene 5-oxide (IV) and from *trans*-thianthrene 5,10-dioxide (V) awaits the completion of deuterium labeling studies which are now in progress.

Table I summarizes the properties of the anion radicals of the thianthrene oxides. From the right-hand column of Table I, the trend toward a progressive narrowing of the total spectral widths for the reduction products of compounds IV–VII can be seen. In Figure 2 a graphical depiction of the lines observed in the e.s.r. spectra is given.

Table I: Summary of E.p.r. Measurements

Compd.	Color reduced	Number of major lines g_H , gauss	Hyperfine lines	Total width, gauss
-S-, -S-, (III)	(Yellow)
-SO-, -S- (IV)	Pale yellow	3	40+ (total)	17
-SO-, -S- (<i>trans</i> (V))	Pale yellow	3	40+ (total)	15.4
-SO-, -S- (<i>cis</i>) (VI)	Pale yellow	5 (2.1)	5/group	9.5
-SO ₂ -, -S- (VII)	Pale yellow	5 (2.11)	1/group	8.9
-SO ₂ -, -SO- (VIII)	Pale brown	5 (2.11)	1/group	8.9
-SO ₂ -, -SO ₂ - (IX)	Pale blue	5 (2.11)	1/group	8.9

In summary, we have shown in this series of radicals prepared from the thianthrene oxides that the effect of sulfoxide groups depends on their stereochemical orientation, and that the presence of sulfone groups causes narrowing of the total widths of the e.s.r. spectra. Increases in the oxidation state of the sulfur-containing groups cause increases in the electron affinity of the molecule. Also, as the oxidation state of these groups in the series IV–VII is increased, decreases are observed in the electron density at the carbon atoms in the outer aromatic rings which bear protons.

Experimental

Equipment. Electron spin resonance spectra were recorded immediately after reduction of the compounds by potassium in 1,2-dimethoxyethane. Two types of instruments were used in the measurements. One was a Varian 100-kc. apparatus, used with the kind permission of Dr. W. B. Moniz of the U. S. Naval Research Laboratory, Washington, D. C., and the other was a spectrometer built at Washington University, St. Louis, which has been described previously.⁷

Reductions. As mentioned earlier in this paper, the anion radicals of the thianthrene oxides were formed in 1,2-dimethoxyethane at -60° by potassium reduction of the parent compounds, and the e.s.r. spectra were measured after the reductions at -70 to -80° . The possibility of the occurrence of some bond cleavage

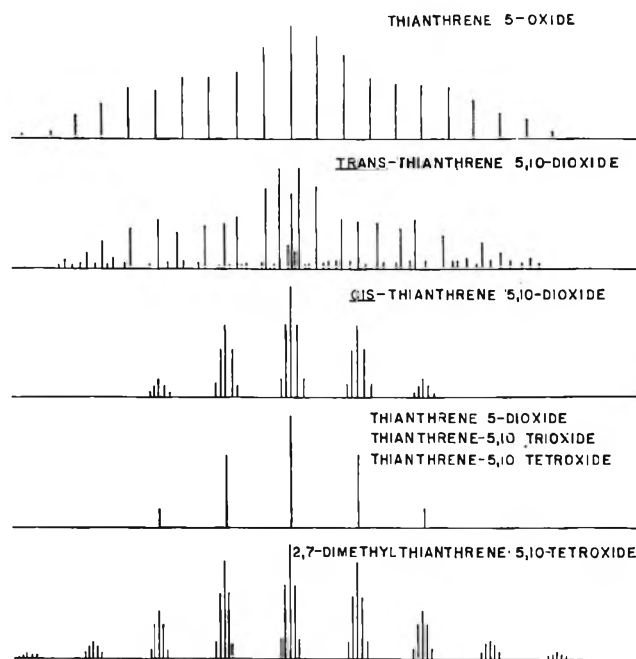


Figure 2.

before the measurement of the spectra seems unlikely for several reasons. Reductions and measurements were carried out at low temperatures (-60 to -80°) which provide mild reaction conditions. Also, the spectra were measured immediately upon the first appearance of color in the reduction solutions. No spectra were produced prior to this appearance of color. In addition, those anion radicals which were obviously unstable at higher temperatures (deepening and changing of color, production of thiophenol-like odors) also lost radical activity at these temperatures, indicating cleavage of bonds and decomposition at the elevated rather than at the lower temperatures.

Materials. Thianthrene was purchased from the Eastman Kodak Co. and recrystallized several times from glacial acetic acid; m.p. 157 – 158° (lit.⁸ m.p. 159°).

Thianthrene 5-oxide was prepared from thianthrene by oxidation with dilute nitric acid; m.p. 143° (lit. m.p. 143° ,⁸ 143 – 143.5° ⁹).

cis and *trans*-thianthrene 5,10-dioxide were prepared by the oxidation of thianthrene with nitric acid of specific gravity 1.2 according to the procedure of Baw, Bennett, and Dearn.^{10a} After recrystallization from acetic acid the *cis* form had m.p. 283 – 284° (lit.¹⁰ m.p. 284°). Recrystallization of the *trans* dioxide from

(7) R. L. Ward and S. I. Weissman, *J. Am. Chem. Soc.*, **79**, 2086 (1957).

(8) K. Fries and W. Vogt, *Ber.*, **42**, 1172 (1909).

(9) H. Gilman and D. R. Swayampati, *J. Am. Chem. Soc.*, **77**, 3387 (1955).

ethanol or from acetic acid gave purified material melting at 248–249° (lit.¹⁰ m.p. 249°).

Thianthrene 5-dioxide was obtained from the reaction of thianthrene 5,10-trioxide with zinc and acetic acid by the method of Gilman and Swayampati.¹¹ Two recrystallizations from glacial acetic acid gave thianthrene 5-dioxide melting at 165.5–166° (lit.¹¹ m.p. 168–169°).

Thianthrene 5,10-trioxide was prepared by the oxidation of thianthrene with chlorine in glacial acetic acid.^{11,12} Recrystallization from 90% acetic acid resulted in trioxide melting at 221–222° (lit.¹¹ m.p. 221.5–222.5°).

Thianthrene 5,10-tetroxide was obtained by the oxidation of thianthrene with excess hydrogen peroxide in glacial acetic acid. The tetroxide was recrystallized from glacial acetic acid, m.p. 323–324° (lit.^{10b} m.p. 321).

(10) (a) H. Baw, G. M. Bennett, and P. Dearnes, *J. Chem. Soc.*, 680 (1934); (b) see F. Krafft and R. E. Lyons, *Ber.*, 29, 435 (1896), for an earlier reference to this method; (c) in both of these papers incorrect stereochemical assignments were made, and these were later corrected by the work of T. W. J. Taylor [*J. Chem. Soc.*, 625 (1935)] and of Hosoya and Wood.^{6a}

(11) H. Gilman and D. R. Swayampati, *J. Am. Chem. Soc.*, 77, 5946 (1955).

(12) K. Fries and W. Vogt, *Ann.*, 381, 312 (1911).

Kinetics of the Nitrous Oxide Decomposition by Mass Spectrometry. A Study to Evaluate Gas-Sampling Methods behind Reflected Shock Waves

by Anthony P. Modica

Avco Corporation, Wilmington, Massachusetts (Received February 4, 1965)

The thermal decomposition of N₂O in the temperature range 2400–3300°K. has been investigated in a mass spectrometer-shock tube apparatus to evaluate two sampling techniques, one involving a simple pinhole and the other a slender Pyrex nozzle protruding into the reflected region. It has been shown that below 3000°K. both methods yield nearly identical experimental results, comparing favorably with those of other investigators. Above this temperature, the effects of the cold end wall on the hot, shocked gas introduce a systematic error in the measured rate constant. The error is slightly less for the nozzle.

Introduction

The shock tube has become a popular laboratory tool to prepare a gas rapidly and homogeneously for high temperature kinetic studies of fast chemical reactions. Until recently, exploitation of the shock tube has been restricted to choice of analytical techniques mainly involving optical spectroscopy, and even then it has been necessary to study simple systems with species of high extinction coefficients.^{1–3} The advent of the time-of-flight mass spectrometer,

with its ability to follow the concentration of several species simultaneously in short resolution times (10 to 50 μsec.), has now made it possible to study a greater variety of reactions behind reflected shock waves.^{4,5}

(1) H. B. Palmer and D. F. Hornig, *J. Chem. Phys.*, 26, 98 (1957).

(2) M. Camac and A. Vaughan, *ibid.*, 34, 460 (1961).

(3) A. P. Modica and D. F. Hornig, "Kinetics of the Thermal Dissociation of N₂F₄ in Shock Waves," Report No. 357-275, Princeton University, Oct. 1963.

A technique, similar to that reported by Bradley and Kistiakowsky,⁴ coupling a Bendix time-of-flight mass spectrometer to a shock tube, has been developed here to study at high temperatures relatively complex reactions which may be of interest to propellant combustion and re-entry ablation. In order to "test" the apparatus, a known kinetic system, the thermal decomposition of nitrous oxide, has been investigated. The objective of this study has been to evaluate experimentally in terms of end-wall effects (*i.e.*, the effects of the cold end wall on the temperature of the sampled gas) two gas-sampling techniques, one involving the usual pinhole and the other a slender conical nozzle protruding into the reflected region.

Apparatus

The operating principles of the Bendix time-of-flight mass spectrometer have been described elsewhere⁶ and may be summarized as follows. Ions are formed in a bunch by a pulsed electron beam, and the ions are then accelerated by a series of grids into a field-free drift tube. Because the ion velocities depend on the charge to mass ratios, the bunch separates into groups of different m/e while moving down the tube. The time between the accelerating pulse and the arrival of each of the mass-resolved groups at the ion-multiplier detector is proportional to $M^{1/2}$ for ions of the same charge. The detector output is displayed on an oscilloscope which is triggered by the accelerating pulses.

In the present research, the mass spectrometer is a Bendix Model 14-206 time-of-flight instrument. Time-intensity profiles of two individual peaks are selected and displayed on an oscilloscope (Tektronix 581) by using the electronic gates of the mass spectrometer to modulate the peak intensities of interest. Permanent records are made with Polaroid film. The downstream end of the shock tube is used to prepare the high temperature reaction mixture, and sampling is performed by allowing the test gas to pass through the end wall directly into the mass spectrometer. The shock tube and end plate are secured to the ion source through the "fast reaction chamber" available on the commercial instrument.

In a number of experiments, the end wall is a 0.0076 cm. thick brass foil having either a 0.0051- or 0.0076-cm. diameter pinhole in its center. Also a small Pyrex nozzle similarly located and protruding into the reflected region has been used. The nozzle is fabricated from Pyrex capillary tubing which has been heated, drawn, and cut to desired specifications. Eastman cement (Type 910) is used to bond the nozzle to the end plate. A typical nozzle (Figure 1) has an entrance and exit diameter of 0.0076 and 0.0254 cm. and a

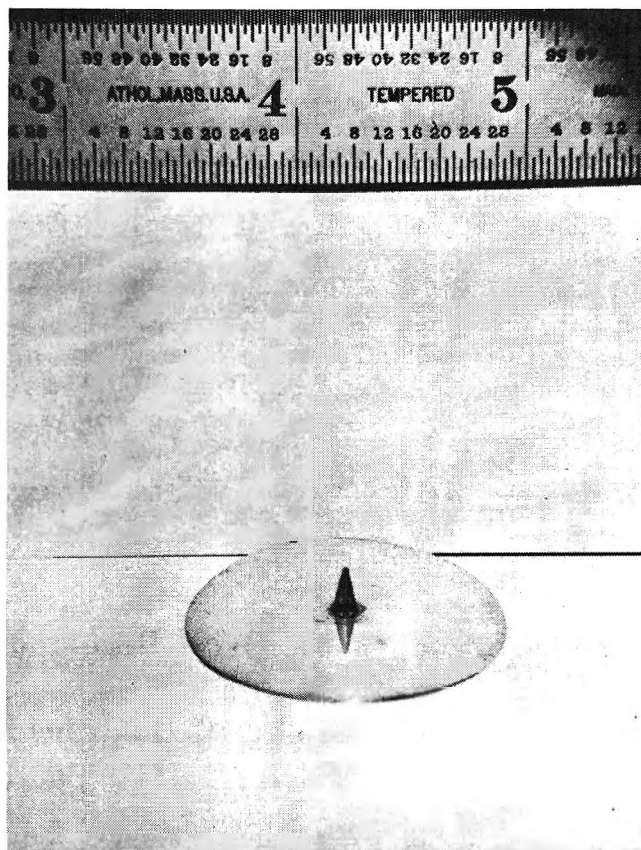


Figure 1. End plate with Pyrex sampling nozzle.

length of 0.475 cm. The nozzle characteristics are such that for an entrance to exit area ratio of 11.1, the exit to entrance temperature and pressure ratios are 8.3 and 200, respectively.⁷ Accordingly, the temperature and pressure of the shocked gas entering the nozzle was changed, for example, from 3000 to 360°K. and 0.24 to 0.0012 atm. (The background pressure in the mass spectrometer before shock arrival varied between 3×10^{-6} and 9×10^{-6} torr.) At the nozzle inlet the gas flow is sonic and becomes supersonic upon expansion. For a flow velocity of 1.02 mm./ μ sec. (speed of sound in a 5:100 N₂O-Ar mixture at 3000°K.), the residence time of the reaction mixture in the nozzle was less than 5 μ sec. With the particle velocity taken as 1 mm./ μ sec. for an average nozzle temperature of 1680°K., the number of collisions with the nozzle wall was about 10^{11} as compared to 10^{10}

(4) J. N. Bradley and G. B. Kistiakowsky, *J. Chem. Phys.*, **35**, 256 (1961).

(5) R. W. Diesen and W. J. Felmlce, *ibid.*, **39**, 2115 (1963).

(6) W. C. Wiley and I. H. McLaren, *Rev. Sci. Instr.*, **26**, 1150 (1955).

(7) For an analysis on nozzle performance see D. Atman, J. M. Carter, S. S. Penner, and M. Summerfield, "Liquid Propellant Rockets," Princeton University Press, Princeton, N. J., 1960, pp. 113-115.

collisions in the gas phase. In view of the large temperature drop and short residence time in the nozzle, chemical reactions taking place there would likely be frozen. The distance from the end plate to the electron beam is approximately 2 mm., so that the particle flight time from the nozzle entrance to the ion source was about 7 μ sec.

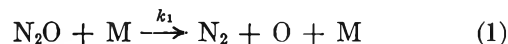
The shock tube is constructed from 2.54-cm. i.d. Pyrex glass pipe with a 4.53-m. driven section separated by a Mylar diaphragm from a 1.51-m. driver. Cold driving with helium was used to pressurize and rupture the diaphragm. The driven section is fitted with four metal inserts which support platinum-film resistance gauges (70-ohm) used for shock velocity measurements. These gauges are placed 76.2 cm. apart. The last gauge approximately 21.8 cm. from the end plate is used to synchronize the shock wave with the mass spectrometer analysis. The outputs of the gauges are displayed on a folded oscilloscope sweep and photographed.

In general, the shock tube is evacuated to 3 μ , and the reactant mixture containing 95% argon (Matheson, 99.9% purity) and 5% nitrous oxide (Matheson, 98% purity) is introduced. The driver section is pressurized with helium until the 0.5-mil Mylar film bursts spontaneously. The shock wave generated passes the first sensing element triggering the speedscope. The last shock detector actuates the sweep of the scope which monitors the time histories of the interesting peaks. A schematic of the shock tube apparatus is shown in Figure 2.

Calculations and Errors

The temperature, pressure, and composition behind the reflected shock wave are calculated from the initial pressure and measured shock velocity with an IBM-7094 computer code (Avco RAD 1360 program)⁸ which couples a thermochemical tape to the Rankine-Hugoniot relations for a moving shock wave. Since the

mixtures contain 5% N₂O in argon, the conditions prevailing behind the reflected shock are not isothermal. The difference in temperature between no dissociation and complete dissociation for the reaction



is 920°K. From the conservation of energy, the condition of temperature in the reflected region before dissociation and during dissociation is given by

$$\begin{aligned} \frac{(1-C)}{M_{\text{Ar}}} \frac{5}{2} R(T_5 - T_1) + \frac{C}{M_{\text{N}_2\text{O}}} \int_{T_1}^{T_5} C_{p\text{N}_2\text{O}} dT = \\ \frac{(1-C)}{M_{\text{Ar}}} \frac{5}{2} R(T_\alpha - T_5) + \frac{(1-\alpha)C}{M_{\text{N}_2\text{O}}} \int_{T_5}^{T_\alpha} C_{p\text{N}_2\text{O}} dT + \\ \frac{\alpha C}{M_{\text{N}_2\text{O}}} (C_{p\text{N}_2} + C_{p\text{O}})(T_\alpha - T_5) + \frac{C\alpha E_D}{M_{\text{N}_2\text{O}}} \quad (2) \end{aligned}$$

where α is the fraction of molecules dissociated, C is the initial weight fraction of N₂O in the system, M is the molecular weight, and E_D is the dissociation energy of N₂O.

During the course of the experiments some shock attenuation has been noticed. The shock velocity over the length of the tube is found to decrease linearly with an attenuation of 0.74%/10 cm. Extrapolation of the shock velocity to the end plate could be done with an accuracy of about 99%. Accordingly, the error introduced in the calculated temperature is <50°K.

Following the procedure in ref. 5, an internal pressure standard (the 20 peak of Ar²⁺) is used to minimize systematic errors encountered in the single-cycle analysis. The electron gun voltage has been adjusted so that the internal pressure standard has approximately the same intensity as the peaks of interest. By this method, fluctuations of the electron gun and nonlinearity of the multiplier are easily corrected.

As pointed out in ref. 4 and 5, inherent to the mass spectrometer-shock tube technique are two new sources of error: the background buildup and background scattering inside the mass spectrometer ion source caused by the sudden increase in density behind the reflected shock and the influence of the cold end wall on the sampled gas from the shock tube.

In this type of experiment there is a continuous pressure increase in the mass spectrometer; however, with the electron beam close to the nozzle exit, Kydd has shown by an approximate calculation that this buildup should be relatively small compared with the effective

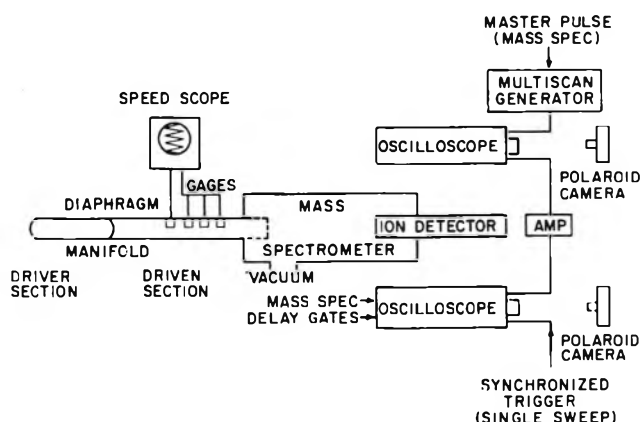


Figure 2. Diagram of apparatus.

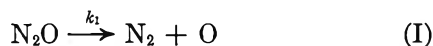
(8) R. D. Gillespie and J. Warga, "A Program for Computing Thermochemical Equilibrium behind a Moving Shock Wave," Avco RAD-TM-63-65, Sept. 23, 1963.

pressure of the sample being analyzed by the electron beam.⁹

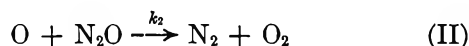
Another problem associated with the technique is whether the gas sample flowing into the mass spectrometer is truly representative of the bulk of the gas behind the reflected wave. According to ref. 4 and 5, the effect of the end plate not only tends to cool the gas being sampled but also allows an opportunity for some of the sampled gas to come into contact with the surface where catalytic recombination of atoms and radicals can take place. Although the absolute magnitudes of these errors are difficult to evaluate analytically, we have attempted to assess the relative temperature influence of the end plate on a reacting gas by comparing results between a pinhole and a protruding nozzle sampling gas far from the end wall.

Experimental Results

The thermal decomposition of N₂O is an example of a quasi-unimolecular decomposition whose mechanism is believed to be



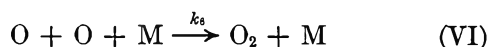
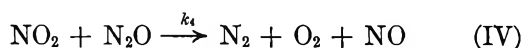
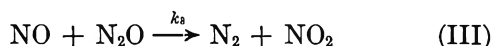
followed by



or



and later still by



Reactions II through VI are not likely to be of importance in the present experiments because of the high dilution and short time available.¹⁰

Johnston¹¹ gives

$$k_1 = 4.4 \times 10^9 \exp(-57,400/RT) \text{ sec.}^{-1} \quad (3)$$

at an N₂O concentration of 2.5×10^{-6} mole/cc. so that the activation energy of reaction I provides a suitable test of the temperature of the gas sample.

In the present experiments, a mixture of 5% N₂O and 95% argon was shock-heated to temperatures between 2400 and 3400°K. at a total concentration of about 10^{-6} mole/cc. The initial conditions of temperature behind the reflected shock were calculated from the Hugoniot relations assuming no dissociation and

with the experimentally determined shock velocity. During the course of the reaction, the temperature of the gas was variable. If one assumes a temperature dependence (ref. 2)

$$T_\alpha = T_0 - B\alpha \quad (4)$$

where T_0 is the initial reflected shock temperature, B is a constant related to the mole ratio of N₂O in the gas mixture (for 5% N₂O, $B = 920^\circ\text{K.}$ as determined from eq. 2), and α is the fraction of molecules dissociated; the rate expression for the N₂O unimolecular reaction when temperature is variable is given by

$$\frac{d\alpha}{dt} = (1 - \alpha)C \exp\{-57,400/R(T_0 - B\alpha)\} \text{ sec.}^{-1} \quad (5)$$

The quantity C is the pre-exponential factor which is to be determined. Upon integration one obtains

$$\Psi = \int_0^{\alpha'} \frac{d\alpha}{(1 - \alpha) \exp\{-57,400/R(T_0 - B\alpha)\}} = Ct \quad (6)$$

The dependence of the rate integral Ψ on α was evaluated numerically with an IBM 7094 computer and is shown in Figure 3 for a number of shock temperatures.

The pre-exponential factor was determined by measuring α at known times from experimental records of the gated outputs of the mass spectrometer. Figure 4 illustrates typical oscillograms depicting the decomposition of N₂O with time. The value of the rate integral for a given measured α was then plotted against time (Figure 5). From the slope of the straight line, C was obtained. The fact that a straight line was observed is considered a test of eq. 5 and of the assumed temperature dependence.

Table I lists the values of C determined over a wide range of initial reflected shock temperatures and for the two sampling techniques. The same data are plotted

(9) G. B. Kistiakowsky and P. H. Kydd, *J. Am. Chem. Soc.*, **79**, 4825 (1957).

(10) The influence of reaction II and II' on the N₂O concentration may be estimated from Kaufman's rate constants [F. Kaufman, N. J. Gerri, and R. E. Bowman, *J. Chem. Phys.*, **25**, 106 (1956)] which give at 3000°K.

$$k_2 = 3 \times 10^{10} \exp(-14,500/RT) = 2.7 \times 10^9 \text{ cc./mole sec.}$$

$$k_2' = 10^{11} \exp(-15,500/RT) = 7.5 \times 10^9 \text{ cc./mole sec.}$$

$$(k_2 + k_2') = 1.02 \times 10^{10} \text{ cc./mole sec.}$$

With [O] taken equal to [N₂O] initially, the half-life of reactions II and II' is $\tau = 1/(k_2 + k_2')[\text{N}_2\text{O}] = 2000 \mu\text{sec.}$ where $[\text{N}_2\text{O}] = 5 \times 10^{-6}$ mole/cc. This half-life is compared to a half-life of about 50 $\mu\text{sec.}$ for reaction I. However, since [O] is actually increasing from zero and [N₂O] is decreasing with time, the half-life of reactions II and II' would be somewhat longer than that indicated above.

(11) H. S. Johnston, *J. Chem. Phys.*, **19**, 663 (1951).

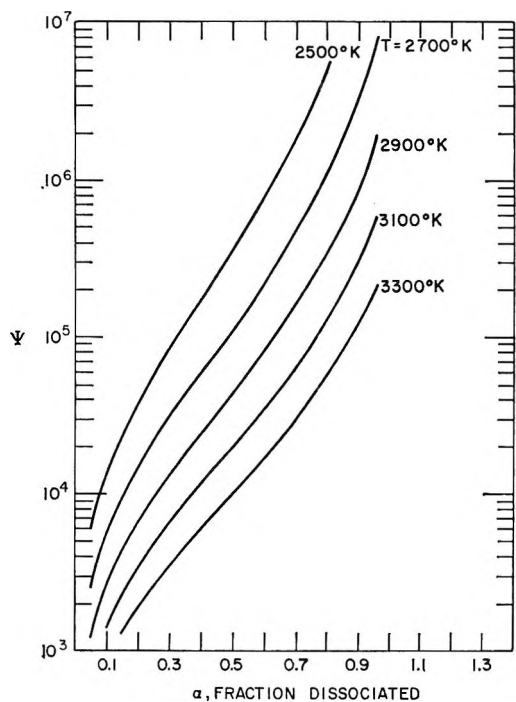


Figure 3. Dependence of rate integral on α for several reflected shock temperatures.

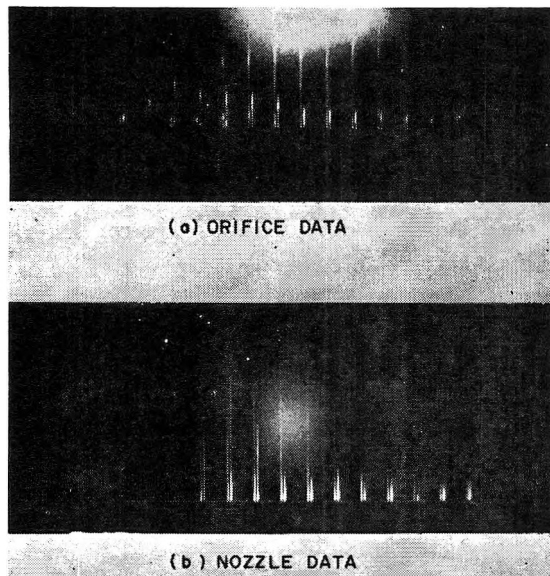


Figure 4. Experimental records of the gated output of the mass spectrometer. Analysis is every $25 \mu\text{sec}$. (a) First peak of doublet is Ar^{2+} ion peak. (b) Second peak represents N_2O^+ ion peak.

in Figure 6. The temperature dependence of the experimental rate constants and those of Bradley (ref. 4) are presented in Figure 7. The solid line is Johnston's extrapolated low temperature data. The dashed line represents the rate expression

$$k = 10^{15} \exp(-61,000/RT) \text{ cm}^3 \text{ mole}^{-1} \text{ sec}^{-1} \quad (7)$$

at a total concentration of 2.5×10^{-6} mole/cc., found by Jost, *et al.*,¹² who used a spectroscopic method to investigate the N_2O reaction at temperatures between 2800 and 4400°K. in shock waves.

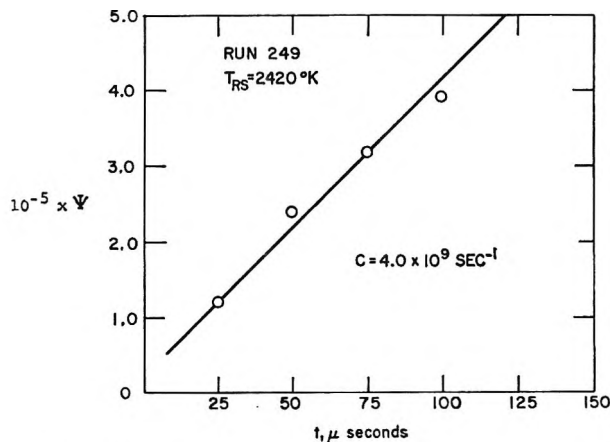


Figure 5. Plot of Ψ vs. time.

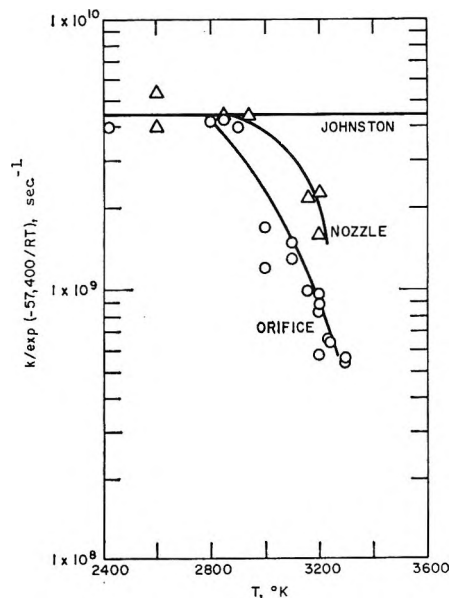


Figure 6. Variation of pre-exponential factor with temperature and method of gas sampling.

Discussion

It can be seen (Figure 6) that below 3000°K. both the simple orifice and nozzle sampling systems give nearly identical experimental results which compare favorably with Johnston's data. With pinhole sam-

(12) W. Jost, *et al.*, Symposium on Chemical Reactions in Shock Tubes, Duke University, April 20, 1964.

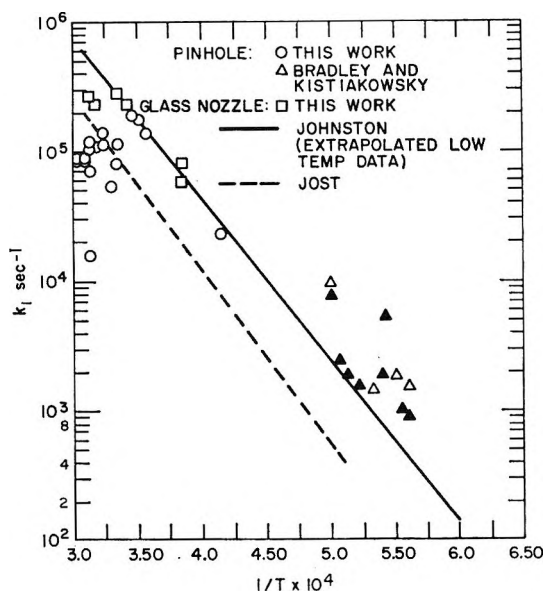


Figure 7. Initial first-order rate constant for N_2O decomposition vs. reciprocal temperature.

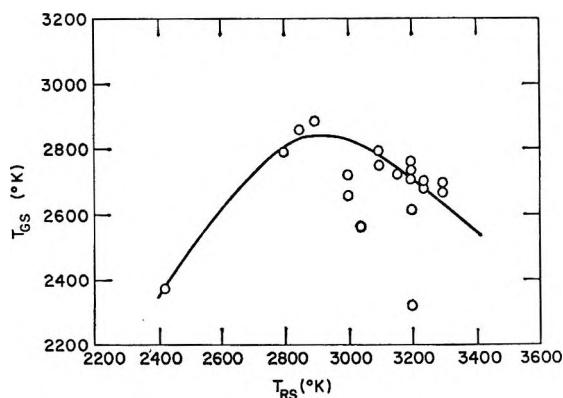


Figure 8. Variation of gas sample temperature with reflected shock temperature for pinhole sampling.

pling, end wall effects above this temperature become important and introduce a large systematic error in the measured rate constant. In the case of the nozzle, the error is only slightly reduced. Since the rate constant is a function of the temperature of the sampled gas, a comparison of the reflected shock temperature and that of the pinhole-sampled gas based on the measured rate constant can be made. The results, shown in Figure 8, indicate an increasing divergence between the reflected shock and sampled gas temperatures above 3000°K. Theoretical work involving an analysis of the flow field in the vicinity of the pinhole is under way in order to correlate the sampled gas temperature and the reflected shock temperature. However, it can be concluded from Figure 8 that, for chemical

Table I: Nitrous Oxide Experimental Rate Constants

Run	Sampling ^a method	Shock velocity, mm./μsec.	T_{RS} , °K.	$k/\exp(-57,400/RT)$, sec. ⁻¹
245	O	1.21	3300	5.4×10^8
246	O	1.21	3300	5.6×10^8
247	O	1.205	3240	6.4×10^8
248	O	1.205	3240	6.6×10^8
249	O	1.04	2420	4.0×10^9
250	O	1.20	3200	5.8×10^8
251	O	1.165	3000	1.2×10^9
255	O	1.175	3040	7.2×10^8
258	O	1.165	3000	1.2×10^9
260	O	1.20	3200	9.8×10^8
261	O	1.185	3100	1.3×10^9
262	O	1.19	3160	1.0×10^9
263	O	1.195	3200	8.8×10^8
264	O	1.20	3200	1.3×10^8
266	O	1.135	2850	4.3×10^8
267	O	1.185	3100	1.5×10^9
269	O	1.17	3000	1.7×10^9
271	O	1.130	2800	4.2×10^8
287	O	1.195	3200	8.4×10^8
292	O	1.145	2900	4.0×10^9
308	N	1.20	3200	2.3×10^9
310	N	1.19	3160	2.2×10^9
312	N	1.20	3200	1.6×10^9
313	N	1.15	2940	4.4×10^9
314	N	1.085	2600	5.4×10^9
315	N	1.135	2850	4.5×10^9
326	N	1.08	2600	4.0×10^9

^a O = orifice, N = nozzle.

reactions below a temperature of 3000°K., end wall effects will not be a serious source of error if neglected from mass spectrometer-shock tube studies.

Another sampling method which has been suggested to avoid end wall difficulties involves a series of expansion nozzles through which the reflected shock gas is passed before being analyzed by the mass spectrometer. Becker and co-workers¹³ have observed that the generation of molecular beams by expanding gases through a Laval nozzle leads to separation of the gas mixture, with heavier components being concentrated in the core of the jet. By yielding a gas sample not typical of the bulk gas in the reflected region, it seems such a multiexpansion sampling method would only serve to complicate the mass spectrometer results.

Acknowledgment. The author wishes to express his thanks to Mr. John LaGraff for assisting in the calculations and the collection and reduction of the data. This research was conducted under U. S. Air Force Contract AF04(094)-498, REST Program.

(13) F. W. Becker and K. Bier, *Z. Naturforsch.*, **9a**, 975 (1954).

Studies of the Hydrogen Held by Solids. VIII. The Decationated Zeolites

by Jan B. Uytterhoeven, L. G. Christner, and W. Keith Hall

Mellon Institute, Pittsburgh, Pennsylvania (Received February 9, 1965)

The sodium forms of the X- and Y-type zeolites contain enough hydrogen to terminate the crystal faces. This was shown by comparing the number of terminal hydroxyl groups, calculated as a function of crystal size, with experimentally measured values. It was found that a 1- μ particle should require 0.15×10^{20} OH/g. to satisfy the residual valences; a 0.1- μ crystal would need 1.4×10^{20} OH/g. The values measured by exchange with D₂ fell within this range. Also, the mean particle size, calculated from electron micrograph distributions, fell within the specified limits. When the zeolites were decationated, the hydrogen contents increased by as much as 50-fold, *i.e.*, to $\sim 10^{21}$ g.⁻¹. A correspondence was found between the decrease in the Na⁺ content and the increase in the hydrogen content. On decationation, a new OH frequency appeared at 3660 cm.⁻¹ in the infrared spectrum indicating that the proton introduced had reacted with the lattice to form a "trigonal aluminum" and an adjacent SiOH group. On adsorption of NH₃, this band decreased and disappeared concomitantly with the development of the NH stretching and bending vibrations of NH₄⁺. The hydrogen content and the intensity of the 3660-cm.⁻¹ absorption band decreased when the zeolite was heated above 500°. This was interpreted as being due to the loss of water from pairs of decationated sites. In this process, one alumina tetrahedron was re-formed while an oxygen from an AlOSi bridge was removed; the negative charge residing on the alumina tetrahedron is balanced by a positive charge on a trigonally coordinated silicon ion.

In their sodium forms, the X- and Y-type zeolites require no hydrogen to satisfy their internal crystal structure; hydroxyl groups are required, however, to terminate the lattice at the crystal faces at points where bonding would occur were the solid phase extended. One or more forms of chemisorbed water may also be present, as could H₃O⁺, corresponding to a cation deficiency. Several studies¹⁻⁵ have been made of the spectra from zeolites in various stages of hydration but the authors have not always agreed on the assignment of infrared bands to particular species. Notably, Bertsch and Habgood⁴ found no evidence of structural surface hydroxyl groups in Na⁺, Li⁺, or K⁺ type-X zeolites after degassing at 500°, whereas Carter, Lucchesi, and Yates⁵ reported three (and sometimes four) distinct OH stretching bands after similar drying. The former authors attributed bands which appeared (at 3695 and 3400 cm.⁻¹) when small amounts of H₂O were "added back" to isolated water molecules adsorbed simultaneously by ion-dipole interaction

with the exchangeable cations and by hydrogen bonding of one of the hydrogens to an oxygen of the zeolite surface. The latter have⁵ attributed bands at 3750 and 3695 cm.⁻¹ to SiOH and AlOH stretching modes, respectively; bands located between 3590 and 3655 cm.⁻¹ were assigned to hydroxyl groups associated with the exchangeable cations. It was concluded that the surfaces of molecular sieves are complex and contain OH groups as impurities in common with surfaces of other less well-crystallized oxides. As somewhat different sample preparation, as well as different spectroscopic, techniques were used in the two investigations,

(1) G. J. C. Frohnsdorff and G. L. Kingston, *Proc. Roy. Soc. (London)*, **A247**, 469 (1958).

(2) H. A. Szymanoski, D. N. Stamires, and G. R. Lynch, *J. Opt. Soc. Am.*, **50**, 1323 (1960).

(3) S. P. Zhadanov, A. V. Kiselev, V. I. Lygin, and T. I. Titanova, *Dokl. Akad. Nauk SSSR*, **150**, 584 (1963).

(4) L. Bertsch and H. W. Habgood, *J. Phys. Chem.*, **67**, 1621 (1963).

(5) J. L. Carter, P. J. Lucchesi, and D. J. C. Yates, *ibid.*, **68**, 1385 (1964).

it was clear that further work was needed to resolve these contradictory conclusions. In particular, it was apparent that a quantitative comparison of the amount of hydrogen present with the amount required to terminate the crystal lattice would be helpful. In the present work, hydrogen contents were determined in three different ways. The amount of hydrogen corresponding to hydroxyl groups necessary to terminate the crystal lattice was theoretically calculated for the particle size distribution determined from several electron micrographs. The total hydrogen contents were then measured by exchange with D_2 and by destructive thermogravimetric determinations carried out under vacuum to 1000° . Aliquots of the samples studied by Bertsch and Habgood⁴ and by Carter, Lucchesi, and Yates⁵ were included in this work.

Earlier workers have noted that structural hydroxyl groups may be present in zeolites due to a hydrolysis of some of the base-exchanged cations during preparation; usually, there is a deficiency of several per cent in the amount of sodium required to just balance the AlO_2^- tetrahedra. So far, however, no detailed study has been made of the decationation process which occurs when part of the Na^+ is replaced by metathesis with NH_4^+ , followed by heating to remove NH_3 . Moreover, the existing infrared data deal almost exclusively with X-type zeolites; only scattered mention of results for Y-type zeolites has appeared. In the present work, a study of the decationation process was made utilizing both infrared spectroscopy and hydrogen content measurements; X- and Y-type zeolites were compared.

Recently, it was suggested⁶ that the protons freed when zeolites are decationated react with Si-O-Al bonds to form a trigonal aluminum ion and an adjacent SiOH group. This suggestion was partially confirmed and the chemistry of decationation was considerably clarified in the present work. The several kinds of acid sites which may be formed are clearly defined.

Experimental

Materials. The X- and Y-type zeolites (Lot No. 137396 and 1280-6, respectively) were supplied by the Linde Co. in the sodium form. The Ca^{2+} and NH_4^+ samples were prepared from the Na^+ forms by conventional cation-exchange procedures using Baker analytical grade $Ca(NO_3)_2$ and NH_4Ac . The preparations were washed free from excess salt by ten centrifugal washings with distilled water followed by two slow sedimentations out of a large excess of distilled water. The degree of ion exchange was determined by flame photometric sodium analyses. The silicon and aluminum analyses were furnished by the Linde Co. The

analytical data are summarized in Table I. Drs. Habgood⁴ and Yates⁵ kindly supplied samples of the Na^+ X used in their respective investigations.

The D_2 was from the Liquid Carbonics Division of General Dynamics Co.; it had a nominal purity of 99.7%, the principal impurity being HD. It was passed through a Pd thimble before use. Linde NH_3 was used. It was purified by a freeze-pump-thaw technique and was double distilled from Dry Ice baths.

Hydrogen Content Measurements. The experimental details of the rising temperature D_2 -exchange method are explained in earlier papers.^{7,8} Initial determinations were made using this technique, terminating at 1040° . As it was found that equilibrium was attained at 500° , the remaining determinations were carried out at this temperature. Care was taken in the initial pretreatment to avoid hydrothermal reaction; 1-2-g. samples were evacuated (at $\sim 10^{-5}$ torr) for 2 hr. at room temperature before heating; the temperature was then raised at a rate of about $5^\circ/\text{min.}$ to the pretreatment temperature specified in Table I as evacuation was continued. The samples were then treated with flowing dry O_2 for 4 hr. to remove any remaining organic impurities and evacuated overnight at the same temperature before contact with D_2 .

Thermogravimetric determinations were carried out in a vacuum thermobalance using a heating program of $1.7^\circ/\text{min.}$, terminating at 1000° . Since the infrared data indicated that molecular H_2O and other impurities were removed by evacuation below 450° , the hydroxyl contents could be calculated from the loss in weight between 500 and 1000° .

Infrared Studies. Thin wafers, transparent to infrared radiation, were prepared by pressing the zeolites between polished stainless steel plates to about 5 tons/ in.^2 . The "thickness" varied between 1.5 and 4 mg./cm.^2 . The platelets were mounted on a platinum support fixed to a quartz slider which enabled them to be moved from between the salt windows to the opposite end of the quartz tube where they could be heated and to be replaced reproducibly for spectroscopic examination. The cell was adopted from Yates and Lucchesi⁹; it could be used in conjunction with a conventional high-vacuum system and the sample could be heated and treated with gases at any desired temperature.

(6) J. G. Larson, H. R. Gerberich, and W. K. Hall, *J. Am. Chem. Soc.*, **87**, 1880 (1965).

(7) W. K. Hall, H. P. Leftin, F. J. Cheselske, and D. E. O'Reilly, *J. Catalysis*, **2**, 506 (1963).

(8) W. K. Hall, F. J. Cheselske, and W. E. Wallace, *J. Phys. Chem.*, **63**, 505 (1959); **65**, 128 (1961).

(9) D. J. C. Yates and P. J. Lucchesi, *ibid.*, **35**, 243 (1961).

Table I: Analytical Data for Zeolites

Zeolite type and base-exchange cation	AlO ₂ ⁻ content, ions/g. × 10 ⁻²⁰	Na ⁺ content, ions/g. × 10 ⁻²⁰	Decationated sites per gram × 10 ⁻²⁰		Pre- treatment temp., °C.	Hydroxyl content		
			Max. ^a	Min. ^b		Deuterium exchange, OH/g. × 10 ⁻²⁰	Thermo- gravimetric, OH/g. × 10 ⁻²⁰	% de- hydroxylation ^c
X (Na ⁺)	34.1	31.7	2.4	0	430	0.56	...	
X (Na ⁺)	34.1	450	0.47	...	
X (Na ⁺)	34.1	31.4	2.7	0	450	0.68	...	
X (Ca ²⁺)	34.1	6.0	530	1.84	...	
X (Ca ²⁺)	34.1	6.0	475	1.47	...	
X (NH ₄ ⁺ I)	34.1	18.4	15.7	13.4	505	6.00	...	58.9
X (NH ₄ ⁺ II)	34.1	15.0	19.1	16.8	500	9.65	...	46.3
X (NH ₄ ⁺ II)	34.1	15.0	19.1	16.8	460	10.24	...	
X (NH ₄ ⁺ III)	34.1	11.0	23.1	20.7	500	3.50	...	84.0
X (NH ₄ ⁺ IV)	34.1	5.8	28.3	25.9	520	2.2	...	91.9
X (NH ₄ ⁺ IV)	34.1	5.8	28.3	25.9	490	5.5	...	
Y (Na ⁺)	26.3	25.7	0.6	0	500	0.29	...	
Y (Ca ²⁺)	26.3	5.3	470	0.61	...	
Y (NH ₄ ⁺)	26.3	5.2	21.0	20.4	440	30.4	25.7	...
Y (NH ₄ ⁺)	26.3	5.2	21.0	20.4	490	11.2	19.5	45.9
Y (NH ₄ ⁺)	26.3	5.2	21.0	20.4	520	12.4	18.3	40.1
Y (NH ₄ ⁺)	26.3	5.2	21.0	20.4	590	2.9	6.7	86.0
Y (NH ₄ ⁺)	26.3	5.2	21.0	20.4	690	2.7	3.3	87.0
Y (NH ₄ ⁺)	26.3	5.2	21.0	20.4	770	0.39	2.5	98.1
X (Na ⁺) ^d	(4%) ^d		500	0.59
X (Na ⁺) ^e	(0%) ^e		500	0.18

^a The maximum number of decationated sites is determined by the difference in the sodium and aluminum content. ^b The minimum number of decationated sites is the difference in the sodium content of a sample from the value as measured for the sodium sample. ^c Per cent dehydroxylation was calculated from the difference between the mean number of decationated sites and the hydroxyl content as measured by deuterium exchange. ^d Reference 5. ^e Reference 4.

Spectra were taken at room temperature using a Beckman IR-7 grating spectrometer; NaCl windows were used on the cell. The spectral region between 1200 and 4000 cm.⁻¹ was examined. The spectrograph was set at a gain of 3.5% in order to obtain a reasonably low noise. The slit was adjusted to effect a transmission of 80% in single beam at 3800 cm.⁻¹ for the OH and NH stretching region and was similarly reset at 1350 cm.⁻¹ for recording spectra in the bending region. The actual slit openings ranged between the standard openings (0.37 mm. at 1350 cm.⁻¹) and 1.5 times the standard opening in the deformation region. Under these operating conditions the resolution was close to 1 cm.⁻¹ in the deformation region and 10 cm.⁻¹ in the stretching region. At high frequencies, the energy loss by scattering was much higher and slit openings of 1-1.5 mm. were required. These values are comparable with, but in general somewhat lower than, those reported by Carter, Lucchesi, and Yates.⁵

The platelets were heated under vacuum to successively higher temperatures and the spectra were taken. After heating to 500°, no difference could be detected between untreated waters and those heated in O₂.

Therefore, the latter step was omitted in most of this work. When NH₃ was adsorbed, small amounts of this gas were admitted from a calibrated volume; the pressure was controlled by condensing excess NH₃ in a thermostat at the temperature of Dry Ice. A single dose contained about 15 μmoles. Water adsorptions were carried out in the same manner with the vapor pressure fixed at 0°.

Results

The pertinent analytical data for the zeolites are contained in Table I along with the results from the D₂-exchange experiments. In the Na⁺ and Ca²⁺ forms, the hydrogen contents (second from last column) were much lower than in the decationated zeolites. Likewise, the amounts of hydrogen present were much less than one atom for each base-exchanged cation or for each AlO₂⁻ tetrahedron. The hydrogen associated with the Ca²⁺ form was always several times larger than with the Na⁺ form. A similar observation was reported by Pickert, Rabo, Dempsey, and Schomaker.¹⁰ The higher values can be explained if, in one way or another, water molecules are associated with the ex-

changeable cations, *e.g.*, as suggested by Bertsch and Habgood.⁴

In order to assess these data, it was necessary to estimate the amount of hydrogen required to terminate the giant molecules at the crystal faces. A model to do this is derived in the Appendix. A particle size count was made from electron micrographs of the Na⁺ X zeolite. In agreement with the information supplied by Linde, most of the particles were in the range 0.1–2 μ ; the size number average was 0.3 μ . The integrated hydrogen content per gram of zeolite was calculated from the distribution with the aid of the theory. The result (0.46×10^{20} OH/g.) agreed, perhaps fortuitously, with the 0.57×10^{20} OH/g. found experimentally. In a similar vein, it was calculated that particles 0.1 and 1 μ along their edges should require 1.9×10^{20} and 0.15×10^{20} OH/g. respectively, to terminate the lattice. It is clear that most of the hydrogen present in the Na zeolite can be accounted for in this way. The data found for the sample of Bertsch and Habgood tend to substantiate this view. These workers removed the smaller particles by a sedimentation procedure. The sample supplied us had an average size of about 1 μ . As expected, the hydroxyl content of this sample was lower than that of the unrefined sieve. The sample supplied by Yates appeared to be quite similar to ours. This difference in particle size may be one of the factors responsible for the discrepancy between the results of Bertsch and Habgood⁴ and of Carter, Lucchesi, and Yates.⁵

When the zeolites were decationated by heating the NH₄⁺ forms, the residual hydrogen contents were several orders of magnitude higher than in the parent Na⁺ forms. No NH₄⁺ remained in samples heated to 500°, however, as was demonstrated by infrared and by Kjeldahl determinations. Thus, the increased hydrogen is evidently due to the protons liberated when NH₃ was driven from the catalyst. There is, in fact, reasonable agreement between the hydrogen contents found for the sieves decationated under optimum conditions and the number of decationated sites. This can be seen by comparing columns 4 and 5 of Table I with columns 7 and 8. The hydrogen contents are now of the same order of magnitude as the concentration of base-exchange cations. Since the exchange with D₂ took place in the same temperature range for the decationated zeolites as was previously found for silica-alumina,⁷ it may be supposed that the protons left to neutralize the negative charge on the alumina tetrahedra reacted with oxygen of the lattice to form hydroxyl groups.

The amount of hydrogen held by decationated Y-zeolites was clearly a function of the temperature of pre-

treatment. It will be shown later that the OH content was a maximum after heating at 290° and that heating to higher temperatures resulted in secondary dehydroxylation.

The data for the X-zeolite indicated that the stability against dehydroxylation was dependent upon the extent of decationation. It is known that the decationated zeolites are less heat resistant than the sodium-saturated forms, the decationated X-type being less stable than the Y. The per cent dehydroxylation (last column of Table I) can be considered as an inverse measure of the stability of the sieves. Dehydroxylation of the Y-type zeolite became critical between 520 and 590°; this was confirmed by the thermogravimetric curves.

If the protons liberated by decomposition of the ammonium ion attacked the lattice as supposed, the hydroxyl groups formed should produce an infrared band. Moreover, the data of Table I indicated that this band should be fairly strong, and its frequency should correspond to that due to the sodium deficiency in the previously studied Na⁺ form.^{2,4,5} Spectra were taken to confirm this prediction. Anhydrous NH₃ was added to test whether NH₄⁺ would re-form, *i.e.*, whether the hydrogen could act as a Brønsted acid.

The frequencies of the infrared bands found in this work and their assignment are listed in Table II. The regions of interest lie between 2800 and 3800 cm.⁻¹, corresponding to the OH and NH stretching frequencies, and between 1300 and 1700 cm.⁻¹, where the corresponding bending vibrations appear. For reference, Lewis-bound NH₃ may best be distinguished from NH₄⁺ by their ν_4 bending vibrations; a band near 1630 cm.⁻¹ is characteristic of chemisorbed NH₃ while NH₄⁺ is characterized by bands between 1400 and 1500 cm.⁻¹. Spectra of H₃O⁺ in crystals^{11,12} have a very broad band in the region between 2900 and 3300 cm.⁻¹, the frequency varying with the environment. A band between 1690 and 1750 cm.⁻¹ seems to be characteristic of these ions for both solids¹¹ and in solution.¹² In agreement with earlier workers, we have found no trace of such a band even when H₂O was "added back" to the zeolite. The characteristic water bending vibration at about 1650 cm.⁻¹ was observed under some circumstances, but could usually be removed by evacuation at room temperature. Similar results have been reported for a silica-alumina catalyst.¹³

(10) P. E. Pickert, J. A. Rabo, E. Dempsey, and V. Schomaker, Proceedings of the 3rd International Congress on Catalysis, Amsterdam, 1964, Preprint No. I. 43.

(11) C. C. Ferisco and D. F. Hornig, *J. Chem. Phys.*, **23**, 1464 (1955).

(12) M. Falk and P. A. Giguere, *Can. J. Chem.*, **35**, 1195 (1957).

(13) M. R. Basila, *J. Phys. Chem.*, **66**, 2223 (1962); M. R. Basila, T. R. Kantner, and K. H. Rhee, *ibid.*, **68**, 3197 (1964).

Table II: The Infrared Absorption Bands Observed with Decationated Zeolites and Their Assignments

Frequency, cm. ⁻¹	Assignment	Zeolite
3660-3680	OH stretching	X and Y
3605	OH stretching	X (NH ₄ ⁺ I and II)
3570	OH stretching	Y and X (NH ₄ ⁺ III and IV)
3423	ν_3 stretching NH ₄ ⁺	X and Y
3385	ν_3 stretching NH ₃ solid ?	X and Y
3320	ν_1 stretching NH ₃	X and Y
3275-3200	ν_3 stretching NH ₄ ⁺	X and Y
3000-2950	ν_3 stretching NH ₄ ⁺	X and Y
1682	NH ₄ ⁺ deformation (probably ν_2)	Y and X (NH ₄ ⁺ III and IV)
1650	H ₂ O deformation	
1630	ν_4 NH ₃ deformation	
1505-1485	ν_4 deformation NH ₄ ⁺	X and Y
1435-1475	ν_4 deformation NH ₄ ⁺	X and Y

When the Na⁺ zeolites were dehydrated above 450°, in agreement with Bertsch and Habgood,⁴ the infrared spectra showed no bands over the entire range. Nevertheless, hydrogen was present, as shown by our assay. This hydrogen could be present in two forms, *i.e.*, SiOH with a band near 3750 cm.⁻¹ and AlOH with an absorption expected near one of the vibrations of alumina.¹⁴ Yates, *et al.*,⁵ observed three bands in the OH stretching region at 3750, 3695, and 3655 cm.⁻¹ which they assigned to SiOH, AlOH, and OH associated with the Na⁺ ion, respectively. We do not question the existence of these bands nor the assignment of the two of higher frequency. As will be shown later, however, their band at 3655 cm.⁻¹ probably corresponded to a few decationated sites. Evidently, they were able to obtain these spectra because of superior spectroscopic techniques, particularly external focusing, which enabled them to increase the transmission so that thicker samples could be used. There is, therefore, really no discrepancy between these works.^{4,5} Rather, the apparent divergence was caused by differences in hydration level, resolution, and limit of detection at the lower hydration levels. Since the workers were not taking spectra of the same entities, both may be correct in their interpretations.

Because of the much higher hydrogen contents of decationated zeolites (Table I), the OH vibrations from these samples were easily detected. The positions of the bands are included in Table II, where the assignments of all bands evidenced in the present work are summarized.

The decationation process was clarified by the data contained in Figures 1-3. When the NH₄⁺ form of a

Y-type zeolite was heated, bands in the OH stretching region developed (Figure 1) while bands in the NH stretching (Figure 2) and bending (Figure 3) regions decreased and finally disappeared. The principal OH vibration was always found near 3660 cm.⁻¹; this had a tendency to shift to higher wave numbers (maximum of 3680 cm.⁻¹) at lower outgassing temperatures. This band corresponded well to the shoulder found at lowest frequency on the Na⁺ zeolite by Yates, *et al.*⁵ Samples which had been decationated to high extents of the total exchange capacity were characterized by a second intense band near 3570 cm.⁻¹ (Figure 1). In the X-type zeolites, the second band was less important and, with samples which had been decationated to less than 10%, was shifted to 3605 cm.⁻¹. Dehydroxylation affected the lower frequency somewhat more than the higher frequency OH band. The 3570-

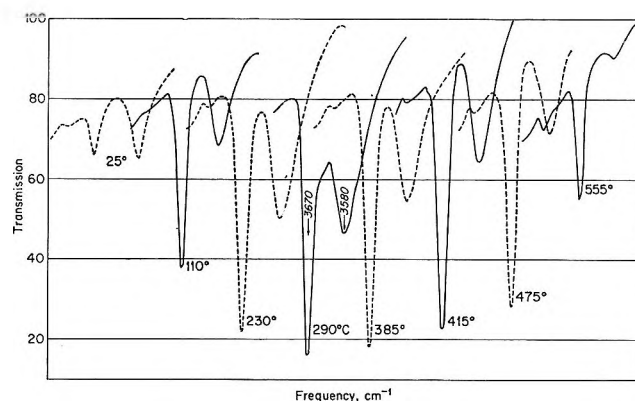


Figure 1. Development of OH stretching bands as a Y-type NH₄⁺ zeolite is decationated by evacuation at increasing temperatures.

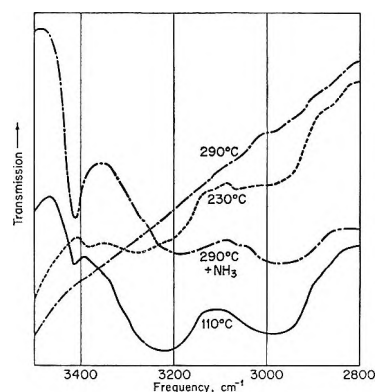


Figure 2. Elimination of NH stretching bands as a Y-type zeolite is decationated; all three are NH₄⁺, ν_3 bands.

(14) J. B. Peri, *Actes. Congr. Intern. Catalyse, 2^e, Paris, 1960*, 1, 1333 (1961).

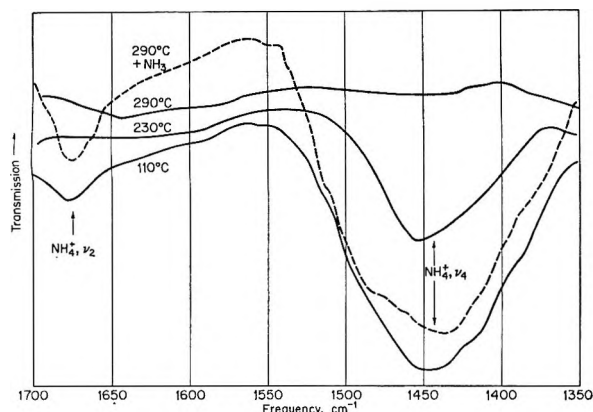


Figure 3. Elimination of NH_4^+ bending modes as a Y-type zeolite is decationated.

cm^{-1} band had completely disappeared in the X-type sieves at 490° , whereas in the Y-type, it was still present, although weak, after evacuation at 555° . This may be considered as another indication of the greater stability of the Y-, as compared with the X-type, sieve.

Table III lists the OH frequencies observed for samples from which increasing amounts of Na^+ had been removed. The per cent dehydroxylation at 520° was evaluated from the infrared data by comparing the absorbance at 3660 cm^{-1} to its maximum value determined for the same sample at 290° . The values are consistent with the dehydroxylation figures listed in Table I and confirm earlier considerations concerning the relative stabilities of the X- and Y-type zeolites.

Table III: Effect of Degree of Decationation on OH Stretching Frequencies

Zeolite	% decationation	OH stretching frequency	Relative intensity ^a
X (NH_4^+ I)	46.4	3660 3605	...
X (NH_4^+ II)	55.6	3660 3640 ^b 3605	30.7
X (NH_4^+ III)	67.4	3660 3570	17.5
X (NH_4^+ IV)	83	3660 3570	5.2
Y (NH_4^+)	80	3660 3570	43.0

^a This is the intensity of the 3660-cm^{-1} band after outgassing at 520° , expressed in percentage of the maximum intensity observed at 290° . ^b Shoulder.

The spectra from unheated NH_4^+ sieves contained bands at 3423 , 3200 , and 2990 cm^{-1} in the stretching region (Figure 2) and at 1435 , 1485 or 1505 , and 1680 cm^{-1} in the bending region (Figure 3). As shown elsewhere,¹⁵ all of these bands may be attributed to

NH_4^+ ions. Although the band at 1680 cm^{-1} is close to the H_3O^+ bending frequency, it cannot be attributed to this species because it could be restored by chemisorption of NH_3 (dashed line, Figure 3). No important difference between X- and Y-type zeolites was found. Evacuation at 290° was sufficient to eliminate the NH_4^+ bands. The OH bands reached their maximum intensity at this same temperature and tended to diminish at higher temperatures. At 500° and above, a very weak band appeared near 3750 cm^{-1} which was attributable to isolated SiOH . This may possibly be due to a small amount of decomposition. Figures 2 and 3 also show that the NH_4^+ ion was regenerated when the sample was contacted with gaseous NH_3 , *i.e.*, that the decationation was reversible.

The results from a more detailed study of the changes which occur on readsorption of NH_3 or $\text{NH}_3 + \text{H}_2\text{O}$ on decationated Y-type zeolites are contained in Figures 4 and 5. In the stretching region, the intensity of the OH bands decreased proportionally with the amount of NH_3 adsorbed; they finally disappeared completely. Simultaneously, bands corresponding to NH_4^+ appeared in both the stretching and the bending regions. In the stretching region, the sharp band at 3423 cm^{-1} appeared first; this was followed by the broader bands at 2990 and 3200 cm^{-1} . In the bending region, the 1435- and 1485-cm^{-1} bands were clearly resolved and the band at 1680 cm^{-1} also appeared. Curves 1-4 of Figures 4 and 5 correspond to spectra taken after 0, 1, 2, and 3 doses of $15 \mu\text{moles}$ of NH_3 were added at

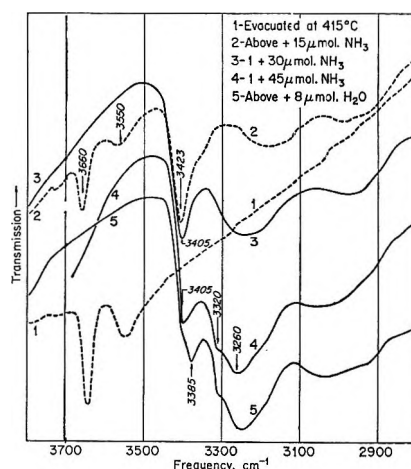


Figure 4. Spectral changes on readsorption of NH_3 or $\text{NH}_3 + \text{H}_2\text{O}$ on a decationated Y-type zeolite after evacuation at 415° : stretching region.

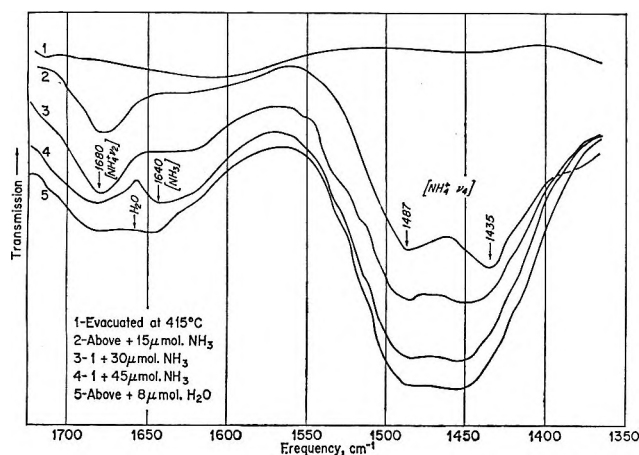


Figure 5. Spectral changes on readsorption of NH₃ or NH₃ + H₂O on a decationated Y-type zeolite after evacuation at 415°: bending region.

room temperature to a film weighing 8 mg. which was about 80% decationated. Since each dose was equivalent to 12×10^{20} NH₃/g., the spectral results are seen to be in excellent agreement with the residual hydrogen associated with the decationated sites (the plate had been pretreated at 415°). The bands corresponding to Lewis-bonded NH₃ were not observed with samples pretreated at temperatures lower than 300° but were evident with samples heated at temperatures where extensive dehydroxylation occurred. Thus, the shoulder at 3320 cm.⁻¹ on curves 4 and 5 of Figure 4 is indicative of this species. The addition of H₂O on top of chemisorbed NH₃ (curve 5) resulted in only minor changes. The NH₄⁺ bands in the 2900–3300- and the 1450–1500-cm.⁻¹ regions strengthened somewhat and the twin band at 1640 and 1680 cm.⁻¹ was merged by the superposition of the bending vibration from adsorbed H₂O at about 1660 cm.⁻¹. The principal difference was the appearance of a new band at 3385 cm.⁻¹ which coincides with the ν_3 frequency of solid ammonia.

Figures 4 and 5 relate to the Y (NH₄⁺) zeolite, but the same behavior was followed with the X zeolites provided that the pretreatment had not caused substantial dehydroxylation. The principal difference was that the 1485-cm.⁻¹ band was shifted to 1505 cm.⁻¹ in the case of the X sieves. The mechanism of NH₃ adsorption was changed when samples were dehydroxylated to an important extent. Figure 6 contains data for X (NH₄⁺ III) pretreated at 530°. In order to observe the same type of behavior for the Y sieve, the sample had to be heated at 600°. When the platelet was contacted with 15 μmoles of NH₃ (curves 2 and B), the NH₄⁺ bands at 3275 and 1475 cm.⁻¹

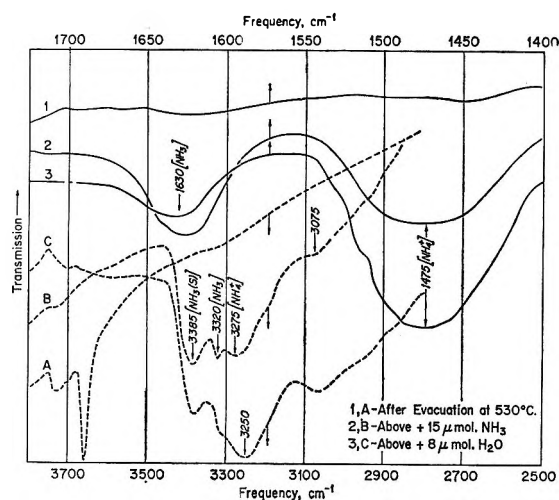


Figure 6. Spectral changes on readsorption of NH₃ or NH₃ + H₂O on a decationated X-type zeolite after evacuation at 530°.

appeared along with the bands for Lewis-bound NH₃ (at 3320 and 1630 cm.⁻¹). The 1680-cm.⁻¹ band, found for the Y-type sieves, was not evident but the ν_3 frequency of solid ammonia (3385 cm.⁻¹) appeared strongly. Addition of 8 μmoles of H₂O (curves 3 and C) resulted in an increase in the NH₄⁺ bands at 3275 and 1475 cm.⁻¹ coupled with a concomitant decrease in the 1630-cm.⁻¹ band of Lewis-bound NH₃. Basila, *et al.*,¹³ observed a similar transformation with silica-alumina when H₂O was added. Similarly, Fripiat and co-workers¹⁶ reported the formation of NH₄⁺ when NH₃ was adsorbed on silica-alumina outgassed at low temperature. These observations differ markedly from those reported for alumina,¹⁷ where the OH groups remained essentially unaffected by the chemisorption of NH₃. With this material, chemisorption appeared to involve the formation of additional OH and NH₂ groups.

Basila¹³ noted a weak band at 1394 cm.⁻¹, which appeared on dehydration of acidic silica-alumina. He tentatively assigned this to an AlO vibration, or overtone, and supposed that it was related to the catalytically active sites. No such band was found in the present work with the decationated zeolites, even though these materials are active cracking catalysts.

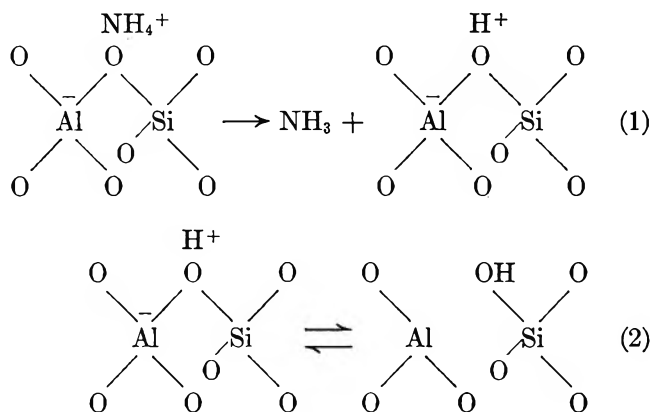
Discussion

The formation of structural OH groups on heating ammonium-exchanged zeolites is not surprising. When NH₃ is released, the protons left to neutralize the negative charge on the alumina tetrahedra can only be

(16) J. J. Fripiat, A. Leona-d, S. Suzuki, and J. B. Uytterhoeven, *J. Phys. Chem.*, in press.

(17) J. B. Peri, *ibid.*, 69, 231 (1965).

screened by reaction with lattice oxygen. The appearance of the OH stretching vibrations at 3570 and 3660 cm.^{-1} indicates that the proton has attached itself to a particular oxygen rather than remaining freely mobile. This chemistry may be represented by eq. 1 and 2.



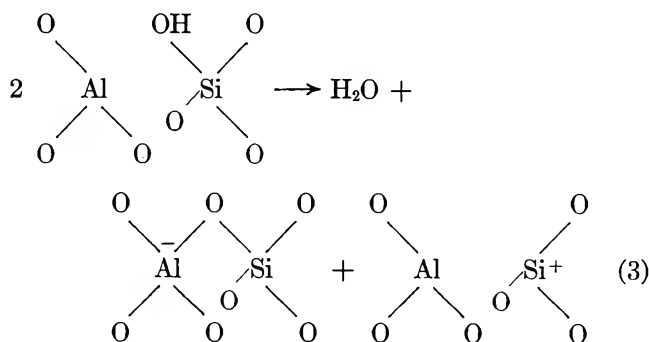
The right-hand member of eq. 1 represents a classical Brønsted acid. The absence of a broad infrared band in the 2900- cm.^{-1} region suggests that this species is not present in substantial quantity at room temperature. Nevertheless, protons can be supplied through the equilibrium of eq. 2, on the approach of a strong base such as NH_3 . With a weaker base, the magnitude of the equilibrium constant may be critical and this will be a function of temperature. If the left-hand member of eq. 2 is an excited state of the right-hand member, *i.e.*, the reaction is exothermic in the direction written, then the concentration of Brønsted acid will increase with temperature. This factor should be considered in the treatment of the kinetics of hydrocarbon reactions.

When a structural hydroxyl group forms at a deca- tionated site, the formal bond between aluminum and oxygen is broken. The question now arises as to whether this "trigonal" aluminum can act as a Lewis acid. Examination of a model of the oxygen lattice revealed that the geometry would change slightly, if at all, when protons react with the lattice. Hence, aluminum ions would not become accessible to the gas unless they passed through the planes of the remaining three oxygens of the original tetrahedra and reacted on the other side. There are three distinct locations for oxygen in the zeolite lattice, *viz.*, on square faces, on hexagonal rings, and on bridges between cuboctahedra. When a hydroxyl group forms at one of the latter two, inversion of the aluminum ion would make it accessible only inside a cuboctahedron, from which all but very small molecules are excluded. At the third location, however, inversion would make an aluminum ion available to the gas inside of the large cavities. This

could act as a Lewis acid, but because the process of eq. 2 neutralizes the electrical charge on the lattice, this would not be a very strong site. Nevertheless, for this very reason such sites could be catalytically important.

The force constant of the OH bond of the deca- tionated zeolite is smaller than that observed for silica gel and for silica-alumina. For both of these materials, the frequency for isolated OH groups appeared at about 3750 cm.^{-1} .¹³ The lower frequency found for the zeolites (3660 cm.^{-1}) suggests that there is considerable interaction between the hydroxyl oxygen and the adjacent aluminum ion. This is consistent with the ready reversibility exhibited by the system. When the deca- tionated zeolite is contacted with NH_3 , the NH_4^+ ion is reconstituted and the original tetrahedra re-form. The occurrence of a second OH band appearing at still lower frequency indicates that all of the OH groups do not have the same environment. As noted above, several distinct oxygen ion sites are present, but the available data do not permit a definite assignment. Although the infrared frequency is a notably poor indication of acid strength, it is of some interest that the OH frequencies from the carboxylic acids fall near those of this work, *e.g.*, 3574 \pm 3 for CH_3COOH ^{18,19} and 3587 cm.^{-1} for CF_3COOH ²⁰⁻²² in the gas phase.

The deamination reaction is not completely reversible when the sample has been partially dehydroxylated. In this case, a new kind of site is formed. The process may be pictured by



The data of Table I establish that most of the hydrogen introduced when the zeolite is deca- tionated can be removed by evacuation above 500°; this was confirmed by the decreasing intensity of the OH stretching bands (Figure 1 and Table III). Evidently, H_2O is lost

(18) S. Bratoz, D. Hadzi, and N. Sheppard, *Spectrochim. Acta*, **8**, 252 (1956).

(19) J. K. Wilmshurst, *J. Chem. Phys.*, **25**, 1171 (1956).

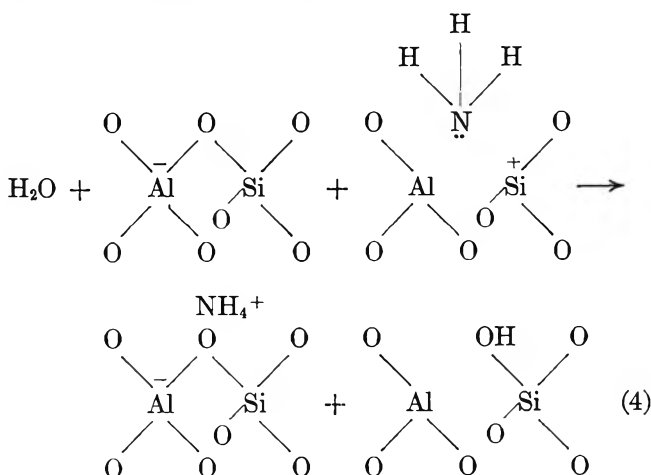
(20) N. Fuson, M. L. Josien, E. A. Jones, and J. R. Lawson, *ibid.*, **20**, 1627 (1952).

(21) R. E. Kagarise, *ibid.*, **27**, 519 (1957).

(22) N. Fuson and M. L. Josien, *J. Opt. Soc. Am.*, **43**, 1102 (1953).

from pairs of decationated sites, reclosing one tetrahedron while an oxygen atom is lost from the other. In this way, accessible trigonal aluminum is formed adjacent to trigonal silicon ions, the latter bearing a net positive charge which balances the negative charge of the reclosed alumina tetrahedra, elsewhere in the structure. Average Si coordination numbers less than 4.0 have been reported²³ for alumina-rich silica-alumina catalysts after evacuation at elevated temperatures. This picture is also supported by the finding of Turkevich and co-workers²⁴ that one molecule of quinoline was capable of poisoning about two decationated sites. Dehydroxylation leads to the formation of extremely strong electrophilic sites (hereinafter called defect sites) which should be capable of abstracting hydride ions from triphenylmethane,²⁵ removing electrons from polynuclear aromatic hydrocarbons,^{24,26,27} or strongly chemisorbing quinoline. Rabo, *et al.*,²⁸ and Stamires and Turkevich²⁶ visualized defect sites identical with these. They also supposed that the protons liberated when NH_3 was evolved would react with lattice oxygen. No spectra were presented, but it was stated²⁸ that a new band appeared at 2.8μ (3570 cm.^{-1}) in decationated sieves. Stamires and Turkevich²⁶ suggested that prior to dehydroxylation the "protons form strong hydrogen bonds with the crystal lattice." We attribute the 3660-cm.^{-1} frequency to a nonhydrogen-bonded OH group, because a study of the model makes hydrogen bonding seem unlikely.

The ammonium ion cannot form on the defect sites because no hydrogen is available; NH_3 must now be chemisorbed in a molecular form. Restated, the Brønsted acid of eq. 1 and 2 has been converted to the Lewis acid of eq. 3. It was demonstrated (Figure 6) that addition of H_2O to the Lewis-bound NH_3 caused the NH_4^+ ion to re-form, *i.e.*



Presumably, when triphenylamine is substituted for

NH_3 , the interaction with the defect sites is strong enough to cause ionization of the substrate to its radical ion.

In conclusion, it may be supposed that the active acid sites of silica-alumina catalysts are formed by analogous processes. The simultaneous presence of Lewis and Brønsted sites on the same surface may be readily understood in these terms. There are, however, a very much larger number of OH groups required to terminate the silica-alumina surface than to terminate the giant molecule crystals of the zeolites. For this reason, the SiOH groups not adjacent to aluminum predominate and generate the 3750-cm.^{-1} band. Brønsted sites, when present, make up only a very small portion of the surface hydroxyl groups as has been pointed out previously.^{6,7} Finally, this difference suggests that the silica-alumina surface resembles the broken crystal faces of the zeolites. Here conventional Lewis acid sites (three coordinated aluminum ions) may exist because the proton freed when NH_3 is evolved can react with the Al-OH to form H_2O .

Acknowledgment. This work was sponsored by the Gulf Research and Development Company as part of the research program of the Multiple Fellowship on Petroleum. J. B. U. gratefully acknowledges a travel and maintenance grant from the North Atlantic Treaty Organization. We are indebted to Dr. R. M. Hexter of the Mellon Institute for use of his infrared spectrometer and for many fruitful discussions. We also thank Mr. W. F. Benusa and Messrs. J. F. Bukowski and M. A. Biss of Gulf Research and Development Company for the thermogravimetric and chemical analyses, respectively.

Appendix

Zeolites, being crystalline aluminum silicates which have no structural hydroxyl groups, should contain no hydrogen except at the crystal faces where they are required to terminate the giant molecule crystals. Thus, the hydrogen held by these materials should vary inversely with crystal size. The problem is to establish a quantitative relationship between these variables.

(23) A. Leonard, S. Suzuki, J. J. Fripiat, and C. DeKimpe, *J. Phys. Chem.*, **68**, 2608 (1964).

(24) J. Turkevich, F. Nozaki, and D. N. Stamires, 3rd International Congress on Catalysis, Amsterdam, 1964, Preprint No. I. 33.

(25) H. P. Leftin and W. K. Hall, *Actes Congr. Intern. Catalyse*, **2**, Paris, 1960, 1, 1353 (1961).

(26) D. N. Stamires and J. Turkevich, *J. Am. Chem. Soc.*, **86**, 749 (1964).

(27) W. K. Hall, *J. Catalysis*, **1**, 53 (1962).

(28) J. A. Rabo, P. E. Pickert, D. N. Stamires, and J. E. Boyle, *Actes Congr. Intern. Catalyse*, **2**, Paris, 1960, 2, 2055 (1961).

The equation derived may depend somewhat on the model used.

The structure of the X- and Y-type zeolites is a cubic (diamond) lattice of cuboctahedra. Each cuboctahedron has eight hexagonal faces and six square faces and is itself composed of elemental tetrahedra of SiO_2 and AlO_2^- . Each cuboctahedron is joined to four others in tetrahedral symmetry.

A single cuboctahedron has 24 corners, each having a residual valence bond to be saturated by a hydroxyl group. The cuboctahedra are joined through the hexagonal faces, each of which has six OH groups. Thus, when two cuboctahedra are linked together, 12 less hydroxyls are required. For N tetrahedra combined with J junctures, the number of hydroxyl groups required to terminate the particle, $F(\text{OH})$, will be given by

$$F(\text{OH}) = 24N - 12J \quad (\text{I})$$

and the number of hydroxyl groups per cuboctahedron is

$$f(\text{OH}) = 12(2 - J/N) \quad (\text{II})$$

Figure 7 depicts the model used to evaluate N and J for a crystal of linear dimension x . It was supposed that the crystal would grow in three dimensions at about equal rates and that rings would close wherever possible. The problem was simplified by considering the crystal to be constructed of h sheets of puckered, closed rings, there being h of these in each direction. Figure 7a shows a single sheet for $h = 3$, whereas Figure 7b indicates the points at which this single sheet would be joined to the one above it. Each corner of a hexagon represents the position of a cuboctahedron and each side the juncture between two cuboctahedra. By letting h take on integral values and by constructing models similar to those shown in the figure, an orderly sequence was established, the general term of which was given by

$$N = 2h^2(h + 2) \quad (\text{III})$$

In a similar way, a sequence was established for the

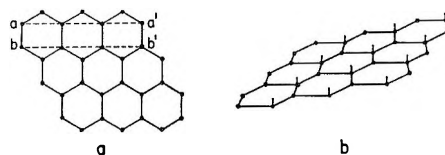


Figure 7. Model used to calculate terminal hydrogen content: corners are cuboctahedra and lines are junctures.

number of junctures in the h separated sheets, *i.e.*

$$hj_s = 3h^3 + 4h^2 - h \quad (\text{IV})$$

The product, hj_s , is not equal to J because it does not include the number of junctions between the sheets, j_1 , which must be added. The three-dimensional zeolite structure is generated by displacing corresponding points in one layer one-half hexagon length in one direction from the layer below it; *i.e.*, a line drawn through aa' (Figure 7a) coincides with bb' of the layer below; a third layer will coincide with the first. From these considerations, it can be shown with the help of Figure 7b that there are h terms equal to $h + 1$ between the sheets. Since there are $h - 1$ spacings between h sheets

$$j_1 = h(h + 1)(h - 1) = h^3 - h \quad (\text{V})$$

Equations IV and V can be combined to give the total number of junctions per particle, *i.e.*

$$J = hj_s + j_1 = 4h^3 + 4h^2 - 2h \quad (\text{VI})$$

Combining eq. II, III, and VI yields

$$f(\text{OH}) = 12(2 - J/N) = 12 \left[2 - \frac{2h^2 + 2h - 1}{h^2 + 2h} \right] \quad (\text{VII})$$

From the crystal structure data published by Bauer,²⁹ it was estimated that

$$x = 1.67 \times 10^{-7}h \text{ cm.} \quad (\text{VIII})$$

where x is the linear dimension of a regular parallelepiped and describes the particle size.

(29) W. H. Bauer, *Am. Mineralogist*, **49**, 697 (1964).

NOTES

On the Interaction of Triphenylamine with Iodine and with Silica-Alumina Catalysts

by Francis R. Dollish and W. Keith Hall

Mellon Institute, Pittsburgh, Pennsylvania
(Received December 12, 1964)

Stamires and Turkevich,¹ in their investigation of the paramagnetic resonance of the triphenylamine-iodine complex in solution, found that the e.p.r. absorption had a hyperfine structure consisting of five lines with a splitting constant of 6.0 gauss. This hyperfine structure was attributed to the formation of a bimolecular triphenylamine radical ion $[(C_6H_5)_3N \cdot N(C_6H_5)_3]^+$. However, the work of Hasegawa² on the optical spectra of aromatic tertiary amines on acid clay and some of our unpublished data on the optical and e.p.r. spectra of triphenylamine on silica-alumina catalysts suggested that the radical ion responsible for this spectrum was the semiquinone of tetraphenylbenzidine. Lewis and Lipkin³ pointed out, many years ago, that the para-hydrogens of the triphenylamine cation radical are exceedingly reactive.

Hasegawa found that the optical spectra of triphenylamine on acid clay consisted of three bands located at 480, 580, and 678 $m\mu$; Hall⁴ reported similar bands at 485 and 660 $m\mu$ for this substrate on silica-alumina. From comparison with the spectra of tri-*p*-tolylamine and tetraphenylbenzidine on acid clay, the bands at 580 and 678 $m\mu$ were assigned² to the triphenylamine radical ion and that at 480 $m\mu$ to the radical ion of tetraphenylbenzidine. It is the purpose of this note to show that similar chemistry occurs with iodine and with silica-alumina.

Experimental

Procedures for the preparation of catalyst samples for e.p.r. and optical study were given earlier.⁴ American Cyanamid Co. Aerocat (AAA) cracking catalyst (22.1% Al_2O_3 , surface area 450 $m^2/g.$) was used. Preparations of triphenylamine and N,N,N',N' -tetraphenylbenzidine complexes with iodine were made according to the procedures of Stamires and Turkevich.¹ The tetraphenylbenzidine was kindly furnished by Mr. Charles Plantz of the Mine Safety Appliances Co. The triphenylamine was 99.99% pure when analyzed by gas-liquid chromatography. All samples were evacuated before use.

Optical spectra were recorded on a Cary Model 14

spectrophotometer using thin platelets (100 mg.) of catalyst, immersed in 10 ml. of $1.4 \times 10^{-4}M$ triphenylamine in isoctane.

For e.p.r. work, 1.5 g. of the catalyst (burned in O_2 for 24 hr. at 540° and then evacuated for 24 hr. at the same temperature) was contacted with 10 ml. of 0.12 M triphenylamine in benzene. After transfer of the reagent onto the catalyst surface, the benzene was removed using an ice bath, then a liquid nitrogen bath, before sealing from the sample under vacuum.

E.p.r. measurements were carried out with a Varian X-band spectrometer (Model V4500) with the microwave bridge in the low power configuration and the magnetic field modulated at 100 kc./sec.

Results and Discussion

Figure 1A illustrates the course of reaction of triphenylamine adsorbed from an isoctane solution onto an optical platelet of silica-alumina. Immediately upon contact, a band developed at 660 $m\mu$ due to the triphenylamine radical ion. After several hours, however, the band observed by Hasegawa for the semiquinone of tetraphenylbenzidine appeared at 485 $m\mu$; after 24 hr. this became the predominant species present.

An investigation of the paramagnetic resonance of triphenylamine on this silica-alumina catalyst at a nominal coverage of 4.8×10^{20} molecules/g. (1×10^{14} molecules/cm.²) showed that immediately upon contact the concentration of free radicals on the dark blue catalyst was 7.2×10^{17} spins/g. The catalyst rapidly turned light orange in color (~ 15 min.), and after 24 hr. the spin concentration decreased to 3.9×10^{17} spins/g. It

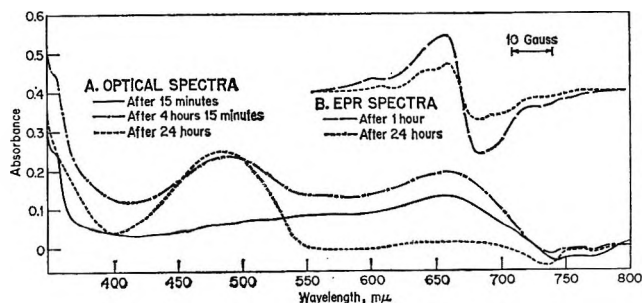


Figure 1. Triphenylamine adsorbed on silica-alumina catalyst.

- (1) D. N. Stamires and J. Turkevich, *J. Am. Chem. Soc.*, **85**, 2557 (1963).
- (2) H. Hasegawa, *J. Phys. Chem.*, **66**, 834 (1962).
- (3) G. N. Lewis and D. Lipkin, *J. Am. Chem. Soc.*, **64**, 2801 (1942).
- (4) W. K. Hall, *J. Catalysis*, **1**, 53 (1962).

Table I: Paramagnetic Complexes with Iodine^a

Reagent	Spins/g.	Hyperfine pattern ^b
A. In solid state (mole ratio of amine/iodine = 0.01)		
Triphenylamine	24.7×10^{16}	Three lines with splitting of 13.06 gauss
N,N,N',N'-Tetraphenylbenzidine	4.3×10^{16}	One Lorentzian line of width at half-height of 13.94 gauss
B. In chloroform solution (0.05 M amine + 0.05 M I ₂) ^c		
Triphenylamine	1.8×10^{16}	Five lines with splitting of 4.736 gauss
N,N,N',N'-Tetraphenylbenzidine	2.6×10^{16}	Five lines with splitting of 4.736 gauss

^a All spin concentrations were measured at ambient temperature at the end of a 24-hr. reaction time. ^b Determined in a dual cavity with hydroquinone in alkaline ethanol ($a_H = 2.368 \pm 0.001$ gauss) as reference. ^c Solutions degassed by repeated freezing and pumping immediately after mixing. The spin concentrations in CHCl₃ were converted from spins/cc. to spins/g. using the density of CHCl₃ at 20° (1.489 g./cc.) as the conversion factor.

is therefore evident that the radicals formed initially undergo further transformations. The hyperfine pattern observed with this (24-hr.) sample (Figure 1B) consists of the superposition of two signals; one arises from the triplet splitting (14–15 gauss) due to the nitrogen-14 nucleus in the triphenylamine radical ion. The other, an unresolved gaussian signal with a width at half-height of about 13 gauss, is due to the unresolved quintet of lines expected for the equal interaction of an electron with the two equivalent nitrogens in the tetraphenylbenzidine radical ion. Thus, the optical and e.p.r. study of triphenylamine on silica-alumina catalyst confirms the reactivity of the triphenylamine radical ion and the presence of two paramagnetic species on the catalyst surface.

The results of the e.p.r. study of the complexes of triphenylamine and tetraphenylbenzidine with iodine, both in the solid state and in chloroform solution, are summarized in Table I. In the solid state, triphenylamine yielded six times as many radical ions as tetraphenylbenzidine, under identical conditions. The hyperfine pattern of the triphenylamine complex consisted of only the triplet splitting due to one nitrogen nucleus. Hence, the conversion of the triphenylamine radical ion to tetraphenylbenzidine in the solid complex at room temperature is small compared with the total number of radicals initially formed. However, the presence of a few per cent of the tetraphenylbenzidine may account for the deviation from the Curie law above 200°K. observed by Stamires and Turkevich for the triphenylamine-iodine complex in the solid state. We were unable to reproduce the reported¹ superhyperfine structure of eleven lines superimposed upon each of the nitrogen triplet lines with either triphenylamine- or tetraphenylbenzidine-iodine complexes.

In chloroform solution, the complexes of these amines with iodine (Table IB) gave concentrations of radical ions of the same order of magnitude and the

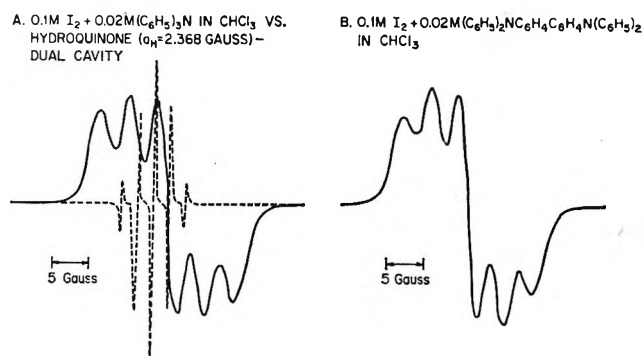


Figure 2. Paramagnetic complexes of triphenylamine and tetraphenylbenzidine with iodine in chloroform.

same hyperfine pattern (Figure 2). Because of the high concentrations of reagents needed to give an unsaturated signal with a good signal to noise ratio, this hyperfine pattern evidences concentration broadening but is otherwise similar to that given in Stamires and Turkevich's Figure 5. The quintet hyperfine pattern is characteristic of radical ions with an unpaired electron equally coupled to two nitrogen atoms and has a hyperfine splitting of 4.736 gauss, as determined by comparison with hydroquinone in a dual cavity (Figure 2A). Stamires and Turkevich report a value of 6.0 gauss for this hyperfine splitting. Similar splittings have been observed for the radical ions of *p*-phenylenediamine ($a_N = 5.29$ gauss)⁵ and N,N,N',N'-tetramethyl-*p*-phenylenediamine ($a_N = 6.99$).⁶ If the paramagnetic species responsible for the hyperfine structure were the bimolecular triphenylamine radical ion proposed by Stamires and Turkevich¹ with coupling through the nitrogen nuclei, then the quintet structure would be

(5) M. T. Melchior and A. H. Maki, *J. Chem. Phys.*, **34**, 471 (1961).

(6) J. R. Bolton, A. Carrington, and J. dos Santos-Veiga, *Mol. Phys.*, **5**, 615 (1962).

expected to have a coupling constant close to 10 gauss, as is found in 1,1-diphenyl-2-picrylhydrazyl.

The use of triphenylamine as a typical electron donor for various donor-acceptor reactions is often complicated by the fact that the triphenylamine radical ions initially formed undergo subsequent reaction to form tetraphenylbenzidine radical ions. Two hydrogen atoms are removed in the coupling reaction; with silica-alumina, it is probable that H₂O is formed and with I₂, HI, *i.e.*, $2(\text{C}_6\text{H}_5)_3\text{N} + \text{Cat-O (or I}_2) \rightarrow (\text{C}_6\text{H}_5)_2\text{-NC}_6\text{H}_4\text{-C}_6\text{H}_4\text{N(C}_6\text{H}_5)_2 + \text{H}_2\text{O (or 2HI)}$. This is reminiscent of Rooney and Pink's observation⁷ that the perylene radical ion formed spontaneously when silica-alumina was contacted with 1,1'-binaphthyl at 200°. It was found that a 15-min. aeration of the triphenylamine-iodine solution before evacuation increased the concentration of paramagnetic species by a factor of 2. This effect of oxygen emphasizes the similarity in behavior of triphenylamine on silica-alumina catalysts and in iodine solutions.

Acknowledgment. This work was sponsored by the Gulf Research and Development Company as part of the research program of the Multiple Fellowship on Petroleum.

(7) J. J. Rooney and R. C. Pink, *Trans. Faraday Soc.*, **58**, 1632 (1962).

Radical Intermediates in the Mercury (³P)

Photosensitized Decomposition of

Cyclopropane^{1a}

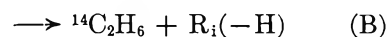
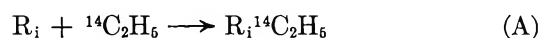
by Richard A. Holroyd^{1b} and George W. Klein

Radiation Research Laboratories, Mellon Institute, Pittsburgh, Pennsylvania (Received January 9, 1965)

Although several studies²⁻⁴ have been made of the mercury (³P) photosensitized decomposition of cyclopropane, it has not been conclusively established what radical intermediates are formed in the quenching process. In addition, there appears to be some disagreement as to the mechanism of polymer formation. A review describing some of the unique aspects of this sensitization has recently been published.⁵ In an investigation of the nature of the polymer it was shown that olefins such as 1,5-hexadiene formed by dimerization of C₃H₅ radicals (either cyclopropyl or allyl) play a major role in the condensation reactions.² The addition reaction of trimethylene diradicals to

unsaturates appears to be an important step in polymer formation. Gunning, *et al.*,^{3a} observed that allyl chloride and *n*-propyl chloride are formed if carbon tetrachloride is present, indicating allyl and *n*-propyl radical intermediates. They propose, however, on the basis of the long induction periods observed in pure cyclopropane, that initially cyclopropyl radicals are formed in the quenching reaction. The work of Setser, *et al.*,⁴ shows that a major quenching process is *cis-trans* isomerization which increases in importance with pressure. Since exchange does not occur, this reaction apparently proceeds *via* an excited state.

In an attempt to establish the identity of the intermediate radicals in the photosensitization, a preliminary investigation has been made utilizing the ¹⁴C₂H₅ radical sampling technique.⁶ In this technique ¹⁴C₂H₅ radicals (generated *in situ* from hydrogen atom addition to ¹⁴C₂H₄) react with the radical intermediates and form (reaction A) labeled hydrocarbons which characterize the initial radical species.



This method is especially advantageous for use in cyclopropane since the ¹⁴C₂H₄ which is added serves a secondary purpose in minimizing complications arising from hydrogen atom addition to the other olefins formed in the sensitization.

Experimental

The details of the experimental method have been described elsewhere.⁶ Matheson cyclopropane was purified by gas chromatography using a 4.5-m. column packed with silicone grease on Celite. This procedure was necessary to eliminate propylene as a principal impurity in the cyclopropane. Propylene seems to have been effectively removed since isopentane-¹⁴C which would be formed from the isopropyl radicals produced by the addition of hydrogen atoms to the propylene was

(1) (a) Supported in part by the Atomic Energy Commission; (b) Atomics International, Canoga Park, Calif.

(2) K. J. Ivin, *J. Chem. Soc.*, 2241 (1956).

(3) (a) H. W. Ford, P. J. Kozak, and H. E. Gunning, Abstracts of the 137th National Meeting of the American Chemical Society, Cleveland, Ohio, April 1960; (b) H. W. Ford, Ph.D. Thesis, Illinois Institute of Technology, 1953.

(4) D. W. Setser, R. S. Rabinovitch, and E. G. Spittler, *J. Chem. Phys.*, **35**, 1840 (1961).

(5) R. J. Cvetanović, "Progress in Reaction Kinetics," Vol. 2, G. Porter, Ed., Pergamon Press, Inc., New York, N. Y., 1964, pp. 83, 84.

(6) R. A. Holroyd and G. W. Klein, *J. Phys. Chem.*, **67**, 2273 (1963).

Table I: Cyclopropane^a

Time, min.	¹⁴ C ₂ H ₄ , μmoles/l.	(c-C ₃ H ₆) (¹⁴ C ₂ H ₅)	Rate, nmole/sec.						X ^c	$\frac{\phi_{\text{allyl}}}{\phi_{^{14}\text{C}_2\text{H}_5}}$	$\phi_{^{14}\text{C}_2\text{H}_5}$
			¹⁴ C ₂ H ₆	¹⁴ C ₄ H ₁₀ ^b	1- ¹⁴ C ₆ H ₁₀	Ethyl- ¹⁴ C- cyclo-C ₃ H ₆	3-Methyl- hexane- ¹⁴ C				
3	12.4	504	...	0.189	0.435	0.020	0.020	0.020	1.08	0.22	
10	11.0	610	0.045	0.145	0.310	0.019	0.040	0.042	0.99	0.17	
10	5.6	1100	0.049	0.109	0.246	0.035	0.045	0.048	1.07	0.15	
3	4.2	1450	...	0.140	0.322	0.025	0.038	0.047	1.10	0.18	

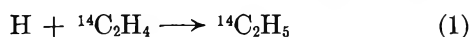
^a Reaction conditions: temperature 25°; quartz cell volume 220 cc.; low pressure mercury arc used, 1849 Å. excluded with a Corning 7910 filter. ^b Calculated on the assumption that the specific activity of the butane is twice that of the other products. ^c On the basis of the retention time on the silicone column used, product X is most likely 5-methylheptene-1.

not detected. Mass spectral analysis revealed no major impurity to be present.

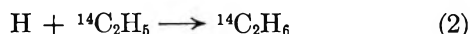
To determine the light intensity at 2537 Å., cyclopropane, for which $\phi_H = 0.8$,⁷ was used as an actinometer. The absorbed light intensity was approximately 4×10^{-9} einstein/sec.

Results

In the mercury-photosensitized decomposition of cyclopropane with ¹⁴C₂H₄ present (at $\sim 10^{-3}$ mole fraction), six carbon-14 labeled products are observed (Table I). The most important products are 1-pentene and *n*-butane, indicating that the predominant radical intermediates present are allyl and ¹⁴C₂H₅. Butane-¹⁴C and ethane-¹⁴C are formed by combination and disproportionation of ¹⁴C₂H₅ radicals. The observation of these products demonstrates that hydrogen atoms are present to generate the ¹⁴C₂H₅ radicals *via* reaction 1. The fact that the ratio ¹⁴C₂H₆:¹⁴C₄H₁₀



exceeds 0.12 is interpreted to mean that reaction 2



is occurring to a small extent.

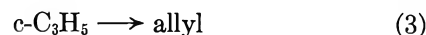
The yield of ¹⁴C₂H₅ radicals as given in the final column of Table I is defined as the total yield of labeled hydrocarbons (see ref. 6). From the observed values of $\phi_{^{14}\text{C}_2\text{H}_6}$ a lower limit of $\phi_H = 0.22$ may be derived. The yield of allyl is also close to 0.22 under our conditions (assuming complete quenching by the cyclopropane) since the ratio of $\phi_{\text{allyl}}/\phi_{^{14}\text{C}_2\text{H}_5}$ ⁸ is nearly unity. Three other labeled products were observed, all formed at a much reduced rate. These were ethylcyclopropane, 3-methylhexane, and a product (X) believed to be 5-methyl-1-heptene on the basis of its retention time. The average value of the ratio of yields of ethylcyclopropane-¹⁴C/1-pentene-¹⁴C is 0.08, *i.e.*, approximately 7% of the C₃ radicals observed are cyclopropyl. It is assumed here that disproportionation (reactions B

and B') for cyclopropyl radicals is negligible. The actual yield of cyclopropyl radicals will be larger than reported to the extent that disproportionation occurs. The fact that the yield of hydrogen atoms is approximately equal to the yield of allyl radicals (Table I, column 10) shows that no significant yield of C₃H₅ radicals was undetected.

Discussion

The results presented here show that allyl radicals are the predominant radical species present. This could mean that allyl radicals and a hydrogen atom are formed in the dissociative quenching reaction. However, this view is inconsistent with the observation by Ford^{3b} of long induction periods in the sensitization during which no observable reaction occurred.

An alternate explanation is that cyclopropane, in quenching excited mercury (³P) atoms, loses a hydrogen atom and a cyclopropyl radical is formed.⁹ With the ethyl-¹⁴C radical sampling method cyclopropyl radicals should then combine with ¹⁴C₂H₅ radicals. However, if the cyclopropyl radical may also isomerize thermally to allyl (reaction 3), the relative yields of these two



radicals would necessarily be dependent on the ¹⁴C₂H₅ radical concentration (and consequently on the light intensity) because of competition of reaction 3 with the combination of cyclopropyl and ¹⁴C₂H₅ radicals. The light intensity employed in this study was low ($\sim 4 \times$

(7) R. L. Stock and H. E. Gunning, *Can. J. Chem.*, **38**, 2295 (1960).

(8) This ratio of yields is derived from the relationship

$$\frac{\phi_{\text{allyl}}}{\phi_{^{14}\text{C}_2\text{H}_5}} = \frac{1\text{-pentene-}^{14}\text{C}}{2(1.12)\text{ butane-}^{14}\text{C}}$$

that is, the ratio of radical yields is given by the ratio of corresponding yields of labeled hydrocarbons adjusted for disproportionation (see ref. 6). (B/A for ethyl plus allyl radicals is assumed to be zero.)

(9) Most other saturated hydrocarbons (including cycloalkanes) lose a hydrogen atom in quenching Hg (³P) atoms and carbon-carbon bond scission does not occur. See, *e.g.*, ref. 6 and 7 and D. W. Beck, D. V. Kniebes, and H. E. Gunning, *J. Chem. Phys.*, **22**, 672 (1954).

10^{-9} einstein/sec.). If it is assumed that the cyclopropyl radicals observed in this study are formed, at least in part, by the quenching reaction and that reaction 3 occurs, then it follows that at greater absorbed light intensities a larger proportion of the cyclopropyl radicals should be scavenged. Further studies along these lines will be necessary to prove if this is indeed the mechanism of allyl radical formation.

The results with added $^{14}\text{C}_2\text{H}_4$ also provide insight into the mechanism of formation of high molecular weight products.¹⁰ It is suggested that the observed labeled 3-methylhexane and 5-methyl-1-heptene (Table I) are formed by secondary reactions in which hydrogen atoms add to the major olefinic products of the sensitization (1-pentene- ^{14}C and 1,5-hexadiene) forming radicals¹¹ which combine with $^{14}\text{C}_2\text{H}_5$ radicals. These results suggest that the polymerization could occur by a series of reactions in which intermediate radicals, formed by hydrogen atom addition to olefin, combine with allyl radicals regenerating olefin which subsequently is attacked by a hydrogen atom, and the process is repeated.

Acknowledgment. The authors wish to thank Dr. Hadley Ford for lending us his Ph.D. thesis and for his criticisms and suggestions during the preparation of this note.

(10) No analysis for polymer was made in this work; visual examination of the cell afterward revealed no deposit.

(11) The radical formed by H-atom addition to 1,5-hexadiene could conceivably rearrange by adding intramolecularly to itself forming a 3-methylcyclopentyl radical. This reaction may be the origin of the cyclopentane rings observed in the polymer.²

Electron Spin Resonance of Aliphatic Semiquinones

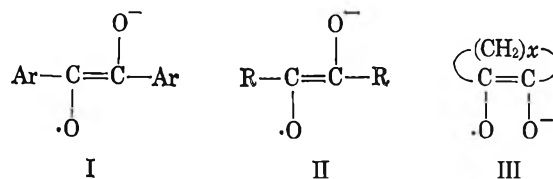
by E. Thomas Strom,

Socony Mobil Field Research Laboratory, Dallas, Texas, and
Pioneering Research Division, U. S. Army Natick Laboratories,
Natick, Massachusetts,¹

Glen A. Russell, and Robert D. Stephens

Department of Chemistry, Iowa State University, Ames, Iowa
(Received January 28, 1965)

Characteristic colors have been observed when compounds of the formula ArCHOHCOAr react with base and oxygen.² Michaelis and Fetcher³ suggested that these species were semiquinones of type I.



The paramagnetic nature of these intermediates has since been demonstrated.⁴

One would not expect the corresponding aliphatic semiquinones (II and III) to be readily observed for two reasons: the absence of aromatic rings in which the electron can be delocalized, and the possibility of condensation reactions occurring in the basic media in which the radicals are usually generated. For example, it was found that the reduction of biacetyl with zinc in basic solution resulted in the formation of the corresponding *p*-benzosemiquinone.⁵

Recent work has shown that the radical anions of cyclic α -diketones (III),⁶ pivalil,⁶⁻⁸ isobutyryl,⁸ and butyryl,⁸ can be formed. Thus, delocalization in the $\cdot\text{O}-\text{C}=\text{C}-\text{O}^-$ system in II and III is sufficient to impart stability to the radical, and cyclization to the benzoquinone is not necessarily an unsurmountable problem.

We have found that ketones of the type $(\text{CH}_3-(\text{CH}_2)_n)_2\text{C}=\text{O}$ readily oxidize in dimethyl sulfoxide (80%)–*t*-butyl alcohol (20%) containing potassium *t*-butoxide to give yellow-green solutions containing semiquinones of type II. Smaller amounts of other radicals are also formed. For semiquinones with $n = 2-10$, the spectra consist of a main quintet, $a^{\text{H}} = 4.68 \pm 0.05$ gauss, due to interaction with the four β -protons. Each peak of the quintet is split further from interaction with the four γ -protons, $a^{\text{H}} = 0.22$ gauss. A typical example is shown in Figure 1. In general, the γ -splitting was a quintet splitting except for $n = 2$ where the first, third, and fifth peaks of the main quintet were split into triplets and the second and fourth peaks into quartets or possibly sextets of which the wing peaks are not observed.

(1) At second address, on military leave of absence.

(2) E. Fischer, *Ann.*, **211**, 214 (1882); A. Hantzsch and W. H. Glower, *Ber.*, **40**, 1520 (1907).

(3) L. Michaelis and E. S. Fetcher, Jr., *J. Am. Chem. Soc.*, **59**, 1246 (1937).

(4) B. Venkataraman and G. K. Fraenkel, *ibid.*, **77**, 2707 (1955); J. L. Ihrig and R. G. Caldwell, *ibid.*, **78**, 2097 (1956); G. A. Russell, E. G. Janzen and E. T. Strom, *ibid.*, **84**, 4155 (1962).

(5) M. Adams, M. S. Blois, Jr., and R. H. Sands, *J. Chem. Phys.*, **28**, 774 (1958).

(6) G. A. Russell and E. T. Strom, *J. Am. Chem. Soc.*, **86**, 744 (1964).

(7) G. R. Luckhurst and L. E. Orgel, *Mol. Phys.*, **7**, 297 (1963).

(8) H. C. Heller, *J. Am. Chem. Soc.*, **86**, 5346 (1964).

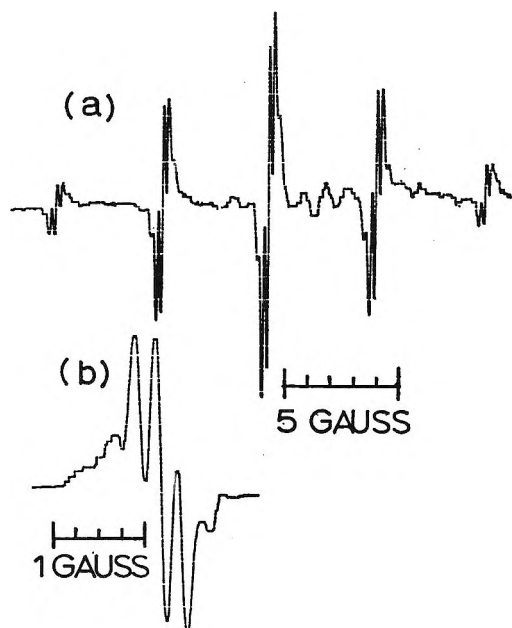


Figure 1. (a) First derivative e.s.r. spectra of *n*-tridecane-6,7-dione radical anion; (b) second multiplet of (a) with expanded scale.

Methyl ketones ($\text{CH}_3\text{COCH}_2\text{R}$) do not form radical anions under these conditions. A superior method for formation of radical anions of the type II even when R or R' is methyl involves the reaction of the α -bromoketone with a basic dimethyl sulfoxide solution. By a modification of this procedure, the semiquinones can be formed directly from ketones. Bromination of the ketones (e.g., 2-butanone) in *t*-butyl alcohol containing potassium *t*-butoxide followed by dilution with dimethyl sulfoxide containing potassium *t*-butoxide forms II spontaneously. A seven-line spectrum, $a_{\text{CH}_3^{\text{H}}} = 6.06$ gauss, is observed for II, R = R' = CH_3 , while for II, R = CH_3 , R' = C_2H_5 , the spectrum yields $a_{\text{CH}_3^{\text{H}}} = 5.96$ and $a_{\text{CH}_2^{\text{H}}} = 4.97$ gauss.

The spin densities at the carbonyl carbon atoms in the radical anions derived from ketones with $n = 2-10$, as evaluated from the equation $a_{\beta}^{\text{H}} = 29.25\rho_{\text{C}}$,^{6,9} are 0.16. This is rather close to the spin density previously calculated [$\rho = 0.12$] for the carbonyl carbon atoms in cyclopentadecane-1,2-dione radical anion, wherein the conformation is frozen relative to spectrometer frequency.^{6,10} That there is not free rotation in the acyclic semiquinones is shown by the nonequivalence of $a_{\text{CH}_3^{\text{H}}}$ and $a_{\text{CH}_2^{\text{H}}}$ noted above. Since $Q_{\text{CCH}_3^{\text{H}}} \cong Q_{\text{CCH}_2\text{R}^{\text{H}}} = 58.5 \cos^2 \theta$, where θ is the time average dihedral angle between the carbonyl carbon p_z orbital and the β -carbon-hydrogen bond, it is possible to calculate relative values of θ for the β -carbon-hydrogen bonds *via* the equation $a^{\text{H}} = Q \cos^2 \theta \rho_{\text{C}}$.⁶ Using

$a_{\text{CH}_3^{\text{H}}} = 6.0$ and $a_{\text{CH}_2^{\text{H}}} = 4.7$ gauss yields $\cos \theta_{\text{-CH}_2\text{-H}} / \cos \theta_{\text{-CH}_3\text{-H}} = 1.13$. Since $\theta_{\text{-CH}_2\text{-H}}$ would be expected to be $\geq 45^\circ$, $\cos \theta_{\text{-CH}_2\text{-H}}$ is ≥ 0.71 ; *i.e.*, R' in R' $\text{CH}_2 = \text{R}$ [formula II] has a preferred *trans* position relative to the carbon-oxygen bond. Using the value of 51° for θ , the spin densities of the carbonyl carbon atoms in II with R = ethyl to *n*-undecyl are calculated to be $\rho_{\text{C}} = 0.205$.

Experimental

E.s.r. spectra were obtained with Varian V-4502 and V-4500 spectrometers with 23- and 15-cm. magnets, respectively, and with 100-kc.p.s. field modulation. Dimethyl sulfoxide (Crown Zellerbach Corp.) was distilled from calcium hydride before use. Potassium *t*-butoxide was purchased from Alfa Inorganics, Inc., and from Mine Safety Appliance Corp. Commercially pure ketones were used without further treatment.

Solutions of the ketone or α -bromoketone ($\sim 0.10 M$) in dimethyl sulfoxide (80%)–*t*-butyl alcohol (20%) and in pure dimethyl sulfoxide were deoxygenated in the U-type mixing cell described previously¹¹ and mixed with a solution of potassium *t*-butoxide in the appropriate solvent. In the case of oxygenation experiments, the cell was then opened to air for 10–20 sec., and the oxidate was shaken down into a flat fused silica e.s.r. cell ("aqueous sample cell").¹²

(9) R. W. Fessenden and R. H. Schuler, *J. Chem. Phys.*, **39**, 2147 (1963).

(10) Even though in some systems $Q_{\text{C-CH}_3^{\text{H}}}$ may be less than 29.25 [C. deWaard and J. C. M. Henning, *Phys. Letters*, **4**, 31 (1963); C. A. McDowell and K. F. G. Paulus, *Mol. Phys.*, **1**, 541 (1963); B. L. Barton and G. K. Fraenkel, *J. Chem. Phys.*, **41**, 1455 (1964); E. T. Strom, G. A. Russell, and R. Konaka, *ibid.*, in press], the indicated similarity would remain unchanged.

(11) G. A. Russell, E. G. Janzen, and E. T. Strom, *J. Am. Chem. Soc.*, **86**, 1807 (1964).

(12) This work was supported in part by a grant from the National Science Foundation.

The Electrostatic Forces within the Carbon Monoxide Molecule¹

by Peter Politzer²

Department of Chemistry, Western Reserve University, Cleveland, Ohio (Received January 28, 1965)

This study was undertaken with the purpose of obtaining more precise knowledge of the roles played by the various molecular orbitals of carbon monoxide. It was hoped that this would lead to a better understand-

ing of the specific effects of the electrons in the individual orbitals upon the properties of the molecule, particularly the strength of the C–O bond.

It was decided that the problem could best be approached by making use of the Hellmann–Feynman theorem³ to calculate the forces exerted by the electrons in the individual molecular orbitals upon the carbon and the oxygen nuclei. Such calculations have been made by Bader and Jones for a number of other molecules,⁴ and their articles give a discussion of this application of the theorem.^{5–7}

According to the Hellmann–Feynman theorem, the force along the molecular axis which is exerted by the electrons in a doubly occupied orbital ϕ_i of a diatomic molecule upon its nucleus "a" of charge Z_a is given by

$$F_{i-a} = 2Z_a e^2 \int \frac{\cos \theta_a}{r_a^2} \phi_i \phi_i^* d\tau \quad (1)$$

All calculations in this paper are in terms of coordinates with centers at the carbon and oxygen nuclei and positive z axes pointing toward each other. The angles θ_c and θ_o are measured away from the respective z axes, and r_a is the radial distance from nucleus a.

The "best-atom" set of LCAO–SCF orbitals which has been determined for carbon monoxide by Ransil⁸ was used in this work. The attraction of the electrons in each of these molecular orbitals for each nucleus in the molecule, as found by eq. 1, is given in Table I. (The individual integrals obtained when ϕ_i is squared were determined by means of published formulas.^{5,9}) Owing to the manner in which the coordinate axes have been defined, a negative force indicates that the particular orbital is pulling that nucleus away from the other one.

Table I: Forces Exerted by the LCAO–SCF Molecular Orbitals of Carbon Monoxide upon the Carbon and Oxygen Nuclei

Molecular orbital	Force on oxygen nucleus, a.u.	Force on carbon nucleus, a.u.
1 σ	0.3125	2.641
2 σ	3.522	0.1231
3 σ	4.554	3.284
4 σ	–4.242	1.477
5 σ	1.088	–1.899
1 π_z	1.058	1.722
1 π_y	1.058	1.722
Totals:	7.351	9.070

Now, according to the Hellmann–Feynman theorem, the net electronic attraction upon each of the two nuclei should be in the direction of the other and should

be exactly balanced by the repulsion between them since at equilibrium the resultant force upon each nucleus should be zero. The internuclear repulsion in this case is 10.560 a.u.¹⁰ So there are clearly large discrepancies between the net attractions, given in Table I as 7.351 and 9.070 a.u., and the repulsion, 10.560 a.u. One must conclude that the electron density predicted by the LCAO–SCF molecular orbitals is not a completely satisfactory representation of the actual distribution in the molecule. Bader and Jones reached similar conclusions for the HF, Li₂, Be₂, C₂, N₂, and F₂ molecules.^{4,6} It should be pointed out, however, that these discrepancies, in themselves, do not necessarily constitute a serious indictment of the LCAO–SCF molecular orbitals since the force calculations are extremely sensitive to the exact form of the orbitals. Thus, slight inaccuracy in the predicted polarization would produce a large effect upon the forces.

In any case, the results which have been obtained provide a quantitative explanation of one of the interesting features of carbon monoxide. It is known experimentally that the loss of an electron, to form CO⁺, leads to a decreased bond length and an increased vibration frequency, implying that the C–O bond is actually strengthened in this ionization process. The reason for this behavior is shown very clearly and directly by a consideration of the forces which are involved. From Ransil's work it is known that the most energetic electrons, one of which is lost in ionization, are in the 5 σ molecular orbital and, furthermore, that this pair of electrons is concentrated near the carbon nucleus, symmetrically around the molecular axis but on the side away from the oxygen. In view of their position, it follows that these electrons must exert a large attractive force on the carbon nucleus and a much smaller one on the more distant oxygen. The effect then, since these electrons are predominantly on the outer side of the carbon nucleus, is to pull this nucleus away from the oxygen—to weaken the bond. These statements are fully supported by the data in Table I. The 5 σ -electrons are seen to exert an attraction of –1.899

(1) This paper is taken from the Ph.D. dissertation of the author, Western Reserve University, 1964.

(2) Chemistry Department, Indiana University, Bloomington, Ind.

(3) R. P. Feynman, *Phys. Rev.*, **56**, 340 (1939).

(4) R. F. W. Bader, *Can. J. Chem.*, **41**, 2303 (1963).

(5) R. F. W. Bader and G. A. Jones, *ibid.*, **39**, 1253 (1961).

(6) R. F. W. Bader and G. A. Jones, *ibid.*, **41**, 586, 2251 (1963).

(7) R. F. W. Bader and G. A. Jones, *J. Chem. Phys.*, **38**, 2791 (1963).

(8) B. J. Ransil, *Rev. Mod. Phys.*, **32**, 245 (1960).

(9) S. Ehrenson and P. E. Phillipson, *ibid.*, **34**, 1224 (1961).

(10) This repulsive force is given by $(6 \times 8)/(2.1320)^2$, where 2.1320 a.u. is the internuclear distance.

a.u. upon the carbon and one of 1.088 a.u. upon the oxygen. Thus, there is a net force of $-1.899 + 1.088 = -0.811$ a.u. tending to separate the carbon from the oxygen. When one of these 5σ -electrons is lost, as by ionization, the attractions upon both nuclei are decreased by some fraction, and the excess pull upon the carbon is therefore also reduced. So the loss of one of the 5σ -electrons diminishes the weakening effect that these electrons have upon the C-O bond and leaves behind a more strongly bound species.

The preceding discussion and the data in Table I should correct an important misconception: the belief that the carbon and oxygen lone-pair electrons in carbon monoxide are essentially nonbonding and have little direct influence on the strength of the C-O bond. In reality, the effect of both electron pairs is to weaken the bond very definitely.

In general, the loss of an electron must be expected to cause a significant rearrangement of the other electrons in a molecule, so that the original orbitals will not be valid for the ion. However, in the particular case of the 5σ -electrons of carbon monoxide, it seemed worthwhile, in view of their rather isolated position, to consider the possibility that as a first approximation they could be treated as being essentially independent of the remaining electrons in the molecule and that the only fundamental effect of ionization was to reduce by one-half their excess pull upon the carbon. This is equivalent then to saying that in forming the CO^+ ion, there is a force of $0.811/2$ a.u. tending to push the carbon toward the oxygen and that the bond length therefore decreases until this force is balanced by the increased nuclear repulsion at the new, shorter distance. This is

expressed mathematically by $0.811/2 = 6 \times 8/d^2 - 6 \times 8/(2.1320)^2$ where d is the internuclear distance in CO^+ . The result obtained is $d = 2.09$ a.u. Since the experimentally observed bond length of CO^+ is 2.11 a.u.,¹¹ the agreement between the calculated and the measured values is certainly very good (1.95% difference). On the other hand, the error is of the same magnitude as the entire difference between CO and CO^+ , 2.13 - 2.11 a.u. In order to decide, therefore, whether or not the accuracy obtained is significant, the above procedure was repeated with some test orbitals occupying approximately the same spatial position in the molecule as the 5σ , but differing in some details. It was found that the value of d can vary over quite a wide range—in one case it came out to be as low as 1.95 a.u. So the closeness of agreement which was obtained using the 5σ -orbital does seem to be meaningful and suggests that as a first approximation the 5σ -electrons of carbon monoxide may perhaps be treated as being essentially independent of the remaining electrons of the molecule.

Acknowledgments. The author wishes to thank Dr. Ralph H. Petrucci for many discussions of this work. He is also most grateful to the National Science Foundation for the support of Cooperative Graduate Fellowships. The force integrals were calculated at the Computation Centers of Case Institute of Technology and Indiana University, and the author wishes particularly to thank Mr. Barry Fell and Mr. Thomas Michels for all of their work with these calculations.

(11) G. Herzberg, "Molecular Spectra and Molecular Structure," Vol. I, D. Van Nostrand Co., Inc., New York, N. Y., 1950, p. 522.

COMMUNICATIONS TO THE EDITOR

Discussion of an Apparent Violation of the Gibbs–Duhem Equation

Sir: Recently, Elliott, *et al.*,¹ have concluded from results of an isopiestic study that Raoult's law is not approached as a limiting law in dilute solutions of gallium in cadmium at 775°K. The argument has been advanced that the solvent, cadmium, need not obey Raoult's law even though the solute, gallium, follows Henry's law at mole fractions of the order of 0.01. Such a state of affairs would represent a violation of the Gibbs–Duhem equation and, indirectly, of the laws of thermodynamics; hence it is inevitable that the results of Elliott, *et al.*, will be thoroughly scrutinized to determine whether the apparent anomaly has dealt a death blow to the laws of dilute solution.

It is well known that gallium forms double molecules in the solid phase^{2,3} and some of the properties of liquid gallium have been explained by assuming that the metal atoms self-associate.⁴ Therefore, it is not impossible that the dimerization equilibrium $2\text{Ga} = \text{Ga}_2$ is important even in dilute solutions of gallium in cadmium. To test this hypothesis, we have attempted to fit the activity data of Elliott, *et al.*, by assuming various values for the dimerization constant, K_2 . Figure 1

in the range of 20 to 25 fit the activity data nearly to within the authors' stated limits of error.

Although it would be desirable to extend the study of Elliott, *et al.*, to determine whether the dimerization hypothesis provides a suitable basis for explaining Ga–Cd activity data over a wide range of conditions, it appears that the data presently available do not provide evidence that Raoult's law is disobeyed as a limiting law. In treating colligative property data for dilute solutions, it is far more reasonable to attribute apparent deviations from Raoult's law to solute association or dissociation than to presume failure of the laws of thermodynamics.

Acknowledgment. The authors thank the U. S. Department of the Interior, Office of Saline Water, for support of this research by Grant No. 14-01-0001-321.

(1) G. R. B. Elliott, J. F. Lemons, and H. S. Swofford, Jr., *J. Phys. Chem.*, **69**, 933 (1965).

(2) A. F. Wells, "Structural Inorganic Chemistry," 3rd Ed., Clarendon Press, Oxford, England, 1962, p. 974.

(3) "International Tables for X-Ray Crystallography," Vol. III, The Kynoch Press, Birmingham, England, p. 279.

(4) B. R. T. Frost, *Progr. Metal Phys.*, **5**, 96 (1954).

THE UNIVERSITY OF OKLAHOMA
NORMAN, OKLAHOMA

SHERRIL D. CHRISTIAN
NORMAN FOGEL

RECEIVED APRIL 2, 1965

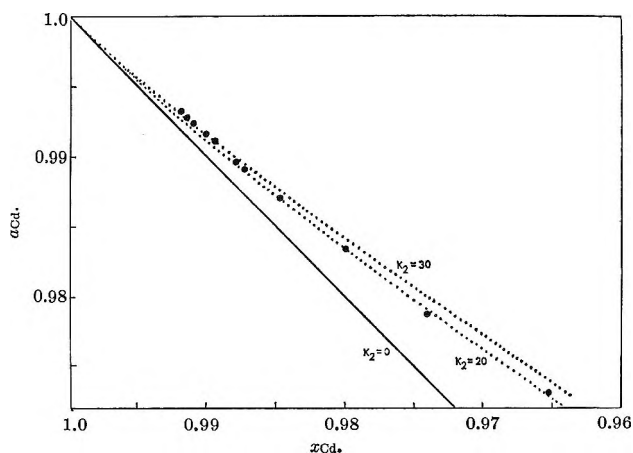


Figure 1. Dependence of cadmium activity on mole fraction at 775°K.

shows experimental values of cadmium activity, a_{Cd} , plotted against cadmium mole fraction, x_{Cd} , as well as the calculated curves corresponding to selected values of K_2 (in reciprocal mole fraction units). Values of K_2

Reply to Discussion of an Apparent Violation of the Gibbs–Duhem Equation

Sir: We appreciate the letter from Professors Christian and Fogel. We believe that the questions which were raised in our paper need further work and discussion.

As Christian and Fogel point out, we have questioned whether certain thermodynamic relationships may be applied to real systems with the exact correlation of theory and reality which has been assumed. In the case of gallium-in-cadmium solutions, we asked whether the cadmium atoms next to a gallium atom in dilute solutions can be totally uninfluenced by the presence of the gallium atom when the gallium behavior is much affected by its cadmium neighbors. This conclusion is implied when one couples Raoult's law for the solvent with Henry's law for the solute as is required by the

Duhem relationship. In answer, we find that our data and Predel's¹ fall on a curve of the form to be expected if the interaction between gallium and cadmium is mutual, each being somewhat repelled by the other (as compared with the interactions of the atoms in the pure liquids).

Christian and Fogel suggest that it would be more reasonable to explain our data as the result of gallium dimerization. In this treatment it is assumed that Ga and Ga₂ molecules behave identically (colligative properties) as far as the cadmium solvent is concerned. We agree that, in the absence of experimental solution studies, it would be reasonable to anticipate possible gallium dimerization in solution. In our judgment, the solution data contradict this conclusion, however. Kleppa² uses first and second powers of the formal atom fraction ($N_{\text{Ga}} = n_{\text{Ga total}} / (n_{\text{Ga total}} + n_{\text{Cd}})$ where n refers to all the gallium or cadmium atoms added) to describe his heat of solution data to 15–20% gallium. Our data also are fitted using the formal atom fraction in first and second powers. The model suggested by Christian and Fogel requires that one turn to a different form, *i.e.*, species fractions ($\mathcal{N}_{\text{Ga}_2} = n_{\text{Ga}_2} / (n_{\text{Ga}_2} + n_{\text{Ga}} + n_{\text{Cd}})$, etc., where n refers to the molecules of a particular species) in seeking a relationship to describe the data.

We believe that our data cannot be described adequately with the dimerization treatment. Using our equation

$$a_{\text{Cd}} = 1 - 0.856N_{\text{Ga}} + 0.943N_{\text{Ga}}^2$$

and considering the first nine points which are little influenced by differences in our results and Predel's, we find a root-mean-square deviation of 0.00013 for the measured activities. The uncertainties which Christian and Fogel refer to are the individual datum uncertainties which are roughly twice as large. At the highest cadmium concentrations where our equation should be most accurate, the line of data and Christian and Fogel's line are separated by about five times our r.m.s. deviation. With the exception of our outermost point, which we discussed as questionable in our paper, Christian and Fogel's equation using $K = 23$ lies everywhere above the data at the larger gallium concentrations and everywhere below the data at the smaller concentrations, and the difference appears to us to be significant.

In fairness to Christian and Fogel's argument it should be pointed out that a different temperature bias (see *Uncertainties* in our paper) could lower the whole group of points while leaving their shape unchanged.

Perhaps such a shift could lead to a better fit on the dimerization assumption. However, the shape of the experimental curve is not one that could ever be fitted well on this assumption.

There is an erroneous statement in our paper which we found too late to correct and would like to correct at this time. Contrary to our statement, oxidation of the gallium before a run was started would alter the slope observed for the data. To rule out this possibility we must turn, first, to the close agreement among three groups of data, our two runs and Predel's; and, second, to our scrupulous removal of oxygen from the container and cadmium and to the excellent metallic sheen of our original and final alloys: an oxidation and removal of 14.4% ($k = 0.856$) of the gallium to a new phase in each case would have created obvious oxide particles or scum, both of which were absent.

While we like to think that our isopiestic balance data give the clearest published evidence supporting our limiting equation, one should not conclude that our data stand alone. As mentioned, the universal limiting Raoult's law is hard to understand chemically. A literature survey,³ not complete but we believe representative, which we carried out showed little experimental support for Raoult's law in dilute solutions if the deviations from Raoult's law were large in the mid-regions. Such systems usually seemed to obey our equation, however. For ideal solutions our equation becomes Raoult's law, of course.

We agree with Christian and Fogel that more gallium-cadmium data would be desirable. We considered undertaking another run, but concluded that measurements of other systems and with other techniques (*e.g.*, e.m.f.) might be more informative. For example, linear negative deviations from Raoult's law, if found, would exclude the association treatment and the atomic nature of the solute would exclude dissociation. Incomplete vapor pressure measurements on Ni-Cd and Cu-Cd solutions⁴ suggest that these systems do indeed have negative deviations.

(1) B. Predel, *Z. Metallk.*, **49**, 226 (1958).

(2) O. J. Kleppa, *Acta Met.*, **6**, 233 (1958).

(3) G. R. B. Elliott, J. F. Lemons, and H. S. Swofford, Jr., "An Alternative Treatment of Solvent Activity in the Raoult's Law Region. The Gallium-Cadmium System," Los Alamos Scientific Laboratory Report LA-2997 (1964).

(4) D. R. Conant, G. R. B. Elliott, and J. F. Lemons, unpublished data.

THE UNIVERSITY OF CALIFORNIA
LOS ALAMOS SCIENTIFIC LABORATORY
LOS ALAMOS, NEW MEXICO

GUY R. B. ELLIOTT
JOE FRED LEMONS

RECEIVED APRIL 29, 1965

Electrical Conductance of Concentrated Aqueous Solutions and Molten Salts: Correlation through Free Volume Transport Model

Sir: Following a successful correlation of electrical conductance data for nitrate melts,¹ both glass-forming and otherwise, by means of the equation

$$\Lambda = AT^{-1/2} \exp(-k/(T - T_0)) \quad (1)$$

(derived from the free volume transport model of Cohen and Turnbull,² T_0 being the temperature below which the liquid contains no free volume, A and k are constants), we have investigated the possibility of extending this type of interpretation of transport phenomena to concentrated aqueous solutions. Such an extension is strongly suggested by reports that, *e.g.*, hot $\text{Mg}(\text{NO}_3)_2\text{-H}_2\text{O}$ solutions, when sufficiently concentrated, yield glassy solids on cooling.^{3,4}

We have measured the electrical conductance of $\text{Mg}(\text{NO}_3)_2\text{-H}_2\text{O}$ solutions as a function of temperature and water content in the range $\text{Mg}:\text{H}_2\text{O} = 1:6$ to $1:2.9$, and of molten $\text{Ca}(\text{NO}_3)_2\cdot 4\text{H}_2\text{O}$ as a function of temperature, and find eq. 1 is satisfied within experimental error with the same limitations found in the case of the water-free $\text{Ca}(\text{NO}_3)_2\text{-KNO}_3$ melts.¹

The T_0 values (theoretical glass transition temperatures) obtained are, not surprisingly, dependent on the charge concentration, ranging from 201°K . for $\text{Ca}(\text{NO}_3)_2\cdot 4\text{H}_2\text{O}$ to 244°K . for $\text{Mg}(\text{NO}_3)_2\cdot 2.9\text{H}_2\text{O}$; *cf.* $306\text{-}330^\circ\text{K}$. for $\text{KNO}_3\text{-Ca}(\text{NO}_3)_2$ glasses. The important finding, however, is that one can predict T_0 for the 1:4 liquids,⁵ to within experimental error ($\pm 5^\circ$), from the T_0 vs. cation charge-to-radius-ratio plot obtained experimentally for the *water-free* $\text{Ca}(\text{NO}_3)_2\text{-KNO}_3$ melts by making the reasonable assumption that the predominant cations in the liquid *at this composition* are quasi-spherical $\text{M}(\text{H}_2\text{O})_4^{2+}$ ($\text{M}^{2+} = \text{Mg}^{2+}, \text{Ca}^{2+}$) species with effective radii ($2r_{\text{H}_2\text{O}} + r_{\text{M}^{2+}}$). Furthermore, the constant k of eq. 1 for the aqueous nitrates is the same within experimental error as for the $\text{Ca}(\text{NO}_3)_2\text{-KNO}_3$ melts. Finally, plots of E_κ vs. T (*e.g.*, Figure 6 (ii) of ref. 1) for the water-free eutectic melts Li , Na , K , NO_3^6 and Na , K , NO_2 , NO_3 form a natural extension to higher temperatures for E_κ vs. T plots of the aqueous melts of about the same T_0 value, thus linking the temperature dependence of conductance of the aqueous and nonaqueous glass-forming liquids and emphasizing the lack of distinction between them.

Thus, despite some ambiguity arising from the treatment of $\text{M}(\text{H}_2\text{O})_4^{2+}$ species as spherical ions, these

observations strongly imply that both the electrical conductance behavior and the glass-forming ability of these solutions may best be interpreted by regarding the aqueous melts as *molten salts of large (i.e., weak field) cations*.

This appears to be a fruitful concept, as it leads one to predict tetrahedral NiCl_4^{2-} complexes in, *e.g.*, hot ($100\text{-}150^\circ$) highly concentrated MgCl_2 solutions by analogy with NiCl_4^{2-} in molten CsCl .⁷ The existence of these complexes, previously unobserved in aqueous systems, is readily demonstrated by test tube experiments and has now been verified by spectroscopic methods.^{8,9}

The free volume approach offers an interpretation of both the temperature dependence of liquid transport properties and the phenomenon of glass formation, and, as glass-forming ability is apparently quite common among concentrated aqueous solutions, this approach may provide a useful new view of concentrated electrolyte solutions in general.

(1) C. A. Angell, *J. Phys. Chem.*, **64**, 218, 1917 (1964).

(2) M. H. Cohen and D. Turnbull, *J. Chem. Phys.*, **31**, 1164 (1959).

(3) J. W. Mellor, "Comprehensive Treatise on Inorganic and Theoretical Chemistry," Vol. IV, Longmans, Green and Co., London, 1940, p. 380.

(4) We now find that many solutions of highly soluble salts have concentration ranges which are glass-forming on sufficient cooling (*e.g.*, quenching into liquid nitrogen) although it seems that only concentrated $\text{Mg}(\text{NO}_3)_2\text{-H}_2\text{O}$ solutions have high enough glass transition temperatures to yield brittle glasses at room temperature.

(5) The 1:4 compositions are the simplest to treat since the higher water content solutions were not glass-forming and thus T_0 could not be determined experimentally, and for lower water contents the choice of species and their effective radii raises difficulties.

(6) L. A. King, C. C. Bissell, and F. R. Duke, *J. Electrochem. Soc.*, **111**, 720, (1964).

(7) D. M. Gruen and R. L. McBeth, *J. Phys. Chem.*, **63**, 393 (1959).

(8) C. A. Angell and D. M. Gruen, to be published.

(9) NiCl_4^{2-} complexes are not found in concentrated CaCl_2 solutions, however, because the Ni^{2+} competes successfully with the Ca^{2+} for the hydration sheath.

(10) Currently on leave at Argonne National Laboratory, Argonne, Ill.

DEPARTMENT OF METALLURGY
UNIVERSITY OF MELBOURNE
PARKVILLE N.2. VICTORIA
AUSTRALIA

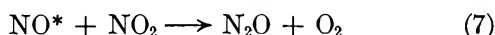
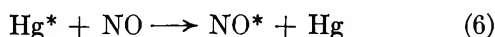
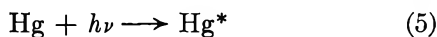
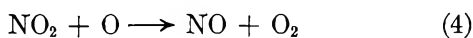
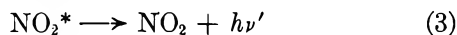
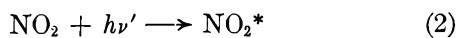
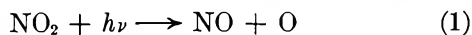
C. A. ANGELL¹⁰

RECEIVED APRIL 9, 1965

Concerning the Reaction $\text{NO}_2 + \text{NO}^* \longrightarrow \text{N}_2\text{O} + \text{O}_2$

Sir: Kistiakowski and co-workers^{1,2} have postulated this reaction as a result of their studies of the flash photolysis of nitrogen dioxide and the reaction of nitrogen atoms with nitrogen dioxide.

We have studied the photolysis of nitrogen dioxide in a flow system using polychromatic radiation of predominantly 3655-Å. wave length. The apparatus and technique used will be described in a succeeding article.³ The kinetics of the photolysis (see Figure 1 and Table I) has led to the postulated mechanism



Reactions 1, 2, 3, and 4 have been studied by numerous investigators.^{4,5} In order to ascertain if reaction 5 occurs, we photolyzed a mixture of nitrous oxide and neopentane (2,2-dimethylpropane) under the same experimental conditions as with nitrogen dioxide. The products of the photolysis of this mixture are nitrogen dioxide, neopentyl alcohol, and the reaction products of neopentyl alcohol and nitrogen dioxide. Since nitrous oxide itself is not decomposed under these conditions, this experiment demonstrates the presence of sufficient mercury vapor in the reaction vessel during the course of a run to initiate the photosensitized decomposition of nitrous oxide.

Reaction 6 has been shown⁶ to be a resonant reaction; *i.e.*, there is essentially no potential energy barrier encountered in going from reactants to products. The excited nitric oxide is in the 4π state.⁷ A transition

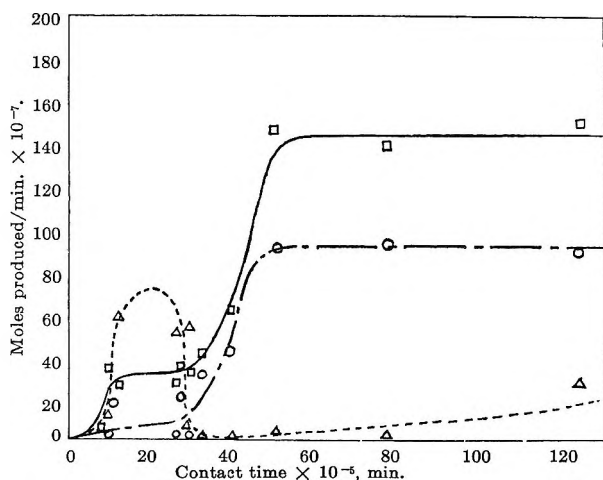
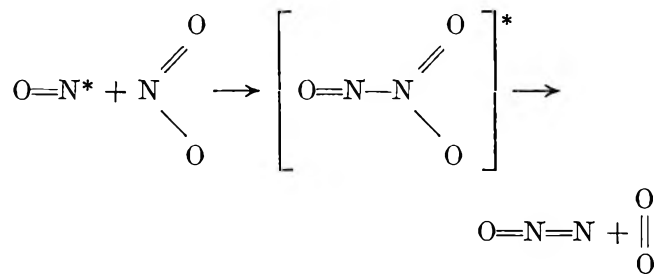


Figure 1. Plots of moles of gas produced per minute vs. contact time: O, nitrous oxide; Δ, nitric oxide; and □, oxygen.

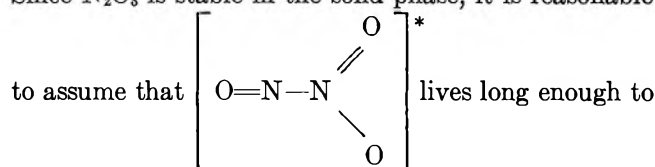
Table I

Run	Contact time × 10 ⁵ min.	Moles of N ₂ O produced/ min. × 10 ⁷	Moles of NO produced/ min. × 10 ⁷	Moles of O ₂ produced/ min. × 10 ⁷
1	124.0	93.4	29.2	154.0
2	63.3	32.4	36.4	83.5
3	11.6	...	59.2	29.5
4	29.0	3.20	54.3	32.0
5	9.38	19.3	13.8	35.7
6	25.8	1.02	52.1	27.6
7	8.62	0.76	11.3	6.81
8	39.0	41.6	0.12	62.5
9	49.5	93.0	4.16	150.0
10	140.0	20.8	146.0	123.0
11	26.8	20.8	4.50	33.7
12	31.6	26.1	2.57	40.2
13	76.5	94.9	0.46	14.3

to this excited state would result in an excited molecule with a long lifetime, since the radiative transition probability of returning to the ground state is exceptionally low.⁶ Consider reaction 7 in detail



This reaction can occur only when the nitrous oxide molecule approaches the nitrogen dioxide molecule in a nitrogen to nitrogen orientation. The nitrogen to nitrogen bond and the oxygen to oxygen bond must be formed and two nitrogen to oxygen bonds broken. Since N₂O₃ is stable in the solid phase, it is reasonable



(1) G. Kistiakowski and P. Kydd, *J. Am. Chem. Soc.*, **79**, 4825 (1957).

(2) G. Kistiakowski and G. Volpi, *J. Chem. Phys.*, **27**, 1141 (1957).

(3) F. Rice and F. Wunderlich, *J. Phys. Chem.*, in press.

(4) F. Ford and N. Endow, *J. Chem. Phys.*, **27**, 1156 (1957).

(5) S. Sato and R. Cvetanović, *Can. J. Chem.*, **36**, 279 (1958).

(6) R. Fallon, J. Vanderslice, and E. Mann, *J. Phys. Chem.*, **63**, 2082 (1959).

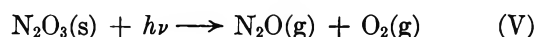
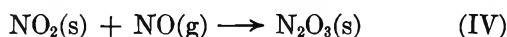
(7) R. P. Frosch and G. W. Robinson, *J. Chem. Phys.*, **41**, 367 (1964).

permit the two oxygen atoms to separate as O_2 . The thermodynamics of the decomposition of N_2O_3 in the gas phase indicates the reaction is exothermic by about 1 kcal./mole.

The activated complex $(N_2O_3)^*$ shown in this mechanism is identical with an excited state of dinitrogen trioxide. Dinitrogen trioxide is formed when an equimolar mixture of nitrogen dioxide and nitric oxide is condensed. Dinitrogen trioxide has never been observed in the gas phase.

From the standpoint of the principle of least motion,⁸ this mechanism would be expected to be more important in the solid phase than in the gas phase. The principle of least motion may be summarized as follows: a low activation energy for an elementary reaction is favored when the motion of the nuclei of the reactant molecules or atoms is minimized. One would thus expect this reaction to be enhanced in the solid phase where the formation of dinitrogen trioxide is ensured.

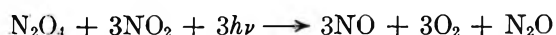
Under experimental conditions which favor reaction in the solid phase, the same products are obtained as in the case of the gas phase photolysis of nitrogen dioxide. The similarity of products is an indication that there may exist reactions in the solid phase analogous to the reactions occurring in the gas phase



Reaction II is less probable than I since the frozen condensate consists mainly of the dimeric species of nitrogen dioxide. Reaction IV is known to occur whenever a gaseous mixture of nitrogen dioxide and nitric oxide is condensed. Reaction V is analogous to reactions 6 and 7 of the postulated gas phase mechanism. Reaction V is more important than reaction 7 of the gas phase mechanism since dinitrogen trioxide is stable in the solid phase. The over-all consecutive reaction in the gas phase is



The analogous consecutive reaction in the solid phase may be written



The reaction postulated by Kistiakowski involving excited nitric oxide molecules and nitrogen dioxide in

the gas phase has as an analogous reaction in the solid phase photochemical decomposition of dinitrogen trioxide.

Acknowledgment. This work was supported in part by the National Science Foundation, Grant G-17434, and in part by the Atomic Energy Commission, Contract At(-40-1) 2590.

(8) F. Rice and E. Teller, *J. Chem. Phys.*, **6**, 489 (1938).

RADIATION LABORATORY
UNIVERSITY OF NOTRE DAME
NOTRE DAME, INDIANA

F. O. RICE

DEPARTMENT OF PHYSICS
GEORGETOWN UNIVERSITY
WASHINGTON, D. C.

F. J. WUNDERLICH

RECEIVED APRIL 19, 1965

Infrared Spectra of Molecules Adsorbed on Metal Powders Obtained from Electrically Exploded Wires

Sir: It has been shown that the electrical explosion of metal wires in an atmosphere ($p \sim 760$ mm.) of a rare gas produces a metal aerosol which, under the proper conditions, consists of spherical particles having a mean diameter of ~ 200 Å.^{1,2} We find that ~ 20 -cm. lengths of *ca.* 0.2-mm. diameter wires may be exploded safely in an argon atmosphere using energies up to 1400 joules in a Pyrex chamber having a 4-l. volume. The condenser bank employs 28.4 μ f. at voltages up to 10 kv. in a circuit having an inductance of 0.3 μ henry.³

The explosion chamber terminates in an 8 cm. o.d. \times 20 cm. closed tube which has been fitted with two diametrically opposed sodium chloride windows. The aerosol is permitted to sediment (~ 2 hr.) onto a salt block which may be moved by magnetic means into the path of an infrared beam which passes through the windows. Spectra were obtained with a Perkin-Elmer Model 521 infrared spectrophotometer.

We have confirmed the particle sizes cited by Karioris, Fish, and Royster² with electron photomicro-

(1) F. G. Karioris and B. R. Fish, *J. Colloid Sci.*, **17**, 155 (1962).

(2) F. G. Karioris, B. R. Fish, and G. W. Royster in "Exploding Wires," Vol. 2, W. G. Chace and H. K. Moore, Ed., Plenum Press, New York, N. Y., 1962, p. 299.

(3) C. P. Nash and C. W. Olsen in ref. 2, p. 5.

graphs of a palladium dispersion and an X-ray line-broadening study of a copper dispersion. When about 5 mg. of aerosol is deposited uniformly on a 6-cm.² salt block, the background transmission in the infrared is $\sim 10\%$.

After the explosion has occurred, the adsorbing gas is introduced, the system is allowed to equilibrate, and the chamber is then evacuated. Systems we have investigated in our initial survey include carbon monoxide on palladium, molybdenum, and copper; and acetylene on copper, nickel, and palladium.

The spectra we observe for carbon monoxide on palladium are in excellent agreement with those discussed by Eischens and Pliskin,⁴ with the single exception that we fail to observe the weak peak at 2065 cm.⁻¹ which these authors find for their silica-supported samples near monolayer coverage. The entire spectrum of carbon monoxide adsorbed on palladium is shifted below the low frequency wing of gaseous CO, so that we were here able to obtain the spectrum of CO adsorbed on aerosols as well as on sedimented powders.

Our spectrum for carbon monoxide on molybdenum, for which a precedent does not exist in the literature, shows a broad, unsymmetrical absorption quite similar to that found in the CO-Pd system, except that the sharp drop in transmission on the high wave number side begins at about 2070 cm.⁻¹ on molybdenum *vs.* 1980 cm.⁻¹ on Pd.

We fail to find any peak which may be attributed to CO adsorbed on copper. This result is in disagreement with the results of Eischens, Pliskin, and Francis,⁵ and Gardner and Petrucci,⁶ all of whom studied silica-supported copper.

The surfaces of our copper samples are far from inactive, however, as evidenced by their behavior toward acetylene. We observe here, in total disagreement with Little, Sheppard, and Yates⁷ (for supported copper), a spectrum having three absorption maxima at 2959, 2924, and 2865 cm.⁻¹, with no others between 3400 and 2700 cm.⁻¹. The striking feature of our result is that both the positions and relative intensities of these peaks are in excellent agreement with the results of Little, *et al.*,⁷ for the adsorbed product obtained when ethylene adsorbed on Vycor-supported palladium was treated with hydrogen. This same spectrum was also obtained by Eischens and Pliskin⁴ by hydrogenating ethylene adsorbed on silica-supported nickel.

If Eischens and Pliskin's⁴ identification of the bound product is correct, we are effecting, spontaneously, a high degree of conversion of adsorbed acetylene to *n*-butyl radicals and carbides. It is clear that substantial amounts of carbide must be present, since a follow-up exposure of our sample to hydrogen produced an increase in the intensity of the spectrum by a factor of about 5, without much alteration in the band shapes.

When explosively dispersed nickel is treated with acetylene, we obtain a spectrum which agrees with that reported by Eischens and Pliskin⁴ for this system and which they attribute to adsorbed ethyl radicals. In our system, as in theirs, hydrogenation leads to an apparent increase in the CH₂:CH₃ ratio. Exposure of a palladium dispersion to acetylene gives rise to adsorbed species which show very weak bands at 2865, 2925, and 2965 cm.⁻¹. We then agree with the recent report of Dunken, Schmidt, and Hobert,⁸ rather than the earlier results of Little, Sheppard, and Yates,⁷ who found only olefinic species until hydrogen gas was added.

From the foregoing, it is clear that the use of exploding wires provides a new and simple means to produce dispersions of any conducting material, whose adsorptive properties may be studied in a manner which should be quite free from extraneous contributions from a supporting medium. That these effects exist may be inferred from the fact that our studies on copper surfaces yield in both cases results which differ markedly from previous investigations.

Acknowledgment. This work was supported by the U. S. Atomic Energy Commission through the Lawrence Radiation Laboratory, Livermore, Calif.

(4) R. P. Eischens and W. A. Pliskin, *Advan. Catalysis*, **10**, 1 (1958).

(5) R. P. Eischens, W. A. Pliskin, and S. A. Francis, *J. Chem. Phys.*, **22**, 1786 (1954).

(6) R. A. Gardner and R. H. Petrucci, *J. Phys. Chem.*, **67**, 1376 (1963).

(7) L. H. Little, N. Sheppard, and D. J. C. Yates, *Proc. Roy. Soc. (London)*, **A259**, 242 (1961).

(8) H. Dunken, K. Schmidt, and H. Hobert, *Z. Chem.*, **4**, 312 (1964).

DEPARTMENT OF CHEMISTRY
UNIVERSITY OF CALIFORNIA
DAVIS, CALIFORNIA 95616

CHARLES P. NASH
ROBERT P. DESIENO

RECEIVED APRIL 12, 1965